

World Journal of *Radiology*

World J Radiol 2017 January 28; 9(1): 1-26





Editorial Board

2014-2017

The *World Journal of Radiology* Editorial Board consists of 365 members, representing a team of worldwide experts in radiology. They are from 36 countries, including Afghanistan (1), Argentina (2), Australia (5), Austria (7), Belgium (2), Brazil (8), Canada (6), Chile (1), China (43), Croatia (1), Denmark (4), Egypt (6), France (5), Germany (22), Greece (10), India (12), Iran (6), Ireland (2), Israel (3), Italy (47), Japan (13), Netherlands (1), New Zealand (1), Pakistan (1), Poland (2), Portugal (1), Serbia (1), Singapore (3), Slovakia (1), South Korea (18), Spain (4), Sweden (2), Switzerland (4), Thailand (1), Turkey (26), United Kingdom (11), and United States (82).

EDITORS-IN-CHIEF

Kai U Juergens, *Bremen*
Edwin JR van Beek, *Edinburgh*
Thomas J Vogl, *Frankfurt*

GUEST EDITORIAL BOARD MEMBERS

Wing P Chan, *Taipei*
Chung-Huei Hsu, *Taipei*
Chin-Chang Huang, *Taipei*
Tsong-Long Hwang, *Taoyuan*
Jung-Lung Hsu, *Taipei*
Chia-Hung Kao, *Taichung*
Yu-Ting Kuo, *Tainan*
Hon-Man Liu, *Taipei*
Hui-Lung Liang, *Kaohsiung*
Chun Chung Lui, *Kaohsiung*
Sen-Wen Teng, *Taipei*
Yung-Liang (William) Wan, *Taoyuan*

MEMBERS OF THE EDITORIAL BOARD



Afghanistan

Takao Hiraki, *Okayama*



Argentina

Patricia Carrascosa, *Vicente Lopez*
Maria C Ziadi, *Rosario*



Australia

Lourens Bester, *Sydney*
Gemma A Figtree, *Sydney*

Stuart M Grieve, *Sydney*
Wai-Kit Lee, *Fitzroy*
Prabhakar Ramachandran, *Melbourne*



Austria

Herwig R Cerwenka, *Graz*
Gudrun M Feuchtnner, *Innsbruck*
Benjamin Henninger, *Innsbruck*
Rupert Lanzenberger, *Vienna*
Shu-Ren Li, *Vienna*
Veronika Schopf, *Vienna*
Tobias De Zordo, *Innsbruck*



Belgium

Steve Majerus, *Liege*
Kathelijne Peremans, *Merelbeke*



Brazil

Clerio F Azevedo, *Rio de Janeiro*
Patrícia P Alfredo, *São Paulo*
Eduardo FC Fleury, *São Paulo*
Edward Araujo Júnior, *São Paulo*
Wellington P Martins, *Ribeirao Preto*
Ricardo A Mesquita, *Belo Horizonte*
Vera MC Salemi, *São Paulo*
Claudia Szobot, *Porto Alegre*
Lilian YI Yamaga, *São Paulo*



Canada

Marie Arsalidou, *Toronto*
Otman A Basir, *Waterloo*

Tarik Zine Belhocine, *Toronto*
James Chow, *Toronto*
Tae K Kim, *Toronto*
Anastasia Oikonomou, *Toronto*



China

Hong-Wei Chen, *Wuxi*
Feng Chen, *Hangzhou*
Jian-Ping Chu, *Guangzhou*
Guo-Guang Fan, *Shenyang*
Bu-Lang Gao, *Shijiazhuang*
Qi-Yong Gong, *Chengdu*
Ying Han, *Beijing*
Xian-Li Lv, *Beijing*
Yi-Zhuo Li, *Guangzhou*
Xiang-Xi Meng, *Harbin*
Yun Peng, *Beijing*
Jun Shen, *Guangzhou*
Ze-Zhou Song, *Hangzhou*
Wai Kwong Tang, *Hong Kong*
Gang-Hua Tang, *Guangzhou*
Jie Tian, *Beijing*
Lu-Hua Wang, *Beijing*
Xiao-bing Wang, *Xi'an*
Yi-Gen Wu, *Nanjing*
Kai Wu, *Guangzhou*
Hui-Xiong Xu, *Shanghai*
Zuo-Zhang Yang, *Kunming*
Xiao-Dan Ye, *Shanghai*
David T Yew, *Hong Kong*
Ting-He Yu, *Chongqing*
Zheng Yuan, *Shanghai*
Min-Ming Zhang, *Hangzhou*
Yudong Zhang, *Nanjing*
Dong Zhang, *Chongqing*
Wen-Bin Zeng, *Changsha*

Yue-Qi Zhu, *Shanghai*



Croatia

Goran Kusec, *Osijek*



Denmark

Poul E Andersen, *Odense*

Lars J Petersen, *Aalborg*

Thomas Z Ramsøy, *Frederiksberg*

Morten Ziebell, *Copenhagen*



Egypt

Mohamed F Bazeed, *Mansoura*

Mohamed Abou El-Ghar, *Mansoura*

Reem HA Mohamed, *Cairo*

Mohamed R Nouh, *Alexandria*

Ahmed AKA Razek, *Mansoura*

Ashraf A Zytoon, *Shebin El-Koom*



France

Sabine F Bensamoun, *Compiègne*

Romarc Loffroy, *Dijon*

Stephanie Nougaret, *Montpellier*

Hassane Oudadesse, *Rennes*

Vincent Vinh-Hung, *Fort-de-France*



Germany

Henryk Barthel, *Leipzig*

Peter Bannas, *Hamburg*

Martin Beeres, *Frankfurt*

Ilja F Ciernik, *Dessau*

A Dimitrakopoulou-Strauss, *Heidelberg*

Peter A Fasching, *Erlangen*

Andreas G Schreyer, *Regensburg*

Philipp Heusch, *Duesseldorf*

Sonja M Kirchhoff, *Munich*

Sebastian Ley, *Munich*

Adel Maataoui, *Frankfurt am Main*

Stephan M Meckel, *Freiburg*

Hans W Muller, *Duesseldorf*

Kay Raum, *Berlin*

Dirk Rades, *Luebeck*

Marc-Ulrich Regier, *Hamburg*

Alexey Surov, *Halle*

Martin Walter, *Magdeburg*

Axel Wetter, *Essen*

Christoph Zilkens, *Düsseldorf*



Greece

Panagiotis Antoniou, *Thessaloniki*

Nikos Efthimiou, *Athens*

Dimitris Karnabatidis, *Patras*

George Latsios, *Athens*

Stylianios Megremis, *Iraklion*

Alexander D Rapidis, *Athens*

Kiki Theodorou, *Larissa*

Ioannis A Tsalafoutas, *Athens*

Evanthia E Tripoliti, *Ioannina*

Athina C Tsili, *Ioannina*



India

Ritesh Agarwal, *Chandigarh*

Chandan J Das, *New Delhi*

Prathamesh V Joshi, *Mumbai*

Naveen Kalra, *Chandigarh*

Chandrasekharan Kesavadas, *Trivandrum*

Jyoti Kumar, *New Delhi*

Atin Kumar, *New Delhi*

Kaushala P Mishra, *Allahabad*

Daya N Sharma, *New Delhi*

Binit Sureka, *New Delhi*

Sanjay Sharma, *New Delhi*

Raja R Yadav, *Allahabad*



Iran

Majid Assadi, *Bushehr*

SeyedReza Najafizadeh, *Tehran*

Mohammad Ali Oghabian, *Tehran*

Amir Reza Radmard, *Tehran*

Ramin Sadeghi, *Mashhad*

Hadi Rokni Yazdi, *Tehran*



Ireland

Tadhg Gleeson, *Wexford*

Frederik JAI Vernimmen, *Cork*



Israel

Dafna Ben Bashat, *Tel Aviv*

Amit Gefen, *Tel Aviv*

Tamar Sella, *Jerusalem*



Italy

Adriano Alippi, *Rome*

Dante Amelio, *Trento*

Michele Anzidei, *Rome*

Filippo F Angileri, *Messinas*

Stefano Arcangeli, *Rome*

Roberto Azzoni, *San Donato milanese*

Tommaso V Bartolotta, *Palermo*

Tommaso Bartalena, *Imola*

Livia Bernardin, *San Bonifacio*

Federico Boschi, *Verona*

Sergio Casciaro, *Lecce*

Emanuele Casciani, *Rome*

Musa M Can, *Napoli*

Alberto Cuocolo, *Napoli*

Michele Ferrara, *Coppito*

Mauro Feola, *Fossano*

Giampiero Francica, *Castel Volturno*

Luigi De Gennaro, *Rome*

Giulio Giovannetti, *Pisa*

Francesca Iacobellis, *Napoli*

Formato Invernizzi, *Monza Brianza*

Francesco Lassandro, *Naples*

Lorenzo Livi, *Florence*

Pier P Mainenti, *Napoli*

Laura Marzetti, *Chieti*

Giuseppe Malinverni, *Crescentino*

Enrica Milanese, *Turin*

Giovanni Morana, *Treviso*

Lorenzo Monti, *Milan*

Silvia D Morbelli, *Genoa*

Barbara Palumbo, *Perugia*

Cecilia Parazzini, *Milan*

Stefano Pergolizzi, *Messina*

Antonio Pinto, *Naples*

Camillo Porcaro, *Rome*

Carlo C Quattrocchi, *Rome*

Alberto Rebonato, *Perugia*

Giuseppe Rizzo, *Rome*

Roberto De Rosa, *Naples*

Domenico Rubello, *Rovigo*

Andrea Salvati, *Bari*

Sergio Sartori, *Ferrara*

Luca M Sconfienza, *Milano*

Giovanni Storto, *Rionero*

Nicola Sverzellati, *Parma*

Alberto S Tagliafico, *Genova*

Nicola Troisi, *Florence*



Japan

Yasuhiko Hori, *Chiba*

Hidetoshi Ikeda, *Koriyama*

Masahito Kawabori, *Sapporo*

Tamotsu Kamishima, *Sapporo*

Hiro Kiyosue, *Yufu*

Yasunori Minami, *Osaka-sayama*

Yasuhiro Morimoto, *Kitakyushu*

Satoru Murata, *Tokyo*

Shigeki Nagamachi, *Miyazaki*

Hiroshi Onishi, *Yamanashi*

Morio Sato, *Wakayama Shi*

Yoshito Tsushima, *Maebashi*

Masahiro Yanagawa, *Suita*



Netherlands

Willem Jan van Rooij, *Tilburg*



New Zealand

W Howell Round, *Hamilton*



Pakistan

Wazir Muhammad, *Abbottabad*



Poland

Maciej S Baglaj, *Wroclaw*

Piotr Czauderna, *Gdansk*



Portugal

Joao Manuel RS Tavares, *Porto*



Serbia

Olivera Ciraj-Bjelac, *Belgrade*



Singapore

Gopinathan Anil, *Singapore*

Terence KB Teo, *Singapore*

Cher Heng Tan, *Singapore*



Slovakia

Stefan Sivak, *Martin*



South Korea

Ki Seok Choo, *Busan*

Seung Hong Choi, *Seoul*

Dae-Seob Choi, *Jinju*

Hong-Seok Jang, *Seoul*

Yong Jeong, *Daejeon*

Chan Kyo Kim, *Seoul*

Se Hyung Kim, *Seoul*

Joong-Seok Kim, *Seoul*

Sang Eun Kim, *Seongnam*

Sung Joon Kwon, *Seoul*

Jeong Min Lee, *Seoul*

In Sook Lee, *Busan*

Noh Park, *Goyang*

Chang Min Park, *Seoul*

Sung Bin Park, *Seoul*

Deuk Jae Sung, *Seoul*

Choongsoo Shin, *Seoul*

Kwon-Ha Yoon, *Iksan*



Spain

Miguel A De Gregorio, *Zaragoza*

Antonio Luna, *Jaén*

Enrique Marco de Lucas, *Santander*

Fernando Ruiz Santiago, *Granada*



Sweden

Dmitry Grishenkov, *Stockholm*

Tie-Qiang Li, *Stockholm*



Switzerland

Nicolau Beckmann, *Basel*

Christian Boy, *Bern*

Giorgio Treglia, *Bellinzona*

Stephan Ulmer, *Kiel*



Thailand

Sirianong Namwongprom, *Chiang Mai*



Turkey

Kubilay Aydin, *Istanbul*

Ramazan Akdemir, *Sakarya*

Serhat Avcu, *Ankara*

Ayşe Aralasmak, *Istanbul*

Oktay Algin, *Ankara*

Nevbahar Akcar, *Meselik*

Bilal Battal, *Ankara*

Zulkif Bozgeyik, *Elazig*

Nazan Ciledag, *Aakara*

Fuldem Y Donmez, *Ankara*

Gulgun Engin, *Istanbul*

Ahmet Y Goktay, *Izmir*

Oguzhan G Gumustas, *Bursa*

Kaan Gunduz, *Ankara*

Pelin Ozcan Kara, *Mersin*

Kivanc Kamburoglu, *Ankara*

Ozgur Kilickesmez, *Istanbul*

Furuzan Numan, *Istanbul*

Cem Onal, *Adana*

Ozgur Oztekin, *Izmir*

Seda Ozbek (Boruban), *Konya*

Selda Sarikaya, *Zonguldak*

Figen Taser, *Kutahya*

Baran Tokar, *Eskisehir*

Ender Uysal, *Istanbul*

Ensar Yekeler, *Istanbul*



United Kingdom

Indran Davagnanam, *London*

M DC Valdés Hernández, *Edinburgh*

Alan Jackson, *Manchester*

Suneil Jain, *Belfast*

Long R Jiao, *London*

Miltiadis Krokidis, *Cambridge*

Pradesh Kumar, *Liverpool*

Peter D Kuzmich, *Derby*

Georgios Plataniotis, *Brighton*

Vanessa Sluming, *Liverpool*



United States

Garima Agrawal, *Saint Louis*

James R Brasic, *Baltimore*

Rajendra D Badgaiyan, *Buffalo*

Ulas Bagci, *Bethesda*

Anat Biegon, *Stony Brook*

Ramon Casanova, *Winston Salem*

Wenli Cai, *Boston*

Zheng Chang, *Durham*

Corey J Chakarun, *Long Beach*

Kai Chen, *Los Angeles*

Hyun-Soon Chong, *Chicago*

Marco Cura, *Dallas*

Ravi R Desai, *Bensalem*

Delia DeBuc, *Miami*

Carlo N De Cecco, *Charleston*

Timm-Michael L Dickfeld, *Baltimore*

Subba R Digumarthy, *Boston*

Huy M Do, *Stanford*

Todd A Faasse, *Grand Rapids*

Salomao Faintuch, *Boston*

Girish M Fatterpekar, *New York*

Dhakshinamoorthy Ganesan, *Houston*

Robert J Griffin, *Little Rock*

Andrew J Gunn, *Boston*

Sandeep S Hedgire, *Boston*

Timothy J Hoffman, *Columbia*

Mai-Lan Ho, *San Francisco*

Juebin Huang, *Jackson*

Abid Irshad, *Charleston*

Matilde Inglese, *New York*

El-Sayed H Ibrahim, *Jacksonville*

Paul R Julsrud, *Rochester*

Pamela T Johnson, *Baltimore*

Ming-Hung Kao, *Tempe*

Sunil Krishnan, *Houston*

Richard A Komoroski, *Cincinnati*

Sandi A Kwee, *Honolulu*

King Kim, *Ft. Lauderdale*

Guozheng Liu, *Worcester*

Yiyan Liu, *Newark*

Venkatesh Mani, *New York*

Lian-Sheng Ma, *Pleasanton*

Rachna Madan, *Boston*

Zeyad A Metwalli, *Houston*

Yilong Ma, *Manhasset*

Hui Mao, *Atlanta*

Feroze B Mohamed, *Philadelphia*

Gul Moonis, *Boston*

John L Noshier, *New Brunswick*

Rahmi Oklu, *Boston*

Aytekun Oto, *Chicago*

Bishnuhari Paudyal, *Philadelphia*

Rajul Pandya, *Youngstown*

Chong-Xian Pan, *Sacramento*

Jay J Pillai, *Baltimore*

Neal Prakash, *Duarte*

Reza Rahbar, *Boston*

Ali S Raja, *Boston*

Gustavo J Rodriguez, *El Paso*

David J Sahn, *Portland*

Steven Schild, *Scottsdale*

Ali R Sepahdari, *Los Angeles*

Li Shen, *Indianapolis*

JP Sheehan, *Charlottesville*

Atul B Shinagare, *Boston*

Sarabjeet Singh, *Boston*

Charles J Smith, *Columbia*

Kenji Suzuki, *Chicago*

Monvadi Srichai-Parsia, *Washington*

Sree H Tirumani, *Boston*

Hebert A Vargas, *New York*

Sachit Verma, *Philadelphia*

Yoichi Watanabe, *Minneapolis*

Li Wang, *Chapel Hill*

Carol C Wu, *Boston*

Shoujun Xu, *Houston*

Min Yao, *Cleveland*

Xiaofeng Yang, *Atlanta*

Qingbao Yu, *Albuquerque*

Aifeng Zhang, *Chicago*

Chao Zhou, *Bethlehem*

Hongming Zhuang, *Philadelphia*



EDITORIAL

- 1 Cutting edge clinical applications in cardiovascular magnetic resonance
De Cecco CN, Muscogiuri G, Varga-Szemes A, Schoepf UJ

MINIREVIEWS

- 5 Functional magnetic resonance imaging and the brain: A brief review
Chow MSM, Wu SL, Webb SE, Gluskin K, Yew DT

ORIGINAL ARTICLE

Retrospective Study

- 10 Impact of contrast-enhanced ultrasound in patients with renal function impairment
Girometti R, Stocca T, Serena E, Granata A, Bertolotto M

Prospective Study

- 17 Multimodality functional imaging using DW-MRI and ¹⁸F-FDG-PET/CT during radiation therapy for human papillomavirus negative head and neck squamous cell carcinoma: Meixoeiro Hospital of Vigo Experience
Aramburu Núñez D, Lopez Medina A, Mera Iglesias M, Salvador Gomez F, Dave A, Hatzoglou V, Paudyal R, Calzado A, Deasy JO, Shukla-Dave A, Muñoz VM

ABOUT COVER

Editorial Board Member of *World Journal of Radiology*, Wenli Cai, PhD, Assistant Professor, Department of Radiology, Massachusetts General Hospital, Harvard Medical School, Boston, MA 02114, United States

AIM AND SCOPE

World Journal of Radiology (*World J Radiol*, *WJR*, online ISSN 1949-8470, DOI: 10.4329) is a peer-reviewed open access academic journal that aims to guide clinical practice and improve diagnostic and therapeutic skills of clinicians.

WJR covers topics concerning diagnostic radiology, radiation oncology, radiologic physics, neuroradiology, nuclear radiology, pediatric radiology, vascular/interventional radiology, medical imaging achieved by various modalities and related methods analysis. The current columns of *WJR* include editorial, frontier, diagnostic advances, therapeutics advances, field of vision, mini-reviews, review, topic highlight, medical ethics, original articles, case report, clinical case conference (clinicopathological conference), and autobiography.

We encourage authors to submit their manuscripts to *WJR*. We will give priority to manuscripts that are supported by major national and international foundations and those that are of great basic and clinical significance.

INDEXING/ABSTRACTING

World Journal of Radiology is now indexed in PubMed, PubMed Central.

FLYLEAF

I-III Editorial Board

EDITORS FOR THIS ISSUE

Responsible Assistant Editor: *Xiang Li*
Responsible Electronic Editor: *Ya-Jing Lu*
Proofing Editor-in-Chief: *Lian-Sheng Ma*

Responsible Science Editor: *Fang-Fang Ji*
Proofing Editorial Office Director: *Xiu-Xia Song*

NAME OF JOURNAL
World Journal of Radiology

ISSN
ISSN 1949-8470 (online)

LAUNCH DATE
January 31, 2009

FREQUENCY
Monthly

EDITORS-IN-CHIEF
Kai U Juergens, MD, Associate Professor, MRT und PET/CT, Nuklearmedizin Bremen Mitte, ZEMODI - Zentrum für morphologische und molekulare Diagnostik, Bremen 28177, Germany

Edwin JR van Beek, MD, PhD, Professor, Clinical Research Imaging Centre and Department of Medical Radiology, University of Edinburgh, Edinburgh EH16 4TJ, United Kingdom

Thomas J Vogl, MD, Professor, Reader in Health Technology Assessment, Department of Diagnostic and Interventional Radiology, Johann Wolfgang Goethe University of Frankfurt, Frankfurt 60590,

Germany

EDITORIAL BOARD MEMBERS
All editorial board members resources online at <http://www.wjnet.com/1949-8470/editorialboard.htm>

EDITORIAL OFFICE
Xiu-Xia Song, Director
World Journal of Radiology
Baishideng Publishing Group Inc
8226 Regency Drive, Pleasanton, CA 94588, USA
Telephone: +1-925-2238242
Fax: +1-925-2238243
E-mail: editorialoffice@wjnet.com
Help Desk: <http://www.wjnet.com/esps/helpdesk.aspx>
<http://www.wjnet.com>

PUBLISHER
Baishideng Publishing Group Inc
8226 Regency Drive,
Pleasanton, CA 94588, USA
Telephone: +1-925-2238242
Fax: +1-925-2238243
E-mail: bpgoffice@wjnet.com
Help Desk: <http://www.wjnet.com/esps/helpdesk.aspx>
<http://www.wjnet.com>

PUBLICATION DATE
January 28, 2017

COPYRIGHT
© 2017 Baishideng Publishing Group Inc. Articles published by this Open-Access journal are distributed under the terms of the Creative Commons Attribution Non-commercial License, which permits use, distribution, and reproduction in any medium, provided the original work is properly cited, the use is non commercial and is otherwise in compliance with the license.

SPECIAL STATEMENT
All articles published in journals owned by the Baishideng Publishing Group (BPG) represent the views and opinions of their authors, and not the views, opinions or policies of the BPG, except where otherwise explicitly indicated.

INSTRUCTIONS TO AUTHORS
<http://www.wjnet.com/bpg/gerinfo/204>

ONLINE SUBMISSION
<http://www.wjnet.com/esps/>

Cutting edge clinical applications in cardiovascular magnetic resonance

Carlo N De Cecco, Giuseppe Muscogiuri, Akos Varga-Szemes, U Joseph Schoepf

Carlo N De Cecco, Akos Varga-Szemes, U Joseph Schoepf, Division of Cardiovascular Imaging, Department of Radiology and Radiological Science, Medical University of South Carolina, Charleston, SC 29425, United States

Giuseppe Muscogiuri, Department of Imaging, Bambino Gesù - Children's Hospital IRCCS, 00146 Rome, Italy

Giuseppe Muscogiuri, Department of Clinical and Molecular Medicine, University of Rome "Sapienza", 00185 Rome, Italy

U Joseph Schoepf, Division of Cardiology, Department of Medicine, Medical University of South Carolina, Charleston, SC 29425, United States

Author contributions: De Cecco CN, Muscogiuri G, Varga-Szemes A and Schoepf UJ all contributed equally to conception, drafting the article and revising it critically for intellectual content.

Conflict-of-interest statement: Dr. U Joseph Schoepf is a consultant for and/or receives research support from Astellas, Bayer, Bracco, GE, Guerbet, Medrad, and Siemens; De Cecco is a consultant for Guerbet and receives financial support from Siemens. The other authors declare no conflict of interest.

Open-Access: This article is an open-access article which was selected by an in-house editor and fully peer-reviewed by external reviewers. It is distributed in accordance with the Creative Commons Attribution Non Commercial (CC BY-NC 4.0) license, which permits others to distribute, remix, adapt, build upon this work non-commercially, and license their derivative works on different terms, provided the original work is properly cited and the use is non-commercial. See: <http://creativecommons.org/licenses/by-nc/4.0/>

Manuscript source: Invited manuscript

Correspondence to: Carlo N De Cecco, MD, PhD, Division of Cardiovascular Imaging, Department of Radiology and Radiological Science, Medical University of South Carolina, 25 Courtenay Drive, MSC 226, Charleston, SC 29425, United States. dececco@musc.edu
Telephone: +1-843-8763185
Fax: +1-843-8763157

Received: September 14, 2016
Peer-review started: September 18, 2016
First decision: October 21, 2016
Revised: November 4, 2016
Accepted: November 27, 2016
Article in press: November 29, 2016
Published online: January 28, 2017

Abstract

Today, the use of cardiovascular magnetic resonance (CMR) is widespread in clinical practice. The increased need to evaluate of subtle myocardial changes, coronary artery anatomy, and hemodynamic assessment has prompted the development of novel CMR techniques including T1 and T2 mapping, non-contrast angiography and four dimensional (4D) flow. T1 mapping is suitable for diagnosing pathologies affecting extracellular volume such as myocarditis, diffuse myocardial fibrosis and amyloidosis, and is a promising diagnostic tool for patients with iron overload and Fabry disease. T2 mapping is useful in depicting acute myocardial edema and estimating the amount of salvageable myocardium following an ischemic event. Novel angiography techniques, such as the self-navigated whole-heart or the quiescent-interval single-shot sequence, enable the visualization of the great vessels and coronary artery anatomy without the use of contrast material. The 4D flow technique overcomes the limitations of standard phase-contrast imaging and allows for the assessment of cardiovascular hemodynamics in the great arteries and flow patterns in the cardiac chambers. In conclusion, the future of CMR is heading toward a more reliable quantitative assessment of the myocardium, an improved non-contrast visualization of the coronary artery anatomy, and a more accurate evaluation of the cardiac hemodynamics.

Key words: Cardiac magnetic resonance; T1 mapping; Magnetic resonance angiography; T2 mapping; Four dimensional flow

© The Author(s) 2017. Published by Baishideng Publishing Group Inc. All rights reserved.

Core tip: The increased need for the evaluation of subtle myocardial changes, coronary artery anatomy, and hemodynamic assessment has prompted the development of novel cardiovascular magnetic resonance (CMR) techniques including T1 and T2 mapping, non-contrast angiography and four dimensional flow. CMR is heading toward a more reliable quantitative assessment of the myocardium, an improved non-contrast visualization of the coronary artery anatomy, and a more accurate evaluation of the cardiac hemodynamics.

De Cecco CN, Muscogiuri G, Varga-Szemes A, Schoepf UJ. Cutting edge clinical applications in cardiovascular magnetic resonance. *World J Radiol* 2017; 9(1): 1-4 Available from: URL: <http://www.wjgnet.com/1949-8470/full/v9/i1/1.htm> DOI: <http://dx.doi.org/10.4329/wjr.v9.i1.1>

Cardiovascular magnetic resonance (CMR) has become a fundamental tool in the diagnostic and therapeutic pathways of several cardiac and vascular diseases. CMR allows for the fast and accurate assessment of cardiac anatomy and function, non-invasive tissue characterization, and blood flow quantification in a single examination. Standard pulse sequences such as T1-weighted and T2-weighted turbo spin echo (TSE) and late gadolinium enhancement (LGE) techniques are widely utilized for myocardial tissue characterization in clinical practice. T1 TSE sequences can depict fatty replacement in arrhythmogenic right ventricular cardiomyopathy, whereas T2-weighted imaging is essential for the evaluation of acute myocardial damage. LGE is important for the assessment of replacement fibrosis and pathologies characterized by myocardial interstitial space expansion.

Although the above techniques have been accepted for clinical application, the use of these sequences for myocardial tissue characterization has a number of limitations. For example, the myocardial signal intensity in T2-weighted images can be influenced by the proximity of the surface coils^[1]. Qualitative evaluation of LGE images is operator-dependent and quantitative assessment is strongly influenced by the designated signal intensity threshold^[2]. The value of the LGE technique may also be limited in cases with diffuse myocardial fibrosis^[3]. Furthermore, it is important to note that LGE requires the administration of contrast agent and is, therefore, not suitable for patients with severe kidney dysfunction.

In order to overcome the aforementioned limitations, CMR sequences including T1 and T2 mapping have recently been developed.

T1 mapping was first introduced to detect diffuse myocardial fibrosis; however, this approach would also be

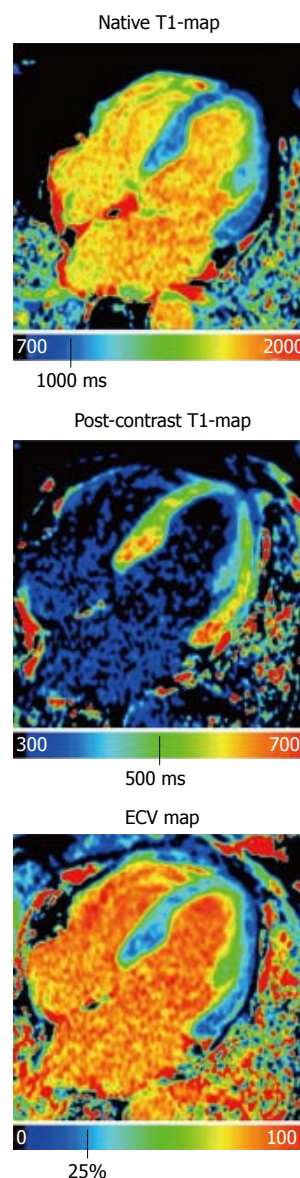


Figure 1 Native T1-map, post-contrast T1-map, and extracellular volume map of the myocardium in a healthy subject. ECV: Extracellular volume.

beneficial in patients with congenital or acquired cardiac pathologies characterized by changes in myocardial extracellular space. In general, T1 mapping can be performed before and after contrast administration. By combining native and post-contrast T1 measurements, the myocardial partition coefficient can be derived, which allows for the calculation of the extracellular volume (ECV) after accounting for the patient's hematocrit (Figure 1)^[4]. Because native T1 correlates with ECV, this technique may allow for tissue characterization in patients with kidney dysfunction, presenting a distinct advantage over LGE imaging techniques. The variation in the range of normal native T1 values stems from the use of different T1 mapping pulse sequences (inversion recovery vs saturation recovery), pulse sequence schemes, magnetic field strengths, etc^[5]. Despite this variation, native T1 mapping has the potential to play a major role in the

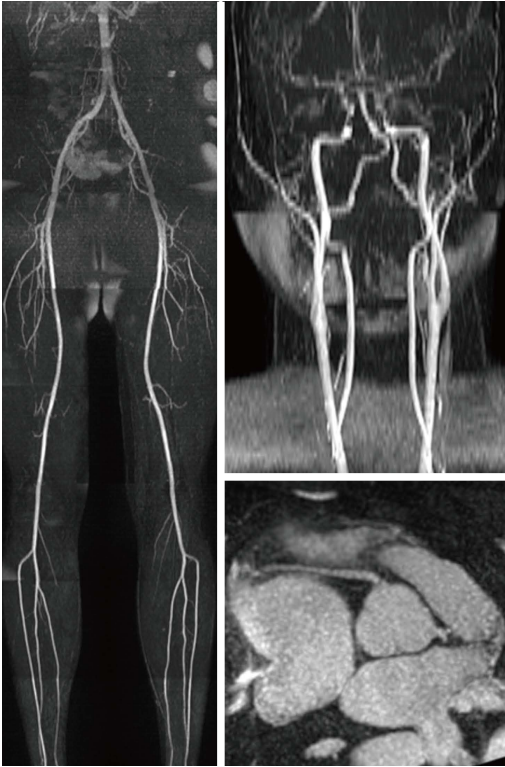


Figure 2 Visualization of the lower extremity, carotid and coronary arteries using quiescent-interval single-shot magnetic resonance angiography.

diagnosis of a variety of cardiac cases. Sado *et al*^[6] showed that T1 mapping improves the detection of mild iron overload. Fontana *et al*^[7] and Banyersad *et al*^[8] showed that native T1 values are significantly higher in patients with cardiac amyloidosis compared to healthy controls and changes in native T1 and ECV can be considered prognostic biomarkers. Additionally, native T1 mapping may be essential in the differential diagnosis of Fabry disease as well as other cardiac diseases characterized by a hypertrophic phenotype^[9].

T2 mapping is based on the collection of different T2-weighted images to sample the T2 decay. T2 mapping is useful for the evaluation of cardiac pathologies characterized by acute myocardial inflammation such as acute myocardial infarction, myocarditis, heart transplant rejection and Takotsubo cardiomyopathy^[10].

Over the past few years, magnetic resonance angiography (MRA) has been surpassed by CT angiography in the clinical arena, mostly due to its faster acquisition time and the concerns related to gadolinium administration-induced nephrogenic systemic sclerosis (NSF). However, recent MR pulse sequence developments show substantial improvement in several aspects. For example, self-navigated whole-heart MRA provides a 3D volume involving the entire heart and the great vessels with an acquisition time of less than 7 min. In addition, it depends less on patient cooperation and can be performed in a free-breathing fashion in a predictable time frame with 100% image acquisition efficiency^[11]. Quiescent-interval single-shot (QISS) MRA (Figure 2), another novel

development, is a robust MRA technique available for both 1.5T and 3T acquisitions. QISS MRA has shown high diagnostic accuracy for the detection of significant arterial stenosis in the lower extremities compared to contrast-enhanced MRA and invasive catheter angiography^[12,13]. QISS MRA has also shown promising results for coronary artery imaging^[14].

The hemodynamic evaluation of blood flow in the great arteries and blood flow patterns in the cardiac chambers also play an important role in patient prognosis, particularly in congenital heart disease assessment. Four dimensional (4D) flow is a promising new technique that proves superior to standard phase-contrast imaging by providing additional information regarding the flow dynamics in the great arteries and flow pathways in both cardiac chambers and great vessels^[15]. This added information about flow pathways in cardiac chambers and great vessels has the potential to aid in identifying left ventricular dysfunction in patients with dilated cardiomyopathy^[16]. In addition, 4D flow allows for wall shear stress evaluation, which helps to better understand the pathologies involving the great vessels^[17].

Considering the variety of new pulse sequences and their potential clinical applications, what is the future of CMR?

T1 and T2 mapping is expected to play a crucial role in depicting subtle myocardial changes. Both techniques may help to eliminate subjectivity in image analysis. The identification of disease-specific T1 and T2 normal ranges would be a great achievement for the accurate quantification of ECV expansion and detection of myocardial involvement. Novel MRA pulse sequences have the potential to broaden the range of clinical indications, providing a valid alternative to CT angiography. Finally, the 4D flow technique may advance understanding of the pathophysiology of different vascular diseases and the hemodynamic impact of flow abnormalities, as well as help with preoperative planning. In addition, a combined T1 mapping and 4D flow approach may provide a better understanding of the relationship between hemodynamics and changes in myocardial tissue^[18].

In conclusion, CMR is heading toward a more reliable quantitative assessment of the myocardium, an improved non-contrast visualization of the coronary artery anatomy, and a more accurate evaluation of cardiac hemodynamics.

REFERENCES

- 1 **Giri S**, Chung YC, Merchant A, Mihai G, Rajagopalan S, Raman SV, Simonetti OP. T2 quantification for improved detection of myocardial edema. *J Cardiovasc Magn Reson* 2009; **11**: 56 [PMID: 20042111 DOI: 10.1186/1532-429X-11-56]
- 2 **McAlindon E**, Pufulete M, Lawton C, Angelini GD, Bucciarelli-Ducci C. Quantification of infarct size and myocardium at risk: evaluation of different techniques and its implications. *Eur Heart J Cardiovasc Imaging* 2015; **16**: 738-746 [PMID: 25736308 DOI: 10.1093/ehjci/ehv111]

- 10.1093/ehjci/jev001]
- 3 **Mewton N**, Liu CY, Croisille P, Bluemke D, Lima JA. Assessment of myocardial fibrosis with cardiovascular magnetic resonance. *J Am Coll Cardiol* 2011; **57**: 891-903 [PMID: 21329834 DOI: 10.1016/j.jacc.2010.11.013]
 - 4 **White SK**, Sado DM, Fontana M, Banyersad SM, Maestrini V, Flett AS, Piechnik SK, Robson MD, Hausenloy DJ, Sheikh AM, Hawkins PN, Moon JC. T1 mapping for myocardial extracellular volume measurement by CMR: bolus only versus primed infusion technique. *JACC Cardiovasc Imaging* 2013; **6**: 955-962 [PMID: 23582361 DOI: 10.1016/j.jcmg.2013.01.011]
 - 5 **Dabir D**, Child N, Kalra A, Rogers T, Gebker R, Jabbour A, Plein S, Yu CY, Otton J, Kidambi A, McDiarmid A, Broadbent D, Higgins DM, Schnackenburg B, Foote L, Cummins C, Nagel E, Puntmann VO. Reference values for healthy human myocardium using a T1 mapping methodology: results from the International T1 Multicenter cardiovascular magnetic resonance study. *J Cardiovasc Magn Reson* 2014; **16**: 69 [PMID: 25384607 DOI: 10.1186/s12968-014-0069-x]
 - 6 **Sado DM**, Maestrini V, Piechnik SK, Banyersad SM, White SK, Flett AS, Robson MD, Neubauer S, Ariti C, Arai A, Kellman P, Yamamura J, Schoennagel BP, Shah F, Davis B, Trompeter S, Walker M, Porter J, Moon JC. Noncontrast myocardial T1 mapping using cardiovascular magnetic resonance for iron overload. *J Magn Reson Imaging* 2015; **41**: 1505-1511 [PMID: 25104503 DOI: 10.1002/jmri.24727]
 - 7 **Fontana M**, Banyersad SM, Treibel TA, Maestrini V, Sado DM, White SK, Pica S, Castelletti S, Piechnik SK, Robson MD, Gilbertson JA, Rowczenio D, Hutt DF, Lachmann HJ, Wechalekar AD, Whelan CJ, Gillmore JD, Hawkins PN, Moon JC. Native T1 mapping in transthyretin amyloidosis. *JACC Cardiovasc Imaging* 2014; **7**: 157-165 [PMID: 24412190 DOI: 10.1016/j.jcmg.2013.10.008]
 - 8 **Banyersad SM**, Fontana M, Maestrini V, Sado DM, Captur G, Petrie A, Piechnik SK, Whelan CJ, Herrey AS, Gillmore JD, Lachmann HJ, Wechalekar AD, Hawkins PN, Moon JC. T1 mapping and survival in systemic light-chain amyloidosis. *Eur Heart J* 2015; **36**: 244-251 [PMID: 25411195 DOI: 10.1093/eurheartj/ehu444]
 - 9 **Thompson RB**, Chow K, Khan A, Chan A, Shanks M, Paterson I, Oudit GY. T+ mapping with cardiovascular MRI is highly sensitive for Fabry disease independent of hypertrophy and sex. *Circ Cardiovasc Imaging* 2013; **6**: 637-645 [PMID: 23922004 DOI: 10.1161/CIRCIMAGING.113.000482]
 - 10 **Ferreira VM**, Piechnik SK, Robson MD, Neubauer S, Karamitsos TD. Myocardial tissue characterization by magnetic resonance imaging: novel applications of T1 and T2 mapping. *J Thorac Imaging* 2014; **29**: 147-154 [PMID: 24576837 DOI: 10.1097/RTI.000000000000077]
 - 11 **Piccini D**, Monney P, Sierro C, Coppo S, Bonanno G, van Heeswijk RB, Chaptin J, Vincenti G, de Blois J, Koestner SC, Rutz T, Littmann A, Zenge MO, Schwitter J, Stuber M. Respiratory self-navigated postcontrast whole-heart coronary MR angiography: initial experience in patients. *Radiology* 2014; **270**: 378-386 [PMID: 24471387 DOI: 10.1148/radiol.13132045]
 - 12 **Hodnett PA**, Koktzoglou I, Davarpanah AH, Scanlon TG, Collins JD, Sheehan JJ, Dunkle EE, Gupta N, Carr JC, Edelman RR. Evaluation of peripheral arterial disease with nonenhanced quiescent-interval single-shot MR angiography. *Radiology* 2011; **260**: 282-293 [PMID: 21502384 DOI: 10.1148/radiol.11101336]
 - 13 **Hodnett PA**, Ward EV, Davarpanah AH, Scanlon TG, Collins JD, Glielmi CB, Bi X, Koktzoglou I, Gupta N, Carr JC, Edelman RR. Peripheral arterial disease in a symptomatic diabetic population: prospective comparison of rapid unenhanced MR angiography (MRA) with contrast-enhanced MRA. *AJR Am J Roentgenol* 2011; **197**: 1466-1473 [PMID: 22109304 DOI: 10.2214/AJR.10.6091]
 - 14 **Edelman RR**, Giri S, Pursnani A, Botelho MP, Li W, Koktzoglou I. Breath-hold imaging of the coronary arteries using Quiescent-Interval Slice-Selective (QISS) magnetic resonance angiography: pilot study at 1.5 Tesla and 3 Tesla. *J Cardiovasc Magn Reson* 2015; **17**: 101 [PMID: 26597281 DOI: 10.1186/s12968-015-0205-2]
 - 15 **Dyverfeldt P**, Bissell M, Barker AJ, Bolger AF, Carlhäll CJ, Ebberts T, Francios CJ, Frydrychowicz A, Geiger J, Giese D, Hope MD, Kilner PJ, Kozerke S, Myerson S, Neubauer S, Wieben O, Markl M. 4D flow cardiovascular magnetic resonance consensus statement. *J Cardiovasc Magn Reson* 2015; **17**: 72 [PMID: 26257141 DOI: 10.1186/s12968-015-0174-5]
 - 16 **Eriksson J**, Bolger AF, Ebberts T, Carlhäll CJ. Four-dimensional blood flow-specific markers of LV dysfunction in dilated cardiomyopathy. *Eur Heart J Cardiovasc Imaging* 2013; **14**: 417-424 [PMID: 22879457 DOI: 10.1093/ehjci/jes159]
 - 17 **Bürk J**, Blanke P, Stankovic Z, Barker A, Russe M, Geiger J, Frydrychowicz A, Langer M, Markl M. Evaluation of 3D blood flow patterns and wall shear stress in the normal and dilated thoracic aorta using flow-sensitive 4D CMR. *J Cardiovasc Magn Reson* 2012; **14**: 84 [PMID: 23237187 DOI: 10.1186/1532-429X-14-84]
 - 18 **van Ooij P**, Allen BD, Contaldi C, Garcia J, Collins J, Carr J, Choudhury L, Bonow RO, Barker AJ, Markl M. 4D flow MRI and T1 -Mapping: Assessment of altered cardiac hemodynamics and extracellular volume fraction in hypertrophic cardiomyopathy. *J Magn Reson Imaging* 2016; **43**: 107-114 [PMID: 26227419 DOI: 10.1002/jmri.24962]

P- Reviewer: Mani V, Ni Y S- Editor: Ji FF L- Editor: A
E- Editor: Lu YJ



Functional magnetic resonance imaging and the brain: A brief review

Maggie SM Chow, Sharon L Wu, Sarah E Webb, Katie Gluskin, DT Yew

Maggie SM Chow, Sharon L Wu, DT Yew, School of Biomedical Science, School of Chinese Medicine, Chinese University of Hong Kong, Hong Kong, China

Sarah E Webb, Division of Life Science, the Hong Kong University of Science and Technology, Hong Kong, China

Katie Gluskin, Department of Neuroscience, St. Mary's College of Maryland, St Marys City, MD 20686, United States

Author contributions: Chow MSM, Wu SL, Webb SE and Gluskin K wrote the paper; Yew DT directed the research.

Conflict-of-interest statement: Authors declare no conflict of interest for this article.

Open-Access: This article is an open-access article which was selected by an in-house editor and fully peer-reviewed by external reviewers. It is distributed in accordance with the Creative Commons Attribution Non Commercial (CC BY-NC 4.0) license, which permits others to distribute, remix, adapt, build upon this work non-commercially, and license their derivative works on different terms, provided the original work is properly cited and the use is non-commercial. See: <http://creativecommons.org/licenses/by-nc/4.0/>

Manuscript source: Invited manuscript

Correspondence to: Dr. Maggie SM Chow, School of Biomedical Science, School of Chinese Medicine, Chinese University of Hong Kong, Hong Kong, China. maggiesmchow@gmail.com
Telephone: +86-852-39434140

Received: June 16, 2016

Peer-review started: June 24, 2016

First decision: August 16, 2016

Revised: September 6, 2016

Accepted: October 22, 2016

Article in press: October 24, 2016

Published online: January 28, 2017

Abstract

Functional magnetic resonance imaging (fMRI) is em-

ployed in many behavior analysis studies, with blood oxygen level dependent- (BOLD-) contrast imaging being the main method used to generate images. The use of BOLD-contrast imaging in fMRI has been refined over the years, for example, the inclusion of a spin echo pulse and increased magnetic strength were shown to produce better recorded images. Taking careful precautions to control variables during measurement, comparisons between different specimen groups can be illustrated by fMRI imaging using both quantitative and qualitative methods. Differences have been observed in comparisons of active and resting, developing and aging, and defective and damaged brains in various studies. However, cognitive studies using fMRI still face a number of challenges in interpretation that can only be overcome by imaging large numbers of samples. Furthermore, fMRI studies of brain cancer, lesions and other brain pathologies of both humans and animals are still to be explored.

Key words: Functional magnetic resonance image; Blood oxygen level dependent imaging; Humans; Pig and rodent models; Aging; Drug effects; Brain lesions and disease

© **The Author(s) 2017.** Published by Baishideng Publishing Group Inc. All rights reserved.

Core tip: We summarize the use of blood oxygen level dependent-contrast imaging in functional magnetic resonance imaging (fMRI) by introducing and comparing the various experimental and analysis methods used, as well as describing the results obtained, and the challenges that might occur in order to derive a hypothesis for further studies and exploration. In addition, an overview of fMRI following sensory stimulation in different specimen groups in both humans and animals is provided.

Chow MSM, Wu SL, Webb SE, Gluskin K, Yew DT. Functional magnetic resonance imaging and the brain: A brief review. *World J Radiol* 2017; 9(1): 5-9 Available from: URL: <http://www.wjgnet.com/1949-8470/full/v9/i1/5.htm> DOI: <http://dx.doi.org/10.4329/wjr.v9.i1.5>

INTRODUCTION

There have recently been a significant number of behavior response analysis studies that have made use of magnetic resonance imaging (MRI), and in particular functional magnetic resonance imaging (fMRI). The majority of these studies make use of blood oxygen level-dependent- (BOLD-) contrast imaging, which involves mapping particular regions of a functioning brain, from the changes in blood oxygen.

BOLD-contrast imaging fMRI has a good enough spatial resolution for the localization of activated brain areas and their delineation from neighbouring regions to be visualised. The voxel representing the area of activation is usually defined as covering a few million neurons^[1]. In addition, the BOLD response lags 1 to 2 s behind the stimulus in order for the vascular system to respond, and in general it peaks at 5 s after the stimulus. A continuation of the same stimulus would downregulate the BOLD response^[1-3]. A refractory period of just a few seconds is frequently inadequate for BOLD imaging after activation to fade (see below), depending on whether the mode of activation is motor, sensory or emotional.

To eliminate noise in the recording, the stimulus must be repeated several times. This process often takes a few minutes to complete, and the results can then be compared across different individuals or animals^[1,4]. With regards to the latter, rodents, pigs and monkeys have all been employed in behavior response analysis studies with BOLD-contrast imaging fMRI^[5-9]. This technique and thus the quality of images generated, has been improved by using both a spin echo pulse and increasing the magnetic strength^[10].

One region of the brain that is popular for fMRI mapping due to it being relatively easy to generate a stimulus, is the sensory part of the brain, including the lateral geniculate bodies and the cortex^[11]. Over the last ten years, our group has employed a number of different inputs of both sensory and motor activations for fMRI mapping, with some success. These include chewing, the opposition of the thumb (in humans) and passively flexing the elbow (in animals). These different types of activation trigger both the motor and the sensory systems, such as proprioception and movement^[12,13]. However, only a limited number of clinical studies on head injuries, Alzheimer's disease and drug use have been documented using this method so far^[4].

QUANTIFYING FMRI RESULTS

In the course of performing fMRI and comparing different specimen groups, it is often necessary to illustrate comparisons with quantitation. This can be achieved *via* a number of methods. For example, the different levels of oxygen usage are frequently illustrated with a pseudocolor scale in the images acquired. In the

commonly used four-color scale, red indicates the highest level of oxygen uptake, yellow is an intermediate level of uptake, green indicates the normal level of oxygen, and blue indicates oxygen levels that are lower than normal (*i.e.*, down-regulation; Figure 1). Utilizing this type of color scale, the researcher can easily compare the volumes of the variously-colored regions either in a specific part of the brain or globally in the whole brain. Indeed, some well-funded research laboratories can afford to purchase software specifically designed to calculate the morphometry for this purpose. Another method used for quantitating fMRI images, which is perhaps more applicable to the smaller, less affluent groups involves manually counting squares on a simple grid. This is placed on successive slices of the fMRI image, after which volume data can be calculated. Though tedious, this method can yield results that are as accurate as those generated from expensive software packages.

In addition to quantitative analysis, qualitative evaluation is also important, for instance to determine the specific regions of the brain that are activated during a particular type of movement. Some of the areas that are activated might be nonspecific, in which case the investigator has to carefully consider each site of activation to determine if any logical deduction might be obtained. In this respect, at least six individuals, when available, should be used for every experiment in each group in order to obtain the n-numbers required to compare the data statistically. Indeed, in some of our previous studies, we aimed to recruit at least a dozen individuals per group. While this was not difficult to achieve with studies using animals, it was sometimes difficult to solicit this number of human volunteers or patients. In addition, we found that fMRI studies are particularly hard to evaluate when the experiments involve cognitive changes that might be affected by emotions. The results of psychometrical tests were variable in different individuals, especially in those with neurosis.

fMRI recordings require the subject (whether human or animal), to perform a particular action in order to trigger a dynamic uptake of oxygen into the brain. This is because fMRI recordings are based on the subsequent increase in oxygen demand from the brain tissue upon the execution of a certain stimulus, whether it is motor, sensory or emotional. One memorable case involved human subjects being asked to repeat a set words in the correct sequence, which elicited a notable increase of blood oxygen levels in the inferior frontal area (BA44) of the brain^[14]. In this study, an uptake of oxygen was normally elicited after repeated and continuous stimulus, and the acquisition of the BOLD-contrast image was usually completed within several seconds after the stimulation ended (in this case after 6 to 18 s). The acquisition of subsequent BOLD-contrast images took > 1 s per slice, *e.g.*, 1.6 s^[14]. The images acquired were then superimposed on the neuroanatomical image of the corresponding slices, which facilitated the localization of

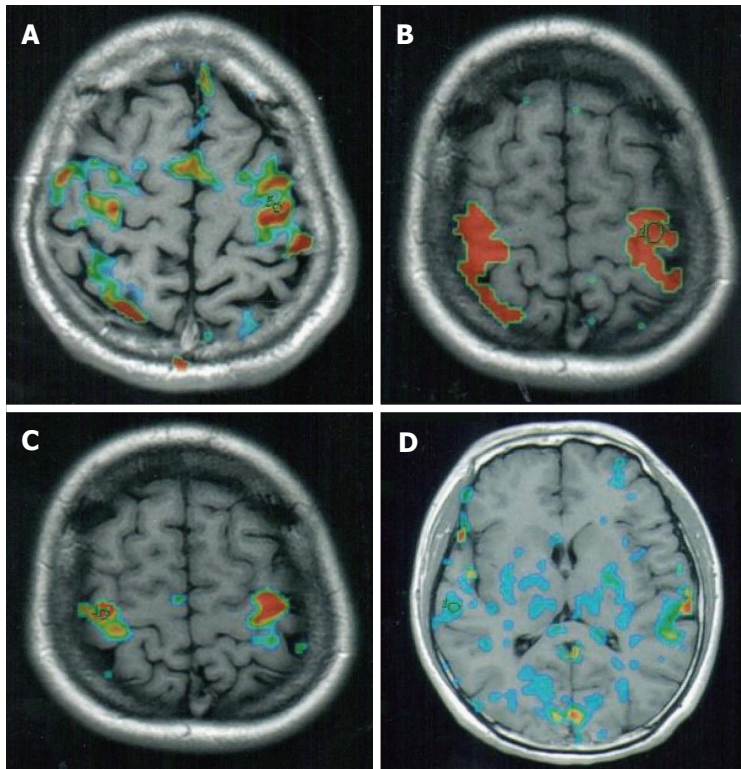


Figure 1 Functional magnetic resonance imaging image of different states. A: fMRI of a short term heroin addict at rest performing no activity and thus have no bodily stimulation. Note some areas still have high BOLD activity (red); B: fMRI of a short term heroin addict when performing motor and sensory activities. Note BOLD image in different regions showing high upregulation of BOLD (red), medium BOLD activity (yellow). While blue indicates downregulation of BOLD activities; C: fMRI of the same individual in (B) at rest after stimulation. There were still some high activity spots of BOLD after stimulation and at rest (red); D: fMRI of a long term (over 7 years) addict of heroin at rest. Many downregulated BOLD spots in the brain (blue). fMRI: Functional magnetic resonance imaging; BOLD: Blood oxygen level dependent.

the sites of recording^[14].

FMRI HUMAN CASES AND DOWNREGULATION

In previous studies, we engaged human volunteers in active movements such as the opposition of the finger and thumb, flexion of the arm or mastication (*e.g.*, by chewing gum)^[12,15]. In animals, such as pigs, rodents and monkeys, however, it is often difficult to capture fMRI images while they are freely and actively moving. Thus, passive movements tend to be performed instead. These include flexion and extension of the limbs and visual stimulation, as well as treatment with drugs.

In order to determine the effect of a specific behaviour on the amount of oxygen uptake in particular regions of the brain using fMRI, images acquired during movement and at rest must be compared. Indeed, valid data can be acquired by subtracting the results recorded at rest from those recorded during movement. Thus, subjects must be imaged as they perform a certain type of movement and then again when they are at rest. It would also be interesting to compare data from fMRI images acquired at different durations of rest after movement, as this might provide useful information regarding changes in the brain that occur during recovery after movement.

A typical example of a standard fMRI recording is depicted in Figure 1. Figure 1A indicates a recording that was acquired when the test subject was at rest. When we conducted this experiment, we were interested to find that in a number of individuals, some sporadic activity occurred in the cortex even at rest. In the recording of

the individual shown in Figure 1, varying levels of activity were registered in the motor, sensory and visual areas of the brain, as well as in the midline of the cortex. Upon stimulation (achieved by thumb and finger opposition), clear and intensive reactions became apparent in the BOLD-contrast images, but these were limited to the motor and sensory areas alone (Figure 1B). Figure 1C depicts the corresponding fMRI image from the same individual following two minutes of stimulation and then one-minute of rest. It is still possible to recognise some residual increased brain activity in the post stimulation resting state. These figures demonstrate the importance of the timing used for the evaluation and comparison of data, as well as the use of the same individual for collecting corresponding sections in each series.

Another comparison method involves depicting of all the active sites of BOLD-contrast fMRI images in the whole brain both at rest and during stimulation. Both of these different methods of comparison are useful in their own way, with the comparison of corresponding slices providing a quantitation of comparison on specific sites, whereas the whole brain images provide a global picture of all the active sites.

In addition to recording the uptake of blood oxygen levels into the brain, the downregulation of blood oxygen has also recently been imaged by fMRI, in order to evaluate subjects with brain damage or brain defects. Figure 1D is an fMRI slice of the brain of long-term heroin addict. The large numbers of blue spots indicate regions of the brain where the blood oxygen levels are lower than normal (as described above, green indicates normal levels of oxygen). In the drug addict's brain, the blood oxygen was low (*i.e.*, downregulated) in the grey

matter, and also in the fibers, especially those in the corpus callosum (Figure 1D). These data confirm those acquired from ordinary MRI of addicts on abusive drugs, which also demonstrated degenerative sites^[16], especially degenerative fibers or grey matter in the cortex, or in groups of nuclei in the cerebellum.

THE USE OF FMRI TO STUDY BRAIN DEVELOPMENT AND DISEASE

fMRI recordings are useful for evaluating the changes in the overall activity of specific brain regions, not only in adults, but also in developing and aging animals. For example, in one study, fMRI was conducted in the neonatal pig. At this stage of development the brain is relatively immature, and it was shown that stimulation of either sensory or motor activities in the body elicited a wide global and non-discrete response in the brain^[7]. Several months later, stimulation of the same activities only produced induced BOLD responses in discrete and related areas of the brain. This example clearly shows that nonselective responses were elicited in the immature brain, whereas in the maturing or fully mature brain, the particular neuronal groups that fired were specific to the related functioning areas. The same type of global nonspecific firing observed in the fMRI of the immature brain can also be observed in some brain diseases such as schizophrenia and bipolar disorders. Follow-up cytochemical and histological studies conducted with the pig concluded that during the development and maturation of the brain, superfluous pathways were pruned significantly, and the number of inhibitory contacts that refine the specificity of each pathway of the brain increased. This study and others, demonstrated the usefulness of utilizing BOLD and fMRI for understanding psychiatric and neurological diseases, and they facilitated the collection of pathological specimens along the way at the same time. The use of fMRI imaging in conjunction with cytochemistry and/or classical pathohistological techniques has the potential to become a very powerful tool to help with the analysis of neurological diseases and mental disorders.

In addition to imaging the developing brain, fMRI can be applied to the aging brain. In a study employing humans of different ages (*i.e.*, young, middle-aged and old), BOLD-contrast imaging of fMRI was recorded in each group as they performed the same motor activities^[12]. The results obtained were interesting and significant. More brain area activations were recorded in individuals in the "old" group (*i.e.*, around 70 years of age), when compared with individuals from the young and middle-aged groups as they conducted the same motor activity. It was concluded that the older brain is less efficient, and so larger areas are required to achieve a certain job. To substantiate this proposition, it was necessary to obtain a similar result in animals. As mentioned previously, specific active movements are a challenge to initiate in animals but passive

movements are easier to control although the results obtained are more difficult to interpret. Therefore, in one a series of experiments we conducted, we used sensory stimulation in order to evaluate the aging hypothesis by applying a weight to the tail of rodents of different ages^[17]. The results obtained with the rodents complimented those of the human studies in that the sensory stimulus triggered increased blood oxygen levels in larger areas of the brains of the older animals than in the young groups. It is therefore tempting to conclude that larger areas of the brain are recruited in the aging groups than in the young groups, to conduct the same functional activity. Perhaps this is due to brains being less efficient overall on aging. On the other hand, it is also possible that on aging it is normal for additional areas of the brain to be used to engage in activities. This would therefore illustrate the plasticity of the brain during aging rather than simply a reduction in the efficiency over time.

CHALLENGES AND FUTURE DIRECTIONS FOR FMRI STUDIES

Cognitive studies using fMRI are extremely important, but the results can be a challenge to interpret. The main difficulties lie in the psychometric nature of the individual to be recorded. For instance, some individuals are very anxious and when they are asked unrelated questions, this elicits responses in areas of the brain that are not normally engaged. Interpretation of data therefore depends on being able to collect a large enough number of samples to be able to exclude false positive results. fMRI imaging has largely been conducted with humans (including normal individuals, patients, addicts, and aged individuals), as well as in animal models of addiction and aging^[18,19]. In the case of patients with various diseases, the way forward for fMRI and its potential are largely still under-explored. However, it might be very insightful to find out how areas of the brain areas react in patients with brain cancer, for example. It would also be interesting to explore any changes that might occur in focal pathological areas and in normal areas surrounding the pathology; as well as what changes take place in the brain as the disease progresses. These are just a few of the studies that might be conducted using BOLD-contrast fMRI.

REFERENCES

- 1 **Huettel SA**, Song AW, McCarthy G. Functional Magnetic resonance imaging. 2nd ed. Sunderland, Mass: Sinauer Associates, 2009: 1-501
- 2 **Dale AM**, Buckner RL. Selective averaging of rapidly presented individual trials using fMRI. *Hum Brain Mapp* 1997; **5**: 329-340 [PMID: 20408237 DOI: 10.1002/(SICI)1097-0193(1997)5: 5<329: : AID-HBM1>3.0.CO; 2-5]
- 3 **Kahn I**, Desai M, Knoblich U, Bernstein J, Henninger M, Graybiel AM, Boyden ES, Buckner RL, Moore CI. Characterization of the functional MRI response temporal linearity via optical control of

- neocortical pyramidal neurons. *J Neurosci* 2011; **31**: 15086-15091 [PMID: 22016542 DOI: 10.1523/JNEUROSCI.0007-11.2011]
- 4 **Rombouts SA**, Bakhof L, Shelten P. Clinical applications of functional brain MRI. 1st edition. Oxford: Oxford University Press, 2008: 1-352
 - 5 **Ogawa S**, Lee TM, Nayak AS, Glynn P. Oxygenation-sensitive contrast in magnetic resonance image of rodent brain at high magnetic fields. *Magn Reson Med* 1990; **14**: 68-78 [PMID: 2161986]
 - 6 **Desai M**, Kahn I, Knoblich U, Bernstein J, Atallah H, Yang A, Kopell N, Buckner RL, Graybiel AM, Moore CI, Boyden ES. Mapping brain networks in awake mice using combined optical neural control and fMRI. *J Neurophysiol* 2011; **105**: 1393-1405 [PMID: 21160013 DOI: 10.1152/jn.00828.2010]
 - 7 **Fang M**, Lorke DE, Li J, Gong X, Yew JC, Yew DT. Postnatal changes in functional activities of the pig's brain: a combined functional magnetic resonance imaging and immunohistochemical study. *Neurosignals* 2005; **14**: 222-233 [PMID: 16301837 DOI: 10.1159/000088638]
 - 8 **Yu H**, Li Q, Wang D, Shi L, Lu G, Sun L, Wang L, Zhu W, Mak YT, Wong N, Wang Y, Pan F, Yew DT. Mapping the central effects of chronic ketamine administration in an adolescent primate model by functional magnetic resonance imaging (fMRI). *Neurotoxicology* 2012; **33**: 70-77 [PMID: 22178134 DOI: 10.1016/j.neuro.2011.11.001]
 - 9 **Sun L**, Li Q, Li Q, Zhang Y, Liu D, Jiang H, Pan F, Yew DT. Chronic ketamine exposure induces permanent impairment of brain functions in adolescent cynomolgus monkeys. *Addict Biol* 2014; **19**: 185-194 [PMID: 23145560 DOI: 10.1111/adb.12004]
 - 10 **Carr VA**, Rissman J, Wagner AD. Imaging the human medial temporal lobe with high-resolution fMRI. *Neuron* 2010; **65**: 298-308 [PMID: 20159444 DOI: 10.1016/j.neuron.2009.12.022]
 - 11 **Kim SG**, Lee SP, Goodyear B, Silva AC, Moonen C, Bandettini PA. Medical Radiology: Diagnostic imaging, Functional MRI: Spatial resolution of BOLD and other fMRI techniques. Berlin: Springer, 2000: 453-463
 - 12 **Fang M**, Li J, Lu G, Gong X, Yew DT. A fMRI study of age-related differential cortical patterns during cued motor movement. *Brain Topogr* 2005; **17**: 127-137 [PMID: 15974472]
 - 13 **Fang M**, Li J, Rudd JA, Wai SM, Yew JC, Yew DT. fMRI mapping of cortical centers following visual stimulation in postnatal pigs of different ages. *Life Sci* 2006; **78**: 1197-1201 [PMID: 16182320 DOI: 10.1016/j.lfs.2005.06.030]
 - 14 **Gore JC**. Principles and practice of functional MRI of the human brain. *J Clin Invest* 2003; **112**: 4-9 [PMID: 12840051 DOI: 10.1172/JCI19010]
 - 15 **Jiang YL**, Tian W, Lu G, Rudd JA, Lai KF, Yeung LY, Wai MS, Li YY, Huang ML, Yew DT. Patterns of cortical activation following motor tasks and psychological-inducing movie cues in heroin users: an fMRI study. *Int J Psychiatry Med* 2014; **47**: 25-40 [PMID: 24956915]
 - 16 **Wang C**, Zheng D, Xu J, Lam W, Yew DT. Brain damages in ketamine addicts as revealed by magnetic resonance imaging. *Front Neuroanat* 2013; **7**: 23 [PMID: 23882190 DOI: 10.3389/fnana.2013.00023]
 - 17 **Zhang L**, Li Q, Wolff LT, Antonio GE, Yeung DK, Zhang A, Wu Y, Yew DT. Changes of brain activity in the aged SAMP mouse. *Biogerontology* 2007; **8**: 81-88 [PMID: 16955218 DOI: 10.1007/s10522-006-9035-9]
 - 18 **Chan WM**, Xu J, Fan M, Jiang Y, Tsui TY, Wai MS, Lam WP, Yew DT. Downregulation in the human and mice cerebella after ketamine versus ketamine plus ethanol treatment. *Microsc Res Tech* 2012; **75**: 258-264 [PMID: 21809417 DOI: 10.1002/jemt.21052]
 - 19 **Wai MS**, Rudd JA, Chan WY, Antonio GE, Yew DT. The effect of Ginkgo biloba on the cerebellum of aging SAMP mouse--a TUNEL, bcl-2, and fMRI study. *Microsc Res Tech* 2007; **70**: 671-676 [PMID: 17405152 DOI: 10.1002/jemt.20452]

P-Reviewer: Gao BL, Pan HC, Takahashi H **S-Editor:** Kong JX

L-Editor: A **E-Editor:** Lu YJ



Retrospective Study

Impact of contrast-enhanced ultrasound in patients with renal function impairment

Rossano Girometti, Tiziano Stocca, Elena Serena, Antonio Granata, Michele Bertolotto

Rossano Girometti, Institute of Diagnostic Radiology, Department of Medical and Biological Sciences, University of Udine, University Hospital "S. Maria della Misericordia", 33100 Udine, Italy

Tiziano Stocca, S.O.C. Radiologia, San Giovanni di Dio Hospital, 34170 Gorizia, Italy

Elena Serena, Michele Bertolotto, Department of Radiology, University of Trieste, Cattinara Hospital, Strada di Fiume, 34149 Trieste, Italy

Antonio Granata, UOC di Nefrologia-Dialisi, "San Giovanni di Dio" Hospital, 92100 Agrigento, Italy

Author contributions: Girometti R and Bertolotto M designed the study; Stocca T and Bertolotto M performed examinations; Stocca T, Serena E, Granata A and Bertolotto M analyzed images; Girometti R, Stocca T, Serena E, Granata A and Bertolotto M analyzed data; Girometti R and Bertolotto M wrote the paper.

Institutional review board statement: The study was reviewed and approved by the Ethical Committee of the Friuli Venezia Giulia, Italy.

Informed consent statement: By Italian regulations (Determinazione Ministeriale 20.03.2008, Delibera del 15.12.2011 del Garante per la Protezione dei Dati personali) informed consent acquisition is waived for retrospective studies.

Conflict-of-interest statement: Nothing to disclose.

Data sharing statement: No additional data are available.

Open-Access: This article is an open-access article which was selected by an in-house editor and fully peer-reviewed by external reviewers. It is distributed in accordance with the Creative Commons Attribution Non Commercial (CC BY-NC 4.0) license, which permits others to distribute, remix, adapt, build upon this work non-commercially, and license their derivative works on different terms, provided the original work is properly cited and the use is non-commercial. See: <http://creativecommons.org/licenses/by-nc/4.0/>

Manuscript source: Invited manuscript

Correspondence to: Rossano Girometti, MD, Institute of Radiology, Department of Medical and Biological Sciences, University of Udine, University Hospital "S. Maria della Misericordia", via Colugna, 33100 Udine, Italy. rgirometti@sirm.org
 Telephone: +39-0432-559266
 Fax: +39-0432-559867

Received: June 11, 2016
 Peer-review started: June 15, 2016
 First decision: July 29, 2016
 Revised: September 18, 2016
 Accepted: November 1, 2016
 Article in press: November 2, 2016
 Published online: January 28, 2017

Abstract

AIM

To investigate the role of contrast enhanced ultrasound (CEUS) in evaluating patients with renal function impairment (RFI) showing: (1) acute renal failure (ARF) of suspicious vascular origin; or (2) suspicious renal lesions.

METHODS

We retrospectively evaluated patients addressed to CEUS over an eight years period to rule-out vascular causes of ARF (first group of 50 subjects) or assess previously found suspicious renal lesions (second group of 41 subjects with acute or chronic RFI). After preliminary grey-scale and color Doppler investigation, each kidney was investigated individually with CEUS, using 1.2-2.4 mL of a sulfur hexafluoride-filled microbubble contrast agent. Image analysis was performed in consensus by two readers who reviewed digital clips of CEUS. We calculated the detection rate of vascular abnormalities in the first group and performed descriptive statistics of imaging findings for the second group.

RESULTS

In the first group, CEUS detected renal infarction or

cortical ischemia in 18/50 patients (36%; 95%CI: 23.3-50.9) and 1/50 patients (2%; 95%CI: 0.1-12), respectively. The detection rate of infarction was significantly higher ($P = 0.0002$; McNemar test) compared to color Doppler ultrasonography (10%). No vascular causes of ARF were identified in the remaining 31/50 patients (62%). In the second group, CEUS detected 41 lesions on 39 patients, allowing differentiation between solid lesions (21/41; 51.2%) vs complex cysts (20/41; 48.8%), and properly addressing 15/39 patients to intervention when feasible based on clinical conditions (surgery and cryoablation in 13 and 2 cases, respectively). Cysts were categorized Bosniak II, IIF, III and IV in 8, 5, 4 and 3 cases, respectively. In the remaining two patients, CEUS found 1 pseudolesion and 1 subcapsular hematoma.

CONCLUSION

CEUS showed high detection rate of renal perfusion abnormalities in patients with ARF, influencing the management of patients with acute or chronic RFI and renal masses throughout their proper characterization.

Key words: Contrast-enhanced ultrasonography; Renal function impairment; Acute renal failure; Renal infarction; Renal lesions; Renal cysts; Bosniak classification

© The Author(s) 2017. Published by Baishideng Publishing Group Inc. All rights reserved.

Core tip: Imaging in patients with renal function impairment (RFI) is challenging because of well-known limitations of conventional color Doppler ultrasound or risks related to the use of contrast media on computed tomography and magnetic resonance imaging. Contrast-enhanced ultrasound is a safer imaging tool in patients with RFI, showing 36% detection rate of renal infarction in patients with acute renal failure of suspicious vascular origin, and the capability of characterizing renal lesions in order to address patients to most proper treatment.

Girometti R, Stocca T, Serena E, Granata A, Bertolotto M. Impact of contrast-enhanced ultrasound in patients with renal function impairment. *World J Radiol* 2017; 9(1): 10-16 Available from: URL: <http://www.wjgnet.com/1949-8470/full/v9/i1/10.htm> DOI: <http://dx.doi.org/10.4329/wjr.v9.i1.10>

INTRODUCTION

Despite technical improvements, imaging of patients with renal function impairment (RFI) is challenging. Contrast-enhanced computed tomography (CT) and magnetic resonance imaging (MRI) provide panoramic representation of the kidneys, perirenal spaces, and vessels, leading to high diagnostic accuracy. However, iodinated contrast agents are potentially harmful in patients with RFI because of the risk of contrast-induced nephropathy (CIN)^[1]. Although risk for nephrogenic systemic fibrosis (NSF) has been better defined over the

last years, concerns still exist for the use of gadolinium chelates in patients with RFI, given uncertainty in pathogenic mechanisms and/or potential additional side effects related to gadolinium accumulation in the brain^[1-4]. In practice, it is recommended to consider alternative imaging modalities in patients at risk with the use of iodinated or gadolinium contrast media^[1].

Color-Doppler ultrasound (US) is the first imaging modality in patients with RFI. It is widely used to rule-out obstruction or investigate renal vessels and parenchymal abnormalities without the use of nephrotoxic agents^[5]. In addition, US permits the detection of incidental, otherwise unknown renal lesions. However, there are well-known limitations of conventional Doppler modes in evaluating these patients, including difficult detection of perfusion abnormalities in globally hypoperfused kidneys, and unreliable characterization of renal masses other than simple cysts^[5-8]. In particular, conventional Doppler modes do not allow differentiation between hypovascular tumors and complicated cysts^[9,10], both of common occurrence in patients with RFI, nor can reliably assess the risk of malignancy of complex cystic masses.

Contrast-enhanced ultrasound (CEUS) has been advocated as the imaging modality of choice to evaluate patients with RFI, given the absence of nephrotoxicity and the ability of representing renal vascularization with excellent sensitivity and high spatial resolution^[9,11]. According to the European federation of societies for ultrasound in medicine and biology (EFSUMB) guidelines, imaging with CEUS should be considered in every patient with RFI, when able to provide the clinically necessary information^[1]. CEUS has the potential to compensate for limitations of conventional Doppler modes with a diagnostic performance comparable or superior to CT in the detection of perfusion abnormalities, lesion characterization (cystic vs solid), and categorization of cysts according to Bosniak criteria^[10,12-14]. To our knowledge, however, evidence supporting the above indications results from reports on patients with normal renal function and experts opinion rather than specifically addressed studies, which currently lack.

The purpose of this study was to investigate the role of CEUS in a population of patients with RFI to assess the cause of renal function deterioration when perfusion abnormalities were clinically suspected or characterize renal lesions.

MATERIALS AND METHODS

Patient's population

Referring institutional review board approved this study and waived for informed consent acquisition due to the retrospective design, in accordance with regulations of our country. By performing a computer search, we identified all patients with RFI who underwent renal CEUS over an 8-years period (January 2004-August 2012) to assess the cause of renal function deterioration, or to attempt characterization of renal masses. Patients

Table 1 Sonographic equipment used in the study

Ultrasound equipment	Contrast-specific mode	No. of patients
MyLab-70 (EsaOte)	CnTI™ (contrast tuned imaging)	7
ATL HDI5000 (Philips)	PIHI™ (pulse inversion harmonic imaging)	15
Sequoia 512 (Acuson Siemens)	CPS™ (contrast pulse sequencing)	54
iU22 (Philips)	PIHI-PM™ (pulse inversion harmonic imaging – power modulation)	15

of the first group were investigated to rule-out a vascular cause for renal function deterioration. They were patients with risk factors for renal infarction manifesting a rapid decline of the estimated glomerular filtration rate (eGFR). In this group, conventional Doppler modes were used to investigate the renal arteries and parenchymal vessels, while CEUS was subsequently performed to rule-out infarcted areas not identified with conventional modes. Patients of the second group had renal masses identified on previous conventional US or unenhanced CT. All of them showed eGFR < 60 mL/min per 1.73 m² estimated from the serum creatinine values using the CKD-EPI equation^[15]. Renal impairment was scored according to the grades of the National Kidney Foundation^[16]. We assessed RFI according to the Kidney disease improving global outcomes (KDIGO) criteria for both acute renal failure (ARF)^[17] and chronic renal failure (CRF)^[18].

A total of 91 patients were enrolled (64 men, 27 women; age range 40-88 years; mean age 71.4 ± 11.02 years), showing renal impairment ranging from grade 3 to grade 5. Indications to CEUS were: (1) assessment of renal function deterioration in 50/91 patients; and (2) characterization of focal renal lesions in the remaining 41/91 patients.

CEUS technique

CEUS was performed using different ultrasound equipment and contrast-specific modes (Table 1). After preliminary grey-scale and color Doppler investigation, CEUS examination was set with low acoustic power to achieve minimum microbubble destruction (mechanical index between 0.06 and 0.2, depending on the equipment used). Each kidney was evaluated separately after *i.v.* injection of a 1.2-2.4 mL dose of a sulfur hexafluoride-filled microbubble contrast agent (SonoVue, BR1, Bracco, Milan, Italy). A 20-gauge cannula was used for contrast injection, followed by a 10 mL normal saline flush. Digital cine-clips were acquired to allow for post-procedure re-evaluation.

Image analysis

One radiologist with 18 years of experience in CEUS performed all the examinations. For the purpose of the study, he and a junior radiologist with five years of experience in this technique reviewed in consensus the images of conventional Doppler modes and the cine-clips of entire CEUS examinations, using a commercially available display workstation (OsiriX MD v.7.5, Pixmeo, Bernex, CH). Readers were blinded to histological

diagnosis and/or follow-up results. No discrepancies were found between image interpretation at the time of examinations and during study review. Readers were asked to assess the presence of renal infarctions, characterize renal lesions as solid or cystic, and classify those with cystic appearance at CEUS according to the Bosniak criteria.

Readers assessed renal infarction on conventional Doppler modes in presence of parenchymal regions lacking color signal^[19]. Concerning CEUS, we used the following diagnostic criteria: (1) infarction was diagnosed in presence of at least one well-defined, wedge-shaped non-enhancing area within an otherwise normal-appearing kidney^[12]; (2) cortical ischemia was diagnosed in presence of enhancing interlobar and arcuate arteries with non-enhancing portions of the cortex^[11]; and (3) a lesion was considered solid if more than half of the volume was represented by enhancing solid tissue, and cystic if composed predominantly of nonenhancing spaces^[10,20]. Cystic lesions were graded according to the Bosniak criteria as previously described^[13,14].

Data analysis

For the group of patients investigated to rule-out a vascular cause for renal function deterioration we calculated the detection rate of vascular abnormalities [(number of positive cases/total number of cases) × 100]. Analysis was performed on a per-patient basis by identifying at least one area of renal involvement. Significance of the difference between techniques in the detection rate of renal infarction was assessed with the McNemar test, using a reference alpha level of 0.01. Analysis was performed with a commercially available software (MedCalc v9.1, Mariakerke, Belgium).

For the group of patients with suspicious renal lesions we performed descriptive statistics of CEUS findings on a per-lesion basis.

RESULTS

Patients with acute RFI of suspicious vascular origin

Of fifty patients, 38 were males and 12 females (mean age: 71 ± 9 years, range 40-88 years). They presented with ARF either in previously well-functioning kidneys (31/50, 62%; 95%CI: 47.2-75.0), or complicating an already known CRF (19/50, 38%; 95%CI: 25.0-52.8). Causes of ARF were established based on clinical history and imaging follow-up in 44/50 cases (88%), renal biopsy in 3/50 cases (6.0%) and autopsy in the

Table 2 Overview of fifty patients with acute renal failure addressed to contrast-enhanced ultrasound to rule-out vascular causes

Findings on CEUS	Side of CEUS findings	Pre-existing renal function	Cause of acute renal failure	No. of patients with biopsy
Renal infarction (<i>n</i> = 18)	Unilateral (<i>n</i> = 13) Bilateral (<i>n</i> = 5)	Chronic RFI (<i>n</i> = 10) No previous history of RFI (<i>n</i> = 8)	Suspicious embolization (<i>n</i> = 2) Placement of aortic endoprosthesis (<i>n</i> = 5) Aortic dissection (<i>n</i> = 2) Ischemia (<i>n</i> = 3) Drug-induced nephrotoxicity (<i>n</i> = 1) Undetermined (<i>n</i> = 5)	None
Acute cortical necrosis pattern (<i>n</i> = 1)	Bilateral (<i>n</i> = 1)	No previous history of RFI (<i>n</i> = 1)	Post-surgical, hypovolemic acute tubular necrosis (<i>n</i> = 1)	None
No vascular abnormalities (<i>n</i> = 31)	None	Chronic RFI (<i>n</i> = 21) No previous history of RFI (<i>n</i> = 10)	Atheroembolic disease (<i>n</i> = 10) Acute pyelonephritis (<i>n</i> = 4) Interstitial nephritis (<i>n</i> = 2) Acute papillary necrosis (<i>n</i> = 1) Antiblastic drug-induced (<i>n</i> = 1) Dehydration (<i>n</i> = 1) Undetermined (<i>n</i> = 12)	1 kidney biopsy, 3 skin biopsy 2 kidney biopsy

CEUS: Contrast enhanced ultrasound; RFI: Renal function impairment.

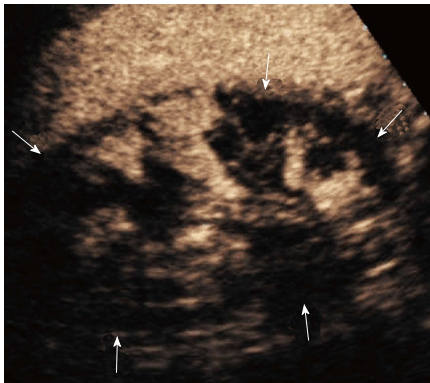


Figure 1 Patient with solitary kidney developing acute renal failure. Contrast enhanced ultrasound showed multiple renal infarctions (arrows) involving a large portion of the parenchyma.

remaining 3/50 cases (6.0%).

Renal infarction was found in 18/50 patients (36%; 95%CI: 23.3-50.9) using CEUS and 5/50 (10%; 95%CI: 3.7-22.6) using color Doppler US, corresponding to a significant difference in detection rate ($P = 0.0002$). In particular, CEUS found infarction in 13 additional subjects compared to color Doppler US (Figure 1). Moreover, CEUS identified acute cortical necrosis in one patient (2%; 95%CI: 0.1-12.0) presenting with non-specific hypoperfusion of the kidneys at color Doppler interrogation (Figure 2).

In the remaining 31/50 patients (62%; 95%CI: 47.2-75.0), there was no evidence of vascular abnormalities both on color Doppler US and CEUS. Final presumptive diagnosis was reached in 20/31 patients based on clinical and laboratory features, course of the disease and kidney biopsy in three subjects (two with interstitial nephritis and one with atheroembolic renal disease, respectively). Other three patients with

atheroembolic renal disease had positive skin biopsy. In the remaining 12 patients, the cause of renal function deterioration remained undetermined. CEUS findings, pre-existing renal function and final diagnosis are reported in Table 2.

Patients with renal lesions

Of 41 patients included in this group, 26 were male and 15 female (mean age: 70 ± 14 years, range 41-90 years). CEUS showed a total of 41 lesions in 39 patients.

Twenty-one/41 lesions were solid in nature (51.2%; 95%CI: 35.4-66.8), whereas 20/41 lesions were assessed as complex cysts (48.8%; 95%CI: 33.2-64.6). Twelve out of 21 solid lesions were removed surgically, with final diagnosis of renal cancer, including 11 clear cell carcinomas (Figure 3) and 1 urothelial carcinoma. The remaining lesions included one oncocytoma diagnosed on autopsy, 7 indeterminate lesions addressed to imaging follow-up because of patients' age and comorbidities contraindicating surgery, and one inoperable lesion addressed to angiographic embolization because of acute intratumoral hemorrhage.

Cysts were classified according to Bosniak categories II, II F, III and IV in 8, 5, 4 and 3 cases, respectively. All category II F lesions, 1/4 category III and 1/3 category IV cysts remained stable over a 3-years imaging follow-up (Figure 4). Two category III cysts were a papillary and a clear cell renal cell carcinoma (RCC) on biopsy performed before percutaneous cryoablation. One category IV lesion was a clear cell RCC at nephrectomy (Figure 5). The remaining two patients (one with category III, one with category IV cysts) were not operated because of clinically relevant comorbidities. Lesions increased in size and complexity over time and were considered presumably malignant. The remaining two patients with suspicious renal tumor on conventional US had a pseudotumour

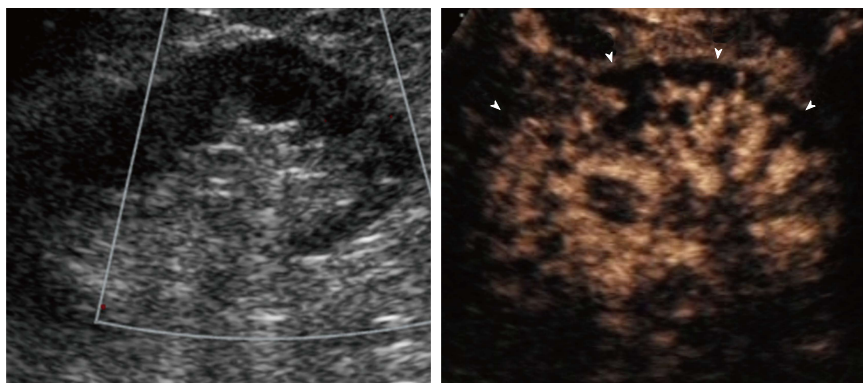


Figure 2 Patient with grade III chronic renal failure developing acute renal failure after Endovascular aortic repair. A: Color Doppler ultrasound showed avascular kidney; B: Contrast enhanced ultrasound showed enhancing hilar vessels and lack of enhancement of large portions of the cortex (arrowheads) consistent with acute cortical necrosis. The contralateral kidney was normal (not shown).

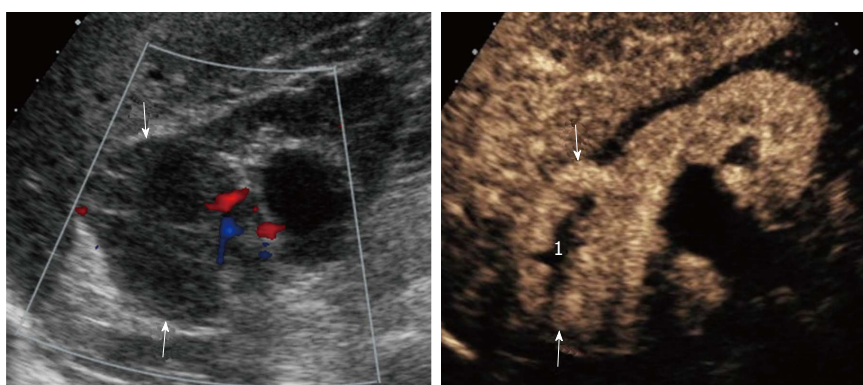


Figure 3 Patient with grade III chronic renal failure. A: Color Doppler ultrasound showed markedly reduced renal parenchyma perfusion and a hypoechoic lesion without obvious vascularity (arrows); B: Contrast enhanced ultrasound showed a solid enhancing mass (arrows) with avascular central portion (1). A clear cell RCC with necrotic central areas was found at surgery. RCC: Renal cell carcinoma.

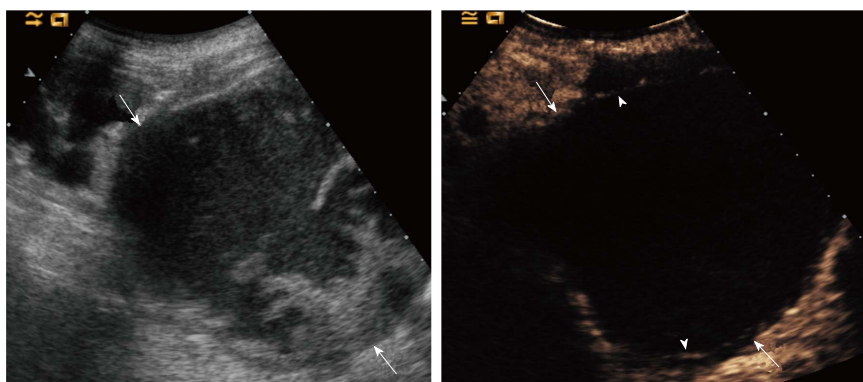


Figure 4 Patient with grade IV chronic renal failure. A: Grey-scale ultrasound showed a complex renal lesion (arrows). Contrast enhanced ultrasound showed no intralesional enhancement, nor vegetations; B: Two thin septa were visible (arrowheads) with minimum enhancement (benign minimally complicated cysts, Bosniak category II).

and a subcapsular hematoma at CEUS, respectively.

DISCUSSION

Current EFSUMB guidelines recommend use of CEUS in patients with RFI^[1]. Indeed, this technique can be performed during the same examination session of color Doppler US, thus acting as first-line and problem-solving imaging modality at the same time^[9,11].

However, indication to CEUS in this scenario is based more on theoretical considerations and experts opinion than on results of validation studies. Indeed, the ability of CEUS to identify renal infarction and to characterize complex cystic masses, pseudolesions, and hypovascular lesions has been mostly demonstrated in patients with well-functioning kidneys^[10,12,13,21]. To our knowledge, no specific studies focused on patients with renal failure. Moreover, there is lack of evidence on whether

information obtained with CEUS in patients with RFI has a clinical impact for patient management.

Our results on a consecutive series of patients with renal failure investigated with CEUS show that this technique is effective in identifying renal infarction and characterizing renal masses. When a vascular cause for the deterioration of the renal function was suspected, CEUS either confirmed the diagnosis or, when negative, prompted further clinical workup and eventually identification of other causes of renal function deterioration. CEUS clearly outperformed US with color Doppler, with a significantly higher detection rate of renal infarction (36% vs 10%) ($P = 0.0002$). Moreover, CEUS was able to differentiate between renal infarctions and cortical ischemia, which showed no definite correspondence on color Doppler US. Therefore, CEUS proved to be effective as problem solving technique in these patients, with the advantage of avoiding radiation

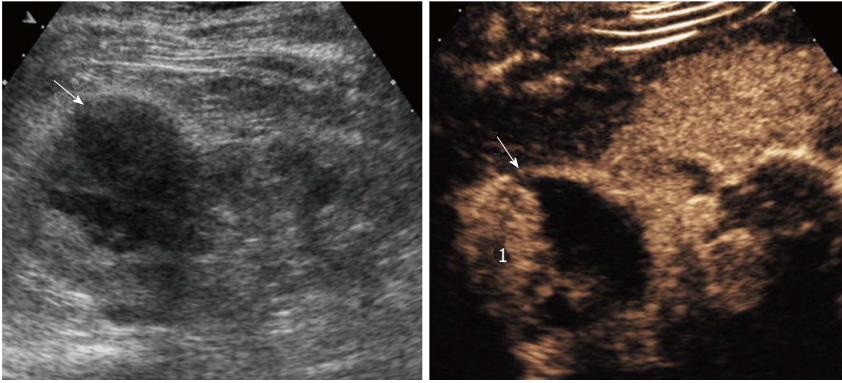


Figure 5 Patient with grade III chronic renal failure that one category IV lesion was a clear cell renal cell carcinoma at nephrectomy. A: Grey-scale ultrasound showed a complex renal lesion (arrow); B: Contrast enhanced ultrasound showed thickened wall with a vegetation (1) consistent for a presumably malignant, Bosniak category IV lesion. A clear cell renal cell carcinoma was found at surgery.

exposure or the use of nephrotoxic contrast agents. When renal lesions were identified in patients with renal failure, CEUS was able to discriminate between solid and cystic ones, as well as to categorize cysts according to the Bosniak criteria. Characterizing lesions with indeterminate appearance on conventional US modes as a presumably benign cysts prevented unnecessary operations in patients with renal failure (usually poor surgical candidates with high risk of complications), and further deterioration of the renal function.

Though cost-effectiveness analysis was beyond the purpose of this study, one can reasonably assume that evaluating the above patients with CEUS would lead to prompt diagnosis and treatment while minimizing patients' risk and costs compared to conventional diagnostic strategy combining US and CT/MRI (including related complications). One might argue that the use of CEUS is often limited to experienced centers, and no randomized controlled trials support the above statements. However, the experience acquired in reference centres and guidelines recommendations (*e.g.*, EFSUMB ones) are now promoting an ever-increasing and widespread use of CEUS, as exemplified by extended indications to paediatric population^[1]. We also believe that our study results might contribute as a reference for the planning of future studies designed to obtain high-level evidence in large populations with normal or impaired renal function. Potential effectiveness of CEUS diagnosis is further emphasized by the fact that this technique can be performed at patients' bedside, which is of special advantage for critically ill ones.

This study has several limitations. The most important one is that the gold standard investigation has not been obtained for the majority of patients with renal function deterioration. Because of the concern for further deterioration of renal function, no additional imaging modalities were performed when the results of CEUS and clinical features were found sufficient for patient's work-up. Only a limited number of patients with suspicious perfusion abnormalities had kidney biopsy (3/50 patients). As a consequence, causative diagnosis for renal function deterioration remained indeterminate in 5 patients with CEUS findings suggestive for renal infarction and 12 patients without CEUS evidence of vascular abnormalities. Gold standard investigation was not available also for 25/41 renal

masses (8/21 solid lesions and 17/20 cysts), whereas 12 patients with presumably malignant renal lesions (7 solid indeterminate lesions, 1 inoperable solid lesion and 4 Bosniak III-IV cysts) were not operated because the surgical risk was considered excessive due to comorbidities. However, all operated or ablated lesions ($n = 15$) were found to have cancer at histological examination, thus emphasizing the effectiveness of CEUS in guiding most proper treatment.

Another major limitation of the present study is its retrospective design. This might have introduced a case-selection bias, because some cases may have not been recorded for inclusion. Additionally, a relatively small number of lesions have been evaluated, reflecting the fact that CEUS has been performed as a problem solving technique to assess very specific diagnostic questions.

Finally, in our series CEUS failed to detect perfusion abnormalities in patients with atheroembolic renal disease. We can only speculate on the anatomic basis for this finding: atheroembolic renal disease consists in patchy embolization of very small arteries (interlobular and afferent arterioles) by cholesterol crystals resulting in cortical ischemic areas which are likely too small to be detected with imaging methods.

In conclusion, our study shows that CEUS has a significant role as a problem-solving technique for detection of perfusion abnormalities and characterization of renal lesions in patients with renal failure. CEUS can be performed in emergency at the bedside. In our series, it was helpful in stratifying treatment decisions, as shown by the fact that all patients with suspicious renal cancer in whom surgery was not contraindicated were operated properly.

ACKNOWLEDGMENTS

The authors thank Dr. Iliana Bednarova from the Institute of Radiology, University of Udine, for her help in revising English language.

COMMENTS

Background

Imaging in patients with acute or chronic renal function impairment (RFI) is challenging because of nephrotoxicity or the risk for nephrogenic systemic fibrosis (NSF) related to the use of computed tomography (CT) and magnetic

resonance imaging contrast agents, respectively. Contrast-enhanced ultrasound (CEUS) is gaining widespread acceptance as the imaging modality of choice to evaluate patients with RFI, given the absence nephrotoxicity and the ability of representing renal vascularization with excellent sensitivity and high spatial resolution. However, the consensus on its use in this setting is related more to experts' opinion and clinical practice than specifically addressed studies. Hence, evidence on this topic still lacks as a basis to support clinical practice and future trials.

Research frontiers

CEUS has a pivotal role in assessing patients with RFI. However, despite the use of CEUS in this scenario, there is paucity of scientific evidence supporting it. The results of the study show that CEUS has a significant impact in managing patients with RFI and might contribute to strengthen the recommendation to use it as the imaging method of choice in this setting.

Innovations and breakthroughs

The authors provided an evidence-based background for supporting the use of CEUS in patients with RFI. CEUS is safer than contrast-enhanced computed tomography and/or magnetic resonance imaging in evaluating patients with RFI. This technique can be performed on patients' bedside, thus allowing prompt diagnosis and management.

Applications

Their study shows that CEUS is a problem-solving technique in detecting perfusion abnormalities and characterizing renal lesions in patients with renal failure.

Terminology

CEUS: An ultrasound technique using microbubble contrast agents.

Peer-review

This is a well-written paper.

REFERENCES

- 1 **Piscaglia F**, Nolsøe C, Dietrich CF, Cosgrove DO, Gilja OH, Bachmann Nielsen M, Albrecht T, Barozzi L, Bertolotto M, Catalano O, Claudon M, Clevert DA, Correia JM, D'Onofrio M, Drudi FM, Eyding J, Giovannini M, Hocke M, Ignee A, Jung EM, Klausner AS, Lassau N, Leen E, Mathis G, Saftoiu A, Seidel G, Sidhu PS, ter Haar G, Timmerman D, Weskott HP. The EFSUMB Guidelines and Recommendations on the Clinical Practice of Contrast Enhanced Ultrasound (CEUS): update 2011 on non-hepatic applications. *Ultraschall Med* 2012; **33**: 33-59 [PMID: 21874631 DOI: 10.1055/s-0031-1281676]
- 2 **Thomsen HS**. Nephrogenic systemic fibrosis: A serious late adverse reaction to gadodiamide. *Eur Radiol* 2006; **16**: 2619-2621 [PMID: 17061066 DOI: 10.1007/s00330-006-0495-8]
- 3 **Thomsen HS**, Morcos SK, Almén T, Bellin MF, Bertolotto M, Bongartz G, Clement O, Leander P, Heinz-Peer G, Reimer P, Stacul F, van der Molen A, Webb JA. Nephrogenic systemic fibrosis and gadolinium-based contrast media: updated ESUR Contrast Medium Safety Committee guidelines. *Eur Radiol* 2013; **23**: 307-318 [PMID: 22865271 DOI: 10.1007/s00330-012-2597-9]
- 4 **Stojanov D**, Aracki-Trenkic A, Benedeto-Stojanov D. Gadolinium deposition within the dentate nucleus and globus pallidus after repeated administrations of gadolinium-based contrast agents-current status. *Neuroradiology* 2016; **58**: 433-441 [PMID: 26873830 DOI: 10.1007/s00234-016-1658-1]
- 5 **Pozzi Mucelli R**, Bertolotto M, Quaià E. Imaging techniques in acute renal failure. *Contrib Nephrol* 2001; **132**: 76-91 [PMID: 11395914]
- 6 **Kim SH**, Cho JY, Kim SY, Moon KC, Kwak C, Kim HH. Ultrasound Evaluation of Renal Masses: Gray-scale, Doppler, and More. *Ultrasound Clinics* 2013; **8**: 565-579 [DOI: 10.1016/j.cult.2013.07.002]
- 7 **Cantisani V**, Bertolotto M, Weskott HP, Romanini L, Grazhdani H, Passamonti M, Drudi FM, Malpassini F, Isidori A, Meloni FM, Calliada F, D'Ambrosio F. Growing indications for CEUS: The kidney, testis, lymph nodes, thyroid, prostate, and small bowel. *Eur J Radiol* 2015; **84**: 1675-1684 [PMID: 26014102 DOI: 10.1016/j.ejrad.2015.05.008]
- 8 **Pozzi Mucelli R**, Bertolotto M. Imaging techniques in acute renal failure. *Kidney Int* 1998; **66**: S102-S105
- 9 **Bertolotto M**, Derchi LE, Cicero C, Iannelli M. Renal Masses as Characterized by Ultrasound Contrast. *Ultrasound Clin* 2013; **8**: 581-592 [DOI: 10.1016/j.cult.2013.07.003]
- 10 **Bertolotto M**, Cicero C, Perrone R, Degraffi F, Cacciato F, Cova MA. Renal Masses With Equivocal Enhancement at CT: Characterization With Contrast-Enhanced Ultrasound. *AJR Am J Roentgenol* 2015; **204**: W557-W565 [PMID: 25905962 DOI: 10.2214/AJR.14.13375]
- 11 **Granata A**, Zanolì L, Insalaco M, Valentino M, Pavlica P, Di Nicolò PP, Scuderi M, Fiorini F, Fatuzzo P, Bertolotto M. Contrast-enhanced ultrasound (CEUS) in nephrology: Has the time come for its widespread use? *Clin Exp Nephrol* 2015; **19**: 606-615 [PMID: 25351822 DOI: 10.1007/s10157-014-1040-8]
- 12 **Bertolotto M**, Martegani A, Aiani L, Zappetti R, Cernic S, Cova MA. Value of contrast-enhanced ultrasonography for detecting renal infarcts proven by contrast enhanced CT. A feasibility study. *Eur Radiol* 2008; **18**: 376-383 [PMID: 17851664 DOI: 10.1007/s00330-007-0747-2]
- 13 **Ascenti G**, Mazziotti S, Zimbaro G, Settineri N, Magno C, Melloni D, Caruso R, Scribano E. Complex cystic renal masses: characterization with contrast-enhanced US. *Radiology* 2007; **243**: 158-165 [PMID: 17392251 DOI: 10.1148/radiol.2431051924]
- 14 **Quaià E**, Bertolotto M, Cioffi V, Rossi A, Baratella E, Pizzolato R, Cova MA. Comparison of contrast-enhanced sonography with unenhanced sonography and contrast-enhanced CT in the diagnosis of malignancy in complex cystic renal masses. *AJR Am J Roentgenol* 2008; **191**: 1239-1249 [PMID: 18806171 DOI: 10.2214/AJR.07.3546]
- 15 **Levey AS**, Stevens LA, Schmid CH, Zhang YL, Castro AF, Feldman HI, Kusek JW, Eggers P, Van Lente F, Greene T, Coresh J. A new equation to estimate glomerular filtration rate. *Ann Intern Med* 2009; **150**: 604-612 [PMID: 19414839]
- 16 **Levey AS**, Eckardt KU, Tsukamoto Y, Levin A, Coresh J, Rossert J, De Zeeuw D, Hostetter TH, Lameire N, Eknoyan G. Definition and classification of chronic kidney disease: a position statement from Kidney Disease: Improving Global Outcomes (KDIGO). *Kidney Int* 2005; **67**: 2089-2100 [PMID: 15882252 DOI: 10.1111/j.1523-1755.2005.00365.x]
- 17 KDIGO Clinical Practice Guideline for Acute Kidney Injury. *Kidney International Supplements* 2012; **2**: 8-12 [DOI: 10.1038/kisup.2012.7]
- 18 **Levey AS**, Coresh J, Balk E, Kausz AT, Levin A, Steffes MW, Hogg RJ, Perrone RD, Lau J, Eknoyan G. National Kidney Foundation practice guidelines for chronic kidney disease: evaluation, classification, and stratification. *Ann Intern Med* 2003; **139**: 137-147 [PMID: 12859163 DOI: 10.7326/0003-4819-139-2-200307150-00013]
- 19 **Hélén O**, el Rody F, Correia JM, Melki P, Chauveau D, Chrétien Y, Moreau JF. Color Doppler US of renovascular disease in native kidneys. *Radiographics* 1995; **15**: 833-854; discussion 854-865 [PMID: 7569132 DOI: 10.1148/radiographics.15.4.7569132]
- 20 **Tamai H**, Takiguchi Y, Oka M, Shingaki N, Enomoto S, Shiraki T, Furuta M, Inoue I, Iguchi M, Yanaoka K, Arai K, Shimizu Y, Nakata H, Shinka T, Sanke T, Ichinose M. Contrast-enhanced ultrasonography in the diagnosis of solid renal tumors. *J Ultrasound Med* 2005; **24**: 1635-1640 [PMID: 16301719]
- 21 **Mazziotti S**, Zimbaro F, Pandolfo A, Racchiusa S, Settineri N, Ascenti G. Usefulness of contrast-enhanced ultrasonography in the diagnosis of renal pseudotumors. *Abdom Imaging* 2010; **35**: 241-245 [PMID: 19194642 DOI: 10.1007/s00261-008-9499-y]

P- Reviewer: Abou El-Ghar M, Markic D, Salvi PF, Scarpioni R, Watanabe T **S- Editor:** Qiu S **L- Editor:** A **E- Editor:** Lu YJ



Prospective Study

Multimodality functional imaging using DW-MRI and ¹⁸F-FDG-PET/CT during radiation therapy for human papillomavirus negative head and neck squamous cell carcinoma: Meixoeiro Hospital of Vigo Experience

David Aramburu Núñez, Antonio Lopez Medina, Moisés Mera Iglesias, Francisco Salvador Gomez, Abhay Dave, Vaïos Hatzoglou, Ramesh Paudyal, Alfonso Calzado, Joseph O Deasy, Amita Shukla-Dave, Victor M Muñoz

David Aramburu Núñez, Antonio Lopez Medina, Francisco Salvador Gomez, Department of Medical Physics and Radiological Protection, Galaria - Meixoeiro, University Hospital Complex of Vigo, 36200 Vigo, Spain

David Aramburu Núñez, Abhay Dave, Ramesh Paudyal, Joseph O Deasy, Amita Shukla-Dave, Department of Medical Physics, Memorial Sloan-Kettering Cancer Center, New York, NY 10065, United States

David Aramburu Núñez, Alfonso Calzado, Department of Radiology, Complutense University, 28040 Madrid, Spain

Moisés Mera Iglesias, Department of Medical Physics, Oncoserv, Santiago de los Caballeros 51000, Dominican Republic

Vaïos Hatzoglou, Amita Shukla-Dave, Department of Radiology, Memorial Sloan-Kettering Cancer Center, New York, NY 10065, United States

Victor M Muñoz, Department of Radiation Oncology, Galaria - Meixoeiro, University Hospital Complex of Vigo, 36200 Vigo, Spain

Author contributions: Aramburu Núñez D, Lopez Medina A and Shukla-Dave A designed the study, performed MRI research, analyzed the data and wrote the paper; Dave A and Paudyal R analyzed the data and reviewed the paper; Mera Iglesias M and Salvador Gomez F performed MRI research and provided software support; Muñoz VM enrolled patients, and performed clinical assessment as per standard of care; Hatzoglou V performed the radiologic assessment; Calzado A and Deasy JO provided support.

Supported by The National Health Institute of Spain: ISCIII Grant PI11/02035 and DTS14/00188; BIOCAPS project (FP7/REGPOT-2012-2013.1), No. 316265; MSKCC internal IMRAS grant; and in part through the NIH/NCI Cancer Center, No. P30

CA008748.

Institutional review board statement: Six patients were enrolled in the Meixoeiro Hospital of Vigo Research Protocol entitled "Radioterapia adaptativa y predicción de la respuesta tumoral basadas en estudios funcionales de RM y PET/CT en cáncer de cabeza y cuello" (ISCIII Grant PI1102035).

Informed consent statement: All patients gave informed consent for their participation in the study approved by the hospital, which was conducted in accordance with the Declaration of Helsinki.

Conflict-of-interest statement: All authors have no conflicts of interest with regard to this manuscript.

Data sharing statement: Upon formal request and with proper motivation, all original data in anonymized format is available from the corresponding author for local inspection, but cannot leave Meixoeiro Hospital of Vigo and Memorial Sloan Kettering Cancer Center.

Open-Access: This article is an open-access article which was selected by an in-house editor and fully peer-reviewed by external reviewers. It is distributed in accordance with the Creative Commons Attribution Non Commercial (CC BY-NC 4.0) license, which permits others to distribute, remix, adapt, build upon this work non-commercially, and license their derivative works on different terms, provided the original work is properly cited and the use is non-commercial. See: <http://creativecommons.org/licenses/by-nc/4.0/>

Manuscript source: Invited manuscript

Correspondence to: Amita Shukla-Dave, PhD, Director Quantitative Imaging, Department of Medical Physics, Memorial Sloan-Kettering Cancer Center, 1275 York Avenue, New York, NY 10065, United States. davea@mskcc.org

Telephone: +1-212-6393184
Fax: +1-212-7173010

Received: August 17, 2016
Peer-review started: August 18, 2016
First decision: October 21, 2016
Revised: October 29, 2016
Accepted: November 21, 2016
Article in press: November 23, 2016
Published online: January 28, 2017

Abstract

AIM

To noninvasively investigate tumor cellularity measured using diffusion-weighted magnetic resonance imaging (DW-MRI) and glucose metabolism measured by ^{18}F -labeled fluorodeoxyglucose positron emission tomography/computed tomography (^{18}F -FDG-PET/CT) during radiation therapy (RT) for human papillomavirus negative (HPV-) head and neck squamous cell carcinoma (HNSCC).

METHODS

In this prospective study, 6 HPV- HNSCC patients underwent a total of 34 multimodality imaging examinations (DW-MRI at 1.5 T Philips MRI scanner [($n = 24$) pre-, during- (2-3 wk), and post-treatment (Tx), and ^{18}F -FDG PET/CT pre- and post-Tx ($n = 10$)]. All patients received RT. Monoexponential modeling of the DW-MRI data yielded the imaging metric apparent diffusion coefficient (ADC) and the mean of standardized uptake value (SUV) was measured from ^{18}F -FDG PET uptake. All patients had a clinical follow-up as the standard of care and survival status was documented at 1 year.

RESULTS

There was a strong negative correlation between the mean of pretreatment ADC ($\rho = -0.67$, $P = 0.01$) and the pretreatment ^{18}F -FDG PET SUV. The percentage (%) change in delta (Δ) ADC for primary tumors and neck nodal metastases between pre- and Wk₂₋₃ Tx were as follows: 75.4% and 61.6%, respectively, for the patient with no evidence of disease, 27.5% and 32.7%, respectively, for those patients who were alive with disease, and 26.9% and 7.31%, respectively, for those who were dead with disease.

CONCLUSION

These results are preliminary in nature and are indicative, and not definitive, trends rendered by the imaging metrics due to the small sample size of HPV- HNSCC patients in a Meixoeiro Hospital of Vigo Experience.

Key words: Diffusion-weighted magnetic resonance imaging; Human papillomavirus negative head and neck squamous cell carcinoma; ^{18}F -labeled fluorodeoxyglucose positron emission tomography/computed tomography

© The Author(s) 2017. Published by Baishideng Publishing Group Inc. All rights reserved.

Core tip: In the modern era of adaptive radiotherapy, it is crucial to understand how different imaging techniques interact and complement each other for application in cancer care. The quantitative imaging metrics, apparent diffusion coefficient and standardized uptake value, play a significant role in understanding the efficacy of the radiotherapy treatment. Tumor cellularity and glucose metabolism were investigated before, during, and after radiotherapy in human papillomavirus negative head and neck squamous cell carcinoma patients using the diffusion-weighted magnetic resonance imaging and ^{18}F -labeled fluorodeoxyglucose positron emission tomography/computed tomography imaging techniques.

Aramburu Núñez D, Lopez Medina A, Mera Iglesias M, Salvador Gomez F, Dave A, Hatzoglou V, Paudyal R, Calzado A, Deasy JO, Shukla-Dave A, Muñoz VM. Multimodality functional imaging using DW-MRI and ^{18}F -FDG-PET/CT during radiation therapy for human papillomavirus negative head and neck squamous cell carcinoma: Meixoeiro Hospital of Vigo Experience. *World J Radiol* 2017; 9(1): 17-26 Available from: URL: <http://www.wjgnet.com/1949-8470/full/v9/i1/17.htm> DOI: <http://dx.doi.org/10.4329/wjcr.v9.i1.17>

INTRODUCTION

The Spanish Cancer Registries reported that in 2014, 241284 new cases of cancer were diagnosed in Spain^[1]. Out of these, 12696 were head and neck (HN) cancers in which approximately 90% were specifically squamous cell carcinomas (SCC)^[2]. The main subgroup for the patients was oropharyngeal SCC wherein 52%-72% of the cases were caused by infection from the human papillomavirus (HPV)^[3]. It has been previously reported that HPV negative (-) HNSCC patients have poor outcomes compared with HPV-positive (HPV+) cancers^[4]. Thus, in an effort to perform biologically guided adaptive radiotherapy, it is critical to understand how different functional imaging techniques interact and potentially complement each other^[5]. Multimodality imaging, such as diffusion-weighted magnetic resonance imaging (DW-MRI) and ^{18}F -labeled fluorodeoxyglucose positron emission tomography/computed tomography (^{18}F -FDG-PET/CT), can provide useful anatomical and functional quantitative imaging metrics.

DW-MRI provides a noninvasive measurement for the degree of random motion of water in tissue; the rate of this diffusion is quantified by a quantitative imaging metric, the apparent diffusion coefficient (ADC)^[6]. The advantage of DW-MRI over traditional anatomical MRI is that it can reflect the tissue cellularity and the integrity of cell membranes^[7]. A recent metaanalysis reported that ADC has an inverse correlation with tissue cell density^[8]. Kim *et al*^[9] have shown that a significant increase in ADC was observed within 1 wk of treatment in HNSCC patients who were complete responders ($P < 0.01$). The Vandecaveye

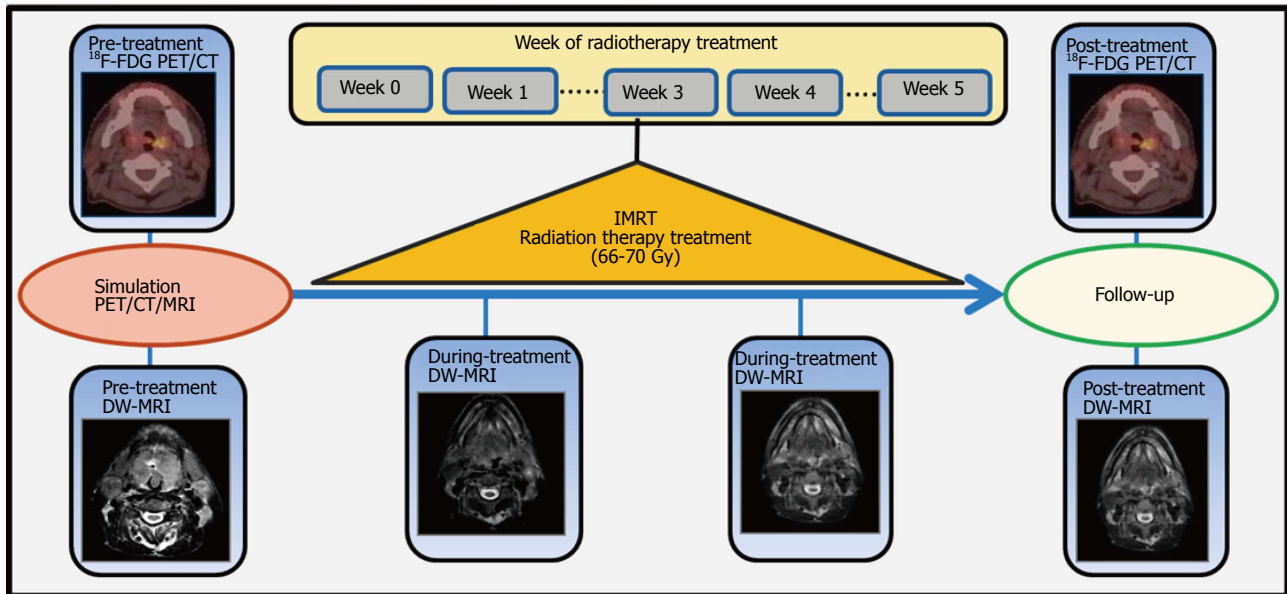


Figure 1 Workflow representing the study design performed in all the patients. ¹⁸F-FDG: Fluorine-18 Fludeoxyglucose; PET/CT: Positron emission tomography/computed tomography; DW-MRI: Diffusion-weighted magnetic resonance imaging.

et al.^[10] study further established the utility of ADC in differentiating responding from non-responding HNSCC by providing a threshold (25% and 20% for primary tumors and lymph node metastases, respectively) for the percent relative (Δ) ADC change between pre-treatment (Tx) and 3 wk post-chemoradiotherapy (post-CRT).

Another quantitative imaging metric, standardized uptake value (SUV), obtained from ¹⁸F-FDG PET is a measure of glucose metabolism. An abnormally elevated SUV can be observed in most primary and metastatic cancers including HNSCC^[11]. The ¹⁸F-FDG PET/CT has an established role in HNSCC management, including staging and monitoring CRT response^[12,13]. The Schwartz *et al.*^[14] study showed that primary tumor SUV was a promising prognostic factor in HNSCC patients.

A better understanding of the association between ¹⁸F-FDG PET/CT and DW-MRI derived quantitative imaging metrics is needed in order for them to become the building blocks for a biologically-guided adaptive radiotherapy. Recently there have been few reports showing correlations between these multimodality imaging techniques and their initial role in the prognosis of HNSCC patients^[15]. However, there are limited studies initiated to explore the use of these techniques together in a treatment planning setting for radiation oncology^[16]. Our study is the first experience in Spain with multimodality imaging in HPV-HNSCC patients for its use in biologically-guided adaptive radiotherapy. The purpose of the current study is to non-invasively investigate tumor cellularity measured using DW-MRI and glucose metabolism measured by ¹⁸F-FDG-PET/CT during RT for HPV- HNSCC.

MATERIALS AND METHODS

Patients

This prospective study was conducted in accordance with

the Declaration of Helsinki^[17]. The study protocol was approved by the local ethics committee; informed consent was obtained from all patients. All patients eligible for this study had biopsy-proven newly diagnosed squamous cell carcinoma of the head and neck. Diagnostic biopsies were also performed to evaluate HPV status. Six HPV- HNSCC patients underwent a total of 34 multimodality imaging examinations [DW-MRI at 1.5 T Philips MRI scanner ($n = 24$) pre-, during (2-3 wk) and post-Tx, and ¹⁸F-FDG PET/CT pre- and post-Tx ($n = 10$)] (Figure 1). All the patients were treated with intensity-modulated radiation therapy (IMRT), and the prescribed doses varied between 66 Gy and 70 Gy to the local planning target volume (PTV). Patient characteristics are given in Table 1.

All the patients had a clinical follow-up as the standard of care and survival status was documented into groups at 1 year. The four groups for patients were as follows: No evidence of disease (NED), alive with disease (AWD), dead of disease (DOD), and dead of other causes (DOC). Additionally, local-regional and distant metastases statuses were noted for all patients^[18].

DWI-MRI

All MRI examinations were performed on a 1.5-Tesla Achieva scanner (Philips Healthcare, The Netherlands) with a Philips Sense Flex coil over the neck. For MRI, all patients were in the supine position with an immobilization system that was also used during the radiotherapy treatment delivery. A thermoplastic mask, head support, and flat table were used to minimize distortion and improve the registration process between the different imaging modalities. The head support and flat table were adapted to the MRI/safety requirements. The MRI protocol consisted of the standard anatomic MRI scans (T1-/T2-weighted images) and DW-MRI.

DW-MRI acquisition was performed using single-shot echo planar imaging (SS-EPI) with three b values ($b =$

Table 1 Characteristics of the patients involved in this study

Characteristics	Value
Demographics	
Mean age (yr)	65
Age range (yr)	52-79
Male/female	5/1
Location of primary tumor	
Oropharynx	6
Metastatic loco-regional nodes	11
Radiation therapy technique	IMRT
Dose (Gy)	66-70
Fractions	32
Outcome	
Alive with disease	3
Dead of disease	2
No evidence of disease	1

0, 600 and 1000 s/mm²). Other parameters included repetition time (TR) = 5000 ms, echo time (TE) = 77-100 ms, number of excitations (NEX) = 2, field of view (FOV): 24 cm, and slice thickness = 6 mm. The total acquisition time for obtaining the DW-MRI data was approximately 5 min. The acquisition matrix of 120 × 97 was zero filled to 256 × 256 during image reconstruction.

¹⁸F-FDG PET/CT

A whole-body PET/CT scan was performed from head to thigh, 60 min after intravenous administration of approximately 370 MBq (± 10%) of ¹⁸F-FDG on a PET/CT Discovery scanner (GE Healthcare Bio-Sciences Corp.). The patient was placed in the supine position, with the same immobilization system as in the radiotherapy treatment delivery. Other parameters included a 70 cm axial FOV, a 218 × 218 matrix. Data was acquired in a 3-D mode. The pixel spacing was 5.47 mm with a slice thickness of 3.27 mm. The spatial resolution varied from 3.99 mm to 4.56 mm. PET images were corrected using the specific software of the equipment for attenuation, scatter, decay, dead time, random coincidences, and slice sensitivity.

Image analysis

All images were registered and analyzed using in-house software (Artfibio-tool)^[19]. The registration for DW-MRI and ¹⁸F-FDG PET/CT datasets was a two-step process: (1) Manual registration: performing a manual alignment (translation and/or rotation) of the images (DWMRI, CT-Scan, PET-CT) interactively on-screen; and (2) Automatic Rigid Registration: Once the images were approximately aligned, a more precise alignment (full rigid transformation) was performed based on an iterative process evaluated by statistical metrics (Viola and Wells mutual information^[20]). Using Artfibio-tool, the signal intensity values were extracted from the whole tumor volumes^[19].

DW-MRI: According to Stejskal and Tanner's^[21] and considering the monoexponential approximation (7), the ADC value was calculated using equation 1:

$$ADC = [\log_e(S_0/S_1)]/(b_1 - b_0). \quad (1)$$

Where S_1 and S_0 are signal values of the images at b_1 values, b_1 and b_0 , respectively, and ADC is the apparent diffusion coefficient.

Regions of Interest (ROIs) were delineated on the primary tumor and neck nodal metastases by an experienced neuroradiologist on the DW-MRI image ($b = 0$ s/mm²). Before contouring the ROIs, the T1-T2-weighted images were used to determine localization and tumor extent.

Finally, a relative percentage (%) change in derived imaging metric (ADC) between pre- and i^{th} intra-Tx week (Wk) was calculated as follows:

$$\Delta ADC (\%) = [(ADC_i - ADC_0)/ADC_0] \times 100. \quad (2)$$

Where i^{th} represents intra-Tx week for ADC metric value and ADC_0 represents the pre-Tx metric value.

¹⁸F-FDG PET/CT: An experienced radiation oncologist matched the ROIs from the MR images with those of the PET/CT images and analyzed them qualitatively and quantitatively using the attenuation-corrected PET emission images. The ROIs were placed over the areas of focal ¹⁸F-FDG uptake in both the primary tumor and neck nodal metastases. The intensity of the ¹⁸F-FDG uptake in the ROIs was measured using the SUV normalized by the dilution volume^[22]. The imaging data available in units of mCi per mL (mCi/mL) per voxel were decay-corrected to the time of injection and converted to SUV units.

Statistical analysis

In the present study, data was analyzed from a total of 34 multimodality imaging studies [DW-MRI ($n = 24$) pre-, during- (2-3 wk) and post-Tx and ¹⁸F-FDG PET/CT pre- and post-Tx ($n = 10$)] to capture treatment response. Values were presented as mean ± SD. The mean value comparison was carried out using the Wilcoxon test. A Spearman correlation analysis was performed between SUV and ADC metric values, which we used to report the correlation and P -values. These correlations were reported using the standard guidelines^[23] in which an absolute correlation of < 0.3 was considered weak, 0.3-0.5 was considered moderate and 0.5-1.0 was considered strong. The significance level was set at $P \leq 0.05$. All data analysis was performed using the R software/environment, an open source project that is distributed under the GNU General Public License^[24].

RESULTS

All 6 patients were untreated at the first time point of multimodality imaging, had biopsy-proven SCC, and were HPV-. Among the 6 patients, a total of 11 neck nodal metastases and 5 primary tumors were analyzed (3 patients had more than one node and 1 patient had an unknown primary tumor site). Patients were grouped as follows based on clinical outcome: NED = 1, AWD = 3, and DOD = 2 (Table 1). A total of 34 multimodality imaging studies [DW-MRI ($n = 24$) and ¹⁸F-FDG PET/

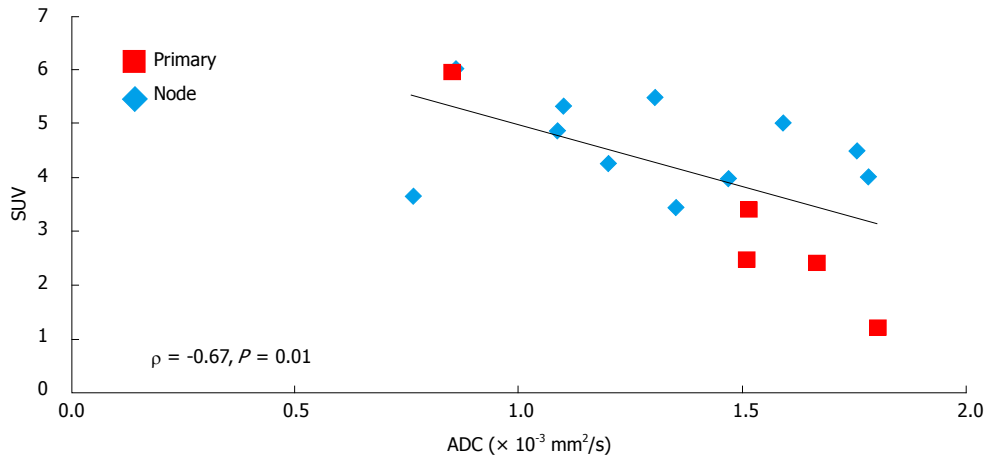


Figure 2 Relationship between pre-Tx mean standardized uptake value and pre-Tx mean apparent diffusion coefficient showing a significant strong negative inverse correlation. SUV: Standardized uptake value; ADC: Apparent diffusion coefficient.

Table 2 Apparent diffusion coefficient metric values for human papillomavirus negative head and neck squamous cell carcinoma patients who were classified based on survival as dead of disease, alive with disease and no evidence of disease before, during and post- radiotherapy

MRI	DOD ADC mean ($\times 10^{-3} \text{ mm}^2/\text{s}$)		AWD ADC mean ($\times 10^{-3} \text{ mm}^2/\text{s}$)		NED ADC mean ($\times 10^{-3} \text{ mm}^2/\text{s}$)	
	Primary	Node	Primary	Node	Primary	Node
Pre-Tx	1.51 ± 0.36	1.43 ± 0.58	1.66 ± 0.41	1.26 ± 0.19	0.85 ± 0.27	0.86 ± 0.20
During Tx (2-3 wk)	1.92 ± 0.33	1.54 ± 0.11	2.12 ± 0.38	1.41 ± 0.38	1.49 ± 0.13	1.39 ± 0.08
Post-Tx	No primary	0.98 ± 0.29	No primary	1.93 ± 0.22	No primary	No node

MRI: Magnetic resonance imaging; ADC: Apparent diffusion coefficient; AWD: Alive with disease; DOC: Dead of other causes; DOD: Dead of disease; NED: No evidence of disease.

CT ($n = 10$)] were analyzed to capture RT response. The results showed a significantly strong negative correlation ($\rho = -0.67$, $P = 0.01$) between the pre-Tx mean SUV and the pre-Tx mean ADC for the 11 lymph nodes and 5 primary tumors (Figure 2).

A summary of the ADC mean for pre-Tx and during-Tx (2nd and 3rd weeks data were combined) from the three different survival groups as DOD, AWD and NED is shown in Table 2. For a single patient who was NED at the last clinical follow-up, the MRI and the ^{18}F -FDG PET/CT post-treatment showed no evidence of disease at the primary tumor site and neck nodal metastases. Figure 3 shows the DW-MRI and ^{18}F -FDG PET/CT images from a patient who was NED. The ADC values (mean \pm SD) for the ROI drawn on the primary tumor were $0.85 \pm 0.27 \times 10^{-3} \text{ mm}^2/\text{s}$, $1.49 \pm 0.13 \times 10^{-3} \text{ mm}^2/\text{s}$ for pre-Tx and Wk₂₋₃ Tx, respectively. The ADC values for the ROIs in neck nodal metastases were as follows $0.86 \pm 0.20 \times 10^{-3} \text{ mm}^2/\text{s}$, $1.39 \pm 0.08 \times 10^{-3} \text{ mm}^2/\text{s}$ for pre-Tx and Wk₂₋₃ Tx (Table 2). Pre-Tx SUV (mean \pm SD) values for primary tumor and neck nodal metastases were 5.99 ± 0.61 and 6.06 ± 0.49 , respectively.

Three patients were AWD on the last clinical follow-up, and 1 patient had an unknown primary tumor site. Both, MRI and ^{18}F -FDG PET/CT post-treatment showed no evidence of disease at the primary tumor site; however the neck nodal metastases were still present.

Figure 4 shows the DW-MRI and ^{18}F -FDG PET/CT images from a patient who was AWD. The ADC values (mean \pm SD) for the primary tumors were $1.66 \pm 0.41 \times 10^{-3} \text{ mm}^2/\text{s}$, $2.12 \pm 0.38 \times 10^{-3} \text{ mm}^2/\text{s}$ for pre-Tx and Wk₂₋₃ Tx, respectively. The ADC values for the neck nodal metastases were $1.26 \pm 0.19 \times 10^{-3} \text{ mm}^2/\text{s}$, $1.41 \pm 0.38 \times 10^{-3} \text{ mm}^2/\text{s}$, and $1.93 \pm 0.22 \times 10^{-3} \text{ mm}^2/\text{s}$ for pre-Tx, Wk₂₋₃ Tx and post-Tx, respectively (Table 2). The SUV mean pre-Tx values for the primary tumor and neck nodal metastases were 1.84 ± 0.83 and 4.85 ± 0.75 , respectively.

The two patients who were DOD died 2 mo and 6 mo post-Tx. Figure 5 shows the DW-MRI and ^{18}F -FDG PET/CT images from a patient who was DOD. The ADC values (mean \pm SD) for the primary tumor were $1.51 \pm 0.36 \times 10^{-3} \text{ mm}^2/\text{s}$ and $1.92 \pm 0.33 \times 10^{-3} \text{ mm}^2/\text{s}$ for pre-Tx and Wk₂₋₃ Tx, respectively. The ADC values for the neck nodal metastases were $1.43 \pm 0.58 \times 10^{-3} \text{ mm}^2/\text{s}$, $1.54 \pm 0.11 \times 10^{-3} \text{ mm}^2/\text{s}$, and $0.98 \pm 0.29 \times 10^{-3} \text{ mm}^2/\text{s}$ for pre-Tx, Wk₂₋₃ Tx and post-Tx, respectively (Table 2). The SUV mean pre-Tx values for the primary tumor and neck nodal metastases were 2.98 ± 0.66 and 3.93 ± 0.45 , respectively.

The ΔADC (%) between pre- and Wk₂₋₃ Tx for primary tumors and neck nodal metastases were as follows: 75.4% and 61.6%, respectively, for the patient with NED, 27.5% and 32.7%, respectively, for those

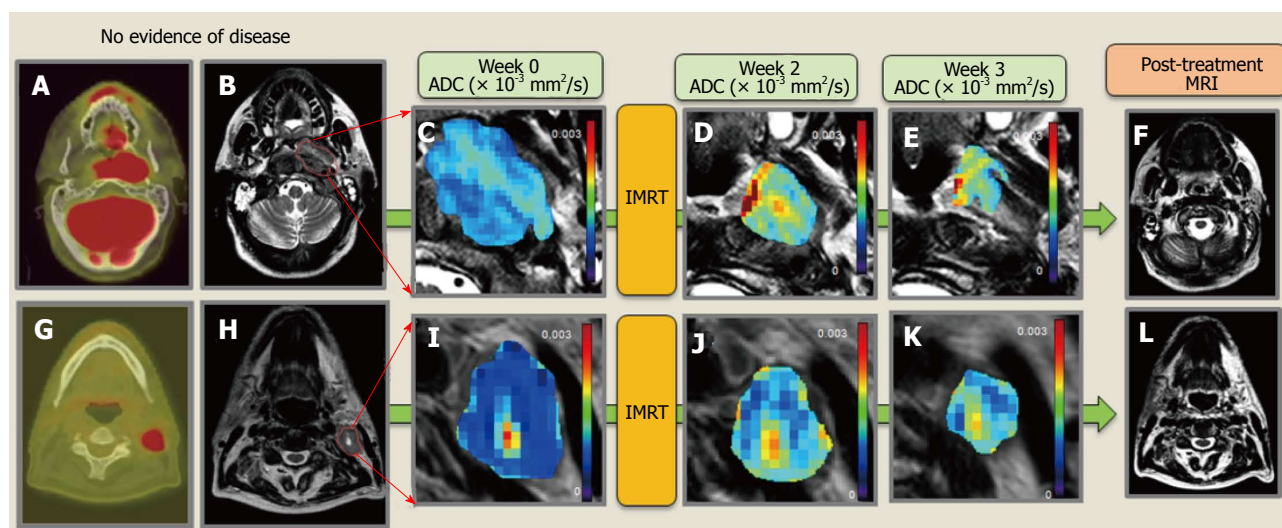


Figure 3 Representative no evidence of disease patient. A and G: Pre-Tx PET/CT of the primary tumor and a neck nodal metastasis; B and H: Primary tumor and representative neck nodal metastasis contoured over a T2-W MRI; C and I: Pre-Tx ADC map overlaid on T2-W MRI; D and J: Wk2-Tx ADC map overlaid on T2-W; E and K: Wk3-Tx ADC map overlaid on T2-W; F and L: T2-W MRI post-Tx with no evidence of primary tumor and neck nodal metastases. PET/CT: Positron emission tomography/computed tomography; MRI: Magnetic resonance imaging; ADC: Apparent diffusion coefficient; IMRT: Intensity modulated radiation therapy.

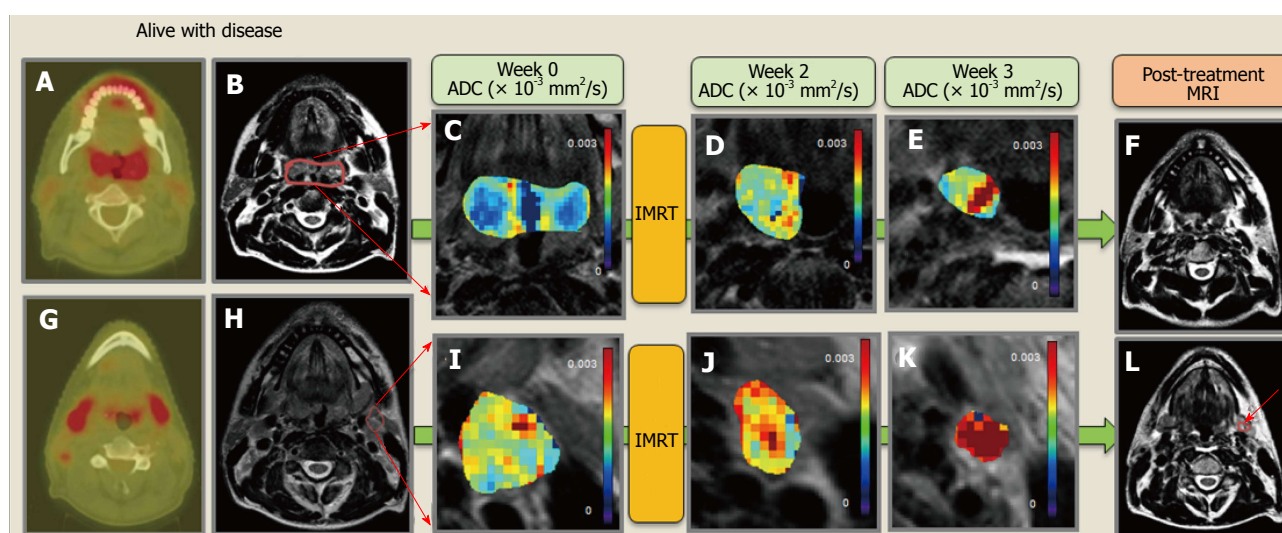


Figure 4 Representative alive with disease patient. A and G: pre-Tx PET/CT of the primary tumor and two neck nodal metastases; B and H: Primary tumor and representative neck nodal metastasis contoured over a T2-W MRI; C and I: Pre-Tx ADC map overlaid on T2-W MRI; D and J: Wk2-Tx ADC map overlaid on T2-W; E and K: Wk3-Tx ADC map overlaid on T2-W; F and L: T2-W MRI post-Tx with no evidence of primary tumor but with presence of neck nodal metastasis. PET/CT: Positron emission tomography/computed tomography; MRI: Magnetic resonance imaging; ADC: Apparent diffusion coefficient; IMRT: Intensity modulated radiation therapy.

patients who were AWD, and 26.9% and 7.31%, respectively, for those who were DOD.

DISCUSSION

This prospective study is the first in Spain conducted in support of integrating functional imaging in a RT setting. We evaluated multimodality imaging in HPV-HNSCC patients for both primary and neck nodal metastases. Specifically, we observed that pretreatment tumor cellularity is inversely proportional to glucose metabolism in these tumors, which was consistent with the previous literature^[15,25,26]. The survival status and

functional metrics show different % change in Δ ADC for the NED, AWD, and DOD survival groups, which would need to be validated in larger patient population studies.

HNSCC is one of the major types of cancer that can be linked to alcohol consumption and tobacco smoking. It typically originates from the mucosal epithelia of the oral cavity, pharynx and larynx^[27]. In oropharyngeal SCC, HPV status is an independent prognostic factor for both overall survival and progression-free survival, which is consistent with the hypothesis that HPV+ and HPV- tumors are distinct and have different causes, risk-factor profiles, and survival outcomes^[28]. HPV-tumors continue to have poor outcomes compared to

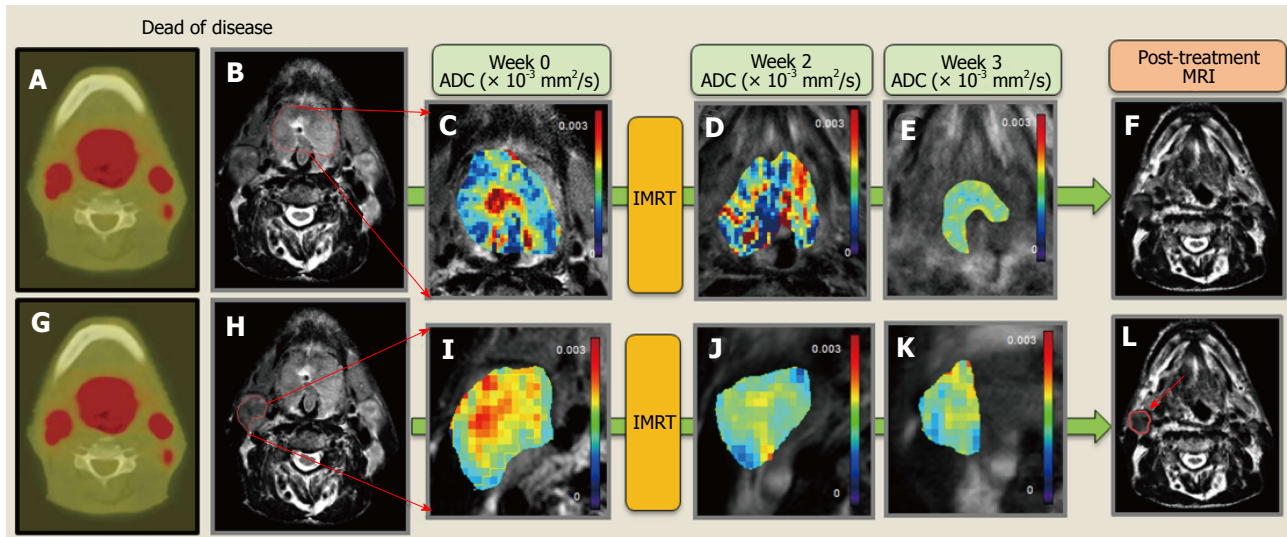


Figure 5 Representative dead of disease patient. A and G: Pre-Tx PET/CT of the primary tumor and three neck nodal metastases; B and H: Primary tumor and representative neck nodal metastasis contoured over a T2-W MRI; C and I: Pre-Tx ADC map overlaid on T2-W MRI; D and J: Wk2-Tx ADC map overlaid on T2-W; E and K: Wk3-Tx ADC map overlaid on T2-W; F and L: T2-W MRI post-Tx with no evidence of primary tumor but with presence of neck nodal metastasis. PET/CT: Positron emission tomography/computed tomography; MRI: Magnetic resonance imaging; ADC: Apparent diffusion coefficient; IMRT: Intensity modulated radiation therapy.

their HPV+ counterparts^[28]. Future clinical trials should be designed specifically for patients with HPV+ or HPV- HNSCC using appropriate, validated quantitative imaging biomarkers. As there is very scarce imaging literature on HPV+ or HPV- alone, it raises an urgent need to study these cohorts independently and assess the value of multimodality imaging for better cancer patient management.

In recent years, studies by Razek have shown that ADC metric has a prognostic value in HNSCC^[29-31]. They reported a mean ADC value in nasopharyngeal carcinoma (NPC) of $0.99 \pm 0.11 \times 10^{-3} \text{ mm}^2/\text{s}$. The ADC value in this study also correlated inversely with tumor volume^[29]. In a separate study by the same group, it was reported that the mean ADC value of residual or recurrent lesions ($1.17 \pm 0.33 \times 10^{-3} \text{ mm}^2/\text{s}$) was less than that observed in post-therapeutic changes ($2.07 \pm 0.25 \times 10^{-3} \text{ mm}^2/\text{s}$)^[30]. They also showed that ADC values with metabolic ratio (Ch/Cr) obtained from 1H-MRS are well correlated with several prognostic parameters of HNSCC^[31].

The use of multimodality imaging (^{18}F -FDG PET/CT, DW-MRI, DCE-MRI) in general HNSCC populations for assessing both the association between the quantitative imaging biomarkers obtained from each imaging technique and their combined or respective roles in prognosis and/or prediction of outcome^[8,25,32,33]. The major technical challenges in IMRT persist in the use of functional images for treatment, one of which includes the identification of a reproducible, RT-compatible patient positioning setup that is consistent between functional techniques and RT. All patients in the present study were in a supine position and fixed in place with the same immobilization system that was used during the RT treatment planning and delivery. A thermoplastic mask, head support, and flat table were used to try

to minimize distortion and to improve the registration process between the different imaging modalities. The head support and flat table were adapted to MRI and PET/CT. This reproducible positioning addressed one of the big hurdles in the acquisition of multimodality images that may be used for adaptive RT in the future^[34,35]. Dirix *et al.*^[36] designed a feasibility, prospective, multimodality imaging study with this prerequisite in mind, recruiting HNSCC patients for dose painting in RT. A pilot study by Subesinghe *et al.*^[37] emphasized the importance of reproducing the positioning for assessing early RT treatment response.

^{18}F -FDG PET/CT and DW-MRI have been the focus of numerous studies in general HNSCC cohorts to determine correlation, if any, between SUV and ADC values, with variable results. SUV and ADC remain exploratory imaging metrics yet to be fully explored and understood in HPV-HNSCC patients. A study by Varoquax *et al.*^[38] involving 24 primary and 10 recurrent HNSCC showed no significant correlation between SUV values (SUV_{max} , SUV_{mean} or SUV_{min}) and ADC values (ADC_{max} , ADC_{mean} or ADC_{min}), nor did Choi *et al.*^[39] find significant correlation between SUV_{mean} and ADC_{mean} in 47 primary HNSCC. Rather, Nakajo *et al.*^[15] found significant negative correlation between SUV_{max} and ADC_{mean} in a study of 28 primary HNSCC tumors and Nakamatsu *et al.*^[26] demonstrated significant negative correlation in 41 neck nodal metastases between SUV values (SUV_{max} , SUV_{mean}) and ADC values (ADC_{mean} , ADC_{min}). In our study, similar results were obtained from a total of 11 neck nodal metastases and 5 primary HPV- HNSCC showing a significant strong negative correlation between the ADC_{mean} and SUV_{mean} pre-Tx ($\rho = -0.67$, $P = 0.01$). Further validation of the correlations with larger patient populations is needed, but was beyond the scope of this

study. Preda *et al.*^[40] concluded in a study with 57 HNSCC primary tumors that “the combination of SUV_{max} and ADC_{min} improves the prognostic role of the two separate parameters”.

The present study showed an increase in ΔADC_{Wk2-3} for the HPV- patient with NED in comparison with the DOD and AWD HPV- patients in both primary tumor and neck nodal metastases, in agreement with above-mentioned studies. Also, the pre-Tx ADC values of the primary tumor and neck nodal metastases for NED is lower than in the group of AWD and DOD, showing that lower pre-Tx ADC values are related to a good response to treatment and are consistent with the previous literature^[9,41].

The % change in ΔADC for primary tumor and neck nodal metastases depict the different Tx responses, suggesting the possibility of identifying HPV- patients with poor prognosis at an early stage to individualize and adapt RT treatment (*i.e.*, through dose-escalation). Vandecaveye *et al.*^[42] showed in neck nodal metastases and primary tumors that ΔADC (Week 2 and Week 4 during CRT) was significantly lower ($P < 0.0001$) in lesions with recurrence than in lesions with a complete response.

Individualization of treatment is especially important in the subgroup of HPV- patients who were part of this study. A limitation of the study was that there were a relatively small number of HPV- patients as the recruitment was highly selective in Spain. However, we felt that this selectivity was justified given that these subtypes of HPV- patients are the ones who have poor prognoses in HNSCC^[28]. The initial results need to be addressed through validation in future studies.

Our study offers insight on how to manage and understand valuable quantitative imaging biomarkers, such as SUV and ADC for HPV- HNSCC, with the objective of integrating them into the development of biological adaptive RT in the future.

These results are preliminary in nature and are indicative, and not definitive, trends rendered by the imaging metrics due to the small sample size of HPV- HNSCC patients in a Meixoeiro Hospital of Vigo Experience.

ACKNOWLEDGMENTS

The authors offer their sincerest thanks to patients who volunteered to participate in this study. Our sincerest thanks to Mr. James Keller, Editor, Department of Medical Physics, Memorial Sloan Kettering Cancer Center for his help in editing this paper. We must be grateful for the exchange program AAPM-SEFM for facilitating the first author's visit to Memorial Sloan Kettering Cancer Center. We thank the National Health Institute of Spain for supporting this work through the ISCIII Grant PI11/02035, DTS14/00018, BIOCAPS, and the Galician Government through the project CN 2012/260 “Consolidation Research Units: AtlantTIC”. This research was also funded in part through the NIH/NCI Cancer Center Support Grant P30 CA008748.

COMMENTS

Background

Human papillomavirus (HPV) negative (-) head and neck squamous cell carcinoma (HNSCC) patients have poor outcomes compared with HPV-positive (HPV+) cancers. Individualization of radiotherapy is especially important in the subgroup of HPV- patients and imaging metrics derived from multimodality imaging can be critical for its implementation.

Research frontiers

In an effort to perform biologically guided adaptive radiotherapy, it is critical to understand how different functional imaging techniques interact and potentially complement each other.

Innovations and breakthroughs

Multimodality imaging in HPV- HNSCC suggests that tumor cell density is inversely proportional to glucose metabolism in a Meixoeiro Hospital of Vigo Experience. These results are promising and need to be validated in larger populations.

Applications

Diffusion-weighted magnetic resonance imaging and ^{18}F -labeled fluoro-deoxyglucose positron emission tomography/computed tomography are two valuable imaging techniques that may help build the framework for adaptive radiotherapy based on functional images in future clinical trials by investigating tumor cellularity and glucose metabolism before, during and after RT in HPV- HNSCC.

Terminology

^{18}F -FDG: Fluorine-18 fludeoxyglucose; ADC: Apparent diffusion coefficient; AWD: Alive with disease; DOC: Dead of other causes; DOD: Dead of disease; DW-MRI: Diffusion-weighted magnetic resonance imaging; HNC: Head and neck cancer; HNSCC: Head and neck squamous cell carcinoma; HPV-: Human papillomavirus negative; HPV+: Human papillomavirus positive; IMRT: Intensity modulated radiation therapy; MRI: Magnetic resonance imaging; NED: No evidence of disease; PET/CT: Positron emission tomography/computed tomography; ROI: Region of interest; RT: Radiotherapy.

Peer-review

This is a good paper.

REFERENCES

- 1 **Galceran.** Europa: Estimaciones de la incidencia y la supervivencia del cáncer en España y su situación en Europa, 2014
- 2 **Sanderson RJ,** Ironside JA. Squamous cell carcinomas of the head and neck. *BMJ* 2002; **325**: 822-827 [PMID: 12376446 DOI: 10.1136/bmj.325.7368.822]
- 3 **Seijas-Tamayo R,** Fernández-Mateos J, Adansa Klain JC, Mesía R, Pastor Borgoñón M, Pérez-Ruiz E, Vázquez Fernández S, Salvador Coloma C, Rueda Domínguez A, Taberna M, Martínez-Trufero J, Bonfill Abella T, Vázquez Estévez S, Pollán M, Del Barco Morillo E, Cruz-Hernández JJ. Epidemiological characteristics of a Spanish cohort of patients diagnosed with squamous cell carcinoma of head and neck: distribution of risk factors by tumor location. *Clin Transl Oncol* 2016; **18**: 1114-1122 [PMID: 27112939 DOI: 10.1007/s12094-016-1493-1]
- 4 **Fakhry C,** Westra WH, Li S, Cmelak A, Ridge JA, Pinto H, Forastiere A, Gillison ML. Improved survival of patients with human papillomavirus-positive head and neck squamous cell carcinoma in a prospective clinical trial. *J Natl Cancer Inst* 2008; **100**: 261-269 [PMID: 18270337 DOI: 10.1093/jnci/djn011]
- 5 **Jansen JF,** Schöder H, Lee NY, Stambuk HE, Wang Y, Fury MG, Patel SG, Pfister DG, Shah JP, Koutcher JA, Shukla-Dave A. Tumor metabolism and perfusion in head and neck squamous cell carcinoma:

- pretreatment multimodality imaging with 1H magnetic resonance spectroscopy, dynamic contrast-enhanced MRI, and [18F]FDG-PET. *Int J Radiat Oncol Biol Phys* 2012; **82**: 299-307 [PMID: 21236594 DOI: 10.1016/j.ijrobp.2010.11.022]
- 6 **Padhani AR**, Liu G, Koh DM, Chenevert TL, Thoeny HC, Takahara T, Dzik-Jurasz A, Ross BD, Van Cauteren M, Collins D, Hammoud DA, Rustin GJ, Taouli B, Choyke PL. Diffusion-weighted magnetic resonance imaging as a cancer biomarker: consensus and recommendations. *Neoplasia* 2009; **11**: 102-125 [PMID: 19186405 DOI: 10.1593/neo.81328]
 - 7 **Chenevert TL**, Stegman LD, Taylor JM, Robertson PL, Greenberg HS, Rehemtulla A, Ross BD. Diffusion magnetic resonance imaging: an early surrogate marker of therapeutic efficacy in brain tumors. *J Natl Cancer Inst* 2000; **92**: 2029-2036 [PMID: 11121466 DOI: 10.1093/jnci/92.24.2029]
 - 8 **Ng SH**, Liao CT, Lin CY, Chan SC, Lin YC, Yen TC, Chang JT, Ko SF, Fan KH, Wang HM, Yang LY, Wang JJ. Dynamic contrast-enhanced MRI, diffusion-weighted MRI and (18)F-FDG PET/CT for the prediction of survival in oropharyngeal or hypopharyngeal squamous cell carcinomas treated with chemoradiation. *Eur Radiol* 2016; **26**: 4162-4172 [PMID: 26911889 DOI: 10.1007/s00330-016-4276-8]
 - 9 **Kim S**, Loevner L, Quon H, Sherman E, Weinstein G, Kilger A, Poptani H. Diffusion-weighted magnetic resonance imaging for predicting and detecting early response to chemoradiation therapy of squamous cell carcinomas of the head and neck. *Clin Cancer Res* 2009; **15**: 986-994 [PMID: 19188170 DOI: 10.1158/1078-0432.CCR-08-1287]
 - 10 **Vandecaveye V**, Dirix P, De Keyser F, Op de Beeck K, Vander Poorten V, Hauben E, Lambrecht M, Nuyts S, Hermans R. Diffusion-weighted magnetic resonance imaging early after chemoradiotherapy to monitor treatment response in head-and-neck squamous cell carcinoma. *Int J Radiat Oncol Biol Phys* 2012; **82**: 1098-1107 [PMID: 21514067 DOI: 10.1016/j.ijrobp.2011.02.044]
 - 11 **Schöder H**, Fury M, Lee N, Kraus D. PET monitoring of therapy response in head and neck squamous cell carcinoma. *J Nucl Med* 2009; **50** Suppl 1: 74S-88S [PMID: 19380408 DOI: 10.2967/jnumed.108.057208]
 - 12 **Ong SC**, Schöder H, Lee NY, Patel SG, Carlson D, Fury M, Pfister DG, Shah JP, Larson SM, Kraus DH. Clinical utility of 18F-FDG PET/CT in assessing the neck after concurrent chemoradiotherapy for Locoregional advanced head and neck cancer. *J Nucl Med* 2008; **49**: 532-540 [PMID: 18344440 DOI: 10.2967/jnumed.107.044792]
 - 13 **Wong RJ**, Lin DT, Schöder H, Patel SG, Gonen M, Wolden S, Pfister DG, Shah JP, Larson SM, Kraus DH. Diagnostic and prognostic value of [(18)F]fluorodeoxyglucose positron emission tomography for recurrent head and neck squamous cell carcinoma. *J Clin Oncol* 2002; **20**: 4199-4208 [PMID: 12377963 DOI: 10.1200/JCO.2002.02.590]
 - 14 **Schwartz DL**, Rajendran J, Yueh B, Coltrera MD, Leblanc M, Eary J, Krohn K. FDG-PET prediction of head and neck squamous cell cancer outcomes. *Arch Otolaryngol Head Neck Surg* 2004; **130**: 1361-1367 [PMID: 15611393 DOI: 10.1001/archotol.130.12.1361]
 - 15 **Nakajo M**, Nakajo M, Kajiya Y, Tani A, Kamiyama T, Yonekura R, Fukukura Y, Matsuzaki T, Nishimoto K, Nomoto M, Koriyama C. FDG PET/CT and diffusion-weighted imaging of head and neck squamous cell carcinoma: comparison of prognostic significance between primary tumor standardized uptake value and apparent diffusion coefficient. *Clin Nucl Med* 2012; **37**: 475-480 [PMID: 22475897 DOI: 10.1097/RLU.0b013e318248524a]
 - 16 **Min M**, Lee MT, Lin P, Holloway L, Wijesekera Dj, Gooneratne D, Rai R, Xuan W, Fowler A, Forstner D, Liney G. Assessment of serial multi-parametric functional MRI (diffusion-weighted imaging and R2*) with (18)F-FDG-PET in patients with head and neck cancer treated with radiation therapy. *Br J Radiol* 2016; **89**: 20150530 [PMID: 26648404 DOI: 10.1259/bjr.20150530]
 - 17 **Goodyear MD**, Krljeza-Jeric K, Lemmens T. The Declaration of Helsinki. *BMJ* 2007; **335**: 624-625 [PMID: 17901471 DOI: 10.1136/bmj.39339.610000.BE]
 - 18 **Bockmühl U**, Ishwad CS, Ferrell RE, Gollin SM. Association of 8p23 deletions with poor survival in head and neck cancer. *Otolaryngol Head Neck Surg* 2001; **124**: 451-455 [PMID: 11283506 DOI: 10.1067/mhn.2001.114794]
 - 19 **Landesa-Vazquez I**, Alba-Castro JL, Mera-Iglesias M, Aramburu-Nunez D, Lopez-Medina A, Munoz-Garzon V. ARTFIBio: A Cross-Platform Image Registration Tool for Tumor Response Quantification in Head and Neck Cancer. *Ieee-Embis International Conference on Biomedical and Health Informatics (Bhi)* 2014: 149-152 [DOI: 10.1109/BHI.2014.6864326]
 - 20 **Mattes D**, Haynor DR, Vesselle H, Lewellen TK, Eubank W. Nonrigid multimodality image registration. *P Soc Photo-Opt Ins* 2001; **2**: 1609-1620 [DOI: 10.1117/12.431046]
 - 21 **Stejskal EO**, Tanner JE. Spin Diffusion Measurements: Spin Echoes in the Presence of a Time-Dependent Field Gradient. *J Chem Phys* 1965; **42**: 288-292 [DOI: 10.1063/1.1695690]
 - 22 **IAEA**. Quantitative Nuclear Medicine Imaging: Concepts, Requirements and Methods. Austria: IAEA Library, 2014
 - 23 **Cohen J**. The statistical power of abnormal-social psychological research: a review. *J Abnorm Soc Psychol* 1962; **65**: 145-153 [PMID: 13880271 DOI: 10.1037/h0045186]
 - 24 **R Project**. GNU Operating System. Available from: URL: <http://www.gnu.org/licenses/gpl.html>
 - 25 **Gawlitza M**, Purz S, Kubiessa K, Boehm A, Barthel H, Kluge R, Kahn T, Sabri O, Stumpp P. In Vivo Correlation of Glucose Metabolism, Cell Density and Microcirculatory Parameters in Patients with Head and Neck Cancer: Initial Results Using Simultaneous PET/MRI. *PLoS One* 2015; **10**: e0134749 [PMID: 26270054 DOI: 10.1371/journal.pone.0134749]
 - 26 **Nakamatsu S**, Matsusue E, Miyoshi H, Kakite S, Kaminou T, Ogawa T. Correlation of apparent diffusion coefficients measured by diffusion-weighted MR imaging and standardized uptake values from FDG PET/CT in metastatic neck lymph nodes of head and neck squamous cell carcinomas. *Clin Imaging* 2012; **36**: 90-97 [PMID: 22370129 DOI: 10.1016/j.clinimag.2011.05.002]
 - 27 **Jemal A**, Siegel R, Xu J, Ward E. Cancer statistics, 2010. *CA Cancer J Clin* 2010; **60**: 277-300 [PMID: 20610543 DOI: 10.3322/caac.20073]
 - 28 **Ang KK**, Harris J, Wheeler R, Weber R, Rosenthal DI, Nguyen-Tân PF, Westra WH, Chung CH, Jordan RC, Lu C, Kim H, Axelrod R, Silverman CC, Redmond KP, Gillison ML. Human papillomavirus and survival of patients with oropharyngeal cancer. *N Engl J Med* 2010; **363**: 24-35 [PMID: 20530316 DOI: 10.1056/NEJMoa0912217]
 - 29 **Abdel Razek AA**, Kamal E. Nasopharyngeal carcinoma: correlation of apparent diffusion coefficient value with prognostic parameters. *La Radiologia medica* 2013; **118**: 534-539 [PMID: 23090251 DOI: 10.1007/s11547-012-0890-x]
 - 30 **Abdel Razek AA**, Kandeel AY, Soliman N, El-shenshawy HM, Kamel Y, Nada N, Denewar A. Role of diffusion-weighted echoplanar MR imaging in differentiation of residual or recurrent head and neck tumors and posttreatment changes. *AJNR American journal of neuroradiology* 2007; **28**: 1146-1152 [PMID: 17569975 DOI: 10.3174/ajnr.A0491]
 - 31 **Razek AA**, Nada N. Correlation of Choline/Creatine and Apparent Diffusion Coefficient values with the prognostic parameters of Head and Neck Squamous Cell Carcinoma. *NMR in biomedicine* 2016; **29**: 483-489 [PMID: 26867020 DOI: 10.1002/nbm.3472]
 - 32 **Han M**, Kim SY, Lee SJ, Choi JW. The Correlations Between MRI Perfusion, Diffusion Parameters, and 18F-FDG PET Metabolic Parameters in Primary Head-and-Neck Cancer: A Cross-Sectional Analysis in Single Institute. *Medicine (Baltimore)* 2015; **94**: e2141 [PMID: 26632740 DOI: 10.1097/MD.0000000000002141]
 - 33 **Shukla-Dave A**, Lee NY, Jansen JF, Thaler HT, Stambuk HE, Fury MG, Patel SG, Moreira AL, Sherman E, Karimi S, Wang Y, Kraus D, Shah JP, Pfister DG, Koutcher JA. Dynamic contrast-enhanced magnetic resonance imaging as a predictor of outcome in head-and-neck squamous cell carcinoma patients with nodal metastases. *Int J Radiat Oncol Biol Phys* 2012; **82**: 1837-1844 [PMID: 21601373 DOI: 10.1016/j.ijrobp.2011.03.006]
 - 34 **van der Heide UA**, Houweling AC, Groenendaal G, Beets-Tan RG, Lambin P. Functional MRI for radiotherapy dose painting. *Magn Reson Imaging* 2012; **30**: 1216-1223 [PMID: 22770686 DOI: 10.1016/j.mri.2011.11.022]

- 10.1016/j.mri.2012.04.010]
- 35 **Thorwarth D**, Beyer T, Boellaard R, de Ruyscher D, Grgic A, Lee JA, Pietrzyk U, Sattler B, Schaefer A, van Elmpt W, Vogel W, Oyen WJ, Nestle U. Integration of FDG-PET/CT into external beam radiation therapy planning: technical aspects and recommendations on methodological approaches. *Nuklearmedizin* 2012; **51**: 140-153 [PMID: 22473130 DOI: 10.3413/Nukmed-0455-11-12]
 - 36 **Dirix P**, Vandecaveye V, De Keyzer F, Stroobants S, Hermans R, Nuyts S. Dose painting in radiotherapy for head and neck squamous cell carcinoma: value of repeated functional imaging with (18)F-FDG PET, (18)F-fluoromisonidazole PET, diffusion-weighted MRI, and dynamic contrast-enhanced MRI. *J Nucl Med* 2009; **50**: 1020-1027 [PMID: 19525447 DOI: 10.2967/jnumed.109.062638]
 - 37 **Subesinghe M**, Scarsbrook AF, Sourbron S, Wilson DJ, McDermott G, Speight R, Roberts N, Carey B, Forrester R, Gopal SV, Sykes JR, Prestwich RJ. Alterations in anatomic and functional imaging parameters with repeated FDG PET-CT and MRI during radiotherapy for head and neck cancer: a pilot study. *BMC Cancer* 2015; **15**: 137 [PMID: 25885109 DOI: 10.1186/s12885-015-1154-8]
 - 38 **Varoquaux A**, Rager O, Lovblad KO, Masterson K, Dulguerov P, Ratib O, Becker CD, Becker M. Functional imaging of head and neck squamous cell carcinoma with diffusion-weighted MRI and FDG PET/CT: quantitative analysis of ADC and SUV. *Eur J Nucl Med Mol Imaging* 2013; **40**: 842-852 [PMID: 23436068 DOI: 10.1007/s00259-013-2351-9]
 - 39 **Choi SH**, Paeng JC, Sohn CH, Pagsisihan JR, Kim YJ, Kim KG, Jang JY, Yun TJ, Kim JH, Han MH, Chang KH. Correlation of 18F-FDG uptake with apparent diffusion coefficient ratio measured on standard and high b value diffusion MRI in head and neck cancer. *J Nucl Med* 2011; **52**: 1056-1062 [PMID: 21680692 DOI: 10.2967/jnumed.111.089334]
 - 40 **Preda L**, Conte G, Bonello L, Giannitto C, Travaini LL, Raimondi S, Summers PE, Mohssen A, Alterio D, Cossu Rocca M, Grana C, Ruju F, Bellomi M. Combining standardized uptake value of FDG-PET and apparent diffusion coefficient of DW-MRI improves risk stratification in head and neck squamous cell carcinoma. *Eur Radiol* 2016 [PMID: 26965504 DOI: 10.1007/s00330-016-4284-8]
 - 41 **Hatakenaka M**, Nakamura K, Yabuuchi H, Shioyama Y, Matsuo Y, Kamitani T, Yonezawa M, Yoshiura T, Nakashima T, Mori M, Honda H. Apparent diffusion coefficient is a prognostic factor of head and neck squamous cell carcinoma treated with radiotherapy. *Jpn J Radiol* 2014; **32**: 80-89 [PMID: 24408077 DOI: 10.1007/s11604-013-0272-y]
 - 42 **Vandecaveye V**, Dirix P, De Keyzer F, de Beeck KO, Vander Poorten V, Roebben I, Nuyts S, Hermans R. Predictive value of diffusion-weighted magnetic resonance imaging during chemoradiotherapy for head and neck squamous cell carcinoma. *Eur Radiol* 2010; **20**: 1703-1714 [PMID: 20179939 DOI: 10.1007/s00330-010-1734-6]

P- Reviewer: Razek AAKA, Xiao NH **S- Editor:** Ji FF **L- Editor:** A
E- Editor: Lu YJ





Published by **Baishideng Publishing Group Inc**

8226 Regency Drive, Pleasanton, CA 94588, USA

Telephone: +1-925-223-8242

Fax: +1-925-223-8243

E-mail: bpgoffice@wjgnet.com

Help Desk: <http://www.wjgnet.com/esps/helpdesk.aspx>

<http://www.wjgnet.com>



World Journal of *Radiology*

World J Radiol 2017 February 28; 9(2): 27-90





Editorial Board

2014-2017

The *World Journal of Radiology* Editorial Board consists of 365 members, representing a team of worldwide experts in radiology. They are from 36 countries, including Afghanistan (1), Argentina (2), Australia (5), Austria (7), Belgium (2), Brazil (8), Canada (6), Chile (1), China (43), Croatia (1), Denmark (4), Egypt (6), France (5), Germany (22), Greece (10), India (12), Iran (6), Ireland (2), Israel (3), Italy (47), Japan (13), Netherlands (1), New Zealand (1), Pakistan (1), Poland (2), Portugal (1), Serbia (1), Singapore (3), Slovakia (1), South Korea (18), Spain (4), Sweden (2), Switzerland (4), Thailand (1), Turkey (26), United Kingdom (11), and United States (82).

EDITORS-IN-CHIEF

Kai U Juergens, *Bremen*
Edwin JR van Beek, *Edinburgh*
Thomas J Vogl, *Frankfurt*

GUEST EDITORIAL BOARD MEMBERS

Wing P Chan, *Taipei*
Chung-Huei Hsu, *Taipei*
Chin-Chang Huang, *Taipei*
Tsong-Long Hwang, *Taoyuan*
Jung-Lung Hsu, *Taipei*
Chia-Hung Kao, *Taichung*
Yu-Ting Kuo, *Tainan*
Hon-Man Liu, *Taipei*
Hui-Lung Liang, *Kaohsiung*
Chun Chung Lui, *Kaohsiung*
Sen-Wen Teng, *Taipei*
Yung-Liang (William) Wan, *Taoyuan*

MEMBERS OF THE EDITORIAL BOARD



Afghanistan

Takao Hiraki, *Okayama*



Argentina

Patricia Carrascosa, *Vicente Lopez*
Maria C Ziadi, *Rosario*



Australia

Lourens Bester, *Sydney*
Gemma A Figtree, *Sydney*



Austria

Herwig R Cerwenka, *Graz*
Gudrun M Feuchtnner, *Innsbruck*
Benjamin Henninger, *Innsbruck*
Rupert Lanzenberger, *Vienna*
Shu-Ren Li, *Vienna*
Veronika Schopf, *Vienna*
Tobias De Zordo, *Innsbruck*



Belgium

Steve Majerus, *Liege*
Kathelijne Peremans, *Merelbeke*



Brazil

Clerio F Azevedo, *Rio de Janeiro*
Patrícia P Alfredo, *São Paulo*
Eduardo FC Fleury, *São Paulo*
Edward Araujo Júnior, *São Paulo*
Wellington P Martins, *Ribeirao Preto*
Ricardo A Mesquita, *Belo Horizonte*
Vera MC Salemi, *São Paulo*
Claudia Szobot, *Porto Alegre*
Lilian YI Yamaga, *São Paulo*



Canada

Marie Arsalidou, *Toronto*
Otman A Basir, *Waterloo*

Tarik Zine Belhocine, *Toronto*
James Chow, *Toronto*
Tae K Kim, *Toronto*
Anastasia Oikonomou, *Toronto*



China

Hong-Wei Chen, *Wuxi*
Feng Chen, *Hangzhou*
Jian-Ping Chu, *Guangzhou*
Guo-Guang Fan, *Shenyang*
Bu-Lang Gao, *Shijiazhuang*
Qi-Yong Gong, *Chengdu*
Ying Han, *Beijing*
Xian-Li Lv, *Beijing*
Yi-Zhuo Li, *Guangzhou*
Xiang-Xi Meng, *Harbin*
Yun Peng, *Beijing*
Jun Shen, *Guangzhou*
Ze-Zhou Song, *Hangzhou*
Wai Kwong Tang, *Hong Kong*
Gang-Hua Tang, *Guangzhou*
Jie Tian, *Beijing*
Lu-Hua Wang, *Beijing*
Xiao-bing Wang, *Xi'an*
Yi-Gen Wu, *Nanjing*
Kai Wu, *Guangzhou*
Hui-Xiong Xu, *Shanghai*
Zuo-Zhang Yang, *Kunming*
Xiao-Dan Ye, *Shanghai*
David T Yew, *Hong Kong*
Ting-He Yu, *Chongqing*
Zheng Yuan, *Shanghai*
Min-Ming Zhang, *Hangzhou*
Yudong Zhang, *Nanjing*
Dong Zhang, *Chongqing*
Wen-Bin Zeng, *Changsha*

Yue-Qi Zhu, *Shanghai*



Croatia

Goran Kusec, *Osijek*



Denmark

Poul E Andersen, *Odense*

Lars J Petersen, *Aalborg*

Thomas Z Ramsøy, *Frederiksberg*

Morten Ziebell, *Copenhagen*



Egypt

Mohamed F Bazeed, *Mansoura*

Mohamed Abou El-Ghar, *Mansoura*

Reem HA Mohamed, *Cairo*

Mohamed R Nouh, *Alexandria*

Ahmed AKA Razek, *Mansoura*

Ashraf A Zytoon, *Shebin El-Koom*



France

Sabine F Bensamoun, *Compiègne*

Romarc Loffroy, *Dijon*

Stephanie Nougaret, *Montpellier*

Hassane Oudadesse, *Rennes*

Vincent Vinh-Hung, *Fort-de-France*



Germany

Henryk Barthel, *Leipzig*

Peter Bannas, *Hamburg*

Martin Beeres, *Frankfurt*

Ilja F Ciernik, *Dessau*

A Dimitrakopoulou-Strauss, *Heidelberg*

Peter A Fasching, *Erlangen*

Andreas G Schreyer, *Regensburg*

Philipp Heusch, *Duesseldorf*

Sonja M Kirchhoff, *Munich*

Sebastian Ley, *Munich*

Adel Maataoui, *Frankfurt am Main*

Stephan M Meckel, *Freiburg*

Hans W Muller, *Duesseldorf*

Kay Raum, *Berlin*

Dirk Rades, *Luebeck*

Marc-Ulrich Regier, *Hamburg*

Alexey Surov, *Halle*

Martin Walter, *Magdeburg*

Axel Wetter, *Essen*

Christoph Zilkens, *Düsseldorf*



Greece

Panagiotis Antoniou, *Thessaloniki*

Nikos Efthimiou, *Athens*

Dimitris Karnabatidis, *Patras*

George Latsios, *Athens*

Stylianios Megremis, *Iraklion*

Alexander D Rapidis, *Athens*

Kiki Theodorou, *Larissa*

Ioannis A Tsalafoutas, *Athens*

Evanthia E Tripoliti, *Ioannina*

Athina C Tsili, *Ioannina*



India

Ritesh Agarwal, *Chandigarh*

Chandan J Das, *New Delhi*

Prathamesh V Joshi, *Mumbai*

Naveen Kalra, *Chandigarh*

Chandrasekharan Kesavadas, *Trivandrum*

Jyoti Kumar, *New Delhi*

Atin Kumar, *New Delhi*

Kaushala P Mishra, *Allahabad*

Daya N Sharma, *New Delhi*

Binit Sureka, *New Delhi*

Sanjay Sharma, *New Delhi*

Raja R Yadav, *Allahabad*



Iran

Majid Assadi, *Bushehr*

SeyedReza Najafizadeh, *Tehran*

Mohammad Ali Oghabian, *Tehran*

Amir Reza Radmard, *Tehran*

Ramin Sadeghi, *Mashhad*

Hadi Rokni Yazdi, *Tehran*



Ireland

Tadhg Gleeson, *Wexford*

Frederik JAI Vernimmen, *Cork*



Israel

Dafna Ben Bashat, *Tel Aviv*

Amit Gefen, *Tel Aviv*

Tamar Sella, *Jerusalem*



Italy

Adriano Alippi, *Rome*

Dante Amelio, *Trento*

Michele Anzidei, *Rome*

Filippo F Angileri, *Messinas*

Stefano Arcangeli, *Rome*

Roberto Azzoni, *San Donato milanese*

Tommaso V Bartolotta, *Palermo*

Tommaso Bartalena, *Imola*

Livia Bernardin, *San Bonifacio*

Federico Boschi, *Verona*

Sergio Casciaro, *Lecce*

Emanuele Casciani, *Rome*

Musa M Can, *Napoli*

Alberto Cuocolo, *Napoli*

Michele Ferrara, *Coppito*

Mauro Feola, *Fossano*

Giampiero Francica, *Castel Volturno*

Luigi De Gennaro, *Rome*

Giulio Giovannetti, *Pisa*

Francesca Iacobellis, *Napoli*

Formato Invernizzi, *Monza Brianza*

Francesco Lassandro, *Naples*

Lorenzo Livi, *Florence*

Pier P Mainenti, *Napoli*

Laura Marzetti, *Chieti*

Giuseppe Malinverni, *Crescentino*

Enrica Milanese, *Turin*

Giovanni Morana, *Treviso*

Lorenzo Monti, *Milan*

Silvia D Morbelli, *Genoa*

Barbara Palumbo, *Perugia*

Cecilia Parazzini, *Milan*

Stefano Pergolizzi, *Messina*

Antonio Pinto, *Naples*

Camillo Porcaro, *Rome*

Carlo C Quattrocchi, *Rome*

Alberto Rebonato, *Perugia*

Giuseppe Rizzo, *Rome*

Roberto De Rosa, *Naples*

Domenico Rubello, *Rovigo*

Andrea Salvati, *Bari*

Sergio Sartori, *Ferrara*

Luca M Sconfienza, *Milano*

Giovanni Storto, *Rionero*

Nicola Sverzellati, *Parma*

Alberto S Tagliafico, *Genova*

Nicola Troisi, *Florence*



Japan

Yasuhiko Hori, *Chiba*

Hidetoshi Ikeda, *Koriyama*

Masahito Kawabori, *Sapporo*

Tamotsu Kamishima, *Sapporo*

Hiro Kiyosue, *Yufu*

Yasunori Minami, *Osaka-sayama*

Yasuhiro Morimoto, *Kitakyushu*

Satoru Murata, *Tokyo*

Shigeki Nagamachi, *Miyazaki*

Hiroshi Onishi, *Yamanashi*

Morio Sato, *Wakayama Shi*

Yoshito Tsushima, *Maebashi*

Masahiro Yanagawa, *Suita*



Netherlands

Willem Jan van Rooij, *Tilburg*



New Zealand

W Howell Round, *Hamilton*



Pakistan

Wazir Muhammad, *Abbottabad*



Poland

Maciej S Baglaj, *Wroclaw*

Piotr Czauderna, *Gdansk*



Portugal

Joao Manuel RS Tavares, *Porto*



Serbia

Olivera Ciraj-Bjelac, *Belgrade*



Singapore

Gopinathan Anil, *Singapore*

Terence KB Teo, *Singapore*

Cher Heng Tan, *Singapore*



Slovakia

Stefan Sivak, *Martin*



South Korea

Ki Seok Choo, *Busan*

Seung Hong Choi, *Seoul*

Dae-Seob Choi, *Jinju*

Hong-Seok Jang, *Seoul*

Yong Jeong, *Daejeon*

Chan Kyo Kim, *Seoul*

Se Hyung Kim, *Seoul*

Joong-Seok Kim, *Seoul*

Sang Eun Kim, *Seongnam*

Sung Joon Kwon, *Seoul*

Jeong Min Lee, *Seoul*

In Sook Lee, *Busan*

Noh Park, *Goyang*

Chang Min Park, *Seoul*

Sung Bin Park, *Seoul*

Deuk Jae Sung, *Seoul*

Choongsoo Shin, *Seoul*

Kwon-Ha Yoon, *Iksan*



Spain

Miguel A De Gregorio, *Zaragoza*

Antonio Luna, *Jaén*

Enrique Marco de Lucas, *Santander*

Fernando Ruiz Santiago, *Granada*



Sweden

Dmitry Grishenkov, *Stockholm*

Tie-Qiang Li, *Stockholm*



Switzerland

Nicolau Beckmann, *Basel*

Christian Boy, *Bern*

Giorgio Treglia, *Bellinzona*

Stephan Ulmer, *Kiel*



Thailand

Sirianong Namwongprom, *Chiang Mai*



Turkey

Kubilay Aydin, *Istanbul*

Ramazan Akdemir, *Sakarya*

Serhat Avcu, *Ankara*

Ayşe Aralasmak, *Istanbul*

Oktay Algin, *Ankara*

Nevbahar Akcar, *Meselik*

Bilal Battal, *Ankara*

Zulkif Bozgeyik, *Elazig*

Nazan Ciledag, *Aakara*

Fuldem Y Donmez, *Ankara*

Gulgun Engin, *Istanbul*

Ahmet Y Goktay, *Izmir*

Oguzhan G Gumustas, *Bursa*

Kaan Gunduz, *Ankara*

Pelin Ozcan Kara, *Mersin*

Kivanc Kamburoglu, *Ankara*

Ozgur Kilickesmez, *Istanbul*

Furuzan Numan, *Istanbul*

Cem Onal, *Adana*

Ozgur Oztekin, *Izmir*

Seda Ozbek (Boruban), *Konya*

Selda Sarikaya, *Zonguldak*

Figen Taser, *Kutahya*

Baran Tokar, *Eskisehir*

Ender Uysal, *Istanbul*

Ensar Yekeler, *Istanbul*



United Kingdom

Indran Davagnanam, *London*

M DC Valdés Hernández, *Edinburgh*

Alan Jackson, *Manchester*

Suneil Jain, *Belfast*

Long R Jiao, *London*

Miltiadis Krokidis, *Cambridge*

Pradesh Kumar, *Liverpool*

Peter D Kuzmich, *Derby*

Georgios Plataniotis, *Brighton*

Vanessa Sluming, *Liverpool*



United States

Garima Agrawal, *Saint Louis*

James R Brasic, *Baltimore*

Rajendra D Badgaiyan, *Buffalo*

Ulas Bagci, *Bethesda*

Anat Biegon, *Stony Brook*

Ramon Casanova, *Winston Salem*

Wenli Cai, *Boston*

Zheng Chang, *Durham*

Corey J Chakarun, *Long Beach*

Kai Chen, *Los Angeles*

Hyun-Soon Chong, *Chicago*

Marco Cura, *Dallas*

Ravi R Desai, *Bensalem*

Delia DeBuc, *Miami*

Carlo N De Cecco, *Charleston*

Timm-Michael L Dickfeld, *Baltimore*

Subba R Digumarthy, *Boston*

Huy M Do, *Stanford*

Todd A Faasse, *Grand Rapids*

Salomao Faintuch, *Boston*

Girish M Fatterpekar, *New York*

Dhakshinamoorthy Ganesan, *Houston*

Robert J Griffin, *Little Rock*

Andrew J Gunn, *Boston*

Sandeep S Hedgire, *Boston*

Timothy J Hoffman, *Columbia*

Mai-Lan Ho, *San Francisco*

Juebin Huang, *Jackson*

Abid Irshad, *Charleston*

Matilde Inglese, *New York*

El-Sayed H Ibrahim, *Jacksonville*

Paul R Julsrud, *Rochester*

Pamela T Johnson, *Baltimore*

Ming-Hung Kao, *Tempe*

Sunil Krishnan, *Houston*

Richard A Komoroski, *Cincinnati*

Sandi A Kwee, *Honolulu*

King Kim, *Ft. Lauderdale*

Guozheng Liu, *Worcester*

Yiyan Liu, *Newark*

Venkatesh Mani, *New York*

Lian-Sheng Ma, *Pleasanton*

Rachna Madan, *Boston*

Zeyad A Metwalli, *Houston*

Yilong Ma, *Manhasset*

Hui Mao, *Atlanta*

Feroze B Mohamed, *Philadelphia*

Gul Moonis, *Boston*

John L Noshier, *New Brunswick*

Rahmi Oklu, *Boston*

Aytekun Oto, *Chicago*

Bishnuhari Paudyal, *Philadelphia*

Rajul Pandya, *Youngstown*

Chong-Xian Pan, *Sacramento*

Jay J Pillai, *Baltimore*

Neal Prakash, *Duarte*

Reza Rahbar, *Boston*

Ali S Raja, *Boston*

Gustavo J Rodriguez, *El Paso*

David J Sahn, *Portland*

Steven Schild, *Scottsdale*

Ali R Sepahdari, *Los Angeles*

Li Shen, *Indianapolis*

JP Sheehan, *Charlottesville*

Atul B Shinagare, *Boston*

Sarabjeet Singh, *Boston*

Charles J Smith, *Columbia*

Kenji Suzuki, *Chicago*

Monvadi Srichai-Parsia, *Washington*

Sree H Tirumani, *Boston*

Hebert A Vargas, *New York*

Sachit Verma, *Philadelphia*

Yoichi Watanabe, *Minneapolis*

Li Wang, *Chapel Hill*

Carol C Wu, *Boston*

Shoujun Xu, *Houston*

Min Yao, *Cleveland*

Xiaofeng Yang, *Atlanta*

Qingbao Yu, *Albuquerque*

Aifeng Zhang, *Chicago*

Chao Zhou, *Bethlehem*

Hongming Zhuang, *Philadelphia*

**EDITORIAL**

- 27 Evaluation of response to immune checkpoint inhibitors: Is there a role for positron emission tomography?
Bauckneht M, Piva R, Sambuceti G, Grossi F, Morbelli S

REVIEW

- 34 Potential role of imaging in assessing harmful effects on spermatogenesis in adult testes with varicocele
Tsili AC, Xiropotamou ON, Sylakos A, Maliakas V, Sofikitis N, Argyropoulou MI

MINIREVIEWS

- 46 Magnetic resonance enterography in Crohn's disease: How we do it and common imaging findings
Mantarro A, Scalise P, Guidi E, Neri E

ORIGINAL ARTICLE**Basic Study**

- 55 Radiology education in Europe: Analysis of results from 22 European countries
Rehani B, Zhang YC, Rehani MM, Palkó A, Lau L, Lette MNM, Dillon WP
- 63 Radiation dose enhancement in skin therapy with nanoparticle addition: A Monte Carlo study on kilovoltage photon and megavoltage electron beams
Zheng XJ, Chow JCL

Retrospective Study

- 72 Magnetic resonance imaging in the assessment of brain involvement in alcoholic and nonalcoholic Wernicke's encephalopathy
Sparacia G, Anastasi A, Speciale C, Agnello F, Banco A

Observational Study

- 79 Feasibility of imaging superficial palmar arch using micro-ultrasound, 7T and 3T magnetic resonance imaging
Pruzan AN, Kaufman AE, Calcagno C, Zhou Y, Fayad ZA, Mani V
- 85 Gastric blunt traumatic injuries: A computed tomography grading classification
Solazzo A, Lassandro G, Lassandro F

Contents

World Journal of Radiology
Volume 9 Number 2 February 28, 2017

ABOUT COVER

Editorial Board Member of *World Journal of Radiology*, Nicola Sverzellati, MD, Academic Research, Department of Surgical Sciences, Section of Radiology, University of Parma, 43121 Parma, Italy

AIM AND SCOPE

World Journal of Radiology (*World J Radiol*, *WJR*, online ISSN 1949-8470, DOI: 10.4329) is a peer-reviewed open access academic journal that aims to guide clinical practice and improve diagnostic and therapeutic skills of clinicians.

WJR covers topics concerning diagnostic radiology, radiation oncology, radiologic physics, neuroradiology, nuclear radiology, pediatric radiology, vascular/interventional radiology, medical imaging achieved by various modalities and related methods analysis. The current columns of *WJR* include editorial, frontier, diagnostic advances, therapeutics advances, field of vision, mini-reviews, review, topic highlight, medical ethics, original articles, case report, clinical case conference (clinicopathological conference), and autobiography.

We encourage authors to submit their manuscripts to *WJR*. We will give priority to manuscripts that are supported by major national and international foundations and those that are of great basic and clinical significance.

INDEXING/ABSTRACTING

World Journal of Radiology is now indexed in PubMed, PubMed Central.

FLYLEAF

I-III Editorial Board

EDITORS FOR THIS ISSUE

Responsible Assistant Editor: *Xiang Li*
Responsible Electronic Editor: *Huan-Liang Wu*
Proofing Editor-in-Chief: *Lian-Sheng Ma*

Responsible Science Editor: *Jin-Xin Kong*
Proofing Editorial Office Director: *Xiu-Xia Song*

NAME OF JOURNAL
World Journal of Radiology

ISSN
ISSN 1949-8470 (online)

LAUNCH DATE
January 31, 2009

FREQUENCY
Monthly

EDITORS-IN-CHIEF
Kai U Juergens, MD, Associate Professor, MRT und PET/CT, Nuklearmedizin Bremen Mitte, ZEMODI - Zentrum für morphologische und molekulare Diagnostik, Bremen 28177, Germany

Edwin JR van Beek, MD, PhD, Professor, Clinical Research Imaging Centre and Department of Medical Radiology, University of Edinburgh, Edinburgh EH16 4TJ, United Kingdom

Thomas J Vogl, MD, Professor, Reader in Health Technology Assessment, Department of Diagnostic and Interventional Radiology, Johann Wolfgang Goethe University of Frankfurt, Frankfurt 60590,

Germany

EDITORIAL BOARD MEMBERS
All editorial board members resources online at <http://www.wjnet.com/1949-8470/editorialboard.htm>

EDITORIAL OFFICE
Xiu-Xia Song, Director
World Journal of Radiology
Baishideng Publishing Group Inc
8226 Regency Drive, Pleasanton, CA 94588, USA
Telephone: +1-925-2238242
Fax: +1-925-2238243
E-mail: editorialoffice@wjnet.com
Help Desk: <http://www.wjnet.com/esps/helpdesk.aspx>
<http://www.wjnet.com>

PUBLISHER
Baishideng Publishing Group Inc
8226 Regency Drive,
Pleasanton, CA 94588, USA
Telephone: +1-925-2238242
Fax: +1-925-2238243
E-mail: bpgoffice@wjnet.com
Help Desk: <http://www.wjnet.com/esps/helpdesk.aspx>
<http://www.wjnet.com>

PUBLICATION DATE
February 28, 2017

COPYRIGHT
© 2017 Baishideng Publishing Group Inc. Articles published by this Open-Access journal are distributed under the terms of the Creative Commons Attribution Non-commercial License, which permits use, distribution, and reproduction in any medium, provided the original work is properly cited, the use is non commercial and is otherwise in compliance with the license.

SPECIAL STATEMENT
All articles published in journals owned by the Baishideng Publishing Group (BPG) represent the views and opinions of their authors, and not the views, opinions or policies of the BPG, except where otherwise explicitly indicated.

INSTRUCTIONS TO AUTHORS
<http://www.wjnet.com/bpg/gerinfo/204>

ONLINE SUBMISSION
<http://www.wjnet.com/esps/>

Evaluation of response to immune checkpoint inhibitors: Is there a role for positron emission tomography?

Matteo Bauckneht, Roberta Piva, Gianmario Sambuceti, Francesco Grossi, Silvia Morbelli

Matteo Bauckneht, Roberta Piva, Gianmario Sambuceti, Silvia Morbelli, Nuclear Medicine Unit, IRCCS San Martino-IST, University of Genoa, 16132 Genoa, Italy

Francesco Grossi, Lung Cancer Unit, IRCCS San Martino-IST, University of Genoa, 16132 Genoa, Italy

Author contributions: Morbelli S conceived and designed the study; Bauckneht M and Morbelli S drafted the manuscript; Bauckneht M and Piva R prepared the tables and figures; Sambuceti G and Grossi F critically revised the manuscript; all the authors approved the final version of the paper.

Conflict-of-interest statement: The authors have no conflicts of interest related to this publication to disclose.

Open-Access: This article is an open-access article which was selected by an in-house editor and fully peer-reviewed by external reviewers. It is distributed in accordance with the Creative Commons Attribution Non Commercial (CC BY-NC 4.0) license, which permits others to distribute, remix, adapt, build upon this work non-commercially, and license their derivative works on different terms, provided the original work is properly cited and the use is non-commercial. See: <http://creativecommons.org/licenses/by-nc/4.0/>

Manuscript source: Invited manuscript

Correspondence to: Silvia Morbelli, MD, PhD, Nuclear Medicine Unit, IRCCS San Martino-IST, University of Genoa, Largo R. Benzi 10, 16132 Genova, Italy. silviadaniela.morbelli@hsanmartino.it
Telephone: +39-010-5552026
Fax: +39-010-5556911

Received: August 20, 2016

Peer-review started: August 23, 2016

First decision: October 21, 2016

Revised: November 2, 2016

Accepted: November 27, 2016

Article in press: November 29, 2016

Published online: February 28, 2017

such as immune checkpoint inhibitors (ICPIs) have demonstrated significant antitumor activity across a wide range of solid tumors. In the clinical practice, the radiological effect of immunotherapeutic agents has raised several more relevant and complex challenges for the determination of their imaging-based response at single patient level. Accordingly, it has been suggested that the conventional Response Evaluation Criteria in Solid Tumors assessment alone, based on dimensional evaluation provided by computed tomography (CT), tends to underestimate the benefit of ICPIs at least in a subset of patients, supporting the need of immune-related response criteria. Different from CT, very few data are available for the evaluation of immunotherapy by means of ^{18}F -fluoro-2-deoxy-D-glucose positron emission tomography (FDG-PET). Moreover, since the antineoplastic activity of ICPIs is highly related to the activation of T cells against cancer cells, FDG accumulation might cause false-positive findings. Yet, discrimination between benign and malignant processes represents a huge challenge for FDG-PET in this clinical setting. Consequently, it might be of high interest to test the complex and variegated response to ICPIs by means of PET and thus it is worthwhile to ask if a similar introduction of immune-related PET-based criteria could be proposed in the future. Finally, PET might offer a new insight into the biology and pathophysiology of ICPIs thanks to a growing number of non-invasive immune-diagnostic approaches based on non-FDG tracers.

Key words: Immune checkpoint inhibitors; Positron emission tomography; Computed tomography; ^{18}F -fluoro-2-deoxy-D-glucose; Non- ^{18}F -fluoro-2-deoxy-D-glucose tracers

© **The Author(s) 2017.** Published by Baishideng Publishing Group Inc. All rights reserved.

Core tip: In the clinical practice, the radiological interpretation of immunotherapy effects represents a huge challenge at single patient level. However, although the computed tomography-based response

Abstract

Strategies targeting intracellular negative regulators

evaluation for immune checkpoint inhibitors (ICPIs) is feasible thanks to the introduction of immune-related response criteria, very few data are available for the potential role of ^{18}F -fluoro-2-deoxy-D-glucose positron emission tomography (FDG-PET). Due to the intrinsic nature of FDG accumulation pathophysiology, it might be central to test the complex and variegated response to ICPIs by means of PET. Finally, PET might offer a new insight into the biology of ICPIs thanks to a growing number of non-invasive immune-diagnostic approaches based on non-FDG tracers.

Bauckneht M, Piva R, Sambuceti G, Grossi F, Morbelli S. Evaluation of response to immune checkpoint inhibitors: Is there a role for positron emission tomography? *World J Radiol* 2017; 9(2): 27-33 Available from: URL: <http://www.wjgnet.com/1949-8470/full/v9/i2/27.htm> DOI: <http://dx.doi.org/10.4329/wjr.v9.i2.27>

TEXT

The function of the immune system is characterized by multiple checkpoints aiming to avoid its over-activation against healthy cells (self-tolerance)^[1]. Cancer cells may take advantage of these checkpoints to escape detection by the immune system. Some of these checkpoints such as cytotoxic T-lymphocyte-associated antigen 4 (CTLA-4) and programmed cell death protein 1 (PD-1) have been extensively studied as targets in the frame of the so-called cancer immunotherapy^[1]. CTLA-4 counteracts the activity of the T cell co-stimulatory receptor CD28 and actively delivers inhibitory signals to the T cell^[2]. PD-1 has two ligands, PD1 ligand 1 (PDL1) and PDL2, and its inhibitory effect is accomplished through a dual mechanism of promoting apoptosis in antigen specific T-cells in lymph nodes while simultaneously reducing apoptosis in regulatory T cells (suppressor T cells)^[3]. In the last few years, the blockade of immune checkpoints has disclosed the potential of the antitumor immune response in a fashion that is transforming human cancer therapeutics. CTLA4 antibodies such as ipilimumab and tremelimumab have been tested in the last ten years in different types of cancer, starting with patients with advanced melanoma^[4]. Ipilimumab was the first therapy to demonstrate a survival benefit for patients with metastatic melanoma. In a study by Hodi *et al.*^[5], ipilimumab significantly improved overall survival in patients with previously treated metastatic melanoma and the drug was approved by the United States Food and Drug Administration (FDA) for the treatment of advanced melanoma in 2011^[5]. Similarly, nivolumab, a humanized anti-PD-1 monoclonal antibody, has demonstrated durable responses in several phase III trials and has received FDA approval in specific clinical settings in patients with melanoma, renal cell cancer, Hodgkin's lymphoma, bladder cancer, and non-small cell lung cancer (NSCLC)^[6-9]. Figure 1 summarizes the

mechanisms of action of the two FDA approved immune checkpoint inhibitors (ICPIs).

Evaluation of response to ICPIs

Historically, the Response Evaluation Criteria in Solid Tumors (RECIST) has been validated and used to evaluate antitumor responses to chemotherapeutic agents^[10] (Table 1 for a more detailed description). These criteria are based on dimensional evaluation and rely on the fact that the cytotoxic effect of chemotherapeutic agents tends to translate into measurable effects in terms of tumor shrinkage from baseline. Furthermore, published studies indicated that achieving a response according to RECIST criteria is predictive of remission and improved survival in specific settings^[11]. Conversely, both RECIST and their revised 1.1 version assumed that an early increase in tumor growth and/or the appearance of new lesions correspond to progressive disease (PD), testifying drug failure and indicating the need of ongoing treatment cessation^[10].

Some exceptions for the use of these criteria have been already suggested in patients treated with target therapies such as tyrosine kinase inhibitors as in this group of patients the lack of tumor shrinkage in the presence of a stable disease has been identified as a potential surrogate end point for improved clinical outcome^[12]. However, in the clinical practice, the radiological effect of immunotherapeutic agents has raised several more relevant and complex challenges for the determination of their imaging-based response at single patient level^[13]. In published studies, while some patients have responded to ICPIs with the expected tumor shrinkage (chemo-like response) or with a stable disease (target therapy-like response), other distinct immune-related patterns of response have been identified. In particular, an initial increase in tumor size, development of new lesions and then a delayed objective response were also observed in patients treated with immunotherapeutic agents^[13]. Specifically, in some patients, the initial increase in total tumor burden was proven to be due to inflammatory cell infiltrates by means of biopsy. In these patients the initial pseudo-progression was followed by a decrease in tumor burden or even disease regression.

As RECIST criteria were not suitable to catch these atypical responses, the so-called immune-related response criteria (irRC) have been proposed to provide more rigorous characterization of all patterns of response observed in the phase II development program for ipilimumab in melanoma^[13-15] (Table 1). The main differences between RECIST 1.1 and irRC rely on the fact that, according to irRC, appearance of new lesions (PD according to the RECIST criteria) will only result in progressive disease in case of a significant ($\geq 25\%$) increase in total tumor burden with respect to baseline. Moreover, different from conventional criteria, if irRC-based PD is evident, it requires further confirmation after one month with the aim of capturing

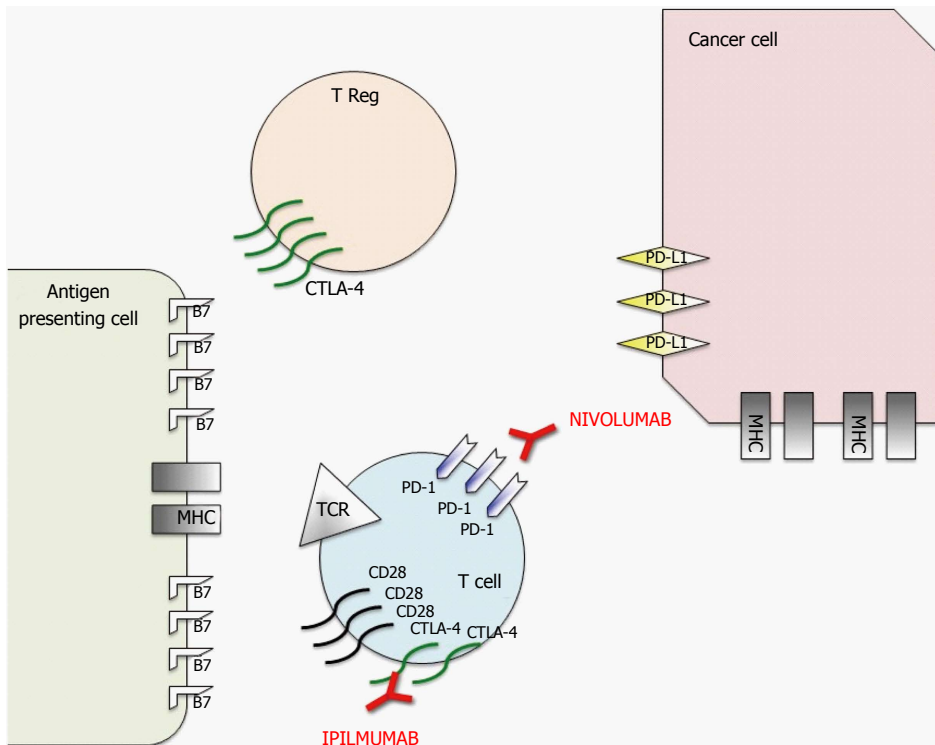


Figure 1 Schematic representation of mechanism of action of nivolumab and ipilimumab, two Food and Drug Administration approved immune checkpoint inhibitors. To prevent autoimmunity, numerous checkpoint pathways regulate the activation of T cells at multiple steps (process known as peripheral tolerance). Central in this process are the cytotoxic T-lymphocyte-associated antigen 4 (CTLA-4) and programmed death 1 (PD-1) immune checkpoints pathways. CTLA-4 is potentially able to stop autoreactive T cells at the initial stage of naive T-cell activation, typically in lymph nodes, while PD-1 regulates previously activated T cells at the later stages of an immune response in peripheral tissues. The binding between T-cell receptor (TCR), which is expressed on T cell surface, with major histocompatibility complex (MHC) expressed on antigen presenting cells (APCs) provides specificity to T-cell activation. However, T cell activation requires more than one stimulatory signal. Among them a central role is played by the binding between B7 molecules (APC) with CD28 (T-Cell). CTLA-4 is a CD28 homolog which does not produce a stimulatory signal but inhibits TCR-MHC binding and thus the T-Cell activation. Different from T-cells in which the amount of CTLA-4 is low, T-Regs highly express CTLA-4. In these cells CTLA-4 might play a role in their suppressive functions. PD-1 is a member of the B7/CD38 family of protein, which is able to bind with two different ligands: Programmed death ligand 1 (PD-L1) and programmed death ligand 2 (PD-L2). PD-1 activation in a T-cell prevents the phosphorylation of key TCR signaling intermediates and thus T-cell activation, resulting in suboptimal control of infections and cancers. Therefore, even though they act at different phases of T-cell activation, the negative effect of PD-1 and CTLA-4 on T-cell activity is similar. Moreover, different from CTLA-4, PD-1 expression is not specific in T-cells, but can be observed also in B-cells and myeloid cells. The rationale for immune checkpoint inhibition (represented in red) for cancer treatment is that CTLA-4 and PD1 pathways are strictly related to cancer survival and thus targeting these molecules or their ligands with monoclonal antibodies permits to impact on cancer growth. Therefore, even if the exact mechanism of action of these monoclonal antibodies in the antitumor response remains unclear, research data suggest that it is at least partially related to an activation and proliferation of T-cells regardless of TCR specificity (due to the inhibition of the inhibitory activity of these checkpoints), which enhances the anti-cancer immune reaction.

delayed response.

Recently, Hodi *et al*^[16] evaluated atypical response patterns and reported the overall survival data in correlation with irRC and RECIST criteria in the context of a retrospective analysis of 327 melanoma patients treated with the PD-1 inhibitor pembrolizumab. This study indicated that the conventional RECIST assessment alone tends to underestimate the benefit of PD-1 inhibitor therapy in a subset of patients, supporting a need of immune-related response evaluation^[16]. IrRC are thus increasingly proposed, but they have not been validated yet in the context of clinical trials and most trials involving ICPIs continue to use RECIST 1.1 to obtain standardized endpoints for regulatory approvals^[15].

However, although the irRC seem better than RECIST, the former has some limitations. The irRC use the bidimensional measurements in line with WHO criteria that are now rarely used in clinical trials and replaced by the unidimensional measurement of the

larger axis of target lesions (RECIST 1.0 and 1.1). The bidimensional measurements introduce a greater variability than unidimensional measurements and make it difficult to compare the responses with studies using the RECIST criteria.

Is there a role for ¹⁸F-fluoro-2-deoxy-D-glucose positron emission tomography in the evaluation of ICPIs?

While optimal CT-based response criteria for ICPIs are in the path of their identification, very few data are available for the evaluation of immunotherapy by means of ¹⁸F-fluoro-2-deoxy-D-glucose positron emission tomography (¹⁸F-FDG-PET), one of the most used imaging techniques in oncology. ¹⁸F-FDG-PET is currently the most widely used molecular imaging modality in the clinical practice for staging and restaging of several cancers. ¹⁸F-FDG-PET is clinically indicated before and after treatment in patients with Hodgkin's lymphoma and NSCLC and it is used in patients with melanoma for

Table 1 Key features of positron emission tomography Response Criteria in Solid Tumors, European Organization for Research and Treatment of Cancer 1999, Response Evaluation Criteria in Solid Tumors 1.1 and immune related Response Criteria

Category	PERCIST	EORTC 1999	RECIST 1.1	irRC
Target lesions	The hottest single tumor lesion (SUL peak) at baseline ¹⁸ F-FDG PET	The most ¹⁸ F-FDG-avid lesions (SUV BSA). Number of lesions not specified	Maximum, 5	Maximum, 15 lesions
New lesion	Results in progressive disease at first appearance	Results in progressive disease at first appearance	Results in progressive disease at first appearance	Up to 10 new visceral and 5 cutaneous lesions may be added to the sum of the products of the two largest perpendicular diameters of all index lesions at any time point
Complete response	CMR: Complete resolution of ¹⁸ F-FDG uptake within the target lesion (< mean liver activity and indistinguishable from background/blood pool and no new ¹⁸ F-FDG-avid lesions)	CMR: Complete absence of ¹⁸ F-FDG uptake	Disappearance of all target and nontarget lesions Nodes must regress to < 10 mm short axis No new lesions Confirmation required	
Partial response	PMR: A reduction of a minimum of 30% in the target tumor ¹⁸ F-FDG SUL peak	PMR: A decrease in SUV > 25%	≥ 30% decrease in tumor burden compared to baseline Confirmation required	≥ 50% decrease in tumor burden compared with baseline ¹ Confirmation required
Progressive disease	PMD: A 30% increase in ¹⁸ F-FDG SUL peak or advent of new ¹⁸ F-FDG-avid lesions	PMD: An increase in SUV > 25% or appearance of new lesions	≥ 20% + 5 mm absolute increase in tumor burden compared with nadir Appearance of new lesions or progression of nontarget lesions	≥ 25% increase in tumor burden compared with baseline, nadir or reset baseline ¹ New lesions added to tumor burden Confirmation required
Stable disease	SMD: Disease other than CMR, PMR or PMD	SMD: Increase in SUV by < 25% or decrease in SUV by < 15%	Neither partial response nor progressive disease	

¹If an increase in tumor burden is observed at the first scheduled assessment, the baseline is reset to the value observed at the first assessment. PERCIST: PET Response Criteria in Solid Tumors; EORTC: European Organization for Research and Treatment of Cancer; RECIST: Response Evaluation Criteria in Solid Tumors; irRC: Immune related Response Criteria; CMR: Complete metabolic response; PMR: Partial metabolic response; PMD: Progressive metabolic disease; SMD: Stable metabolic disease; SUL: SUV normalized to lean body mass; SUV BSA: SUV normalized for body surface area; SUV: Standardized uptake value.

specific clinical indications^[17-19]. The use of ¹⁸F-FDG-PET in post-treatment settings is based on the assumption that tumor size changes are only the final step in a sequence of complex metabolic and functional processes during and after treatment^[20]. Two different types of criteria have been proposed for the identification of ¹⁸F-FDG-PET-based response in solid tumors: The European Organization for Research and Treatment of Cancer (EORTC) and the PET Response Criteria in Solid Tumors (PERCIST) criteria^[21,22] (Table 1). Both criteria target the most metabolically active part of patient's tumor burden, which is regarded as the most viable and aggressive disease site. In both cases, the so-called standardized uptake value (SUV) is measured at baseline and after treatment. However, they differ for some relevant aspects. The EORTC criteria were published in 1999 and are based on the evaluation of a lesion-specific region of interest (ROI) chosen as the most ¹⁸F-FDG-avid at baseline and followed in the after-treatment scans^[22]. The PERCIST criteria were proposed in 2009 by Wahl *et al.*^[21] and rely on the use of a 1 cm³ ROI on the most ¹⁸F-FDG-avid part of the single most metabolically active lesion at each PET/CT scan (which is not necessarily located in the same lesion in all scans).

Relatively few papers have compared the two

methods in solid tumors and good agreement, similar responses and survival outcomes have been highlighted in the available studies^[23]. However, for the EORTC criteria, no recommendations on the number of target lesions or on whether computing SUV max or average SUV for response calculation are given while the PERCIST criteria recommend the use of lean body mass for SUV normalization (SUL). In this framework, some studies have demonstrated a higher accuracy with respect to RECIST for both metabolic response based criteria in patients treated with target therapies such as erlotinib. This finding is due to the relative lower tumor shrinkage characterizing this type of treatment^[24]. Similarly, an ¹⁸F-FDG-PET-based five-point scale (5-PS), the so-called Deauville criteria, has been demonstrated to be superior to CT-based response by scoring images in the assessment of response at the middle and end of treatment in HD patients^[18]. Again these findings testify that functional changes always precede morphological changes in the course of pathological processes. In this regard it might be of interest to test the complex and variegated response to ICPIs by means of PET-based criteria. In fact, on one hand, functional imaging may capture different features of treatment with ICPIs in terms of entity and time course of response. On

the other hand, it has been reported that the initial increase in tumor size, later followed by tumor volume reduction in part of the patients treated with ICPIs, is due to inflammatory cell infiltrates. Accordingly, given the well-known high metabolic activity characterizing inflammatory cells, this feature may also hamper the evaluation of ^{18}F -FDG-PET-based response to ICPIs. Sachpekidis *et al.*^[20] evaluated the role of ^{18}F -FDG-PET/CT after two cycles of ipilimumab in predicting the final response to therapy in 22 patients with metastatic melanoma. They evaluated response to treatment by means of the EORTC criteria and found that ^{18}F -FDG-PET/CT after two cycles of ipilimumab is predictive of the final treatment outcome in patients with progressive metabolic disease (PMD) and stable metabolic disease (SMD)^[20]. However, two patients were initially falsely classified as early SMD, but they later demonstrated new metastatic lesions, “upgrading” them to late PMD. Similarly, early evaluation by means of ^{18}F -FDG-PET did not identify responders to treatment as the two patients eventually characterized with PMR were initially classified with early PMD due to new lesions^[20]. In fact, both RECIST 1.1 and PET-based criteria consider the identification of new (metabolically active) lesions as progressive disease. Therefore, presently proposed PET-based metabolic criteria suffer from at least one of the same limitations that have resulted in the underestimation of response to treatment with ICPIs by means of RECIST 1.1. Similarly, in the phase 2 study by Younes *et al.*^[9], nivolumab resulted in frequent responses in patients with classical Hodgkin’s lymphoma after failure of ASCT and brentuximab vedotin. Most of these responses were maintained through the reported follow-up period with an acceptable safety profile. In this study ^{18}F -FDG-PET was performed at baseline and at weeks 17 and 25. A negative ^{18}F -FDG-PET scan, visually assessed by an independent radiological review committee (IRRC), was required for confirmation of complete remission. The study demonstrated a general reduction of tumor burden. Yet, discordance in complete remission between IRRC and investigator assessments was largely based on the interpretation of ^{18}F -FDG-PET scans and standardized uptake values were not collected as part of this study. The vast majority of other available data on the potential utility of ^{18}F -FDG-PET after ICPIs are case reports more often describing underlying challenges of monitoring radiologic response in these patients and showing ^{18}F -FDG-PET features of inflammatory reactions. PET-highlighted autoimmune pancolitis, splenic sarcoidosis-like lesion and exacerbation of sarcoidosis as a potential confounder in the assessment of tumor response in a melanoma patient treated with ipilimumab have all been described^[25-27]. Similarly, Koo *et al.*^[26] illustrated a series of inflammatory reactions with avid FDG uptake in patients treated with ipilimumab, including those with thyroiditis, hypophysitis, granulomatous inflammation in the lymph nodes and skin, and enterocolitis.

Accordingly, the potential and challenges of ^{18}F -FDG-

PET imaging in the evaluation of patients treated with ICPIs still need to be clarified and deeply addressed. Given the relatively greater experience of CT-based evaluation in this setting and the fact that irRC CT-based criteria seem to better in capturing response to ICPIs, it is worthwhile to ask if a similar modification of PET-based criteria could be proposed in the future.

Potential new PET-based approaches to evaluate the effect of ICPIs

As mentioned above, due to its intrinsic nature, ^{18}F -FDG-PET displays not only cancer cell’s metabolic activity but also inflammation. Since the antineoplastic activity of ICPIs is highly related to the activation of T cells against cancer cells, ^{18}F -FDG accumulation might cause false-positive findings. Yet, discrimination between benign and malignant processes represents a huge challenge for ^{18}F -FDG-PET in this clinical setting. Together with the need of the clinicians to discriminate between responders and non-responders, allowing individual therapy optimization and avoiding adverse effects brought about by ineffective therapy, several studies have been recently conducted to explore the possible role of non-FDG radiotracers in the field of ICPIs. These studies, mainly performed with labeled monoclonal antibodies, open the new era of the so-called “Immuno-PET”. Accordingly, in 2014, Higashikawa *et al.*^[28] developed a molecular imaging probe that is able to evaluate CTLA-4 expression prior to CTLA-4 targeting in cancer. This ^{64}Cu labeled radiotracer is basically composed of DOTA protein together with a CTLA-4 specific antibody and is able to display CTLA-4 expression *in vivo*. Similarly, specific experimental radiotracers were proposed for the visualization of PD-1 and PD-L1 cellular expression^[29-32]. Maute *et al.*^[29] measured PD-L1 expression by radiolabeling a PD-L1 high affinity protein (HAC) with ^{64}Cu and tested its feasibility in a living mouse, while Hettich *et al.*^[30] developed two ^{64}Cu labeled immunoPET tracers for imaging of both PD-1 and PD-L1. Also one SPECT study with radiolabeled anti-murine PD-L1 in mice has been conducted^[32]. More recently, a ^{89}Zr labeled CD3 PET imaging agent was proposed by Larimer *et al.*^[33]. CD3 is a part of the TCR complex that serves as a global T lymphocyte marker. By serving as a marker of total T-cell infiltration, CD3 may represent a more direct approach than pre-treatment biopsy or genetic screening to monitoring tumor immune response, by directly examining active recruitment of T cells responsible for cancer cell death. In this study the authors showed that CD3 PET imaging revealed two distinct groups of mice, stratified by PET signal intensity. While high-CD3 PET uptake was correlated with subsequent reduced tumor volume, low uptake was predictive of suboptimal response. Altogether these non-invasive approaches allow simultaneous imaging of the entire cancer mass and associated metastases, which may differ from the primary tumor in CTLA-4, PD-1 or PD-L1 expression status. Immune imaging can be used for repeated assessment of the same tumor at different

time points (e.g., before and after treatment), thereby yielding a richer set of diagnostic information that would be difficult or impossible to achieve with traditional approaches. Furthermore, although further investigations are needed before their potential introduction in the clinical setting, these non-invasive immune-diagnostic approaches might yield novel insights into the biology and pathophysiological importance of ICPIs as cancer therapeutics.

REFERENCES

- Pardoll DM.** The blockade of immune checkpoints in cancer immunotherapy. *Nat Rev Cancer* 2012; **12**: 252-264 [PMID: 22437870 DOI: 10.1038/nrc3239]
- Walunas TL, Lenschow DJ, Bakker CY, Linsley PS, Freeman GJ, Green JM, Thompson CB, Bluestone JA.** CTLA-4 can function as a negative regulator of T cell activation. *Immunity* 1994; **1**: 405-413 [PMID: 7882171]
- Francisco LM, Sage PT, Sharpe AH.** The PD-1 pathway in tolerance and autoimmunity. *Immunol Rev* 2010; **236**: 219-242 [PMID: 20636820 DOI: 10.1111/j.1600]
- O'Day SJ, Hamid O, Urba WJ.** Targeting cytotoxic T-lymphocyte antigen-4 (CTLA-4): a novel strategy for the treatment of melanoma and other malignancies. *Cancer* 2007; **110**: 2614-2627 [PMID: 18000991 DOI: 10.1002/cncr.23086]
- Hodi FS, O'Day SJ, McDermott DF, Weber RW, Sosman JA, Haanen JB, Gonzalez R, Robert C, Schadendorf D, Hassel JC, Akerley W, van den Eertwegh AJ, Lutzky J, Lorigan P, Vaubel JM, Linette GP, Hogg D, Ottensmeier CH, Lebbé C, Peschel C, Quirt I, Clark JI, Wolchok JD, Weber JS, Tian J, Yellin MJ, Nichol GM, Hoos A, Urba WJ.** Improved survival with ipilimumab in patients with metastatic melanoma. *N Engl J Med* 2010; **363**: 711-723 [PMID: 20525992 DOI: 10.1056/NEJMoa1003466]
- Giri A, Walia SS, Gajra A.** Clinical Trials Investigating Immune Checkpoint Inhibitors in Non-Small-Cell Lung Cancer. *Rev Recent Clin Trials* 2016; **11**: 297-305 [PMID: 27457350]
- Carlo MI, Voss MH, Motzer RJ.** Checkpoint inhibitors and other novel immunotherapies for advanced renal cell carcinoma. *Nat Rev Urol* 2016; **13**: 420-431 [PMID: 27324121 DOI: 10.1038/nrurol.2016.103]
- Ball MW, Allaf ME, Drake CG.** Recent advances in immunotherapy for kidney cancer. *Discov Med* 2016; **21**: 305-313 [PMID: 27232516]
- Younes A, Santoro A, Shipp M, Zinzani PL, Timmerman JM, Ansell S, Armand P, Fanale M, Ratanatharathorn V, Kuruvilla J, Cohen JB, Collins G, Savage KJ, Trneny M, Kato K, Farsaci B, Parker SM, Rodig S, Roemer MG, Ligon AH, Engert A.** Nivolumab for classical Hodgkin's lymphoma after failure of both autologous stem-cell transplantation and brentuximab vedotin: a multicentre, multicohort, single-arm phase 2 trial. *Lancet Oncol* 2016; **17**: 1283-1294 [PMID: 27451390 DOI: 10.1016/S1470-2045(16)30167]
- Eisenhauer EA, Therasse P, Bogaerts J, Schwartz LH, Sargent D, Ford R, Dancey J, Arbuck S, Gwyther S, Mooney M, Rubinstein L, Shankar L, Dodd L, Kaplan R, Lacombe D, Verweij J.** New response evaluation criteria in solid tumours: revised RECIST guideline (version 1.1). *Eur J Cancer* 2009; **45**: 228-247 [PMID: 19097774 DOI: 10.1016/j.ejca.2008.10.026]
- von Minckwitz G, Sinn HP, Raab G, Loibl S, Blohmer JU, Eidtmann H, Hilfrich J, Merkle E, Jackisch C, Costa SD, Caputo A, Kaufmann M.** Clinical response after two cycles compared to HER2, Ki-67, p53, and bcl-2 in independently predicting a pathological complete response after preoperative chemotherapy in patients with operable carcinoma of the breast. *Breast Cancer Res* 2008; **10**: R30 [PMID: 18380893 DOI: 10.1186/bcr1989]
- Tsuji K, Shiraishi J, Tsuji T, Kurata T, Kawaguchi T, Kubo A, Takada M.** Is response rate increment obtained by molecular targeted agents related to survival benefit in the phase III trials of advanced cancer? *Ann Oncol* 2010; **21**: 1668-1674 [PMID: 20064832 DOI: 10.1093/annonc/mdp588]
- Wolchok JD, Hoos A, O'Day S, Weber JS, Hamid O, Lebbé C, Maio M, Binder M, Bohnsack O, Nichol G, Humphrey R, Hodi FS.** Guidelines for the evaluation of immune therapy activity in solid tumors: immune-related response criteria. *Clin Cancer Res* 2009; **15**: 7412-7420 [PMID: 19934295 DOI: 10.1158/1078-0432]
- Hodi FS, Sznol M, Kluger HM, McDermott DF, Carvajal RD, Lawrence DP, Topalian SL, Atkins MB, Powderly JD, Sharfman WH, Puzanov I, Smith DC, Leming PD, Lipson EJ, Taube JM, Anders R, Horak CE, Kollia G, Gupta AK, Sosman JA.** Long term survival of ipilimumab-naïve patients (pts) with advanced melanoma (MEL) treated with nivolumab (anti-PD-1, BMS-936558, ONO-4538) in a phase I trial. ASCO Annual Meeting 2014 May 30- Jun 3; Chicago, Illinois, USA. *J Clin Oncol* 2014; **32**: 5s (suppl; abstr 9002)
- Chiou VL, Burotto M.** Pseudoprogression and Immune-Related Response in Solid Tumors. *J Clin Oncol* 2015; **33**: 3541-3543 [PMID: 26261262 DOI: 10.1200/JCO.2015.61.6870]
- Hodi FS, Hwu WJ, Kefford R, Weber JS, Daud A, Hamid O, Patnaik A, Ribas A, Robert C, Gangadhar TC, Joshua AM, Hersey P, Dronca R, Joseph R, Hille D, Xue D, Li XN, Kang SP, Ebbinghaus S, Perrone A, Wolchok JD.** Evaluation of Immune-Related Response Criteria and RECIST v1.1 in Patients With Advanced Melanoma Treated With Pembrolizumab. *J Clin Oncol* 2016; **34**: 1510-1517 [PMID: 26951310 DOI: 10.1200/JCO.2015.64.0391]
- Gould MK, Donington J, Lynch WR, Mazzzone PJ, Midthun DE, Naidich DP, Wiener RS.** Evaluation of individuals with pulmonary nodules: when is it lung cancer? Diagnosis and management of lung cancer, 3rd ed: American College of Chest Physicians evidence-based clinical practice guidelines. *Chest* 2013; **143**: e93S-120S [PMID: 23649456 DOI: 10.1378/chest.12-2351]
- Cheson BD, Fisher RI, Barrington SF, Cavalli F, Schwartz LH, Zucca E, Lister TA.** Recommendations for initial evaluation, staging, and response assessment of Hodgkin and non-Hodgkin lymphoma: the Lugano classification. *J Clin Oncol* 2014; **32**: 3059-3068 [PMID: 25113753 DOI: 10.1200/JCO.2013.54.8800]
- Morbelli S, Capitanio S, De Carli F, Bongioanni F, De Astis E, Miglino M, Verardi MT, Buschiazzo A, Fiz F, Marini C, Pomposelli E, Sambucetti G.** Baseline and ongoing PET-derived factors predict detrimental effect or potential utility of 18F-FDG PET/CT (FDG-PET/CT) performed for surveillance in asymptomatic lymphoma patients in first remission. *Eur J Nucl Med Mol Imaging* 2016; **43**: 232-239 [PMID: 26283504 DOI: 10.1007/s00259-015-3164-9]
- Sachpekidis C, Larribere L, Pan L, Haberkorn U, Dimitrakopoulou-Strauss A, Hassel JC.** Predictive value of early 18F-FDG PET/CT studies for treatment response evaluation to ipilimumab in metastatic melanoma: preliminary results of an ongoing study. *Eur J Nucl Med Mol Imaging* 2015; **42**: 386-396 [PMID: 25359635 DOI: 10.1007/s00259-014-2944-y]
- Wahl RL, Jacene H, Kasamony Y, Lodge MA.** From RECIST to PERCIST: Evolving Considerations for PET response criteria in solid tumors. *J Nucl Med* 2009; **50** Suppl 1: 122S-150S [PMID: 19403881 DOI: 10.2967/jnumed.108.057307]
- Young H, Baum R, Cremerius U, Herholz K, Hoekstra O, Lammertsma AA, Pruim J, Price P.** Measurement of clinical and subclinical tumour response using [18F]-fluorodeoxyglucose and positron emission tomography: review and 1999 EORTC recommendations. European Organization for Research and Treatment of Cancer (EORTC) PET Study Group. *Eur J Cancer* 1999; **35**: 1773-1782 [PMID: 10673991]
- Skougaard K, Nielsen D, Jensen BV, Hendel HW.** Comparison of EORTC criteria and PERCIST for PET/CT response evaluation of patients with metastatic colorectal cancer treated with irinotecan and cetuximab. *J Nucl Med* 2013; **54**: 1026-1031 [PMID: 23572497 DOI: 10.2967/jnumed.112.111757]
- Stefano A, Russo G, Ippolito M, Cosentino S, Murè G, Baldari S, Sabini MG, Sardina D, Valastro LM, Bordonaro R, Messa C, Gilardi MC, Soto Parra H.** Evaluation of erlotinib treatment response in non-small cell lung cancer using metabolic and anatomic criteria. *Q*

- J Nucl Med Mol Imaging* 2014 May 9; Epub ahead of print [PMID: 24809275]
- 25 **Goethals L**, Wilgenhof S, De Geeter F, Everaert H, Neyns B. 18F-FDG PET/CT imaging of an anti-CTLA-4 antibody-associated autoimmune pancolitis. *Eur J Nucl Med Mol Imaging* 2011; **38**: 1390-1391 [PMID: 21365253 DOI: 10.1007/s00259-011-1749-5]
 - 26 **Koo PJ**, Klingensmith WC, Lewis KD, Bagrosky BM, Gonzalez R. Anti-CTLA4 antibody therapy related complications on FDG PET/CT. *Clin Nucl Med* 2014; **39**: e93-e96 [PMID: 23657138 DOI: 10.1097/RLU.0b013e318292a775]
 - 27 **Perng P**, Marcus C, Subramaniam RM. (18)F-FDG PET/CT and Melanoma: Staging, Immune Modulation and Mutation-Targeted Therapy Assessment, and Prognosis. *AJR Am J Roentgenol* 2015; **205**: 259-270 [PMID: 26204273 DOI: 10.2214/AJR.14.13575]
 - 28 **Higashikawa K**, Yagi K, Watanabe K, Kamino S, Ueda M, Hiromura M, Enomoto S. 64Cu-DOTA-anti-CTLA-4 mAb enabled PET visualization of CTLA-4 on the T-cell infiltrating tumor tissues. *PLoS One* 2014; **9**: e109866 [PMID: 25365349]
 - 29 **Maute RL**, Gordon SR, Mayer AT, McCracken MN, Natarajan A, Ring NG, Kimura R, Tsai JM, Manglik A, Kruse AC, Gambhir SS, Weissman IL, Ring AM. Engineering high-affinity PD-1 variants for optimized immunotherapy and immuno-PET imaging. *Proc Natl Acad Sci USA* 2015; **112**: E6506-E6514 [PMID: 26604307 DOI: 10.1073/pnas.1519623112]
 - 30 **Hettich M**, Braun F, Bartholomä MD, Schirmbeck R, Niedermann G. High-Resolution PET Imaging with Therapeutic Antibody-based PD-1/PD-L1 Checkpoint Tracers. *Theranostics* 2016; **6**: 1629-1640 [PMID: 27446497 DOI: 10.7150/thno.15253]
 - 31 **Heskamp S**, Hobo W, Molkenboer-Kuennen JD, Olive D, Oyen WJ, Dolstra H, Boerman OC. Noninvasive Imaging of Tumor PD-L1 Expression Using Radiolabeled Anti-PD-L1 Antibodies. *Cancer Res* 2015; **75**: 2928-2936 [PMID: 25977331 DOI: 10.1158/0008-5472.CAN-14-3477]
 - 32 **Josefsson A**, Nedrow JR, Park S, Banerjee SR, Rittenbach A, Jammes F, Tsui B, Sgouros G. Imaging, Biodistribution, and Dosimetry of Radionuclide-Labeled PD-L1 Antibody in an Immunocompetent Mouse Model of Breast Cancer. *Cancer Res* 2016; **76**: 472-479 [PMID: 26554829 DOI: 10.1158/0008-5472.CAN-15-2141]
 - 33 **Larimer BM**, Wehrenberg-Klee E, Caraballo A, Mahmood U. Quantitative CD3 PET Imaging Predicts Tumor Growth Response to Anti-CTLA-4 Therapy. *J Nucl Med* 2016; **57**: 1607-1611 [PMID: 27230929 DOI: 10.2967/jnumed.116.173930]

P- Reviewer: Morris DLL, Palumbo B **S- Editor:** Ji FF

L- Editor: Wang TQ **E- Editor:** Wu HL



Potential role of imaging in assessing harmful effects on spermatogenesis in adult testes with varicocele

Athina C Tsili, Olga N Xiropotamou, Anastasios Sylakos, Vasilios Maliakas, Nikolaos Sofikitis, Maria I Argyropoulou

Athina C Tsili, Olga N Xiropotamou, Vasilios Maliakas, Maria I Argyropoulou, Department of Clinical Radiology, University of Ioannina, Medical School, University Campus, 45110 Epirus, Greece

Anastasios Sylakos, Nikolaos Sofikitis, Department of Urology, University of Ioannina, Medical School, University Campus, 45110 Epirus, Greece

Author contributions: Tsili AC and Xiropotamou ON contributed equally to this work; Tsili AC, Sofikitis N and Argyropoulou MI designed the research; Xiropotamou ON, Sylakos A and Maliakas V performed the research and analyzed the data; Tsili AC and Xiropotamou ON wrote the paper; all authors approved the final version of the article to be published.

Conflict-of-interest statement: The authors declare no conflicts of interest related to this publication.

Open-Access: This article is an open-access article which was selected by an in-house editor and fully peer-reviewed by external reviewers. It is distributed in accordance with the Creative Commons Attribution Non Commercial (CC BY-NC 4.0) license, which permits others to distribute, remix, adapt, build upon this work non-commercially, and license their derivative works on different terms, provided the original work is properly cited and the use is non-commercial. See: <http://creativecommons.org/licenses/by-nc/4.0/>

Manuscript source: Invited manuscript

Correspondence to: Athina C Tsili, MD, Assistant Professor, Department of Clinical Radiology, University of Ioannina, Medical School, University Campus, Ioannina, 45110 Epirus, Greece. a_tsili@yahoo.gr
Telephone: +30-69-76510904
Fax: +30-26-51007862

Received: August 10, 2016

Peer-review started: August 11, 2016

First decision: September 12, 2016

Revised: November 2, 2016

Accepted: December 16, 2016

Article in press: December 19, 2016

Published online: February 28, 2017

Abstract

Varicocele is characterized by an abnormal dilatation and retrograde blood flow in the spermatic veins. Varicocele is the leading correctable cause of male infertility. Although it is highly prevalent in infertile men, it is also observed in individuals with normal fertility. Determining which men are negatively affected by varicocele would enable clinicians to better select those men who will benefit from treatment. To assess the functional status of the testes in men with varicocele, color Doppler sonographic parameters were evaluated. Testicular arterial blood flow was significantly reduced in men with varicocele, reflecting an impairment of spermatogenesis. An improvement in the testicular blood supply was found after varicocelectomy on spectral Doppler analysis. Testicular contrast harmonic imaging and elastography might improve our knowledge about the influence of varicocele on intratesticular microcirculation and tissue stiffness, respectively, providing possible information on the early damage of testicular structure by varicocele. Magnetic resonance imaging (MRI), with measurement of apparent diffusion coefficient has been used to assess the degree of testicular dysfunction and to evaluate the effectiveness of varicocele repair. Large prospective studies are needed to validate the possible role of functional sonography and MRI in the assessment of early defects of spermatogenesis in testes with varicocele.

Key words: Varicocele; Spermatogenesis; Diagnostic imaging; Ultrasonography; Doppler ultrasound imaging; Magnetic resonance imaging; Functional

© The Author(s) 2017. Published by Baishideng Publishing Group Inc. All rights reserved.

Core tip: Varicocele is known as one of the main causes of male infertility. However, many controversies exist regarding the effect of varicocele on male reproductive potential, which patients to treat and whether repair leads to an improvement of the fertility status. Non-

invasive imaging modalities, including functional sonography and magnetic resonance imaging, might provide useful information on the early damage of testicular structure by varicoceles, therefore helping clinicians target repair efforts to those men who will benefit from varicocele treatment.

Tsili AC, Xiropotamou ON, Sylakos A, Maliakas V, Sofikitis N, Argyropoulou MI. Potential role of imaging in assessing harmful effects on spermatogenesis in adult testes with varicocele. *World J Radiol* 2017; 9(2): 34-45 Available from: URL: <http://www.wjgnet.com/1949-8470/full/v9/i2/34.htm> DOI: <http://dx.doi.org/10.4329/wjr.v9.i2.34>

INTRODUCTION

Male infertility is a social problem, representing the causal factor for infertility in 50% of cases and the sole cause in 30% of infertile couples^[1-3]. Varicocele is the most common andrological disorder between adolescents and adult males. Its clinical significance is mainly related to fertility, as it represents the most common cause of impaired male fertility and the most common treatable cause of infertility^[4-10]. The origin of the word varicocele comes from varico (a combining form meaning "varix" in Latin) and cele (a combining form meaning "tumor" in Greek) and dates to 1730-1740.

Varicocele has been one of the most controversial topics of debate in the fields of andrology and urology, regarding the effect of varicocele on male infertility and whether repair leads to improvement of fertility status^[4-10]. While most men with varicocele are able to father children, most evidence suggests that varicocele has detrimental effects on male reproductive potential. A non-invasive imaging technique providing answers to questions regarding which patients with varicocele are at risk for infertility and which will benefit from varicocele repair, would be extremely useful.

DEFINITION AND EPIDEMIOLOGY

Varicocele is clinically defined as an abnormal dilation of the veins of the pampiniform venous plexus and the testicular veins with continuous or intermittent reflux of venous blood^[4,5,11]. Primary varicoceles are due to venous reflux into the pampiniform plexus from the internal spermatic vein because of incompetent venous valves, and they usually occur on the left side. Secondary varicoceles are the result of increased pressure in the testicular veins, which can be related to several causes, such as hydronephrosis, abdominal and retroperitoneal neoplasms, and the so-called nutcracker phenomenon, which involves compression of the left renal vein between the superior mesenteric artery and aorta^[4,12-15]. Although varicoceles are almost always

more common and larger on the left side, they are bilateral in 50% of cases^[14]. The uncommon, isolated right-sided varicocele always necessitates further investigation, as this finding may be associated with situs inversus or retroperitoneal malignancies^[4,14].

Varicocele epidemiology is incompletely understood^[14]. A clinical varicocele is found in approximately 15% of all adult males, up to 35% of infertile men and 81% of men presenting with secondary infertility. When classified according to semen analysis parameters, 12% of infertile men with normal semen analyses and 25.4% of those with abnormal results were found to have clinical varicocele^[4,5,8,12,14]. This disorder may be present at birth or in young children, but the incidence substantially increases in adolescents coinciding with pubertal development^[4,5,14]. The prevalence of varicocele also increases with advancing age, with an increase of approximately 10% per decade of life, probably because of the aging of venous valves^[14].

An association between varicocele and varicose veins of the lower extremities and an inverse relationship between the prevalence of varicocele and body mass index have been suggested^[4-16]. Hereditary factors may also play a role in the prevalence of varicocele^[14,17].

ETIOLOGY AND PATHOGENESIS

The exact etiology of varicocele is still unknown, but it is probably multifactorial^[4,5,12,13,18]. The cause for the high incidence of left varicocele is that the left internal spermatic vein runs vertically to drain into the ipsilateral renal vein at a right angle, when the man is in the standing position, and thus, the endoluminal pressure in the renal vein is transmitted backward, opposing flow from the internal spermatic vein. On the right side, the internal spermatic vein runs tangentially to join the inferior vena cava, resulting in less flow turbulence and back pressure in the vein and therefore in a lower incidence of venous dilation on the right side. However, Gat *et al*^[19] reported that varicocele is mainly a bilateral disease, expressed earlier on the left side, with a right-sided venous return problem presenting in 86% of infertile men with clinically significant varicocele.

Several other theories related to the etiological factors of varicocele have been proposed, including the following: Incompetence or absence of venous valves in the spermatic veins, obstructed venous drainage, vascular contractions of the left testicular vein caused by catecholamines from the left adrenal gland and the so-called nutcracker phenomenon^[4,5,12,13,18,20,21].

CLINICAL FINDINGS-CLASSIFICATION

Clinically, varicocele is characterized by an abnormal enlargement of the spermatic veins of the venous plexus, which drains the blood from the testes, associated with an anomalous intermittent or continuous backflow of blood into the plexus. In adult males, most cases are

asymptomatic, often revealed during an investigation related to infertility and/or because of an unfavorable outcome of semen analysis^[5]. Rarely, it may present with scrotal pain or create esthetic problems or discomfort due to the presence of significant enlargement of the scrotum^[5,12].

Clinical varicocele was found to be a significant risk factor for decreased sperm count, motility and morphology in adult infertile men^[22,23]. A study conducted by the World Health Organization (WHO) reported that both sperm concentration and motility were lower in men with varicocele compared to individuals without varicocele^[22]. Recently, Agarwal *et al.*^[23] in a systematic review assessing the effects of varicocele on semen parameters based on the new 2010 WHO laboratory criteria for the examination of the human semen, reported that varicocele was associated with reduced sperm count, motility and morphology^[23].

Physical examination represents the gold standard for the diagnosis of clinically significant varicoceles^[5,8,12,24]. It is used by clinical urologists and pediatricians, consisting of palpation performed with the patient in the standing position and observation of the scrotum during the Valsalva maneuver. The classification system published by Dubin and Amelar in 1970 is the most commonly used and includes the following three degrees of varicocele: Grade 1, varicocele detectable by palpation only during the Valsalva maneuver; Grade 2, varicocele detectable by simple palpation; and, Grade 3, varicocele visible on inspection and palpation^[24]. However, this system has limitations because its diagnostic accuracy is closely associated with physician's experience. A study involving experienced andrologists and clinicians identified a significant inter-observer and intra-observer variability in the grading of varicoceles based on the above classification^[12].

Histology from a testicular biopsy in men with varicocele has shown depressed spermatogenesis with maturation arrest, sloughing of the spermatogenic epithelium, profusion of Leydig cells, thickening of the tubular basement membrane and interstitial blood vessel wall with luminal narrowing, and increased deposition of interstitial fibrous tissue^[25].

PATHOPHYSIOLOGY

The pathophysiology of impaired spermatogenesis in varicocele is multifactorial. A combination of several factors affects spermatogenesis and sperm function, and the relative involvement of these factors is different in each patient^[4,7,8,25]. Several pathophysiologic mechanisms resulting in impairment of spermatogenesis in left varicocele have been proposed, including heat stress, notch signaling, cadmium accumulation, insufficiency of the hypothalamo-pituitary-gonadal axis, retrograde flow of adrenal or renal metabolites, possible disruptions of blood-testis barrier, testicular hypoxia and alterations in testicular extracellular fluid dynamics^[4,7,8,25]. Interstitial

lesions, including the proliferation of Leydig cells, thickening of the tubular basement membrane and blood vessel wall with luminal narrowing, and increased deposition of interstitial collagen fibers may also play an important role in varicocele-related testicular dysfunction^[25].

Current evidence suggests the primary role of reactive oxygen species (ROS) and the resultant oxidative stress (OS) in the pathogenesis of varicocele-associated male infertility^[4,7,8,18,25,26]. Excessive ROS has also been associated with sperm DNA fragmentation (SDF), which may mediate the clinical manifestation of poor sperm function and infertility related to varicocele^[4,7,8,18,25-27]. A significantly less total acrosin activity in the spermatozoa of infertile men with varicocele and an abnormal retention of cytoplasmic droplets by human spermatozoa, which is negatively correlated with sperm motility, are other potential contributing factors for the diminished sperm function in individuals with varicocele^[4,28].

Using animal models, bilateral detrimental effects on testicular temperature, blood flow, and histology have been reported to occur in cases of unilateral varicocele, probably related either to the dilatation of the right testicular vein in individuals with left varicocele or the role of the sympathetic nervous system^[4,29,30]. The development of a unilateral varicocele affecting bilateral Leydig cell secretory function results in a significant reduction in bilateral intratesticular testosterone content, which, in turn, affects the Sertoli cell secretory function and epididymal maturation process, all contributing to the reduced male reproductive potential^[4]. Recent advances in biomolecular techniques and mass spectrometry equipment have allowed us to better understand the molecular pathways associated with varicocele and male infertility^[25,31,32].

DIAGNOSIS

In the past, various diagnostic imaging modalities were used for the evaluation of varicoceles, including venography, scintigraphy, and thermography^[33-35]. Labeled blood-pool scintigraphy was reported as an accurate and noninvasive method for the detection and grading of varicocele. The main contribution of radionuclide blood-pool imaging of the scrotum was in the detection and grading of subclinical varicocele in infertile men with no other cause of infertility. The technique was also accurate in the diagnosis of recurrent varicocele^[33-35]. However, the above methods have been replaced by less invasive and more easily performed diagnostic tools, especially ultrasonographic examination of the scrotum.

Ultrasonography (US) is currently the most established and widely used modality for the study of varicoceles, with 97% sensitivity and 94% specificity in the diagnosis of clinical varicocele and 83%-95% sensitivity in the diagnosis of subclinical varicocele^[5,12,13,33,36,37]. The classic US features of a varicocele is that of "multiple,

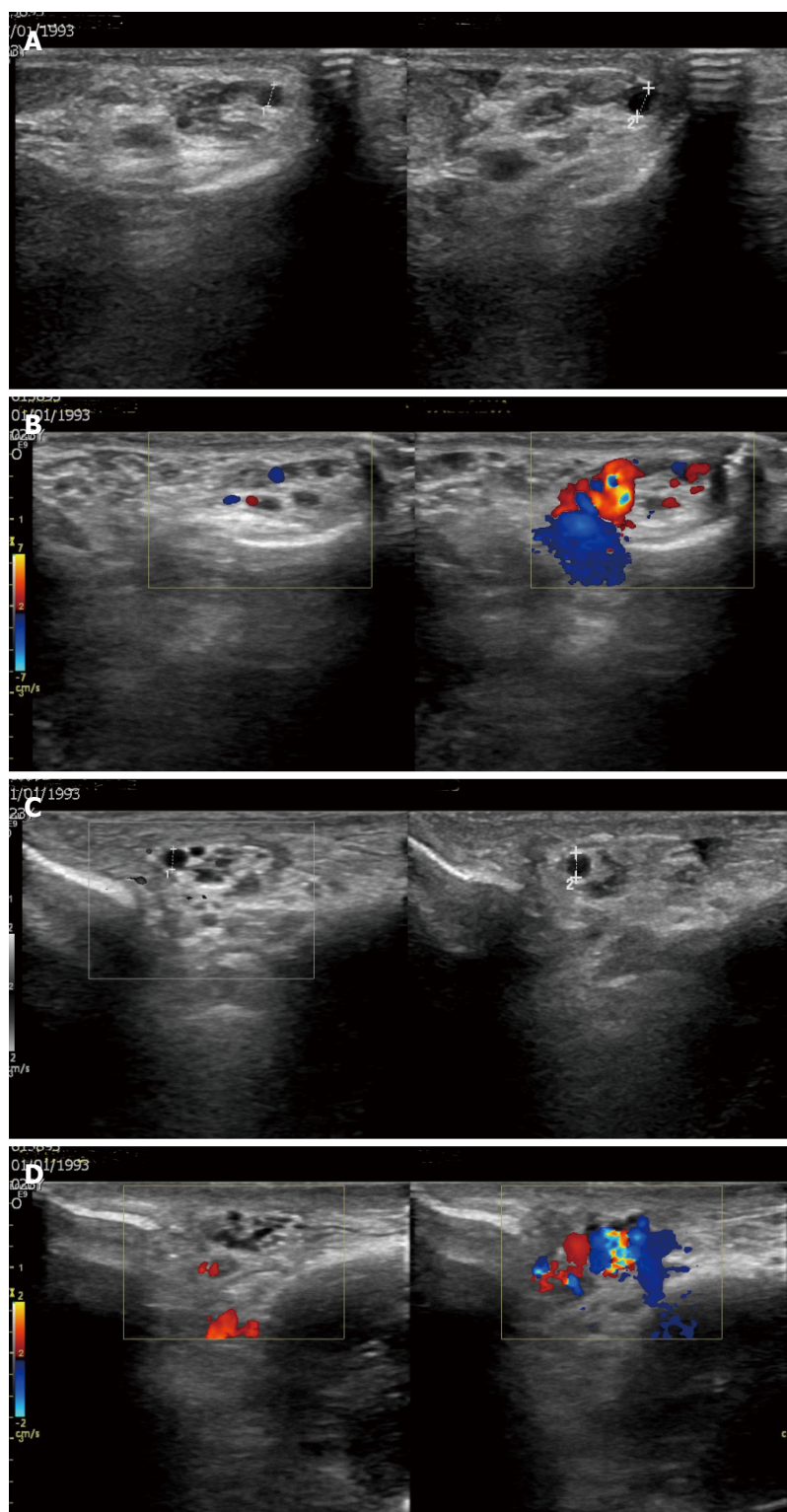


Figure 1 A 24-year-old man with bilateral varicocele. A: Gray-scale sonographic images, longitudinal sections at the suprastesticular region of the left hemiscrotum at rest and during the Valsalva maneuver. The maximal diameter of the left spermatic veins is 2.5 mm at rest and 3.5 mm during the Valsalva maneuver; B: Color Doppler sonographic images, longitudinal sections same level show blood flow reversal after Valsalva maneuver; C: Gray-scale sonographic images, longitudinal sections at the right suprastesticular region. The maximal diameter of the right spermatic veins is 2.3 mm at rest and 2.8 mm during the Valsalva maneuver; D: Color Doppler sonographic images, longitudinal sections show flow reversal with Valsalva maneuver.

anechoic, serpiginous, tubular structures” near the superior and lateral aspects of the testis. Color, power, or spectral Doppler US with settings optimized for low flow velocities is used complimentary to aid in the diagnosis

of varicoceles. Typical Doppler findings include venous flow at rest, with intermittent or continuous flow reversal with Valsalva maneuver (Figures 1 and 2)^[5,33].

However, there are no homogeneous US criteria

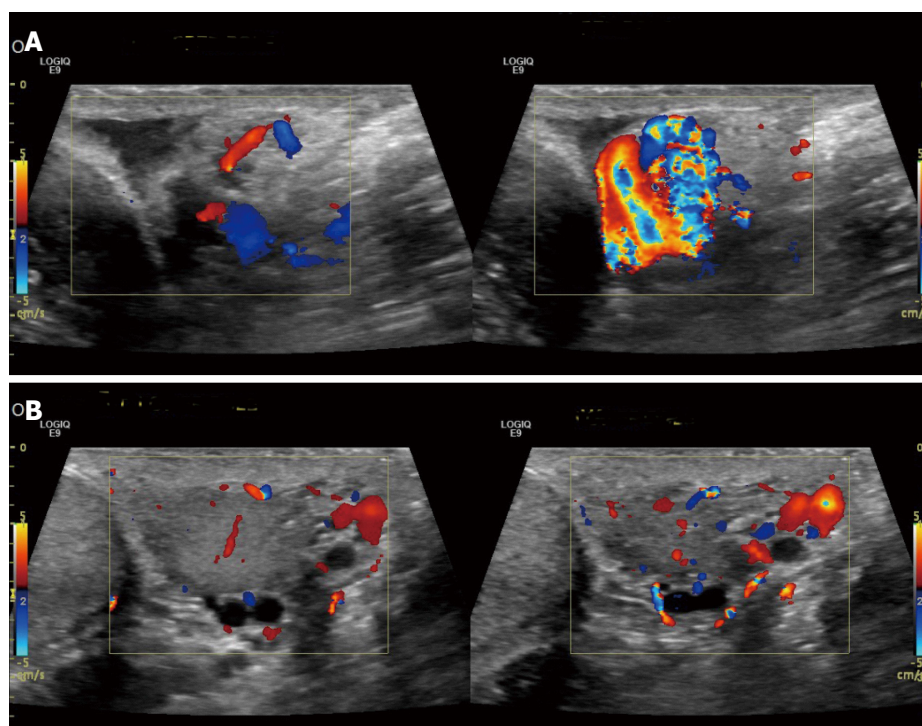


Figure 2 A 36-year-old man with left varicocele. Color Doppler sonographic images, longitudinal sections at the level of the upper (A) and lower pole (B) of the left testis depict flow reversal seen during the Valsalva maneuver.

Table 1 Sarteschi classification

Grade	Characteristics
1	Venous reflux at the emergence of the scrotal vein only during the Valsalva maneuver; hypertrophy of the venous wall without stasis
2	Supratesticular reflux only during the Valsalva maneuver; venous stasis without varicosities
3	Peritesticular reflux during the Valsalva maneuver; overt varicocele with early stage varices of the cremasteric vein
4	Spontaneous basal reflux that increases during the Valsalva maneuver; possible testicular hypotrophy, overt varicocele, varicosities in the pampiniform plexus
5	Spontaneous basal reflux that does not increase during the Valsalva maneuver; testicular hypotrophy, overt varicocele, varicosities in the pampiniform plexus

regarding the extent of venous dilation or reflux that must be present to meet the definition of a varicocele^[5,12,13,36-45]. A widely accepted US criterion for the diagnosis of varicocele is the existence of veins larger than 2 mm in diameter, with 95% sensitivity^[38]. In general, clinicians agree that clinically relevant varicoceles are more than 2.5-3 mm in diameter^[33]. Multiple grading systems exist for classifying the US findings of varicocele; however, all have a low predictive value in terms of impairment of spermatogenesis, which is the main indication for any therapeutic plan^[5,12,13,31,46,47]. The Sarteschi (Table 1) and Chiou *et al.*^[47] (Table 2) classifications systems are among the most commonly used.

Advances in US and magnetic resonance imaging (MRI) provide the potential to expand the role of imaging beyond that of visual confirmation and characterization of varicoceles. The ability to identify the early signs of testicular dysfunction based on imaging findings may have implications for the selection of patients for varicocele repair.

US IN THE EVALUATION OF INTRATESTICULAR MICROCIRCULATION IN TESTES WITH VARICOCELE

The testis gets its arterial supply mainly from the testicular artery (TA) supplemented with the cremasteric artery and the deferential artery, all coursing through the deep inguinal canal to enter the spermatic cord^[48-51]. TA penetrates the tunica albuginea along the posterior surface of the testis and divides into capsular arteries. These capsular branches then give rise to the centripetal arteries which carry blood from the capsular surface, centrally towards the mediastinum along the testicular septa. Branches of the centripetal arteries then course backward towards the capsular surface, known as recurrent rami. In approximately 50% of testes, the transtesticular artery can also be seen passing directly from the testicular artery at the mediastinum into the parenchyma^[48-51]. Testicular perfusion can be evaluated with color Doppler (CD), power Doppler, and spectral

Table 2 Chiou *et al.*^[47] classification (total score of ≥ 4 defined as varicocele)

Characteristics	Grade
Maximum vein diameter (mm)	
< 2.5	0
2.5-2.9	1
3-3.9	2
≥ 4	3
Plexus/sum of diameter of veins	
No plexus identified	0
Plexus (+) with sum diameter < 3 mm	1
Plexus (+) with sum diameter 3-5.9 mm	2
Plexus (+) with sum diameter ≥ 6 mm	3
Change of flow velocity on Valsalva maneuver	
< 2 cm/s or duration < 1 s	0
2-4.9	1
5-9.9	2
≥ 10	3
Total score	0-9

Doppler US. The spectral waveform of the intratesticular arteries characteristically has a low-resistance pattern, with a mean resistive index (RI) in adults and postpubertal boys of 0.62 (range, 0.48-0.75)^[48].

Several clinical studies have assessed the effects of varicocele on testicular blood flow by US^[49,50-56]. In an early study, Ross *et al.*^[52] compared the testicular blood flow in 248 patients with varicocele and 34 fertile volunteers with color Doppler ultrasonography (CDUS) and reported no significant differences^[52]. A similar result was reported by Grasso Leanza *et al.*^[53]. In this study, the peak systolic velocity (PSV) of the testicular arteries was evaluated in men with varicocele and healthy subjects with normal or impaired spermatogenesis using CDUS. No significant difference was found in relation to the presence or degree of varicocele^[53].

However, in subsequent studies, CDUS proved to be sensitive in assessing alterations in intratesticular circulation in testes with clinical varicocele^[37,49,54-56]. A significant decrease in testicular arterial blood flow and an increase in RI and PSV in testes with clinical varicocele were reported^[37,49,54-56]. Semiz *et al.*^[37] concluded that spectral Doppler parameters might be used as a noninvasive method to assess the hemodynamic changes and testicular microcirculation in cases of clinical varicocele^[37]. The PSV, end-diastolic velocity (EDV), RI and pulsatility index (PI) from capsular and intratesticular arteries in 50 men with clinical varicocele were measured and correlated with semen analysis parameters, including count, motility, volume and morphology. PSV significantly correlated with sperm count in men with unilateral and bilateral varicocele. No significant correlation between EDV, RI, PI and semen analysis results was found^[37]. Unsal *et al.*^[54] evaluated the effects of clinical varicocele on testicular microcirculation comparing PSV, EDV, RI and PI from capsular and intratesticular arteries in 15 men with left clinical varicocele and 34 controls^[54]. The authors found

a significantly greater RI and PI of capsular branches of the left testes (RI = 0.68 ± 0.04 ; PI = 1.22 ± 0.15) compared to the control group (RI = 0.64 ± 0.06 ; PI = 1.07 ± 0.18)^[54].

Biagiotti *et al.*^[55] reported that spectral Doppler traces from the TA can be used to differentiate the various causes of impaired spermatogenesis^[55]. The RI and PSV proved the most reliable indicators for routine clinical use to identify infertile men in this study, whereas EDV, FSH and TV were not. Specifically, men with varicoceles or, varicoceles and male accessory glands inflammation or fertile men with varicoceles had the highest PSV and RI^[55].

In cases of subclinical varicocele, no significant changes in intratesticular perfusion are probably seen on CDUS^[50]. Akcar *et al.*^[50] assessed the testicular volume (TV) and the RI from centripetal intratesticular arteries in 27 men with left varicocele, 96% of which were subclinical. The authors found that subclinical varicocele is not associated with testicular atrophy and does not affect the intratesticular arterial resistance^[50].

Testicular contrast harmonic imaging has been proposed as an adjuvant diagnostic tool in the assessment of the effects of varicocele on intratesticular microcirculation^[57]. Caretta *et al.*^[57] in a study of 90 patients with left varicocele, associated with either normozoospermia or oligospermia calculated contrast material arrival time in the arteriolar circulation (wash-in), time to peak arterial circulation, arrival time in the venular circulation (washout) and mean transit time in each testis after intravenous administration of contrast agent containing phospholipid stabilized microbubbles filled with sulfur hexafluoride. All parameters were significantly higher in patients with varicocele plus normozoospermia or oligospermia compared to controls, although they did not correlate with varicocele grading. A negative linear correlation between total sperm count and left mean transit time was found in patients with varicocele. In the multivariate analysis, left mean transit time was the only independent predicting parameter of oligospermia in this study^[57].

Tissue elastography (TE) is a relatively new imaging technique that measures the stiffness of tissue^[58-60]. TE has been reported as a useful diagnostic tool, further enhancing the characterization of focal testicular lesions^[58-60]. Acoustic radiation force impulse (ARFI) elastography represents one of the main types of elastography currently in use, involving the estimation of shear wave speed. In a prospective controlled study of 30 men with clinical varicocele and 30 controls, Dede *et al.*^[61] concluded that ARFI elastography may be used to assess the early damage of testicular structure by varicocele^[61]. Mean elastography results were significantly different between the two groups and significantly lower in testes with varicoceles. Significant negative correlations between FSH and testis elasticity was also reported. Additionally, a negative correlation was determined between varicocele grade and elasticity

of testes^[61].

ROLE OF MRI

Although US represents the primary imaging modality in the assessment of scrotal diseases, MRI has recently emerged as an important supplemental diagnostic tool, used both as a problem-solving technique in patients with inconclusive US findings and as a primary imaging modality^[62-64]. Recently, functional MRI techniques, including diffusion-weighted imaging (DWI), dynamic contrast-enhanced (DCE) MRI and MR spectroscopy have added important diagnostic information to the interpretation of testicular diseases^[65-75].

DWI, with the calculation of apparent diffusion coefficient (ADC), is an evolving technique that can be used to improve tissue characterization if interpreted in combination with the findings of conventional MR sequences. DWI applications in scrotal pathology include characterization of intratesticular lesions, diagnosis of testicular torsion and detection and localization of nonpalpable undescended testes^[65-67]. Karakas *et al.*^[72] in a preliminary study of 25 men with varicocele and 25 healthy volunteers recommended the potential role of DWI for the early detection and the determination of the degree of testicular damage due to varicocele^[72]. The authors found lower ADC both in the ipsilateral and contralateral testicular parenchyma of patients with varicocele, compared to that of healthy volunteers. A significant negative correlation between the mean ADC and venous diameter was also found^[72]. Decreased ADC of the ipsilateral testis in patients with varicocele might be associated with hypoxia and fibrosis. Decreased ADC of the contralateral testis might be related to hormonal and autoimmune factors and heat stress^[72].

DCE-MRI evaluates the kinetics of the distribution of the paramagnetic contrast medium in the microvessels and the interstitial spaces of the tissues used. The technique has been useful in the characterization of scrotal lesions and the discrimination of various causes of acute scrotal pain^[68,69,73-75]. Normal testes enhance slowly, moderately and homogeneously with a linear increase in signal intensity during the entire dynamic period (type I curve)^[68,69]. This pattern of enhancement is probably related to an intact "blood-testis" barrier. Minor disruptions of the blood-testis barrier could be associated with alterations of testicular perfusion in testes with varicocele and could be detected using DCE-MRI^[73].

Although MRI is not routinely used in the assessment of testes with varicocele, large prospective studies evaluating functional MRI data might validate the possible role of this technique in the investigation of harmful effects on spermatogenesis.

TREATMENT

There are numerous surgical and non-surgical techniques for treating clinically significant varicocele, although

there is no consensus on which might be considered the treatment of choice^[4,5,7,8,11,25,76-78]. Microsurgical varicocelectomy is the most recommended type of therapy and is associated with fewer complications and lower recurrence rates, compared to the other techniques^[4,11].

Varicocele embolization represents a technically feasible, minimally invasive and outpatient treatment option for men with varicocele, with high success rates. A major advantage of embolization over surgery is the ability to simultaneously perform intra-operative venography^[79-83]. Postoperative recurrence of varicocele has been mainly attributed to the persistence of collaterals or anomalous veins missed during surgical ligation^[84-86]. Better anatomic delineation on pre-embolization venography enables the identification of these veins, therefore reducing the possibility of future recurrences^[79-86]. Embolization may be suggested for patients with recurrence, although no strong evidence to recommend the ideal treatment for recurrent varicocele exists^[79-86].

The diagnosis and treatment of varicoceles are embraced by the American Society for Reproductive Medicine (ASRM), American Urological Association (AUA) and European Urological Association, and the recommendations are presented in Table 3^[8,76-78]. If varicocele repair is decided, it is advisable to include both sides, if a clinically palpable varicocele is present bilaterally. For now, the available data indicate no benefit for subclinical varicocele treatment^[11].

Another controversial topic in urology is the effects of varicocele treatment on male infertility^[11]. Several studies indicated that varicocele repair improves semen parameters, including sperm density, count, concentration, motility and morphology and the percentage of progressively motile sperm in most treated men with clinical varicocele and abnormal semen parameters^[4,5,9]. In addition to the improvement in semen parameters, varicocele repair may allow a couple with severely impaired semen parameters to have less invasive treatment. Men with severe oligospermia who would otherwise require *in vitro* fertilization/intra cytoplasmic sperm injection (IVF-ICSI) to conceive may have adequate improvement in semen analysis to allow intrauterine insemination instead of IVF-ICSI, and those with oligospermia may have sufficient improvement in semen parameters to allow natural conception in some cases. Surgical varicocele repair also proved useful in alleviating OS-associated infertility and improving sperm nuclear DNA integrity. Temporal changes in the testicular histology after varicocelectomy, including maturation of the germ cells, with the absence of meiotic abnormalities and normalization of the number of Leydig cells, have been reported^[8].

The debate about the role of varicocele repair in male infertility mainly lies on its actual positive effect on improving natural fertility. Several studies attempting to investigate this issue have yielded equivocal results. However, most of the existing data agree that varicocele repair increases natural pregnancy rates and mitigates

Table 3 Summary of recommendations for the diagnosis and treatment of varicoceles

	ASRM/SMRU	AUA	EAU
Guideline title	Report on varicocele and infertility: A committee opinion	The optimal evaluation of the infertile male: AUA best practice statement	Guidelines on male infertility
Infertile male evaluation	Medical and reproductive history, physical examination and at least two semen analyses	Complete medical history, physical examination by a urologist or other specialist in male reproduction and at least two semen analyses	Medical history and physical examination, including semen analysis: One semen analysis is sufficient if normal, two will be performed if the first one is abnormal based on WHO 2010 criteria
Optimal method to detect varicocele	Physical examination; varicoceles graded, 1 to 3	Physical examination; varicoceles graded, 1 to 3	Physical examination; varicoceles graded, 1 to 3
Role of scrotal US	For inconclusive physical examination	Indicated in those patients in whom physical examination is difficult or inadequate or a testicular mass is suspected	Used to confirm presence of varicocele identified on physical examination
Indications for treatment of varicocele	If the male partner of a couple attempting to conceive has a varicocele, treatment should be considered if most or all the following are met: clinically palpable varicocele; abnormal semen parameters; known infertility; female partner has normal fertility or a potentially treatable cause of infertility; time to conception is not a concern. An adult male who is not currently attempting to achieve conception but has a palpable varicocele, abnormal semen analyses and a desire for future fertility, and/or pain related to the varicocele is also a candidate for varicocele repair	Not stated	Varicocele repair may be effective in men with abnormal semen analysis, a clinical varicocele and otherwise unexplained infertility of duration > 2 yr
Contraindications to treatment	Patients with either normal semen analysis, isolated teratozoospermia, or a subclinical varicocele; and, if IVF or IVF-ICSI is otherwise required for the treatment of a female factor infertility	Not stated	
Method of treatment	There are two types of varicocele management, surgical repair and percutaneous embolization. Multiple types exist within each category. None of these has been proven superior to the others in its ability to improve fertility, although there are differences in recurrence rates with microsurgical subinguinal varicocelectomy having the lowest recurrence rates	Not stated	Reviews all types of treatment within guidelines and provides complication and recurrence rates of each, without specific recommendations

ASRM: American Society of Reproductive Medicine; SMRU: Society of Male Reproduction and Urology; AUA: American Urological Association; EAU: European Association of Urology; WHO: World Health Organization; IVF: *In vitro* fertilization; ICSI: Intracytoplasmic sperm injection.

the need for multiple assisted reproductive technology cycles^[87-89]. Recently, there is increased evidence that clinically significant varicocele may influence testosterone production, and some researchers advocate varicocele repair in cases of decreased testosterone levels, including patients with non-obstructive azoospermia^[90-92].

US ASSESSMENT OF TESTICULAR BLOOD FLOW AFTER VARICOCELE REPAIR

Several groups have assessed the effects of varicocelectomy on testicular arterial blood flow by CDUS^[51,93-98]. Sun *et al*^[93] used CDUS to assess the changes in testicular perfusion following laparoscopic varicocele clipping in 14 children and reported no significant change^[93]. However, the authors evaluated only the

magnitude of arterial perfusion, not using any arterial flow parameters^[93]. Student *et al*^[94] reported no major changes in RI after laparoscopic varicocelectomy in comparing cases with spermatic artery ligation to those with spermatic artery preservation^[94]. Tanriverdi *et al*^[96] compared microsurgery and high ligation varicocelectomy by evaluating intratesticular arterial flow 7 d after surgery and reported no significant difference between the preoperative and postoperative RI in both groups^[96]. A similar study comparing two laparoscopic surgical methods of varicocelectomy at 3 mo follow-up demonstrated that mean RI in the group of patients with spermatic artery ligation was comparable to the group of spermatic artery preservation.

However, subsequent studies reported a correlation between CDUS parameters and the effects of varicocele repair^[51,97,98]. Balci *et al*^[97] assessed the long-term effects of varicocele repair on intratesticular arterial RI in 26 infertile men with left varicocele, undergoing

subinguinal varicocelectomy. CDUS was performed before and 6 mo after the operation, and spectral Doppler indexes were measured in the intratesticular arteries and correlated with semen analysis results. RI, PI and EDV decreased significantly after surgery, but no significant change was observed in PSV. Surgery resulted in a significant increase in total sperm count, motility, morphology, and total motile sperm count, although no significant correlation was found between sperm parameters and RI^[97]. CDUS was performed by Tarhan *et al.*^[98] in 30 men with left clinical varicocele who underwent a microsurgical inguinal varicocelectomy before, 3 and 6 mo after surgery^[98]. Spectral Doppler parameters, including PSV, EDV, RI and PI, were measured from testicular, capsular, and intratesticular arteries and were correlated with preoperative and postoperative semen analysis results. A significant improvement in both testicular blood supply and sperm parameters was found. Specifically, PSV and EDV in the left TA increased, whereas RI and PI in the left capsular and intratesticular arteries decreased significantly after surgery, both reflecting an increase in testicular arterial blood flow. Regarding semen analysis, significant increases in sperm concentration, morphology percentage, and total motile sperm concentration were seen 3 mo after surgery^[98]. Recently, Zhang *et al.*^[51] evaluated the effects of laparoscopic varicocelectomy (LV) and microsurgical subinguinal varicocelectomy (MV) on testicular microcirculation using CDUS and concluded that the RI and the PI of ipsilateral capsular artery (CA) and intratesticular artery (ITA) probably represent important indexes for the prognosis after varicocelectomy^[51]. Specifically, the authors found a significant decrease in the mean values of PSV, PI and RI of CA and ITA after LV and MV, but no significant change in EDV. In comparing the two groups, the RI and PI of left CA and ITA in the third month and of ITA in the sixth month postoperatively in the MV group were significantly lower than those in the LV group. Both types of surgery resulted in a significant increase in the sperm density, morphology and total motile sperm count. Moreover, the PI and RI of ipsilateral CA and ITA seemed negatively correlated with sperm quality^[51].

CONCLUSION

Varicocele is a common medical condition entangled with many controversies. Determining which patients are negatively affected by varicocele would help clinicians better select those men who will benefit the most from therapy. Functional imaging techniques, including US and MRI, might provide early indications of testicular dysfunction in testes with varicocele. Large prospective studies are needed to validate the potential role of non-invasive imaging, including US and MRI, in the assessment of the functional status of the testis in men with varicocele, thereby helping to differentiate causal from incidental varicocele.

REFERENCES

- 1 **Simpson WL**, Rausch DR. Imaging of male infertility: pictorial review. *AJR Am J Roentgenol* 2009; **192**: S98-107 (Quiz S108-11) [PMID: 19458104 DOI: 10.2214/AJR.07.7109]
- 2 **Ammar T**, Sidhu PS, Wilkins CJ. Male infertility: the role of imaging in diagnosis and management. *Br J Radiol* 2012; **85** Spec No 1: S59-S68 [PMID: 22763036 DOI: 10.1259/bjr/31818161]
- 3 **Donkol RH**. Imaging in male-factor obstructive infertility. *World J Radiol* 2010; **2**: 172-179 [PMID: 21161032 DOI: 10.4329/wjr.v2.i5.172]
- 4 **Sofikitis N**, Stavrou S, Skouros S, Dimitriadis F, Tsounapi P, Takenaka A. Mysteries facts and fiction in varicocele pathophysiology and treatment. *European Urology Supplements* 2014; **13**: 89-99 [DOI: 10.1016/j.eursup.2014.07.002]
- 5 **Valentino M**, Bertolotto M, Derchi L, Pavlica P. Children and adults varicocele: diagnostic issues and therapeutical strategies. *J Ultrasound* 2014; **17**: 185-193 [PMID: 25177391 DOI: 10.1007/s40477-014-0088-3]
- 6 **Chiba K**, Ramasamy R, Lamb DJ, Lipshultz LI. The varicocele: diagnostic dilemmas, therapeutic challenges and future perspectives. *Asian J Androl* 2016; **18**: 276-281 [PMID: 26698233 DOI: 10.4103/1008-682X.167724]
- 7 **Esteves SC**, Agarwal A. Afterword to varicocele and male infertility: current concepts and future perspectives. *Asian J Androl* 2016; **18**: 319-322 [PMID: 26780876 DOI: 10.4103/1008-682X.172820]
- 8 **Shridharani A**, Owen RC, Elkelany OO, Kim ED. The significance of clinical practice guidelines on adult varicocele detection and management. *Asian J Androl* 2016; **18**: 269-275 [PMID: 26806081 DOI: 10.4103/1008-682X.172641]
- 9 **Tiseo BC**, Esteves SC, Cocuzza MS. Summary evidence on the effects of varicocele treatment to improve natural fertility in subfertile men. *Asian J Androl* 2016; **18**: 239-245 [PMID: 26806080 DOI: 10.4103/1008-682X.172639]
- 10 **Will MA**, Swain J, Fode M, Sonksen J, Christman GM, Ohl D. The great debate: varicocele treatment and impact on fertility. *Fertil Steril* 2011; **95**: 841-852 [PMID: 21272869 DOI: 10.1016/j.fertnstert.2011.01.002]
- 11 **Baazeem A**, Belzile E, Ciampi A, Dohle G, Jarvi K, Salonia A, Weidner W, Zini A. Varicocele and male factor infertility treatment: a new meta-analysis and review of the role of varicocele repair. *Eur Urol* 2011; **60**: 796-808 [PMID: 21733620 DOI: 10.1016/j.eururo.2011.06.018]
- 12 **Iosa G**, Lazzarini D. Hemodynamic classification of varicoceles in men: our experience. *J Ultrasound* 2013; **16**: 57-63 [PMID: 24294344 DOI: 10.1007/s40477-013-0016-y]
- 13 **Pauroso S**, Di Leo N, Fulle I, Di Segni M, Alessi S, Maggini E. Varicocele: Ultrasonographic assessment in daily clinical practice. *J Ultrasound* 2011; **14**: 199-204 [PMID: 23396816 DOI: 10.1016/j.jus.2011.08.001]
- 14 **Alsaikhan B**, Alrabeeah K, Delouya G, Zini A. Epidemiology of varicocele. *Asian J Androl* 2016; **18**: 179-181 [PMID: 26763551 DOI: 10.4103/1008-682X.172640]
- 15 **Gulleroglu K**, Gulleroglu B, Baskin E. Nutcracker syndrome. *World J Nephrol* 2014; **3**: 277-281 [PMID: 25374822 DOI: 10.5527/wjn.v3.i4.277]
- 16 **Nielsen ME**, Zderic S, Freedland SJ, Jarow JP. Insight on pathogenesis of varicoceles: relationship of varicocele and body mass index. *Urology* 2006; **68**: 392-396 [PMID: 16904459 DOI: 10.1016/j.urology.2006.02.005]
- 17 **Gökçe A**, Davarci M, Yalçinkaya FR, Güven EO, Kaya YS, Helvacı MR, Balbay MD. Hereditary behavior of varicocele. *J Androl* 2010; **31**: 288-290 [PMID: 19834129 DOI: 10.2164/jandrol.109.008698]
- 18 **Cho CL**, Esteves SC, Agarwal A. Novel insights into the pathophysiology of varicocele and its association with reactive oxygen species and sperm DNA fragmentation. *Asian J Androl* 2016; **18**: 186-193 [PMID: 26732105 DOI: 10.4103/1008-682X.170441]

- 19 **Gat Y**, Bachar GN, Everaert K, Levinger U, Gornish M. Induction of spermatogenesis in azoospermic men after internal spermatic vein embolization for the treatment of varicocele. *Hum Reprod* 2005; **20**: 1013-1017 [PMID: 15618245 DOI: 10.1093/humrep/deh706]
- 20 **Sofikitis N**, Dritsas K, Miyagawa I, Koutselinis A. Anatomical characteristics of the left testicular venous system in man. *Arch Androl* 1993; **30**: 79-85 [PMID: 8470944 DOI: 10.3109/01485019308987738]
- 21 **Sofikitis N**, Miyagawa I. Experimental models for the study of varicocele: a selected review. *Jpn J Fertil Steril* 1993; **38**: 168-177
- 22 The influence of varicocele on parameters of fertility in a large group of men presenting to infertility clinics. World Health Organization. *Fertil Steril* 1992; **57**: 1289-1293 [PMID: 1601152 DOI: 10.1016/S0015-0282(16)55089-4]
- 23 **Agarwal A**, Sharma R, Harlev A, Esteves SC. Effect of varicocele on semen characteristics according to the new 2010 World Health Organization criteria: a systematic review and meta-analysis. *Asian J Androl* 2016; **18**: 163-170 [PMID: 26780872 DOI: 10.4103/1008-682X.172638]
- 24 **Dubin L**, Amelar RD. Varicocele size and results of varicocelectomy in selected subfertile men with varicocele. *Fertil Steril* 1970; **21**: 606-609 [PMID: 5433164]
- 25 **Shiraishi K**, Matsuyama H, Takiyama H. Pathophysiology of varicocele in male infertility in the era of assisted reproductive technology. *Int J Urol* 2012; **19**: 538-550 [PMID: 22417329 DOI: 10.1111/j.1442-2042.2012.02982.x]
- 26 **Agarwal A**, Prabakaran S, Allamaneni SS. Relationship between oxidative stress, varicocele and infertility: a meta-analysis. *Reprod Biomed Online* 2006; **12**: 630-633 [PMID: 16790111 DOI: 10.1016/S1472-6483(10)61190-X]
- 27 **Wang YJ**, Zhang RQ, Lin YJ, Zhang RG, Zhang WL. Relationship between varicocele and sperm DNA damage and the effect of varicocele repair: a meta-analysis. *Reprod Biomed Online* 2012; **25**: 307-314 [PMID: 22809864 DOI: 10.1016/j.rbmo.2012.05.002]
- 28 **Sofikitis N**, Miyagawa I, Zavos PM, Inaga S, Iino A, Toda T, Harada T, Mio Y, Terakawa N. Acrosin profiles of human spermatozoa recovered from the new Sperm Prep II filtration column. *Tohoku J Exp Med* 1992; **166**: 451-457 [PMID: 1502691 DOI: 10.1620/tjem.166.451]
- 29 **Sofikitis N**, Takahashi C, Nakamura I, Hirakawa S, Miyagawa I. Surgical repair of secondary right varicocele in rats with primary left varicocele: effects on fertility, testicular temperature, spermatogenesis, and sperm maturation. *Arch Androl* 1992; **28**: 43-52 [PMID: 1550427 DOI: 10.3109/01485019208987679]
- 30 **Oztürk H**, Tander B, Aydın A, Okumus Z, Cetinkursun S. The effects of chemical sympathectomy on testicular injury in varicocele. *BJU Int* 2001; **87**: 232-234 [PMID: 11167648 DOI: 10.1046/j.1464-410x.2001.01987.x]
- 31 **Camargo M**, Intasqui P, Bertolla RP. Proteomic profile of seminal plasma in adolescents and adults with treated and untreated varicocele. *Asian J Androl* 2016; **18**: 194-201 [PMID: 26643563 DOI: 10.4103/1008-682X.168788]
- 32 **Agarwal A**, Sharma R, Samanta L, Durairajanayagam D, Sabanegh E. Proteomic signatures of infertile men with clinical varicocele and their validation studies reveal mitochondrial dysfunction leading to infertility. *Asian J Androl* 2016; **18**: 282-291 [PMID: 26732106 DOI: 10.4103/1008-682X.170445]
- 33 **Belay RE**, Huang GO, Shen JK, Ko EY. Diagnosis of clinical and subclinical varicocele: how has it evolved? *Asian J Androl* 2016; **18**: 182-185 [PMID: 26780869 DOI: 10.4103/1008-682X.169991]
- 34 **Freund J**, Handelsman DJ, Bautovich GJ, Conway AJ, Morris JG. Detection of varicocele by radionuclide blood-pool scanning. *Radiology* 1980; **137**: 227-230 [PMID: 7422850 DOI: 10.1148/radiology.137.1.7422850]
- 35 **Paz A**, Melloul M. Comparison of radionuclide scrotal blood-pool index versus gonadal venography in the diagnosis of varicocele. *J Nucl Med* 1998; **39**: 1069-1074 [PMID: 9627346 DOI: 10.1097/00005392-199901000-00129]
- 36 **Kim YS**, Kim SK, Cho IC, Min SK. Efficacy of scrotal Doppler ultrasonography with the Valsalva maneuver, standing position, and resting-Valsalva ratio for varicocele diagnosis. *Korean J Urol* 2015; **56**: 144-149 [PMID: 25685302 DOI: 10.4111/kju.2015.56.2.144]
- 37 **Semiz I**, Tokgöz O, Tokgoz H, Voyvoda N, Serifoglu I, Erdem Z. The investigation of correlation between semen analysis parameters and intraparenchymal testicular spectral Doppler indices in patients with clinical varicocele. *Ultrasound Q* 2014; **30**: 33-40 [PMID: 24901777 DOI: 10.1097/RUQ.0000000000000055]
- 38 **Gonda RL**, Karo JJ, Forte RA, O'Donnell KT. Diagnosis of subclinical varicocele in infertility. *AJR Am J Roentgenol* 1987; **148**: 71-75 [PMID: 3024475 DOI: 10.2214/ajr.148.1.71]
- 39 **Aydos K**, Baltaci S, Salih M, Anafarta K, Bedük Y, Gülsoy U. Use of color Doppler sonography in the evaluation of varicoceles. *Eur Urol* 1993; **24**: 221-225 [PMID: 8375443]
- 40 **Cina A**, Minnetti M, Pirroni T, Vittoria Spampinato M, Canadè A, Oliva G, Ribatti D, Bonomo L. Sonographic quantitative evaluation of scrotal veins in healthy subjects: normative values and implications for the diagnosis of varicocele. *Eur Urol* 2006; **50**: 345-350 [PMID: 16542771 DOI: 10.1016/j.eururo.2006.02.055]
- 41 **Kocakoc E**, Serhatlioglu S, Kiris A, Bozgeyik Z, Ozdemir H, Bodakci MN. Color Doppler sonographic evaluation of interrelations between diameter, reflux and flow volume of testicular veins in varicocele. *Eur J Radiol* 2003; **47**: 251-256 [PMID: 12927671 DOI: 10.1016/S0720-048X(02)00182-1]
- 42 **Lee J**, Binsaleh S, Lo K, Jarvi K. Varicoceles: the diagnostic dilemma. *J Androl* 2008; **29**: 143-146 [PMID: 18077824 DOI: 10.2164/jandrol.107.003467]
- 43 **Pilatz A**, Altinkilic B, Köhler E, Marconi M, Weidner W. Color Doppler ultrasound imaging in varicoceles: is the venous diameter sufficient for predicting clinical and subclinical varicocele? *World J Urol* 2011; **29**: 645-650 [PMID: 21607575 DOI: 10.1007/s00345-011-0701-4]
- 44 **Stahl P**, Schlegel PN. Standardization and documentation of varicocele evaluation. *Curr Opin Urol* 2011; **21**: 500-505 [PMID: 21926627 DOI: 10.1097/MOU.0b013e32834b8698]
- 45 **Eskew LA**, Watson NE, Wolfman N, Bechtold R, Scharling E, Jarow JP. Ultrasonographic diagnosis of varicoceles. *Fertil Steril* 1993; **60**: 693-697 [PMID: 8405527 DOI: 10.1016/S0090-4295(97)00452-4]
- 46 **Sarteschi LM**, Liguori G, Trombetta C. Varicocele. In: Sarteschi LM, Menchini-Fabris GF. *Ecografia andrologica*. Athena Srl: Modena, 2003: 139-155
- 47 **Chiou RK**, Anderson JC, Wobig RK, Rosinsky DE, Matamoros A, Chen WS, Taylor RJ. Color Doppler ultrasound criteria to diagnose varicoceles: correlation of a new scoring system with physical examination. *Urology* 1997; **50**: 953-956 [PMID: 9426729 DOI: 10.1016/S0090-4295(97)00452-4]
- 48 **Dogra VS**, Gottlieb RH, Oka M, Rubens DJ. Sonography of the scrotum. *Radiology* 2003; **227**: 18-36 [PMID: 12616012 DOI: 10.1148/radiol.2271001744]
- 49 **Schurich M**, Aigner F, Frauscher F, Pallwein L. The role of ultrasound in assessment of male fertility. *Eur J Obstet Gynecol Reprod Biol* 2009; **144** Suppl 1: S192-S198 [PMID: 19303691 DOI: 10.1016/j.ejogrb.2009.02.034]
- 50 **Akcar N**, Turgut M, Adapinar B, Ozkan IR. Intratesticular arterial resistance and testicular volume in infertile men with subclinical varicocele. *J Clin Ultrasound* 2004; **32**: 389-393 [PMID: 15372446 DOI: 10.1002/jcu.20059]
- 51 **Zhang M**, Du L, Liu Z, Qi H, Chu Q. The effects of varicocelectomy on testicular arterial blood flow: laparoscopic surgery versus microsurgery. *Urol J* 2014; **11**: 1900-1906 [PMID: 25361712]
- 52 **Ross JA**, Watson NE, Jarow JP. The effect of varicoceles on testicular blood flow in man. *Urology* 1994; **44**: 535-539 [PMID: 7941192 DOI: 10.106/S0090-4295(94)80053-7]
- 53 **Grasso Leanza F**, Pepe P, Panella P, Pepe F. Volocimetric evaluation of spermatic vessels with echo color doppler in patients with idiopathic varicocele. *Minerva Urol Nefrol* 1997; **49**: 179-182 [PMID: 9557498]
- 54 **Unsal A**, Turgut AT, Taşkın F, Koşar U, Karaman CZ. Resistance and pulsatility index increase in capsular branches of testicular artery: indicator of impaired testicular microcirculation in

- varicocele? *J Clin Ultrasound* 2007; **35**: 191-195 [PMID: 17366558 DOI: 10.1002/jcu.20331]
- 55 **Biagiotti G**, Cavallini G, Modenini F, Vitali G, Gianaroli L. Spermatogenesis and spectral echo-colour Doppler traces from the main testicular artery. *BJU Int* 2002; **90**: 903-908 [PMID: 12460354 DOI: 10.1046/j.1464-410X.2002.03033.x]
 - 56 **Gordon SJ**, Campbell S, Bhardwa J, Nargund VH. Spermatogenesis and spectral echo-colour Doppler traces from the main testicular artery. *BJU Int* 2003; **91**: 897-898 [PMID: 12780864 DOI: 10.1046/j.1464-410X.2003.t01-3-04246.x]
 - 57 **Caretta N**, Palego P, Schipilliti M, Torino M, Pati M, Ferlin A, Foresta C. Testicular contrast harmonic imaging to evaluate intratesticular perfusion alterations in patients with varicocele. *J Urol* 2010; **183**: 263-269 [PMID: 19942233 DOI: 10.1016/j.juro.2009.08.140]
 - 58 **Huang DY**, Sidhu PS. Focal testicular lesions: colour Doppler ultrasound, contrast-enhanced ultrasound and tissue elastography as adjuvants to the diagnosis. *Br J Radiol* 2012; **85** Spec No 1: S41-S53 [PMID: 22674702 DOI: 10.1259/bjr/30029741]
 - 59 **Aigner F**, De Zordo T, Pallwein-Prettner L, Junker D, Schäfer G, Pichler R, Leonhartsberger N, Pinggera G, Dogra VS, Frauscher F. Real-time sonoelastography for the evaluation of testicular lesions. *Radiology* 2012; **263**: 584-589 [PMID: 22396607 DOI: 10.1148/radiol.12111732]
 - 60 **Goddi A**, Sacchi A, Magistretti G, Almolla J, Salvatore M. Real-time tissue elastography for testicular lesion assessment. *Eur Radiol* 2012; **22**: 721-730 [PMID: 22028111 DOI: 10.1007/s00330-011-2312-2]
 - 61 **Dede O**, Teke M, Daggulli M, Utangaç M, Baş O, Penbegül N. Elastography to assess the effect of varicoceles on testes: a prospective controlled study. *Andrologia* 2016; **48**: 257-261 [PMID: 26011193 DOI: 10.1111/and.12440]
 - 62 **Tsili AC**, Giannakis D, Sylakos A, Ntorkou A, Sofikitis N, Argyropoulou MI. MR imaging of scrotum. *Magn Reson Imaging Clin N Am* 2014; **22**: 217-38, vi [PMID: 24792679 DOI: 10.1016/j.mric.2014.01.007]
 - 63 **Aganovic L**, Cassidy F. Imaging of the scrotum. *Radiol Clin North Am* 2012; **50**: 1145-1165 [PMID: 23122043 DOI: 10.1016/j.rcl.2012.08.003]
 - 64 **Cassidy FH**, Ishioka KM, McMahon CJ, Chu P, Sakamoto K, Lee KS, Aganovic L. MR imaging of scrotal tumors and pseudotumors. *Radiographics* 2010; **30**: 665-683 [PMID: 20462987 DOI: 10.1148/rg.303095049]
 - 65 **Tsili AC**, Argyropoulou MI, Giannakis D, Tsampalas S, Sofikitis N, Tsampoulas K. Diffusion-weighted MR imaging of normal and abnormal scrotum: preliminary results. *Asian J Androl* 2012; **14**: 649-654 [PMID: 22367182 DOI: 10.1038/aja.2011.172]
 - 66 **Maki D**, Watanabe Y, Nagayama M, Ishimori T, Okumura A, Amoh Y, Nakashita S, Terai A, Dodo Y. Diffusion-weighted magnetic resonance imaging in the detection of testicular torsion: feasibility study. *J Magn Reson Imaging* 2011; **34**: 1137-1142 [PMID: 21928380 DOI: 10.1002/jmri.22698]
 - 67 **Kantarci M**, Doganay S, Yalcin A, Aksoy Y, Yilmaz-Cankaya B, Salman B. Diagnostic performance of diffusion-weighted MRI in the detection of nonpalpable undescended testes: comparison with conventional MRI and surgical findings. *AJR Am J Roentgenol* 2010; **195**: W268-W273 [PMID: 20858788 DOI: 10.2214/AJR.10.4221]
 - 68 **Tsili AC**, Argyropoulou MI, Astrakas LG, Ntoulia EA, Giannakis D, Sofikitis N, Tsampoulas K. Dynamic contrast-enhanced subtraction MRI for characterizing intratesticular mass lesions. *AJR Am J Roentgenol* 2013; **200**: 578-585 [PMID: 23436847 DOI: 10.2214/AJR.12.9064]
 - 69 **Watanabe Y**, Dohke M, Ohkubo K, Ishimori T, Amoh Y, Okumura A, Oda K, Hayashi T, Dodo Y, Arai Y. Scrotal disorders: evaluation of testicular enhancement patterns at dynamic contrast-enhanced subtraction MR imaging. *Radiology* 2000; **217**: 219-227 [PMID: 11012448 DOI: 10.1148/radiology.217.1.r00oc41219]
 - 70 **Aaronson DS**, Iman R, Walsh TJ, Kurhanewicz J, Turek PJ. A novel application of 1H magnetic resonance spectroscopy: non-invasive identification of spermatogenesis in men with non-obstructive azoospermia. *Hum Reprod* 2010; **25**: 847-852 [PMID: 20124393 DOI: 10.1093/humrep/dep475]
 - 71 **Tsili AC**, Astrakas LG, Ntorkou A, Giannakis D, Stavrou S, Maliakas V, Sofikitis N, Argyropoulou MI. MR Spectra of Normal Adult Testes and Variations with Age: Preliminary Observations. *Eur Radiol* 2016; **26**: 2261-2267 [PMID: 26474986 DOI: 10.1007/s00330-015-4055-y]
 - 72 **Karakas E**, Karakas O, Cullu N, Badem OF, Boyacı FN, Gulum M, Cece H. Diffusion-weighted MRI of the testes in patients with varicocele: a preliminary study. *AJR Am J Roentgenol* 2014; **202**: 324-328 [PMID: 24450672 DOI: 10.2214/AJR.13.10594]
 - 73 **Choyke PL**. Dynamic contrast-enhanced MR imaging of the scrotum: reality check. *Radiology* 2000; **217**: 14-15 [PMID: 11012418 DOI: 10.1148/radiology.217.1.r00oc4414]
 - 74 **Terai A**, Yoshimura K, Ichioke K, Ueda N, Utsunomiya N, Kohei N, Arai Y, Watanabe Y. Dynamic contrast-enhanced subtraction magnetic resonance imaging in diagnostics of testicular torsion. *Urology* 2006; **67**: 1278-1282 [PMID: 16765192 DOI: 10.1016/j.urology.2005.12.021]
 - 75 **Watanabe Y**, Nagayama M, Okumura A, Amoh Y, Suga T, Terai A, Dodo Y. MR imaging of testicular torsion: features of testicular hemorrhagic necrosis and clinical outcomes. *J Magn Reson Imaging* 2007; **26**: 100-108 [PMID: 17659558 DOI: 10.1002/jmri.20946]
 - 76 **Practice Committee of the American Society for Reproductive Medicine; Society for Male Reproduction and Urology**. Report on varicocele and infertility: a committee opinion. *Fertil Steril* 2014; **102**: 1556-1560 [PMID: 25458620 DOI: 10.1016/j.fertnstert.2014.10.007]
 - 77 **American Urological Association Education and Research, Inc.** Report on Varicocele and Infertility: An AUA Best Practice Policy and ASRM Practice Committee Report. Linthicum, MD: American Urological Association, Inc.; Birmingham, AL: American Society for Reproductive Medicine; 2001. Available from: URL: <http://www.auanet.org/common/pdf/education/clinical-guidance/Varicocele-Archive.pdf>
 - 78 **Jungwirth A**, Giwercman A, Tournaye H, Diemer T, Kopa Z, Dohle G, Krausz C. European Association of Urology guidelines on Male Infertility: the 2012 update. *Eur Urol* 2012; **62**: 324-332 [PMID: 22591628 DOI: 10.1016/j.eururo.2012.04.048]
 - 79 **Halpern J**, Mittal S, Pereira K, Bhatia S, Ramasamy R. Percutaneous embolization of varicocele: technique, indications, relative contraindications, and complications. *Asian J Androl* 2016; **18**: 234-238 [PMID: 26658060 DOI: 10.4103/1008-682X.169985]
 - 80 **Nabi G**, Asterlings S, Greene DR, Marsh RL. Percutaneous embolization of varicoceles: outcomes and correlation of semen improvement with pregnancy. *Urology* 2004; **63**: 359-363 [PMID: 14972491 DOI: 10.1016/j.urology.2003.09.026]
 - 81 **Sze DY**, Kao JS, Frisoli JK, McCallum SW, Kennedy WA, Razavi MK. Persistent and recurrent postsurgical varicoceles: venographic anatomy and treatment with N-butyl cyanoacrylate embolization. *J Vasc Interv Radiol* 2008; **19**: 539-545 [PMID: 18375298 DOI: 10.1016/j.jvir.2007.11.009]
 - 82 **Rais-Bahrami S**, Montag S, George AK, Rastinehad AR, Palmer LS, Siegel DN. Angiographic findings of primary versus salvage varicoceles treated with selective gonadal vein embolization: an explanation for surgical treatment failure. *J Endourol* 2012; **26**: 556-560 [PMID: 22077657 DOI: 10.1089/end.2011.0387]
 - 83 **Jargiello T**, Drelich-Zbroja A, Falkowski A, Sojka M, Pyra K, Szczerbo-Trojanowska M. Endovascular transcatheter embolization of recurrent postsurgical varicocele: anatomic reasons for surgical failure. *Acta Radiol* 2015; **56**: 63-69 [PMID: 24413222 DOI: 10.1177/0284185113519624]
 - 84 **Rotker K**, Sigman M. Recurrent varicocele. *Asian J Androl* 2016; **18**: 229-233 [PMID: 26806078 DOI: 10.4103/1008-682X.171578]
 - 85 **Cayan S**, Shavakhabov S, Kadioğlu A. Treatment of palpable varicocele in infertile men: a meta-analysis to define the best technique. *J Androl* 2016; **30**: 33-40 [PMID: 18772487 DOI: 10.2164/jandrol.108.005967]
 - 86 **Cayan S**, Kadioğlu TC, Tefekli A, Kadioğlu A, Tellaloglu S. Comparison of results and complications of high ligation surgery and microsurgical high inguinal varicocelectomy in the treatment of varicocele. *Urology* 2000; **55**: 750-754 [PMID: 10792094 DOI: 10.1016/j.juro.2000.05.007]

- 10.2164/jandrol.112.016444]
- 87 **Chiles KA**, Schlegel PN. Cost-effectiveness of varicocele surgery in the era of assisted reproductive technology. *Asian J Androl* 2016; **18**: 259-261 [PMID: 26732113 DOI: 10.4103/1008-682X.172644]
 - 88 **Esteves SC**, Roque M, Agarwal A. Outcome of assisted reproductive technology in men with treated and untreated varicocele: systematic review and meta-analysis. *Asian J Androl* 2016; **18**: 254-258 [PMID: 26510504 DOI: 10.4103/1008-682X.163269]
 - 89 **Pathak P**, Chandrashekar A, Hakky TS, Pastuszak AW. Varicocele management in the era of in vitro fertilization/intracytoplasmic sperm injection. *Asian J Androl* 2016; **18**: 343-348 [PMID: 27030086]
 - 90 **Schlegel PN**, Goldstein M. Alternate indications for varicocele repair: non-obstructive azoospermia, pain, androgen deficiency and progressive testicular dysfunction. *Fertil Steril* 2011; **96**: 1288-1293 [PMID: 22130099 DOI: 10.1016/j.fertnstert.2011.10.033]
 - 91 **Esteves SC**, Miyaoka R, Roque M, Agarwal A. Outcome of varicocele repair in men with nonobstructive azoospermia: systematic review and meta-analysis. *Asian J Androl* 2016; **18**: 246-253 [PMID: 26680033 DOI: 10.4103/1008-682X.169562]
 - 92 **Dabaja AA**, Goldstein M. When is a varicocele repair indicated: the dilemma of hypogonadism and erectile dysfunction? *Asian J Androl* 2016; **18**: 213-216 [PMID: 26696437 DOI: 10.4103/1008-682X.169560]
 - 93 **Sun N**, Cheung TT, Khong PL, Chan KL, Tam PK. Varicocele: Laparoscopic clipping and color Doppler follow-up. *J Pediatr Surg* 2001; **36**: 1704-1707 [PMID: 11685706 DOI: 10.1053/jpsu.2001.27967]
 - 94 **Student V**, Zátura F, Scheinar J, Vrtal R, Vrána J. Testicle hemodynamics in patients after laparoscopic varicocelectomy evaluated using color Doppler sonography. *Eur Urol* 1998; **33**: 91-93 [PMID: 9471047]
 - 95 **Tarhan S**, Gümüş B, Gündüz I, Ayyıldız V, Gökten C. Effect of varicocele on testicular artery blood flow in men--color Doppler investigation. *Scand J Urol Nephrol* 2003; **37**: 38-42 [PMID: 12745742 DOI: 10.1080/00365590310008677]
 - 96 **Tanriverdi O**, Miroglu C, Horasanli K, Altay B, Caliskan KC, Gumus E. Testicular blood flow measurements and mean resistive index values after microsurgical and high ligation varicocelectomy. *Urology* 2006; **67**: 1262-1265 [PMID: 16765187 DOI: 10.1016/j.urol.2005.12.033]
 - 97 **Balci A**, Karazincir S, Gorur S, Sumbas H, Egilmez E, Inandi T. Long-term effect of varicocele repair on intratesticular arterial resistance index. *J Clin Ultrasound* 2008; **36**: 148-152 [PMID: 18088054 DOI: 10.1002/jcu.20439]
 - 98 **Tarhan S**, Ucer O, Sahin MO, Gumus B. Long-term effect of microsurgical inguinal varicocelectomy on testicular blood flow. *J Androl* 2011; **32**: 33-39 [PMID: 20671143 DOI: 10.2164/jandrol.109.009977]

P- Reviewer: Chen SS, Rais-Bahrami S, Seo JT **S- Editor:** Qiu S
L- Editor: A **E- Editor:** Wu HL



Magnetic resonance enterography in Crohn's disease: How we do it and common imaging findings

Annalisa Mantarro, Paola Scalise, Elisa Guidi, Emanuele Neri

Annalisa Mantarro, Paola Scalise, Elisa Guidi, Emanuele Neri, Department of Translational Research and New Technologies in Medicine and Surgery, Diagnostic Radiology, 56126 Pisa, Italy

Author contributions: Mantarro A wrote the paper; Scalise P performed research; Guidi E analysed data; Neri E designed research.

Conflict-of-interest statement: No potential conflicts of interest and no financial support.

Open-Access: This article is an open-access article which was selected by an in-house editor and fully peer-reviewed by external reviewers. It is distributed in accordance with the Creative Commons Attribution Non Commercial (CC BY-NC 4.0) license, which permits others to distribute, remix, adapt, build upon this work non-commercially, and license their derivative works on different terms, provided the original work is properly cited and the use is non-commercial. See: <http://creativecommons.org/licenses/by-nc/4.0/>

Manuscript source: Invited manuscript

Correspondence to: Emanuele Neri, MD, Professor of Radiology at the University of Pisa, Department of Translational Research and New Technologies in Medicine and Surgery, Diagnostic Radiology, Radiodiagnostica 3 Ospedale S, Chiara - Edificio 18, Via Roma 67, 56126 Pisa, Italy. emanuele.neri@med.unipi.it
Telephone: +39-050-992509
Fax: +39-050-551461

Received: April 30, 2016

Peer-review started: May 4, 2016

First decision: July 20, 2016

Revised: October 22, 2016

Accepted: December 13, 2016

Article in press: December 14, 2016

Published online: February 28, 2017

Abstract

Crohn's disease (CD) is a chronic inflammatory disease

of the gastrointestinal tract, with unpredictable clinical course by phases of relapses alternating with other of quiescence. The etiology is multifactorial and is still not completely known; globally the westernization of lifestyle is causing an increasing incidence of CD, with peak age of 20-30 years. The diagnostic workup begins with the evaluation of the clinical history, physical examination and laboratory tests. However, the clinical assessment is subjected to interobserver variability and, occasionally, the symptoms of acute and chronic inflammation may be indistinguishable. In this regards, the role of magnetic resonance (MR) enterography is crucial to determine the extension, the disease activity and the presence of any complications without ionizing radiations, making this method very suitable for young population affected by CD. The purpose of this review article is to illustrate the MR enterography technique and the most relevant imaging findings of CD, allowing the detection of small bowel involvement and the assessment of disease activity.

Key words: Crohn's disease; Disease activity; Magnetic resonance sequences; Small bowel; Magnetic resonance enterography

© The Author(s) 2017. Published by Baishideng Publishing Group Inc. All rights reserved.

Core tip: Magnetic resonance (MR) enterography represents a non-invasive technique for Crohn's disease (CD) diagnosis, allowing morphological and functional evaluation of the small bowel loops. For all these reasons, MR enterography is assuming a prominent role as first-choice radiological examination in patients affected by CD. In this setting, the purpose of this review article is to illustrate the MR enterography technique and the most relevant imaging findings of CD, in order to discriminate among the various subtypes of CD (active, fistulizing/perforating or chronic subtype) and to assess disease activity.

Mantarro A, Scalise P, Guidi E, Neri E. Magnetic resonance enterography in Crohn's disease: How we do it and common imaging findings. *World J Radiol* 2017; 9(2): 46-54 Available from: URL: <http://www.wjgnet.com/1949-8470/full/v9/i2/46.htm> DOI: <http://dx.doi.org/10.4329/wjrr.v9.i2.46>

INTRODUCTION

Crohn's disease (CD) is a type of chronic inflammatory bowel disease, characterized by typical fluctuating course with relapses alternating with periods of remission^[1]. The incidence of CD is increasing worldwide, but the highest has been reported in Northern Europe, United Kingdom, and North America, occurring 20%-30% more frequently in women, with age of onset during young adulthood and, in a small subset of patients, between the 60 and 80 years of age^[2]. Nowadays, the etiopathogenesis is not completely known; however the development of CD depends on several factors (immunological, genetic, and environmental, such as diet or smoking), which lead to a dysregulated immune response to commensal flora or common antigens, in genetically susceptible hosts^[3,4]. Usually, CD may manifest with increased frequency of bowel movements, diarrhoea, abdominal pain and weight loss; while symptoms like asthenia, anorexia, nausea, vomiting, fever and extra-intestinal manifestations (*i.e.*, arthritis, uveitis, episcleritis, skin rashes, erythema nodosum, pyoderma gangrenosum) occur in about a quarter of patients^[5].

Moreover, CD may affect any portion of the gastrointestinal tract from mouth to anus, mainly involving the ileocaecal region (about one half of all cases), following by the ileum and colon (30% and 20% of patients, respectively)^[6]. Both the transmural chronic inflammation and the discontinuous involvement ("skip lesions") of affected bowel loops, alternating inflamed and uninvolved segments, are typical features of CD^[7]. During the active phase of inflammatory response, the enteric mucosa appears as irregular due to neutrophils and mononuclear cell infiltration, alternating ulceration and edema ("cobblestoning" pattern), associated with cryptitis, crypt microabscesses, and sometimes non-caseating granulomas. When the inflammation becomes chronic, the superficial aphthoid ulcers can penetrate into the bowel wall resulting in deep ulcerations, sinus tracts or fistula formation, thus extending into mesentery, lymph nodes and adjacent structures (*i.e.*, other bowel loops, bladder, uterus, vagina or skin).

Moreover, the chronic inflammatory response promotes smooth muscle cell proliferation, collagen accumulation, wall thickening, stenosis and fibrosis of the affected bowel segments with mesenteric fibro-fatty proliferation^[8,9].

Given this context, the management and staging of patients with CD requires the correct determination of inflammatory lesion location, extension, activity and

severity, in order to choose appropriate therapeutic strategies^[10,11]. Since the clinical presentation of acute and chronic inflammation may be overlapped, the cross-sectional imaging techniques are useful for distinguishing them and preventing the development of potential complications. Among imaging modalities, magnetic resonance (MR) enterography provides the advantages of high-tissue-contrast evaluation with optimal detection of fluid and submucosal edema, multiplanar capability, multiparametric assessment and functional informations (motility, perfusion, diffusion) without ionizing radiations, making this method very suitable for young population affected by CD^[12].

The purpose of this article is to review MR enterography technique and the most relevant imaging findings of CD, in order to provide an overview of the current state-of-art of MR imaging in CD, highlighting the recent MR innovations that allow a better evaluation of disease activity.

TECHNIQUE

MR enterography requires fast imaging techniques, luminal distension and 6-h fasting before the procedure^[11]. In this regard, an adequate colonic distension is mandatory to better identify wall thickening and parietal enhancement on the post-contrastographic images. The oral contrast agents used to obtain a well-distended lumen are classified based on their effects on T1 and T2-weighted images. The positive contrast agents (diluted gadolinium, some fruit juices or milk) yield the advantage of high intraluminal signal due to their high T2, but they may interfere with the detection of mucosal enhancement in T1-weighted sequences after gadolinium administration due to T1 shortening effect. By contrast, the use of negative contrast agents, as superparamagnetic iron oxide, determines a low intraluminal signal (low T2 and T1) and allows a better evaluation of the bowel walls^[13]. However the widest accepted contrast agents are the biphasic ones (methylcellulose, mannitol, polyethylene glycol), characterized by hyperosmolar effect, that promotes luminal distention. Furthermore, they permit the assessment of wall thickening thanks to high signal intensity on T2-weighted sequences (positive effect), in which the bowel walls appear as hypointense, while the lumen is hyperintense. On T1-weighted images after gadolinium administration, these biphasic contrast agents maximize the depiction of wall enhancement by means of low intraluminal signal (negative effect)^[14]. As above mentioned the biphasic contrast agent are more frequently preferred for MR enterography in CD. The patients are instructed to ingest about 1.5-2 L of water solution with biphasic contrast agent 45 min preceding the procedure^[15]. The patient is positioned in prone decubitus in order to increase bowel loop separation and decrease both the peristalsis and the acquired abdominal volume in MR sequences, consequently

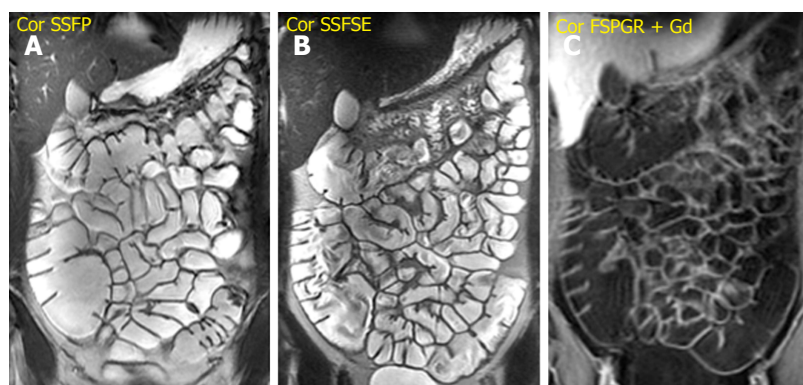


Figure 1 Assessment of small bowel anatomy, disease localization and segmental extension. A: Steady-state free precession (SSFP); B: T2-weighted single shot fast spin echo (SSFSE) sequence; C: Gadolinium-enhanced fat-suppressed 3D spoiled gradient-echo (FSPGR) sequence.

reducing blurring and bowel motility artifacts. The supine position is required for noncompliant patients with abdominal stomas or entero-cutaneous fistulas. Moreover, before T2-weighted sequences and contrast medium injection, endovenous administration of 20 mg of hyoscine butylbromide is recommended to further reduce bowel peristalsis^[16]. MR enterography is performed using phased-array coils to improve signal-to-noise ratio and spatial resolution, simultaneously minimizing the acquisition time with faster sequences and parallel imaging.

The MR study protocol consists of the following sequences.

Steady-state free precession sequence - (FIESTA, General Electric; True-FISP, Siemens)

It is a very fast sequence thanks to a short repetition and echo time, providing high-contrast MR images dependent on T2*/T1 ratio. It allows motion-free images, ensuring a good visualization of the small bowel, mesentery, vascularization and lymphadenopathy in coronal and axial view. Furthermore, this sequence may provide cine assessment of the bowel loops, facilitating the discrimination between fibrotic stricture and functional stenosis. However, the images suffer from magnetic susceptibility artifacts, caused by the presence of gas or ferromagnetic materials, and chemical shift artifacts resulting in a "black boundary" effect around structures, which may hamper a correct definition of bowel wall thickening^[17].

T2-weighted SSFSE (Single Shot Fast Spin Echo, General Electric) or HASTE (Half-fourier Acquisition Single-shot Turbo spin-Echo, Siemens)

It allows to obtain high-contrast resolution MR images in coronal and axial planes for the depiction of wall thickening, fold pattern changes, ulceration, intramural bowel edema and extraluminal fluid collections (particularly with fat-suppressed images). It is a fast sequence with a long echo train, which utilizes the partial Fourier encoding of K-space data for reducing the acquisition time, nevertheless decreasing signal-to-noise ratio of MR

images. It is not sensitive to magnetic susceptibility or chemical shift artifacts, allowing an optimal evaluation of wall thickening. However, this sequence is sensitive to intraluminal flow voids, blurring and bowel motility artifacts; in this regard, the endovenous administration of spasmolytic agent is recommended to reduce bowel peristalsis^[13].

Gadolinium-enhanced fat-suppressed 3D spoiled gradient-echo sequence

It is performed after the intravenous injection of 0.1-0.2 mmol/kg of gadopentetate dimeglumine (Gd-DTPA) with a delay time of 40-80 s; the acquisition of arterial phase after 25 s is optional. It is very useful to evaluate bowel wall enhancement, which is highlighted by endoluminal low-signal intensity caused by positive contrast agent administration. Moreover, it provides relevant information about vasculature, lymph nodes, fistulas or abscesses. Frequently the sequence is performed in the coronal plane; axial acquisitions may be useful for evaluating the pathological and thickened bowel loops^[18] (Figure 1).

Diffusion-weighted imaging sequence

Diffusion-weighted imaging sequence in the axial plane has been proposed to better identify the inflamed bowel loops in active phase^[16].

MR enterography advantages

Several studies have compared the accuracy of different non-invasive diagnostic methods in the assessment of CD.

In this setting, MR enterography is more effective than ultrasound (US), particularly in the evaluation of the entire gastrointestinal tract, perianal region and complications; although US permits a rapid and accurate examination of the terminal ileum^[19].

Moreover, Lee *et al*^[20] have demonstrated that the effectiveness of MR enterography is comparable to that of CT enterography, with the advantage of not using ionizing radiations, making this modality ideal in imaging the youth.

MR ENTEROGRAPHY INDICATIONS

The clinical indications of MR enterography include the following conditions: (1) assesment of small bowel anatomy, disease localization and segmental extension; (2) morphological evaluation (bowel wall, mesentery, vascular supply and lymph nodes); (3) dynamic evaluation (disease activity and neoangiogenesis); (4) classification of CD into three subtypes based on inflammatory activity, including active inflammatory, fistulizing/perforating and fibrostenosing categories; (5) follow-up of patients with diagnosed CD; (6) exclusion of CD diagnosis in symptomatic patients; (7) suspected disease relapse, stricturing disease and/or extraluminal complications; (8) monitoring therapeutic response or failure; and (9) planning of surgical intervention^[17].

The assessment of CD subtypes is required by clinicians for the therapeutic planning, through the detection of linear and aphthoid ulcers, wall edema, skip lesions, fistulas, abscess or strictures; and their correlation with clinical data^[21]. Frequently, acute and chronic changes may coexist in the same bowel segment with a wide variety of intestinal and extra-intestinal abnormalities. In this context, the bowel wall lesions characterizing active disease are managed medically, whereas fibrotic strictures with bowel obstruction are frequently treated with surgical intervention^[22].

Active inflammatory subtype

The typical pathological findings of active CD comprehend: Aphthoid and deep ulceration, wall thickening (greater than 4 mm), intramural and mesenteric edema, stratified enhancement pattern of bowel wall, increased mesenteric vascularity, reactive lymphadenopathy^[13].

Ulcers: The aphthoid ulcers, typical findings of CD in the early stages, can only be detected through an adequate luminal distension and high-resolution MR imaging, they appear as a nidus of high signal intensity in T2-weighted images, surrounded by a rim of moderate signal intensity^[23]. Advanced inflammation may produce other changes, such as deep and transmural (linear) ulcerations. The typical "cobblestone" mucosal appearance result from confluent (longitudinal and transverse) ulcerations combined with bulging of the edematous mucosa^[12].

Fold thickening: The SSFSE sequence allows to identify fold thickening and distortion caused by mucosal ulceration^[24].

Wall thickening: It is easily identified on steady-state free precession (SSFP), T2-weighted (SSFSE) and fat-suppressed 3D spoiled gradient-echo (FSPGR) (after Gd-DTPA administration) sequences, previous adequate distension of the small bowel loops. Nevertheless, the SSFP sequence hampers the correct definition of wall thickening, because of the chemical shift artefact. For this reason, the measurement of wall thickness

should be performed in SSFSE images. The degree of wall thickening correlates with both the presence of inflammation and the degree of disease activity. Particularly, a wall thickening greater than 3 mm is indicative of inflammation, while a thickening ranging from 5 to 10 mm is suggestive of CD^[25].

Intramural edema: This is a typical sign of active inflammation resulting in submucosal thickening, which appears as hyperintensity on T2-weighted (SSFSE) images with fat saturation^[26].

Mesenteric changes: In some cases of advanced inflammation, the mesentery may be edematous around the inflamed intestinal loops. Typically, the mesenteric edema is associated with both submucosal edema and stratified enhancement of the bowel wall; all these findings are suggestive of active inflammation. The mesenteric fibro-fatty proliferation (or fat-wrapping) represents another sign of advanced CD with consolidated transmural inflammation. It can be defined as an increase of mesenteric fat, which can determine mass effect with consequent anatomical displacement of the mesenteric vessels or the adjacent abdominal viscera, increasing the separation among the bowel loops. Moreover, the vascular engorgement produces an increased mesenteric vascularity ("comb sign"), resulting in hyperenhancement of mesenteric vessels supplying inflamed bowel loops^[16,21] (Figure 2).

Stratified enhancement pattern: The bowel wall enhancement, evaluated after Gd-DTPA intravenous administration, represents the parameter that most closely correlates to both the degree of inflammation and clinical indices of disease activity. The mucosal hyperemia of the affected loops is represented by hyperenhancement, which is significantly higher than normal loops; it decreases decrease in response to therapy. The typical stratified enhancement pattern ("target sign") is produced by mucosal and muscle/serosa increased enhancement with intermediate hypointensity of edematous submucosa^[27] (Figure 3).

Reactive mesenteric lymphadenopathy: Hyperenhancement, enlargement, and edema of lymph nodes can be present in active disease, but they are not specific of CD. These findings are easily identified with SSFP and FSPGR (after Gd-DTPA administration) sequences^[28].

Fistulizing/perforating subtype

It is characterized by the presence of deep penetrating ulcers, which can lead to the creation of sinus tract, fistulas and/or abscesses. The sinus tracts appear as hyperintense blind-ending tracts on T2-weighted images, that arise from bowel wall without ever reaching the surface of another structure (Figure 4). By contrast, fistulas originate from deep transmural ulcers, which communicate with adjacent epithelial

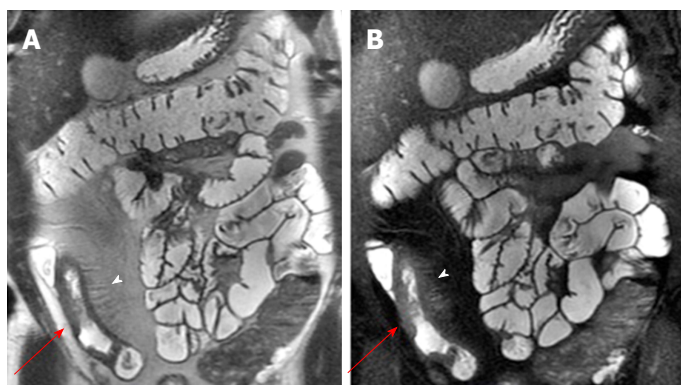


Figure 2 Wall thickening and mesenteric changes. SSFSE (A) and gadolinium-enhanced FSPGR (B) sequences show wall thickening (red arrows) of terminal ileum with comb signs (arrowhead) and mesenteric fat proliferation. SSFSE: Single shot fast spin echo; FSPGR: Fat-suppressed 3D spoiled gradient-echo.

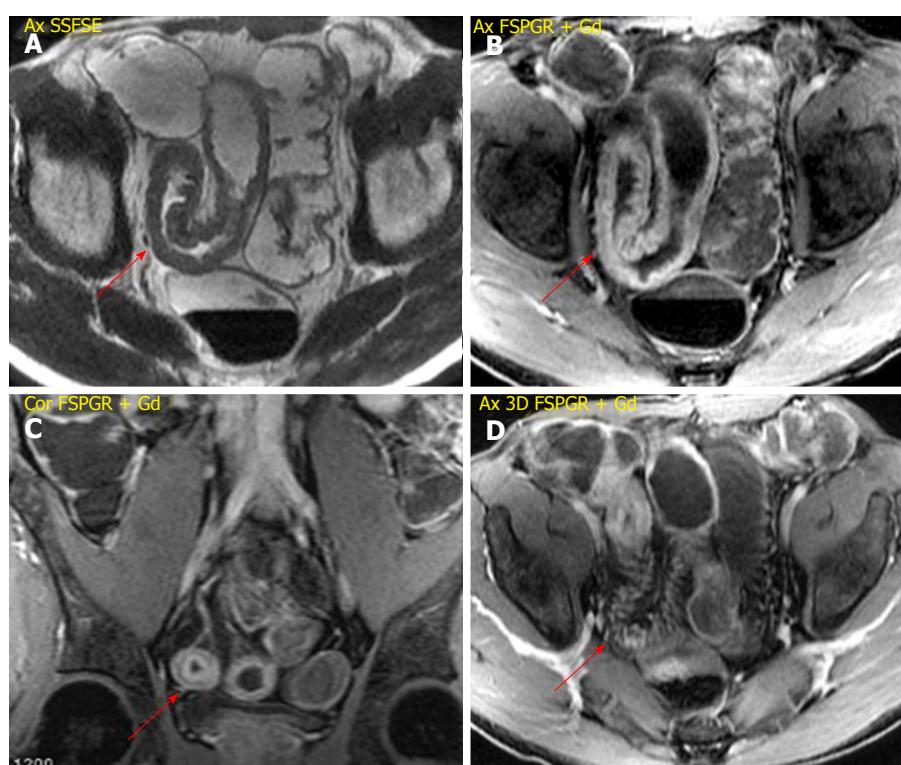


Figure 3 Active inflammation. A: Wall thickening (10 mm) of terminal ileum extending for about 18 cm detected on SSFSE sequence; B: Gadolinium-enhanced FSPGR sequence shows the stratified enhancement pattern characterized by mucosal and muscle/serosa increased enhancement with intermediate hypointensity of edematous submucosa; C: Coronal FSPGR sequence revealing typical "target sign" due to stratified enhancement of bowel wall; D: Mesenteric fat thickening and vascular engorgement of vasa recta (comb sign) displayed on gadolinium-enhanced image. SSFSE: Single shot fast spin echo; FSPGR: Fat-suppressed 3D spoiled gradient-echo.

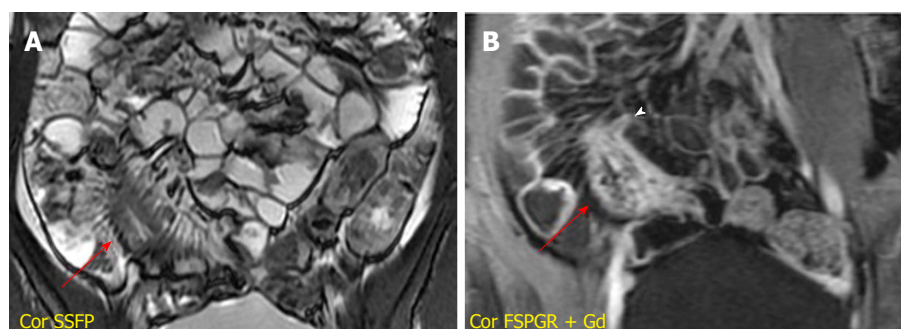


Figure 4 Subacute and stenotic disease with sinus tract. A: SSFP sequence showing wall thickening (11 mm; red arrow) of terminal ileum with comb sign and mesenteric fat thickening; B: Post-gadolinium image reveals diffuse enhancement of the stenotic bowel loop and sinus tract (arrowhead), which is a blind-ending tract arising from the bowel wall. SSFP: Steady-state free precession; FSPGR: Fat-suppressed 3D spoiled gradient-echo.

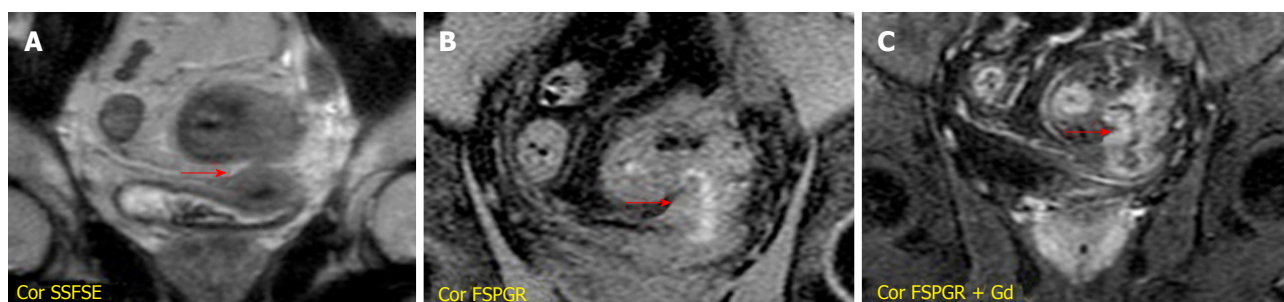


Figure 5 Entero-vesical fistula. A: Coronal SSFSE sequence detects wall thickening of the sigmoid colon with entero-vesical fistula (red arrow); B: FSPGR without gadolinium administration highlights the entero-vesical fistula, which appears hyperintense due to colonic content; C: Entero-vesical fistula appears as hyperintense transmurals lines in post-gadolinium sequence. SSFSE: Single shot fast spin echo; FSPGR: Fat-suppressed 3D spoiled gradient-echo.

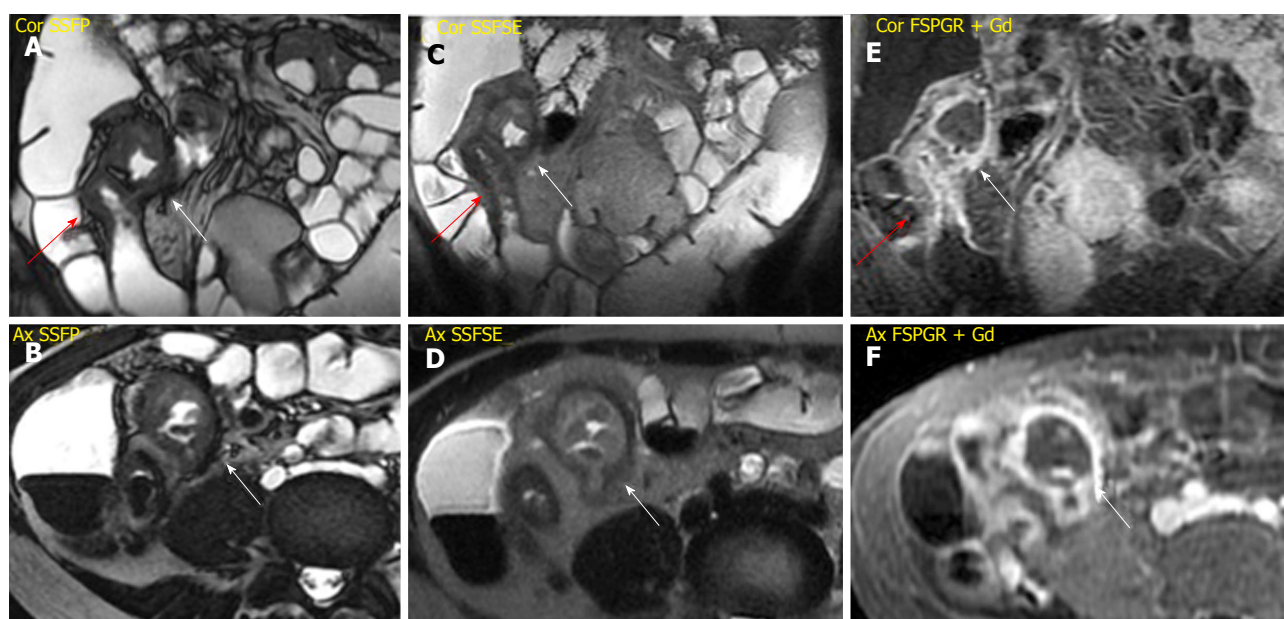


Figure 6 Peri-ileal abscess. A-D: SSFP and SSFSE sequences display wall thickening of the terminal ileum associated (red arrow) with contiguous encapsulated collection of pus and inhomogeneous content (abscess, white arrow); E and F: FSPGR sequence shows mucosal enhancement with hypointense deep layers of the bowel wall (fibrotic disease), associated with enhancing peripheral rim of the capsulated collection (abscess, white arrow). SSFP: Steady-state free precession; SSFSE: Single shot fast spin echo; FSPGR: Fat-suppressed 3D spoiled gradient-echo.

surfaces (bowel loops or other organs), appearing as hyperintense transmural lines on FSPGR (after Gd-DTPA administration) sequences^[29,30]. The fistulas can penetrate into contiguous bowel loops (enteroenteric or enterocolic fistulas) or into other structures (*i.e.*, bladder, uterus, vagina or skin); however, their identification in the earliest phase is very difficult due to low spatial resolution and partial volume averaging of MR images (Figure 5). An accurate high-resolution MR study associated with the use of multiplanar imaging can help to reveal the presence of fistulas. The desmoplastic reaction in the mesenteric tissue contributes to produce stellate appearance of fistulas, with spiculated margins^[31].

Other locoregional complications of CD comprehend the development of phlegmon and abscesses. The penetrating process may lead to a localized inflammatory reaction resulting into phlegmon formation, which is an inflammatory mass with mild/moderate increase signal on T2-weighted and post-gadolinium sequences^[32]. An

abscess is an encapsulated collection of pus, which has MR characteristics similar to those of fluid collections (hyperintense on T2-weighted and hypointense on T1-weighted images), but with inhomogeneous content because of solid and gaseous components, delimited by an enhancing peripheral rim^[13] (Figure 6).

Fibrostenotic subtype

The chronic inflammation of the bowel wall tends to progress towards fibrostenotic and irreversible complications (bowel strictures and obstruction), as consequence of prolonged intestinal injury^[33]. During chronic disease, the deposition of submucosal fat is promoted resulting in stratified appearance on T2-weighted images. This finding may be distinguished by submucosal edema on T2-weighted images thanks to fat saturation, which reduces the signal of fat in chronic disease^[34]. Moreover, the bowel wall enhancement differs from the stratified pattern, typical of active

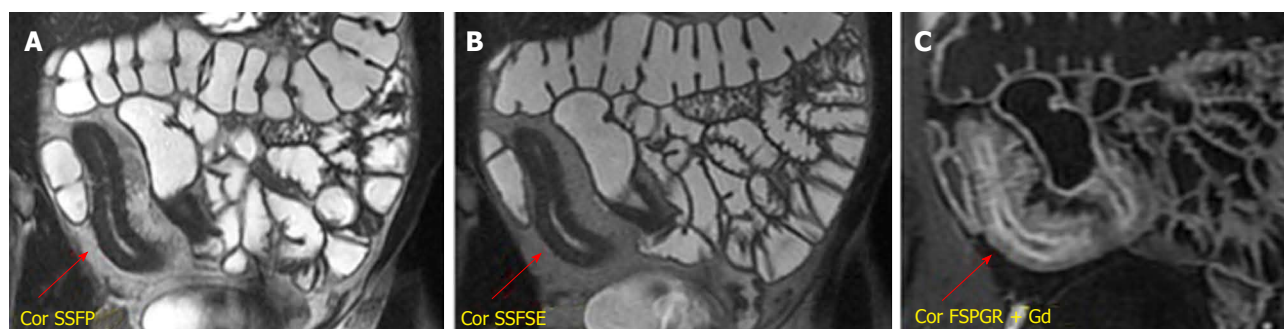


Figure 7 Chronic disease. A and B: Coronal SSFP and SSFSE sequences detect wall thickening (10 mm, red arrows) of neo-terminal ileum, after ileo-cecal resection, extending for about 19 cm; C: Coronal FSPGR sequence shows mucosal enhancement with hypointensity of the deep layers indicating the fibrotic disease. SSFP: Steady-state free precession; SSFSE: Single shot fast spin echo; FSPGR: Fat-suppressed 3D spoiled gradient-echo.

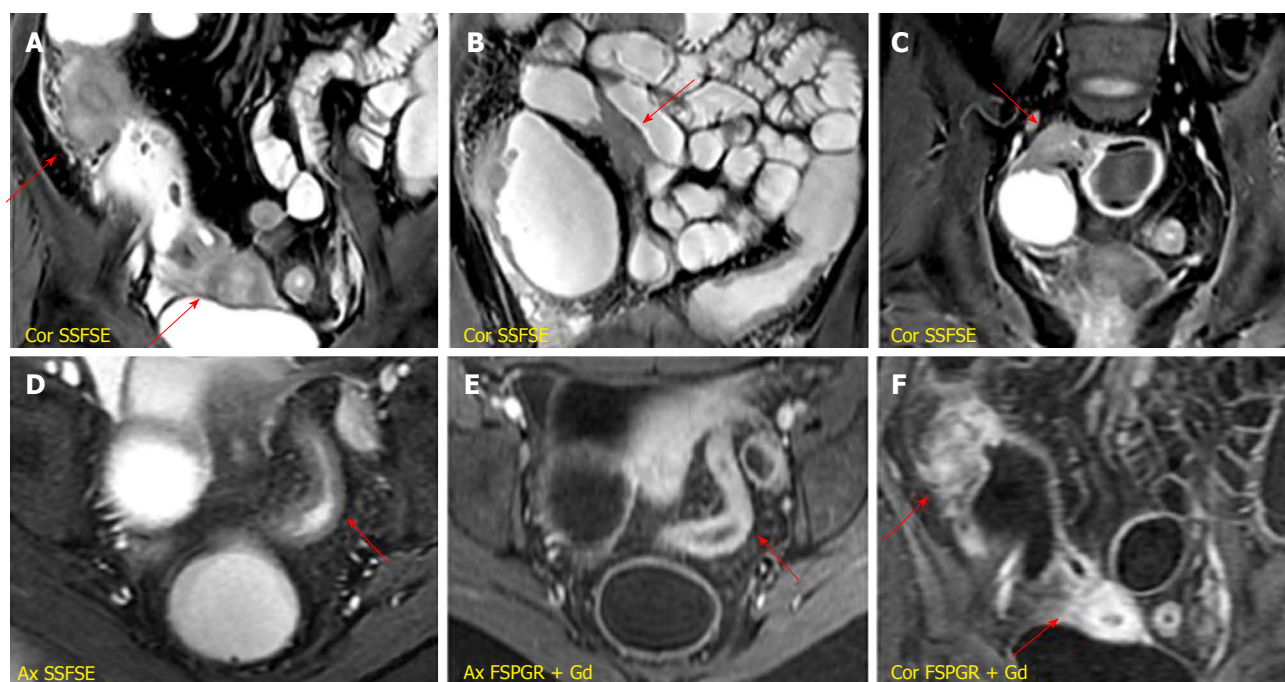


Figure 8 Fibrostenotic disease. A-C: Multiple fibrotic strictures of the small bowel alternating with prestenotic dilated tracts detected on SSFSE sequences; D: Wall thickening of the sigmoid colon producing luminal narrowing displayed on SSFSE image; E and F: Post-gadolinium sequences reveal a diffuse and homogeneous enhancement in sigmoid colon (E) and small bowel (F) suggestive of subacute inflammation. SSFSE: Single shot fast spin echo; FSPGR: Fat-suppressed 3D spoiled gradient-echo.

disease. On this ground, the thickened and fibrotic bowel wall shows diffuse and homogeneous enhancement during subacute transmural inflammation, while the moderate mucosal enhancement with hypointensity of the deep layers suggests fibrotic disease^[35] (Figure 7). In chronic disease, fibrosis may lead to stricture formation with high risk of small bowel obstruction of the affected segment, and consequent prestenotic dilatation (Figure 8). The fibrotic stricture appears as fixed luminal narrowing without any high signal intensity on T2-weighted images; by contrast the inflamed stricture, in acute disease, shows submucosal edema with the typical stratified enhancement pattern. It is important to identify the presence of fibrotic strictures because they are not responsive to medical therapy, but require prompt surgical approach to avoid complications such as

bowel obstruction^[12,36]. Furthermore, MR enterography is useful for detecting asymmetric bowel fibrosis on the mesenteric border with apparent dilatation (pseudodiverticula) on the antimesenteric side, and rare complications such as small bowel adenocarcinoma^[37].

Reading and reporting MR enterography

The recommended reading strategy for MR enterography examinations should integrate previous morphological evaluation, followed by functional assessment of the small bowel loops. The clinical information received and the specific diagnostic query are crucial for the radiologist, in order to better adapt the examination technique to the specific patient conditions.

According to the RSNA reporting initiative, consisting of a library of report templates, the MR entero-

graphy report should include these criteria: (1) clinical indication; (2) description of imaging technique and quality; (3) small bowel findings (*i.e.*, distension, peristalsis, bowel wall thickening, post-contrast findings, fistulas and/or abscess, lymph nodes); (4) collateral findings in abdominal organs; and (5) final impression indicating location and activity of disease, complications and extra-enteric findings^[38].

CONCLUSION

MR enterography is now considered a well-established imaging technique for small bowel evaluation. It plays an increasingly important role as non-invasive and effective method to evaluate the small-bowel involvement and the possible intestinal and extra-intestinal complications, in patients affected by CD.

Nevertheless, MR enterography examination should be tailored both to the patient and diagnostic query, in order to guide the clinical management.

REFERENCES

- Ananthakrishnan AN. Epidemiology and risk factors for IBD. *Nat Rev Gastroenterol Hepatol* 2015; **12**: 205-217 [PMID: 25732745 DOI: 10.1038/nrgastro.2015.34]
- Cosnes J, Gower-Rousseau C, Seksik P, Cortot A. Epidemiology and natural history of inflammatory bowel diseases. *Gastroenterology* 2011; **140**: 1785-1794 [PMID: 21530745 DOI: 10.1053/j.gastro.2011.01.055]
- Baumgart DC, Sandborn WJ. Crohn's disease. *Lancet* 2012; **380**: 1590-1605 [PMID: 22914295 DOI: 10.1016/S0140-6736(12)60026-9]
- Sartor RB. Mechanisms of disease: pathogenesis of Crohn's disease and ulcerative colitis. *Nat Clin Pract Gastroenterol Hepatol* 2006; **3**: 390-407 [PMID: 16819502 DOI: 10.1038/ncpgasthep0528]
- Di Sabatino A, Rovedatti L, Vidali F, Macdonald TT, Corazza GR. Recent advances in understanding Crohn's disease. *Intern Emerg Med* 2013; **8**: 101-113 [PMID: 21553239 DOI: 10.1007/s11739-011-0599-2]
- Hart A, Ng SC. Crohn's disease. *Medicine* 2011; **39**: 229-236 [DOI: 10.1016/j.mpmed.2011.01.004]
- Laass MW, Roggenbuck D, Conrad K. Diagnosis and classification of Crohn's disease. *Autoimmun Rev* 2014; **13**: 467-471 [PMID: 24424189 DOI: 10.1016/j.autrev.2014.01.029]
- Alzoghaibi MA. Neutrophil expression and infiltration into Crohn's intestine. *Saudi J Gastroenterol* 2005; **11**: 63-72 [PMID: 19861848 DOI: 10.4103/1319-3767.33322]
- Randall CW, Vizcete JA, Martinez N, Alvarez JJ, Garapati KV, Malakouti M, Taboada CM. From historical perspectives to modern therapy: a review of current and future biological treatments for Crohn's disease. *Therap Adv Gastroenterol* 2015; **8**: 143-159 [PMID: 25949527 DOI: 10.1177/1756283X15576462]
- Wilkins T, Jarvis K, Patel J. Diagnosis and management of Crohn's disease. *Am Fam Physician* 2011; **84**: 1365-1375 [PMID: 22230271]
- Panes J, Bouhnik Y, Reinisch W, Stoker J, Taylor SA, Baumgart DC, Danese S, Halligan S, Marincak B, Matos C, Peyrin-Biroulet L, Rimola J, Rogler G, van Assche G, Ardizzone S, Ba-Salamah A, Bali MA, Bellini D, Biancone L, Castiglione F, Ehehalt R, Grassi R, Kucharzik T, Maccioni F, Maconi G, Magro F, Martin-Comin J, Morana G, Pendsé D, Sebastian S, Signore A, Tolan D, Tielbeek JA, Weishaupt D, Wiarda B, Laghi A. Imaging techniques for assessment of inflammatory bowel disease: joint ECCO and ESGAR evidence-based consensus guidelines. *J Crohns Colitis* 2013; **7**: 556-585 [PMID: 23583097 DOI: 10.1016/j.crohns.2013.02.020]
- Leyendecker JR, Bloomfield RS, DiSantis DJ, Waters GS, Mott R, Bechtold RE. MR enterography in the management of patients with Crohn disease. *Radiographics* 2009; **29**: 1827-1846 [PMID: 19959524 DOI: 10.1148/rg.296095510]
- Tolan DJ, Greenhalgh R, Zealley IA, Halligan S, Taylor SA. MR enterographic manifestations of small bowel Crohn disease. *Radiographics* 2010; **30**: 367-384 [PMID: 20228323 DOI: 10.1148/rg.302095028]
- Laghi A, Paolantonio P, Iafrate F, Borrelli O, Dito L, Tomei E, Cucchiara S, Passariello R. MR of the small bowel with a biphasic oral contrast agent (polyethylene glycol): technical aspects and findings in patients affected by Crohn's disease. *Radiol Med* 2003; **106**: 18-27 [PMID: 12951547]
- Kuehle CA, Ajaj W, Ladd SC, Massing S, Barkhausen J, Lauenstein TC. Hydro-MRI of the small bowel: effect of contrast volume, timing of contrast administration, and data acquisition on bowel distention. *AJR Am J Roentgenol* 2006; **187**: W375-W385 [PMID: 16985108 DOI: 10.2214/AJR.05.1079]
- Griffin N, Grant LA, Anderson S, Irving P, Sanderson J. Small bowel MR enterography: problem solving in Crohn's disease. *Insights Imaging* 2012; **3**: 251-263 [PMID: 22696087 DOI: 10.1007/s13244-012-0154-3]
- Furukawa A, Saotome T, Yamasaki M, Maeda K, Nitta N, Takahashi M, Tsujikawa T, Fujiyama Y, Murata K, Sakamoto T. Cross-sectional imaging in Crohn disease. *Radiographics* 2004; **24**: 689-702 [PMID: 15143222 DOI: 10.1148/rg.243035120]
- Gourtsoyannis N, Papanikolaou N, Grammatikakis J, Maris T, Prassopoulos P. MR enteroclysis protocol optimization: comparison between 3D FLASH with fat saturation after intravenous gadolinium injection and true FISP sequences. *Eur Radiol* 2001; **11**: 908-913 [PMID: 11419161 DOI: 10.1007/s003300000805]
- Stasi C, Falchini M, Milani S. Imaging modalities for the noninvasive assessment of fibrosis in Crohn's disease. *ScientificWorldJournal* 2012; **2012**: 450151 [PMID: 22654607 DOI: 10.1100/2012/450151]
- Lee SS, Kim AY, Yang SK, Chung JW, Kim SY, Park SH, Ha HK. Crohn disease of the small bowel: comparison of CT enterography, MR enterography, and small-bowel follow-through as diagnostic techniques. *Radiology* 2009; **251**: 751-761 [PMID: 19276325 DOI: 10.1148/radiol.2513081184]
- Fidler JL, Guimaraes L, Einstein DM. MR imaging of the small bowel. *Radiographics* 2009; **29**: 1811-1825 [PMID: 19959523 DOI: 10.1148/rg.296095507]
- Maglinte DD, Gourtsoyannis N, Rex D, Howard TJ, Kelvin FM. Classification of small bowel Crohn's subtypes based on multimodality imaging. *Radiol Clin North Am* 2003; **41**: 285-303 [PMID: 12659339 DOI: 10.1016/S0033-8389(02)00117-3]
- Sinha R, Rajiah P, Murphy P, Hawker P, Sanders S. Utility of high-resolution MR imaging in demonstrating transmural pathologic changes in Crohn disease. *Radiographics* 2009; **29**: 1847-1867 [PMID: 19959525 DOI: 10.1148/rg.296095503]
- Sinha R, Verma R, Verma S, Rajesh A. MR enterography of Crohn disease: part 2, imaging and pathologic findings. *AJR Am J Roentgenol* 2011; **197**: 80-85 [PMID: 21701014 DOI: 10.2214/AJR.11.6740]
- Sempere GA, Martinez Sanjuan V, Medina Chulia E, Benages A, Tome Toyosato A, Canelles P, Bulto A, Quiles F, Puchades I, Cuquerella J, Celma J, Orti E. MRI evaluation of inflammatory activity in Crohn's disease. *AJR Am J Roentgenol* 2005; **184**: 1829-1835 [PMID: 15908538 DOI: 10.2214/ajr.184.6.01841829]
- Yoon K, Chang KT, Lee HJ. MRI for Crohn's Disease: Present and Future. *Biomed Res Int* 2015; **2015**: 786802 [PMID: 26413543 DOI: 10.1155/2015/786802]
- Del Vescovo R, Sansoni I, Caviglia R, Ribolsi M, Perrone G, Leoncini E, Grasso RF, Cicala M, Zobel BB. Dynamic contrast enhanced magnetic resonance imaging of the terminal ileum: differentiation of activity of Crohn's disease. *Abdom Imaging* 2008; **33**: 417-424 [PMID: 17639383 DOI: 10.1007/s00261-007-9267-4]
- Prassopoulos P, Papanikolaou N, Grammatikakis J, Rousomoustakaki M, Maris T, Gourtsoyannis N. MR enteroclysis imaging of Crohn disease. *Radiographics* 2001; **21** Spec No: S161-S172 [PMID: 11598255 DOI: 10.1148/radiographics.21.suppl.1.g01oc02s161]
- Scharl M, Rogler G. Pathophysiology of fistula formation in Crohn's

- disease. *World J Gastrointest Pathophysiol* 2014; **5**: 205-212 [PMID: 25133023 DOI: 10.4291/wjgp.v5.i3.205]
- 30 **Maccioni F**, Bruni A, Viscido A, Colaiacomo MC, Cocco A, Montesani C, Caprilli R, Marini M. MR imaging in patients with Crohn disease: value of T2- versus T1-weighted gadolinium-enhanced MR sequences with use of an oral superparamagnetic contrast agent. *Radiology* 2006; **238**: 517-530 [PMID: 16371574 DOI: 10.1148/radiol.2381040244]
 - 31 **Herrmann KA**, Michaely HJ, Zech CJ, Seiderer J, Reiser MF, Schoenberg SO. Internal fistulas in Crohn disease: magnetic resonance enteroclysis. *Abdom Imaging* 2006; **31**: 675-687 [PMID: 16447079 DOI: 10.1007/s00261-005-0400-y]
 - 32 **Cullen G**, Vaughn B, Ahmed A, Peppercorn MA, Smith MP, Moss AC, Cheifetz AS. Abdominal phlegmons in Crohn's disease: outcomes following antitumor necrosis factor therapy. *Inflamm Bowel Dis* 2012; **18**: 691-696 [PMID: 21648022 DOI: 10.1002/ibd.21783]
 - 33 **Latella G**, Di Gregorio J, Flati V, Rieder F, Lawrance IC. Mechanisms of initiation and progression of intestinal fibrosis in IBD. *Scand J Gastroenterol* 2015; **50**: 53-65 [PMID: 25523556 DOI: 10.3109/00365521.2014.968863]
 - 34 **Maccioni F**, Viscido A, Broglia L, Marrollo M, Masciangelo R, Caprilli R, Rossi P. Evaluation of Crohn disease activity with magnetic resonance imaging. *Abdom Imaging* 2000; **25**: 219-228 [PMID: 10823437 DOI: 10.1007/s002610000004]
 - 35 **Punwani S**, Rodriguez-Justo M, Bainbridge A, Greenhalgh R, De Vita E, Bloom S, Cohen R, Windsor A, Obichere A, Hansmann A, Novelli M, Halligan S, Taylor SA. Mural inflammation in Crohn disease: location-matched histologic validation of MR imaging features. *Radiology* 2009; **252**: 712-720 [PMID: 19635832 DOI: 10.1148/radiol.2523082167]
 - 36 **Rimola J**, Planell N, Rodríguez S, Delgado S, Ordás I, Ramírez-Morros A, Ayuso C, Aceituno M, Ricart E, Jauregui-Amezaga A, Panés J, Cuatrecasas M. Characterization of inflammation and fibrosis in Crohn's disease lesions by magnetic resonance imaging. *Am J Gastroenterol* 2015; **110**: 432-440 [PMID: 25623654 DOI: 10.1038/ajg.2014.424]
 - 37 **Cahill C**, Gordon PH, Petrucci A, Boutros M. Small bowel adenocarcinoma and Crohn's disease: any further ahead than 50 years ago? *World J Gastroenterol* 2014; **20**: 11486-11495 [PMID: 25206256 DOI: 10.3748/wjg.v20.i33.11486]
 - 38 MR Enterography Template. [accessed 2016 Apr 23]. Available from: URL: <http://www.radreport.org/template/0000051>

P- Reviewer: Anzola LK, Giudici F **S- Editor:** Gong ZM
L- Editor: A **E- Editor:** Wu HL



Basic Study

Radiology education in Europe: Analysis of results from 22 European countries

Bhavya Rehani, Yi C Zhang, Madan M Rehani, András Palkó, Lawrence Lau, Miriam N Mikhail Lette, William P Dillon

Bhavya Rehani, Yi C Zhang, William P Dillon, Department of Radiology and Biomedical Imaging, University of California, San Francisco, CA 94110, United States

Madan M Rehani, Department of Radiology, Massachusetts General Hospital, Harvard Medical School, Boston, MA 02115, United States

András Palkó, Department of Radiology, University of Szeged, H-6720 Szeged, Hungary

Lawrence Lau, Consultant Radiologist, Melbourne, 3103 Victoria, Australia

Miriam N Mikhail Lette, Consultant Diagnostic Radiologist, RAD-AID International, 1110 Geneva, Switzerland

Author contributions: Rehani B, Zhang YC and Dillon WP made substantial contributions to conception and design of the study and acquisition of data, and the remaining authors made substantial contributions to acquisition of data, or analysis and interpretation of data; all authors made substantial contributions to drafting the article or making critical revisions related to important intellectual content of the manuscript; all authors gave final approval of the version of the article to be published.

Institutional review board statement: The University of California San Francisco IRB does not consider this project as human subject research.

Conflict-of-interest statement: Bhavya Rehani is the recipient of a RSNA Education Scholar grant for development of RISEMed.org. All other authors have no conflict of interest to disclose.

Data sharing statement: Technical appendix, statistical code, and dataset available from the corresponding author at bhavya.rehani@ucsf.edu. Consent was not obtained but the potential benefits of sharing these data outweigh the potential harms because the data does not contain any personal information. The data only pertains to radiology education infrastructure on a national level.

Open-Access: This article is an open-access article which was

selected by an in-house editor and fully peer-reviewed by external reviewers. It is distributed in accordance with the Creative Commons Attribution Non Commercial (CC BY-NC 4.0) license, which permits others to distribute, remix, adapt, build upon this work non-commercially, and license their derivative works on different terms, provided the original work is properly cited and the use is non-commercial. See: <http://creativecommons.org/licenses/by-nc/4.0/>

Manuscript source: Unsolicited manuscript

Correspondence to: Bhavya Rehani, MD, Assistant Professor, Department of Radiology and Biomedical Imaging, University of California, 1001 Potrero Ave, San Francisco, CA 94110, United States. bhavya.rehani@ucsf.edu
Telephone: +1-415-2068024
Fax: +1-415-4760616

Received: July 30, 2016

Peer-review started: July 31, 2016

First decision: September 2, 2016

Revised: October 25, 2016

Accepted: December 1, 2016

Article in press: December 2, 2016

Published online: February 28, 2017

Abstract

AIM

To assess the state of radiology education across Europe by means of a survey study.

METHODS

A comprehensive 23-item radiology survey was distributed *via* email to the International Society of Radiology members, national radiological societies, radiologists and medical physicists. Reminders to complete the survey were sent and the results were analyzed over a period of 4 mo (January-April 2016). Survey questions include length of medical school and residency training;

availability of fellowship and subspecialty training; number of residency programs in each country; accreditation pathways; research training; and medical physics education. Descriptive statistics were used to analyze and summarize data.

RESULTS

Radiology residency training ranges from 2-6 years with a median of 5 years, and follows 1 year of internship training in 55% (12 out of 22) European countries. Subspecialty fellowship training is offered in 55% (12 out of 22) European countries. Availability for specialization training by national societies is limited to eight countries. For nearly all respondents, less than fifty percent of radiologists travel abroad for specialization. Nine of 22 (41%) European countries have research requirements during residency. The types of certifying exam show variation where 64% (14 out of 22) European countries require both written and oral boards, 23% (5 out of 22) require oral examinations only, and 5% (1 out of 22) require written examinations only. A degree in medical physics is offered in 59% (13 out of 22) European countries and is predominantly taught by medical physicists. Nearly all respondents report that formal examinations in medical physics are required.

CONCLUSION

Comparative learning experiences across the continent will help guide the development of comprehensive yet pragmatic infrastructures for radiology education and collaborations in radiology education worldwide.

Key words: Radiology education; European radiology survey; Radiology training; Residency; Radiology research

© **The Author(s) 2017.** Published by Baishideng Publishing Group Inc. All rights reserved.

Core tip: The authors report survey results of radiology education across 22 European countries with respect to length of training, subspecialty fellowship availability, research opportunities, and national certification and credentialing. Given the diversity in training requirements and its impact on cross-border training recognition, our results provide important insights to understand radiology education and its potential on portability across different countries in Europe.

Rehani B, Zhang YC, Rehani MM, Palkó A, Lau L, Lette MNM, Dillon WP. Radiology education in Europe: Analysis of results from 22 European countries. *World J Radiol* 2017; 9(2): 55-62 Available from: URL: <http://www.wjgnet.com/1949-8470/full/v9/i2/55.htm> DOI: <http://dx.doi.org/10.4329/wjr.v9.i2.55>

INTRODUCTION

Radiology provides cutting-edge imaging information that guides clinical decision-making. As our under-

standing of disease processes has grown more complex, radiology itself has branched into increasingly subspecialized fields. The number of distinct subspecialties in the broader scope of the discipline has significant implications for radiology teaching. Radiology training programs around the world face a challenging task in both teaching a common knowledge base across all the imaging modalities and in imparting deep subspecialty knowledge within each specialty domain.

A paucity of literature exists regarding the radiology education infrastructure worldwide^[1]. This gap in the literature can be challenging for radiologists who would like to collaborate, contribute and learn from differences, similarities and challenges in radiology education systems outside their country. Highlighting the variations in residency training may encourage exchange of best practices and experiences to better prepare trainees for an ever-evolving practice environment. There is a wide range of training infrastructure and assessment methods across the globe with respect to pre-clinical qualifications, radiology residency structure, on-call requirements, access to teaching, and certifying national or board examinations^[2].

The goal of this paper is to understand the radiology education infrastructure across the European continent, share common practices and explore different perspectives to better prepare the next generation of radiologists leaders.

MATERIALS AND METHODS

Medical school, internship, radiology residency

A comprehensive radiology survey (Table 1) was created to analyze the state of Radiology education worldwide. Each survey consisted of questions assessing medical school, radiology residency, internship, fellowships and subspecialties, medical physics, research, and accreditation, along with supplemental questions specifically targeted to their specific audience.

Subspecialty training

Apart from the overall infrastructure of radiology residency and subspecialty training, we also inquired about the number of radiology residency programs in the country, availability and type of subspecialty fellowship programs and the percentage of radiologists who have to travel outside the country for further training. We surveyed fellowship availability in the following subspecialties: Neuroradiology, Interventional Radiology, Musculoskeletal Radiology, Chest Radiology, Abdominal Radiology, Interventional Neuroradiology, Nuclear Medicine, Ultrasound, Breast Imaging, Cardiovascular Imaging, and Pediatric Radiology.

National or university based board certifying exam and research

The type of national or university based board certifying exam was questioned. Research requirements to finish

Table 1 List of survey questions

Survey questions	
A	How long is medical school in your country excluding internship?
B	Is internship required in your country?
C	How long is the radiology residency/post-graduate training in your country including internship in number of years?
D	Please provide the number of radiology residency programs in your country (rough estimate if exact figure is not known)
E	Is subspecialty radiology fellowship training available in your country?
F	Which subspecialty fellowship trainings are available in your country?
G	What percentage of radiology residents travel outside your country for subspecialized radiology training?
H	Approximately how many radiologists are there in your country?
I	If subspecialty training is not present in your country, are week- or month-long courses for advanced training and credentialing in a particular subspecialty available from your national societies?
J	Are there research requirements for radiology residents/trainees to finish training?
K	If there is a research requirement to finish training, please explain. Otherwise, please skip this question
L	What kind of national certifying exam or university based exam is required for residents to be certified in radiology?
M	How many MRI scanners are available in your country?
N	What percentage of radiology/medical imaging procedures is done by non-radiologists?
O	Is there a degree option like MSc in medical physics in your country?
P	Who teaches medical physics to radiology residents in your country?
Q	Are radiology residents formally examined for medical physics?

Table 2 Medical school, internship, and residency responses

Country	Length of medical school (excluding internship)	Internship requirement	Length of radiology residency (internship included)	Number of radiology residency programs
Armenia	6	No	2	1-5
Austria	6	Yes	6	6-10
Bulgaria	6	No	4	1-5
Croatia	6	Yes	5	6-10
Denmark	6	Yes	5	41-50
Estonia	5	No	4	1-5
Greece	6	No	5	11-20
Hungary	6	No	5	6-10
Italy	6	Yes	4	31-40
Lithuania	5	No	5	1-5
Malta	5	Yes	5	1-5
Norway	6	No	5	--
Poland	6	Yes	5	41-50
Portugal	6	Yes	5	> 80
Romania	5	Yes	4	21-30
Serbia	6	Yes	4	> 80
Slovakia	6	No	5	6-10
Slovenia	6	Yes	5	1-5
Spain	6	No	4	> 80
Sweden	6	Yes	7	51-100
Switzerland	6	No	5	21-30
United Kingdom	5	Yes	5	41-50

residency training were assessed.

Medical physics

Availability of masters programs in medical physics, medical physicists for education, and national radiation safety programs was queried.

The 23-item survey was distributed *via* email to the International Society of Radiology members, national radiological societies, radiologists and medical physicists. Reminders to complete the survey were sent and the results were analyzed over a period of 4 mo (January-April 2016).

To check the accuracy of information submitted we contacted radiologists, representatives of national radiology and neuroradiology societies by email who validated the responses and answered specific discordant questions. Descriptive statistics were used to analyze and summarize data.

RESULTS

Medical school, internship, radiology residency (Table 2)

We gathered data for 22 European countries based upon responses from national radiological society representatives or radiologists (Figure 1). Seventy-seven percent (17 out of 22) respondents report six-year medical school training. Radiology residency training ranges from 2-6 years with a median of 5 years, and follows 1 year of internship training in 55% (12 out of 22) European countries.

Subspecialty training (Table 3)

Subspecialty fellowship training is offered in 55% (12 out of 22) European countries. Within those countries, interventional radiology fellowship is the most common subspecialty followed by neuroradiology, pediatrics, and nuclear medicine fellowships. Switzerland offers the greatest variety of fellowship opportunities including neuroradiology, interventional, neuro-interventional, musculoskeletal, nuclear medicine, and pediatrics training. In contrast, Austria, Estonia and Sweden offer only one fellowship subspecialty. Availability for specialization training by national societies is limited to eight countries. For nearly all respondents, less than fifty percent of radiologists travel abroad for specialization.

Research opportunities (Table 4)

Nine of 22 (41%) European countries have research requirements during residency, which range from 1-mo to 9-mo research blocks, or at least one publication



Figure 1 Survey responses representing countries (place markers) across the European continent.

during residency with an open time frame of research commitment.

National or university based board certifying exam (Table 4)

The types of certifying exam show variation where 64% (14 out of 22) European countries require both written and oral boards, 23% (5 out of 22) require oral examinations only, and 5% (1 out of 22) require written examinations only.

Medical physics education (Table 5)

A degree in medical physics is offered in 59% (13 out of 22) European countries and is predominantly taught by medical physicists. Nearly all respondents report that formal examinations in medical physics are required.

DISCUSSION

Europe is the third most populous continent after Asia and Africa with a wide diversity of cultures and languages. Similarly, there is diversity in radiology education systems. Although medical school training is six years long in the majority of European countries included in our study, there are differences in clinical

internship requirement and length of residency training, which may vary by up to two years^[3]. Given the diversity in training requirements and its impact on cross-border training recognition, our results provide important insights to understand radiology education and its potential on portability across different countries in Europe.

While some countries have greater than eighty radiology residency programs, others like Armenia, Bulgaria, Estonia, Lithuania, Malta and Slovenia have only one to five radiology residency programs in the entire country. It is unclear if the number of residency programs is sufficient, given the size and population of these countries.

Fellowship training is available in 50% of the respondent countries in our study. The countries that offer at least one fellowship include Austria, Croatia, Estonia, Greece, Hungary, Romania, Serbia, Slovakia, Sweden, Switzerland, and United Kingdom. The most common fellowship offered is interventional radiology. Ultrasound fellowship is only available in one respondent country (Croatia), while none of the respondent countries have chest radiology fellowships.

Compared to the 2004 EAR Education Survey^[3], there has been an increase in both the number of

Table 3 Subspecialty fellowship responses

Country	Subspecialty	Types of available subspecialties											Percent radiologists traveling abroad for specialization	Approx. number of radiologists	Specialization training by national society
		Neuro	IR	MSK	Chest	Abd	Neuro-IR	NM	US	Breast	CV	Ped			
Armenia	N												< 50%	201-400	Y
Austria	Y	Y											< 50%	> 400	Y
Bulgaria	N												< 50%	Difficult to estimate	N
Croatia	Y	Y	Y						Y				< 50%	201-400	N
Denmark	N												< 50%	> 400	N
Estonia	Y		Y										< 50%	--	N
Greece	Y		Y	Y		Y						Y	< 50%	--	--
Hungary	Y	Y	Y				Y			Y		Y	< 50%	> 400	Y
Italy	N												< 50%	> 400	Y
Lithuania	N												< 50%	201-400	Y
Malta	N												> 50%	< 50	Y
Norway	---												< 50%	> 400	--
Poland	N												< 50%	> 400	N
Portugal	N												< 50%	> 400	N
Romania	Y	Y				Y		Y					< 50%	> 400	N
Serbia	Y		Y			Y							< 50%	101-200	N
Slovakia	Y		Y							Y	Y	Y	--	> 400	N
Slovenia	N												< 50%	101-200	N
Spain	N												< 50%	> 400	N
Sweden	Y							Y					0%	--	--
Switzerland	Y	Y	Y	Y			Y	Y				Y	< 50%	> 400	--
United Kingdom	Y	Y	Y				Y	Y					< 50%	> 400	N

Neuro: Neuroradiology; IR: Interventional radiology; MSK: Musculoskeletal radiology; Chest: Chest radiology; Abd: Abdominal radiology; Neuro-IR: Interventional neuroradiology; NM: Nuclear medicine; US: Ultrasound; Breast: Breast imaging; CV: Cardiovascular imaging; Ped: Pediatric radiology; Y: Yes; N: No.

countries that offer fellowship training as well as in the variety of available subspecialties. For example, fellowship training in Switzerland now encompasses interventional radiology (IR), musculoskeletal (MSK), Neurointerventional, and Nuclear Medicine. Similarly, Slovakia increased fellowship training to include Interventional Radiology, Breast, Cardiovascular, and Pediatrics. Estonia, Greece, Hungary, and Romania are additional examples of countries that expanded subspecialty training.

Given rapid innovation across many imaging modalities, increasing exposure to fellowship training is fast becoming a priority to ensure that residents learn up-to-date subspecialty knowledge worldwide. Our results show that less than 50% of radiologists travel outside their respective countries for training. It has been discussed that practicing radiologists understandably face the challenge of meeting clinical demands while maintaining teaching responsibilities^[4]. Individual didactic teaching sessions may not be feasible in a high-volume work environment^[5].

This creates a potential role for interactive e-learning teaching modules^[6-9] and virtual education^[10] to supplement education in a particular subspecialty for self-motivated learners. Accessible electronic modules have served as useful extensions to radiology teaching^[11,12]. The European Society of Radiology (ESR) offers accre-

dited electronic modules categorized by subspecialty content with optional self assessments^[13]. The ESR has also implemented and continuously updated the European Training Curriculum, a subspecialty-specific framework organized by training level that enhances the quality of radiology education throughout Europe^[14].

The European Society of Radiology offers courses to help prepare trainees for the European Diploma in Radiology (EDiR)^[15]. The EDiR, a certificate of excellence, helps standardize radiology training in the setting of varied certification methods across Europe as demonstrated in our survey results.

Basic and translational research exposure form a significant component of radiology education and should be made widely available^[16]. Residents can make considerable contributions to the field because they have a unique perspective on the day-to-day practice from an "in-the-trenches" point of view, ranging from image interpretation to workflow management and on-call demands. Residents also have first hand experiences with different technology platforms and thus can bring new ideas that drive innovation in radiology. In our surveyed European countries, fewer than half of European countries have dedicated research blocks during residency. Challenges in promoting research include limited finances, lack of incentives for researchers, issues of career planning, and gender

Table 4 Certification and research responses

Country	Research requirement for residency	If yes, describe research requirement	Type of certifying exam required	Number of MRI scanners	Percentage of radiology procedures by non-radiologists
Armenia	No	---	Oral	6-10	---
Austria	Yes	9-mo research	Written and oral	> 100	15%-20%
Bulgaria	No	---	Oral	10-50	> 20%
Croatia	Yes	Indexed publication	Written and oral	10-50	---
Denmark	Yes	1-mo research	Oral	10-50	0%-5%
Estonia	No	---	Oral	---	---
Greece	Yes	---	Written and oral	---	---
Hungary	No	---	Written and oral	5-10	---
Italy	Yes	At least one research project	Written and oral	> 100	0%-5%
Lithuania	Yes	Research presentation	Written and oral	10-50	---
Malta	No	---	Written and oral	6-10	---
Norway	---	---	---	> 100	---
Poland	No	---	Written and oral	> 100	15%-20%
Portugal	No	---	Oral	51-100	> 20%
Romania	No	---	Written and oral	< 5	---
Serbia	No	---	Written and oral	10-50	5%-10%
Slovakia	No	---	Written and oral	10-50	---
Slovenia	Yes	At least one publication during residency	Written and oral	10-50	10%-15%
Spain	No	---	Written	> 100	10%-15%
Sweden	Yes	---	---	---	---
Switzerland	No	---	Written and oral	51-100	> 20%
United Kingdom	Yes	Basic research competency	Written and oral	> 100	> 20%

Table 5 Medical physics responses

Country	Medical physics degree	Medical physics taught by	Formal examination of medical physics
Armenia	Yes	Radiologist	Yes, there is a question paper combined with another subject Only oral test
Austria	No	Radiologist	Only written test
Bulgaria	No	Radiologist	Yes, there is a separate question paper on this subject Radiologists review the answer sheets for medical physics portion
Croatia	No	Radiologist	Radiologists review the answer sheets for medical physics part Radiologists conduct oral exam in medical physics and radiation safety
Denmark	Yes	Medical physicist	Yes, there is a separate question paper on this subject Only written test Radiologists review the answer sheets for medical physics portion
Estonia	Yes	---	---
Greece	Yes	Medical physicist	Only oral test
Hungary	Yes	Medical physicist	There is both oral and written test
Italy	No	Medical physicist	Only oral test
Lithuania	No	Medical physicist	Yes, there is a separate question paper on this subject Yes, there is a question paper combined with another subject
Malta	Yes	Medical physicist	Yes, there is a question paper combined with another subject Only written test
Norway	No	Medical physicist	Yes, there is a question paper combined with another subject
Poland	Yes	Radiologist	Only written test
Portugal	No	Other	---
Romania	No	Medical physicist	Yes there is a question paper along combined with another subject Radiologists review the answer sheets for medical physics part
Serbia	Yes	Medical physicist	Yes, there is a separate question paper on this subject Yes, there is a question paper combined with another subject
Slovakia	Yes	Medical physicist	Yes, there is a question paper combined with another subject There is both oral and written test
Slovenia	No	Medical physicist	Radiologists review the answer sheets for medical physics portion
Spain	Yes	Medical physicist	Only written test
Sweden	Yes	Medical physicist	Yes, there is a separate question paper on this subject
Switzerland	Yes	Medical physicist	Yes, there is a separate question paper on this subject Only written test
United Kingdom	Yes	Medical physicist	Radiologists review the answer sheets for medical physics portion Yes, there is a separate question paper on this subject Radiologists review the answer sheets for medical physics portion

issues^[16]. This also seems to be a challenge worldwide and increased emphasis on research during residency has been encouraged^[17-19]. Increasing time and mentorship resources for research will help establish radiology innovation early in the career pathway. Radiologists around the world could assist in mentoring trainees in research outside their programs to encourage future world leaders in radiology.

Medical physics and radiation safety is particularly important given the reported radiation injuries due to imaging^[20-22]. The ESR recently noted an increase in inappropriate exposure to ionizing radiation along with significant variations in dosimetry for the same examination^[23]. To reduce patient exposure to unnecessary radiation, the ESR plans to implement individual patient dose tracking, mobile dose information for physicians, and radiation protection training with certification^[23]. Nearly all survey respondents reported that formal examination in medical physics is required in Europe. In addition, 70% had medical physics training from medical physicist rather than a radiologist. Medical physics degree programs are also offered by majority of respondent European countries.

Each European country included in our study offers a unique perspective on radiology education based on what is feasible for resident teaching, subspecialty training, and research. Comparative learning experiences across the continent will help guide the development of comprehensive yet pragmatic infrastructures for radiology education and collaborations in radiology education worldwide.

Limitations of our study include a sample size of twenty out of a total of forty-eight European countries. As such, our data may not be representative of the radiologic education landscape across all of Europe. In addition, our survey response rate indicates that our results represent only a fraction of all countries in Europe, likely due to the approach in questionnaire distribution and collection. Our survey channels through the International Society of Radiology also may have introduced bias in selecting for countries that are its participating members.

Future research may involve potential collaboration with the European Society of Radiology to gain insight into the radiology infrastructure across a greater number of European countries. E-learning modules may help augment the variety of fellowship training and increase resident engagement with real time communication and feedback. Innovative technology platforms that offer indexed and searchable didactic content will contribute to a sustainable solution for international radiology education.

ACKNOWLEDGMENTS

We would like to profoundly thank International Society of Radiology for collaboration and radiologists in Europe who participated in this survey.

COMMENTS

Background

The status of radiology education in Europe, particularly in specialty fellowship training and research, merits an in-depth study in order to gain an understanding of challenges and potential collaborations among the regional training programs.

Research frontiers

Recent advances in technology platforms for web-based applications and mobile tools have enabled trainees to gain access to specialty training that may supplement availability of radiology education at their home institutions.

Innovations and breakthroughs

This study demonstrates that subspecialty fellowship training is offered in approximately half of European countries and the availability for specialization training by national societies is limited to eight countries. Other differences in board certifications and medical physics curricula differ among the regional training programs. The European Training Curriculum serves as a reference for the establishment and revision of national training programs and sets the basis for the European Diploma in Radiology exam.

Applications

Practical applications of this study include the use of country-specific training availability data to augment radiology education and in providing access to online teaching curricula to supplement radiology education.

Peer-review

This is a well-written paper regarding radiology education in Europe.

REFERENCES

- 1 **Di Marco L**, Conway WF, Chapin R. Radiology Resident Education in France from Medical School Through Board Certification. *J Am Coll Radiol* 2015; **12**: 1097-1102 [PMID: 26435123 DOI: 10.1016/j.jacr.2015.06.030]
- 2 **Willatt JM**, Mason AC. Comparison of radiology residency programs in ten countries. *Eur Radiol* 2006; **16**: 437-444 [PMID: 15702337 DOI: 10.1007/s00330-004-2635-3]
- 3 **European Society of Radiology**. Radiological Training Programmes in Europe: EAR Education Survey - Analysis of Results. 2004 EAR Education Committee. [accessed 2016 May 8]. Available from: URL: https://www.myesr.org/html/img/pool/ESR_brochure_05.pdf
- 4 **Gunderman RB**, Kang YP, Fraley RE, Williamson KB. Teaching the teachers. *Radiology* 2002; **222**: 599-603 [PMID: 11867772 DOI: 10.1148/radiol.2223010825]
- 5 **Cohen MD**, Gunderman RB. Academic radiology: sustaining the mission. *Radiology* 2002; **224**: 1-4 [PMID: 12091654 DOI: 10.1148/radiol.2241011741]
- 6 **Colucci PG**, Kostandy P, Shrauner WR, Arleo E, Fuortes M, Griffin AS, Huang YH, Juluru K, Tsiouris AJ. Development and utilization of a web-based application as a robust radiology teaching tool (radstax) for medical student anatomy teaching. *Acad Radiol* 2015; **22**: 247-255 [PMID: 25964956]
- 7 **Carriero A**, Bonomo L, Calliada F, Campioni P, Colosimo C, Cotroneo A, Cova M, Ettorre GC, Fugazzola C, Garlaschi G, Macarini L, Mascalchi M, Meloni GB, Midiri M, Mucelli RP, Rossi C, Sironi S, Torricelli P, Beomonte BZ, Zompatori M, Zuiani C. E-learning in radiology: an Italian multicentre experience. *Eur J Radiol* 2012; **81**: 3936-3941 [PMID: 22902406 DOI: 10.1016/j.ejrad.2012.07.007]
- 8 **Pinto A**, Brunese L, Pinto F, Acampora C, Romano L. E-learning and education in radiology. *Eur J Radiol* 2011; **78**: 368-371 [PMID: 21255951 DOI: 10.1016/j.ejrad.2010.12.029]
- 9 **Zafar S**, Safdar S, Zafar AN. Evaluation of use of e-Learning in undergraduate radiology education: a review. *Eur J Radiol* 2014; **83**: 2277-2287 [PMID: 25242658 DOI: 10.1016/j.ejrad.2014.08.017]
- 10 **RISE**: Real-time International Student Education. [accessed 2016 June 27]. Available from: URL: <http://www.risemed.org>

- 11 **Farkhondeh A**, Geist JR. Evaluation of Web-Based Interactive Instruction in Intraoral and Panoramic Radiographic Anatomy. *J Mich Dent Assoc* 2015; **97**: 34-38 [PMID: 26292503]
- 12 **Scherer A**, Kröpil P, Heusch P, Buchbender C, Sewerin P, Blondin D, Lanzman RS, Miese F, Ostendorf B, Bölke E, Mödler U, Antoch G. Case-based interactive PACS learning: introduction of a new concept for radiological education of students. *Radiologe* 2011; **51**: 969-970, 973-977 [PMID: 22033604 DOI: 10.1007/s00117-011-2241-8]
- 13 eLearning - Education on Demand. [accessed 2016 June 27]. Available from: URL: <https://cslide.ctimeetingtech.com/library/esr/home>
- 14 European Training Curriculum for Radiology. [accessed 2016 June 27]. Available from: URL: http://www.myesr.org/cms/website.php?id=en/education_training/european_training_curriculum_for_radiology.htm
- 15 EDiR - European Diploma in Radiology. [accessed 2016 June 23]. Available from: URL: http://www.myesr.org/cms/website.php?id=29634/en/education_training/elearning/european_diploma_in_radiology_edir.htm
- 16 **European Society of Radiology (ESR)**. Research education in Europe: an opinion paper by the European Society of Radiology. *Insights Imaging* 2015; **6**: 157-162 [PMID: 25763995 DOI: 10.1007/s13244-015-0397-x]
- 17 **Alderson PO**, Bresolin LB, Becker GJ, Thrall JH, Dunnick NR, Hillman BJ, Lee JK, Nagy EC. Enhancing research in academic radiology departments: recommendations of the 2003 Consensus Conference. *J Am Coll Radiol* 2004; **1**: 591-596 [PMID: 17411658 DOI: 10.1016/j.jacr.2004.03.011]
- 18 **Barker CF**. Making imaging research a part of radiology resident training. *Acad Radiol* 2013; **20**: 135-136 [PMID: 23395241 DOI: 10.1016/j.acra.2012.11.003]
- 19 **Costello JR**, Mullins ME, Votaw JR, Karolyi DR, Kalb B, Gonzales P, Fornwalt B, Meltzer CC. Establishing a new radiology residency research track. *Acad Radiol* 2013; **20**: 243-248 [PMID: 23085410 DOI: 10.1016/j.acra.2012.08.011]
- 20 **Valk PE**, Dillon WP. Radiation injury of the brain. *AJNR Am J Neuroradiol* 1991; **12**: 45-62 [PMID: 7502957]
- 21 **Sodickson A**, Baeyens PF, Andriole KP, Prevedello LM, Nawfel RD, Hanson R, Khorasani R. Recurrent CT, cumulative radiation exposure, and associated radiation-induced cancer risks from CT of adults. *Radiology* 2009; **251**: 175-184 [PMID: 19332852 DOI: 10.1148/radiol.2511081296]
- 22 **Schonfeld SJ**, Lee C, Berrington de González A. Medical exposure to radiation and thyroid cancer. *Clin Oncol (R Coll Radiol)* 2011; **23**: 244-250 [PMID: 21296564 DOI: 10.1016/j.clon.2011.01.159]
- 23 **European Society of Radiology**. ESR statement on radiation protection: globalisation, personalised medicine and safety (the GPS approach). *Insights Imaging* 2013; **4**: 737-739 [PMID: 24092563 DOI: 10.1007/s13244-013-0287-z]

P- Reviewer: Boffano P, Gao BL, Pinto A, Quattrocchi CC, Wan YL
S- Editor: Kong JX **L- Editor:** A **E- Editor:** Wu HL



Basic Study

Radiation dose enhancement in skin therapy with nanoparticle addition: A Monte Carlo study on kilovoltage photon and megavoltage electron beams

Xiao J Zheng, James C L Chow

Xiao J Zheng, Department of Physics, Ryerson University, Toronto, ON M5B 2K3, Canada

James C L Chow, Radiation Medicine Program, Princess Margaret Cancer Centre, Department of Radiation Oncology, University of Toronto, Toronto, ON M5G 2M9, Canada

Author contributions: Zheng XJ performed the Monte Carlo experiments and data analyses which were reviewed by Chow JCL; the figures of the manuscript were prepared by Zheng XJ and Chow JCL; Chow JCL designed the study and wrote the manuscript.

Institutional review board statement: This study does not involve any human or animal subject.

Informed consent statement: This study does not involve any human subject.

Conflict-of-interest statement: The authors declare no conflicts of interest regarding this manuscript.

Open-Access: This article is an open-access article which was selected by an in-house editor and fully peer-reviewed by external reviewers. It is distributed in accordance with the Creative Commons Attribution Non Commercial (CC BY-NC 4.0) license, which permits others to distribute, remix, adapt, build upon this work non-commercially, and license their derivative works on different terms, provided the original work is properly cited and the use is non-commercial. See: <http://creativecommons.org/licenses/by-nc/4.0/>

Manuscript source: Invited manuscript

Correspondence to: James C L Chow, PhD, Radiation Medicine Program, Princess Margaret Cancer Centre, Department of Radiation Oncology, University of Toronto, 610 University Avenue, Toronto, ON M5G 2M9, Canada. james.chow@rmp.uhn.on.ca
Telephone: +1-416-9464501
Fax: +1-416-9466566

Received: August 11, 2016

Peer-review started: August 11, 2016

First decision: September 28, 2016

Revised: October 24, 2016

Accepted: December 7, 2016

Article in press: December 9, 2016

Published online: February 28, 2017

Abstract

AIM

To investigate the dose enhancement due to the incorporation of nanoparticles in skin therapy using the kilovoltage (kV) photon and megavoltage (MV) electron beams. Monte Carlo simulations were used to predict the dose enhancement when different types and concentrations of nanoparticles were added to skin target layers of varying thickness.

METHODS

Clinical kV photon beams (105 and 220 kVp) and MV electron beams (4 and 6 MeV), produced by a Gulmay D3225 orthovoltage unit and a Varian 21 EX linear accelerator, were simulated using the EGSnrc Monte Carlo code. Doses at skin target layers with thicknesses ranging from 0.5 to 5 mm for the photon beams and 0.5 to 10 mm for the electron beams were determined. The skin target layer was added with the Au, Pt, I, Ag and Fe₂O₃ nanoparticles with concentrations ranging from 3 to 40 mg/mL. The dose enhancement ratio (DER), defined as the dose at the target layer with nanoparticle addition divided by the dose at the layer without nanoparticle addition, was calculated for each nanoparticle type, nanoparticle concentration and target layer thickness.

RESULTS

It was found that among all nanoparticles, Au had the

highest DER (5.2-6.3) when irradiated with kV photon beams. Dependence of the DER on the target layer thickness was not significant for the 220 kVp photon beam but it was for 105 kVp beam for Au nanoparticle concentrations higher than 18 mg/mL. For other nanoparticles, the DER was dependent on the atomic number of the nanoparticle and energy spectrum of the photon beams. All nanoparticles showed an increase of DER with nanoparticle concentration during the photon beam irradiations regardless of thickness. For electron beams, the Au nanoparticles were found to have the highest DER (1.01-1.08) when the beam energy was equal to 4 MeV, but this was drastically lower than the DER values found using photon beams. The DER was also found affected by the depth of maximum dose of the electron beam and target thickness. For other nanoparticles with lower atomic number, DERs in the range of 0.99-1.02 were found using the 4 and 6 MeV electron beams.

CONCLUSION

In nanoparticle-enhanced skin therapy, Au nanoparticle addition can achieve the highest dose enhancement with 105 kVp photon beams. Electron beams, while popular for skin therapy, did not produce as high dose enhancements as kV photon beams. Additionally, the DER is dependent on nanoparticle type, nanoparticle concentration, skin target thickness and energies of the photon and electron beams.

Key words: Skin therapy; Monte Carlo simulation; Nanoparticle; Dose enhancement; Photon and electron beams

© The Author(s) 2017. Published by Baishideng Publishing Group Inc. All rights reserved.

Core tip: This paper investigated the dose enhancement effect due to nanoparticle addition using the kilovoltage (kV) photon and megavoltage (MV) electron beams in skin therapy. Dose enhancements of skin layers with different thicknesses were studied with various nanoparticle types, nanoparticle concentrations, radiation beam types and beam energies using Monte Carlo simulation. From the results, it is found that kV photon beams can achieve much higher dose enhancements at the skin compared to MV electron beams. Moreover, gold nanoparticles, which had the highest atomic number in our study, provided the highest dose enhancement for nanoparticle-enhanced skin therapy.

Zheng XJ, Chow JCL. Radiation dose enhancement in skin therapy with nanoparticle addition: A Monte Carlo study on kilovoltage photon and megavoltage electron beams. *World J Radiol* 2017; 9(2): 63-71 Available from: URL: <http://www.wjgnet.com/1949-8470/full/v9/i2/63.htm> DOI: <http://dx.doi.org/10.4329/wjr.v9.i2.63>

INTRODUCTION

In cancer treatment, chemotherapy and radiotherapy are two popular methods to control the tumour cell. Chemotherapy uses anticancer drugs at molecular, cellular and tissue levels through various mechanisms such as enhancing the double-strand break due to the conformation changes in chromatin and DNA, and inhibiting the DNA repair processes leading to the conversion of sublethal DNA damage^[1-5]. In radiotherapy, on the other hand, it is necessary to provide conformal dose coverage at the target (tumour) while sparing the surrounding normal tissues. Target dose escalation is therefore desired to increase the tumour control probability, but at the same time decrease normal tissue complication probabilities for organs-at-risk (OARs). Under such circumstances, nanoparticle-enhanced radiotherapy is suggested for providing dose enhancement in the target^[6-8]. There are two advantages of accumulating heavy-atom nanoparticles within the tumour. First, due to the increased compositional atomic number of tumours with nanoparticles, imaging contrast is increased due to the enhancement of photoelectric absorption when using a kilovoltage (kV) photon source (e.g., computed tomography)^[9,10]. Such contrast enhancement can help the radiation staff to identify and outline the target during radiation treatment planning. Second, the increase in the photoelectric cross-section due to the addition of nanoparticles increases the dose absorption of the target^[11,12]. This results in dose enhancement at the target and improved treatment outcome. Preclinical results of Au nanoparticle enhanced radiotherapy have proven that the addition of 1.9 nm Au nanoparticles to mammary cancer cells of mice can lead to a significant increase in survival rate of 86% compared to 20% with radiotherapy alone and 0% with Au nanoparticle addition alone^[13]. For radiotherapy of EGFR-positive cancer, a facile synthetic method of indium-111 to Au nanoparticle was developed with high payload to enhance the delivery of radioactivity to the tumour^[14]. Au nanoparticle was also studied as a drug-delivery platform in transient anti-angiogenic therapies to induce tumour vascular normalization and enhance the efficacy of the cytotoxic drugs^[15]. Moreover, tumour radiosensitizations for breast and prostate with Au nanoparticle addition were studied both *in vitro* and *in vivo* based on the cell-line and small-animal model^[16,17].

Since dose enhancement is due to an increase in the photoelectric cross-section by raising the compositional atomic number through heavy-atom nanoparticle addition, such enhancement decreases when using megavoltage (MV) instead of kV range photon beams where Compton interactions dominate. Unlike preclinical models using kV photon beams, human radiotherapy requires MV energies for deep-seated targets. This is due to the considerable differences in size and thickness for humans compared to small animals and therefore higher penetrative MV photon beams are required^[18].

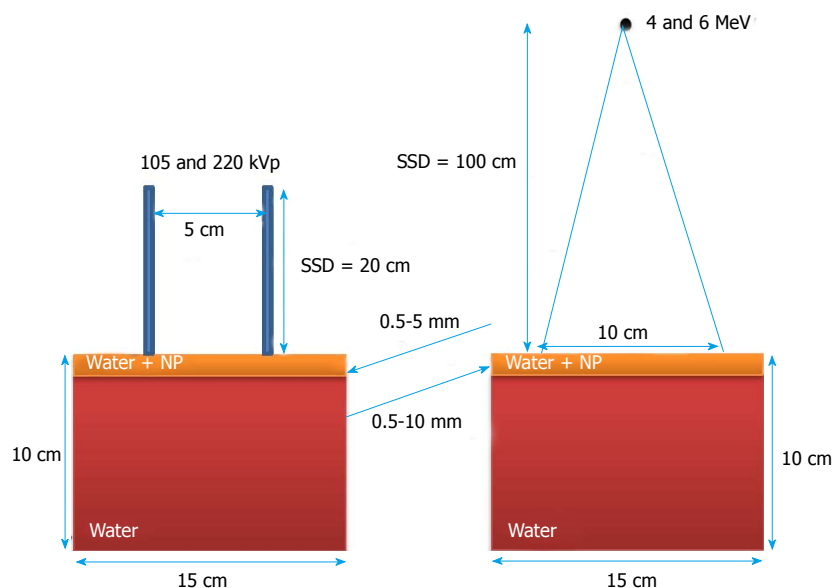


Figure 1 Schematic diagrams (not-to-scale) showing the experimental setups of the kilovoltage photon beams (left) and megavoltage electron beams (right). The thicknesses of the skin target layer (water mixed with nanoparticles) ranged from 0.5-5 mm for the photon beams and 0.5-10 mm for the electron beams. SSD: Source-to-surface distance.

Dose enhancement using MV photon beams is lower than kV beams when treating deep-seated tumours in radiotherapy. In skin therapy, however, kV photon beams are used to treat superficial lesions as the target is located on the patient's surface. Therefore, sufficient dose enhancement at the target can be achieved using kV (e.g., 105 and 220 kVp) photon beams^[19,20]. The aim of this study is to investigate the dose enhancement due to nanoparticle addition of various types, concentrations, beam energies for several skin target thicknesses. For dosimetric comparison, similar nanoparticle additions using electron beams were carried out because electron therapy is also popular in skin lesion treatment. In this study, lower electron beam energies of 4 and 6 MeV with relatively short electron paths were focused on as they were clinically used to treat superficial lesions^[19].

Monte Carlo simulations using EGSnrc^[21] were used to calculate doses of the skin target using the macroscopic approach^[22]. Heterogeneous phantoms were used with the clinical kV photon and MV electron beams from the orthovoltage unit and medical linear accelerator in this study, respectively. The dose enhancement ratio (DER), defined here as the ratio of the dose in the skin target with nanoparticle addition to the dose of target without nanoparticle addition, was determined with variations of the nanoparticle type, concentration and skin target thickness using the photon and electron beams.

MATERIALS AND METHODS

Calculation geometry

Figure 1 shows the calculation geometry used in the Monte Carlo simulations. A water phantom with dimensions of 15 × 15 × 10 cm³ was used in this study. The top skin target layers with thicknesses ranging from 0.5-5 mm for the photon beams and 0.5-10 mm for the electron beams. While varying the skin target thickness, the height of the phantom was

kept constant at 10 cm. For the target layer, different nanoparticles consisting of Au, Pt, I, Ag and Fe₂O₃ with atomic numbers equal to 79, 78, 53, 47 and 23 were mixed with water for 5 concentrations (3, 7, 18, 30 and 40 mg/mL).

For the kV photon beam irradiations, the 105 and 220 kVp beams produced by a Gulmay D3225 orthovoltage unit were used. The photon beams were conformed by a standard circular applicator of 5 cm diameter with a source-to-surface distance (SSD) equal to 20 cm. In the electron beam irradiations, the 4 and 6 MeV electron beams produced by a Varian 21 EX linear accelerator were used with a 10 × 10 cm² standard square cutout in the bottom of a 10 × 10 cm² applicator (not shown in Figure 1). The SSD of the electron beam irradiation was set to 100 cm. It should be noted that both the photon and electron beam irradiations were based on typical clinical geometries for skin therapy.

Monte Carlo simulation

The EGSnrc code developed by the National Research Council Canada was used in this study^[21]. For the kV photon beams, the spectral shape in this code was improved by implementing the electron impact ionization model. In addition, the directional bremsstrahlung splitting approach was used to enhance the efficiency of energy transitions from the electron current to photons^[23].

Phase-space files of 105 and 220 kVp photon beams, produced by a Gulmay D3225 orthovoltage machine using a standard open circular applicator with diameter of 5 cm, were generated using the BEAMnrc code^[24]. The SSD was set at 20 cm. The treatment head model in simulation included the X-ray tube, primary collimator, filter, ionization chamber and applicator with material and geometry information provided by the manufacturer. Phase-space files containing 36 million particles were generated including information on energy, orientation,

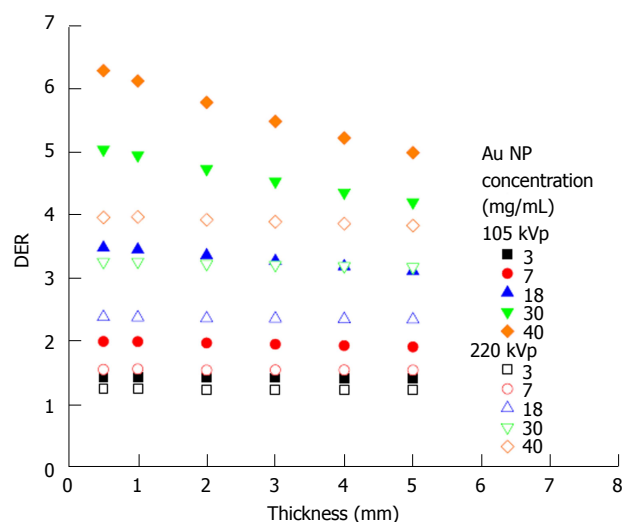


Figure 2 Relationship between the dose enhancement ratio and skin target thickness with variation of Au nanoparticle concentration using the 105 and 220 kVp photon beams. DER: Dose enhancement ratio.

type, charge and position of particles crossing the scoring plane at the bottom of the applicator. The phase-space files were verified by comparing the percentage depth doses and beam profiles in water measured by a parallel-plate ionization chamber and water tank elsewhere^[19]. For the 4 and 6 MeV electron beams produced by the Varian 21 EX linear accelerator, phase-space files were generated from BEAMnrc using a $10 \times 10 \text{ cm}^2$ applicator with an SSD of 100 cm. Details of the geometries and materials of the treatment head were provided by the linear accelerator manufacturer, and the parameter reduced electron step transport algorithm II (PRESTA II) was used as the electron-step algorithm^[25]. The phase-space files for the electron beams contained 55 million particles, and were verified elsewhere by comparing the percentage depth doses and beam profiles between the Monte Carlo and measurement results using radiographic film, ionization chamber and solid water phantom^[19].

The material data sets for different concentrations of nanoparticles were created using the EGSnrc-based PEGS4 code^[21]. Data sets regarding particle interaction cross-sections for various concentrations (3, 7, 18, 30 and 40 mg/mL) of Au, Pt, I, Ag and Fe_2O_3 nanoparticles mixed with water were generated. DOSXYZnrc was used to calculate the dose at the skin target layer irradiated by the photon and electron beams^[26]. For the 105 and 220 kVp photon beams, 150 million histories were run for each calculation with the energy cut-off for the electron (ECUT) and photon (PCUT) transport set to 521 keV and 1 keV. The PRESTA II was used for the electron-step algorithm, and the spin effect, bound Compton scattering, Rayleigh scattering, atomic relaxation and electron impact ionization options were all used in the simulation. For the simulation using the electron beams, the ECUT, PCUT and ESTEPE were set to 521 keV, 10 keV and 25%, respectively^[27]. Two hundred million histories were simulated in Monte

Carlo for the 4 and 6 MeV electron beams. Under these approaches, the relative dose error (statistical uncertainty as a fraction of dose in the voxel) was found to be around 1% according to the Monte Carlo output files^[21].

DER

The doses determined from the skin target layer with different thicknesses, nanoparticle concentrations, and types using Monte Carlo simulations were used to calculate the DER, defined in this study as:

$$\text{DER} = \frac{\text{Dose with nanoparticle addition in the target layer}}{\text{Dose without nanoparticle addition in the target layer}} \quad (1)$$

It can be seen from Eq. (1) that due to the general dose enhancement effect from nanoparticle addition, the DER is typically close to or larger than one.

RESULTS

The dependency of the DER on skin target thickness using Au nanoparticles with increasing concentration (3–40 mg/mL) and kV photon beams is shown in Figure 2. The target thickness ranged from 0.5 to 5 mm. For other nanoparticle materials, dependence of the DER on target thickness is shown in Figure 3 for nanoparticle concentrations equal to 7, 18 and 40 mg/mL using the 105 and 220 kVp photon beams. Figure 4 reveals the relationship between the DER and Au nanoparticle concentration for different target thicknesses. In addition, Figure 5 shows relationships between the DER and nanoparticle concentration for different nanoparticle types with target thicknesses equal to 0.5, 3 and 5 mm, respectively. For the 4 and 6 MeV electron beam irradiations, Figure 6 shows the dependence of the DER on the target thickness for the Au nanoparticles with different concentrations. Variations of the DER for the Au nanoparticles with different target thicknesses are shown in Figure 7 using 4 and 6 MeV electron beams, respectively. The relationship between the DER and nanoparticle concentration for different nanoparticle types are shown in Figure 8 with the target thickness equal to 2 mm.

DISCUSSION

Kilovoltage photon beams

Dependence of the DER on skin target thickness:

It can be seen from Figure 2 that the dependence of the DER on the skin target thickness was not significant, when the Au nanoparticle was added with concentrations ranging from 3 to 40 mg/mL using the 220 kVp photon beams. For the 105 kVp photon beams, however, the DER was found increasing with a decrease of target thickness when the nanoparticle concentration was higher than 18 mg/mL. This shows that the dose enhancement effect on the target thickness was more

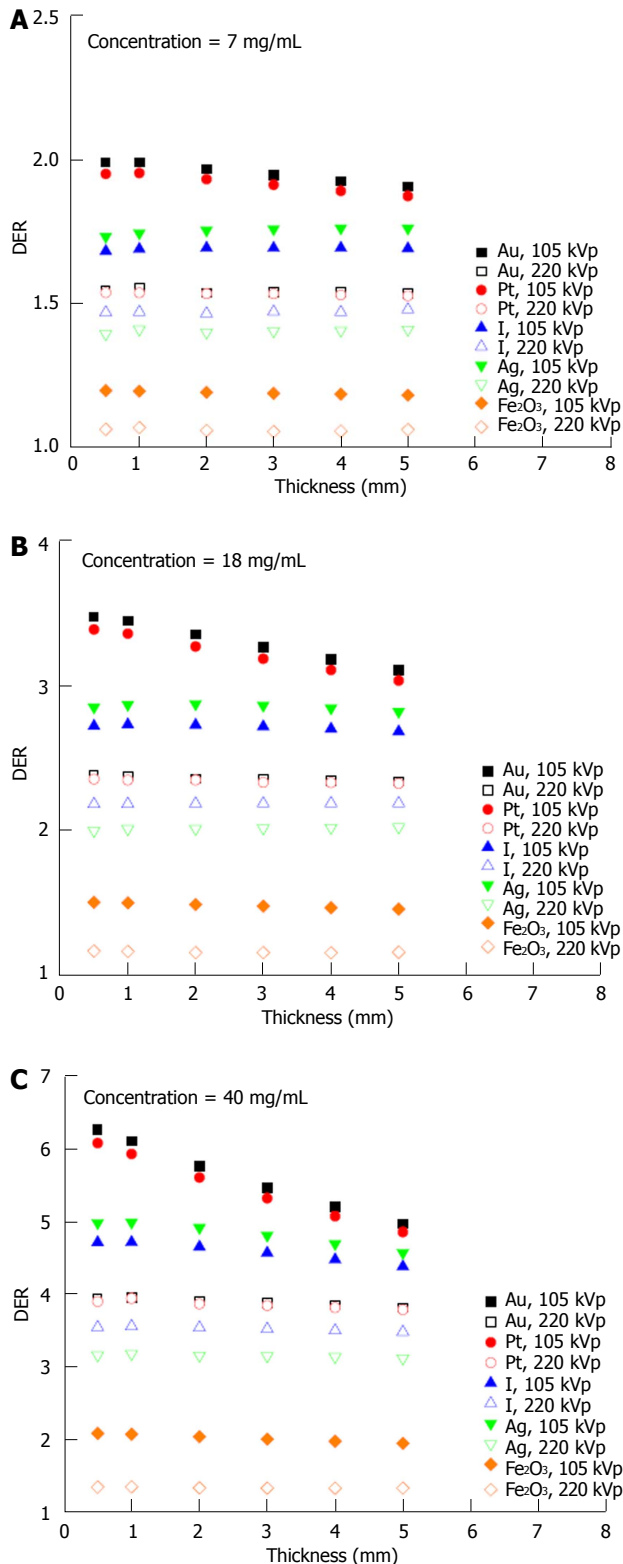


Figure 3 Relationship between the dose enhancement ratio and skin target thickness with nanoparticle concentrations of (A) 7, (B) 18 and (C) 40 mg/mL using the Au, Pt, I, Ag and Fe₂O₃ nanoparticles for the 105 and 220 kVp photon beams. DER: Dose enhancement ratio.

sensitive to lower energy photon beams and higher nanoparticle concentration.

For the dependence of the DER on skin target thickness for other nanoparticles, Figure 3 shows the

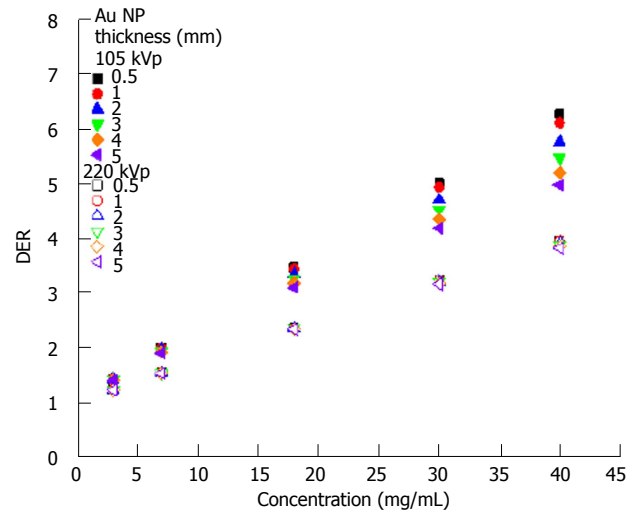


Figure 4 Relationship between the dose enhancement ratio and Au nanoparticle concentration with variation of the skin target thickness using the 105 and 220 kVp photon beams. DER: Dose enhancement ratio.

relationship between the two for nanoparticle concentrations equal to 7, 18 and 40 mg/mL. In Figure 3, it is seen that the dose enhancement was generally affected by the atomic number of the nanoparticle and the quality of the kV photon beams. The DER for the Ag nanoparticles was slightly higher than for I for the 105 kVp photon beams. However, the atomic number of Ag (47) is smaller than I (53). This may be due to the energy spectrum of the polyenergetic 105 kVp photon beam produced by the orthovoltage machine^[20]. In Figure 3, the Au nanoparticles are seen to have the highest DERs of 2, 3.5 and 6.3 when the nanoparticle concentration was 7, 18 and 40 mg/mL, respectively. A higher DER was found for higher nanoparticle concentrations and thinner target thicknesses due to the higher depth-dose gradient from the 105 kVp photon beams compared to 220 kVp^[28]. Moreover, dependence of the DER on the target thickness was not significant for the Pt, I, Ag and Fe₂O₃ nanoparticles using 220 kVp photon beams.

Dependence of the DER on nanoparticle concentration: In Figure 4, it can be seen that the DER increased with an increase of Au nanoparticle concentration from 3 to 40 mg/mL using the 105 and 220 kVp photon beams. For the 220 kVp photon beams, the increase of the DER in the nanoparticle concentration did not vary with the target thickness significantly. For the 105 kVp photon beams, however, the rate of change of the DER with nanoparticle concentration was found to increase with a decrease of target thickness. When the Au nanoparticle concentration increased from 3 to 40 mg/mL, the DER was found to increase from 1.4 to 6.3 when using 105 kVp photon beams, respectively.

The degree of DER variation on the nanoparticle concentration was found to be more significant when the atomic number of the nanoparticles increased, with the Au nanoparticles producing the highest DER

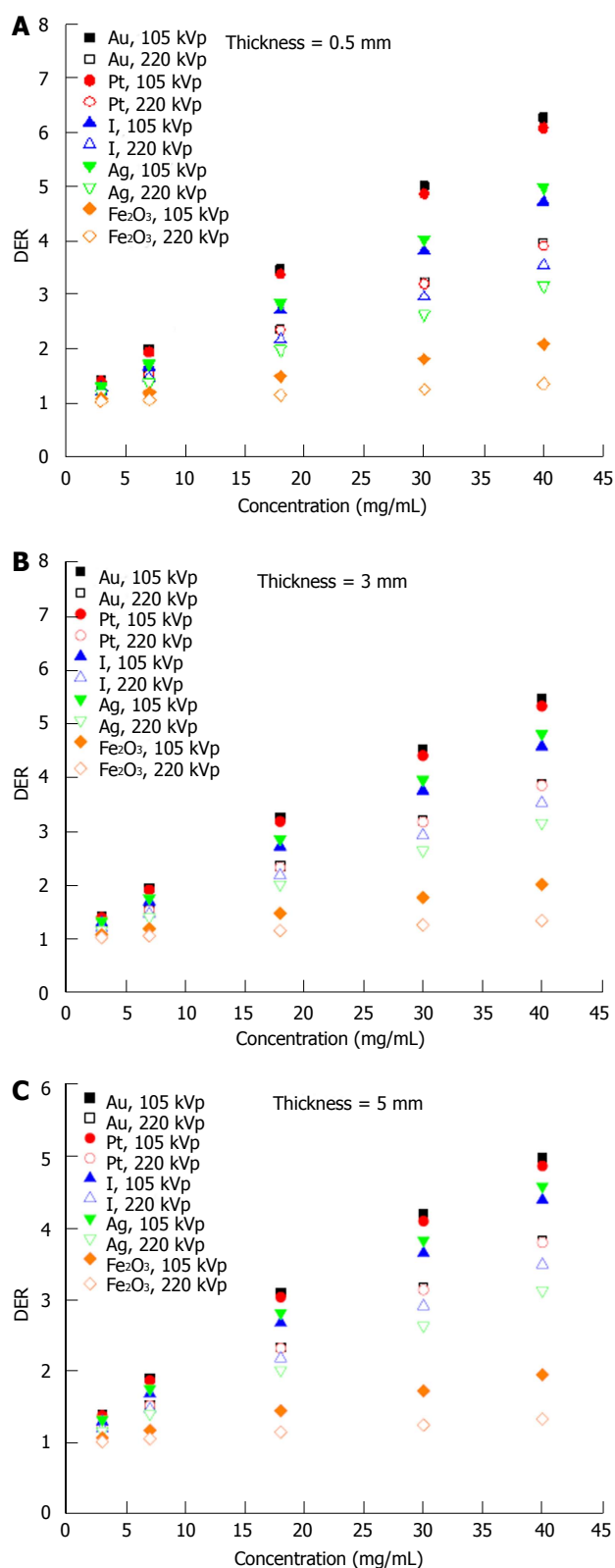


Figure 5 Relationship between the dose enhancement ratio and nanoparticle concentration with skin target thickness equal to (A) 0.5, (B) 3 and (C) 5 mm using the Au, Pt, I, Ag and Fe₂O₃ nanoparticles for the 105 and 220 kVp photon beams. DER: Dose enhancement ratio.

when using a 105 kVp photon beam. When the target thickness decreased from 5 mm to 0.5 mm (Figure 5), the DER increased for 105 kVp photon beams. In

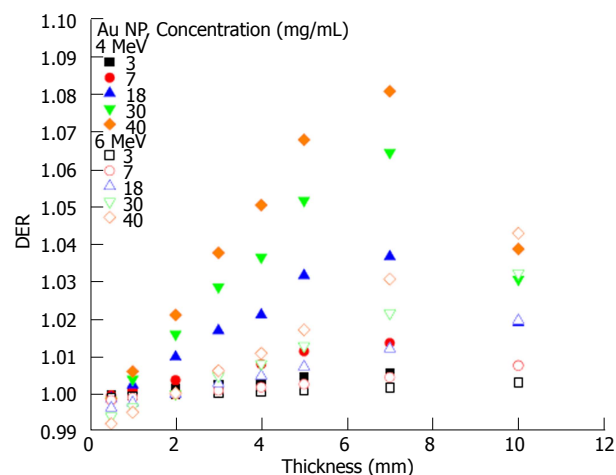


Figure 6 Relationship between the dose enhancement ratio and skin target thickness with different Au nanoparticle concentrations using the 4 and 6 MeV electron beams. DER: Dose enhancement ratio.

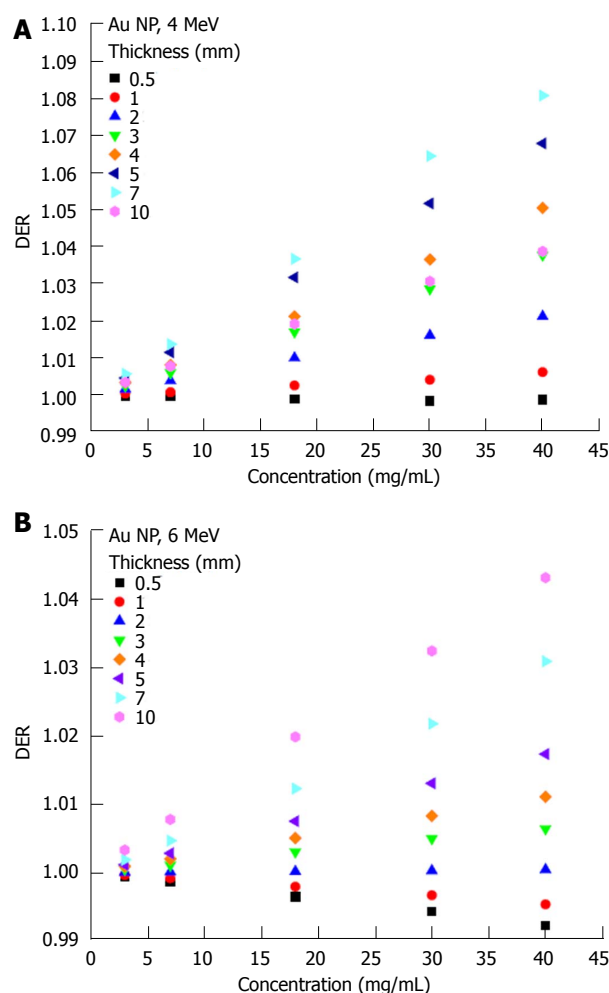


Figure 7 Relationship between the dose enhancement ratio and Au nanoparticle concentration with variation of skin target thickness using the (A) 4 and (B) 6 MeV electron beams. DER: Dose enhancement ratio.

Figure 5, though it can be seen that the DER for the Fe₂O₃ nanoparticles was only in the range of 1 to 2 in the concentration range of 3–40 mg/mL, DER of higher

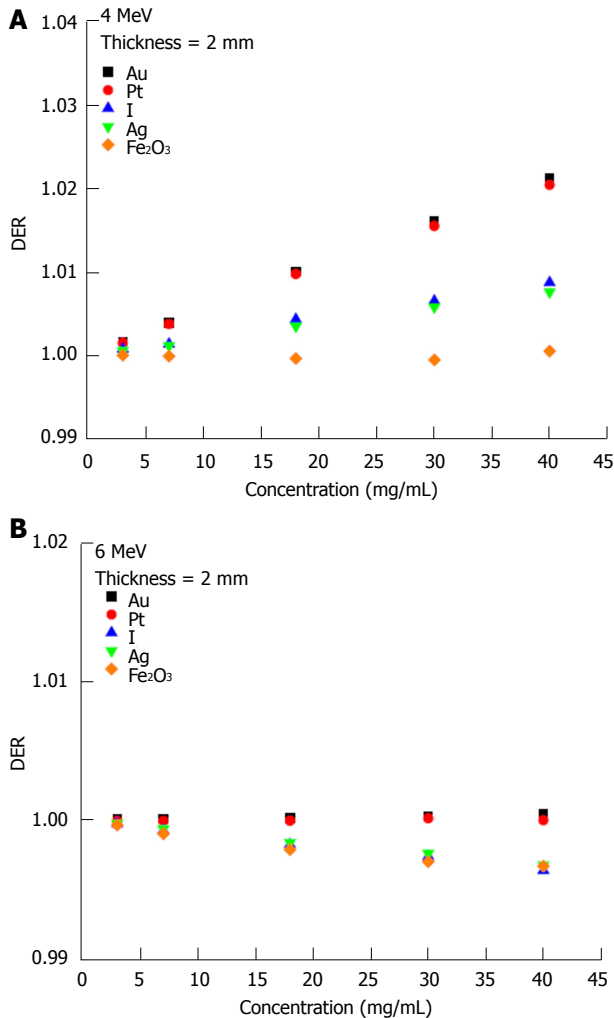


Figure 8 Relationship between the dose enhancement ratio and nanoparticle concentrations of the Au, Pt, I, Ag and Fe_2O_3 using the (A) 4 and (B) 6 MeV electron beams. The thickness of the target layer is equal to 2 mm. DER: Dose enhancement ratio.

than 5 can be achieved for the Au and Pt nanoparticles using the 105 kVp photon beams. It is found that dose enhancement was higher when using the lower energy 105 kVp photon beams, whenever the target thickness or nanoparticle concentration varied.

Megavoltage electron beams

Dependence of the DER on skin target thickness:

For the Au nanoparticles, it can be seen in Figure 6 that variation of the DER on the skin target thickness became significant when the electron beam energy decreased from 6 to 4 MeV. However, when the nanoparticle concentration was equal to 40 mg/mL, the DER decreased when varying the target thickness from 7 to 10 mm. Such an effect can also be observed in Figure 7A. Typically, the DER was found to increase as the target thickness increased from 0.5 to 10 mm. Unlike the kV range photon beams, we can see in Figure 6 that the DER only varied between 0.99 and 1.1 for the Au nanoparticle, having the highest atomic number in this study. This is due to the fact that photoelectric effect,

which is dominant in the kV photon beam range, does not contribute to the energy absorption of the 4 and 6 MeV electron beams^[11].

Dependence of the DER on nanoparticle concentration:

Dependence of the DER on nanoparticle concentration was found to vary with the target thickness. For the 4 MeV electron beams, variation of the DER with Au nanoparticle concentration was not significant when the target thickness was small. For a nanoparticle concentration of 40 mg/mL in Figure 7A, it is seen that the DER increased when the target thickness increased from 0.5 mm to 7 mm. A decrease of DER was seen at a target thickness equal to 10 mm (also Figure 6). This is because the depth of maximum dose of the 4 MeV beam (7 mm) was smaller than the target thickness of 10 mm. For the 6 MeV electron beam with a deeper depth of maximum dose (15 mm), the highest DER can be found at the 10 mm target layer as shown in Figure 7B. Moreover, it is interesting to see that the DER was smaller than one when the target thickness was in the range of 0.5–2 mm for the 6 MeV electron beams. This shows that electron beams with higher energy (6 MeV) would not show dose enhancement (*i.e.*, $\text{DER} \leq 1$) with Au nanoparticle addition when the target thickness was lower than 2 mm.

When the skin target thickness was equal to 2 mm, it can be seen from Figure 8 that only Au, Pt, I and Ag nanoparticles had slight dose enhancement using the 4 MeV electron beams (Figure 8A). The DER was found to be smaller than one when the 6 MeV electron beams were used (Figure 8B) with low atomic number nanoparticles (*e.g.*, Fe_2O_3) having the smallest DER in the range of nanoparticle concentration between 3 and 40 mg/mL.

In conclusion, different thicknesses of skin target layers with nanoparticle additions were irradiated by clinical kV photon and MV electron beams. The DER was calculated with variations of the target thickness, nanoparticle type, nanoparticle concentration and beam energy. It is found that with kV photon beams there was a higher DER than MV electron beams, with the Au nanoparticles having the highest DER compared to the other simulated materials (Pt, I, Ag and Fe_2O_3). For the kV photon beams, the 105 kVp beams showed higher dose enhancement than using a 220 kVp beam. It is therefore concluded that the kV photon beams and Au nanoparticles would be the most appropriate for use in nanoparticle-enhanced skin therapy. Moreover, higher nanoparticle concentration was shown to benefit dose enhancement.

ACKNOWLEDGMENTS

The authors would like to thank Amada Tulk from Gulmay Medical to allow us to share the Monte Carlo input data from Dr T Knoos in the Lund University Hospital for the verification of the kV photon beams.

The authors would also like to thank Varti Vartanian and Mitch Spiegel of Varian Medical Systems for providing detailed information about the 21 EX linear accelerator, and Dr F Verhaegen of Maastricht Clinic for sharing his BEAMnrc input files for verification of the electron beam simulations. The authors would like to thank Dr D Markel of the Princess Margaret Cancer Centre/ University of Toronto for editing this manuscript.

COMMENTS

Background

This work studied the dose enhancement due to nanoparticle addition in skin therapy using the clinical kilovoltage photon and megavoltage electron beams.

Research frontiers

The Monte Carlo results can guide the radiation staff which combination of nanoparticle type, nanoparticle concentration, beam type and beam energy should be used for different skin lesion thickness.

Innovations and breakthroughs

This Monte Carlo study combined all practical nanoparticle types, nanoparticle concentrations, clinical radiation beams and beam energies in treating skin lesions.

Applications

Nanoparticle-enhanced skin radiotherapy.

Peer-review

This is a well-written paper.

REFERENCES

- 1 Ali I, Lone MN, Al-Othman ZA, Al-Warthan A, Sanagi MM. Heterocyclic Scaffolds: Centrality in Anticancer Drug Development. *Curr Drug Targets* 2015; **16**: 711-734 [PMID: 25751009 DOI: 10.2174/1389450116666150309115922]
- 2 Ali I, Wani WA, Haque A, Saleem K. Glutamic acid and its derivatives: candidates for rational design of anticancer drugs. *Future Med Chem* 2013; **5**: 961-978 [PMID: 23682571 DOI: 10.4155/fmc.13.62]
- 3 Ali I, Haque A, Saleem K, Hsieh MF. Curcumin-I Knoevenagel's condensates and their Schiff's bases as anticancer agents: synthesis, pharmacological and simulation studies. *Bioorg Med Chem* 2013; **21**: 3808-3820 [PMID: 23643901 DOI: 10.1016/j.bmc.2013.04.018]
- 4 Ali I, Wani WA, Saleem K, Haque A. Platinum compounds: a hope for future cancer chemotherapy. *Anticancer Agents Med Chem* 2013; **13**: 296-306 [PMID: 22583420 DOI: 10.2174/1871520611313020016]
- 5 Ali I. Nano anti-cancer drugs: pros and cons and future perspectives. *Curr Cancer Drug Targets* 2011; **11**: 131-134 [PMID: 21062238 DOI: 10.2174/156800911794328457]
- 6 Her S, Jaffray DA, Allen C. Gold nanoparticles for applications in cancer radiotherapy: Mechanisms and recent advancements. *Adv Drug Deliv Rev* 2017; **109**: 84-101 [PMID: 26712711 DOI: 10.1016/j.addr.2015.12.012]
- 7 Coulter JA, Butterworth KT, Jain S. Prostate cancer radiotherapy: potential applications of metal nanoparticles for imaging and therapy. *Br J Radiol* 2015; **88**: 20150256 [PMID: 26051659 DOI: 10.1259/bjr.20150256]
- 8 Chow JCL. Characteristic of secondary electrons from irradiated gold nanoparticle in radiotherapy, 2015. Handbook of nanoparticle, Switzerland: Springer, 2015 [DOI: 10.1007/978-3-319-13188-7_10-2]
- 9 Cormode DP, Naha PC, Fayad ZA. Nanoparticle contrast agents for computed tomography: a focus on micelles. *Contrast Media Mol Imaging* 2014; **9**: 37-52 [PMID: 24470293 DOI: 10.1002/cmmi.1551]
- 10 Chow JCL. Photon and electron interactions with gold nanoparticles: a Monte Carlo study on gold nanoparticle-enhanced radiotherapy. 2016 Nanobiomaterials in medical imaging: applications of nanobiomaterials, Amsterdam: Elsevier, 2016; in press [DOI: 10.1016/b978-0-323-41736-5.00002-9]
- 11 Chow JC, Leung MK, Jaffray DA. Monte Carlo simulation on a gold nanoparticle irradiated by electron beams. *Phys Med Biol* 2012; **57**: 3323-3331 [PMID: 22572475 DOI: 10.1088/0031-9155/57/11/3323]
- 12 Leung MK, Chow JC, Chithrani BD, Lee MJ, Oms B, Jaffray DA. Irradiation of gold nanoparticles by x-rays: Monte Carlo simulation of dose enhancements and the spatial properties of the secondary electrons production. *Med Phys* 2011; **38**: 624-631 [PMID: 21452700 DOI: 10.1118/1.3539623]
- 13 Hainfeld JF, Slatkin DN, Smilowitz HM. The use of gold nanoparticles to enhance radiotherapy in mice. *Phys Med Biol* 2004; **49**: N309-N315 [PMID: 15509078]
- 14 Song L, Falzone N, Vallis KA. EGF-coated gold nanoparticles provide an efficient nano-scale delivery system for the molecular radiotherapy of EGFR-positive cancer. *Int J Radiat Biol* 2016; **92**: 716-723 [PMID: 26999580 DOI: 10.3109/09553002.2016.1145360]
- 15 Li W, Zhao X, Du B, Li X, Liu S, Yang XY, Ding H, Yang W, Pan F, Wu X, Qin L, Pan Y. Gold Nanoparticle-Mediated Targeted Delivery of Recombinant Human Endostatin Normalizes Tumour Vasculature and Improves Cancer Therapy. *Sci Rep* 2016; **6**: 30619 [PMID: 27470938 DOI: 10.1038/srep30619]
- 16 Chattopadhyay N, Cai Z, Kwon YL, Lechtman E, Pignol JP, Reilly RM. Molecularly targeted gold nanoparticles enhance the radiation response of breast cancer cells and tumor xenografts to X-radiation. *Breast Cancer Res Treat* 2013; **137**: 81-91 [PMID: 23160926 DOI: 10.1007/s10549-012-2338-4]
- 17 Butterworth KT, Nicol JR, Ghita M, Rosa S, Chaudhary P, McGarry CK, McCarthy HO, Jimenez-Sanchez G, Bazzi R, Roux S, Tillement O, Coulter JA, Prise KM. Preclinical evaluation of gold-DTTPA nanoparticles as theranostic agents in prostate cancer radiotherapy. *Nanomedicine (Lond)* 2016; **11**: 2035-2047 [PMID: 27463088 DOI: 10.2217/nnm-2016-0062]
- 18 Chow JC, Leung MK, Lindsay PE, Jaffray DA. Dosimetric variation due to the photon beam energy in the small-animal irradiation: a Monte Carlo study. *Med Phys* 2010; **37**: 5322-5329 [PMID: 21089767 DOI: 10.1118/1.3488979]
- 19 Chow JC, Jiang R. Bone and mucosal dosimetry in skin radiation therapy: a Monte Carlo study using kilovoltage photon and megavoltage electron beams. *Phys Med Biol* 2012; **57**: 3885-3899 [PMID: 22642985 DOI: 10.1088/0031-9155/57/12/3885]
- 20 Chow JC, Owringi AM. Surface dose reduction from bone interface in kilovoltage X-ray radiation therapy: a Monte Carlo study of photon spectra. *J Appl Clin Med Phys* 2012; **13**: 3911 [PMID: 22955657 DOI: 10.1120/jacmp.v13i5.3911]
- 21 Kawrakow I, Rogers DWO. The EGSnrc code system: Monte Carlo simulation of electron and photon transport, technique report PIRS-701. National Research Council of Canada: Ottawa, Canada
- 22 Cho SH. Estimation of tumour dose enhancement due to gold nanoparticles during typical radiation treatments: a preliminary Monte Carlo study. *Phys Med Biol* 2005; **50**: N163-N173 [PMID: 16030374 DOI: 10.1088/0031-9155/50/15/N01]
- 23 Knoos T, Rosenschold P, Wieslander E. Modelling of an orthovoltage x-ray therapy unit with the EGSnrc Monte Carlo package. *J Phys Conf Ser* 2007; **74**: 012009 [DOI: 10.1088/1742-6596/74/1/012009]
- 24 Rogers DWO, Walters B, Kawrakow I. BEAMnrc user manual. NRC Report PIRS-0509: Ottawa, Canada: NRCC, 2006
- 25 Bielajew AF, Rogers DWO. PRESTA: The parameter reduced electron-step transport algorithm for electron Monte Carlo transport. *Nucl Instrum Methods B* 1986; **18**: 165-171, 174-181 [DOI: 10.1016/S0168-583X(86)80027-1]
- 26 Ma CM, Reckwerdt P, Holmes M, Rogers DWO, Geiser B. DOSXYZ user manual. NRC Report PIRS 509b, Ottawa, Canada: NRCC, 1995

- 27 **Chow JC**, Owraangi AM. Solid water as phantom material for dosimetry of electron backscatter using low-energy electron beams: a Monte Carlo evaluation. *Med Phys* 2009; **36**: 1587-1594 [PMID: 19544774 DOI: 10.1118/1.3110107]
- 28 **Chow JC**, Grigorov GN. Effect of the bone heterogeneity on the dose prescription in orthovoltage radiotherapy: A Monte Carlo study. *Rep Pract Oncol Radiother* 2011; **17**: 38-43 [PMID: 24376995 DOI: 10.1016/j.rpor.2011.09.001]

P-Reviewer: Cerwenka HR, Loomba RS, Moskowitz SI
S-Editor: Qiu S **L-Editor:** A **E-Editor:** Wu HL



Retrospective Study

Magnetic resonance imaging in the assessment of brain involvement in alcoholic and nonalcoholic Wernicke's encephalopathy

Gianvincenzo Sparacia, Andrea Anastasi, Claudia Speciale, Francesco Agnello, Aurelia Banco

Gianvincenzo Sparacia, Andrea Anastasi, Claudia Speciale, Francesco Agnello, Aurelia Banco, Department of Radiology, University of Palermo, 90127 Palermo, Italy

Author contributions: Sparacia G contributed to guarantor of integrity of entire study, study design, text editing, literature research; Anastasi A, Speciale C and Agnello F contributed to imaging data collecting, drafting the article, literature research; Banco A contributed to imaging data collecting.

Institutional review board statement: This was a retrospective study approved by the Institutional Review Board of the University of Palermo, Department of Radiology, Palermo, Italy.

Informed consent statement: All patients had given written consent for this retrospective study.

Conflict-of-interest statement: All authors have no conflict-of-interest.

Data sharing statement: Participants gave informed consent for data sharing and the presented data are anonymized to avoid the risk of identification. No additional data are available.

Open-Access: This article is an open-access article which was selected by an in-house editor and fully peer-reviewed by external reviewers. It is distributed in accordance with the Creative Commons Attribution Non Commercial (CC BY-NC 4.0) license, which permits others to distribute, remix, adapt, build upon this work non-commercially, and license their derivative works on different terms, provided the original work is properly cited and the use is non-commercial. See: <http://creativecommons.org/licenses/by-nc/4.0/>

Manuscript source: Unsolicited manuscript

Correspondence to: Gianvincenzo Sparacia, MD, Department of Radiology, University of Palermo, Via del Vespro 127, 90127 Palermo, Italy. sparacia@yahoo.com
Telephone: +39-091-6552385
Fax: +39-091-6552302

Received: August 24, 2016

Peer-review started: August 26, 2016

First decision: October 8, 2016

Revised: December 6, 2016

Accepted: December 27, 2016

Article in press: December 28, 2016

Published online: February 28, 2017

Abstract

AIM

To present the typical and atypical magnetic resonance (MR) imaging findings of alcoholic and non-alcoholic Wernicke's encephalopathy.

METHODS

This study included 7 patients with Wernicke's encephalopathy (2 men, 5 women; mean age, 52.3 years) that underwent brain MR examination between January 2012 and March 2016 in a single institution. Three patients were alcoholics and 4 patients were non-alcoholics. MR protocol included a T2-weighted sequence, a fluid attenuation inversion recovery (FLAIR) sequence, a diffusion-weighted sequence ($b = 0$ and 1000 s/mm^2), and a contrast-enhanced MR sequence. All MR images were retrospectively reviewed at baseline and follow-up by two radiologists.

RESULTS

All patients with Wernicke's encephalopathy had bilateral areas showing high signal intensity on both T2-weighted and FLAIR MR images in the typical sites (*i.e.*, the periaqueductal region and the tectal plate). Signal intensity abnormalities in the atypical sites (*i.e.*, the cerebellum and the cerebellar vermis) were seen in 4 patients, all of which had no history of alcohol abuse. Six patients had areas with restricted diffusion

in the typical and atypical sites. Four patients had areas showing contrast-enhancement in the typical and atypical sites. Follow-up MR imaging within 6 mo after therapy (intravenous administration of thiamine) was performed in 4 patients, and demonstrated a complete resolution of all the signal intensities abnormalities previously seen in all patients.

CONCLUSION

MR imaging is valuable in the diagnosis of Wernicke's encephalopathy particularly in patients presenting with atypical clinical symptoms, or with no history of alcohol abuse.

Key words: Brain; Magnetic resonance imaging; Neurodegenerative disorder; Wernicke's encephalopathy

© The Author(s) 2017. Published by Baishideng Publishing Group Inc. All rights reserved.

Core tip: The purpose of this study was to describe the typical and atypical magnetic resonance (MR) imaging findings of alcoholic and nonalcoholic Wernicke's encephalopathy. Bilateral increased T2-weighted and fluid attenuation inversion recovery MR signal intensity in the typical areas were seen in all patients. Signal-intensity alterations in atypical sites were seen only in nonalcoholic patients. This study demonstrated that MR imaging was useful in supporting the diagnosis of Wernicke's encephalopathy.

Sparacia G, Anastasi A, Speciale C, Agnello F, Banco A. Magnetic resonance imaging in the assessment of brain involvement in alcoholic and nonalcoholic Wernicke's encephalopathy. *World J Radiol* 2017; 9(2): 72-78 Available from: URL: <http://www.wjgnet.com/1949-8470/full/v9/i2/72.htm> DOI: <http://dx.doi.org/10.4329/wjor.v9.i2.72>

INTRODUCTION

Wernicke's encephalopathy (WE) is a neurologic disease caused by thiamine (vitamin B1) deficiency^[1]. Thiamine is involved in sustainment of the osmotic gradients of cell membranes and in the maintenance of membrane integrity. A thiamine deficiency could lead intra and extra cellular edema, as due to an inability of cell membranes to maintain osmotic gradient.

Thiamine deficiency is a consequence of inadequate dietary intake and of impaired absorption of the vitamin. Alcohol abuse is the most common cause of WE, other causes could be gastrointestinal surgery, hyperemesis gravidarum, anorexia nervosa and protracted parenteral therapy. Usually nonalcoholic WE is more difficult to diagnose. In previous study only 20% or less of patients with nonalcoholic WE were diagnosed premortem^[1].

However, in industrialized countries, 90% of the cases of thiamine deficiency are associated with alcohol abuse^[2]. Alcohol chronic abuse can cause a thiamine

deficiency directly and indirectly with inadequate dietary intake, impaired intestinal absorption and poor intracellular use of thiamine.

The typical clinical presentation of WE is characterized by a triad of symptoms: Ocular manifestations (like nystagmus, bilateral lateral rectus palsies, ophthalmoplegia and conjugate gaze palsies), ataxia and global confusion. In the clinical practice, this typical triad occurs in only 13%-18% of all patients with WE^[3-5].

The prognosis of WE patients depends on prompt and early intravenous administration of thiamine supplementation^[3]. Sometimes WE become irreversible because the diagnosis is delayed or is misdiagnosed based on ambiguous symptoms such as dizziness, weakness, anorexia, and memory disturbance^[4]. Magnetic resonance (MR) imaging may be valuable for the diagnosis especially when the clinical diagnosis is difficult.

In the periventricular regions, there is a high rate of thiamine-related glucose and oxidative metabolism, which has been considered the cause of blood-brain barrier deficiency of these regions in WE^[6].

The typical MR imaging findings in acute WE are represented by a symmetrical increased T2-weighted and fluid-attenuated inversion recovery (FLAIR) signal intensity of periaqueductal area, medial thalami, mammillary bodies, tectal plate and periventricular region of third and fourth ventricles^[5]. In these areas, the maintenance of cellular osmotic gradients is considered to be strictly related to thiamine levels.

The atypical MR imaging findings are represented by abnormal signal-intensity involving the cerebellum, the cerebellar vermis, the cranial nerve nuclei, the red nuclei, the dentate nuclei, the caudate nuclei, the corpus callosum, and the cerebral cortex^[5,7-21].

In this article the typical and atypical MRI findings of alcoholic and nonalcoholic Wernicke's encephalopathy are presented and the value of MR imaging in the diagnosis and follow-up of the disorder is discussed.

MATERIALS AND METHODS

Patient population

The institutional review board of our institution approved this retrospective study and written informed consent was obtained from all patients. All patients were referenced with the suspect of WE. There were a total of 7 patients (2 men, 5 women; age 28-75 years; mean age, 52.3 years) that underwent MR examination between January 2012 and March 2016 in a single institution. Four out of 7 patients underwent to MR imaging follow-up within 2 mo after intravenous administration of thiamine. Demographic and epidemiologic data are summarized in Table 1.

Three patients had a history of chronic alcohol abuse: (1) patient #1 (male, 50 years) was hospitalized for fatigue, malnutrition, and stupor; clinical examination showed a bilateral paralysis of the abductens, lateral nystagmus in both eyes, mental confusion and

Table 1 Patient population affected by Wernicke's encephalopathy

Patient	Age (yr)	Gender	Predisposing causes
1	50	M	Alcoholic
2	55	F	Alcoholic
3	67	F	Alcoholic
4	45	F	Parental nutrition
5	75	F	Leukemia in chemotherapy treatment
6	28	F	Pregnancy
7	53	M	Stomach cancer

M: Male; F: Female.

disorientation; (2) patient #2 (female, 55 years) was hospitalized for loss of consciousness, nystagmus, bilateral lateral rectus palsies and conjugate gaze palsies; and (3) patient #3 (female, 67 years) was admitted with ataxia and global confusion.

The remaining 4 patients hadn't history of alcohol abuse: (1) patient #4 (female, of 45 years) was in parental nutrition from some weeks for acute pancreatitis, she showed sudden onset of nystagmus, disorientation, and ataxia; (2) patient #5 (female, 75 years), affected by leukemia, was treated with chemotherapy and parenteral nutrition, presented with vomiting, nausea, hallucinations, behavioral disturbances; (3) patient #6 (female, 28 years), at 32nd weeks of pregnancy, had hyperemesis gravidarum with neurological disorders; and (4) patient #7 (male, 53 years) had a stomach cancer with pyloric stenosis demonstrated at gastroscopy and was hospitalized for walking disorders, nausea, and vomiting.

MR imaging examination

All MR examinations were performed on a 1.5T MR scanner (Signa Excite, GE Medical Systems, Milwaukee, United States). MR imaging protocol included axial and sagittal fast spin-echo (FSE) T2W [5100/110 (TR/TE)] images, axial FLAIR [8000/140/2400 (TR/TE/TI)] images, along with axial, sagittal, and coronal non-enhanced and contrast-enhanced (0.1 mmol/Kg gadobutrol - Gadovist, Bayer, Germany) FSE T1W [650/15 (TR/TE)] images with a field of view (FOV) of 22 cm, matrix 512 × 512, slice thickness 5 mm, intersection gap 1 mm, number of excitations 2. Diffusion-weighted imaging (DWI) with echo-planar (TR 6500/TE 125) technique was obtained in all patients.

RESULTS

Typical and atypical MRI findings in WE patients are summarized in Table 2.

In all patients, high signal intensity on T2W and FLAIR sequences was demonstrated in the periaqueductal area and in the tectal plate in association with signal abnormalities around the mammillary bodies in 1 alcoholic WE (Figure 1) patient and in 2 nonalcoholics WE patients. Concomitant involvement of the medial

Table 2 Typical and atypical sites for magnetic resonance signal abnormalities in alcoholic and nonalcoholic Wernicke's encephalopathy patients

Patient	Typical site					Atypical site
	Periaqueductal	Thalami	Tectal plate	Floor of the fourth ventricle	Mammillary bodies	
1	X ¹	X	X	X		
2	X ¹ , r	X	X		X ¹ , r	
3	X ¹ , r	X	X	X	r	
4	X ¹	X	X		X	X, r
5	X	X	X			X, r
6	X	X	X	X	X	X, r
7	X		X			X, r

¹Contrast-enhancement on T1W sequences. X: High signal intensity on T2W and FLAIR MR sequences; r: Restricted diffusion; FLAIR: Fluid-attenuated inversion recovery.

thalami was seen in 2 alcoholics WE patients and in 3 nonalcoholics WE patients.

In the 4 nonalcoholics WE patients, in adjunction to the signal abnormalities in the periaqueductal area and in the tectal plate, high signal intensity on T2W and FLAIR images was seen in the cerebellar vermis and in the cerebellar hemispheres with restricted diffusion in these areas (Figure 2).

Restricted diffusion was demonstrated in the periaqueductal grey matter and around the mammillary bodies in 2 alcoholics WE patients in the acute phase of the disease (Figure 3).

Three alcoholics and 1 nonalcoholic WE patients presented contrast-enhancement of the periaqueductal grey matter. One of the 3 alcoholic WE patients presented a concomitant contrast-enhancement of the mammillary bodies in the acute phase of the disease (Figure 4).

MR imaging follow-up, performed within 6 mo after intravenous administration of thiamine in 4 (2 alcoholic and 2 nonalcoholics WE) patients, demonstrated disappearance of the signal abnormalities seen on T2-weighted, FLAIR, and diffusion-weighted images (Figure 5) previously observed concomitant with clinical recovery.

DISCUSSION

Our results confirm that MR imaging can assist the diagnosis of WE, particularly in patients presenting with atypical clinical symptoms, or with no history of alcohol abuse, and in the acute phase of the disease by using DWI sequences and contrast-enhanced MR imaging.

The pathology of the alterations detected in Wernicke's encephalopathy was not completely understood. Thiamine deficiency could lead an inability in sustainment of osmotic gradients of cell membranes and in the maintenance of membrane integrity with following intra and extra cellular edema.

In the periventricular regions, there is a high rate of thiamine-related glucose and oxidative metabolism

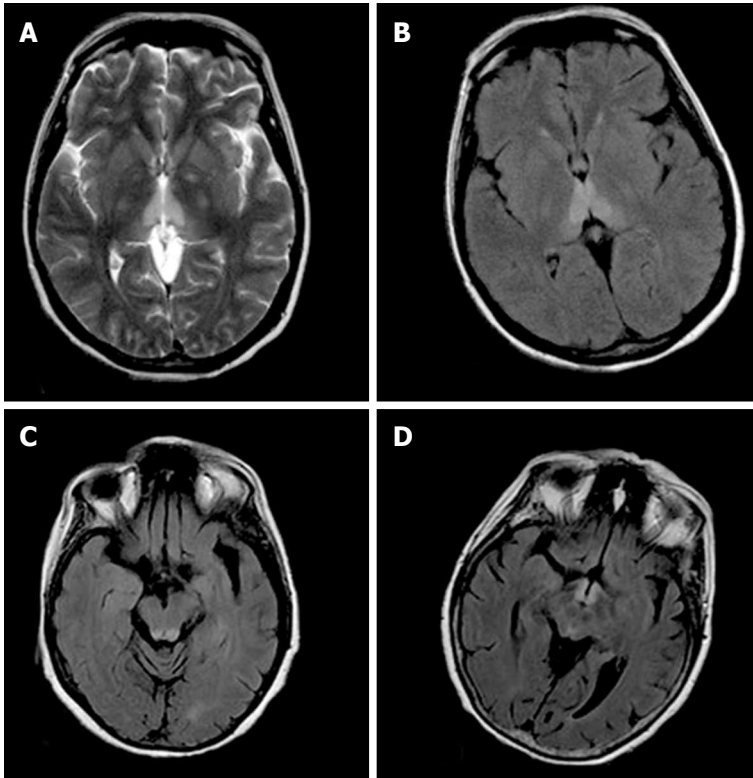


Figure 1 Magnetic resonance images in a patient with alcoholic Wernicke's encephalopathy. A: Axial T2-weighted image shows symmetrical high signal intensity lesions in the medial thalami; B: Axial fluid-attenuated inversion recovery (FLAIR) image shows symmetrical high signal intensity lesions in the medial thalami; C: Axial FLAIR image shows symmetrical high signal intensity lesions in the periaqueductal area; D: Axial FLAIR image shows symmetrical high signal intensity lesions around the mammillary bodies.

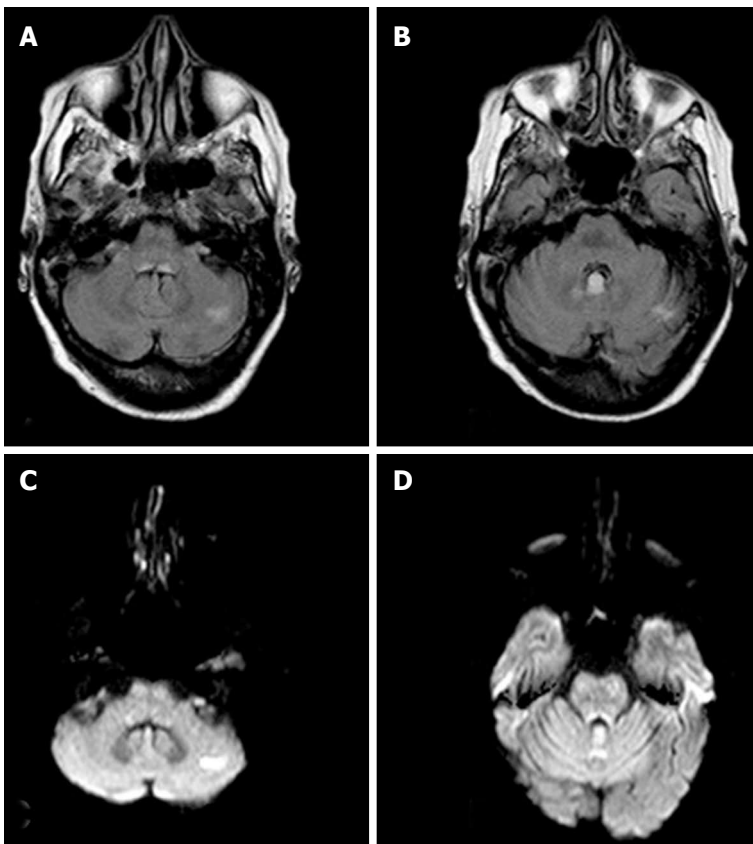


Figure 2 Magnetic resonance images in a patient with nonalcoholic Wernicke's encephalopathy. A: Axial FLAIR image shows a high signal intensity lesion in the left cerebellar hemisphere; B: Axial FLAIR image shows a high signal intensity lesion in the cerebellar vermis; C: Axial DWI shows a high signal intensity lesion in the left cerebellar hemisphere; D: Axial DWI shows a high signal intensity lesion in the cerebellar vermis. FLAIR: Fluid-attenuated inversion recovery; DWI: Diffusion-weighted imaging.

and it can account as the cause of blood-brain barrier deficiency of these regions^[11,12].

Cytotoxic edema is considered the most distinctive lesion of acute WE, and it is easily shown on DWI images as it detects changes in the diffusion of water

molecules.

However, the presence of high signal intensities on DWI and decreased apparent diffusion coefficient values must be carefully evaluated as it could result from T2 shine-through effects^[10]. Signal alterations on DWI most

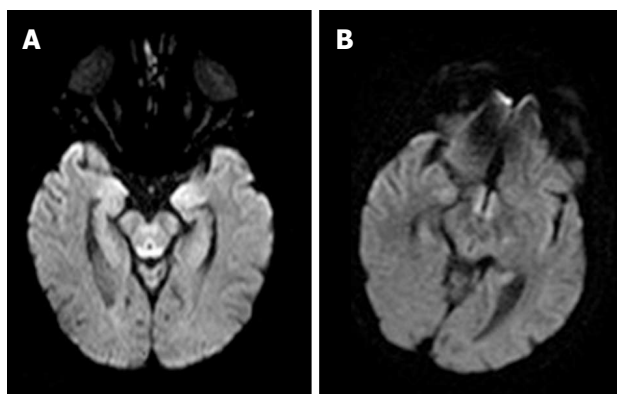


Figure 3 Axial diffusion weighted image magnetic resonance images in a patient with alcoholic Wernicke's encephalopathy in the acute phase. A: Diffusion weighted image shows restricted diffusion in the periaqueductal grey matter; B: Diffusion weighted image shows restricted diffusion around the mammillary bodies.

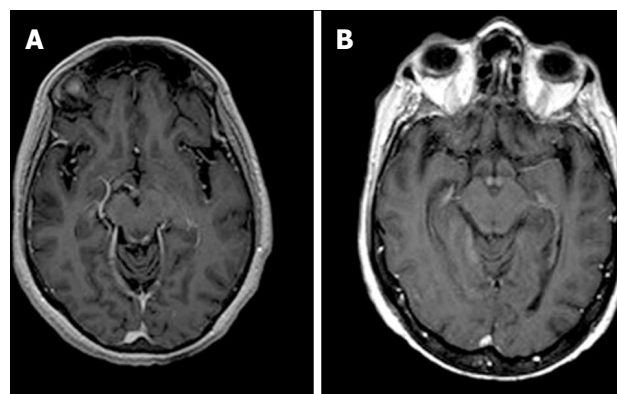


Figure 4 Axial T1-weighted magnetic resonance images after contrast material administration in a patient with alcoholic Wernicke's encephalopathy. A: Enhanced axial T1-weighted image shows contrast-enhancement of the periaqueductal grey matter; B: Enhanced axial T1-weighted image shows contrast-enhancement around the mammillary bodies.

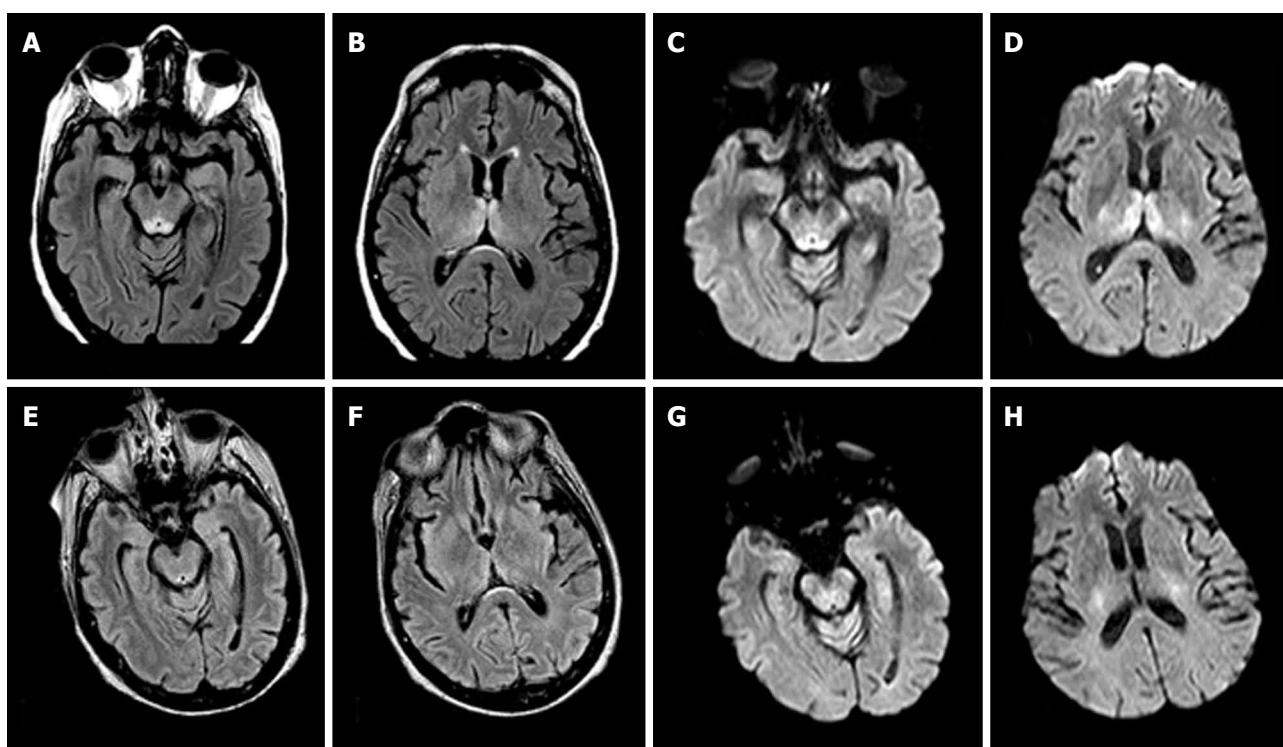


Figure 5 Magnetic resonance images in a patient affected by alcoholic Wernicke's encephalopathy. A-D: MR images before intravenous administration of thiamine therapy; E-H: MR images after intravenous administration of thiamine therapy. Axial FLAIR images (A,B) and DWI images (C,D) show signal abnormalities in the periaqueductal area and in the medial thalami. Axial FLAIR (E,F) and DWI (G,H) follow-up MR images, after intravenous administration of thiamine therapy, show resolution of the signal abnormalities previously observed. MR: Magnetic resonance; FLAIR: Fluid-attenuated inversion recovery; DWI: Diffusion weighted image.

likely represent tissue at risk, similar to the cells in the ischemic penumbra, related to the cytotoxic edema and can be reversible^[21]. In this study restricted diffusion was seen in 4 nonalcoholics and 2 alcoholics WE patients. At follow-up MR imaging obtained in 4 patients within 6 mo after thiamine therapy, resolution of these alterations was demonstrated confirming that restricted diffusion can be reversible (Figure 5).

According to previous reports^[13,22], contrast enhancement was observed more frequently in the mammillary

bodies in alcoholic patients (Figure 4), suggesting that mammillary bodies may be particularly susceptible to the toxic effects of alcohol.

Mammillary bodies enhancement, without mammillary body atrophy, is a finding that was associated with the acute phase of the disease, thus can allow an earlier diagnosis and treatment^[22].

If not treated or inappropriately treated, Wernicke's encephalopathy can lead to irreversible brain damage and, in 20% of cases, to death. Initial improvements in

acute symptoms can be observed within the first week after thiamine administration, but usually, one to 3 mo are needed to resolve^[15,22].

Our result confirms that MR signal abnormalities in WE can be reversible if a prompt therapy is established as demonstrated at follow-up MR imaging in 4 (2 alcoholic and 2 nonalcoholics WE) patients in our series (Figure 5).

The main limitation of this study is that it is a retrospective study without predefined criteria for diagnosis, which may have lead to a selection bias. Specifically, some patients with WE may not have been identified due to missed clinical diagnosis, particularly if they had atypical clinical manifestations and no history of alcohol abuse.

Despite these limitations, the diagnosis was confirmed in all patients as they clinically recovered after thiamine therapy and in 4 out of 7 patients resolution of the signal intensities abnormalities previously seen was demonstrated at follow-up MR imaging.

In conclusion, MR imaging is valuable in supporting the diagnosis of WE in patients with or without a history of alcohol abuse, especially in patients without the classic clinical presentation. Bilateral and symmetric increased T2-weighted and FLAIR MR signal intensity in the typical areas (periaqueductal area, medial thalami, mammillary bodies, tectal plate) are more often seen in alcoholic WE patients. Signal-intensity alterations in atypical sites (cerebellum, cranial nerve nuclei, and cerebral cortex) are found more frequently in nonalcoholic patients. Contrast-enhanced MR imaging and DWI MR imaging provides additional information to help diagnosis, especially in the acute phase of the disease, and should be included in the standard MR protocol in patients suspected to have WE. Knowledge of these MR imaging findings may be useful in the early diagnosis of WE and in reducing the complications associated with the disease.

COMMENTS

Background

Wernicke's encephalopathy (WE) is a serious neurologic disease, with acute onset, caused by thiamine deficiency. Alcohol abuse is the most common cause. Typical clinical presentation is characterized by a triad of symptoms: Ocular manifestations, ataxia and global confusion. However, this triad occurs in only 13%-18% of patients. Thus, magnetic resonance imaging (MRI) results are of utmost importance for the diagnosis of WE.

Research frontiers

This study demonstrated that MR imaging can assist the diagnosis of WE, especially in patients with atypical clinical symptoms, or with no history of alcohol abuse.

Applications

MR imaging is useful in supporting the diagnosis of WE. Knowledge of MR imaging findings can help radiologist in the early diagnosis, thus reducing the risk of complications.

Terminology

Wernicke's encephalopathy: Acute neurologic disease caused by thiamine (vitamin B1) deficiency.

Peer-review

Well written article. Nicely summarises brain imaging findings in WE including typical and atypical cases.

REFERENCES

- 1 **Gui QP**, Zhao WQ, Wang LN. Wernicke's encephalopathy in nonalcoholic patients: clinical and pathologic features of three cases and literature reviewed. *Neuropathology* 2006; **26**: 231-235 [PMID: 16771180 DOI: 10.1111/j.1440-1789.2006.00665.x]
- 2 **Thomson AD**, Marshall EJ. The natural history and pathophysiology of Wernicke's Encephalopathy and Korsakoff's Psychosis. *Alcohol Alcohol* 2006; **41**: 151-158 [PMID: 16384871 DOI: 10.1093/alcalc/agh249]
- 3 **Zuccoli G**, Gallucci M, Capellades J, Regnicolo L, Tumiatì B, Giadàs TC, Bottari W, Mandrioli J, Bertolini M. Wernicke encephalopathy: MR findings at clinical presentation in twenty-six alcoholic and nonalcoholic patients. *AJNR Am J Neuroradiol* 2007; **28**: 1328-1331 [PMID: 17698536 DOI: 10.3174/ajnr.A0544]
- 4 **Fei GQ**, Zhong C, Jin L, Wang J, Zhang Y, Zheng X, Zhang Y, Hong Z. Clinical characteristics and MR imaging features of nonalcoholic Wernicke encephalopathy. *AJNR Am J Neuroradiol* 2008; **29**: 164-169 [PMID: 18192344 DOI: 10.3174/ajnr.A0827]
- 5 **Nolli M**, Barbieri A, Pinna C, Pasetto A, Nicosia F. Wernicke's encephalopathy in a malnourished surgical patient: clinical features and magnetic resonance imaging. *Acta Anaesthesiol Scand* 2005; **49**: 1566-1570 [PMID: 16223408 DOI: 10.1111/j.1399-6576.2-005.00879.x]
- 6 **Bonucchi J**, Hassan I, Policeni B, Kaboli P. Thyrotoxicosis associated Wernicke's encephalopathy. *J Gen Intern Med* 2008; **23**: 106-109 [PMID: 18026802 DOI: 10.1007/s11606-007-0438-3]
- 7 **Blanco-Muñoz O**, Suárez-Gauthier A, Martín-García H, Díaz-Konrad V, San Antonio-Román V, Cabello A. Unusual cortical compromise in a case of Wernicke's encephalopathy. *Rev Neurol* 2006; **42**: 596-599 [PMID: 16703527]
- 8 **Lindboe CF**, Løberg EM. Wernicke's encephalopathy in non-alcoholics. An autopsy study. *J Neurol Sci* 1989; **90**: 125-129 [PMID: 2723677 DOI: 10.1016/0022-510X(89)90095-6]
- 9 **Asato R**, Okumura R, Konishi J. "Fogging effect" in MR of cerebral infarct. *J Comput Assist Tomogr* 1991; **15**: 160-162 [PMID: 1987190 DOI: 10.1097/00004728-199101000-00029]
- 10 **Zuccoli G**, Pipitone N. Neuroimaging findings in acute Wernicke's encephalopathy: review of the literature. *AJR Am J Roentgenol* 2009; **192**: 501-508 [PMID: 19155417 DOI: 10.2214/AJR.07.3959]
- 11 **Bae SJ**, Lee HK, Lee JH, Choi CG, Suh DC. Wernicke's encephalopathy: atypical manifestation at MR imaging. *AJNR Am J Neuroradiol* 2001; **22**: 1480-1482 [PMID: 11559494]
- 12 **Gallucci M**, Bozzao A, Splendiani A, Masciocchi C, Passariello R. Wernicke encephalopathy: MR findings in five patients. *AJNR Am J Neuroradiol* 1990; **11**: 887-892 [PMID: 2120991 DOI: 10.2214/ajr.155.6.2122685]
- 13 **Sun GH**, Yang YS, Liu QS, Cheng LF, Huang XS. Pancreatic encephalopathy and Wernicke encephalopathy in association with acute pancreatitis: a clinical study. *World J Gastroenterol* 2006; **12**: 4224-4227 [PMID: 16830380 DOI: 10.3748/wjg.v12.i26.4224]
- 14 **Antunez E**, Estruch R, Cardenal C, Nicolas JM, Fernandez-Sola J, Urbano-Marquez A. Usefulness of CT and MR imaging in the diagnosis of acute Wernicke's encephalopathy. *AJR Am J Roentgenol* 1998; **171**: 1131-1137 [PMID: 9763009 DOI: 10.2214/ajr.171.4.9763009]
- 15 **Zhong C**, Jin L, Fei G. MR Imaging of nonalcoholic Wernicke encephalopathy: a follow-up study. *AJNR Am J Neuroradiol* 2005; **26**: 2301-2305 [PMID: 16219836]
- 16 **Park SH**, Kim M, Na DL, Jeon BS. Magnetic resonance reflects the pathological evolution of Wernicke encephalopathy. *J Neuroimaging* 2001; **11**: 406-411 [PMID: 11677881 DOI: 10.1111/j.1552-6569.2001.tb00070.x]
- 17 **Liu YT**, Fuh JL, Lirmg JF, Li AF, Ho DM, Wang SJ. Correlation of magnetic resonance images with neuropathology in acute Wernicke's encephalopathy. *Clin Neurol Neurosurg* 2006; **108**: 682-687

- [PMID: 15992992 DOI: 10.1016/j.clineuro.2005.05.010]
- 18 **Shogry ME**, Curnes JT. Mamillary body enhancement on MR as the only sign of acute Wernicke encephalopathy. *AJNR Am J Neuroradiol* 1994; **15**: 172-174 [PMID: 8141051]
 - 19 **D'Aprile P**, Gentile MA, Carella A. Enhanced MR in the acute phase of Wernicke encephalopathy. *AJNR Am J Neuroradiol* 1994; **15**: 591-593 [PMID: 8197963]
 - 20 **Zuccoli G**, Santa Cruz D, Bertolini M, Rovira A, Gallucci M, Carollo C, Pipitone N. MR imaging findings in 56 patients with Wernicke encephalopathy: nonalcoholics may differ from alcoholics. *AJNR Am J Neuroradiol* 2009; **30**: 171-176 [PMID: 18945789 DOI: 10.3174/ajnr.A1280]
 - 21 **Manzo G**, De Gennaro A, Cozzolino A, Serino A, Fenza G, Manto A. MR imaging findings in alcoholic and nonalcoholic acute Wernicke's encephalopathy: a review. *Biomed Res Int* 2014; **2014**: 503596 [PMID: 25050351 DOI: 10.1155/2014/503596]
 - 22 **Sparacia G**, Banco A, Lagalla R. Reversible MRI abnormalities in an unusual paediatric presentation of Wernicke's encephalopathy. *Pediatr Radiol* 1999; **29**: 581-584 [PMID: 10415181 DOI: 10.1007/s002470050652]

P- Reviewer: Kumar A, Prakash N **S- Editor:** Kong JX
L- Editor: A **E- Editor:** Wu HL



Observational Study**Feasibility of imaging superficial palmar arch using micro-ultrasound, 7T and 3T magnetic resonance imaging**

Alison N Pruzan, Audrey E Kaufman, Claudia Calcagno, Yu Zhou, Zahi A Fayad, Venkatesh Mani

Alison N Pruzan, Audrey E Kaufman, Claudia Calcagno, Yu Zhou, Zahi A Fayad, Venkatesh Mani, Translational and Molecular Imaging Institute, Department of Radiology, Icahn School of Medicine at Mount Sinai, New York, NY 10029, United States

Author contributions: Pruzan AN, Kaufman AE and Mani V designed the study and performed the research; Zhou Y helped perform the research and helped acquire ultrasound data; Calcagno C provided her imaging expertise and helped with MRI acquisition; Pruzan AN and Kaufman AE drafted the article and made critical revisions related to the intellectual content of the manuscript; Fayad ZA and Mani V helped with data analysis and interpretation; all authors reviewed and approved the manuscript content; Pruzan AN and Kaufman AE contributed equally to this research.

Institutional review board statement: This study was conducted in conformance with institutional policies with regard to human subject protections after informed consent and ethical permission were obtained.

Conflict-of-interest statement: There are no conflicts of interest to disclose.

Data sharing statement: No additional data are available.

Open-Access: This article is an open-access article which was selected by an in-house editor and fully peer-reviewed by external reviewers. It is distributed in accordance with the Creative Commons Attribution Non Commercial (CC BY-NC 4.0) license, which permits others to distribute, remix, adapt, build upon this work non-commercially, and license their derivative works on different terms, provided the original work is properly cited and the use is non-commercial. See: <http://creativecommons.org/licenses/by-nc/4.0/>

Manuscript source: Invited manuscript

Correspondence to: Venkatesh Mani, PhD, Translational and Molecular Imaging Institute, Department of Radiology, Icahn School of Medicine at Mount Sinai, 1470 Madison Avenue New York, NY 10029, United States. venkatesh.mani@mssm.edu
Telephone: +1-212-8248538

Received: October 8, 2016

Peer-review started: October 10, 2016

First decision: December 13, 2016

Revised: December 17, 2016

Accepted: January 11, 2017

Article in press: January 14, 2017

Published online: February 28, 2017

Abstract**AIM**

To demonstrate feasibility of vessel wall imaging of the superficial palmar arch using high frequency micro-ultrasound, 7T and 3T magnetic resonance imaging (MRI).

METHODS

Four subjects (ages 22-50 years) were scanned on a micro-ultrasound system with a 45-MHz transducer (Vevo 2100, VisualSonics). Subjects' hands were then imaged on a 3T clinical MR scanner (Siemens Biograph MMR) using an 8-channel special purpose phased array carotid coil. Lastly, subjects' hands were imaged on a 7T clinical MR scanner (Siemens Magnetom 7T Whole Body Scanner) using a custom built 8-channel transmit receive carotid coil. All three imaging modalities were subjectively analyzed for image quality and visualization of the vessel wall.

RESULTS

Results of this very preliminary study indicated that vessel wall imaging of the superficial palmar arch was feasible with a whole body 7T and 3T MRI in comparison with micro-ultrasound. Subjective analysis of image quality (1-5 scale, 1: poorest, 5: best) from B mode, ultrasound, 3T SPACE MRI and 7T SPACE MRI indicated that the image quality obtained at 7T was superior to both 3T MRI and micro-ultrasound. The 3D SPACE sequence at both 7T and 3T MRI with isotropic voxels allowed for multi-planar

reformatting of images and allowed for less operator dependent results as compared to high frequency micro-ultrasound imaging. Although quantitative analysis revealed that there was no significant difference between the three methods, the 7T Tesla trended to have better visibility of the vessel and its wall.

CONCLUSION

Imaging of smaller arteries at the 7T is feasible for evaluating atherosclerosis burden and may be of clinical relevance in multiple diseases.

Key words: Superficial Palmar Arch; 7T and 3T magnetic resonance imaging; Micro-ultrasound; Atherosclerosis; Cardiovascular disease

© **The Author(s) 2017.** Published by Baishideng Publishing Group Inc. All rights reserved.

Core tip: The evaluation of smaller arteries in the hand may be clinically useful in a variety of vascular diseases. Imaging the vessel wall of such small caliber arteries (2.5 mm to 3.1 mm) requires very high spatial resolution and the use of either high frequency micro-ultrasound or 7 Tesla magnetic resonance imaging (MRI) would be the ideal tool to acquire these images. We sought to demonstrate feasibility of vessel wall imaging of the superficial palmar arch using 7T and 3T MRI in comparison with very high frequency micro-ultrasound.

Pruzan AN, Kaufman AE, Calcagno C, Zhou Y, Fayad ZA, Mani V. Feasibility of imaging superficial palmar arch using micro-ultrasound, 7T and 3T magnetic resonance imaging. *World J Radiol* 2017; 9(2): 79-84 Available from: URL: <http://www.wjgnet.com/1949-8470/full/v9/i2/79.htm> DOI: <http://dx.doi.org/10.4329/wjrr.v9.i2.79>

INTRODUCTION

A variety of pathological processes can affect the hand, including atherosclerosis, scleroderma, thromboangiitis obliterans (TO), hypothenar hammer syndrome and acute arterial thrombosis related to intraarterial injection^[1].

Atherosclerosis is a chronic complex process involving multiple factors including inflammation, oxidative stress, endothelial dysfunction, smooth muscle cell proliferation, platelet activation, and thrombosis, all leading to pathologic changes in the arterial wall with plaque formation^[2]. The plaque is primarily composed of inflammatory cells, lipids, and calcium^[3]. Chronic atherosclerosis can cause peripheral vascular occlusive disease in the extremities. In the upper extremity, atherosclerosis is more prevalent in the proximal subclavian artery but can occur in smaller distal vessels with resultant morbidity^[4]. For example, young diabetics who have diffuse distal atherosclerosis, end-stage

renal disease and are on renal dialysis are at high risk for developing finger gangrene^[5]. In the autoimmune disorder scleroderma, ultrasound evaluation has shown that the ulnar artery proximal to the wrist is specifically targeted^[6]. The vasculopathy of scleroderma can cause secondary Raynaud's phenomenon, as well as digital ulcers. Doppler sonography has proven useful in assessing palmar and digital arteries in these cases^[7,8]. TO also known as Buerger's disease, is a panarteritis of unknown origin, which demonstrates a strong concurrence with tobacco use. It affects both small and medium-sized vessels of the extremities. The thrombotic and inflammatory changes associated with TO cause vascular changes with associated arteriographic findings^[9-11]. Hypothenar hammer syndrome, a post-traumatic pathology arising from repetitive hitting of the hypothenar region of the hand, can cause ulnar artery occlusive disease with thromboembolism and resulting ischemia to the digits^[12,13]. The thrombosis secondary to TO and hypothenar hammer syndrome may be relatively localized, whereas diffuse arterial thrombosis of the hand may occur secondary to intraarterial injection of medications or illegal substances^[14]. Visualizing atherosclerotic changes in small arteries such as the superficial palmar arch may provide valuable clinical insights into the progression of these disease states.

Imaging the vessel wall of smaller caliber arteries requires higher resolution imaging when compared to imaging larger vessels such as the aorta and carotid arteries. For this purpose we conducted MR evaluation of the superficial palmar arch using 7T and 3T whole body MR scanners and compared the images acquired with high frequency micro-ultrasound imaging. The superficial palmar arch is the continuation of the ulnar artery as it passes distal to the flexor retinaculum in the hypothenar region of the palm. We chose to focus on the superficial palmar arch because it is easily and consistently visualized using the modalities employed. We hypothesize that 7T MRI will provide better delineation of the vessel wall as compared to 3T and may be a suitable method to visualize small arteries in the hand. We also believe that ultrasound may be a convenient alternative compared to 3T and 7T due to its image acquisition speed and wide availability. But, conventional clinical ultrasound (about 3-7 MHz) may lack resolution, so the use of a high frequency (45-MHz) micro-ultrasound typically used in animal models may be better suited for superficial structures such as the palmar arch.

MATERIALS AND METHODS

Study population

Four subjects (ages 22-50 years) were scanned on a micro-ultrasound system with a 45-MHz transducer (Vevo 2100, VisualSonics, Toronto, Canada) (Figure 1A). While this system is primarily used in animal studies, it has been successfully and safely used in

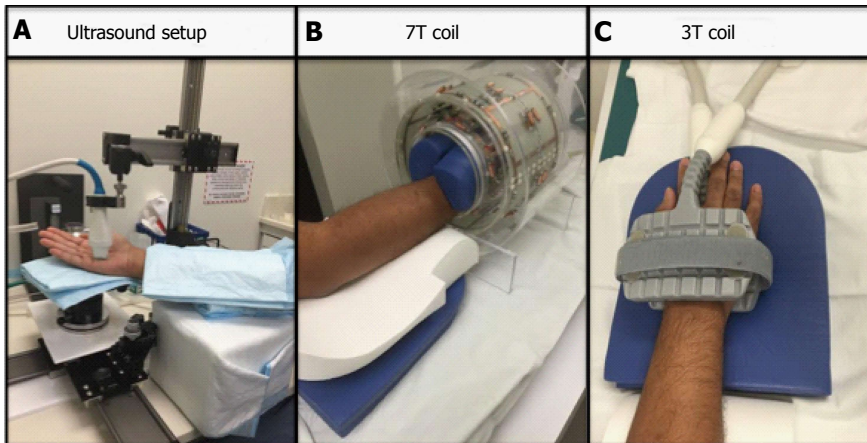


Figure 1 The figure shows the set up for the ultrasound (A), the 7T (B) and the 3T (1) respectively.

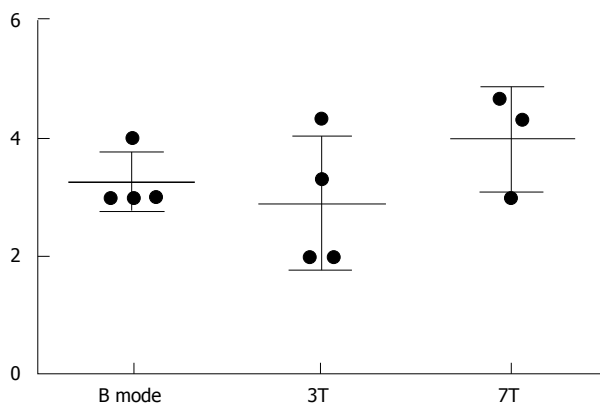


Figure 2 Data from 3 subjective analyses of image quality (1-5 scale). Error bars included.

clinical studies, which include infants and children.^[15,16] Subjects' hands were then imaged on a 3T clinical MR scanner (Siemens Biograph MMR) using an 8-channel special purpose phased array carotid coil (Figure 1C). Lastly, subjects' hands were imaged on a 7T clinical MR scanner (Siemens Magnetom 7T Whole Body Scanner) using a custom built 8-channel transmit receive carotid coil (Figure 1B).

Micro-ultrasound imaging and protocol

The Vevo Imaging Station (Vevo 2100, VisualSonics, Toronto, Canada) was used for mounting the transducer and for stabilizing the position of the hand. The subject was seated during the scan with the hand in supine position with slight rotation toward neutral. Padding was also used under the hand and arm for stabilization and comfort purposes (Figure 1A). With this positioning, images in B mode, Power mode, Doppler mode and M mode of the superficial palmar arch were obtained. Images were then subjectively analyzed for image quality. Three readers rated the images on a score: (1) is a non-visible vessel with non-visible walls and poor image quality; (2) represents a vessel with indistinct vessel walls and poor image quality; (3) is a vessel with adequate image quality with walls moderately well seen; (4) represents a vessel with

Table 1 Imaging protocol for both 3T and 7T magnetic resonance imaging

Parameter	7T T2 SPACE	3T T2 SPACE	7T TOF	3T TOF
TE	101	77	2.81	3.23
TR	1500	1600	60	21
Slice thickness	625.00 μ m	630.00 μ m	160.00 mm	1.00 mm
Pixel size	0.600/0.600	0.625/0.625	0.3125/0.3125	0.234/0.234
Number of averages	2	4	1	1
Field of view	136 \times 160	100 \times 160	160 \times 160	107 \times 120

distinct vessel walls and good image quality; and (5) is excellent visualization of the vessel and image quality. Results from the three readers were averaged. Criteria used for subjective evaluation were the overall image quality, visualization of the vessel wall, adequate flow suppression and absence of artifacts. We also obtained measures of average peak Doppler velocity, intima media thickness, wall thickness, lumen diameter, and total vessel diameter.

MR imaging and protocol

Subjects' hands were imaged on a 3T clinical MR scanner (Siemens Biograph MMR) using an 8-channel special purpose phased array carotid coil (Figure 1C). Subjects' hands were imaged on a 7T clinical MR scanner (Siemens Magnetom 7T Whole Body Scanner) using a custom built 8-channel transmit receive carotid coil (Figure 1B). Subjects were imaged in a head first prone position with hand extended above the head. The imaging protocols between 3T and 7T were matched as closely as possible. Total scan time was approximately 20 min each. We acquired a localizer, a 3D time-of-flight (TOF) MR angiography sequence followed by a 3D T2 weighted Sampling Perfection with Application optimized Contrasts using different flip angle Evolution (SPACE) sequence^[1,17,18] and a 0.6 mm isotropic resolution in all dimensions (Table 1). MR images were also subjectively analyzed for image quality and visualization of the vessel wall. The imaging criteria used were similar to that for the ultrasound. Furthermore, we also measured

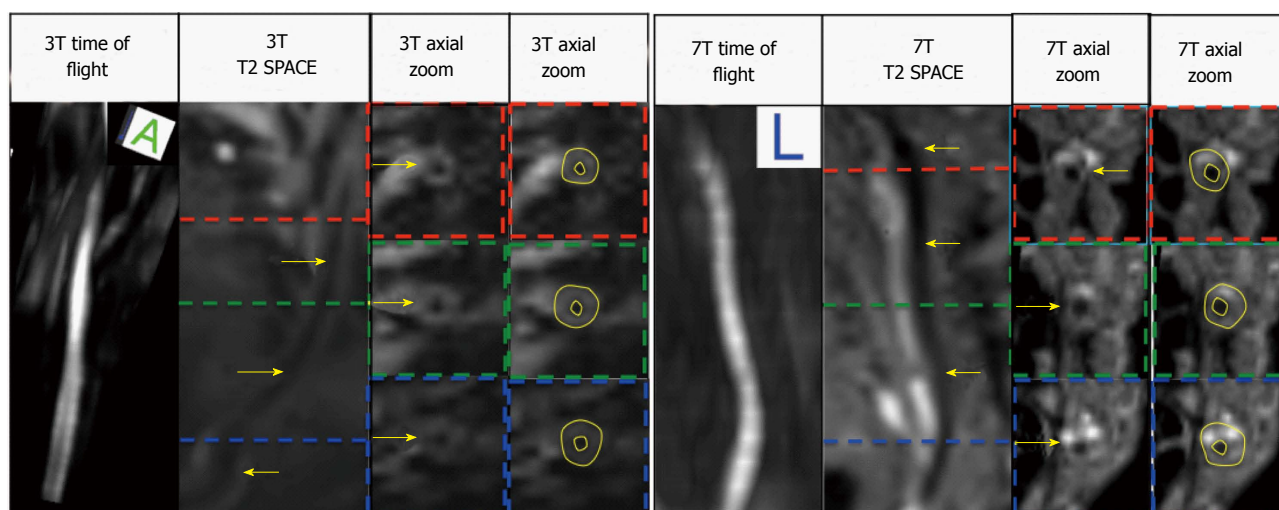


Figure 3 Displays the 3T images (Left) and the 7T images (Right) the arrows point to vessel wall.

Table 2 Data from 3 subjective analyses of image quality with average and standard deviation

Subject	B mode	3T	7T
1	3.00	3.33	3.00
2	3.00	2.00	Not available
3	3.00	4.33	4.67
4	4.00	2.00	4.33
Average	3.25	2.92	4.00
Standard deviation	0.50	1.13	0.882

Table 3 RM one-way ANOVA and Tukey's multiple comparisons test

Vessel wall measurements	P value
Lumen area	0.3152
Wall area	0.0628
Total vessel area	0.0573
Normalized wall index	0.0362 ^a
Wall thickness	0.0519

^a $P < 0.05$, significant.

wall thickness, lumen and outer diameters from the MR images. The order of the imaging tests was randomized.

Statistical analysis

The data were expressed as the mean \pm SD. For the statistics, a RM one-way ANOVA and Tukey's multiple comparisons test were used. $P < 0.05$ was considered as statistically significant.

RESULTS

Subjective analysis of image quality was performed (1-5 scale, 1: Vessel non-visible, 5: Clearly visible vessel wall) from B mode, ultrasound, 3T SPACE MRI and 7T SPACE MRI. These results are shown in Table 2 and Figure 2.

In addition, lumen area, wall area, total vessel area, and wall thickness were automatically calculated by a MatLab script (MATLAB and Statistics Toolbox Release 2012b, The MathWorks, Inc., Natick, Massachusetts, United States) for the manually drawn contours on the 3T and 7T images using a customized software program (Vessel Mass Software, Leiden University Medical Center, The Netherlands) (Figure 3). Sonographic images were analyzed on the micro-ultrasound machine using the software on the B and M Mode photos (Figure 4) and data was extracted and used to calculate the aforementioned measurements by hand in Microsoft Excel.

DISCUSSION

Qualitative analysis indicated that the image quality obtained at 7T trended to be superior to both 3T MRI and micro-ultrasound (Figure 2 and Table 2). Compared to the 3D Time of Flight, the 3D SPACE sequence with isotropic voxels allowed for multi-planar reformatting of images and allowed for less operator dependent results as compared to high frequency micro-ultrasound imaging. Although there was no significant difference between the three methods ($P = 0.5647$, One-Way ANOVA), the 7T Tesla trended to have better visibility of the vessel and its wall (Table 2, Figures 2 and 3).

The One-Way ANOVA between all 3 imaging modalities showed that 7T, 3T and micro-ultrasound imaging are all comparable imaging methods with no statistical difference between extracted values, (lumen area, wall area, total vessel area, wall thickness)^[19,20] [$P > 0.05$ (Table 3)]. *Post hoc* test using Tukey's correction however showed significant differences when comparing 3T and micro-ultrasound for wall thickness.

Results of this very preliminary study indicated that vessel wall imaging of the superficial palmar arch was feasible with a whole body 7T MRI with subjective evaluations indicating that the image quality obtained at 7T is superior to both 3T MRI and micro-ultrasound. The 3D SPACE sequence with isotropic voxels allowed

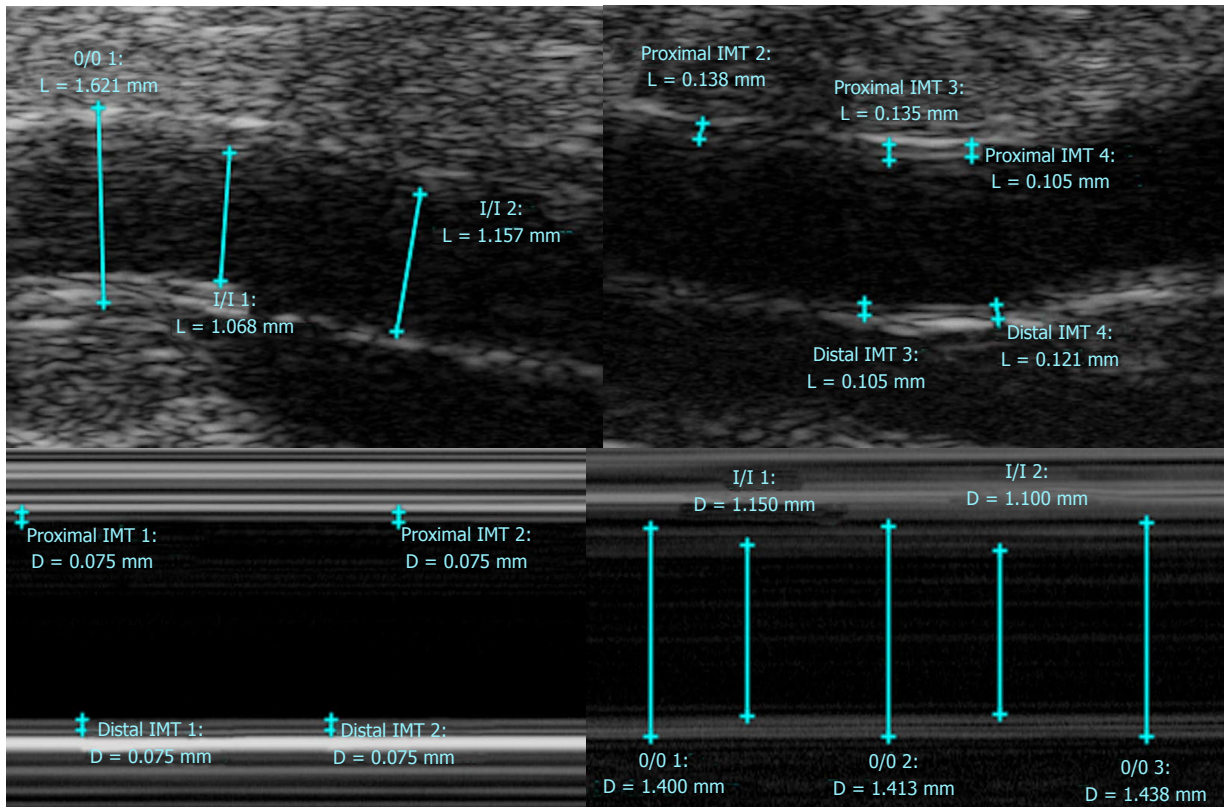


Figure 4 Ultrasound Images (B mode, M mode).

multi-planar reformatting of images and allows for less operator dependent results as compared to ultrasound imaging. Scanning time for the micro-ultrasound portion of the study approached that of the MR scan times, however with more operator experience the micro-ultrasound scan time could improve. The time spent on post-processing image analysis was similar across all modalities. Limitations of this study include a very small sample size and the fact that only healthy individuals without any atherosclerotic disease were examined. Future investigation should study individuals with diseased conditions in a larger sample size. Additionally, methods to optimize image quality could include warming the region of interest prior and during imaging to dilate the vessel and provide better contrast between the lumen and the vessel wall structures. This technique has been shown to optimize image quality in peripheral 2D TOF MRA evaluation^[21].

In conclusion, imaging of the superficial palmar arch at the 7T is feasible with high frequency micro-ultrasound, 3T and 7T MRI and should be considered for evaluating arterial pathology. This may be of clinical relevance in specific disease conditions such as atherosclerosis, scleroderma, diabetes, TO, hypothenar hammer syndrome and acute arterial thrombosis related to intraarterial injection. Future studies need to be performed in diseased individuals and in a larger number of subjects to better establish clinical feasibility of the approach.

COMMENTS

Background

Imaging the vessel wall of smaller caliber arteries requires higher resolution imaging when compared to imaging larger vessels such as the aorta and carotid arteries. For this purpose the authors conducted MR evaluation of the superficial palmar arch using 7T and 3T whole body MR scanners and compared the images acquired with high frequency ultrasound imaging. The author chose to focus on the superficial palmar arch because it is easily and consistently visualized using the modalities employed.

Research frontiers

A variety of pathological processes can affect the hand, including atherosclerosis, scleroderma, thromboangitis obliterans, hypothenar hammer syndrome and acute arterial thrombosis related to intraarterial injection. These diseases are currently evaluated using sonography, arteriography, and standard 1.5 or 3T MRI. The intent of the investigation is to improve and potentially advance imaging techniques for evaluation of these diseases.

Innovations and breakthroughs

A thorough search of medical literature shows few if any prior investigations related to imaging the superficial palmar arch on a 7T MRI and therefore this is a novel application.

Applications

Future evaluation for atherosclerosis and other diseases may involve non-invasive 3T or 7T MR as well as micro-ultrasound imaging of the superficial palmar arch.

Peer-review

Imaging of smaller artery is feasible using micro-ultrasound and 3T and 7T MRI. Interesting and good study enough for publication.

REFERENCES

- 1 **Wong SK**, Mobolaji-lawal M, Arama L, Cambe J, Biso S, Alie N, Fayad ZA, Mani V. Atherosclerosis imaging using 3D black blood TSE SPACE vs 2D TSE. *World J Radiol* 2014; **6**: 192-202 [PMID: 24876923 DOI: 10.4329/wjr.v6.i5.192]
- 2 **Faxon DP**, Fuster V, Libby P, Beckman JA, Hiatt WR, Thompson RW, Topper JN, Annex BH, Rundback JH, Fabunmi RP, Robertson RM, Loscalzo J. Atherosclerotic Vascular Disease Conference: Writing Group III: pathophysiology. *Circulation* 2004; **109**: 2617-2625 [PMID: 15173044 DOI: 10.1161/01.CIR.0000128520.37674.EF]
- 3 **Alie N**, Eldib M, Fayad ZA, Mani V. Inflammation, Atherosclerosis, and Coronary Artery Disease: PET/CT for the Evaluation of Atherosclerosis and Inflammation. *Clin Med Insights Cardiol* 2014; **8**: 13-21 [PMID: 25674025 DOI: 10.4137/CMC.S17063]
- 4 **Zimmerman NB**. Occlusive vascular disorders of the upper extremity. *Hand Clin* 1993; **9**: 139-150 [PMID: 8444972]
- 5 **Yeager RA**, Moneta GL, Edwards JM, Landry GJ, Taylor LM, McConnell DB, Porter JM. Relationship of hemodialysis access to finger gangrene in patients with end-stage renal disease. *J Vasc Surg* 2002; **36**: 245-249; discussion 249 [PMID: 12170204]
- 6 **Stafford L**, Englert H, Gover J, Bertouch J. Distribution of macrovascular disease in scleroderma. *Ann Rheum Dis* 1998; **57**: 476-479 [PMID: 9797553]
- 7 **Lescoat A**, Coiffier G, Rouil A, Droitcourt C, Cazalets C, de Carlan M, Perdriger A, Jégo P. Vascular evaluation of the hand by Power Doppler Ultrasonography provides new predictive markers of ischemic digital ulcers in systemic sclerosis. *Arthritis Care Res (Hoboken)* 2016 Jul 7; Epub ahead of print [PMID: 27390194 DOI: 10.1002/acr.22965]
- 8 **Chikui T**, Izumi M, Eguchi K, Kawabe Y, Nakamura T. Doppler spectral waveform analysis of arteries of the hand in patients with Raynaud's phenomenon as compared with healthy subjects. *AJR Am J Roentgenol* 1999; **172**: 1605-1609 [PMID: 10350298 DOI: 10.2214/ajr.172.6.10350298]
- 9 **Rivera-Chavarría IJ**, Brenes-Gutiérrez JD. Thromboangiitis obliterans (Buerger's disease). *Ann Med Surg (Lond)* 2016; **7**: 79-82 [PMID: 27144003 DOI: 10.1016/j.amsu.2016.03.028]
- 10 **Gallagher KA**, Tracci MC, Scovell SD. Vascular arteritides in women. *J Vasc Surg* 2013; **57**: 27S-36S [PMID: 23522715 DOI: 10.1016/j.jvs.2012.10.119]
- 11 **Fazeli B**, Rezaee SA. A review on thromboangiitis obliterans pathophysiology: thrombosis and angiitis, which is to blame? *Vascular* 2011; **19**: 141-153 [PMID: 21652666 DOI: 10.1258/vasc.2010.ra0045]
- 12 **Marie I**, Hervé F, Primard E, Cailleux N, Levesque H. Long-term follow-up of hypothernar hammer syndrome: a series of 47 patients. *Medicine (Baltimore)* 2007; **86**: 334-343 [PMID: 18004178 DOI: 10.1097/MD.0b013e31815c95d3]
- 13 **Carpentier PH**, Biro C, Jiguet M, Maricq HR. Prevalence, risk factors, and clinical correlates of ulnar artery occlusion in the general population. *J Vasc Surg* 2009; **50**: 1333-1339 [PMID: 19837535 DOI: 10.1016/j.jvs.2009.07.076]
- 14 **Iannuzzi NP**, Higgins JP. Acute Arterial Thrombosis of the Hand. *J Hand Surg Am* 2015; **40**: 2099-2106 [PMID: 26408378 DOI: 10.1016/j.jhsa.2015.04.015]
- 15 **Ymalay R**, Sadanala U, Tinney JP, Kriss V, Keller BB. Initial Observations and Limitations of Vevo 2100 High Resolution Ultrasound Imaging in Neonates. *J Invest Med* 2012; **60**: 379
- 16 **Kaufman CL**, Ouseph R, Blair B, Kutz JE, Tsai TM, Scheker LR, Tien HY, Moreno R, Ozyurekoglu T, Banegas R, Murphy E, Burns CB, Zaring R, Cook DF, and Marvin MR. Graft Vasculopathy in Clinical Hand Transplantation. *Am J Transplant* 2012; **12**: 1004-1016 [DOI: 10.1111/j.1600-6143.2011.03915]
- 17 **Mihai G**, Chung YC, Merchant A, Simonetti OP, Rajagopalan S. T1-weighted-SPACE dark blood whole body magnetic resonance angiography (DB-WBMRA): initial experience. *J Magn Reson Imaging* 2010; **31**: 502-509 [PMID: 20099365 DOI: 10.1002/jmri.22049]
- 18 **Zhang Z**, Fan Z, Carroll TJ, Chung Y, Weale P, Jerecic R, Li D. Three-dimensional T2-weighted MRI of the human femoral arterial vessel wall at 3.0 Tesla. *Invest Radiol* 2009; **44**: 619-626 [PMID: 19692844 DOI: 10.1097/RLI.0b013e3181b4c218]
- 19 **Fayad ZA**, Mani V, Woodward M, Kallend D, Abt M, Burgess T, Fuster V, Ballantyne CM, Stein EA, Tardif JC, Rudd JH, Farkouh ME, Tawakol A. Safety and efficacy of dalcetrapib on atherosclerotic disease using novel non-invasive multimodality imaging (dal-PLAQUE): a randomised clinical trial. *Lancet* 2011; **378**: 1547-1559 [PMID: 21908036 DOI: 10.1016/S0140-6736(11)61383-4]
- 20 **Balu N**, Chu B, Hatsukami TS, Yuan C, Yarnykh VL. Comparison between 2D and 3D high-resolution black-blood techniques for carotid artery wall imaging in clinically significant atherosclerosis. *J Magn Reson Imaging* 2008; **27**: 918-924 [PMID: 18383253 DOI: 10.1002/jmri.21282]
- 21 **Blackband SJ**, Buckley DL, Knowles AJ, Gibbs P, Turnbull LW, Horsman A. Improved peripheral MR angiography with temperature regulation in healthy patients. *Radiology* 1996; **198**: 899-902 [PMID: 8628890 DOI: 10.1148/radiology.198.3.8628890]

P- Reviewer: Chow J, Gumustas OG, Tang GH **S- Editor:** Qi Y
L- Editor: A **E- Editor:** Wu HL



Observational Study

Gastric blunt traumatic injuries: A computed tomography grading classification

Antonio Solazzo, Giulia Lassandro, Francesco Lassandro

Antonio Solazzo, Department of Radiology, AO Bolognini di Seriate, 24068 Seriate, Italy

Giulia Lassandro, Department of Radiology, Federico II University, 80131 Naples, Italy

Francesco Lassandro, Department of Radiology, Monaldi Hospital, 80131 Naples, Italy

Author contributions: Solazzo A and Lassandro G analyzed and interpreted the data and drafted the article; Lassandro F designed the study, acquired data and critically revised the article; all the authors approved the version for publication.

Institutional review board statement: Approved by ethical committee of SUN-Monaldi n.940 August 2, 2016.

Informed consent statement: Participants informed consent was not obtained to be enrolled in this study, but data are anonymized and risk of identification is low.

Conflict-of-interest statement: All the authors have no conflict of interests.

Data sharing statement: No addition data are available.

Open-Access: This article is an open-access article which was selected by an in-house editor and fully peer-reviewed by external reviewers. It is distributed in accordance with the Creative Commons Attribution Non Commercial (CC BY-NC 4.0) license, which permits others to distribute, remix, adapt, build upon this work non-commercially, and license their derivative works on different terms, provided the original work is properly cited and the use is non-commercial. See: <http://creativecommons.org/licenses/by-nc/4.0/>

Manuscript source: Invited manuscript

Correspondence to: Francesco Lassandro, MD, Department of Radiology, Monaldi Hospital, via Leonardo Bianchi, 80131 Naples, Italy. f.lassandro@gmail.com
Telephone: +39-081-5786114
Fax: +39-081-5786114

Received: July 13, 2016

Peer-review started: July 16, 2016

First decision: September 2, 2016

Revised: October 30, 2016

Accepted: December 1, 2016

Article in press: December 2, 2016

Published online: February 28, 2017

Abstract

AIM

To produce a radiological grading of gastric traumatic injuries.

METHODS

In our study, we retrospectively analyzed 32 cases of blunt gastric traumatic injuries and compared computed tomography (CT) data with patients' surgical or medical development. In all cases, a basal phase was acquired, and an intravenous contrast material was administered *via* an antecubital venous catheter with acquisition in the venous phase (70-90 s). In addition, a further set of delayed scans was performed 4-5 min after the first scanning session, without supplementary intravenous contrast material, to identify or better define areas of active bleeding. All CT examinations were retrospectively reviewed by two radiologists, with more than 5 years of experience in emergency radiology, to detect signs of gastric injuries and/or associated abdominal lesions according to literature data. Specific CT findings for gastric rupture include luminal content extravasation and discontinuity of the gastric wall, while CT findings suggestive of injury consisted of free peritoneal fluid, extraluminal air, pneumatosis, and thickening and hematoma of gastric wall.

RESULTS

We found 32 gastric traumatic injuries. In 22 patients

(68.8%), the diagnosis was based on the surgical findings; in the other 10 patients (31.2%), the diagnosis was based on the clinical and CT radiological data. We observed discontinuity of the gastric wall and luminal content extravasation in 1 patient (3.1%); in 10 patients (31.2%), there was extra-luminal air in the peritoneum. In 28 patients (87.5%), there was peritoneal fluid, which was blood in 14 patients (hematoma in 11 patients and contrast material extravasation from active bleeding in 3 patients). In 15 patients (46.9%), there was gastric wall thickening. In 3 patients, it was possible to identify a prevalent involvement of the external layer of the gastric wall, whereas, in 2 patients, the inner side of the gastric wall presented with major involvement. In 3 patients (9.4%), pneumatosis of the gastric wall was detected. In 19 (59.4%) patients, the stomach was full. The fundus was the most frequently damaged part of the stomach because it was involved in 17 patients (53.1%). Based on the observed data, we identified four grades of gastric lesions.

CONCLUSION

A radiologic score is helpful for guiding the diagnosis and management (surgical or conservative) of gastric blunt traumatic injuries and stratify patients according to short-term outcomes.

Key words: Gastric injuries; Blunt trauma; Computed tomography grading; Emergency radiology; Stomach rupture

© **The Author(s) 2017.** Published by Baishideng Publishing Group Inc. All rights reserved.

Core tip: Although a wide spectrum of computed tomography findings has been described for gastric blunt traumas, no systematic instrumental approach exists in this setting. In this study the authors produced a radiological grading of gastric traumatic injuries that might play a role in both the diagnostic phase of the emergency setting and prognostic stratification of these patients.

Solazzo A, Lassandro G, Lassandro F. Gastric blunt traumatic injuries: A computed tomography grading classification. *World J Radiol* 2017; 9(2): 85-90 Available from: URL: <http://www.wjgnet.com/1949-8470/full/v9/i2/85.htm> DOI: <http://dx.doi.org/10.4329/wjr.v9.i2.85>

INTRODUCTION

In Europe, blunt trauma is the main cause of death in the first four decades of life, and there is a substantial rate of permanent disability^[1,2].

Blunt trauma involving the stomach is infrequent with a reported incidence of 0.4%-1.7%^[3-5]; however, such trauma may cause extremely high individual and social consequences^[6].

Management of traumatic injuries requires a high index of suspicion, rapid investigation, accurate classification and well-defined treatment protocols to ensure optimal outcomes and reduce long-term disabilities^[7].

Clinical signs and symptoms of gastrointestinal injuries often require hours before they appear, and a delayed diagnosis may prolong the period of peritoneal contamination, increasing the incidence of intra-abdominal complications, such as abscess, sepsis, and mortality^[8,9]. Moreover, the differentiating between injuries requiring surgery and those that can be treated conservatively may be very challenging^[10].

The widespread introduction of traumatic injury classifications, based on clinical and instrumental findings for most of the abdominal organs, has greatly improved the management of patients with traumatic injuries^[7]. Although a wide spectrum of computed tomography (CT) findings has been described for gastric blunt traumas, no systematic instrumental approach exists in this setting^[11]. For this reason, we sought to produce a radiological grading of gastric traumatic injuries in our study that might play a role in both the diagnostic phase of the emergency setting and prognostic stratification of these patients.

MATERIALS AND METHODS

Over a 14-year period, from January 2002 to December 2015, a total of 32 patients (22 males and 10 females; age range 16-82 years, mean age: 41.34) with evidence of blunt gastric traumatic injuries were retrospectively identified based on the final surgical and radiological reports.

The diagnosis of gastric injury was based on the surgical findings in 22 patients, whereas the diagnosis for 10 patients was based on the clinical and radiological findings. CT scan was performed in all patients.

CT scans were performed with different scanners over time, reflecting the evolution of the technique, ranging from single slice helical CT to 64-row detector CT. In all cases, a basal phase was acquired, and an intravenous contrast material was administered *via* an antecubital venous catheter with acquisition in the venous phase (70-90 s). In addition, a further set of delayed scans was performed 4-5 min after the first scanning session, without supplementary intravenous contrast material, to identify or better define areas of active bleeding.

All CT examinations were retrospectively reviewed by two radiologists, with more than 5 years of experience in emergency radiology, to detect signs of gastric injuries and/or associated abdominal lesions according to literature data. Specific CT findings for gastric rupture include luminal content extravasation and discontinuity of the gastric wall, while CT findings suggestive of injury consisted of free peritoneal fluid, extraluminal air, pneumatosis, and thickening and hematoma of gastric wall^[11].

Table 1 Computed tomography signs of gastric blunt traumatic injuries

CT signs of gastric blunt traumatic injuries (n. 57 in 32)	
Gastric wall discontinuity	1
Extraluminal air	10
Peritoneal fluid	28
Hematoma	11
Contrast material	3
Luminal content extravasation	1
Gastric wall thickening	15
Pneumatosis of gastric wall	3

CT: Computed tomography.

Table 2 Abdominal associated lesions

Abdominal associated lesions (n. 33 in 27 patients)	
Large bowel	2
Spleen	14
Liver	9
Left kidney	3
Right kidney	1
Pancreas	1
Mesentery	3

We evaluated the relevance of each instrumental pattern of gastric blunt injury, comparing the radiological signs with surgical findings or clinical follow-up, to propose a radiologic classification for this type of injury.

RESULTS

We found 32 gastric traumatic injuries. In 22 patients (68.8%), the diagnosis was based on the surgical findings; in the other 10 patients (31.2%), the diagnosis was based on the clinical and CT radiological data.

We observed (Table 1) discontinuity of the gastric wall and luminal content extravasation in 1 patient (3.1%); in 10 patients (31.2%), there was extra-luminal air in the peritoneum (it was linked to pneumoretroperitoneum in 2 patients and to pneumomediastinum in 1 patient). In 28 patients (87.5%), there was peritoneal fluid, which was blood in 14 patients (hematoma in 11 patients and contrast material extravasation from active bleeding in 3 patients). In 15 patients (46.9%), there was gastric wall thickening. In 3 patients, it was possible to identify a prevalent involvement of the external layer of the gastric wall, whereas, in 2 patients, the inner side of the gastric wall presented with major involvement. In 3 patients (9.4%), pneumatosis of the gastric wall was detected. In 19 (59.4%) patients, the stomach was full.

Twenty-seven patients (84.4%) presented with associated abdominal lesions. The spleen was the most frequently involved organ (43.8%), which was followed by the liver (28.1%), kidneys (12.5%), large bowel (6.3%), mesentery (9.4%) and pancreas (3.1%) (Table 2).

The fundus was the most frequently damaged part of the stomach because it was involved in 17 patients

Table 3 Location of gastric lesions

Location of gastric lesions	
Fundus	17
Body	15
Anterior wall	7
Greater curvature	2
Small curvature	1
Posterior surface	3
Antrum	3
Not detectable	1

(53.1%) (Table 3).

All patients with extraluminal air and/or peritoneal hematic collections underwent surgery. Among the 22 patients with a surgical diagnosis of gastric lesions, 14 showed radiological signs that were directly related to gastric involvement (thickening of the gastric wall, extraluminal air in proximity to the gastric wall and discontinuity of the gastric wall) (66.6%). In the other 8 patients, a gastric lesion was diagnosed during surgery, but it was not detected on the CT scan.

Peritoneal fluid was detected in all patients who underwent surgery, but it was also present in 6 of 10 patients who were conservatively treated (60%).

Nine out of 10 patients who had not undergone surgery showed a thickened gastric wall on CT. Perigastric pneumatosis was the only sign in one patient.

Pneumatosis of the gastric wall was observed in 3 patients (9.4%), two with significant gastric lesion requiring surgery and one who recovered spontaneously.

Based on the observed data, we identified four grades of gastric lesions.

Cases with minor contusion with parietal thickening alone (Figure 1), which did not involve the fundus and was not associated with the peritoneal fluid, and only included portal pneumatosis (Figure 2) detected by CT scan, do not require surgical intervention (grade 1 lesion). Cases of minor lacerations with high attenuating focal thickening involving the mucosal side and with a small level without hematic peritoneal fluid (Figure 3) require monitoring (grade 2 lesion). Cases with partial laceration with parietal hematoma and/or stretching of the external layer and peritoneal hematic collection (Figure 4) require careful monitoring (grade 3 lesion). Cases with full thickness rupture, necrosis, food in peritoneal cavity, vascular involvement and contrast media extravasation (Figure 5) require intervention (grade 4 lesion) (Table 4).

DISCUSSION

Trauma currently represents a major social and sanitary problem with characteristics of an epidemic illness involving especially young people and with a high residual morbidity.

Gastric blunt traumas often occur after high velocity impact involving the epigastric region when the stomach is full, in the post-prandial phase^[12-14], due to

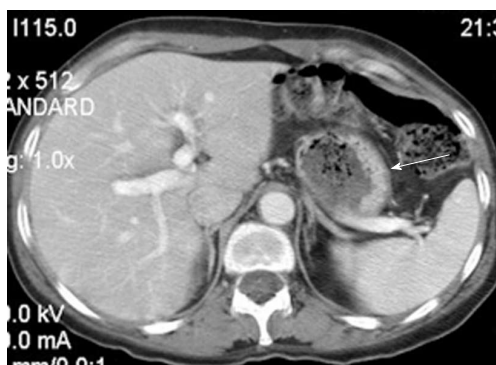


Figure 1 Wall thickening of the gastric body (arrow). Surgery was not required. Grade 1 lesion.

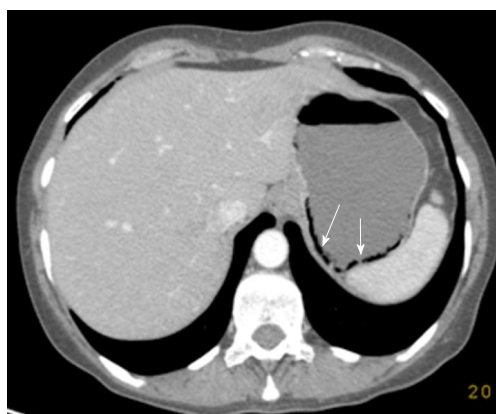


Figure 2 Isolated gastric pneumatosis after abdominal trauma (arrows). Spontaneous recovery. Grade 1 lesion.



Figure 3 Blood in the gastric lumen (arrow). Follow-up without surgery. Grade 2 lesion.

the positive correlation between the wall pressure and cavity radius, as explained in Laplace's law. These data were confirmed by an experimental model of rats that also demonstrated a higher frequency and grade of injury of other parenchymal organs in rats with full stomachs^[15]. Moreover, a full thickness rupture is more frequently observed at the level of the fundus^[11,16]. The mechanisms responsible for gastric injuries in blunt trauma include tangential tearing along fixed points,

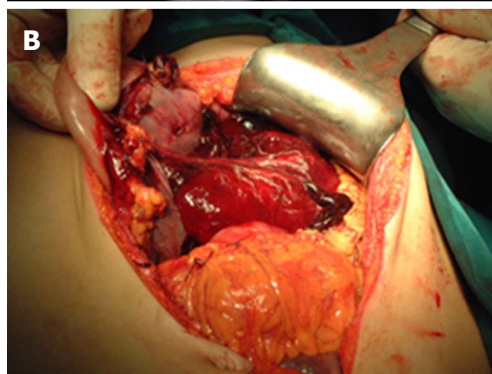


Figure 4 Parietal hematoma. A: Parietal hematoma: Thickening with high-attenuation in the external layer of gastric wall (arrows). Grade 3 lesion. Follow-up with subsequent surgery for worsening symptoms and peritoneal reaction; B: External layer gastric wall hematoma confirmed at surgery.

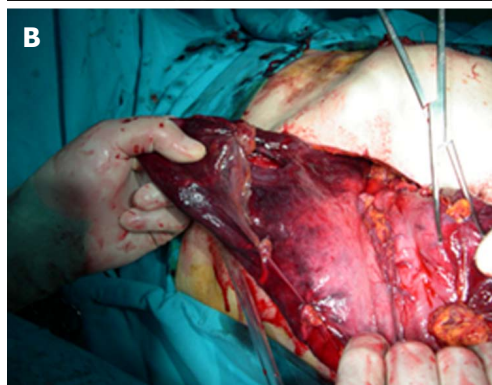
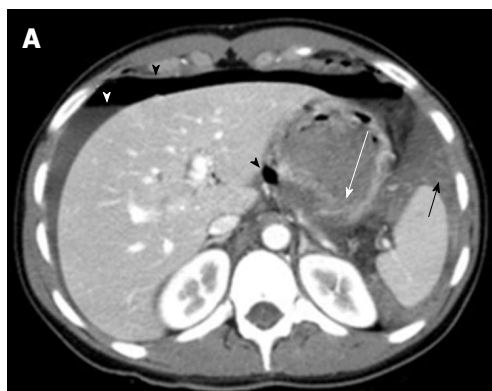


Figure 5 Gastric rupture. A: Gastric wall rupture (white arrow): Peritoneal fluid (white arrowhead) with homogeneous hyperdense components from blood (black arrow), pneumoperitoneum with a bubble of gas located close to the gastric lesion (black arrowheads). Grade 4 lesion; B: Gastric rupture confirmed at surgery.

Table 4 Grading computed tomography of gastric blunt traumatic injuries

	Pathology	CT signs	Treatment
Grade 1	Gastric contusion	Gastric wall thickening No peritoneal fluid	No surgery
Grade 2	Minor lacerations involving the mucosal side	Perigastric pneumatosis High-attenuation hematoma confined to the inner side, blood in the gastric lumen	Follow-up
Grade 3	Partial laceration with parietal hematoma and/or stretching of the external layer	Small amount of non-bloody peritoneal fluid Peritoneal hematoma collection, gastric wall thickening with high-attenuation of the external side	Close follow-up/ surgery
Grade 4	Full thickness rupture Vascular involvement (necrosis or active bleeding)	Extraluminal air Luminal content extravasation Contrast material extravasation	Emergency surgery

CT: Computed tomography.

increased intraluminal pressure, and crushing against vertebral bodies^[17].

In the management of trauma patients, diagnostic imaging plays a key role, especially CT, which is considered the gold standard for accurate and fast detection of abdominal injuries.

To standardize and improve clinical outcomes, especially for prompt identification of patients who need to be referred to surgery, radiological scores have been widely used.

Although they represent 0.4%-1.7% of all abdominal traumas^[12,18-20], gastric blunt traumatic injuries have rarely been described in the medical literature^[12,18-21], and a CT grading classification is not yet available. For this reason, we propose a radiological score based on our experience and literature data to better classify these lesions (Table 4).

Full thickness rupture of the stomach requires prompt surgical intervention, which is also the cases with vascular involvement, infarct or hemorrhage. However, in several cases, a parietal thickening may be observed on CT scans, bringing attention to the stomach without necessarily requiring surgery.

In some cases, the gas content of the stomach, which usually plays a protective role, can dissect the mucosal layer and pass into the gastric veins, causing perigastric pneumatosis and, subsequently, portal pneumatosis^[10,11,22], a condition that could be related to more serious conditions, such as an intestinal infarction from traumatic shock.

Extraluminal air, hematic peritoneal collection and active bleeding suggest patients should be referred to surgery. Proximal lesions with fundus involvement more often require surgery. In other cases, less aggressive treatment and surveillance may be indicated.

However, in 33.3% of our patients who required surgery, a gastric injury was detected on surgical intervention without any previous radiological suspicion. The use of a simple classification could help guide medical practice.

In conclusion, traumatic injuries require a careful and systematic treatment approach because of their economic and social relevance. For these reasons,

uncommon lesions require attention, and a meta-analysis should be performed.

COMMENTS

Background

Gastric injuries after blunt trauma have rarely been reported in the literature; however, preoperative recognition and staging of these lesions play a critical role in patient management.

Research frontiers

The widespread introduction of traumatic injury classifications, based on clinical and instrumental findings for most of the abdominal organs, has greatly improved the management of patients with traumatic injuries. Although a wide spectrum of computed tomography findings has been described for gastric blunt traumas, no systematic instrumental approach exists in this setting.

Innovations and breakthroughs

The authors produced a radiological grading of gastric traumatic injuries.

Applications

The study results suggest that a radiological grading of gastric traumatic injuries might play a role in both the diagnostic phase of the emergency setting and prognostic stratification of these patients.

Peer-review

The authors investigated gastric blunt traumatic injuries about computed tomography classification. The work is good and well designed.

REFERENCES

- 1 Bode PJ, Edwards MJ, Kruit MC, van Vugt AB. Sonography in a clinical algorithm for early evaluation of 1671 patients with blunt abdominal trauma. *AJR Am J Roentgenol* 1999; **172**: 905-911 [PMID: 10587119 DOI: 10.2214/ajr.172.4.10587119]
- 2 van Beeck EF, van Roijen L, Mackenbach JP. Medical costs and economic production losses due to injuries in the Netherlands. *J Trauma* 1997; **42**: 1116-1123 [PMID: 9210552 DOI: 10.1097/00005373-199706000-00023]
- 3 Takabe K, Ohtani T, Muto I, Takano Y, Miyauchi T, Kato H, Sekido H, Ohki S, Hatakeyama K, Shimada H. Computed tomography (CT) findings of gastric rupture after blunt trauma. *Hepato-gastroenterology* 2000; **47**: 901-903 [PMID: 10919058]
- 4 Oncel D, Malinoski D, Brown C, Demetriades D, Salim A. Blunt gastric injuries. *Am Surg* 2007; **73**: 880-883 [PMID: 17939417]
- 5 Brusca V, Coimbra R, Rasslan S, Abrantes WL, Souza HP, Neto G, Dalcin RR, Drumond DA, Ribas JR. Blunt gastric injury. A

- multicentre experience. *Injury* 2001; **32**: 761-764 [PMID: 11754882 DOI: 10.1016/S0020-1383(01)00081-X]
- 6 **Hoyt DB**, Coimbra R, Potenza BM. Trauma System, Triage, and Transport. In: Feliciano DV, Mattox KL, Moore EE, Bonnie RJ, Fulco CE, Liverman CT, editors. *Magnitude and Costs. Reducing the burden of injury. Advancing Prevention and Treatment*. Washington, DC, United States: National Academy Press, 1999
- 7 **Oniscu GC**, Parks RW, Garden OJ. Classification of liver and pancreatic trauma. *HPB* (Oxford) 2006; **8**: 4-9 [PMID: 18333232 DOI: 10.1080/13651820500465881]
- 8 **Brody JM**, Leighton DB, Murphy BL, Abbott GF, Vaccaro JP, Jagminas L, Cioffi WG. CT of blunt trauma bowel and mesenteric injury: typical findings and pitfalls in diagnosis. *Radiographics* 2000; **20**: 1525-1536; discussion 1536-1537 [PMID: 11112806 DOI: 10.1148/radiographics.20.6.g00nv021525]
- 9 **Butela ST**, Federle MP, Chang PJ, Thaete FL, Peterson MS, Dorvault CJ, Hari AK, Soni S, Branstetter BF, Paisley KJ, Huang LF. Performance of CT in detection of bowel injury. *AJR Am J Roentgenol* 2001; **176**: 129-135 [PMID: 11133551 DOI: 10.2214/ajr.176.1.1760129]
- 10 **Scaglione M**, de Lutio di Castelguidone E, Scialpi M, Merola S, Dietrich AI, Lombardo P, Romano L, Grassi R. Blunt trauma to the gastrointestinal tract and mesentery: is there a role for helical CT in the decision-making process? *Eur J Radiol* 2004; **50**: 67-73 [PMID: 15093237 DOI: 10.1016/j.ejrad.2003.11.016]
- 11 **Lassandro F**, Romano S, Rossi G, Muto R, Cappabianca S, Grassi R. Gastric traumatic injuries: CT findings. *Eur J Radiol* 2006; **59**: 349-354 [PMID: 16787728 DOI: 10.1016/j.ejrad.2006.04.028]
- 12 **Courcy PA**, Soderstrom C, Brotman S. Gastric rupture from blunt trauma. A plea for minimal diagnostics and early surgery. *Am Surg* 1984; **50**: 424-427 [PMID: 6331779]
- 13 **Siemens RA**, Fulton RL. Gastric rupture as a result of blunt trauma. *Am Surg* 1977; **43**: 229-233 [PMID: 851294]
- 14 **Takabe K**, Hatakeyama K. Computed tomography is useful for preoperative workup of gastric rupture caused by blunt trauma. *Surg Today* 2009; **39**: 1109 [PMID: 19997812 DOI: 10.1007/s00595-009-4069-7]
- 15 **Kafadar H**, Kafadar S, Tokdemir M. Comparison of internal organ injuries by blunt abdominal trauma in rats with empty or full stomach. *Ulus Travma Acil Cerrahi Derg* 2014; **20**: 395-400 [PMID: 25541917 DOI: 10.5505/tjtes.2014.92331]
- 16 **Shinkawa H**, Yasuhara H, Naka S, Morikane K, Furuya Y, Niwa H, Kikuchi T. Characteristic features of abdominal organ injuries associated with gastric rupture in blunt abdominal trauma. *Am J Surg* 2004; **187**: 394-397 [PMID: 15006569 DOI: 10.1016/j.amjsurg.2003.12.018]
- 17 **Madiba TE**, Hlophe M. Gastric trauma: a straightforward injury, but no room for complacency. *S Afr J Surg* 2008; **46**: 10-13 [PMID: 18468416]
- 18 **Brunsting LA**, Morton JH. Gastric rupture from blunt abdominal trauma. *J Trauma* 1987; **27**: 887-891 [PMID: 3612865 DOI: 10.1097/00005373-198708000-00007]
- 19 **Pikoulis E**, Delis S, Tsatsoulis P, Leppäniemi A, Derlopas K, Koukoulides G, Mantonakis S. Blunt injuries of the stomach. *Eur J Surg* 1999; **165**: 937-939 [PMID: 10574100 DOI: 10.1080/110241599750008035]
- 20 **Semel L**, Frittelli G. Gastric rupture from blunt abdominal trauma. *N Y State J Med* 1981; **81**: 938-939 [PMID: 6940012]
- 21 **Nanji SA**, Mock C. Gastric rupture resulting from blunt abdominal trauma and requiring gastric resection. *J Trauma* 1999; **47**: 410-412 [PMID: 10452486 DOI: 10.1097/00005373-199908000-00040]
- 22 **Kingsley DD**, Albrecht RM, Vogt DM. Gastric pneumatosis and hepatoportal venous gas in blunt trauma: clinical significance in a case report. *J Trauma* 2000; **49**: 951-953 [PMID: 11086792 DOI: 10.1097/00005373-200011000-00027]

P- Reviewer: Bazeed MF, Gao BL, Shen J **S- Editor:** Gong XM

L- Editor: A **E- Editor:** Wu HL





Published by **Baishideng Publishing Group Inc**

8226 Regency Drive, Pleasanton, CA 94588, USA

Telephone: +1-925-223-8242

Fax: +1-925-223-8243

E-mail: bpgoffice@wjgnet.com

Help Desk: <http://www.wjgnet.com/esps/helpdesk.aspx>

<http://www.wjgnet.com>



World Journal of *Radiology*

World J Radiol 2017 March 28; 9(3): 91-147





Editorial Board

2014-2017

The *World Journal of Radiology* Editorial Board consists of 365 members, representing a team of worldwide experts in radiology. They are from 36 countries, including Afghanistan (1), Argentina (2), Australia (5), Austria (7), Belgium (2), Brazil (8), Canada (6), Chile (1), China (43), Croatia (1), Denmark (4), Egypt (6), France (5), Germany (22), Greece (10), India (12), Iran (6), Ireland (2), Israel (3), Italy (47), Japan (13), Netherlands (1), New Zealand (1), Pakistan (1), Poland (2), Portugal (1), Serbia (1), Singapore (3), Slovakia (1), South Korea (18), Spain (4), Sweden (2), Switzerland (4), Thailand (1), Turkey (26), United Kingdom (11), and United States (82).

EDITORS-IN-CHIEF

Kai U Juergens, *Bremen*
Edwin JR van Beek, *Edinburgh*
Thomas J Vogl, *Frankfurt*

GUEST EDITORIAL BOARD MEMBERS

Wing P Chan, *Taipei*
Chung-Huei Hsu, *Taipei*
Chin-Chang Huang, *Taipei*
Tsong-Long Hwang, *Taoyuan*
Jung-Lung Hsu, *Taipei*
Chia-Hung Kao, *Taichung*
Yu-Ting Kuo, *Tainan*
Hon-Man Liu, *Taipei*
Hui-Lung Liang, *Kaohsiung*
Chun Chung Lui, *Kaohsiung*
Sen-Wen Teng, *Taipei*
Yung-Liang (William) Wan, *Taoyuan*

MEMBERS OF THE EDITORIAL BOARD



Afghanistan

Takao Hiraki, *Okayama*



Argentina

Patricia Carrascosa, *Vicente Lopez*
Maria C Ziadi, *Rosario*



Australia

Lourens Bester, *Sydney*
Gemma A Figtree, *Sydney*



Austria

Herwig R Cerwenka, *Graz*
Gudrun M Feuchtnner, *Innsbruck*
Benjamin Henninger, *Innsbruck*
Rupert Lanzenberger, *Vienna*
Shu-Ren Li, *Vienna*
Veronika Schopf, *Vienna*
Tobias De Zordo, *Innsbruck*



Belgium

Steve Majerus, *Liege*
Kathelijne Peremans, *Merelbeke*



Brazil

Clerio F Azevedo, *Rio de Janeiro*
Patrícia P Alfredo, *São Paulo*
Eduardo FC Fleury, *São Paulo*
Edward Araujo Júnior, *São Paulo*
Wellington P Martins, *Ribeirao Preto*
Ricardo A Mesquita, *Belo Horizonte*
Vera MC Salemi, *São Paulo*
Claudia Szobot, *Porto Alegre*
Lilian YI Yamaga, *São Paulo*



Canada

Marie Arsalidou, *Toronto*
Otman A Basir, *Waterloo*

Tarik Zine Belhocine, *Toronto*
James Chow, *Toronto*
Tae K Kim, *Toronto*
Anastasia Oikonomou, *Toronto*



China

Hong-Wei Chen, *Wuxi*
Feng Chen, *Hangzhou*
Jian-Ping Chu, *Guangzhou*
Guo-Guang Fan, *Shenyang*
Bu-Lang Gao, *Shijiazhuang*
Qi-Yong Gong, *Chengdu*
Ying Han, *Beijing*
Xian-Li Lv, *Beijing*
Yi-Zhuo Li, *Guangzhou*
Xiang-Xi Meng, *Harbin*
Yun Peng, *Beijing*
Jun Shen, *Guangzhou*
Ze-Zhou Song, *Hangzhou*
Wai Kwong Tang, *Hong Kong*
Gang-Hua Tang, *Guangzhou*
Jie Tian, *Beijing*
Lu-Hua Wang, *Beijing*
Xiao-bing Wang, *Xi'an*
Yi-Gen Wu, *Nanjing*
Kai Wu, *Guangzhou*
Hui-Xiong Xu, *Shanghai*
Zuo-Zhang Yang, *Kunming*
Xiao-Dan Ye, *Shanghai*
David T Yew, *Hong Kong*
Ting-He Yu, *Chongqing*
Zheng Yuan, *Shanghai*
Min-Ming Zhang, *Hangzhou*
Yudong Zhang, *Nanjing*
Dong Zhang, *Chongqing*
Wen-Bin Zeng, *Changsha*

Yue-Qi Zhu, *Shanghai*



Croatia

Goran Kusec, *Osijek*



Denmark

Poul E Andersen, *Odense*

Lars J Petersen, *Aalborg*

Thomas Z Ramsøy, *Frederiksberg*

Morten Ziebell, *Copenhagen*



Egypt

Mohamed F Bazeed, *Mansoura*

Mohamed Abou El-Ghar, *Mansoura*

Reem HA Mohamed, *Cairo*

Mohamed R Nouh, *Alexandria*

Ahmed AKA Razek, *Mansoura*

Ashraf A Zytoon, *Shebin El-Koom*



France

Sabine F Bensamoun, *Compiègne*

Romarc Loffroy, *Dijon*

Stephanie Nougaret, *Montpellier*

Hassane Oudadesse, *Rennes*

Vincent Vinh-Hung, *Fort-de-France*



Germany

Henryk Barthel, *Leipzig*

Peter Bannas, *Hamburg*

Martin Beeres, *Frankfurt*

Ilja F Ciernik, *Dessau*

A Dimitrakopoulou-Strauss, *Heidelberg*

Peter A Fasching, *Erlangen*

Andreas G Schreyer, *Regensburg*

Philipp Heusch, *Duesseldorf*

Sonja M Kirchhoff, *Munich*

Sebastian Ley, *Munich*

Adel Maataoui, *Frankfurt am Main*

Stephan M Meckel, *Freiburg*

Hans W Muller, *Duesseldorf*

Kay Raum, *Berlin*

Dirk Rades, *Luebeck*

Marc-Ulrich Regier, *Hamburg*

Alexey Surov, *Halle*

Martin Walter, *Magdeburg*

Axel Wetter, *Essen*

Christoph Zilkens, *Düsseldorf*



Greece

Panagiotis Antoniou, *Thessaloniki*

Nikos Efthimiou, *Athens*

Dimitris Karnabatidis, *Patras*

George Latsios, *Athens*

Stylianios Megremis, *Iraklion*

Alexander D Rapidis, *Athens*

Kiki Theodorou, *Larissa*

Ioannis A Tsalafoutas, *Athens*

Evanthia E Tripoliti, *Ioannina*

Athina C Tsili, *Ioannina*



India

Ritesh Agarwal, *Chandigarh*

Chandan J Das, *New Delhi*

Prathamesh V Joshi, *Mumbai*

Naveen Kalra, *Chandigarh*

Chandrasekharan Kesavadas, *Trivandrum*

Jyoti Kumar, *New Delhi*

Atin Kumar, *New Delhi*

Kaushala P Mishra, *Allahabad*

Daya N Sharma, *New Delhi*

Binit Sureka, *New Delhi*

Sanjay Sharma, *New Delhi*

Raja R Yadav, *Allahabad*



Iran

Majid Assadi, *Bushehr*

SeyedReza Najafizadeh, *Tehran*

Mohammad Ali Oghabian, *Tehran*

Amir Reza Radmard, *Tehran*

Ramin Sadeghi, *Mashhad*

Hadi Rokni Yazdi, *Tehran*



Ireland

Tadhg Gleeson, *Wexford*

Frederik JAI Vernimmen, *Cork*



Israel

Dafna Ben Bashat, *Tel Aviv*

Amit Gefen, *Tel Aviv*

Tamar Sella, *Jerusalem*



Italy

Adriano Alippi, *Rome*

Dante Amelio, *Trento*

Michele Anzidei, *Rome*

Filippo F Angileri, *Messinas*

Stefano Arcangeli, *Rome*

Roberto Azzoni, *San Donato milanese*

Tommaso V Bartolotta, *Palermo*

Tommaso Bartalena, *Imola*

Livia Bernardin, *San Bonifacio*

Federico Boschi, *Verona*

Sergio Casciaro, *Lecce*

Emanuele Casciani, *Rome*

Musa M Can, *Napoli*

Alberto Cuocolo, *Napoli*

Michele Ferrara, *Coppito*

Mauro Feola, *Fossano*

Giampiero Francica, *Castel Volturno*

Luigi De Gennaro, *Rome*

Giulio Giovannetti, *Pisa*

Francesca Iacobellis, *Napoli*

Formato Invernizzi, *Monza Brianza*

Francesco Lassandro, *Naples*

Lorenzo Livi, *Florence*

Pier P Mainenti, *Napoli*

Laura Marzetti, *Chieti*

Giuseppe Malinverni, *Crescentino*

Enrica Milanese, *Turin*

Giovanni Morana, *Treviso*

Lorenzo Monti, *Milan*

Silvia D Morbelli, *Genoa*

Barbara Palumbo, *Perugia*

Cecilia Parazzini, *Milan*

Stefano Pergolizzi, *Messina*

Antonio Pinto, *Naples*

Camillo Porcaro, *Rome*

Carlo C Quattrocchi, *Rome*

Alberto Rebonato, *Perugia*

Giuseppe Rizzo, *Rome*

Roberto De Rosa, *Naples*

Domenico Rubello, *Rovigo*

Andrea Salvati, *Bari*

Sergio Sartori, *Ferrara*

Luca M Sconfienza, *Milano*

Giovanni Storto, *Rionero*

Nicola Sverzellati, *Parma*

Alberto S Tagliafico, *Genova*

Nicola Troisi, *Florence*



Japan

Yasuhiko Hori, *Chiba*

Hidetoshi Ikeda, *Koriyama*

Masahito Kawabori, *Sapporo*

Tamotsu Kamishima, *Sapporo*

Hiro Kiyosue, *Yufu*

Yasunori Minami, *Osaka-sayama*

Yasuhiro Morimoto, *Kitakyushu*

Satoru Murata, *Tokyo*

Shigeki Nagamachi, *Miyazaki*

Hiroshi Onishi, *Yamanashi*

Morio Sato, *Wakayama Shi*

Yoshito Tsushima, *Maebashi*

Masahiro Yanagawa, *Suita*



Netherlands

Willem Jan van Rooij, *Tilburg*



New Zealand

W Howell Round, *Hamilton*



Pakistan

Wazir Muhammad, *Abbottabad*



Poland

Maciej S Baglaj, *Wroclaw*

Piotr Czauderna, *Gdansk*



Portugal

Joao Manuel RS Tavares, *Porto*



Serbia

Olivera Ciraj-Bjelac, *Belgrade*



Singapore

Gopinathan Anil, *Singapore*

Terence KB Teo, *Singapore*

Cher Heng Tan, *Singapore*



Slovakia

Stefan Sivak, *Martin*



South Korea

Ki Seok Choo, *Busan*

Seung Hong Choi, *Seoul*

Dae-Seob Choi, *Jinju*

Hong-Seok Jang, *Seoul*

Yong Jeong, *Daejeon*

Chan Kyo Kim, *Seoul*

Se Hyung Kim, *Seoul*

Joong-Seok Kim, *Seoul*

Sang Eun Kim, *Seongnam*

Sung Joon Kwon, *Seoul*

Jeong Min Lee, *Seoul*

In Sook Lee, *Busan*

Noh Park, *Goyang*

Chang Min Park, *Seoul*

Sung Bin Park, *Seoul*

Deuk Jae Sung, *Seoul*

Choongsoo Shin, *Seoul*

Kwon-Ha Yoon, *Iksan*



Spain

Miguel A De Gregorio, *Zaragoza*

Antonio Luna, *Jaén*

Enrique Marco de Lucas, *Santander*

Fernando Ruiz Santiago, *Granada*



Sweden

Dmitry Grishenkov, *Stockholm*

Tie-Qiang Li, *Stockholm*



Switzerland

Nicolau Beckmann, *Basel*

Christian Boy, *Bern*

Giorgio Treglia, *Bellinzona*

Stephan Ulmer, *Kiel*



Thailand

Sirianong Namwongprom, *Chiang Mai*



Turkey

Kubilay Aydin, *Istanbul*

Ramazan Akdemir, *Sakarya*

Serhat Avcu, *Ankara*

Ayşe Aralasmak, *Istanbul*

Oktay Algin, *Ankara*

Nevbahar Akcar, *Meselik*

Bilal Battal, *Ankara*

Zulkif Bozgeyik, *Elazig*

Nazan Ciledag, *Aakara*

Fuldem Y Donmez, *Ankara*

Gulgun Engin, *Istanbul*

Ahmet Y Goktay, *Izmir*

Oguzhan G Gumustas, *Bursa*

Kaan Gunduz, *Ankara*

Pelin Ozcan Kara, *Mersin*

Kivanc Kamburoglu, *Ankara*

Ozgur Kilickesmez, *Istanbul*

Furuzan Numan, *Istanbul*

Cem Onal, *Adana*

Ozgur Oztekin, *Izmir*

Seda Ozbek (Boruban), *Konya*

Selda Sarikaya, *Zonguldak*

Figen Taser, *Kutahya*

Baran Tokar, *Eskisehir*

Ender Uysal, *Istanbul*

Ensar Yekeler, *Istanbul*



United Kingdom

Indran Davagnanam, *London*

M DC Valdés Hernández, *Edinburgh*

Alan Jackson, *Manchester*

Suneil Jain, *Belfast*

Long R Jiao, *London*

Miltiadis Krokidis, *Cambridge*

Pradesh Kumar, *Liverpool*

Peter D Kuzmich, *Derby*

Georgios Plataniotis, *Brighton*

Vanessa Sluming, *Liverpool*



United States

Garima Agrawal, *Saint Louis*

James R Brasic, *Baltimore*

Rajendra D Badgaiyan, *Buffalo*

Ulas Bagci, *Bethesda*

Anat Biegon, *Stony Brook*

Ramon Casanova, *Winston Salem*

Wenli Cai, *Boston*

Zheng Chang, *Durham*

Corey J Chakarun, *Long Beach*

Kai Chen, *Los Angeles*

Hyun-Soon Chong, *Chicago*

Marco Cura, *Dallas*

Ravi R Desai, *Bensalem*

Delia DeBuc, *Miami*

Carlo N De Cecco, *Charleston*

Timm-Michael L Dickfeld, *Baltimore*

Subba R Digumarthy, *Boston*

Huy M Do, *Stanford*

Todd A Faasse, *Grand Rapids*

Salomao Faintuch, *Boston*

Girish M Fatterpekar, *New York*

Dhakshinamoorthy Ganesan, *Houston*

Robert J Griffin, *Little Rock*

Andrew J Gunn, *Boston*

Sandeep S Hedgire, *Boston*

Timothy J Hoffman, *Columbia*

Mai-Lan Ho, *San Francisco*

Juebin Huang, *Jackson*

Abid Irshad, *Charleston*

Matilde Inglese, *New York*

El-Sayed H Ibrahim, *Jacksonville*

Paul R Julsrud, *Rochester*

Pamela T Johnson, *Baltimore*

Ming-Hung Kao, *Tempe*

Sunil Krishnan, *Houston*

Richard A Komoroski, *Cincinnati*

Sandi A Kwee, *Honolulu*

King Kim, *Ft. Lauderdale*

Guozheng Liu, *Worcester*

Yiyan Liu, *Newark*

Venkatesh Mani, *New York*

Lian-Sheng Ma, *Pleasanton*

Rachna Madan, *Boston*

Zeyad A Metwalli, *Houston*

Yilong Ma, *Manhasset*

Hui Mao, *Atlanta*

Feroze B Mohamed, *Philadelphia*

Gul Moonis, *Boston*

John L Noshier, *New Brunswick*

Rahmi Oklu, *Boston*

Aytekun Oto, *Chicago*

Bishnuhari Paudyal, *Philadelphia*

Rajul Pandya, *Youngstown*

Chong-Xian Pan, *Sacramento*

Jay J Pillai, *Baltimore*

Neal Prakash, *Duarte*

Reza Rahbar, *Boston*

Ali S Raja, *Boston*

Gustavo J Rodriguez, *El Paso*

David J Sahn, *Portland*

Steven Schild, *Scottsdale*

Ali R Sepahdari, *Los Angeles*

Li Shen, *Indianapolis*

JP Sheehan, *Charlottesville*

Atul B Shinagare, *Boston*

Sarabjeet Singh, *Boston*

Charles J Smith, *Columbia*

Kenji Suzuki, *Chicago*

Monvadi Srichai-Parsia, *Washington*

Sree H Tirumani, *Boston*

Hebert A Vargas, *New York*

Sachit Verma, *Philadelphia*

Yoichi Watanabe, *Minneapolis*

Li Wang, *Chapel Hill*

Carol C Wu, *Boston*

Shoujun Xu, *Houston*

Min Yao, *Cleveland*

Xiaofeng Yang, *Atlanta*

Qingbao Yu, *Albuquerque*

Aifeng Zhang, *Chicago*

Chao Zhou, *Bethlehem*

Hongming Zhuang, *Philadelphia*

**EDITORIAL**

- 91 Laser ablation of liver tumors: An ancillary technique, or an alternative to radiofrequency and microwave?
Sartori S, Di Vece F, Ermili F, Tombesi P

REVIEW

- 97 Complementary roles of interventional radiology and therapeutic endoscopy in gastroenterology
Ray DM, Srinivasan I, Tang SJ, Vilmann AS, Vilmann P, McCowan TC, Patel AM
- 112 Three-dimensional radiation dosimetry using polymer gel and solid radiochromic polymer: From basics to clinical applications
Watanabe Y, Warmington L, Gopishankar N

ORIGINAL ARTICLE**Retrospective Study**

- 126 Reporting rotator cuff tears on magnetic resonance arthrography using the Snyder's arthroscopic classification
Aliprandi A, Messina C, Arrigoni P, Bandirali M, Di Leo G, Longo S, Magnani S, Mattiuz C, Randelli F, Sdao S, Sardanelli F, Sconfienza LM, Randelli P

Observational Study

- 134 Multimodality imaging using proton magnetic resonance spectroscopic imaging and ¹⁸F-fluorodeoxyglucose-positron emission tomography in local prostate cancer
Shukla-Dave A, Wassberg C, Pucar D, Schöder H, Goldman DA, Mazaheri Y, Reuter VE, Eastham J, Scardino PT, Hricak H
- 143 Computed tomography pulmonary angiography using a 20% reduction in contrast medium dose delivered in a multiphasic injection
Chen M, Mattar G, Abdulkarim JA

Contents

World Journal of Radiology
Volume 9 Number 3 March 28, 2017

ABOUT COVER

Editorial Board Member of *World Journal of Radiology*, Samer Ezziddin, MD, PhD, Professor, Klinik für Nuklearmedizin, Universitätsklinikum des Saarlandes, 66421 Homburg, Germany

AIM AND SCOPE

World Journal of Radiology (*World J Radiol*, *WJR*, online ISSN 1949-8470, DOI: 10.4329) is a peer-reviewed open access academic journal that aims to guide clinical practice and improve diagnostic and therapeutic skills of clinicians.

WJR covers topics concerning diagnostic radiology, radiation oncology, radiologic physics, neuroradiology, nuclear radiology, pediatric radiology, vascular/interventional radiology, medical imaging achieved by various modalities and related methods analysis. The current columns of *WJR* include editorial, frontier, diagnostic advances, therapeutics advances, field of vision, mini-reviews, review, topic highlight, medical ethics, original articles, case report, clinical case conference (clinicopathological conference), and autobiography.

We encourage authors to submit their manuscripts to *WJR*. We will give priority to manuscripts that are supported by major national and international foundations and those that are of great basic and clinical significance.

INDEXING/ABSTRACTING

World Journal of Radiology is now indexed in PubMed, PubMed Central.

FLYLEAF

I-III Editorial Board

EDITORS FOR THIS ISSUE

Responsible Assistant Editor: *Xiang Li*
Responsible Electronic Editor: *Dan Li*
Proofing Editor-in-Chief: *Lian-Sheng Ma*

Responsible Science Editor: *Fang-Fang Ji*
Proofing Editorial Office Director: *Xiu-Xia Song*

NAME OF JOURNAL
World Journal of Radiology

ISSN
ISSN 1949-8470 (online)

LAUNCH DATE
January 31, 2009

FREQUENCY
Monthly

EDITORS-IN-CHIEF
Kai U Juergens, MD, Associate Professor, MRT und PET/CT, Nuklearmedizin Bremen Mitte, ZEMODI - Zentrum für morphologische und molekulare Diagnostik, Bremen 28177, Germany

Edwin JR van Beek, MD, PhD, Professor, Clinical Research Imaging Centre and Department of Medical Radiology, University of Edinburgh, Edinburgh EH16 4TJ, United Kingdom

Thomas J Vogl, MD, Professor, Reader in Health Technology Assessment, Department of Diagnostic and Interventional Radiology, Johann Wolfgang Goethe University of Frankfurt, Frankfurt 60590,

Germany

EDITORIAL BOARD MEMBERS
All editorial board members resources online at <http://www.wjgnet.com/1949-8470/editorialboard.htm>

EDITORIAL OFFICE
Xiu-Xia Song, Director
World Journal of Radiology
Baishideng Publishing Group Inc
8226 Regency Drive, Pleasanton, CA 94588, USA
Telephone: +1-925-2238242
Fax: +1-925-2238243
E-mail: editorialoffice@wjgnet.com
Help Desk: <http://www.wjgnet.com/esps/helpdesk.aspx>
<http://www.wjgnet.com>

PUBLISHER
Baishideng Publishing Group Inc
8226 Regency Drive,
Pleasanton, CA 94588, USA
Telephone: +1-925-2238242
Fax: +1-925-2238243
E-mail: bpgoffice@wjgnet.com
Help Desk: <http://www.wjgnet.com/esps/helpdesk.aspx>
<http://www.wjgnet.com>

PUBLICATION DATE
March 28, 2017

COPYRIGHT
© 2017 Baishideng Publishing Group Inc. Articles published by this Open-Access journal are distributed under the terms of the Creative Commons Attribution Non-commercial License, which permits use, distribution, and reproduction in any medium, provided the original work is properly cited, the use is non commercial and is otherwise in compliance with the license.

SPECIAL STATEMENT
All articles published in journals owned by the Baishideng Publishing Group (BPG) represent the views and opinions of their authors, and not the views, opinions or policies of the BPG, except where otherwise explicitly indicated.

INSTRUCTIONS TO AUTHORS
<http://www.wjgnet.com/bpg/gerinfo/204>

ONLINE SUBMISSION
<http://www.wjgnet.com/esps/>

Laser ablation of liver tumors: An ancillary technique, or an alternative to radiofrequency and microwave?

Sergio Sartori, Francesca Di Vece, Francesca Ermili, Paola Tombesi

Sergio Sartori, Francesca Di Vece, Francesca Ermili, Paola Tombesi, Section of Interventional Ultrasound, St Anna Hospital, 44100 Ferrara, Italy

Author contributions: Sartori S, Di Vece F, Ermili F and Tombesi P contributed equally to this paper with conception and design of the study, literature review and analysis, drafting and critical revision and editing, and final approval of the final version.

Conflict-of-interest statement: The authors declare no conflict of interest.

Open-Access: This article is an open-access article which was selected by an in-house editor and fully peer-reviewed by external reviewers. It is distributed in accordance with the Creative Commons Attribution Non Commercial (CC BY-NC 4.0) license, which permits others to distribute, remix, adapt, build upon this work non-commercially, and license their derivative works on different terms, provided the original work is properly cited and the use is non-commercial. See: <http://creativecommons.org/licenses/by-nc/4.0/>

Manuscript source: Invited manuscript

Correspondence to: Sergio Sartori, MD, Section of Interventional Ultrasound, St Anna Hospital, via A. Moro 8, 44100 Ferrara, Italy. srs@unife.it
Telephone: +39-0532-239480
Fax: +39-0532-239613

Received: July 31, 2016

Peer-review started: August 2, 2016

First decision: September 28, 2016

Revised: December 23, 2016

Accepted: January 11, 2017

Article in press: January 14, 2017

Published online: March 28, 2017

Abstract

Radiofrequency ablation (RFA) is currently the most popular and used ablation modality for the treatment of

non surgical patients with primary and secondary liver tumors, but in the last years microwave ablation (MWA) is being technically improved and widely rediscovered for clinical use. Laser thermal ablation (LTA) is by far less investigated and used than RFA and MWA, but the available data on its effectiveness and safety are quite good and comparable to those of RFA and MWA. All the three hyperthermia-based ablative techniques, when performed by skilled operators, can successfully treat all liver tumors eligible for thermal ablation, and to date in most centers of interventional oncology or interventional radiology the choice of the technique usually depends on the physician's preference and experience, or technical availability. However, RFA, MWA, and LTA have peculiar advantages and limitations that can make each of them more suitable than the other ones to treat patients and tumors with different characteristics. When all the three thermal ablation techniques are available, the choice among RFA, MWA, and LTA should be guided by their advantages and disadvantages, number, size, and location of the liver nodules, and cost-saving considerations, in order to give patients the best treatment option.

Key words: Radiofrequency ablation; Liver neoplasm; Laser ablation; Microwave ablation; Hepatocellular carcinoma; Liver metastases

© **The Author(s) 2017.** Published by Baishideng Publishing Group Inc. All rights reserved.

Core tip: Radiofrequency ablation, microwave ablation, and laser thermal ablation, when performed by skilled operators, can successfully treat all liver tumors eligible for thermal ablation. However, each of them has peculiar advantages and limitations that can make one technique more suitable than the other ones to treat patients and tumors with different characteristics. When all the three techniques are available, the choice should be guided by their advantages and disadvantages, number, size and location of the liver nodules, and cost-

saving considerations, in order to give patients the best treatment option.

Sartori S, Di Vece F, Ermili F, Tombesi P. Laser ablation of liver tumors: An ancillary technique, or an alternative to radiofrequency and microwave? *World J Radiol* 2017; 9(3): 91-96 Available from: URL: <http://www.wjgnet.com/1949-8470/full/v9/i3/91.htm> DOI: <http://dx.doi.org/10.4329/wjrv.9.i3.91>

INTRODUCTION

Temperatures in excess of 60 °C are known to cause relatively instantaneous cell death, and thermal ablation by heating neoplastic tissue to cytotoxic temperatures is becoming increasingly important for treating primary and secondary liver cancer^[1]. Radiofrequency ablation (RFA) is currently the most popular and used ablation modality, but in the last years microwave ablation (MWA) is being technically improved and widely rediscovered for clinical use^[2-6]. RFA energy is delivered as an alternating current at a frequency of about 400 MHz, resulting in molecular frictional agitation and heat generation known as the joule effect^[1,7]. Tissues nearest to the electrode are heated directly, while more peripheral areas are less effectively heated by thermal conduction^[8]. MWA is a special case of dielectric heating where the dielectric material is tissue containing water. MWA induces a high-speed (between 900 and 2450 MHz) alternating electric field, causing the rotation of water molecules and generating heat^[1,7,9,10]. In contrast to RFA, energy radiates into the tissue with direct heating of the lesion, and charring and vaporization in the proximity of the needle are not obstacles to the delivery of energy^[10,11].

The effectiveness and limits of RFA have widely and extensively been reported worldwide. Due to the physical limitations in energy deposition, the effectiveness of RFA in local tumor control decreases with the increase of tumor size^[10]. Local control rates over 90% have been reported for nodules up to 3 cm in diameter, and only 6%-10% for tumors greater than 5 cm^[12]. Moreover, tumor location close to large vessels can also influence ablation success, because thermal energy is partially shunted away by the cooler blood (the so-called heat-sink effect)^[13,14].

The recent technical developments of MWA technology, such as the introduction of a cooling jacket around the MWA antenna and a miniaturized device for MW confinement into the distal portion of the antenna, have minimized the main limits of the earlier MWA systems, allowing for the reduction of back heating effects, increase of the ablation time, and amount of power that can be safely delivered^[2,6]. Due to these technical improvements and the characteristics of heat production and energy delivery^[9-11], MWA has recently been reported to achieve larger ablation areas than RFA^[3,4,15], and appears to be less susceptible to the heat-sink effect^[10,11].

Most studies investigating the effectiveness of MWA were conducted before the introduction into clinical practice of the most recent advancements in MWA technology, and at present the best available evidence suggests similar outcomes for RFA and MWA. Reported three- and 5-year survival rates of Child's class A patients with single hepatocellular carcinoma (HCC) less than 5 cm, or up to three HCC less than 3 cm, range from 60% to 78%, and from 50% to 64%, respectively, for RFA^[16-18], and from 72% to 73%, and 51%-57%, respectively, for MWA^[19,20]. The outcomes of RFA and MWA in patients with up to 6 metastases from colorectal cancer with a maximum diameter of 6 cm are also comparable, with 3-year survival rates of 28%-46% and 46%-51%, respectively, and 5-year survival rates of 25%-46% and 17%-32%, respectively^[21-24].

LASER THERMAL ABLATION - WHY CINDERELLA?

However, there is a third hyperthermia-based ablation technique, which uses laser optical fibers to deliver high-energy laser radiation to the tissue. Because of light absorption, temperatures of up to 150 °C are reached, leading to coagulative necrosis^[7,9,11]. Neodymium:Yttrium Aluminum Garnet (Nd:YAG, wavelength of 1064 nm) and diode (wavelength of 800-980 nm) lasers are most commonly used, as penetration of light is optimal in the near infrared spectrum. Light is delivered *via* flexible quartz fibers with a diameter from 300 to 600 µm. Conventional bare-tip fibers provide an almost spherical thermal lesion of 12-15 mm in diameter, and a beam-splitting device or a multi-source device allow for the use of up to four fibers, simultaneously delivering the light into each single fiber^[11,25,26]. Moreover, interstitial quartz fibers with flat or cylindrical diffusing tips have been reported to achieve larger ablation areas^[9]. Laser-induced interstitial thermotherapy is a special form of laser technique that uses a unique saline-cooled power laser application system to increase the volume of coagulative necrosis while preventing carbonization at the tip of the laser applicator^[10]. The device consists of a 9 French catheter with centimetre markings and a 7 French sheathed catheter with irrigated double lumina. Room temperature saline is used as the irrigation fluid, and a pump is integrated with the laser. This permits reliable cooling of the applicator and expansion of the laser-induced necrosis zone, resulting particularly useful for the treatment of liver metastases that require large safety margins to take care of microscopic disease around the lesions^[27].

Laser thermal ablation (LTA) is by far less investigated and used than RFA and MWA, but the available data on its effectiveness and safety are quite good. Most of the studies on LTA are focused on the treatment of HCC. Complete response rates ranging from 82% to 97%, and cumulative 3-year survival rates up to 73% were reported in Child's class A patients with single HCC ≤ 5

cm or up to three nodules ≤ 3 cm treated with multiple bare fibers^[28,29]. Moreover, median survival of 3.5 years was achieved in patients with nodules ≤ 5 cm located at high-risk sites by using water-cooled higher power LTA^[30]. To date, there are in literature just two randomized trials comparing LTA and RFA in the treatment of HCC, and both of them did not find any significant difference between the two techniques in terms of local tumor control, overall survival, and safety^[31,32]. A multicenter study investigating the safety of LTA in five hundred-twenty patients with 647 HCC treated by 1004 LTA sessions reported mortality and major complication rates of 0.8% and 1.5%, respectively^[33]. Likewise, also the outcomes of patients with liver metastases from colorectal cancer with diameter up to 5 cm treated with LTA appear comparable to those reported for RFA and MWA, with 3- and 5-year survival rates ranging from 28% to 72.4%, and from 10% to 37%, respectively^[9,34-36].

Despite these excellent results, LTA is frequently not considered an effective ablation technique, and the vast majority of reviews, consensus, or position papers dealing with the efficacy or safety of thermal ablation of liver tumors does not even mention LTA among the ablative techniques that are to date available^[1,10,37-41].

We do not agree with such an attitude. Although it is true that LTA has been investigated less vigorously than the other ablation techniques, it is also true that the relatively low number of published studies dealing with LTA seems to be due to an unjustified prejudice, rather than to an actual lower efficacy of LTA in comparison with RFA or MWA. All the three hyperthermia-based ablative techniques, when performed by skilled operators, can successfully treat all liver tumors eligible for thermal ablation, and to date in most centers of interventional oncology or interventional radiology the choice of the technique usually depends on the physician's preference and experience, or technical availability. However, in our opinion RFA, MWA and LTA have peculiar advantages and limitations that can make each of them more suitable than the other ones to treat patients and tumors with different characteristics. For instance, RFA is surely the best established thermal technique, and its efficacy has been largely proven, but lesions larger than 2-2.5 cm require multiple overlapping ablations to create an adequate safety margin, and sub-capsular or high-risk location of the tumors is considered a relative contraindication to RFA, even though some reports documented its feasibility^[42,43]. Moreover, tumors strictly close to large vessels can be incompletely treated because of the heat-sink effect. MWA has less sensitivity to the heat-sink effect, deeper penetration of energy and better propagation across the poorly conductive tissue than RFA, and can achieve larger ablation volumes. On the other hand, microwave energy is more difficult to distribute than RF energy, is carried in wavelengths which are more cumbersome than the small wires used to feed energy to RF electrodes, and are prone to heating when carrying large amount of power^[11]. Consequently, MWA appears less feasible than RFA in the treatment of high-

risk located and sub-capsular nodules. Moreover, the latest versions of MWA devices provided with the most recent technical advances are more expensive than RFA.

As regards LTA, the technique proposed by Pacella *et al.*^[28] and improved by Di Costanzo *et al.*^[44] uses 300- μ m bare optical fibers introduced into the tumor through 21-gauge needles. The diameter of the needles is considerably smaller than RFA electrodes and MWA antennas, making LTA safer and more suitable for ablating lesions in at-risk location or in locations that are difficult to reach^[11,45]. Moreover, a multisource device allows to use from one to four fibers at once, enabling to achieve ablation areas from one to 4-5 cm in diameter, and consequently to treat tumors ranging from 5-6 mm to 3 cm in diameter obtaining an acceptable safety margin. Furthermore, in western countries LTA has been reported to be the cheapest ablation technique when up to three fibers are used, and cheaper than MWA when four fibers are used^[11]. For these characteristics, LTA has been proposed as a valid alternative to RFA for lesions up to 2 cm^[46], and it has been suggested as the technique of choice in presence of multiple small and variably sized liver tumors^[45]. On the other hand, the correct placement of the fibers can be challenging, particularly if more than two fibers are needed, and should be performed by very skill operators^[11]. Moreover, like RFA, also the efficacy of LTA can be limited by the heat-sink effect.

FINAL CONSIDERATIONS

In the last years, multimodality anti-tumor strategies including surgery, chemotherapy, radiotherapy, ablation techniques, and catheter-based treatments are being more and more advocated, to tailor the best treatment options to patient and tumor characteristics^[45,47-49]. Such an approach is often adopted not only to choose the most suitable treatment options, but also to choose the most suitable technique available for each treatment option. For instance, patients candidate to catheter-based treatments can undergo bland embolization, transarterial chemoembolization with lipiodol or with drug-eluting beads, or radioembolization, according to the type of tumor, liver function, and presence or absence of portal venous thrombosis. Likewise, patients candidate to liver surgery can undergo wedge resection, segmentectomy, lobectomy, or transplantation according to the liver function, and number, size, and location of the tumors.

In our opinion, the choice among the thermal ablation techniques should also be based on the same criteria whenever possible. Some authors suggested that the reference centers for thermal ablation should be equipped with all the available techniques so as to be able to use the best and the most suitable one for each type of tumor^[26]. Recently, an algorithm has been proposed to tailor thermal ablation on each single patient, according to advantages and disadvantages of RFA, MWA and LTA, number, size, and location of the liver nodules, and cost-saving considerations (Figures 1 and 2)^[11]. On the basis of this algorithm, all the three ablation techniques have

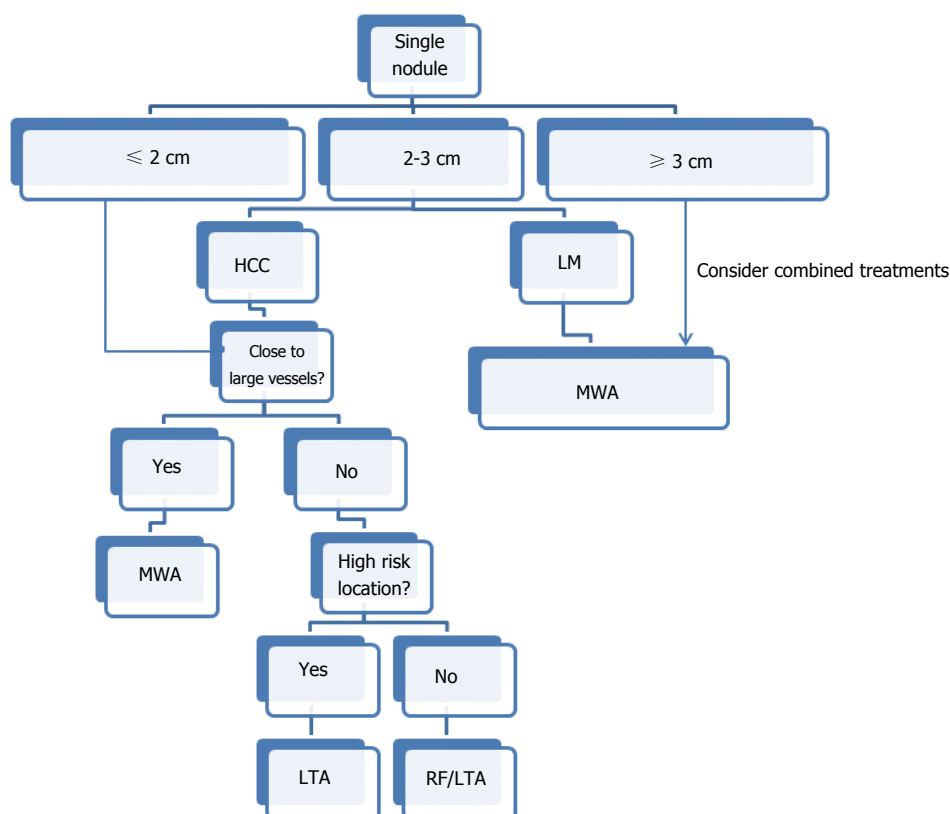


Figure 1 Algorithm proposed by Tombesi *et al*^[11] for thermal ablation of single liver tumor. HCC: Hepatocellular carcinoma; MWA: Microwave ablation; LTA: Laser thermal ablation; RF: Radiofrequency.

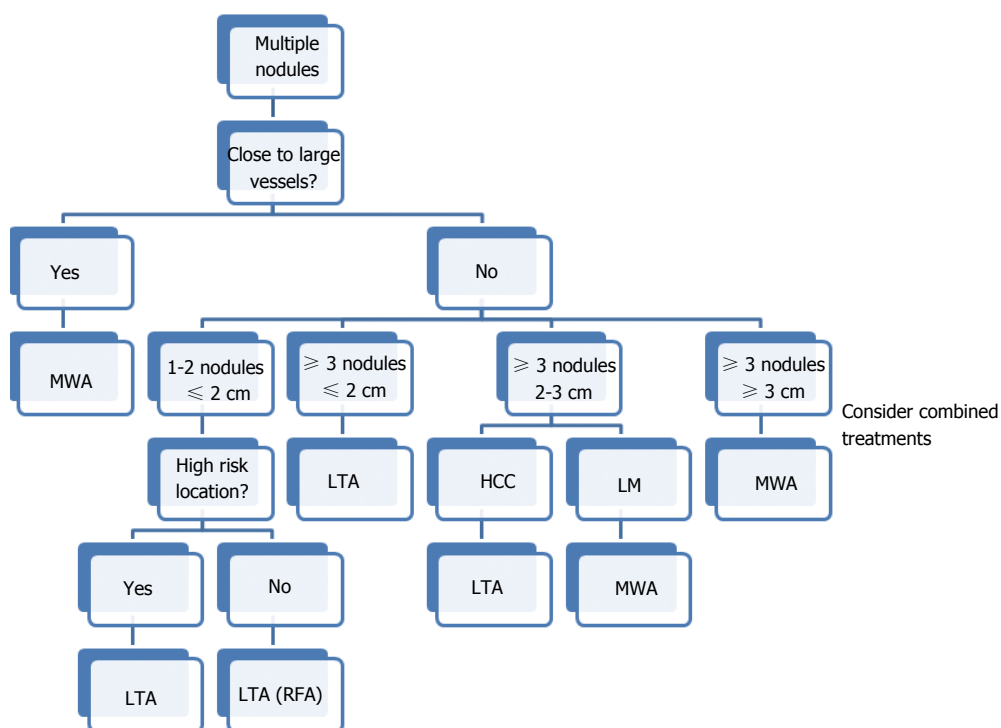


Figure 2 Algorithm proposed by Tombesi *et al*^[11] for thermal ablation of multiple liver tumors. HCC: Hepatocellular carcinoma; MWA: Microwave ablation; LTA: Laser thermal ablation; RFA: Radiofrequency ablation.

a preferential role in some specific circumstances. For instance, a single nodule 2 cm or smaller in size can be

efficaciously treated using all the thermal modalities, but RFA and LTA are cheaper than MWA and should

be preferred. Conversely, MWA should be considered the technique of choice when the tumor is ≥ 3 cm in diameter or is close to large vessels independently of its size, as MWA can achieve larger ablation volumes and is not affected by the heat-sink effect. Multiple small and variably sized lesions should be treated with LTA, and so on (Figures 1 and 2). This algorithm reflects the personal experience and opinion of the authors, and it can surely be modified and improved. However, it is also based on objective considerations that can largely be shared, and in our opinion it could represent the basis for a consensus on the optimal and reasoned use of the thermal ablation modalities.

In conclusion, at present there is no ideal ablation technique that outclasses the other ones. There are ablation techniques that share some main technical aspects and are usually comparable, but each of them has peculiar characteristics that make it the "ideal" technique in some particular settings. We believe we should exploit such peculiarities to give patients the best treatment option.

REFERENCES

- 1 **Brace CL.** Radiofrequency and microwave ablation of the liver, lung, kidney, and bone: what are the differences? *Curr Probl Diagn Radiol* 2009; **38**: 135-143 [PMID: 19298912 DOI: 10.1067/j.cpradiol.2007.10.001]
- 2 **Inokuchi R,** Seki T, Ikeda K, Kawamura R, Asayama T, Yanagawa M, Umehara H, Okazaki K. Percutaneous microwave coagulation therapy for hepatocellular carcinoma: increased coagulation diameter using a new electrode and microwave generator. *Oncol Rep* 2010; **24**: 621-627 [PMID: 20664966]
- 3 **Qian GJ,** Wang N, Shen Q, Sheng YH, Zhao JQ, Kuang M, Liu GJ, Wu MC. Efficacy of microwave versus radiofrequency ablation for treatment of small hepatocellular carcinoma: experimental and clinical studies. *Eur Radiol* 2012; **22**: 1983-1990 [PMID: 22544225 DOI: 10.1007/s00330-012-2442-1]
- 4 **Cavagnaro M,** Amabile C, Bernardi P, Pisa S, Tosoratti N. A minimally invasive antenna for microwave ablation therapies: design, performances, and experimental assessment. *IEEE Trans Biomed Eng* 2011; **58**: 949-959 [PMID: 21172749 DOI: 10.1109/TBME.2010.2099657]
- 5 **Goldberg SN.** Science to practice: Can we expand focal interventional oncologic ablation treatments into an effective systemic therapy? *Radiology* 2013; **267**: 321-323 [PMID: 23610091 DOI: 10.1148/radiol.13130140]
- 6 **Wang Y,** Sun Y, Feng L, Gao Y, Ni X, Liang P. Internally cooled antenna for microwave ablation: results in ex vivo and in vivo porcine livers. *Eur J Radiol* 2008; **67**: 357-361 [PMID: 17768024 DOI: 10.1016/j.ejrad.2007.07.015]
- 7 **Loffroy R,** Estivalet L, Favelier S, Pottecher P, Genson PY, Cercueli JP, Krausé D. Interventional radiology therapies for liver cancer. *Hepatoma Res* 2016; **2**: 1-9 [DOI: 10.4103/2394-5079.167439]
- 8 **Ahmed M,** Brace CL, Lee FT, Goldberg SN. Principles of and advances in percutaneous ablation. *Radiology* 2011; **258**: 351-369 [PMID: 21273519 DOI: 10.1148/radiol.10081634]
- 9 **Vogl TJ,** Farshid P, Naguib NN, Darvishi A, Bazrafshan B, Mbalisike E, Burkhard T, Zangos S. Thermal ablation of liver metastases from colorectal cancer: radiofrequency, microwave and laser ablation therapies. *Radiol Med* 2014; **119**: 451-461 [PMID: 24894923 DOI: 10.1007/s11547-014-0415-y]
- 10 **Foltz G.** Image-guided percutaneous ablation of hepatic malignancies. *Semin Intervent Radiol* 2014; **31**: 180-186 [PMID: 25071304 DOI: 10.1055/s-0034-1373792]
- 11 **Tombesi P,** Di Vece F, Sartori S. Radiofrequency, microwave, and laser ablation of liver tumors: time to move toward a tailored ablation technique? *Hepatoma Res* 2015; **1**: 52-57 [DOI: 10.4103/2394-5079.155697]
- 12 **Livraghi T,** Goldberg SN, Lazzaroni S, Meloni F, Ierace T, Solbiati L, Gazelle GS. Hepatocellular carcinoma: radio-frequency ablation of medium and large lesions. *Radiology* 2000; **214**: 761-768 [PMID: 10715043 DOI: 10.1148/radiology.214.3.r00mr02761]
- 13 **Mulier S,** Ni Y, Jamart J, Ruers T, Marchal G, Michel L. Local recurrence after hepatic radiofrequency coagulation: multivariate meta-analysis and review of contributing factors. *Ann Surg* 2005; **242**: 158-171 [PMID: 16041205 DOI: 10.1097/01.sla.0000171032.99149.fe]
- 14 **Lu DS,** Raman SS, Limanond P, Aziz D, Economou J, Busuttil R, Sayre J. Influence of large peritumoral vessels on outcome of radiofrequency ablation of liver tumors. *J Vasc Interv Radiol* 2003; **14**: 1267-1274 [PMID: 14551273 DOI: 10.1097/01.RVI.0000092666.72261.6B]
- 15 **Di Vece F,** Tombesi P, Ermili F, Maraldi C, Sartori S. Coagulation areas produced by cool-tip radiofrequency ablation and microwave ablation using a device to decrease back-heating effects: a prospective pilot study. *Cardiovasc Intervent Radiol* 2014; **37**: 723-729 [PMID: 24196263 DOI: 10.1007/s00270-013-0733-9]
- 16 **Lencioni R,** Cioni D, Crocetti L, Franchini C, Pina CD, Lera J, Bartolozzi C. Early-stage hepatocellular carcinoma in patients with cirrhosis: long-term results of percutaneous image-guided radiofrequency ablation. *Radiology* 2005; **234**: 961-967 [PMID: 15665226 DOI: 10.1148/radiol.2343040350]
- 17 **Choi D,** Lim HK, Rhim H, Kim YS, Yoo BC, Paik SW, Joh JW, Park CK. Percutaneous radiofrequency ablation for recurrent hepatocellular carcinoma after hepatectomy: long-term results and prognostic factors. *Ann Surg Oncol* 2007; **14**: 2319-2329 [PMID: 17522947 DOI: 10.1007/s00330-006-0461-5]
- 18 **Guglielmi A,** Ruzzenente A, Sandri M, Pachera S, Pedrazzani C, Tasselli S, Iacono C. Radio frequency ablation for hepatocellular carcinoma in cirrhotic patients: prognostic factors for survival. *J Gastrointest Surg* 2007; **11**: 143-149 [PMID: 17390163 DOI: 10.1007/s11605-006-0082-y]
- 19 **Liang P,** Dong B, Yu X, Yu D, Wang Y, Feng L, Xiao Q. Prognostic factors for survival in patients with hepatocellular carcinoma after percutaneous microwave ablation. *Radiology* 2005; **235**: 299-307 [PMID: 15731369 DOI: 10.1148/radiol.2351031944]
- 20 **Dong B,** Liang P, Yu X, Su L, Yu D, Cheng Z, Zhang J. Percutaneous sonographically guided microwave coagulation therapy for hepatocellular carcinoma: results in 234 patients. *AJR Am J Roentgenol* 2003; **180**: 1547-1555 [PMID: 12760916 DOI: 10.2214/ajr.180.6.1801547]
- 21 **Gillams AR,** Lees WR. Radiofrequency ablation of colorectal liver metastases. *Abdom Imaging* 2005; **30**: 419-426 [PMID: 15759208 DOI: 10.1007/s00261-004-0256-6]
- 22 **Hildebrand P,** Leibecke T, Kleemann M, Mirow L, Birth M, Bruch HP, Bürk C. Influence of operator experience in radiofrequency ablation of malignant liver tumours on treatment outcome. *Eur J Surg Oncol* 2006; **32**: 430-434 [PMID: 16520015 DOI: 10.1016/j.ejso.2006.01.006]
- 23 **Liang P,** Dong B, Yu X, Yang Y, Yu D, Su L, Xiao Q, Sheng L. Prognostic factors for percutaneous microwave coagulation therapy of hepatic metastases. *AJR Am J Roentgenol* 2003; **181**: 1319-1325 [PMID: 14573427 DOI: 10.2214/ajr.181.5.1811319]
- 24 **Tanaka K,** Shimada H, Nagano Y, Endo I, Sekido H, Togo S. Outcome after hepatic resection versus combined resection and microwave ablation for multiple bilobar colorectal metastases to the liver. *Surgery* 2006; **139**: 263-273 [PMID: 16455336 DOI: 10.1016/j.surg.2005.07.036]
- 25 **Francica G,** Petrolati A, Di Stasio E, Pacella S, Stasi R, Pacella CM. Effectiveness, safety, and local progression after percutaneous laser ablation for hepatocellular carcinoma nodules up to 4 cm are not affected by tumor location. *AJR Am J Roentgenol* 2012; **199**: 1393-1401 [PMID: 23169736 DOI: 10.2214/AJR.11.7850]
- 26 **Di Costanzo GG,** Francica G, Pacella CM. Laser ablation for small

- hepatocellular carcinoma: State of the art and future perspectives. *World J Hepatol* 2014; **6**: 704-715 [PMID: 25349642 DOI: 10.4254/wjh.v6.i10.704]
- 27 **Vogl TJ**, Straub R, Zangos S, Mack MG, Eichler K. MR-guided laser-induced thermotherapy (LITT) of liver tumours: experimental and clinical data. *Int J Hyperthermia* 2004; **20**: 713-724 [PMID: 15675667 DOI: 10.1080/02656730400007212]
 - 28 **Pacella CM**, Bizzarri G, Magnolfi F, Cecconi P, Caspani B, Anelli V, Bianchini A, Valle D, Pacella S, Manenti G, Rossi Z. Laser thermal ablation in the treatment of small hepatocellular carcinoma: results in 74 patients. *Radiology* 2001; **221**: 712-720 [PMID: 11719667 DOI: 10.1148/radiol.2213001501]
 - 29 **Pacella CM**, Francica G, Di Lascio FM, Arienti V, Antico E, Caspani B, Magnolfi F, Megna AS, Pretolani S, Regine R, Sponza M, Stasi R. Long-term outcome of cirrhotic patients with early hepatocellular carcinoma treated with ultrasound-guided percutaneous laser ablation: a retrospective analysis. *J Clin Oncol* 2009; **27**: 2615-2621 [PMID: 19332729 DOI: 10.1200/JCO.2008.19.0082]
 - 30 **Eichler K**, Zangos S, Gruber-Rouh T, Vogl TJ, Mack MG. Magnetic resonance-guided laser-induced thermotherapy in patients with oligonodular hepatocellular carcinoma: long-term results over a 15-year period. *J Clin Gastroenterol* 2012; **46**: 796-801 [PMID: 22955262 DOI: 10.1097/MCG.0b013e3182641806]
 - 31 **Ferrari FS**, Megliola A, Scorzelli A, Stella A, Vigni F, Drudi FM, Venezia D. Treatment of small HCC through radiofrequency ablation and laser ablation. Comparison of techniques and long-term results. *Radiol Med* 2007; **112**: 377-393 [PMID: 17447018 DOI: 10.1007/s11547-007-0148-2]
 - 32 **Di Costanzo GG**, Tortora R, D'Adamo G, De Luca M, Lampasi F, Addario L, Galeota Lanza A, Picciotto FP, Tartaglione MT, Cordone G, Imperato M, Matterna S, Pacella CM. Radiofrequency ablation versus laser ablation for the treatment of small hepatocellular carcinoma in cirrhosis: a randomized trial. *J Gastroenterol Hepatol* 2015; **30**: 559-565 [PMID: 25251043 DOI: 10.1111/jgh.12791]
 - 33 **Arienti V**, Pretolani S, Pacella CM, Magnolfi F, Caspani B, Francica G, Megna AS, Regine R, Sponza M, Antico E, Di Lascio FM. Complications of laser ablation for hepatocellular carcinoma: a multicenter study. *Radiology* 2008; **246**: 947-955 [PMID: 18195382 DOI: 10.1148/radiol.2463070390]
 - 34 **Eickmeyer F**, Schwarzmaier HJ, Müller FP, Nakic Z, Yang Q, Fiedler V. [Survival after laser-induced interstitial thermotherapy of colorectal liver metastases--a comparison of first clinical experiences with current therapy results]. *Rofo* 2008; **180**: 35-41 [PMID: 18008194 DOI: 10.1055/s-2007-963565]
 - 35 **Puls R**, Langner S, Rosenberg C, Hegenscheid K, Kuehn JP, Noeckler K, Hosten N. Laser ablation of liver metastases from colorectal cancer with MR thermometry: 5-year survival. *J Vasc Interv Radiol* 2009; **20**: 225-234 [PMID: 19109037 DOI: 10.1016/j.jvir.2008.10.018]
 - 36 **Vogl TJ**, Dommermuth A, Heinle B, Nour-Eldin NE, Lehnert T, Eichler K, Zangos S, Bechstein WO, Naguib NN. Colorectal cancer liver metastases: long-term survival and progression-free survival after thermal ablation using magnetic resonance-guided laser-induced interstitial thermotherapy in 594 patients: analysis of prognostic factors. *Invest Radiol* 2014; **49**: 48-56 [PMID: 24056114 DOI: 10.1097/RLI.0b013e3182a6094e]
 - 37 **Bertot LC**, Sato M, Tateishi R, Yoshida H, Koike K. Mortality and complication rates of percutaneous ablative techniques for the treatment of liver tumors: a systematic review. *Eur Radiol* 2011; **21**: 2584-2596 [PMID: 21858539 DOI: 10.1007/s00330-011-2222-3]
 - 38 **Pepple PT**, Gerber DA. Laparoscopic-assisted ablation of hepatic tumors: a review. *Semin Intervent Radiol* 2014; **31**: 125-128 [PMID: 25053864 DOI: 10.1055/s-0034-1373787]
 - 39 **Wells SA**, Hinshaw JL, Lubner MG, Ziemlewicz TJ, Brace CL, Lee FT. Liver Ablation: Best Practice. *Radiol Clin North Am* 2015; **53**: 933-971 [PMID: 26321447 DOI: 10.1016/j.rcl.2015.05.012]
 - 40 **Gillams A**, Goldberg N, Ahmed M, Bale R, Breen D, Callstrom M, Chen MH, Choi BI, de Baere T, Dupuy D, Gangi A, Gervais D, Helmberger T, Jung EM, Lee F, Lencioni R, Liang P, Livraghi T, Lu D, Meloni F, Pereira P, Piscaglia F, Rhim H, Salem R, Sofocleous C, Solomon SB, Soulen M, Tanaka M, Vogl T, Wood B, Solbiati L. Thermal ablation of colorectal liver metastases: a position paper by an international panel of ablation experts, The Interventional Oncology Sans Frontières meeting 2013. *Eur Radiol* 2015; **25**: 3438-3454 [PMID: 25994193 DOI: 10.1007/s00330-015-3779-z]
 - 41 **Meyer J**, Toomay S. Update on treatment of liver metastases: focus on ablation therapies. *Curr Oncol Rep* 2015; **17**: 420 [PMID: 25416314 DOI: 10.1007/s11912-014-0420-2]
 - 42 **Sartori S**, Tombesi P, Macario F, Nielsen I, Tassinari D, Catellani M, Abbasciano V. Subcapsular liver tumors treated with percutaneous radiofrequency ablation: a prospective comparison with nonsubcapsular liver tumors for safety and effectiveness. *Radiology* 2008; **248**: 670-679 [PMID: 18519740 DOI: 10.1148/radiol.2482071690]
 - 43 **Teratani T**, Yoshida H, Shiina S, Obi S, Sato S, Tateishi R, Mine N, Kondo Y, Kawabe T, Omata M. Radiofrequency ablation for hepatocellular carcinoma in so-called high-risk locations. *Hepatology* 2006; **43**: 1101-1108 [PMID: 16628706 DOI: 10.1002/hep.21164]
 - 44 **Di Costanzo GG**, D'Adamo G, Tortora R, Zanfardino F, Matterna S, Francica G, Pacella CM. A novel needle guide system to perform percutaneous laser ablation of liver tumors using the multifiber technique. *Acta Radiol* 2013; **54**: 876-881 [PMID: 23761559 DOI: 10.1177/0284185113489825]
 - 45 **Tombesi P**, Di Vece F, Sartori S. Laser ablation for hepatic metastases from neuroendocrine tumors. *AJR Am J Roentgenol* 2015; **204**: W732 [PMID: 26001265]
 - 46 **Orlacio A**, Bolacchi F, Chegai F, Bergamini A, Costanzo E, Del Giudice C, Angelico M, Simonetti G. Comparative evaluation of percutaneous laser and radiofrequency ablation in patients with HCC smaller than 4 cm. *Radiol Med* 2014; **119**: 298-308 [PMID: 24277510 DOI: 10.1007/s11547-013-0339-y]
 - 47 **Oberg K**, Astrup L, Eriksson B, Falkmer SE, Falkmer UG, Gustafsen J, Haglund C, Knigge U, Vatn MH, Välimäki M. Guidelines for the management of gastroenteropancreatic neuroendocrine tumours (including bronchopulmonary and thymic neoplasms). Part I-general overview. *Acta Oncol* 2004; **43**: 617-625 [PMID: 15545182 DOI: 10.1080/02841860410018502]
 - 48 **Govaert KM**, van Kessel CS, Lolkema M, Ruers TJ, Borel Rinkes IH. Does Radiofrequency Ablation Add to Chemotherapy for Unresectable Liver Metastases? *Curr Colorectal Cancer Rep* 2012; **8**: 130-137 [PMID: 22611343 DOI: 10.1007/s11888-012-0122-9]
 - 49 **Sartori S**, Tombesi P, Di Vece F. Thermal ablation in colorectal liver metastases: Lack of evidence or lack of capability to prove the evidence? *World J Gastroenterol* 2016; **22**: 3511-3515 [PMID: 27053843 DOI: 10.3748/wjg.v22.i13.3511]

P- Reviewer: Oto A, Vogl TJ S- Editor: Kong JX L- Editor: A
E- Editor: Li D



Complementary roles of interventional radiology and therapeutic endoscopy in gastroenterology

David M Ray, Indu Srinivasan, Shou-Jiang Tang, Andreas S Vilmann, Peter Vilmann, Timothy C McCowan, Akash M Patel

David M Ray, Timothy C McCowan, Akash M Patel, Department of Radiology, Division of Interventional Radiology, University of Mississippi Medical Center, Jackson, MS 39216, United States

Indu Srinivasan, Shou-Jiang Tang, Division of Digestive Diseases, Department of Medicine, University of Mississippi Medical Center, Jackson, MS 39216, United States

Andreas S Vilmann, Peter Vilmann, GastroUnit, Division of Endoscopy, Copenhagen University Hospital Herlev, 2730 Herlev, Denmark

Author contributions: All authors were involved in the planning the design and conduct of the review paper, and equally in revising the manuscript and approving the final version; the initial research was conducted by Ray DM and Srinivasan I; Ray DM, Srinivasan I, Patel AM and Tang SJ were involved in drafting the manuscript.

Conflict-of-interest statement: Drs. David M Ray, Indu Srinivasan, Shou-Jiang Tang, Andreass S Vilmann, Timothy C McCowan, and Akash M Patel have no conflict of interest or financial to disclose related to this review. Peter Vilmann is a consultant at MediGlobe GmbH, Grassau, Germany.

Open-Access: This article is an open-access article which was selected by an in-house editor and fully peer-reviewed by external reviewers. It is distributed in accordance with the Creative Commons Attribution Non Commercial (CC BY-NC 4.0) license, which permits others to distribute, remix, adapt, build upon this work non-commercially, and license their derivative works on different terms, provided the original work is properly cited and the use is non-commercial. See: <http://creativecommons.org/licenses/by-nc/4.0/>

Manuscript source: Invited manuscript

Correspondence to: Akash M Patel, MD, Department of Radiology, Division of Interventional Radiology, University of Mississippi Medical Center, 2500 North State Street, Jackson, MS 39216, United States. ampatel@umc.edu
Telephone: +1-601-9840454

Received: July 28, 2016

Peer-review started: July 31, 2016

First decision: September 2, 2016

Revised: November 12, 2016

Accepted: January 11, 2017

Article in press: January 14, 2017

Published online: March 28, 2017

Abstract

Acute upper and lower gastrointestinal bleeding, enteral feeding, cecostomy tubes and luminal strictures are some of the common reasons for gastroenterology service. While surgery was initially considered the main treatment modality, the advent of both therapeutic endoscopy and interventional radiology have resulted in the paradigm shift in the management of these conditions. In this paper, we discuss the patient's work up, indications, and complementary roles of endoscopic and angiographic management in the settings of gastrointestinal bleeding, enteral feeding, cecostomy tube placement and luminal strictures. These conditions often require multidisciplinary approaches involving a team of interventional radiologists, gastroenterologists and surgeons. Further, the authors also aim to describe how the fields of interventional radiology and gastrointestinal endoscopy are overlapping and complementary in the management of these complex conditions.

Key words: Gastrointestinal hemorrhage; Enteral nutrition; Interventional radiology; Gastroenterology; Endoscopy

© **The Author(s) 2017.** Published by Baishideng Publishing Group Inc. All rights reserved.

Core tip: This paper reviews the current information and dissects the similarities, differences, and complementary roles of gastroenterologists and interventional radiologists

in the management of various luminal gastrointestinal conditions such as gastrointestinal bleeding, enteral feeding, placement of cecostomy tubes and strictures. We discuss the multidisciplinary approach, indications, contraindications and management of these conditions in an attempt to provide an educational experience for all your esteemed readers.

Ray DM, Srinivasan I, Tang SJ, Vilmann AS, Vilmann P, McCowan TC, Patel AM. Complementary roles of interventional radiology and therapeutic endoscopy in gastroenterology. *World J Radiol* 2017; 9(3): 97-111 Available from: URL: <http://www.wjgnet.com/1949-8470/full/v9/i3/97.htm> DOI: <http://dx.doi.org/10.4329/wjr.v9.i3.97>

INTRODUCTION

Various gastrointestinal (GI) diseases such as acute GI bleeding, esophageal strictures, strictures associated with inflammatory bowel disease and enteral feedings were traditionally managed by the surgeons alone. However, surgery has been associated with high morbidity and mortality rates, thus leading on to a search for other modalities that were less invasive and equally or better efficacious. Though the first endoluminal visualization of the stomach was performed by Kussmaul in 1868, it was not until 1958 that the first fibroscope was introduced by Hirschowitz *et al*^[1]. From then, the field of endoscopy has evolved rapidly with various innovations such as charged couple devices, video chip to hemostatic clips, biopsy forceps, snares, banding kit, etc. These innovations have expanded the horizons of endoscopy, changing it from a mere diagnostic tool to one of therapeutics. Endoscopists are now able to treat GI bleeding, perform biopsies, remove polyps, dilate strictures, place stents and feeding tubes. Similar to gastroenterology, the field of interventional radiology (IR) has had its share of technological advances. Fluoroscopy advanced during the early 1900s. The first angioplasty by Dotter in 1964 was a landmark in vascular interventions^[2]. Embolization, angioplasty, and other fluoroscopic guided techniques significantly advanced have also decreased the need for first line surgery in many patients^[2,3].

Interventional endoscopy and radiology are two minimally invasive disciplines that overlap and complement one another in the care of multiple complex GI disease processes. Acute GI bleeding is a common presentation to the emergency room which can be life threatening. Management of this often times requires a collaboration between a gastroenterologist, radiologist, and a surgeon. However, with the advent of therapeutic endoscopy and interventional radiology, in many cases, the role of surgery is now limited to technically challenging cases not amenable to endoscopic or radiological intervention. Though few articles addressing the need for multidisciplinary approach in treating GI bleeding have been published, there is a paucity of literature for other

above mentioned conditions. Thus, in this article we hope to not only outline the role of endoscopists and radiologists in managing various GI conditions but also their complementary roles to overcome their individual shortcomings. Since this is an expansive topic we will be only focusing on endoluminal conditions such as GI bleeding, access for enteral nutrition, cecostomy tube placement and strictures. Hepatobiliary pathology including variceal bleeding, portal hypertensive gastropathy, biliary drainage, endoscopic ultrasound (EUS) guided internal drainage, EUS guided celiac block and tissue biopsy will be described elsewhere.

LITERATURE RESEARCH

We conducted an English literature review of the various GI topics. Searches were performed for GI hemorrhage with respect to management, endoscopy and interventional radiology. Searches for hemorrhage were further subdivided into upper and lower GI bleeding. Similar review was performed for enteral feeding, cecostomy tubes, and stricture management. Further literature was reviewed by evaluating references. Also, since many patients are complex and require the opinion of several specialists in the outpatient and emergent setting, the authors added the opinion of our institution when appropriate.

Acute upper GI bleed

Acute life threatening GI bleeding once considered a surgical emergency with significant mortality continues to have a high mortality rate despite tremendous advances made in endoscopic and radiographic techniques. The incidence of GI bleeding tends to increase with age and ranges between 37 and 172/100000 adults^[4,5]. It has been reported to account for approximately 350000 hospital admissions per year in the United States alone^[6]. Rebleeding following interventions remains relatively high at reported rates of 7%-16%^[4]. It is a frequent presenting symptom to the hospital and requires management by a multidisciplinary team comprising of gastroenterologists, surgeons, interventional radiologists, and anesthesiologists^[7].

GI bleeding is usually arbitrarily divided between upper and lower bleeds. Upper GI bleed constitutes any bleed that originates in the GI tract proximal to ligament of Treitz while anything distal constitutes a lower GI bleed. Upper GI hemorrhage may manifest as hematemesis, coffee ground emesis, bloody return through nasogastric tube or feeding tube, melena or as brisk hematochezia with hemodynamic compromise. Lower GI bleeding usually presents as melena (if from the right colon or distal small bowel) or hematochezia. The most common cause of nonvariceal upper GI bleed is peptic ulcer disease^[8]. Other etiologies include neoplasms, inflammation, iatrogenic, trauma, ischemia, and vascular malformations (such as Dieulafoy's lesions and angiodysplasia) with more than one diagnosis noted in 16%-20% of cases^[4].

When a patient presents to the emergency room with

GI bleeding, initial assessment must be made to ensure hemodynamic stability of the patient and determine the need for urgent intervention. Resuscitation with crystalloids and blood transfusion must be performed. In patients suspected with nonvariceal upper GI bleed, proton pump inhibitors must be initiated as they reduce the chances of finding high risk stigmata during endoscopy^[9]. If the patient is stable enough to undergo upper endoscopy, then it must be performed next as it can be both diagnostic and therapeutic. The patient is placed in a left lateral position with head bend forward to facilitate the insertion of the endoscope. At the time of upper endoscopy, there are various endoscopic treatment modalities available to help achieve hemostasis. Traditionally, endoscopic therapy has been broadly categorized into injection, thermal and mechanical methods.

Injection therapy

Injection therapy includes administration of epinephrine (1:10000) around the bleeding vessel. This was first described by Soehendra *et al*^[10]. In 1988, Chung *et al*^[11] presented the first randomized trial comparing injection therapy to medical therapy in 68 patients and reported reduced surgery, transfusion requirements and shorter hospital stay in the group with injection therapy. This is performed by placing multiple aliquots of 0.5 to 1 mL of diluted epinephrine (1:10000) 1 to 2 mm away from the bleeding vessel. This technique works by a combination of tamponade and transient vasoconstriction. Typically, 5 mL can be administered in one setting but on occasion as high as 25 mL have also been administered with no significant side effects except transient tachycardia. However, it should be avoided in patients with active ongoing cardiac ischemia. After injection of epinephrine blanching of the surrounding mucosa is noticed. Studies^[12,13] have demonstrated that epinephrine alone is effective, but epinephrine in combination with another endoscopic modality is superior to epinephrine alone. This is most likely due to its transient duration of action.

More recently hemostatic powders have gained popularity. These are designed to be delivered *via* a catheter passed through the accessory channel of the endoscope. Hemospray is an inorganic powder that is metabolically inert and nontoxic. This acts in two ways; the first is upon coming in contact with water it forms a stable mechanical barrier over the vessel and stops the bleeding. Secondly, it acts by increasing the local concentration of clotting factors and promoting clot formation^[14]. The adherent clot that it forms sloughs off within 24-72 h and is eliminated from the GI tract^[15]. In 2011, Sung *et al*^[15] conducted a pilot study in 20 patients with active peptic ulcer bleeding. Hemostasis was achieved in all but one patient (95%). It has also proven to be efficacious in tumor related bleeding^[16] given its ease of application to large surfaces even in difficult positions. In a small study, Holster *et al*^[17] evaluated the efficacy of this novel technique in patients on antithrombotic agents and concluded that endoscopic hemostasis by Hemospray is not decreased by systemic antithrombotic effects such

as Plavix, aspirin, or vitamin K antagonists. Thus, though initial reports are fascinating, further trials with larger populations are needed.

THERMAL METHODS

Thermal devices can be divided into contact devices such as heater probe and bipolar probe and noncontact devices such as argon plasma coagulation (APC). Contact probes are ideal for bleeding vessels that are less than 2 to 3 mm in size. The goal of a contact probe is to apply firm pressure on the visible vessel to interrupt the blood flow and then to apply enough heat to weld the walls of the vessel together^[18]. Heater probes contain a nonstick Teflon coated heating element directly delivering heat to the vessel. It also contains three irrigation ports on the sides to wash out the clots and allow better visualization of the vessel. The heat is then delivered for a preset amount of time by tapping the coagulation pedal. For the treatment of actively bleeding ulcer four pulses of 30 Joules must be applied^[18].

Bipolar probes work by delivering electrical current from an electrosurgical generator to electrodes situated at the tip of the probe. Tissue coagulation is obtained indirectly by conversion of electrical energy to heat energy. Similar to heater probes they also contain a water channel which is, however, centrally located. Unlike the heater probe coagulation time is determined by the amount of time the endoscopist presses the coagulation foot pedal. For bleeding peptic ulcers, a setting of 20 watts for a contact period of 7 to 10 s is suggested^[19]. APC is a non-contact monopolar thermal method which acts by delivering high frequency electrical current conducted *via* argon gas (that has been ionized) to the tissue. This method, however, produces superficial coagulation only, and once the tissue gets desiccated, it loses its electrical conductivity. Hence, the maximum depth is about 3 mm to 4 mm which is a safety feature to prevent deep tissue injury. The probe can be circumferential, end or side fearing, and should be held 1-2 mm away from the target. However, owing to its superficial effect it is not routinely used for peptic ulcer disease.

MECHANICAL METHODS

Mechanical hemostasis can be achieved by causing a physical tamponade of the bleeding site. Currently two types of instruments are widely used: Clips and banding kits. The use of through-the-scope clips was first reported in 1975 by Hayashi *et al*^[20] for endoscopic hemostasis. Since then, tremendous improvements have been made in both the clip designs and their deployment devices. They are either single use clips or reusable clips which can be rotated, closed and reopened multiple times. They are deployed over the bleeding vessel and act by clamping the bleeding point. They slough off within few days to weeks. They are most beneficial for accessible lesions that do not have a hard fibrotic base. Based on

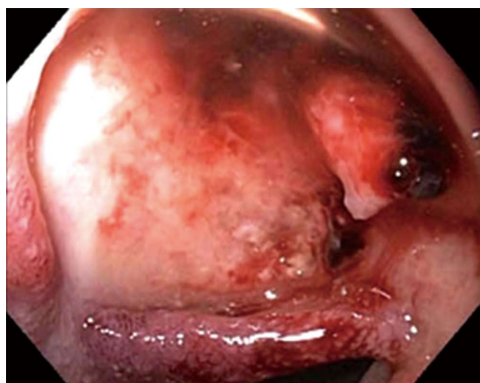


Figure 1 Endoscopic image showing a large ulcer in the superior wall of the bulb with a large visible vessel. Attempted endoclip placement after epinephrine injection resulted in major bleeding and a loss of endoscopic view and patient was then emergently transferred to interventional radiology.

historical data, the vessel should be ≤ 2 mm in size. Recently, over-the-scope clipping devices have become available and can be applied to larger vessels. Banding devices are mostly used for esophageal varices, which will not be discussed in this review.

Etiologies

The two most common etiologies for peptic ulcers include non-steroidal anti-inflammatory drugs and helicobacter pylori infection. These are easily visualized at the time of endoscopy, and certain endoscopic features such as active bleeding, spurting arterial vessel, adherent clot and non-bleeding visible vessel, predict high rate of rebleeding and hence require endoscopic therapy and/or interventional embolization therapy^[21]. While treating a high risk stigmata ulcer, it is recommended that injection therapy should not be used alone as studies^[12,13] demonstrated that the combination therapy of epinephrine with clips or thermal devices was superior to injection alone. APC have not been demonstrated to be useful in peptic ulcer bleeding. Through-the-scope Hemoclips and contact thermal devices have found to be equally efficacious in treating vessels less than 2 mm in size^[22]. Placing a clip may be challenging in difficult to access locations such as the posterior wall of the duodenal bulb where contact thermocoagulation should be attempted. In cases with oozing without a visible vessel monotherapy is adequate. Treating ulcers with adherent clots is challenging as meta-analysis^[22] has shown conflicting results regarding endoscopic treatment vs medical management.

Dieulafoy's lesions which are characterized by a large submucosal vessel eroding through the mucosa and then rupturing were first described almost a hundred years ago. Endoscopically it is identified when there is visible or an active bleeding vessel with no ulcer. Treatment is usually similar to actively bleeding vessel in peptic ulcer disease and includes injection therapy, clips, banding devices, heater probe and bipolar probe. Studies have shown that monotherapy with injection should not be attempted. Bipolar probes should be set at 20 watts and applied for 10 to 12 s, and heater probes should be set

at 30 joules and 4 pulse should be administered.

Mallory Weiss tears are usually self-limited bleeds and do not need endoscopic therapy. However, in the presence of ongoing active bleeding clips are preferred, though other devices such as band devices and electrocautery have also been reported^[23,24]. The settings for bipolar and heater probes include 15-20 watts for 4 s and 15-20 joules for 3 pulses respectively. However, there are no trials comparing the various treatment modalities.

Angioectasias and gastric antral vascular ectasias (GAVE) usually cause chronic and obscure GI bleeding. These are usually treated with APC. The probe should be set at 45 watts with 1 L/min argon flow rate for vascular ectasia; whereas for GAVE, 60 watts with 1 L/min is applied for deeper tissue penetration. Though other previously mentioned methods have been used, there are again no prospective comparison trials.

However, despite the advances made in therapeutic endoscopies there are still certain instances where we fail to achieve hemostasis endoscopically. Thus, it is important to realize the limitations of various modalities and be aware of other options that we may have. Large bleeding vessels more than 2 mm to 3 mm in size, or high stigmata ulcer in posterior wall of the duodenal bulb may not be amenable to endoscopic intervention. Rarely interventions in such instances may fuel a massive GI bleed requiring IR intervention (Figures 1-3).

Pre-intervention imaging

If a patient is stable enough during presentation and plans are not made for immediate endoscopy, pre-procedure imaging can be performed to attempt localization of the culprit vessel or other underlying etiologies. Computerized tomography (CT) scanning is readily available in many centers and can tolerate patients with a tenuous clinical picture due to the speed of image acquisition. Multiphasic CT is usually performed without contrast followed by three contrasted series of images in the arterial, venous, and delayed phases to assist in localizing the bleed. A positive study occurs when there is contrast extravasation into the bowel lumen or identification of an abnormal vessel, mass, or other underlying etiology; the same is true for conventional catheter based angiography^[8,25]. CT angiography can detect bleeds with a reported sensitivity of 0.5 cc/min of active extravasation which is compared to the sensitivity of catheter arteriography rate of detection of at least 1 cc/min^[25].

Another imaging modality for patients is technetium labeled red blood cell scintigraphy. In this study, patient's red blood cells are tagged with technetium and imaged for 60-90 min. Pooling of radiotracer is considered to be positive. Typical rates of bleeding required for detection of bleeding have been reported between 0.05-0.5 cc/min^[25]. A benefit of this study is the ability to detect arterial or venous bleeding; a disadvantage, in turn, becomes the lack of precisely identifying the location of the bleed. Sensitivity and specificity of this study are 91% and 95%

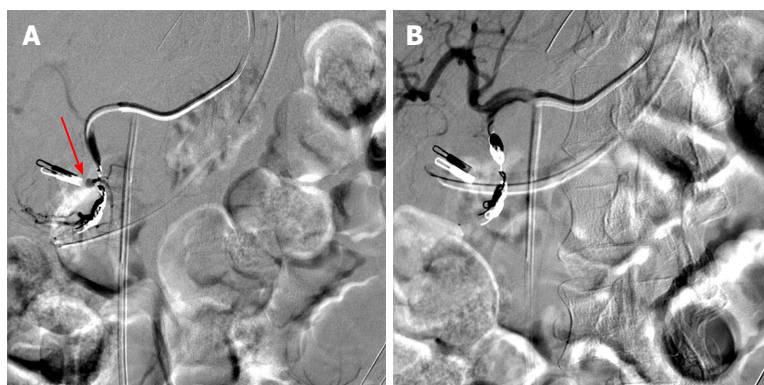


Figure 2 During interventional angiography, selected fluoroscopic images showing a pseudoaneurysm of the gastroduodenal artery (A, red arrow) that was successfully coiled with subsequent hemostasis via the sandwich technique (B). Previously placed Endoclip is visible and can act as a fluoroscopic marker during angiography.

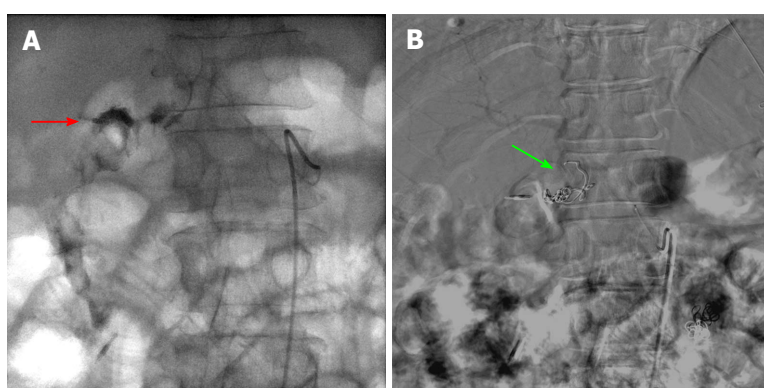


Figure 3 Fluoroscopic images of a case of 2-3 cm bleeding duodenal ulcer that failed endoscopic hemostasis with Endoclip application. A: Fluoroscopic image following contrast injection to the right gastric artery showing active extravasation into the lumen. The bleeding vessel (red arrow) is identified which is near the endoscopically placed clip; B: Digital subtraction angiography post coiling of the right gastric artery (green arrow).

respectively and are improved with increasing volume of extravasation^[25].

As mentioned earlier, if endoscopy is unsuccessful at either identifying or stopping the bleeding source, transcatheter arteriography is the next step at intervention. Typically, the femoral artery is used as the site for arterial access unless other factors prevent this approach; however, radial approach is an alternative which has been gaining interest at some centers^[26]. If upper GI bleeding is suspected, the celiac artery is usually cannulated first^[8]. Superselective evaluations are performed based on any prior studies used to help localize the location of the bleed. If a culprit vessel is identified, multiple methods of embolization have been described^[8,27]. Patient breathing causes motion which can make visualization of bleeding difficult on angiography. Also, bowel gas and bowel movement can cause further limitations during catheter angiography.

There are many different techniques for embolization and controlling active hemorrhage. These include placing covered stents, endovascular coils/plugs, and embolic glue. In some instances, the microcatheter used to evaluate the culprit vessel will occlude and stop the hemorrhage temporarily. This can be utilized in temporary situations to spasm an artery to achieve hemostasis without per-

manently occluding an artery. Care must be taken to evaluate the vasculature in the region of bleeding as many sites in the GI tract have collateral blood flow. In sites that have collateral flow, a sandwich technique can be utilized; this requires identifying the bleeding site and embolizing the distal and proximal side branches to provide occlusion ensuring no distal reconstitution and decreasing chances of re-bleeding^[8].

In some instances, patients are too hemodynamically unstable to obtain imaging and may need to go directly to the angiography suite or the endoscopy lab. Close communication between the emergency room physicians, anesthesiologists, surgeons, gastroenterologists, and interventional radiologists must be encouraged in order to provide optimal care for these critically ill patients. One important caveat to consider regarding angiography over endoscopy as a first line intervention is that angiography will only be positive if there is active bleeding, an abnormal vessel, or tumor blush. Also, active bleeding with high clinical suspicion of the approximate location of a bleed can be an appropriate indication of taking the patient directly to angiography in order to identify and treat the site of bleeding as active bleeding may terminate during the time taken to obtain imaging^[28]. Hyperemia can be identified by angiography but subtle



Figure 4 A male patient presented with massive bright red blood per rectum which was unresponsive to transfusions. A representative computed tomography scan image demonstrates active contrast extravasation in the rectum (white arrow).

mucosal abnormalities will be more readily identified with endoscopic management. Additionally, in cases of high risk ulcers which have had either successful or unsuccessful endoscopy, catheter arteriography has been shown to play a key role in preventing rebleeding by performing prophylactic embolization^[29]. Surgical consultation is always recommended and performed at our hospital.

ACUTE LOWER GI BLEEDING

Acute lower gastrointestinal bleeding is defined as bleeding of recent duration (< 3 d), hemodynamic instability, anemia or requirement of blood transfusion^[30]. Though most lower GI bleeds resolve spontaneously, mortality and morbidity is increased in elderly patients and those with comorbid medical conditions^[31]. Bleeding rate and total blood loss become a critical factor in determining correct patient management. Initial management and assessment is similar to upper GI bleeds. A multi-disciplinary approach is crucial for providing the best care for these critically ill patients.

Lower GI bleeding accounts for approximately 30% of all GI hemorrhage and has many etiologies^[32]. The most common causes of lower GI bleeding are diverticula, angiodysplasia, anorectal neoplasm, and colitis^[32,33]. The incidence increases with age with mean age of presentation ranging from 63 to 77 years of age. It has been estimated that lower GI bleeding is 200 times more likely in an 80 years old than a 20 years old^[32]. Although bleeding can be life threatening, unlike upper GI bleeding, most cases of lower bleeding tend to be self-limited. Of the cases considered a lower bleed, the colon is the source in approximately 80% of cases^[28]. Many patients with bleeding associated with diverticulosis can stop spontaneously in up to 80% of patients^[32,33]. Mortality rates have been reported at less than 5%^[34].

Initial management includes determination of the need for urgent evaluation and resuscitation with crystalloids and blood products and correction of coagulation factors in applicable. If stable, imaging plays a key role in

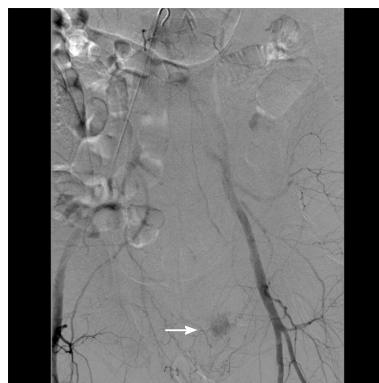


Figure 5 During interventional angiography, contrast extravasation is visualized into the colon via a distal branch artery from the internal iliac artery (white arrow). The culprit vessel was occluded by spasm or dissection at the ostium with no residual active bleeding. During follow-up lower endoscopy, an endoscopic image showed no active bleeding with discrete large sized clean based ulcers, consistent with ischemic colitis.

identifying the source and etiology of the bleeding. As stated previously, CT and tagged red blood cell scintigraphy are excellent non-invasive options to assist with acute management decisions (Figures 4 and 5). Other useful tools in the management of patients with small bowel bleeding distal to the ligament of Treitz include capsule endoscopy and CT enterography to evaluate for a specific lesion or site of bleeding. Though diagnostic testing helps to localize the lesion, studies have shown that the diagnostic yield of colonoscopy ranges from 45% to 100%^[34] which is higher than radiological evaluation. If stable enough, patients should undergo urgent colonoscopy within 8 to 24 h of admission as that improves diagnostic yield and likelihood of therapeutic intervention. This was also demonstrated by Strate and Syngal^[35] in 2003 where they studied 144 patients and concluded that endoscopic therapy was successful in 29% of colonoscopies performed within 12 h and this dropped to 4% when performed between 24 to 48 h. These patients need to undergo rapid purge prep which involves drinking 1L of Golytely every 30 to 45 min until no fecal matter is noted in the effluent^[36]. However, performing a colonoscopy at the time of active significant bleeding is often not useful as the bleeding impairs visualization in the colon; this is in contrast to angiography, which usually requires active extravasation to detect the hemorrhage. The various hemostatic devices are similar to the one discussed in the upper GI bleeding section. In cases of intermittent scant hematochezia, if hemodynamically stable, healthy individual less than 40 years of age can be considered for flexible sigmoidoscopy^[37].

Diverticular bleeding accounts for 20% to 65% of acute lower GI bleeds^[32] and causes significant bleeding in 3% to 15%^[38] of the cases (Figure 6). The bleeding is characterized as painless hematochezia which stops simultaneously in 75% to 80% of the cases but recurs in about 25% to 40% of the cases within 4 years^[38]. Endoscopic management involves using clipping or thermal

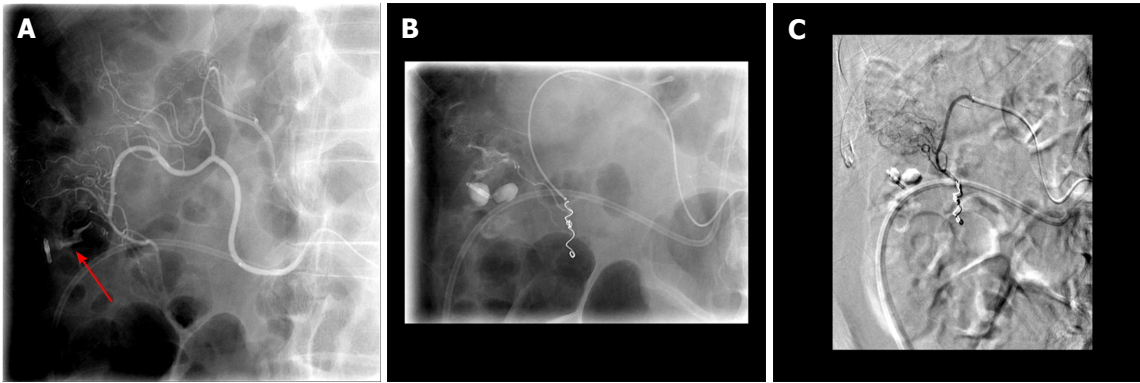


Figure 6 Fluoroscopic images of a case of colon diverticular bleeding that failed endoscopic hemostasis with Endoclip application. A: Active extravasation at the site of the clip (red arrow); B: Ongoing extravasation superior to the clip after initial coils placed in the inferior branch of the middle colic artery; C: Digital subtraction angiography following additional coils with no extravasation.

contact modalities either alone or in conjugation with injection technique. Due to thinner walls of the right sided colon, perforation is a concern. Endoclip placement is often preferred to treat the bleeding or visible vessel at the neck or bottom of the diverticulum. If thermal methods are used care should be taken to apply lower setting for short periods of time only. Typically 10-15 joules (heater probe) or 10 to 16 watts (bipolar) should be applied for 2 to 3 second pulse contacts and mild pressure^[39,40]. Endoscopic clips can be either deployed over the bleeding vessel or use to oppose the walls to act as a tamponade effect and prevent bleeding^[41]. Kaltenbach *et al.*^[42] described using EndoCap to evert the diverticulum and placing the clip.

Ischemic colitis affects about 1% to 19% of the cases^[35] and typically presents as painful hematochezia^[43] affecting the watershed areas of the colon: Splenic flexure and rectosigmoid junction. The majority of patients respond to conservative management and treatment of the underlying condition. Angiography is recommended in patients with severe ischemic colitis, right sided colitis or suspicion of underlying thromboembolism or concurrent mesenteric ischemia^[44]. Radiation proctitis is caused by radiation induced endarteritis obliterans with resultant telangiectasia and neovascularization in the rectum^[45]. Effective treatment includes serial management with APC.

The other etiologies for colitis such as *Clostridium difficile* colitis, inflammatory bowel disease, viral, bacterial and parasitic infections, diversion colitis can also present with hematochezia and usually managed by treating the underlying conditions.

Angiectasias account for 3% to 15% of cases with lower GI bleeding^[30], and their incidence also increase with age^[46]. They range from 2 mm to several centimeters and are characterized by ectatic blood vessels radiating from a central feeding vessel^[46]. Though both contact and non-contact thermal methods are used for its treatment, APC is the preferred treatment modality^[47]. Owing to thin walls of the right side of the colon power settings of 15 W to 30 W at 1 L/min argon flow rate is utilized. Short pulses of 1 to 2 s are applied and the probe is held 1 to 3 mm

away from the mucosa^[40]. Lee *et al.*^[48] in 2010 described application of Hemoclips in conjugation with APC to control bleeding.

Hemorrhoids are present in 75% of colonoscopies^[46] but are indicated in only 2% to 10% of acute lower GI bleeds^[49]. Bleeding hemorrhoids are usually managed with banding devices. Like esophageal varices they are also conducted in series with no more than 3 bands placed in one setting.

Management of rectal ulcers and Dieulafoy's lesion are similar to upper GI bleeds and achieved by thermal or mechanical methods or dual therapy, including injection technique. Hence, as stated above most cases of lower GI bleeding are self-limited, but occasionally patients may present with massive GI bleeding where they are too unstable to undergo colonoscopy or despite drinking the prep the colon is still filled with blood obscuring endoscopic evaluation. In such cases, it is IR that can prove invaluable. Surgery is typically reserved as a last resort since even with location identified mortality is high, and mortality increases when the bleed cannot be localized.

Angiography is similar regarding lower GI bleeds compared to upper bleeds. A major advantage compared to colonoscopy is that no bowel prep is needed. Typically, the interventional radiologist will begin with the superior mesenteric artery (SMA) as this will be the major supply to the distal small bowel, ascending and transverse colon. The inferior mesenteric artery (IMA) supplies the descending sigmoid colon as well as the rectum and anus. Branches of the internal iliac artery also supply the rectosigmoid colon and anus and become the main supply in cases of an occluded or diminutive IMA. Many collaterals and normal anatomic variants exist which must be evaluated prior to any interventions^[28]. For instance, the SMA may provide arterial supply to the entire colon in the event the IMA is occluded *via* the arc of Riouan or marginal artery of Drummond which are arterio-arterio anastomoses between the superior and inferior mesenteric arteries^[50].

Ideally, a selective embolization is performed if the etiology is discovered by angiography. When distal

branches are able to be cannulated, the risk of developing colonic ischemia is low and perhaps subclinical. Other methods such as vasospasm can prove useful to maintain normal blood flow while clot and hemostasis develop as demonstrated in Figures 4 and 5.

GASTROSTOMY TUBE

Though feeding tubes have been in place for over 400 years it was not until 1980 that the first description of percutaneous endoscopic gastrostomy tube was attempted by Gauderer *et al*^[51]. Subsequently, in 1981 the first percutaneous gastrostomy tube was placed under radiological guidance^[52]. This was initially developed for cases where endoscopy could not be performed or was too risky to be attempted^[52,53]. Since then, these two approaches have widely replaced surgical open gastrostomy owing to its minimally invasive nature, reduced cost and ease of tube placement^[54]. These tubes are not only used for feeding but can also be used for decompression. Typical indications for gastrostomy tube are for providing nutrition in patients with an inability to obtain adequate nutrition but with intact and functional GI tract. Impaired swallowing mechanism associated with neurological conditions and neoplastic conditions of the oropharynx, larynx and esophagus are some of the common indications^[55,56]. It can also be performed to attain gastric decompression in patients with gastroparesis or obstruction such as peritoneal carcinomatosis.

Absolute contraindications to this procedure are an uncorrectable coagulopathy, thrombocytopenia, peritonitis, or bowel ischemia. Large gastric varices, if known, can pose an increased risk of internal hemorrhage. Ascites or peritoneal dialysis is a relative contraindication given potential for pericatheter leakage and life threatening peritonitis respectively. In these patients, paracentesis can provide assistance to make the procedure safe^[57]. In peritoneal dialysis patients, the procedure should be discussed with patient's nephrologist. Contraindications specific for endoscopic placement include inability to bring the gastric wall in apposition with the anterior abdominal wall, facial fractures, skull fractures and upper GI obstruction^[58]. In these cases, radiologically placed gastrostomy tube is preferred. Specific contraindications to radiologically placed feeding tubes include inability to travel to the radiology suite in patients with hemodynamic instability^[58]. Also, prior gastric surgery can make the anatomical window smaller and more challenging suggesting the need for CT guidance^[55,56].

For percutaneous endoscopic gastrostomy tube placement, there are currently three techniques: (1) "pull" or Pomskey-Gauderer technique^[51]: This involves insufflating the stomach and selecting an appropriate site by indenting the abdominal wall with a finger. Sterile precautions should then be followed and the site anesthetized with lidocaine. Subsequently the needle is advanced in to the stomach while withdrawing the plunger. The endoscopist confirms that the gastric puncture of

the needle corresponds to the air in the syringe. This is essential to ensure the absence of any intervening bowel. A small skin incision is made and trocar is introduced into the stomach. A guidewire is then fed through the trocar and grasped endoscopically and pulled out through the mouth along with the endoscope. The feeding tube is then attached to the guidewire and pulled through the esophagus, stomach and abdominal wall and held in place by both internal and external bumper; (2) "push" or Sacks-vine technique^[59]. This technique is similar to pull technique till the guidewire is placed. Then an introducer tube is threaded over the guidewire and pushed till it emerges through the abdominal wall and then is grasped manually and secured in position; and (3) introducer technique or Russell technique^[60], this was developed in 1984 and has recently gained popularity to be used in cases with head and neck cancer to avoid seeding of the gastrostomy tract^[61]. This uses a transabdominal approach. In this technique once the access to stomach is obtained endoscopically, gastropexy is performed next using either T fasteners^[62] or gastropexy sutures^[63]. Subsequently, the stomach is accessed with a needle and a guidewire. The tract is then dilated with a dilating catheter and finally a balloon tip gastrostomy catheter is placed into the stomach through the peel away sheath.

Interventional radiological gastrostomy tube can be placed with either fluoroscopic, CT, or ultrasound guidance. These procedures can be performed with excellent success rates^[55]. Success typically depends on the appropriate anatomic window in order to make a percutaneous approach into the stomach. Previous cross sectional imaging is utilized to evaluate for appropriate anatomical window for gastrostomy tube placement. Patients are administered barium orally or *via* nasogastric/orogastric tube at least 12 h prior to the procedure in order to opacify the transverse colon. Upon the patient entering the IR suite, a nasogastric tube is inserted if not already present. At our institution, we then use ultrasound to evaluate the liver margin and outline prior to the procedure. The insertion site is chosen below the costal margin, above the transverse colon, and to the left of midline. Some institutions, including ours, will administer 0.5-1 mg of intravenous glucagon to inhibit gastric motility during the procedure. The stomach is then insufflated with air. Gastropexy is next performed with T-fasteners in order to apply the stomach to the abdominal wall. An incision is then made between the gastropexy sutures. A needle is inserted into the stomach which is confirmed by aspirating air at an angle directed towards the pylorus. Care must be taken during these next steps to ensure the stomach remains insufflated with air; typically, a technologist will assist with insufflating air as needed. A wire is then inserted and the tract is dilated to the appropriate tube size. The gastrostomy tube is then inserted by using a peel-away sheath. Gastrostomy tubes may have a pigtail or balloon to secure within the stomach; we use tubes with balloons for securing the tube location. Contrast is then injected and both AP and lateral fluoroscopic views obtained to ensure the tube has been placed into the

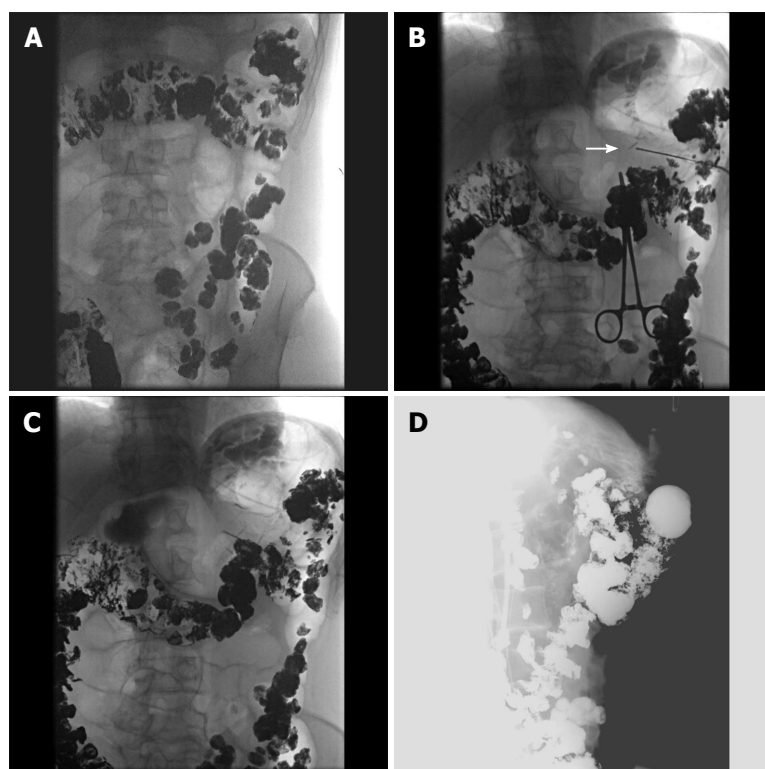


Figure 7 Selected fluoroscopic images demonstrating fluoroscopically guided gastrostomy placement. A: Contrast seen throughout the transverse colon; B: The first T-tac (white arrow) is deployed following needle insertion into the gastric lumen; C: Two more T-tacs placed; D: Static lateral image of the gastrostomy tube against abdominal wall and not in the colon. The contrast is injected into the tube to demonstrate intraluminal placement.

stomach only and is secured to the abdominal wall. This procedure is illustrated in Figure 7. Occasionally, this method will be adjusted and performed under CT guidance for patients with a narrow anatomic window. Percutaneous sonographic gastrostomy which was initially described by Gebel *et al*^[64] in 1991 for patients with upper GI tract obstruction is yet another technique. This procedure is currently not widely performed in United States, though is still popular in Europe. This process involves passage of a nasogastric tube into the stomach, followed by instillation 500 to 1500 cc of water. The stomach is then localized by ultrasound. The puncture site into the stomach is identified after establishing absence of vessels and colon or small intestine interposition with ultrasound and Doppler. A small skin incision is made, and a needle is introduced into the stomach. A wire is then passed through the stomach into the duodenum. The puncture site is then dilated with serial dilators and gastrostomy tube placed. In 1998 Bleck *et al*^[65], reported successful placement of feeding tube in 38 patients *via* this method with no major complications reported in a 4 mo follow-up period. Major complications can include internal hemorrhage, catheter dislodgement, peritonitis/sepsis, or death. Minor complications are catheter leakage and clogging requiring exchange.

Thus, though studies have proven them to have equal success rates with both endoscopic and radiological tube placement, each procedure has a distinct advantage over the other^[66]. With endoscopic placement, the procedure can be performed at the bed side and have diagnostic capabilities. In a study published in 1990, 10%-71%

of patients were found to have abnormal endoscopy findings out of which management had to be altered in 36% of patients^[67]. Also the endoscopic procedure reduces the radiation exposure. Meanwhile, radiological placement is possible in patients who fail endoscopic management such as those who are morbidly obese or have severe upper GI luminal narrowing^[68]. Hence it is of utmost importance that practitioners are aware of these indications so that the patient can be sent to appropriate discipline for gastrostomy tube placement.

CECOSTOMY TUBES

Cecostomy tubes can be placed surgically or percutaneously with endoscopic or image guidance^[69]. These tubes are mainly indicated in patients with neurological disorder with resultant fecal incontinence to facilitate cleansing enemas^[70], in the assistance of bowel training in the pediatric population, neurogenic bowel due to any issue, chronic colonic pseudo obstruction and colonic obstruction^[71]. The contraindications are similar to gastrostomy tube^[72,73].

Placement of a percutaneous endoscopic cecostomy tube is similar to endoscopic percutaneous gastrostomy tube placement^[74]. The night before the procedure 4 liters of Golytely is administered to clean the colon. In patients with chronic constipation more prolonged prep may be needed^[75]. The colonoscope is then advanced all the way to the cecum which is insufflated. An appropriate site is selected by finger indentation in the right lower

quadrant and transillumination is performed. The rest of the procedure is similar to percutaneous endoscopic gastrostomy tube placement *via* the “pull” technique. The cecum needs to be fixed to the abdominal wall with the help of a “fixation” device to prevent leakage of the fecal content^[69].

IR can perform these procedures either under fluoroscopic or CT guidance. The bowel will be prepped prior to the procedure similar to endoscopic procedures. Similar to gastrostomy tubes, the colon is insufflated with air and glucagon administered to decrease bowel contractions. A needle is inserted, T-tacks used to secure the position of the cecum, a wire inserted with subsequent dilation, and a tube is then inserted. This has been reported as a safe procedure although not commonly performed at our institution^[72]. Though only small case series have been described, the procedure is easily performed and has a good success rate. However, the complication rate has been reported to be as high as 42% and includes wound infection, bleeding, perforation leading to peritonitis and buried bumper syndrome^[76]. Buried bumper syndrome (BBS) which is a well-known complication of gastrostomy tube placement, occurs due to excessive outward traction on the tube. In 2011 Rao *et al.*^[77] described its occurrence in a patient who had undergone percutaneous endoscopic cecostomy tube placement about 1.5 years prior to the presentation. BBS usually presents with peristomal cellulitis owing to the presence of intraluminal stool. If the tract is immature, BBS can lead to fecal peritonitis and intra-abdominal sepsis. Management involves antibiotics and removal of the tube. Cecostomy tubes should not be removed by external traction as it can lead to colonic laceration. Instead, the tube should be cut externally and removed endoscopically with the help of a snare. This complication can potentially be prevented with the usage of balloon tube or by avoiding excessive traction. In 2006, Uno^[78], described the introducer technique to reduce the incidence of wound infection. In 2015, Duchalais *et al.*^[79] published a prospective trial to evaluate the efficacy of constipation in patients undergoing percutaneous endoscopic cecostomy tube placement and reported successful results in three quarters of the patient population. However, chronic wound pain prompted the removal in the other one fourth of the patient population. Currently there are no trials comparing the efficacy of endoscopic and fluoroscopically placed percutaneous cecostomy tubes.

STRICTURES

Esophageal strictures are routinely seen in practice. The common causes include peptic strictures which develop as a sequel to GERD and account for almost 80% of benign strictures^[80]. Their incidence seems to be decreasing in recent years with the more widespread use of proton pump inhibitors. Other causes include: Schatzki's ring, radiation, caustic injury, anastomotic stricture, pill induced esophagitis, esophageal web, eosinophilic esophagitis

and malignancy^[81]. They can be further divided into simple and complex strictures^[82]. Simple strictures are symmetric, < 2 cm in length, with a diameter of greater than equal to 12 mm, and allow easy passage of an upper endoscope. Complex strictures, however, are asymmetric, have a diameter < 12 mm, more than > 2 cm long, and do not allow the passage of the scope. Most of these strictures are amenable to treatment with dilation and stent placement which can be done both endoscopically and radiographically.

These patients present with dysphagia and should undergo initial endoscopic evaluation as that not only helps in diagnosis but can also aid in performing possible therapeutic intervention such as dilation^[83]. Further, they can also assess to see if they are any predisposing factors such as angulated stricture, diverticula, and hiatal hernia which may increase the risk of complications. Most benign strictures respond to dilation unlike malignant strictures which have a greater risk of complications^[84]. Active esophageal perforation is an absolute contraindication to dilation^[85]. There are currently three types of dilators: Maloney bougie (without a guidewire), Savory-Gilliard (passed over a guidewire) and through the scope (TTS) balloon dilators^[86]. Prior to dilation, the endoscopist should consider the method of dilation, the diameter to which the obstruction should be dilated, need for wire guidance and need for radiographic screening^[85]. Benign esophageal strictures are usually dilated to about 13 to 15 mm. However Schatzki's ring can be dilated to about 16 to 20 mm^[85]. Maloney dilators range from 16F to 60F and exert both longitudinal and radial force. This can be done blindly or under fluoroscopic guidance. These dilators can also be used for self-dilation without sedation^[82]. Patients with benign esophageal stricture requiring frequent dilations are ideal candidates for self-dilation. The Maloney dilator is usually marked at two points: 20 cm from the entry site and 10 cm beyond the distal end of the stricture. The procedure is performed with the patient in sitting position. The dilator is lubricated with water and introduced over the tongue into the oropharynx. Once the patient visualizes the 20 cm marking, the tube is in the esophagus. The dilator is then advanced until the second marking is seen at the level of incisors, which confirms the passage of maximal diameter of the dilator across the stricture. Lastly, the dilator is carefully withdrawn.

Similarly, Savory dilators also range from 16F to 60F and have the same mechanism of action. The rigid tip is passed over a guidewire. They are also marked with radiopaque band at their maximal diameter. The guidewire is usually passed to the antrum and can be done endoscopically or fluoroscopically. Subsequently, the dilator is passed over the guidewire till the maximal diameter is beyond the stricture. If no force is experienced, then the dilator is slowly removed in one to one exchange manner to ensure the positioning of the guidewire. This uses tactile perception to determine the amount of resistance encountered. Sequential dilation is performed but usually in one setting no greater than

3 dilators are passed though studies have shown no increased risks with passing > 3 dilators in cases of a benign simple esophageal stricture^[87]. TTS balloons work by exerting only radial force. They can usually increase up to 3 diameters and are useful for serial dilations with a single balloon. The endoscope is usually positioned proximal to the stricture and the balloon dilator is advanced through the stricture. The balloon is then inflated under direct endoscopic visualization and the pressure is held for 30 to 60 s.

Studies have shown similar efficacy in treating peptic strictures *via* any of the above mentioned methods^[88,89]. In the treatment of postesophagectomy anastomotic strictures these methods show a similar efficacy of 93%; however, they have a high recurrence rate and need multiple sessions^[90,91]. Though most procedures are performed under endoscopic guidance, fluoroscopy is important in the setting of complex strictures as it aids in dilation^[85]. Further in cases where an endoscope is unable to cross proximal lesions, fluoroscopic dilation must be performed.

Fluoroscopic or other image guided balloon dilatation has been described in the literature as a safe method for stricture treatment of the esophagus in various disease states^[92,93]. However, this has not been a common procedure in our IR department. In cases of refractory benign strictures, steroid injection into the stricture prior to dilation has shown to be effective in increasing post dilation diameter, reducing the need for repeat dilation and increasing the interval between dilations. Temporary esophageal stenting is also an option. A systemic review published regarding the use of plastic stents in benign esophageal strictures reported successful dilation in 52% of the cases. However, stent migration was reported in 24% of the population^[94]. Song *et al*^[95] in 2000 published a study where fully covered metal stents were placed in 25 patients, but migration was noted in 80% while 48% of them developed a new stricture. Few studies^[96,97] have also been published regarding the use of biodegradable stents without promising results.

Similar to the upper GI tract, patients with inflammatory bowel disease are known to develop strictures. This is more common in Crohn's disease where 40% of patients with ileal disease develop strictures^[98]. Further studies demonstrate that 60% of patients with strictures would undergo surgery within the next 20 years^[99]. Strictures in Crohn's disease can occur *de novo*, at the site of bowel anastomosis, or at the ileal pouch. They can be divided into inflammatory vs fibrotic^[100]. Inflammatory strictures can be treated with medical management. However, fibrotic strictures were traditionally treated with only surgical management^[101]. Studies have shown that stricturoplasty tends to preserve bowel length and is associated with high recurrence rate leading to frequent operations. In younger adults, the course tends to be more aggressive leading to frequent operations and finally short bowel syndrome^[102]. Endoscopic managements have been devised in an attempt to reduce this dreaded complication. Prior to any therapy

endoscopic evaluation and biopsy, assessment of the stricture must be performed to rule out malignancy especially in the setting of ulcerative colitis. Endoscopic management includes dilation therapy, local injection of steroids, needle-knife stricturotomy and stent placement^[103]. The technique of balloon dilation (TTS) is similar to the one described for esophageal stricture. Endoscopic balloon dilation has shown to both avoid or delay the need for surgery, though frequent dilations may be needed. In a systemic review published by Hassan *et al*^[104] in patients with Crohn's disease related strictures, endoscopic dilation achieved success in 86% of the patients with long term clinical efficacy obtained in 56% of them. In a multivariate analysis, stricture length of < 4 cm was the only predictor for surgery free follow up period. The mean adverse events (perforation and bleeding) were less than 2%. In 2010, Mueller *et al*^[105] published a prospective single center study of 55 patients. They reported an initial success rate of 95% with 76% of those patients not requiring surgery during the follow-up period. Given the high relapsing rate, addition of steroid injection to the stricture at the time of dilation has been studied. However, currently the data is conflicting^[106,107]. More recently stent placement at the time of endoscopy in this patient population has been evaluated. However, studies using self-expandable metallic stents (SEMS)^[108] and biodegradable stents^[109] have reported high rates of stent migration and other adverse events. In 2012 Loras *et al*^[110] published a small series of 25 SEMS placement with technical success obtained in 92% of the stent placements that was maintained for a 4 wk follow-up period.

Similar to upper GI strictures, fluoroscopic guided balloon dilatation and/or stent placement has also been described for the lower GI tract for patients as a pre-surgical or palliative relief^[111,112]. Typically, the procedure involves placing the patient supine on the fluoroscopy table. A wire is then inserted through the anus retrograde to the level of the obstruction. Once the wire passes the obstruction and is proximal, a catheter is inserted for the purpose of water soluble contrast injection. This step is critical to evaluate the dimensions of the stent and type of delivery system used. Appropriate stents should cover the lesion with 1-2 cm extension beyond the obstruction. Covered stents are not recommended due to risk of migration^[111]. Water-soluble contrasted enema can be repeated immediately or any time after the procedure to evaluate placement. However, this is also another procedure not commonly performed in our IR department.

CONCLUSION

Advances in the medical field have been to the advantage of the patient in many disease processes as discussed above. In today's era of minimally invasive procedures, surgery as a first choice of management is getting less popular. Therapeutic endoscopy and interventional radiology have come a long way from their

initial inception to being main modalities of treatment. Treatment modality of choice is often based on availability of the services, clinical stability of the patients and their presentation. However, these are complex patients that often require close collaboration between gastroenterologists, radiologists and surgeons.

REFERENCES

- Hirschowitz BI, Curtiss LE, Peters CW, Pollard HM. Demonstration of a new gastroscope, the fibroscope. *Gastroenterology* 1958; **35**: 50; discussion 51-53 [PMID: 13562387]
- Rösch J, Keller FS, Kaufman JA. The birth, early years, and future of interventional radiology. *J Vasc Interv Radiol* 2003; **14**: 841-853 [PMID: 12847192 DOI: 10.1097/01.RVI.0000083840.97061.5b]
- Rösch J, Dotter CT, Brown MJ. Selective arterial embolization. A new method for control of acute gastrointestinal bleeding. *Radiology* 1972; **102**: 303-306 [PMID: 4536688 DOI: 10.1148/102.2.303]
- van Leerdam ME. Epidemiology of acute upper gastrointestinal bleeding. *Best Pract Res Clin Gastroenterol* 2008; **22**: 209-224 [PMID: 18346679 DOI: 10.1016/j.bpg.2007.10.011]
- Sildiroglu O, Muasher J, Arslan B, Sabri SS, Saad WE, Angle JF, Matsumoto AH, Turba UC. Outcomes of patients with acute upper gastrointestinal nonvariceal hemorrhage referred to interventional radiology for potential embolotherapy. *J Clin Gastroenterol* 2014; **48**: 687-692 [PMID: 25014238 DOI: 10.1097/MCG.0000000000000181]
- Eisen GM, Dominitz JA, Faigel DO, Goldstein JL, Kalloo AN, Petersen BT, Raddawi HM, Ryan ME, Vargo JJ, Young HS, Fanelli RD, Hyman NH, Wheeler-Harbaugh J, American Society for Gastrointestinal Endoscopy. Standards of Practice C. An annotated algorithmic approach to upper gastrointestinal bleeding. *Gastrointest Endosc* 2001; **53**: 853-858 [DOI: 10.1016/S0016-5107(01)70304-5]
- Andersen PE, Duvnjak S. Endovascular treatment of nonvariceal acute arterial upper gastrointestinal bleeding. *World J Radiol* 2010; **2**: 257-261 [DOI: 10.4329/wjr.v2.i7.257]
- Loffroy R, Rao P, Ota S, De Lin M, Kwak BK, Geschwind JF. Embolization of acute nonvariceal upper gastrointestinal hemorrhage resistant to endoscopic treatment: results and predictors of recurrent bleeding. *Cardiovasc Interv Radiol* 2010; **33**: 1088-1100 [DOI: 10.1007/s00270-010-9829-7]
- Hwang JH, Fisher DA, Ben-Menachem T, Chandrasekhara V, Chathadi K, Decker GA, Early DS, Evans JA, Fanelli RD, Foley K, Fukami N, Jain R, Jue TL, Khan KM, Lightdale J, Malpas PM, Maple JT, Pasha S, Saltzman J, Sharaf R, Shergill AK, Dominitz JA, Cash BD, Standards of Practice Committee of the American Society for Gastrointestinal E. The role of endoscopy in the management of acute non-variceal upper GI bleeding. *Gastrointest Endosc* 2012; **75**: 1132-1138 [DOI: 10.1016/j.gie.2012.02.033]
- Soehendra NWB. New techniques for endoscopic treatment of bleeding gastric ulcer. *Endoscopy* 1976; **8**: 2 [PMID: 862577 DOI: 10.1055/s-0028-1098382]
- Chung SC, Leung JW, Steele RJ, Crofts TJ, Li AK. Endoscopic injection of adrenaline for actively bleeding ulcers: a randomised trial. *Br Med J (Clin Res Ed)* 1988; **296**: 1631-1633 [PMID: 3135047 DOI: 10.1136/bmj.296.6637.1631]
- Calvet X, Vergara M, Brullet E, Gisbert JP, Campo R. Addition of a second endoscopic treatment following epinephrine injection improves outcome in high-risk bleeding ulcers. *Gastroenterology* 2004; **126**: 441-450 [PMID: 14762781 DOI: 10.1053/j.gastro.2003.11.006]
- Vergara M, Calvet X, Gisbert JP. Epinephrine injection versus epinephrine injection and a second endoscopic method in high risk bleeding ulcers. *Cochrane Database Syst Rev* 2007; CD005584 [DOI: 10.1002/14651858.CD005584.pub2]
- Bustamante-Balén M, Plumé G. Role of hemostatic powders in the endoscopic management of gastrointestinal bleeding. *World J Gastrointest Pathophysiol* 2014; **5**: 284-292 [PMID: 25133029 DOI: 10.4291/wjgp.v5.i3.284]
- Sung JJ, Luo D, Wu JC, Ching JY, Chan FK, Lau JY, Mack S, Ducharme R, Okolo P, Canto M, Kalloo A, Giday SA. Early clinical experience of the safety and effectiveness of Hemospray in achieving hemostasis in patients with acute peptic ulcer bleeding. *Endoscopy* 2011; **43**: 291-295 [DOI: 10.1055/s-0030-1256311]
- Hui AJ, Sung JJ. Gastrointestinal bleeding. *Endoscopy* 2013; **45**: 276-280 [PMID: 23440586 DOI: 10.1055/s-0032-1326226]
- Holster IL, Kuipers EJ, Tjwa ET. Hemospray in the treatment of upper gastrointestinal hemorrhage in patients on antithrombotic therapy. *Endoscopy* 2013; **45**: 63-66 [PMID: 23208778 DOI: 10.1055/s-0032-1325793]
- Johnston JH, Jensen DM, Auth D. Experimental comparison of endoscopic yttrium-aluminum-garnet laser, electrosurgery, and heater probe for canine gut arterial coagulation. Importance of compression and avoidance of erosion. *Gastroenterology* 1987; **92**: 1101-1108 [DOI: 10.1016/S0016-5085(87)91065-1]
- Jensen DM. Heat probe for hemostasis of bleeding peptic ulcers: technique and results of randomized controlled trials. *Gastrointest Endosc* 1990; **36**: S42-S49 [PMID: 2242811]
- Hayashi TYM, Kuwabara T, Kudoh I. The study on staunch clip for the treatment by endoscopy. *Gastroenterol Endosc* 1975; **17**: 92-101
- Jensen DM. Spots and clots - leave them or treat them? Why and how to treat. *Can J Gastroenterol* 1999; **13**: 413-415 [PMID: 10377473 DOI: 10.1155/1999/703461]
- Laine L, McQuaid KR. Endoscopic therapy for bleeding ulcers: an evidence-based approach based on meta-analyses of randomized controlled trials. *Clin Gastroenterol Hepatol* 2009; **7**: 33-47; quiz 1-2 [DOI: 10.1016/j.cgh.2008.08.016]
- Lecleire S, Antonietti M, Iwanicki-Caron I, Duclos A, Ramirez S, Ben-Soussan E, Herve S, Ducrotte P. Endoscopic band ligation could decrease recurrent bleeding in Mallory-Weiss syndrome as compared to haemostasis by hemoclips plus epinephrine. *Aliment Pharmacol Ther* 2009; **30**: 399-405 [DOI: 10.1111/j.1365-2036.2009.04051.x]
- Papp JP. Electrocoagulation of actively bleeding Mallory-Weiss tears. *Gastrointest Endosc* 1980; **26**: 128-130 [PMID: 7450460 DOI: 10.1016/S0016-5107(80)73301-1]
- Laing CJ, Tobias T, Rosenblum DI, Banker WL, Tseng L, Tamarkin SW. Acute gastrointestinal bleeding: emerging role of multidetector CT angiography and review of current imaging techniques. *Radiographics* 2007; **27**: 1055-1070 [DOI: 10.1148/rf.274065095]
- Posham R, Biederman DM, Patel RS, Kim E, Tabori NE, Nowakowski FS, Lookstein RA, Fischman AM. Transradial Approach for Noncoronary Interventions: A Single-Center Review of Safety and Feasibility in the First 1,500 Cases. *J Vasc Interv Radiol* 2016; **27**: 159-166 [DOI: 10.1016/j.jvir.2015.10.026]
- Dixon S, Chan V, Shrivastava V, Anthony S, Uberoi R, Bratby M. Is there a role for empiric gastroduodenal artery embolization in the management of patients with active upper GI hemorrhage? *Cardiovasc Interv Radiol* 2013; **36**: 970-977 [DOI: 10.1007/s00270-012-0511-0]
- Walker TG. Acute gastrointestinal hemorrhage. *Tech Vasc Interv Radiol* 2009; **12**: 80-91 [PMID: 19853226 DOI: 10.1053/j.tvir.2009.08.002]
- Laursen SB, Hansen JM, Andersen PE, Schaffalitzky de Muckadell OB. Supplementary arterial embolization an option in high-risk ulcer bleeding--a randomized study. *Scand J Gastroenterol* 2014; **49**: 75-83 [DOI: 10.3109/00365521.2013.854829]
- Zuckerman GR, Prakash C. Acute lower intestinal bleeding: part I: clinical presentation and diagnosis. *Gastrointest Endosc* 1998; **48**: 606-617 [DOI: 10.1016/S0016-5107(98)70043-4]
- Strate LL, Ayanian JZ, Kotler G, Syngal S. Risk factors for mortality in lower intestinal bleeding. *Clin Gastroenterol Hepatol* 2008; **6**: 1004-1010; quiz 955 [PMID: 18558513 DOI: 10.1016/j.cgh.2008.03.021]
- Lee EW, Laberge JM. Differential diagnosis of gastrointestinal bleeding. *Tech Vasc Interv Radiol* 2004; **7**: 112-22 [PMID: 16015555 DOI: 10.1053/j.tvir.2004.12.001]
- Zuccaro G. Epidemiology of lower gastrointestinal bleeding. *Best*

- Pract Res Clin Gastroenterol* 2008; **22**: 225-232 [PMID: 18346680 DOI: 10.1016/j.bpg.2007.10.009]
- 34 **Strate LL**. Lower GI bleeding: epidemiology and diagnosis. *Gastroenterol Clin North Am* 2005; **34**: 643-664 [PMID: 16303575 DOI: 10.1016/j.gtc.2005.08.007]
 - 35 **Strate LL**, Syngal S. Timing of colonoscopy: impact on length of hospital stay in patients with acute lower intestinal bleeding. *Am J Gastroenterol* 2003; **98**: 317-322 [PMID: 12591048 DOI: 10.1111/j.1572-0241.2003.07232.x]
 - 36 **Elta GH**. Urgent colonoscopy for acute lower-GI bleeding. *Gastrointest Endosc* 2004; **59**: 402-408 [PMID: 14997144 DOI: 10.1016/S0016-5107(03)02721-4]
 - 37 **Eckardt VF**, Schmitt T, Kanzler G, Eckardt AJ, Bernhard G. Does scant hematochezia necessitate the performance of total colonoscopy? *Endoscopy* 2002; **34**: 599-603 [PMID: 12173078 DOI: 10.1055/s-2002-33249]
 - 38 **McGuire HH**. Bleeding colonic diverticula. A reappraisal of natural history and management. *Ann Surg* 1994; **220**: 653-656 [PMID: 7979613 DOI: 10.1097/0000658-199411000-00008]
 - 39 **Bloomfield RS**, Rockey DC, Shetzline MA. Endoscopic therapy of acute diverticular hemorrhage. *Am J Gastroenterol* 2001; **96**: 2367-2372 [PMID: 11513176 DOI: 10.1111/j.1572-0241.2001.04048.x]
 - 40 **Wong Kee Song LM**, Baron TH. Endoscopic management of acute lower gastrointestinal bleeding. *Am J Gastroenterol* 2008; **103**: 1881-1887 [PMID: 18796089 DOI: 10.1111/j.1572-0241.2008.02075.x]
 - 41 **Yen EF**, Ladabaum U, Muthusamy VR, Cello JP, McQuaid KR, Shah JN. Colonoscopic treatment of acute diverticular hemorrhage using endoclips. *Dig Dis Sci* 2008; **53**: 2480-2485 [DOI: 10.1007/s10620-007-0151-4]
 - 42 **Kaltenbach T**, Watson R, Shah J, Friedland S, Sato T, Shergill A, McQuaid K, Soetikno R. Colonoscopy with clipping is useful in the diagnosis and treatment of diverticular bleeding. *Clin Gastroenterol Hepatol* 2012; **10**: 131-137 [PMID: 22056302 DOI: 10.1016/j.cgh.2011.10.029]
 - 43 **Chait MM**. Lower gastrointestinal bleeding in the elderly. *World J Gastrointest Endosc* 2010; **2**: 147-154 [PMID: 21160742 DOI: 10.4253/wjge.v2.i5.147]
 - 44 **Elder K**, Lashner BA, Al Solaiman F. Clinical approach to colonic ischemia. *Cleve Clin J Med* 2009; **76**: 401-409 [PMID: 19570972 DOI: 10.3949/ccjm.76a.08089]
 - 45 **Barnert J**, Messmann H. Diagnosis and management of lower gastrointestinal bleeding. *Nat Rev Gastroenterol Hepatol* 2009; **6**: 637-646 [PMID: 19881516 DOI: 10.1038/nrgastro.2009.167]
 - 46 **Bounds BC**, Kelsey PB. Lower gastrointestinal bleeding. *Gastrointest Endosc Clin N Am* 2007; **17**: 273-288, vi. [PMID: 17556148 DOI: 10.1016/j.giec.2007.03.010]
 - 47 **Kwan V**, Bourke MJ, Williams SJ, Gillespie PE, Murray MA, Kaffes AJ, Henriquez MS, Chan RO. Argon plasma coagulation in the management of symptomatic gastrointestinal vascular lesions: experience in 100 consecutive patients with long-term follow-up. *Am J Gastroenterol* 2006; **101**: 58-63 [DOI: 10.1111/j.1572-0241.2006.00370.x]
 - 48 **Lee TY**, Yeh HZ, Yang SS, Chang CS. Successful application of haemoclips plus argon plasma coagulation for angioectasia bleeding with underlying arteriovenous malformation in the colon. *Colorectal Dis* 2010; **12**: e180-1 [DOI: 10.1111/j.1463-1318.2009.02059.x]
 - 49 **Longstreth GF**. Epidemiology and outcome of patients hospitalized with acute lower gastrointestinal hemorrhage: a population-based study. *Am J Gastroenterol* 1997; **92**: 419-424 [PMID: 9068461]
 - 50 **Walker TG**, Salazar GM, Waltman AC. Angiographic evaluation and management of acute gastrointestinal hemorrhage. *World J Gastroenterol* 2012; **18**: 1191-1201 [PMID: 22468082 DOI: 10.3748/wjg.v18.i11.1191]
 - 51 **Gauderer MW**, Ponsky JL, Izant RJ, Jr. Gastrostomy without laparotomy: a percutaneous endoscopic technique. *J Pediatr Surg* 1980; **15**: 872-875 [DOI: 10.1016/S0022-3468(80)80296-X]
 - 52 **de Baere T**, Chapot R, Kuoch V, Chevallier P, Delille JP, Domenge C, Schwaab G, Roche A. Percutaneous gastrostomy with fluoroscopic guidance: single-center experience in 500 consecutive cancer patients. *Radiology* 1999; **210**: 651-654 [DOI: 10.1148/radiology.210.3.r99mr40651]
 - 53 **Ozmen MN**, Akhan O. Percutaneous radiologic gastrostomy. *Eur J Radiol* 2002; **43**: 186-195 [PMID: 12204401 DOI: 10.1016/S0720-048X(02)00155-9]
 - 54 **Grant JP**. Comparison of percutaneous endoscopic gastrostomy with Stamm gastrostomy. *Ann Surg* 1988; **207**: 598-603 [PMID: 3377569 DOI: 10.1097/0000658-198805000-00014]
 - 55 **Wollman B**, D'Agostino HB, Walus-Wigle JR, Easter DW, Beale A. Radiologic, endoscopic, and surgical gastrostomy: an institutional evaluation and meta-analysis of the literature. *Radiology* 1995; **197**: 699-704 [PMID: 7480742 DOI: 10.1148/radiology.197.3.7480742]
 - 56 **Lyon SM**, Pascoe DM. Percutaneous gastrostomy and gastrojejunostomy. *Semin Intervent Radiol* 2004; **21**: 181-189 [PMID: 21331127 DOI: 10.1055/s-2004-860876]
 - 57 **Kynci JA**, Chodash HB, Tsang TK. PEG in a patient with ascites and varices. *Gastrointest Endosc* 1995; **42**: 100-101 [PMID: 7557165 DOI: 10.1016/S0016-5107(95)70259-8]
 - 58 **Itkin M**, DeLegge MH, Fang JC, McClave SA, Kundu S, d'Othee BJ, Martinez-Salazar GM, Sacks D, Swan TL, Towbin RB, Walker TG, Wojak JC, Zuckerman DA, Cardella JF, Society of Interventional R, American Gastroenterological Association I, Canadian Interventional Radiological A, Cardiovascular, Interventional Radiological Society of E. Multidisciplinary practical guidelines for gastrointestinal access for enteral nutrition and decompression from the Society of Interventional Radiology and American Gastroenterological Association (AGA) Institute, with endorsement by Canadian Interventional Radiological Association (CIRA) and Cardiovascular and Interventional Radiological Society of Europe (CIRSE). *Gastroenterology* 2011; **141**: 742-765 [DOI: 10.1053/j.gastro.2011.06.001]
 - 59 **Sacks BA**, Vine HS, Palestrant AM, Ellison HP, Shropshire D, Lowe R. A nonoperative technique for establishment of a gastrostomy in the dog. *Invest Radiol* 1983; **18**: 485-487 [PMID: 6642944 DOI: 10.1097/00004424-198309000-00015]
 - 60 **Russell TR**, Brotman M, Norris F. Percutaneous gastrostomy. A new simplified and cost-effective technique. *Am J Surg* 1984; **148**: 132-137 [PMID: 6430111 DOI: 10.1016/0002-9610(84)90300]
 - 61 **Choudhry U**, Barde CJ, Markert R, Gopalswamy N. Percutaneous endoscopic gastrostomy: a randomized prospective comparison of early and delayed feeding. *Gastrointest Endosc* 1996; **44**: 164-167 [DOI: 10.1016/S0016-5107(96)70134-7]
 - 62 **Terry NE**, Boswell WC, Carney DE, Beck A, Lowe L, Rittmeyer C. Percutaneous endoscopic gastrostomy with T-bar fixation in children and infants. *Surg Endosc* 2008; **22**: 167-170 [PMID: 17522924 DOI: 10.1007/s00464-007-9402-x]
 - 63 **Dormann AJ**, Wejda B, Kahl S, Huchzermeyer H, Ebert MP, Malfertheiner P. Long-term results with a new introducer method with gastroscopy for percutaneous endoscopic gastrostomy. *Am J Gastroenterol* 2006; **101**: 1229-1234 [PMID: 16771943 DOI: 10.1111/j.1572-0241.2006.00541.x]
 - 64 **Gebel MLP**, Muller MJ. New technique: US-guided percutaneous gastrostomy. *J Ultrasound Med* 1991; **10**: 1
 - 65 **Bleck JS**, Reiss B, Gebel M, Wagner S, Strassburg CP, Meier PN, Boozari B, Schneider A, Caselitz M, Westhoff-Bleck M, Manns M. Percutaneous sonographic gastrostomy: method, indications, and problems. *Am J Gastroenterol* 1998; **93**: 941-945 [DOI: 10.1111/j.1572-0241.1998.00283.x]
 - 66 **Galaski A**, Peng WW, Ellis M, Darling P, Common A, Tucker E. Gastrostomy tube placement by radiological versus endoscopic methods in an acute care setting: a retrospective review of frequency, indications, complications and outcomes. *Can J Gastroenterol* 2009; **23**: 109-114 [PMID: 19214286 DOI: 10.1155/2009/801925]
 - 67 **Wolfsen HC**, Kozarek RA, Ball TJ, Patterson DJ, Botoman VA, Ryan JA. Value of diagnostic upper endoscopy preceding percutaneous gastrostomy. *Am J Gastroenterol* 1990; **85**: 249-251 [PMID: 1689950]
 - 68 **Thornton FJ**, Varghese JC, Haslam PJ, McGrath FP, Keeling F, Lee MJ. Percutaneous gastrostomy in patients who fail or are unsuitable

- for endoscopic gastrostomy. *Cardiovasc Intervent Radiol* 2000; **23**: 279-284 [PMID: 10960541 DOI: 10.1007/s002700010069]
- 69 **Lynch CR**, Jones RG, Hilden K, Wills JC, Fang JC. Percutaneous endoscopic cecostomy in adults: a case series. *Gastrointest Endosc* 2006; **64**: 279-282 [PMID: 16860089 DOI: 10.1016/j.gie.2006.02.037]
- 70 **Chait PG**, Shandling B, Richards HM, Connolly BL. Fecal incontinence in children: treatment with percutaneous cecostomy tube placement--a prospective study. *Radiology* 1997; **203**: 621-624 [DOI: 10.1148/radiology.203.3.9169678]
- 71 **Chevallier P**, Marcy PY, Francois E, Peten EP, Motamedi JP, Padovani B, Bruneton JN. Controlled transperitoneal percutaneous cecostomy as a therapeutic alternative to the endoscopic decompression for Ogilvie's syndrome. *Am J Gastroenterol* 2002; **97**: 471-474 [DOI: 10.1111/j.1572-0241.2002.05457.x]
- 72 **Marker DR**, Perosi N, Ul Haq F, Morefield W, Mitchell S. Percutaneous Cecostomy in Adult Patients: Safety and Quality-of-Life Results. *J Vasc Interv Radiol* 2015; **26**: 1526-1532 e1 [PMID: 26208742 DOI: 10.1016/j.jvir.2015.06.014]
- 73 **Khan WU**, Satkunasingham J, Moineddin R, Jamal I, Afzal S, Chait P, Parra D, Amaral JG, Temple MJ, Connolly BL. The percutaneous cecostomy tube in the management of fecal incontinence in children. *J Vasc Interv Radiol* 2015; **26**: 189-195 [DOI: 10.1016/j.jvir.2014.10.015]
- 74 **Ponsky JL**, Aszodi A, Perse D. Percutaneous endoscopic cecostomy: a new approach to nonobstructive colonic dilation. *Gastrointest Endosc* 1986; **32**: 108-111 [DOI: 10.1016/S0016-5107(86)71907-X]
- 75 **Holm AN**, Baron TH. Palliative use of percutaneous endoscopic gastrostomy and percutaneous endoscopic cecostomy tubes. *Gastrointest Endosc Clin N Am* 2007; **17**: 795-803 [DOI: 10.1016/j.giec.2007.07.002]
- 76 **Bertolini D**, De Saussure P, Chilcott M, Girardin M, Dumonceau JM. Severe delayed complication after percutaneous endoscopic colostomy for chronic intestinal pseudo-obstruction: a case report and review of the literature. *World J Gastroenterol* 2007; **13**: 2255-2257 [PMID: 17465514 DOI: 10.3748/wjg.v13.i15.2255]
- 77 **Rao AS**, Loftus CG, Baron TH. Buried bumper syndrome arising from a percutaneous endoscopic cecostomy tube. *Gastrointest Endosc* 2011; **73**: 168-169 [DOI: 10.1016/j.gie.2010.04.039]
- 78 **Uno Y**. Introducer method of percutaneous endoscopic cecostomy and antegrade continence enema by use of the Chait Trapdoor cecostomy catheter in patients with adult neurogenic bowel. *Gastrointest Endosc* 2006; **63**: 666-673 [DOI: 10.1016/j.gie.2005.12.035]
- 79 **Duchalais E**, Meurette G, Mantoo SK, Le Rhun M, Varannes SB, Lehur PA, Coron E. Percutaneous endoscopic caecostomy for severe constipation in adults: feasibility, durability, functional and quality of life results at 1 year follow-up. *Surg Endosc* 2015; **29**: 620-626 [DOI: 10.1007/s00464-014-3709-1]
- 80 **Richter JE**. Peptic strictures of the esophagus. *Gastroenterol Clin North Am* 1999; **28**: 875-891, vi [PMID: 10695007 DOI: 10.1016/S0889-8553(05)70095-9]
- 81 **Standards of Practice Committee**, Egan JV, Baron TH, Adler DG, Davila R, Faigel DO, Gan SL, Hirota WK, Leighton JA, Lichtenstein D, Qureshi WA, Rajan E, Shen B, Zuckerman MJ, VanGuilder T, Fanelli RD. Esophageal dilation. *Gastrointest Endosc* 2006; **63**: 755-760 [PMID: 16650533 DOI: 10.1016/j.gie.2006.02.031]
- 82 **Hernandez LV**, Jacobson JW, Harris MS. Comparison among the perforation rates of Maloney, balloon, and Savary dilation of esophageal strictures. *Gastrointest Endosc* 2000; **51**: 460-462 [DOI: 10.1016/S0016-5107(00)70448-2]
- 83 **ASGE Standards of Practice Committee**, Pasha SF, Acosta RD, Chandrasekhara V, Chathadi KV, Decker GA, Early DS, Evans JA, Fanelli RD, Fisher DA, Foley KQ, Fonkalsrud L, Hwang JH, Jue TL, Khashab MA, Lightdale JR, Muthusamy VR, Sharaf R, Saltzman JR, Shergill AK, Cash B. The role of endoscopy in the evaluation and management of dysphagia. *Gastrointest Endosc* 2014; **79**: 191-201 [PMID: 24332405 DOI: 10.1016/j.gie.2013.07.042]
- 84 **Tietjen TG**, Pasricha PJ, Kalloo AN. Management of malignant esophageal stricture with esophageal dilation and esophageal stents. *Gastrointest Endosc Clin N Am* 1994; **4**: 851-862 [PMID: 7529118]
- 85 **Riley SA**, Attwood SE. Guidelines on the use of oesophageal dilatation in clinical practice. *Gut* 2004; **53** Suppl 1: i1-i6 [PMID: 14724139 DOI: 10.1136/gut.53.suppl_1.i1]
- 86 **Committee AT**, Siddiqui UD, Banerjee S, Barth B, Chauhan SS, Gottlieb KT, Konda V, Maple JT, Murad FM, Pfau PR, Pleskow DK, Tokar JL, Wang A, Rodriguez SA. Tools for endoscopic stricture dilation. *Gastrointest Endosc* 2013; **78**: 391-404 [DOI: 10.1016/j.gie.2013.04.170]
- 87 **Kozarek RA**, Patterson DJ, Ball TJ, Gelfand MG, Jiranek GE, Bredfeldt JE, Brandabur JJ, Wolfson HW, Raltz SL. Esophageal dilation can be done safely using selective fluoroscopy and single dilating sessions. *J Clin Gastroenterol* 1995; **20**: 184-188 [PMID: 7797822 DOI: 10.1097/00004836-199504000-00003]
- 88 **Scolapio JS**, Pasha TM, Gostout CJ, Mahoney DW, Zinsmeister AR, Ott BJ, Lindor KD. A randomized prospective study comparing rigid to balloon dilators for benign esophageal strictures and rings. *Gastrointest Endosc* 1999; **50**: 13-17 [DOI: 10.1016/S0016-5107(99)70337-8]
- 89 **Saeed ZA**, Winchester CB, Ferro PS, Michaletz PA, Schwartz JT, Graham DY. Prospective randomized comparison of polyvinyl bougies and through-the-scope balloons for dilation of peptic strictures of the esophagus. *Gastrointest Endosc* 1995; **41**: 189-195 [DOI: 10.1016/S0016-5107(95)70336-5]
- 90 **Marjanovic G**, Schrag HJ, Fischer E, Hopt UT, Fischer A. Endoscopic bougienage of benign anastomotic strictures in patients after esophageal resection: the effect of the extent of stricture on bougienage results. *Dis Esophagus* 2008; **21**: 551-557 [DOI: 10.1111/j.1442-2050.2008.00819.x]
- 91 **Ikeya T**, Ohwada S, Ogawa T, Tanahashi Y, Takeyoshi I, Koyama T, Morishita Y. Endoscopic balloon dilation for benign esophageal anastomotic stricture: factors influencing its effectiveness. *Hepatogastroenterology* 1999; **46**: 959-966 [PMID: 10370646]
- 92 **Sabharwal T**, Adam A. Balloon dilatation of esophageal strictures/achalasia. *Semin Intervent Radiol* 2004; **21**: 149-155 [PMID: 21331124 DOI: 10.1055/s-2004-860873]
- 93 **Thyoka M**, Barnacle A, Chippington S, Eaton S, Drake DP, Cross KM, De Coppi P, Kiely EM, Pierro A, Curry JJ, Roebuck DJ. Fluoroscopic balloon dilation of esophageal atresia anastomotic strictures in children and young adults: single-center study of 103 consecutive patients from 1999 to 2011. *Radiology* 2014; **271**: 596-601 [DOI: 10.1148/radiol.13122184]
- 94 **Repici A**, Hassan C, Sharma P, Conio M, Siersema P. Systematic review: the role of self-expanding plastic stents for benign oesophageal strictures. *Aliment Pharmacol Ther* 2010; **31**: 1268-1275 [DOI: 10.1111/j.1365-2036.2010.04301.x]
- 95 **Song HY**, Jung HY, Park SI, Kim SB, Lee DH, Kang SG, Il Min Y. Covered retrievable expandable nitinol stents in patients with benign esophageal strictures: initial experience. *Radiology* 2000; **217**: 551-557 [DOI: 10.1148/radiology.217.2.r00nv03551]
- 96 **Saito Y**, Tanaka T, Andoh A, Minematsu H, Hata K, Tsujikawa T, Nitta N, Murata K, Fujiyama Y. Usefulness of biodegradable stents constructed of poly-L-lactic acid monofilaments in patients with benign esophageal stenosis. *World J Gastroenterol* 2007; **13**: 3977-3980 [PMID: 17663513 DOI: 10.3748/wjg.v13.i29.3977]
- 97 **Hirdes MM**, Siersema PD, van Boeckel PG, Vleggaar FP. Single and sequential biodegradable stent placement for refractory benign esophageal strictures: a prospective follow-up study. *Endoscopy* 2012; **44**: 649-654 [DOI: 10.1055/s-0032-1309818]
- 98 **Cosnes J**, Gower-Rousseau C, Seksik P, Cortot A. Epidemiology and natural history of inflammatory bowel diseases. *Gastroenterology* 2011; **140**: 1785-1794 [PMID: 21530745 DOI: 10.1053/j.gastro.2011.01.055]
- 99 **Peyrin-Biroulet L**, Harmsen WS, Tremaine WJ, Zinsmeister AR, Sandborn WJ, Loftus EV, Jr. Surgery in a population-based cohort of Crohn's disease from Olmsted County, Minnesota (1970-2004). *Am J Gastroenterol* 2012; **107**: 1693-1701 [DOI: 10.1038/ajg.2012.298]

- 100 **Lichtenstein GR**, Olson A, Travers S, Diamond RH, Chen DM, Pritchard ML, Feagan BG, Cohen RD, Salzberg BA, Hanauer SB, Sandborn WJ. Factors associated with the development of intestinal strictures or obstructions in patients with Crohn's disease. *Am J Gastroenterol* 2006; **101**: 1030-1038 [PMID: 16606351 DOI: 10.1111/j.1572-0241.2006.00463.x]
- 101 **Vrabie R**, Irwin GL, Friedel D. Endoscopic management of inflammatory bowel disease strictures. *World J Gastrointest Endosc* 2012; **4**: 500-505 [PMID: 23189221 DOI: 10.4253/wjge.v4.i11.500]
- 102 **Dietz DW**, Laureti S, Strong SA, Hull TL, Church J, Remzi FH, Lavery IC, Fazio VW. Safety and longterm efficacy of strictureplasty in 314 patients with obstructing small bowel Crohn's disease. *J Am Coll Surg* 2001; **192**: 330-337; discussion 337-338 [DOI: 10.1016/S1072-7515(01)00775-X]
- 103 **Paine E**, Shen B. Endoscopic therapy in inflammatory bowel diseases (with videos). *Gastrointest Endosc* 2013; **78**: 819-835 [PMID: 24139079 DOI: 10.1016/j.gie.2013.08.023]
- 104 **Hassan C**, Zullo A, De Francesco V, Ierardi E, Giustini M, Pitidis A, Taggi F, Winn S, Morini S. Systematic review: Endoscopic dilatation in Crohn's disease. *Aliment Pharmacol Ther* 2007; **26**: 1457-1464 [DOI: 10.1111/j.1365-2036.2007.03532.x]
- 105 **Mueller T**, Rieder B, Bechtner G, Pfeiffer A. The response of Crohn's strictures to endoscopic balloon dilation. *Aliment Pharmacol Ther* 2010; **31**: 634-639 [PMID: 20047581 DOI: 10.1111/j.1365-2036.2009.04225.x]
- 106 **Di Nardo G**, Oliva S, Passariello M, Pallotta N, Civitelli F, Frediani S, Gualdi G, Gandullia P, Mallardo S, Cucchiara S. Intralesional steroid injection after endoscopic balloon dilation in pediatric Crohn's disease with stricture: a prospective, randomized, double-blind, controlled trial. *Gastrointest Endosc* 2010; **72**: 1201-1208 [DOI: 10.1016/j.gie.2010.08.003]
- 107 **East JE**, Brooker JC, Rutter MD, Saunders BP. A pilot study of intrastricture steroid versus placebo injection after balloon dilatation of Crohn's strictures. *Clin Gastroenterol Hepatol* 2007; **5**: 1065-1069 [DOI: 10.1016/j.cgh.2007.04.013]
- 108 **Attar A**, Maunoury V, Vahedi K, Vernier-Massouille G, Vida S, Bulois P, Colombel JF, Bouhnik Y, Getaïd. Safety and efficacy of extractible self-expandable metal stents in the treatment of Crohn's disease intestinal strictures: a prospective pilot study. *Inflamm Bowel Dis* 2012; **18**: 1849-1854 [DOI: 10.1002/ibd.22844]
- 109 **Rejchrt S**, Kopacova M, Brozik J, Bures J. Biodegradable stents for the treatment of benign stenoses of the small and large intestines. *Endoscopy* 2011; **43**: 911-917 [DOI: 10.1055/s-0030-1256405]
- 110 **Loras C**, Perez-Roldan F, Gornals JB, Barrio J, Igea F, Gonzalez-Huix F, Gonzalez-Carro P, Perez-Miranda M, Espinos JC, Fernandez-Banares F, Esteve M. Endoscopic treatment with self-expanding metal stents for Crohn's disease strictures. *Aliment Pharmacol Ther* 2012; **36**: 833-839 [DOI: 10.1111/apt.12039]
- 111 **de Gregorio MA**, Mainar A, Rodriguez J, Alfonso ER, Tejero E, Herrera M, Medrano J, D'Agostino H. Colon stenting: a review. *Semin Intervent Radiol* 2004; **21**: 205-216 [PMID: 21331130 DOI: 10.1055/s-2004-860941]
- 112 **Paul L**, Pinto I, Gomez H, Fernandez-Lobato R, Moyano E. Metallic stents in the treatment of benign diseases of the colon: preliminary experience in 10 cases. *Radiology* 2002; **223**: 715-722 [DOI: 10.1148/radiol.2233010866]

P-Reviewer: Andersen PE, Francica G, Lassandro F
S-Editor: Kong JX **L-Editor:** A **E-Editor:** Li D



Three-dimensional radiation dosimetry using polymer gel and solid radiochromic polymer: From basics to clinical applications

Yoichi Watanabe, Leighton Warmington, N Gopishankar

Yoichi Watanabe, Leighton Warmington, Department of Radiation Oncology, University of Minnesota, Minneapolis, MN 55455, United States

N Gopishankar, All India Institutes of Medical Sciences, Delhi 110029, India

Author contributions: Watanabe Y wrote the article; Warmington L provided the data and reviewed the manuscript; Gopishankar N reviewed the manuscript and made suggestions for improvement.

Conflict-of-interest statement: Authors declare no conflict of interests for this article.

Open-Access: This article is an open-access article which was selected by an in-house editor and fully peer-reviewed by external reviewers. It is distributed in accordance with the Creative Commons Attribution Non Commercial (CC BY-NC 4.0) license, which permits others to distribute, remix, adapt, build upon this work non-commercially, and license their derivative works on different terms, provided the original work is properly cited and the use is non-commercial. See: <http://creativecommons.org/licenses/by-nc/4.0/>

Manuscript source: Invited manuscript

Correspondence to: Yoichi Watanabe, PhD, Department of Radiation Oncology, University of Minnesota, 420 Delaware St. SE, MMC494, Minneapolis, MN 55455, United States. watan016@umn.edu
Telephone: +1-612-6266708
Fax: +1-612-6267060

Received: October 10, 2016

Peer-review started: October 13, 2016

First decision: November 30, 2016

Revised: December 31, 2016

Accepted: January 16, 2017

Article in press: January 18, 2017

Published online: March 28, 2017

Abstract

Accurate dose measurement tools are needed to evaluate the radiation dose delivered to patients by using modern and sophisticated radiation therapy techniques. However, the adequate tools which enable us to directly measure the dose distributions in three-dimensional (3D) space are not commonly available. One such 3D dose measurement device is the polymer-based dosimeter, which changes the material property in response to radiation. These are available in the gel form as polymer gel dosimeter (PGD) and ferrous gel dosimeter (FGD) and in the solid form as solid plastic dosimeter (SPD). Those are made of a continuous uniform medium which polymerizes upon irradiation. Hence, the intrinsic spatial resolution of those dosimeters is very high, and it is only limited by the method by which one converts the dose information recorded by the medium to the absorbed dose. The current standard methods of the dose quantification are magnetic resonance imaging, optical computed tomography, and X-ray computed tomography. In particular, magnetic resonance imaging is well established as a method for obtaining clinically relevant dosimetric data by PGD and FGD. Despite the likely possibility of doing 3D dosimetry by PGD, FGD or SPD, the tools are still lacking wider usages for clinical applications. In this review article, we summarize the current status of PGD, FGD, and SPD and discuss the issue faced by these for wider acceptance in radiation oncology clinic and propose some directions for future development.

Key words: Optical computed tomography; Three-dimensional dose measurement; Solid radiochromic polymer; Magnetic resonance imaging; Polymer gel

© **The Author(s) 2017.** Published by Baishideng Publishing Group Inc. All rights reserved.

Core tip: Polymer gel and solid radiochromic polymer dosimeters are promising tools for measuring the radiation dose distributions in three-dimensional space. The techniques have been studied for last 20 years, but are not used for routine clinical applications to improve the radiation delivery quality. In this review, we summarize the current status and discuss the necessary development to make these tools more accessible for wider usages.

Watanabe Y, Warmington L, Gopishankar N. Three-dimensional radiation dosimetry using polymer gel and solid radiochromic polymer: From basics to clinical applications. *World J Radiol* 2017; 9(3): 112-125 Available from: URL: <http://www.wjgnet.com/1949-8470/full/v9/i3/112.htm> DOI: <http://dx.doi.org/10.4329/wjor.v9.i3.112>

INTRODUCTION

The accurate quantification of radiation dose absorbed by the medium is the fundamental requirement in radiation physics. Particularly, when the radiation is used for medical purpose, the high accuracy of dose determination delivered to a patient is mandatory. In radiation therapy, the amount of the radiation dose absorbed by the tissue strongly correlates to the killing probability of both cancer cells and healthy cells^[1]. Hence, the radiation must be delivered precisely to the planned location. The absolute dose can be very accurately measured by ion-chambers^[2]; hence, it serves as a starting point for evaluating the overall accuracy of dose delivery methods. With the introduction of sophisticated technologies, for example, the intensity modulated radiation therapy (IMRT), the volumetrically modulated arc therapy (VMAT), and the stereotactic ablative radiation therapy, we can deliver the radiation dose distributed in an ideal three-dimensional (3D) shape with the maximum dose delivered to the cancer cells and the minimum dose to the healthy cells^[3]. Many factors make the delivered dose very different from the ideal dose distributions. Therefore, the validation of the dose delivered to the patient in comparison to the planned dose is the most important task which one needs to perform before the actual application of the new technologies to patients.

A modern treatment planning requires sophisticated software, which can reproduce the actual radiation delivery and compute the radiation dose to the patient. The treatment planning system (TPS) uses the 3D model of the beam for the dose calculations. The beam data necessary for this process must be supplied by the users, who collect the data by using a 3D water scanning system consisting of a water phantom and an appropriate dosimeter. Hence, the main application of 3D dosimeters is the validation of the dose delivery technique through the comparison of the 3D dose distributions calculated by the TPS with the actual dose delivered to the patient or in a phantom that mimics the patient as a surrogate of the

patient.

There are many measurement tools available for characterizing the dose distribution in multi-dimensional space. One can move a point detector, such as an ionization chamber and a silicon diode in a 3D space to cover a volume of interest. An extension of this line of thought is to place many point detectors such as ionization chambers, silicon diodes, thermoluminescent detectors (TLD), in a line, or in the one dimension, and on a flat plane or curved surface in the two dimensions (2D). One of the limitations of this approach is the achievable spatial resolution. Note that the moving point detector method may be able to remedy this problem to some extent with longer measurement time.

The spatial resolution problem can be solved by using a real multi-dimensional detector such as radiographic and radiochromic films. The films can record the dose on a microscopic scale, but it requires specialized equipment to decipher the recorded dose information. The concept of these 2D dose measurement tools can be easily extended into the 3D space. Some materials change its material characteristics when they are irradiated. Hence, if we can build an appropriate instrument to convert the changes to the absorbed dose, we can measure the dose in 3D.

The Fricke ferrous sulfate dosimeter, a type of chemical dosimeters, was developed in early 20th century and was capable of recording the dose in a 3D space^[4]. Besides the lack of adequate dose quantification method, the dosimeter suffered a major drawback because the recorded dose distribution quickly fades out due to the diffusion of the ferrous ions. The problem was finally solved by the invention of a non-ferrous solution such as the acrylamide-based polymer gel in the mid-1990s. The first of such material was the BANANA gel manufactured and sold by the MGS Research (now 3D Dosimetry Inc., Madison, CT, United States). Later the dosimeter went through a few cycles of improvement, and it is now available commercially as BANG from the same company. A major drawback of the first polymer gel dosimeter (PGD) was its high sensitivity to the oxygen contamination, which necessitated a hypoxic environment for the manufacturing, for example, in a glove box, and often lead to an incorrect radiation response in the area where the oxygen interacted with the gel. A solution to this problem was the introduction of polymer gels with much-reduced sensitivity to oxygen. The first of these was called MAGIC (Methacrylic and Ascorbic acid in Gelatin Initiated by Copper)^[5]. Subsequently, many other groups developed variations of MAGIC. In the same time period, a 3D dosimeter in the solid form, the solid plastic dosimeter (SPD), was commercialized as PRESAGE (Heuris Inc., Skillman, NJ, United States)^[6]. For the last 20 years, there have been very active research and development in the field of 3D dosimetry. In this review article, we summarize the current status of the 3D dosimeters and discuss the issue faced by these for wider acceptance in radiation oncology clinic and propose some directions for future development.

Table 1 Summary of polymer gel dosimeter

Dosimeter name	Type	Base	Monomer	Crosslinker	Catalyzer/ stabilizer	Scavenger/ antioxidant	Key investigator	Country	Ref.
BANANA	PAG	Agarose	Acrylamide	BIS		Nitrous oxide	Maryanski	United States	[58]
BANG	PAG	Gelatin	Acrylamide	BIS		Ammonium- persulphate, TEMED	Maryanski	United States	[59,60]
BANG-2	PAG	Gelatin	MAA	BIS	Sodium Hydroxide	AA	Maryanski	United States	[42]
BANG-3	MAG	Gelatin	MAA		CuSO ₄ ·5H ₂ O	AA	Maryanski	United States	[61]
MAGIC	MAG	Gelatin	MAA		CuSO ₄ ·5H ₂ O, Hydroquinone	AA	Gore	United States	[5]
MAGAT	MAG	Gelatin	MAA			THPC	Baldock	Australia	[62]
nPAG	PAG	Gelatin	Acrylamide	BIS		THPS	De Deene	Belgium	[63]
nMAG	MAG	Gelatin	MAA			THPS	De Deene	Belgium	[63]
nMAG	MAG	Gelatin	MAA			THP	Ceberg	Sweden	[64]
MAGIC-f	MAG	Gelatin	MAA	Formaldehyde	CuSO ₄ ·5H ₂ O	AA	Baffa	Brazil	[65]
HEA		Gelatin	HEA	BIS			Baldock	Australia	[66]
VIPAR		Gelatin	VIPAR	BIS			Pappas	Greece	[67]
NIPAM		Gelatin	NIPAM	BIS		THPC	Schreiner	Canada	[68]
Genipin gel	MAG	Gelatin	MAA, genipin			Sulfuric acid	Jordan	Canada	[69]
LCV micelle radiochromic gel		Gelatin	LCV, surfactant- Triton, TCAA	Formaldehyde			Jordan	Canada	[70]
PAG	PAG	Gelatin	Acrylamide	BIS	NaI	THPC	Elleume	France	[71]
nMAG	nMAG	Agarose, Gelatin	MAA			THPC	Yoshioka	Japan	[72]
nMAG	nMAG	Gelatin	HEMA, TGMEMA, 9G			THPC	Hiroki	Japan	[73]
Radiochromic gel	RGD	Gelatin	SDS, Chloroform, TCAA		LMG dye		De Deene	Australia	[10]

BIS: N,N'-methylene-bis-acrylamide; MAA: Methacrylic acid; AA: Ascorbic acid; THPC: Tetrakis (hydroxymethyl) phosphonium chloride; THPS: Tetrakis (hydroxymethyl) phosphonium sulfate; NIPAM: N-isopropylacrylamide; LCV: Leuco crystal violet; TCAA: TriChloro Acetic Acid (CCl₃COOH); VIPAR: N-vinylpyrrolidone argon; HEA: 2-hydroxyethylacrylate; HEMA: 2-hydroxyethyl methacrylate; TGMEMA: Triethylene glycol monoethyl ether monomethacrylate; 9G: Polyethylene glycol 400 dimethacrylate; SDS: Sodium dodecyl sulfate.

3D DOSIMETER

Here we define 3D dosimeter as a dose measurement device, which can record the 3D dose distribution in a continuous medium. Consequently, the spatial resolution of this dosimeter is mostly determined by the read-out technique used with this dosimeter. In contrast, a dosimeter which is made of many point-like detectors at discrete points and a non-negligible distance among those can be called as pseudo 3D dosimeter. In this review, we will minimize the discussion on the pseudo 3D dosimeter. The following 3D dosimeters are currently available commercially or in research laboratories: The PGD; the Fricke gel dosimeter (FGD); the SPD.

Furthermore, we cannot ignore two other 3D dosimeters, scintillators, and Cherenkov-radiation detectors. The former is a rather old technology, but it has not gained much attention as a 3D dosimetry tool mostly because the material has mass density and effective atomic number very different from those of the water^[7]. The Cherenkov detector has been studied by one group for last few years and has a potential to be an excellent 3D dosimeter^[8], but it needs further extensive studies by many different investigators before clinical applications. Therefore, we focus on PGD, FGD and SPD in the rest of this article.

PGD

PGD is composed of five chemical components: water, gelatin, monomer, catalyzer, and oxygen scavenger^[9]. Note that the oxygen scavenger is added to make PGD more resistant to oxygen contamination. Such a PGD is called normoxic PGD or nPGD. Usually, we can group PGD/nPGD into two groups. Those with methacrylic as a monomer are called MAGAT/nMAG and those with acrylamide are called PAGAT/nPAG. There are many variations of those depending on the chemical agents. We summarized the MAGAT/nMAG and PAGAT/nPAG in Table 1. Notably, Vandecasteele *et al.*^[10] recently developed the radiochromic gel dosimeter (RGD), which is composed of 92% weight of water, gelatin, sodium dodecyl sulfate, trichloroacetic acid (CCl₃COOH) and leuco-malachite green (LMG). The RGD was mainly developed to be used with an optical computed tomography (OCT) scanner as a read-out method^[10]. The list is certainly incomplete, but can show a significant contribution from many investigators in many countries and demonstrate the international nature of this field. The photo in Figure 1 shows the PAGAT dosimeter. The white cloud in the center of the clear PAGAT gel contained in a cylindrical plastic container indicates the high radiation dose volume generated by a 6MV photon beam.

Table 2 Summary of ferrous gel dosimeter

Dosimeter	Type	Base	Monomer	Key investigator	Country	Ref.
Fricke	Fluid	None	Ammonium ferrous sulfate	Gore	United States	[11]
FeMRI	FGD	Agarose	Seaplaque, seagel	Olsson	Sweden	[74]
PVA-FX	FGD	Hydrogel	PVA, FBX	Chu	Canada	[75]
FAX	FGD	Agarose	XO, ferrous	Leong	Malaysia	[76]
FX	FGD	Gelatin	Ferrous ammonium sulfate, XO, sulfuric acid	Jordan	Canada	[70]
PVA cryogel	FGD	Hydrogel	FBX, PVA, dimethyl sulfoxide	Eyadeh	Canada	[77]
XO-PVA	FGD	Hydrogel	PVA, XO, ferrous sulfate, sulfuric acid	Trapp	Australia	[78]
NC-FG	FGD	Gelatin	Nano-clay, ammonium iron (II) sulfate, Perchloric acid	Maeyama	Japan	[41]

PVA: Polyvinyl alcohol; XO: Xylenol orange; FBX: Ferrous benzoic xylenol orange (= ferrous ammonium sulfate, XO, H₂SO₄); FGD: Ferrous gel dosimeter; MRI: Magnetic resonance imaging; NC-FG: Nano-composite Fricke gel.

**Figure 1** The photo of PAGAT polymer gel dosimeter.**Figure 2** The photo of solid plastic dosimeter.

FGD

Fricke ferrous sulfate dosimeter is a type of chemical dosimeter. The radiation induces a chemical change as Fe²⁺ ions convert to Fe³⁺ ions^[11]. The concentration of the ferric ions can be measured by absorption photo-spectrometry. Since the ferric ion concentration strongly affects its magnetic property, magnetic resonance imaging (MRI) is an ideal tool to determine the ferric ion distribution. Later, to prevent the diffusive motion of the ferric ions, which blurs the dose distribution, hydrogels were introduced as the background material^[12,13]. Babic *et al.*^[13] used radiochromic ferrous xylenol orange with the Fricke gel so that it changes the color upon irradiation, allowing the utilization of an optical technique for 3D dose quantification. FGD is summarized in Table 2.

SPD

The SPD, often called a solid radiochromic dosimeter, is a new type of 3D dosimeters. Some plastic material such as polydiacetylene polymerizes when it interacts with photons. The characteristic of the photopolymerization can be amplified by adding coloring dye to produce a radiation responding medium. Radiochromic or gafchromic films were developed from this material. Those are commercially available as EBT series products (Ashland Inc., Covington, KY, United States). The same chemical principle can be realized in a 3D material. Adamovics *et al.*^[6] produced the first 3D radiochromic dosimeter based on polyurethane with LMG. The radiation sensitivity

was enhanced by adding chemical catalyzer such as chloroform^[6]. This dosimeter is available commercially as PRESAGE and may contain proprietary ingredients. As shown in Table 3, there are only a few investigators who currently produce SPD in-house. Fortunately, the production of SPD is rather straightforward since there is a commercial product which was developed for artwork. A mixture of Clear Poly A and B (Smooth-On Inc., Easton, PA) can cast in any shape. By adding LMG, this material can be quickly turned into SPD^[14]. Figure 2 shows the SPD manufactured in-house. The green bar vertically running in the middle of the cylindrical phantom indicates the beam path of 18 MV photons with 1 cm × 1 cm field size.

Water equivalency

One of the requirements for a dosimeter is its ability to measure the dose absorbed by water in water^[4]. The detectors, therefore, must be placed in a water equivalent medium, which includes the actual water, such as the 3D water scanning system, and a solid phantom that is equivalent to water such as the white water and solid water^[15]. The equivalency, however, needs a special consideration when the atomic composition of the material is different from that of water. The actual equivalency of radiological characteristics means that the photon and electron scattering cross sections are the same as those of water for all energy of photons and electrons. This definition of water equivalency also applies to heavier charged particles such as protons and heavy ions. It is

Table 3 Summary of solid plastic dosimeter

Dosimeter	Type	A	B	Initiator	Dye	Key investigator	Country	Ref.
SPD	SPD	Diacetylene	Ethyl trichloroacetate, heptachloropropane, <i>etc.</i>	Radiochromic (fuschin cyanide, <i>etc.</i>)	Leuco crystal violet, or LMG	Patel	United States	[79]
PRESAGE	SPD	Polyol_A, diacyanate	Polyol_B	Carbon tetrachloride, methylene chloride, tetra-chloroethane, Chloroform	LMG	Adamovics	United States	[6]
PRESAGE	SPD	Crystal clear A	Crystal clear B	Carbon tetrachloride	LMG	Hashemi	Iran	[80]
PRESAGE	SPD	Crystal clear A	Crystal clear B	Chloroform, bromoform, or iodoform	LMG	Geso	Australia	[81]
PRESAGE	SPD	Crystal clear A	Crystal clear B	Bromoform	LMG	Watanabe	United States	[14]

LMG: Leuco-malachite green; SPD: Solid plastic dosimeter.

Table 4 Water equivalency of three-dimensional dosimeters

Dosimeter	Type	Relative effective atomic number	Relative mass density	Relative electron density
PAGAT	PGD	1.013 ¹	1.026 ⁴	0.928 ⁴
MAGAT	PGD	1.014 ¹ , 0.984 ³	1.032 ³	0.993 ³
nMAG	PGD	1.018 ¹		
MAGIC	PGD	1.018 ¹ , 0.987 ³	1.037 ³	0.990 ³
Genipin gel	PGD	1.014 ²	1.001 ²	0.9982 ²
PRESAGE-A	SPD	1.037 ²	1.054 ²	0.977 ²
Water		1.00 (Z _{eff} = 7.42)	1.000	1.0 (3.343 × 10 ²³ Electrons/g)

The numbers in parentheses indicate the references. ¹Ref. [82] (for 18MeV photon energy); ²Ref. [83]; ³Ref. [84]; ⁴Ref. [85]. PGD: Polymer gel dosimeter; SPD: Solid plastic dosimeter.

important to remember that the radiological quantity often depends on the radiation energy.

To simplify the discussion, we focus on the photons and electrons in this section. Then, the cross sections can be replaced by the photon attenuation coefficients and electron stopping power. To quantify the radiological quantity of the materials, we can use the effective atomic number, mass density, and electron density. We use the photon energy above the energy of gamma rays produced by Cobalt-60, or 1.25 MeV, and below 20 MeV, which is the maximum photon and electron energy currently clinically in use. For this range of energy, we might assume three quantities mentioned above can be evaluated for one energy, say, at 6 MeV. In Table 4 we summarized those for some of the standard 3D dosimeters. Note that the genipin PGD has the radiological quantities the closest to those of water.

DOSE QUANTIFICATION TECHNIQUES

All 3D dosimeters under review are not absolute dosimeters in the sense of calorimeter or ionization chambers since those do not quantify either energy absorbed by a medium or the number of ion-electron pairs produced in a medium. Those rather rely on a monotonic relationship between the expected absorbed dose and the amount of the quantitative changes of the characteristic of the dosimeter material. PGD material polymerizes when the radiation interacts with the material. The polymerization occurs among the monomers which are suspended in the gelatin matrix. This process, in turn, causes a change in the

molecular structure and the mass density. Consequently, these changes lead to an alteration of the mechanical, optical, and magnetic properties. FGD relies on a mechanism different from PGD. In FGD, new ferrous ions are produced by radiation. The change in the concentration of ferrous ions is closely related to the absorbed dose. In SPD, the radiation causes copolymerization of the monomers and the change of color at the same time. It is noteworthy that we always need to obtain a calibration relationship between the dose absorbed by the 3D dosimeter and the amount of quantitative changes measured by the dose quantification tool for the dose measurement.

Here, we discuss three dose quantification techniques; MRI, OCT, and X-ray computed tomography (XCT). There are other techniques such as the ultrasound device, but those will not be considered in this review because they are not readily available in clinics or their unproven measurement accuracy. Each system has its advantages and disadvantages. In Table 5, we summarized the cons and pros of those systems. Note that since the technology keeps changing and improving, some of the disadvantages may disappear in the future.

MRI

The most common method of the dose quantification of PGD and FGD is MRI. MRI can measure the changes of the transverse (or spin-lattice) relaxation time (T₁), the lateral (or spin-spin) relaxation time (T₂), the magnetization transfer, the susceptibility, and radio-frequency spectra. Because of the solid nature, MRI cannot be used with SPD.

Table 5 Comparison of dose quantification techniques

Method	Pros	Cons
MRI	Commonly available at a hospital	Low SNR
	Easily accessible scan protocol	Image artifacts
	Known accuracy and precision	Limited spatial resolution
OCT	Linear dose response	Long scan time
	High spatial resolution	Optical artifacts
	Small physical size or compact	Needs refractive index matching
XCT	Easy and free access if owned	
	Easy access at hospital	Low image contrast
	High SNR	
	Very fast scan	

SNR: Signal-to-noise ratio; MRI: Magnetic resonance imaging; OCT: Optical computer tomography; XCT: X-ray computed tomography.

The T2 change is most noticeable in PGD; hence, it is the most important parameter. The 3D distribution of T2 or the inverse of T2, the spin-spin relaxation rate (R2), can be measured by using a multiple spin echo pulse sequence such as Car-Purcell-Meiboom-Gill^[16]. The T1 change is quantified for FGD since the ions strongly influence the spin-lattice relaxation^[17].

OCT

The change in the mass density in PGD and the color change of SPD naturally lead to an optical method for the dose quantification. By borrowing the ideas from both the optical densitometer used for radiographic and radiochromic films and the X-ray CT, the 3D distribution of the change in the optical properties can be measured by OCT. There are three types of OCT systems. The first generation OCT uses the line of laser light with a pair of a light source and a point photon detector. The entire 3D volume can be covered by moving the laser light and the sensor together both in the transverse and longitudinal directions while the sample is rotated. The standard image reconstruction algorithm can be used to obtain full 3D dose distribution data. The second generation scanner uses a mirror to sweep the light ray along the transverse direction to speed up the scanning time. For an even quicker scan, the third generation OCT uses a broad cone beam of laser light, either parallel beam or a divergent beam in the object, and a charge coupled detector camera as the sensor. Some researchers proposed a fan-beam type scanning system by generating a horizontal fan beam^[14,18]. OCT measures the attenuation of photons, and this is represented by the optical density (OD). Hence, the dose must be estimated by using an appropriate calibration relationship between OD and the dose.

XCT

XCT relies on the photon attenuation by the object. Since the radiation changes the density of PGD, the dose pattern can be visualized by using XCT. This approach might be the most attractive method for routine applications of the 3D dosimetry because of the wide-spread use of the XCT in the radiation therapy clinic. However,

the practicality of XCT as the readout tool yet needs to be proven.

Comparison of dose quantification methods

Important factors which determine the quality of the dose quantification methods are the accuracy, the precision, the spatial resolution, the speed, and the cost. The accuracy depends on the quality of the calibration data which are used to convert the measured physical parameters to dose to the dosimeter (or often to the water). Hence, a parameter more important than the accuracy is the uncertainty or the precision of the measurement. We compare these parameters of MRI, OCT and XCT, based on the published results. The scanning speed and the precision are strongly correlated for MRI, to some extent, for both OCT and XCT. For example, the repeated acquisition of MR images decreases the image noise, though the noise only decreases with the square root of the number of image acquisition, resulting in a significant increase in the scanning time or slower scanning speed. Note that among these, only OCT is not used in radiation oncology clinics as a standard imaging tool for routine clinical work and needs to be purchased specifically for the 3D dosimetry purpose.

For dosimetric applications, the precision must be high, and it should be smaller than 5%. In Table 6, we summarize the precision quoted in literature. It is, however, worth mentioning that those values are a combination of the precision stemming from the dosimeter itself and the dose quantification tool. Furthermore, many items in Table 6 are not known, and systematic studies are needed to quantify those uncertainty values.

Long scanning time is acceptable if the scanning system is used solely for the 3D dosimetry such as a dedicated OCT system. Otherwise, the system should be capable of acquiring 3D dose data in a reasonable time frame, *i.e.*, shorter than one hour and at most 2 h.

The cost of the dose data quantification is user fees for MRI and XCT. Usually, the fee is about \$500 per hour at the most institutions in the United States if any payment is needed. Note that in this review the cost is estimated at the United States dollars. The cost of OCT, if purchased, could range from \$10000 to \$50000. Hence, for repeated uses, OCT could be the most economical system unless the MRI and XCT are available for free.

ACCURACY AND PRECISION

Accuracy of absolute dose measurement

The primary purpose of 3D dose measurements is not the absolute quantification of the absorbed dose, but rather it is often a measurement of the relative 3D distribution of the dose produced by a radiation delivery technique. Hence, the capability of the absolute dose measurement is not the most important requirement for the 3D dosimeters. However, the 3D dosimeters can be used as an absolute dosimeter if the radiation response is adequately characterized.

Table 6 Precision (or uncertainty) of three-dimensional dosimetry^[22]

Uncertainty type	Source	Factor	PGD	FGD	SPD
A	Physicochemical	Chemical composition	< 2%		< 2%
		Temperature variation			
		Temporal and spatial integrity			
	Irradiation	Dose rate	< 0.4% (3 mm ³)	1 mm	2%
		Energy			
		Temperature			
		Phantom position setup			
		Image noise			
		Image noise			
	MRI	The standard deviation of CT number	2% to 8%		
	OCT				
	XCT				
B	MRI	B0 non-uniformity	< 3%		
		B1 non-uniformity			
		Gradient non-uniformity			
		Temperature during scanning			
		Non-uniform refractive index			
	Medium OCT	Refractive index matching			
		Unstable light source			
		Ambient stray light			
		Desynchronization between galvanic mirror and detector			
		Misalignment of light, subject, and detector			
	XCT	Image processing	5%		
		Calibration equation			

MRI: Magnetic resonance imaging; OCT: Optical computer tomography; XCT: X-ray computed tomography; FGD: Ferrous gel dosimeter; PGD: Polymer gel dosimeter; SPD: Solid plastic dosimeter.

The accuracy of the dose measured by a detector depends on the accuracy of the original signal recorded inside the 3D dosimeter medium and the precision of the dose-response data or the calibration equation, which is used to convert the raw signal data to the absorbed dose^[16,19]. To study this more quantitatively, let us assume the calibration equation represented by a second order polynomial, which is the most common response characteristics of the 3D dosimeters. For the raw data X recorded by the 3D dosimeter, the absolute dose D can be now expressed by

$$D = aX^2 + bX + c \quad (1)$$

It is well known that the uncertainty of D can be given as the function of the uncertainties of the raw data X , and the three coefficients, a , b and c , in Eq.(1):

$$\delta D = \{(X^2\delta a)^2 + (X\delta b)^2 + (\delta c)^2 + [(2aX + b)\delta X]^2\}^{1/2} \quad (2)$$

If the calibration equation (1) is exact, *i.e.*, $\delta a = \delta b = \delta c = 0$, Eq.(2) can be modified as

$$\delta D/D = (X/D) \times (dD/dX) (\delta X/X) = \{[(2aX + b)X]/D\} \times (\delta X/X) \quad (3)$$

Eq.(3) implies that the relative uncertainty of D is proportional to the relative uncertainty of X ; in other words, the smaller the uncertainty of X the smaller the uncertainty of the dose. In reality, however, the uncertainty of the coefficients, a , b and c , is not negligible; hence, the uncertainty of D can be much larger than the uncertainty given by Eq.(3). Another point which is often forgotten is that the uncertainty of dose also depends on the dose

itself because the proportional constant in Eq.(3) is a function of X and D .

Precision

The precision or the uncertainty of the measured dose is a summation of the uncertainty due to the random errors (or Type A) and systematic errors (Type B). The Type A uncertainty can be estimated by Eq.(2) or a similar equation derived for a particular calibration equation. It is not simple, however, to characterize the Type B errors.

MacDougall *et al.*^[20] attempted to estimate the measurement uncertainty of PGD and FGD in 2002. They gave a rather pessimistic estimate of the accuracy obtainable, *i.e.*, 10% for PGD and 5% for FGD, and the estimated uncertainty was 1.5% for FGD only. Since that time, the dose read-out technique and the quality of 3D dosimeter have improved. The issues of the measurement uncertainty with the 3D dosimeters were, again, reviewed by De Deene and Andrew^[21] in 2015. The nominal uncertainty values from this article are summarized in Table 6. The data are still sparse mainly because the uncertainty is unique to every measurement and dosimeter quality and there is a significant variation in the quality of both measurements and the dosimeters. It is important to note that there are many boxes which are not filled in Table 6. Those are not easily measurable and not well characterized yet. However, eventually, all those uncertainty factors must be estimated to provide a reliable 3D dosimetry tool to the medical community.

PRECLINICAL APPLICATIONS

Besides the highly 3D nature of the dose distribution delivered by modern radiation therapy devices, three

factors affect the dose, consequently the treatment effectiveness. The human body is mostly made of water, or about 50%-65% with the rest composed of higher density tissue, such as bone and lower density material such as lung or air cavity. Furthermore, some patients receive implants often made of high-density material for medical reasons. The dose distribution drastically changes in the vicinity of or near the interface between media with different mass density. The heterogeneity of the medium generates the highly complex dosage patterns and often the current dose calculation algorithms used by the TPS system cannot handle this circumstance accurately. Hence, the effect of tissue heterogeneity must be studied through experimental measurements. Another factor significantly impacting the dose to the tissue is that the temporal change of the human body, consequently the changes in the shape and the material density distribution during a radiation therapy. Such a temporal change is more important when more fractions are used. Note that radiotherapy for the treatment may last for even longer than two months. The effect on the 3D dose distributions can be studied by taking many CT scans. However, what is not known is that the motion of specific points in 3D space and the accumulated dose at that point. We cannot figure out where a tissue volume at a point A on day 1 is on day 2 when the body is deformed. Perhaps, this problem could be solved by creating a mechanical model of the inside of the human body. Alternatively, we can measure the exact accumulated 3D dose distribution to the volume at the end of the treatment with an appropriate dosimetric tool. The third factor is the size of the volume in which the dose must be measured. If the volume is less than 1 cm³ and we need to obtain the 3D dose distribution in this volume, there is a lack of adequate dosimetry tools, currently.

Heterogeneity effects

The interface dosimetry in which one addresses the dose distribution near the tissue and non-tissue interface is well studied at least in a simple geometry such as in the vicinity of a planar heterogeneous material. When we move to heterogeneous materials with more complex 3D shape, the standard dose measurement tools such as ionization chambers, TLD, silicon diodes, radiographic and radiochromic films, are not useful because those cannot provide a real 3D dose distribution with high spatial resolution and add extra heterogeneity due to the measurement tool itself. For this type of measurements, the 3D dosimeters, PGD, FGD and SPD, are ideal dosimeters. There are only a few studies addressing the 3D interface dosimetry by the 3D dosimeters. Since the current deterministic dose calculation methods may not be accurate for this problem, one need to use Monte Carlo simulation methods to create a reference data, to which the measured data are compared to the evaluation of the measurements^[22,23].

Deformable object

There is commercially available software such as Velocity

(Varian Medical Systems, Palo Alto, CA, United States) and MIM Maestro (MIM Software Inc., Cleveland, OH, United States), which can deform the shape of the body image and provide the sum of the doses delivered to many differently deformed objects. Experimental measurements should validate the algorithms of this software. The shape of soft material can be easily deformed. Hence, by implanting many small detectors, *i.e.*, silicon diodes or MOSFET, in the material, we can track the dose to points. At the end of such a study, we can obtain the accumulated dose. The more attractive approach is to use a deformable material which can measure 3D dose distributions. PGD and FGD are ideal for this study because of their flexible nature of the material and the ability to record the dose in 3D space. Applications of PGD in this area of research are not advanced at all, and only a few researchers are currently working on this topic, including the De Deene's group^[24].

Small field

When the size of the radiation beam is small, *e.g.*, less than 1 cm, the only currently available measurement tool is either radiographic/radiochromic films or the 3D dosimeters. There are a few publications on applications of PGD/FGD/SPD^[25-30], and more studies on this topic are needed.

CLINICAL APPLICATIONS

3D dosimeters can be used in clinical practice in radiation oncology. Currently, it is used for evaluation of new tools and radiation delivery techniques. It is also being used as an external QA auditing tool to monitor the quality of dose delivery^[31]. In Figure 3, we present a standard measurement and analysis procedure when we use the 3D dosimeter for evaluation of the delivered dose in comparison to the dose predicted by the TPS.

3D dosimetry products

BANG series dosimeter (nMAG-type PGD) is manufactured and sold by 3D Dosimetry Inc. The same company recently introduced the RGD as CrystalBall™^[32]. PRESAGE SPD is available from Heuris Inc., owned by Dr. Adamovic. The most common imaging device for the dose quantification of PGD/FGD is the MRI system, and it is readily available at most medical facilities. There are only two companies which supply OCT systems for PGD/FGD/SPD. The 3D Dosimetry, Inc. sells its OCTOPUS series system. Modus Medical, Inc. (London, ON, Canada) manufactures two types of cone-beam-based OCT systems, named as Vista.

Analysis software

The analysis software should be able to process the raw image data acquired by the imaging device and convert the raw data to the 3D dose. Also, it is desirable for the software to be able to perform the evaluation of the measured dose in comparison to the reference data from

Process flow diagram for 3D validation of radiation delivery techniques

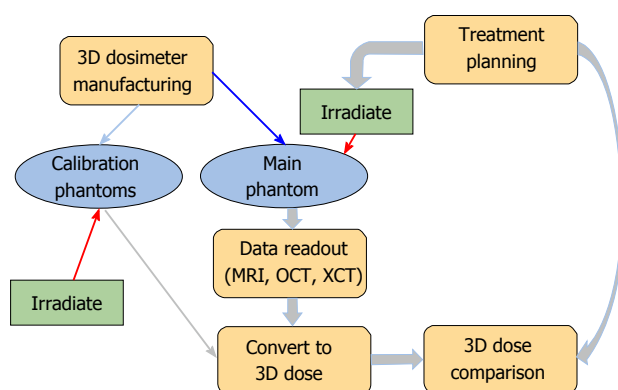


Figure 3 The process flow for dose evaluation using the three-dimensional dosimeters. MRI: Magnetic resonance imaging; OCT: Optical computer tomography; XCT: X-ray computed tomography; 3D: Three-dimensional.

TPS, Monte Carlo code, or other 3D dose measurement tools. The gamma index analysis capability in addition to volumetric analysis, such as generation of dose volume histograms (DVH) using the contour data from TPS is the desired function.

The commercial OCT systems, OCTOPUS and Vista, come with the analysis software. The OCTOPUS system from the 3D Dosimetry Inc. comes with built-in VOLQA™ software. A commercial software PolyGeVero is available from the GeVero Co (Lotz, Poland). Additionally, RTSafe, P.C. (Athens, Greece) and 3D Dosimetry Inc. provide the dosimetry analysis service.

Most research groups in this field developed own data analysis software. Those cannot be used for the work directly related to routine patient treatments, but are excellent tools for research related to new equipment and delivery techniques. These can be easily available for free from the developers^[33].

Routine quality assurance

The regular quality assurance (QA) involves the measurements of beam output and the evaluation of mechanical and dosimetric accuracy^[34]. Other regular QA includes the dosimetric validation of the treatment plans for every IMRT/VMAT treatment^[34]. Thorough dosimetric measurements performed at the acquisition of the new accelerator, or the annual QA can be included in this category. The 3D dosimeters are not used for this purpose currently.

Testing new dosimetry equipment

Pseudo 3D dosimetry tools are being introduced into clinics for routine applications. The device must be tested, and its accuracy must be evaluated before actual applications for patients. PGD/FGD/SPD are ideal tools for such evaluation studies. One example in this area is the assessment of the ArcCHECK device (SUN NUCLEAR, Melbourne, FL, United States). This device contains 1383 small silicon detectors arranged helically on the cylindrical surface. The device measures the radiation dose deposited by both incident and exiting beams. The device is specifically designed for QA of VMAT. Furthermore, special software

3DVH can be used to reconstruct the radiation dose distribution inside the cylinder where there is no detector or in the patient by using the dose data measured by ArcCHECK. The 3D dose data can be mathematically reconstructed from the available fluence data. Hence, this device can provide the users a 3D dose distribution data in a phantom or a patient. Since the device is based on a new idea and its design is very innovative, the evaluation of its performance is essential. Watanabe and Nakaguchi, hence, undertook an assessment study by using BANG3^[33]. They measured the 3D dose distribution generated by VMAT and compared the results with those obtained by ArcCHECK. Their results demonstrated a satisfactory agreement between those two measurement techniques, hence, confirming the measurement accuracy of the new device as a pseudo-3D dosimeter. This application of PGD is a critical step to demonstrate its value and suggests that the PGD should be invaluable. PGD may become the standard tool for evaluation of pseudo-3D dosimeters which will be developed in the future.

End-to-end QA

A task group of AAPM, TG-142, recommends the end-to-end test of a new dose delivery system such as SRS and IMRT/VMAT^[34]. Such a test can be accomplished the most adequately by using the 3D dosimeter because the shape of a patient can be simulated easily by using these tools. The earliest application of PGD was made to the end-to-end QA of Gamma Knife stereotactic radiosurgery (GKSRS). One of the studies could, in fact, point out a non-negligible geometric error associated with the imaging, which was not considered or quantified before^[35]. As a matter of fact, all the MRI-based PGD of GKSRS is considered as an end-to-end test of the dose delivered when the dose delivery is planned on the MR image which was taken before planning and radiation delivery.

SRS

The application of 3D dosimeters for GKSRS is well established as discussed before. Applications of 3D dosimeters to other types of SRS technique have not been performed as often as GKSRS for an unknown reason. Björelund *et al.*^[36] used nMAG for the dosimetric evaluation of a linac-based hypofractionated SRS system. PAGAT was used for QA of SRS by multi-leaf collimator (MLC), m3 (BrainLab)^[37].

IMRT/VMAT/tomotherapy

The dose delivery technique of IMRT and VMAT (including tomotherapy) requires very sophisticated mechanical maneuver of the MLC, jaws, and the angles of gantry and collimator. The radiation delivery is, in essence, four-dimensional because the positions of all these components move during a single delivery of treatment. Hence, the precision of delivering dose is affected by the composite of many factors. An individual test of this element is not sufficient. Hence, the actual 3D dose evaluation of these technologies should be performed at least once before the introduction to clinical usages.

Table 7 IMRT/VMAT/tomotherapy three-dimensional dosimetry

Ref.	Dosimeter	Read-out method	Treatment site	Delivery type	Photon energy/ number of fields	Comparison on the plane or in volume	Gamma index criteria % dose difference (global/ local)/DTA (mm)/ threshold (%)	Gamma index passing rate
[86]	MAGIC	MRI/T2	Model	IMRT/GKSRS	6MV/Co-60	Volume	3/3/	50.3%
[87]	FX gel	OCT/Vista	Head and Neck	IMRT	6MV	Volume	3/3/none	84.1%
[88]	BANG3	MRI/T2	Prostate	Tomotherapy	6MV/Arc	Volume	3/3	53%
[89]	PRESAGE	DLOS	Brain	IMRT	6MV	Volume	3/3	95%
[90]	MAGIC-f	MRI/T2	Prostate	Tomotherapy	6MV/Arc	Plane	3/3	88.4%
[91]	nPAG	OCTOPUS-IQ	Prostate	IMRT	/7fields	Volume		95.3%
[10]	PAGAT	MRI/T2	Pituitary	IMRT	6MV/7fields	Volume	2/2	99.4%
[33]	BANG3	MRI/T2	Prostate	VMAT (Elekta)	6MV/Arc	Volume	3 (global)/3/25	95.7%
[92]	BANG3	MRI/T2	Prostate	VMAT (Varian)	6MV/Arc	Volume	3 (global)/3/50	90.0%
[93]	PRESAGE	DMOS	Brain	IMRT	6MV/5fields	Volume	3 (global)/3/10	99.4%
[94]	NIPAM	MRI/T2	Eye	IMRT	6MV/5fields	Plane	3/3/	98.5%

MRI: Magnetic resonance imaging; DTA: Distance to agreement; DMOS: Duke Mid-Sized Optical-CT Scanner; DLOS: Duke Large field-of-view Optical-CT Scanner.

The 3D dosimetry tools can be used effectively for this purpose.

The major goal of the 3D dosimetry, hence, is the validation of the 3D dose distribution predicted by TPS by comparing with the measured dose which reflects the performance of the radiation delivery system. There are many studies on this topic. In Table 7, we summarize the published studies, which provide the gamma index passing rates. There are many other studies, most of which are earlier publications without the gamma analysis.

Proton/heavy ions

Because of its unique depth dose generated by ion beams such as protons and heavy ions, *i.e.*, carbon-12, a tremendous interest in those technologies exists. In fact, the use of protons for radiation therapy is rapidly expanding. The desirable depth-dose characteristics, mainly due to the existence of the Bragg peak at a particular range, however, suffers from a significant uncertainty of the actual location of the sharp peak in the dose. This issue is sometimes called as range uncertainty. The measurement of the depth dose of particle beams, hence, is an important task, which every new facility should perform. The 3D dosimeter can be a good candidate for this type of applications if those materials are tailored to adequately simulate the linear energy transfer (LET) of particles in water or tissue.

Gustavsson *et al.*^[38] used BANG3 for the measurement of the central axis depth dose curve of a 68MeV proton beam. They found that the dose at the Bragg peak was underestimated by a factor of two by BANG3 because of the “quenching”. The quenching or under-response of the BANG3 occurred because the proton energy changes as those travel into deeper locations. LET depends on the proton energy. Thus, calibration data obtained by a specific energy at a shallow depth cannot be applied to the depth dose measurement. We can solve this problem by using the estimated proton energy as the function of depth theoretically, for example, by Monte Carlo simulation^[38]. The introduction of BANG3-Pro eventually solved the issue of PGD due to the LET dependence of its

radiation response. The new PGD had gelatin matrix with higher viscosity than the original BANG3^[39]. PGD was also tested with heavy ion beams^[40]. Recently, Maeyama *et al.* used the nano-composite Fricke gel (NC-FG), a type of FGD, with carbon and argon ion beams, whose LET ranged from 10 to 3000 eV/ μm ^[41]. NC-FG showed a consistent dose response for the range of LET tested in their study.

Brachytherapy

Brachytherapy uses the small size of the radioactive material as radiation sources for radiation therapy. It is easy to expect, hence, that the dose distributions generated by single brachytherapy source or multiple sources are highly three-dimensional. Because of the large dose gradient, the 3D dosimeters are potentially an ideal dose measurement device. Therefore, 3D dosimeters were widely used with radioactive sources. The primary application is in the 3D dose distribution measurement of the single radioactive source. The results can be compared with the standard data of TG53 which are clinically in use. The measurements were done with various types of radioactive sources: Iridium-192 high dose rate (HDR) source^[42-48], low dose rate (LDR) Iodine-125 seed^[49,50], and LDR Cesium-137 source^[51]. Additionally, the 3D dosimeters were used for the dosimetry of beta-emitting radioactive sources such as Ruthenium-103^[52], Rhenium-188^[53], and Yttrium-90^[54]. The SPD was also used with a radioactive source^[55,56].

For many brachytherapy procedures using LDR and HDR sources, the high dose is delivered to a large volume by placing many sources or moving a single HDR source over the volume. There is a lack of 3D dosimetry study in this more clinically useful source configuration.

DISCUSSION AND SUMMARY

Current technical issues

An ultimate goal of the 3D dosimeter study is to produce a tool for 3D dosimetry, which can be routinely used in all radiation therapy clinics all over the world. This goal

is yet to be reached. It seems that even institutions with sufficient expertise in this field are not using the tool routinely except occasional applications, mostly, for research purpose or evaluation of new devices or software. There are two major factors for this somewhat depressing situation after over 20 years of extensive research. The first factor is the precision of the measurements in comparison to the existing tools. As discussed in the precision section, the state-of-art methods in PGD, FGD, and SPD can achieve $\pm 5\%$ uncertainty with 95% confidence if the measurements and instruments are well prepared and managed. This accuracy is still less than that of other more standard tools such as a 3D water scanning system with an ionization chamber, which can provide a 3D dose distribution, but with coarser measurement grids than PGD and SPD. Note that the 3D water scanning is faster than PGD and SPD when the measurement time includes the preparation and the data analysis. Hence, the current 3D dosimeters cannot replace the 3D water scanning system, which is always used for commissioning and annual QA of the accelerator.

Therefore, the improvement of the measurement precision should be the primary goal of the 3D dosimetry community. The uncertainty is composed of the random errors (Type A), which are caused by the random nature of the signal acquired by the measurement device, and the uncertainty of the calibration data, which is again strongly affected by the random errors during the calibration. However, a larger uncertainty stems from other factors (Table 6): (1) the non-uniformity of the detector medium; (2) the reproducibility of dosimetric properties; and (3) the uncertainty associated with the dose quantification device.

The issues (1) and (2) can be overcome by improving the manufacturing process and the distribution (or delivery of the product to the customer) system. The issue (3) can be solved by using an imaging device specifically designed for the 3D dosimetry. MRI cannot be easily made just for the 3D dosimetry. Since MRI is a diagnostic tool, it is not suited for the quantitative measurement. However, the situation will improve because the community is now more interested in the "quantitative" imaging. On the other hand, OCTs are designed for the 3D dosimetry to provide the most accurate result, although the current system still requires further improvement.

The cost of the 3D dosimetry is another obstacle preventing its widespread acceptance as a routine measurement tool. Let us examine this issue further by using an example. Suppose we would like to use PGD for the regular patient specific IMRT/VMAT QA. Assume that the current standard is the use of ArcCHECK and the price of the ArcCHECK system is \$50000. Now, then we purchase a commercial PGD, whose price is \$500 for an 18-cm diameter 20-cm long cylindrical phantom containing PGD. The cost of the dose quantification device is zero if MRI is used or \$30000 if a commercial OCT system is purchased. Assume we use an OCT system. Then, the difference of the device costs between the ArcCHECK and PGD approach is \$20000 by excluding the cost of PGD.

This difference can cover 40 PGD phantoms, which are the number needed for one year of patient specific QA at a typical radiation oncology department. If we assume that we use these systems for five years, the total cost of the ArcCHECK approach is still \$50000. However, the total cost of PGD is \$130000. Hence, there is a tremendous disadvantage of the PGD over the ArcCHECK regarding the cost. However, this cost analysis does not diminish the value of the 3D dosimeter approach as we discuss next. It is evident from this analysis, furthermore, that the development of reusable 3D dosimeters could lead to significant cost saving^[57].

Now, let us consider the information obtained by these tools. The information is quantified by the number of pixels and voxels, which record the dose data, for PGD, and the number of diode detectors in ArcCHECK, which is 1386. The voxel size of typical OCT scan is $1\text{ mm} \times 1\text{ mm} \times 1\text{ mm}$ or 1 mm^3 ($= 0.001\text{ cm}^3$). The volume of dose measurement is a 20-cm diameter and 20-cm long; hence, this volume is 833 cm^3 and contains 833000 voxels. Assume we use the system for $40 \times 5 = 200$ times in five years. The dollar per the data point or information is 18 cents for the ArcCHECK method; whereas it is 0.08 cents for PGD. Therefore, PGD is much more cost effective if all the acquired data can be utilized to improve the treatment quality.

CONCLUSION

The 3D dosimeters have been under development for many years and were studied by researchers all over the world. It seems that the lack of the acceptance for wider radiation oncology applications stems from the inherent or unknown uncertainty of the tools and the cost needed for everyday usages. These issues should be addressed in the future. More focused studies are needed to resolve these problems.

REFERENCES

- 1 **Hall EJ**, Giaccia AJ. Radiobiology for the Radiologist. 7th ed. Philadelphia, PA: Lippincott Williams & Wilkins, 2011
- 2 **Johns HE**, Cunningham JR. The Physics of Radiology. Springfield, IL: Charles C. Thomas, 1983
- 3 **Khan FM**, Gibbons JP. Khan's The Physics of Radiation Therapy. 5th ed. Philadelphia: Lippincott Williams and Wilkins, 2014
- 4 **Attix AF**. Introduction to Radiological Physics and Radiation Dosimetry. Weinheim, Germany: Wiley-VCH Verlag GmbH & Co. KGaA, 2004
- 5 **Fong PM**, Keil DC, Does MD, Gore JC. Polymer gels for magnetic resonance imaging of radiation dose distributions at normal room atmosphere. *Phys Med Biol* 2001; **46**: 3105-3113 [PMID: 11768494 DOI: 10.1088/0031-9155/46/12/303]
- 6 **Adamovics J**, Maryanski MJ. Characterisation of PRESAGE: A new 3-D radiochromic solid polymer dosimeter for ionising radiation. *Radiat Prot Dosimetry* 2006; **120**: 107-112 [PMID: 16782984 DOI: 10.1093/rpd/nci555]
- 7 **Beddar AS**. Water equivalent plastic scintillation detectors in radiation therapy. *Radiat Prot Dosimetry* 2006; **120**: 1-6 [PMID: 16882685 DOI: 10.1093/rpd/nci694]
- 8 **Glaser AK**, Zhang R, Gladstone DJ, Pogue BW. Optical dosimetry of radiotherapy beams using Cherenkov radiation: the relationship

- between light emission and dose. *Phys Med Biol* 2014; **59**: 3789-3811 [PMID: 24938928 DOI: 10.1088/0031-9155/59/14/3789]
- 9 **Baldock C**, De Deene Y, Doran S, Ibbott G, Jirasek A, Lepage M, McAuley KB, Oldham M, Schreiner LJ. Polymer gel dosimetry. *Phys Med Biol* 2010; **55**: R1-63 [PMID: 20150687 DOI: 10.1088/0031-9155/55/5/R01]
 - 10 **Vandecasteele J**, De Deene Y. Evaluation of radiochromic gel dosimetry and polymer gel dosimetry in a clinical dose verification. *Phys Med Biol* 2013; **58**: 6241-6262 [PMID: 23965800 DOI: 10.1088/0031-9155/58/18/6241]
 - 11 **Gore JC**, Kang YS, Schulz RJ. Measurement of radiation dose distributions by nuclear magnetic resonance (NMR) imaging. *Phys Med Biol* 1984; **29**: 1189-1197 [PMID: 6494247]
 - 12 **Olsson LE**, Petersson S, Ahlgren L, Mattsson S. Ferrous sulphate gels for determination of absorbed dose distributions using MRI technique: basic studies. *Phys Med Biol* 1989; **34**: 43-52 [PMID: 2928377 DOI: 10.1088/0031-9155/34/1/004]
 - 13 **Babic S**, Battista J, Jordan K. An apparent threshold dose response in ferrous xylenol-orange gel dosimeters when scanned with a yellow light source. *Phys Med Biol* 2008; **53**: 1637-1650 [PMID: 18367793 DOI: 10.1088/0031-9155/53/6/009]
 - 14 **Brost E**, Senthikumar S, Warmington L, Watanabe Y. SU-F-T-434: Development of a Fan-Beam Optical Scanner Using CMOS Array for Small Field Dosimetry. *Med Phys* 2016; **43**: 3563 [PMID: 28048592 DOI: 10.1118/1.4956619]
 - 15 **Watanabe Y**, Constantinou C. Phantom Materials in Radiology. *Encyclopedia of Medical Devices and Instrumentation*: John Wiley & Sons, Inc., 2006
 - 16 **Watanabe Y**, Kubo H. A variable echo-number method for estimating R2 in MRI-based polymer gel dosimetry. *Med Phys* 2011; **38**: 975-982 [PMID: 21452734 DOI: 10.1118/1.3544659]
 - 17 **Kron T**, Pope JM. Dose distribution measurements in superficial x-ray beams using NMR dosimetry. *Phys Med Biol* 1994; **39**: 1337-1349 [PMID: 15552108 DOI: 10.1088/0031-9155/39/9/003]
 - 18 **Campbell WG**, Rudko DA, Braam NA, Wells DM, Jirasek A. A prototype fan-beam optical CT scanner for 3D dosimetry. *Med Phys* 2013; **40**: 061712 [PMID: 23718591 DOI: 10.1118/1.4805111]
 - 19 **Watanabe Y**, Akimitsu T, Hirokawa Y, Mooij RB, Perera GM. Evaluation of dose delivery accuracy of Gamma Knife by polymer gel dosimetry. *J Appl Clin Med Phys* 2005; **6**: 133-142 [PMID: 16143798 DOI: 10.1120/jacmp.v6i3.2110]
 - 20 **MacDougall ND**, Pitchford WG, Smith MA. A systematic review of the precision and accuracy of dose measurements in photon radiotherapy using polymer and Fricke MRI gel dosimetry. *Phys Med Biol* 2002; **47**: R107-R121 [PMID: 12433119 DOI: 10.1088/0031-9155/47/20/201]
 - 21 **De Deene Y**, Andrew J. Uncertainty in 3D gel dosimetry. *Journal of Physics: Conference Series*, 2015: 012008 [DOI: 10.1088/1742-6596/573/1/012008]
 - 22 **Watanabe Y**, Mooij R, Perera GM, Maryanski MJ. Heterogeneity phantoms for visualization of 3D dose distributions by MRI-based polymer gel dosimetry. *Med Phys* 2004; **31**: 975-984 [PMID: 15191281 DOI: 10.1118/1.1688210]
 - 23 **Warmington L**, Watanabe Y. SU-E-T-734: The Feasibility of Using Polymer Gel Dosimetry to Measure the Dose Around Thin High Z Materials Irradiated with High Energy Photon Beams. *Medical Physics* 2015; **42**: 3505 [DOI: 10.1118/1.4925098]
 - 24 **De Deene Y**, Skyt PS, Hil R, Booth JT. FlexyDos3D: a deformable anthropomorphic 3D radiation dosimeter: radiation properties. *Phys Med Biol* 2015; **60**: 1543-1563 [PMID: 25615261 DOI: 10.1088/0031-9155/60/4/1543]
 - 25 **Wong CJ**, Ackerly T, He C, Patterson W, Powell CE, Ho A, Qiao G, Solomon DH, Meder R, Geso M. High-resolution measurements of small field beams using polymer gels. *Appl Radiat Isot* 2007; **65**: 1160-1164 [PMID: 17574428 DOI: 10.1016/j.apradiso.2007.04.005]
 - 26 **Pantelis E**, Antypas C, Petrokokkinos L, Karaikos P, Papagiannis P, Kozicki M, Georgiou E, Sakellidou L, Seimenis I. Dosimetric characterization of CyberKnife radiosurgical photon beams using polymer gels. *Med Phys* 2008; **35**: 2312-2320 [PMID: 18649464 DOI: 10.1118/1.2919099]
 - 27 **Pappas E**, Maris TG, Zacharopoulou F, Papadakis A, Manolopoulos S, Green S, Wojnecki C. Small SRS photon field profile dosimetry performed using a PinPoint air ion chamber, a diamond detector, a novel silicon-diode array (DOSI), and polymer gel dosimetry. Analysis and intercomparison. *Med Phys* 2008; **35**: 4640-4648 [PMID: 18975710 DOI: 10.1118/1.2977829]
 - 28 **Olding T**, Holmes O, Dejean P, McAuley KB, Nkongchu K, Santyr G, Schreiner LJ. Small field dose delivery evaluations using cone beam optical computed tomography-based polymer gel dosimetry. *J Med Phys* 2011; **36**: 3-14 [PMID: 21430853 DOI: 10.4103/0971-6203.75466]
 - 29 **Hassani H**, Nedaie HA, Zahmatkesh MH, Shirani K. A dosimetric study of small photon fields using polymer gel and Gafchromic EBT films. *Med Dosim* 2014; **39**: 102-107 [PMID: 24388694 DOI: 10.1016/j.meddos.2013.10.007]
 - 30 **Shih TY**, Wu J, Shih CT, Lee YT, Wu SH, Yao CH, Hsieh BT. Small-Field Measurements of 3D Polymer Gel Dosimeters through Optical Computed Tomography. *PLoS One* 2016; **11**: e0151300 [PMID: 26974434 DOI: 10.1371/journal.pone.0151300]
 - 31 **Juang T**, Grant R, Adamovics J, Ibbott G, Oldham M. On the feasibility of comprehensive high-resolution 3D remote dosimetry. *Med Phys* 2014; **41**: 071706 [PMID: 24989375 DOI: 10.1118/1.4884018]
 - 32 **Avery S**, Kraus J, Lin L, Kassaei A, Maryanski M. MO-F-CAMPUS-T-02: Dosimetric Accuracy of the CrystalBall₄,[®] New Reusable Radiochromic Polymer Gel Dosimeter for Patient QA in Proton Therapy. *Medical Physics* 2015; **42**: 3581 [DOI: 10.1118/1.4925477]
 - 33 **Watanabe Y**, Nakaguchi Y. 3D evaluation of 3DVH program using BANG3 polymer gel dosimeter. *Med Phys* 2013; **40**: 082101 [PMID: 23927338 DOI: 10.1118/1.4813301]
 - 34 **Klein EE**, Hanley J, Bayouth J, Yin FF, Simon W, Dresser S, Serago C, Aguirre F, Ma L, Arjomandy B, Liu C, Sandin C, Holmes T. Task Group 142 report: quality assurance of medical accelerators. *Med Phys* 2009; **36**: 4197-4212 [PMID: 19810494 DOI: 10.1118/1.3190392]
 - 35 **Watanabe Y**, Perera GM, Mooij RB. Image distortion in MRI-based polymer gel dosimetry of gamma knife stereotactic radio-surgery systems. *Med Phys* 2002; **29**: 797-802 [PMID: 12033575 DOI: 10.1118/1.1470204]
 - 36 **Björrelund A**, Lindvall P, Karlsson A, Gustavsson H, Bäck SA, Karlsson M, Bergenheim TA. Liquid ionization chamber calibrated gel dosimetry in conformal stereotactic radiotherapy of brain lesions. *Acta Oncol* 2008; **47**: 1099-1109 [PMID: 18607837 DOI: 10.1080/02841860801888781]
 - 37 **Kairn T**, Taylor ML, Crowe SB, Dunn L, Franich RD, Kenny J, Knight RT, Trapp JV. Monte Carlo verification of gel dosimetry measurements for stereotactic radiotherapy. *Phys Med Biol* 2012; **57**: 3359-3369 [PMID: 22572565 DOI: 10.1088/0031-9155/57/11/3359]
 - 38 **Gustavsson H**, Bäck SA, Medin J, Grusell E, Olsson LE. Linear energy transfer dependence of a normoxic polymer gel dosimeter investigated using proton beam absorbed dose measurements. *Phys Med Biol* 2004; **49**: 3847-3855 [PMID: 15470909 DOI: 10.1088/0031-9155/49/17/002]
 - 39 **Zeidan OA**, Sriprisan SI, Lopatiuk-Tirpak O, Kupelian PA, Meeks SL, Hsi WC, Li Z, Palta JR, Maryanski MJ. Dosimetric evaluation of a novel polymer gel dosimeter for proton therapy. *Med Phys* 2010; **37**: 2145-2152 [PMID: 20527548 DOI: 10.1118/1.3388869]
 - 40 **Ramm U**, Moog J, Spielberger B, Bankamp A, Bottcher HD, Kraft G. Investigations of dose response of BANG polymer-gels to carbon ion irradiation. *Radiother Oncol* 2004; **73** Suppl 2: S99-101 [PMID: 15971320 DOI: 10.1016/S0167-8140(04)80025-2]
 - 41 **Maeyama T**, Fukunishi N, Ishikawa KL, Fukasaku K, Fukuda S. Radiological properties of nanocomposite Fricke gel dosimeters for heavy ion beams. *J Radiat Res* 2016; **57**: 318-324 [PMID: 26968632 DOI: 10.1093/jrr/trw025]
 - 42 **Maryanski MJ**, Ibbott GS, Eastman P, Schulz RJ, Gore JC. Radiation therapy dosimetry using magnetic resonance imaging of polymer gels. *Med Phys* 1996; **23**: 699-705 [PMID: 8724743 DOI: 10.1118/1.597717]

- 43 **McJury M**, Tapper PD, Cosgrove VP, Murphy PS, Griffin S, Leach MO, Webb S, Oldham M. Experimental 3D dosimetry around a high-dose-rate clinical ¹⁹²Ir source using a polyacrylamide gel (PAG) dosimeter. *Phys Med Biol* 1999; **44**: 2431-2444 [PMID: 10533920 DOI: 10.1088/0031-9155/44/10/305]
- 44 **De Deene Y**, Reynaert N, De Wagter C. On the accuracy of monomer/polymer gel dosimetry in the proximity of a high-dose-rate ¹⁹²Ir source. *Phys Med Biol* 2001; **46**: 2801-2825 [PMID: 11720348 DOI: 10.1088/0031-9155/46/11/304]
- 45 **Papagiannis P**, Pappas E, Kipouros P, Angelopoulos A, Sakelliou L, Baras P, Karaikos P, Seimenis I, Sandilos P, Baltas D. Dosimetry close to an ¹⁹²Ir HDR source using N-vinylpyrrolidone based polymer gels and magnetic resonance imaging. *Med Phys* 2001; **28**: 1416-1426 [PMID: 11488573 DOI: 10.1118/1.1382603]
- 46 **Kipouros P**, Anagnostopoulos G, Angelopoulos A, Baltas D, Baras P, Drolapas A, Karaikos P, Pantelis E, Papagiannis P, Sakelliou L, Seimenis I. Dosimetric calculations and VIPAR polymer gel dosimetry close to the microSelectron HDR. *Z Med Phys* 2002; **12**: 252-259 [PMID: 12575439]
- 47 **Kipouros P**, Papagiannis P, Sakelliou L, Karaikos P, Sandilos P, Baras P, Seimenis I, Kozicki M, Anagnostopoulos G, Baltas D. 3D dose verification in ¹⁹²Ir HDR prostate monotherapy using polymer gels and MRI. *Med Phys* 2003; **30**: 2031-2039 [PMID: 12945969 DOI: 10.1118/1.1590437]
- 48 **Senkesen O**, Tezcanli E, Buyuksarac B, Ozbay I. Comparison of 3D dose distributions for HDR ¹⁹²Ir brachytherapy sources with normoxic polymer gel dosimetry and treatment planning system. *Med Dosim* 2014; **39**: 266-271 [PMID: 24933316 DOI: 10.1016/j.meddos.2014.04.003]
- 49 **Farajollahi AR**, Bonnett DE, Ratcliffe AJ, Aukett RJ, Mills JA. An investigation into the use of polymer gel dosimetry in low dose rate brachytherapy. *Br J Radiol* 1999; **72**: 1085-1092 [PMID: 10700826 DOI: 10.1259/bjr.72.863.10700826]
- 50 **Papagiannis P**, Pantelis E, Georgiou E, Karaikos P, Angelopoulos A, Sakelliou L, Stiliaris S, Baltas D, Seimenis I. Polymer gel dosimetry for the TG-43 dosimetric characterization of a new ¹²⁵I interstitial brachytherapy seed. *Phys Med Biol* 2006; **51**: 2101-2111 [PMID: 16585848 DOI: 10.1088/0031-9155/51/8/010]
- 51 **Fragoso M**, Love PA, Verhaegen F, Nalder C, Bidmead AM, Leach M, Webb S. The dose distribution of low dose rate Cs-137 in intracavitary brachytherapy: comparison of Monte Carlo simulation, treatment planning calculation and polymer gel measurement. *Phys Med Biol* 2004; **49**: 5459-5474 [PMID: 15724536 DOI: 10.1088/0031-9155/49/24/005]
- 52 **Chan MF**, Fung AY, Hu YC, Chui CS, Amols H, Zaider M, Abramson D. The measurement of three dimensional dose distribution of a ruthenium-106 ophthalmological applicator using magnetic resonance imaging of BANG polymer gels. *J Appl Clin Med Phys* 2001; **2**: 85-89 [PMID: 11604053 DOI: 10.1120/1.1351776]
- 53 **Wuu CS**, Schiff P, Maryanski MJ, Liu T, Borzillary S, Weinberger J. Dosimetry study of Re-188 liquid balloon for intravascular brachytherapy using polymer gel dosimeters and laser-beam optical CT scanner. *Med Phys* 2003; **30**: 132-137 [PMID: 12607830 DOI: 10.1118/1.1533749]
- 54 **Massillon-JI G**, Minniti R, Mitch MG, Maryanski MJ, Soares CG. The use of gel dosimetry to measure the 3D dose distribution of a ⁹⁰Sr/⁹⁰Y intravascular brachytherapy seed. *Phys Med Biol* 2009; **54**: 1661-1672 [PMID: 19242054 DOI: 10.1088/0031-9155/54/6/017]
- 55 **Wai P**, Adamovics J, Krstajic N, Ismail A, Nisbet A, Doran S. Dosimetry of the microSelectron-HDR Ir-192 source using PRESAGE and optical CT. *Appl Radiat Isot* 2009; **67**: 419-422 [PMID: 18684629 DOI: 10.1016/j.apradiso.2008.06.038]
- 56 **Vidovic AK**, Juang T, Meltsner S, Adamovics J, Chino J, Steffey B, Craciunescu O, Oldham M. An investigation of a PRESAGE® in vivo dosimeter for brachytherapy. *Phys Med Biol* 2014; **59**: 3893-3905 [PMID: 24957850 DOI: 10.1088/0031-9155/59/14/3893]
- 57 **Juang T**, Adamovics J, Oldham M. Characterization of a reusable PRESAGE (R) 3D dosimeter. 8th International Conference on 3d Radiation Dosimetry (Ic3ddose), 2015: 012039 [DOI: 10.1088/1742-6596/573/1/012039]
- 58 **Maryanski MJ**, Gore JC, Kennan RP, Schulz RJ. NMR relaxation enhancement in gels polymerized and cross-linked by ionizing radiation: a new approach to 3D dosimetry by MRI. *Magn Reson Imaging* 1993; **11**: 253-258 [PMID: 8455435 DOI: 10.1016/0730-725X(93)90030-H]
- 59 **Maryanski MJ**, Schulz RJ, Ibbott GS, Gatenby JC, Xie J, Horton D, Gore JC. Magnetic resonance imaging of radiation dose distributions using a polymer-gel dosimeter. *Phys Med Biol* 1994; **39**: 1437-1455 [PMID: 15552115 DOI: 10.1088/0031-9155/39/9/010]
- 60 **Mather ML**, Charles PH, Baldock C. Measurement of ultrasonic attenuation coefficient in polymer gel dosimeters. *Phys Med Biol* 2003; **48**: N269-N275 [PMID: 14620069 DOI: 10.1088/0031-9155/48/20/N01]
- 61 **Maryanski MJ**. Scavenging is no magic. *Phys Med Biol* 2002; **47**: L11-L2; author reply L11-L2; [PMID: 12108780 DOI: 10.1088/0031-9155/47/11/011]
- 62 **Venning AJ**, Mather ML, Baldock C. Investigation of vacuum pumping on the dose response of the MAGAS normoxic polymer gel dosimeter. *Australas Phys Eng Sci Med* 2005; **28**: 105-110 [PMID: 16060316 DOI: 10.1088/0031-9155/50/16/015]
- 63 **De Deene Y**, Pittomvils G, Visalatchi S. The influence of cooling rate on the accuracy of normoxic polymer gel dosimeters. *Phys Med Biol* 2007; **52**: 2719-2728 [PMID: 17473347 DOI: 10.1088/0031-9155/52/10/006]
- 64 **Ceberg S**, Lepage M, Bäck SÅ, Gustafsson H, Ceberg C. Modelling the dynamic dose response of an nMAG polymer gel dosimeter. *Phys Med Biol* 2012; **57**: 4845-4853 [PMID: 22797664 DOI: 10.1088/0031-9155/57/15/4845]
- 65 **Fernandes JP**, Pastorello BF, de Araujo DB, Baffa O. Formaldehyde increases MAGIC gel dosimeter melting point and sensitivity. *Phys Med Biol* 2008; **53**: N53-N58 [PMID: 18263941 DOI: 10.1088/0031-9155/53/4/N04]
- 66 **Gustavsson H**, Bäck SA, Lepage M, Rintoul L, Baldock C. Development and optimization of a 2-hydroxyethylacrylate MRI polymer gel dosimeter. *Phys Med Biol* 2004; **49**: 227-241 [PMID: 15083668 DOI: 10.1088/0031-9155/49/2/004]
- 67 **Pappas E**, Maris T, Angelopoulos A, Paparigopoulou M, Sakelliou L, Sandilos P, Voyiatzi S, Vlachos L. A new polymer gel for magnetic resonance imaging (MRI) radiation dosimetry. *Phys Med Biol* 1999; **44**: 2677-2684 [PMID: 10533935 DOI: 10.1088/0031-9155/44/10/320]
- 68 **Senden RJ**, De Jean P, McAuley KB, Schreiner LJ. Polymer gel dosimeters with reduced toxicity: a preliminary investigation of the NMR and optical dose-response using different monomers. *Phys Med Biol* 2006; **51**: 3301-3314 [PMID: 16825731 DOI: 10.1088/0031-9155/51/14/001]
- 69 **Jordan K**. Sci-Fri PM: Planning-08: Zero diffusion radiochromic genipin-gelatin dosimeter. *Medical Physics* 2008; **35**: 3413 [DOI: 10.1118/1.2965980]
- 70 **Babic S**, McNiven A, Battista J, Jordan K. Three-dimensional dosimetry of small megavoltage radiation fields using radiochromic gels and optical CT scanning. *Phys Med Biol* 2009; **54**: 2463-2481 [PMID: 19336848 DOI: 10.1088/0031-9155/54/8/014]
- 71 **Gastaldo J**, Boudou C, Lamalle L, Tropès I, Corde S, Sollier A, Rucka G, Elleaume H. Normoxic polyacrylamide gel doped with iodine: response versus X-ray energy. *Eur J Radiol* 2008; **68**: S118-S120 [PMID: 18602237 DOI: 10.1016/j.ejrad.2008.04.053]
- 72 **Yoshioka M**, Hayashi S, Usui S, Haneda K, Numasaki H, Teshima T, Tominaga T. A new polymer gel dosimeter composed of methacrylic acid, agarose gel and THPC with gelatin. *Journal of Physics: Conference Series*, 2009; **164**: 012013 [DOI: 10.1088/1742-6596/164/1/012013]
- 73 **Hiroki A**, Sato Y, Nagasawa N, Ohta A, Seito H, Yamabayashi H, Yamamoto T, Taguchi M, Tamada M, Kojima T. Preparation of polymer gel dosimeters based on less toxic monomers and gellan gum. *Phys Med Biol* 2013; **58**: 7131-7141 [PMID: 24052135 DOI: 10.1088/0031-9155/58/20/7131]
- 74 **Olsson LE**, Fransson A, Ericsson A, Mattsson S. MR imaging of absorbed dose distributions for radiotherapy using ferrous sulphate gels. *Phys Med Biol* 1990; **35**: 1623-1631 [PMID: 2284333 DOI: 10.1088/0031-9155/35/10/006]

- 10.1088/0031-9155/35/12/003]
- 75 **Chu KC**, Jordan KJ, Battista JJ, Van Dyk J, Rutt BK. Polyvinyl alcohol-Fricke hydrogel and cryogel: two new gel dosimetry systems with low Fe³⁺ diffusion. *Phys Med Biol* 2000; **45**: 955-969 [PMID: 10795984 DOI: 10.1088/0031-9155/45/4/311]
 - 76 **Leong LH**, Kandaiya S, Seng NB. Characterisation of a Ferrous Agarose Xylenol (FAX) gel for radiotherapy dose measurement. *Australas Phys Eng Sci Med* 2007; **30**: 135-140 [PMID: 17682403 DOI: 10.1007/BF03178418]
 - 77 **Eyadeh MM**, Farrell TJ, Diamond KR. Evaluation of a ferrous benzoic xylenol orange transparent PVA cryogel radiochromic dosimeter. *Phys Med Biol* 2014; **59**: 1773-1787 [PMID: 24619200 DOI: 10.1088/0031-9155/59/7/1773]
 - 78 **Smith ST**, Masters KS, Hosokawa K, Blinco JP, Crowe SB, Kairn T, Trapp JV. Technical Note: Preliminary investigations into the use of a functionalised polymer to reduce diffusion in Fricke gel dosimeters. *Med Phys* 2015; **42**: 6798-6803 [PMID: 26632037 DOI: 10.1118/1.4934827]
 - 79 **Patel GN**. Thick radiation sensitive devices. Google Patents, 2004
 - 80 **Mostaer A**, Hashemi B, Zahmatkesh MH, Aghamiri SM, Mahdavi SR. A basic dosimetric study of PRESAGE: the effect of different amounts of fabricating components on the sensitivity and stability of the dosimeter. *Phys Med Biol* 2010; **55**: 903-912 [PMID: 20071770 DOI: 10.1088/0031-9155/55/3/023]
 - 81 **Alqathami M**, Blencowe A, Qiao G, Butler D, Geso M. Optimization of the sensitivity and stability of the PRESAGE (TM) dosimeter using trihalomethane radical initiators. *Radiat Phys Chem* 2005; **35**: 327-330 [DOI: 10.1016/j.radphyschem.2012.03.022]
 - 82 **Warmington LL**. Three-dimensional dosimetry around small distributed high-Z materials [Doctoral dissertation]. Minneapolis, MN: University of Minnesota, 2016
 - 83 **Gorjiara T**, Hill R, Kuncic Z, Bosi S, Davies JB, Baldock C. Radiological characterization and water equivalency of genipin gel for x-ray and electron beam dosimetry. *Phys Med Biol* 2011; **56**: 4685-4699 [PMID: 21734335 DOI: 10.1088/0031-9155/56/15/004]
 - 84 **Venning AJ**, Nitschke KN, Keall PJ, Baldock C. Radiological properties of normoxic polymer gel dosimeters. *Med Phys* 2005; **32**: 1047-1053 [PMID: 15895589 DOI: 10.1118/1.1881812]
 - 85 **Brown S**, Venning A, De Deene Y, Vial P, Oliver L, Adamovics J, Baldock C. Radiological properties of the PRESAGE and PAGAT polymer dosimeters. *Appl Radiat Isot* 2008; **66**: 1970-1974 [PMID: 18693028 DOI: 10.1016/j.apradiso.2008.06.005]
 - 86 **Crescenti RA**, Scheib SG, Schneider U, Gianolini S. Introducing gel dosimetry in a clinical environment: customization of polymer gel composition and magnetic resonance imaging parameters used for 3D dose verifications in radiosurgery and intensity modulated radiotherapy. *Med Phys* 2007; **34**: 1286-1297 [PMID: 17500460 DOI: 10.1118/1.2712042]
 - 87 **Babic S**, Battista J, Jordan K. Three-dimensional dose verification for intensity-modulated radiation therapy in the radiological physics centre head-and-neck phantom using optical computed tomography scans of ferrous xylenol-orange gel dosimeters. *Int J Radiat Oncol Biol Phys* 2008; **70**: 1281-1291 [PMID: 18313533 DOI: 10.1016/j.ijrobp.2007.11.032]
 - 88 **Watanabe Y**, Gopishankar N. Three-dimensional dosimetry of TomoTherapy by MRI-based polymer gel technique. *J Appl Clin Med Phys* 2010; **12**: 3273 [PMID: 21330972 DOI: 10.1120/jacmp.v12i1.3273]
 - 89 **Oldham M**, Thomas A, O'Daniel J, Juang T, Ibbott G, Adamovics J, Kirkpatrick JP. A quality assurance method that utilizes 3D dosimetry and facilitates clinical interpretation. *Int J Radiat Oncol Biol Phys* 2012; **84**: 540-546 [PMID: 22361085 DOI: 10.1016/j.ijrobp.2011.12.015]
 - 90 **Pavoni JF**, Pike TL, Snow J, DeWerd L, Baffa O. Tomotherapy dose distribution verification using MAGIC-f polymer gel dosimetry. *Med Phys* 2012; **39**: 2877-2884 [PMID: 22559660 DOI: 10.1118/1.4704496]
 - 91 **Skyt PS**, Petersen JB, Yates ES, Poulsen PR, Ravkilde TL, Balling P, Muren LP. Dosimetric verification of complex radiotherapy with a 3D optically based dosimetry system: dose painting and target tracking. *Acta Oncol* 2013; **52**: 1445-1450 [PMID: 23957684 DOI: 10.3109/0284186X.2013.813965]
 - 92 **Hayashi N**, Malmin RL, Watanabe Y. Dosimetric verification for intensity-modulated arc therapy plans by use of 2D diode array, radiochromic film and radiosensitive polymer gel. *J Radiat Res* 2014; **55**: 541-552 [PMID: 24449714 DOI: 10.1093/jrr/rrt139]
 - 93 **Jackson J**, Juang T, Adamovics J, Oldham M. An investigation of PRESAGE® 3D dosimetry for IMRT and VMAT radiation therapy treatment verification. *Phys Med Biol* 2015; **60**: 2217-2230 [PMID: 25683902 DOI: 10.1088/0031-9155/60/6/2217]
 - 94 **Cheng KY**, Hsieh LL, Shih CT. A Comprehensive Evaluation of NIPAM Polymer Gel Dosimeters on Three Orthogonal Planes and Temporal Stability Analysis. *PLoS One* 2016; **11**: e0155797 [PMID: 27192217 DOI: 10.1371/journal.pone.0155797]

P- Reviewer: Arisan V, Tomizawa M, Tsalafoutas IA **S- Editor:** Ji FF

L- Editor: A **E- Editor:** Li D



Retrospective Study

Reporting rotator cuff tears on magnetic resonance arthrography using the Snyder's arthroscopic classification

Alberto Aliprandi, Carmelo Messina, Paolo Arrigoni, Michele Bandirali, Giovanni Di Leo, Stefano Longo, Sandro Magnani, Chiara Mattiuz, Filippo Randelli, Silvana Sdao, Francesco Sardanelli, Luca Maria Sconfienza, Pietro Randelli

Alberto Aliprandi, Michele Bandirali, Giovanni Di Leo, Silvana Sdao, Francesco Sardanelli, Servizio di Radiologia, IRCCS Policlinico San Donato, 20097 San Donato Milanese, Italy

Carmelo Messina, Sandro Magnani, Chiara Mattiuz, Scuola di Specializzazione in Radiodiagnostica, Università degli Studi di Milano, 20122 Milano, Italy

Paolo Arrigoni, Unità Operativa di Ortopedia e Traumatologia II, IRCCS Policlinico San Donato, 20097 San Donato Milanese, Italy

Stefano Longo, Francesco Sardanelli, Luca Maria Sconfienza, Pietro Randelli, Dipartimento di Scienze Biomediche per la Salute, Università degli Studi di Milano, 20139 Milano, Italy

Filippo Randelli, Unità Operativa di Ortopedia e Traumatologia V, IRCCS Policlinico San Donato, 20097 San Donato Milanese, Italy

Luca Maria Sconfienza, Unità Operativa di Radiologia/Diagnostica per Immagini con Servizio di Radiologia Interventistica, IRCCS Istituto Ortopedico Galeazzi, 20161 Milano, Italy

Pietro Randelli, Unità Operativa Complessa, I Divisione, Istituto Ortopedico Gaetano Pini, 20122 Milano, Italy

Author contributions: Aliprandi A, Arrigoni P, Randelli F, Sardanelli F and Randelli P designed the research and substantially contributed to study conception; Messina C, Bandirali M, Magnani S, Mattiuz C and Sdao S acquired the data and performed the research; Di Leo G and Longo S contributed to study design and data interpretation/analysis; Messina C, Bandirali M, Magnani S, Mattiuz C and Sdao S drafted the article; Aliprandi A, Arrigoni P, Randelli F, Sardanelli F and Sconfienza LM made critical revision related to important content of the manuscript; all authors approved the final version of the manuscript to be published.

Institutional review board statement: The study was

reviewed and approved by the Comitato Etico ASL Milano Due Institutional Review Board.

Informed consent statement: Informed consent was waived from Institutional Review Board.

Conflict-of-interest statement: All authors declare no conflicts of interest.

Data sharing statement: Technical appendix, statistical code, and dataset available from the corresponding author at (io@lucasconfienza.it). Consent was not obtained but the presented data are anonymized and risk of identification is low.

Open-Access: This article is an open-access article which was selected by an in-house editor and fully peer-reviewed by external reviewers. It is distributed in accordance with the Creative Commons Attribution Non Commercial (CC BY-NC 4.0) license, which permits others to distribute, remix, adapt, build upon this work non-commercially, and license their derivative works on different terms, provided the original work is properly cited and the use is non-commercial. See: <http://creativecommons.org/licenses/by-nc/4.0/>

Manuscript source: Invited manuscript

Correspondence to: Dr. Luca Maria Sconfienza, Dipartimento di Scienze Biomediche per la Salute, Università degli Studi di Milano, Via Mangiagalli 31, 20139 Milano, Italy. io@lucasconfienza.it
Telephone: +39-02-66214497

Received: August 24, 2016

Peer-review started: August 24, 2016

First decision: October 20, 2016

Revised: December 12, 2016

Accepted: January 2, 2017

Article in press: January 3, 2017

Published online: March 28, 2017

Abstract

AIM

To determine diagnostic performance of magnetic resonance arthrography (MRA) in evaluating rotator cuff tears (RCTs) using Snyder's classification for reporting.

METHODS

One hundred and twenty-six patients (64 males, 62 females; median age 55 years) underwent shoulder MRA and arthroscopy, which represented our reference standard. Surgical arthroscopic reports were reviewed and the reported Snyder's classification was recorded. MRA examinations were evaluated by two independent radiologists (14 and 5 years' experience) using Snyder's classification system, blinded to arthroscopy. Agreement between arthroscopy and MRA on partial- and full-thickness tears was calculated, first regardless of their extent. Then, analysis took into account also the extent of the tear. Interobserver agreement was also calculated the quadratically-weighted Cohen kappa statistics.

RESULTS

On arthroscopy, 71/126 patients (56%) had a full-thickness RCT. The remaining 55/126 patients (44%) had a partial-thickness RCT. Regardless of tear extent, out of 71 patients with arthroscopically-confirmed full-thickness RCTs, 66 (93%) were correctly scored by both readers. All 55 patients with arthroscopic diagnosis of partial-thickness RCT were correctly assigned as having a partial-thickness RCT at MRA by both readers. Interobserver reproducibility analysis showed total agreement between the two readers in distinguishing partial-thickness from full-thickness RCTs, regardless of tear extent ($k = 1.000$). With regard to tear extent, in patients in whom a complete tear was correctly diagnosed, correct tear extent was detected in 61/66 cases (92%); in the remaining 5/66 cases (8%), tear extent was underestimated. Agreement was $k = 0.955$. Interobserver agreement was total ($k = 1.000$).

CONCLUSION

MRA shows high diagnostic accuracy and reproducibility in evaluating RCTs using the Snyder's classification for reporting. Snyder's classification may be adopted for routine reporting of MRA.

Key words: Arthroscopy; Magnetic resonance imaging; Shoulder; Arthrography; Supraspinatus tendon; Rotator cuff tear

© The Author(s) 2017. Published by Baishideng Publishing Group Inc. All rights reserved.

Core tip: In the present study we determined the diagnostic performance of magnetic resonance arthrography (MRA) in evaluating rotator cuff tears (RCTs) using Snyder's classification for reporting. One hundred and twenty-six patients underwent MRA and arthroscopy, which represented our reference standard. Agreement between arthroscopy and MRA on partial- and full-

thickness tears was calculated. Arthroscopy findings: 71/126 patients (56%) had a full-thickness RCTs, while 55/126 patients (44%) had a partial-thickness RCTs. MRA showed high diagnostic accuracy and reproducibility in evaluating RCTs using the Snyder's classification for reporting. Snyder's classification may be adopted for routine reporting of MRA.

Aliprandi A, Messina C, Arrigoni P, Bandirali M, Di Leo G, Longo S, Magnani S, Mattiuz C, Randelli F, Sdao S, Sardanelli F, Sconfienza LM, Randelli P. Reporting rotator cuff tears on magnetic resonance arthrography using the Snyder's arthroscopic classification. *World J Radiol* 2017; 9(3): 126-133 Available from: URL: <http://www.wjgnet.com/1949-8470/full/v9/i3/126.htm> DOI: <http://dx.doi.org/10.4329/wjr.v9.i3.126>

INTRODUCTION

The shoulder joint is a complex anatomic structure consisting of static and dynamic stabilizers, which confers functional stability and high degree of mobility at the same time^[1]. Rotator cuff (RC) acts as a dynamic stabilizer contributing to shoulder stability: It consists of four muscles (supraspinatus, subscapularis, infraspinatus and teres minor), which tendons fuse to form a continuous structure near their insertions. Together with long head of biceps tendon, RC tendons create an ideal configuration to actively compress the humeral head into the glenoid's cavity^[2]. Nevertheless, due to the glenohumeral joint high-grade of mobility, RC tears (RCTs) are commonly encountered, implying shoulder pain and dysfunction, often associated with loss of biomechanical balance and instability and subacromial impingement^[3,4]. The prevalence of full-thickness RCTs is almost 25% of individuals in their 60s and 50% of individuals in their 80s, with the supraspinatus being the most frequently involved tendon^[5].

Both ultrasound and magnetic resonance imaging (MRI) are accurate techniques in identifying shoulder pathologic conditions and RCTs^[6,7]. Magnetic resonance arthrography (MRA) has been shown to improve diagnostic performance of conventional MRI, as contrast material distends the joint capsule and outlines intra-articular structures; thus, MRA is particularly useful for RC partial-thickness tears as well as labrum and glenohumeral ligament tears and degeneration^[7,8].

Several orthopaedic classifications of RCTs were proposed throughout years. In 1934, Codman^[9] described the development of supraspinatus partial-thickness tears. In 1983, Neer^[10] classified RCTs into three progressive stages of impingement. In 1984, DeOrio and Cofield^[11] used the length of the greatest diameter of the tear to categorize the tear in four degrees. In 1990, Ellman^[12] further developed the classification of Neer, popularizing for the first time a system to classify partial thickness tears based on intra-operative findings. Recently, Davidson and Burkhart^[13] developed a geometric classification system

Table 1 Snyder's classification of rotator cuff tears

Location	
A	Articular side
B	Bursal side
C	Full-thickness tears, connecting A and B sides
Severity of partial tears (A and B side)	
0	Normal cuff, with smooth coverings of synovium and bursa
1	Minimal, superficial bursal or synovial irritation or slight capsular fraying in a small, localized area; usually < 1 cm
2	Actually fraying and failure of some rotator cuff fibres in addition to synovial, bursal, or capsular injury; usually < 2 cm
3	More severe rotator cuff injury, including fraying and fragmentation of tendons fibers, often involving the whole surface of a cuff tendon; usually < 3 cm
4	Very severe partial rotator cuff tear that usually contains, in addition to fraying and fragmentation of tendon tissue, a sizable flap tear and often encompasses more than a single tendon
Severity of complete tears (C)	
1	Small, complete tear, such as a puncture wound
2	Moderate tear, (usually < 2 cm) that still encompasses only one of the rotator cuff tendons with no retraction of the torn ends
3	Large, complete tear involving an entire tendon with minimal retraction of the torn edge; usually 3 to 4 cm
4	Massive rotator cuff tear involving two or more rotator cuff tendons, frequently with associated retraction and scarring of the remaining tendon

Modified from Millstein and Snyder^[16].

based on pre-operative (MRI)^[14]. At our institution, shoulder orthopaedic surgeons use the Snyder's arthroscopic classification of RCTs, which includes three parameters: The location of the lesion, the extent of the lesion, *i.e.*, partial-thickness or full-thickness - and the number of involved tendons (Table 1)^[15,16]. In particular, Snyder's classification separates RCTs into articular-sided, bursal-sided, and complete tears.

Despite many orthopaedic classifications, these never entered into radiological practice and radiologists still descriptively report tears of the RC^[17]. A recent study from Bosmans *et al*^[18] showed that, although radiology report remains an indispensable tool for medical practice, there is still a consistent percentage of referring physicians that remains unsatisfied with them. In fact, communication is a critical aspect when providing medical care, and a discrepancy in the language used between physicians (*i.e.*, radiologists and orthopaedic surgeons) may not convey the correct message and generate confusion^[19]. Thus, the aim of our study was to evaluate the diagnostic performance of MRA in evaluating RCTs using the Snyder's classification system for reporting MRA findings, having arthroscopy as reference standard.

MATERIALS AND METHODS

Study population and design

This retrospective study was reviewed and approved by the Institutional Review Board (Comitato Etico ASL Milano Due) and patients' informed consent was waived. Between June 2006 and December 2013, a series of 1324 consecutive shoulder MRA were performed at our institution in patients presenting with pain and functional limitation of the shoulder. From this database, we selected all patients who underwent arthroscopic surgery at our Institution, for a total of 126 patients (64 males and 62 females; age range 15-79 years; median age 55

years; 25th-75th percentile 38-63 years). Inclusion criteria for the study were: (1) MRA performed at our Institution following a standardised protocol; and (2) surgery performed at our Institution.

MRA - ultrasound-guided intra-articular injection of contrast material

Intra-articular injection of contrast agent was performed under ultrasound-guidance using a high frequency probe with anterior approach, as described by Sconfienza *et al*^[20] and Messina *et al*^[21]. Patients were positioned supine with the shoulder under investigation slightly extra-rotated, with the arm outstretched along the body. After careful skin disinfection, a 19-G needle was introduced in the joint and contrast material was injected. The procedure ended after injection of up to 20 mL of 0.0025 mmol/mL of gadoterate meglumine (Gd-DOTA, Dotarem pre-filled syringes; Guerbet, Paris, France). After injection, patient's arm was gently intra and extra-rotated for better contrast distribution into the joint capsule.

MRA - image acquisition

MRA was performed within 10 min from contrast agent injection using a 1.5-T system (Magnetom Sonata Maestro Class, Siemens Medical Solution, Erlangen, Germany) equipped with a 40 mT/m gradient power and a dedicated phased-array surface coil. The following imaging protocol was acquired: 3 plane (axial, coronal oblique and sagittal oblique) turbo spin-echo T1-weighted fat-saturated sequences (TR/TE = 763/15 ms; slice thickness = 4 mm; FOV = 190 mm × 190 mm; matrix = 256 × 256); oblique coronal turbo spin-echo T2-weighted fat-saturated sequences (TR/TE = 4000/74 ms; slice thickness = 4 mm with 0.8-mm interslice gap; FOV = 240 mm × 240 mm; matrix = 256 × 256); three-dimensional dual echo steady state (3D-DESS, TR/TE = 17/6 ms, slice thickness = 0.8 mm, voxel = 0.8 mm × 0.8

Table 2 Adaptation to magnetic resonance arthrography of arthroscopic Snyder's classification of rotator cuff partial tears

Lesion's grade	Severity of partial tears (A or B lesion)
1	Subtle irregularities of the tendon surface with preserved thickness
2	Major irregularities of the tendon surface with preserved thickness
3	Lesions involve less than 50% of tendon diameter and lesion extension is less than 3 cm
4	Lesions involve more than 50% of tendon's diameter with an extension of more than 3 cm or the lesion involves two tendons

A: Articular side; B: Bursal side.

Table 3 Distribution of lesion severity degree on articular and bursal sides of 55 patients with a partial rotator cuff tear at the arthroscopic assessment

		Articular side tear				
		A0	A1	A2	A3	A4
Bursal side tear	B0	-	1	1	2	1
	B1	3	8	0	0	0
	B2	4	5	5	3	1
	B3	0	0	1	5	2
	B4	0	0	0	1	12

A: Articular side; B: Bursal side.

mm × 0.8 mm).

Imaging evaluation and RCTs classification

As a pilot attempt to classify RCTs using Snyder's classification, in the present study we only considered RCTs involving the supraspinatus tendon. The Snyder's arthroscopic classification (Table 1) was used as reference for evaluating complete tears. For partial-thickness tears, the Snyder's classification was modified according to what reported in Table 2. Images were reviewed by two independent radiologists with 14 (reader 1) and 5 years' (reader 2) experience in musculoskeletal MRA, respectively, blinded to arthroscopic findings.

Surgical classification of RCTs

Arthroscopy was performed by one of three orthopaedic surgeons with 5 to 17 years' experience in shoulder arthroscopy. Surgical reports were reviewed and the reported Snyder's classification was recorded.

Statistical analysis

For analysis of lesion extent accuracy, data obtained by the most experienced reader (reader 1) was used and compared to reference standard. We calculated first the agreement between arthroscopy and MRA on partial- and full-thickness tears, regardless of their extent. Then, we performed a deeper analysis taking into account also the extent of the tear, still separately for partial- and full-thickness tears. Interobserver agreement was also calculated the quadratically-weighted Cohen kappa statistics was used.

RESULTS**Reference standard**

Arthroscopy was performed after a median of 137 d

Table 4 Data regarding the 5 patients with a complete tear at the reference standard assigned with a partial score at the magnetic resonance arthrography by the most experienced reader (reader 1)

Reader 1		Reference standard
Articular side	Bursal side	Complete tear
A 2	B 1	C 1
A 3	B 4	C 1
A 2	B 3	C 1
A 4	B 4	C 1
A 4	B 4	C 1

A: Articular side; B: Bursal side.

from MRA (25th-75th percentile 72-211 d). At arthroscopic assessment, 71/126 patients (56%) had a full-thickness RCT with different severity grade: C1, $n = 27$; C2, $n = 25$; C3, $n = 15$; C4, $n = 4$. The remaining 55/126 patients (44%) had a partial-thickness RCT. Distribution of the articular and bursal location of the tear is reported in Table 3 according to the most experienced reader (reader 1).

Accuracy vs the reference standard regardless of tear extent

Out of 71 patients with arthroscopically-confirmed full-thickness RCTs, 66 (93%) were correctly scored by both readers; in the remaining 5 patients (7%), both readers assigned a partial-thickness tear instead of a full-thickness tear. Table 4 shows data about the 5 patients with a complete tear at arthroscopy who were assigned with a partial score by the most experienced reader (reader 1). Figures 1-3 show MRA findings and corresponding arthroscopic confirmation.

All 55 patients with arthroscopic diagnosis of partial-thickness tear were correctly assigned as having a partial-thickness tear at MRA by both readers (Figure 3).

Interobserver reproducibility analysis showed total agreement between the two readers in distinguishing partial-thickness from full-thickness RCTs, regardless of tear extent ($k = 1.000$).

Accuracy vs the reference standard considering tear extent

In patients in whom a complete tear was correctly diagnosed, correct tear extent was detected in 61/66 cases (92%); in the remaining 5/66 cases (8%), tear extent was underestimated, as both readers assigned C1 instead of C2. Agreement with arthroscopy was $k = 0.955$.

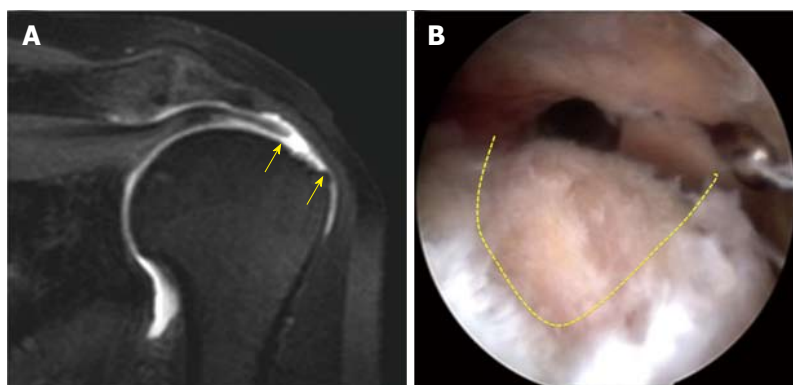


Figure 1 Magnetic resonance arthrography of a C2 lesion of the supraspinatus tendon. A: MRA, coronal TSE T1w fat sat. Full tear with fiber retraction of supraspinatus tendon. Yellow arrows show the bare area of foot print lesion (C2 lesion according to Snyder classification); B: Arthroscopic view. Dotted line shows the crescent shape lesion. MRA: Magnetic resonance arthrography.

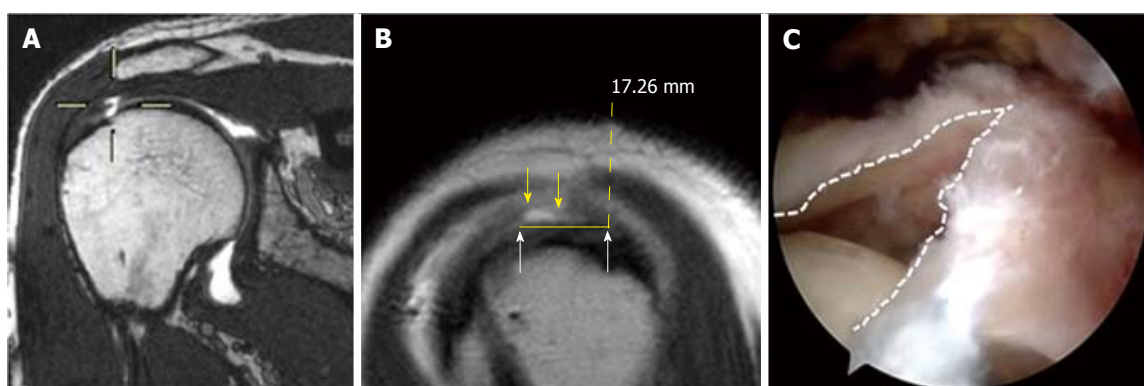


Figure 2 Magnetic resonance arthrography of a C1 tear of the supraspinatus tendon. A: MRA coronal, double echo steady state. Viewfinder shows the hyperintense signal in supraspinatus tendon, expression of full tear (C1 lesion according to Snyder classification); B: MRA Sagittal TSE T1w. Yellow arrows show the full tear (C1 lesion according to Snyder classification). White arrows show the degenerative tendon matrix, later removed by the surgeon; C: Arthroscopic view. White dotted line show a full, V-shape, tear of supraspinatus tendon completed to C2 according to Snyder classification by the surgeon. MRA: Magnetic resonance arthrography.

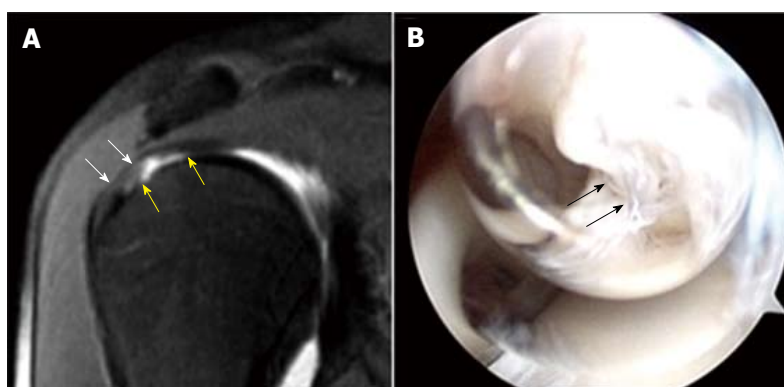


Figure 3 Magnetic resonance arthrography and arthroscopy of an A4 tear of the supraspinatus tendon. A: MRA, coronal TSE T1w fat sat. The yellow arrows show the articular asymmetric profile, expression of erosion and partial tear of supraspinatus tendon (A4 lesion according to Snyder classification). White arrows show the regular bursal profile; B: Arthroscopic view. The black arrows show the mangy and flap of supraspinatus tendon. MAR: Magnetic resonance arthrography.

Interobserver agreement was total ($k = 1.000$).

In 55 patients in whom a partial-thickness tear was diagnosed, agreement in terms of tear extent was $k = 0.878$ for the articular side and $k = 0.837$ for the bursal side, respectively. Full data are reported in Tables 5 and 6, respectively. Regarding interobserver agreement, the two readers disagreed at maximum for 1 degree

for either articular or bursal side of the supraspinatus tendon, with $k = 0.947$ and $k = 0.969$, respectively.

DISCUSSION

When managing a patient affected with a RCT, both clinical and imaging evaluation play a crucial role^[22].

Table 5 Data on agreement of the severity degree assigned on the articular side for partial tear between magnetic resonance arthrography (according to the most experienced reader) and arthroscopy

		Reader 1				
		A0	A1	A2	A3	A4
Arthroscopy	A0	7	0	0	0	0
	A1	8	6	0	0	0
	A2	2	2	3	0	0
	A3	0	0	4	7	0
	A4	0	0	0	8	8

Quadratically weighted Cohen kappa = 0.878. A: Articular side.

The role of diagnostic imaging is to help in the choice between surgical or nonsurgical treatment. Ultrasound, unenhanced MR and MRA have become the most common imaging techniques by which a RCT is diagnosed. Ultrasound is as accurate as unenhanced MR, but MRA remains the most sensitive and specific technique and is generally performed in cases in which ultrasound and unenhanced MR are not definitive^[7].

The use of a common RCTs classification by radiologists and orthopaedists may allow for a more direct comparison, leading to better clinical diagnosis and letting the patient to decide a treatment option with clearer information. Snyder proposed a classification system for the evaluation of RCTs measuring both their extent and number of tendons involved, providing indications for surgery or conservative treatment on the basis of the obtained score^[16]. In the present study we adopted the Snyder's classification as it was already successfully used by orthopaedics surgeons at our Institution, as a tentative to achieve a better communication with them.

In our study we found a high agreement in diagnosing RCTs for both radiologists having arthroscopy as reference standards. These results are in line with what is already reported in a recent systematic review about the accuracy of MRA in diagnosing RCTs using conventional descriptive reporting systems^[23]. Moreover, we found a very high interobserver reproducibility between the two readers, with a perfect agreement for full-thickness RCTs; regarding partial-thickness RCTs, the two readers rarely disagreed. This means that also the less experienced reader showed a very good diagnostic performance. As a consequence, we can think that the Snyder's classification system may have a value also when used in reporting MRA, even though originally created for arthroscopy.

A deeper analysis of the results showed that radiologists tend to underestimate the damage of the tendon, for both full-thickness and partial-thickness RCTs. This data deserves some considerations. The margins of a tendon tear are usually made by degenerated tendon matrix. During arthroscopy, the orthopaedic surgeon debrides the degenerated area to have more consistent margins for repair^[24]. Thus, final evaluation of tear extent by the orthopaedic surgeon may be larger compared to

Table 6 Data on agreement of the severity degree assigned on the bursal side for partial lesions between magnetic resonance arthrography and arthroscopic assessment

		Reader 1				
		B0	B1	B2	B3	B4
Arthroscopy	B0	5	0	0	0	0
	B1	7	4	0	0	0
	B2	4	7	7	0	0
	B3	0	0	3	5	0
	B4	0	0	0	3	10

Quadratically weighted Cohen kappa = 0.837. B: Bursal side.

what previously seen on MRA.

Regarding partial-thickness RCTs, reproducibility of MRA is still high but lower than for full-thickness RCTs. This was expected, as it is known that both MRI and MRA have higher performance in assessing the full-thickness RCTs rather than partial-thickness RCTs^[25-27]. However, the difference between the radiologist and the arthroscopy was only 1 degree in the majority of cases and 2 degrees in a few patients: These discrepancies are expected to not affect significantly the patients' management^[28]. Moreover, similarly to what happens for full-thickness RCTs, the radiologist always tends to underestimate the lesion degree of partial RCTs. Again, the main reason for this underestimation may be related to the fact that partial-tear tendon debridement procedure could be performed by the surgeon on wider area of the tendon, with a consequent extension of the Snyder's arthroscopic score^[28]. Overall, we should also consider the time elapsed from MRA to surgery (median delay 137 d) which could represent a factor for progression of mild damage of the tendon. It is known that tendon injuries, if left untreated, can progress by determining the transition from small partial injury to a greater degree and from partial to complete tears^[29].

This study has some limitations. First, it was performed retrospectively. Second, arthroscopy was performed by several orthopaedic surgeons with different experience in RCTs repair. Thus, certain degree of variability in RCTs scoring at the reference standard may be expected and may have slightly influenced our results. The same can be said for the delay between MRA and arthroscopy, which limited the reliability of the reference standard. In fact, the median delay of 137 d between MRA and arthroscopy could be seen as a long time between the two exams; nevertheless, this kind of delays may be common in everyday hospital practice, as patients usually attempt conservative treatments before undergoing surgery.

In conclusion, our study demonstrates high reproducibility of MRA in evaluating RCTs using the Snyder's classification as a method for reporting. This allows to conclude that not only MRA but also the Snyder's classification has an intrinsic high diagnostic value. Even though originally created for arthroscopy, Snyder's classification is well suitable and may be adopted for routine reporting of

MRA.

COMMENTS

Background

The shoulder joint is a complex anatomic structure consisting of static and dynamic stabilizers, which confers functional stability and high degree of mobility at the same time. Rotator cuff acts as a dynamic stabilizer contributing to shoulder stability. Rotator cuff tears (RCTs) are commonly encountered, implying shoulder pain and dysfunction, often associated with loss of biomechanical balance and instability and subacromial impingement.

Research frontiers

Magnetic resonance arthrography (MRA) is particularly useful for rotator cuff partial-thickness tears as well as labrum and glenohumeral ligament tears and degeneration. Several orthopaedic classifications of RCTs were proposed throughout years; At the authors' institution, shoulder orthopaedic surgeons use the Snyder's arthroscopic classification of RCTs, which includes three parameters: The location of the lesion, the extent of the lesion - and the number of involved tendons.

Innovations and breakthroughs

Despite many orthopaedic classifications, these never entered into radiological practice and radiologists still descriptively report tears of the RC, with referring physicians that may remains unsatisfied with them. The authors evaluated the diagnostic performance of MRA in evaluating RCTs using the Snyder's classification system for reporting MRA findings, evaluating its accuracy using arthroscopy as reference standard.

Applications

MRA showed high diagnostic accuracy and reproducibility in evaluating RCTs using the Snyder's classification for reporting. Snyder's classification may be adopted for routine reporting of MRA.

Terminology

MRA is an examination of magnetic resonance imaging that is performed after the injection of contrast material (gadolinium) into the joint, with the aim to increase its diagnostic performance. RCTs may involve the articular or bursal side, and can be classified as partial or complete according to thickness tendon involvement.

Peer-review

The authors evaluate the diagnostic performance of MRA in evaluating RCTs using the Snyder's classification system for reporting MRA findings, evaluating its accuracy using arthroscopy as reference standard. They demonstrated high reproducibility of MRA in evaluating RCTs using the Snyder's classification as a method for reporting.

REFERENCES

- Huegel J, Williams AA, Soslowsky LJ. Rotator cuff biology and biomechanics: a review of normal and pathological conditions. *Curr Rheumatol Rep* 2015; **17**: 476 [PMID: 25475598 DOI: 10.1007/s11926-014-0476-x]
- Longo UG, Berton A, Papapietro N, Maffulli N, Denaro V. Biomechanics of the rotator cuff: European perspective [Internet]. In: Rotator Cuff Tear. 2011. [cited 2016 Aug 17]. Available from: URL: <http://www.ncbi.nlm.nih.gov/pubmed/21986041>
- Gombera MM, Sekiya JK. Rotator cuff tear and glenohumeral instability : a systematic review. *Clin Orthop Relat Res* 2014; **472**: 2448-2456 [PMID: 24043432 DOI: 10.1007/s11999-013-3290-2]
- Longo S, Corradi A, Michielon G, Sardanelli F, Sconfienza LM. Ultrasound evaluation of the subacromial space in healthy subjects performing three different positions of shoulder abduction in both loaded and unloaded conditions. *Phys Ther Sport* 2016 Aug 12; Epub ahead of print [PMID: 27776926 DOI: 10.1016/j.ptsp.2016.08.007]
- Tashjian RZ. Epidemiology, natural history, and indications for treatment of rotator cuff tears. *Clin Sports Med* 2012; **31**: 589-604 [PMID: 23040548 DOI: 10.1016/j.csm.2012.07.001]
- Corazza A, Orlandi D, Fabbro E, Ferrero G, Messina C, Sartoris R, Perugin Bernardi S, Arcidiacono A, Silvestri E, Sconfienza LM. Dynamic high-resolution ultrasound of the shoulder: how we do it. *Eur J Radiol* 2015; **84**: 266-277 [PMID: 25466650 DOI: 10.1016/j.ejrad.2014.11.007]
- de Jesus JO, Parker L, Frangos AJ, Nazarian LN. Accuracy of MRI, MR arthrography, and ultrasound in the diagnosis of rotator cuff tears: a meta-analysis. *AJR Am J Roentgenol* 2009; **192**: 1701-1707 [PMID: 19457838 DOI: 10.2214/AJR.08.1241]
- Hodler J, Kursunoglu-Brahme S, Snyder SJ, Cervilla V, Karzel RP, Schweitzer ME, Flannigan BD, Resnick D. Rotator cuff disease: assessment with MR arthrography versus standard MR imaging in 36 patients with arthroscopic confirmation. *Radiology* 1992; **182**: 431-436 [PMID: 1489363 DOI: 10.1148/radiology.182.2.1489363]
- Codman EA. The shoulder: rupture of the supraspinatus tendon and other lesions in or about the subacromial bursa. Boston, United States: Thomas Todd, 1934: 123-177
- Neer CS. Impingement lesions. *Clin Orthop Relat Res* 1983; **(173)**: 70-77 [PMID: 6825348 DOI: 10.1097/00003086-198303000-00010]
- DeOrio JK, Cofield RH. Results of a second attempt at surgical repair of a failed initial rotator-cuff repair. *J Bone Joint Surg Am* 1984; **66**: 563-567 [PMID: 6707035 DOI: 10.2106/00004623-198466040-00011]
- Ellman H. Diagnosis and treatment of incomplete rotator cuff tears. *Clin Orthop Relat Res* 1990; **(254)**: 64-74 [PMID: 2182260 DOI: 10.1097/00003086-199005000-00010]
- Davidson J, Burkhart SS. The geometric classification of rotator cuff tears: a system linking tear pattern to treatment and prognosis. *Arthroscopy* 2010; **26**: 417-424 [PMID: 20206053 DOI: 10.1016/j.arthro.2009.07.009]
- Sconfienza LM, Orlandi D, Fabbro E, Ferrero G, Martini C, Savarino E, Silvestri E. Ultrasound assessment of the rotator cuff cable: comparison between young and elderly asymptomatic volunteers and interobserver reproducibility. *Ultrasound Med Biol* 2012; **38**: 35-41 [PMID: 22104526 DOI: 10.1016/j.ultrasmedbio.2011.10.010]
- Snyder S. Arthroscopic classification of rotator cuff lesions and surgical decision making. In: Wilkins LW. Philadelphia: Shoulder Arthroscopy, 2003: 201-207
- Millstein ES, Snyder SJ. Arthroscopic management of partial, full-thickness, and complex rotator cuff tears: indications, techniques, and complications. *Arthroscopy* 2003; **19** Suppl 1: 189-199 [PMID: 14673438 DOI: 10.1016/j.arthro.2003.10.033]
- Robertson PL, Schweitzer ME, Mitchell DG, Schlesinger F, Epstein RE, Frieman BG, Fenlin JM. Rotator cuff disorders: interobserver and intraobserver variation in diagnosis with MR imaging. *Radiology* 1995; **194**: 831-835 [PMID: 7862988 DOI: 10.1148/radiology.194.3.7862988]
- Bosmans JM, Weyler JJ, De Schepper AM, Parizel PM. The radiology report as seen by radiologists and referring clinicians: results of the COVER and ROVER surveys. *Radiology* 2011; **259**: 184-195 [PMID: 21224423 DOI: 10.1148/radiol.10101045]
- Larson DB, Froehle CM, Johnson ND, Towbin AJ. Communication in diagnostic radiology: meeting the challenges of complexity. *AJR Am J Roentgenol* 2014; **203**: 957-964 [PMID: 25341133 DOI: 10.2214/AJR.14.12949]
- Sconfienza LM, Serafini G, Silvestri E. Ultrasound-guided musculoskeletal procedures - the upper limb. Milan, Italy: Springer-Verlag Mailand, 2012
- Messina C, Banfi G, Aliprandi A, Mauri G, Secchi F, Sardanelli F, Sconfienza LM. Ultrasound guidance to perform intra-articular injection of gadolinium-based contrast material for magnetic resonance arthrography as an alternative to fluoroscopy: the time is now. *Eur Radiol* 2016; **26**: 1221-1225 [PMID: 26253260 DOI: 10.1007/s00330-015-3945-3]
- Lansdown DA, Feeley BT. Evaluation and treatment of rotator

- cuff tears. *Phys Sportsmed* 2012; **40**: 73-86 [PMID: 22759608 DOI: 10.3810/psm.2012.05.1967]
- 23 **Lenza M**, Buchbinder R, Takwoingi Y, Johnston RV, Hanchard NC, Faloppa F. Magnetic resonance imaging, magnetic resonance arthrography and ultrasonography for assessing rotator cuff tears in people with shoulder pain for whom surgery is being considered. *Cochrane Database Syst Rev* 2013; (9): CD009020 [PMID: 24065456 DOI: 10.1002/14651858.CD009020.pub2]
 - 24 **Castagna A**, Borroni M, Garofalo R, Rose GD, Cesari E, Padua R, Conti M, Gumina S. Deep partial rotator cuff tear: transtendon repair or tear completion and repair? A randomized clinical trial. *Knee Surg Sports Traumatol Arthrosc* 2015; **23**: 460-463 [PMID: 23689964 DOI: 10.1007/s00167-013-2536-6]
 - 25 **Aliprandi A**, Sdao S, Cannaò PM, Khattak YJ, Longo S, Sconfienza LM, Sardanelli F. Imaging of shoulder pain in overhead throwing athletes. *Sport Sci Health* 2013; **9**: 81-88 [DOI: 10.1007/s11332-013-0151-z]
 - 26 **Waldt S**, Bruegel M, Mueller D, Holzapfel K, Imhoff AB, Rummeny EJ, Woertler K. Rotator cuff tears: assessment with MR arthrography in 275 patients with arthroscopic correlation. *Eur Radiol* 2007; **17**: 491-498 [PMID: 16969638 DOI: 10.1007/s00330-006-0370-7]
 - 27 **Magee T**, Shapiro M, Williams D. Comparison of high-field-strength versus low-field-strength MRI of the shoulder. *AJR Am J Roentgenol* 2003; **181**: 1211-1215 [PMID: 14573405 DOI: 10.2214/ajr.181.5.1811211]
 - 28 **Fukuda H**. The management of partial-thickness tears of the rotator cuff. *J Bone Joint Surg Br* 2003; **85**: 3-11 [PMID: 12585570 DOI: 10.1302/0301-620X.85B1.13846]
 - 29 **Yamanaka K**, Matsumoto T. The joint side tear of the rotator cuff. A followup study by arthrography. *Clin Orthop Relat Res* 1994; (304): 68-73 [PMID: 8020236]

P- Reviewer: Gao BL, Li YZ **S- Editor:** Gong XM **L- Editor:** A
E- Editor: Li D



Observational Study

Multimodality imaging using proton magnetic resonance spectroscopic imaging and ^{18}F -fluorodeoxyglucose-positron emission tomography in local prostate cancer

Amita Shukla-Dave, Cecilia Wassberg, Darko Pucar, Heiko Schöder, Debra A Goldman, Yousef Mazaheri, Victor E Reuter, James Eastham, Peter T Scardino, Hedvig Hricak

Amita Shukla-Dave, Heiko Schöder, Yousef Mazaheri, Hedvig Hricak, Department of Radiology, Memorial Sloan-Kettering Cancer Center, New York, NY 10065, United States

Amita Shukla-Dave, Yousef Mazaheri, Department of Medical Physics, Memorial Sloan-Kettering Cancer Center, New York, NY 10065, United States

Cecilia Wassberg, Department of Diagnostic Radiology, Karolinska University Hospital, 17176 Solna, Sweden

Darko Pucar, Department of Radiology, Augusta University, Augusta, GA 30912, United States

Debra A Goldman, Department of Epidemiology-Biostatistics, Memorial Sloan-Kettering Cancer Center, New York, NY 10065, United States

Victor E Reuter, Department of Pathology, Memorial Sloan-Kettering Cancer Center, New York, NY 10065, United States

James Eastham, Peter T Scardino, Department of Urology, Memorial Sloan-Kettering Cancer Center, New York, NY 10065, United States

Author contributions: Shukla-Dave A, Wassberg C, Pucar D, Schöder H, Mazaheri Y and Hricak H designed the study, performed MRI and PET research, analyzed the data and wrote the paper; Goldman DA performed the statistical analysis; Reuter VE performed the pathology assessment for the study; Eastham J and Scardino PT enrolled patients, and performed clinical assessment as per standard of care; all authors reviewed the final manuscript.

Supported by National Institutes of Health grant, No. #R01 CA76423; and in part through the NIH/NCI Cancer Center Support grant, No. P30 CA008748.

Institutional review board statement: Our study was compliant with the Health Insurance Portability and Accountability Act. Twenty-two patients who were referred from the Urology

department for endorectal MRI/MRSI examinations and ^{18}F -FDG-PET/CT and then underwent prostatectomy as primary or salvage treatment were included in the study.

Informed consent statement: Patient data were collected and handled in accordance with institutional and federal guidelines.

Conflict-of-interest statement: All authors have no conflicts of interest with regard to this manuscript.

Data sharing statement: Upon formal request and with proper motivation, all original data in anonymized format is available from the corresponding author for local inspection, but cannot leave Memorial Sloan Kettering Cancer Center.

Open-Access: This article is an open-access article which was selected by an in-house editor and fully peer-reviewed by external reviewers. It is distributed in accordance with the Creative Commons Attribution Non Commercial (CC BY-NC 4.0) license, which permits others to distribute, remix, adapt, build upon this work non-commercially, and license their derivative works on different terms, provided the original work is properly cited and the use is non-commercial. See: <http://creativecommons.org/licenses/by-nc/4.0/>

Manuscript source: Invited manuscript

Correspondence to: Amita Shukla-Dave, PhD, Department of Medical Physics, Memorial Sloan-Kettering Cancer Center, 1275 York Avenue, New York, NY 10065, United States. davea@mskcc.org
Telephone: +1-212-6393184
Fax: +1-212-7173010

Received: October 31, 2016

Peer-review started: November 2, 2016

First decision: December 15, 2016

Revised: December 22, 2016

Accepted: January 11, 2017

Article in press: January 14, 2017

Published online: March 28, 2017

Abstract

AIM

To assess the relationship using multimodality imaging between intermediary citrate/choline metabolism as seen on proton magnetic resonance spectroscopic imaging (^1H -MRSI) and glycolysis as observed on ^{18}F -fluorodeoxyglucose positron emission tomography/computed tomography (^{18}F -FDG-PET/CT) in prostate cancer (PCa) patients.

METHODS

The study included 22 patients with local PCa who were referred for endorectal magnetic resonance imaging/ ^1H -MRSI (April 2002 to July 2007) and ^{18}F -FDG-PET/CT and then underwent prostatectomy as primary or salvage treatment. Whole-mount step-section pathology was used as the standard of reference. We assessed the relationships between PET parameters [standardized uptake value (SUVmax and SUVmean)] and MRSI parameters [choline + creatine/citrate (CC/Cmax and CC/Cmean) and total number of suspicious voxels] using spearman's rank correlation, and the relationships of PET and ^1H -MRSI index lesion parameters to surgical Gleason score.

RESULTS

Abnormal intermediary metabolism on ^1H -MRSI was present in 21/22 patients, while abnormal glycolysis on ^{18}F -FDG-PET/CT was detected in only 3/22 patients. Specifically, index tumor localization rates were 0.95 (95%CI: 0.77-1.00) for ^1H -MRSI and 0.14 (95%CI: 0.03-0.35) for ^{18}F -FDG-PET/CT. Spearman rank correlations indicated little relationship ($\rho = -0.36$ -0.28) between ^1H -MRSI parameters and ^{18}F -FDG-PET/CT parameters. Both the total number of suspicious voxels ($\rho = 0.55$, $P = 0.0099$) and the SUVmax ($\rho = 0.46$, $P = 0.0366$) correlated weakly with the Gleason score. No significant relationship was found between the CC/Cmax, CC/Cmean or SUVmean and the Gleason score ($P = 0.15$ -0.79).

CONCLUSION

The concentration of intermediary metabolites detected by ^1H MRSI and glycolytic flux measured ^{18}F -FDG PET show little correlation. Furthermore, only few tumors were FDG avid on PET, possibly because increased glycolysis represents a late and rather ominous event in the progression of PCa.

Key words: Proton magnetic resonance spectroscopic imaging; ^{18}F -fluorodeoxyglucose-positron emission tomography; Prostate cancer

© The Author(s) 2017. Published by Baishideng Publishing Group Inc. All rights reserved.

Core tip: Although metabolic imaging is increasingly utilized in prostate cancer (PCa), the mechanisms leading to cancer-related metabolic rearrangements and consequent imaging findings remain poorly understood. This

study compared two modalities utilizing distinct metabolic pathways, proton magnetic resonance spectroscopic imaging (^1H -MRSI) and ^{18}F -fluorodeoxyglucose positron emission tomography/computed tomography (^{18}F -FDG-PET/CT), in local PCa. Abnormal intermediary metabolism on ^1H -MRSI was present in 21/22 patients, while abnormal glycolysis on ^{18}F -FDG-PET/CT was detected in only 3/22 patients. This study provides an insight why metabolic PET agents promising for detection of PCa target intermediary metabolism. On the other hand, elevated glycolysis may have ominous prognostic implications in PCa.

Shukla-Dave A, Wassberg C, Pucar D, Schöder H, Goldman DA, Mazaheri Y, Reuter VE, Eastham J, Scardino PT, Hricak H. Multimodality imaging using proton magnetic resonance spectroscopic imaging and ^{18}F -fluorodeoxyglucose-positron emission tomography in local prostate cancer. *World J Radiol* 2017; 9(3): 134-142 Available from: URL: <http://www.wjgnet.com/1949-8470/full/v9/i3/134.htm> DOI: <http://dx.doi.org/10.4329/wjrv.9.i3.134>

INTRODUCTION

Multimodality imaging is performed in patients with cancer to understand metabolism, however the mechanisms leading to metabolic rearrangements remains poorly understood. By decoding the connections between cancer signaling and metabolism, it may be possible to better understand the clinical implications of imaging findings and develop new imaging strategies.

In patients with prostate cancer (PCa), two key functional imaging modalities, proton magnetic resonance spectroscopic imaging (^1H -MRSI) and ^{18}F -fluorodeoxyglucose positron emission tomography/computed tomography (^{18}F -FDG-PET/CT), are used to identify cancer-induced changes in cellular metabolism^[1-3]. On ^1H -MRSI, decreased levels of citrate (a Krebs cycle and fatty acid synthesis intermediate) and polyamines (amino acid metabolism intermediates) and elevated choline (a precursor of membrane synthesis) are a signature of PCa^[2,4-7]. On ^{18}F -FDG-PET, increased glucose uptake by glucose transporters and glucose phosphorylation to glucose-6-phosphate by hexokinase are used for identifying PCa and other cancers^[3,8]. The indications for ^1H -MRSI and ^{18}F -FDG-PET/CT examinations in patients with PCa are very different^[9,10]. ^1H -MRSI adds incremental value to standard prostate magnetic resonance imaging (MRI) in the detection of primary or recurrent loco-regional PCa and in the evaluation of its aggressiveness (Gleason Grade)^[9-14]. ^1H -MRSI can also be used prior to treatment to predict biochemical relapse of PCa after radical prostatectomy or the presence of insignificant PCa^[14-17]. In contrast, ^{18}F -FDG-PET/CT is not recommended for the detection and initial evaluation of PCa or detection of early recurrence. Various other PET agents, such as ^{18}F - or ^{11}C -labeled choline or acetate, several various amino acids, and agents binding to the

transmembrane PSMA molecule are available for this purpose^[18-24]. ¹⁸F-FDG plays a role in the characterization of advanced metastatic PCa^[8,25]. The clinical significance of the current study lies in exploring the use of multimodality imaging in local PCa. In this study, we wanted to explore the relationship using multimodality imaging between concentrations of intermediary metabolites citrate and choline, measured by ¹H-MRSI, and glycolysis as noted on ¹⁸F-FDG PET/CT in local PCa.

MATERIALS AND METHODS

Patient demographics

Our study was compliant with the Health Insurance Portability and Accountability Act. Patient data were collected and handled in accordance with institutional and federal guidelines. Twenty-two patients who were referred from the Urology department for endorectal MRI/MRSI examinations (April 2002 to July 2007) and ¹⁸F-FDG-PET/CT and then underwent prostatectomy as primary or salvage treatment were included in the study. Whole-mount step-section pathology of the surgical specimen was available for all the patients. Of the 22 patients, 11 were imaged before treatment while 11 were imaged after external beam radiation therapy. The institutional review board approved our retrospective review of multimodality imaging using MRI/MRSI and ¹⁸F-FDG-PET/CT studies, pathology data (from surgical pathology), and clinical follow-up data and waived the informed consent requirement. The mean time between the MRSI and PET exams was 11 ± 37 d (\pm SD).

Endorectal MRI/MRSI data acquisition and processing

Data were acquired on a 1.5-Tesla GE Signa Horizon scanner. MRI was done using a pelvic phased-array coil and an expandable endorectal coil; T1- and T2-weighted spin-echo MR images were obtained using a previously described standard prostate imaging protocol (total time, approximately 30 min)^[4]. MR image acquisition was followed by a standard MRSI protocol with point-resolved spectroscopic voxel excitation and water and lipid suppression (total time, 17 min) in a voxel array and the SI dimension zero filled to 16 slices (3-mm resolution) with a voxel size of 0.12 to 0.16 cm³^[4]. MRSI data were overlaid on the corresponding T2-weighted images, including the raw spectra and the metabolic ratio [choline + creatine to citrate (CC/C)]^[4]. Tumors were identified by dedicated radiologists with > 5 years of experience in prostate imaging.

¹H-MRSI data interpretation

An MRI physicist with > 10 years of experience in prostate MRSI retrospectively interpreted the ¹H-MRSI studies using established metabolic criteria for the evaluation of PCa in the peripheral and transition zones^[6,14,26,27]. The physicist, who was blinded to clinical data and surgical pathology, recorded the location and total number of suspicious voxels (tumor volume estimation), maximum

(max) CC/C, and mean CC/C for the index lesion^[6,14,26,27].

¹⁸F-FDG-PET/CT data acquisition and processing

Details of the ¹⁸F-FDG-PET/CT imaging procedure have been described previously^[28]. Briefly, a low-dose CT scan (120-140 kV, approximately 80 mA), which is used for attenuation correction of PET emission images as well as for anatomic localization of PET abnormalities, was acquired first. This was followed by acquisition of PET emission images of the lower pelvis including of the prostate for 5 min per bed position. Images were reconstructed using iterative algorithms with average slice thickness of 3 mm and a 128 × 128 matrix size. Patients were scanned in the supine position. Before the examination, patients fasted for at least 6 h, but liberal intake of water was allowed. Patients were injected intravenously with 444-555 MBq of ¹⁸F-FDG and a PET/CT scan started after an uptake period of approximately 60 min. Plasma glucose level was < 200 mg at the time of imaging in all patients.

¹⁸F-FDG-PET/CT data interpretation

All ¹⁸F-FDG-PET/CT data were available for retrospective review on a standard clinical workstation (PACS with Advance Work Station extension; General Electric). One board-certified radiologist/nuclear medicine physician, who had > 10 years of experience in PET and > 5 years of experience in prostate imaging, reviewed the ¹⁸F-FDG-PET/CT studies. PET images were analyzed in three orthogonal planes (transaxial, coronal, sagittal) both visually and quantitatively. For quantitative PET analysis, maximum standardized uptake value (SUVmax) and average SUV (SUVmean) of the index lesion were determined using a Volume of Interest with 40% threshold of SUVmax. All SUVs were normalized to body weight.

Pathology

Whole-mount transverse serial sections of the prostate were prepared as described previously^[29]. The distal 5-mm portion of the apex was amputated and coned. The remainder of the gland was serially sectioned from the apex to the base at 3-4-mm intervals and submitted in its entirety for paraffin-embedded whole mounts. Cancer foci were outlined in ink on whole-mount, apical, and seminal vesicle sections and photographed. The photographs constituted the tumor maps. The primary and secondary Gleason grades as well as the pathologic tumor node stage were also determined. The index lesion was identified in all cases as the tumor with the largest volume. Tissue sections stained with H and E were examined by one uro-pathologist blinded to imaging and clinical data.

Matching of MRI/MRSI data, ¹⁸F-FDG-PET/CT and pathology data

The matching of imaging and pathology for the index lesion was performed in consensus by two dually-boarded radiologists/nuclear medicine physicians with

Table 1 Patient characteristics

		<i>n</i> (%)
Clinical stage ¹	T1c	10 (45.5)
	T2a	4 (18.2)
	T2b	4 (18.2)
	T2c	1 (4.5)
	T3	1 (4.5)
	T3a	2 (9.1)
Biopsy Gleason score	0 + 0	1 (4.5)
	3 + 3	3 (13.6)
	3 + 4	5 (22.7)
	4 + 3	5 (22.7)
	4 + 4	4 (18.2)
	4 + 5	4 (18.2)
Pathology stage	pT2a	3 (13.6)
	pT2b	5 (22.7)
	pT3a	7 (31.8)
	pT3b	6 (27.3)
	pT4	1 (4.5)
	Not Graded ²	1 (4.5)
Pathology Gleason score	3 + 3	1 (4.5)
	3 + 4	8 (36.4)
	4 + 3	4 (18.2)
	4 + 4	4 (18.2)
	4 + 5	3 (13.6)
	5 + 4	1 (4.5)
Prior radiation treatment	EBRT	11 (50)
	Untreated	11 (50)

¹Clinical stage was determined prior to primary or salvage surgery; ²One index tumor was not graded due to treatment effect. EBRT: External beam radiation therapy.

> 5 years and > 15 years of experience in prostate imaging. The histopathologic axial step sections were visually matched with corresponding axial T2-weighted transverse MR images with superimposed MRSI data and fused ¹⁸F-FDG PET/CT data with a precision of ± 1 slice based on established anatomic landmarks^[12]. Because the spectroscopic data were acquired in the same position and with the same gradients as the imaging data, registration of the spectroscopic data with the T2-weighted images was automatic, and the spectroscopic data could be compared with the most closely corresponding histopathologic step section.

Statistical analysis

Clinical and pathological characteristics were described using medians and ranges for continuous variables and frequencies and percents or proportions for categorical variables. Gleason grades were summed into Gleason scores of 6, 7, 8 or 9.

The localization rates of ¹⁸F-FDG-PET/CT and ¹H-MRSI were calculated along with exact 95% confidence intervals. The relationships between PET parameters (SUVmax and SUVmean) and MRSI parameters (CC/Cmax, CC/Cmean, Total # Voxels) were assessed using Spearman's rank correlation and graphically displayed with scatter plots and 95% confidence bands. Additionally, the relationships of PET and MRSI parameters to surgical Gleason score were assessed with Spearman's rank

correlation and, given the Gleason score's ordinal nature, graphically illustrated with box plots. *P*-values less than 0.05 were considered statistically significant. All analyses were done using SAS 9.4 (The SAS Institute, Cary, NC).

RESULTS

Patient characteristics are summarized in Table 1. The patients had a median age of 58 years (range: 47-70 years) and median PSA of 4.81 ng/mL (range: 0.11-96.53 ng/mL).

Index tumor localization rates were 0.95 (95%CI: 0.77-1.00) for ¹H-MRSI and 0.14 (95%CI: 0.03-0.35) for ¹⁸F-FDG-PET/CT, with 21 out of 22 index tumors found on pathology identified on ¹H-MRSI and only 3 of those 21 index lesions identified on ¹⁸F-FDG-PET/CT. Figure 1 shows ¹H-MRSI, ¹⁸F-FDG-PET/CT and whole-mount step-section pathology from a patient in whom the tumor seen at pathology was observed by multimodality imaging. Figure 2 shows ¹H-MRSI, ¹⁸F-FDG-PET/CT and whole-mount step-section pathology from a patient in whom the tumor seen at pathology was observed by ¹H-MRSI only. In the 3 patients with positive PET findings, the total tumor volumes measured by PET were 10.9, 11.1 and 10.4 cc and the SUVmax values were 3.3, 3.5 and 4.5. On ¹H-MRSI in the 21 positive patients, CC/Cmax (median 6.4, range: 0.5-37.4), CC/Cmean (median 2.0, range: 0.5-18.5) and number of suspicious voxels (median 9.0, range 2-32) showed more profound alterations for all patients. Both the scatter plots (Figure 3 and Table 2) and the Spearman rank correlations indicated little relationship between ¹H-MRSI parameters and ¹⁸F-FDG-PET/CT. Spearman's ρ ranged between -0.362 and 0.28 (*P*-values range: 0.10-0.66). No clear pattern of association was detected in the graphs.

Gleason scores ranged from 6 (8/22, 36%) to 9 (4/22, 18.1%) with one patient lacking a score due to treatment effect. This patient was excluded from further analysis. Both the total number of voxels ($\rho = 0.55$, *P* = 0.0099) and the SUVmax ($\rho = 0.46$, *P* = 0.0366) correlated with the Gleason score. No significant relationship was found between the CC/Cmax, CC/Cmean or SUVmean and the Gleason score (*P* = 0.15-0.79, Table 3). The box plots demonstrate an upward trend for total number of voxels and SUVmax with each subsequent Gleason score (Figure 4).

DISCUSSION

Multimodality imaging in PCa detection on ¹H-MRSI is based on the detection of decreased citrate and polyamines with elevated choline^[2,4]. This is reflected in the high CC/Cmax (median 9.0) and CC/Cmean (median: 2.0) for the prostate index lesions. On ¹⁸F-FDG-PET/CT, PCa is identified based on increased glucose uptake by glucose transporters (GLUT) and glucose phosphorylation to glucose-6-phosphate by hexokinase^[3,8]. The present study adds to the literature for patients with local or loco-regional primary or recurrent PCa and shows that the

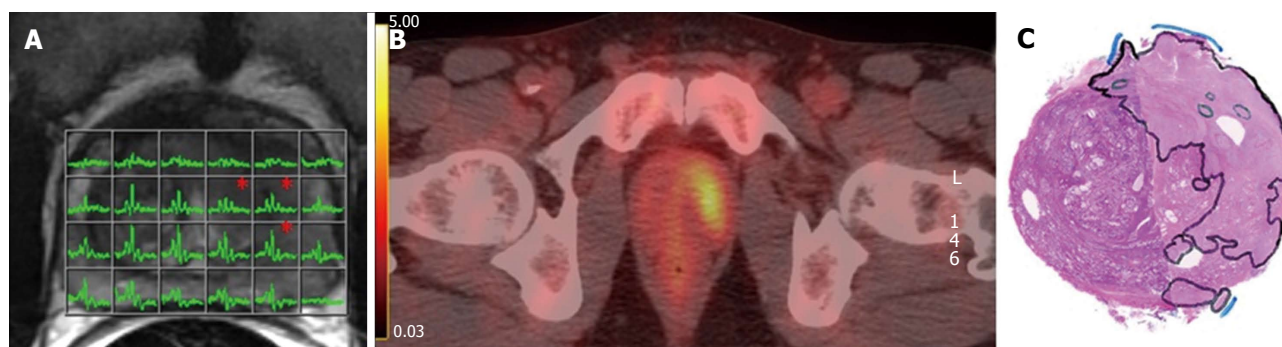


Figure 1 Representative 1.5T magnetic resonance imaging/magnetic resonance spectroscopic imaging in a 58-year-old patient with prostate specific antigen 96.53 ng/mL, clinical stage T3 and surgical Gleason score 4 + 5. A: Axial T2-weighted image and overlaid point-resolved spectroscopic box indicating excitation region selected and 3D MRSI demonstrating three suspicious voxels marked with asterisks; B: ^{18}F -FDG-PET/CT fusion image shows a focal uptake in the left prostate; C: Whole-mount step-section histopathology after radical prostatectomy shows a large cancer in the left prostate. MRSI: Magnetic resonance spectroscopic imaging; ^{18}F -FDG-PET/CT: ^{18}F -fluorodeoxyglucose positron emission tomography/computed tomography.

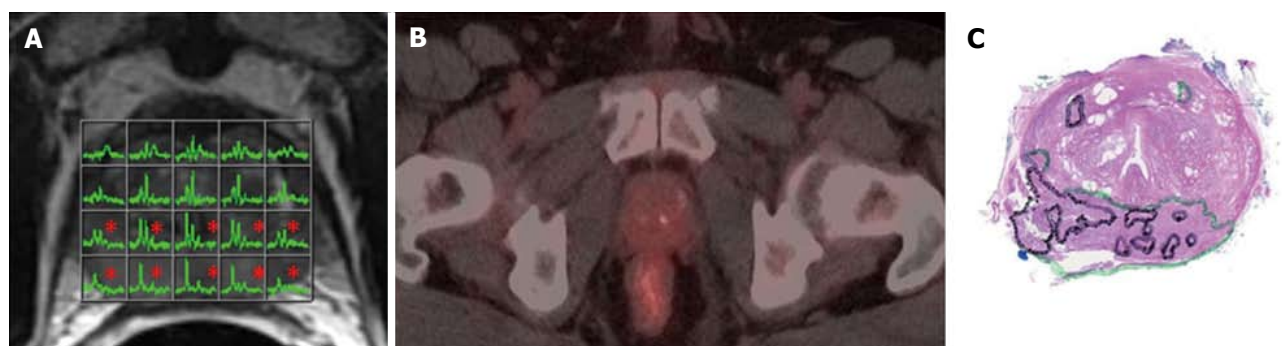


Figure 2 Representative 1.5T magnetic resonance imaging/magnetic resonance spectroscopic imaging in a 64-year-old patient with prostate specific antigen 4.9 ng/mL, clinical stage T3 and surgical Gleason score 4 + 3. A: Axial T2-weighted image and overlaid point-resolved spectroscopic box indicating excitation region selected and 3D MRSI demonstrating ten suspicious voxels marked with asterisks; B: ^{18}F -FDG-PET/CT fusion image shows no focal uptake in the prostate; C: Whole-mount step-section histopathology after radical prostatectomy shows a large cancer extending from medial to right side of the prostate. MRSI: Magnetic resonance spectroscopic imaging; ^{18}F -FDG-PET/CT: ^{18}F -fluorodeoxyglucose positron emission tomography/computed tomography.

Table 2 Spearman correlations between proton magnetic resonance spectroscopic imaging and ^{18}F -fluorodeoxyglucose data ($n = 22$)

^1H -MRSI	^{18}F -FDG	Rho (ρ)	P-value
CC/Cmax	SUVmax	-0.281	0.21
	SUVmean	-0.101	0.66
CC/Cmean	SUVmax	-0.362	0.10
	SUVmean	-0.158	0.48
Total # Voxels	SUVmax	0.2565	0.25
	SUVmean	0.2783	0.21

^1H -MRSI: Proton magnetic resonance spectroscopic imaging; ^{18}F -FDG: ^{18}F -fluorodeoxyglucose.

Table 3 Spearman correlations between proton magnetic resonance spectroscopic imaging and ^{18}F -fluorodeoxyglucose data and surgical Gleason score ($n = 22$)

^{18}F -FDG/ ^1H -MRSI	With Gleason score	
	Rho (ρ)	P-value
CC/Cmax	0.2165	0.35
CC/Cmean	0.0624	0.79
Total # Voxels	0.5493	0.0099
SUVmean	0.3225	0.15
SUVmax	0.4584	0.0366

^1H -MRSI: Proton magnetic resonance spectroscopic imaging; ^{18}F -FDG: ^{18}F -fluorodeoxyglucose.

citrate decrease in PCa was both much more frequent and pronounced than was the elevation in ^{18}F -FDG uptake. This is in-line with the known low sensitivity of ^{18}F -FDG-PET/CT for detecting localized primary PCa. Further research is needed to develop a clearer understanding of the underlying genomic and metabolic mechanisms and to confirm whether metabolic alterations progress stepwise from early abnormalities in citrate metabolism to late abnormalities in glucose metabolism. Since our

patients were imaged at only one time point, the data appear consistent with this understanding. Improved understanding of PCa metabolism could help in determining the most appropriate imaging modalities (including imaging with radiotracers) for different clinical stages of PCa and possibly also in identifying and monitoring novel targeted therapies.

For instance, according to the "bioenergetic theory of prostate malignancy"^[1,17], the normal prostate produces

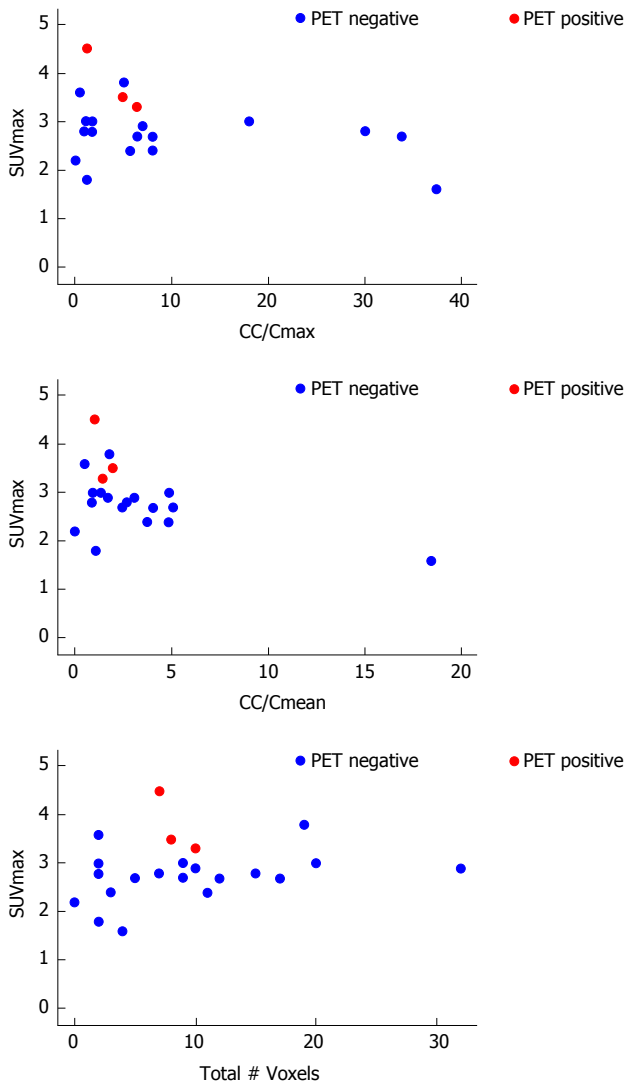


Figure 3 Scatter plots demonstrating the relationships between proton magnetic resonance spectroscopic imaging and ^{18}F -fluorodeoxyglucose positron emission tomography parameters ($n = 22$). PET: Positron emission tomography.

and secretes an enormous amount of citrate; this is achieved by zinc-induced inhibition of m-aconitase, a Krebs cycle enzyme that converts citrate to isocitrate. With this truncated Krebs cycle, the normal prostate sacrifices ATP production for citrate secretion^[17]. Conversely, in PCa, down-regulation of multiple membrane zinc transporters and zinc decline lead to activation of the full Krebs cycle, oxidation and a consequent decrease in intracellular and secreted citrate and increase in ATP production supporting malignancy^[30-32]. However, the decline of citrate in PCa could also be related to its conversion to AcCoA by cytosolic ATP citrate lyase (ACLY) and subsequent utilization for fatty acid synthesis^[30,33,34]. Activation of ACLY seems to be critical for biosynthesis and growth in various cancer models^[30,34]. Thus, based on this bioenergetic theory, two possible scenarios could explain the low ^{18}F -FDG uptake in early, slow-growing PCa: (1) early PCa exhibits only a mildly increased

cellular energy demand that is matched by activation of the mitochondrial Krebs cycle (bioenergetic mode); or (2) early PCa exhibits an unchanged energy demand and retains a persistently truncated Krebs cycle, but it diverts cytosolic citrate from secretion to fatty acid synthesis (biosynthetic mode).

Biochemical alterations in PCa may be linked to signaling pathways implicated in PCa initiation and progression. For example, the PTEN/PI-3-Kinase pathway, one of the central pathways in early PCa, is closely linked to cellular metabolism^[35]. PTEN tumor suppressor loss, with subsequent activation of the PI-3-Kinase pathway and downstream effectors such as AKT and mTOR^[36,37], has anabolic effects leading to increased glucose and amino acid uptake for the purposes of protein, fatty acid, and membrane synthesis, as well as the expression and membrane localization of glucose transporters^[38]. Other consequences of PTEN loss include hexokinase translocation to the mitochondrial membrane^[39], FA synthesis *via* ACLY^[40,41], steroid hormone-dependent FA synthesis^[42], glycogen synthesis, membrane localization of amino-acid transporters, amino-acid uptake, and protein synthesis^[43]. Other signaling alterations that typically occur later in PCa progression may also eventually upregulate glycolysis. Loss of p53, for example, is associated with increased glycolysis through GLUT3 expression^[44]. We therefore summarize the following: In early PCa, citrate is diverted from secretion to AKT-dependent FA synthesis and/or to zinc-deficiency-induced oxidation in the Krebs cycle, leading to a decline in citrate signal on ^1H -MRSI. While AKT-dependent stimulation of glycolysis alone is insufficient to produce a detectable increase in ^{18}F -FDG uptake in PCa, the subsequent loss of p53 further promotes glycolysis, resulting in a detectable difference in ^{18}F -FDG uptake between PCa and normal prostate tissue. We are hoping that future studies which include genomic and proteomic tissue analysis, may eventually link tumor biology and imaging in PCa. Such links have been made in other studies. For instance, the extent of changes in intermediary metabolism on ^1H -MRSI has been shown to correlate with the Gleason grade^[14]. Similarly, risk scoring based on metabolic changes on ^1H -MRSI has been found to correlate with treatment outcome in patients with high-risk PCa who underwent neoadjuvant chemotherapy/hormone therapy before radical prostatectomy or radiation therapy^[15]. Conversely, near-normal intermediary metabolism on pre-treatment ^1H -MRSI has been found to predict very-low-risk PCa in radical prostatectomy specimens^[16].

Certain PET tracers are superior to ^{18}F -FDG in detecting early PCa and early recurrence after radical prostatectomy or radiation therapy^[18-24]. In contrast, in the most-advanced form of PCa, castration-resistant disease, ^{18}F -FDG-PET/CT is predictive of survival^[28,45], supporting the statement that increased glycolysis represents a late and ominous event in the progression of PCa. Of note, ^{18}F -FDG-PET/CT has been established as predictive of outcome in multiple other cancers, with high ^{18}F -FDG avidity predicting poor outcome^[46-49]. The present study

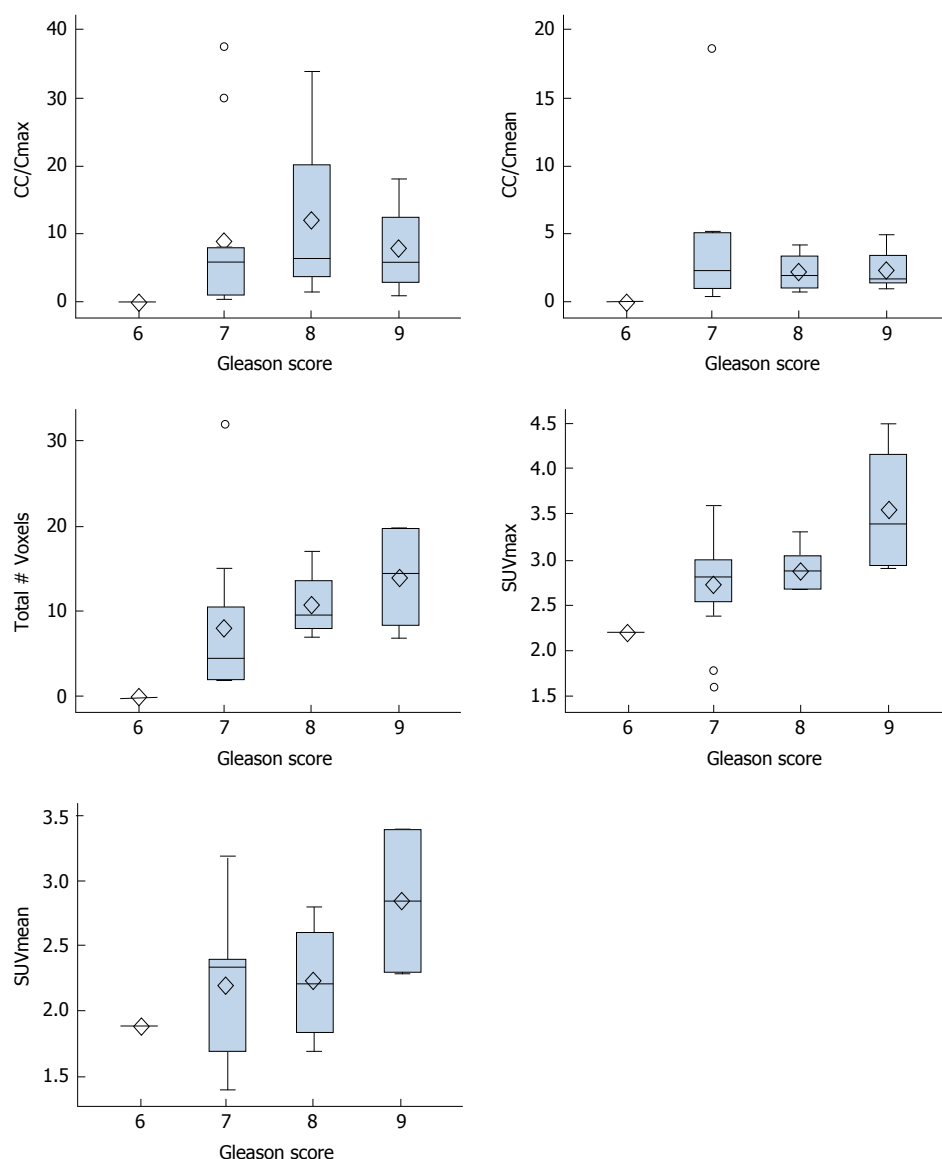


Figure 4 Box plots demonstrating the relationships between surgical Gleason score and imaging parameters ($n = 22$).

has a few limitations given its retrospective study design and the fact that we could not control for treatment. Also, due to a low sample size, it was not feasible to estimate survival. However, this study met its purpose of exploring the relationship using multimodality imaging between ^1H -MRSI and ^{18}F -FDG-PET/CT in PCa patients. To optimize PCa multimodality imaging, it is critical to understand how different metabolic imaging techniques interact and how they can be used to develop the most effective imaging protocols.

The present study suggests that the concentration of intermediary metabolites detected by ^1H MRSI and glycolytic flux measured ^{18}F -FDG PET show little correlation. Furthermore, only few tumors were FDG avid on PET, possibly because increased glycolysis represents a late and rather ominous event in the progression of PCa.

ACKNOWLEDGMENTS

The authors thank Ada Muellner, MS for editing the manuscript.

COMMENTS

Background

Although metabolic imaging is increasingly utilized in prostate cancer (PCa), the mechanisms leading to cancer-related metabolic rearrangements and consequent imaging findings remain poorly understood. The aim of the study was to better understand the sequence of metabolic changes in localized PCa.

Research frontiers

To optimize PCa multimodality imaging, it is critical to understand how different metabolic imaging techniques interact and how they can be used to develop the most effective imaging protocols.

Innovations and breakthroughs

Comparison of proton magnetic resonance spectroscopic imaging (^1H -MRSI) and ^{18}F -fluorodeoxyglucose positron emission tomography/computed tomography (^{18}F -FDG-PET/CT) findings in local PCa demonstrated that abnormal choline intermediary metabolism on ^1H -MRSI precedes the changes in glycolysis on ^{18}F -FDG-PET/CT.

Applications

In principle, imaging analysis of distinct metabolic pathways in PCa can be utilized to predict patient outcome, optimize management, and plan future

diagnostic and therapeutic trials in PCa.

Terminology

¹H-MRSI: Proton magnetic resonance spectroscopic imaging; ¹⁸F-FDG-PET: ¹⁸F-FDG-positron emission tomography; PCa: Prostate cancer.

Peer-review

The topic is actual and interesting.

REFERENCES

- Costello LC, Franklin RB. Citrate metabolism of normal and malignant prostate epithelial cells. *Urology* 1997; **50**: 3-12 [PMID: 9218011 DOI: 10.1016/S0090-4295(97)00124-6]
- Kurhanewicz J, Vigneron DB, Hricak H, Narayan P, Carroll P, Nelson SJ. Three-dimensional H-1 MR spectroscopic imaging of the in situ human prostate with high (0.24-0.7-cm3) spatial resolution. *Radiology* 1996; **198**: 795-805 [PMID: 8628874]
- Schöder H, Larson SM. Positron emission tomography for prostate, bladder, and renal cancer. *Semin Nucl Med* 2004; **34**: 274-292 [PMID: 15493005]
- Shukla-Dave A, Hricak H, Moskowitz C, Ishill N, Akin O, Kuroiwa K, Spector J, Kumar M, Reuter VE, Koutcher JA, Zakian KL. Detection of prostate cancer with MR spectroscopic imaging: an expanded paradigm incorporating polyamines. *Radiology* 2007; **245**: 499-506 [PMID: 17890357 DOI: 10.1148/radiol.2452062201]
- Swanson MG, Vigneron DB, Tabatabai ZL, Males RG, Schmitt L, Carroll PR, James JK, Hurd RE, Kurhanewicz J. Proton HR-MAS spectroscopic and quantitative pathologic analysis of MRI/3D-MRSI-targeted postsurgical prostate tissues. *Magn Reson Med* 2003; **50**: 944-954 [PMID: 14587005]
- Mazaheri Y, Shukla-Dave A, Muellner A, Hricak H. MRI of the prostate: clinical relevance and emerging applications. *J Magn Reson Imaging* 2011; **33**: 258-274 [PMID: 21274967 DOI: 10.1002/jmri.22420]
- Sciarra A, Barents J, Bjartell A, Eastham J, Hricak H, Panebianco V, Witjes JA. Advances in magnetic resonance imaging: how they are changing the management of prostate cancer. *Eur Urol* 2011; **59**: 962-977 [PMID: 21367519 DOI: 10.1016/j.eururo.2011.02.034]
- Schöder H, Herrmann K, Gönen M, Hricak H, Eberhardt S, Scardino P, Scher HI, Larson SM. 2-[¹⁸F]fluoro-2-deoxyglucose positron emission tomography for the detection of disease in patients with prostate-specific antigen relapse after radical prostatectomy. *Clin Cancer Res* 2005; **11**: 4761-4769 [PMID: 16000572 DOI: 10.1158/1078-0432.CCR-05-0249]
- Hricak H, Choyke PL, Eberhardt SC, Leibel SA, Scardino PT. Imaging prostate cancer: a multidisciplinary perspective. *Radiology* 2007; **243**: 28-53 [PMID: 17392247]
- Pucar D, Sella T, Schöder H. The role of imaging in the detection of prostate cancer local recurrence after radiation therapy and surgery. *Curr Opin Urol* 2008; **18**: 87-97 [PMID: 18090496]
- Yu KK, Scheidler J, Hricak H, Vigneron DB, Zaloudek CJ, Males RG, Nelson SJ, Carroll PR, Kurhanewicz J. Prostate cancer: prediction of extracapsular extension with endorectal MR imaging and three-dimensional proton MR spectroscopic imaging. *Radiology* 1999; **213**: 481-488 [PMID: 10551230 DOI: 10.1148/radiology.213.2.r99nv26481]
- Pucar D, Shukla-Dave A, Hricak H, Moskowitz CS, Kuroiwa K, Olgac S, Eboria LE, Scardino PT, Koutcher JA, Zakian KL. Prostate cancer: correlation of MR imaging and MR spectroscopic with pathologic findings after radiation therapy-initial experience. *Radiology* 2005; **236**: 545-553 [PMID: 15972335 DOI: 10.1148/radiol.2362040739]
- Wefer AE, Hricak H, Vigneron DB, Coakley FV, Lu Y, Wefer J, Mueller-Lisse U, Carroll PR, Kurhanewicz J. Sextant localization of prostate cancer: comparison of sextant biopsy, magnetic resonance imaging and magnetic resonance spectroscopic imaging with step section histology. *J Urol* 2000; **164**: 400-404 [PMID: 10893595]
- Zakian KL, Sircar K, Hricak H, Chen HN, Shukla-Dave A, Eberhardt S, Muruganandham M, Eboria L, Kattan MW, Reuter VE, Scardino PT, Koutcher JA. Correlation of proton MR spectroscopic imaging with gleason score based on step-section pathologic analysis after radical prostatectomy. *Radiology* 2005; **234**: 804-814 [PMID: 15734935 DOI: 10.1148/radiol.2343040363]
- Pucar D, Koutcher JA, Shah A, Dyke JP, Schwartz L, Thaler H, Kurhanewicz J, Scardino PT, Kelly WK, Hricak H, Zakian KL. Preliminary assessment of magnetic resonance spectroscopic imaging in predicting treatment outcome in patients with prostate cancer at high risk for relapse. *Clin Prostate Cancer* 2004; **3**: 174-181 [PMID: 15636684]
- Shukla-Dave A, Hricak H, Kattan MW, Pucar D, Kuroiwa K, Chen HN, Spector J, Koutcher JA, Zakian KL, Scardino PT. The utility of magnetic resonance imaging and spectroscopic for predicting insignificant prostate cancer: an initial analysis. *BJU Int* 2007; **99**: 786-793 [PMID: 17223922]
- Costello LC, Franklin RB. The clinical relevance of the metabolism of prostate cancer; zinc and tumor suppression: connecting the dots. *Mol Cancer* 2006; **5**: 17 [PMID: 16700911]
- Breeuwsma AJ, Rybalov M, Leliveld AM, Pruim J, de Jong IJ. Correlation of [¹¹C]choline PET-CT with time to treatment and disease-specific survival in men with recurrent prostate cancer after radical prostatectomy. *Q J Nucl Med Mol Imaging* 2012; **56**: 440-446 [PMID: 23069923]
- Giovacchini G, Picchio M, Garcia-Parra R, Briganti A, Abdollah F, Gianolli L, Schindler C, Montorsi F, Messa C, Fazio F. ¹¹C-choline PET/CT predicts prostate cancer-specific survival in patients with biochemical failure during androgen-deprivation therapy. *J Nucl Med* 2014; **55**: 233-241 [PMID: 24408897 DOI: 10.2967/jnumed.113.123380]
- Kwee SA, Lim J, Watanabe A, Kromer-Baker K, Coel MN. Prognosis Related to Metastatic Burden Measured by ¹⁸F-Fluorocholine PET/CT in Castration-Resistant Prostate Cancer. *J Nucl Med* 2014; **55**: 905-910 [PMID: 24676753 DOI: 10.2967/jnumed.113.135194]
- Morris MJ, Scher HI. (¹¹C)-acetate PET imaging in prostate cancer. *Eur J Nucl Med Mol Imaging* 2007; **34**: 181-184 [PMID: 17238014 DOI: 10.1007/s00259-006-0281-5]
- Núñez R, Macapinlac HA, Yeung HW, Akhurst T, Cai S, Osman I, Gonen M, Riedel E, Scher HI, Larson SM. Combined ¹⁸F-FDG and ¹¹C-methionine PET scans in patients with newly progressive metastatic prostate cancer. *J Nucl Med* 2002; **43**: 46-55 [PMID: 11801702]
- Ren J, Yuan L, Wen G, Yang J. The value of anti-1-amino-3-¹⁸F-fluorocyclobutane-1-carboxylic acid PET/CT in the diagnosis of recurrent prostate carcinoma: a meta-analysis. *Acta Radiol* 2016; **57**: 487-493 [PMID: 25907118 DOI: 10.1177/0284185115581541]
- Turkbey B, Mena E, Shih J, Pinto PA, Merino MJ, Lindenberg ML, Bernardo M, McKinney YL, Adler S, Owenius R, Choyke PL, Kurdziel KA. Localized prostate cancer detection with ¹⁸F FACBC PET/CT: comparison with MR imaging and histopathologic analysis. *Radiology* 2014; **270**: 849-856 [PMID: 24475804 DOI: 10.1148/radiol.13130240]
- Cimitan M, Bortolus R, Morassut S, Canzonieri V, Garbeglio A, Baresic T, Borsatti E, Drigo A, Trovò MG. [¹⁸F]fluorocholine PET/CT imaging for the detection of recurrent prostate cancer at PSA relapse: experience in 100 consecutive patients. *Eur J Nucl Med Mol Imaging* 2006; **33**: 1387-1398 [PMID: 16865395]
- Shukla-Dave A, Hricak H, Eberhardt SC, Olgac S, Muruganandham M, Scardino PT, Reuter VE, Koutcher JA, Zakian KL. Chronic prostatitis: MR imaging and ¹H MR spectroscopic imaging findings--initial observations. *Radiology* 2004; **231**: 717-724 [PMID: 15163811 DOI: 10.1148/radiol.2313031391]
- Zakian KL, Eberhardt S, Hricak H, Shukla-Dave A, Kleinman S, Muruganandham M, Sircar K, Kattan MW, Reuter VE, Scardino PT, Koutcher JA. Transition zone prostate cancer: metabolic characteristics at ¹H MR spectroscopic imaging--initial results. *Radiology* 2003; **229**: 241-247 [PMID: 12920178]
- Meirelles GS, Schöder H, Ravizzini GC, Gönen M, Fox JJ, Humm J, Morris MJ, Scher HI, Larson SM. Prognostic value of baseline

- [18F] fluorodeoxyglucose positron emission tomography and 99mTc-MDP bone scan in progressing metastatic prostate cancer. *Clin Cancer Res* 2010; **16**: 6093-6099 [PMID: 20975102 DOI: 10.1158/1078-0432.CCR-10-1357]
- 29 **Aihara M**, Wheeler TM, Ohori M, Scardino PT. Heterogeneity of prostate cancer in radical prostatectomy specimens. *Urology* 1994; **43**: 60-66; discussion 66-67 [PMID: 8284886]
- 30 **Bauer DE**, Hatzivassiliou G, Zhao F, Andreadis C, Thompson CB. ATP citrate lyase is an important component of cell growth and transformation. *Oncogene* 2005; **24**: 6314-6322 [PMID: 16007201 DOI: 10.1038/sj.onc.1208773]
- 31 **Desouki MM**, Geradts J, Milon B, Franklin RB, Costello LC. hZip2 and hZip3 zinc transporters are down regulated in human prostate adenocarcinomatous glands. *Mol Cancer* 2007; **6**: 37 [PMID: 17550612 DOI: 10.1186/1476-4598-6-37]
- 32 **Franklin RB**, Feng P, Milon B, Desouki MM, Singh KK, Kajdacsy-Balla A, Bagasra O, Costello LC. hZIP1 zinc uptake transporter down regulation and zinc depletion in prostate cancer. *Mol Cancer* 2005; **4**: 32 [PMID: 16153295]
- 33 **Halliday KR**, Fenoglio-Preiser C, Sillerud LO. Differentiation of human tumors from nonmalignant tissue by natural-abundance ¹³C NMR spectroscopic. *Magn Reson Med* 1988; **7**: 384-411 [PMID: 2459580]
- 34 **Hatzivassiliou G**, Zhao F, Bauer DE, Andreadis C, Shaw AN, Dhanak D, Hingorani SR, Tuveson DA, Thompson CB. ATP citrate lyase inhibition can suppress tumor cell growth. *Cancer Cell* 2005; **8**: 311-321 [PMID: 16226706 DOI: 10.1016/j.ccr.2005.09.008]
- 35 **Trotman LC**, Niki M, Dotan ZA, Koutcher JA, Di Cristofano A, Xiao A, Khoo AS, Roy-Burman P, Greenberg NM, Van Dyke T, Cordon-Cardo C, Pandolfi PP. Pten dose dictates cancer progression in the prostate. *PLoS Biol* 2003; **1**: E59 [PMID: 14691534]
- 36 **Manning BD**, Cantley LC. AKT/PKB signaling: navigating downstream. *Cell* 2007; **129**: 1261-1274 [PMID: 17604717 DOI: 10.1016/j.cell.2007.06.009]
- 37 **Plas DR**, Thompson CB. Akt-dependent transformation: there is more to growth than just surviving. *Oncogene* 2005; **24**: 7435-7442 [PMID: 16288290 DOI: 10.1038/sj.onc.1209097]
- 38 **Calera MR**, Martinez C, Liu H, Jack AK, Birnbaum MJ, Pilch PF. Insulin increases the association of Akt-2 with Glut4-containing vesicles. *J Biol Chem* 1998; **273**: 7201-7204 [PMID: 9516411]
- 39 **Majewski N**, Nogueira V, Bhaskar P, Coy PE, Skeen JE, Gottlob K, Chandel NS, Thompson CB, Robey RB, Hay N. Hexokinase-mitochondria interaction mediated by Akt is required to inhibit apoptosis in the presence or absence of Bax and Bak. *Mol Cell* 2004; **16**: 819-830 [PMID: 15574336 DOI: 10.1016/j.molcel.2004.11.014]
- 40 **Berwick DC**, Hers I, Heesom KJ, Moule SK, Tavaré JM. The identification of ATP-citrate lyase as a protein kinase B (Akt) substrate in primary adipocytes. *J Biol Chem* 2002; **277**: 33895-33900 [PMID: 12107176 DOI: 10.1074/jbc.M204681200]
- 41 **Pierce MW**, Palmer JL, Keutmann HT, Hall TA, Avruch J. The insulin-directed phosphorylation site on ATP-citrate lyase is identical with the site phosphorylated by the cAMP-dependent protein kinase in vitro. *J Biol Chem* 1982; **257**: 10681-10686 [PMID: 6286669]
- 42 **Bandyopadhyay S**, Pai SK, Watabe M, Gross SC, Hirota S, Hosobe S, Tsukada T, Miura K, Saito K, Markwell SJ, Wang Y, Huggenvik J, Pauza ME, Iiizumi M, Watabe K. FAS expression inversely correlates with PTEN level in prostate cancer and a PI 3-kinase inhibitor synergizes with FAS siRNA to induce apoptosis. *Oncogene* 2005; **24**: 5389-5395 [PMID: 15897909 DOI: 10.1038/sj.onc.1208555]
- 43 **Edinger AL**, Thompson CB. Akt maintains cell size and survival by increasing mTOR-dependent nutrient uptake. *Mol Biol Cell* 2002; **13**: 2276-2288 [PMID: 12134068 DOI: 10.1091/mbc.01-12-0584]
- 44 **Kawauchi K**, Araki K, Tobiume K, Tanaka N. p53 regulates glucose metabolism through an IKK-NF-kappaB pathway and inhibits cell transformation. *Nat Cell Biol* 2008; **10**: 611-618 [PMID: 18391940 DOI: 10.1038/ncb1724]
- 45 **Morris MJ**, Akhurst T, Larson SM, Ditullio M, Chu E, Siedlecki K, Verbel D, Heller G, Kelly WK, Slovin S, Schwartz L, Scher HI. Fluorodeoxyglucose positron emission tomography as an outcome measure for castrate metastatic prostate cancer treated with antimicrotubule chemotherapy. *Clin Cancer Res* 2005; **11**: 3210-3216 [PMID: 15867215 DOI: 10.1158/1078-0432.CCR-04-2034]
- 46 **Bahri H**, Laurence L, Edeline J, Leghzi H, Devillers A, Raoul JL, Cuggia M, Mesbah H, Clement B, Boucher E, Garin E. High prognostic value of 18F-FDG PET for metastatic gastroenteropancreatic neuroendocrine tumors: a long-term evaluation. *J Nucl Med* 2014; **55**: 1786-1790 [PMID: 25286923 DOI: 10.2967/jnumed.114.144386]
- 47 **Binderup T**, Knigge U, Loft A, Federspiel B, Kjaer A. 18F-fluorodeoxyglucose positron emission tomography predicts survival of patients with neuroendocrine tumors. *Clin Cancer Res* 2010; **16**: 978-985 [PMID: 20103666 DOI: 10.1158/1078-0432.CCR-09-1759]
- 48 **Noy A**, Schöder H, Gönen M, Weissler M, Ertelt K, Cohler C, Portlock C, Hamlin P, Yeung HW. The majority of transformed lymphomas have high standardized uptake values (SUVs) on positron emission tomography (PET) scanning similar to diffuse large B-cell lymphoma (DLBCL). *Ann Oncol* 2009; **20**: 508-512 [PMID: 19139176 DOI: 10.1093/annonc/mdn657]
- 49 **Robbins RJ**, Wan Q, Grewal RK, Reibke R, Gonen M, Strauss HW, Tuttle RM, Drucker W, Larson SM. Real-time prognosis for metastatic thyroid carcinoma based on 2-[18F]fluoro-2-deoxy-D-glucose-positron emission tomography scanning. *J Clin Endocrinol Metab* 2006; **91**: 498-505 [PMID: 16303836 DOI: 10.1210/jc.2005-1534]

P- Reviewer: Hekal IA, Huang SP, Simone G **S- Editor:** Ji FF
L- Editor: A **E- Editor:** Li D



Observational Study

Computed tomography pulmonary angiography using a 20% reduction in contrast medium dose delivered in a multiphasic injection

Mitchell Chen, Gaith Mattar, Jamal A Abdulkarim

Mitchell Chen, Jamal A Abdulkarim, Department of Radiology, George Eliot Hospital NHS Trust, Nuneaton, Warwickshire CV10 7DJ, United Kingdom

Gaith Mattar, Department of Radiology, University Hospitals Birmingham NHS Trust, Birmingham B15 2TH, United Kingdom

Author contributions: Abdulkarim JA designed the experiment; Chen M and Abdulkarim JA conducted literature research; Mattar G and Abdulkarim JA performed the data collection; Chen M analysed the data; Chen M and Abdulkarim JA prepared the manuscript.

Institutional review board statement: The study was reviewed and approved by the George Eliot Hospital NHS Trust Directorate of Audit and Research.

Informed consent statement: Individual consent from patients was not obtained as this is retrospective observational study. All patient data were fully anonymised.

Conflict-of-interest statement: Chen M declares no conflict of interest. Mattar G declares no conflict of interest. Abdulkarim JA declares no conflict of interest.

Data sharing statement: Technical appendix, statistical code, and dataset available from the corresponding author at jamal.abdulkarim@geh.nhs.uk. Consent was not obtained for data sharing but the presented data are anonymised and risk of identification is low.

Open-Access: This article is an open-access article which was selected by an in-house editor and fully peer-reviewed by external reviewers. It is distributed in accordance with the Creative Commons Attribution Non Commercial (CC BY-NC 4.0) license, which permits others to distribute, remix, adapt, build upon this work non-commercially, and license their derivative works on different terms, provided the original work is properly cited and the use is non-commercial. See: <http://creativecommons.org/licenses/by-nc/4.0/>

Manuscript source: Invited manuscript

Correspondence to: Jamal A Abdulkarim, FRCR, Consultant Radiologist, Department of Radiology, George Eliot Hospital NHS Trust, College Street, Nuneaton, Warwickshire CV10 7DJ, United Kingdom. jamal.abdulkarim@geh.nhs.uk
Telephone: +44-247-6351351
Fax: +44-247-6865175

Received: October 5, 2016

Peer-review started: October 9, 2016

First decision: November 29, 2016

Revised: December 30, 2016

Accepted: January 16, 2017

Article in press: January 18, 2017

Published online: March 28, 2017

Abstract

AIM

To evaluate the feasibility of reducing the dose of iodinated contrast agent in computed tomography pulmonary angiography (CTPA).

METHODS

One hundred and twenty-seven patients clinically suspected of having pulmonary embolism underwent spiral CTPA, out of whom fifty-seven received 75 mL and the remaining seventy a lower dose of 60 mL of contrast agent. Both doses were administered in a multiphasic injection. A minimum opacification threshold of 250 Hounsfield units (HU) in the main pulmonary artery is used for assessing the technical adequacy of the scans.

RESULTS

Mean opacification was found to be positively correlated to patient age (Pearson's correlation 0.4255, $P < 0.0001$) and independent of gender (male:female, 425.6 vs 450.4,

$P = 0.34$). When age is accounted for, the study and control groups did not differ significantly in their mean opacification in the main (436.8 *vs* 437.9, $P = 0.48$), left (416.6 *vs* 419.8, $P = 0.45$) or the right pulmonary arteries (417.3 *vs* 423.5, $P = 0.40$). The number of sub-optimally opacified scans (the mean opacification in the main pulmonary artery < 250 HU) did not differ significantly between the study and control groups (7 *vs* 10).

CONCLUSION

A lower dose of iodine contrast at 60 mL can be feasibly used in CTPA without resulting in a higher number of sub-optimally opacified scans.

Key words: Computed tomography pulmonary angiography; Contrast dose; Contrast induced nephropathy; Acute kidney disease; Contrast safety; Contrast dose reduction; Multiphasic injection

© The Author(s) 2017. Published by Baishideng Publishing Group Inc. All rights reserved.

Core tip: Computed tomography pulmonary angiography scanning using a lower dose of contrast agent (60 mL) is proposed. Comparisons were made to patients in a control group who have received a standard dose of contrast medium (75 mL) at our Trust. There is no statistical difference in the degree of opacification in the main pulmonary artery between the two groups. The rate of rejection due to inadequate opacification is not affected by the reduction in contrast dose. The feasibility of using a reduced contrast dose at 60 mL is clearly demonstrated.

Chen M, Mattar G, Abdulkarim JA. Computed tomography pulmonary angiography using a 20% reduction in contrast medium dose delivered in a multiphasic injection. *World J Radiol* 2017; 9(3): 143-147 Available from: URL: <http://www.wjgnet.com/1949-8470/full/v9/i3/143.htm> DOI: <http://dx.doi.org/10.4329/wjr.v9.i3.143>

INTRODUCTION

Computed tomography pulmonary angiography (CTPA) is the *de facto* gold standard investigation for detecting or ruling out the presence of pulmonary embolism (PE)^[1]. The degree of pulmonary arterial opacification defines the technical adequacy of a CTPA scan. It is proportional to the rate and dose of contrast medium administration^[2]. A good quality scan is essential for optimising its negative predictive value. However, using a high dose of contrast medium can lead to contrast induced-acute kidney injury (CI-AKI), formerly known as contrast-induced nephropathy, when there is a sudden rise in serum creatinine following the exposure to iodinated contrast media, that is not linked to another nephrotoxic event. The condition is normally self-limiting but can lead to increased morbidity and mortality^[3]. Certain patient groups are at

an increased risk of developing CI-AKI; such as those affected by hypertension, chronic kidney disease (CKD), diabetes mellitus, congestive heart failure, reduced intravascular volume, advanced age and recent exposure to nephrotoxic drugs^[4]. For this reason, the dose of contrast should be kept to a minimum provided that it does not affect the overall quality of the image.

Recent advances in computed tomography (CT) technology have enabled faster image acquisition times, thus reducing the time required during which the pulmonary vasculature must be opacified. This has made it possible to consider reducing the dose of contrast medium used in CTPA^[5]. At our Trust, the current protocol is to administer 75 mL of 350 mg/mL iodine/iodersol delivered *via* a multiphasic injection. In this study, we have tested the hypothesis that the scan is technically adequate using only a 60 mL dose of the contrast medium at the same concentration. The dose reduction is intended to enhance patient safety as well reducing the overall scanning cost.

MATERIALS AND METHODS

Patient selection

One hundred and twenty-seven patients clinically suspected of having PE underwent spiral CTPA between the months of January to April 2015; of these subjects, seventy received a higher dose of 75 mL (control group) and the remaining fifty-seven, 60 mL (study group) of 350 mg/mL iodine/iodersol contrast agent (Omnipaque 350, GE Healthcare, United States). The dose reduction of 20% was chosen in conjunction with the CT scanner manufacturer (Siemens AG). In this observational study, both patient cohorts were studied retrospectively. Patient cohort allocation was not randomised due to the nature of this study.

In the control group, there were 32 male and 38 female patients, whose mean age was 65.7 years [range (34-93)]. In the study group, there were 23 male and 34 female patients, with a mean age of 62.7 years [range (16-92)]. Characteristics of the study population are given in Table 1. Patient data were fully anonymised.

CTPA protocol

Scans were performed on a 128-slice CT scanner (Somatom Definition AS+, Siemens AG, Berlin and Munich, Germany), and acquired with a radiation dose of 120 kV and a tube output of a minimum of 666 mAs/80 kW for 5 s, 0.3 s rotation time, pitch 0.6, 0.6 mm slice thickness with 38.4 mm collimation.

The contrast medium was given *via* an 18G cannula, placed in the ante-cubital fossa and delivered *via* a power injector (Ulrich Inject CT Motion, Ulrich Medical, Buchbrunnweg, Germany) at a rate of 5 mL/s, with a saline chaser of 25 mL at the same injection rate. The overall injection time is 12 s for 60 mL of contrast and 15 s for 75 mL of contrast.

We used a bolus tracking method to control the scan initiation. We first acquired an initial low-dose monitoring image six seconds after contrast injection and repeated

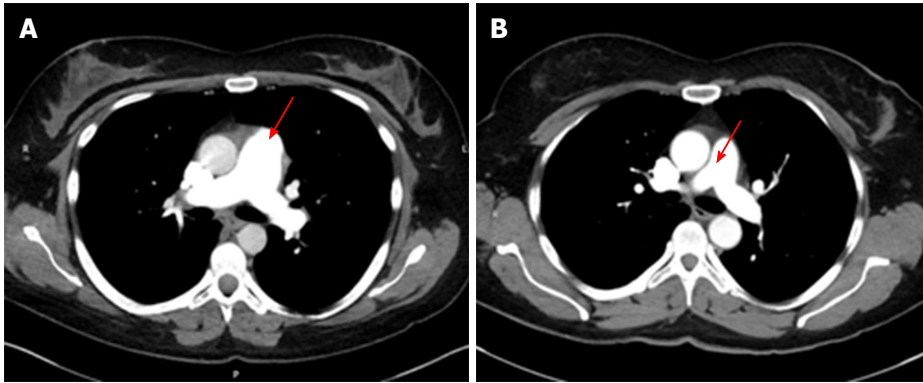


Figure 1 Sample axial image slices showing the good opacification in the main pulmonary artery with intravenous contrast in the two groups (red arrows). A: 60 mL; B: 75 mL.

Table 1 Characteristics of the study population

	60 mL	75 mL (control)
Size	57	70
Gender (M:F)	23:34	32:38
Mean age (yr)	65.7	62.7
Age range (yr)	34-93	16-92

M: Male; F: Female.

every 1.5 s thereafter. Upon reaching a threshold of 100 Hounsfield units (HU) in the main pulmonary artery, the scan was initiated. The scan table is then moved from the monitoring to the starting position; during which time patients were instructed to breath-hold for 4–6 s. CTPA scans were acquired in a cranio-caudal direction. The images were reconstructed using Siemens iterative reconstruction method, SAFIRE (Sinogram Affirmed Iterative Reconstruction, strength 3).

Patients' age and gender were obtained retrospectively from their medical notes. Patient weight was not examined in this study.

Image data assessment

A radiology registrar with 3 year of experience performed the image data analysis retrospectively on an Insignia Picture Archiving and Communication System workstation (Basingstoke, United Kingdom). We measured image opacification in the main, left and right pulmonary arteries. An acceptance threshold of a 250 HU for main pulmonary artery opacification was adopted for our study, as it was the figure used widely in various literatures^[6].

Statistical analysis

We used the χ^2 test to analyse categorical variables such as gender and number of rejected scans and Pearson's coefficient for the correlation studies. We performed all statistical tests with a significance level of $P < 0.05$. Statistical calculations were performed using Microsoft Excel 2010 (Microsoft Corp, United States).

RESULTS

We found no significant difference between the two groups in either age (P value: 0.35) or gender (P value: 0.42).

Sample axial images from the 60 and 75 mL groups are given in Figure 1, showing the good opacification of the main pulmonary arteries.

The mean opacification values in the main, right and left pulmonary arteries are shown in Table 2. Even though the reported degree of opacification was higher with 75 mL of contrast medium, the difference did not affect the overall image quality, as shown in the discussion below.

We found the mean opacification to be positively correlated to patient age (Pearson's correlation 0.426, $P < 0.0001$). When age is accounted for by introducing an age-dependent linear regression coefficient to the mean opacification measure, the two groups did not differ significantly in terms of their mean opacification in the main (437 vs 438, $P = 0.48$), left (417 vs 420, $P = 0.45$) or the right pulmonary arteries (417 vs 424, $P = 0.40$). Taking an acceptance threshold of 250 HU, the rate of rejected scans did not differ significantly between the two groups, as shown in Table 3.

DISCUSSION

Various past literature have reported on the use of a smaller dose of contrast media in CTPA^[7–9]. In a former study carried out at our centre^[7], we have established the feasibility of using a 75 mL of contrast in a higher concentration (350 mg/mL Iodine/Ioversol), compared to 100 mL of a standard concentration (300 mg/mL Iodine/Ioversol). This finding was also reported in a Randomised Clinical Trial published in the same year^[8], which further established the use of a lower energy tube (80 kVp vs 100 kVp) for a reduced dose of radiation. In a different single cohort study^[9], the authors have evaluated the practicality of CTPA with 30 mL of contrast medium in patients with renal impairment. Although it was stated that only one out of 24 scans were non-diagnostic, the reported average opacification (247 HU) in the main

Table 2 A comparison of mean opacification values in the pulmonary arteries between the two groups

	Mean opacification \pm standard deviation		Mean difference (95%CI)
	60 mL of contrast agent	75 mL of contrast agent	
Main pulmonary artery	437 \pm 121	438 \pm 142	1 (-45 to 47)
Right pulmonary artery	417 \pm 115	420 \pm 130	3 (-41 to 47)
Left pulmonary artery	417 \pm 110	424 \pm 140	7 (-38 to 50)

All values are given in Hounsfield units.

Table 3 Number of sub-optimal studies in each group

Group	Number of sub-optimal studies
75 mL	10
60 mL	7
$P = 0.96$	

pulmonary arteries is notably lower than that found in our study and is below the 250 HU threshold that we have used. Furthermore, their work was a single cohort study and reported no comparisons to a control group.

The risk of CI-AKI in the general population is low (less than 2%) but would greatly increase to up to 40% in patients with certain risk factors (diabetes mellitus, cardiac failure, CKD, older age and recent exposure to nephrotoxic drugs)^[3]. Since the risk of CI-AKI is known to be dose-dependent^[3], the goal would be to keep the dose of contrast medium to a minimum. Additionally, a reduction in contrast medium dose can lower the cost by about 15% per scan, which is in line with figures cited in a related study^[10].

Our study utilised a lower dose (60 mL) of contrast agent compared to the normal dose (75 mL) currently used in clinical practice at our Trust. The study results show that a further reduction in contrast agent dose in CTPA is possible, without impairing pulmonary arterial enhancement.

To highlight sub-optimally opacified scans, we used an acceptance threshold of 250 HU. It is important to note that there is no overall consensus on this cut-off figure and various other figures have been quoted in past literature^[5,11]. The threshold of 250 HU was chosen based on the authors' own clinical experience: When reporting on CTPA scans, a single radiodensity measurement is made in the main pulmonary artery and as such, PE can not be confidently ruled out if the minimum opacification was less than 250 HU. With this figure, the experimental and control groups have yielded a scan acceptance rate of 89% and 86%, respectively. This is comparable to the 88.9% acceptance rate quoted in Nazaroglu *et al.*^[12]. We note that the Hounsfield Unit is not the optimal quality measure for indeterminate scans, such as those affected by flow or streak artefacts. Given these artefacts are more prominent at a lower contrast dose, alternative quality measures such as a visual grading system or reporter confidence can be employed to potentially better assess our data.

Some patient factors are known to influence the

degree of vascular opacification. Most notably, age has been demonstrated to have a positive correlation with the degree of opacification^[11], which is reflected in our results. Body weight is yet another factor with a negative impact on image opacification^[5], this was not assessed given the retrospective nature of our study.

Another limitation of our study is that the patients were not monitored for any change in their renal function, as this was not routinely done in our hospital but only reserved for those with a clinical suspicion of CI-AKI. Therefore, we were not able to assess the impact of using a lower dose of contrast medium on the incidence of CI-AKI. Moreover, given the small study size and the low incidence of CI-AKI in the general population, it might have been difficult to establish compelling evidence on this even had such test results been available. A potential improvement can be achieved by prospectively recruiting patients who are at a higher risk of developing CI-AKI and monitor for any incidence difference of CIN in the low contrast dose group. However, even without this result, knowing the dose-dependent nature of CI-AKI, it would still be sensible to strive for any contrast dose reduction when possible, especially for patients more prone to developing this condition^[13].

Finally, we have focused our measurements on the central pulmonary vasculature whereas pulmonary emboli can also be found in the peripheries. It should be noted that the isolation and sampling of smaller peripheral vessel would be technically challenging and potentially inaccurate, and it is therefore impractical to incorporate peripheral vessel measurements at this stage.

In summary, our study demonstrated that using a reduced dose of contrast medium (60 mL vs 75 mL) is a clinically feasible without adversely affecting the image quality and diagnostic value of CTPA for PE. We propose the lower contrast dose of 60 mL should be used as standard practice in all patients undergoing CTPA.

ACKNOWLEDGMENTS

We would like to thank Mr Adam Ryder and the rest of the CT team at the George Eliot Hospital for their help during this study.

COMMENTS

Background

Computed tomography pulmonary angiography (CTPA) is the *de facto* gold standard for visualising the pulmonary arteries to detect the presence of

pulmonary emboli (PE). However, the use of contrast agent in this modality can lead to contrast-induced acute kidney injury (CI-AKI). To enhance the safety of CTPA for patients prone to developing CI-AKI, such as the elderly and those with diabetes mellitus, cardiac failure or chronic kidney disease, a dose reduction is desirable and has been rendered feasible with recent technological advancements in computed tomography image acquisition and multiphasic contrast injection.

Research frontiers

The focus in this research area has been on reducing the dose of contrast used in CTPA to achieve better patient safety, while still producing technically satisfactory imaging data for PE detection.

Innovations and breakthroughs

The authors have demonstrated the feasibility of using a lower dose (60 mL) of contrast agent compared to the normal dose (75 mL) currently used at this Trust. The study results have shown that CTPA can be performed at this reduced contrast dose level without rendering pulmonary arterial enhancement inadequate.

Applications

The result can be applied to clinical radiology practice where a lower dose of contrast can be used to produce technically adequate imaging data. Future works include the inclusion of patient body weight, a large sample size and a study of the specific effect of contrast medium dose on patients' kidney function. A further reduction in contrast dose can also be considered.

Peer-review

This study utilised a lower dose (60 mL) of contrast agent compared to the normal dose (75 mL) currently used in clinical practice. The experimental results have shown that a reduction in contrast agent dose can be achieved without adversely affecting pulmonary arterial enhancement in CTPA. They demonstrated that using a reduced dose of contrast medium (60 mL vs 75 mL) is a clinically feasible without adversely affecting the image quality and diagnostic value of CTPA for PE. They proposed the lower contrast dose of 60 mL should be used as standard practice in all patients undergoing CTPA. The dose reduction is intended to enhance patient safety as well reducing the overall scanning cost. The dose reduction is a hot issue at present. This is a useful paper for the patient's health care.

REFERENCES

- 1 **National Institute for Health and Care Excellence.** Venous thromboembolic diseases: the management of venous thromboembolic diseases and the role of thrombophilia testing, CG144. London: National Institute for Health and Care Excellence, 2012
- 2 **Fleischmann D.** How to design injection protocols for multiple detector-row CT angiography (MDCTA). *Eur Radiol* 2005; **15** Suppl 5: E60-E65 [PMID: 18637231]
- 3 **Thomsen HS, Morcos SK, Barrett BJ.** Contrast-induced nephropathy: the wheel has turned 360 degrees. *Acta Radiol* 2008; **49**: 646-657 [PMID: 18568557 DOI: 10.1080/02841850801995413]
- 4 **Lewington A, MacTier R, Hoefield R, Sutton A, Smith D, Downes M.** Prevention of contrast induced acute kidney injury (CI-AKI) in adult patients. Royal College of Radiologist Guidelines, 2013
- 5 **Bae KT, Tao C, Gürel S, Hong C, Zhu F, Gebke TA, Milite M, Hildebolt CF.** Effect of patient weight and scanning duration on contrast enhancement during pulmonary multidetector CT angiography. *Radiology* 2007; **242**: 582-589 [PMID: 17255426 DOI: 10.1148/radiol.2422052132]
- 6 **Ramadan SU, Kosar P, Sonmez I, Karahan S, Kosar U.** Optimisation of contrast medium volume and injection-related factors in CT pulmonary angiography: 64-slice CT study. *Eur Radiol* 2010; **20**: 2100-2107 [PMID: 20437179 DOI: 10.1007/s00330-010-1782-y]
- 7 **Goble EW, Abdulkarim JA.** CT pulmonary angiography using a reduced volume of high-concentration iodinated contrast medium and multiphasic injection to achieve dose reduction. *Clin Radiol* 2014; **69**: 36-40 [PMID: 24070908 DOI: 10.1016/j.crad.2013.07.023]
- 8 **Szucs-Farkas Z, Christe A, Megyeri B, Rohacek M, Vock P, Nagy EV, Heverhagen JT, Schindera ST.** Diagnostic accuracy of computed tomography pulmonary angiography with reduced radiation and contrast material dose: a prospective randomized clinical trial. *Invest Radiol* 2014; **49**: 201-208 [PMID: 24473367 DOI: 10.1097/RLI.000000000000016]
- 9 **Singh T, Lam KV, Murray C.** Low volume contrast CTPA in patients with renal dysfunction. *J Med Imaging Radiat Oncol* 2011; **55**: 143-148 [PMID: 21501402 DOI: 10.1111/j.1754-9485.2011.02243.x]
- 10 **Tsuchiya K, Honya K, Yoshida M, Gomyo M, Nitatori T.** Cerebral CT angiography using a reduced dose of contrast material at high iodine concentration in combination with a saline flush. *Clin Radiol* 2008; **63**: 1332-1335 [PMID: 18996263 DOI: 10.1016/j.crad.2008.07.007]
- 11 **Roggenland D, Peters SA, Lemburg SP, Holland-Letz T, Nicolas V, Heyer CM.** CT angiography in suspected pulmonary embolism: impact of patient characteristics and different venous lines on vessel enhancement and image quality. *AJR Am J Roentgenol* 2008; **190**: W351-W359 [PMID: 18492877 DOI: 10.2214/AJR.07.3402]
- 12 **Nazaroglu H, Ozmen CA, Akay HO, Kiliç I, Bilici A.** 64-MDCT pulmonary angiography and CT venography in the diagnosis of thromboembolic disease. *Am J Roentgenol* 2009; **192**: 654-661 [PMID: 19234261 DOI: 10.2214/AJR.07.3939]
- 13 **Lee CH, Goo JM, Lee HJ, Kim KG, Im JG, Bae KT, Lee CH, Goo JM, Lee HJ, Kim KG, Im JG, Bae KT.** Determination of optimal timing window for pulmonary artery MDCT angiography. *Am J Roentgenol* 2007; **188**: 313-317 [PMID: 17242236 DOI: 10.2214/AJR.06.0078]

P- Reviewer: Chow J, Gao BL, Li YZ **S- Editor:** Song XX
L- Editor: A **E- Editor:** Li D





Published by **Baishideng Publishing Group Inc**

8226 Regency Drive, Pleasanton, CA 94588, USA

Telephone: +1-925-223-8242

Fax: +1-925-223-8243

E-mail: bpgoffice@wjgnet.com

Help Desk: <http://www.wjgnet.com/esps/helpdesk.aspx>

<http://www.wjgnet.com>



World Journal of *Radiology*

World J Radiol 2017 April 28; 9(4): 148-216





Editorial Board

2014-2017

The *World Journal of Radiology* Editorial Board consists of 365 members, representing a team of worldwide experts in radiology. They are from 36 countries, including Afghanistan (1), Argentina (2), Australia (5), Austria (7), Belgium (2), Brazil (8), Canada (6), Chile (1), China (43), Croatia (1), Denmark (4), Egypt (6), France (5), Germany (22), Greece (10), India (12), Iran (6), Ireland (2), Israel (3), Italy (47), Japan (13), Netherlands (1), New Zealand (1), Pakistan (1), Poland (2), Portugal (1), Serbia (1), Singapore (3), Slovakia (1), South Korea (18), Spain (4), Sweden (2), Switzerland (4), Thailand (1), Turkey (26), United Kingdom (11), and United States (82).

EDITORS-IN-CHIEF

Kai U Juergens, *Bremen*
Edwin JR van Beek, *Edinburgh*
Thomas J Vogl, *Frankfurt*

GUEST EDITORIAL BOARD MEMBERS

Wing P Chan, *Taipei*
Chung-Huei Hsu, *Taipei*
Chin-Chang Huang, *Taipei*
Tsong-Long Hwang, *Taoyuan*
Jung-Lung Hsu, *Taipei*
Chia-Hung Kao, *Taichung*
Yu-Ting Kuo, *Tainan*
Hon-Man Liu, *Taipei*
Hui-Lung Liang, *Kaohsiung*
Chun Chung Lui, *Kaohsiung*
Sen-Wen Teng, *Taipei*
Yung-Liang (William) Wan, *Taoyuan*

MEMBERS OF THE EDITORIAL BOARD



Afghanistan

Takao Hiraki, *Okayama*



Argentina

Patricia Carrascosa, *Vicente Lopez*
Maria C Ziadi, *Rosario*



Australia

Lourens Bester, *Sydney*
Gemma A Figtree, *Sydney*

Stuart M Grieve, *Sydney*
Wai-Kit Lee, *Fitzroy*
Prabhakar Ramachandran, *Melbourne*



Austria

Herwig R Cerwenka, *Graz*
Gudrun M Feuchtnner, *Innsbruck*
Benjamin Henninger, *Innsbruck*
Rupert Lanzenberger, *Vienna*
Shu-Ren Li, *Vienna*
Veronika Schopf, *Vienna*
Tobias De Zordo, *Innsbruck*



Belgium

Steve Majerus, *Liege*
Kathelijne Peremans, *Merelbeke*



Brazil

Clerio F Azevedo, *Rio de Janeiro*
Patrícia P Alfredo, *São Paulo*
Eduardo FC Fleury, *São Paulo*
Edward Araujo Júnior, *São Paulo*
Wellington P Martins, *Ribeirao Preto*
Ricardo A Mesquita, *Belo Horizonte*
Vera MC Salemi, *São Paulo*
Claudia Szobot, *Porto Alegre*
Lilian YI Yamaga, *São Paulo*



Canada

Marie Arsalidou, *Toronto*
Otman A Basir, *Waterloo*

Tarik Zine Belhocine, *Toronto*
James Chow, *Toronto*
Tae K Kim, *Toronto*
Anastasia Oikonomou, *Toronto*



China

Hong-Wei Chen, *Wuxi*
Feng Chen, *Hangzhou*
Jian-Ping Chu, *Guangzhou*
Guo-Guang Fan, *Shenyang*
Bu-Lang Gao, *Shijiazhuang*
Qi-Yong Gong, *Chengdu*
Ying Han, *Beijing*
Xian-Li Lv, *Beijing*
Yi-Zhuo Li, *Guangzhou*
Xiang-Xi Meng, *Harbin*
Yun Peng, *Beijing*
Jun Shen, *Guangzhou*
Ze-Zhou Song, *Hangzhou*
Wai Kwong Tang, *Hong Kong*
Gang-Hua Tang, *Guangzhou*
Jie Tian, *Beijing*
Lu-Hua Wang, *Beijing*
Xiao-bing Wang, *Xi'an*
Yi-Gen Wu, *Nanjing*
Kai Wu, *Guangzhou*
Hui-Xiong Xu, *Shanghai*
Zuo-Zhang Yang, *Kunming*
Xiao-Dan Ye, *Shanghai*
David T Yew, *Hong Kong*
Ting-He Yu, *Chongqing*
Zheng Yuan, *Shanghai*
Min-Ming Zhang, *Hangzhou*
Yudong Zhang, *Nanjing*
Dong Zhang, *Chongqing*
Wen-Bin Zeng, *Changsha*

Yue-Qi Zhu, *Shanghai*



Croatia

Goran Kusec, *Osijek*



Denmark

Poul E Andersen, *Odense*

Lars J Petersen, *Aalborg*

Thomas Z Ramsøy, *Frederiksberg*

Morten Ziebell, *Copenhagen*



Egypt

Mohamed F Bazeed, *Mansoura*

Mohamed Abou El-Ghar, *Mansoura*

Reem HA Mohamed, *Cairo*

Mohamed R Nouh, *Alexandria*

Ahmed AKA Razek, *Mansoura*

Ashraf A Zytoon, *Shebin El-Koom*



France

Sabine F Bensamoun, *Compiègne*

Romarc Loffroy, *Dijon*

Stephanie Nougaret, *Montpellier*

Hassane Oudadesse, *Rennes*

Vincent Vinh-Hung, *Fort-de-France*



Germany

Henryk Barthel, *Leipzig*

Peter Bannas, *Hamburg*

Martin Beeres, *Frankfurt*

Ilja F Ciernik, *Dessau*

A Dimitrakopoulou-Strauss, *Heidelberg*

Peter A Fasching, *Erlangen*

Andreas G Schreyer, *Regensburg*

Philipp Heusch, *Duesseldorf*

Sonja M Kirchhoff, *Munich*

Sebastian Ley, *Munich*

Adel Maataoui, *Frankfurt am Main*

Stephan M Meckel, *Freiburg*

Hans W Muller, *Duesseldorf*

Kay Raum, *Berlin*

Dirk Rades, *Luebeck*

Marc-Ulrich Regier, *Hamburg*

Alexey Surov, *Halle*

Martin Walter, *Magdeburg*

Axel Wetter, *Essen*

Christoph Zilkens, *Düsseldorf*



Greece

Panagiotis Antoniou, *Thessaloniki*

Nikos Efthimiou, *Athens*

Dimitris Karnabatidis, *Patras*

George Latsios, *Athens*

Stylianios Megremis, *Iraklion*

Alexander D Rapidis, *Athens*

Kiki Theodorou, *Larissa*

Ioannis A Tsalafoutas, *Athens*

Evanthia E Tripoliti, *Ioannina*

Athina C Tsili, *Ioannina*



India

Ritesh Agarwal, *Chandigarh*

Chandan J Das, *New Delhi*

Prathamesh V Joshi, *Mumbai*

Naveen Kalra, *Chandigarh*

Chandrasekharan Kesavadas, *Trivandrum*

Jyoti Kumar, *New Delhi*

Atin Kumar, *New Delhi*

Kaushala P Mishra, *Allahabad*

Daya N Sharma, *New Delhi*

Binit Sureka, *New Delhi*

Sanjay Sharma, *New Delhi*

Raja R Yadav, *Allahabad*



Iran

Majid Assadi, *Bushehr*

SeyedReza Najafizadeh, *Tehran*

Mohammad Ali Oghabian, *Tehran*

Amir Reza Radmard, *Tehran*

Ramin Sadeghi, *Mashhad*

Hadi Rokni Yazdi, *Tehran*



Ireland

Tadhg Gleeson, *Wexford*

Frederik JAI Vernimmen, *Cork*



Israel

Dafna Ben Bashat, *Tel Aviv*

Amit Gefen, *Tel Aviv*

Tamar Sella, *Jerusalem*



Italy

Adriano Alippi, *Rome*

Dante Amelio, *Trento*

Michele Anzidei, *Rome*

Filippo F Angileri, *Messinas*

Stefano Arcangeli, *Rome*

Roberto Azzoni, *San Donato milanese*

Tommaso V Bartolotta, *Palermo*

Tommaso Bartalena, *Imola*

Livia Bernardin, *San Bonifacio*

Federico Boschi, *Verona*

Sergio Casciaro, *Lecce*

Emanuele Casciani, *Rome*

Musa M Can, *Napoli*

Alberto Cuocolo, *Napoli*

Michele Ferrara, *Coppito*

Mauro Feola, *Fossano*

Giampiero Francica, *Castel Volturno*

Luigi De Gennaro, *Rome*

Giulio Giovannetti, *Pisa*

Francesca Iacobellis, *Napoli*

Formato Invernizzi, *Monza Brianza*

Francesco Lassandro, *Naples*

Lorenzo Livi, *Florence*

Pier P Mainenti, *Napoli*

Laura Marzetti, *Chieti*

Giuseppe Malinverni, *Crescentino*

Enrica Milanese, *Turin*

Giovanni Morana, *Treviso*

Lorenzo Monti, *Milan*

Silvia D Morbelli, *Genoa*

Barbara Palumbo, *Perugia*

Cecilia Parazzini, *Milan*

Stefano Pergolizzi, *Messina*

Antonio Pinto, *Naples*

Camillo Porcaro, *Rome*

Carlo C Quattrocchi, *Rome*

Alberto Rebonato, *Perugia*

Giuseppe Rizzo, *Rome*

Roberto De Rosa, *Naples*

Domenico Rubello, *Rovigo*

Andrea Salvati, *Bari*

Sergio Sartori, *Ferrara*

Luca M Sconfienza, *Milano*

Giovanni Storto, *Rionero*

Nicola Sverzellati, *Parma*

Alberto S Tagliafico, *Genova*

Nicola Troisi, *Florence*



Japan

Yasuhiko Hori, *Chiba*

Hidetoshi Ikeda, *Koriyama*

Masahito Kawabori, *Sapporo*

Tamotsu Kamishima, *Sapporo*

Hiro Kiyosue, *Yufu*

Yasunori Minami, *Osaka-sayama*

Yasuhiro Morimoto, *Kitakyushu*

Satoru Murata, *Tokyo*

Shigeki Nagamachi, *Miyazaki*

Hiroshi Onishi, *Yamanashi*

Morio Sato, *Wakayama Shi*

Yoshito Tsushima, *Maebashi*

Masahiro Yanagawa, *Suita*



Netherlands

Willem Jan van Rooij, *Tilburg*



New Zealand

W Howell Round, *Hamilton*



Pakistan

Wazir Muhammad, *Abbottabad*



Poland

Maciej S Baglaj, *Wroclaw*

Piotr Czauderna, *Gdansk*



Portugal

Joao Manuel RS Tavares, *Porto*



Serbia

Olivera Ciraj-Bjelac, *Belgrade*



Singapore

Gopinathan Anil, *Singapore*

Terence KB Teo, *Singapore*

Cher Heng Tan, *Singapore*



Slovakia

Stefan Sivak, *Martin*



South Korea

Ki Seok Choo, *Busan*

Seung Hong Choi, *Seoul*

Dae-Seob Choi, *Jinju*

Hong-Seok Jang, *Seoul*

Yong Jeong, *Daejeon*

Chan Kyo Kim, *Seoul*

Se Hyung Kim, *Seoul*

Joong-Seok Kim, *Seoul*

Sang Eun Kim, *Seongnam*

Sung Joon Kwon, *Seoul*

Jeong Min Lee, *Seoul*

In Sook Lee, *Busan*

Noh Park, *Goyang*

Chang Min Park, *Seoul*

Sung Bin Park, *Seoul*

Deuk Jae Sung, *Seoul*

Choongsoo Shin, *Seoul*

Kwon-Ha Yoon, *Iksan*



Spain

Miguel A De Gregorio, *Zaragoza*

Antonio Luna, *Jaén*

Enrique Marco de Lucas, *Santander*

Fernando Ruiz Santiago, *Granada*



Sweden

Dmitry Grishenkov, *Stockholm*

Tie-Qiang Li, *Stockholm*



Switzerland

Nicolau Beckmann, *Basel*

Christian Boy, *Bern*

Giorgio Treglia, *Bellinzona*

Stephan Ulmer, *Kiel*



Thailand

Sirianong Namwongprom, *Chiang Mai*



Turkey

Kubilay Aydin, *Istanbul*

Ramazan Akdemir, *Sakarya*

Serhat Avcu, *Ankara*

Ayşe Aralasmak, *Istanbul*

Oktay Algin, *Ankara*

Nevbahar Akcar, *Meselik*

Bilal Battal, *Ankara*

Zulkif Bozgeyik, *Elazig*

Nazan Ciledag, *Aakara*

Fuldem Y Donmez, *Ankara*

Gulgun Engin, *Istanbul*

Ahmet Y Goktay, *Izmir*

Oguzhan G Gumustas, *Bursa*

Kaan Gunduz, *Ankara*

Pelin Ozcan Kara, *Mersin*

Kivanc Kamburoglu, *Ankara*

Ozgur Kilickesmez, *Istanbul*

Furuzan Numan, *Istanbul*

Cem Onal, *Adana*

Ozgur Oztekin, *Izmir*

Seda Ozbek (Boruban), *Konya*

Selda Sarikaya, *Zonguldak*

Figen Taser, *Kutahya*

Baran Tokar, *Eskisehir*

Ender Uysal, *Istanbul*

Ensar Yekeler, *Istanbul*



United Kingdom

Indran Davagnanam, *London*

M DC Valdés Hernández, *Edinburgh*

Alan Jackson, *Manchester*

Suneil Jain, *Belfast*

Long R Jiao, *London*

Miltiadis Krokidis, *Cambridge*

Pradesh Kumar, *Liverpool*

Peter D Kuzmich, *Derby*

Georgios Plataniotis, *Brighton*

Vanessa Sluming, *Liverpool*



United States

Garima Agrawal, *Saint Louis*

James R Brasic, *Baltimore*

Rajendra D Badgaiyan, *Buffalo*

Ulas Bagci, *Bethesda*

Anat Biegon, *Stony Brook*

Ramon Casanova, *Winston Salem*

Wenli Cai, *Boston*

Zheng Chang, *Durham*

Corey J Chakarun, *Long Beach*

Kai Chen, *Los Angeles*

Hyun-Soon Chong, *Chicago*

Marco Cura, *Dallas*

Ravi R Desai, *Bensalem*

Delia DeBuc, *Miami*

Carlo N De Cecco, *Charleston*

Timm-Michael L Dickfeld, *Baltimore*

Subba R Digumarthy, *Boston*

Huy M Do, *Stanford*

Todd A Faasse, *Grand Rapids*

Salomao Faintuch, *Boston*

Girish M Fatterpekar, *New York*

Dhakshinamoorthy Ganesan, *Houston*

Robert J Griffin, *Little Rock*

Andrew J Gunn, *Boston*

Sandeep S Hedgire, *Boston*

Timothy J Hoffman, *Columbia*

Mai-Lan Ho, *San Francisco*

Juebin Huang, *Jackson*

Abid Irshad, *Charleston*

Matilde Inglese, *New York*

El-Sayed H Ibrahim, *Jacksonville*

Paul R Julsrud, *Rochester*

Pamela T Johnson, *Baltimore*

Ming-Hung Kao, *Tempe*

Sunil Krishnan, *Houston*

Richard A Komoroski, *Cincinnati*

Sandi A Kwee, *Honolulu*

King Kim, *Ft. Lauderdale*

Guozheng Liu, *Worcester*

Yiyan Liu, *Newark*

Venkatesh Mani, *New York*

Lian-Sheng Ma, *Pleasanton*

Rachna Madan, *Boston*

Zeyad A Metwalli, *Houston*

Yilong Ma, *Manhasset*

Hui Mao, *Atlanta*

Feroze B Mohamed, *Philadelphia*

Gul Moonis, *Boston*

John L Noshier, *New Brunswick*

Rahmi Oklu, *Boston*

Aytekun Oto, *Chicago*

Bishnuhari Paudyal, *Philadelphia*

Rajul Pandya, *Youngstown*

Chong-Xian Pan, *Sacramento*

Jay J Pillai, *Baltimore*

Neal Prakash, *Duarte*

Reza Rahbar, *Boston*

Ali S Raja, *Boston*

Gustavo J Rodriguez, *El Paso*

David J Sahn, *Portland*

Steven Schild, *Scottsdale*

Ali R Sepahdari, *Los Angeles*

Li Shen, *Indianapolis*

JP Sheehan, *Charlottesville*

Atul B Shinagare, *Boston*

Sarabjeet Singh, *Boston*

Charles J Smith, *Columbia*

Kenji Suzuki, *Chicago*

Monvadi Srichai-Parsia, *Washington*

Sree H Tirumani, *Boston*

Hebert A Vargas, *New York*

Sachit Verma, *Philadelphia*

Yoichi Watanabe, *Minneapolis*

Li Wang, *Chapel Hill*

Carol C Wu, *Boston*

Shoujun Xu, *Houston*

Min Yao, *Cleveland*

Xiaofeng Yang, *Atlanta*

Qingbao Yu, *Albuquerque*

Aifeng Zhang, *Chicago*

Chao Zhou, *Bethlehem*

Hongming Zhuang, *Philadelphia*

**EDITORIAL**

- 148 New era of electronic brachytherapy
Ramachandran P

REVIEW

- 155 "Beyond saving lives": Current perspectives of interventional radiology in trauma
Singh A, Kumar A, Kumar P, Kumar S, Gamanagatti S

MINIREVIEWS

- 178 Imaging spectrum of spinal dysraphism on magnetic resonance: A pictorial review
Kumar J, Afsal M, Garg A

ORIGINAL ARTICLE**Basic Study**

- 191 Segmentations of the cartilaginous skeletons of chondrichthyan fishes by the use of state-of-the-art computed tomography
McQuiston AD, Crawford C, Schoepf UJ, Varga-Szemes A, Canstein C, Renker M, De Cecco CN, Baumann S, Naylor GJP
- 199 Gd-EOB-DTPA based magnetic resonance imaging for predicting liver response to portal vein embolization
Szklaruk J, Luersen G, Ma J, Wei W, Underwood M

Retrospective Study

- 206 C-reactive protein and radiographic findings of lower respiratory tract infection in infants
Twomey M, Fleming H, Moloney F, Murphy KP, Crush L, O'Neill SB, Flanagan O, James K, Bogue C, O'Connor OJ, Maher MM
- 212 Computed tomography-guided catheter drainage with urokinase and ozone in management of empyema
Li B, Liu C, Li Y, Yang HF, Du Y, Zhang C, Zheng HJ, Xu XX

ABOUT COVER

Editorial Board Member of *World Journal of Radiology*, Cher Heng Tan, MD, Assistant Professor, Department of Diagnostic Radiology, Tan Tock Seng Hospital, Singapore 308433, Singapore

AIM AND SCOPE

World Journal of Radiology (*World J Radiol*, *WJR*, online ISSN 1949-8470, DOI: 10.4329) is a peer-reviewed open access academic journal that aims to guide clinical practice and improve diagnostic and therapeutic skills of clinicians.

WJR covers topics concerning diagnostic radiology, radiation oncology, radiologic physics, neuroradiology, nuclear radiology, pediatric radiology, vascular/interventional radiology, medical imaging achieved by various modalities and related methods analysis. The current columns of *WJR* include editorial, frontier, diagnostic advances, therapeutics advances, field of vision, mini-reviews, review, topic highlight, medical ethics, original articles, case report, clinical case conference (clinicopathological conference), and autobiography.

We encourage authors to submit their manuscripts to *WJR*. We will give priority to manuscripts that are supported by major national and international foundations and those that are of great basic and clinical significance.

INDEXING/ABSTRACTING

World Journal of Radiology is now indexed in PubMed, PubMed Central, and Emerging Sources Citation Index(Web of Science).

FLYLEAF

I-III Editorial Board

EDITORS FOR THIS ISSUE

Responsible Assistant Editor: *Xiang Li*
Responsible Electronic Editor: *Huan-Liang Wu*
Proofing Editor-in-Chief: *Lian-Sheng Ma*

Responsible Science Editor: *Fang-Fang Ji*
Proofing Editorial Office Director: *Xiu-Xia Song*

NAME OF JOURNAL
World Journal of Radiology

ISSN
ISSN 1949-8470 (online)

LAUNCH DATE
January 31, 2009

FREQUENCY
Monthly

EDITORS-IN-CHIEF
Kai U Juergens, MD, Associate Professor, MRT und PET/CT, Nuklearmedizin Bremen Mitte, ZEMODI - Zentrum für morphologische und molekulare Diagnostik, Bremen 28177, Germany

Edwin JR van Beek, MD, PhD, Professor, Clinical Research Imaging Centre and Department of Medical Radiology, University of Edinburgh, Edinburgh EH16 4TJ, United Kingdom

Thomas J Vogl, MD, Professor, Reader in Health Technology Assessment, Department of Diagnostic and Interventional Radiology, Johann Wolfgang Goethe University of Frankfurt, Frankfurt 60590,

Germany

EDITORIAL BOARD MEMBERS
All editorial board members resources online at <http://www.wjnet.com/1949-8470/editorialboard.htm>

EDITORIAL OFFICE
Xiu-Xia Song, Director
World Journal of Radiology
Baishideng Publishing Group Inc
7901 Stoneridge Drive, Suite 501, Pleasanton, CA 94588, USA
Telephone: +1-925-2238242
Fax: +1-925-2238243
E-mail: editorialoffice@wjnet.com
Help Desk: <http://www.f6publishing.com/helpdesk>
<http://www.wjnet.com>

PUBLISHER
Baishideng Publishing Group Inc
7901 Stoneridge Drive, Suite 501, Pleasanton, CA 94588, USA
Telephone: +1-925-2238242
Fax: +1-925-2238243
E-mail: bpgoffice@wjnet.com
Help Desk: <http://www.f6publishing.com/helpdesk>
<http://www.wjnet.com>

PUBLICATION DATE
April 28, 2017

COPYRIGHT
© 2017 Baishideng Publishing Group Inc. Articles published by this Open-Access journal are distributed under the terms of the Creative Commons Attribution Non-commercial License, which permits use, distribution, and reproduction in any medium, provided the original work is properly cited, the use is non commercial and is otherwise in compliance with the license.

SPECIAL STATEMENT
All articles published in journals owned by the Baishideng Publishing Group (BPG) represent the views and opinions of their authors, and not the views, opinions or policies of the BPG, except where otherwise explicitly indicated.

INSTRUCTIONS TO AUTHORS
<http://www.wjnet.com/bpg/gerinfo/204>

ONLINE SUBMISSION
<http://www.f6publishing.com>

New era of electronic brachytherapy

Prabhakar Ramachandran

Prabhakar Ramachandran, Department of Physical Sciences,
Peter MacCallum Cancer Centre, Melbourne, VIC 3165, Australia

Author contributions: Ramachandran P contributed to this paper.

Conflict-of-interest statement: Ramachandran P declares no conflict of interest related to this publication.

Open-Access: This article is an open-access article which was selected by an in-house editor and fully peer-reviewed by external reviewers. It is distributed in accordance with the Creative Commons Attribution Non Commercial (CC BY-NC 4.0) license, which permits others to distribute, remix, adapt, build upon this work non-commercially, and license their derivative works on different terms, provided the original work is properly cited and the use is non-commercial. See: <http://creativecommons.org/licenses/by-nc/4.0/>

Manuscript source: Invited manuscript

Correspondence to: Prabhakar Ramachandran, MSc, MCA, PhD, MACPSEM, MARPS, MinstP, DABR, Lead Physicist, Associate Professor, Department of Physical Sciences, Peter MacCallum Cancer Centre, 305 Grattan St, Melbourne, VIC 3165, Australia. ramachandran.prabhakar@petermac.org
Telephone: +61-3-99288964

Received: August 30, 2016

Peer-review started: September 2, 2016

First decision: September 26, 2016

Revised: December 15, 2016

Accepted: January 16, 2017

Article in press: January 18, 2017

Published online: April 28, 2017

Abstract

Traditional brachytherapy refers to the placement of radioactive sources on or inside the cancer tissues. Based on the type of sources, brachytherapy can be classified as radionuclide and electronic brachytherapy. Electronic brachytherapy uses miniaturized X-ray

sources instead of radionuclides to deliver high doses of radiation. The advantages of electronic brachytherapy include low dose to organs at risk, reduced dose to treating staff, no leakage radiation in off state, less shielding, and no radioactive waste. Most of these systems operate between 50 and 100 kVp and are widely used in the treatment of skin cancer. Intrabeam, Xofigo and Papillon systems are also used in the treatment of intra-operative radiotherapy to breast in addition to other treatment sites. The rapid fall-off in the dose due to its low energy is a highly desirable property in brachytherapy and results in a reduced dose to the surrounding normal tissues compared to the Ir-192 source. The Xofigo Axxent brachytherapy system uses a 2.25 mm miniaturized X-ray tube and the source almost mimics the high dose rate Ir-192 source in terms of dose rate and it is the only electronic brachytherapy system specifically used in the treatment of cervical cancers. One of the limiting factors that impede the use of electronic brachytherapy for interstitial application is the source dimension. However, it is highly anticipated that the design of miniaturized X-ray tube closer to the dimension of an Ir-192 wire is not too far away, and the new era of electronic brachytherapy has just begun.

Key words: Brachytherapy; Electronic brachytherapy; Intrabeam; Xofigo; Cervical cancer

© **The Author(s) 2017.** Published by Baishideng Publishing Group Inc. All rights reserved.

Core tip: Electronic brachytherapy is a new form of radiotherapy that delivers a very high dose of radiation inside or very close to the cancer tissues. These devices utilize a miniaturized X-ray source to deliver radiation at relatively high dose rates to the target volume. Electronic brachytherapy eliminates some of the accidents related to radionuclide brachytherapy such as loss of sources, radiation leakage in off state, transportation accidents and radioactive waste. It finds wide applications in the treatment of cancers including skin, breast, endometrium, cervix and spinal metastasis. Electronic brachytherapy is a promising technology of

the future and could potentially replace radionuclide brachytherapy.

Ramachandran P. New era of electronic brachytherapy. *World J Radiol* 2017; 9(4): 148-154 Available from: URL: <http://www.wjgnet.com/1949-8470/full/v9/i4/148.htm> DOI: <http://dx.doi.org/10.4329/wjr.v9.i4.148>

INTRODUCTION

Brachytherapy is a form of radiotherapy treatment technique that delivers a high dose of radiation inside or very close to the cancer tissues. The term brachytherapy was originally derived from the Greek words βραχύς (brachys) and θεραπεία (therapeía) which means "short" and "curing or healing" respectively. The history of brachytherapy dates back to the 1910s; soon after the discovery of radioactivity, Pierre Curie suggested the idea of using radioactive sources for brachytherapy, and it was first utilized in the treatment of lupus and gradually extended to other sites. Traditionally, brachytherapy involves the use of sealed radioactive sources. It is extensively used in the treatment of brain, eye, base of tongue, floor of mouth, tongue, oropharynx, lip, nasopharynx, trachea, esophagus, breast, cervix, endometrium, prostate, rectum, skin, sarcoma and many other treatment sites^[1-6]. Brachytherapy can be used alone or in conjunction with conventional external beam radiotherapy.

Based on the type of sources, brachytherapy can now be classified as radionuclide and electronic brachytherapy. The concept of electronic brachytherapy was first envisaged by Alan Sliski of the Photoelectron Corporation^[7,8]. He designed a miniaturized, low power X-ray source that can operate in the range of approximately 10 to 90 kV using small currents between 1 nA and 100 μ A. The system uses a mini accelerator that generates low energy X-rays at the tip of a needle-like probe. Most of the current electronic brachytherapy systems utilize a miniaturized X-ray source to deliver radiation at relatively high dose rates to the target volume. Miniature X-ray sources have several advantages over the most common radionuclide based brachytherapy. Table 1 highlights some of the strengths and weaknesses of electronic brachytherapy compared to radionuclide based brachytherapy. The low kilovoltage electronic X-ray sources require relatively less shielding as opposed to Co-60, Cs-137 and Ir-192 sources which require heavily shielded bunkers. The highlighting feature of X-ray based sources is the absence of radiation when the source is not in use.

RATIONALE FOR ELECTRONIC BRACHYTHERAPY

The International Commission on Radiation Protection

published a report in 2005 that reviewed all the radiotherapy accidents associated with high dose rate brachytherapy^[9]. The report showed that radionuclide based brachytherapy resulted in 500 accidents including one death along the entire chain of procedures from radioactive source packaging to dose delivery. Some of the accidents were related to loss of sources, radiation leakage and inaccurate calibration of sources. Radiation accidents with radionuclide brachytherapy can also occur due to the use of the wrong isotope, leaking sources, and failure to remove temporary implants^[10]. There are occasions when the source may not retract due to a power outage, a kink in the catheter or interlock failure. These conditions may lead to an excessive dose to the treating staff and unwanted doses to the patient while trying to retract the source. It is expected that the introduction of electronic brachytherapy would eliminate most of these accidents associated with radionuclide brachytherapy. Electronic brachytherapy systems do not emit radiation in the off state, which eliminates likely accidents with source packaging, transportation and mishandling of sources related to radionuclide brachytherapy. They can be operated in a standard treatment room with minimal shielding due to low energy and no radiation leakage in the off state. There is also no radioactive waste and hence no concerns with source transportation unlike radionuclides which require a special license for source transportation and radioactive waste disposal.

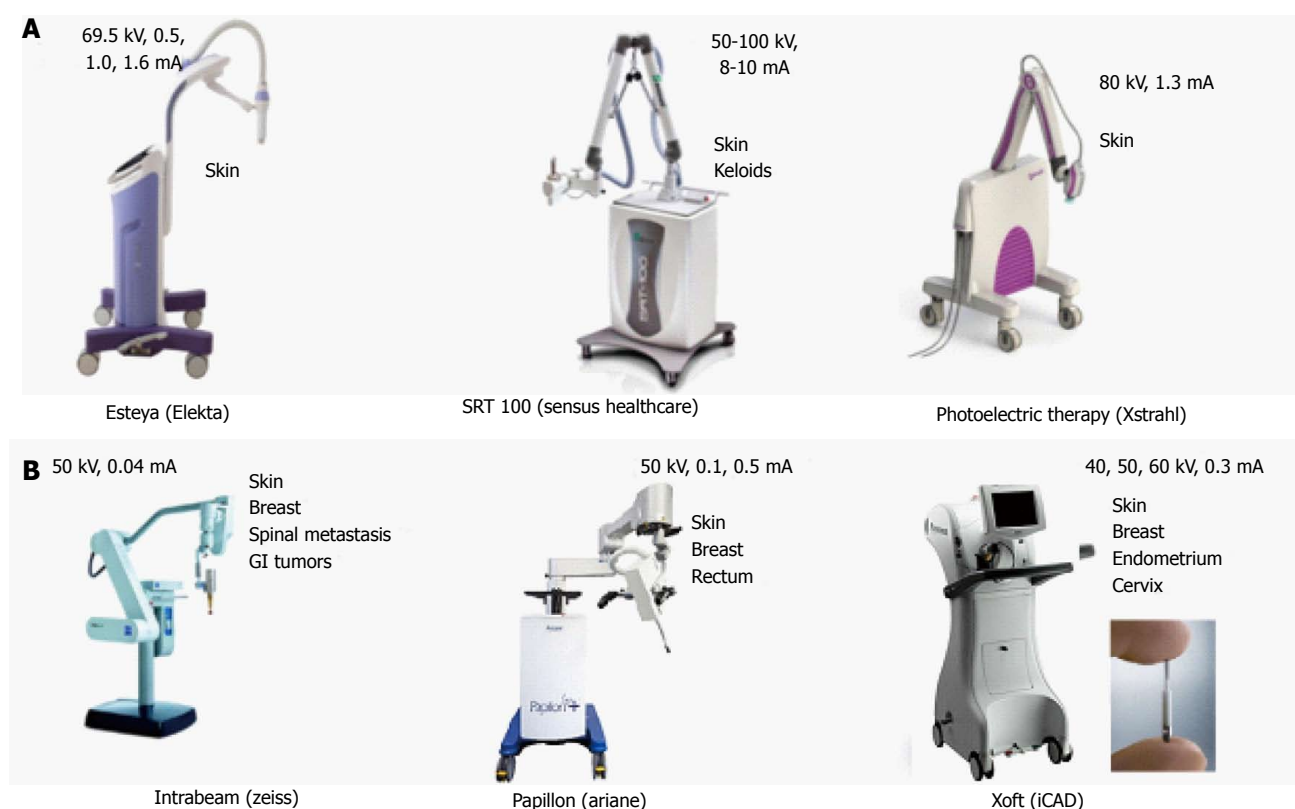
ELECTRONIC BRACHYTHERAPY MACHINES

Currently, six different types of electronic brachytherapy systems (Figure 1) are available, which includes Intrabeam (Zeiss), Xofig (iCAD), Papillon (Ariane), Photoelectric Therapy (Xstrahl), Esteya (Elekta) and SRT 100 (Sensus Healthcare). Most of these systems operate between 50 and 100 kVp. Esteya delivers 69.5 kV X-ray beam at a dose rate of 2.7 Gy/min at 3 mm and is used to treat non-melanoma skin cancer, including basal cell carcinoma and squamous cell carcinoma^[11]. Papillon from Ariane Medical Systems is used to treat breast, rectum, and skin cancers. This X-ray system operates at 30 and 50^[12] kVp with a dose rate of > 8 Gy/min and > 20 Gy/min at 20 cm focus to surface distance. The SRT-100 system operates between 50 and 100 kVp and can be used to treat non-melanoma skin cancer including basal cell carcinoma skin and keloids^[13]. Intrabeam and Xofig electronic brachytherapy have a wide variety of applicators to treat multiple sites^[14-19]. The heart of the intrabeam system is an XS4 miniaturized linear accelerator with an inbuilt internal radiation monitor that monitors the dose delivered to the patients in real time. A mini accelerator section accelerates the electrons emitted by a cathode gun, and the existing electron beam is focussed onto a gold target to generate X-rays. The intrabeam system is employed in the treatment

Table 1 Comparison of radionuclide and electronic brachytherapy sources

Source	Strengths	Weaknesses
Radionuclide	Small source Fixed energy spectrum Easy to predict the output at any point in time using half-life Used in combination with EBRT/alone Rapid dose fall-off Lower dose to organs at risk Proven clinical application Well-established protocols and treatment procedures	Radiation leakage – Off condition Radioactive waste – A big concern Frequent source replacement (depends on half-life) Output correction due to source decay Source transportation related radiation accidents Fixed-dose rate and dosimetric properties Limited treatment sites compared to EBRT Relatively large source size
Electronic brachytherapy	No radiation leakage in off condition User adjustable energy and current (dose rate) No radioactive waste Source transportation - not an issue Relatively stable output during the life of the X-ray tube Less exposure to staff	Limited treatment sites compared to radionuclide brachytherapy Minimal experience compared to radionuclide-based brachytherapy

EBRT: External beam radiation therapy.

**Figure 1 Electronic brachytherapy systems operating.** A: The range between 50 and 100 kVp; B: The range between 40 and 60 kVp.

of breast, skin, GI and spinal metastases. This system uses X-rays produced by a gold target, and the Xofter Axxent uses a tungsten target to generate X-rays. The size of a conventional diagnostic/therapeutic X-ray tube typically varies between 30 and 50 cm along the long axis and 20 cm in diameter. As opposed to the standard X-ray tube, the Xofter Axxent brachytherapy X-ray tube is the only system currently available with a diameter of 2.25 mm with a full assembly diameter of 5.4 mm which incorporates an extra space outside the cathode-anode assembly of the X-ray tube for water circulation

to extract the heat during X-ray emission. This system can be used to treat cancers of the skin, breast, and endometrium. When compared to other existing electronic brachytherapy systems, the Xofter source almost mimics a Ir-192 source in terms of dose rate. It is the only electronic brachytherapy system closer to a wired radionuclide source such as Ir-192/Co-60 currently available to treat cancer of the cervix. The nominal dose rate of the Axxent HDR X-ray source is 0.6 Gy/min at 3 cm in water. The maximum anode current, at 50 kVp is 300 μ A. The Xofter Axxent brachytherapy is

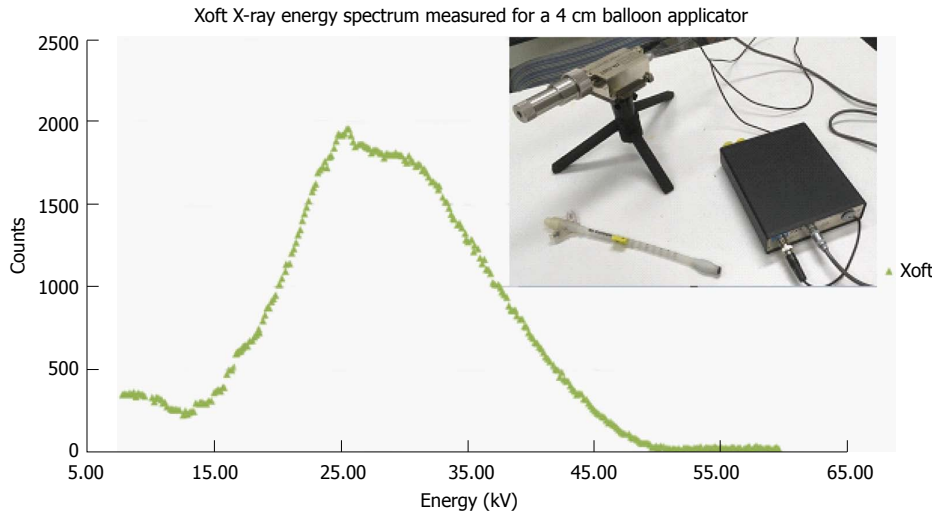


Figure 2 Xoft X-ray energy spectrum measured using an Amptek spectrometer.

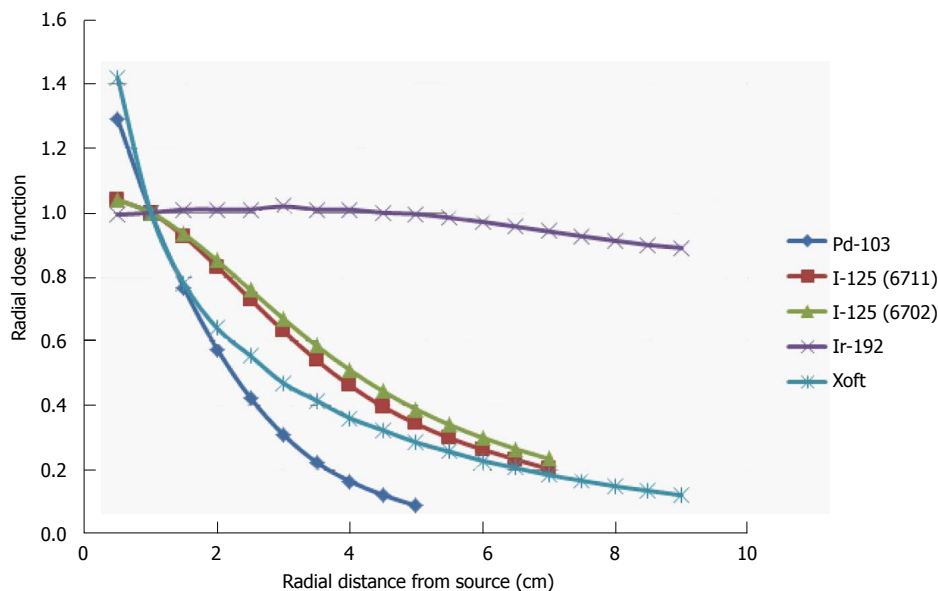


Figure 3 Radial dose function [Pd-103, I-125 (6711), I-125 (6702), Ir-192 and Xoft].

a comprehensive system with an inbuilt electrometer and a well-type chamber which enables Physicists to measure and verify the output just before treatment.

Figure 2 shows the energy spectra measured using an Amptek spectrometer placed close to a 3-4 cm spherical balloon applicator and it also indicates that the maximum energy of the Xoft X-ray source approaching 50 keV. The average energy of the Xoft Axxent X-ray source is between 26 and 35 keV which enables the systems to be used in a CT or diagnostic X-ray bunker for treatment. The dose fall-off with 50 kVp X-rays is quite rapid compared to the Ir-192 source which would help the treating physician to reduce the complications to adjacent normal tissues and may also contribute to dose escalation. Figure 3 shows that the Xoft Axxent X-ray source mimics the dose fall-off characteristics of low energy isotopes with an average energy lying between I-125 and Pd-103 radioactive sources and still

maintains the high dose rate property of the Ir-192 source. Figure 4 compares the dose fall-off of the Xoft 50 kV source, 6 MV, 6 MV 60° wedge and 18 MV beams. The dose fall-off measurement was conducted for a bare Xoft X-ray source and the X-ray source placed inside a 3-4 cm balloon applicator in a Welhofer radiation field analyzer. It is evident from the figure that the dose fall-off with electronic brachytherapy is quite rapid compared to megavoltage beams.

CLINICAL APPLICATIONS AND LIMITATIONS

Electronic brachytherapy is currently used to treat cancers of breast, skin, keloids, spinal metastasis, GI, endometrium, cervix, and rectum. Some of the existing electronic brachytherapy systems such as Esteya and

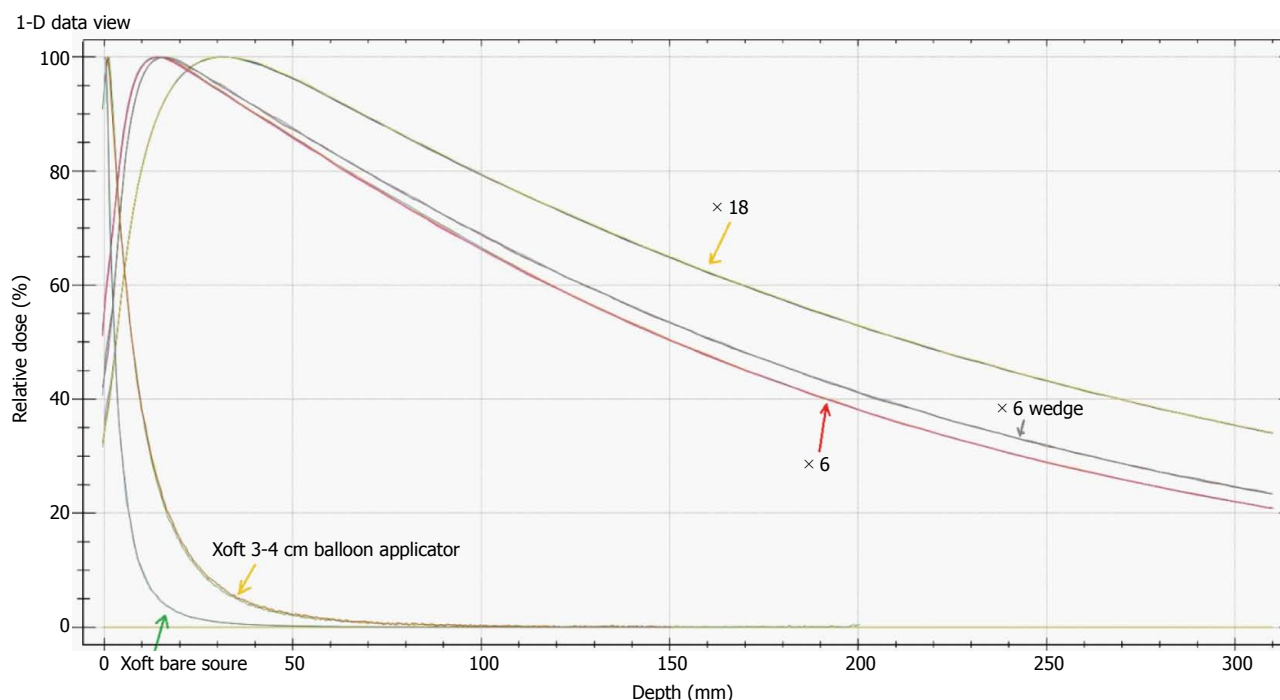


Figure 4 Comparison of 6MV, 6MV wedge, 18 MV, Xoft bare source and Xoft 3-4 cm balloon applicator profiles.

Photoelectric Therapy are limited to small skin cancers due to their specific design. The papillon+, intrabeam, Xoft and SRT-100 electronic brachytherapy systems are also used in the treatment of skin cancers. Most of these systems use a small flattening filter to flatten the beam for the treatment of skin cancers. Several studies have demonstrated that these systems result in lower toxicity and provides excellent cosmesis^[18]. Intrabeam uses a special needle applicator with a diameter of 4.4 mm for the treatment of vertebral metastases. The papillon+, intrabeam, and xoft electronic brachytherapy systems produce an isotropic distribution which is highly desirable for breast intraoperative radiotherapy. The TARGIT trial is the largest IORT trial to date using electronic brachytherapy in conjunction with breast conservation surgery. This trial studied a total of 3451 patients wherein 1721 subjects were randomized to TARGIT and 1730 to external beam radiotherapy. The 5-year results of the local control and overall survival from the TARGIT-A randomized trial published in Lancet 2014 concluded that a risk-adapted approach should be considered for patients treated with electronic brachytherapy^[20]. In 2010, the first multi-center study to evaluate the safety and device performance of Xoft Electronic Brachytherapy was published by Mehta *et al*^[21]. This study enrolled a total of 65 patients between March 2007 and March 2008 and had completely resected invasive ductal carcinoma or ductal carcinoma insitu with N0, M0. The fractionated regimen of 34 Gy over 10 fractions prescribed 1 cm beyond the balloon surface show similar acute toxicities to other high dose rate approaches for accelerated partial breast irradiation.

According to the World Health Organization, cervical cancer is the second most common cancer in women worldwide and every year more than 270000 women die from cervical cancer^[22]. Brachytherapy is one of the most common treatment modalities used in the treatment of cervical cancer. Traditionally, radionuclide-based brachytherapy has been administered alone or in combination with external beam radiotherapy for cervical cancer patients. The majority of the centers in developing countries have a remote afterloading treatment unit for delivering this modality. Most of the radiation accidents associated with these sorts of procedures could be eliminated with the use of electronic brachytherapy. The Xoft Axxent requires relatively fewer resources compared to the standard radionuclide based brachytherapy. Recent studies have shown that Ir-192, Co-60, and Xoft based cervical brachytherapy dosimetry are comparable and could result in reduced dose to the bladder and rectum^[23]. Figure 5 shows a simulated intracavitary treatment plan planned using the Xoft X-ray source for a predefined dwell positions. The rapid dose fall-off of 50 kV compared to Ir-192 is one of the main reasons for this reduced dose to the bladder and rectum. Recently, Xoft introduced a Henschke type applicator that could enable the delivery of radiation to cervical cancers. The cervical Henschke type applicators are made of a titanium material with 0°, 15°, 30° and 45° tandem angles and 2.0, 2.5 and 3 cm ovoid diameters. The standard flexible source channel used for cancers other than cervical is 25 cm and exclusively for cervical brachytherapy the source channel is 50 cm (Figure 6). Xoft also provides a set of vaginal applicators for the treatment of endometrial cancers.

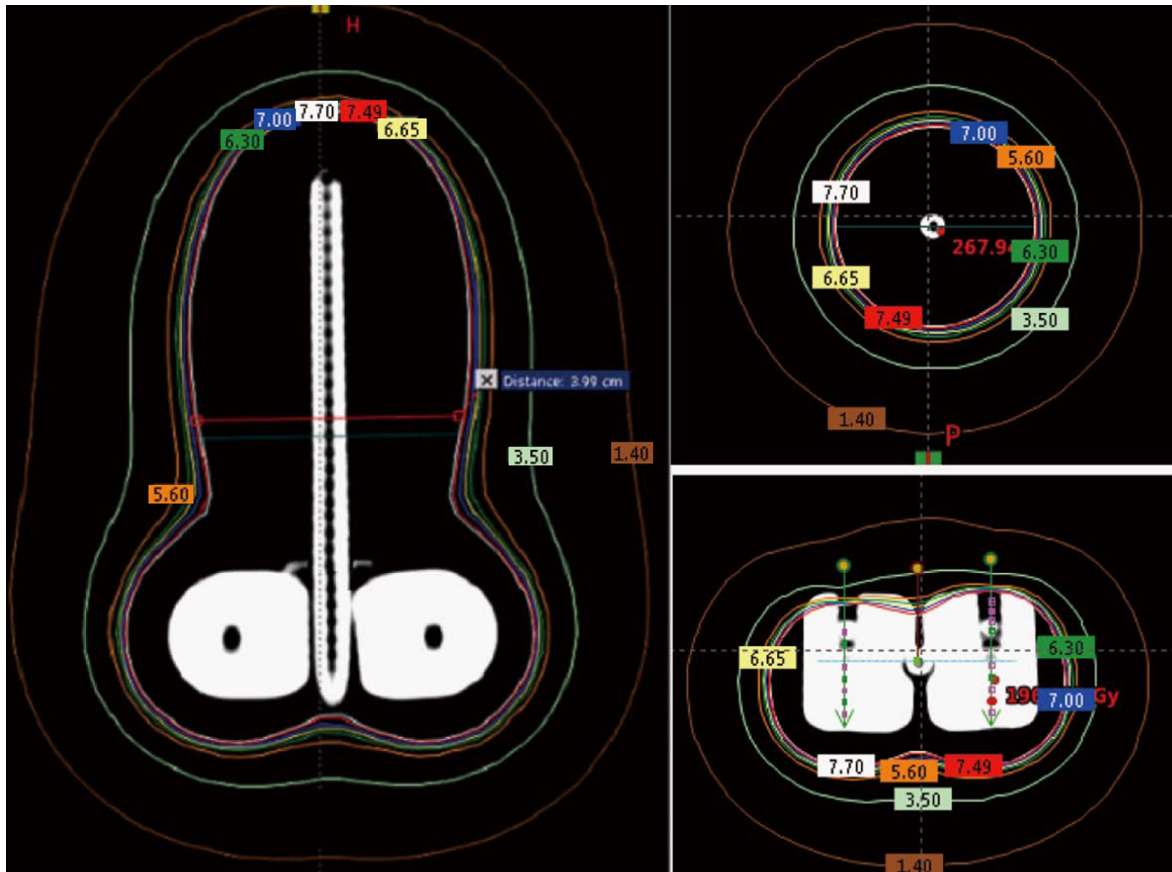


Figure 5 Simulation of a Tandem and Ovoid applicators planned in a Brachyvision software for a predefined Xoft X-ray source dwell positions.

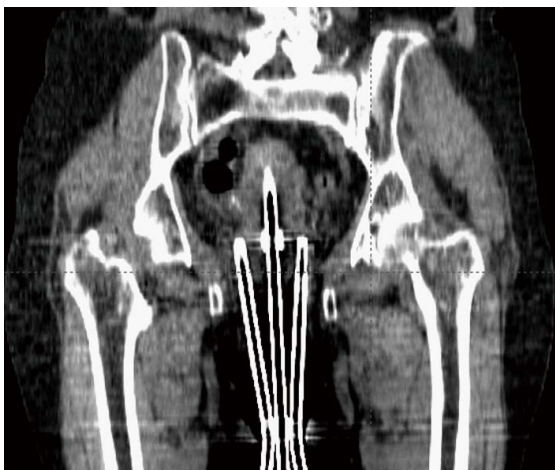


Figure 6 Coronal view of the Xoft Henschke applicator.

The existing miniaturized X-ray tube has few limitations in its longevity and source size. With radionuclide-based brachytherapy, the specific activity of the source determines the size of the source. Radionuclide sources such as Iridium-192 have a high specific activity which enables the manufacturers to produce small sources with high activity. Due to this, conventional radionuclide-based brachytherapy has wider applications and can deliver interstitial brachytherapy to multiple treatment

sites. Head and neck based interstitial brachytherapy such as the base of tongue and floor of mouth require a loop technique where the smaller size source would help to make the sharp bend. The diameter of the Axxent xoft brachytherapy source is 2.25 mm, and when housed inside a cooling tube it increases the effective source diameter to 5 mm. However, this limits its application to interstitial brachytherapy. With a rapid growth in the field of computer technology and biomedical engineering could one day lead to the design of a stable sub-millimetre X-ray tube. Such a miniaturized X-ray tube would enable the expansion of electronic brachytherapy to most sites currently treated by Ir-192 sources.

CONCLUSION

The ever-growing technological advancements have led to the development of a miniaturized X-ray tube and this has been explored for various treatment sites. Electronic brachytherapy is a promising technology that has more potential to replace the existing radionuclide-based brachytherapy procedures. One of the limiting factors that impede the use of electronic brachytherapy for interstitial application is the source dimension. However, it is highly anticipated that the design of miniaturized X-ray tube closer to the dimension of an Ir-192 wire is not too far away, and the new era of electronic

brachytherapy has just begun.

ACKNOWLEDGMENTS

The author would like to thank Associate Professor Moshi Geso, RMIT University for providing the Amptek X-ray spectrometer. The author would also like to thank Dr. Steven David, Dr. Derrick Wanigaratne and Mr Karl Roozen for helping with this manuscript.

REFERENCES

- 1 **Orton CG**, Seyedsadr M, Somnay A. Comparison of high and low dose rate remote afterloading for cervix cancer and the importance of fractionation. *Int J Radiat Oncol Biol Phys* 1991; **21**: 1425-1434 [PMID: 1938550]
- 2 **Homs MY**, Steyerberg EW, Eijkenboom WM, Tilanus HW, Stalpers LJ, Bartelsman JF, van Lanschoot JJ, Wijrdeman HK, Mulder CJ, Reinders JG, Boot H, Aleman BM, Kuipers EJ, Siersema PD. Single-dose brachytherapy versus metal stent placement for the palliation of dysphagia from oesophageal cancer: multicentre randomised trial. *Lancet* 2004; **364**: 1497-1504 [PMID: 15500894 DOI: 10.1016/S0140-6736(04)17272-3]
- 3 **Mohanti BK**, Bansal M, Bahadur S, Shukla NK, Deo SV, Prabhakar R, Rath GK. Interstitial brachytherapy with or without external beam irradiation in head and neck cancer: Institute Rotary Cancer Hospital experience. *Clin Oncol (R Coll Radiol)* 2001; **13**: 345-352 [PMID: 11716227]
- 4 **Radek A**, Grochal M, Gasiński P, Zieliński K, Kopczyński J, Sobotkowski J, Grzelak M, Lyczak P, Błaszczyk B. Stereotactic biopsy and brachytherapy in the diagnostics and treatment of brain tumors--preliminary report. *Neurol Neurochir Pol* 2001; **35** Suppl 5: 5-11 [PMID: 11935681]
- 5 **King TA**, Bolton JS, Kuske RR, Fuhrman GM, Scroggins TG, Jiang XZ. Long-term results of wide-field brachytherapy as the sole method of radiation therapy after segmental mastectomy for T(is,1,2) breast cancer. *Am J Surg* 2000; **180**: 299-304 [PMID: 11113440]
- 6 **Ragde H**, Grado GL, Nadir BS. Brachytherapy for clinically localized prostate cancer: thirteen-year disease-free survival of 769 consecutive prostate cancer patients treated with permanent implants alone. *Arch Esp Urol* 2001; **54**: 739-747 [PMID: 11692443]
- 7 **Peter M**, Nomikos PM, Dinsmore MT, Sliski AP. Miniaturized low power x-ray source. United States patent US 5153900. 1992 Oct 6
- 8 **Dinsmore M**, Harte KJ, Sliski AP, Smith DO, Nomikos PM, Dalterio MJ, Boom AJ, Leonard WF, Oettinger PE, Yanch JC. A new miniature x-ray source for interstitial radiosurgery: device description. *Med Phys* 1996; **23**: 45-52 [PMID: 8700032 DOI: 10.1118/1.597790]
- 9 **Valentin J**. Prevention of high-dose-rate brachytherapy accidents. ICRP Publication 97. *Ann ICRP* 2005; **35**: 1-51 [PMID: 16243099 DOI: 10.1016/j.icrp.2005.05.002]
- 10 **Kaulich TW**, Becker G, Lamprecht U, Nüsslin F, Bamberg M. Emergency rescue in accidents with HDR afterloading units. *Strahlenther Onkol* 1999; **175**: 524-529 [PMID: 10554648]
- 11 **Garcia-Martinez T**, Chan JP, Perez-Calatayud J, Ballester F. Dosimetric characteristics of a new unit for electronic skin brachytherapy. *J Contemp Brachytherapy* 2014; **6**: 45-53 [PMID: 24790622 DOI: 10.5114/jcb.2014.40770]
- 12 **Myint AS**. Novel radiation techniques for rectal cancer. *J Gastrointest Oncol* 2014; **5**: 212-217 [PMID: 24982769 DOI: 10.3978/j.issn.2078-6891.2014.031]
- 13 **Sheu RD**, Powers A, Lo YC. Commissioning a 50-100 kV X-ray unit for skin cancer treatment. *J Appl Clin Med Phys* 2015; **16**: 5182 [PMID: 26103186]
- 14 **Dickler A**. Xofig Axxent electronic brachytherapy: a new device for delivering brachytherapy to the breast. *Nat Clin Pract Oncol* 2009; **6**: 138-142 [PMID: 19174776 DOI: 10.1038/nponc1319]
- 15 **Rong Y**, Welsh JS. Surface applicator calibration and commissioning of an electronic brachytherapy system for nonmelanoma skin cancer treatment. *Med Phys* 2010; **37**: 5509-5517 [PMID: 21089786 DOI: 10.1118/1.3489379]
- 16 **Hepel JT**, Hiatt JR, Cardarelli GA, Wazer DE. Modeling study for optimization of skin dose for partial breast irradiation using Xofig Axxent electronic brachytherapy applicator. *Brachytherapy* 2010; **9**: 81-85 [PMID: 19850533 DOI: 10.1016/j.brachy.2009.08.005]
- 17 **Richardson S**, Garcia-Ramirez J, Lu W, Myerson RJ, Parikh P. Design and dosimetric characteristics of a new endocavitary contact radiotherapy system using an electronic brachytherapy source. *Med Phys* 2012; **39**: 6838-6846 [PMID: 23127076 DOI: 10.1118/1.4757915]
- 18 **Goubert M**, Parent L. Dosimetric characterization of INTRABEAM® miniature accelerator flat and surface applicators for dermatologic applications. *Phys Med* 2015; **31**: 224-232 [PMID: 25687416 DOI: 10.1016/j.ejmp.2015.01.009]
- 19 **Williams NR**, Pigott KH, Brew-Graves C, Keshtgar MR. Intra-operative radiotherapy for breast cancer. *Gland Surg* 2014; **3**: 109-119 [PMID: 25083504 DOI: 10.3978/j.issn.2227-684X.2014.03.03]
- 20 **Vaidya JS**, Wenz F, Bulsara M, Tobias JS, Joseph DJ, Keshtgar M, Flyger HL, Massarut S, Alvarado M, Saunders C, Eiermann W, Metaxas M, Sperk E, Sütterlin M, Brown D, Esserman L, Roncadin M, Thompson A, Dewar JA, Holtveg HM, Pigorsch S, Falzon M, Harris E, Matthews A, Brew-Graves C, Potyka I, Corica T, Williams NR, Baum M. Risk-adapted targeted intraoperative radiotherapy versus whole-breast radiotherapy for breast cancer: 5-year results for local control and overall survival from the TARGIT-A randomised trial. *Lancet* 2014; **383**: 603-613 [PMID: 24224997 DOI: 10.1016/S0140-6736(13)61950-9]
- 21 **Mehta VK**, Algan O, Griem KL, Dickler A, Haile K, Wazer DE, Stevens RE, Chadha M, Kurtzman S, Modin SD, Dowlatshahi K, Elliott KW, Rusch TW. Experience with an electronic brachytherapy technique for intracavitary accelerated partial breast irradiation. *Am J Clin Oncol* 2010; **33**: 327-335 [PMID: 20375833 DOI: 10.1097/COC.0b013e3181d79d9e]
- 22 **WHO guidance note**. Comprehensive cervical cancer prevention and control - a healthier future for girls and women, 2012. Switzerland
- 23 **Mobit PN**, Packianathan S, He R, Yang CC. Comparison of Axxent-Xofig, (192)Ir and (60)Co high-dose-rate brachytherapy sources for image-guided brachytherapy treatment planning for cervical cancer. *Br J Radiol* 2015; **88**: 20150010 [PMID: 25996576 DOI: 10.1259/bjr.20150010]

P- Reviewer: Chen F, Chow J, Dickler A S- Editor: Song XX

L- Editor: A E- Editor: Wu HL



"Beyond saving lives": Current perspectives of interventional radiology in trauma

Anuradha Singh, Atin Kumar, Pawan Kumar, Subodh Kumar, Shivanand Gamanagatti

Anuradha Singh, Atin Kumar, Pawan Kumar, Shivanand Gamanagatti, Department of Radiodiagnosis, All India Institute of Medical Sciences, Ansari Nagar, New Delhi 110029, India

Subodh Kumar, Department of Surgical Disciplines, All India Institute of Medical Sciences, Ansari Nagar, New Delhi 110029, India

Author contributions: Gamanagatti S contributed equally to conception, article design, and image preparation; Singh A helped with the literature search and article drafting; Kumar A helped to procure the images, and final approval of version of article to be published; Kumar P and Kumar S contributed in critical revision article concept, revision literature search and image preparation.

Conflict-of-interest statement: The authors have nothing to disclose.

Open-Access: This article is an open-access article which was selected by an in-house editor and fully peer-reviewed by external reviewers. It is distributed in accordance with the Creative Commons Attribution Non Commercial (CC BY-NC 4.0) license, which permits others to distribute, remix, adapt, build upon this work non-commercially, and license their derivative works on different terms, provided the original work is properly cited and the use is non-commercial. See: <http://creativecommons.org/licenses/by-nc/4.0/>

Manuscript source: Unsolicited manuscript

Correspondence to: Shivanand Gamanagatti, MD, Additional Professor, Department of Radiodiagnosis, All India Institute of Medical Sciences, Room no 81-B, Ansari Nagar, New Delhi 110029, India. shiv223@gmail.com
Telephone: +91-11-26594567
Fax: +91-11-26588500

Received: September 25, 2016
Peer-review started: September 28, 2016
First decision: November 2, 2016
Revised: December 30, 2016
Accepted: January 16, 2017
Article in press: January 18, 2017
Published online: April 28, 2017

Abstract

Interventional radiology (IR) has become an integral part in the management of traumatic injuries. There is an ever-increasing role of IR in traumatic injuries of solid abdominal organs, pelvic and peripheral arteries to control active bleeding by therapeutic embolization or vascular reconstruction using stent grafts. Traditionally, these endovascular treatments have been offered to hemodynamically stable patients. However, in recent times endovascular approach has become preferable to surgery even in hemodynamically unstable patients with injury of surgically difficult-to-access sites. With shifting trends towards non operative management coupled with availability of the current state-of-the-art equipments, hardware and technical expertise, IR has gained an impeccable role in trauma management. However, due to lack of awareness and widespread acceptance, IR continues to remain an ocean of unexplored potentialities.

Key words: Blunt abdominal trauma; Pelvic trauma; Peripheral arterial injury; Interventional radiology; Embolization

© **The Author(s) 2017.** Published by Baishideng Publishing Group Inc. All rights reserved.

Core tip: Over the past two decades, there has been a paradigm shift in the management of traumatic injuries with inception of the concept of non operative management (NOM), which is followed if there are no peritoneal signs or hollow viscus injury. Interventional radiology (IR) is an extension of NOM which not only saves lives by achieving hemostasis at the site of vascular injury or difficult to access surgical sites but also controls rebleeding following surgery. Time and again it has proven to be a highly effective management option which successfully bridges the conservative management and emergency laparotomy. In current scenario, in vascular injury, IR can obviate emergency

laparotomy not only in hemodynamically stable but unstable patients as well, as evidenced by the recent literature. Ignorance and lack of acceptance have limited the utilization of IR significantly, which if practiced judiciously will provide expedient hemodynamic control as well as faster restoration to physiological status.

Singh A, Kumar A, Kumar P, Kumar S, Gamanagatti S. "Beyond saving lives": Current perspectives of interventional radiology in trauma. *World J Radiol* 2017; 9(4): 155-177 Available from: URL: <http://www.wjgnet.com/1949-8470/full/v9/i4/155.htm> DOI: <http://dx.doi.org/10.4329/wjcr.v9.i4.155>

INTRODUCTION

Trauma continues to be the leading cause of mortality in young population. Uncontrolled exsanguination is the most common cause of the early trauma related mortality, accounting for nearly 30%-40% of such fatalities. At initial hospitalization following trauma, resuscitation is done as per the standard advanced trauma life support guidelines. Patient management as per these guidelines is divided into two categories—primary and secondary survey. Primary survey aims at performing immediate lifesaving interventions. It is defined by the mnemonic ABCDE which include control of Airway, Breathing, Circulation, Disability assessment (neurological) and Exposure of the patient to rule out any injury to unexposed part. In secondary survey, trauma related brief clinical details are obtained and examination is performed. Afterwards, on the basis of clinical status (hemodynamic stability), mechanism of injury and the presence of hemoperitoneum, patients are triaged into surgical and nonsurgical candidates. Surgical candidates are immediately shifted to the operation-theatre without any further investigation, for exploration. On the contrary, hemodynamically stable non-surgical candidates are further subjected to cross-sectional imaging to evaluate the extent and severity of injuries, besides localizing the site of active bleeding, if any^[1,2].

Recent times have witnessed an increasing role of IR in the management of acutely injured polytrauma patients. Similar to the shifting trends towards minimally invasive procedures as in other surgical disciplines, therapeutic embolization by endovascular route is the next benchmark in the non operative management (NOM) of hemodynamically stable patients which considerably decreases the morbidity and duration of hospitalization apart from imminently saving an endangered life^[1].

Currently, interventional radiology (IR) procedures are targeted at managing vascular injuries in a hemodynamically stable non-surgical patient. Whereas, in hemodynamically unstable patients, surgery is the mainstay of treatment. However, exception to this rule is the bleeding at certain surgically difficult-to-access

sites which are preferably managed by endovascular interventions irrespective of the hemodynamic status. Nonetheless, when and how to intervene by endovascular route depends on a multitude of parameters including clinical stability, type and location of injury. Although, IR procedures may not reduce overall mortality, there is definite immediate survival benefit, especially in traumatic vascular injuries^[3].

On the basis of mechanism of injury, traumatic injuries may be classified into blunt or penetrating. This has implications in management as penetrating injuries are more commonly associated with hollow visceral organs and mesenteric injury as compared to blunt trauma, and hence, they more often undergo surgery. Contrast-enhanced CT (CECT) is imperative in all those cases of penetrating trauma where depth of wound is critical (based on surgeon's discretion), provided the patient is hemodynamically stable. Nonetheless, the indications and technique of radiological interventions remain same regardless of the mechanism of injury^[1-3].

The purpose of this article is to review the principles and techniques of IR used in the treatment of arterial injuries of solid organs, pelvic fractures and extremities along with an abridged recommended protocol practiced at the author's institute. Also, an overview of the scope of endovascular interventions as well as non-vascular interventions is briefed.

CURRENT STATUS OF INTERVENTIONAL RADIOLOGIST IN A TRAUMA TEAM

Managing traumatic injury is a multidisciplinary approach with the interventional radiologist increasingly becoming an integral part of the trauma team. Importance of IR lies in the fact that it has now emerged as a separate sub-specialty of radiology. Tools and techniques of IR include image guidance to approach the bleeding site through endovascular route and clog the bleeder by a host of embolizing agents such as coil, gelfoam or particles. Apart from this, IR also has a definite role in the management of peripheral vascular injuries by reconstruction of the vessel through stent graft. The old adage "time is money" holds true in managing critically injured patients. Hence, a dedicated IR team is imperative round the clock to perform these non-invasive interventions, thereby, minimizing the patient's morbidity besides saving lives^[1,2].

Role of IR in trauma^[1,4]

In traumatic injuries, IR procedures may be useful as the sole definitive treatment or as a temporary adjunct prior to surgery.

Definitive indications

Most common indication of IR in trauma is endovascular embolization in vascular injury of solid abdominal organs. Besides, endovascular route is preferred in injuries at anatomically complex sites like pelvis and maxillofacial

regions, even if the patient is hemodynamically unstable. Re-bleeding following surgery is preferably managed through endovascular route as there may be anatomical distortion and coagulopathy which can complicate re-laparotomy. Further, interventions like transcatheter-embolization or stent placements have shown promising results in peripheral vascular injuries by controlling the ongoing bleeding as well as maintaining the vascular continuity; hence, preventing limb ischemia. Nowadays, if the facility is available, endovascular interventions are favored over surgery wherever feasible as there is less morbidity and mortality associated with the former^[1,4].

Temporary indications

Endovascular interventions can also be used as a temporary adjunct to definitive surgery to prevent massive exsanguination. For example, Balloon occlusion of the internal iliac arteries or abdominal aorta/ its branches may be done in cases of life-threatening hemorrhage prior to emergency laparotomy. Prophylactic embolization may be done in high grade (≥ 4) solid visceral organ injuries (liver, spleen) even without any vascular injury as these are more likely to fail with NOM^[1-4].

Principles, tools and techniques of IR in the setting of trauma^[1,2,4]

General principles of IR remain the same as in elective procedures, however, in trauma, aim is to save life by rapidly controlling exsanguinating hemorrhage. Hence, many a times balance needs to be struck between precision vs suboptimal embolization. The chief mechanism of action of the embolic agents include reduction in perfusion pressure which subsequently reduces or halts the ongoing bleeding. Furthermore, embolization should be as close to the site of vascular injury as possible. However, drawbacks of too proximal embolization include recruitment of collaterals leading to re-bleeding whereas distal embolization will result in infarct.

SPECIAL CONSIDERATIONS FOR ENDOVASCULAR INTERVENTIONS IN TRAUMA^[1,2,4]

In traumatic injuries, ongoing hemorrhage and hypovolemia frequently leads to arterial spasm. Hence, catheterization should be as super-selective as possible as this may aid in detection of injuries which may be occult on initial non-selective angiograms.

Technique of the embolization, *i.e.*, selective vs non-selective depends on the site and size of vessel injured, *e.g.*, bleeding from an end-artery may be seen in certain organs like liver, kidney, spleen, and sacrificing it by embolization whether temporary or permanent is acceptable. In order to minimize the loss of functioning parenchyma and tissue necrosis, embolizing agent should be delivered as proximal to the target site as

possible. Reaching the peripheral most terminal branch super-selectively which gradually narrows in calibre, requires the use of micro-catheters which can tolerate small pieces of gel-foam, coils or particles. However, in hemodynamically unstable patients, if there is difficulty in reaching the site of bleeding more selectively, procedure should be expedited by settling for non-selective proximal embolization with an intent to save life over an organ^[1,4].

At certain sites with rich anastomotic network, like the buttock or pelvis, the goal is to occlude the arteries of small calibre while preserving the distal anastomoses. These small arteries are filled with small pieces of gelfoam followed by occlusion of the proximal branch by coil. In another modification of this technique, if catheterization distal to the site of vascular injury (*e.g.*, pseudoaneurysm) is achieved, then coils are deployed from distal to proximal, spanning the injured site, also called "sandwich technique". This technique avoids the risk of procedure failure that would result from retrograde blood flow by collateral circulation leading to vascular leakage. Due to the similar risks of rebleeding due to collaterals in pelvic trauma, contralateral internal iliac artery angiography and embolization should be done.

If there is a rent in large calibre arteries like aorta or iliac artery, it is repaired by covered stent grafts whereas bleeding from smaller vessels is dealt with material embolization. Similarly, restoration of the injured non-expandable conduit vessels of extremities require either surgery or stent graft. Other embolizing agents (except for non-axial branches, *vide infra*) are not used as there is risk of ischemia due to paucity of collateral circulation^[2,4].

It is worthwhile to mention that the most important determinant for the successful control of bleeding by embolizing agents is an intact coagulation cascade which helps in clot formation. Hence, early endovascular intervention is desirable before hypothermia, acidosis or coagulopathy sets in. Before concluding a negative angiogram, possibility of variant anatomy needs consideration. Of the numerous variants, following are the commonest^[5]: (1) celiac axis angiogram: Dorsal pancreatic artery arising from celiac trunk (approximately 10%), not to be mistaken for contrast extravasation; (2) superior mesenteric artery angiogram: Replaced accessory right hepatic artery (approximately 12%); and (3) pelvic angiogram: Origin of obturator artery from inferior epigastric or common femoral artery requiring catheterization of external iliac artery.

ESSENTIALS OF RADIOLOGICAL INTERVENTIONS^[1-4]

Pre-procedure preparation

Ongoing resuscitation measures (airway maintenance, fluid, medications and blood transfusion) is imperative during all aspects of trauma care even during angio-

graphic intervention. Review of available imaging such as CT scan if already performed plays an important role in the detection, location and description of the visceral and vascular injuries (*e.g.*, the extent of organ injuries, presence of active contrast extravasation, pseudoaneurysm, dissection or arterio-venous fistula).

Laboratory studies are not prerequisite for trauma angiography and the procedure should not be delayed for results of coagulation profile. Management plan should be discussed with the trauma surgeon and also with the family. Informed consent must always be obtained.

Procedure

Initial steps of angiographic intervention for trauma are similar regardless of the location of injury. Arterial access is usually obtained *via* common femoral artery and vascular sheath is placed (6F for adults and 5 F for pediatric patients) after ascertaining the puncture site by fluoroscopy. In cases of severe hemodynamic shock, the femoral pulses may not be palpable, and in such cases ultrasound guidance may be used to gain vascular access. If pre-procedural imaging findings are known, then angiography should be targeted immediately to the site of injury to achieve haemostasis. In cases where patient has been shifted directly to IR suite without any prior imaging, then diagnostic angiography should be extensive enough to include all the potential sites of injury (solid abdominal viscera, mesenteric and pelvic vasculature). Angiographic findings suggestive of vascular injury include contrast extravasation, arterial occlusion, arteriovenous fistula, pseudoaneurysm and diffuse abnormal blush. Super-selective catheterization (*e.g.*, proper hepatic artery, gastroduodenal artery, splenic artery, renal artery, superior mesenteric artery, anterior and posterior division of internal iliac artery) is imperative not only to identify the potential site of injury but also helps in targeted embolization. It is prudent to perform multiple angiographic views as just one angiographic view or run can miss significant findings. Based on the angiographic findings and site of injury, appropriate embolizing material is used (*vide infra*).

Occasionally, nonselective gelfoam embolization of the internal iliac arteries without angiographic evidence of vascular injury especially of bilateral internal iliac arteries as in pelvic trauma may help in controlling venous bleeds, however its potential benefit is controversial. Post-embolization or post stent placement angiography is critical to confirm hemostasis prior to removal of the access sheath.

Special situations^[2,3]

False negative diagnostic angiography: Discrepancies between CT and angiography leading to negative diagnostic angiography may result from intermittent vasospasm, spontaneous occlusion, non-arterial bleeder (venous or capillary), failure to achieve selective catheterization which may miss vascular injuries especially if ongoing bleeding is slow/from a terminal

branch or if there is a variant arterial anatomy (*vide supra*). Occasionally, there may not be any flow through the ruptured vessel at the time of examination which is also referred as “cut-off” sign on angiography.

Pelvic trauma: In severe pelvic trauma, usually branches of bilateral internal iliac arteries are injured. In such cases, both the internal iliac arteries can be accessed through a single arterial puncture with the help of specially designed uterine artery catheter.

Teaching point: Not all arterial injuries require prompt management. Bleeding from small arterial branches (1-2 mm) are usually self-limiting, provided the patient is normothermic with an intact coagulation cascade.

Embolizing agents^[4,6-10]

Selection of embolization agent depends on the type and site of injury, selectivity of catheterization, level of permanence of procedure (temporary vs permanent), coagulation profile (Figure 1) amiliarity and comfort level of interventional radiologist performing the procedure (Tables 1 and 2).

According to the mechanism of delivery coils can be categorized into two types - pushable or detachable coils. Once deployed, pushable coils cannot be repositioned unlike detachable coils. Method of deployment of detachable coils can be mechanical, electrolytic or hydrolytic. Amongst these, Guglielmi detachable coil which is detached electrolytically is most widely used. Due to the benefits of controlled and precise delivery at the target sits, these coils are most commonly used in cerebral aneurysms. However, they are not commonly used in trauma due to the longer time needed for their delivery. Besides, they are expensive and require more expertise^[8-10].

Embolizing agents which can be used in coagulopathy

Choice of embolizing material in traumatic injuries is a special concern due to frequent prevalence of coagulopathy in these patients as compared to the general population. As mentioned above, most of the commonly used embolizing agents like gelfoam or coils need an intact coagulation mechanism for clot formation. On the contrary, mechanism of clot formation in liquid embolic agents is independent of the coagulation profile. However, the major limitation precluding their widespread use is tissue infarction which is especially more with absolute alcohol and sclerosants. Nevertheless, few other liquid embolic agents like N-butyl cyanoacrylate or ethylene vinyl alcohol co-polymer (onyx) with better safety profile may be used in coagulopathy. Nevertheless, these agents are costly and require expertise for controlled administration at target site so as to limit the complications.

Another alternative in coagulopathy is hydrogel coil which is a platinum coil coated with an expandable polymer. After polymerization, there is an increase in the volume of coil by up to nine-fold. This property of

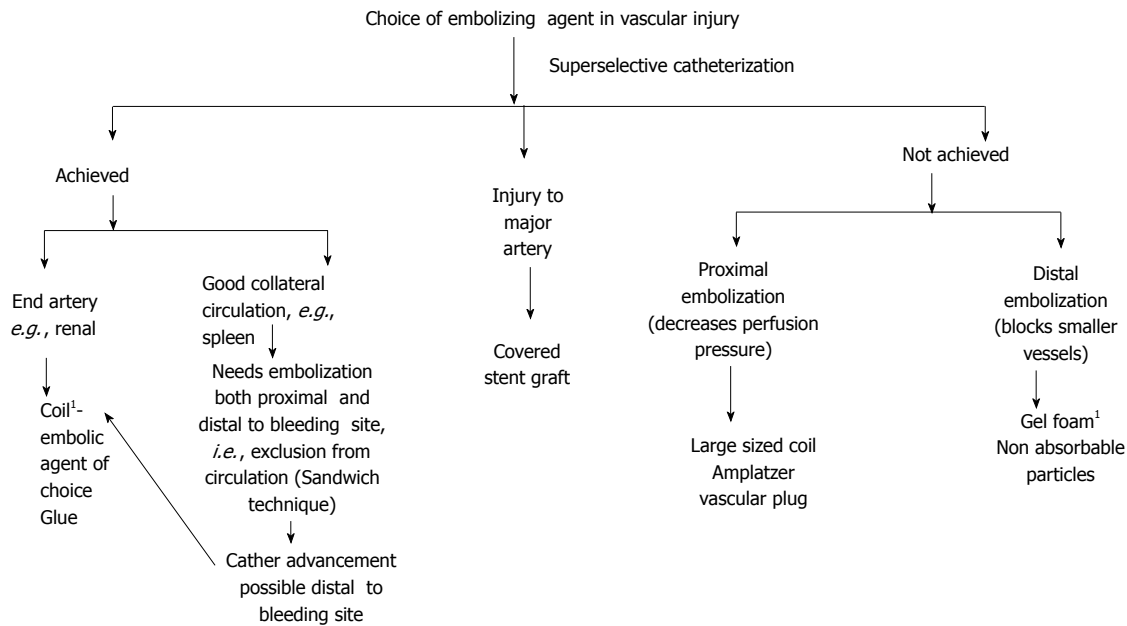


Figure 1 Choice of embolizing agent in vascular injury. ¹Workhorse of IR in trauma. IR: Interventional radiology.

Table 1 Embolizing agents used in traumatic injuries

Embolizing agent	Indications	Advantages	Demerits
Permanent			
Coil (covered with thrombogenic fibers) (Size of coil should be 20%-30% more than the target vessel size)	Active contrast extravasation Pseudoaneurysm	Rapid and effective control of bleeding Agent of choice when site of bleeding can be approached superselectively Relatively cheap (standard coils)	Reduced effectiveness in coagulopathy which hampers effective thrombosis Limited utility when target site can not be selectively approached
Non-absorbable particles (e.g., Polyvinyl alcohol)	Injury to terminal vessels	Permanent control of bleeding Adjunct to gelfoam	Tendency to clump and aggregate at the catheter site leading to proximal embolization, catheter block Non targeted embolization due to small size Tissue necrosis
Liquid embolic agent [e.g., glue(N-butyl cyanoacrylate)]	As an alternative to coil especially in rebleeding	Rapid control of bleeding in hemodynamically unstable patients	No added benefit over gelfoam, incurs additional cost Expertise for controlled delivery at target site Propensity for non targeted distal embolization leading to infarct or necrosis Rarely glue embolization of pulmonary circulation
Amplatzer vascular plug (AGA Medical Corporation, Plymouth, MN, United States) Available in various sizes	Large caliber vessel or large AVF (large size plug)	Single device (mesh shaped metal coil): Deployed with much greater accuracy and replaces the need of multiple coils	Costly Less beneficial in cases of distal vascular injury with good collateralization as it is deployed in proximal larger branch
Temporary			
Gelatin sponge (CuraMedical, Assendelft, the Netherlands) Either in the form of pledgets (cut from gelfoam sheet) or slurry (non-ionic iodinated contrast mixed with gelfoam)	Cornerstone of IR in trauma: Controls majority of haemorrhage	Rapid, effective temporary occlusion of bleeding site Easily available and cheap Can be easily refashioned to the size of target artery	Non-targeted embolization to proximal branches can occur in case of rapid injection Resorbed after 3 wk: Potential risk of delayed haemorrhage Reduced effectiveness in impaired hemostasis Small risk of infection due to entrapped air during preparation
Autologous clot	Nonselective and rapid control of haemorrhage	Easy availability No cost	Clot dissolution in cases of coagulopathy and hemodilution
Starch microparticles	Usually complete reperfusion after 60 min, less tissue damage	Temporary occlusion is usually complete Uniform distribution	Allergic, non-target embolization

expansion ensures more complete occlusion which is especially beneficial in large aneurysms. However, cost

and possible blockage in incompatible delivery system are its major disadvantages^[5,8,9].

Table 2 Embolizing agents precluded in traumatic injuries^[6-10]

Embolizing agent	Reason
Powdered form gelatin sponge	Obliteration of small caliber vessels; May lead to infarction or abscess Large caliber vessels; Risk of rebleeding due to potential collateralization from neighboring undamaged parenchyma
Non absorbable particles of small size (e.g., polyvinyl alcohol), liquid embolic agents (glue) Alcohol	Difficult to handle: Striking balance between selective embolization <i>vs</i> optimizing end point of embolization an issue Non-targeted embolization: Irreversible unwanted tissue damage Extensive tissue necrosis Difficult to the handle while delivering at the target site



Figure 2 High grade liver injury with active contrast extravasation. Case of blunt trauma abdomen, FAST positive, hemodynamically stable (A) CECT abdomen showed extensive laceration, intraparenchymal hematoma consistent with Grade V liver injury along with diffuse active contrast extravasation (arrow) within the lacerated segment VIII (arrow) of liver with resultant hemoperitoneum (B) Selective hepatic artery angiogram revealed active contrast extravasation from anterior division of right hepatic artery with increased conspicuity in (C) superselective right hepatic artery angiogram which was subsequently embolized by microcoils (D) Post embolization angiogram revealed faint opacification of branches of anterior division of RHA (arrow) with subsidence of extravasation. FAST: Focused assessment with sonography in trauma; RHA: Right hepatic artery; CECT: Contrast enhanced computed tomography.

Teaching point: Specific indications and options for embolization are based on location and type of injury

It is of utmost importance that the ultimate goal of radiological interventions as well as the choice of embolizing material is to treat the patient and not just the imaging findings.

Endovascular management in various traumatic injuries

Liver injury: Liver is the second most commonly injured organ in the blunt abdominal trauma following spleen. In majority of these cases, clinically significant hemorrhage occurs due to the injury to hepatic artery. However, venous injury (central hepatic or portal vein) is even more dreadful which mandates surgical repair irrespective of the hemodynamic status.

After initial resuscitation, hemodynamically stable

patients initially undergo NOM which may include endovascular interventions, if needed. Hepatic artery embolization (HAE) in this subset is indicated if there is injury to the hepatic artery or may be done prophylactically in high grade liver injuries (Figures 2-4). Surgery is not the preliminary treatment of choice in these cases as during surgery only the main hepatic artery is ligated with potential chances of re-bleeding due to collateralization. On the contrary, in endovascular interventions, site-specific distal embolization can be performed which obviates collateralization^[11]. If superselective catheterization is not feasible or if bleeding is from multiple sites, then non-selective gelfoam embolization can be done without any undue prolongation of the procedural time (Figure 5). If hemodynamic instability persists despite resuscitative

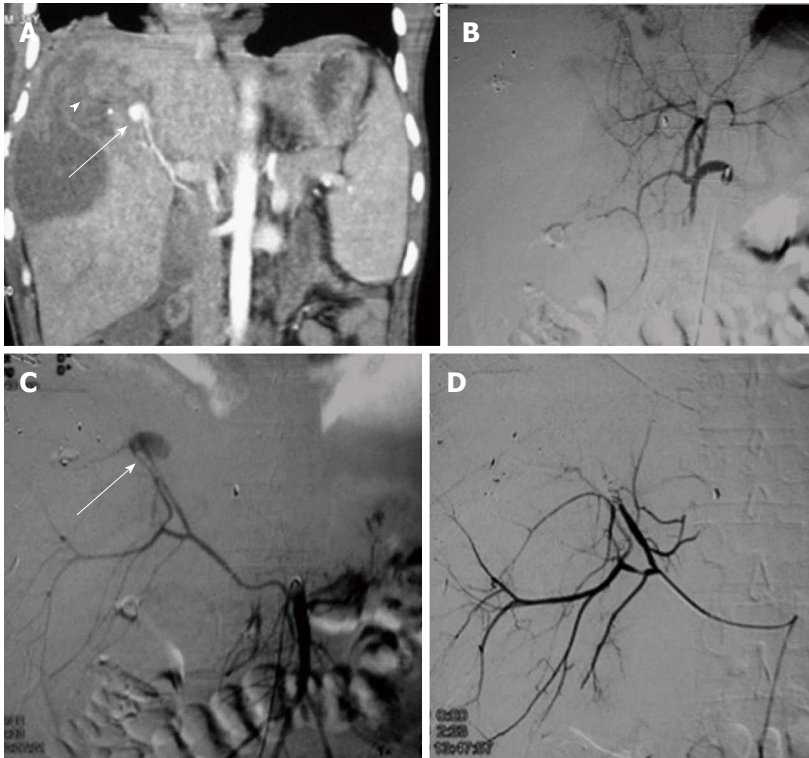


Figure 3 Gun shot injury with hepatic artery pseudoaneurysm. A 38-year male with gunshot injury presented after a week with falling hematocrit. A: CECT showed a contrast filled outpouching in segment VIII of liver paralleling the attenuation of adjacent hepatic artery branch s/o PsA (arrow) with adjacent subcapsular hematoma (arrowhead) subsequently DSA was done; B: Initial hepatic angiogram showed opacification of only branches of left lobe of liver, no opacification of right hepatic artery -s/o variant anatomy; C: SMA angiogram showed replaced right hepatic artery with PsA arising from the terminal end of anterior division (arrow). Due to smaller caliber and spasm, neck of the PsA could not be negotiated, hence, proximal embolization with microcoils was performed; D: Post embolization angiogram showed faint opacification of branches of anterior division of RHA along with exclusion of PsA. CECT: Contrast enhanced computed tomography; RHA: Right hepatic artery; PsA: Pseudoaneurysm; SMA: Superior mesentery artery; DSA: Digital subtraction angiography.

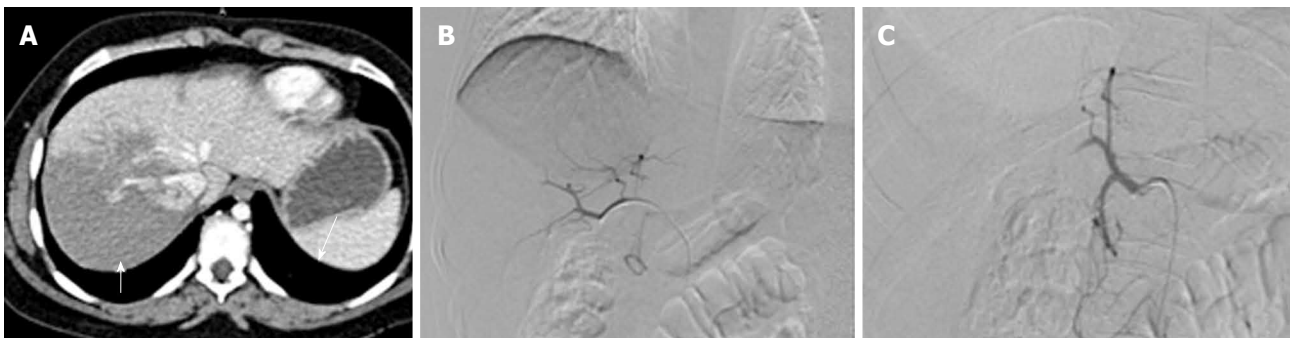


Figure 4 Prophylactic embolization of right hepatic artery in high grade liver injury. A: CECT abdomen of a 35 years old male, c/o BTA showed extensive deep lacerations and intraparenchymal contusions in the right lobe of liver s/o Grade IV injury. Majority of these lacerations were reaching upto the hepatic surface (arrow) with possible capsular breach. Mild hemoperitoneum was present in pelvis; no active contrast extravasation or pseudoaneurysm; B: In view of high grade injury involving right lobe, prophylactic gelfoam embolization of right hepatic artery was done; C: Post embolization, there was non-opacification of RHA. CECT: Contrast enhanced computed tomography; BTA: Blunt trauma abdomen; RHA: Right hepatic artery.

efforts, then the patients are straightway taken to the operating room for rapid “damage control surgery” (DCS) with extensive peri-hepatic packing and temporary abdominal closure^[12-14].

It has been observed that despite refinement of the surgical skills, there is risk of intraparenchymal re-bleeding, especially with high grade injuries. In such scenarios, a re-laparotomy is not preferred due to the ensuing acidosis and metabolic derangements coupled with difficulty in accessing the site of vascular injury which may be either remotely located or anatomically distorted by the previous surgery^[11]. In such demanding situations, HAE has emerged as a complementary tool in managing complex hepatic injuries with favorable outcomes. Even in hemodynamically unstable patients, recent studies have shown that HAE has an edge over

the traditional management due to the uniqueness of angioembolization to reach the targeted site; thus providing a better control at the site of vascular injury^[6,15].

Complications of HAE: It is an essentially safe procedure with only few complications observed. These include delayed hemorrhage, infarction/ necrosis, abscess, bilioma or biliary fistula. Risk of complications are more in high grade liver injuries with extensive vascular and biliary disruption^[15,16].

Technical success: HAE is successful in approximately 80%-100% of cases. Risk of technical failure is higher in those cases who have initially undergone laparotomy^[17]. Nevertheless, even in such cases, results of HAE is

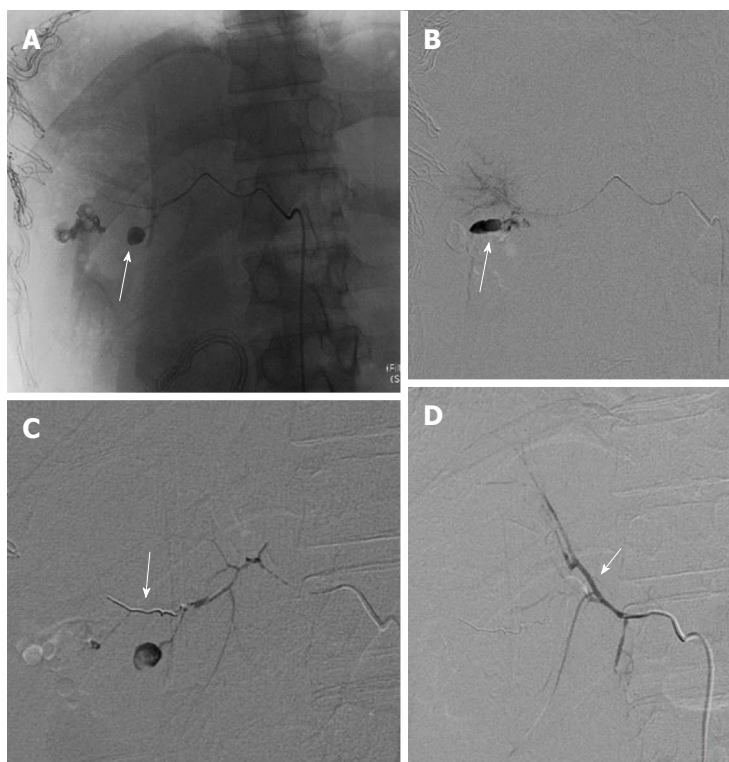


Figure 5 Re-bleed after perihepatic packing. A 38-year-old male with BTA, hemodynamically unstable and taken directly to OR for perihepatic packing. DSA was contemplated in view of persistent hypotension after perihepatic packing. A and B: Selective right hepatic angiogram showed PsA arising from its posterior division (arrow). Subsequently, guidewire followed by micro catheter manipulation was done across its neck; C: Microcoil was deployed across the neck of PsA from distal to proximal followed by gelfoam embolization; D: Post embolization angiographic run showed faint opacification of posterior branch due to sluggish flow. Note brilliant opacification of anterior branch of RHA (arrow) due to reflux of contrast. OR: Operating room; RHA: Right hepatic artery; BTA: Blunt trauma abdomen; DSA: Digital subtraction angiography.

excellent with significant reduction in morbidity and mortality as compared to re-laparotomy. In one series, therapeutic angioembolization was performed in 21 of the 24 patients after DCS and none of these cases had delayed hemorrhage^[13]. In another major Norwegian study comprising of 114 patients with liver injury, it was observed that with the inclusion of endovascular management, there was significant reduction in the laparotomy rate from 58% to 34% and complication rate by 40% (including abscess, biloma, and bile leak), although overall survival rate remained stable at 89%-90%^[18].

Other studies have reported significant reduction in mortality when higher grades of liver injury (Grade IV-V) were managed by multidisciplinary approach; especially, with the availability of expertise of angioembolization at the need of hour^[11,19]. In a retrospective series by Lin *et al.*^[20] consisting of 16 cases of ongoing haemorrhage, DCS was immediately followed by transarterial embolization (TAE) which undoubtedly had the survival benefit, saving lives in about 50% cases. The authors further propounded that the duration of DCS should be as short as possible and to be closely followed by TAE without any undue delay.

At our level I trauma center, HAE is done in hepatic artery injury or prophylactically in high grade liver injury, if the patient is hemodynamically stable (Figure 6). Further, it is also done if the patient continues to remain

hemodynamically unstable despite DCS. This protocol has been adopted from the inception of our center (2007) and it has lowered the need for laparotomy and complications like abscess, biloma, and biliary leak.

Splenic injury

Spleen is the most commonly injured solid organ in blunt abdominal trauma. Splenectomy, which once used to be performed in all splenic injuries, is not the preliminary choice in every case due to the concern for the long term immunity. Nowadays, it is restricted to high grade injury with unsalvageable spleen or failure of endovascular interventions to control the bleeding. Management protocol for splenic injury is essentially similar to that of liver injury. In hemodynamically stable patients, splenic artery embolization (SAE) is indicated in arterial injury or prophylactically in high grade splenic injuries. This approach offers the advantage of preserving the functioning splenic parenchyma unlike surgery^[1,6,21,22].

In SAE, initially celiac axis angiogram is done followed by selective splenic artery angiogram. There are two embolization options available - proximal or distal, the choice of which is guided by the angiographic findings. Proximal embolization is non-selective which sufficiently reduces the inflow and pulp pressure. Hence, it is preferred in intrasplenic hemorrhage. Additionally, collateral circulation from the small pancreatic branches

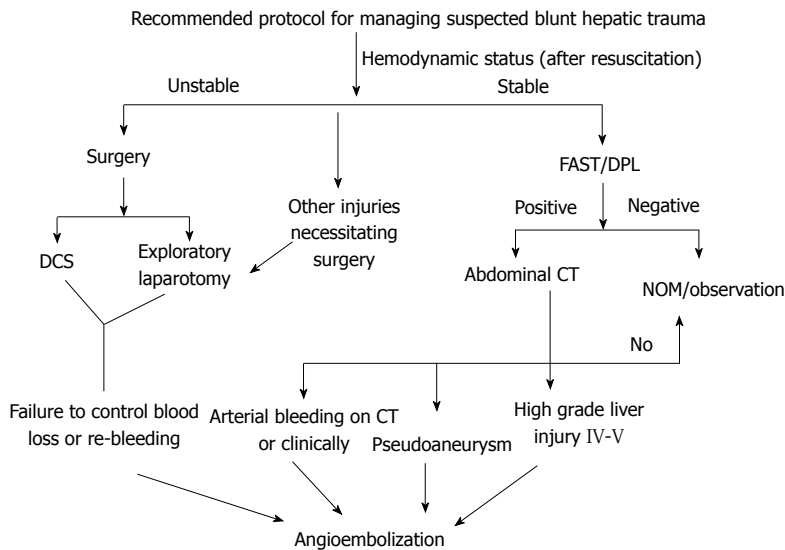


Figure 6 Recommended protocol for managing suspected blunt hepatic trauma. CT: Computed tomography; DCS: Damage control surgery; FAST: Focused assessment with sonography in trauma; DPL: Diagnostic peritoneal lavage.

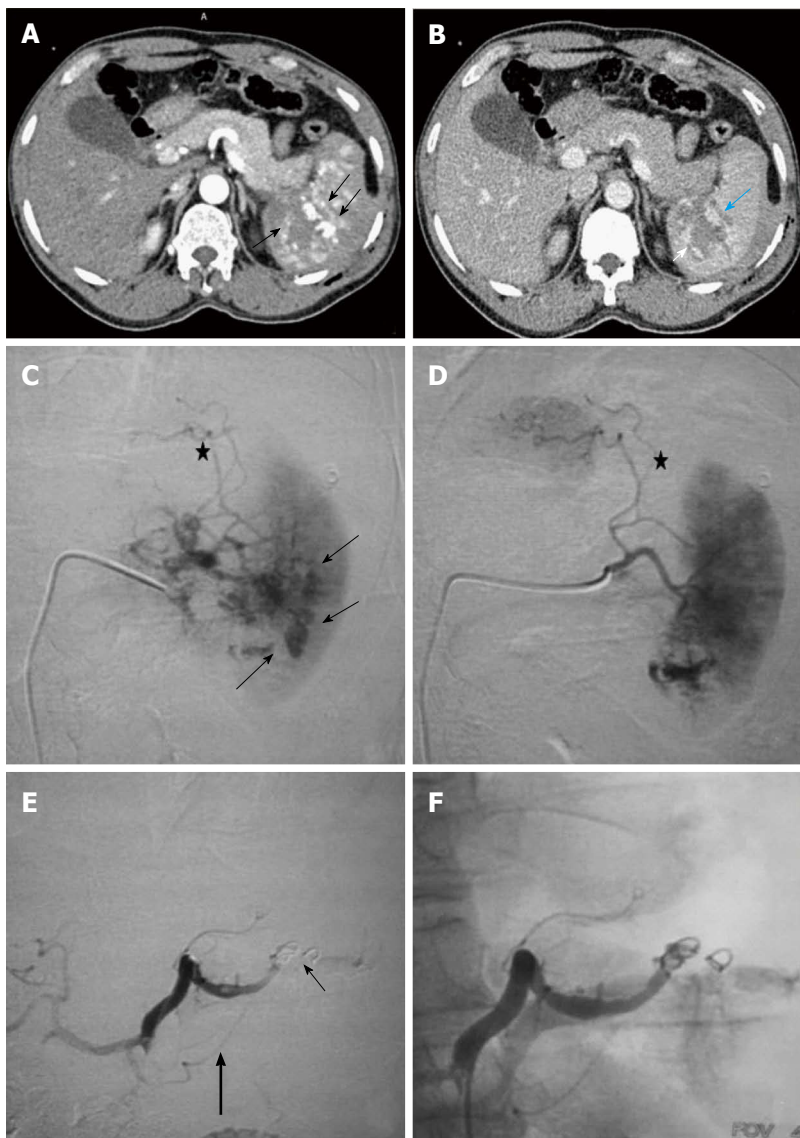


Figure 7 Grade IV splenic injury with active contrast extravasation in a 29-year-old male with blunt trauma abdomen, hemodynamically stable and FAST positive. Arterial phase image (A) showing blobs of contrast (arrow) marginating the deep splenic laceration. In portovenous phase (B), lacerations are better appreciated, few of which are involving splenic hilum. Also, blobs of contrast in the arterial images has slight increased in size (arrow), nonetheless, remain localised s/o focal active contrast extravasation. DSA was done (C and D), selective splenic artery angiogram showed multiple areas of active contrast extravasation from trabecular arteries of lower pole (arrow) with disruption of parenchymal continuity due to laceration (asterisk). Proximal embolization of splenic artery was done with coil followed by gelfoam instillation (E). Note coils (thin arrow) are deployed distal to the origin of dorsal pancreatic artery (thick arrow). Post embolization angiographic run (F) showed proximal contrast stasis with no opacification distal to embolization site. DSA: Digital subtraction angiography; FAST: Focused assessment with sonography in trauma.

is preserved; thus, lowering the risk of splenic infarction. In this technique, size of the coil size should be approximately 20%-25% larger than the diameter of the splenic artery to avoid its proximal or distal migration. It

is positioned just distal to the origin of dorsal pancreatic artery and proximal to arteria pancreatica magna (anatomical landmark is lateral to the left transverse process of L2 vertebra) (Figure 7).

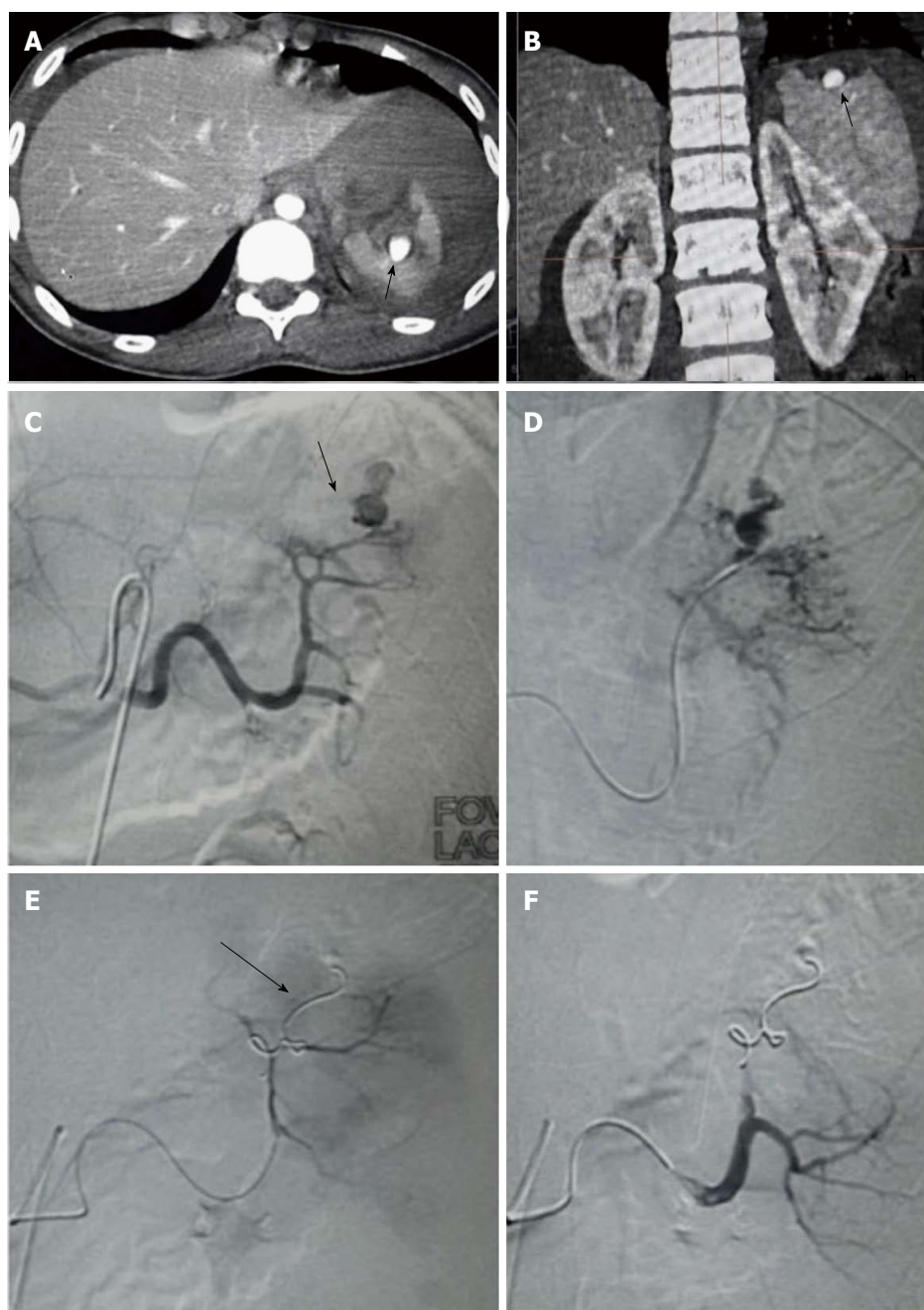


Figure 8 Splenic artery pseudoaneurysm. Case of 39-year-old female with BTA, FAST positive, hemodynamically stable. CECT revealed (A and B) Extensive lacerations involving spleen with presence of contrast filled intrasplenic outpouching paralleling the aortic attenuation s/o pseudoaneurysm. Splenic artery angiogram showed (C) PsA (arrow) arising from the upper polar branch which on delayed phases showed contrast spillage s/o leaking PsA (D). Subsequently, upper pole branch was selectively catheterised by microcatheter followed by deployment of microcoils (arrow) across the neck of PsA (distal embolization) (E). Post embolization angiography (F) showed no flow distal to coil with exclusion of PsA and good contrast opacification of lower pole branch. CECT: Contrast enhanced computed tomography; BTA: Blunt trauma abdomen; PsA: Pseudoaneurysm; FAST: Focused assessment with sonography in trauma.

Distal or selective embolization, on the other hand, is done in extrasplenic haemorrhage or if there is localized site of injury like in pseudoaneurysm or AV fistula. In this, with the help of co-axial microcatheter system, site specific distal embolization is performed to achieve maximum hemostatic control (Figure 8). Embolization is done by the placement of smaller sized coils, gelfoam pledgets or combination of both^[6,23].

Proximal splenic artery embolization in traumatic injuries has a success rate of 90%-95% with low

incidence of splenic infarction. Distal embolization is also associated with similar success rate for hemostasis but there is higher risk for splenic infarction. Overall procedural time and radiation exposure is more in proximal than distal embolization. Choosing one technique over the other is solely left to the discretion of interventional radiologist and at times combination of both may be required (Figure 9)^[1,21-23].

Complication of SAE: Results of SAE are excellent with

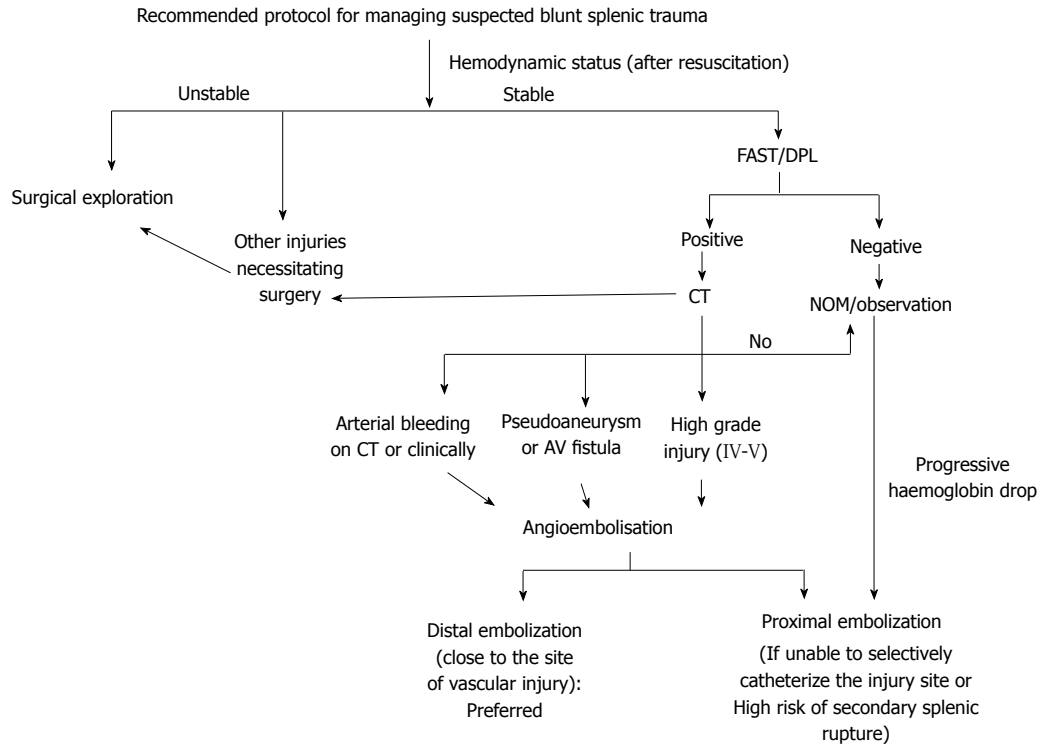


Figure 9 Recommended protocol for managing suspected blunt splenic trauma. CT: Computed tomography; FAST: Focused assessment with sonography in trauma; DPL: Diagnostic peritoneal lavage; NOM: Non operative management.

faster recuperation as compared to surgery. Although infrequent, there is risk of certain complications like recurrent hemorrhage, splenic abscess, post embolization syndrome, coil migration or symptomatic infarct necessitating splenectomy^[1,6,15,21,24].

Technical success rate: Reported success rate of SAE in various series ranges from 73%-100% which has markedly increased the success rate of NOM to over 90%. Several studies suggest that in haemodynamically stable patients, survival rates of angioembolization and splenectomy are comparable^[1,23]. In a study by Gaarder *et al*^[25], it was found that performing angiography with embolization (if needed) in all the cases of high grade splenic injury increased the success rates of NOM from 75%-96% as delayed bleeding was the most important reason for the failure of NOM. Also, there was increase in splenic salvage rate with fewer complications than the historical controls when angiography was empirically performed in high grade splenic injuries.

Renal injury

Injuries involving the renal arteries usually occur in conjunction with other solid visceral injuries. A vast majority of blunt renal injuries are minor which usually get resolved NOM. Nephrectomy is reserved only if the organ is non-salvageable like shattered kidney or vascular pedicle avulsion. However, in special circumstances like solitary functioning kidney, nephron sparing surgery is the aim rather than nephrectomy which may render the subsequent need for renal replacement therapy.

Nowadays, most of the endovascular injuries (active bleeding, pseudoaneurysm or arteriovenous fistula) are preferably managed by endovascular interventions. These minimally invasive procedures offer the advantage of rapid control of ongoing hemorrhage besides obviating the surgery and the associated risks^[26]. Selection of embolization technique is based on the site and nature of vascular injury (Table 3). The technique of angioembolization in renovascular injury is essentially similar to other organs. An important highlight of the renal circulation is that it is an end arterial supply with paucity of collateral circulation unlike liver or spleen. The corollary to the fact is that, there is high risk of tissue infarction which limits the leverage of non-selective embolization in renal vasculature, which may be performed in liver or spleen in special circumstances. Hence, as a rule, embolization in renovascular injury should be as selective as possible in order to maximize the preservation of viable and perfused renal tissue. Proximal renal artery embolization, on the other hand, is primarily reserved for diffuse renal injury with little or no salvageable renal parenchyma. It is done with an intent to control the life threatening exsanguination besides avoiding surgery (Figures 10-12)^[1,26,27].

Complications of renal artery embolization

Although there is limited data available on the long term success rate of angioembolization; as per the literature it is an extremely well tolerated procedure. Complications which may be occasionally encountered include renal infarction, renal abscess or hypertension. Nevertheless, renal function is largely preserved^[28].

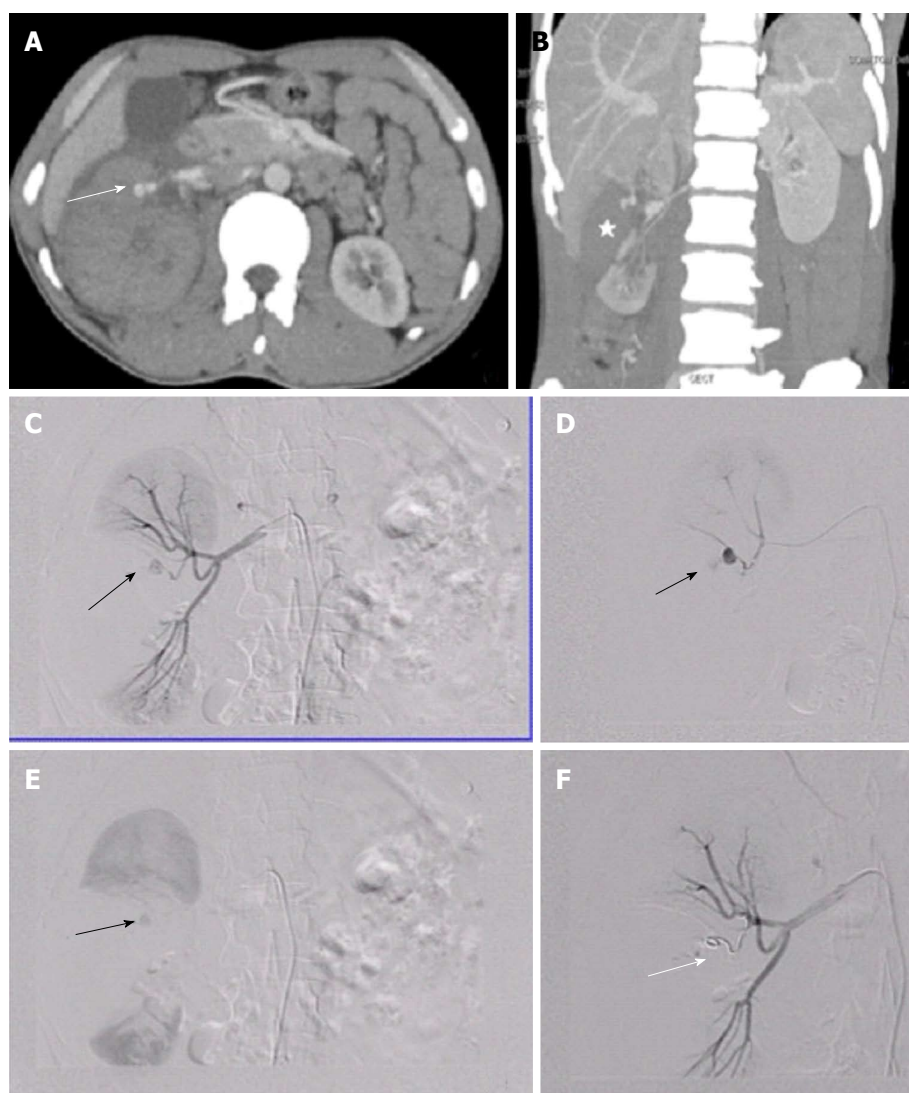


Figure 10 Renovascular injury: 35 years old male with blunt trauma abdomen. A, B: CECT abdomen showed deep lacerations involving the interpole of right kidney extending upto the renal hilum (asterisk). A pseudoaneurysm (arrow) was seen arising from upper polar branch along with presence of perinephric hematoma; C, D: DSA with catheterisation of right main renal artery confirmed the presence of pseudoaneurysm (arrow); E: In view of end arterial supply, involved branch was selectively accessed and catheter was subsequently manipulated across the neck of PsA with the help of microwire followed by deployment of coil; F: Post embolization angiography showed non opacification distal to the coil (arrow). CECT: Contrast enhanced computed tomography; PsA: Pseudoaneurysm; DSA: Digital subtraction angiography.

Table 3 Endovascular interventions in renal artery injury^[27]

Vascular injury Site and type of injury	Endovascular management	Comments
Main renal artery-dissection, laceration, contrast extravasation	Stent graft	Preserves flow across the site of injury if negotiated safely and successfully
Main renal artery occlusion	Intra-arterial thrombolysis using urokinase or tissue plasminogen activator	Salvages kidney if administered within 6 h of injury
Intra-renal haemorrhage or pseudoaneurysm	Superselective embolization <i>via</i> microcatheter system and microcoils	Targeted embolization: Preserves functioning renal parenchyma
Arterio-venous or arterio-calyceal fistula	Embolization just proximal to fistulous site	Targeted embolization: Preserves functioning renal parenchyma

Technical success: Endovascular approach has a high success rate in managing renovascular injury. As per the literature, the procedure (including repeat angioembolization) is successful in > 95% of cases in achieving hemostasis and preserving renal function,

besides obviating nephrectomy^[29-31].

In a study by Hotaling *et al*^[29], of the 77 patients undergoing angioembolization for renovascular injuries, 68 patients further required some additional treatment. Technical success rate was especially lower with higher

grade renal injuries (IV and V). However, result of the repeat angioembolization were quite dramatic, with an overall success rate of 92%. Similar results of low success rates in initial angioembolization were observed in studies by Van der Wilden *et al.*^[30] and Menaker *et al.*^[31], highlighting the importance of carefully scrutinizing such patients for signs of recurrent hemorrhage. There are limited reports of thrombolysis in posttraumatic renal artery occlusion.

A high initial failure rate of endovascular interventions in renal injuries has been attributed variously to the high fluid and transfusion requirements, older age group (> 55 years), concomitant injury to other abdominal organs and metabolic derangements (especially acidosis)^[32,33].

Prospects of stent-grafting in renovascular injuries^[27]

There is limited data available on the long term effects of stent graft placement in renal artery injuries. However, few reports suggest a higher propensity for refractory hypertension and renal atrophy in traumatic injuries as compared to the general population. Although the procedure remains similar irrespective of the causative etiology of renal artery occlusion; the low technical success rate in traumatic injuries may be due to below mentioned factors.

In traumatic injuries, duration of renal ischemia is the most critical determinant of the technical success of the endovascular stenting as well as restoration of the renal vitality. For optimal results, total duration of ischemia should be < 3 h in complete and < 6 h in incomplete arterial occlusion. Further, to prevent stent occlusion, anticoagulation should be administered immediately after stent placement. However, in trauma due to ongoing bleeding or potential risk of re-bleeding, anticoagulation is not recommended, which increases the likelihood of stent occlusion. Another important determinant is the extent of collateralization and patency of renal vein which increases the tolerance to the ischemic event; thereby, increasing the success rate of stenting.

Pelvic fracture

Management of severe pelvic injuries continue to remain an enigma for trauma surgeons. Mortality in pelvic injury ranges from 2%-23% and nearly 54% of the early deaths are attributed to the ongoing hemorrhage. As hemodynamic instability adversely influence the prognosis of these severely injured patients, prompt and effective management is warranted. Pelvis stabilization with binders or external fixators is the most vital step in the preliminary management of pelvic injuries which serves as an adjunct to IR to limit the bleeding until embolization can be performed. This acts by reducing the pelvic volume as well as approximation of the fracture ends which prevents further bleeding and leads to hematoma formation which provides tamponade to the bleeding site, especially, if it is from the end of the fracture or venous injury. Pelvic fractures are often associated with other abdominal injuries; hence, CT is

imperative before planning further management^[3,6,33-38].

As compared to other sites, bleeding in pelvic injury may be of multifactorial etiology like venous, arterial or osseous. Amongst these, venous bleeding is the most common and is due to the disruption of presacral venous plexus which leads to the pelvic retroperitoneal hemorrhage (PRH). Arterial injury may result from the shearing pelvic injury, avulsion/ transection of artery from the sharp bony fragment or iatrogenic while managing pelvic fractures. Internal pudendal and superior gluteal arteries are the most commonly injured arteries. Clinically, arterial injury may be suggested by hemodynamic instability requiring massive blood transfusions. In such cases, there is a nearly 43%-78% incidence of positive angiographic findings. Musculoskeletal injury is another cause of pelvic hemorrhage due to the fracture of vascular cancellous bone or intramuscular hematoma. As mentioned above, venous and osseous bleeding usually get controlled by pelvic stabilization. On the contrary, arterial bleeding due to the high pressure circulation, usually needs to intervened^[3,6,36,37].

Pelvic fracture related retroperitoneal hemorrhage may be managed either by surgery or endovascular embolization. Surgical management consists of intra-operative fixation with or without pre-peritoneal packing. Urgent laparotomy is indicated in persistent hypotension, gross hemoperitoneum or polytrauma with other indication of surgical exploration^[6]. However, there are several limitations in pelvic surgery which increases the risk of complications. Amongst these, complex anatomy of the pelvis is the most important determinant which may hinder the accessibility to the bleeding site. Due to difficult access, there is increased intra-operative risk of destabilization of already formed clot which may be disturb its tamponade effect at the site of bleeding. Furthermore, arterial bleeding is usually due to multiple small peripheral branches which may be difficult to access or identify during surgery. Even, bilateral internal iliac ligation may prove futile in these cases due to the rich collateral circulation in pelvis^[6,39,40].

Angiographic embolization (Figure 13-15) in pelvic injury is indicated in major pelvic fracture with signs of ongoing bleeding despite ruling out other non-pelvic sources of blood loss. These include persistent hypotension even after administration of fluid and/or transfusion requirements exceeding 4 units of blood/24 h or > 6 units/4 h. It is also done in inadequately controlled hemorrhage after surgical exploration or if there is large expanding hematoma during laparotomy. Endovascular embolization is also indicated if there are CT findings suggestive of pelvic vascular injury which may be active contrast extravasation, pseudoaneurysm or pelvic hematoma exceeding 600 cc in volume. CT angiography is highly sensitive in diagnosing such injuries with a negative predictive value of 99.6%. Accordingly, catheter angiography is usually not performed if CT angiography does not reveal any findings suggestive of vascular injury. Embolization may also be a temporary

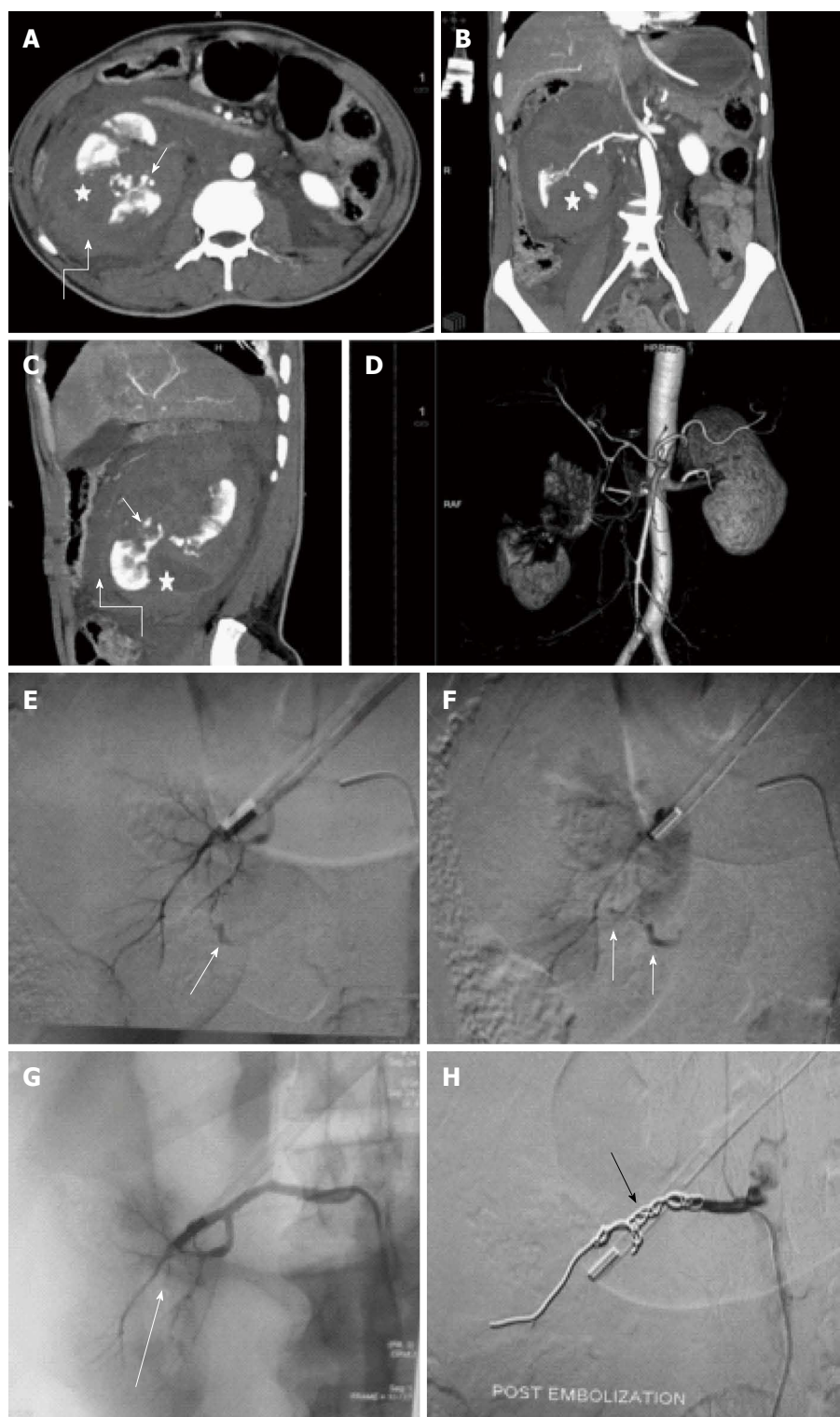


Figure 11 Main renal artery injury. A-D: CECT in a 22 years old male following road traffic accident revealed multiple deep lacerations (asterisk) involving entire thickness of right kidney resulting in shattered kidney. Few areas of active contrast extravasation (thin arrow) were noted at the edge of laceration along with presence of extensive perinephric hematoma (curved arrow). Although, main renal artery was showing good luminal opacification, however, less than 25 % remaining functioning renal parenchyma precluded salvagability. Due to high post operative morbidity, angiography was resorted over nephrectomy; E, F: Selective catheterisation of main renal artery showed multiple areas of active contrast extravasation (arrow); G: Subsequently, in view of potentially life threatening haemorrhage and non-salvageable kidney, coil embolization (arrow) of main renal artery was contemplated; H: Post embolization angiography showed opacification of only proximal stump of renal artery. Following conservative management, patient was then discharged 8 d later. CECT: Contrast enhanced computed tomography.

adjunct before the definitive surgery^[6,36,37,39,40].

Pelvic angioembolization may be selective if the site of vascular injury may be negotiated precisely. However,

non-selective embolization may be done if selective catheterization is not achieved or prophylactically if angiography does not reveal any evidence of vascular

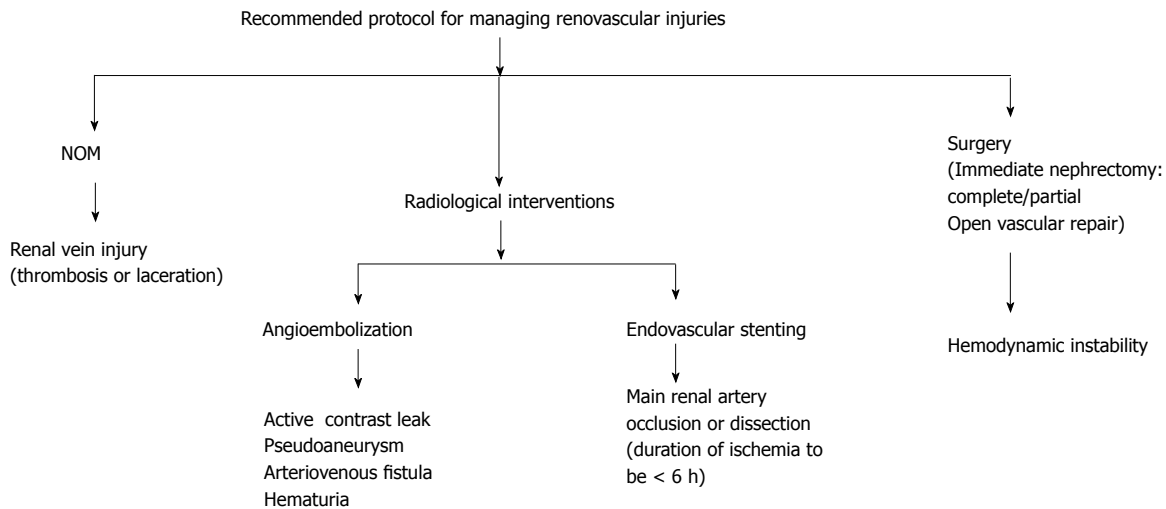


Figure 12 Recommended protocol for managing renovascular injuries. NOM: Non operative management.

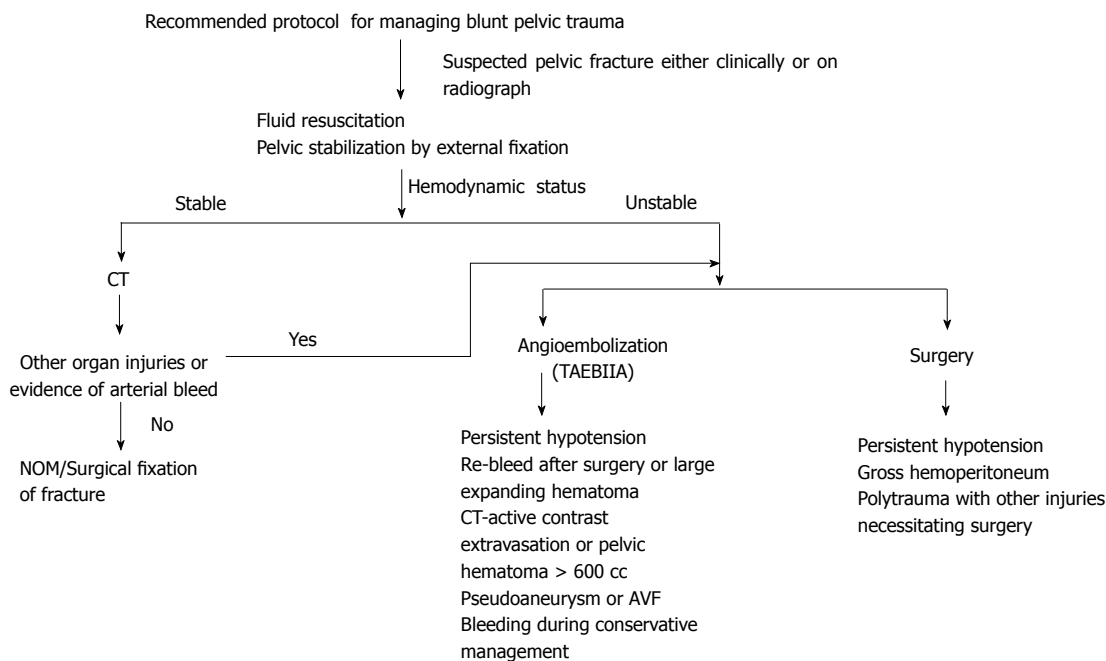


Figure 13 Recommended protocol for managing blunt pelvic trauma. NOM: Non operative management; TAE/IIA: Transarterial embolization of bilateral iliac artery; CT: Computed tomography; AVF: Arterio-venous fistula.

injury. If non-selective, then both the internal iliac arteries are embolized as there may be chances of re-bleeding due to extensive collateral circulation in pelvis. For the similar reason, embolization should be as peripheral as possible for effectively controlling the bleeding. Other causes of re-bleeding include anomalous or accessory branches of the external iliac and inferior mesenteric artery. Choice of embolizing agent is dependent on the selectiveness of catheterization achieved as well coagulation profile. In nonselective embolization of bilateral internal iliac artery, bleeding is most effectively controlled by flow-directed particulate embolization using Gelfoam slurry. It is easily available, inexpensive, and temporary measure which leads to mechanical occlusion. It is prepared by diluting Gelfoam

shavings with iodinated non-ionic contrast through a three-way stop-cock between two 10-cc syringes. Since this embolization approach is non-targeted, it results in occlusion of multiple vessels in a traumatized vascular bed (as compared to multiple selective catheterizations). On the contrary, coil is preferred when the bleeding vessel can be selectively approached. It achieves rapid and permanent vascular occlusion. For effective clot formation, coagulation profile must be intact. It should not be used if transfusion requirements ≥ 8 packed cell units or hypothermia both of which can induce coagulopathy^[6,37,39,40].

There are several advantages of angioembolization over surgery. Angioembolization rapidly controls the bleeding without disturbing the tamponade effect of

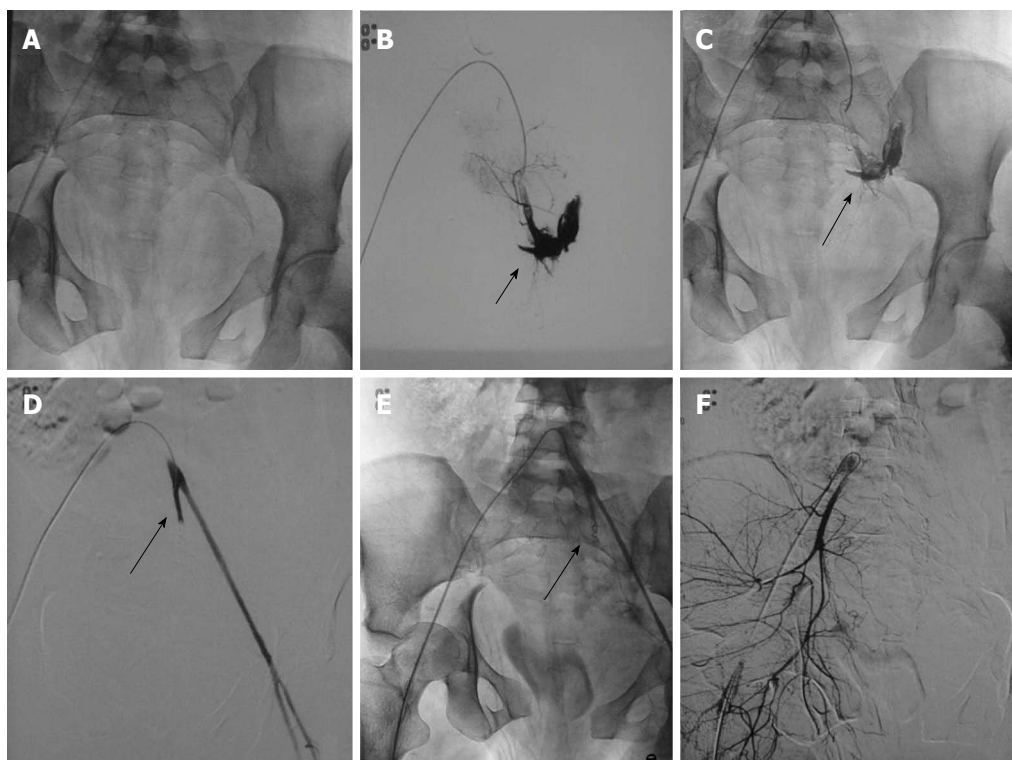


Figure 14 Pelvic fractures with injury of left internal iliac artery. DSA of 24-year-old hemodynamically unstable patient with extensive pelvic fractures. A-C: Selective catheterization of left common iliac artery showed active contrast extravasation from left internal iliac artery subjacent to the disrupted left sacroiliac articulation which was subsequently embolized with coil; D, E: Angiography post embolization showed non-opacification of internal iliac artery distal to coil (arrow) with complete disappearance of contrast extravasation. Left external iliac artery showed good opacification; F: Subsequently, right common iliac artery was cannulated which revealed no vascular injury. DSA: Digital subtraction angiography.

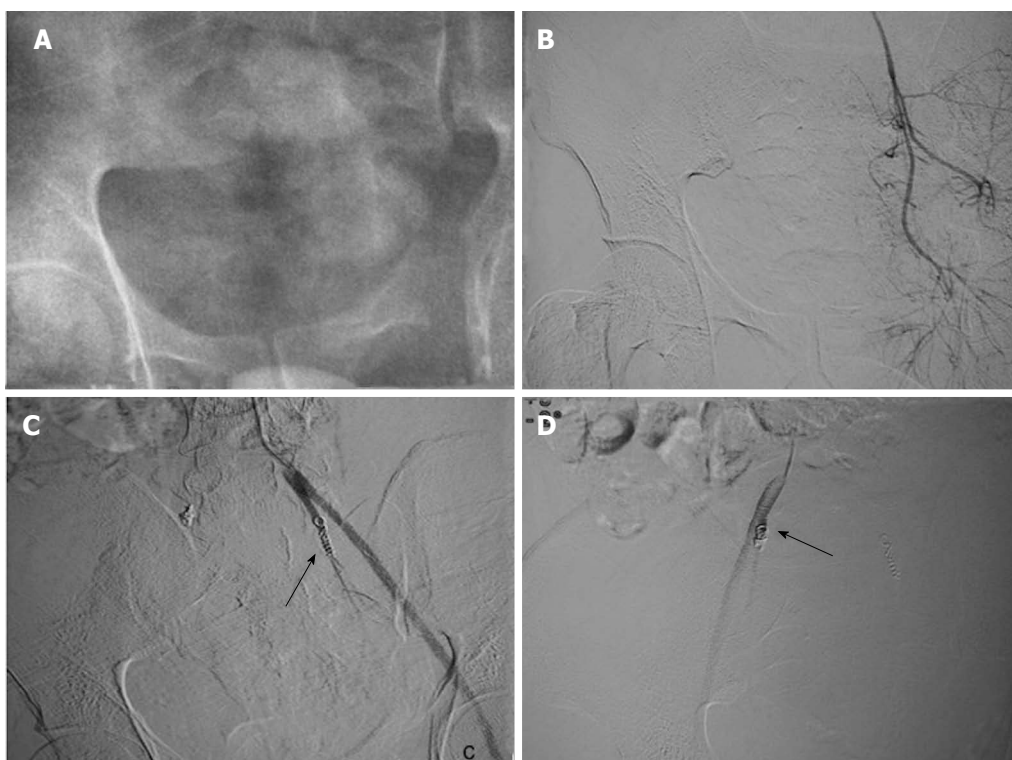


Figure 15 Transarterial embolization of bilateral internal iliac artery: Another case of severe pelvic injury with persistent hypotension. A-D: Bilateral internal iliac arteries were selectively cannulated, however, no vascular injury present. Prophylactic coil embolization of bilateral internal iliac artery was done (arrow). Few hours later patient became normotensive.

hematoma (Figures 13-15). Irrespective of the pelvic anatomy, embolization may access even the remote site of vascular injury with maintained tissue barriers unlike surgery. Besides, the procedure can be done under local anaesthesia as opposed to general anaesthesia needed for surgery^[36,37,39,40].

As mentioned above, pelvic hemorrhage is one of the exceptions to the general rules of radiological interventions in traumatic injuries, as it is always a preferred option over surgery irrespective of the hemodynamic status of the patient. However, optimal therapeutic approach remains controversial which largely depends on the expertise and availability of subspecialty physicians and support staff^[6,36,37,39,40].

Complications of pelvic embolization include failure to control the bleeding which may be due to rapid bleeding due to extensive injuries, failure to achieve selective catheterization or prolonged delay since the time of injury to angiographic intervention. Further, re-bleeding may occur in 5.8%-7.5% of cases requiring repetition of the procedure. Rarely, there may be ischemic necrosis of the rectum or gluteal muscles, peripheral nerve damage with paralysis or paresthesia, colonic or ureteric injury or sexual dysfunction^[39-41].

Technical success: Angioembolization has become the cornerstone in management of the pelvic injuries with a reported success rate of about 85%-90% in controlling pelvic hemorrhage^[6]. A positive angiogram is reported in 28% to 100% of studies of traumatic PRH. Time from the onset hemorrhage to shifting to IR suite is a crucial determinant as reported in a study by Agolini *et al*^[42] in which authors found a significant reduction in the mortality when this duration was < 3 h. In another study by Velmahos *et al*^[43], it was reported that of the 30 patients, angiographic embolization could control haemorrhage and achieve hemodynamic stability in 27 patients (90%) which additionally increased to 97% after repeat angiography. Temporary arterial embolization of the bilateral internal iliac arteries (TAEBIIA) is a safe, rapid and extremely safe method to control PRH. Theoretically TAEBIIA can cause pelvic ischemia, although has never been reported till date. Nonetheless, the reported mortality rate remains high at 5% to 35% which is usually due to concomitant organ injuries or multiple organ failure^[40].

Peripheral vascular injuries

Peripheral vascular injuries (PVI) require meticulous triage to identify hard (distal pulselessness, expanding or pulsatile hematoma/bleeding, thrill or bruit and critical limb ischemia) or soft signs (pallor, cold limbs, non-expanding hematoma, neurological deficit or unexplained hypotension). Presence of hard signs heralds further surgical or endovascular management^[4,6].

PVI can be broadly classified into limb threatening (active contrast extravasation, laceration, pseudoaneurysm, AV fistula, transection or thrombosis) or non-limb threatening (attenuation, spasm, small AV

fistula or pseudoaneurysm in non-critical branches). All these injuries can further be typified into ischemic or hemorrhagic based on clinical presentation which has therapeutic implications. Patients with ischemic type of peripheral vascular injuries are usually managed by surgical exploration whereas hemorrhagic type of injuries are managed either by surgical or by endovascular approach, which depends on hemodynamic status, amount and rapidity of bleeding, availability of local resources and technical expertise^[41,42].

IR is an adjunct to surgical management of peripheral vascular injuries. If the patient is hemodynamically stable, endovascular treatment plays an important role in managing the hemorrhagic type of peripheral vascular injuries. In PVI, endovascular interventions include embolization and vascular reconstruction (Figures 16-18). Choice of procedure depends on the type (end vs main branch) and size (small, medium sized or large) of injured vessel as well as nature of vascular injury (pseudoaneurysm, arteriovenous fistula, active leak) (Figures 19 and 20)^[42,43].

Endovascular treatment has certain advantages over conventional surgical techniques like reduced operative time, estimated blood loss and complication rates. At times in situations where definitive endovascular treatment is not possible, simple technique such as temporary balloon occlusion can control ongoing hemorrhage before proceeding for definitive surgical repair. If indicated, endovascular interventions are treatment of choice as there is significant reduction in morbidity and mortality as compared to surgery. Further in IR procedures, general anaesthesia is usually not required, hence can be performed even in patients with head injury^[4].

Contraindications of endovascular interventions in peripheral vascular trauma (Table 4)^[44,45]

Only absolute contraindication for endovascular interventions is inability to negotiate the vascular injury with guidewire unless embolization is aimed. Endovascular approach is not preferred for stenting at anatomically mobile sites like common femoral, popliteal or axillary arteries, especially if surgical access is not difficult.

Bowel and mesentery injury

Bowel and mesenteric injuries rank next to the liver and spleen in incidence in the blunt trauma abdomen. There is no role of endovascular IR in bowel injury which essentially undergo surgical repair. On the other hand, isolated mesenteric vascular injuries without any associated bowel injury may be managed endovascularly. Such injuries include active bleeding or pseudoaneurysm and are preferably managed surgically. The caveat in endovascular management of the mesenteric injuries is the potential risk of bowel ischemia or infarction due to high risk of non-selective or non-target embolization. Moreover, these complications are more if there is injury to peripheral branches which are extremely difficult for selective catheterization due

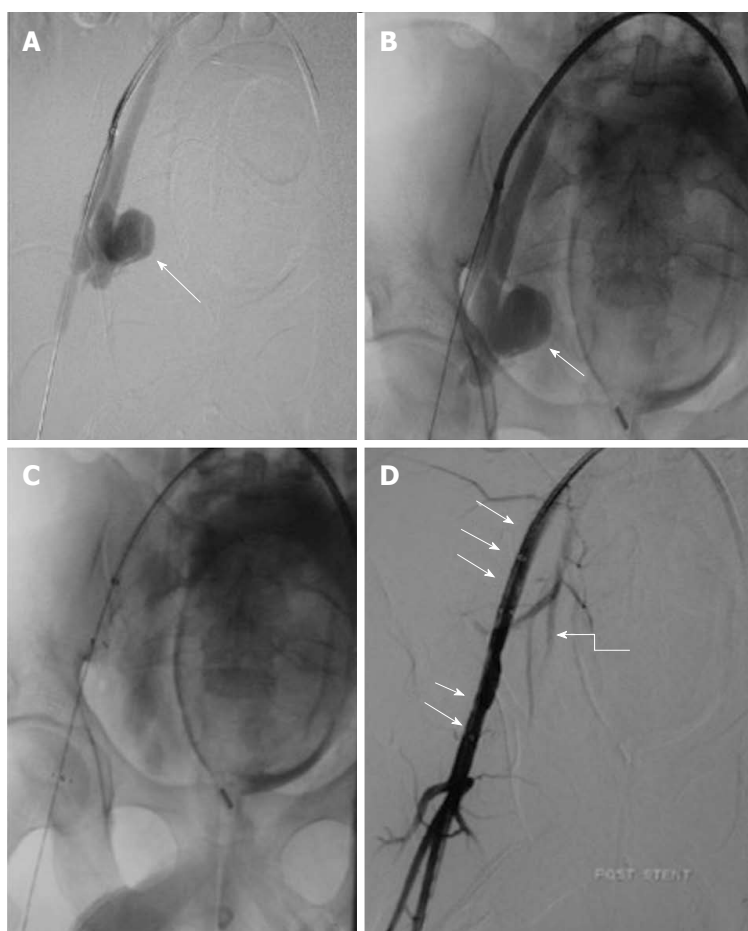


Figure 16 Stent grafting in pseudoaneurysm. Case of gun shot injury, CECT showed presence of PsA from right internal iliac artery (not shown). A, B: Arterial access was obtained through the left common femoral artery and a long arterial sheath was placed. Angiogram showed a large pseudoaneurysm (arrow) arising from the proximal portion of anterior division of right internal iliac artery with no contrast opacification distally (except for a short stump); C, D: Subsequently, a covered stent graft (arrow) was placed in right external iliac artery. Post procedural angiography showed preservation of flow across the right external iliac artery and branches of right internal iliac artery (curved arrow). CECT: Contrast enhanced computed tomography; PsA: Pseudoaneurysm.

Table 4 Permanent embolization in peripheral vascular injury^[4]

Indication	Contraindication
Non vital branches Proximal non-axial branches, <i>e.g.</i> , profunda brachii and profunda femoris	Major vessels like axillary, brachial, superficial femoral and popliteal arteries due to risk of critical limb ischemia

to small calibre or angulated course. Accordingly, choice of embolizing agent may vary depending on the final position of the catheter's tip, type and site of vascular injury, and the preference of the operator. Various embolic agents which can be used include microcoils, glue and gelfoam^[46].

Injury to aorta and its branches

Aortic injuries are usually incurred in high velocity thoraco-abdominal injuries. Spectrum of injury to aorta and its branches include aortic transection, dissection, pseudoaneurysm and minimal aortic injuries. Majority of these injuries prove detrimental due to fatal exsanguination. Common sites of aortic injury in the descending order are aortic isthmus, root of the ascending aorta and descending aorta at the

level of diaphragm due to relative immobility at these sites. These injuries are usually diagnosed on CECT/CT angiography in most of the cases. Endovascular management is usually reserved for the dissection and pseudoaneurysm in the hemodynamically stable patients. Endovascular management options include placement of the stent to maintain the luminal integrity. Additionally, other embolizing agent like coil, glue etc may be used for packing of the sac of pseudoaneurysm. Nowadays, endovascular management of aortic injuries is preferred over surgery wherever feasible due to less mortality and morbidity in the former^[47,48].

Face and neck injuries

Cervico-facial injuries whether blunt or penetrating may potentially injure the carotid and/or vertebral

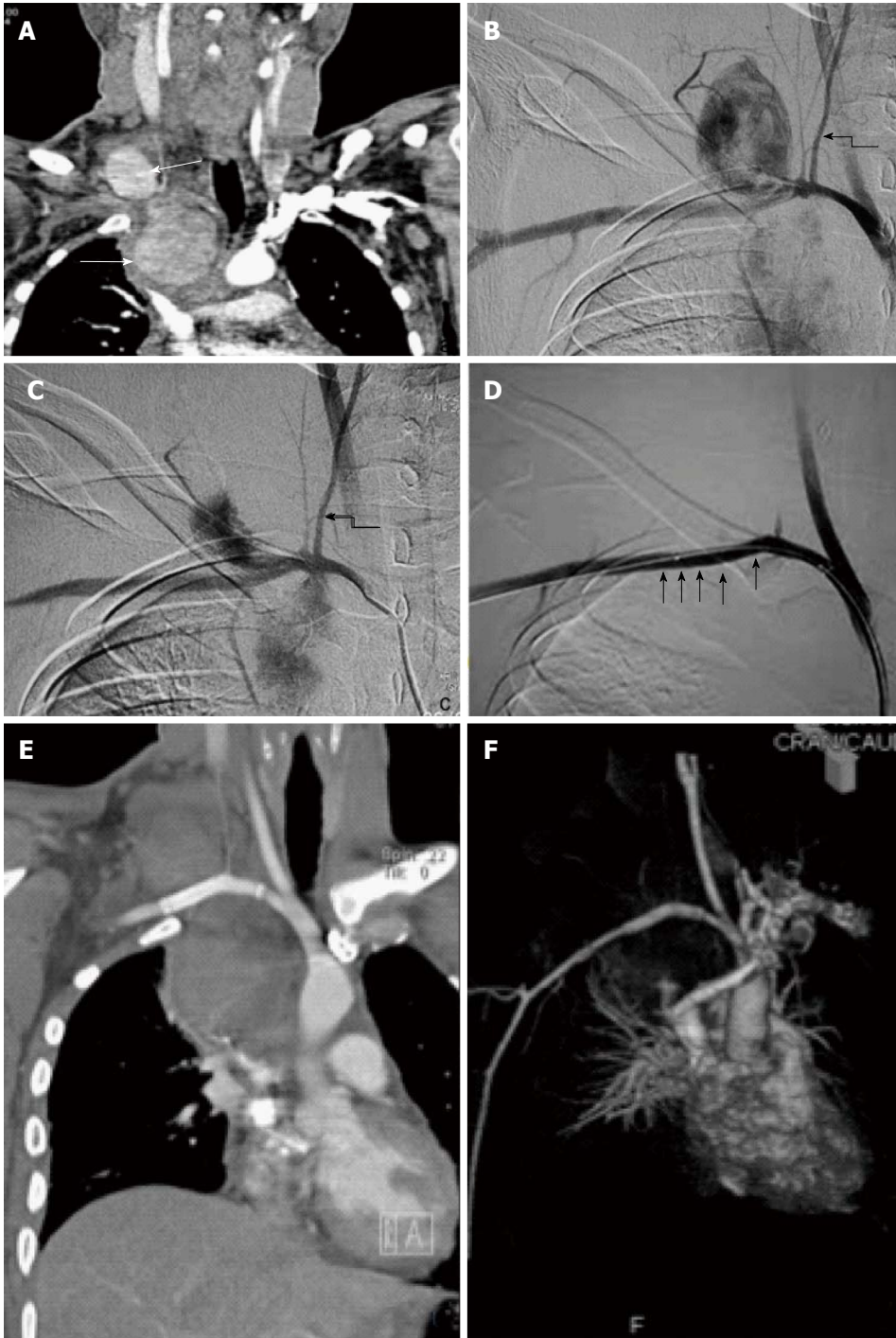


Figure 17 Peripheral vascular injury. A 56-year-old male with multiple rib fractures and neck swelling following road traffic accident. A: CT angiography showed two distinct pseudoaneurysms arising from the proximal right subclavian artery, one cervical and other intrathoracic (arrow). However, there was good opacification of distal subclavian artery with no disruption in continuity, ruling out transection (curved arrow); B, C: DSA corroborated CT findings and revealed two large pseudoaneurysms arising from the proximal right subclavian artery, lateral to the origin of thyrocervical branch (arrow); D: Subsequently, guidewire was manipulated across the PsA and covered stent graft (arrow) was deployed, excluding the origin of right common carotid artery. Post stenting angiography showed no opacification of pseudoaneurysm with good flow in distal subclavian artery; E, F: Follow up CT angiography done 2 wk later revealed both the pseudoaneurysm to be thrombosed. The stent (arrow) was optimally placed stent (arrow) with preservation of distal flow across it. PsA: Pseudoaneurysm; DSA: Digital subtraction angiography.

arteries. Besides causing exsanguination, there is risk of compromise to the central nervous system blood supply. These major vascular injuries may be managed conservatively, surgically or by endovascular interventions. This in turn depends on multiple factors which include hemodynamic and neurological status,

any additional injury which mandates surgery, site of injury and extent of collateral circulation.

In a hemodynamically stable patient, CT angiography may be done to characterize the type and site of vascular injury. CT also helps in evaluation of injury to other structures. Nowadays, surgery in cerebrovascular



Figure 18 Pseudoaneurysm from right profunda femoris artery: 21-year-old male with stab injury. A: DSA showed a large PsA arising from right profunda femoris artery with no distal flow, likely vascular transection with pseudoaneurysm of proximal end; B: As guidewire could not be negotiated across the pseudoaneurysm due to possible discontinuity, proximal coil embolization (arrow) was done. Post embolization angiography showed complete exclusion of pseudoaneurysm. Note the presence of collaterals (curved arrow) along the course of profunda femoris artery. PsA: Pseudoaneurysm; DSA: Digital subtraction

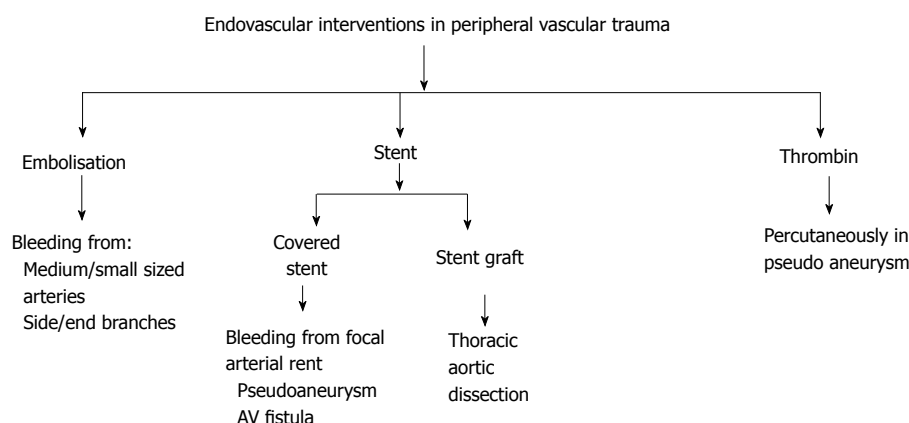


Figure 19 Endovascular interventions in peripheral vascular trauma. AV: Arterio-venous.

injuries is preferred only in those cases which are hemodynamically unstable, other surgical indication or if endovascular embolization is risky which may be either due to non-selective catheterization or inadequate collateralization. Cerebrovascular injuries are now increasingly indicated in such injuries as this approach is minimally invasive, rapid and access even the complex anatomical sites. Initially diagnostic angiography is done to localize/ characterize the site and type of vascular and adequacy of the collateral circulation. Choice of embolizing agent depends on the calibre of the vessel, collateral network and selectiveness of catheterization. If vascular patency can be sacrificed without the risk of ischemia then gel foam, coils or NBCA may be used. If luminal conduit needs to be maintained as in injury to large or medium calibre vessels, then endovascular

stenting may be done^[49].

Non vascular interventions

Non vascular interventions are frequently used in the management of the sequelae of traumatic injuries either alone or as an interim to surgery. Percutaneous drainage is done for the collections or hematoma under imaging guidance. Moreover, percutaneous hepatobiliary (Percutaneous transhepatic biliary drainage) and renal (Percutaneous nephrostomy) interventions may be done in obstruction or biliary/urinary leak.

CIRSE guidelines for quality improvement in endovascular treatment of traumatic injuries

Cardiovascular and interventional radiological society of Europe (CIRSE, 2012) has laid down the guidelines for

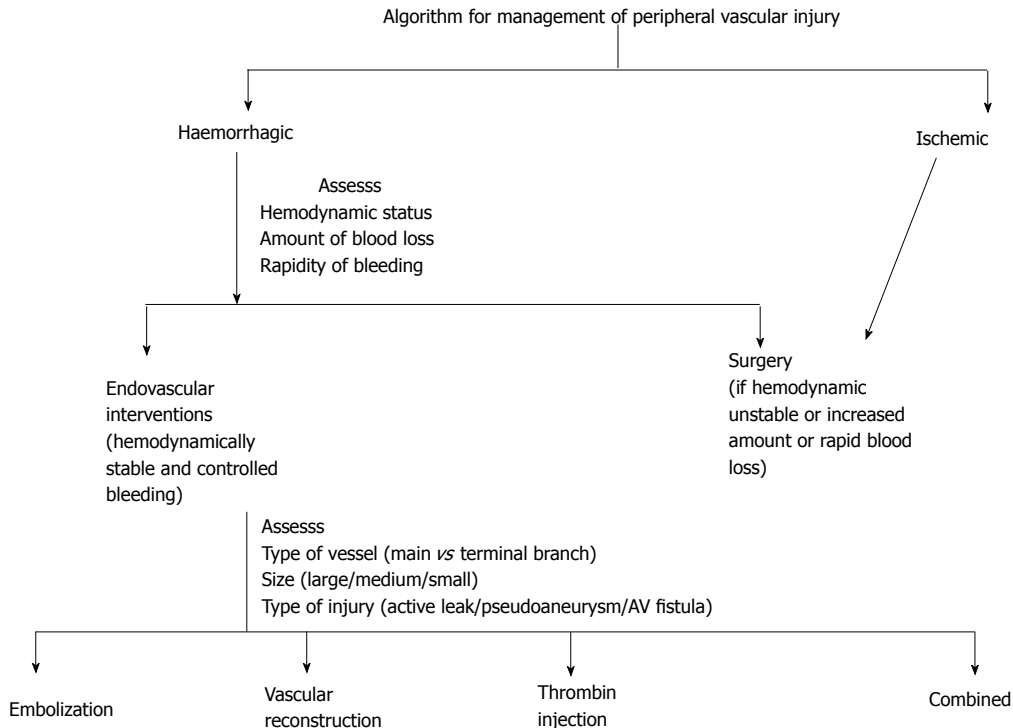


Figure 20 Algorithm for management of peripheral vascular injury.

imaging and radiological interventions in the traumatic injuries. These are evidence based guidelines which mention the indications and contraindications of IR in various injuries. It is intended to maximize the safety of radiological interventions by providing levels of evidence and recommendations^[26].

Recent trends: IR in hemodynamically unstable patients

Until now interventional radiological procedures were reserved for hemodynamically stable patients as an adjunct to NOM or surgery. However, recently concept of time conscious trauma management protocol "Prompt and Rapid Endovascular Strategies in Traumatic Occasions" (PRESTO) has been introduced which conceptualizes initiating the role of interventional radiologist right from the time of hospital entry. Akin to DCS which aims at lifesaving measures, specifically tailored interventional radiological procedure as per this protocol has been termed as "Damage control IR". The idea is to save a potentially life threatening exsanguination even if it is achieved at the cost of organ sacrifice. As per this protocol, as soon as patient arrives, IR team is informed and during primary survey itself femoral arterial sheath is placed, which potentiates and supplements ongoing resuscitative efforts by providing a quick access route for resuscitative endovascular balloon occlusion of the aorta, thus maintaining the normal pressure. This approach buys time for shifting the patient for surgery/IR suite or CT scan and provides access for subsequent endovascular interventions.

If the patient can be shifted, then pan CT is performed also termed as FACT (focused assessment with

CT) which includes head, chest, abdomen and pelvis scan and rapid assessment of acquired images by a special reading mode which is programmed to detect preselected severe injuries within 3 min. If the patient is taken directly to IR suite, then diagnostic angiography is performed with allotted time of approximately 10 min for each major vessel. In cases if CT is done, then targeted angiography is done aiming at site of vascular injury. Procedure should not be prolonged for want of selective embolization and rapidly wound up by doing proximal embolization. Regarding embolizing agents, glue (N-Cyanobutylacrylate) is preferred as its mechanism of action is not hampered by coagulopathy. Hydrocoil and onyx are other alternative embolizing agents in coagulopathy and are comparatively easier to handle. With unprecedented success of IR in NOM for hemodynamically stable patients, it can be forecasted that if strictly followed then PRESTO may not only reduce the early trauma related mortality but will also redefine the status of IR marking the beginning of new era in trauma management^[50].

CONCLUSION

Recent times have witnessed a paradigm shift in the management of traumatic injuries with trend towards NOM. Integration of IR procedures is an extension of such approach requiring minimally invasive interventions to achieve hemostasis. Uniqueness of endovascular techniques lies in approaching site of vascular injury without altering the normal tissue barrier or tamponade effect of hematoma coupled with expeditiously controlling

life threatening hemorrhage by embolization. Not only has it helped in reducing mortality but a considerable reduction in morbidity with faster recuperation. Along with the availability of new generation CT scanners which permits faster image acquisition and hence providing an overview of extent of injuries, surgical expertise is now sought mainly for managing penetrating injuries, multiple bleeding sites or in case of hemodynamically instability.

REFERENCES

- 1 **Wallis A**, Kelly MD, Jones L. Angiography and embolisation for solid abdominal organ injury in adults - a current perspective. *World J Emerg Surg* 2010; **5**: 18 [PMID: 20584325 DOI: 10.1186/1749-7922-5-18]
- 2 **Lopera JE**. Embolization in trauma: principles and techniques. *Semin Intervent Radiol* 2010; **27**: 14-28 [PMID: 21359011 DOI: 10.1055/s-0030-1247885]
- 3 **Khanna P**, Phan H, Hardy AH, Nolan T, Dong P. Multidisciplinary management of blunt pelvic trauma. *Semin Intervent Radiol* 2012; **29**: 187-191 [PMID: 23997410 DOI: 10.1055/s-0032-1326927]
- 4 **Bauer JR**, Ray CE. Transcatheter arterial embolization in the trauma patient: a review. *Semin Intervent Radiol* 2004; **21**: 11-22 [PMID: 21331105 DOI: 10.1055/s-2004-831401]
- 5 **Moore HM**, List A, Holden A, Osborne TM. Therapeutic embolization for acute haemorrhage in the abdomen and pelvis. *Australas Radiol* 2000; **44**: 161-168 [PMID: 10849978]
- 6 **Gould JE**, Vedantham S. The role of interventional radiology in trauma. *Semin Intervent Radiol* 2006; **23**: 270-278 [PMID: 21326773 DOI: 10.1055/s-2006-948766]
- 7 **Hoffer EK**, Borsa JJ, Bloch RD, Fontaine AB. Endovascular techniques in the damage control setting. *Radiographics* 1999; **19**: 1340-1348 [PMID: 10489186]
- 8 **Medsing A**, Zajko A, Orons P, Amesur N, Santos E. A case-based approach to common embolization agents used in vascular interventional radiology. *AJR Am J Roentgenol* 2014; **203**: 699-708 [PMID: 25247933 DOI: 10.2214/AJR.14.12480]
- 9 **Lubarsky M**, Ray CE, Funaki B. Embolization agents-which one should be used when? Part 1: large-vessel embolization. *Semin Intervent Radiol* 2009; **26**: 352-357 [PMID: 21326545 DOI: 10.1055/s-0029-1242206]
- 10 **Lubarsky M**, Ray C, Funaki B. Embolization agents-which one should be used when? Part 2: small-vessel embolization. *Semin Intervent Radiol* 2010; **27**: 99-104 [PMID: 21359018 DOI: 10.1055/s-0030-1247891]
- 11 **Doklešić K**, Stefanović B, Gregorić P, Ivančević N, Lončar Z, Jovanović B, Bumbaširević V, Jeremić V, Vujadinović ST, Stefanović B, Milić N, Karamarković A. Surgical management of AAST grades III-V hepatic trauma by Damage control surgery with perihaptic packing and Definitive hepatic repair-single centre experience. *World J Emerg Surg* 2015; **10**: 34 [PMID: 26236391 DOI: 10.1186/s13017-015-0031-8]
- 12 **Prichayudh S**, Sirinawin C, Sriussadaporn S, Pak-art R, Kritayakirana K, Samorn P, Sriussadaporn S. Management of liver injuries: predictors for the need of operation and damage control surgery. *Injury* 2014; **45**: 1373-1377 [PMID: 24613610 DOI: 10.1016/j.injury.2014.02.013]
- 13 **Asfar S**, Khoursheed M, Al-Saleh M, Alfawaz AA, Farghaly MM, Nur AM. Management of liver trauma in Kuwait. *Med Princ Pract* 2014; **23**: 160-166 [PMID: 24457986 DOI: 10.1159/000358126]
- 14 **Pereira BM**. Non-operative management of hepatic trauma and the interventional radiology: an update review. *Indian J Surg* 2013; **75**: 339-345 [PMID: 24426473 DOI: 10.1007/s12262-012-0712-4]
- 15 **Bilbao JI**, Martínez-Cuesta A, Urtasun F, Cosín O. Complications of embolization. *Semin Intervent Radiol* 2006; **23**: 126-142 [PMID: 21326756 DOI: 10.1055/s-2006-941443]
- 16 **Mohan B**, Bhoday HS, Aslam N, Kaur H, Chhabra S, Sood N, Wander G. Hepatic vascular injury: clinical profile, endovascular management and outcomes. *Indian Heart J* 2013; **65**: 59-65 [PMID: 23438614 DOI: 10.1016/j.ihj.2012.12.011]
- 17 **Gaarder C**, Naess PA, Eken T, Skaga NO, Pillgram-Larsen J, Klow NE, Buanes T. Liver injuries--improved results with a formal protocol including angiography. *Injury* 2007; **38**: 1075-1083 [PMID: 17706220]
- 18 **Asensio JA**, Petrone P, García-Núñez L, Kimbrell B, Kuncir E. Multidisciplinary approach for the management of complex hepatic injuries AAST-OIS grades IV-V: a prospective study. *Scand J Surg* 2007; **96**: 214-220 [PMID: 17966747]
- 19 **Asensio JA**, Roldán G, Petrone P, Rojo E, Tillou A, Kuncir E, Demetriades D, Velmahos G, Murray J, Shoemaker WC, Berne TV, Chan L. Operative management and outcomes in 103 AAST-OIS grades IV and V complex hepatic injuries: trauma surgeons still need to operate, but angioembolization helps. *J Trauma* 2003; **54**: 647-653; discussion 653-654 [PMID: 12707525]
- 20 **Lin BC**, Wong YC, Lim KE, Fang JF, Hsu YP, Kang SC. Management of ongoing arterial haemorrhage after damage control laparotomy: optimal timing and efficacy of transarterial embolisation. *Injury* 2010; **41**: 44-49 [PMID: 19539285 DOI: 10.1016/j.injury.2009.01.007]
- 21 **Gaba RC**, Katz JR, Parvinian A, Reich S, Omene BO, Yap FY, Owens CA, Knuttinen MG, Bui JT. Splenic artery embolization: a single center experience on the safety, efficacy, and clinical outcomes. *Diagn Interv Radiol* 2013; **19**: 49-55 [PMID: 22875411 DOI: 10.4261/1305-3825]
- 22 **Bessoud B**, Denys A, Calmes JM, Madoff D, Qanadli S, Schnyder P, Doenz F. Nonoperative management of traumatic splenic injuries: is there a role for proximal splenic artery embolization? *AJR Am J Roentgenol* 2006; **186**: 779-785 [PMID: 16498106 DOI: 10.2214/AJR.04.1800]
- 23 **Raikhlin A**, Baerlocher MO, Asch MR, Myers A. Imaging and transcatheter arterial embolization for traumatic splenic injuries: review of the literature. *Can J Surg* 2008; **51**: 464-472 [PMID: 19057735]
- 24 **Ekeh AP**, Khalaf S, Ilyas S, Kauffman S, Walusimbi M, McCarthy MC. Complications arising from splenic artery embolization: a review of an 11-year experience. *Am J Surg* 2013; **205**: 250-254; discussion 254 [PMID: 23375704 DOI: 10.1016/j.amjsurg.2013.01.003]
- 25 **Gaarder C**, Dormagen JB, Eken T, Skaga NO, Klow NE, Pillgram-Larsen J, Buanes T, Naess PA. Nonoperative management of splenic injuries: improved results with angioembolization. *J Trauma* 2006; **61**: 192-198 [PMID: 16832270]
- 26 **Chakraverty S**, Flood K, Kessel D, McPherson S, Nicholson T, Ray CE, Robertson I, van Delden OM. CIRSE guidelines: quality improvement guidelines for endovascular treatment of traumatic hemorrhage. *Cardiovasc Intervent Radiol* 2012; **35**: 472-482 [PMID: 22271075 DOI: 10.1007/s00270-012-0339-7]
- 27 **Bittenbinder EN**, Reed AB. Advances in renal intervention for trauma. *Semin Vasc Surg* 2013; **26**: 165-169 [PMID: 25220322 DOI: 10.1053/j.semvasc.2014.06.012]
- 28 **Stewart AF**, Brewer ME, Daley BJ, Klein FA, Kim ED. Intermediate-term follow-up of patients treated with percutaneous embolization for grade 5 blunt renal trauma. *J Trauma* 2010; **69**: 468-470 [PMID: 20699760 DOI: 10.1097/TA.0b013e3181e5407a]
- 29 **Hotaling JM**, Sorensen MD, Smith TG, Rivara FP, Wessells H, Voelzke BB. Analysis of diagnostic angiography and angioembolization in the acute management of renal trauma uSingh A national data set. *J Urol* 2011; **185**: 1316-1320 [PMID: 21334643 DOI: 10.1016/j.juro.2010.12.003]
- 30 **van der Wilden GM**, Velmahos GC, Joseph DK, Jacobs L, Debusk MG, Adams CA, Gross R, Burkott B, Agarwal S, Maung AA, Johnson DC, Gates J, Kelly E, Michaud Y, Charash WE, Winchell RJ, Desjardins SE, Rosenblatt MS, Gupta S, Gaeta M, Chang Y, de Moya MA. Successful nonoperative management of the most severe blunt renal injuries: a multicenter study of the research consortium of New England Centers for Trauma. *JAMA Surg* 2013; **148**: 924-931 [PMID: 23945834 DOI: 10.1001/jamasurg.2013.2747]
- 31 **Menaker J**, Joseph B, Stein DM, Scalea TM. Angiointervention: high rates of failure following blunt renal injuries. *World J Surg* 2011; **35**:

- 520-527 [PMID: 21190111 DOI: 10.1007/s00268-010-0927-0]
- 32 **Brewer ME**, Strnad BT, Daley BJ, Currier RP, Klein FA, Mobley JD, Kim ED. Percutaneous embolization for the management of grade 5 renal trauma in hemodynamically unstable patients: initial experience. *J Urol* 2009; **181**: 1737-1741 [PMID: 19233429 DOI: 10.1016/j.juro.2008.11.100]
 - 33 **Starr AJ**, Griffin DR, Reinert CM, Frawley WH, Walker J, Whitlock SN, Borer DS, Rao AV, Jones AL. Pelvic ring disruptions: prediction of associated injuries, transfusion requirement, pelvic arteriography, complications, and mortality. *J Orthop Trauma* 2002; **16**: 553-561 [PMID: 12352563]
 - 34 **Smith W**, Williams A, Agudelo J, Shannon M, Morgan S, Stahel P, Moore E. Early predictors of mortality in hemodynamically unstable pelvis fractures. *J Orthop Trauma* 2007; **21**: 31-37 [PMID: 17211266]
 - 35 **Pohlemann T**, Bosch U, Gänsslen A, Tschern H. The Hannover experience in management of pelvic fractures. *Clin Orthop Relat Res* 1994; **(305)**: 69-80 [PMID: 8050249]
 - 36 **Eastridge BJ**, Burgess AR. Pedestrian pelvic fractures: 5-year experience of a major urban trauma center. *J Trauma* 1997; **42**: 695-700 [PMID: 9157205]
 - 37 **Riemer BL**, Butterfield SL, Diamond DL, Young JC, Raves JJ, Cottingham E, Kislak K. Acute mortality associated with injuries to the pelvic ring: the role of early patient mobilization and external fixation. *J Trauma* 1993; **35**: 671-675 discussion 676-677 [PMID: 8230327]
 - 38 **Balogh Z**, King KL, Mackay P, McDougall D, Mackenzie S, Evans JA, Lyons T, Deane SA. The epidemiology of pelvic ring fractures: a population-based study. *J Trauma* 2007; **63**: 1066-1073; discussion 1072-1073 [PMID: 17993952]
 - 39 **Hoffer EK**. Transcatheter embolization in the treatment of hemorrhage in pelvic trauma. *Semin Intervent Radiol* 2008; **25**: 281-292 [PMID: 21326518 DOI: 10.1055/s-0028-1085928]
 - 40 **Broadwell SR**, Ray CE. Transcatheter embolization in pelvic trauma. *Semin Intervent Radiol* 2004; **21**: 23-35 [PMID: 21331106 DOI: 10.1055/s-2004-831402]
 - 41 **Fu CY**, Wang YC, Wu SC, Chen RJ, Hsieh CH, Huang HC, Huang JC, Lu CW, Huang YC. Angioembolization provides benefits in patients with concomitant unstable pelvic fracture and unstable hemodynamics. *Am J Emerg Med* 2012; **30**: 207-213 [PMID: 21159470 DOI: 10.1016/j.ajem.2010.11.005]
 - 42 **Agolini SF**, Shah K, Jaffe J, Newcomb J, Rhodes M, Reed JF. Arterial embolization is a rapid and effective technique for controlling pelvic fracture hemorrhage. *J Trauma* 1997; **43**: 395-399 [PMID: 9314298]
 - 43 **Velmahos GC**, Chahwan S, Hanks SE, Murray JA, Berne TV, Asensio J, Demetriades D. Angiographic embolization of bilateral internal iliac arteries to control life-threatening hemorrhage after blunt trauma to the pelvis. *Am Surg* 2000; **66**: 858-862 [PMID: 10993617]
 - 44 **Salazar GM**, Walker TG. Evaluation and management of acute vascular trauma. *Tech Vasc Interv Radiol* 2009; **12**: 102-116 [PMID: 19853228 DOI: 10.1053/j.tvir.2009.08.004]
 - 45 **Katsanos K**, Sabharwal T, Carrell T, Dourado R, Adam A. Peripheral endografts for the treatment of traumatic arterial injuries. *Emerg Radiol* 2009; **16**: 175-184 [PMID: 18941810 DOI: 10.1007/s10140-008-0771-9]
 - 46 **Shin JS**, Shin JH, Ko HK, Kim JW, Yoon HK. Transcatheter arterial embolization for traumatic mesenteric bleeding: a 15-year, single-center experience. *Diagn Interv Radiol* 2016; **22**: 385-389 [PMID: 27306658 DOI: 10.5152/dir.2016.15413]
 - 47 **Steenburg SD**, Ravenel JG, Ikonidis JS, Schönholz C, Reeves S. Acute traumatic aortic injury: imaging evaluation and management. *Radiology* 2008; **248**: 748-762 [PMID: 18710974 DOI: 10.1148/radiol.2483071416]
 - 48 **Brenner ML**, Moore LJ, DuBose JJ, Tyson GH, McNutt MK, Albarado RP, Holcomb JB, Scalea TM, Rasmussen TE. A clinical series of resuscitative endovascular balloon occlusion of the aorta for hemorrhage control and resuscitation. *J Trauma Acute Care Surg* 2013; **75**: 506-511 [PMID: 24089121 DOI: 10.1097/TA.0b013e31829e5416]
 - 49 **Radvany MG**, Gailloud P. Endovascular management of neurovascular arterial injuries in the face and neck. *Semin Intervent Radiol* 2010; **27**: 44-54 [PMID: 21359014 DOI: 10.1055/s-0030-1247888]
 - 50 **Matsumoto J**, Lohman BD, Morimoto K, Ichinose Y, Hattori T, Taira Y. Damage control interventional radiology (DCIR) in prompt and rapid endovascular strategies in trauma occasions (PRESTO): A new paradigm. *Diagn Interv Imaging* 2015; **96**: 687-691 [PMID: 26119866 DOI: 10.1016/j.diii.2015.06.001]

P- Reviewer: Andersen PE, Kambadakone A, Tarazov PG

S- Editor: Kong JX **L- Editor:** A **E- Editor:** Wu HL



Imaging spectrum of spinal dysraphism on magnetic resonance: A pictorial review

Jyoti Kumar, Muhammed Afsal, Anju Garg

Jyoti Kumar, Muhammed Afsal, Anju Garg, Department of Radiodiagnosis, Maulana Azad Medical College and Associated Lok Nayak Hospital, New Delhi 110002, India

Author contributions: Kumar J and Afsal M substantially contributed towards the conception of study, data collection and drafting the article; Garg A analysed the data and critically revised to assess intellectual content in the article.

Conflict-of-interest statement: Authors declare no conflict of interests for this article.

Open-Access: This article is an open-access article which was selected by an in-house editor and fully peer-reviewed by external reviewers. It is distributed in accordance with the Creative Commons Attribution Non Commercial (CC BY-NC 4.0) license, which permits others to distribute, remix, adapt, build upon this work non-commercially, and license their derivative works on different terms, provided the original work is properly cited and the use is non-commercial. See: <http://creativecommons.org/licenses/by-nc/4.0/>

Manuscript source: Invited manuscript

Correspondence to: Dr. Jyoti Kumar, Department of Radiodiagnosis, Maulana Azad Medical College and Associated Lok Nayak Hospital, Bahadur Shah Zafar Road, New Delhi 110002, India. drjyotikumar@gmail.com
Telephone: +91-99-68604361

Received: October 13, 2016

Peer-review started: October 17, 2016

First decision: January 16, 2017

Revised: February 16, 2017

Accepted: February 28, 2017

Article in press: March 2, 2017

Published online: April 28, 2017

Magnetic resonance imaging (MRI) is now considered the imaging modality of choice for diagnosing these conditions. The purpose of this article is to review the normal development of spinal cord and spine and reviewing the MRI features of spinal dysraphism. Although imaging of spinal dysraphism is complicated, a systematic approach and correlation between neuro-radiological, clinical and developmental data helps in making the correct diagnosis.

Key words: Spinal dysraphism; Magnetic resonance imaging; Open spinal dysraphism; Meningomyelocele; Closed spinal dysraphism

© The Author(s) 2017. Published by Baishideng Publishing Group Inc. All rights reserved.

Core tip: Imaging of spinal dysraphism may appear complicated as it is a group of diverse conditions which can have variable imaging appearance. It includes a heterogeneous group of anomalies which result from faulty closure of midline structures during development. Magnetic resonance imaging is now considered the imaging modality of choice for diagnosing these conditions. A systematic approach and correlation with neuroradiological, clinical and developmental data helps in making the correct diagnosis.

Kumar J, Afsal M, Garg A. Imaging spectrum of spinal dysraphism on magnetic resonance: A pictorial review. *World J Radiol* 2017; 9(4): 178-190 Available from: URL: <http://www.wjgnet.com/1949-8470/full/v9/i4/178.htm> DOI: <http://dx.doi.org/10.4329/wjr.v9.i4.178>

Abstract

Congenital malformations of spine and spinal cord are collectively termed as spinal dysraphism. It includes a heterogeneous group of anomalies which result from faulty closure of midline structures during development.

INTRODUCTION

Congenital malformations of spine and spinal cord are collectively termed as spinal dysraphism. It includes

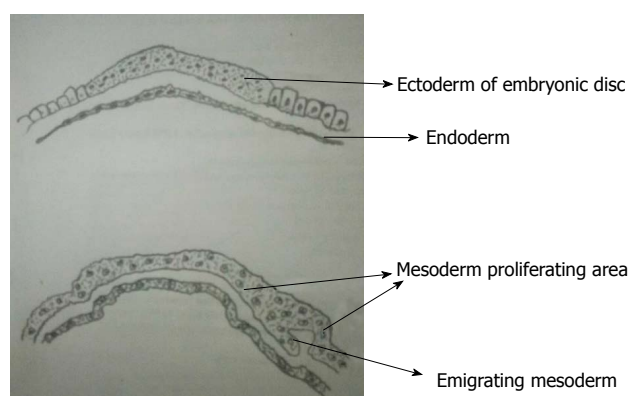


Figure 1 Gastrulation. During gastrulation, the bilaminar embryonic disc is converted to a trilaminar disc by the formation of mesoderm. There is rapid division of cells in embryonic disc which then detach and migrate between endoderm and ectoderm to form mesoderm. Notochord later develops from mesoderm.

a heterogeneous group of anomalies resulting from incomplete midline closure of osseous, mesenchymal and nervous tissue^[1]. Most of these conditions are diagnosed at or soon after birth, but some are discovered late in childhood or in adulthood because of absence of clinical manifestations. Magnetic resonance imaging (MRI) is the imaging modality of choice for diagnosing spinal dysraphism because of its superior soft tissue characterisation and multiparametric imaging capabilities^[2]. The purpose of this article is to review the normal development of spinal cord and MRI features of spinal dysraphism with clinico-embryologic and radiological correlation.

EMBRYOLOGY

Development of spinal cord occurs during early embryogenesis (between 2-6 wk of gestation) in three main stages - gastrulation, primary neurulation and secondary neurulation^[3,4]. During the stage of gastrulation, the bilaminar embryonic disc composed of ectoderm and endoderm is converted to a trilaminar disc by the formation of mesoderm (Figure 1).

Notochord which is formed from midline mesoderm interacts with overlying ectoderm resulting in the formation of neuroectoderm and neural plate^[5]. Primary neurulation begins with the formation of neural plate and ends with the closure of caudal end of neural plate (Figure 2). A small depression develops along the central axis of neural plate to form neural groove and neural folds are formed on both sides of the neural groove. The neural plate then bends and neural folds fuse together converting the linear neural plate into a cylindrical neural tube. Closure of neural groove proceeds bidirectionally with the cephalic end (anterior or rostral neuropore) closing on day 25 and the caudal end (posterior or caudal neuropore) closing on day 27 or 28^[6].

During secondary neurulation there is formation of caudal cell mass composed of undifferentiated pluripotent cells from the caudal end of neural tube and notochord distal to caudal neuropore. Neurons and

Table 1 Classification of spinal dysraphisms

Open spinal dysraphisms
Myelomeningocele
Myelocele
Hemimyelomeningocele
Hemimyocele
Closed spinal dysraphisms
With subcutaneous mass
Lipomyelomeningocele
Lipomyelocele
Terminal myelocystocele
Meningocele
Myelocystocele
Without subcutaneous mass
Simple dysraphic states
Intradural lipoma
Filar lipoma
Tight filum terminale
Persistent terminal ventricle
Dermal sinus
Complex dysraphic states
Dorsal enteric fistula
Neurenteric cyst
Diastematomyelia
Caudal agenesis
Segmental spinal dysgenesis

vacuoles develop within the caudal cell mass. Vacuoles then coalesce and eventually connect to the central canal by the process called cavitation. Finally the cells of caudal cell mass undergo retrograde differentiation during which cells undergo programmed cell death or apoptosis to form conus medullaris, filum terminale and ventriculus terminalis (Figure 3)^[7,8].

Various disorders due to defective primary neurulation include open spinal dysraphism (OSD), closed spinal dysraphism (CSD) and dorsal dermal sinus while defects during secondary neurulation results in filar lipoma, tight filum terminale, caudal agenesis and sacrococcygeal teratoma. Defective development of notochord results in diastematomyelia, neurenteric cyst, caudal agenesis and segmental spinal dysgenesis^[9].

CLASSIFICATION

On the basis of presence or absence of overlying skin covering, spinal dysraphism is divided into open and closed types^[10-12] (Table 1). In OSD overlying skin covering is absent and the neural elements are exposed to the external environment whereas, in closed type the neural elements have a skin covering (Figure 4). CSD can be further divided based on the presence or absence of associated subcutaneous mass.

In our review, we will follow the clinic-radiological classification as it is easier to understand and is more prevalent in use.

OSDS

Myelomeningocele and myelocele

OSDs result from faulty primary neurulation due to defective closure of the neural tube. About 98.8% of

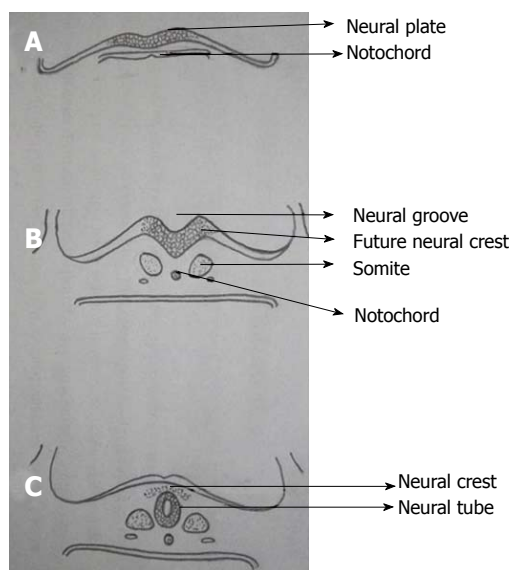


Figure 2 Primary neurulation. A: Thickening of embryonic ectoderm is seen dorsal to notochord to form neuroectoderm and neural plate; B: Neural plate invaginates along its central axis to form neural groove. Neural folds are formed on both sides of the neural groove; C: The neural plate then bends and neural folds fuse together to form neural tube and simultaneously separate from surface ectoderm (dysjunction).

all OSDs are constituted by Myelomeningocele (MMC) where both the neural placode and meningeal lining protrude through the bony and cutaneous defect in the midline^[3]. OSDs are commonly diagnosed clinically as the neonate presents with a midline reddish exposed neural placode and immediate surgical repair is usually done, so imaging studies are not always performed. It usually involves the lower lumbar and sacral regions (98%) and is rare in cervical and upper thoracic spine, probably because the lesion in these areas are more severe leading to fetal demise^[4,13].

In MMC, the protruding neural placode extends beyond the skin surface as there is enlargement of the adjacent subarachnoid space (Figure 5)^[5]. This helps to distinguish MMC from the far rarer myelocele, where the placode is flush with the skin surface (Figures 6 and 7). About 80% of myelocele and MMC have associated hydrocephalus and 100% patients have Chiari II malformation which involves cerebellum, brain stem, skull base, spine and spinal column (Figure 8)^[3,4]. Studies have shown that defective neural tube closure resulting in abnormal drainage of CSF and hence decompression of the primitive ventricular system resulting in various manifestations of Chiari II malformation^[14,15].

Advancements in prenatal diagnosis permit diagnosis of neural tube defects in fetus as early as first trimester, and now most of the cases of MMC are diagnosed prenatally during screening sonography. Although sonography is the modality of choice for screening fetus for any gross congenital anomalies, MRI is being increasingly used for prenatal evaluation of CNS anomalies with the advent of faster MR sequences (Figure 9)^[16,17].

Prenatal diagnosis and developments in fetal sur-

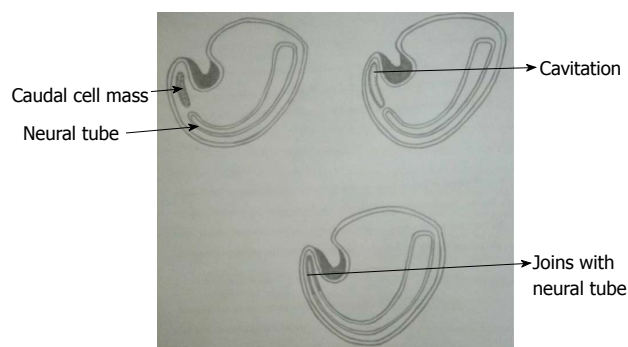


Figure 3 Secondary neurulation. Schematic diagram of caudal end of embryo showing secondary neurulation which forms the distal part of spinal cord. There is formation of solid caudal cell mass distal to the caudal neuropore which then develops a lumen by a process called "cavitation". This then becomes continuous with the central cavity of neural tube.

gery has made possible in utero repair of the neural tube defects which can arrest the development of other malformations developing secondary to abnormal tube closure. The Management of Myelomeningocele Study trial, a prospective randomized study done in United States has shown that fetal surgery for MMC in second trimester preserves neurologic function, reverses the changes of Chiari II malformation and reduces the need for postnatal ventriculoperitoneal shunt^[18-21].

Hemimyelomeningocele and hemimyelocele

These conditions are extremely rare and are caused by defective gastrulation and primary neurulation^[22]. Diastematomyelia is a common association with OSDs but only when one of the hemicords shows defective neurulation, the malformation is labelled hemimyelo(meningo)cele^[3]. Here one of the two hemicords exhibits a myelomeningocele or myelocele while the other hemicord can be normal or is tethered.

CSDS WITH SUBCUTANEOUS MASS

Lipomas with dural defect - lipomyelocele and lipomyelomeningocele

Lipomyelocele and Lipomyelomeningocele result from defective primary neurulation where there is premature focal disjunction of cutaneous ectoderm and neuroectoderm allowing mesenchyme to enter the neural tube. This mesenchyme later forms the lipomatous tissue for unknown reasons^[23,24]. Clinically they are characterized by the presence of subcutaneous fatty mass lesion above the intergluteal line which may extend to buttocks. Sagittal T1 WI images show high intensity fat on the dorsal aspect of the placode which is continuous with the adjacent subcutaneous fat. T1 weighted fat saturated images show suppression of fat signal. Lipomyelocele and Lipomyelomeningocele are differentiated based on the position of neural placode - lipoma interface (Figure 10). It lies within or at the edge of the spinal canal in lipomyelocele and outside the spinal canal in lipomyelomeningocele (Figure 11)^[11].



Figure 4 Open and closed spinal dysraphism. Clinical pictures of open (A) and closed (B) spinal dysraphism. In open spinal dysraphism, a case of cervical myelomeningocele the neural placode is directly exposed to the environment and is surrounded by partially epithelized skin (arrow in A). In closed spinal dysraphism with subcutaneous mass there is continuous skin coverage over the abnormality (arrow in B).

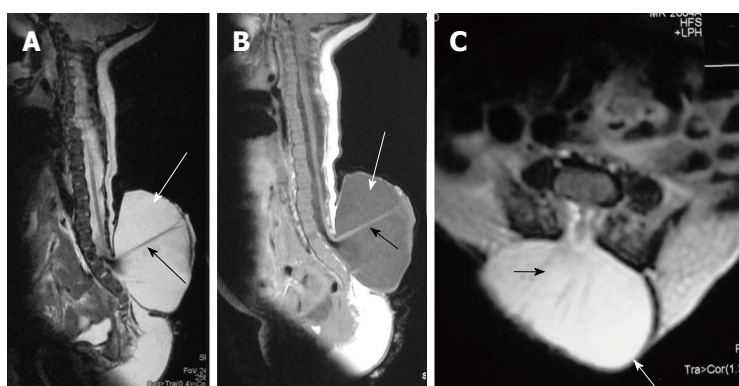


Figure 5 Lumbar myelomeningocele. T2 weighted sagittal (A), T1 weighted sagittal (B) and T2 weighted axial (C) images of lumbar spine showing myelomeningocele. There is posterior herniation of a CSF filled sac (white arrows) containing cord and nerve fibers (black arrows). There is absence of skin covering with interruption of subcutaneous fat.

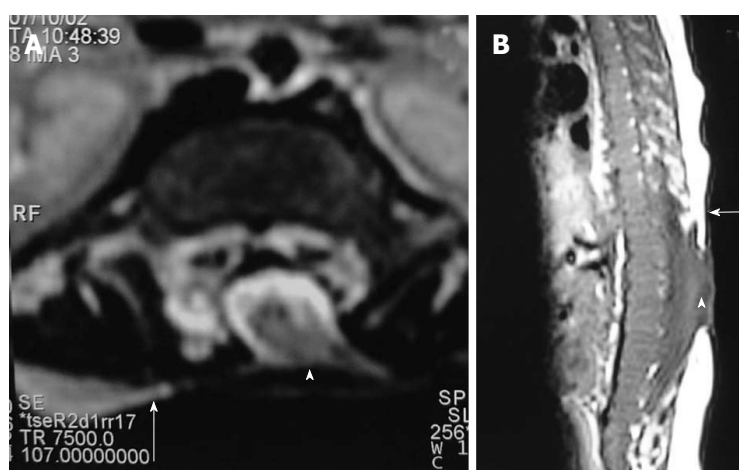


Figure 6 Myelocele. Axial T2 weighted (A) and sagittal T1 weighted (B) images of dorsolumbar spine in a case of myelocele showing the neural placode (arrowhead) flush with the skin surface (arrow). Skin covering is absent over the myelocele.

In lipomyelomeningocele there is expansion of subarachnoid space anterior to the cord pushing the neural placode - lipoma interface posteriorly to lie outside the boundaries of spinal canal. In hemilipomyelocele or hemilipomyelomeningocele there is associated diastematomyelia with one of the hemicord showing lipomyelocele or lipomyelomeningocele respectively (Figure 12).

Meningocele

Meningocele refers to herniation of CSF filled sac lined by dura and arahnoid mater. The exact embryogenesis is unknown but is thought to be caused by ballooning

of meninges due to CSF pulsation. By definition, spinal cord should not be seen within the meningocele but may be seen tethered to its neck. Meningocele may contain nerve roots and or filum terminale which usually appear hypertrophied.

Posterior meningocele is due to herniation of meningeal lining through posterior spina bifida (Figure 13). It is usually lumbosacral in location but can be seen in other locations also. Anterior meningocele is almost always presacral in location^[25].

Terminal myelocystocele

Terminal myelocystocele involves herniation of a

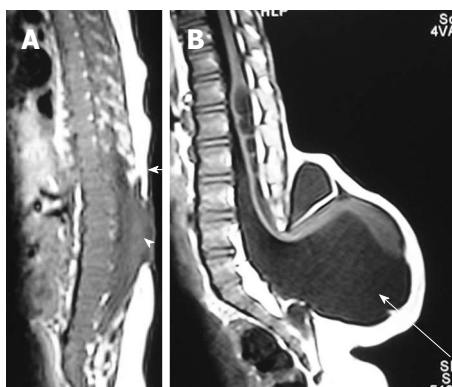


Figure 7 Myelocele and myelomeningocele. Sagittal T1 weighted images of spine in cases of myelocele (A) and myelomeningocele (B). In myelocele the placode (arrowhead) is flush with the skin surface (arrow). In myelomeningocele (B), the protruding neural placode extends beyond the skin surface as there is enlargement of the underlying subarachnoid space (arrow).

dilated terminal central canal forming terminal syringohydromyelia (syringocele) through a posterior vertebral defect into an expanded CSF filled dural sheath (meningocele). It results from defective secondary neurulation which affects the CSF flow dynamics. The inner terminal syrinx communicates with the central canal of the spinal cord and the outer meningocele is continuous with the spinal subarachnoid space. The syringocele and meningocele usually do not communicate with each other^[26-28].

CSDS WITHOUT SUBCUTANEOUS MASS

Simple dysraphic states

These are a heterogeneous group of conditions which arise due to abnormalities of primary and secondary neurulation and are the most common type of spinal dysraphism seen in older children^[29]. Simple dysraphic states include intradural lipoma, filar lipoma, tight filum terminale, dermal sinus and persistent terminal ventricle.

Intradural lipoma

It is a midline lipoma located in the groove of unopposed neural placode in its dorsal surface within an intact dural sac. The intact dura help to differentiate this from lipomyelocele and lipomyelomeningocele. They are usually seen in lumbosacral region and are associated with tethered cord syndrome. Large lipomas may cause cord displacement. On MRI lipomas follow the signal intensity of subcutaneous fat on all sequences (Figure 14)^[10].

Filar lipoma

Filar lipoma is an abnormality of secondary neurulation which shows fibrolipomatous thickening of the filum terminale. On imaging filar lipoma appears hyperintense on T1 and T2 weighted images within a thickened filum terminale (Figure 15). One point five percent to 5% of normal adult population may show fat within filum

terminale on MRI and hence the finding is considered a normal variant (Figure 16) unless it is associated with tethered cord syndrome^[30,31]. Tethered cord syndrome is characterized clinically by progressive neurological deficit and on imaging, there is low lying conus medullaris with a short thick filum terminale which is tethered to dural sac^[32].

Tight filum terminale

It is characterized by shortening and hypertrophy of filum terminale which cause tethering of cord and impairs the ascent of conus medullaris. Embryologically the defect lies in retrogressive differentiation during secondary neurulation.

On imaging it is characterized by a thick filum terminale (thickness measuring > 2 mm) and a low lying conus medullaris - below L2 vertebral body (Figure 17)^[8]. It is usually seen in association with other malformations and isolated cases are rare.

Dermal sinus

It is an epithelial lined fistulous communication between CNS or its meningeal covering and skin. It results from focal incomplete disjunction between neuroectoderm and cutaneous ectoderm.

Clinically a midline dimple or ostium is found on the cutaneous surface and is commonly associated with cutaneous stigmata of underlying occult spinal dysraphism like hairy nevus, hemangioma or hyperpigmentation. The tract then ascends and opens into spinal canal (Figure 18). Dermal sinus may be associated with intraspinal dermoids or epidermoids which show variable imaging findings depending on their contents^[33,34]. Dermoids usually appear hyperintense on both T1 and T2 weighted images while epidermoids are hypointense on T1 weighted and hyperintense on T2 weighted images. CNS infection is a common complication because of fistulous communication and hence these cases require early surgical repair (Figure 19).

Persistent terminal ventricle

Terminal ventricle is a small, ependyma lined cavity within conus medullaris (Figures 13 and 17). Embryologically incomplete regression of terminal ventricle during the stage of secondary neurulation is responsible for the condition. Location just above filum terminale helps to differentiate it from hydromyelia and lack of enhancement is the differentiating feature from intramedullary tumors^[35].

COMPLEX DYRAPHIC STATES

Any abnormality occurring at the time of gastrulation affects the spinal cord and various other structures which are derived from notochord resulting in complex anomalies^[36]. Most of these abnormalities are covered by skin and subcutaneous masses are absent. On the basis of their embryogenesis complex dysraphic states are divided into two subtypes - disorders of midline

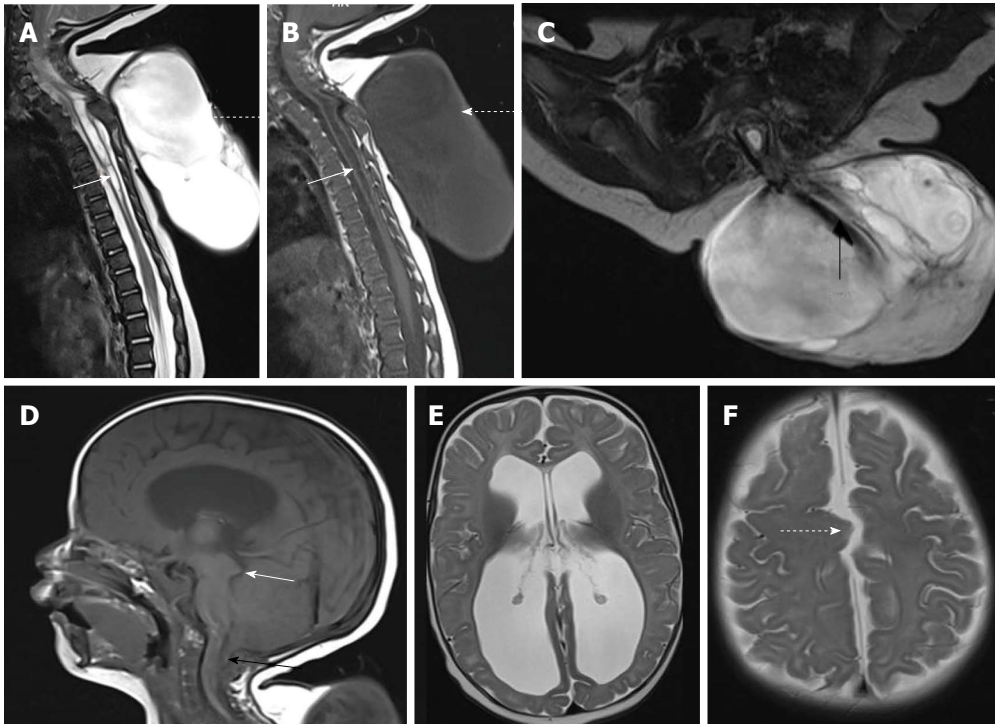


Figure 8 Cervico-dorsal myelomeningocele with Chiari II malformation. T2 weighted sagittal (A), T1 weighted sagittal (B) and T2 weighted axial (C) images of cervicodorsal spine showing myelomeningocele. There is posterior herniation of a CSF filled sac (dashed arrows) containing nerve fibers (black arrow). Spinal cord show kinking at the same level and dilated central canal (white arrow) suggestive of syringohydromyelia. There is no overlying skin cover. Sagittal T1 weighted (D) and axial T2 weighted (E and F) images of brain shows herniation of cerebellar tonsils (black arrow) with tectal beaking (white arrow). Fourth ventricle is elongated and tubular shaped. There is colpocephaly suggestive of corpus callosal agenesis (in E) and interdigitating gyri (dashed arrow in F) suggestive of fenestrated falx.

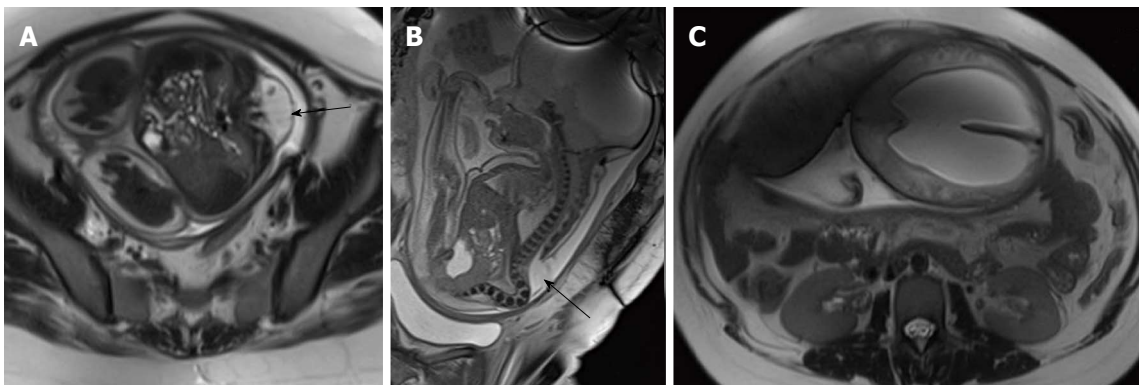


Figure 9 Fetal Myelomeningocele with Chiari II malformation. Axial (A) and sagittal (B) T2 weighted images of lumbar spine of fetus showing splaying of posterior elements of lumbar vertebrae with herniation of spinal canal contents (black arrow) suggestive of MMC. Axial T2 weighted image of brain (C) shows associated hydrocephalus. Hydrocephalus in the setting of MMC in a fetus is considered highly suggestive of Chiari II malformation. MMC: Myelomeningocele.

notochordal integration and disorders of notochordal formation.

Disorders of midline notochordal integration

The process of fusion of paired notochordal anlagen to form a single midline notochordal process is called midline notochordal integration^[3]. Any abnormality at this stage results in longitudinal splitting of spinal cord. Most important entities in this group are neurenteric cyst and diastematomyelia.

Neurenteric cyst: Most severe form of disorder of

midline notochordal integration is dorsal enteric fistula - a fistulous communication between skin surface and bowel - which is an extremely rare condition. Neurenteric cyst is a localized form of dorsal enteric fistula and is seen anterior to spinal cord with adjacent vertebral anomalies. These cysts are typically seen in extramedullary intradural compartment of cervicothoracic spine, however may be seen in other locations too^[37]. On MRI, neurenteric cysts usually appear iso- to hyperintense to CSF on both T1 and T2 weighted images due to high protein content and show absent contrast enhancement (Figure 20)^[38,39].

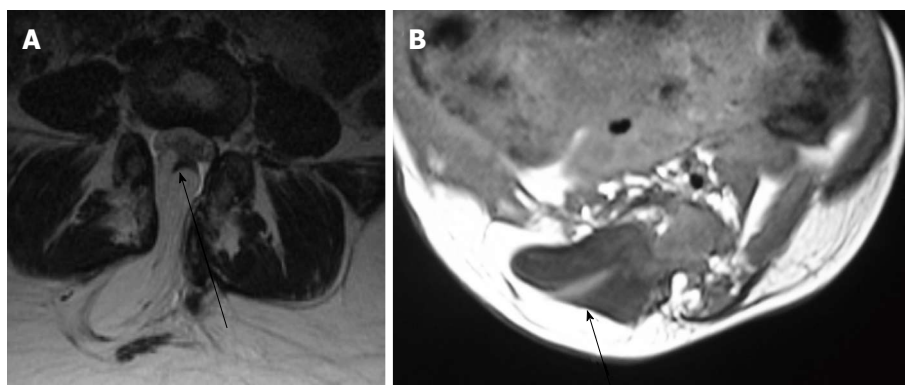


Figure 10 Lipoma placode interface in lipomyelocele and lipomyelomeningocele. Axial T2 weighted images in cases of lipomyelocele (A) and axial T1 weighted images in case of lipomyelomeningocele (B) showing high intensity fat on the dorsal aspect of the neural placode which is continuous with the adjacent subcutaneous fat. The lipoma placode interface (black arrow) is within the spinal canal in lipomyelocele and outside the spinal canal in lipomyelomeningocele. Both these conditions have intact skin covering.

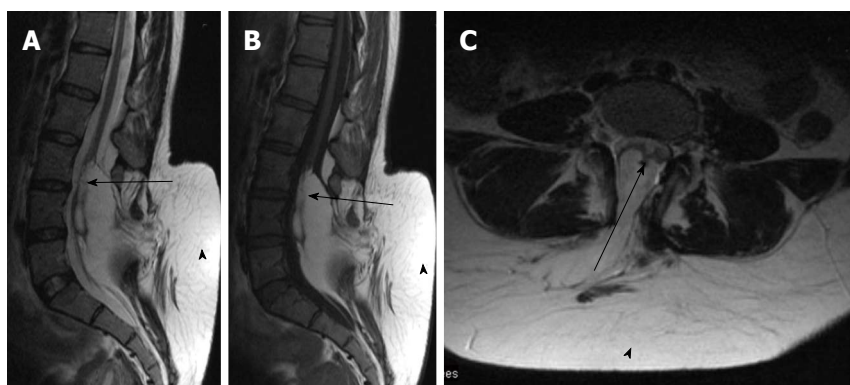


Figure 11 Lipomyelocele. T2 weighted sagittal (A), T1 weighted sagittal (B) and T2 weighted axial (C) images of lumbosacral spine in a case of lumbar lipomyelocele. High intensity fat is seen on the dorsal aspect of the neural placode which is continuous with the adjacent subcutaneous fat (arrowhead) through an open defect in the posterior aspect of spinal canal. The placode lipoma interface is within the spinal canal (arrow).

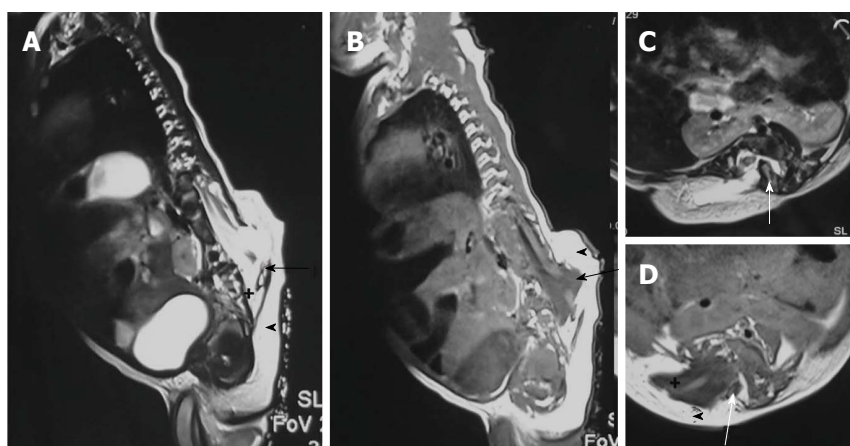


Figure 12 Hemilipomyelomeningocele. T2 weighted sagittal (A), T1 weighted sagittal (B), T2 weighted axial (C) and T1 weighted axial (D) images in a case of hemilipomyelomeningocele. There is diastematomyelia with bony septum (white arrow) suggestive of type I diastematomyelia. There is defect in the posterior spinal canal on the right side through which the spinal canal contents herniate with intact overlying skin and subcutaneous tissue (arrowhead). There is expansion of subarachnoid space (+) anterior to the cord pushing the neural placode - lipoma interface posteriorly to lie outside the boundaries of spinal canal (arrow).

Diastematomyelia: It is the most common form of defective midline notochordal integration. Due to defective midline integration there are two notochordal processes each of which induces formation of separate

neural plate with intervening primitive streak tissue. The development of the primitive streak tissue decides the type of diastematomyelia. In type I diastematomyelia the intervening primitive streak develops into bone

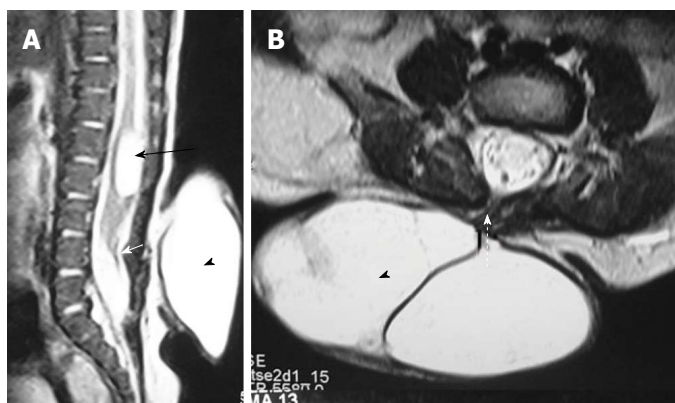


Figure 13 Posterior meningocele with persistent terminal ventricle. T2 weighted sagittal (A) and axial (B) images of lumbosacral spine showing posterior meningocele and persistent terminal ventricle. There is herniation of a CSF filled sac (arrowhead) through a posterior spina bifida (dashed arrow) consistent with posterior meningocele. No neural tissue is noted within the CSF sac. There is another CSF attenuation lesion in conus medullaris (black arrow) suggestive of persistent terminal ventricle. The filum terminale is short and thick (white arrow) with low lying spinal cord suggestive of tight filum terminale. CSF: Cerebrospinal fluid.

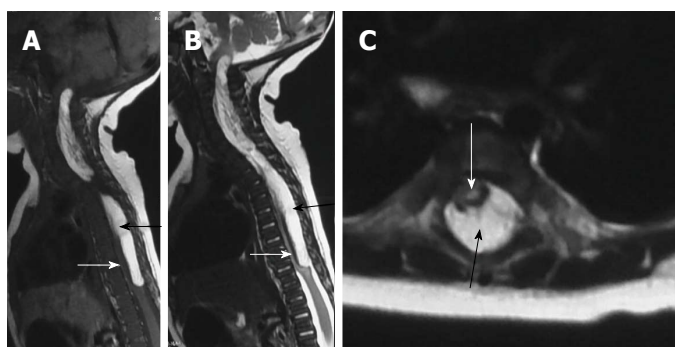


Figure 14 Dural lipoma. T2 weighted sagittal (A), T1 weighted sagittal (B) and T2 weighted axial (C) images of cervico-dorsal spine showing a T1 and T2 hyperintense lesion in the spinal canal (black arrow) causing compression and anterior displacement of the spinal cord (white arrow). The lesion is isointense to subcutaneous fat on all sequences.

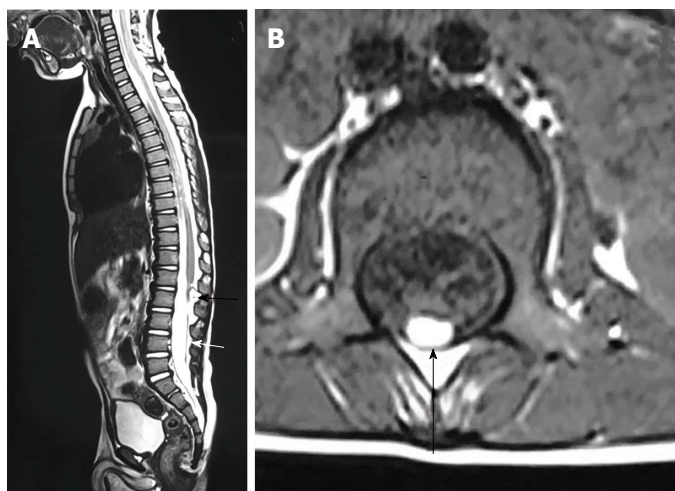


Figure 15 Filarlipoma. T2 weighted sagittal (A) and T1 weighted axial images of lumbosacral spine in a case of filar lipoma. The lesion (black arrow) appears hyperintense on both T1 and T2 weighted images and follows the signal of subcutaneous fat on all sequences. Filum terminale is thickened and is tethered (white arrow).

or cartilage, resulting in two hemicords in different dural sacs separated by an osteocartilaginous septum (Figure 12). In type II diastematomyelia, the primitive streak is reabsorbed or forms a fibrous septum with the hemicords lying within the same dural sac (Figure 21)^[40]. Diastematomyelia is commonly associated with vertebral anomalies and hydromyelia. A high lying hairy tuft over a child's back is a reliable indicator for underlying diastematomyelia^[41].

Disorders of notochordal formation

Apoptosis or programmed cell death is an important process occurring during different steps of embryogenesis. Abnormal apoptosis results in disorders of notochord formation and these disorders include caudal

agenesis and segmental spinal dysgenesis^[29].

Caudal agenesis: It is characterized by partial or total agenesis of spinal column and is commonly associated with genital anomalies, anal imperforation, pulmonary hypoplasia, renal aplasia or dysplasia and limb abnormalities. Caudal agenesis (CA) is broadly divided into two types.

In type I CA both caudal cell mass and notochord formation is affected, resulting in high position (most commonly at the level of D12 vertebra) and abnormal termination of conus medullaris. There is accompanying varying degree of vertebral aplasia, with the last vertebra as L5 through S2 in majority of patients.

In type II CA there is abnormal development of



Figure 16 Fat in filumterminale. T2 weighted (A) and T1 weighted (B) sagittal images of lumbosacral spine in a 60-year-old male showing linear T1 and T2 hyperintense focus in filumterminale (arrow) noted incidentally. Spinal cord is not low lying and there is no tethering of cauda equina fibres. Note is made of degenerative changes in lumbar spine.

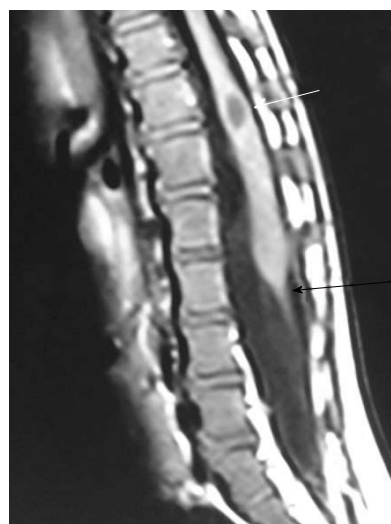


Figure 17 Tight filumterminale. T1 weighted sagittal image of the lumbosacral spine showing thick and short filum terminale (black arrow) with low lying spinal cord. There is a CSF attenuation lesion in conus medullaris (white arrow) suggestive of syrinx. CSF: Cerebrospinal fluid.

only caudal cell mass with unaffected true notochord formation. Hence, there is defective secondary neurulation with normal primary neurulation. As a result only the most caudal part of conus medullaris is absent in type II CA (Figure 22). Vertebral dysgenesis is less severe in these cases and these patients present with tethered cord syndrome as the conus in these cases is stretched and tethered^[42,43].

Segmental spinal dysgenesis: This is an extremely rare condition characterized by: (1) segmental agenesis or dysgenesis of lumbar or thoracolumbar spine; (2) segmental abnormality of spinal cord or nerve roots; (3) congenital paraparesis or paraplegia; and (4) congenital lower limb deformities. This occurs due to notochordal abnormality occurring during gastrulation which involves an intermediate segment of notochord^[29,44].



Figure 18 Dermal sinus. T2 weighted sagittal images of lumbosacral spine showing a T2 hypointense tract extending from the posterior skin surface to the spinal canal (black arrow). There is associated tethered cord.

SACROCOCCYGEAL TERATOMA

Sacroccocygeal teratoma, although a tumor, needs special mentioning as it develops from the pluripotent cells of caudal cell mass. It is the most common tumor of fetus and new born and commonly present as a large complex solid cystic mass caudal to coccyx. Most of the teratomas are benign and contains derivatives from all three germ layers. Based on the presence of external and internal components they are divided into four types - type I: Primarily external, type II: Equal external and internal portions, type III: Primarily internal and type IV: Entirely internal.

On MRI, sacroccocygeal teratoma has variable signal on T1 and T2 weighted images depending on the internal contents (fat, soft tissue, fluid, calcium). On post contrast images, there is heterogeneous

enhancement of the solid portion (Figure 23)^[45,46]. This may also be picked up on antenatal scan where MRI can accurately depict its extension into the pelvis and its mass effect on pelvic organs (Figure 24).

POST-OPERATIVE IMAGING

Surgery is the treatment of choice for spinal dysraphism and surgery includes closure of the neural tube defect and detethering followed by lifelong supportive care and follow up. During follow-up, worsening of symptoms

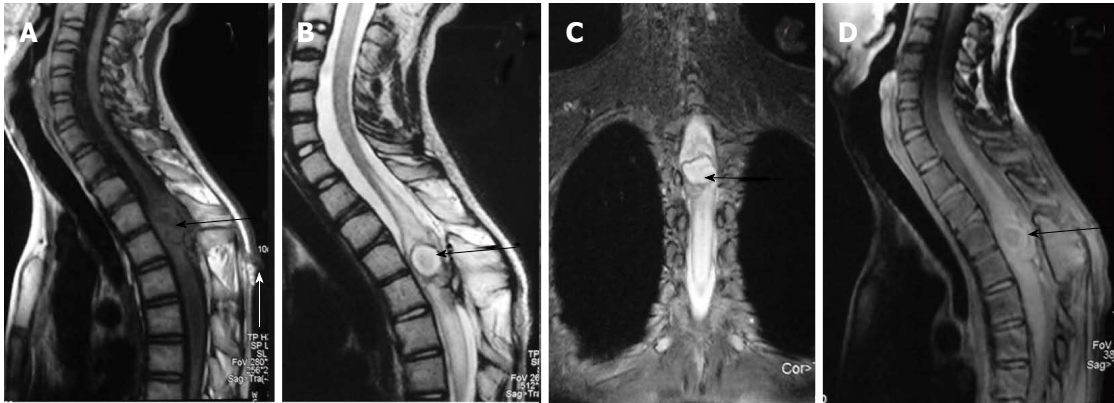


Figure 19 Infected dermal sinus with intraspinal dermoid. T1 weighted sagittal image (A) showing a dermal sinus (white arrow) with an intraspinal lesion (black arrow) showing mildly hyperintense signal with expansion of spinal cord. On T2 weighted sagittal (B) and STIR coronal (C) images the intraspinal lesion appears hyperintense with well defined hypointense rim. On post contrast image (D) there is peripheral enhancement of the intraspinal lesion and the tract.

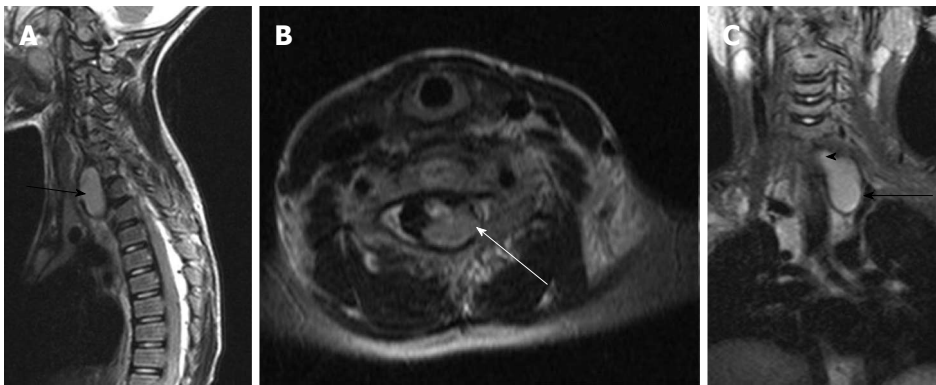


Figure 20 Neuroenteric cyst. T2 weighted images of cervicodorsal spine in sagittal (A), axial (B) and coronal (C) planes show a bilobed lesion with both extraspinal (black arrow) and intraspinal extramedullary component (white arrow). The communication between them (arrowhead) is better appreciated in the coronal plane (C).

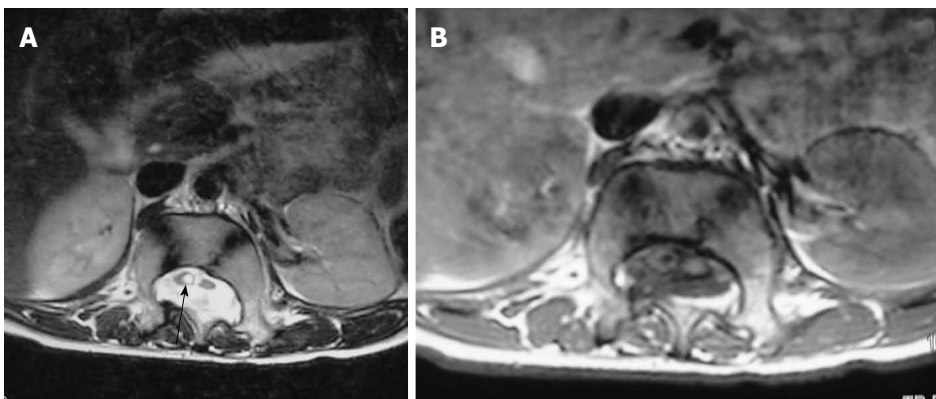


Figure 21 Diastematomyelia II. Axial T2 weighted (A) and T1 weighted (B) scan of lumbar spine showing two hemicords. No intervening bony septum was noted. The hemicord on the right shows dilated central canal or syringohydromyelia (arrow).

should be looked for and MRI should be done at the earliest suspicion. During post-operative imaging, various immediate and late complications of spinal surgery like wound infection, shunt infection, wound dehiscence, cerebrospinal fluid leak, problems related to kyphectomy, adhesions with retethering or dermoid formation should be looked for (Figure 25). Retethering is due to post-surgical fibrosis resulting in tethering of

cauda equine fibres. MRI may be done in prone position to look for CSF dorsal to the conus for ruling out retethering^[47].

CONCLUSION

Imaging of spinal dysraphism may appear complicated as it is a group of diverse conditions which can have

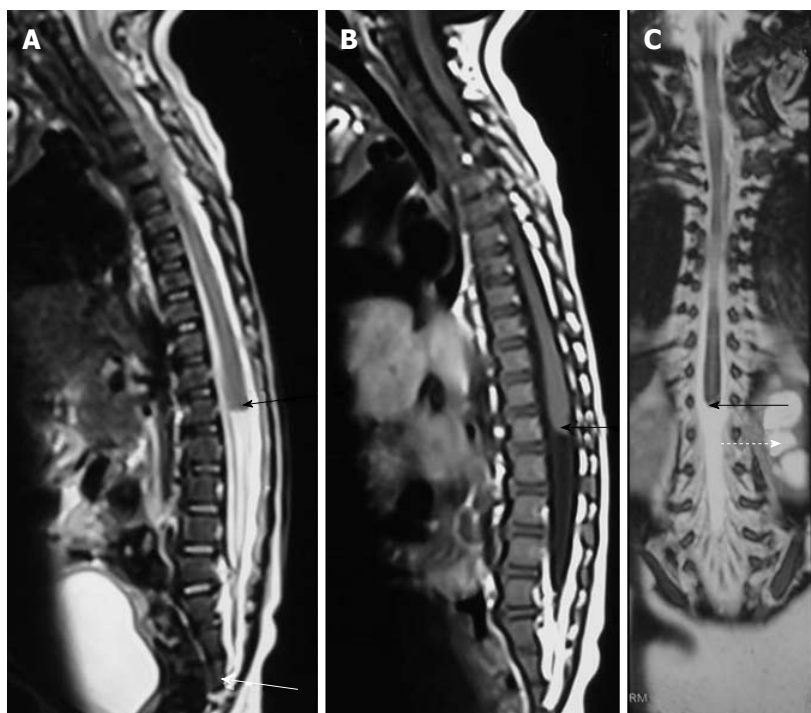


Figure 22 Caudal agenesis. T2 weighted sagittal (A), T1 weighted sagittal (B) and T2 weighted coronal (C) MR images showing type II caudal agenesis. There is non-development of distal sacral vertebra (white arrow in A) with abnormal termination of conus medullaris (black arrow). The child also has associated left hydronephrosis (dashed arrow in C).

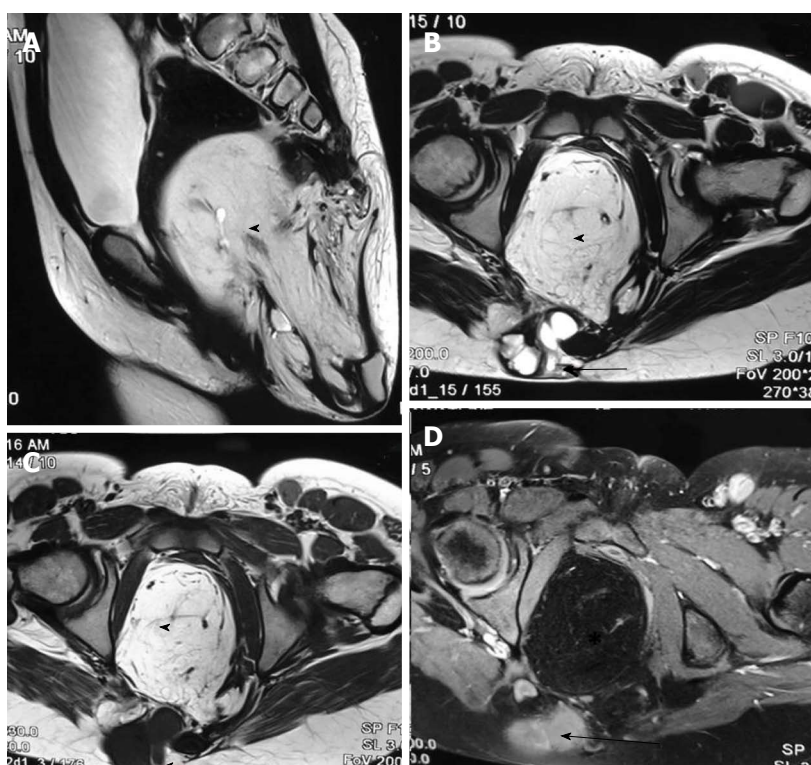


Figure 23 Sacrococcygeal teratoma (type III). T2 weighted sagittal (A), T2 weighted axial (B), T1 weighted axial (C) and T1 weighted fat suppressed axial post contrast (D) images show a large heterogeneous presacral lesion. It has a large internal component which is predominately fat (arrowhead) appearing hyperintense on both T1 and T2 weighted images with signal suppression on post contrast fat saturated image. It also has a small complex solid cystic external component (arrow) appearing hyperintense on T2 weighted and hypointense on T1 weighted with enhancement on post contrast images.

variable imaging appearance. A systematic approach and correlation with neuroradiological, clinical and develop-

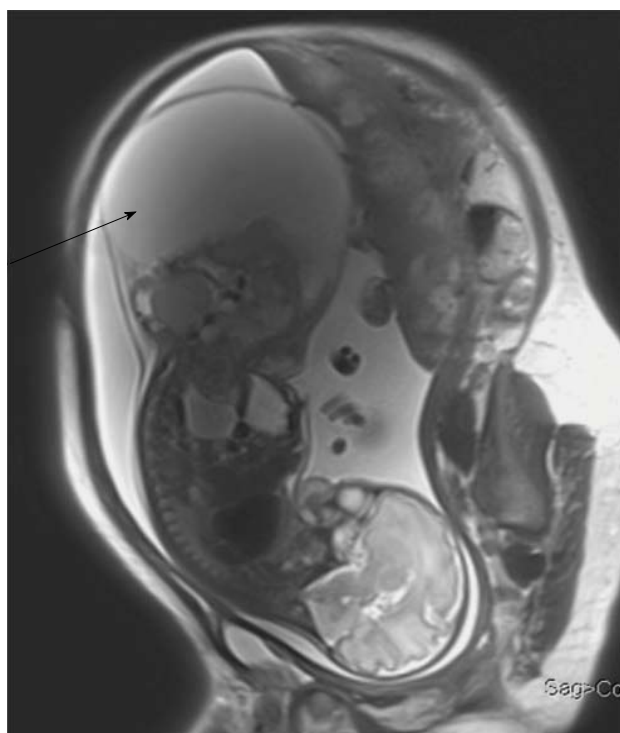


Figure 24 Fetal sacrococcygeal teratoma. T2 weighted sagittal scans through the fetus show a large heterogeneous lesion in the lumbosacral region (arrow) with extension into the pelvis. The lesion shows both solid and cystic components consistent with sacrococcygeal teratoma.

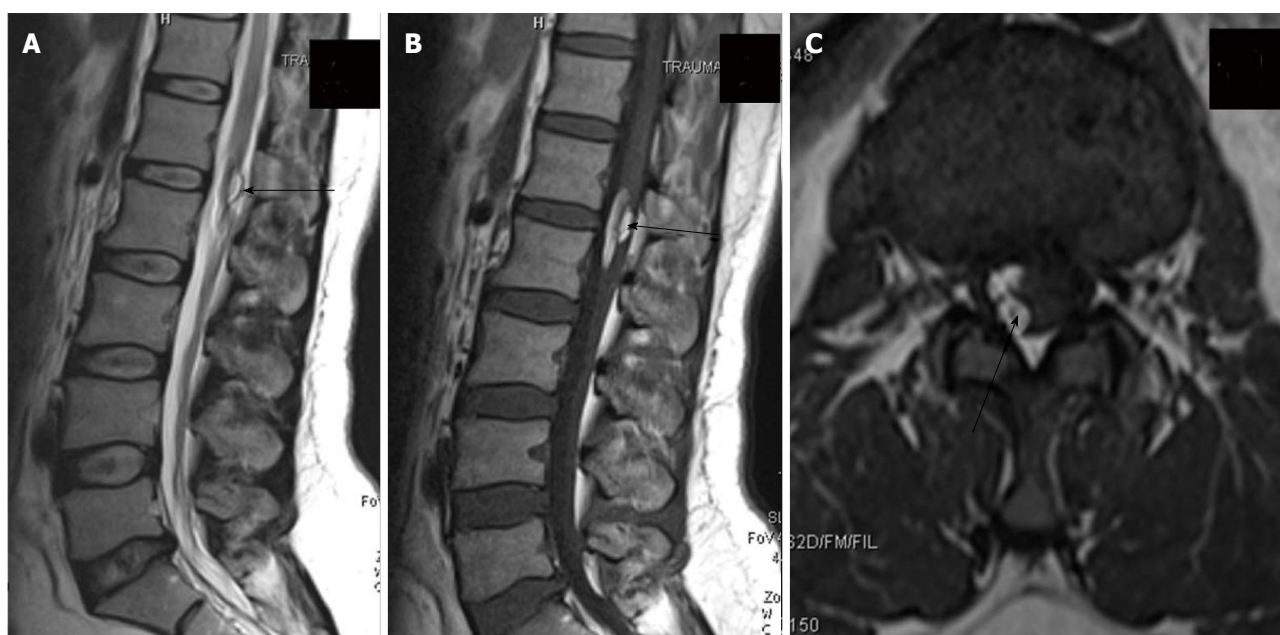


Figure 25 Post-operative dermoid. In a post-operative case of spinal dysraphism, T2 weighted sagittal, T1 weighted sagittal and T1 weighted axial images of lumbosacral spine showing a T1 and T2 hyperintense lesion in the conus medullaris and filum terminale consistent with dermoid formation (black arrow).

mental data helps in making the correct diagnosis.

REFERENCES

- 1 French BN. The embryology of spinal dysraphism. *Clin Neurosurg* 1983; **30**: 295-340 [PMID: 6365396]
- 2 Rossi A, Cama A, Piatelli G, Ravegnani M, Biancheri R, Tortori-Donati P. Spinal dysraphism: MR imaging rationale. *J Neuroradiol* 2004; **31**: 3-24 [PMID: 15026728 DOI: 10.1016/S0150-9861(04)96875-7]
- 3 Tortori-Donati P, Rossi A, Cama A. Spinal dysraphism: a review of neuroradiological features with embryological correlations and proposal for a new classification. *Neuroradiology* 2000; **42**: 471-491 [PMID: 10952179 DOI: 10.1007/s002340000325]
- 4 Barkovich AJ. *Pediatric neuroradiology*, 4th ed. Philadelphia, PA: Lippincott Williams & Wilkins, 2011: 857-916
- 5 Naidich TP, Blaser SI, Delman BN. Congenital Anomalies of the Spine and Spinal Cord: Embryology and Malformations. In: Atlas SW eds. *Magnetic Resonance Imaging of the Brain and Spine*, 4th ed. Philadelphia: Lippincott Williams & Wilkins, 2009: 1364-1447
- 6 Müller F, O'Rahilly R. The first appearance of the neural tube and optic primordium in the human embryo at stage 10. *Anat Embryol (Berl)* 1985; **172**: 157-169 [PMID: 4051192 DOI: 10.1007/BF00319598]
- 7 Catala M. Genetic control of caudal development. *Clin Genet*

- 2002; **61**: 89-96 [PMID: 11940082 DOI: 10.1034/j.1399-0004.2002.610202.x]
- 8 **Warder DE**. Tethered cord syndrome and occult spinal dysraphism. *Neurosurg Focus* 2001; **10**: e1 [PMID: 16749753 DOI: 10.3171/foc.2001.10.1.2]
 - 9 **Huisman TA**, Rossi A, Tortori-Donati P. MR imaging of neonatal spinal dysraphia: what to consider? *Magn Reson Imaging Clin N Am* 2012; **20**: 45-61 [PMID: 22118592 DOI: 10.1016/j.mric.2011.08.010]
 - 10 **Tortori-Donati P**, Rossi A, Biancheri R, Cama A. Magnetic resonance imaging of spinal dysraphism. *Top Magn Reson Imaging* 2001; **12**: 375-409 [PMID: 11744877 DOI: 10.1097/00002142-200112000-00003]
 - 11 **Rossi A**, Biancheri R, Cama A, Piatelli G, Ravegnani M, Tortori-Donati P. Imaging in spine and spinal cord malformations. *Eur J Radiol* 2004; **50**: 177-200 [PMID: 15081131 DOI: 10.1016/j.ejrad.2003.10.015]
 - 12 **Thompson D**. Spinal dysraphic anomalies; classification, presentation and management. *Paediatrics and Child Health* 2010; **20**: 397-403 [DOI: 10.1016/j.paed.2010.03.011]
 - 13 **Osaka K**, Matsumoto S, Tanimura T. Myeloschisis in early human embryos. *Childs Brain* 1978; **4**: 347-359 [PMID: 679772 DOI: 10.1159/000119791]
 - 14 **McLone DG**, Naidich TP. Developmental morphology of the subarachnoid space, brain vasculature, and contiguous structures, and the cause of the Chiari II malformation. *AJNR Am J Neuroradiol* 1992; **13**: 463-482 [PMID: 1566711]
 - 15 **McLone DG**, Knepper PA. The cause of Chiari II malformation: a unified theory. *Pediatr Neurosci* 1989; **15**: 1-12 [PMID: 2699756 DOI: 10.1159/000120432]
 - 16 **von Koch CS**, Glenn OA, Goldstein RB, Barkovich AJ. Fetal magnetic resonance imaging enhances detection of spinal cord anomalies in patients with sonographically detected bony anomalies of the spine. *J Ultrasound Med* 2005; **24**: 781-789 [PMID: 15914682 DOI: 10.7863/jum.2005.24.6.781]
 - 17 **Reddy UM**, Filly RA, Copel JA. Prenatal imaging: ultrasonography and magnetic resonance imaging. *Obstet Gynecol* 2008; **112**: 145-157 [PMID: 18591320 DOI: 10.1097/01.AOG.0000318871.95090.d9]
 - 18 **Adzick NS**, Thom EA, Spong CY, Brock JW, Burrows PK, Johnson MP, Howell LJ, Farrell JA, Dabrowiak ME, Sutton LN, Gupta N, Tulipan NB, D'Alton ME, Farmer DL. A randomized trial of prenatal versus postnatal repair of myelomeningocele. *N Engl J Med* 2011; **364**: 993-1004 [PMID: 21306277 DOI: 10.1056/NEJMoa1014379]
 - 19 **Adzick NS**. Fetal surgery for spina bifida: past, present, future. *Semin Pediatr Surg* 2013; **22**: 10-17 [PMID: 23395140 DOI: 10.1053/j.sempedsurg.2012.10.003]
 - 20 **Adzick NS**. Fetal surgery for myelomeningocele: trials and tribulations. Isabella Forshall Lecture. *J Pediatr Surg* 2012; **47**: 273-281 [PMID: 22325376 DOI: 10.1016/j.jpedsurg.2011.11.021]
 - 21 **Grivell RM**, Andersen C, Dodd JM. Prenatal versus postnatal repair procedures for spina bifida for improving infant and maternal outcomes. *Cochrane Database Syst Rev* 2014; **(10)**: CD008825 [PMID: 25348498 DOI: 10.1002/14651858.cd008825.pub2]
 - 22 **Parmar H**, Patkar D, Shah J, Maheshwari M. Diastematomyelia with terminal lipomyelocystocele arising from one hemicord: case report. *Clin Imaging* 2003; **27**: 41-43 [PMID: 12504320 DOI: 10.1016/S0899-7071(02)00522-3]
 - 23 **Naidich TP**, Blaser SI, Delman BN, McLone DG, Dias MS, Zimmerman RA, Raybaud CA, Birschansky SB, Altman NR, Braffman BH. Embryology of the spine and spinal cord. *ASNR* 2002; **3**: 13
 - 24 **Naidich TP**, McLone DG, Mutluer S. A new understanding of dorsal dysraphism with lipoma (lipomyeloschisis): radiologic evaluation and surgical correction. *AJR Am J Roentgenol* 1983; **140**: 1065-1078 [PMID: 6344595 DOI: 10.2214/ajr.140.6.1065]
 - 25 **Lee KS**, Gower DJ, McWhorter JM, Albertson DA. The role of MR imaging in the diagnosis and treatment of anterior sacral meningocele. Report of two cases. *J Neurosurg* 1988; **69**: 628-631 [PMID: 3418399 DOI: 10.3171/jns.1988.69.4.0628]
 - 26 **Byrd SE**, Harvey C, Darling CF. MR of terminal myelocystoceles. *Eur J Radiol* 1995; **20**: 215-220 [PMID: 8536754 DOI: 10.1016/0720-048X(95)00659-E]
 - 27 **Peacock WJ**, Murovic JA. Magnetic resonance imaging in myelocystoceles. Report of two cases. *J Neurosurg* 1989; **70**: 804-807 [PMID: 2709123 DOI: 10.3171/jns.1989.70.5.0804]
 - 28 **McLone DG**, Naidich TP. Terminal myelocystocele. *Neurosurgery* 1985; **16**: 36-43 [PMID: 3883218 DOI: 10.1227/00006123-198501000-00008]
 - 29 **Tortori-Donati P**, Fondelli MP, Rossi A, Raybaud CA, Cama A, Capra V. Segmental spinal dysgenesis: neuroradiologic findings with clinical and embryologic correlation. *AJNR Am J Neuroradiol* 1999; **20**: 445-456 [PMID: 10219410]
 - 30 **Uchino A**, Mori T, Ohno M. Thickened fatty filum terminale: MR imaging. *Neuroradiology* 1991; **33**: 331-333 [PMID: 1922748 DOI: 10.1007/BF00587817]
 - 31 **Brown E**, Matthes JC, Bazan C, Jinkins JR. Prevalence of incidental intraspinal lipoma of the lumbosacral spine as determined by MRI. *Spine (Phila Pa 1976)* 1994; **19**: 833-836 [PMID: 8202803 DOI: 10.1097/00007632-199404000-00018]
 - 32 **EHefnawy AS**, Wadie BS. Effect of detethering on bladder function in children with myelomeningocele: Urodynamic evaluation. *J Pediatr Neurosci* 2009; **4**: 70-72 [PMID: 21887186 DOI: 10.4103/1817-1745.57324]
 - 33 **Kanev PM**, Park TS. Dermoids and dermal sinus tracts of the spine. *Neurosurg Clin N Am* 1995; **6**: 359-366 [PMID: 7620359]
 - 34 **Thompson DN**. Spinal inclusion cysts. *Childs Nerv Syst* 2013; **29**: 1647-1655 [PMID: 24013335 DOI: 10.1007/s00381-013-2147-z]
 - 35 **Coleman LT**, Zimmerman RA, Rorke LB. Ventriculus terminalis of the conus medullaris: MR findings in children. *AJNR Am J Neuroradiol* 1995; **16**: 1421-1426 [PMID: 7484626]
 - 36 **Dias MS**, Walker ML. The embryogenesis of complex dysraphic malformations: a disorder of gastrulation? *Pediatr Neurosurg* 1992; **18**: 229-253 [PMID: 1476931 DOI: 10.1159/000120670]
 - 37 **Harris CP**, Dias MS, Brockmeyer DL, Townsend JJ, Willis BK, Apfelbaum RI. Neurenteric cysts of the posterior fossa: recognition, management, and embryogenesis. *Neurosurgery* 1991; **29**: 893-897; discussion 897-898 [PMID: 1758603 DOI: 10.1227/00006123-199112000-00015]
 - 38 **Simon JA**, Olan WJ, Santi M. Intracranial neurenteric cysts: a differential diagnosis and review. *Radiographics* 1997; **17**: 1587-1593 [PMID: 9397466 DOI: 10.1148/radiographics.17.6.9397466]
 - 39 **Rufener S**, Ibrahim M, Parmar HA. Imaging of congenital spine and spinal cord malformations. *Neuroimaging Clin N Am* 2011; **21**: 659-676, viii [PMID: 21807317 DOI: 10.1016/j.nic.2011.05.011]
 - 40 **Pang D**, Dias MS, Ahab-Barmada M. Split cord malformation: Part I: A unified theory of embryogenesis for double spinal cord malformations. *Neurosurgery* 1992; **31**: 451-480 [PMID: 1407428 DOI: 10.1227/00006123-199209000-00010]
 - 41 **Barkovich AJ**, Edwards MS, Cogen PH. MR evaluation of spinal dermal sinus tracts in children. *AJNR Am J Neuroradiol* 1991; **12**: 123-129 [PMID: 1903240]
 - 42 **Estin D**, Cohen AR. Caudal agenesis and associated caudal spinal cord malformations. *Neurosurg Clin N Am* 1995; **6**: 377-391 [PMID: 7620361]
 - 43 **Rufener SL**, Ibrahim M, Raybaud CA, Parmar HA. Congenital spine and spinal cord malformations--pictorial review. *AJR Am J Roentgenol* 2010; **194**: S26-S37 [PMID: 20173174 DOI: 10.2214/AJR.07.7141]
 - 44 **Zana E**, Chalard F, Mazda K, Sebag G. An atypical case of segmental spinal dysgenesis. *Pediatr Radiol* 2005; **35**: 914-917 [PMID: 15933868 DOI: 10.1007/s00247-005-1483-x]
 - 45 **Danzer E**, Hubbard AM, Hedrick HL, Johnson MP, Wilson RD, Howell LJ, Flake AW, Adzick NS. Diagnosis and characterization of fetal sacrococcygeal teratoma with prenatal MRI. *AJR Am J Roentgenol* 2006; **187**: W350-W356 [PMID: 16985105 DOI: 10.2214/AJR.05.0152]
 - 46 **Kocaoglu M**, Frush DP. Pediatric presacral masses. *Radiographics* 2006; **26**: 833-857 [PMID: 16702458 DOI: 10.1148/rg.263055102]
 - 47 **Venkataramana NK**. Spinal dysraphism. *J Pediatr Neurosci* 2011; **6**: S31-S40 [PMID: 22069428 DOI: 10.4103/1817-1745.85707]

P- Reviewer: Battal B, Doglietto F S- Editor: Ji FF L- Editor: A

E- Editor: Wu HL



Basic Study

Segmentations of the cartilaginous skeletons of chondrichthyan fishes by the use of state-of-the-art computed tomography

Andrew D McQuiston, Callie Crawford, U Joseph Schoepf, Akos Varga-Szemes, Christian Canstein, Matthias Renker, Carlo N De Cecco, Stefan Baumann, Gavin J P Naylor

Andrew D McQuiston, U Joseph Schoepf, Akos Varga-Szemes, Matthias Renker, Carlo N De Cecco, Stefan Baumann, Division of Cardiovascular Imaging, Department of Radiology and Radiological Sciences, Medical University of South Carolina, Charleston, SC 29425, United States

Callie Crawford, Christian Canstein, Gavin J P Naylor, Hollings Marine Laboratory, College of Charleston, Charleston, SC 29425, United States

Matthias Renker, Department of Internal Medicine I, Cardiology/Angiology, Giessen University, 430011 Giessen, Germany

Carlo N De Cecco, Department of Radiological Sciences, Oncology and Pathology, University of Rome "Sapienza"-Polo Pontino, 04100 Latina, Italy

Stefan Baumann, First Department of Medicine, Faculty of Medicine Mannheim, University Medical Centre Mannheim, University of Heidelberg, 68305 Mannheim, Germany

Author contributions: All the authors contributed to the manuscript.

Institutional animal care and use committee statement: This study used preserved museum specimens and was exempt from IACUC approval.

Institutional review board statement: Not applicable.

Conflict-of-interest statement: U Joseph Schoepf, MD is a consultant for and/or receives research support from Astellas, Bayer, Bracco GE Healthcare, Guerbet, Medrad, and Siemens Healthineers. Drs. Akos Varga-Szemes and Carlo N. De Cecco were consultants for and/or received research support from Guerbet and Siemens. Christian Canstein, MSc is an employee of Siemens. The other authors declare that they have no conflicts-of-interest.

Data sharing statement: No additional data are available.

Open-Access: This article is an open-access article which was

selected by an in-house editor and fully peer-reviewed by external reviewers. It is distributed in accordance with the Creative Commons Attribution Non Commercial (CC BY-NC 4.0) license, which permits others to distribute, remix, adapt, build upon this work non-commercially, and license their derivative works on different terms, provided the original work is properly cited and the use is non-commercial. See: <http://creativecommons.org/licenses/by-nc/4.0/>

Manuscript source: Unsolicited manuscript

Correspondence to: U Joseph Schoepf, MD, Professor of Radiology, Medicine and Pediatrics, Director, Division of Cardiovascular Imaging, Department of Radiology and Radiological Sciences, Medical University of South Carolina, Ashley River Tower, 25 Courtenay Drive, Charleston, SC 29425, United States. schoepf@musc.edu
Telephone: +1-843-7922633
Fax: +1-843-7920409

Received: August 7, 2016

Peer-review started: August 8, 2016

First decision: September 28, 2016

Revised: October 25, 2016

Accepted: December 13, 2016

Article in press: December 14, 2016

Published online: April 28, 2017

Abstract

AIM

To apply dual-source multidetector computed tomography (DSCT) scanning technology in conjunction with computationally assisted segmentation in order to explore and document skeletal variation that has occurred over the course of evolution.

METHODS

We examined 4 divergent species of elasmobranchs

with high-resolution 3rd generation DSCT. The formalin prepared species examined were: *Aptychotrema vincentiana*, *Mitsukurina owstoni*, *Negaprion brevirostris* and *Dactylobatus armatus*.

RESULTS

All three structures of the hyoid arch (hyomandibular, ceratohyal, and basihyal) were clearly visible whereas in the two batoids, the hyomandibular was the prominent feature, the ceratohyal was not visible and the basihyal was more reduced and closer to the gill arches. The general shape of the puboischiadic bar, or pelvic girdle, illustrated a closer relationship between the two sharks and the two batoids than between the two groups.

CONCLUSION

In exquisite detail, DSCT imaging revealed important morphological variations in various common structures in the four elasmobranch specimens studied, providing insights into their evolutionary diversification.

Key words: Computed tomography imaging; Comparative biology; Sharks; Rays

© The Author(s) 2017. Published by Baishideng Publishing Group Inc. All rights reserved.

Core tip: Computed tomography is a helpful noninvasive imaging tool for comparative biology. The skeletal variations observed through our data will increase our understanding of how the anatomy of these organisms has changed over the course of evolution. The data collected allows for a more comprehensive understanding regarding the evolutionary history of the group.

McQuiston AD, Crawford C, Schoepf UJ, Varga-Szemes A, Canstein C, Renker M, De Cecco CN, Baumann S, Naylor GJP. Segmentations of the cartilaginous skeletons of chondrichthyan fishes by the use of state-of-the-art computed tomography. *World J Radiol* 2017; 9(4): 191-198 Available from: URL: <http://www.wjgnet.com/1949-8470/full/v9/i4/191.htm> DOI: <http://dx.doi.org/10.4329/wjr.v9.i4.191>

INTRODUCTION

About 450 million years ago, the evolutionary lineage that lead to sharks, skates, and rays split from the main trunk of the vertebrate tree^[1]. One lineage gave rise to bony fishes, tetrapods, amniotes and mammals - including humans - while the other gave rise to modern sharks and rays. The two lineages have been experimenting with different ways of solving environmental challenges for nearly half a billion years. Because they are evolutionarily independent, it is likely that each lineage has developed different solutions to similar challenges and that each harbors architectural attributes and innovations that are lineage specific.

Considerable effort has been put into studying the adaptations that have made the lineage leading to humans so successful, but almost nothing is known about the corresponding innovations and adaptations that have made sharks and rays so successful^[2,3].

Comparative biology provides an efficient way to reconstruct evolutionary history and to better understand how lineages have overcome environmental challenges. The approach involves exploring the diversity of traits in a suite of related organisms and then organizing the information into an evolutionary hierarchy that reveals how traits have changed over the course of time^[4,5]. Traits can be molecular, cellular, physiological or anatomical.

Computed tomography (CT) is an important 3-dimensional (3D) imaging tool for medical and non-medical purposes. Beyond clinical radiology, this modality has previously been described in literature for use in a variety of different fields, including but not limited to aviation security, forensic minimally invasive autopsy, archaeology, and visualization of sarcophagi and mummies^[6-8]. Due to its high spatial resolution and non-destructive nature, CT enables the display of distinct skeletal characteristics of different representatives of shark and ray lineages. Furthermore, the high spatial resolution of modern CT technology renders increased material differentiation possible, which may facilitate the assessment of minute disparities within the cartilaginous structures of sharks, skates and rays.

The work presented is a subset of the Chondrichthyan Tree of Life (CToL) project, a multi-institutional endeavor to create a database of evolutionary information for Chondrichthyan fishes (sharks, skates, rays and chimeras). Chondrichthyes are subdivided into two subclasses: Elasmobranchii (sharks, rays and skates) and Holocephali (chimeras). The goal of the CToL is to reconstruct the evolutionary lineages of all extant sharks, skates, rays and chimeras to better understand how these organisms have addressed environmental challenges by collecting both anatomical and genetic information. Thus, we sought to contribute to this body of knowledge through the application of DSCT and computer assisted segmentation to document variations in preserved specimens of sharks and rays.

MATERIALS AND METHODS

Study specimens

DSCT scans of 4 highly divergent elasmobranchs: *Aptychotrema vincentiana* (CSIRO MUW101), *Mitsukurina owstoni* (HUMZ 204610), *Negaprion brevirostris* (GBML uncatalogued) and *Dactylobatus armatus* (UF 41302), were collected. The geographical distribution associated with each species can be seen in Figure 1. The specimens were preserved with formalin and kept in 70% Ethanol or 50% Isopropanol, sealed and stored in a dark environment and shipped from museums around the world to our institution. Specimens were loaned

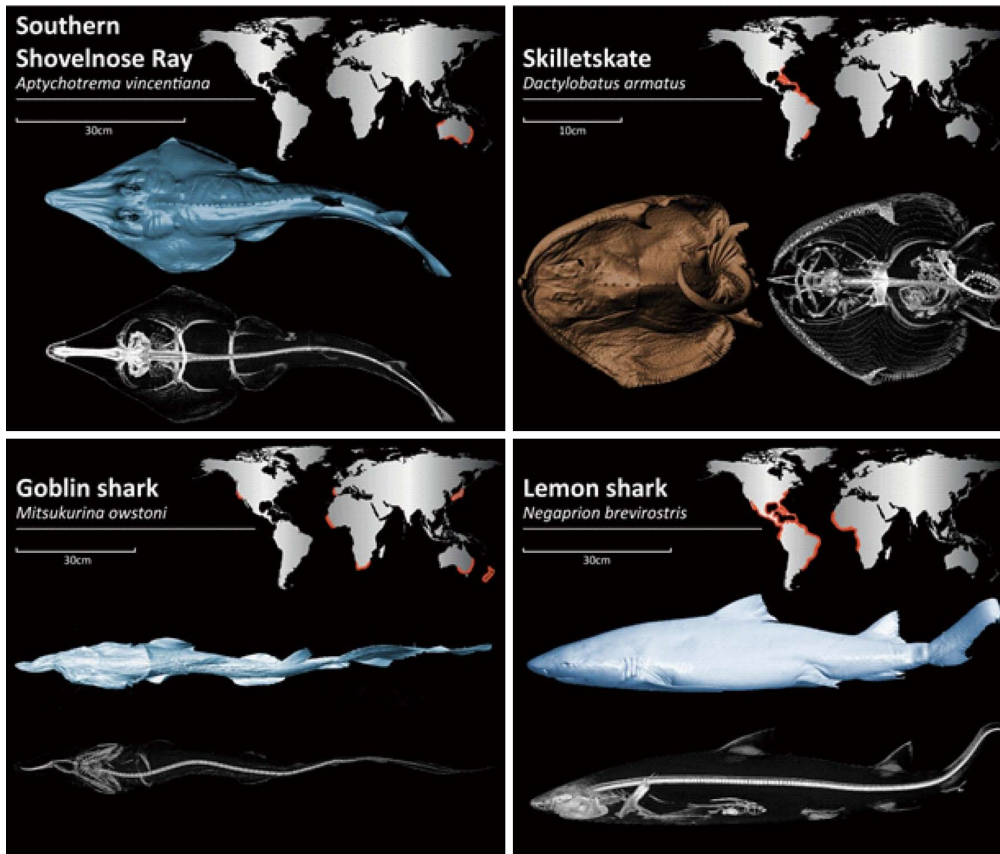


Figure 1 Three-dimensional reconstructions and global distribution, represented by orange highlights, of the four representative species in our study.

from Commonwealth Scientific and Industrial Research Organisation (CSIRO; Clayton South, Australia), Hokkaido University (HUMZ; Sapporo, Hokkaido, Japan), Grice Marine Biological Laboratory (GMBL; Charleston, South Carolina, United States), and the University of Florida (UF; Gainesville, Florida, United States). Table 1 provides an overview of the four species. As this study used preserved museum specimens, it was exempt from IACUC approval.

Southern Shovelnose ray (*Aptychotrema vincentiana*)

Endemic to Australia, the Southern Shovelnose ray resides primarily in shallow waters on sandy substrates where they feed on crustaceans, molluscs, worms, and other invertebrates^[9]. It is easily distinguished by its long triangular snout. They are usually sandy-colored with scattered dark spots, assisting with camouflage on the ocean floor. Reproduction is ovoviparous, with litters reaching 14-16 in number^[10].

Goblin shark (*Mitsukurina owstoni*)

Typically found at depths of up to 1300 m, goblin sharks have a nearly global distribution^[10]. This shark is distinguished by its disproportionately long, thin snout overhanging rows of sharp, non-serrated fang-like teeth. The highly protrusive jaws extend anteriorly, enabling the Goblin shark to capture cephalopods, crustaceans and bony fish^[10]. Goblin sharks have a

relatively small optic tectum, indicating that vision is less important to this species; instead they rely heavily on their electro-sensitive snout. Nevertheless, unlike most deep-sea sharks, they have fully functional irises suggesting that they do use vision to some extent. Although a pregnant female is yet to be captured, these sharks are thought to be ovoviparous. Little is known about their social behavior^[10].

Lemon sharks (*Negaprion brevirostris*)

Lemon sharks inhabit coral reefs, enclosed sounds, bays, river mouths, and mangrove fringes of coastal inshore waters of the Western Atlantic and Eastern Pacific oceans. They are large, stocky, and blunt nosed with a pair of similar sized dorsal fins; the first just posterior to the pectoral fins and the second just anterior to the origin of the anal fin. They are commonly found in warm, shallow water at depths usually not exceeding 100 m. This species feeds mostly on bony fish^[10], however, intra-specific predation of juvenile lemon sharks by adults has been observed^[11]. Group living and social behavior is frequently observed among juveniles and thought to be important to survival, possibly reducing the risk from predation. Some believe lemon sharks exhibit social learning and cooperation, based on a relative brain mass overlapping that of mammals and birds^[12]. Lemon sharks gather for reproduction in special nursery areas located in shallow water. A 10-12 mo gestation period

Table 1 Overview of the study specimens

	Southern Shovelnose ray	Skilletskate	Goblin shark	Lemon shark
Scientific name	<i>Aptychotrema vincentiana</i>	<i>Dactylobatus armatus</i>	<i>Mitsukurina owstoni</i>	<i>Negaprion brevirostris</i>
Kingdom	Animalia	Animalia	Animalia	Animalia
Phylum	Chordata	Chordata	Chordata	Chordata
Class	Chondrichthyes	Chondrichthyes	Chondrichthyes subclass:	Chondrichthyes subclass:
			Elasmobranchii	Elasmobranchii
Order	Rajiformes	Rajiformes	Lamniformes	Carcharhiniformes
Family	Rhinobatidae	Rajidae	Mitsukurinidae	Carcharhinidae
Genus	Aptychotrema	Dactylobatus	Mitsukurina	Negaprion
Species authority	Haacke, 1885	Bean and Weed, 1909	Jordan, 1898	Poey, 1868
Distribution	Eastern Indian Ocean: endemic to Australia (20°S - 40°S)	Western Central Atlantic: South Carolina, United States to the Gulf of Mexico and along Central America to Venezuela Also found on middle continental slope off southern Brazil (35°N - 35°S, 30°W - 98°W)	Western Atlantic: Guyana, Suriname and French Guiana Eastern Atlantic: France (Bay of Biscay), Madeira, Portugal, and South Africa Western Indian Ocean: off South Africa. Western Pacific: Japan, Australia (South Australia, New South Wales), New Zealand Eastern Pacific: United States (southern California) (8°N - 55°S, 180°W - 180°E)	Western Atlantic: New Jersey, United States to southern Brazil, including the Gulf of Mexico, the Bahamas, and the Caribbean; also in Gulf of Mexico Northeast Atlantic: Senegal, Côte d'Ivoire and probably wide-ranging off West Africa, but this requires confirmation. Eastern Pacific: southern Baja California, Mexico and the Gulf of California to Ecuador (45°N - 39°S, 114°W - 0°)
Environment	Marine; demersal;	Marine; bathydemersal;	Marine; bathydemersal;	Marine; brackish; reef-associated; oceano-dromous
	Depth range: 0-32 m	Depth range: 300-900 m (usually 300-700 m)	Depth range: 30-1300 m (usually 270-960 m)	Depth range: 0-92 m
Size (cm)	Maximum length: 79.0 cm	Maximum length: 32.0 cm	Maximum length: 617.0 cm	Maximum length: 340.0 cm
	Presented specimen: 72.9 cm	Presented specimen: 23.5 cm	Presented specimen: 119.5 cm	Presented specimen: 95.6 cm
Red list category	Least concern	Data deficient	Least concern	Near Threatened
Threat to humans	Harmless	Harmless	Harmless	Minor Threat

follows spring and early summer mating, which yields average litters of 4-17 offspring^[13].

Skilletskate (*Dactylobatus armatus*)

The skilletskate is a deepwater species first discovered in 1905 (Figure 2). It can be found sporadically throughout the western Atlantic on the muddy bottoms of the continental slope, and is occasionally caught by commercial deepwater fisheries. Similar to others in the order Rajiformes, skates are presumed to be oviparous, but little is known about the biology of the skilletskate. The species is presently considered data deficient^[14].

DSCT protocol and technique

All examinations were performed with a high-resolution 3rd generation dual-source multidetector computed tomography (DSCT) scanner (Somatom Force, Siemens, Forchheim, Germany). 3D CT scans of the skeletal anatomy for each species were performed using a high resolution imaging protocol that was optimized for each individual specimen by maximizing the tube current. Acquisitions were performed in dual-energy mode at tube voltages of 80 and 150 kV with the specimen placed along the isocenter Z-axis of the CT gantry (Figure 2). The imaging data were processed with 0.5 mm

section thickness, allowing for reconstruction of the 3D skeletal structure and surface anatomy using advanced modelled iterative reconstruction. The cranium was virtually re-sliced in the sagittal, coronal, and frontal planes and movies of rotations of each specimen were generated. Further CT imaging parameters are listed in Table 2.

Three-dimensional reconstruction

Segmentation and three-dimensional rendering of the cartilaginous skeletons were manually completed with various tools in MIMICS Research version 17.0 64-bit software (Materialise, Leuven, Belgium). Specific cartilaginous elements were color coded to facilitate comparison across species (Figure 3). The 3D images were handled electronically on a workstation, displaying areas of interest in multiple dimensions. The data from the scans will be added to an anatomical database as part of the CTOL project which will allow for a more rigorous interpretation of the fossil record.

RESULTS

We were able to acquire high quality images and generate 3D reconstructions without the presence of artifacts

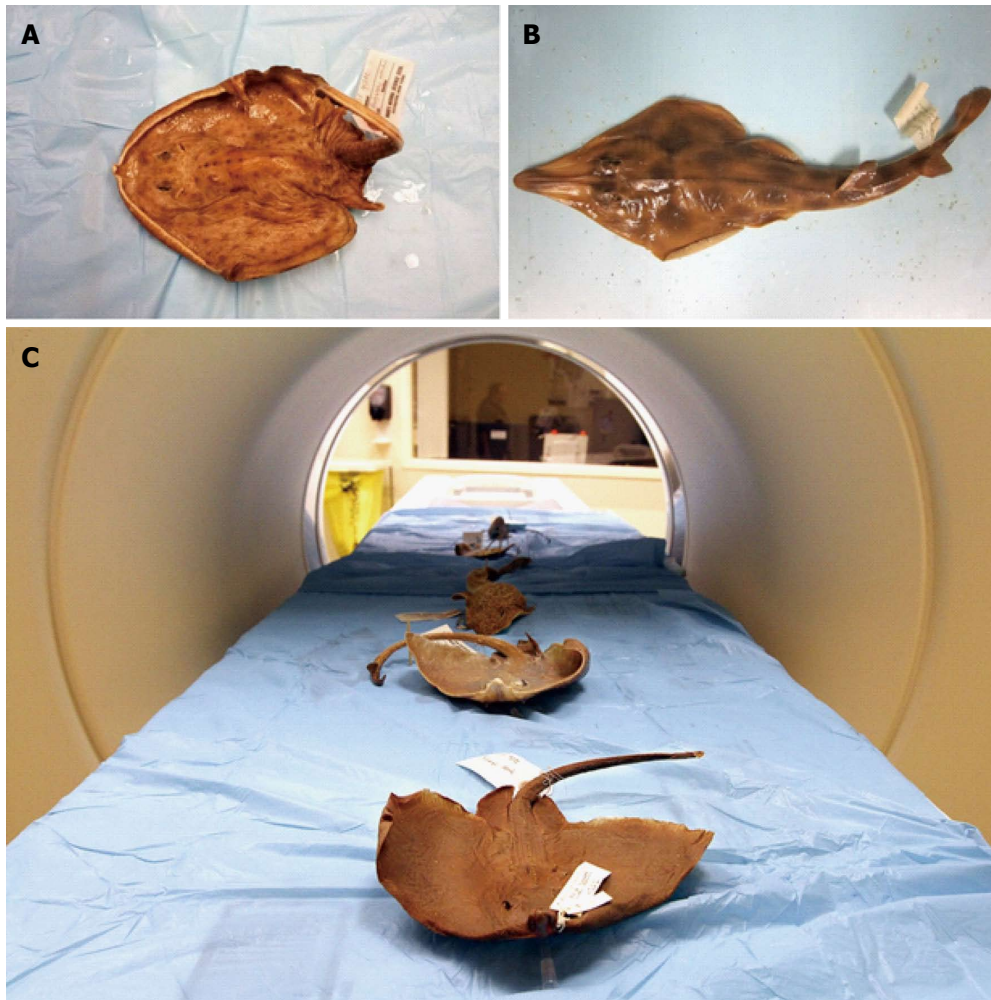


Figure 2 Formalin-preserved specimens positioned in the computed tomography scanner. A: Skilleyskate (*Dactylobatus armatus*); B: Southern Shovelnose ray (*Aptychotrema vincentiana*); C: The processes of the scan.

Table 2 Computed tomography protocol

Acquisition parameters	Thorax Hd	DE Thorax
Section collimation	192 mm × 0.6 mm	192 mm × 0.6 mm
Slice thickness (mm)	0.5	0.5
Increment (mm)	0.3	0.5
Rotation time (s)	0.5	0.3
Pitch	0.35	0.65
Tube voltage (kV)	120	80 + 150
Effective tube current-time product (mAs)	37-104	1107/615
DLP (mGy/cm)	2.3-6.23	17.55-27.76
Reconstruction kernel	Bf32/Br54 Admire 3	Qr32/Qr54 Admire 3

in all specimens. Anatomical structures present in all specimens are color coded and shown in Figure 3. Each colored structure corresponds to the structure of the same color in the other panels, illustrating how it has changed in each of the four species over the course of evolutionary history. The following examples demonstrate such structures, which share a common

origin but have somewhat diverged in terms of overall structure and function.

Hyoid arch

Figure 4 shows the structures of the hyoid arch in pale green for each of the specimens in the current study. In the two shark species, all three structures of the hyoid arch (hyomandibular, ceratohyal, and basihyal) were clearly visible whereas in the two batoids, the hyomandibular was a prominent feature while the ceratohyal was not visible and the basihyal was much more reduced and closer to the gill arches.

Puboischiadic bar

The pink structure shown in all panels of Figure 3 represents the pelvic fins for each specimen. The general shape of the puboischiadic bar, or pelvic girdle, illustrated a closer relationship between the two sharks and the two batoids than between the two groups. With greater coverage of the families and genera of these two groups of elasmobranchs, the characteristics of the structures can be used to discern relationships in the phylogeny.

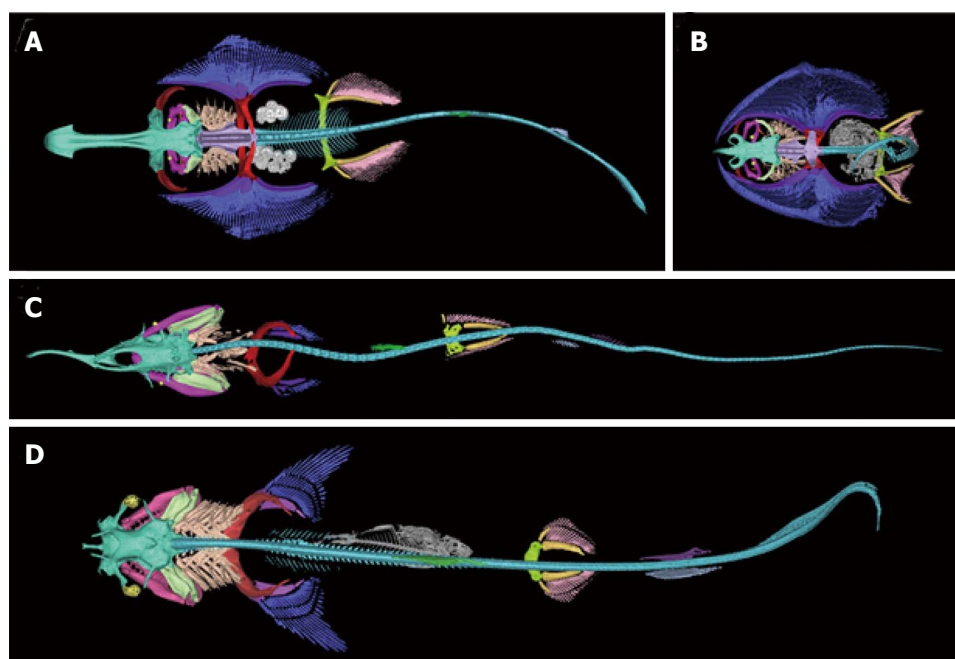


Figure 3 Dorsal view of three-dimensional reconstructions of the skeleton. A: Shovelnose ray (*Aptychotrema vincentiana*); B: Skilleyskate (*Dactylobatus armatus*); C: Lemon shark (*Negaprion brevirostris*); D: Goblin Shark (*Mitsukurina owstoni*). Skeletal element color coding: turquoise, chondrocranium; maroon, antorbital; magenta, jaws (palatoquadrate, meckel's cartilage, and labial cartilage); orange, spiracular cartilage; yellow, eye cup and lens; pale green, hyoid arch (hyomandibular, ceratohyal, and basihyal); peach, gill arches (pharyngobranchials, epibranchials, ceratobranchials, hypobranchials, basibranchial, and branchial rays); violet, synarcual; cyan, vertebral column; red, scapulocoracoid; purple, pectoral basal cartilages; blue, pectoral radials; gray, ingested fish (flounder and teleost vertebral column); white, eggs; green, anterior dorsal fin; skyblue, posterior dorsal fin; deep purple, anal fin; greenyellow, puboischiadic bar; gold, pelvic basal cartilages; pink, pelvic radials.

DISCUSSION

About 530 million years ago, the Cambrian explosion gave rise to the first vertebrates. About 80 million years later, the Chondrichthyan lineage of all modern sharks, skates, rays and chimaeras departed from the main vertebrate lineage. This lineage gave rise to all modern elasmobranchs (Kyne, 2007 #174)^[15]. The other lineage gave rise to the bony fishes, which in turn gave rise to the well-studied tetrapod, amniotes and mammal diversifications. Both lineages developed jaws prior to diverging, one of the defining features of early vertebrates. However, while most members of the bony fish lineage went on to acquire features more commonly associated with extant vertebrates (*e.g.*, lungs, bone), the elasmobranchs maintained gills and developed a cartilaginous skeleton. Of course, these characteristics should not be thought of as subordinate-rather, they allowed for their extraordinarily lengthy survival over the course of evolutionary history, making these features especially intriguing. It would also be incorrect to think that sharks, skates, and rays have not evolved since they diverged from the main vertebrate trunk. Their main design has remained relatively fixed in comparison with the bony fish lineage, which has diversified incredibly into all extant amphibians, reptiles, birds and mammals. The fact that sharks, skates, and rays are extant today means that they and their ancestors survived at least five global mass extinctions over the last half billion years, one of which (Permian-Triassic

extinction) killed 96% of all marine species^[16], and are among the oldest groups of surviving vertebrates. To put this into context, ancestors specific to the elasmobranch lineage date back more than 200 million years before the appearance of the first dinosaur. Around 65 million years ago at the end of the Cretaceous period, the most recent mass extinction event occurred, wiping out 75% of extant species during that time, along with all dinosaurs^[17]. Some species of elasmobranchs of course survived, giving rise to all modern sharks, skates, and rays.

The superorder Batoidea, including all modern skates and rays, represent a flattened variation of the common ancestor they share with modern sharks, which was likely much more shark-like. Ancient batoid remains as old as 150 million years have been recovered, but they are thought to have first appeared in the late Triassic. By flattening their bodies, batoids adopted an anatomy better suited for occupying the ocean floor. They share many of the same feeding niches with sharks, pursuing krill, crush shelled molluscs, and fish (including sharks). However, the flattened batoid face and resulting ventrally located mouth make the ram feeding mode employed by sharks impossible^[18].

Although elasmobranch fossils exist, the fossil record is less complete compared to other vertebrates whose skeletons are better calcified. Teeth, having mineralogical stability, have a significantly increased chance of undergoing fossilization and have provided the majority of the information to biologists studying elasmobranch

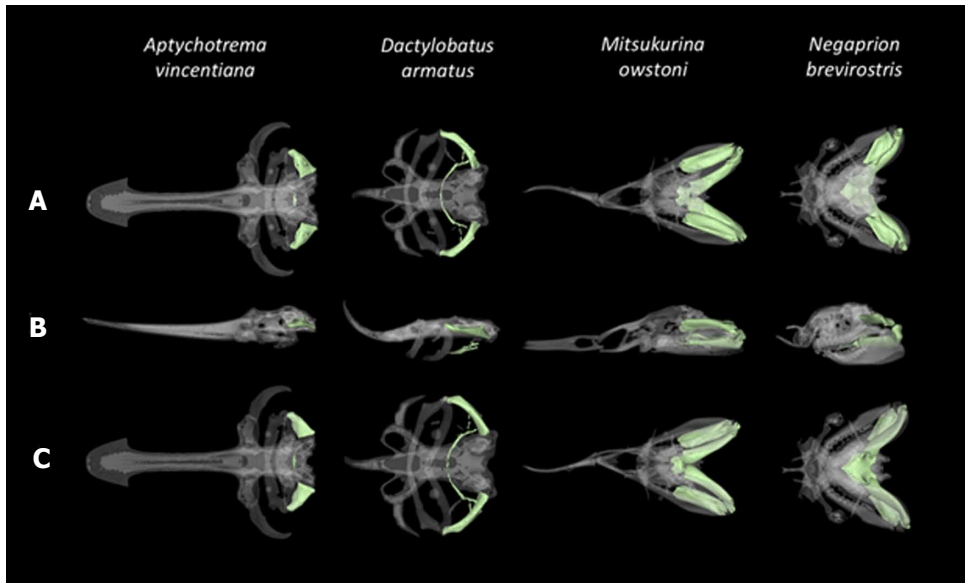


Figure 4 Close-up dorsal, lateral, and ventral views of the cranial skeleton of four elasmobranchs. A: Shovelnose ray (*Aptychotrema vincentiana*); B: The Skillet skate (*Dactylobatus armatus*); C: The Goblin Shark (*Mitsukurina owstoni*) and the Lemon shark (*Negaprion brevirostris*), reconstructed in 3D with the hyoid arch highlighted in pale green.

evolution through fossils. However, elasmobranch teeth cannot paint the whole picture, making other methods for studying their evolution important. Genetic evidence represents the primary alternative to fully articulated fossils. CT imaging constitutes another important method for studying the phylogeny of different species, providing the opportunity to obtain scan data for segmentations of the cartilaginous skeleton of Chondrichthyan. Obtaining CT data and the subsequent segmentation was used to determine the shape, angle, and size of various structures in a noninvasive manner, avoiding the destructive dissections that are generally required to measure these structures. Dissection was not possible for most of the specimens examined due to their frailty and rarity.

Morphology of the hyoid arch, a central component of the jaw protrusion apparatus, has diverged considerably among extant elasmobranchs and those observed in the fossil record^[19]. Jaw protrusion is believed to have conferred a distinct advantage for prey capture, and has been well studied^[20]. Shape and angle of the hyoid arch may be used to determine whether an elasmobranch is likely to use suction or ram feeding strategies^[21], and is often used to infer ancestral feeding mechanisms when vestigial elements remain. We were able to identify the hyoid arch and the shape and angle of its components in each of the four species studied.

The pelvic fins, including the puboischiadic bar, pelvic radials, pelvic propterygium, and pelvic metapterygium have also diverged within the elasmobranchs. In males, this structure also includes the claspers which are often used in species identification. In batoids, the pelvic fins can be used for punting, and sometimes walking as observed in the leg-skates whereas in sharks, the pelvic fins are used more for stabilization, although some sharks have been observed using pelvic fins for walking

and punting (Macesic and Kaijura).

Although we did not explore the Micro-CT (MCT) modality in this study due to the fact that the species were too large for the limited field-of-view of MCT; MCT imaging would likely provide significantly more detailed resolution of elasmobranch anatomical structures. The MCT unit at our institution (Siemens Inveon Micro-CT/PET, Siemens Medical Solutions, Knoxville, TN) allows for 30-80 kVp tube potential with a 9 cm × 6 cm maximum field of view. The dual-modality system can produce images with a resolution as low as 15 μm. While size restrictions would severely limit which specimens could be imaged, smaller elasmobranchs such as the cigar shark (*Isistius brasiliensis*), measuring less than 4 cm in diameter, would fit into the machine's bore. Furthermore, elasmobranch embryos and some newborn pups would make good candidates for MCT imaging. In some cases, however, embryos and very young individuals are not well calcified, resulting in low-quality images of skeletal structures.

CT-based comparative anatomy of modern elasmobranchs will be used to document anatomical variation among the major elasmobranch lineages for an ongoing CTOL project. The skeletal variations observed are expected to increase our understanding of how the anatomy in these organisms has changed over the course of evolution. Completed segmentations will be entered into an online database which will also contain information for the other components of the CTOL project.

COMMENTS

Background

The work presented is a subset of the chondrichthyan tree of life (CTOL) project, a multi-institutional endeavor to create a database of evolutionary information for

Chondrichthyan fishes (sharks, skates, rays and chimeras). Chondrichthyes are subdivided into two subclasses: Elasmobranchii (sharks, rays and skates) and Holocephali (chimeras). The goal of the CTOL is to reconstruct the evolutionary lineages of all extant sharks, skates, rays, and chimeras to better understand how these organisms have addressed environmental challenges by collecting both anatomical and genetic information.

Research frontiers

Computed tomography (CT) is an important 3-dimensional (3D) imaging tool for medical as well as non-medical purposes. Due to its high spatial resolution and non-destructive nature, CT enables the display of distinct skeletal characteristics of different representatives of shark and ray lineages. Furthermore, the high spatial resolution of modern CT technology renders increased material differentiation possible, which may facilitate the assessment of minute disparities within the cartilaginous structures of sharks, skates, and rays.

Innovations and breakthroughs

The skeletal variations observed are expected to increase the understanding of how the anatomy in these organisms has changed over the course of evolution.

Applications

CT-based comparative anatomy of modern elasmobranchs will be used to document anatomical variation among the major elasmobranch lineages for an ongoing CTOL project. Completed segmentations will be entered into an online database which will also contain information for the other components of the CTOL project.

Terminology

Chondrichthyan Tree of Life (CToL) project: A multi-institutional endeavor to create a database of evolutionary information for Chondrichthyan fishes. Chondrichthyan fishes: Sharks, skates, rays and chimeras. Chondrichthyes are subdivided into two subclasses: Elasmobranchii (sharks, rays and skates) and Holocephali (chimeras).

Peer-review

This is an interesting study on the documentation of skeletal variation in 4 divergent species of elasmobranchs with high-resolution 3rd generation DSC.

REFERENCES

- 1 Maisey J, Chesek C, Miller D. Discovering fossil fishes. New York, NY: Henry Holt and Company, 1996: 223
- 2 Myers RA, Baum JK, Shepherd TD, Powers SP, Peterson CH. Cascading effects of the loss of apex predatory sharks from a coastal ocean. *Science* 2007; **315**: 1846-1850 [PMID: 17395829 DOI: 10.1126/science.1138657]
- 3 Carrier JC, Musick JA, Heithaus MR. Biology of sharks and their relatives. 2nd ed. Boca Raton: CRC Press/Taylor & Francis Group, 2012: 3-4 [DOI: 10.1201/b11867]
- 4 Compagno L. Sharks of the order Carcharhiniformes. Princeton, NJ: Princeton University Press, 1988: 12-71, 341-345
- 5 Shirai S. Squalan phylogeny: a new framework of "squaloid" sharks and related taxa. Sapporo: Hokkaido University Press, 1992: 151
- 6 Huppertz A, Wildung D, Kemp BJ, Nentwig T, Asbach P, Rasche FM, Hamm B. Nondestructive insights into composition of the sculpture of Egyptian Queen Nefertiti with CT. *Radiology* 2009; **251**: 233-240 [PMID: 19332855 DOI: 10.1148/radiol.2511081175]
- 7 Jansen RJ, Poulus M, Kottman J, de Groot T, Huisman DJ, Stoker J. CT: a new nondestructive method for visualizing and characterizing ancient Roman glass fragments in situ in blocks of soil. *Radiographics* 2006; **26**: 1837-1844 [PMID: 17102054 DOI: 10.1148/rgr.266065079]
- 8 Weustink AC, Hunink MG, van Dijke CF, Renken NS, Krestin GP, Oosterhuis JW. Minimally invasive autopsy: an alternative to conventional autopsy? *Radiology* 2009; **250**: 897-904 [PMID: 19244053 DOI: 10.1148/radiol.2503080421]
- 9 Last P, Stevens JD. Sharks and Rays of Australia. Melbourne, Australia: CSIRO, 1994
- 10 Castro J. The Sharks of North America. Oxford: Oxford University Press, 2011: 201-205, 481-485
- 11 Guttridge T, Gruber SH, Franks BR, Kessel ST, Gledhill KS, Uphill J, Krause J, Sims DW. Deep danger: intra-specific predation risk influences habitat use and aggregation formation of juvenile lemon shark *Negaprion brevirostris*. *Marine Ecology Progress Series* 2012; **445**: 279-291 [DOI: 10.3354/meps09423]
- 12 Guttridge TL, van Dijk S, Stamhuis EJ, Krause J, Gruber SH, Brown C. Social learning in juvenile lemon sharks, *Negaprion brevirostris*. *Anim Cogn* 2013; **16**: 55-64 [PMID: 22933179 DOI: 10.1007/s10071-012-0550-6]
- 13 Compagno L. FAO Species Catalogue. In: Ichthyology JSIo, editor Sharks of the World. Rome, 1984
- 14 McEachran J, de Carvalho MR Batoid Fishes. In: University OD, editor The Living Marine Resources of the Western Central Atlantic. Rome, 2002: 508-529
- 15 Kyne P, Simpfendorfer CA. A Collation and Summarization of Available Data on Deepwater Chondrichthyan: Biodiversity, Life History and Fisheries (Marine Conservation Biology Institute, 2007). Available from: URL: http://www.iucnssg.org/uploads/5/4/1/2/54120303/kyne_simpfendorfer_2007.pdf
- 16 Labandeira CC, Sepkoski JJ. Insect diversity in the fossil record. *Science* 1993; **261**: 310-315 [PMID: 11536548 DOI: 10.1126/science.11536548]
- 17 Raup DM, Sepkoski JJ. Mass extinctions in the marine fossil record. *Science* 1982; **215**: 1501-1503 [PMID: 17788674 DOI: 10.1126/science.215.4539.1501]
- 18 Dean MN, Bizzarro JJ, Summers AP. The evolution of cranial design, diet, and feeding mechanisms in batoid fishes. *Integr Comp Biol* 2007; **47**: 70-81 [PMID: 21672821 DOI: 10.1093/icb/pcm034]
- 19 Wilga C. Evolutionary divergence in the feeding mechanism of fishes. *Acta Geologica Polonica* 2008; **58**: 113-120
- 20 Wilga C, Hueter RE, Wainwright PC, Motta PJ. Evolution of the upper jaw protrusion mechanisms in elasmobranchs. *American Zoologist* 2002; **41**: 1248-1257
- 21 Tomita T, Sato K, Suda K, Kawauchi J, Nakaya K. Feeding of the megamouth shark (Pisces: Lamniformes: Megachasmaidae) predicted by its hyoid arch: a biomechanical approach. *J Morphol* 2011; **272**: 513-524 [PMID: 21381075 DOI: 10.1002/jmor.10905]

P- Reviewer: Chen F, Iurita J, Verlinden O S- Editor: Qiu S
L- Editor: A E- Editor: Wu HL



Basic Study

Gd-EOB-DTPA based magnetic resonance imaging for predicting liver response to portal vein embolization

Janio Szklaruk, Gustavo Luersen, Jingfei Ma, Wei Wei, Michelle Underwood

Janio Szklaruk, Jingfei Ma, Wei Wei, Michelle Underwood, Department of Diagnostic Radiology, the University of Texas MD Anderson Cancer Center, Houston, TX 77030, United States

Gustavo Luersen, Hospital Moinhos de Vento, Rua Goncalo de Carvalho, Porto Alegre, RS 90035-170, Brazil

Author contributions: All authors contributed to the study design, manuscript preparation, data analysis and data acquisition (except Wei W he did not work on Data Acquisition); the statistical methods were reviewed by Wei W who is a Principal statistical analyst.

Supported by The NIH/NCI and used the Department of Biostatistics Resource Group, No. P30CA016672.

Institutional review board statement: This study was approved by the University of Texas MD Anderson Cancer Center Institutional Review Board as a prospective project.

Conflict-of-interest statement: All others declare that they have nothing to disclose except for Dr. Jingfei Ma. Dr. Ma has ongoing financial relationships with GE Healthcare and Siemens Healthcare and there are no family members that present a potential conflict of interest.

Data sharing statement: No additional data are available.

Open-Access: This article is an open-access article which was selected by an in-house editor and fully peer-reviewed by external reviewers. It is distributed in accordance with the Creative Commons Attribution Non Commercial (CC BY-NC 4.0) license, which permits others to distribute, remix, adapt, build upon this work non-commercially, and license their derivative works on different terms, provided the original work is properly cited and the use is non-commercial. See: <http://creativecommons.org/licenses/by-nc/4.0/>

Manuscript source: Invited manuscript

Correspondence to: Janio Szklaruk, MD, PhD, Professor, Department of Diagnostic Radiology, the University of Texas MD Anderson Cancer Center, 1515 Holcombe Blvd., Unit 1473,

Houston, TX 77030, United States. jszklaruk@mdanderson.org
Telephone: +1-713-7453230
Fax: +1-713-7451302

Received: August 26, 2016
Peer-review started: August 29, 2016
First decision: December 13, 2016
Revised: January 11, 2017
Accepted: February 28, 2017
Article in press: March 2, 2017
Published online: April 28, 2017

Abstract

AIM

To evaluate the correlation between degree of kinetic growth (kGR) of the liver following portal vein embolization (PVE) liver and the enhancement of the during the hepatobiliary phase of contrast administration and to evaluate if the enhancement can be used to predict response to PVE prior to the procedure.

METHODS

Seventeen patients were consented for the prospective study. All patients had an MR of the abdomen with Gd-EOB-DTPA. Fourteen patients underwent PVE. The correlation between the kGR of the liver and the degree of enhancement was evaluated with linear regression (strong assumptions) and Spearman's correlation test (rank based, no assumptions). The correlation was examined for the whole liver, segments I, VIII, VII, VI, V, IV, right liver and left liver.

RESULTS

There was no correlation between the degree of enhancement during the hepatobiliary phase and kGR for any segment, lobe of the liver or whole liver ($P = 0.19$ to 0.91 by Spearman's correlation test).

CONCLUSION

The relative enhancement of the liver during the hepatobiliary phase with Gd-EOB-DTPA cannot be used to predict the liver response to PVE.

Key words: Gd-EOB-DTPA; Liver magnetic resonance imaging; Portal vein embolization; Resection; Kinetic growth

© **The Author(s) 2017.** Published by Baishideng Publishing Group Inc. All rights reserved.

Core tip: Our hypothesis was that the degree of enhancement of the liver during the hepatobiliary phase will correlate with the degree of liver response to portal vein embolization. This will be able to be used as a screen method for patients scheduled for portal vein embolization (PVE). The use of Gd-EOB-DTPA in the assessment of liver function has been correlated with clinical assessment of liver function classification. We evaluated the correlation between degree of kinetic growth (kGR) of the liver following PVE liver and the enhancement of the during the hepatobiliary phase of contrast administration. There was no correlation between the degree of enhancement during the hepatobiliary phase and kGR.

Sklaruk J, Luersen G, Ma J, Wei W, Underwood M. Gd-EOB-DTPA based magnetic resonance imaging for predicting liver response to portal vein embolization. *World J Radiol* 2017; 9(4): 199-205 Available from: URL: <http://www.wjgnet.com/1949-8470/full/v9/i4/199.htm> DOI: <http://dx.doi.org/10.4329/wjr.v9.i4.199>

INTRODUCTION

Portal vein embolization (PVE) is performed to redirect portal flow to the liver remnant in order to increase liver volume. PVE is increasingly used to induce hypertrophy of the anticipated liver remnant in the management of patients with liver metastases undergoing liver resection. The rationale for PVE is to reduce suboptimal post-resection liver size and resulting morbidities^[1-5].

The minimum reported safe functioning liver remnant (FLR) is 20% of total liver volume (TLV) in patients with normal liver and 40% of TLV in compromised liver such as cirrhotic patients^[1,2,6]. The evaluation of FLR following PVE is recommended at 21 d following the procedure^[2,7]. At this time, a FLR of less than 20% or a degree of hypertrophy of less than 5% predicted the likelihood of hepatic resection dysfunction. These patients with suboptimal FLR are reported to have major liver-centered complications, including hepatic dysfunction, and insufficiency following surgery^[2,7].

In addition to the FLR, kinetic growth rate (kGR) has been reported to be a better predictor of postoperative morbidity and mortality after liver resection for small

FLR than conventional measured volume parameters^[7,8]. The kGR calculates the change in FLR as function of time. A kGR of < 2% per week correlates with poor rates of hepatic insufficiency and liver-related 90-d mortality^[7,9-11]. At this time there is no predictor of liver hypertrophy response to PVE prior to the procedure. This results in unnecessary PVE in the patient population that do not respond to treatment. These unnecessary PVE have inherent morbidities^[1,3,6].

Gadoxetic acid disodium (Gd-EOB-DTPA) is a hepatobiliary contrast agent. The enhancement of the liver with Gd-EOB-DTPA depends on liver function^[9-13].

The purpose of this project is to evaluate the response to PVE (based on kGR calculations) and the degree of hepatic function (based on the enhancement of the liver with Gd-EOB-DTPA). Our hypothesis is that the degree of enhancement of the liver following the intravenous administration of Gd-EOB-DTPA at the hepatobiliary phase will correlate and predict the kinetic growth rate of the liver following portal vein embolization. This prediction in kGR will allow the selection of patients who will respond to PVE. This will then limit a number of unnecessary PVE procedures for patients that predictably will not respond to treatment.

MATERIALS AND METHODS

This is a prospective IRB approved project. The inclusion criteria were all patients who were scheduled for a PVE. Patients who consented to this project were offered an MR examination of the liver with Gd-EOB-DTPA. This MR was performed before the PVE procedure.

MRI protocol

All patients had an MR examination of the liver with Gd-EOB-DTPA (Table 1). All MR exams were performed in the same scanner at 1.5T (GE Wisconsin, United States). The examination consisted of T1 (in/out-of-phase at 5/0 mm), T2 (Fast Spine Echo at 5/0 mm), DWI at b = 50, 400, 800 mm²/s, and pre- and post-pre-contrast and post-Gd-EOB-DTPA injected at 1 cc/s. 3D spoiled gradient echo Liver Acquisition Volume Acquisition (LAVA, GEMS, Milwaukee Wisconsin). The LAVA images were obtained during the late arterial phase, portal venous phase, delayed phase, excretory phase, 10 min and 20 min post-Gd-EOB-DTPA. For an internal standard all images were acquired with a test tube (1 cm × 10 cm) of Gd-EOB-DTPA diluted with water placed on the side of the patient. This was used to standardize signal intensity between the different phases of contrast administration.

Evaluation of enhancement

One radiologist with over 20 years of experience in body MR placed multiple regions of interests in the liver. The diameter of the ROI in the liver measure ranged from 1 to 2 cm. The ROI in the liver were placed outside major vessels, bile ducts, or liver masses. A ROI was

Table 1 Magnetic resonance imaging pulse sequence protocol

	T1 (OOP) 2D FSPGR	T1 (IP) 2D FSPGR	T2 (FS)	Pre- and Post-Gd 3D FSPGR	DWI EPI (B-0, 400, 800)
# ECHOES/SHOTS	2	2	1	1	1
TE1/TE2 (ms)	2.2-2.4	4.2-4.8	85	min	min (about 50-60)
TR/#R-R (ms)	120	120			
FLIP ANGLE	85	85		15	
ETL			16		
FOV (cm)	48	48	48	48	48
SCAN THK (mm)	6	6	6	5-6 (-2.5)	6
FREQ × PHASE	256 × 160	256 × 160	256 × 160	256 × 128	100 × 160
NEX	1	1	4	1	1, 4, 6
PHASE FOV	0.9-1.0	0.9-1.0	0.75-1.0	0.75-1.0	0.75-1.0

Post-Gd images were obtained at late arterial phase (fluoro-triggered), 60 s, 180 s, 300 s, and 20 min post-Gd injection. Gd-EOB-DTPA was injected at 0.25 mmol/kg at 1 cc/s. TR: Repetition time; TE: Echo time; ETL: Echo train length; FS: Fat Saturated; FOV: Field of view; THK: Thickness; NEX: Number of averages; FSPGR: Fast spoiled gradient echo; DWI: Diffusion weighted imaging; EPI: Echo planar imaging; FREQ: Frequency; SEG: Segment.

also placed in the external test tube. Multiple ROIs were placed in each patient. One ROI was placed for each liver segment evaluated (IV, V, VI, VII, VIII) and one for segments II/III. The multiple ROIs were placed to evaluate the correlation of segmental enhancement of the liver with kGR.

The percentage of enhancement (%E) was calculated by subtracting the signal intensity (SI) during the hepatobiliary phase (HBP) from the SI during the pre-contrast phase corrected by the signal intensity of the external test tube (t): The %E was calculated for segments VIII, VII, VI, V, IV, left liver average, right liver average and whole liver average. $\% E_{(\text{segment-x})} = [SI_{\text{hbp}} / SI_{\text{t}}]_{(\text{segment-x})} - (SI_{\text{pre}} / SI_{\text{t}})_{(\text{segment-x})} / (SI_{\text{pre}} / SI_{\text{t}})_{(\text{segment-x})} \times 100$.

Evaluation of kGR

The kGR was calculated by evaluating the degree of hypertrophy (DH) divided by the time period (in days) from the PVE to the post-PVE scan: $kGR = DH / \text{Time Period (days)}^{[7]}$. DH was calculated by comparing the FLR post-PVE minus FLR pre-PVE: $DH = \% \text{ FLR}_{\text{post-PVE}} - \% \text{ FLR}_{\text{pre-PVE}}^{[7]}$. The functional liver reserve for time period (i) was calculated: $FLR_i = (FLR_i / sTLV)^{[7]}$. The standardized total liver volume (sTLV) was calculated: $sTLV = 794.41 + 1267.28 \times \text{body surface area (m}^2)^{[2,7]}$. One radiologist with over 20 years of experience in body imaging demarcated the segments. The segmental and total liver volumes were calculated from the axial MR/CT images with standard software: GE Advantage Workstation AW4.1_06 Volume Viewer Voxtool 3.0.64z (General Electric, Wisconsin, United States)^[2,7].

Statistical analysis

Summary statistics of enhancement and kGR were provided in mean, SD, and range by site. Association between kGR and enhancement during the hepatobiliary phase were estimated using linear regression (linearity and normality assumptions) and Spearman's correlation test (rank based, no assumptions). All tests were two-sided and *P* values of 0.05 or less were considered statistically significant. Statistical analysis was carried

out using SAS version 9 (SAS Institute, Cary, NC). Biomedical statistical review was performed by one of the authors, Mr. Wei W, who is a biomedical statistician.

RESULTS

Seventeen patients were consented for this prospective project: 10 males and 17 females. Age range was 21-65 years old. The primary diagnosis was colorectal cancer in all patients. Three patients did not undergo a portal vein embolization and were therefore excluded.

The % E for each segment, lobe and whole liver is shown in Table 2. The %E ranged from 82% to 199%. For all patients, the kGR ranged from -0.34 to 3.73 (Figure 1). The average kGR was 1.97%. Nine patients were above the 2% cut-off for decreased morbidity^[7]. The FLR pre-PVE and post-PVE is shown in Figure 2. The relationship between the kGR and the degree of enhancement for various segments, lobes and whole liver are shown in Figure 3 and Table 3. Based on linear regression (strong assumptions) and Spearman's correlation test (rank based, no assumptions), there was no significant correlation between enhancement and kGR.

DISCUSSION

Our hypothesis was that the degree of enhancement of the liver during the hepatobiliary phase will correlate with the degree of liver response to portal vein embolization. Our results, unfortunately, did not support our hypothesis.

A possibility that our hypothesis was not demonstrated is that the patient population was not representative of the published data on portal vein embolization. However, the average kGR of 1.97% in our study compares favorably with the reported average kGR in the initial publications on PVE of 2.4^[7]. In addition, the cut-off of 2% in kGR is reported as the threshold for complications and hepatic failure^[7]. In our patient population 9 patients were above the threshold and 6 patients were below the threshold. This is a relative low

Table 2 Percent in enhancement calculated between the pre-contrast phase and hepatobiliary phase of contrast administration

Average left liver	Average right liver	Average whole liver	SEG IV	SEG VIII	SEG VII	SEG V	SEG VI
118.27	129.14	123.1	137.3	118.06	129.77	146.59	122.15
106.69	124.13	114.44	96.6	112.28	129.85	129.01	125.38
131.41	132.71	132.15	122.9	126.81	139.86	121.72	142.46
133.22	130	131.79	111.85	124.87	133.4	142.06	119.66
166.19	176.9	172.31	161.17	176.29	184.49	147.19	199.65
81.83	113.24	95.79	77.14	101.13	122.32	104.6	124.92
102.63	113.57	107.5	83.77	108.26	131.64	112.28	102.11
157.2	160.56	158.88	161.62	146.42	158.69	174.57	162.57
114.15	134.94	123.39	110.28	131.55	138.96	130.07	139.16
104.98	129.04	115.68	103.53	130.94	116.86	142.72	125.66
117.83	148.94	131.66	123.38	141.55	145.57	164.26	144.37
132.54	151.34	140.9	119.4	158.55	156.5	125.41	164.92
102.2	113.12	107.06	108.72	132.15	127.38	74.83	118.13
123.9	124.27	124.07	124.09	105.84	131.57	139.36	120.32

The data are shown for segments IV, V, VI, VII, and VIII. Also the data were calculated using the average enhancement of the right liver, left liver, and whole liver.

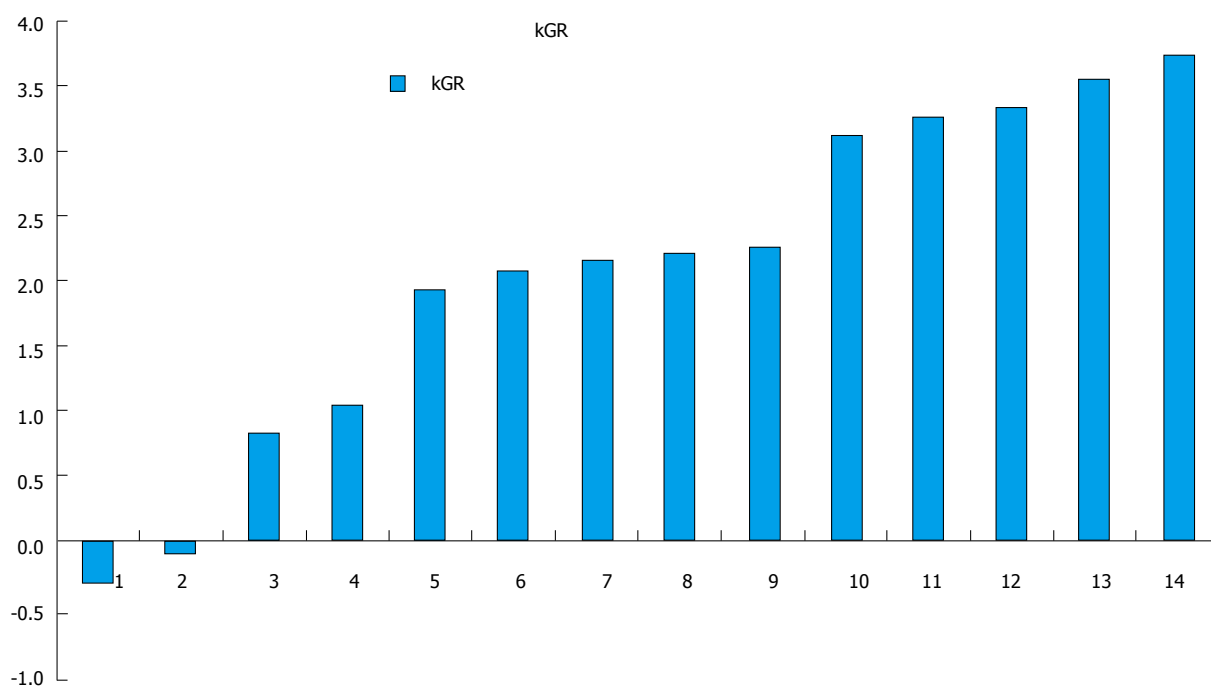


Figure 1 kinetic growth for each of the 14 patients. The data are displayed at increasing values. A cut-off below 2% is considered sub-optimal for liver resection. Patients 1-5 did not show a kGR above the 2% threshold. kGR: Kinetic growth rate.

number of patients but this was distributed between the < 2% or > 2% kGR group. The range of kGR in our study population of -0.33%-3.73% was narrower than that on the prior reports of (0.2-9.4%)^[7]. The average DH of our patient population was 9.60%. This also compares favorably with the DH of 10.1% on the original report^[7]. The range of DH on our patient population of -1.3%-17.8% was narrower than on prior results (0.1%-39.9%)^[7,14]. In summary, our patient population appears to represent the two groups of responders and non-responders to PVE.

The enhancement of the liver with Gd-EOB-DTPA depends on the expression of various transporters^[11,15].

This includes organic anion transport factor 8 and organic transporter TP^[11,15-17]. The enhancement also depends on the expression of multidrug resistance protein 2^[16,17]. The use of Gd-EOB-DTPA to assess liver function has been reported following portal vein embolization^[18,19].

The use of Gd-EOB-DTPA in the assessment of liver function has been correlated with clinical assessment of liver function such as in the evaluation of the degree of cirrhosis and in the stratification with the Child-Pugh classification^[10,20,21]. The lack of correlation between the degree of liver enhancement and response to PVE seems to indicate that the response of hypertrophy

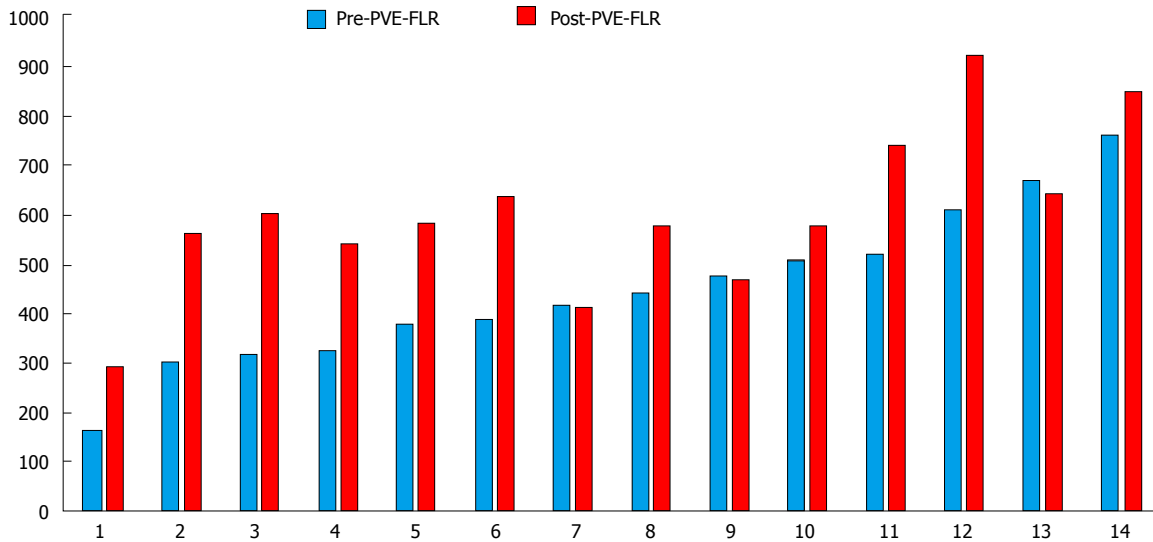
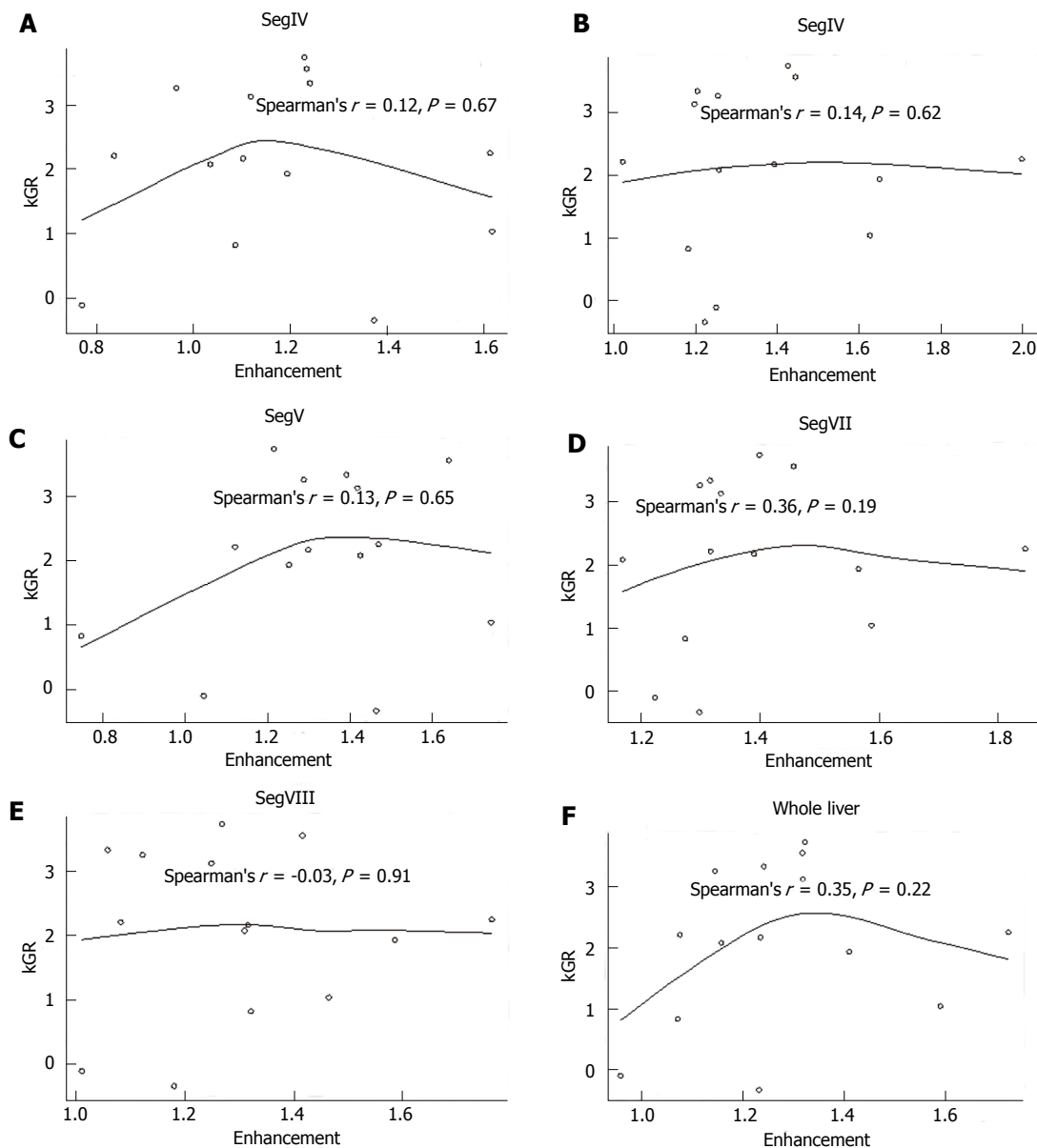


Figure 2 For each of the 14 patients the functioning liver remnant pre- and post-portal vein embolization. This data was ordered from smallest to largest FLR based on the pre-PVE exam for each patient. These patient's number do not correlate with Figure 1 patient number. Patients 7, 9, and 13 on this Figure did not show interval increase in FLR. FLR: Functional liver reserve; PVE: Portal vein embolization; .



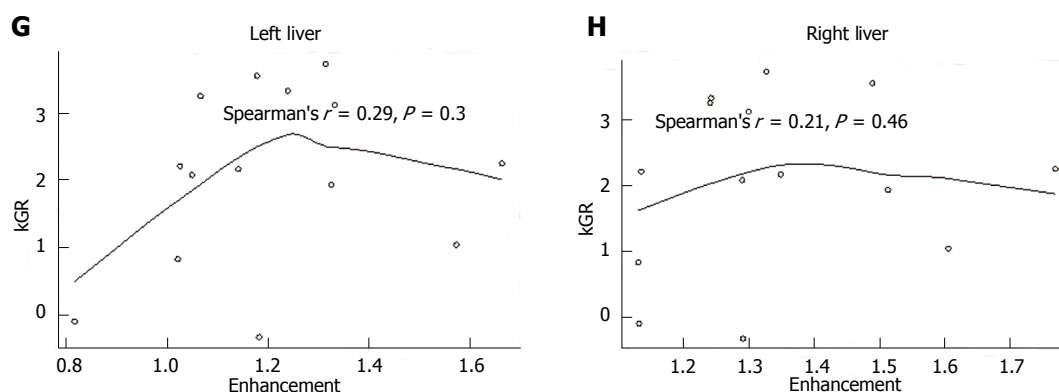


Figure 3 Correlation of the kinetic growth for each patient as a function of the degree of liver enhancement on the hepatobiliary phase. A: Segment IV of the liver; B: Segment VI of the liver; C: Segment V of the liver; D: Segment VII of the liver; E: Segment VIII of the liver; F: Whole liver; G: Left liver; H: Right liver; kGR: Kinetic growth rate.

Table 3 Summary of linear regression model results correlating enhancement and kinetic growth

Site	Estimated Slope	95% LCL	95% UCL	P value
Left liver	1.43	-2.14	5.01	0.4
Right liver	1.08	-3.24	5.4	0.6
SegIV	0.04	-3.3	3.38	0.98
SegV	1.23	-1.98	4.43	0.42
SegVI	0.35	-2.92	3.62	0.82
SegVII	1.05	-3.59	5.69	0.63
SegVIII	0.49	-3.41	4.4	0.79
Whole liver	1.37	-2.57	5.32	0.46

Linear regression assumes normality for both enhancement and kGR, it also assumes a linear relationship between the two. The estimated slope shows how much KGR increases with 1 unit increase of enhancement. P value based on test of slope against zero. If P value < 0.05 then there is significant correlation between enhancement and KGR. Conclusion: Enhancement was NOT significantly correlated with KGR in any of the site measured (all slopes not significantly different from zero, i.e., a flat line). PVE: Portal vein embolization; kGR: Kinetic growth rate; FLR: Functional liver reserve; LAVA: Liver acquisition volume acquisition; ROI: Region of interest; LCL: Lower confidence level; UCL: Upper confidence level.

of the liver to PVE is not only based on liver function but also on other factors such as clonal activity of the hepatocytes. This clonal activity does not affect liver enhancement with Gd-EOB-DTPA.

In conclusion, it is unfortunate that the enhancement of the liver during the hepatobiliary phase did not predict response to treatment with PVE. This would have resulted in a robust screening process for patients schedule for a PVE. Our result should alert other groups to seek alternative screening test to PVE that include evaluation of clonal activity rather than functional liver activity. Although Gd-EOB-DTPA has increasingly shown to be a very powerful tool for the evaluation of liver disease, the enhancement of this agent during the hepatobiliary phase does not predict the degree of liver hypertrophy following PVE.

ACKNOWLEDGMENTS

Ms. Palencia Lewis in the preparation of the documents.

COMMENTS

Background

Hepatic resection is commonly used to cure metastatic disease to the liver. The success of the resection depends on the functional liver reserve post-hepatectomy. To decreased morbidity portal vein embolization is commonly used. Not all patients respond to portal vein embolization (PVE) and PVE has inherent risk factors. The authors were looking for a method to predict response to PVE. Gd-EOB-DTPA is a hepatobiliary agent for MR. The enhancement at 20 min post-Gd has been associated with liver function. The authors wanted to explore if Gd-EOB-DTPA enhanced MR could provide information to predict which patients will response to PVE. This may be then used as a screening tool for patients undergoing PVE.

Research frontiers

This is a novel project and the area there are no publications on prediction of response to PVE with MR.

Innovations and breakthroughs

The results of this project did not prove the hypothesis. The enhancement on the hepatobiliary phase of Gd-EOB-DTPA enhanced MR cannot predict liver response to PVE. The breakthrough is that very likely the response of the liver to PVE is likely a clonal response rather than a liver function response.

Applications

The results did not prove the hypothesis. This suggests that new methodology should be considered to evaluate predictors of response to PVE. This new methodology may include evaluation of clonal activity rather than liver function.

Terminology

PVE: Procedure performed to induce regrowth on one side of the liver in advance of a planned hepatic resection on the other side. This is frequently used in hepatomas and colorectal metastases; Kinetic growth rate (kGR): Defined as the degree of liver hypertrophy at initial volume assessment divided by number of weeks elapsed after PVE; Gd-EOB-DTPA: Is the only approved liver specific MR contrast agent. Enhancement at the hepatobiliary phase, at 20 min, correlates with the degree of liver function. The enhancement is also a function of expression of OTPB and multidrug resistance proteins.

Peer-review

The authors evaluated the response to PVE (based on kGR calculations) and the degree of hepatic function (based on the enhancement of the liver with Gd-EOB-DTPA). Their hypothesis is that the degree of enhancement of the liver following the intravenous administration of Gd-EOB-DTPA at the hepatobiliary phase will correlate and predict the kinetic growth rate of the liver following portal vein embolization. They demonstrated that although Gd-EOB-DTPA has increasingly shown to be a very powerful tool for the evaluation of liver disease,

the enhancement of this agent during the hepatobiliary phase does not predict the degree of liver hypertrophy following PVE.

REFERENCES

- 1 **Abdalla EK**, Hicks ME, Vauthey JN. Portal vein embolization: rationale, technique and future prospects. *Br J Surg* 2001; **88**: 165-175 [PMID: 11167863 DOI: 10.1046/j.1365-2168.2001.01658.x]
- 2 **Vauthey JN**, Chaoui A, Do KA, Bilimoria MM, Fenstermacher MJ, Charnsangavej C, Hicks M, Alsasser G, Lauwers G, Hawkins IF, Caridi J. Standardized measurement of the future liver remnant prior to extended liver resection: methodology and clinical associations. *Surgery* 2000; **127**: 512-519 [PMID: 10819059 DOI: 10.1067/msy.2000.105294]
- 3 **Ganeshan DM**, Szklaruk J. Portal vein embolization: cross-sectional imaging of normal features and complications. *AJR Am J Roentgenol* 2012; **199**: 1275-1282 [PMID: 23169719 DOI: 10.2214/AJR.12.8636]
- 4 **van Gulik TM**, van den Esschert JW, de Graaf W, van Lienden KP, Busch OR, Heger M, van Delden OM, Laméris JS, Gouma DJ. Controversies in the use of portal vein embolization. *Dig Surg* 2008; **25**: 436-444 [PMID: 19212116 DOI: 10.1159/000184735]
- 5 **Madoff DC**, Gaba RC, Weber CN, Clark TW, Saad WE. Portal Venous Interventions: State of the Art. *Radiology* 2016; **278**: 333-353 [PMID: 26789601 DOI: 10.1148/radiol.2015141858]
- 6 **Avritscher R**, Duke E, Madoff DC. Portal vein embolization: rationale, outcomes, controversies and future directions. *Expert Rev Gastroenterol Hepatol* 2010; **4**: 489-501 [PMID: 20678021 DOI: 10.1586/egh.10.41]
- 7 **Shindoh J**, Truty MJ, Aloia TA, Curley SA, Zimmitti G, Huang SY, Mahvash A, Gupta S, Wallace MJ, Vauthey JN. Kinetic growth rate after portal vein embolization predicts posthepatectomy outcomes: toward zero liver-related mortality in patients with colorectal liver metastases and small future liver remnant. *J Am Coll Surg* 2013; **216**: 201-209 [PMID: 23219349 DOI: 10.1016/j.jamcollsurg.2012.10.018]
- 8 **Croome KP**, Hernandez-Alejandro R, Parker M, Heimbach J, Rosen C, Nagorney DM. Is the liver kinetic growth rate in ALPPS unprecedented when compared with PVE and living donor liver transplant? A multicentre analysis. *HPB (Oxford)* 2015; **17**: 477-484 [PMID: 25728543 DOI: 10.1111/hpb.12386]
- 9 **Jhaveri K**, Cleary S, Audet P, Balaa F, Bhayana D, Burak K, Chang S, Dixon E, Haider M, Molinari M, Reinhold C, Sherman M. Consensus statements from a multidisciplinary expert panel on the utilization and application of a liver-specific MRI contrast agent (gadoteric acid). *AJR Am J Roentgenol* 2015; **204**: 498-509 [PMID: 25714278 DOI: 10.2214/AJR.13.12399]
- 10 **Kim HY**, Choi JY, Park CH, Song MJ, Song DS, Kim CW, Bae SH, Yoon SK, Lee YJ, Rha SE. Clinical factors predictive of insufficient liver enhancement on the hepatocyte-phase of Gd-EOB-DTPA-enhanced magnetic resonance imaging in patients with liver cirrhosis. *J Gastroenterol* 2013; **48**: 1180-1187 [PMID: 23354621 DOI: 10.1007/s00535-012-0740-7]
- 11 **Nilsson H**, Blomqvist L, Douglas L, Nordell A, Janczewska I, Näslund E, Jonas E. Gd-EOB-DTPA-enhanced MRI for the assessment of liver function and volume in liver cirrhosis. *Br J Radiol* 2013; **86**: 20120653 [PMID: 23403453 DOI: 10.1259/bjr.20120653]
- 12 **Geisel D**, Lüdemann L, Keuchel T, Malinowski M, Seehofer D, Stockmann M, Hamm B, Gebauer B, Denecke T. Increase in left liver lobe function after preoperative right portal vein embolisation assessed with gadolinium-EOB-DTPA MRI. *Eur Radiol* 2013; **23**: 2555-2560 [PMID: 23652847 DOI: 10.1007/s00330-013-2859-1]
- 13 **Saito K**, Ledsam J, Sourbron S, Otaka J, Araki Y, Akata S, Tokuyue K. Assessing liver function using dynamic Gd-EOB-DTPA-enhanced MRI with a standard 5-phase imaging protocol. *J Magn Reson Imaging* 2013; **37**: 1109-1114 [PMID: 23086736 DOI: 10.1002/jmri.23907]
- 14 **Zeile M**, Bakal A, Volkmer JE, Stavrou GA, Dautel P, Hoeltje J, Stang A, Oldhafer KJ, Brünig R. Identification of cofactors influencing hypertrophy of the future liver remnant after portal vein embolization-the effect of collaterals on embolized liver volume. *Br J Radiol* 2016; **89**: 20160306 [PMID: 27730840 DOI: 10.1259/bjr.20160306]
- 15 **Narita M**, Hatano E, Arizono S, Miyagawa-Hayashino A, Isoda H, Kitamura K, Taura K, Yasuchika K, Nitta T, Ikai I, Uemoto S. Expression of OATP1B3 determines uptake of Gd-EOB-DTPA in hepatocellular carcinoma. *J Gastroenterol* 2009; **44**: 793-798 [PMID: 19404564 DOI: 10.1007/s00535-009-0056-4]
- 16 **Kimura Y**, Sato S, Hitomi E, Ohyama M, Adachi K, Inagaki Y, Yamakawa Y, Hirano A, Kawai H, Tsuchida K, Senoo K, Katsumi K, Joh T. Coexpression of organic anion-transporting polypeptides 1B3 and multidrug-resistant proteins 2 increases the enhancement effect of gadolinium-ethoxybenzyl-diethylenetriamine pentaacetic acid on hepatocellular carcinoma in magnetic resonance imaging. *Hepatol Res* 2014; **44**: 327-337 [PMID: 23607695 DOI: 10.1111/hepr.12128]
- 17 **Tsuda N**, Harada K, Matsui O. Effect of change in transporter expression on gadolinium-ethoxybenzyl-diethylenetriamine pentaacetic acid-enhanced magnetic resonance imaging during hepatocarcinogenesis in rats. *J Gastroenterol Hepatol* 2011; **26**: 568-576 [PMID: 21332553 DOI: 10.1111/j.1440-1746.2010.06494.x]
- 18 **Akiba A**, Murata S, Mine T, Onozawa S, Sekine T, Amano Y, Kawano Y, Uchida E, Kumita S. Volume change and liver parenchymal signal intensity in Gd-EOB-DTPA-enhanced magnetic resonance imaging after portal vein embolization prior to hepatectomy. *Biomed Res Int* 2014; **2014**: 684754 [PMID: 25302304 DOI: 10.1155/2014/684754]
- 19 **Geisel D**, Raabe P, Lüdemann L, Malinowski M, Stockmann M, Seehofer D, Pratschke J, Hamm B, Denecke T. Gd-EOB-DTPA-enhanced MRI for monitoring future liver remnant function after portal vein embolization and extended hemihepatectomy: A prospective trial. *Eur Radiol* 2016 Dec 13; Epub ahead of print [PMID: 27966044 DOI: 10.1007/s00330-016-4674-y]
- 20 **Kamimura K**, Fukukura Y, Yoneyama T, Takumi K, Tateyama A, Umanodan A, Shindo T, Kumagai Y, Ueno S, Koriyama C, Nakajo M. Quantitative evaluation of liver function with T1 relaxation time index on Gd-EOB-DTPA-enhanced MRI: comparison with signal intensity-based indices. *J Magn Reson Imaging* 2014; **40**: 884-889 [PMID: 24677659 DOI: 10.1002/jmri.24443]
- 21 **Lee S**, Choi D, Jeong WK. Hepatic enhancement of Gd-EOB-DTPA-enhanced 3 Tesla MR imaging: Assessing severity of liver cirrhosis. *J Magn Reson Imaging* 2016; **44**: 1339-1345 [PMID: 27197633 DOI: 10.1002/jmri.25288]

P- Reviewer: Akamatsu N, Li YZ, Tarazov PG S- Editor: Qi Y
L- Editor: A E- Editor: Wu HL



Retrospective Study

C-reactive protein and radiographic findings of lower respiratory tract infection in infants

Maria Twomey, Hannah Fleming, Fiachra Moloney, Kevin P Murphy, Lee Crush, Siobhan B O'Neill, Oisín Flanagan, Karl James, Conor Bogue, Owen J O'Connor, Michael M Maher

Maria Twomey, Hannah Fleming, Fiachra Moloney, Kevin P Murphy, Lee Crush, Siobhan B O'Neill, Oisín Flanagan, Karl James, Conor Bogue, Owen J O'Connor, Michael M Maher, Department of Radiology, Cork University Hospital, Wilton, T12 DC4A Cork, Ireland

Author contributions: Twomey M drafted the manuscript; Fleming H collected the data and drafted the manuscript; Moloney F collected data and performed statistical analysis; Murphy KP collected the data; Crush L collected data and reported the chest radiographs; O'Neill SB collected the data and performed data analysis; Flanagan O was involved in data analysis, drafting the manuscript and editing; James K redrafted and revised the manuscript, created the audio file and added supplementary comments; Bogue C edited the manuscript; O'Connor OJ edited the manuscript; Maher MM designed the research study and oversaw all aspects of the study.

Institutional review board statement: The study was reviewed and approved by the Cork Clinical Research Ethics Committee, Lancaster Hall, Cork, Ireland.

Informed consent statement: Informed consent was not deemed necessary for this study. Clinical and radiological data was collected retrospectively in an anonymised fashion and no patient underwent additional procedures or investigations as a result of recruitment to the study. Ethical approval was granted without a requirement for informed consent.

Conflict-of-interest statement: All authors wish to declare no conflicts of interest.

Data sharing statement: The technical appendix, statistical code, and dataset are available from the corresponding author at drkarlames@outlook.com. Informed consent was not obtained but the presented data are anonymised and the risk of identification is low.

Open-Access: This article is an open-access article which was selected by an in-house editor and fully peer-reviewed by external reviewers. It is distributed in accordance with the Creative Commons Attribution Non Commercial (CC BY-NC 4.0) license, which permits others to distribute, remix, adapt, build upon this

work non-commercially, and license their derivative works on different terms, provided the original work is properly cited and the use is non-commercial. See: <http://creativecommons.org/licenses/by-nc/4.0/>

Manuscript source: Unsolicited manuscript

Correspondence to: Karl James, FFR RCSI, Department of Radiology, Cork University Hospital, 1 Bishopstown Road, Wilton, T12 DC4A Cork, Ireland. drkarlames@outlook.com
Telephone: +353-021-4920288
Fax: +353-021-4922002

Received: June 14, 2016

Peer-review started: June 17, 2016

First decision: July 27, 2016

Revised: August 10, 2016

Accepted: October 17, 2016

Article in press: October 18, 2016

Published online: April 28, 2017

Abstract**AIM**

To evaluate the association between C-reactive protein (CRP) and radiological evidence of lower respiratory tract infection (LRTI) in infants.

METHODS

All patients aged less than 4 years who presented with suspected lower respiratory tract infection, who received a peri-presentation chest radiograph and CRP blood measurement over an 18-mo period were included in the study. Age, gender, source of referral, CRP, white cell count, neutrophil count along with the patients' symptoms and radiologist's report were recorded.

RESULTS

Three hundred and eleven patients met the inclusion

criteria. Abnormal chest radiographs were more common in patients with elevated CRP levels ($P < 0.01$). Radiologic signs of LRTI were identified in 73.7% of chest radiographs when a patient had a CRP level between 50-99 mg/L. CRP levels were a better predictor of positive chest radiograph findings for those aged greater than 1 year compared to those 1 year or less.

CONCLUSION

CRP may be used in patients with suspected LRTI diagnosis to select those who are likely to have positive findings on chest radiograph, thus reducing unnecessary chest radiographs.

Key words: Chest radiograph; C-reactive protein; Chest infection; Respiratory infection; Pediatric

© The Author(s) 2017. Published by Baishideng Publishing Group Inc. All rights reserved.

Core tip: Abnormal chest radiograph findings are significantly more common in patients with elevated C-reactive protein (CRP) levels. Young children are most likely to have abnormal chest radiograph findings if they have all three of the following; a CRP level of 50-99 mg/L, respiratory symptoms and if they are aged greater than 1 year.

Twomey M, Fleming H, Moloney F, Murphy KP, Crush L, O'Neill SB, Flanagan O, James K, Bogue C, O'Connor OJ, Maher MM. C-reactive protein and radiographic findings of lower respiratory tract infection in infants. *World J Radiol* 2017; 9(4): 206-211 Available from: URL: <http://www.wjgnet.com/1949-8470/full/v9/i4/206.htm> DOI: <http://dx.doi.org/10.4329/wjr.v9.i4.206>

INTRODUCTION

Despite the very low effective dose imparted during the acquisition of a chest radiograph this investigation is common and may be subject to excessive and unjustified use. Children have a greater risk of cancer when exposed to diagnostic ionizing radiation due to their larger proportion of dividing cells and also due to their longer life expectancy during which a potential radiation induced cancer can be expressed^[1-3]. Post natal exposure to diagnostic ionizing radiation is associated with an increased risk of childhood acute lymphoblastic leukaemia^[1] and brain neoplasms^[3] and therefore use of all diagnostic imaging modalities which employ ionizing radiation should be limited and justified in young patients. There is also the issue of cost associated with performance of unnecessary radiological tests and also the issue of stress to patients and parents of performing radiological examinations in infants and young children.

In addition to chest radiography, non-specific serum inflammatory markers are commonly requested in

paediatric patients with suspected lower respiratory tract infection (LRTI). Measurement of C-reactive protein (CRP) in these patients is commonplace and often helps to substantiate the clinical diagnosis, to establish the severity of infection and in some cases to monitor the therapeutic management of LRTI^[4-11]. Routinely measured CRP levels may potentially be of additional clinical use to physicians and radiologists if they could aid in the selection and justification of performance of chest radiography in the setting of infantile lower respiratory tract infection. No previous study has examined the association between CRP and objective radiological evidence of LRTI in infants. Therefore we designed a retrospective study to determine whether an increased CRP level in paediatric patients presenting with acute respiratory symptoms, is associated with abnormal findings on chest radiography and to determine if other haematological and clinical parameters may additionally predict the presence of chest radiograph abnormalities.

MATERIALS AND METHODS

This institutional ethical review board approved, retrospective study was conducted between January 2009 and August 2011. Infants aged between 28 d and 4 years who presented to a single institution with clinically suspected lower respiratory tract infection and who had undergone chest radiography and CRP blood measurement within a 24-h period were included in the study. Patients with chronic lung diseases such as cystic fibrosis were excluded from the study. Presenting symptoms were recorded from the patient medical records for each patient and CRP level, white cell count and neutrophil count were recorded in all cases from the hospital electronic laboratory database. The presence of consolidation, pneumonic infiltrates, bronchial wall thickening, peribronchial cuffing, collapse or effusion were retrospectively recorded in each case by 2 reviewers in consensus (HF, 2-year experience; SON, 4-year experience) following examination of the radiology reports in an unblinded fashion. The CRP level in all patients was measured in mg/L (normal 0-5 mg/L) using the Beckman Coulter Latex Enhanced Turbidometric assay.

Statistical analysis

Data analysis involved the use of both descriptive and inferential statistics using SPSS 17 (IBM Computers, New York, United States). Descriptive methods employed included one-way and two-way frequencies along with mean and standard deviation. Inferential statistics consisted of χ^2 tests and t tests. Correlation coefficient tests explored the relationship between quantitative measures. A threshold P value below 0.05 was deemed as statistically significant. Numerical averages are presented as mean \pm SD unless otherwise stated.

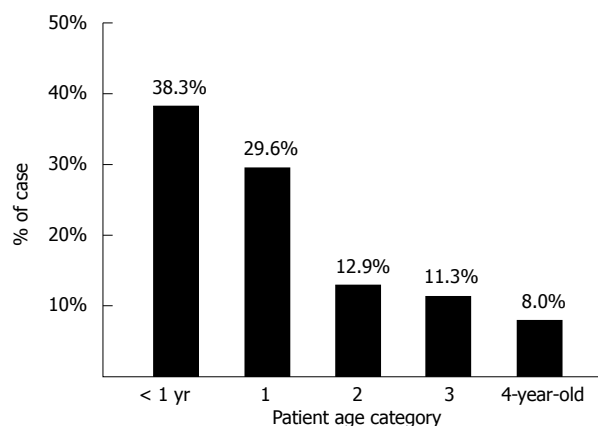


Figure 1 Age distribution of patient cohort.

RESULTS

Three hundred and eleven patients were included in the study. There were 164 males (52.7%) and 147 females (47.3%) with ages ranging from 28 d to 4 years (mean age 1.2 years \pm 1.3) (Figure 1). The distribution of age was very similar for both genders, with females being just slightly older (1.3 \pm 1.3 years) than males (1.1 \pm 1.3 years).

Over half of all cases (53.2%) had been admitted directly to hospital following general practitioner (GP) referral, 37.2% were from the emergency department (ED) and the remaining 9.6% were outpatients. Patients aged less than one year of age were significantly more likely to be inpatients ($P < 0.01$). Forty-seven point five percent of all children who were inpatients were aged less than one year whereas 17.2% of all outpatients and 33% of all ED cases were in this age category. Outpatients were on average over double the age of inpatient cases. This age discrepancy by location is likely explained by a high rate of direct hospital admissions following GP referral, for younger patients as per hospital policy.

Twenty-five point one percent of all CRP measurements were in the "normal" range (0-5 mg/L), 40.2% were in the range 5-49 mg/L, 18.3% were in the 50-99 mg/L range and 16.4% of patients had a CRP of greater than 100 mg/L (Table 1).

Fifty point four percent had both respiratory and systemic symptoms whereas 24.8% had respiratory symptoms alone. The remainder (24.8%) had no respiratory symptoms and CRP and chest radiograph were performed for investigation of fever. CRP levels were significantly higher in patients with systemic symptoms (68.6 \pm 86.2 mg/L vs 32.7 \pm 55.2 mg/L) ($P < 0.01$). Patients who were seen initially in the ED had statistically significant lower CRP readings (28.5 \pm 38.6 mg/L) than inpatients (57.8 \pm 66.0 mg/L) ($P < 0.001$) or outpatients (74.6 \pm 108.6 mg/L) ($P < 0.001$). This could reflect lower threshold for performance of chest radiography in the ED setting.

Serum white cell count (WCC) (normal range:

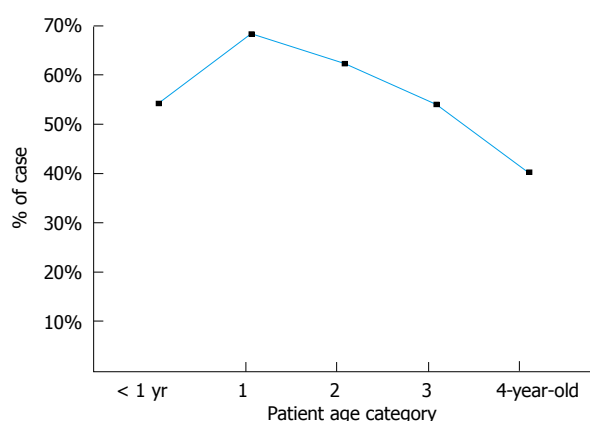


Figure 2 Rate of radiographic evidence of lower respiratory tract infection according to patient age.

4-11 $\times 10^9$ /L) ranged from 3.1-55.6 $\times 10^9$ /L, with a mean of 13.9 \pm 7.2 $\times 10^9$ /L. Serum neutrophil levels (normal range: 1.8-8 $\times 10^9$ /L) ranged from 0.6 to 38.1 $\times 10^9$ /L with a mean of 8.2 \pm 5.7 $\times 10^9$ /L. There was no significant difference in WCC or neutrophil counts between inpatient, outpatients and ED patients. CRP levels correlated positively and strongly with WCC and neutrophil counts ($P < 0.001$).

Fifty-eight point five percent of all chest radiographs were abnormal and abnormal findings were most frequently encountered in 1-year-old patients (68.5%) (Figure 2). Abnormal chest radiograph findings were significantly more common in patients with elevated CRP levels ($P < 0.01$) (Figure 3). However, when patients were sub-grouped according to their age it was found that an elevated CRP level was significantly predictive of an abnormal findings on chest radiography in patients greater than 1 year of age ($P < 0.01$) but was not predictive of an abnormal chest radiograph in patients aged less than 1 year of age ($P = 0.56$). It is worth noting that a CRP of > 100 mg/L was less predictive of an abnormal chest radiograph than a CRP level of 55-99 mg/L (Figure 3). This was especially true in patients under one year of age where only 37.5% of chest radiographs were positive when the CRP exceeded 100 mg/L (Figure 4). Interestingly WCC and neutrophil counts were not predictive of an abnormal chest radiograph across the entire cohort or in sub-groups aged less than or greater than 1 year.

The presence of respiratory symptoms (cough, wheeze, tachypnea, respiratory distress, dyspnoea) was more predictive of an abnormal chest radiograph than systemic symptoms alone (Figure 5). Infants aged less than one year with both respiratory symptoms and elevated CRP levels of 50-99 mg/L, were significantly more likely to have an abnormal chest radiograph ($P < 0.01$) (Figure 5). The combination of these 2 elements yielded a positive predictive value (PPV) of 62% for an abnormal chest radiograph whereas the absence of either had a negative predictive value (NPV) of 62%. Those aged 1-4 years presenting with both respiratory

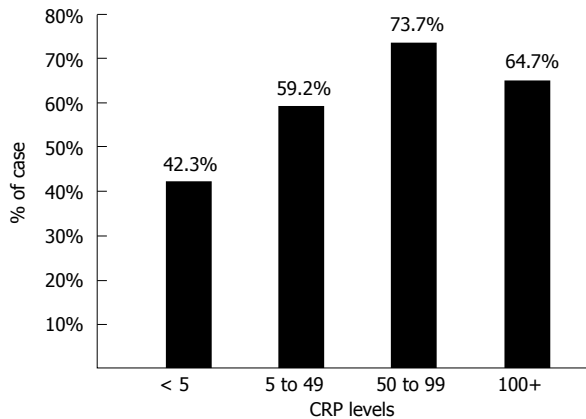


Figure 3 Rate of radiographic evidence of lower respiratory tract infection according to patient C-reactive protein levels. CRP: C-reactive protein.

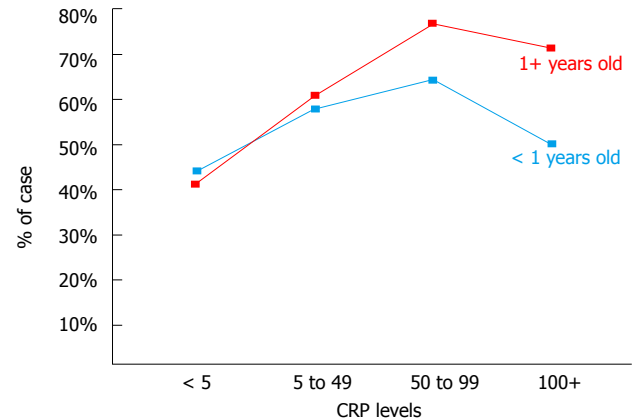


Figure 4 Rate of radiographic evidence of lower respiratory tract infection according to patient age and C-reactive protein level. CRP: C-reactive protein.

Table 1 Distribution of C-reactive protein levels in the patient cohort

CRP category (mg/L)	Frequency (n)	Percentage
< 5	78	25.1
5-49	125	40.2
50-99	57	18.3
> 100	51	16.4

CRP: C-reactive protein.

symptoms and a CRP of 50-99 mg/L had a PPV of 64% for an abnormal chest radiograph and the absence of either yielded a NPV of 75% for chest radiograph findings.

DISCUSSION

The major finding of our study is that abnormal chest radiograph findings were significantly more common in patients with elevated CRP levels. This finding suggests that CRP levels may predict findings on chest radiographs in infants with suspected LRTI. A CRP range of 50-99 mg/L was most predictive of an abnormal chest radiograph. We also found that patients who were less than 1 year frequently have normal chest radiographs in the presence of CRP level elevations above 100 mg/L. This finding may be explained by the fact that the presenting complaints of patients aged less than 1 year may often be non-specific and possibly that those aged less than one year have an increased likelihood of having other possible infectious pathologies such as gastroenteritis or urinary tract infection, which are both common in this age group. The presence of respiratory symptoms was, as expected, a predictor of positive chest radiograph findings along with systemic symptoms. Patients aged greater than 1 year were also more likely to yield a finding on chest radiograph.

A single prospective case control study by Almirall *et al.*^[12] of patients greater than 14 years complements our own results by finding that CRP was an independent

predictor of LRTI. It concluded that a serum CRP level > 33 mg/L can differentiate patients with true alveolar infection from patients with LRTI other than pneumonia. In our study, patients with a CRP of > 33 mg/L had a 68.2% likelihood of an abnormal chest radiograph, as opposed to a 24.7% chance of a normal radiograph. A CRP level of < 33 mg/L in children aged 1 to 4 had an NPV of 50% in predicting a normal chest radiograph. Almirall *et al.*^[12] also found that patients requiring inpatient care had higher CRP levels than outpatients and that CRP levels varied significantly with patient age in keeping with our findings.

In another study involving the adult population, Hopstaken *et al.*^[7] found that both ESR and CRP had a higher odds ratio at predicting pneumonia than clinical signs alone and therefore concluded that CRP along with clinical signs had sufficient sensitivity to predict the presence of LRTI. The authors of that study advise that it may be possible to safely withhold antibiotic treatment in adult patients with a CRP value of < 20 mg/L among other criteria. Again, this complements our findings in a pediatric setting, which suggest that a normal CRP may negate the need for chest radiography in patients aged 1 to 4, particularly in the absence of respiratory symptoms. Chest radiograph omission would have a beneficial impact in terms of radiation dose reduction to infants and their parents, workload reduction for radiographers/radiology technicians in a cohort of patients in which chest radiography can be challenging, decreased stress to sick infants and reduced economic costs.

Numerous previous studies examined the utility of non-specific inflammatory markers such as CRP and findings on chest radiographs in determining the nature of the infectious pathogen responsible for LRTI. These studies found little or no value of CRP levels or chest radiograph findings in the differentiation between bacterial and viral pneumonia^[4,5,10,11]. As a result of these previous studies, attempts at differentiating between viral and bacterial pathogens was not undertaken in our study.

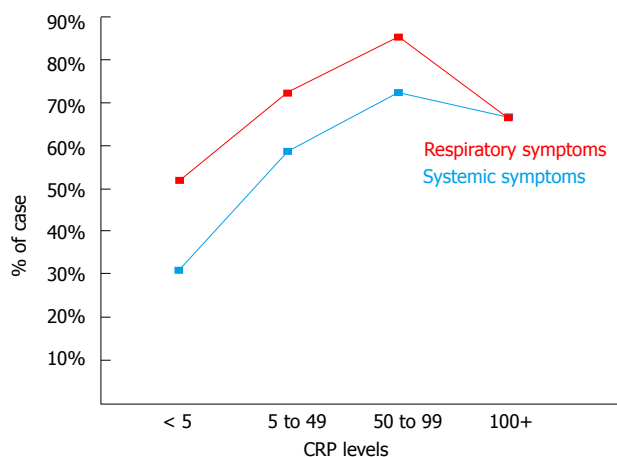


Figure 5 Rate of radiographic evidence of lower respiratory tract infection according to patient symptoms and C-reactive protein level. CRP: C-reactive protein.

The issue of investigation and management of community-acquired pneumonia (CAP) in children has been extensively investigated recently. Recent studies, including a study by Neuman *et al.*^[13], have investigated the use of investigations including chest radiography and subsequent management of children presenting to hospital with CAP. The study investigated a mean of 375000 ED visits for CAP annually, during the study period from 2001-2009. Among children discharged from EDs with CAP, full blood count was performed during 30% of visits, chest radiography during 83%, and viral testing in only 13%^[13]. A recommendation from the study was that efforts should be made to reduce the performance of certain diagnostic testing, such as a full blood count and chest radiography^[13]. Another very recent study by Florin *et al.*^[14] examined variability across hospitals in diagnostic test utilisation for children diagnosed with CAP during ED evaluation and to determine if test utilisation is associated with hospitalisation and ED revisits. This study analysed a total of 100615 ED visits were analysed. Full blood count (28.7%), blood culture (27.9%), and chest radiograph (75.7%) were the most commonly ordered ED diagnostic tests. There was significant variation in the utilisation of these investigations between hospitals. An interesting finding was that hospitals, which had increased rates of utilisation of these investigations, had increased likelihood of hospital admission compared to hospitals that utilised these investigations less frequently. However, ED revisits between the low- and high-utilising hospitals were not significant. The study concluded that an opportunity exists to reduce diagnostic testing for CAP without negatively affecting outcomes^[14]. Recently, the Pediatric Infectious Diseases Society, have published guidelines on the management of CAP in infants and children older than 3 mo of age^[15]. These guidelines suggest that routine chest radiographs are not necessary for the confirmation of suspected CAP in patients well enough to be treated in the outpatient setting and that chest radiography (posteroanterior and lateral)

should only be obtained in children with suspected or documented hypoxemia or significant respiratory distress and in those with failed initial antibiotic therapy, to verify the presence or absence of complications of pneumonia, including parapneumonic effusions, necrotising pneumonia, and pneumothorax^[15]. The findings of our study would suggest that serum CRP levels may play a role in guiding the decision of whether to perform or not perform a chest radiograph in this setting.

Limitations of our study include the retrospective design and that reviewers retrospectively analysed chest radiograph reports and findings. Prospective data collection may be more applicable in normal clinical practice than double or consensus read interpretations. Although CRP elevation is a useful biomarker for infection in the immunocompromised patient^[16], we did not attempt to identify and separate individuals who might be particularly at risk of complications from a respiratory tract infection (such as those with immunodeficiency) and we cannot confidently state that our findings apply to children with a known history of immunodeficiency or malignancy. Ideally, further studies in a larger cohort of patients should be considered to evaluate the role of CRP in the triage and justification of chest radiography in the diagnosis and follow-up of LRTI in the infant population.

In conclusion, this study found that abnormal chest radiograph findings were significantly more common in patients with elevated CRP levels. Young children are most likely to have abnormal chest radiograph findings if they have all three of the following; a CRP level of 50-99 mg/L, respiratory symptoms and if they are aged greater than 1 year. We found no association between an abnormal chest radiograph and elevated WCC and neutrophil count.

COMMENTS

Background

There is an on-going and laudable drive to lower patient exposure to ionising radiation whenever possible. This is especially true when dealing with infants and young children who are at higher risk of malignancy from ionising radiation exposure. The authors acknowledge that the radiation exposure associated with chest radiography is very low. There is however, also the issue of cost associated with performance of unnecessary radiological tests and also the issue of stress to patient and parents of performing radiological examinations in infants and young children. For those reasons, the performance of radiological studies should be limited to clinical situations where it will aid diagnosis or alter management in a young patient cohort. The authors undertook a retrospective study to examine the relationship between serum C-reactive protein (CRP) levels to abnormal findings on chest radiographs to ascertain if raised CRP levels could predict abnormal chest radiograph findings.

Research frontiers

A previous study in adults had shown that low CRP levels could help predict those that require antibiotic treatment for lower respiratory tract infection. No previous studies have looked at using CRP levels in a pediatric population to predict those that may or may not require chest radiography.

Innovations and breakthroughs

The results of this study found that children aged between 1-4 with an elevated CRP were significantly more likely to have an abnormal chest radiograph.

Conversely, the negative predictive value of a normal CRP in a patient with respiratory symptoms or a raised CRP without respiratory symptoms in this age group was 75%.

Applications

The authors' findings may help guide clinicians regarding the need to perform chest imaging when dealing with a child presenting with respiratory symptoms but without hypoxaemia or severe respiratory distress. The ultimate goal being the reduction of unnecessary ionising radiation exposure and reducing cost and potential stress to young patients and their parents.

Terminology

CRP is an acute phase protein released into the blood stream from the liver under the influence of circulating interleukin-6, secreted by T-cell and macrophages. It is used as a marker for inflammation.

Peer-review

The authors investigated CRP and radiographic findings of lower respiratory tract infection in infants. It is a well written paper.

REFERENCES

- 1 **Bartley K**, Metayer C, Selvin S, Ducore J, Buffler P. Diagnostic X-rays and risk of childhood leukaemia. *Int J Epidemiol* 2010; **39**: 1628-1637 [PMID: 20889538 DOI: 10.1093/ije/dyq162]
- 2 **Brenner DJ**, Hall EJ. Computed tomography--an increasing source of radiation exposure. *N Engl J Med* 2007; **357**: 2277-2284 [PMID: 18046031 DOI: 10.1056/NEJMr072149]
- 3 **Pearce MS**, Salotti JA, Little MP, McHugh K, Lee C, Kim KP, Howe NL, Ronckers CM, Rajaraman P, Sir Craft AW, Parker L, Berrington de González A. Radiation exposure from CT scans in childhood and subsequent risk of leukaemia and brain tumours: a retrospective cohort study. *Lancet* 2012; **380**: 499-505 [PMID: 22681860 DOI: 10.1016/S0140-6736(12)60815-0]
- 4 **Clark JE**, Hammal D, Spencer D, Hampton F. Children with pneumonia: how do they present and how are they managed? *Arch Dis Child* 2007; **92**: 394-398 [PMID: 17261579 DOI: 10.1136/adc.2006.097402]
- 5 **Don M**, Valent F, Korppi M, Canciani M. Differentiation of bacterial and viral community-acquired pneumonia in children. *Pediatr Int* 2009; **51**: 91-96 [PMID: 19371285 DOI: 10.1111/j.1442-200X.2008.02678.x]
- 6 **Esposito S**, Bosis S, Cavagna R, Faelli N, Begliatti E, Marchisio P, Blasi F, Bianchi C, Principi N. Characteristics of Streptococcus pneumoniae and atypical bacterial infections in children 2-5 years of age with community-acquired pneumonia. *Clin Infect Dis* 2002; **35**: 1345-1352 [PMID: 12439797 DOI: 10.1086/344191]
- 7 **Hopstaken RM**, Muris JW, Knottnerus JA, Kester AD, Rinkens PE, Dinant GJ. Contributions of symptoms, signs, erythrocyte sedimentation rate, and C-reactive protein to a diagnosis of pneumonia in acute lower respiratory tract infection. *Br J Gen Pract* 2003; **53**: 358-364 [PMID: 12830562]
- 8 **Korppi M**, Heiskanen-Kosma T, Leinonen M. White blood cells, C-reactive protein and erythrocyte sedimentation rate in pneumococcal pneumonia in children. *Eur Respir J* 1997; **10**: 1125-1129 [PMID: 9163657 DOI: 10.1183/09031936.97.10051125]
- 9 **Korppi M**. Non-specific host response markers in the differentiation between pneumococcal and viral pneumonia: what is the most accurate combination? *Pediatr Int* 2004; **46**: 545-550 [PMID: 15491381 DOI: 10.1111/j.1442-200X.2004.01947.x]
- 10 **Nohynek H**, Valkeila E, Leinonen M, Eskola J. Erythrocyte sedimentation rate, white blood cell count and serum C-reactive protein in assessing etiologic diagnosis of acute lower respiratory infections in children. *Pediatr Infect Dis J* 1995; **14**: 484-490 [PMID: 7667052]
- 11 **Virkki R**, Juven T, Rikalainen H, Svedström E, Mertsola J, Ruuskanen O. Differentiation of bacterial and viral pneumonia in children. *Thorax* 2002; **57**: 438-441 [PMID: 11978922 DOI: 10.1136/thorax.57.5.438]
- 12 **Almirall J**, Bolibar I, Toran P, Pera G, Boquet X, Balanzó X, Sauca G. Contribution of C-reactive protein to the diagnosis and assessment of severity of community-acquired pneumonia. *Chest* 2004; **125**: 1335-1342 [PMID: 15078743]
- 13 **Neuman MI**, Shah SS, Shapiro DJ, Hersh AL. Emergency department management of childhood pneumonia in the United States prior to publication of national guidelines. *Acad Emerg Med* 2013; **20**: 240-246 [PMID: 23517255 DOI: 10.1111/acem.12088]
- 14 **Florin TA**, French B, Zorc JJ, Alpern ER, Shah SS. Variation in emergency department diagnostic testing and disposition outcomes in pneumonia. *Pediatrics* 2013; **132**: 237-244 [PMID: 23878049 DOI: 10.1542/peds.2013-0179]
- 15 **Bradley JS**, Byington CL, Shah SS, Alverson B, Carter ER, Harrison C, Kaplan SL, Mace SE, McCracken GH, Moore MR, St Peter SD, Stockwell JA, Swanson JT. The management of community-acquired pneumonia in infants and children older than 3 months of age: clinical practice guidelines by the Pediatric Infectious Diseases Society and the Infectious Diseases Society of America. *Clin Infect Dis* 2011; **53**: e25-e76 [PMID: 21880587 DOI: 10.1093/cid/cir531]
- 16 **Pepys MB**, Hirschfield GM. C-reactive protein: a critical update. *J Clin Invest* 2003; **111**: 1805-1812 [PMID: 12813013 DOI: 10.1172/JCI18921]

P- Reviewer: Gao BL, Gumustas OG **S- Editor:** Gong XM
L- Editor: A **E- Editor:** Wu HL



Retrospective Study

Computed tomography-guided catheter drainage with urokinase and ozone in management of empyema

Bing Li, Chuan Liu, Yang Li, Han-Feng Yang, Yong Du, Chuan Zhang, Hou-Jun Zheng, Xiao-Xue Xu

Bing Li, Chuan Liu, Yang Li, Han-Feng Yang, Yong Du, Chuan Zhang, Hou-Jun Zheng, Xiao-Xue Xu, Sichuan Key Laboratory of Medical Imaging, Department of Radiology, Affiliated Hospital of North Sichuan Medical College, Nanchong 637000, Sichuan Province, China

Author contributions: Li B and Xu XX designed the study; Li B, Li Y, Zhang C, Liu C and Zheng HJ performed examinations and collected the data; Yang HF, Du Y and Xu XX contributed to the analysis and supervised the report; Li B and Liu C wrote this paper together; Li B, Liu C and Xu XX revised the paper.

Institutional review board statement: This study was approved by the Institutional Review Board of the Affiliated Hospital of North Sichuan Medical College, Department of Radiology - Sichuan Province, China.

Informed consent statement: All patients had given written consent for this study.

Conflict-of-interest statement: All authors have no conflict-of-interest.

Data sharing statement: Participants gave informed consent for data sharing, and no additional data are available.

Open-Access: This article is an open-access article which was selected by an in-house editor and fully peer-reviewed by external reviewers. It is distributed in accordance with the Creative Commons Attribution Non Commercial (CC BY-NC 4.0) license, which permits others to distribute, remix, adapt, build upon this work non-commercially, and license their derivative works on different terms, provided the original work is properly cited and the use is non-commercial. See: <http://creativecommons.org/licenses/by-nc/4.0/>

Manuscript source: Unsolicited manuscript

Correspondence to: Xiao-Xue Xu, MD, Sichuan Key Laboratory of Medical Imaging, Department of Radiology, Affiliated Hospital of North Sichuan Medical College, 63 Wenhua Road, Nanchong 637000, Sichuan Province, China. littleknownnc@qq.com
Fax: +86-817-2222856

Received: November 5, 2016

Peer-review started: November 8, 2016

First decision: January 16, 2017

Revised: January 31, 2017

Accepted: February 28, 2017

Article in press: March 2, 2017

Published online: April 28, 2017

Abstract

AIM

To retrospectively compare the outcomes of catheter drainage, urokinase and ozone in management of empyema.

METHODS

Retrospective study included 209 patients (111 males and 98 females; age range 19 to 72 years) who were diagnosed with empyema. The patients were divided into 3 groups based on the therapy instituted: catheter drainage only (group I); catheter drainage and urokinase (group II); catheter drainage, urokinase and ozone (group III). Drainage was considered successful if empyema was resolved with closure of cavity, clinical symptoms were resolved, and need for any further surgical procedure was avoided. Success rate, length of stay (LOS), need for further surgery and hospital costs were compared between the three groups using the Kruskal-Wallis nonparametric test, with $P < 0.05$ considered significant.

RESULTS

Of the 209 patients with empyema, all catheters were placed successfully under CT guidance. Sixty-three patients were treated with catheters alone (group I), 64 with catheters and urokinase (group II), and 82 with catheters, urokinase and ozone (group III). Group I, group II and group III had success rates of 62%, 83% and 95% respectively ($P < 0.05$). Group I and group

II had statistically longer LOS ($P < 0.05$) and higher hospital costs ($P < 0.05$) compared to group III. There were statistically significant differences between the three groups when comparing patients who converted into further surgery.

CONCLUSION

The combination of chest tube drainage, urokinase and ozone is a safe and effective therapeutic modality in thoracic empyema.

Key words: Computed tomography-guided; Catheter drainage; Urokinase; Ozone; Empyema

© **The Author(s) 2017.** Published by Baishideng Publishing Group Inc. All rights reserved.

Core tip: The use of ozone as an auxiliary antibacterial agent has achieved a relative good result. CT imaging-based guidance offers precise targeting, which is crucial to the success rates of therapeutic treatment. The combination of chest catheter drainage, urokinase and ozone is a safe and effective therapeutic treatment in thoracic empyema.

Li B, Liu C, Li Y, Yang HF, Du Y, Zhang C, Zheng HJ, Xu XX. Computed tomography-guided catheter drainage with urokinase and ozone in management of empyema. *World J Radiol* 2017; 9(4): 212-216 Available from: URL: <http://www.wjgnet.com/1949-8470/full/v9/i4/212.htm> DOI: <http://dx.doi.org/10.4329/wjr.v9.i4.212>

INTRODUCTION

Empyema refers to a collection of pus in the pleural cavity that can occur due to lung infection, trauma or surgery, with a mortality rate approaching 20% in adults^[1]. Treatment options in the management of empyema include antibiotic therapy, thoracentesis, drainage using intercostal catheter (ICC) with or without adjunctive fibrinolytic therapy, thoracoscopy, and open thoracotomy and decortications^[2].

Image-guided percutaneous catheter drainage (IGPCD) has been shown to be a safer and more effective alternative to ICC, because IGPCD provides direct demonstration of the fluid collection. Thus, considering the advantages of IGPCD, which has less pain and lower postoperative morbidity as well as fewer complications, it has become a reasonable procedure to address various stages of empyema. But there remains much controversy, especially in multiloculated pleural empyema^[3-6]. Some studies showed a higher rate of conversions to open decortications during the drainage procedure.

Intrapleural administration of fibrinolytic agents have been used both in pediatric and adult populations without subjection to surgical procedures^[7,8]. Ozone has bactericidal, antiviral and antifungal properties and is

used empirically for the treatment of chronic wounds, such as trophic ulcers, ischemic ulcers and diabetic wounds^[9]. The purpose of this study was to compare the outcomes of simple catheter drainage alone against its treatment with urokinase and the combined treatment of urokinase with ozone for the management of empyema. To our knowledge there has not been a similar study published to date.

MATERIALS AND METHODS

Approval was obtained from the Hospital Institutional Review Board to perform a retrospective review of patients between January 2012 and September 2016. The study included 209 patients (111 males, 98 females; mean age: 34.5 years, range: 19-72 years) who were diagnosed with empyema. All patients were at the fibropurulent stages of empyema. Patients who were at organizational stage were excluded. Of the 209 patients, 75 patients had postoperative empyema, and 134 had para-pneumonic empyema. Patients with tuberculosis or diabetes were excluded from this study.

The patients were divided into three groups based on the therapy instituted: Catheter drainage only (group I); catheter drainage with urokinase (group II); and catheter drainage with the combined treatment of urokinase and ozone (group III). CT scans were performed on all patients to define the extent, location, and number of locations.

All catheters were placed by CT-guided procedures and were performed under local anesthesia. By using the Seldinger technique, 8F to 14F pigtail catheters (total 240) were placed into the patients. The choice of catheter depended on the viscosity of the initial aspirate.

In group II, 50000 units of urokinase (Everbright Pharmaceutical Co., Ltd. Shengyang, China) diluted in 20.0 mL normal saline was injected into the pleural space *via* a pigtail catheter. The catheter was clamped for 4 h following urokinase injection. Then, the catheter was left unclamped for 20 min to allow for open drainage. In group III, in addition to urokinase, 10.0-20.0 mL (according to the size of the empyema cavity) oxygen-ozone gas mixture (ozone concentration 25 µg/mL) was administered through the catheter per day. The oxygen-ozone gas mixture was produced immediately prior to injection by using an ozone generator (Herrmann, Kleinwallstadt, Germany).

Drainage was considered successful when: (1) clinical symptoms were resolved; (2) the empyema cavity was closed; and/or (3) no further surgical procedure was needed. The patients were referred for further surgical management when: (1) the empyema failed to resolve; (2) if the follow-up imaging showed the development of a thick pleural peel with the absence of re-expansion of the lung; or (3) if the patients failed to show clinical improvement.

The difference of patient characteristics among the three groups were evaluated as well as the technical success of catheter placement and length of hospital

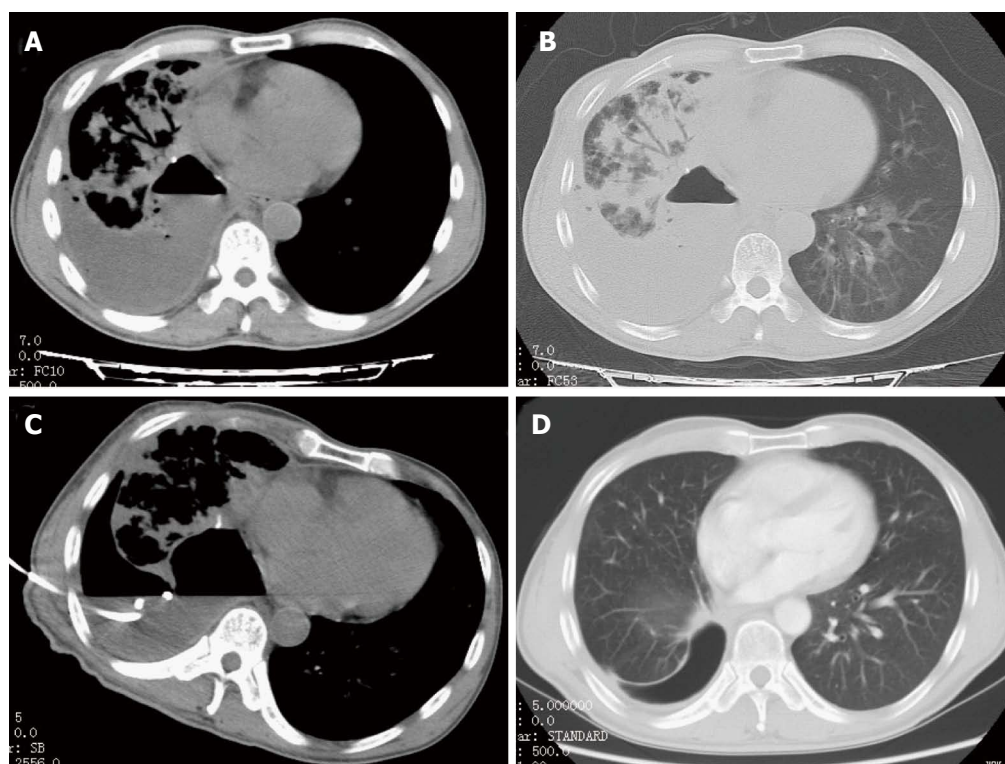


Figure 1 A 36-year-old male presented with fever and chest pain after right lung cancer resection. A and B: Unenhanced transverse CT shows empyema in right pleura with liquid-gas plane, and infections can be seen in right lung; C: Catheter was placed under CT-guidance; D: Empyema and infections were absorbed after 2 mo.

stay (LOS). Clinical details such as hospital stay, fever (morning oral temperature of $> 37.5^{\circ}\text{C}$), conversion into further surgery and average hospital charges were also recorded.

Statistical analysis was used to compare the three groups. Mean and standard deviation (SD) of variables from each group were obtained. Statistical differences among groups were calculated by using the Kruskal-Wallis non-parametric test, with a P value < 0.05 considered significant. Descriptive statistical analysis was also performed. All statistical analyses were conducted with SPSS software (version 19.0; IBM Corporation, Armonk, NY, United States).

RESULTS

For the 209 patients with empyema, all catheters were successfully placed under CT-guidance (Figure 1). Sixty-three (30.1%) patients were treated with catheters alone (group I), 64 (30.6%) with catheters and urokinase (group II), and 82 (39.3%) patients with catheters, urokinase and ozone (group III). All of the different variables from the three treatment groups are listed in Table 1. The three groups of patients were similar in mean age.

Although duration of symptoms, initial white blood cell count, and lymphocytes were different in three groups, the differences were not significant among the three groups. Groups I, II and III demonstrated a success rate of 62%, 83% and 95% respectively (P

< 0.05) (Table 2). Moreover, compared to group III, groups I and II had a statistically longer LOS ($P < 0.05$), longer duration of fever ($P < 0.05$) and higher hospital costs ($P < 0.05$). Hospital charges for groups I and II were statistically higher than for group III.

There were also statistically significant differences between the three groups when comparing patients who converted into further surgery. There were no statistically significant differences between groups I and II when comparing LOS, duration of fever, and hospital charges. Complications appeared in 4 patients who had a small amount of asymptomatic pneumothorax. No other complications were noted.

DISCUSSION

Many institutions are now using antibiotics with image-guided catheter drainage and fibrinolytics as first-line therapy^[10,11]. However, higher mortality rates (10%-15%) have been reported for drainage and irrigation of empyema even in early stages, whereas decortications in series including chronic cases have produced a mortality rate of 4%-13% only^[7]. The study by Maskell *et al.*^[12] showed that the intra-pleural instillation of fibrinolysis did not reduce mortality. They associated the failure of conservative treatment with loculated collections; fibrinolysis alone did not produce sufficient clearance of pleural fluid, possibly because the infected pleural fluid was viscous, lumpy, and resistant to tube drainage^[12].

Table 1 Comparison of preadmission variables among treatment groups

Variable	Group I	Group II	Group III
Patients, <i>n</i>	63	64	82
Average age in years	36.7 (14.3)	29.6 (12.6)	38.2 (19.1)
Duration of symptoms in days	12.4 (8.2)	14.8 (6.3)	13.7 (5.9)
Initial WBC, $\times 10^3$	16.4 (8.8)	16.9 (7.6)	17.1 (8.7)
Total lymphocytes, $\times 10^3$	13.2 (6.9)	14.4 (7.4)	14.7 (7.3)

Data are presented as mean (SD). WBC: White blood cell count.

To improve the effects of treatment, in the present study, catheter drainage was combined with urokinase and ozone treatment for empyema, and achieved an overall success rate of 95%. This was a relatively higher success rate than reported from previous studies, which had 72%-87% success rates in various smaller series^[11,13]. And, as a result, LOS and hospital costs were decreased significantly in our series.

Ozone therapy has been utilized and its benefits studied for more than a century now. Ozone, in the gaseous or aqueous phase, has been shown to be a powerful and reliable anti-microbial agent against bacteria, fungi, protozoa and viruses^[14]. It acts by inactivating bacteria, viruses, fungi, yeast and protozoa, which stimulates oxygen metabolism and the immune system^[14]. The oxidant potential of ozone induces the destruction of cell walls and the cytoplasmic membranes of bacteria and fungi by acting on glycoproteins, glycolipids and other amino acids, as well as inhibiting the key enzymes of the cells resulting in the increased membrane permeability and death^[14].

Because most patients have mixed infections, the use of antibiotics cannot reach adequate results. Also, the longtime use of antibiotics can lead to bacterial resistance^[15]. Even then, sometimes the causative organism may not be identified as the patients might have been partially treated before any specimen could be obtained for sensitivity testing. The use of ozone as an auxiliary antibacterial agent has achieved a relatively good result.

In the management of chronic wounds, such as trophic ulcers, ischemic ulcers and diabetic wounds, ozone has been used empirically as a clinical therapeutic agent^[16]. The beneficial effects of ozone on wound healing might be assumed to be due to ameliorated impaired dermal wounds healing or increased oxygen tension by ozone exposure in the wound area^[16].

Ozone exposure has been associated with activation of transcription factors that are required for regulation of the inflammatory response and the entire process of wound healing^[14]. In addition, ozone can be fully diffused into the abscess cavity, causing abscess wall dehydration. It can also split the inflammatory separations and expand drug solution distribution^[14]. So, the combined treatment with urokinase and ozone has a synergistic effect in the treatment for empyema.

The present study was performed under CT-

Table 2 Comparison of hospitalization and outcome variables among treatment groups

Variable	Group I	Group II	Group III
Technical success of catheter placement	100%	100%	100%
Success rate of management	62%	83%	95%
Length of hospital stay in days	21.0 (7.4)	19.4 (5.7)	12.8 (5.4)
Duration of fever in days	4.2 (3.0)	3.7 (2.6)	2.1 (1.8)
Converted into further surgery	8 (32%)	8 (25%)	5 (12%)
Average hospital charges in RMB¥	25057	19814	15871

Data are presented as mean (SD) or *n* (%).

guidance. CT imaging-based guidance offers precise targeting, which is crucial to the success rate of therapeutic treatment. By such procedures, a better therapeutic effect was obtained compared to the standard ICC treatment. The use of CT imaging was also advantageous when the presence of air resulted in poorly defined collection under ultrasound guidance or collection volume was small and adjacent to mediastinal structures. CT imaging can display the package of empyema clearly, and provide the best puncture path for the use of the catheter to separate the loculated empyema.

Complications of catheter drainage include hemorrhage from intercostal vessel injury, subcutaneous emphysema, pneumothorax and catheter-related pain^[1,3,6]. The patients in this study did not encounter any major complications nor did any of the patients in group II and III have any significant clinical bleeding.

The results presented in this study are retrospective and represent an institutional bias. A larger prospective randomized trial is warranted to further evaluate the role of urokinase with ozone in treating this important clinical scenario.

In conclusion, urokinase and ozone are a useful adjunct in the management of empyema. This technique used early in the exudative and fibropurulent stage of effusion, can decrease the rate of surgical interventions and the length of hospital stay, with minor associated morbidity. It can be concluded that the combined treatment of chest catheter drainage, urokinase and ozone is a safe and effective therapeutic procedure in thoracic empyema, rather than catheter drainage only.

COMMENTS

Background

In daily clinical work, the treatment of empyema is not satisfactory. And, according to recent reports, the mortality rates range from approximately 10% to 15% in early stages of drainage and irrigation of empyema. The authors sought to improve the effects of this treatment further. Ozone, in the gaseous or aqueous phase, has been shown to be a powerful and reliable antimicrobial agent against bacteria, fungi, protozoa and viruses.

Research frontiers

Now, many institutions are using antibiotics with image-guided catheter drainage and fibrinolytics as first-line therapy of empyema. And, to date, the application of

ozone in the treatment of empyema has been infrequently reported.

Innovations and breakthroughs

The use of ozone combined with urokinase in the management of empyema is unusual. The authors compared the outcomes of three groups and found that the combination of chest catheter drainage, urokinase and ozone is a safe and effective therapeutic treatment of thoracic empyema. In addition, CT imaging-based guidance offers precise targeting, which is crucial to the success rate of therapeutic treatment.

Applications

Urokinase and ozone are a useful adjunct in the management of empyema, and the patients in this study obtained a preferable outcome.

Terminology

IGPCD: Image-guided percutaneous catheter drainage; LOS: Length of hospital stay.

Peer-review

The article is good.

REFERENCES

- 1 **Chung JH**, Lee SH, Kim KT, Jung JS, Son HS, Sun K. Optimal timing of thoracoscopic drainage and decortication for empyema. *Ann Thorac Surg* 2014; **97**: 224-229 [PMID: 24119984 DOI: 10.1016/j.athoracsur.2013.08.039]
- 2 **Heffner JE**, Klein JS, Hampson C. Interventional management of pleural infections. *Chest* 2009; **136**: 1148-1159 [PMID: 19809058 DOI: 10.1378/chest.08-2956]
- 3 **Maier A**, Domej W, Anegg U, Woltsche M, Fell B, Pinter H, Smolle-Jüttner FM. Computed tomography or ultrasonically guided pigtail catheter drainage in multiloculated pleural empyema: a recommended procedure? *Respirology* 2000; **5**: 119-124 [PMID: 10894100 DOI: 10.1046/j.1440-1843.2000.00237.x]
- 4 **Thourani VH**, Brady KM, Mansour KA, Miller JJ, Lee RB. Evaluation of treatment modalities for thoracic empyema: a cost-effectiveness analysis. *Ann Thorac Surg* 1998; **66**: 1121-1127 [PMID: 9800792 DOI: 10.1016/S0003-4975(98)00767-X]
- 5 **Carr JA**, Fales C, Shaikh IA, Foulds K. Computed tomographic modeling before and after treatment for posttraumatic empyema: early decortication is superior to catheter drainage. *Ann Thorac Surg* 2011; **91**: 1723-1728 [PMID: 21529770 DOI: 10.1016/j.athoracsur.2011.02.046]
- 6 **Yu D**, Buchvald F, Brandt B, Nielsen KG. Seventeen-year study shows rise in parapneumonic effusion and empyema with higher treatment failure after chest tube drainage. *Acta Paediatr* 2014; **103**: 93-99 [PMID: 24117621 DOI: 10.1111/apa.12426]
- 7 **Gates RL**, Hogan M, Weinstein S, Arca MJ. Drainage, fibrinolytics, or surgery: a comparison of treatment options in pediatric empyema. *J Pediatr Surg* 2004; **39**: 1638-1642 [PMID: 15547825 DOI: 10.1016/j.jpedsurg.2004.07.015]
- 8 **Mahant S**, Cohen E, Weinstein M, Wadhwa A. Video-assisted thoracoscopic surgery vs chest drain with fibrinolytics for the treatment of pleural empyema in children: a systematic review of randomized controlled trials. *Arch Pediatr Adolesc Med* 2010; **164**: 201-203 [PMID: 20124153 DOI: 10.1001/archpediatrics.2009.271]
- 9 **Kim HS**, Noh SU, Han YW, Kim KM, Kang H, Kim HO, Park YM. Therapeutic effects of topical application of ozone on acute cutaneous wound healing. *J Korean Med Sci* 2009; **24**: 368-374 [PMID: 19543419 DOI: 10.3346/jkms.2009.24.3.368]
- 10 **Cremonesini D**, Thomson AH. How should we manage empyema: antibiotics alone, fibrinolytics, or primary video-assisted thoracoscopic surgery (VATS)? *Semin Respir Crit Care Med* 2007; **28**: 322-332 [PMID: 17562502 DOI: 10.1055/s-2007-981653]
- 11 **Misthos P**, Sepsas E, Konstantinou M, Athanassiadi K, Skottis I, Lioulas A. Early use of intrapleural fibrinolytics in the management of postpneumonic empyema. A prospective study. *Eur J Cardiothorac Surg* 2005; **28**: 599-603 [PMID: 16129614 DOI: 10.1016/j.ejcts.2005.07.005]
- 12 **Maskell NA**, Davies CW, Nunn AJ, Hedley EL, Gleeson FV, Miller R, Gabe R, Rees GL, Peto TE, Woodhead MA, Lane DJ, Darbyshire JH, Davies RJ. U.K. Controlled trial of intrapleural streptokinase for pleural infection. *N Engl J Med* 2005; **352**: 865-874 [PMID: 15745977 DOI: 10.1056/NEJMoa042473]
- 13 **Silverman SG**, Mueller PR, Saini S, Hahn PF, Simeone JF, Forman BH, Steiner E, Ferrucci JT. Thoracic empyema: management with image-guided catheter drainage. *Radiology* 1988; **169**: 5-9 [PMID: 3047789 DOI: 10.1148/radiology.169.1.3047789]
- 14 **Elvis AM**, Ekta JS. Ozone therapy: A clinical review. *J Nat Sci Biol Med* 2011; **2**: 66-70 [PMID: 22470237 DOI: 10.4103/0976-9668.82319]
- 15 **Kwon YS**. Pleural infection and empyema. *Tuberc Respir Dis (Seoul)* 2014; **76**: 160-162 [PMID: 24851128 DOI: 10.4046/trd.2014.76.4.160]
- 16 **Andreula C**. Ozone therapy. *Neuroradiology* 2011; **53** Suppl 1: S207-S209 [PMID: 21863433 DOI: 10.1007/s00234-011-0930-7]

P- Reviewer: Lassandro F, Martusevich AK, Markic D, Sartori S, Schoenhagen P **S- Editor:** Ji FF **L- Editor:** Filipodia **E- Editor:** Wu HL





Published by **Baishideng Publishing Group Inc**
7901 Stoneridge Drive, Suite 501, Pleasanton, CA 94588, USA
Telephone: +1-925-223-8242
Fax: +1-925-223-8243
E-mail: bpgoffice@wjgnet.com
Help Desk: <http://www.f6publishing.com/helpdesk>
<http://www.wjgnet.com>



World Journal of *Radiology*

World J Radiol 2017 May 28; 9(5): 217-252





Editorial Board

2014-2017

The *World Journal of Radiology* Editorial Board consists of 365 members, representing a team of worldwide experts in radiology. They are from 36 countries, including Afghanistan (1), Argentina (2), Australia (5), Austria (7), Belgium (2), Brazil (8), Canada (6), Chile (1), China (43), Croatia (1), Denmark (4), Egypt (6), France (5), Germany (22), Greece (10), India (12), Iran (6), Ireland (2), Israel (3), Italy (47), Japan (13), Netherlands (1), New Zealand (1), Pakistan (1), Poland (2), Portugal (1), Serbia (1), Singapore (3), Slovakia (1), South Korea (18), Spain (4), Sweden (2), Switzerland (4), Thailand (1), Turkey (26), United Kingdom (11), and United States (82).

EDITORS-IN-CHIEF

Kai U Juergens, *Bremen*
Edwin JR van Beek, *Edinburgh*
Thomas J Vogl, *Frankfurt*

GUEST EDITORIAL BOARD MEMBERS

Wing P Chan, *Taipei*
Chung-Huei Hsu, *Taipei*
Chin-Chang Huang, *Taipei*
Tsong-Long Hwang, *Taoyuan*
Jung-Lung Hsu, *Taipei*
Chia-Hung Kao, *Taichung*
Yu-Ting Kuo, *Tainan*
Hon-Man Liu, *Taipei*
Hui-Lung Liang, *Kaohsiung*
Chun Chung Lui, *Kaohsiung*
Sen-Wen Teng, *Taipei*
Yung-Liang (William) Wan, *Taoyuan*

MEMBERS OF THE EDITORIAL BOARD



Afghanistan

Takao Hiraki, *Okayama*



Argentina

Patricia Carrascosa, *Vicente Lopez*
Maria C Ziadi, *Rosario*



Australia

Lourens Bester, *Sydney*
Gemma A Figtree, *Sydney*



Austria

Herwig R Cerwenka, *Graz*
Gudrun M Feuchtnner, *Innsbruck*
Benjamin Henninger, *Innsbruck*
Rupert Lanzenberger, *Vienna*
Shu-Ren Li, *Vienna*
Veronika Schopf, *Vienna*
Tobias De Zordo, *Innsbruck*



Belgium

Steve Majerus, *Liege*
Kathelijne Peremans, *Merelbeke*



Brazil

Clerio F Azevedo, *Rio de Janeiro*
Patrícia P Alfredo, *São Paulo*
Eduardo FC Fleury, *São Paulo*
Edward Araujo Júnior, *São Paulo*
Wellington P Martins, *Ribeirao Preto*
Ricardo A Mesquita, *Belo Horizonte*
Vera MC Salemi, *São Paulo*
Claudia Szobot, *Porto Alegre*
Lilian YI Yamaga, *São Paulo*



Canada

Marie Arsalidou, *Toronto*
Otman A Basir, *Waterloo*

Tarik Zine Belhocine, *Toronto*
James Chow, *Toronto*
Tae K Kim, *Toronto*
Anastasia Oikonomou, *Toronto*



China

Hong-Wei Chen, *Wuxi*
Feng Chen, *Hangzhou*
Jian-Ping Chu, *Guangzhou*
Guo-Guang Fan, *Shenyang*
Bu-Lang Gao, *Shijiazhuang*
Qi-Yong Gong, *Chengdu*
Ying Han, *Beijing*
Xian-Li Lv, *Beijing*
Yi-Zhuo Li, *Guangzhou*
Xiang-Xi Meng, *Harbin*
Yun Peng, *Beijing*
Jun Shen, *Guangzhou*
Ze-Zhou Song, *Hangzhou*
Wai Kwong Tang, *Hong Kong*
Gang-Hua Tang, *Guangzhou*
Jie Tian, *Beijing*
Lu-Hua Wang, *Beijing*
Xiao-bing Wang, *Xi'an*
Yi-Gen Wu, *Nanjing*
Kai Wu, *Guangzhou*
Hui-Xiong Xu, *Shanghai*
Zuo-Zhang Yang, *Kunming*
Xiao-Dan Ye, *Shanghai*
David T Yew, *Hong Kong*
Ting-He Yu, *Chongqing*
Zheng Yuan, *Shanghai*
Min-Ming Zhang, *Hangzhou*
Yudong Zhang, *Nanjing*
Dong Zhang, *Chongqing*
Wen-Bin Zeng, *Changsha*

Yue-Qi Zhu, *Shanghai*



Croatia

Goran Kusec, *Osijek*



Denmark

Poul E Andersen, *Odense*

Lars J Petersen, *Aalborg*

Thomas Z Ramsøy, *Frederiksberg*

Morten Ziebell, *Copenhagen*



Egypt

Mohamed F Bazeed, *Mansoura*

Mohamed Abou El-Ghar, *Mansoura*

Reem HA Mohamed, *Cairo*

Mohamed R Nouh, *Alexandria*

Ahmed AKA Razek, *Mansoura*

Ashraf A Zytoon, *Shebin El-Koom*



France

Sabine F Bensamoun, *Compiègne*

Romarc Loffroy, *Dijon*

Stephanie Nougaret, *Montpellier*

Hassane Oudadesse, *Rennes*

Vincent Vinh-Hung, *Fort-de-France*



Germany

Henryk Barthel, *Leipzig*

Peter Bannas, *Hamburg*

Martin Beeres, *Frankfurt*

Ilja F Ciernik, *Dessau*

A Dimitrakopoulou-Strauss, *Heidelberg*

Peter A Fasching, *Erlangen*

Andreas G Schreyer, *Regensburg*

Philipp Heusch, *Duesseldorf*

Sonja M Kirchhoff, *Munich*

Sebastian Ley, *Munich*

Adel Maataoui, *Frankfurt am Main*

Stephan M Meckel, *Freiburg*

Hans W Muller, *Duesseldorf*

Kay Raum, *Berlin*

Dirk Rades, *Luebeck*

Marc-Ulrich Regier, *Hamburg*

Alexey Surov, *Halle*

Martin Walter, *Magdeburg*

Axel Wetter, *Essen*

Christoph Zilkens, *Düsseldorf*



Greece

Panagiotis Antoniou, *Thessaloniki*

Nikos Efthimiou, *Athens*

Dimitris Karnabatidis, *Patras*

George Latsios, *Athens*

Stylianios Megremis, *Iraklion*

Alexander D Rapidis, *Athens*

Kiki Theodorou, *Larissa*

Ioannis A Tsalafoutas, *Athens*

Evanthia E Tripoliti, *Ioannina*

Athina C Tsili, *Ioannina*



India

Ritesh Agarwal, *Chandigarh*

Chandan J Das, *New Delhi*

Prathamesh V Joshi, *Mumbai*

Naveen Kalra, *Chandigarh*

Chandrasekharan Kesavadas, *Trivandrum*

Jyoti Kumar, *New Delhi*

Atin Kumar, *New Delhi*

Kaushala P Mishra, *Allahabad*

Daya N Sharma, *New Delhi*

Binit Sureka, *New Delhi*

Sanjay Sharma, *New Delhi*

Raja R Yadav, *Allahabad*



Iran

Majid Assadi, *Bushehr*

SeyedReza Najafizadeh, *Tehran*

Mohammad Ali Oghabian, *Tehran*

Amir Reza Radmard, *Tehran*

Ramin Sadeghi, *Mashhad*

Hadi Rokni Yazdi, *Tehran*



Ireland

Tadhg Gleeson, *Wexford*

Frederik JAI Vernimmen, *Cork*



Israel

Dafna Ben Bashat, *Tel Aviv*

Amit Gefen, *Tel Aviv*

Tamar Sella, *Jerusalem*



Italy

Adriano Alippi, *Rome*

Dante Amelio, *Trento*

Michele Anzidei, *Rome*

Filippo F Angileri, *Messinas*

Stefano Arcangeli, *Rome*

Roberto Azzoni, *San Donato milanese*

Tommaso V Bartolotta, *Palermo*

Tommaso Bartalena, *Imola*

Livia Bernardin, *San Bonifacio*

Federico Boschi, *Verona*

Sergio Casciaro, *Lecce*

Emanuele Casciani, *Rome*

Musa M Can, *Napoli*

Alberto Cuocolo, *Napoli*

Michele Ferrara, *Coppito*

Mauro Feola, *Fossano*

Giampiero Francica, *Castel Volturno*

Luigi De Gennaro, *Rome*

Giulio Giovannetti, *Pisa*

Francesca Iacobellis, *Napoli*

Formato Invernizzi, *Monza Brianza*

Francesco Lassandro, *Naples*

Lorenzo Livi, *Florence*

Pier P Mainenti, *Napoli*

Laura Marzetti, *Chieti*

Giuseppe Malinverni, *Crescentino*

Enrica Milanese, *Turin*

Giovanni Morana, *Treviso*

Lorenzo Monti, *Milan*

Silvia D Morbelli, *Genoa*

Barbara Palumbo, *Perugia*

Cecilia Parazzini, *Milan*

Stefano Pergolizzi, *Messina*

Antonio Pinto, *Naples*

Camillo Porcaro, *Rome*

Carlo C Quattrocchi, *Rome*

Alberto Rebonato, *Perugia*

Giuseppe Rizzo, *Rome*

Roberto De Rosa, *Naples*

Domenico Rubello, *Rovigo*

Andrea Salvati, *Bari*

Sergio Sartori, *Ferrara*

Luca M Sconfienza, *Milano*

Giovanni Storto, *Rionero*

Nicola Sverzellati, *Parma*

Alberto S Tagliafico, *Genova*

Nicola Troisi, *Florence*



Japan

Yasuhiko Hori, *Chiba*

Hidetoshi Ikeda, *Koriyama*

Masahito Kawabori, *Sapporo*

Tamotsu Kamishima, *Sapporo*

Hiro Kiyosue, *Yufu*

Yasunori Minami, *Osaka-sayama*

Yasuhiro Morimoto, *Kitakyushu*

Satoru Murata, *Tokyo*

Shigeki Nagamachi, *Miyazaki*

Hiroshi Onishi, *Yamanashi*

Morio Sato, *Wakayama Shi*

Yoshito Tsushima, *Maebashi*

Masahiro Yanagawa, *Suita*



Netherlands

Willem Jan van Rooij, *Tilburg*



New Zealand

W Howell Round, *Hamilton*



Pakistan

Wazir Muhammad, *Abbottabad*



Poland

Maciej S Baglaj, *Wroclaw*

Piotr Czauderna, *Gdansk*



Portugal

Joao Manuel RS Tavares, *Porto*



Serbia

Olivera Ciraj-Bjelac, *Belgrade*



Singapore

Gopinathan Anil, *Singapore*

Terence KB Teo, *Singapore*

Cher Heng Tan, *Singapore*



Slovakia

Stefan Sivak, *Martin*



South Korea

Ki Seok Choo, *Busan*

Seung Hong Choi, *Seoul*

Dae-Seob Choi, *Jinju*

Hong-Seok Jang, *Seoul*

Yong Jeong, *Daejeon*

Chan Kyo Kim, *Seoul*

Se Hyung Kim, *Seoul*

Joong-Seok Kim, *Seoul*

Sang Eun Kim, *Seongnam*

Sung Joon Kwon, *Seoul*

Jeong Min Lee, *Seoul*

In Sook Lee, *Busan*

Noh Park, *Goyang*

Chang Min Park, *Seoul*

Sung Bin Park, *Seoul*

Deuk Jae Sung, *Seoul*

Choongsoo Shin, *Seoul*

Kwon-Ha Yoon, *Iksan*



Spain

Miguel A De Gregorio, *Zaragoza*

Antonio Luna, *Jaén*

Enrique Marco de Lucas, *Santander*

Fernando Ruiz Santiago, *Granada*



Sweden

Dmitry Grishenkov, *Stockholm*

Tie-Qiang Li, *Stockholm*



Switzerland

Nicolau Beckmann, *Basel*

Christian Boy, *Bern*

Giorgio Treglia, *Bellinzona*

Stephan Ulmer, *Kiel*



Thailand

Sirianong Namwongprom, *Chiang Mai*



Turkey

Kubilay Aydin, *Istanbul*

Ramazan Akdemir, *Sakarya*

Serhat Avcu, *Ankara*

Ayşe Aralasmak, *Istanbul*

Oktay Algin, *Ankara*

Nevbahar Akcar, *Meselik*

Bilal Battal, *Ankara*

Zulkif Bozgeyik, *Elazig*

Nazan Ciledag, *Aakara*

Fuldem Y Donmez, *Ankara*

Gulgun Engin, *Istanbul*

Ahmet Y Goktay, *Izmir*

Oguzhan G Gumustas, *Bursa*

Kaan Gunduz, *Ankara*

Pelin Ozcan Kara, *Mersin*

Kivanc Kamburoglu, *Ankara*

Ozgur Kilickesmez, *Istanbul*

Furuzan Numan, *Istanbul*

Cem Onal, *Adana*

Ozgur Oztekin, *Izmir*

Seda Ozbek (Boruban), *Konya*

Selda Sarikaya, *Zonguldak*

Figen Taser, *Kutahya*

Baran Tokar, *Eskisehir*

Ender Uysal, *Istanbul*

Ensar Yekeler, *Istanbul*



United Kingdom

Indran Davagnanam, *London*

M DC Valdés Hernández, *Edinburgh*

Alan Jackson, *Manchester*

Suneil Jain, *Belfast*

Long R Jiao, *London*

Miltiadis Krokidis, *Cambridge*

Pradesh Kumar, *Liverpool*

Peter D Kuzmich, *Derby*

Georgios Plataniotis, *Brighton*

Vanessa Sluming, *Liverpool*



United States

Garima Agrawal, *Saint Louis*

James R Brasic, *Baltimore*

Rajendra D Badgaiyan, *Buffalo*

Ulas Bagci, *Bethesda*

Anat Biegon, *Stony Brook*

Ramon Casanova, *Winston Salem*

Wenli Cai, *Boston*

Zheng Chang, *Durham*

Corey J Chakarun, *Long Beach*

Kai Chen, *Los Angeles*

Hyun-Soon Chong, *Chicago*

Marco Cura, *Dallas*

Ravi R Desai, *Bensalem*

Delia DeBuc, *Miami*

Carlo N De Cecco, *Charleston*

Timm-Michael L Dickfeld, *Baltimore*

Subba R Digumarthy, *Boston*

Huy M Do, *Stanford*

Todd A Faasse, *Grand Rapids*

Salomao Faintuch, *Boston*

Girish M Fatterpekar, *New York*

Dhakshinamoorthy Ganesan, *Houston*

Robert J Griffin, *Little Rock*

Andrew J Gunn, *Boston*

Sandeep S Hedgire, *Boston*

Timothy J Hoffman, *Columbia*

Mai-Lan Ho, *San Francisco*

Juebin Huang, *Jackson*

Abid Irshad, *Charleston*

Matilde Inglese, *New York*

El-Sayed H Ibrahim, *Jacksonville*

Paul R Julsrud, *Rochester*

Pamela T Johnson, *Baltimore*

Ming-Hung Kao, *Tempe*

Sunil Krishnan, *Houston*

Richard A Komoroski, *Cincinnati*

Sandi A Kwee, *Honolulu*

King Kim, *Ft. Lauderdale*

Guozheng Liu, *Worcester*

Yiyan Liu, *Newark*

Venkatesh Mani, *New York*

Lian-Sheng Ma, *Pleasanton*

Rachna Madan, *Boston*

Zeyad A Metwalli, *Houston*

Yilong Ma, *Manhasset*

Hui Mao, *Atlanta*

Feroze B Mohamed, *Philadelphia*

Gul Moonis, *Boston*

John L Noshier, *New Brunswick*

Rahmi Oklu, *Boston*

Aytekun Oto, *Chicago*

Bishnuhari Paudyal, *Philadelphia*

Rajul Pandya, *Youngstown*

Chong-Xian Pan, *Sacramento*

Jay J Pillai, *Baltimore*

Neal Prakash, *Duarte*

Reza Rahbar, *Boston*

Ali S Raja, *Boston*

Gustavo J Rodriguez, *El Paso*

David J Sahn, *Portland*

Steven Schild, *Scottsdale*

Ali R Sepahdari, *Los Angeles*

Li Shen, *Indianapolis*

JP Sheehan, *Charlottesville*

Atul B Shinagare, *Boston*

Sarabjeet Singh, *Boston*

Charles J Smith, *Columbia*

Kenji Suzuki, *Chicago*

Monvadi Srichai-Parsia, *Washington*

Sree H Tirumani, *Boston*

Hebert A Vargas, *New York*

Sachit Verma, *Philadelphia*

Yoichi Watanabe, *Minneapolis*

Li Wang, *Chapel Hill*

Carol C Wu, *Boston*

Shoujun Xu, *Houston*

Min Yao, *Cleveland*

Xiaofeng Yang, *Atlanta*

Qingbao Yu, *Albuquerque*

Aifeng Zhang, *Chicago*

Chao Zhou, *Bethlehem*

Hongming Zhuang, *Philadelphia*

**MINIREVIEWS**

- 217 Diffusion weighted imaging for the detection and evaluation of cholesteatoma
Henninger B, Kremser C

ORIGINAL ARTICLE**Basic Study**

- 223 Correlation of lumbar lateral recess stenosis in magnetic resonance imaging and clinical symptoms
Splettstößer A, Khan MF, Zimmermann B, Vogl TJ, Ackermann H, Middendorp M, Maataoui A
- 230 Cystic lesions of peripheral nerves: Are we missing the diagnosis of the intraneural ganglion cyst?
Panwar J, Mathew A, Thomas BP

Retrospective Study

- 245 Transarterial chemoembolization using 40 µm drug eluting beads for hepatocellular carcinoma
Greco G, Cascella T, Facciorusso A, Nani R, Lanocita R, Morosi C, Vaiani M, Calareso G, Greco FG, Ragnanese A, Bongini MA, Marchianò AV, Mazzaferro V, Spreafico C

ABOUT COVER

Editorial Board Member of *World Journal of Radiology*, Mohamed F Bazeed, MSc, PhD, Associate Professor, Department of Radiology, Faculty of Medicine, Mansoura University, Mansoura 35111, Egypt

AIM AND SCOPE

World Journal of Radiology (*World J Radiol*, *WJR*, online ISSN 1949-8470, DOI: 10.4329) is a peer-reviewed open access academic journal that aims to guide clinical practice and improve diagnostic and therapeutic skills of clinicians.

WJR covers topics concerning diagnostic radiology, radiation oncology, radiologic physics, neuroradiology, nuclear radiology, pediatric radiology, vascular/interventional radiology, medical imaging achieved by various modalities and related methods analysis. The current columns of *WJR* include editorial, frontier, diagnostic advances, therapeutics advances, field of vision, mini-reviews, review, topic highlight, medical ethics, original articles, case report, clinical case conference (clinicopathological conference), and autobiography.

We encourage authors to submit their manuscripts to *WJR*. We will give priority to manuscripts that are supported by major national and international foundations and those that are of great basic and clinical significance.

INDEXING/ABSTRACTING

World Journal of Radiology is now indexed in PubMed, PubMed Central, and Emerging Sources Citation Index (Web of Science).

FLYLEAF

I-III Editorial Board

EDITORS FOR THIS ISSUE

Responsible Assistant Editor: *Xiang Li*
Responsible Electronic Editor: *Dan Li*
Proofing Editor-in-Chief: *Lian-Sheng Ma*

Responsible Science Editor: *Jin-Xin Kong*
Proofing Editorial Office Director: *Xiu-Xia Song*

NAME OF JOURNAL
World Journal of Radiology

ISSN
ISSN 1949-8470 (online)

LAUNCH DATE
January 31, 2009

FREQUENCY
Monthly

EDITORS-IN-CHIEF
Kai U Juergens, MD, Associate Professor, MRT und PET/CT, Nuklearmedizin Bremen Mitte, ZEMODI - Zentrum für morphologische und molekulare Diagnostik, Bremen 28177, Germany

Edwin JR van Beek, MD, PhD, Professor, Clinical Research Imaging Centre and Department of Medical Radiology, University of Edinburgh, Edinburgh EH16 4TJ, United Kingdom

Thomas J Vogl, MD, Professor, Reader in Health Technology Assessment, Department of Diagnostic and Interventional Radiology, Johann Wolfgang Goethe University of Frankfurt, Frankfurt 60590,

Germany

EDITORIAL BOARD MEMBERS
All editorial board members resources online at <http://www.wjnet.com/1949-8470/editorialboard.htm>

EDITORIAL OFFICE
Xiu-Xia Song, Director
World Journal of Radiology
Baishideng Publishing Group Inc
7901 Stoneridge Drive, Suite 501, Pleasanton, CA 94588, USA
Telephone: +1-925-2238242
Fax: +1-925-2238243
E-mail: editorialoffice@wjnet.com
Help Desk: <http://www.f6publishing.com/helpdesk>
<http://www.wjnet.com>

PUBLISHER
Baishideng Publishing Group Inc
7901 Stoneridge Drive, Suite 501, Pleasanton, CA 94588, USA
Telephone: +1-925-2238242
Fax: +1-925-2238243
E-mail: bpgoffice@wjnet.com
Help Desk: <http://www.f6publishing.com/helpdesk>
<http://www.wjnet.com>

PUBLICATION DATE
May 28, 2017

COPYRIGHT
© 2017 Baishideng Publishing Group Inc. Articles published by this Open-Access journal are distributed under the terms of the Creative Commons Attribution Non-commercial License, which permits use, distribution, and reproduction in any medium, provided the original work is properly cited, the use is non commercial and is otherwise in compliance with the license.

SPECIAL STATEMENT
All articles published in journals owned by the Baishideng Publishing Group (BPG) represent the views and opinions of their authors, and not the views, opinions or policies of the BPG, except where otherwise explicitly indicated.

INSTRUCTIONS TO AUTHORS
<http://www.wjnet.com/bpg/gerinfo/204>

ONLINE SUBMISSION
<http://www.f6publishing.com>

Diffusion weighted imaging for the detection and evaluation of cholesteatoma

Benjamin Henninger, Christian Kremser

Benjamin Henninger, Christian Kremser, Department of Radiology, Medical University of Innsbruck, 6020 Innsbruck, Austria

Author contributions: Henninger B wrote the paper; Kremser C performed proofreading and wrote the physical part.

Conflict-of-interest statement: Authors declare no conflict of interests for this article.

Open-Access: This article is an open-access article which was selected by an in-house editor and fully peer-reviewed by external reviewers. It is distributed in accordance with the Creative Commons Attribution Non Commercial (CC BY-NC 4.0) license, which permits others to distribute, remix, adapt, build upon this work non-commercially, and license their derivative works on different terms, provided the original work is properly cited and the use is non-commercial. See: <http://creativecommons.org/licenses/by-nc/4.0/>

Manuscript source: Invited manuscript

Correspondence to: Dr. Benjamin Henninger, PD, Department of Radiology, Medical University of Innsbruck, Anichstraße 35, 6020 Innsbruck, Austria. benjamin.henninger@i-med.ac.at
Telephone: +43-512-50480914
Fax: +43-512-50422758

Received: October 28, 2016

Peer-review started: November 2, 2016

First decision: February 15, 2017

Revised: February 23, 2017

Accepted: March 12, 2017

Article in press: March 13, 2017

Published online: May 28, 2017

Abstract

Cholesteatoma is a collection of keratinous debris and stratified squamous epithelium. It is trapped in the middle ear and can lead to bony erosion. The disease is treated surgically often followed by a second-look procedure to check for residual tissue or

recurrence. Cholesteatoma has specific signal-intensity characteristics on magnetic resonance imaging with very high signal intensity on diffusion weighted imaging (DWI). Various DWI techniques exist: Echo-planar imaging (EPI)-based and non-EPI-based techniques as well as new approaches like multi-shot EPI DWI. This article summarizes all techniques, discusses the significance in detecting cholesteatoma and mentions actual studies. Further recommendations for daily clinical practise are provided.

Key words: Cholesteatoma; Diffusion weighted imaging; Computed tomography; Magnetic resonance imaging; Echo-planar imaging; Non-echo-planar imaging

© **The Author(s) 2017.** Published by Baishideng Publishing Group Inc. All rights reserved.

Core tip: Imaging cholesteatoma is either performed by computed tomography (CT) or by magnetic resonance imaging (MRI). CT is the method of choice for detection and for assessing exact location and extent. MRI with diffusion weighted imaging (DWI) is a powerful tool for the detection of local recurrence or residual cholesteatoma. Many DWI-techniques are available today; this review article gives an overview of the different sequences and the diagnostic procedure when using DWI with a clinical focus.

Henninger B, Kremser C. Diffusion weighted imaging for the detection and evaluation of cholesteatoma. *World J Radiol* 2017; 9(5): 217-222 Available from: URL: <http://www.wjgnet.com/1949-8470/full/v9/i5/217.htm> DOI: <http://dx.doi.org/10.4329/wjr.v9.i5.217>

INTRODUCTION

Cholesteatomas are defined as enlarging collections of keratinous debris within a sack of stratified squamous

epithelium trapped in the middle ear^[1]. It is a common inflammatory disease that grows progressively as the debris increases. It is seen as a kind of chronic otitis media with cell proliferation due to repeated inflammation or for congenital reason. Clinically the complications of cholesteatoma are related to bony erosion and destruction which is thought to be related to mechanical pressure. Even small cholesteatoma can cause ossicular chain erosions with the threat of a conductive hearing loss. The diagnosis is usually made on clinical features.

Cholesteatomas of the middle ear are managed by surgery, generally with complete excision of the lesion with tympanoplasty or radical or modified radical mastoidectomy. This is often followed by a second-look procedure performed to check for residual or recurrent disease. This second-look is conducted 6-18 mo after the initial operation because most recur within the first 2 postoperative years, with 60% occurring during the first year after surgery^[2,3]. The second-look surgery is mainly to assess residual or recurrent disease because both cannot adequately be diagnosed solely by clinical examination^[4].

COMPUTED TOMOGRAPHY

Computed tomography (CT) of the temporal bone is widely accepted to detect or confirm cholesteatoma and to assess the extension, the exact location and possible complications of the disease. Therefore it is mandatory for the initial preoperative description of the extent of cholesteatoma and for correct surgical planning. CT is further recommended for the evaluation of recurrent disease but it is not reliable when the postoperative, formed cavity is completely filled with a soft-tissue mass or partially filled with nonspecific imaging abnormalities^[5,6]. This can be caused by recurrent cholesteatoma, granulation or fibrous tissue. This differential diagnosis is important since recurrent cholesteatoma needs middle ear surgery but there is no need for surgery if only granulation tissue is detected.

MAGNETIC RESONANCE IMAGING

Magnetic resonance imaging (MRI) has several advantages over CT in detecting recurrent or residual disease: Beside delayed contrast-enhanced T1-weighted spin-echo (SE) imaging^[7], diffusion weighted imaging (DWI) shows promising results in the data published so far^[8-12]. Contrast-enhanced MRI can discriminate between the non-enhancing cholesteatoma and other contrast-enhancing findings, *e.g.*, inflammation, scar or granulation tissue^[7,13]. DWI is more practical with a shorter examination time than delayed contrast material-enhanced imaging; there is also no need for contrast injection. The technique relies on the principles of the Brownian motion of water molecules^[14]. Cholesteatomas appear hyperintense on DWI obtained with b-factors of 800 or 1000 s/mm² where the b-factor is a measure of the strength of the respective

diffusion weighting. This visual characteristic is similar to a histologically identical lesion, the epidermoid cyst^[15] - granulation tissue, fibrous tissue, cholesterol granuloma or serous fluid, on the other hand, have low signal intensity on DWI (at a b-factor of 800 s/mm²). Visual assessment of DWI images obtained with a b-factor of 800 s/mm² without calculation of the apparent diffusion coefficient (ADC) is sufficient for the respective diagnostic analysis^[9,12]. The reason for the high signal intensity is assumed to be due to a T2 shine-through effect or due to the restricted molecular diffusion of cholesteatoma. The T2 shine-through effect is observed in lesions with a prolonged relaxation time. Nevertheless, the real reason for the increased signal intensity on DWI is still unknown and under discussion in literature. DWI is a valuable tool to prevent unnecessary second-look surgeries in patients suspected for cholesteatomas and is therefore a reliable alternative to CT^[16]. However, numerous artefacts can be generated during the acquisition of DWI, *as, e.g.*, susceptibility artefacts, motion artefacts, ghosting artefacts and eddy current artefacts with the risk of false positive results^[17].

So far a variety of different DWI-techniques has been used, which basically can be divided into echo-planar imaging (EPI)-based and non-EPI-based techniques. The choice of the actually used technique is thereby mainly influenced by the fact that imaging has to be performed near the skull base where problems due to different artefacts (*e.g.*, motion, field inhomogeneities) can occur.

In addition DWI MRI is extremely useful for the assessment of possible complications such as erosion of the semicircular canal or invasion of the membranous labyrinth or the middle cranial fossa and to assess abscess formations^[17].

EPI-DWI

Single-shot (SS) EPI-DWI can be seen as a widely available standard DWI technique. It is relatively insensitive to motion but prone to susceptibility artefacts, chemical shift and geometric distortion^[14]. These artefacts can mask areas of restricted diffusion in a cholesteatoma^[18]. A further limitation of EPI-DWI is its low spatial resolution and relatively thick sections. The size limit to detect a cholesteatoma with EPI-DWI is approximately 5 mm^[9,11].

Non-EPI-DWI

Turbo spin-echo (TSE)-based DWI is a spin-echo based SS or multi-shot (MS) technique with longer echo time and a higher signal-to-noise ratio than SS EPI-DWI. The sequence is known to lack significant image distortions and it does not show the susceptibility artefacts that are observed with standard EPI-DWI. Therefore a better spatial resolution in the middle ear is possible and it permits fast multiplanar imaging^[19]. Furthermore thinner slices can be obtained than with EPI-sequences. This so called non-EPI sequence has therefore hardly any false-positive findings. False-negative findings are mostly a consequence of motion or empty retraction pockets^[20].

The signal intensity of other postoperative findings has been reported much lower than that of residual and/or recurrent cholesteatoma^[19,21].

In a study by Geoffroy *et al.*^[22] non-EPI DWI was reliable to diagnose recurrent cholesteatoma also in children with a high sensitivity (87%) and specificity (71%). Nevertheless, they concluded that follow-up must be prolonged because small recurrence less than 5 mm may be missed.

The TSE-DWI can be combined with half-Fourier acquisition single-shot turbo spin-echo (HASTE), a single-shot technique with excellent motion insensitivity. HASTE is also less prone to susceptibility artefacts and geometric distortion than the EPI-Sequence^[23,24]. The sensitivity and specificity of non-EPI DWI in depicting residual or recurrent cholesteatoma is very high, in literature it is between 90%-100% and also postulated higher than with EPI DWI^[19-21,23-25]. The study by De Foer *et al.*^[25] prospectively evaluated a SS TSE-DWI sequence in detecting cholesteatoma with evaluation of the size of the middle ear cholesteatoma. They found 21 middle ear cholesteatomas at surgery with a size between 2 mm and 19 mm and 19/21 could be detected with DWI. Years later another study by De Foer *et al.*^[26] compared non-EPI DWI, delayed gadolinium-enhanced T1-weighted MRI and the combination of both techniques in the evaluation of patients with cholesteatoma. Sensitivity and specificity was 56.7%/67.6% with the delayed gadolinium-enhanced T1-weighted images, 82.6%/87.2% with the non-EPI DWI images and 84.2%/88.2% for the combination of both kinds of images. They concluded that for the detection of cholesteatoma non-EPI DWI can be used alone.

Non-EPI sequences with periodically rotated overlapping parallel lines with enhanced reconstruction (PROPELLER, GE Medical Systems, Milwaukee, Wisconsin/BLADE, Siemens Medical Solutions, Erlangen, Germany) have been reported as useful in avoiding geometric distortions. The k-space data are acquired in the form of rotating sections (blades). The resulting oversampling of the central k-space leads to an improved signal-to-noise ratio (SNR) and to the reduction of motion and susceptibility artefacts^[23,27,28]. MS TSE-based DWI increases sensitivity, specificity and diagnostic accuracy compared to conventional single-shot EPI DWI^[29].

In a systematic review of DWI in the assessment of postoperative cholesteatoma by Jindal *et al.*^[30] a combined sensitivity of 91.4% and positive predictive value of 97.3% was calculated for the non-EPI sequences. Non-EPI also showed a negative predictive value of 85% which means that it is very useful in avoiding second-look operations in healthy ears^[30].

MS EPI DWI

Recently it has been shown that an improved, MS EPI approach can provide high-resolution DWI with reduced geometric distortions, however, with longer imaging time^[31-33]. Readout-segmented echo-planar (RESOLVE) DWI is a new approach for obtaining DWI images with

high quality delivering sharp images at high spatial resolution and reduced slice thickness. Therefore it is possible to detect even small cholesteatomas. It uses the same diffusion preparation as SS EPI. By dividing the k-space trajectory into multiple segments in the phase encoding direction TE can be reduced to increase the quality of the acquired images. Further RESOLVE DWI is largely free of distortions, susceptibility and T2* blurring artefacts. As we mentioned before non-EPI seems to be superior to the EPI techniques in diagnosing recurrent or residual cholesteatoma, however, at the time of the systematic review by Jindal *et al.*^[30] the RESOLVE technique was not yet available. To date there are only few studies that evaluated this new approach, however, with promising results^[31]. In our daily clinical routine RESOLVE has been proven as a robust and reliable approach for the detection of recurrent cholesteatoma.

DWI FOR THE DAILY CLINICAL PRACTISE

DWI is a powerful tool that can replace CT and delayed gadolinium enhanced T1-weighted sequences. At our department and others contrast agent is not used anymore^[26]. The best approach is to use non-EPI sequences or (if available) newer EPI-techniques as RESOLVE which provides high resolution and allows thinner slice-thickness. Single-shot EPI-DWI techniques are not recommended as they can provide false positive results due to artefacts. Further anatomical sequences (T1- and T2-weighted) should be added in coronal and/or axial orientation to better localize suspected lesions. Our department uses an axial T1 and T2 TSE sequence and a coronal T2 TSE sequence with fat-saturation. The fat saturation can help to detect fatty content of any detected lesion or structure. These sequences can also help to differentiate, *e.g.*, the characteristic T1 hyperintensity of cholesterol granuloma. Dremmen *et al.*^[20] suggested to use conventional sequences to decrease the risk of misdiagnosis because transplanted fat within a postoperative cavity may show increased signal on DWI. Slice-thickness for the DWI (and its corresponding anatomical T1- or T2-weighted sequence) should not exceed 3 mm. If available, coloured image-fusion of DWI and anatomic sequences helps to better demonstrate the findings to patients or clinicians. On the basis of the findings by Steens *et al.*^[34] repeated follow-up DWI after surgery of cholesteatoma is recommended. Their study showed an evidence of cholesteatoma in 31% of the patients on repeated follow-up DWI.

For the interpretation of DWI the reporting radiologist should look for hyperintense lesions on high b-values (800 or 1000 s/mm²), ADC-values should not be taken into the diagnostic decision as cholesteatomas can be hyperintense in ADC because of the T2 shine-through effect. If a lesion is detected the next step should be an anatomical correlation and signal interpretation on T1- and T2-contrast. This minimizes false positive results.

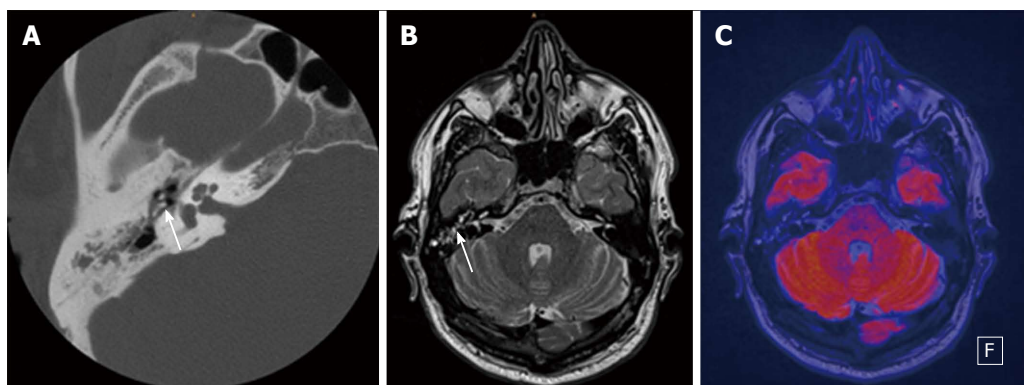


Figure 1 Thirty-nine-year-old male patient with clinically suspected cholesteatoma in the right middle ear. A: Axial CT of the temporal bone with soft-tissue mass in the tympanic space adjacent to malleolus and incus (white arrow); B: Axial T2-weighted MR depicts fluid-like signal in the tympanic space (white arrow); C: Fused axial T2-weighted image and axial EPI DWI RESOLVE without any sign of restriction. Therefore there is no evidence of cholesteatoma; the findings are consistent with chronic otitis media. CT: Computed tomography; DWI: Diffusion weighted imaging; EPI: Echo-planar imaging; RESOLVE: Readout-segmented echo-planar.

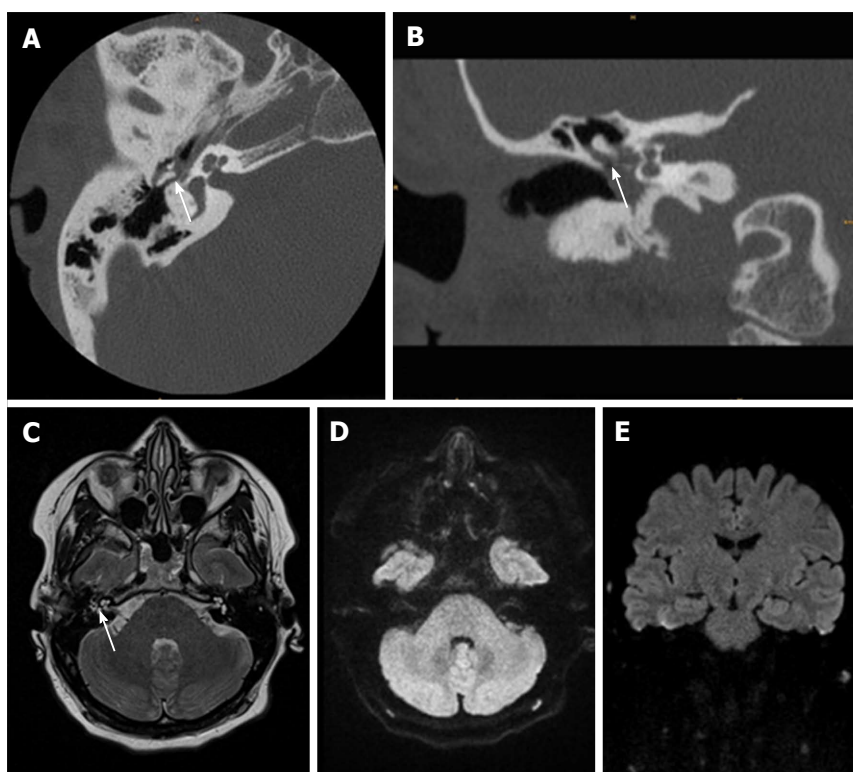


Figure 2 Thirty-one-year-old female after surgery for cholesteatoma. A, B: CT show a soft-tissue mass in the tympanic space adjacent to malleolus and scutum with suspected bony erosion (white arrow); C-E: Axial T2 weighted image shows fluid-like signal (white arrow) that has no restriction in EPI DWI RESOLVE (axial in D and coronal in E). There was no sign of recurrent cholesteatoma on follow-up surgery. CT: Computed tomography; DWI: Diffusion weighted imaging; EPI: Echo-planar imaging; RESOLVE: Readout-segmented echo-planar.

Clinical examples are provided in Figures 1-3.

CONCLUSION

In conclusion, MRI with DWI can prevent unnecessary revision surgery in patients who are suspected of having

recurrent or residual disease. Many techniques exist but non-EPI DWI and new MS EPI approaches (RESOLVE) are recommended to avoid false positive results due to different artefacts. The interpretation is simple but additional anatomical sequences are needed for exact localisation and differential diagnosis.

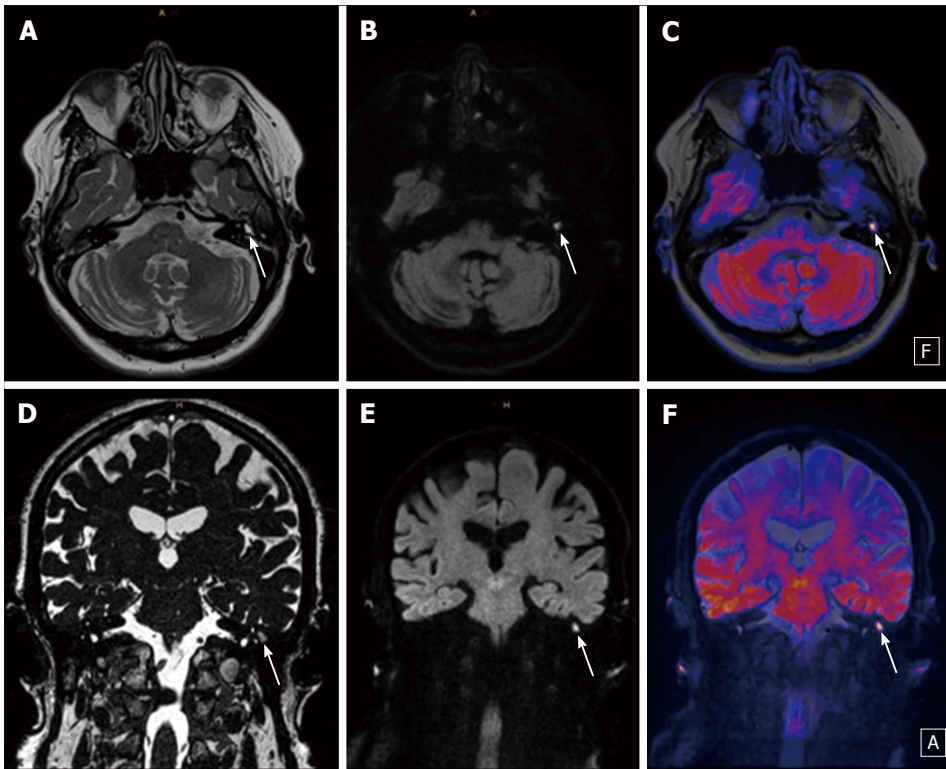


Figure 3 Twenty-three-year-old male patient with a typical cholesteatoma detected with diffusion weighted imaging. A, D: T2 weighted images (A and D) show a fluid-like mass in the left middle ear (white arrow); B, C, E, F: EPI DWI RESOLVE (B and E) depict a hyperintense signal (white arrow) consistent with restriction due to a small cholesteatoma that is better demonstrated on fused images (C and F). DWI: Diffusion weighted imaging; EPI: Echo-planar imaging; RESOLVE: Readout-segmented echo-planar.

REFERENCES

- Swartz JD. Cholesteatomas of the middle ear. Diagnosis, etiology, and complications. *Radiol Clin North Am* 1984; **22**: 15-35 [PMID: 6709867]
- Shelton C, Sheehy JL. Tympanoplasty: review of 400 staged cases. *Laryngoscope* 1990; **100**: 679-681 [PMID: 2362526 DOI: 10.1288/00005537-199007000-00001]
- Gyo K, Sasaki Y, Hinohira Y, Yanagihara N. Residue of middle ear cholesteatoma after intact canal wall tympanoplasty: surgical findings at one year. *Ann Otol Rhinol Laryngol* 1996; **105**: 615-619 [PMID: 8712631]
- Yigiter AC, Pinar E, Imre A, Erdogan N. Value of Echo-Planar Diffusion-Weighted Magnetic Resonance Imaging for Detecting Tympanomastoid Cholesteatoma. *J Int Adv Otol* 2015; **11**: 53-57 [PMID: 26223719 DOI: 10.5152/iao.2015.447]
- Williams MT, Ayache D. Imaging of the postoperative middle ear. *Eur Radiol* 2004; **14**: 482-495 [PMID: 14749948 DOI: 10.1007/s00330-003-2198-8]
- Blaney SP, Tierney P, Oyarazabal M, Bowdler DA. CT scanning in "second look" combined approach tympanoplasty. *Rev Laryngol Otol Rhinol (Bord)* 2000; **121**: 79-81 [PMID: 10997063]
- Williams MT, Ayache D, Alberti C, Héran F, Lafitte F, Elmaleh-Bergès M, Piekarski JD. Detection of postoperative residual cholesteatoma with delayed contrast-enhanced MR imaging: initial findings. *Eur Radiol* 2003; **13**: 169-174 [PMID: 12541126 DOI: 10.1007/s00330-002-1423-1]
- Fitzek C, Mewes T, Fitzek S, Mentzel HJ, Hunsche S, Stoeter P. Diffusion-weighted MRI of cholesteatomas of the petrous bone. *J Magn Reson Imaging* 2002; **15**: 636-641 [PMID: 12112513 DOI: 10.1002/jmri.10118]
- Aikele P, Kittner T, Offergeld C, Kaftan H, Hüttenbrink KB, Laniado M. Diffusion-weighted MR imaging of cholesteatoma in pediatric and adult patients who have undergone middle ear surgery. *AJR Am J Roentgenol* 2003; **181**: 261-265 [PMID: 12818870 DOI: 10.2214/ajr.181.1.1810261]
- Maheshwari S, Mukherji SK. Diffusion-weighted imaging for differentiating recurrent cholesteatoma from granulation tissue after mastoidectomy: case report. *AJNR Am J Neuroradiol* 2002; **23**: 847-849 [PMID: 12006291]
- Vercruysse JP, De Foer B, Pouillon M, Somers T, Casselman J, Offeciers E. The value of diffusion-weighted MR imaging in the diagnosis of primary acquired and residual cholesteatoma: a surgical verified study of 100 patients. *Eur Radiol* 2006; **16**: 1461-1467 [PMID: 16514469 DOI: 10.1007/s00330-006-0160-2]
- Bergui M, Zhong J, Bradac GB, Sales S. Diffusion-weighted images of intracranial cyst-like lesions. *Neuroradiology* 2001; **43**: 824-829 [PMID: 11688697]
- Lemma MM, De Foer B, VandeVyver V, Vercruysse JP, Verstraete KL. Imaging of the opacified middle ear. *Eur J Radiol* 2008; **66**: 363-371 [PMID: 18339504 DOI: 10.1016/j.ejrad.2008.01.020]
- Bammer R. Basic principles of diffusion-weighted imaging. *Eur J Radiol* 2003; **45**: 169-184 [PMID: 12595101]
- Chen S, Ikawa F, Kurisu K, Arita K, Takaba J, Kanou Y. Quantitative MR evaluation of intracranial epidermoid tumors by fast fluid-attenuated inversion recovery imaging and echo-planar diffusion-weighted imaging. *AJNR Am J Neuroradiol* 2001; **22**: 1089-1096 [PMID: 11415903]
- Cimsit NC, Cimsit C, Baysal B, Ruhi IC, Ozbilgen S, Aksoy EA. Diffusion-weighted MR imaging in postoperative follow-up: reliability for detection of recurrent cholesteatoma. *Eur J Radiol* 2010; **74**: 121-123 [PMID: 19231123 DOI: 10.1016/j.ejrad.2009.01.025]
- De Foer B, Vercruysse JP, Pilet B, Michiels J, Vertriest R, Pouillon M, Somers T, Casselman JW, Offeciers E. Single-shot, turbo spin-echo, diffusion-weighted imaging versus spin-echo-planar, diffusion-weighted imaging in the detection of acquired middle ear cholesteatoma. *AJNR Am J Neuroradiol* 2006; **27**: 1480-1482

- [PMID: 16908562]
- 18 **Attenberger UI**, Runge VM, Stemmer A, Williams KD, Naul LG, Michaely HJ, Schoenberg SO, Reiser MF, Wintersperger BJ. Diffusion weighted imaging: a comprehensive evaluation of a fast spin echo DWI sequence with BLADE (PROPELLER) k-space sampling at 3 T, using a 32-channel head coil in acute brain ischemia. *Invest Radiol* 2009; **44**: 656-661 [PMID: 19724235 DOI: 10.1097/RLI.0b013e3181af3f0e]
 - 19 **Dubrule F**, Souillard R, Chechin D, Vaneeecloo FM, Desaulty A, Vincent C. Diffusion-weighted MR imaging sequence in the detection of postoperative recurrent cholesteatoma. *Radiology* 2006; **238**: 604-610 [PMID: 16304085 DOI: 10.1148/radiol.2381041649]
 - 20 **Dremmen MH**, Hofman PA, Hof JR, Stokroos RJ, Postma AA. The diagnostic accuracy of non-echo-planar diffusion-weighted imaging in the detection of residual and/or recurrent cholesteatoma of the temporal bone. *AJNR Am J Neuroradiol* 2012; **33**: 439-444 [PMID: 22194383 DOI: 10.3174/ajnr.A2824]
 - 21 **Dhepnorrarat RC**, Wood B, Rajan GP. Postoperative non-echo-planar diffusion-weighted magnetic resonance imaging changes after cholesteatoma surgery: implications for cholesteatoma screening. *Otol Neurotol* 2009; **30**: 54-58 [PMID: 19092558 DOI: 10.1097/MAO.0b013e31818edf4a]
 - 22 **Geoffray A**, Guesmi M, Nebbia JF, Leloutre B, Bailleux S, Maschi C. MRI for the diagnosis of recurrent middle ear cholesteatoma in children--can we optimize the technique? Preliminary study. *Pediatr Radiol* 2013; **43**: 464-473 [PMID: 23160645 DOI: 10.1007/s00247-012-2502-3]
 - 23 **Schwartz KM**, Lane JJ, Bolster BD, Neff BA. The utility of diffusion-weighted imaging for cholesteatoma evaluation. *AJNR Am J Neuroradiol* 2011; **32**: 430-436 [PMID: 20488909 DOI: 10.3174/ajnr.A2129]
 - 24 **De Foer B**, Vercruysse JP, Bernaerts A, Deckers F, Pouillon M, Somers T, Casselman J, Offeciers E. Detection of postoperative residual cholesteatoma with non-echo-planar diffusion-weighted magnetic resonance imaging. *Otol Neurotol* 2008; **29**: 513-517 [PMID: 18520587 DOI: 10.1097/MAO.0b013e31816c7c3b]
 - 25 **De Foer B**, Vercruysse JP, Bernaerts A, Maes J, Deckers F, Michiels J, Somers T, Pouillon M, Offeciers E, Casselman JW. The value of single-shot turbo spin-echo diffusion-weighted MR imaging in the detection of middle ear cholesteatoma. *Neuroradiology* 2007; **49**: 841-848 [PMID: 17768611 DOI: 10.1007/s00234-007-0268-3]
 - 26 **De Foer B**, Vercruysse JP, Bernaerts A, Meersschaert J, Kenis C, Pouillon M, De Beuckeleer L, Michiels J, Bogaerts K, Deckers F, Somers T, Hermans R, Offeciers E, Casselman JW. Middle ear cholesteatoma: non-echo-planar diffusion-weighted MR imaging versus delayed gadolinium-enhanced T1-weighted MR imaging--value in detection. *Radiology* 2010; **255**: 866-872 [PMID: 20501723 DOI: 10.1148/radiol.10091140]
 - 27 **Forbes KP**, Pipe JG, Karis JP, Heiserman JE. Improved image quality and detection of acute cerebral infarction with PROPELLER diffusion-weighted MR imaging. *Radiology* 2002; **225**: 551-555 [PMID: 12409594 DOI: 10.1148/radiol.2252011479]
 - 28 **Más-Estellés F**, Mateos-Fernández M, Carrascosa-Bisquert B, Facal de Castro F, Puchades-Román I, Morera-Pérez C. Contemporary non-echo-planar diffusion-weighted imaging of middle ear cholesteatomas. *Radiographics* 2012; **32**: 1197-1213 [PMID: 22787002 DOI: 10.1148/rg.324115109]
 - 29 **Elefante A**, Cavaliere M, Russo C, Caliendo G, Marseglia M, Cicala D, Piccolo D, Di Lullo A, Brunetti L, Palma A, Iengo M, Brunetti A. Diffusion weighted MR imaging of primary and recurrent middle ear cholesteatoma: an assessment by readers with different expertise. *Biomed Res Int* 2015; **2015**: 597896 [PMID: 25722983 DOI: 10.1155/2015/597896]
 - 30 **Jindal M**, Riskalla A, Jiang D, Connor S, O'Connor AF. A systematic review of diffusion-weighted magnetic resonance imaging in the assessment of postoperative cholesteatoma. *Otol Neurotol* 2011; **32**: 1243-1249 [PMID: 21921855 DOI: 10.1097/MAO.0b013e31822e938d]
 - 31 **Yamashita K**, Yoshiura T, Hiwatashi A, Kamano H, Dashjams T, Shibata S, Tamae A, Honda H. Detection of middle ear cholesteatoma by diffusion-weighted MR imaging: multishot echo-planar imaging compared with single-shot echo-planar imaging. *AJNR Am J Neuroradiol* 2011; **32**: 1915-1918 [PMID: 21778245 DOI: 10.3174/ajnr.A2651]
 - 32 **Skare S**, Newbould RD, Clayton DB, Albers GW, Nagle S, Bammer R. Clinical multishot DW-EPI through parallel imaging with considerations of susceptibility, motion, and noise. *Magn Reson Med* 2007; **57**: 881-890 [PMID: 17457876 DOI: 10.1002/mrm.21176]
 - 33 **Flook E**, Izzat S, Ismail A. Cholesteatoma imaging using modified echo-planar diffusion-weighted magnetic resonance imaging. *J Laryngol Otol* 2011; **125**: 10-12 [PMID: 20831846 DOI: 10.1017/S0022215110001805]
 - 34 **Steens S**, Venderink W, Kunst D, Meijer A, Mylanus E. Repeated Postoperative Follow-up Diffusion-weighted Magnetic Resonance Imaging to Detect Residual or Recurrent Cholesteatoma. *Otol Neurotol* 2016; **37**: 356-361 [PMID: 26905824 DOI: 10.1097/MAO.0000000000000985]

P- Reviewer: Lim SM S- Editor: Song XX L- Editor: A
E- Editor: Li D



Basic Study

Correlation of lumbar lateral recess stenosis in magnetic resonance imaging and clinical symptoms

Annina Splettstößer, M Fawad Khan, Bernd Zimmermann, Thomas J Vogl, Hanns Ackermann, Marcus Middendorp, Adel Maataoui

Annina Splettstößer, Radprax MVZ, 40721 Hilden, Germany

M Fawad Khan, Bernd Zimmermann, Thomas J Vogl, Adel Maataoui, Institute for Diagnostic and Interventional Radiology, Goethe University, 60590 Frankfurt/Main, Germany

Hanns Ackermann, Institute of Biostatistics and Mathematical Modeling, Goethe University, 60590 Frankfurt/Main, Germany

Marcus Middendorp, Department of Nuclear Medicine, Goethe University, 60590 Frankfurt/Main, Germany

Author contributions: Middendorp M and Maataoui A contributed equally to this work; Maataoui A and Vogl TJ supervised the project; Splettstößer A, Middendorp M, and Maataoui A wrote the main paper; all authors were involved in the study design, data analysis, and discussion of the results at all stages.

Institutional review board statement: The study inclusive of patient information and consent form was reviewed and approved by the ethics committee of the State Authorisation Association for Medical Issues of Hessen, Germany (FF 48/2014). Patients were not required to give informed consent to the study because the analysis used anonymous clinical data that were obtained after each patient agreed to examination by written consent.

Conflict-of-interest statement: All authors ensure that there are no conflicts of interest.

Data sharing statement: Consent was not obtained but the presented data are anonymized and risk of identification is very low. No additional data are available.

Open-Access: This article is an open-access article which was selected by an in-house editor and fully peer-reviewed by external reviewers. It is distributed in accordance with the Creative Commons Attribution Non Commercial (CC BY-NC 4.0) license, which permits others to distribute, remix, adapt, build upon this work non-commercially, and license their derivative works on different terms, provided the original work is properly cited and the use is non-commercial. See: <http://creativecommons.org/licenses/by-nc/4.0/>

Manuscript source: Invited manuscript

Correspondence to: Adel Maataoui, MD, Institute for Diagnostic and Interventional Radiology, Goethe University, Theodor-Stern-Kai 7, 60590 Frankfurt/Main, Germany. adel.maataoui@gmx.de
Telephone: +49-69-63015534
Fax: +49-69-63014222

Received: October 7, 2016

Peer-review started: October 14, 2016

First decision: November 11, 2016

Revised: February 22, 2017

Accepted: March 16, 2017

Article in press: March 17, 2017

Published online: May 28, 2017

Abstract

AIM

To assess the correlation of lateral recess stenosis (LRS) of lumbar segments L4/5 and L5/S1 and the Oswestry Disability Index (ODI).

METHODS

Nine hundred and twenty-seven patients with history of low back pain were included in this uncontrolled study. On magnetic resonance images (MRI) the lateral recesses (LR) at lumbar levels L4/5 and L5/S1 were evaluated and each nerve root was classified into a 4-point grading scale (Grade 0-3) as normal, not deviated, deviated or compressed. Patient symptoms and disability were assessed using ODI. The Spearman's rank correlation coefficient was used for statistical analysis ($P < 0.05$).

RESULTS

Approximately half of the LR revealed stenosis (grade 1-3; 52% at level L4/5 and 42% at level L5/S1) with 2.2% and 1.9% respectively reveal a nerve root compression.

The ODI score ranged from 0%-91.11% with an arithmetic mean of $34.06\% \pm 16.89\%$. We observed a very weak statistically significant positive correlation between ODI and LRS at lumbar levels L4/5 and L5/S1, each bilaterally (L4/5 left: $\rho < 0.105$, $P < 0.01$; L4/5 right: $\rho < 0.111$, $P < 0.01$; L5/S1 left: $\rho 0.128$, $P < 0.01$; L5/S1 right: $\rho < 0.157$, $P < 0.001$).

CONCLUSION

Although MRI is the standard imaging tool for diagnosing lumbar spinal stenosis, this study showed only a weak correlation of LRS on MRI and clinical findings. This can be attributed to a number of reasons outlined in this study, underlining that imaging findings alone are not sufficient to establish a reliable diagnosis for patients with LRS.

Key words: Low back pain; Lumbar spine; Magnetic resonance imaging; Lateral recess stenosis; Oswestry Disability Score; Lumbar spinal canal stenosis

© The Author(s) 2017. Published by Baishideng Publishing Group Inc. All rights reserved.

Core tip: In the presented study lateral recesses of nearly 1000 patients with low back pain were evaluated on magnetic resonance imaging (MRI) and correlated with patient symptoms. Though MRI is the method of choice for diagnosing lumbar spinal stenosis, we revealed only a very weak correlation of lateral recess stenosis (LRS) and patient symptoms. This can be attributed to numerous reasons outlined in this study, underlining that imaging findings alone are not sufficient for an adequate diagnostic approach of patients with LRS.

Splettstößer A, Khan MF, Zimmermann B, Vogl TJ, Ackermann H, Middendorp M, Maataoui A. Correlation of lumbar lateral recess stenosis in magnetic resonance imaging and clinical symptoms. *World J Radiol* 2017; 9(5): 223-229 Available from: URL: <http://www.wjgnet.com/1949-8470/full/v9/i5/223.htm> DOI: <http://dx.doi.org/10.4329/wjcr.v9.i5.223>

INTRODUCTION

After arthritis and rheumatism^[1] low back pain (LBP) is the second most cause of disability in United States adults, and thus is a major social and economic issue^[2]. With the aging population the prevalence is even drastically rising^[3]. Lumbar spinal stenosis (LSS) is one main cause of LBP. As a distinct syndrome LSS was already described by Verbiest *et al*^[4] in 1954. Most studies about LSS focus on the central LSS. Failure to recognize or adequately treat lateral recess stenosis (LRS) is considered to be the main reason for failed back surgery on the lumbar spine^[5]. On account of this we focused on the LRS in the presented study. Regarding imaging analyses LSS is defined by the reduced size of the spinal canal. Based on the anatomical regions,

LSS is generally subdivided in central spinal stenosis, LRS and foraminal stenosis. The LRS affects the lateral region of the lumbar spinal canal that is bordered laterally by the pedicle, posteriorly by the superior articular facet, and anteriorly by the vertebral body, endplate margin, and disc margin^[6] (Figure 1). LRS is most commonly caused by degenerative changes of the spine such as facet joint osteoarthritis, ligamentum flavum hypertrophy, intervertebral disc degeneration and endplate spur. Congenital abnormalities, bone diseases, tumors or trauma are rare causes of LRS^[7]. According to Bartynski *et al*^[8] two pathways for the development of degenerative LRS exist. On the one hand the congenital or acquired trefoil canal in which the nerve root remains in its position in the LR and the narrowing of the LR develops in an anteroposterior fashion. Regarding the acquired trefoil canal first of all facet joint osteoarthritis causes the trefoil-shape, subsequent following endplate and disc degeneration result in LRS. The second pathway is called acute angular pinch. The narrowing occurs simultaneously from all directions due to endplate, disc and facet joint degeneration. The nerve root is either deviated medially or compressed in the LR. Magnetic resonance imaging (MRI) is considered the standard imaging technique for evaluation of LSS^[9-11] due to the best soft tissue contrast^[7]. Although LSS as a distinct syndrome has already been described more than 60 years ago, the radiological classification systems remain inconsistent^[12,13]. In 2014 the "Consensus conference of core radiological parameters to describe lumbar stenosis" with 15 internationally renowned experts focused on this problem^[12]. Concerning the LRS they recommend the classification system of Bartynski *et al*^[8] which focuses on the compression and the localization of the nerve root in the LR. In short Bartynski *et al*^[8] divided the LRS in 4 grades: Normal (grade 0), small without root compression (grade 1), small with root compression (grade 2) and severe root compression (grade 3). LSS is usually diagnosed by clinical findings in correlation with imaging results. However in the daily routine we frequently experience a mismatch between LBP and MRI results. The aim of our study was to verify this mismatch regarding LBP and LRS. To the best of our knowledge there are no previous studies investigating the correlation of LBP and MRI findings of LRS in such a large group of patients.

MATERIALS AND METHODS

Study participants

The study was approved by the ethical committee. In total the study involved lumbar MR images of 927 patients (410 men and 517 women). The mean age of the patients included was 47.7 years (ranging from 13 to 92 years). All patients included in the study had suffered from LBP without any history of spinal surgery. Criteria for exclusion of patients were confirmed disc herniation, spinal stenosis, scoliosis and vertebral fractures. The MR images were gathered over a time of one year with

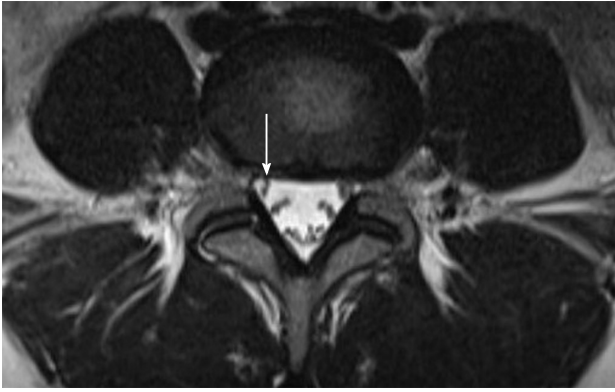


Figure 1 Axial T2-weighted magnetic resonance image of lumbar level L4/5 shows the lateral recess that is bordered laterally by the pedicle, posteriorly by the superior articular facet, and anteriorly by the vertebral body, endplate margin, and disc margin.

suspected disc herniation and facet joint degeneration being the main reasons for MRI.

Imaging technique

MRI of the lumbar spine was conducted with a 1.5 Tesla MRI system (Magnetom® Avanto, Siemens AG, Erlangen, Germany) and a dedicated receive only spine coil. For imaging analysis axial T2-weighted images were obtained using fast spin-echo sequences. The sequence parameters were: TR 3550; TE 90; matrix 448; field of view 210 mm; slice thickness 4 mm; interslice gap 10%, number of excitations.

Image analysis

All MR images were assessed in consensus by two blinded authors (Adel Maataoui, M Fawad Khan). Both authors are board certified radiologists with longstanding experience in imaging of the musculoskeletal system. Degeneration of lumbar spine concerns mostly segments L4/5 and L5/S1, for which reason the LR of these segments were graded on axial T2-weighted fast spin-echo images. All in all, an overall number of 3708 lateral recesses were rated.

Our grading system of LRS was based on Bartynski's classification. We defined grade 0 as a normal LR in which the nerve root is bathed in cerebrospinal fluid. There is no contact to the adjacent structures. Grade 1 represents a narrowing of the LR without root deviation. Grade 2 additionally reveals a root deviation. Grade 3 describes a compression of the nerve root (Table 1, Figure 2).

Oswestry Disability Index

By means of the Oswestry Disability Index (ODI) functional status was assessed. The ODI is one of the principle outcome measure questionnaires for LBP - it measures pain and disability, which are core items in patients with LBP^[14]. We used the german version of the ODI developed by Mannion *et al.*^[15]. This standardized, self-administered questionnaire contains ten sections: One section about pain intensity and nine sections

about limitations of various activities of daily life, namely personal care (washing, dressing, etc.), lifting, walking, sitting, standing, sleeping, sex life, social life and travelling^[16]. The question about sex life was excluded on grounds of ethical aspects. Each section is scored on a scale of 0-5 points with 0 representing no disability and 5 the greatest disability. Section 2 "personal care" for example contains the following statements and scores: I can look after myself normally without causing extra pain (0); I can look after myself normally but it is very painful (1); It is painful to look after myself and I am slow and careful (2); I need some help but manage most of my personal care (3); I need help every day in most aspects of self care (4); and I do not get dressed, wash with difficulty and stay in bed (5)^[16].

Finally the index is calculated by dividing the summed score by the total possible score (which has to be reduced by 5 for every question not answered). The result is then multiplied by 100 and expressed as a percentage. The result is interpreted as follows: Score of 0%-20%, minimal disability; 20%-40%, moderate disability; 40%-60%, severe disability; 60%-80%, crippled; 80%-100%, patients are bedbound.

Statistical analysis

Data were analysed with the use of the BIAS software package (Epsilon publisher, Frankfurt a.M., Germany). In order to evaluate the correlation of LRS and ODI Spearman's coefficient of rank correlation was determined. *P* value < 0.05 were considered statistically significant.

RESULTS

Grades of LRS in the patient cohort

Three thousand seven hundred and eight LR of 927 patients were assessed at lumbar level L4/5 and L5/S1. Table 2 presents the number of LR according to the relative grade of stenosis. The image evaluation revealed 430/461 grade 0 stenosis (48.1%), 357/349 grade 1 stenosis (38.1%), 113/103 grade 2 stenosis (11.7%) and 27/14 grade 3 stenosis (2.2%) for the left/right side of lumbar level L4/5 and 528/548 grade 0 stenosis (58%), 303/316 grade 1 stenosis (33.4%), 75/49 grade 2 stenosis (6.7%) and 21/14 grade 3 stenosis (1.9%) for the left/right side of lumbar level L5/S1, respectively.

Symptoms and disability

According to ODI scores patient symptoms and disability ranged from a minimal score of 0% to a maximal score of 91.11%. The mean value amounted to 34.06% ± 16.89%. Most patients (48.39%) showed a moderate functional disability (21%-40%). Regarding sex no statistical difference between the ODI scores could be revealed: Men 32.47% ± 16.55% and women 35.58% ± 16.55%.

The mean ODI scores for LRS grade 0, 1, 2, 3 of lumbar level L4/5 on the right side were 31.53% ± 15.46%, 31.53% ± 17.60%, 33.01% ± 17.17% and

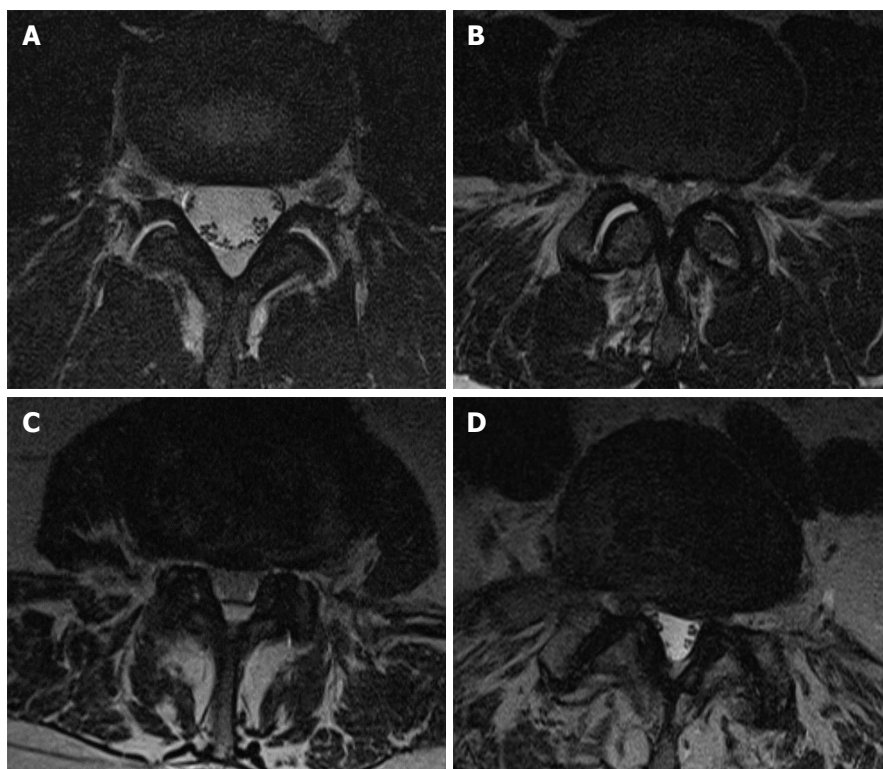


Figure 2 Axial T2-weighted magnetic resonance images illustrate the grading system of lateral recess stenosis. A: Grade 0 bilaterally; B: Grade 1 bilaterally; C: Grade 2 bilaterally; D: Grade 3 on the left, Grade 1 on the right.

Table 1 Grading system of lateral recess stenosis

Grade	Nerve root in the lateral recess
0	Normal
1	No deviation
2	Deviation
3	Compression

33.03% \pm 16.89%. There was no statistical difference between the ODI score and the grade of LRS on lumbar level L4/5 on the right.

The mean ODI scores for LRS grade 0, 1, 2, 3 of lumbar level L4/5 on the left side were 30.75% \pm 17.85%, 30.74% \pm 17.03%, 32.39% \pm 16.97% and 33.25% \pm 16.90%. There was no statistical difference between the ODI score and the grade of LRS on lumbar level L4/5 on the left.

The mean ODI scores for LRS grade 0, 1, 2, 3 of lumbar level L5/S1 on the right side were 32.03% \pm 16.58%, 32.03% \pm 16.60%, 33.24% \pm 16.41% and 33.88% \pm 16.76%. There was no statistical difference between the ODI score and the grade of LRS on lumbar level L5/S1 on the right.

The mean ODI scores for LRS grade 0, 1, 2, 3 of lumbar level L5/S1 on the left side were 32.14% \pm 16.90%, 33.15% \pm 16.62%, 33.13% \pm 16.60% and 33.46% \pm 16.78%. There was no statistical difference between the ODI score and the grade of LRS on lumbar level L5/S1 on the left.

Table 2 Number of grades of lateral recess stenosis for lumbar levels L4/5 and L5/S1

Lumbar level	Grades			
	0	1	2	3
L4/5 left	430	357	113	27
L4/5 right	461	349	103	14
L5/S1 left	528	303	75	21
L5/S1 right	548	316	49	14

Correlation of ODI and LRS

We observed a very weak statistically significant positive correlation between ODI and LRS at lumbar levels L4/5 and L5/S1, each bilaterally.

L4/5 left and ODI: $\rho < 0.105$, $P < 0.01$; L4/5 right and ODI: $\rho < 0.111$, $P < 0.01$; L5/S1 left and ODI: $\rho < 0.128$, $P < 0.01$; L5/S1 right and ODI: $\rho < 0.157$, $P < 0.001$.

DISCUSSION

Despite the high prevalence of LSS and that the combination of clinical and imaging findings are the standard diagnostic tools^[17] clinical and imaging findings often do not correlate. Haig *et al.*^[9] and Geisser *et al.*^[18] could not find any difference between symptomatic and asymptomatic patients based on the size of the lumbar spinal canal measured on MR images. Lohmann *et al.*^[19] did also not detect a correlation between clinical findings and LSS on computed tomography (CT) images.

The aim of our study was to verify if the results of these studies which focused on central LSS, do also apply to LRS. In the presented study with a cohort of more than 900 patients we found only a very weak positive correlation between the severity of LBP and the severity of LRS. Our findings are supported by the results of Kuittinen *et al.*^[20]: By MR imaging and electromyography they evaluated 140 nerve roots of 14 patients, who were selected for surgical treatment of LRS. The findings were correlated with each other as well as with the clinical symptoms, measured by different tests including the ODI. In this little cohort they revealed a positive correlation between MR-findings and EMG and between EMG and patient symptoms. But they revealed no correlation between MR findings and patient symptoms. The study is limited by the very small cohort of patients and the fact that also neuroforaminal stenosis was included.

It is unclear why clinical and imaging findings do often not correlate. The compression of the nerve root is considered to be one of the main causes of symptoms in patients with LRS^[21-23]. In an experimental study Lacroix-Fralish *et al.*^[24] observed that a nerve root ligation in a rat model produced mechanical allodynia. Mechanical root compression in a dog model revealed intraradicular edema and Wallerian degeneration^[25]. Using a silicon tube Saal^[26] and Xue *et al.*^[27] produced lumbar nerve root compression in a rat model, which resulted in disappearing of the myelin sheath and activation of microglia, which is assumed to participate in the genesis and maintenance of pain^[24].

Thus, it must be considered that a possible reason for the discrepancy between MRI findings and patient symptoms could be that MRI does not sufficiently identify nerve compression. Bartynski *et al.*^[8] assessed the accuracy of MRI in 26 patients with symptomatic nerve root compression in the LR at lumbar levels L2/3 - L5/S1. Each patient underwent MRI, conventional myelography and CT myelography; the root compression was confirmed surgically and a post-operative pain improvement could be observed. In MRI the root compression was underestimated in nearly 30%.

LSS, in addition, has an important dynamic component. MRI was performed, as usual, with the patient lying in the supine position. Yet it is known and even a key feature for LSS that patient symptoms increase under axial loading and lumbar extension while they decrease under axial distraction and flexion^[17,28]. This can be explained by anatomic alterations: Flexion and extension can change the size of the central lumbar canal, the LR and the neural foramen and can consecutively result in changes of the cauda equina as well as in isolated nerve root compression in the LR^[29]. In experimental studies axial loading has caused alterations of the size of the lumbar canal and the neural foramen^[30]. In the upright position axial loading can cause displacement of peridiscal structures that lead to a nerve root compression which is not observable in the supine position^[31]. In addition the pressure in the lumbar canal can be altered by postural changes^[32,33].

Two other aspects should be considered as possible explanations for the weak correlation. On the one hand the nerve root can be compressed without clinical symptoms. On the other hand clinical symptoms can be evident without imaging findings of root compression. Although there are single studies which reveal nerve root compression in approximately 20% of asymptomatic individuals^[34], there is in total only a small number of asymptomatic individuals who reveal nerve root compression in MRI. In a study presented by Weishaupt *et al.*^[35] with 60 asymptomatic volunteers only one single root compression was observed in MRI by one of the readers. A study of nearly 100 asymptomatic elite junior tennis players revealed a nerve root compression in only 2%^[36]. Boos *et al.*^[37] reported a "major nerve deformation" in 4% of asymptomatic adults.

A possible explanation for clinical symptoms without evident nerve root compression in imaging is the inflammation of the nerve root caused by inflammatory mediators^[38,39], for example, Interleukin $\beta 1$ ^[40]. It is hypothesized, that these substances can diffuse in the spinal canal from the facet joints, the ligamentum flavum^[40] and from the intervertebral disc^[26,41].

Beside the nerve root nearly all lumbar structures are potential sources of LBP, such as the facet joints, the intervertebral discs, bones, fascial structures and muscles^[42]. Especially facet joint osteoarthritis is known for radiating pain without evidence of nerve root compression^[43,44]. Because of the fact that LRS is based on facet joint osteoarthritis, intervertebral disc degeneration, ligamentum flavum hypertrophy and endplate spur we have to consider that in our study each of these structures could be the crucial factor for patient symptoms.

LBP rarely causes objective endpoints so outcomes are best measured with patient-reported metrics^[45]. We assessed patient symptoms by means of the ODI. It is one of the most commonly used measures of disability in back pain^[46]. It has established psychometric properties, is easy to use and has a low administrative burden^[46]. Yet, based on self-reported symptoms, the ODI remains subjective. Furthermore it does not measure nerve root level specific symptoms. A limitation of the presented study is that results of clinical, more objective, examinations were not included and that we assessed no nerve root level specific symptoms. In addition the LRS were not proved surgically.

In conclusion, in our broad study population we only found a very weak statistically significant positive correlation between LBP and LRS on MR-images, thus confirming the well-known problem that in the context of diagnosing LBP clinical and imaging findings often do not correlate. Our results underline the necessity not to evaluate LRS isolated on imaging but in relation to clinical findings.

COMMENTS

Background

Low back pain (LBP) is an important issue for healthcare systems all over the

world. One reason of LBP is lumbar spinal stenosis (LSS), with lateral recess stenosis (LRS) not gaining as much attention as central spinal stenosis, a fact that is assumed to be the main reason for failed back surgery. Concerning imaging techniques magnetic resonance imaging (MRI) is the standard imaging tool for evaluating LSS. However in the daily routine people frequently experience a mismatch between LBP and MRI results. The aim of this study was to verify this mismatch regarding LBP and LRS.

Research frontiers

The problem that in the context of LBP clinical and imaging findings often do not correlate has been the objective of numerous studies in the past. Yet the LRS as one reason of LBP is underrepresented and most studies have a small study population.

Innovations and breakthroughs

The authors assessed the correlation between LBP and LRS in a very broad study population including nearly 1000 patients. Functional status was assessed by means of the Oswestry Disability Index (ODI), and LRS was assessed on axial magnetic resonance images of lumbar level L4/5 and L5/S1 by evaluating the nerve root in the lateral recess on a 4 point grading scale. The authors revealed a very weak statistically significant positive correlation between ODI and LRS at the L4/5 segment as well as the L5/S1 segment.

Applications

The presented findings underline the necessity not to evaluate LRS isolated on imaging but in relation with the clinical findings.

Terminology

Lateral recess stenosis: It describes the stenosis of the lateral part of the lumbar spinal canal that is bordered laterally by the pedicle, posteriorly by the superior articular facet, and anteriorly by the vertebral body, endplate margin, and disc margin. It is most commonly caused by degenerative changes; Oswestry Disability Index: The Oswestry Disability Index is one of the principle outcome measure questionnaires for low back pain focussing on disability and pain.

Peer-review

The authors studied the correlation of lumbar recess stenosis in MRI with clinical symptoms.

REFERENCES

- From the Centers for Disease Control and Prevention. Prevalence of disabilities and associated health conditions among adults--United States, 1999. *JAMA* 2001; **285**: 1571-1572 [PMID: 11302137]
- Balagué F, Mannion AF, Pellisé F, Cedraschi C. Non-specific low back pain. *Lancet* 2012; **379**: 482-491 [PMID: 21982256 DOI: 10.1016/s0140-6736(11)60610-7]
- Freburger JK, Holmes GM, Agans RP, Jackman AM, Darter JD, Wallace AS, Castel LD, Kalsbeek WD, Carey TS. The rising prevalence of chronic low back pain. *Arch Intern Med* 2009; **169**: 251-258 [PMID: 19204216 DOI: 10.1001/archinternmed.2008.543]
- Verbiest H. A radicular syndrome from developmental narrowing of the lumbar vertebral canal. *J Bone Joint Surg Br* 1954; **36-B**: 230-237 [PMID: 13163105]
- Burton CV, Kirkaldy-Willis WH, Yong-Hing K, Heithoff KB. Causes of failure of surgery on the lumbar spine. *Clin Orthop Relat Res* 1981; **(157)**: 191-199 [PMID: 7249453]
- Lee CK, Rauschnig W, Glenn W. Lateral lumbar spinal canal stenosis: classification, pathologic anatomy and surgical decompression. *Spine (Phila Pa 1976)* 1988; **13**: 313-320 [PMID: 3388117]
- Andreisek G, Hodler J, Steurer J. Uncertainties in the diagnosis of lumbar spinal stenosis. *Radiology* 2011; **261**: 681-684 [PMID: 22095990 DOI: 10.1148/radiol.11111086]
- Bartynski WS, Lin L. Lumbar root compression in the lateral recess: MR imaging, conventional myelography, and CT myelography comparison with surgical confirmation. *AJNR Am J Neuroradiol* 2003; **24**: 348-360 [PMID: 12637281]
- Haig AJ, Geisser ME, Tong HC, Yamakawa KS, Quint DJ, Hoff JT, Chiodo A, Miner JA, Phalke VV. Electromyographic and magnetic resonance imaging to predict lumbar stenosis, low-back pain, and no back symptoms. *J Bone Joint Surg Am* 2007; **89**: 358-366 [PMID: 17272451 DOI: 10.2106/jbjs.e.00704]
- Sasiadek MJ, Bladowska J. Imaging of degenerative spine disease--the state of the art. *Adv Clin Exp Med* 2012; **21**: 133-142 [PMID: 23214277]
- Malfair D, Beall DP. Imaging the degenerative diseases of the lumbar spine. *Magn Reson Imaging Clin N Am* 2007; **15**: 221-238, vi [PMID: 17599641 DOI: 10.1016/j.mric.2007.04.001]
- Andreisek G, Deyo RA, Jarvik JG, Porchet F, Winklhofer SF, Steurer J. Consensus conference on core radiological parameters to describe lumbar stenosis - an initiative for structured reporting. *Eur Radiol* 2014; **24**: 3224-3232 [PMID: 25079488 DOI: 10.1007/s00330-014-3346-z]
- Andreisek G, Imhof M, Wertli M, Winklhofer S, Pfirrmann CW, Hodler J, Steurer J. A systematic review of semiquantitative and qualitative radiologic criteria for the diagnosis of lumbar spinal stenosis. *AJR Am J Roentgenol* 2013; **201**: W735-W746 [PMID: 24147503 DOI: 10.2214/ajr.12.10163]
- Deyo RA, Battie M, Beurskens AJ, Bombardier C, Croft P, Koes B, Malmivaara A, Roland M, Von Korf M, Waddell G. Outcome measures for low back pain research. A proposal for standardized use. *Spine (Phila Pa 1976)* 1998; **23**: 2003-2013 [PMID: 9779535]
- Mannion AF, Junge A, Fairbank JC, Dvorak J, Grob D. Development of a German version of the Oswestry Disability Index. Part 1: cross-cultural adaptation, reliability, and validity. *Eur Spine J* 2006; **15**: 55-65 [PMID: 15856341]
- Fairbank JC, Pynsent PB. The Oswestry Disability Index. *Spine (Phila Pa 1976)* 2000; **25**: 2940-2952; discussion 2952 [PMID: 11074683]
- Genevay S, Atlas SJ. Lumbar spinal stenosis. *Best Pract Res Clin Rheumatol* 2010; **24**: 253-265 [PMID: 20227646 DOI: 10.1016/j.berh.2009.11.001]
- Geisser ME, Haig AJ, Tong HC, Yamakawa KS, Quint DJ, Hoff JT, Miner JA, Phalke VV. Spinal canal size and clinical symptoms among persons diagnosed with lumbar spinal stenosis. *Clin J Pain* 2007; **23**: 780-785 [PMID: 18075405 DOI: 10.1097/AJP.0b013e31815349bf]
- Lohman CM, Tallroth K, Kettunen JA, Lindgren KA. Comparison of radiologic signs and clinical symptoms of spinal stenosis. *Spine (Phila Pa 1976)* 2006; **31**: 1834-1840 [PMID: 16845360 DOI: 10.1097/01.brs.0000227370.65573.ac]
- Kuittinen P, Sipola P, Aalto TJ, Määttä S, Parviainen A, Saari T, Sinikallio S, Savolainen S, Turunen V, Kröger H, Airaksinen O, Leinonen V. Correlation of lateral stenosis in MRI with symptoms, walking capacity and EMG findings in patients with surgically confirmed lateral lumbar spinal canal stenosis. *BMC Musculoskelet Disord* 2014; **15**: 247 [PMID: 25051886 DOI: 10.1186/1471-2474-15-247]
- Shobeiri E, Khalatbari MR, Taheri MS, Tofighirad N, Moharamzad Y. Magnetic resonance imaging characteristics of patients with low back pain and those with sciatica. *Singapore Med J* 2009; **50**: 87-93 [PMID: 19224091]
- Ciric I, Mikhael MA, Tarkington JA, Vick NA. The lateral recess syndrome. A variant of spinal stenosis. *J Neurosurg* 1980; **53**: 433-443 [PMID: 7420163 DOI: 10.3171/jns.1980.53.4.0433]
- Epstein JA EN. Lumbar spondylosis and spinal stenosis. In: Wilkins RH RS, eds., editor Neurosurgery. New York: McGraw Hill, 1996: 3831-3840
- Lacroix-Fralish ML, Tawfik VL, Tanga FY, Spratt KF, DeLeo JA. Differential spinal cord gene expression in rodent models of radicular and neuropathic pain. *Anesthesiology* 2006; **104**: 1283-1292 [PMID: 16732101]
- Kobayashi S, Yoshizawa H, Yamada S. Pathology of lumbar nerve root compression. Part 1: Intraradicular inflammatory changes induced by mechanical compression. *J Orthop Res* 2004; **22**: 170-179 [PMID: 14656677 DOI: 10.1016/s0736-0266(03)00131-1]

- 26 **Saal JS.** The role of inflammation in lumbar pain. *Spine* (Phila Pa 1976) 1995; **20**: 1821-1827 [PMID: 7502140]
- 27 **Xue F, Wei Y, Chen Y, Wang Y, Gao L.** A rat model for chronic spinal nerve root compression. *Eur Spine J* 2014; **23**: 435-446 [PMID: 24141952 DOI: 10.1007/s00586-013-2990-3]
- 28 **Schönström N, Lindahl S, Willén J, Hansson T.** Dynamic changes in the dimensions of the lumbar spinal canal: an experimental study in vitro. *J Orthop Res* 1989; **7**: 115-121 [PMID: 2908901 DOI: 10.1002/jor.1100070116]
- 29 **Penning L, Wilmink JT.** Posture-dependent bilateral compression of L4 or L5 nerve roots in facet hypertrophy. A dynamic CT-myelographic study. *Spine* (Phila Pa 1976) 1987; **12**: 488-500 [PMID: 3629399]
- 30 **Nowicki BH, Yu S, Reinartz J, Pinter F, Yoganandan N, Haughton VM.** Effect of axial loading on neural foramina and nerve roots in the lumbar spine. *Radiology* 1990; **176**: 433-437 [PMID: 2367657 DOI: 10.1148/radiology.176.2.2367657]
- 31 **Beattie PF, Meyers SP, Stratford P, Millard RW, Hollenberg GM.** Associations between patient report of symptoms and anatomic impairment visible on lumbar magnetic resonance imaging. *Spine* (Phila Pa 1976) 2000; **25**: 819-828 [PMID: 10751293]
- 32 **Olmarker K, Rydevik B, Hansson T, Holm S.** Compression-induced changes of the nutritional supply to the porcine cauda equina. *J Spinal Disord* 1990; **3**: 25-29 [PMID: 2134408]
- 33 **Takahashi K, Kagechika K, Takino T, Matsui T, Miyazaki T, Shima I.** Changes in epidural pressure during walking in patients with lumbar spinal stenosis. *Spine* (Phila Pa 1976) 1995; **20**: 2746-2749 [PMID: 8747254]
- 34 **van Rijn JC, Klemetso N, Reitsma JB, Majoie CB, Hulsmans FJ, Peul WC, Bossuyt PM, Heeten GJ, Stam J.** Symptomatic and asymptomatic abnormalities in patients with lumbosacral radicular syndrome: Clinical examination compared with MRI. *Clin Neurol Neurosurg* 2006; **108**: 553-557 [PMID: 16289310 DOI: 10.1016/j.clineuro.2005.10.003]
- 35 **Weishaupt D, Zanetti M, Hodler J, Boos N.** MR imaging of the lumbar spine: prevalence of intervertebral disk extrusion and sequestration, nerve root compression, end plate abnormalities, and osteoarthritis of the facet joints in asymptomatic volunteers. *Radiology* 1998; **209**: 661-666 [PMID: 9844656 DOI: 10.1148/radiology.209.3.9844656]
- 36 **Rajeswaran G, Turner M, Gissane C, Healy JC.** MRI findings in the lumbar spines of asymptomatic elite junior tennis players. *Skeletal Radiol* 2014; **43**: 925-932 [PMID: 24691895 DOI: 10.1007/s00256-014-1862-1]
- 37 **Boos N, Rieder R, Schade V, Spratt KF, Semmer N, Aebi M.** 1995 Volvo Award in clinical sciences. The diagnostic accuracy of magnetic resonance imaging, work perception, and psychosocial factors in identifying symptomatic disc herniations. *Spine* (Phila Pa 1976) 1995; **20**: 2613-2625 [PMID: 8747239]
- 38 **Cavanaugh JM.** Neural mechanisms of lumbar pain. *Spine* (Phila Pa 1976) 1995; **20**: 1804-1809 [PMID: 7502138]
- 39 **Siddall PJ, Cousins MJ.** Pain mechanisms and management: an update. *Clin Exp Pharmacol Physiol* 1995; **22**: 679-688 [PMID: 8575103]
- 40 **Igarashi A, Kikuchi S, Konno S.** Correlation between inflammatory cytokines released from the lumbar facet joint tissue and symptoms in degenerative lumbar spinal disorders. *J Orthop Sci* 2007; **12**: 154-160 [PMID: 17393271 DOI: 10.1007/s00776-006-1105-y]
- 41 **McCarron RF, Wimpee MW, Hudkins PG, Laros GS.** The inflammatory effect of nucleus pulposus. A possible element in the pathogenesis of low-back pain. *Spine* (Phila Pa 1976) 1987; **12**: 760-764 [PMID: 2961088]
- 42 **Allegrì M, Montella S, Salici F, Valente A, Marchesini M, Compagnone C, Baciarello M, Manferdini ME, Fanelli G.** Mechanisms of low back pain: a guide for diagnosis and therapy. *F1000Res* 2016; **5**: pii: F1000 Faculty Rev-1530 [PMID: 27408698 DOI: 10.12688/f1000research.8105.1]
- 43 **Epstein JA, Epstein BS, Rosenthal AD, Carras R, Lavine LS.** Sciatica caused by nerve root entrapment in the lateral recess: the superior facet syndrome. *J Neurosurg* 1972; **36**: 584-589 [PMID: 5026544 DOI: 10.3171/jns.1972.36.5.0584]
- 44 **V. M. Facet syndrome.** In: Weinstein JN WS, eds., editor *The lumbar spine: The International Society for the Study of the Lumbar Spine*. Philadelphia: WB Saunders Company, 1990: 422-441
- 45 **Werneke M.** A proposed set of metrics for standardized outcome reporting in the management of low back pain. *Acta Orthop* 2016; **87**: 88 [PMID: 26610164 DOI: 10.3109/17453674.2015.1120127]
- 46 **Smeets R, Köke A, Lin CW, Ferreira M, Demoulin C.** Measures of function in low back pain/disorders: Low Back Pain Rating Scale (LBPRS), Oswestry Disability Index (ODI), Progressive Isoinertial Lifting Evaluation (PILE), Quebec Back Pain Disability Scale (QBPDS), and Roland-Morris Disability Questionnaire (RDQ). *Arthritis Care Res* (Hoboken) 2011; **63** Suppl 11: S158-S173 [PMID: 22588742 DOI: 10.1002/acr.20542]

P- Reviewer: Cerwenka HR, Gao BL **S- Editor:** Song XX

L- Editor: A **E- Editor:** Li D



Basic Study

Cystic lesions of peripheral nerves: Are we missing the diagnosis of the intraneural ganglion cyst?

Jyoti Panwar, Anil Mathew, Binu P Thomas

Jyoti Panwar, Department of Radiology, Christian Medical College, Vellore 632004, India

Jyoti Panwar, Joint Department of Medical Imaging, University Health Network, University of Toronto, Toronto, Ontario M5G 2N2, Canada

Anil Mathew, Binu P Thomas, Department of Hand Surgery and Leprosy Reconstructive Surgery, Christian Medical College, Vellore 632004, India

Author contributions: Panwar J and Mathew A participated in the conception, acquisition, analysis, interpretation of the data and drafted the initial manuscript; Panwar J was the guarantor and designed the study; Thomas BP revised the article critically for important intellectual content; language revision and final approval of the version of the article was done by Mathew A and Thomas BP.

Institutional review board statement: The study was reviewed and approved by the Institutional review board, Christian Medical College, Vellore, India.

Informed consent statement: Not applicable given the retrospective design of our study.

Conflict-of-interest statement: There are no conflicts of interest to report.

Data sharing statement: No additional data is available.

Open-Access: This article is an open-access article which was selected by an in-house editor and fully peer-reviewed by external reviewers. It is distributed in accordance with the Creative Commons Attribution Non Commercial (CC BY-NC 4.0) license, which permits others to distribute, remix, adapt, build upon this work non-commercially, and license their derivative works on different terms, provided the original work is properly cited and the use is non-commercial. See: <http://creativecommons.org/licenses/by-nc/4.0/>

Manuscript source: Invited manuscript

Correspondence to: Jyoti Panwar, MD, FRCR, Musculo-

skeletal Radiology Fellow, Joint Department of Medical Imaging, University Health Network, University of Toronto, 585 University Avenue, Toronto, Ontario M5G 2N2, Canada. drjyotimch@gmail.com
Telephone: +1-416-3403372

Received: September 26, 2016

Peer-review started: September 28, 2016

First decision: October 20, 2016

Revised: January 17, 2017

Accepted: March 16, 2017

Article in press: March 17, 2017

Published online: May 28, 2017

Abstract

AIM

To highlight the salient magnetic resonance imaging (MRI) features of the intraneural ganglion cyst (INGC) of various peripheral nerves for their precise diagnosis and to differentiate them from other intra and extra-neural cystic lesions.

METHODS

A retrospective analysis of the magnetic resonance (MR) images of a cohort of 245 patients presenting with nerve palsy involving different peripheral nerves was done. MR images were analyzed for the presence of a nerve lesion, and if found, it was further characterized as solid or cystic. The serial axial, coronal and sagittal MR images of the lesions diagnosed as INGC were studied for their pattern and the anatomical extent along the course of the affected nerve and its branches. Its relation to identifiable anatomical landmarks, intra-articular communication and presence of denervation changes in the muscles supplied by involved nerve was also studied.

RESULTS

A total of 45 cystic lesions in the intra or extraneural

locations of the nerves were identified from the 245 MR scans done for patients presenting with nerve palsy. Out of these 45 cystic lesions, 13 were diagnosed to have INGC of a peripheral nerve on MRI. The other cystic lesions included extraneural ganglion cyst, paralabral cyst impinging upon the suprascapular nerve, cystic schwannoma and nerve abscesses related to Hansen's disease involving various peripheral nerves. Thirteen lesions of INGC were identified in 12 patients. Seven of these affected the common peroneal nerve with one patient having a bilateral involvement. Two lesions each were noted in the tibial and suprascapular nerves, and one each in the obturator and proximal sciatic nerve. An intra-articular connection along the articular branch was demonstrated in 12 out of 13 lesions. Varying stages of denervation atrophy of the supplied muscles of the affected nerves were seen in 7 cases. Out of these 13 lesions in 12 patients, 6 underwent surgery.

CONCLUSION

INGC is an important cause of reversible mono-neuropathy if diagnosed early and surgically treated. Its classic MRI pattern differentiates it from other lesions of the peripheral nerve and aid in its therapeutic planning. In each case, the joint connection has to be identified preoperatively, and the same should be excised during surgery to prevent further cyst recurrence.

Key words: Intra-neural; Magnetic resonance imaging; Peripheral nerves; Extra-neural; Ganglion cyst

© The Author(s) 2017. Published by Baishideng Publishing Group Inc. All rights reserved.

Core tip: This is a retrospective study to emphasize the characteristic magnetic resonance imaging (MRI) features of the intra-neural ganglion cyst (INGC) of the peripheral nerves. The radiologist should recognize the classic MRI pattern of the INGC, its joint connection and imaging anatomy of the involved nerve. This would aid surgeons in complete removal of the cyst, prevent its recurrence and hence improved patient outcomes. Both radiologists and surgeons should be aware of other neurogenic lesions and the extra neural ganglion cyst which may also have a joint connection.

Panwar J, Mathew A, Thomas BP. Cystic lesions of peripheral nerves: Are we missing the diagnosis of the intra-neural ganglion cyst? *World J Radiol* 2017; 9(5): 230-244 Available from: URL: <http://www.wjgnet.com/1949-8470/full/v9/i5/230.htm> DOI: <http://dx.doi.org/10.4329/wjr.v9.i5.230>

INTRODUCTION

Patients presenting with thickened peripheral nerves and nerve palsy are often diagnosed as Hansen's disease (HD) in endemic areas when other diagnostic tests

come back inconclusive^[1-4]. These patients may be thus treated with long term empirical multi-drug therapy for the same^[3-6]. An intra-neural ganglion cyst (INGC) is a non-neoplastic mucinous cyst within the epineurium of a nerve and commences from an adjoining joint^[7-13]. These cysts are filled with a mucinous material which is walled off by a fibrous layer^[7-9]. As these cysts expand within the epineurium, they displace and compress the adjacent nerve fascicles leading to pain, paresthesia, tingling and muscle paralysis in the distribution of the involved nerve^[14,15]. It may follow trivial trauma to the joint^[7]. The clinical evaluation of an involved nerve will show thickening if superficial and a variable degree of sensory-motor disturbance along its distribution^[13-15]. This presentation of variable motor palsy and sensory symptoms of acute onset may mimic other conditions like lumbosacral disc disease, pelvic or shoulder pathologies and may delay early detection^[14,16]. The diagnosis of INGC can be confirmed by imaging techniques like magnetic resonance imaging (MRI) and high resolution ultrasonography^[14-19]. The nerve paralysis is usually reversible if the nerve is surgically decompressed early. Its articular connection should be identified and disconnected during surgery to prevent recurrence^[14,15,20].

MATERIALS AND METHODS

This study was approved by the institutional review board, and consent from all patients was waived. This research did not receive any specific grant from funding agencies in the public, commercial, or not-for-profit sectors.

Patient selection

All MR images of the patients presenting with peripheral nerve palsy from July 2005 to December 2015 were selected from our radiology database. A computer search was also performed for the term "ganglion cyst" of proximal tibiofibular (PTF) joint, "paralabral cyst", "intra-neural ganglion cyst", ganglion cyst of knee, shoulder, elbow and hip joints in the radiology information system database. From this cohort of images, all nerves with solid and cystic lesions were first identified. Among the cystic lesions thus identified the images showing elongated cystic lesions of the peripheral nerve along its course and those that fulfilled one or more of the inclusion criteria for INGC (Table 1) were selected. Thirteen such lesions were identified and their MR images, available clinical details, follow-up information and histopathology were reviewed by a musculoskeletal radiologist.

Image acquisition

Images were obtained by a variety of MRI scanners, including 0.5-T units ($n = 1$; NT Intera, Philips Healthcare, Netherland), 1.5-T units ($n = 2$; Magnetom Avanto, Siemens Healthcare, Erlangen, Germany), and 3-T units ($n = 6$; Intera Achieva, Philips Healthcare, Best,

Table 1 Inclusion criteria for intraneural ganglion cyst

Multilobular elongated hyperintense cystic mass on T2 weighted imaging
Distributed along the course of a peripheral nerve and its branches
Extension along the articular branch to the adjacent joint
Denervation changes of the muscles supplied by involved nerve

Netherlands). The imaging protocol and parameters also varied from case to case. The images were acquired in all three orthogonal planes including axial, coronal and sagittal in all patients. Fast spin echo T2-weighted axial, coronal and sagittal images with or without fat suppression and T1-weighted axial images were done in all patients scanned in the 0.5-T and 1.5-T MR scanner. Proton density fat suppressed axial, coronal and sagittal images along with T1-weighted axial images were available for all cases done in the 3-T MR scanner.

Image analysis

The MR images of all cystic lesions were reviewed by a musculoskeletal radiologist on a General Electric® (GE) picture archiving and communication system workstation. The images were evaluated, specifically looking for the presence of the following features: (1) the presence of T2/fat suppressed (T2 or proton density) hyperintense cystic lesion, along the nerve or its branches; (2) the exact anatomical site, intra or extra-neural location; (3) any communication to the adjacent joint along an articular branch; (4) the morphology of the cyst in terms of shape and pattern; and (5) denervation changes of the affected muscle compartment was also assessed.

RESULTS

Clinical findings

The mean age of the patients was 38.2 years (range 9-67 years). There were ten males and two females in this series. Pain along the distribution of the involved nerve and weakness of muscles supplied by the same were the most common presenting symptoms and was present in all 12 patients. One lesion was asymptomatic. The same was discovered incidentally on the contralateral side during routine imaging. Four cases of INGCS involving the common peroneal nerve (CPN) were primarily diagnosed as cystic schwannoma and one suprascapular and obturator nerves lesion were labeled as a paralabral and obturator foramen ganglion cysts respectively. However, no labral tear was seen on MR imaging in either case. Of the 13 lesions, 6 cysts were excised or decompressed by surgery. The articular connection was excised during surgery in 4 out of 5 patients with CPN (PTF joint connection) and in one patient with suprascapular nerve (AC joint connection) involvement.

The other cystic lesions included: 9 cases of extra-neural ganglion cyst (ENGCS) of PTF joint in close relation with CPN, one ENGCS of radio-humeral (elbow) joint impinging upon the deep branch of radial nerve, 6 cases of paralabral cyst impinging upon the suprascapular

nerve, 8 cases of cystic schwannoma and 8 cases of nerve abscesses related to HD involving various peripheral nerves. Table 2 summarizes the clinical details of patients with cystic lesions related to and of the nerve.

MRI findings

INGCS: An elongated multi-lobulated cystic lesion, oriented longitudinally along the course of the nerve was seen in all 13 INGC lesions. An extension of the cyst along the articular branch with intra-articular communication was demonstrated in 12 of these lesions (Figures 1 and 2).

Out of the 13 lesions, 7 involved the peroneal nerve with one patient having bilateral lesions of which one side was asymptomatic. The tibial (Figures 3-5) and suprascapular nerves (Figure 6) were involved in 2 patients.

One case each of the obturator (Figures 7 and 8) and proximal sciatic nerves (Figures 9 and 10) were also identified.

A variable extension of cysts along the branches of the parent nerve was seen in 12 cases (Figures 1-5, 8 and 11). Varying stages of denervation of the supplied muscles were seen in 7 cases (Figures 3-5, 8 and 11).

Six patients underwent surgery and their diagnoses were confirmed by histo-pathological evaluation of the biopsied specimens. The intraoperative images of one of these patients are shown in Figure 12.

In one tibial nerve INGC, in addition to PTF joint connection, a second posterior knee joint connection was also noted (Figure 4). In four cases with CPN involvement, the INGC could also be seen extending distally for a variable length along the deep (Figures 2) and superficial peroneal (Figure 11) nerve branches. The obturator nerve cyst also extended along its anterior branch (Figure 8) the tibial nerve lesions extended along the branch to the popliteus and tibialis posterior muscles (Figure 3-5). Table 3 summarizes the MRI findings of INGC of the peripheral nerves in this series.

Other cystic lesions

ENGCS: These are most commonly seen around the PTF joint in close relation with CPN and its branches. Its characteristic MR features are described in Figure 13 and its differentiation from INGC on imaging is illustrated in Figure 14 and summarized in Table 4.

Cystic schwannoma: Schwannomas represent the most common peripheral nerve sheath tumor^[21] and are mostly solid or heterogeneous tumors. However, cystic schwannomas of the peripheral nerve are uncommon^[22,23] and may mimic other extra or intraneural cystic lesions. MR features of cystic schwannoma of CPN are illustrated in Figure 15.

Paralabral cyst: Paralabral cysts of the shoulder joint are commonly seen in the middle aged men and cause impingement of the suprascapular nerve. They are commonly located at the posterosuperior glenoid region, secondary to a labral tear. They can extend into

Table 2 Epidemiological data of patients diagnosed with cystic lesions related to the nerve

Patient data	Intraneural ganglion cyst	Extraneural ganglion cyst	Para-labral cyst	Cystic schwannoma	Nerve abscess
Total number of lesions	13	10	6	8	8
Mean age (yr)	38.2	30.5	32	42.6	28.2
SD	14.66	16.42	3.94	10.79	12.84
Common symptoms	Pain along distribution of nerve, motor weakness	Pain and swelling	Pain and weakness of external rotators	Parasthesia, pain along distribution of nerve	Parasthesia and weakness
Male:female ratio	10:2	6:4	6:0	5:3	8:0
Nerves involved	CPN 7 Tibial 2 Suprascapular 2 Prox. Sciatic 1 Obturator 1	Near CPN 9 Radial 1	Near SSN 6	CPN 3 Median 2 Sciatic 1 Tibial 1 Radial 1	Ulnar 5 ¹ CPN 2 ¹ Median 3 Radial 3 ¹
Number who underwent surgery	6/13	10/10	6/6	8/8	3/8
Correct diagnosis on MRI	7/13	8/10	6/6	8/8	8/8

¹Combined involvement of multiple nerves. MRI: Magnetic resonance imaging; CPN: Common peroneal nerve.

Table 3 Summary of magnetic resonance imaging findings of intraneural ganglion cyst of peripheral nerves

SN	Involved nerve	Extension			Labral or capsular tear	Joint abnormality	Muscle denervation
		Anatomical extent along the parent nerve	Branches	Intra-articular extension			
1	Right CPN	Upto sciatic bifurcation	Recurrent articular	Anterior aspect of PTF joint	Negative	-	Muscles of anterolateral compartment of leg
2	Left CPN	Upto posterolateral fibular head	Recurrent articular, deep peroneal	Anterior aspect of PTF joint	Negative	-	-
3	Right CPN	Upto sciatic bifurcation	Recurrent articular, superficial and deep peroneal	Anterior aspect of PTF joint	Negative	-	Muscles of anterolateral compartment of leg
4	Left CPN	Upto posterolateral fibular head	Recurrent articular, deep peroneal	Anterior aspect of PTF joint	Negative	-	-
5	Left CPN	Upto posterolateral fibular head	Recurrent articular, deep peroneal	Anterior aspect of PTF joint	Negative	-	Muscles of anterolateral compartment of leg
6	Right CPN	Upto posterolateral fibular head	Recurrent articular	Anterior aspect of PTF joint	Negative	-	Muscles of anterolateral compartment of leg
7	Right CPN	Upto neck of fibula	Recurrent articular	Anterior aspect of PTF joint	Negative	-	-
8	Right obturator	Along the lateral pelvic wall to pelvic brim	Anterior division	Anteromedial aspect of hip joint	Negative	-	Adductor brevis and magnus
9	Right suprascapular	Suprascapular to spinoglenoid notch	-	-	Negative	-	Supra and infraspinatus
10	Left proximal sciatic	At sciatic notch	Articular	Posteromedial aspect of hip joint	Negative	-	-
11	Right tibial	Upto tibial nerve	Articular, branch to popliteus muscle	Posterior aspect of PTF joint	Negative	-	-
12	Left tibial	Upto sciatic bifurcation	Articular, branch to popliteus muscle, branch to tibialis posterior muscle	Posterior aspect of PTF and knee joints	Negative	-	Popliteus and tibialis posterior
13	Right suprascapular	From the level of AC joint to below the spinoglenoid notch	Articular branch to AC joint	AC joint	Negative	-	-

PTF: Proximal tibiofibular; AC: Acromioclavicular; CPN: Common peroneal nerve.

the spinoglenoid notch and can cause compression of the suprascapular nerve (Figure 16).

Nerve abscess related to HD: Granulomatous nerve lesions of HD may show central breakdown and abscess formation. These are relatively uncommon and are seen

in the tuberculoid form of the leprosy (Figure 17).

DISCUSSION

INGC is often referred to as a rare non-neoplastic mucinous cyst located within the epineurium of peripheral

Table 4 Magnetic resonance features differentiating intraneural ganglion cyst from extraneural ganglion cyst

	Intraneural ganglion cyst	Extraneural ganglion cyst
Cyst size	Small	Large
Cyst shape	Tubular beaded configuration	Globular
Cyst pattern and location	It is along the course of the nerve and its branches with no fat plane between the cyst and the nerve	It does not follow the course of the nerve; the nerve is seen separately from the cyst with an intervening preserved fat plane; usually located in between the fibula and peroneus longus muscle, with or without an intramuscular extension
PTF joint connection	Is present and the tail lies anteromedial to proximal fibula between 10-12 o'clock position on axial MR images	Is present but located more superiorly and anterolateral to the proximal fibula at 12-2 o'clock position on axial MR images
Relation with fibula	The extension of the cyst along the articular branch appears to cross the fibula from medial to lateral ("Transverse limb sign")	The cyst never crosses the fibula and always lies anterior, anterolateral or lateral to the fibula (Absent "Transverse limb sign")
Muscle denervation	Common	Uncommon

MR: Magnetic resonance; PTF: Proximal tibiofibular.

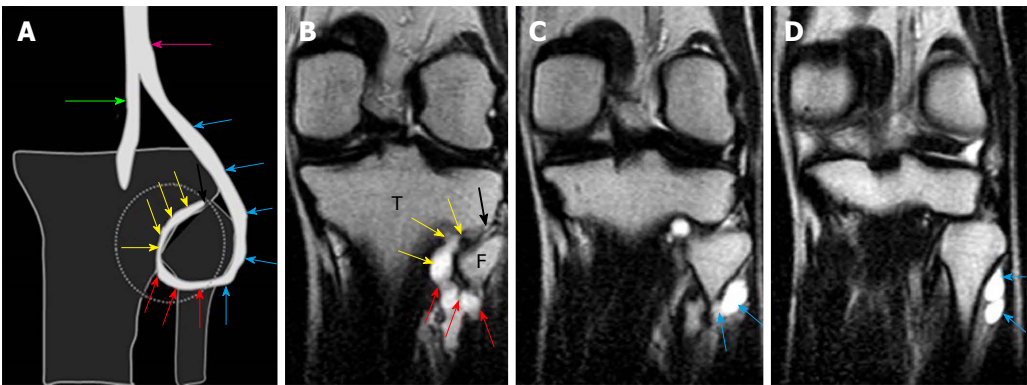


Figure 1 A shows a diagrammatic representation of the intraneural ganglion cyst associated with the proximal tibiofibular joint in the coronal plane; B-D are serial, coronal, T2-weighted, fast spin echo images of the knee show the origin of the lobulated tubular cyst from the proximal tibiofibular joint also called the "tail sign" demonstrated by the black arrows. The further extension along the descending limb (yellow arrows) of the articular branch represents the "vertical limb sign". The ascending limb of the articular branch (red arrows) demonstrates the "transverse limb sign" which continues to the CPN (blue arrows). Extension of the cyst into the two limbs of the articular branch and further ascent into the parent nerve represents the "u-sign". T: Tibia; F: Fibula; CPN: Common peroneal nerve.

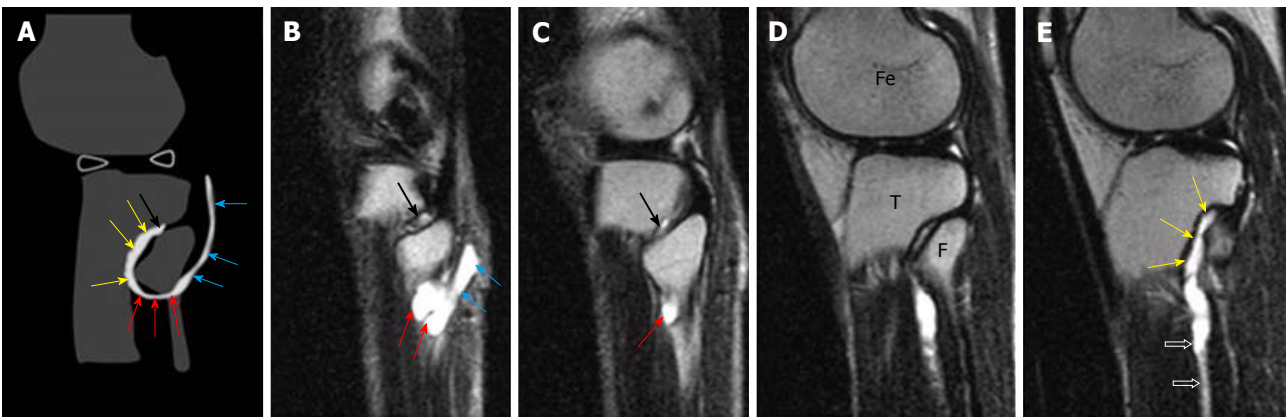


Figure 2 A shows a diagrammatic representation of the intraneural ganglion cyst associated with the proximal tibiofibular joint in the sagittal plane; B-E serial, sagittal, T2-weighted, fast spin echo images of the knee show the origin of the lobulated tubular cyst from the proximal tibiofibular joint represents the "tail sign" (black arrows). The further extension along the descending limb (yellow arrows) represents the "vertical limb sign" and ascending limb (red arrows) of the articular branch demonstrates the "transverse limb sign"; which continues to the CPN (blue arrows). The cyst also extends along the deep peroneal nerve (open arrows) in image E. T: Tibia; F: Fibula; CPN: Common peroneal nerve; Fe: Femur.

nerves and is closely related to an adjoining joint^[7-11,20,24,25]. These lesions commonly affect the peroneal nerve at the knee but can involve the other peripheral nerves^[7,26,27]

as shown in this series. They usually present with mild symptoms and remain undiagnosed initially^[27]. MRI plays an important role in diagnosing this condition and can

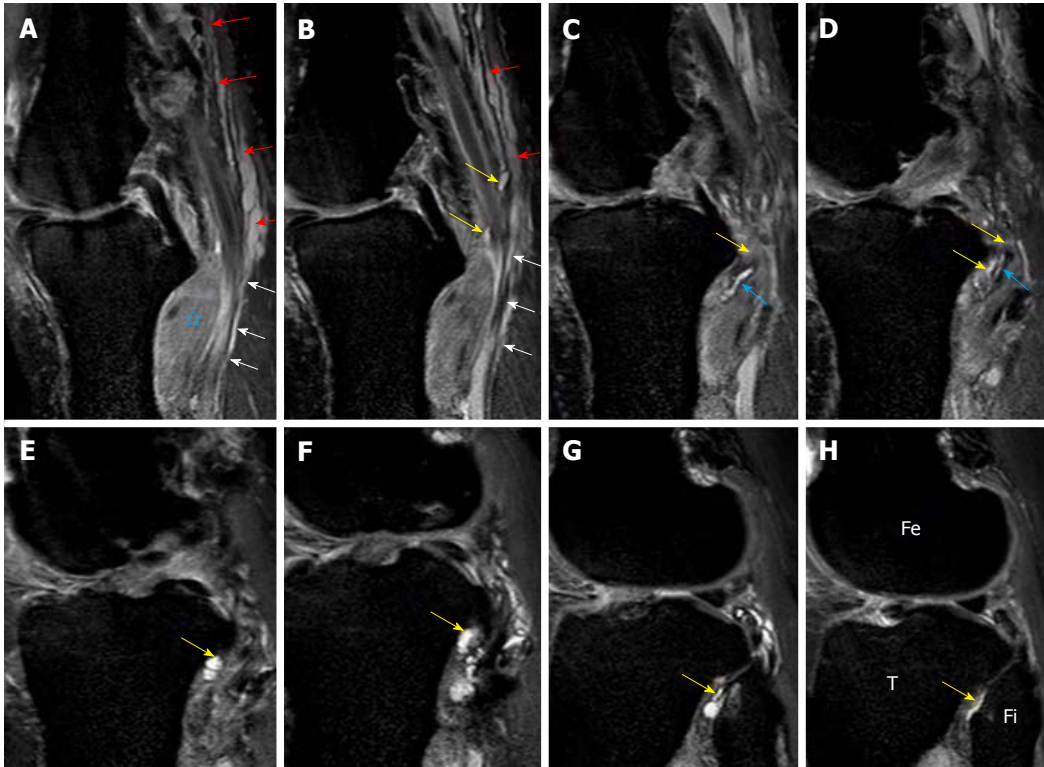


Figure 3 Images A-H show serial, proton density-weighted fat suppressed sagittal sections of the knee demonstrate the longitudinally oriented cystic lesion in the tibial nerve (red arrows) with extension along the articular branch to proximal tibiofibular joint (yellow arrows), branch to popliteus (blue arrows) and tibialis posterior muscles (white arrows). Note the denervation edema in the popliteus muscle (star). T: Tibia; Fi: Fibula; Fe: Femur.

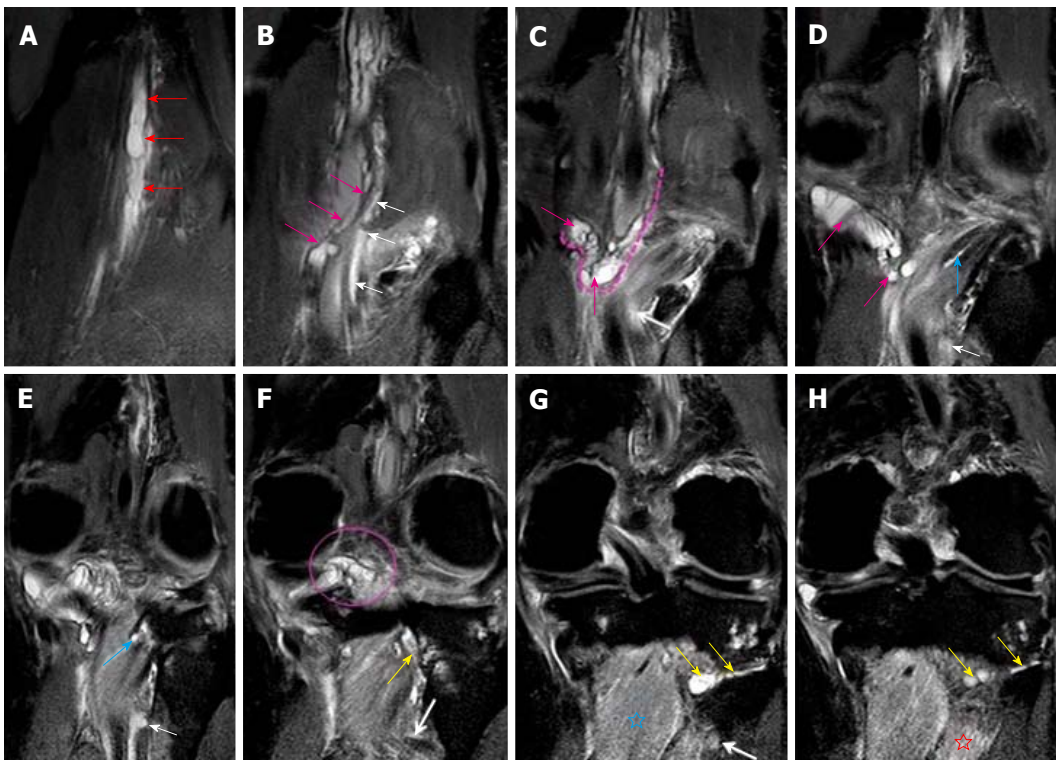


Figure 4 Images A-H show serial, proton density-weighted fat suppressed coronal sections of the knee demonstrate the longitudinal extent of intraneural cyst in the tibial nerve (red arrows), with propagation of cyst along the articular branches that communicate with the posterior aspect of knee joint (pink arrows, dashed line and circle) and to the postero-inferior part of proximal tibiofibular joint (yellow arrows). This represents a dual joint connection (knee and proximal tibiofibular) from the same intraneural ganglion cyst. The cyst also extends along the branch to the popliteus (blue arrows) and tibialis posterior muscles (white arrows). Note the denervation edema in the popliteus (blue star) and tibialis posterior (red star) muscles. Superiorly, the cyst extends up to the bifurcation of the sciatic nerve in the distal third of the thigh.

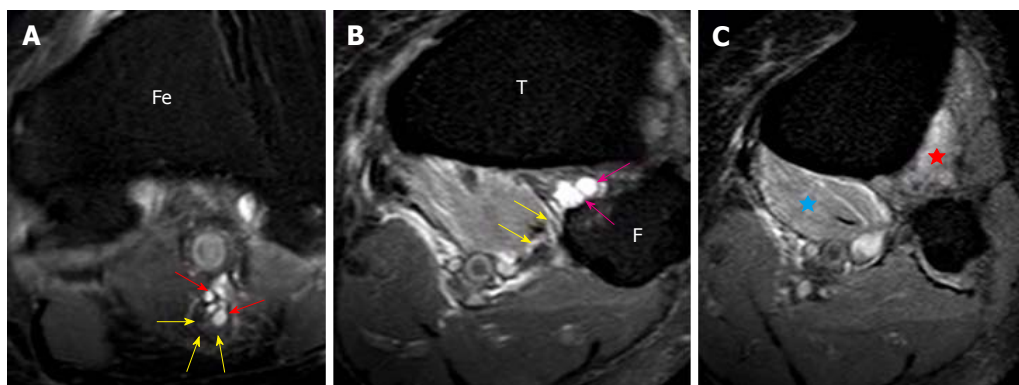


Figure 5 Images A-C show serial, proton density-weighted fat suppressed axial images of the knee demonstrate the eccentric cyst (red arrows) within the epineurium of tibial nerve displacing the nerve fascicles (yellow arrows) which represents the “signet ring sign” (A). The joint connection (pink arrows) is well appreciated where the cyst arises from the posterior aspect of the PTF joint. This represents the “tail sign” (B). The cyst (yellow arrows) extends along the posterior surface of the popliteus muscle into the branch to popliteus muscle. Denervation edema is seen in the popliteus (blue star) and tibialis posterior (red star) muscles. T: Tibia; F: Fibula; Fe: Femur; PTF: Proximal tibiofibular.

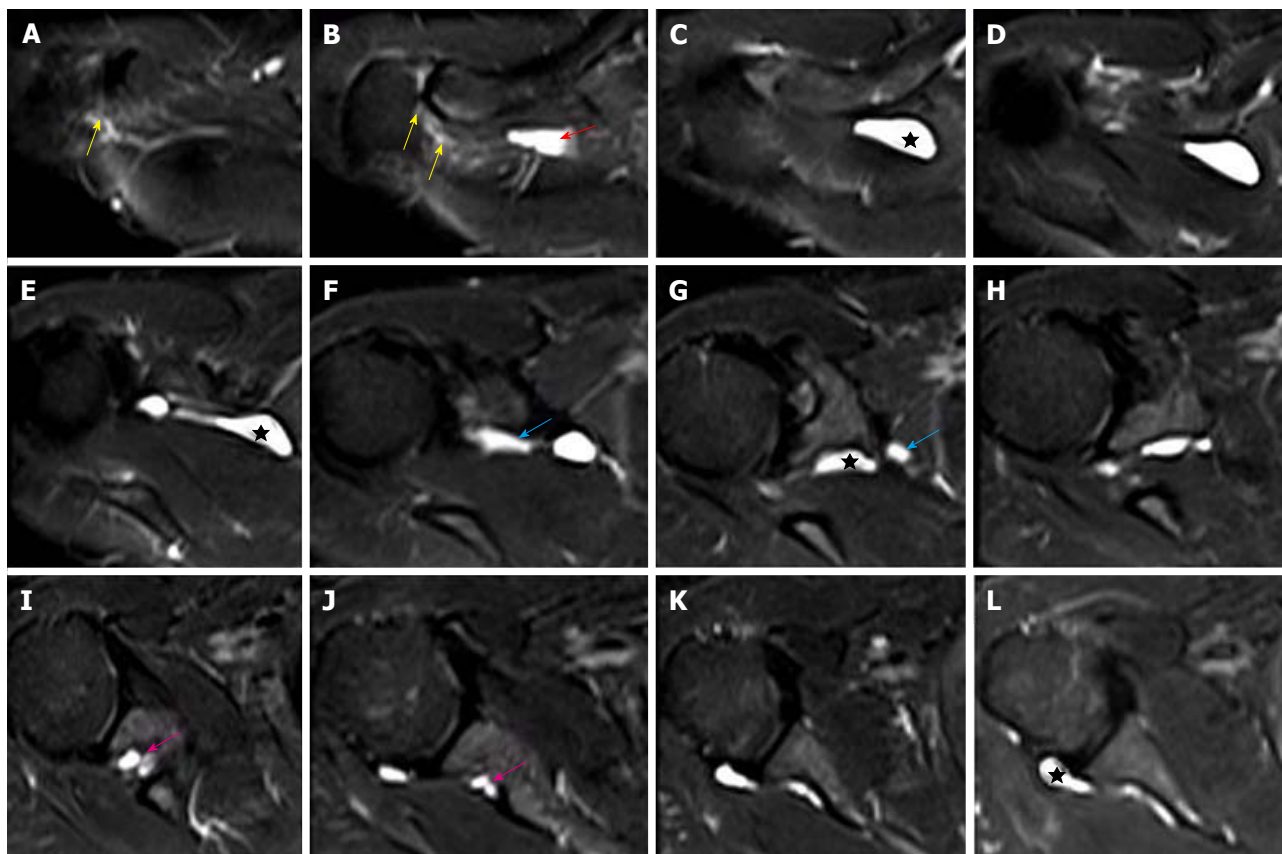


Figure 6 Images A-L show serial T2-weighted fat suppressed axial sections of the right shoulder, outlines the longitudinally oriented cyst (stars) along the course of the suprascapular nerve. The cyst extends from the level of the acromioclavicular joint (B) to the posterior aspect of glenohumeral joint (L). A narrow joint connection extends along the expected course of the articular branch of the suprascapular nerve to the acromioclavicular joint (yellow arrows). Further descent of the intraneural cyst through the posterior triangle into the suprascapular and spinoglenoid notches are demonstrated by red, blue and pink arrows respectively. No obvious labral or capsular tear or degeneration of joint is noted on magnetic resonance imaging.

reliably demonstrate the presence and the pattern of the cystic lesion and the exact level of communication of the cyst to the adjacent joint^[8,20,28,29]. This typical imaging pattern and its consistent anatomical location within the nerves and the communication with adjoining joints, distinguish the intraneural cyst from the other neurogenic or extra neural cystic lesions^[8,28,29]. Recognition of its articular connection on MR further helps in complete

removal of the cyst, thus avoiding cyst recurrences^[20,29].

The exact pathogenesis of the INGC is still not known. There are numerous hypotheses for its pathogenesis ranging from recurrent trauma, intra-neural hemorrhage, mucoid degeneration, *de novo* formation from haematomatous cell rests^[7,11,30-32] and the more recent “unified articular theory”^[20,29,33,34]. According to the latter, the INGC originates from an adjoining joint and dissects

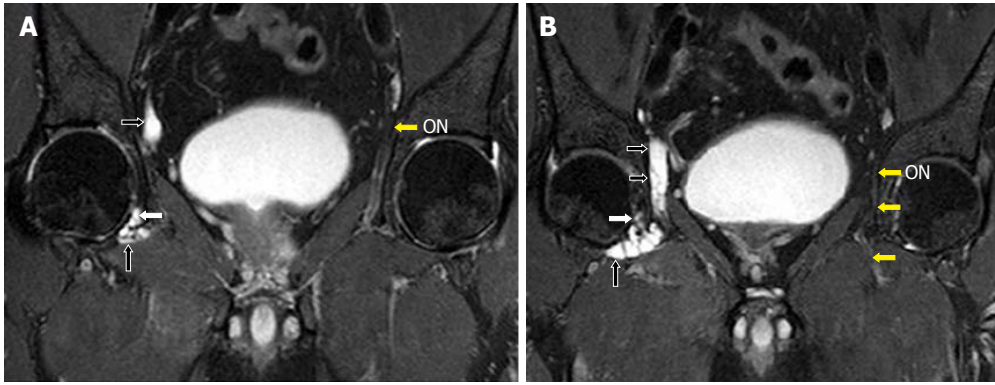


Figure 7 Images A, B show serial, T2-weighted fat suppressed coronal sections of the pelvis that demonstrates the longitudinally oriented intraneural cyst in the right obturator nerve (black arrows). The extension along the articular branch to the anteromedial aspect of right hip joint (white arrows) is also seen. Note the normal left obturator nerve (ON, yellow arrows). Reprinted with permission from Acta Neurologica Belgica.

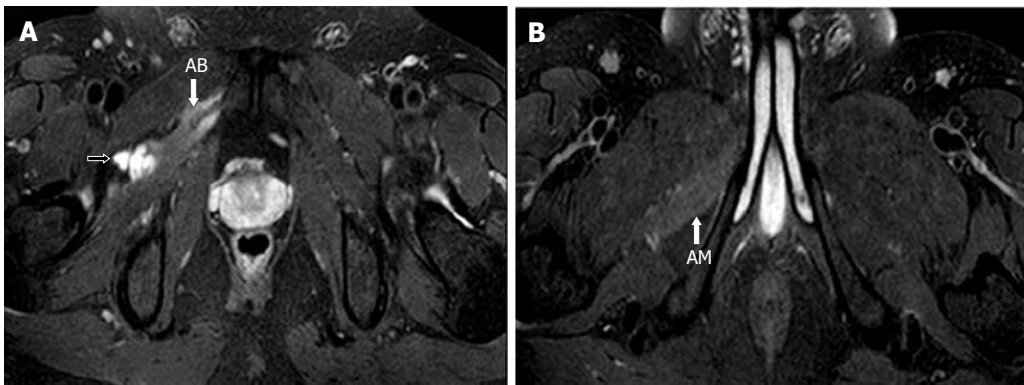


Figure 8 Image A, B show serial, T2-weighted fat suppressed axial images of the pelvis that demonstrates the further inferior extension of the cyst along the anterior branch of the obturator nerve (black arrow). Note the denervation atrophy of adductor brevis (AB) and magnus (AM) muscles. Reprinted with permission from Acta Neurologica Belgica.

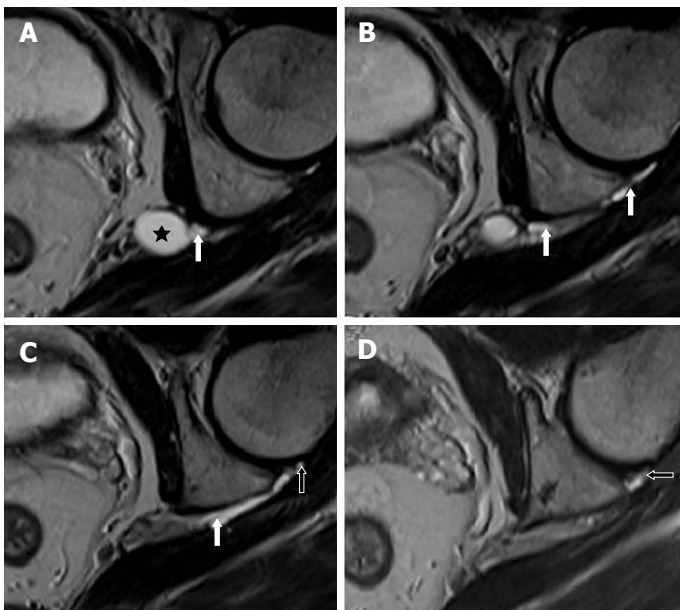


Figure 9 Image A-D show serial, T2-weighted, fast spin echo axial sections of the left hip joint highlighting a cyst (star) at the level of the left sciatic notch. An extension along the expected course of the articular branch of the sciatic nerve (white arrows) communicating with the posteromedial aspect of the ipsilateral hip joint (open arrows) is also seen.

along the articular branch into the parent nerve. The cyst dissects along the path of least resistance, namely the

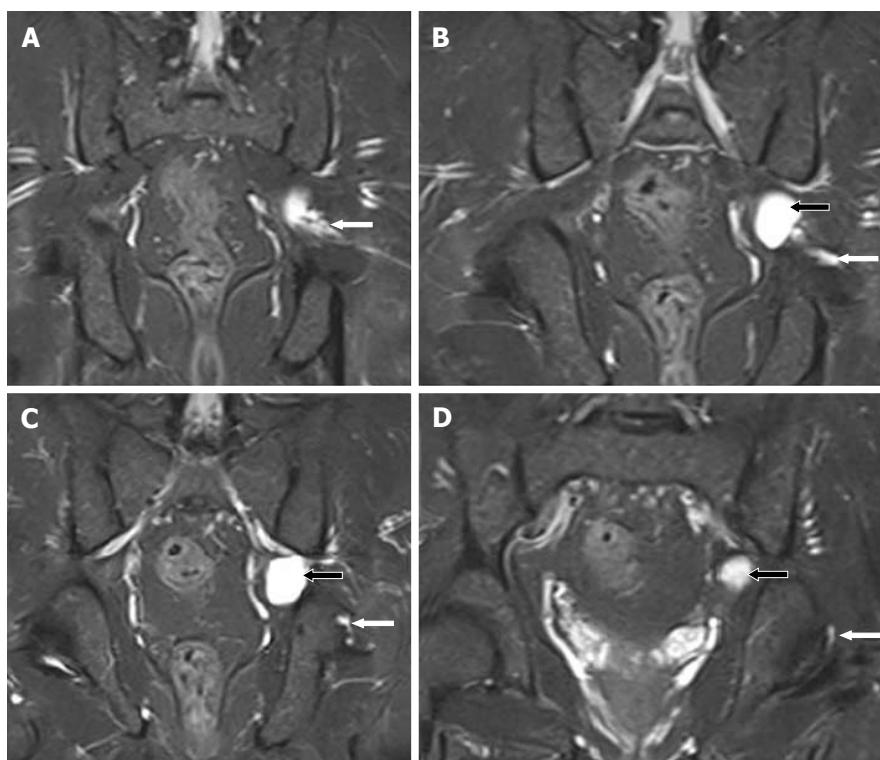


Figure 10 Images A-D show serial, T2-weighted fat suppressed coronal sections of the pelvis, demonstrate a cyst (black arrows) at the level of the left sciatic notch. The cyst extends along the articular branch of the sciatic nerve (white arrows) and communicates with the posteromedial aspect of the ipsilateral hip joint (D). No obvious labral or capsular tear or degeneration of joint is noted.

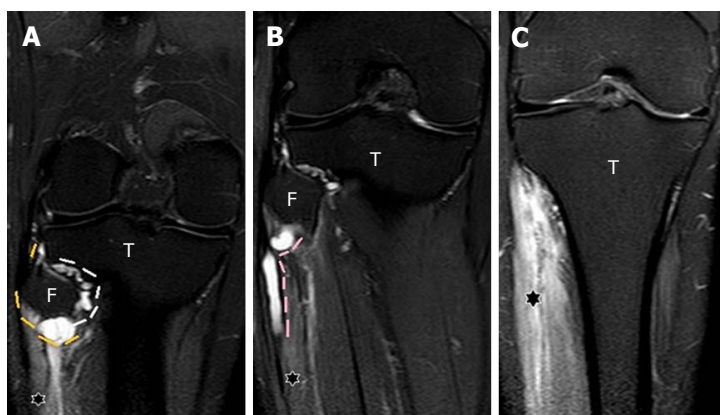


Figure 11 Images A-C show serial, coronal, proton density fat suppressed sections of the knee and proximal leg. The entire extent of the cyst within the articular branch (white dashes) to the PTF joint extending to the CPN (yellow dashes) at the posterolateral fibular neck is seen, demonstrating the "u-sign" (A). The cyst extends into the proximal portion of the superficial peroneal nerve (pink dashes) for a length of approximately 5 cm (B). Denervation hyperintensity of the muscles (stars) of anterior and peroneal compartments of the leg is also seen. T: Tibia; F: Fibula; PTF: Proximal tibiofibular; CPN: Common peroneal nerve.

perineural tissue of the nerve^[11,30,31].

The diagnostic work-up includes clinical examination, electrophysiological studies and imaging. The ganglion cyst usually presents with pain, motor weakness and paraesthesia along the distribution of involved nerve^[13-15,35]. Electrophysiological studies including electromyography and nerve conduction studies may indicate muscle denervation and conduction latency, respectively^[35-38]. MRI is the imaging of choice for the nerve and its surrounding soft tissues^[37,39-41]. It helps in defining the lesion along the course of the nerve.

On MR, these cysts are small in size and demonstrate the typical, tubular beaded configuration oriented longitudinally along the course of the involved nerve and its branches^[8,9,19,38,40]. They appear as low signal on T1-weighted and high signal on T2-weighted images^[42,43]. The joint connection and the extension of the cyst along the articular branch of nerve when present, can be well demonstrated^[20,29,30,36,38,39]. Further denervation muscle edema as T2 hyperintensity and muscle atrophy as T1 hyperintensity can be seen^[8,10,38]. In the peroneal intraneural cyst, the PTF joint connection and a cyst

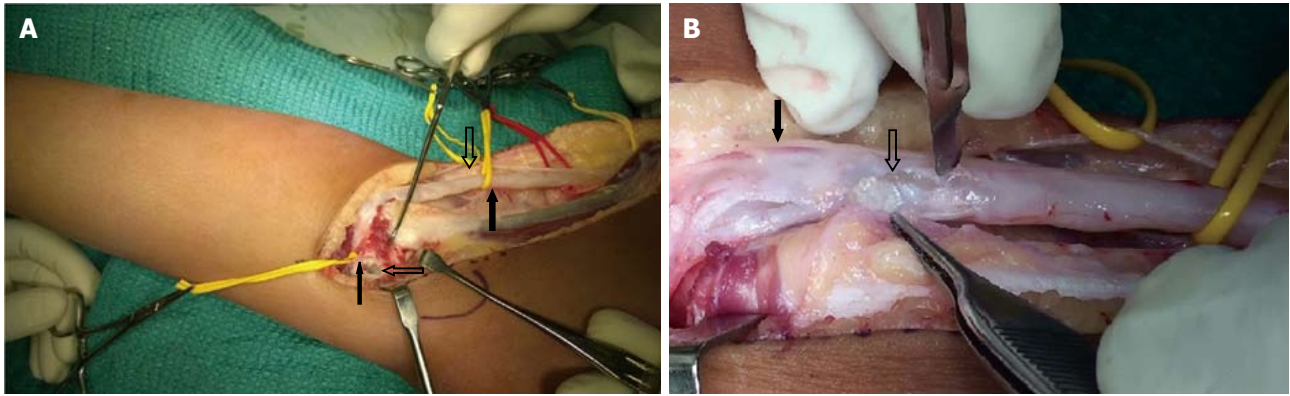


Figure 12 The intraoperative images of one of these patients. A: Surgical exposure and decompression of the CPN in a 9-year-old girl presenting with foot drop. The intraoperative picture shows a thickened CPN (thick block arrow); the sural communicating branch of the CPN (thick hollow arrow); the articular branch of the CPN (thin block arrow) and the arthrotomy of the PTF joint and a mucinous cyst within it (thin hollow arrow); B: Close up of the CPN, being decompressed with multiple stab incisions with mucin (hollow arrow) within the substance of the nerve. The superficial peroneal branch of the nerve (block arrow) appeared unaffected which correlated clinically. PTF: Proximal tibiofibular; CPN: Common peroneal nerve.

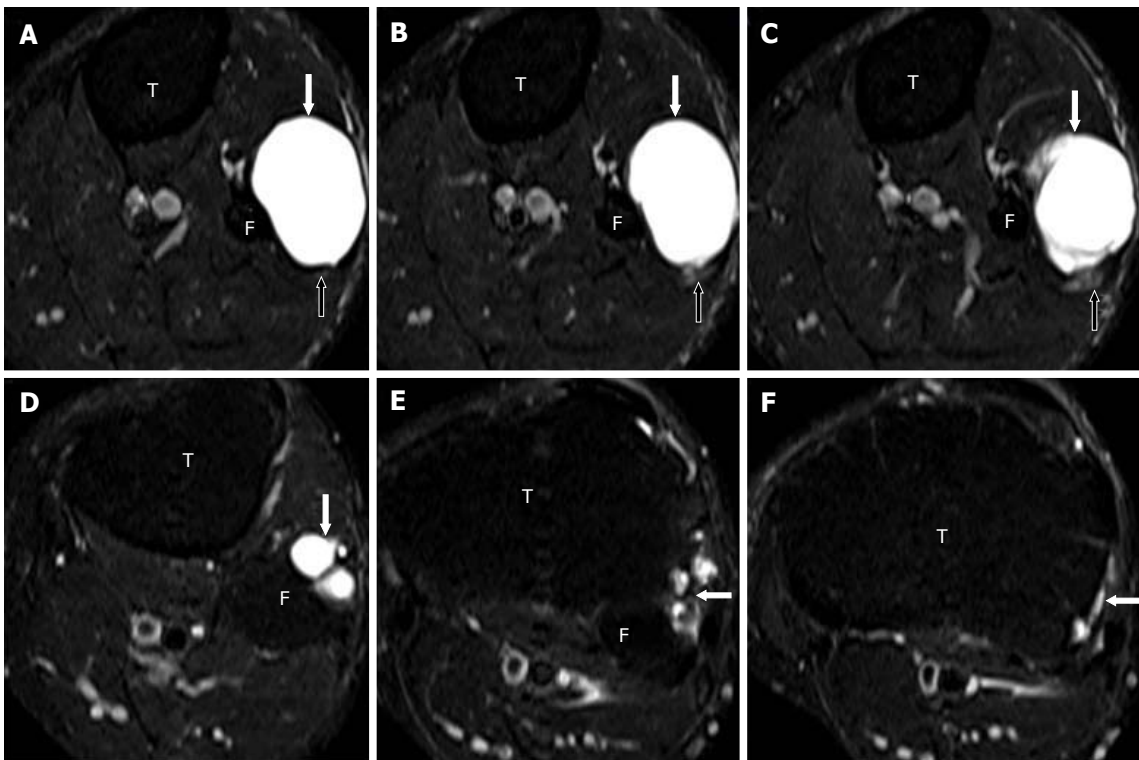


Figure 13 Images A-F show serial, T2-weighted fat suppressed axial sections of the proximal leg and demonstrate a large multilobulated globular extra-neural ganglion cyst (block arrows). The ENG is antero-lateral to the proximal fibula and indenting the peroneus longus muscle anteriorly (A-C). The CPN (open arrows) lies posterior to the cyst but is seen separate from it. The tail of the cyst (arrows in D-F) extends superiorly and communicates with the superior aspect of the PTF joint. PTF: Proximal tibiofibular; CPN: Common peroneal nerve; ENG: Extranural ganglion cyst; T: Tibia; F: Fibula.

along the descending and ascending limb of articular branch of CPN can be seen in all the three orthogonal planes^[20,24,29,38,39]. As described by Spinner *et al.*^[24,29,30] in 2008, on serial axial sections, the joint connection is interpreted as the “tail sign” (Figures 1-5 and 14) and the extension of the cyst in the ascending limb of the articular branch as the “transverse limb sign” (Figures 1, 2 and 14). An eccentric cyst within the outer epineurium of the CPN is interpreted as the “signet ring sign” (Figures 3-5 and 14). In all our seven CPN lesions, we found that

they had evidence of joint connection; presence of cysts along the articular branch; variable proximal ascent of the intra-neural cyst along the CPN and distal descent along its branches. On coronal images this extension of the cyst along the descending and ascending portions of the articular branch is interpreted as “u-sign” (Figures 1, 2 and 11).

In the lower extremity, less commonly, they can involve the lumbosacral plexus, sciatic, obturator and tibial nerves^[9,12,28,44]. The sciatic nerve can be involved in its

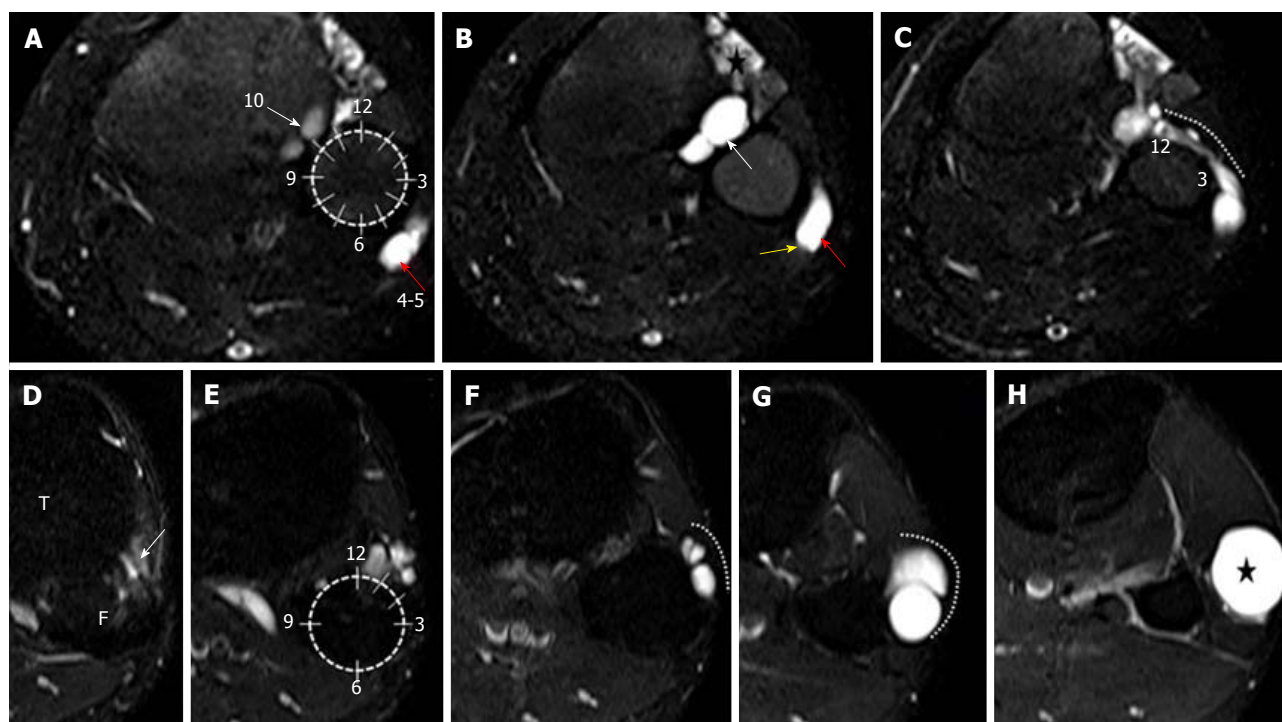


Figure 14 Axial, T2-weighted fat suppressed images A-H of the proximal leg show the left clock face model to differentiate intraneural ganglion cyst from extraneural ganglion cyst. A-C represent INGC where images A, B (at the upper-mid fibular head level) depict the joint connection of the cyst at the 10 o'clock (white arrows) which signifies the "tail sign". The cyst (red arrows) within the outer epineurium of the CPN (yellow arrow), between the 4 and 5 o'clock position represents the "signet ring sign". Image C, (at the level of fibular neck) shows the extension of the cyst along the ascending limb of the articular branch (dotted white line) depicting the "transverse limb sign". It crosses the anterior surface of fibula from the PTF joint and progresses clockwise from 12-3 o'clock position around the fibular head. On the other hand, images D-H, depicting ENGCG show a more superiorly located joint connection (white arrow) in between 12-2 o'clock position in images D, E. It lies anterolateral to the fibula (dotted white line) and never crosses it as seen in images F, G. The cyst (star) is more globular and lying in the intermuscular plane as seen in the image H. INGC: Intraneural ganglion cyst; CPN: Common peroneal nerve; ENGCG: Extraneural ganglion cyst; T: Tibia; F: Fibula.

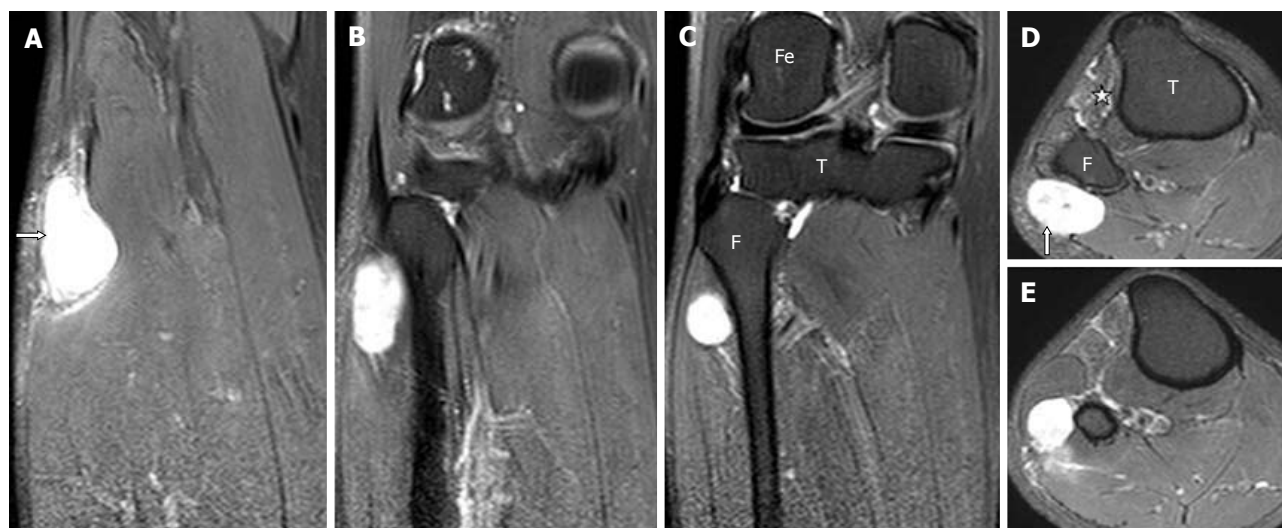


Figure 15 Serial, coronal (images A-C), and axial (images D-E), proton density fat suppressed sections show a well-defined oval cystic lesion at the posterolateral aspect of upper fibula along the expected course of common peroneal nerve which does not communicate within the proximal tibiofibular joint. Mild denervation edema is seen in the anterior compartment muscles (star). This is a case of cystic schwannoma involving the CPN. T: Tibia; F: Fibula; Fe: Femur; CPN: Common peroneal nerve.

proximal or distal portion. We have seen in our case, the presence of intra-neural sciatic ganglion cyst at the sacral notch, with characteristic tubular connection to the posteromedial hip joint on MR. There were no obvious degenerative changes in the joint, labral tears or other

structural problems on both the conventional MR and radiographs in the case reported herein. However, intra-articular contrast was not given and hence, the common underlying pathology of labral tear or capsular rent with intra-neural extension from a paralabral or para-articular

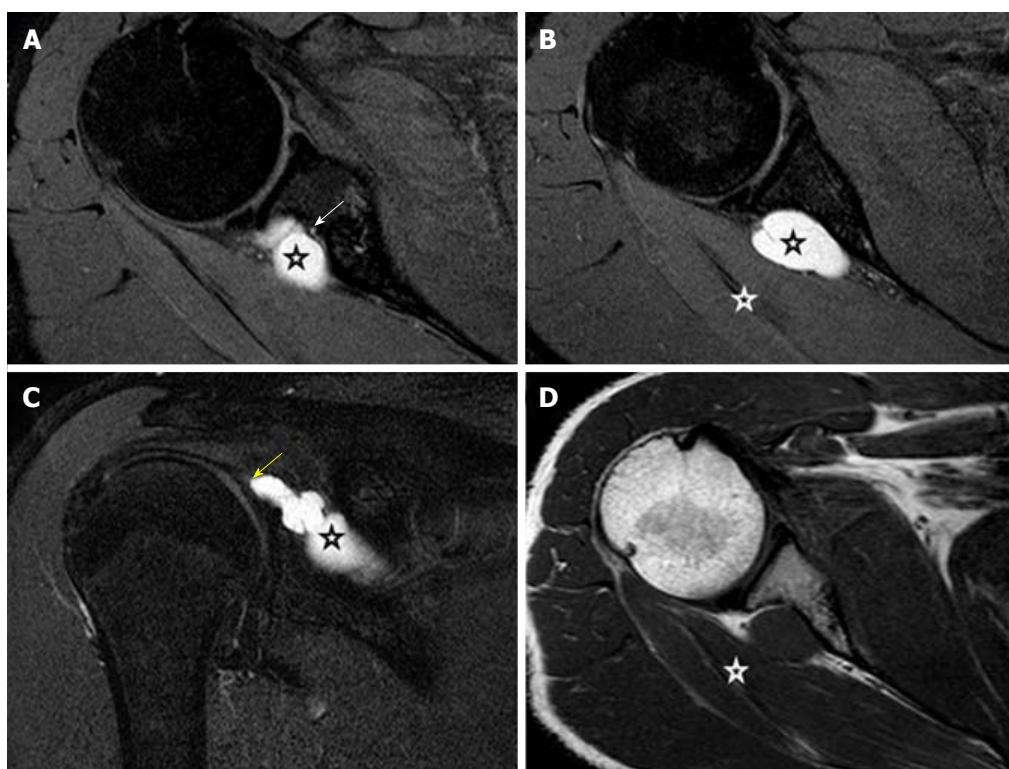


Figure 16 Proton density fat suppressed, serial axial (A, B), coronal (C) and T1-weighted, axial (D) show a well-defined lobulated slightly elongated cystic lesion (black stars) at the spinoglenoid notch compressing upon the suprascapular nerve (white arrow), which is seen separately from the cyst with preserved fat plane. There is a tail like communication (yellow arrow) of the cyst with the posterior labrum. This suggests labral tear with paralabral cyst formation. Denervation edema and mild volume loss in the infraspinatus muscle (white stars) is seen.

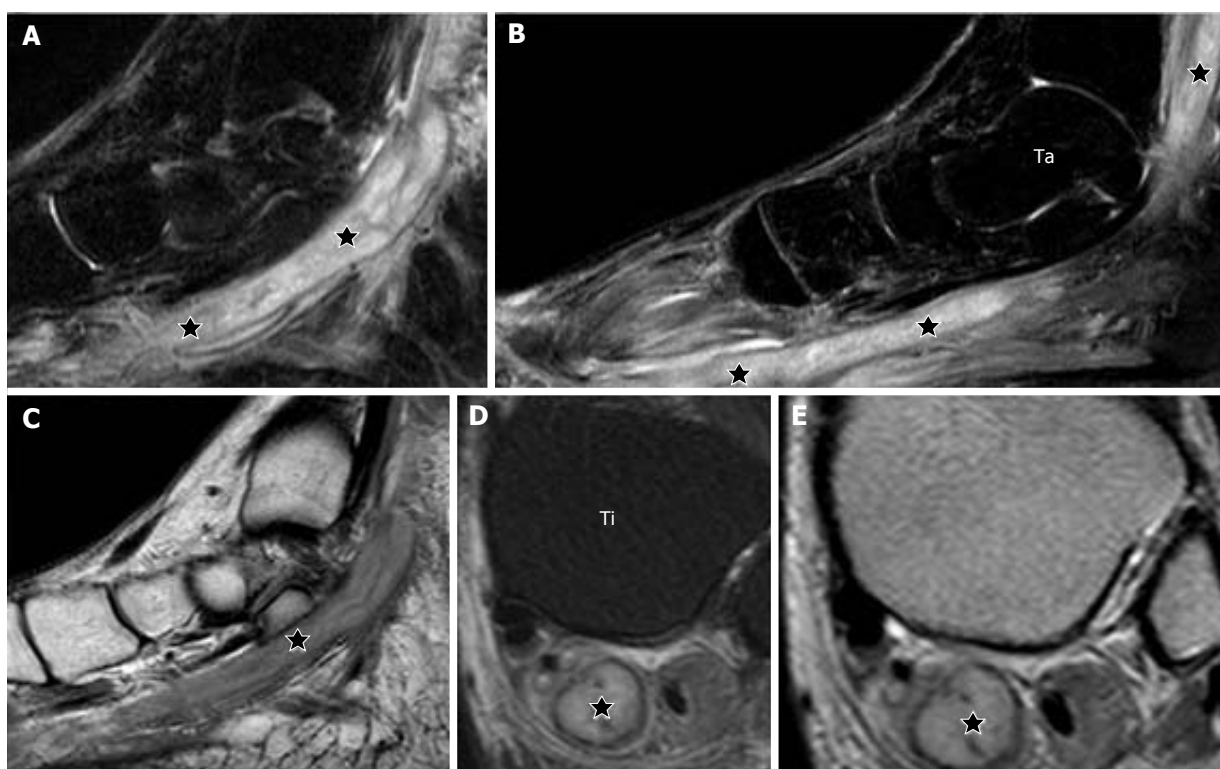


Figure 17 T2-weighted fat suppressed, serial sagittal (A, B); T1-weighted, sagittal (C); T2-weighted fat suppressed, axial (D) and proton density-weighted, axial (E) show an elongated tubular cystic lesion (stars) along the posterior tibial nerve at the lower leg, ankle and foot. The lesion is seen within the substance of the nerve and has a central cystic component (stars) and a peripheral thin wall consistent with an abscess (D, E). This is a case of Hansen's disease with posterior tibial nerve abscess; Ta: Talus; Ti: Tibia.

cyst cannot be completely excluded. In Spinner's series of INGC around the hip and pelvic region^[44], four out of five cases showed a cyst at the sciatic notch with an articular communication with the ipsilateral hip joint and further extension of the same into the sciatic nerve. Likewise, the obturator INGC also has a known joint connection with the anteromedial hip joint^[44,45] as seen in our case. The propagation of the cyst along the articular branch and further dissection of the cyst along the parent nerve and its anterior and posterior branches has been described^[45] and is demonstrated in the current case. Variable atrophy and denervation hyperintensity of ipsilateral adductor brevis and magnus muscles was also seen in our case.

Various case reports have described the involvement of tibial nerve in the popliteal fossa by the INGC^[7,12,36,40,46,47]. These tibial INGCs are the posterior counterpart of the peroneal INGCs and demonstrate an intraneural cyst and its connection to the adjacent joint *via* the articular branch to the PTF joint^[40,47,48]. In one of our cases there was evidence of dual communication of the tibial intra-neural cyst to both the knee and PTF joint through its corresponding articular branches (Figures 3-5) and further extension of cyst into the popliteus and tibialis posterior nerve branches (Figures 3-5). Denervation edema was noted in both popliteus and tibialis posterior muscles (Figures 3-5).

In the upper extremity, less commonly, they can involve the suprascapular, ulnar or median nerves^[8,49]. INGC is a common cause of suprascapular nerve impingement at the suprascapular and more commonly at the spino-glenoid notch originating from gleno-humeral joint and often associated with tears of the glenoid labrum^[50,51]. It may also arise from the acromioclavicular (AC) joint as articular branch of the suprascapular nerve innervate the AC joint^[52]. They track along the articular branch into the parent nerve and can be associated with a labral tear or capsular rent^[53]. However, in one of our cases, the joint connection could not be demonstrated. In the other case there was an AC joint connection (Figure 6). In contrast to this extra neural paralabral cyst where the nerve is seen separately from the cyst with a preserved fat plane in between, an INGC affecting the suprascapular nerve evolves within the epineurium of the nerve as seen in other peripheral nerve INGCs^[53-55].

In our series of 245 cases of peripheral nerve palsy for which imaging was done, 45 cases of cystic lesions were identified. Of these 45 cystic lesions, more than a fourth (13 cases), were diagnosed to be INGC retrospectively. Although the exact incidence of INGC is not known, in our series it was the commonest cause for the cystic nerve lesions. The fact that these lesions are reported as rare^[7-11] may be incorrect since they are often underdiagnosed as shown in our series. The primary radiological diagnosis of INGC in our series was correct in only 60% of the cases, *i.e.*, the last 7 cases in this series. Lack of knowledge of this pathological entity and absence of this entity in standard radiological textbooks were

probable reasons for its under-diagnosis among the early cases in this series. INGC as an entity was little known before the 90s even in western literature, being reported as rare case reports or case series prior to that^[14,56,57]. The others cystic lesions in this series varied from cystic schwannoma, extra-neural ganglion cysts, paralabral cysts and nerve abscesses. All of these cystic lesions were correctly diagnosed primarily except two ENGCS which were mistaken as cystic schwannoma.

This article endeavors to describe different INGCs at varying anatomical locations, to emphasize the fact that it is the single largest cause of surgically treatable mono-neuropathy due to a cystic nerve lesion. These lesions have a classic configuration, anatomical location within the nerve and extensions along its branches. Most have defined communications to the nearby joint and the innervated muscles show signs of denervation. Identification of the articular branch and disconnecting it is important to prevent recurrence. The youngest patient in this series had surgery, 7 mo after the onset of nerve palsy due to the late presentation at the hospital. The cysts were decompressed and the articular branch disconnected during the surgery. The innervated muscles showed MRC grade 4 recovery about one year after surgery, in spite of the late intervention.

In conclusion, over the past years, INGC has been increasingly recognized as a radio-pathologic entity. It is a cause of peripheral neuropathy that can be treated by surgery, but is often under-diagnosed. This research looked at a historic cohort of patients that were imaged for mono-neuropathy and within that the subsets of patients with cystic lesions were looked at, in greater detail. We were certainly missing the diagnosis of the INGC until recently. The surgical treatment of a cystic schwannoma is enucleation as opposed to the INGC where the nerve is decompressed and the articular branch is excised. This study re-emphasizes that any elongated cystic lesion along the course of a peripheral nerve and in the vicinity of a joint should be considered as an INGC unless proved otherwise. This will ensure that both the radiologist and the surgeon would diligently search for the articular (branch) connection and hence prevent a misdiagnosis and a possible recurrence.

COMMENTS

Background

Intraneural ganglion cysts (INGCs) of peripheral nerves occur within the epineurium and related to the adjoining joint were thought of as a relatively uncommon entity. They are generally formed when the joint fluid tracks into the epineural sheath of the articular branch of the nerve and further along the path of least resistance. They commonly present with sensory-motor symptoms along the distribution of the involved nerve. If these are identified and treated early, symptoms are reversible. The articular branch disconnection of the cyst will avoid the recurrence of the cyst. In this study, they evaluated 13 such cases involving the different peripheral nerves.

Research frontiers

Magnetic resonance imaging (MRI) is the most important modality to diagnose this condition. It also allows differentiating it from other intra or juxtra-neural

lesions like neurogenic tumors and the extra-neural ganglion cyst. Though it has been described as a rare disease in literature, the results of this study showed that it is the single largest cause of surgically treatable mono-neuropathy caused by a cystic nerve lesion.

Innovations and breakthroughs

In this study, the classic MRI pattern of the INGC was a useful tool in diagnosing this condition and to differentiate it from other intra or extraneural cystic lesions. These results agree with prior literature. However, in this study, 40% of cases representing the initial cases in this series were misdiagnosed preoperatively and were mistaken for neurogenic tumor. This emphasizes the diagnostic knowledge of this condition. An early diagnosis and surgical intervention will improve patient outcomes.

Applications

In the order of differential diagnosis of cystic nerve lesions arising in the vicinity of a joint, the INGC comes first. This research re-emphasizes that the knowledge of the classic MRI pattern is paramount in diagnosing the INGC. An early surgical intervention will cause significant reversal of neurologic symptoms.

Terminology

INGC: Intraneural ganglion cyst, cyst occurring within the epineurium of nerve; ENG: Extraneural ganglion cyst, cyst adjacent to nerve but outside the epineurial sheath; CPN: Common peroneal nerve, a nerve in the lower leg that provides sensation and motor function to parts of the lower leg.

Peer-review

This review article has well described the use and dose optimisation of computed tomography in patients with cystic nerve lesions, it is well-organized and useful for clinical practice, especially for the western radiology society.

REFERENCES

- 1 van Brakel WH, Nicholls PG, Das L, Barkataki P, Suneetha SK, Jadhav RS, Maddali P, Lockwood DN, Wilder-Smith E, Desikan KV. The INFIR Cohort Study: investigating prediction, detection and pathogenesis of neuropathy and reactions in leprosy. Methods and baseline results of a cohort of multibacillary leprosy patients in north India. *Lepr Rev* 2005; **76**: 14-34 [PMID: 15881033]
- 2 de Freitas MR, Nascimento OJ, Quaglino EA, Oliveira A, Hahn MD. Small-fiber polyneuropathy in leprosy without skin changes: study of 17 cases. *Arq Neuropsiquiatr* 2003; **61**: 542-546 [PMID: 14513154 DOI: 10.1590/S0004-282X2003000400003]
- 3 World Health Organization, Global leprosy situation, Relevé Épidémiologique Hebd. Sect. Hygiène Secrétariat Société Nations Wkly Epidemiol Rec Health Sect Secr Leag Nation 2005; **80**: 289-295
- 4 Scollard DM, Adams LB, Gillis TP, Krahenbuhl JL, Truman RW, Williams DL. The continuing challenges of leprosy. *Clin Microbiol Rev* 2006; **19**: 338-381 [DOI: 10.1128/CMR.19.2.338-381.2006]
- 5 Joyce M, Scollard D. *Lepr. Hansens Dis. Conns Curr. Ther.*, edition 1, Saunders, Philadelphia, 2004: 100-105
- 6 Ustianowski AP, Lockwood DN. Leprosy: current diagnostic and treatment approaches. *Curr Opin Infect Dis* 2003; **16**: 421-427 [PMID: 14501994 DOI: 10.1097/01.qco.0000092813.64370.be]
- 7 Patel P, Schucany WG. A rare case of intraneural ganglion cyst involving the tibial nerve. *Proc (Bayl Univ Med Cent)* 2012; **25**: 132-135 [PMID: 22481843]
- 8 Uetani M, Hashmi R, Hayashi K, Nagatani Y, Narabayashi Y, Imamura K. Peripheral nerve intraneural ganglion cyst: MR findings in three cases. *J Comput Assist Tomogr* 1998; **22**: 629-632 [PMID: 9676458 DOI: 10.1097/00004728-199807000-00023]
- 9 Harbaugh KS, Tiel RL, Kline DG. Ganglion cyst involvement of peripheral nerves. *J Neurosurg* 1997; **87**: 403-408 [PMID: 9285606 DOI: 10.3171/jns.1997.87.3.0403]
- 10 Spinner RJ, Desy NM, Rock MG, Amrami KK. Peroneal intraneural ganglia. Part I. Techniques for successful diagnosis and treatment. *Neurosurg Focus* 2007; **22**: E16 [PMID: 17613207 DOI: 10.3171/foc.2007.22.6.17]
- 11 Jacobs RR, Maxwell JA, Kepes J. Ganglia of the nerve. Presentation of two unusual cases, a review of the literature, and a discussion of pathogenesis. *Clin Orthop Relat Res* 1975: 135-144 [PMID: 172271 DOI: 10.1097/00003086-197511000-00020]
- 12 Adn M, Hamlat A, Morandi X, Guegan Y. Intraneural ganglion cyst of the tibial nerve. *Acta Neurochir (Wien)* 2006; **148**: 885-889; discussion 889-890 [PMID: 16775659 DOI: 10.1007/s00701-006-0803-8]
- 13 Johnston JA, Lyne DE. Intraneural ganglion cyst of the peroneal nerve in a four-year-old girl: a case report. *J Pediatr Orthop* 2007; **27**: 944-946 [PMID: 18209620 DOI: 10.1097/BPO.0b013e3181558c05]
- 14 Tehli O, Celikmez RC, Birgili B, Solmaz I, Celik E. Pure peroneal intraneural ganglion cyst ascending along the sciatic nerve. *Turk Neurosurg* 2011; **21**: 254-258 [PMID: 21534214 DOI: 10.5137/1019-5149.JTN.2660-09.1]
- 15 Liang T, Panu A, Crowther S, Low G, Lambert R. Ultrasound-guided aspiration and injection of an intraneural ganglion cyst of the common peroneal nerve. *HSS J* 2013; **9**: 270-274 [PMID: 24426879 DOI: 10.1007/s11420-013-9345-9]
- 16 Lang CJ, Neubauer U, Qiayumi S, Fahlbusch R. Intraneural ganglion of the sciatic nerve: detection by ultrasound. *J Neurol Neurosurg Psychiatry* 1994; **57**: 870-871 [PMID: 8021688 DOI: 10.1136/jnnp.57.7.870-a]
- 17 Leijten FS, Arts WF, Puylaert JB. Ultrasound diagnosis of an intraneural ganglion cyst of the peroneal nerve. Case report. *J Neurosurg* 1992; **76**: 538-540 [PMID: 1310730 DOI: 10.3171/jns.1992.76.3.0538]
- 18 Masciocchi C, Innacoli M, Cisternino S, Barile A, Rossi F, Passariello R. Myxoid intraneural cysts of external popliteal ischiadic nerve. Report of 2 cases studied with ultrasound, computed tomography and magnetic resonance imaging. *Eur J Radiol* 1992; **14**: 52-55 [PMID: 1314178 DOI: 10.1016/0720-048X(92)90062-E]
- 19 McCarthy CL, McNally EG. The MRI appearance of cystic lesions around the knee. *Skeletal Radiol* 2004; **33**: 187-209 [PMID: 14991250 DOI: 10.1007/s00256-003-0741-y]
- 20 Spinner RJ, Atkinson JL, Scheithauer BW, Rock MG, Birch R, Kim TA, Kliot M, Kline DG, Tiel RL. Peroneal intraneural ganglia: the importance of the articular branch. Clinical series. *J Neurosurg* 2003; **99**: 319-329 [PMID: 12924707 DOI: 10.3171/jns.2003.99.2.0319]
- 21 Martinez Algarra JC, Gastaldi Rodrigo P, Palomares Talens E. [Multiple schwannoma of the sciatic nerve. Apropos of a case]. *Rev Chir Orthop Reparatrice Appar Mot* 1999; **85**: 632-635 [PMID: 10575727]
- 22 Parmar H, Patkar D, Gadani S, Shah J. Cystic lumbar nerve sheath tumours: MRI features in five patients. *Australas Radiol* 2001; **45**: 123-127 [PMID: 11380354 DOI: 10.1046/j.1440-1673.2001.00891.x]
- 23 Wu D, Ba Z, Huang Y, Zhao W, Shen B, Kan H. Totally cystic schwannoma of the lumbar spine. *Orthopedics* 2013; **36**: e679-e682 [PMID: 23672923 DOI: 10.3928/01477447-20130426-36]
- 24 Spinner RJ, Carmichael SW, Wang H, Parisi TJ, Skinner JA, Amrami KK. Patterns of intraneural ganglion cyst descent. *Clin Anat* 2008; **21**: 233-245 [PMID: 18330922 DOI: 10.1002/ca.20614]
- 25 Nicholson TR, Cohen RC, Grattan-Smith PJ. Intraneural ganglion of the common peroneal nerve in a 4-year-old boy. *J Child Neurol* 1995; **10**: 213-215 [PMID: 7642891 DOI: 10.1177/088307389501000310]
- 26 Kim TS, Jo YH, Paik SS, Kim SJ. Intraneural Ganglion Cyst of the Peripheral Nerve: Two Cases Report. *J Korean Bone Jt Tumor Soc* 2013; **19**: 83 [DOI: 10.5292/jkbjts.2013.19.2.83]
- 27 Haller JM, Potter MQ, Sinclair M, Hutchinson DT. Intraneural ganglion in superficial radial nerve mimics de quervain tenosynovitis. *J Wrist Surg* 2014; **3**: 262-264 [PMID: 25364639 DOI: 10.1055/s-0034-1384746]
- 28 Swartz KR, Wilson D, Boland M, Fee DB. Proximal sciatic nerve intraneural ganglion cyst. *Case Rep Med* 2009; **2009**: 810973 [PMID: 20069041 DOI: 10.1155/2009/810973]
- 29 Spinner RJ, Luthra G, Desy NM, Anderson ML, Amrami KK. The clock face guide to peroneal intraneural ganglia: critical "times" and sites for accurate diagnosis. *Skeletal Radiol* 2008; **37**:

- 1091-1099 [PMID: 18641980 DOI: 10.1007/s00256-008-0545-1]
- 30 **Spinner RJ**, Amrami KK, Wang H, Kliot M, Carmichael SW. Cross-over: a generalizable phenomenon necessary for secondary intraneural ganglion cyst formation. *Clin Anat* 2008; **21**: 111-118 [PMID: 18220283 DOI: 10.1002/ca.20590]
- 31 **Krishnan KG**, Schackert G. Intraneural ganglion cysts: a case of sciatic nerve involvement. *Br J Plast Surg* 2003; **56**: 183-186 [PMID: 12791372 DOI: 10.1016/S0007-1226(03)00036-5]
- 32 **Colbert SH**, Le MH. Case report: intraneural ganglion cyst of the ulnar nerve at the wrist. *Hand (NY)* 2011; **6**: 317-320 [PMID: 22942857 DOI: 10.1007/s11552-011-9329-5]
- 33 **Spinner RJ**, Amrami KK, Wolanskyj AP, Desy NM, Wang H, Benarroch EE, Skinner JA, Rock MG, Scheithauer BW. Dynamic phases of peroneal and tibial intraneural ganglia formation: a new dimension added to the unifying articular theory. *J Neurosurg* 2007; **107**: 296-307 [PMID: 17695383 DOI: 10.3171/JNS-07/08/0296]
- 34 **Elangovan S**, Odegard GM, Morrow DA, Wang H, Hébert-Blouin MN, Spinner RJ. Intraneural ganglia: a clinical problem deserving a mechanistic explanation and model. *Neurosurg Focus* 2009; **26**: E11 [PMID: 19435441 DOI: 10.3171/FOC.2009.26.2.E11]
- 35 **Greer-Bayramoglu RJ**, Nimigan AS, Gan BS. Compression neuropathy of the peroneal nerve secondary to a ganglion cyst. *Can J Plast Surg* 2008; **16**: 181-183 [PMID: 19721802 DOI: 10.4172/plastic-surgery.1000570]
- 36 **Spinner RJ**, Desy NM, Amrami KK. Sequential tibial and peroneal intraneural ganglia arising from the superior tibiofibular joint. *Skeletal Radiol* 2008; **37**: 79-84 [PMID: 17968541 DOI: 10.1007/s00256-007-0400-9]
- 37 **Kukreja MM**, Telang VG. Common Peroneal Nerve Palsy Secondary to a Proximal Tibiofibular Joint "Ganglion Cyst"—A Case Report and Review of Literature. [accessed 2016 Jun 19]. Available from: URL: http://file.scirp.org/pdf/OJO_2015112014185133.pdf
- 38 **Coakley FV**, Finlay DB, Harper WM, Allen MJ. Direct and indirect MRI findings in ganglion cysts of the common peroneal nerve. *Clin Radiol* 1995; **50**: 168-169 [PMID: 7889707 DOI: 10.1016/S0009-9260(05)82993-9]
- 39 **Spinner RJ**, Amrami KK, Rock MG. The use of MR arthrography to document an occult joint communication in a recurrent peroneal intraneural ganglion. *Skeletal Radiol* 2006; **35**: 172-179 [PMID: 16333654 DOI: 10.1007/s00256-005-0036-6]
- 40 **Spinner RJ**, Atkinson JL, Harper CM, Wenger DE. Recurrent intraneural ganglion cyst of the tibial nerve. Case report. *J Neurosurg* 2000; **92**: 334-337 [PMID: 10659022 DOI: 10.3171/jns.2000.92.2.0334]
- 41 **Leon J**, Marano G. MRI of peroneal nerve entrapment due to a ganglion cyst. *Magn Reson Imaging* 1987; **5**: 307-309 [PMID: 3657403 DOI: 10.1016/0730-725X(87)90009-9]
- 42 **Dubuisson AS**, Stevenaert A. Recurrent ganglion cyst of the peroneal nerve: radiological and operative observations. Case report. *J Neurosurg* 1996; **84**: 280-283 [PMID: 8592235 DOI: 10.3171/jns.1996.84.2.0280]
- 43 **Iverson DJ**. MRI detection of cysts of the knee causing common peroneal neuropathy. *Neurology* 2005; **65**: 1829-1831 [PMID: 16344535 DOI: 10.1212/01.wnl.0000187098.42938.b6]
- 44 **Spinner RJ**, Hébert-Blouin MN, Trousdale RT, Midha R, Russell SM, Yamauchi T, Sasaki S, Amrami KK. Intraneural ganglia in the hip and pelvic region. Clinical article. *J Neurosurg* 2009; **111**: 317-325 [PMID: 19374493 DOI: 10.3171/2009.2.JNS081720]
- 45 **Sureka J**, Panwar S, Mullapudi I. Intraneural ganglion cysts of obturator nerve causing obturator neuropathy. *Acta Neurol Belg* 2012; **112**: 229-230 [PMID: 22426671 DOI: 10.1007/s13760-012-0041-1]
- 46 **Spinner RJ**, Hébert-Blouin MN, Amrami KK, Rock MG. Peroneal and tibial intraneural ganglion cysts in the knee region: a technical note. *Neurosurgery* 2010; **67**: ons71-ons8; discussion ons78 [PMID: 20679946 DOI: 10.1227/01.NEU.0000374683.91933.0E]
- 47 **Davis GA**, Cox IH. Tibial intraneural ganglia at the ankle and knee: incorporating the unified (articular) theory in adults and children. *J Neurosurg* 2011; **114**: 236-239 [PMID: 20415523 DOI: 10.3171/2010.3.JNS10427]
- 48 **Jerath NU**, Chen JJ, Miller BJ, Reddy CG. Teaching NeuroImages: intraneural ganglion cyst of the tibial nerve. *Neurology* 2014; **82**: e174-e175 [PMID: 24843041 DOI: 10.1212/WNL.0000000000000429]
- 49 **Wang H**, Terrill RQ, Tanaka S, Amrami KK, Spinner RJ. Adherence of intraneural ganglia of the upper extremity to the principles of the unifying articular (synovial) theory. *Neurosurg Focus* 2009; **26**: E10 [PMID: 19435440 DOI: 10.3171/FOC.2009.26.2.E10]
- 50 **Lee BC**, Yegappan M, Thiagarajan P. Suprascapular nerve neuropathy secondary to spinoglenoid notch ganglion cyst: case reports and review of literature. *Ann Acad Med Singapore* 2007; **36**: 1032-1035 [PMID: 18185886]
- 51 **Limucci N**, Rossi F, Salvati F, Pistoia LM, Barile A, Masciocchi C. Bilateral suprascapular nerve entrapment by glenoid labral cysts associated with rotator cuff damage and posterior instability in an amateur weightlifter. *J Sports Med Phys Fitness* 2010; **50**: 64-67 [PMID: 20308974]
- 52 **Ebraheim NA**, Whitehead JL, Alla SR, Moral MZ, Castillo S, McCollough AL, Yeasting RA, Liu J. The suprascapular nerve and its articular branch to the acromioclavicular joint: an anatomic study. *J Shoulder Elbow Surg* 2011; **20**: e13-e17 [PMID: 21194975 DOI: 10.1016/j.jse.2010.09.004]
- 53 **Spinner RJ**, Amrami KK, Kliot M, Johnston SP, Casañas J. Suprascapular intraneural ganglia and glenohumeral joint connections. *J Neurosurg* 2006; **104**: 551-557 [PMID: 16619659 DOI: 10.3171/jns.2006.104.4.551]
- 54 **Spinner RJ**, Amrami KK. Intraneural ganglion of the suprascapular nerve: Case report. *J Hand Surg Am* 2006; **31**: 1698-1699 [PMID: 17145396 DOI: 10.1016/j.jhsa.2006.09.015]
- 55 **Sanger J**, Cortes W, Yan JG. Intraneural ganglion of the suprascapular nerve: case report. *J Hand Surg Am* 2006; **31**: 40-44 [PMID: 16443102 DOI: 10.1016/j.jhsa.2005.08.010]
- 56 **Parkes A**. Intraneural ganglion of the lateral popliteal nerve. *J Bone Joint Surg Br* 1961; **43-B**: 784-790 [PMID: 14038186]
- 57 **Bacigalupo LE**, Damasio MB, Zuccarino F, Succio G, Silversti E, Bianchi S, Martinoli C. US and MR imaging of peroneal intraneural ganglia: Emphasis on the articular branch. *Skeletal Radiol* 2005; **34**: 588 [DOI: 10.1007/s00256-005-0959-y]

P- Reviewer: Ju CI, Reddy CG, Squires JH **S- Editor:** Song XX
L- Editor: A **E- Editor:** Li D



Retrospective Study

Transarterial chemoembolization using 40 μ m drug eluting beads for hepatocellular carcinoma

Giorgio Greco, Tommaso Cascella, Antonio Facciorusso, Roberto Nani, Rodolfo Lanocita, Carlo Morosi, Marta Vaiani, Giuseppina Calareso, Francesca G Greco, Antonio Ragnanese, Marco A Bongini, Alfonso V Marchianò, Vincenzo Mazzaferro, Carlo Spreafico

Giorgio Greco, Tommaso Cascella, Rodolfo Lanocita, Carlo Morosi, Marta Vaiani, Giuseppina Calareso, Francesca G Greco, Alfonso V Marchianò, Carlo Spreafico, Department of Radiology, Interventional Radiology, Nuclear Medicine and Radiotherapy, National Cancer Institute, 20133 Milan, Italy

Antonio Facciorusso, Gastroenterology Unit, Ospedali Riuniti Foggia, University of Foggia, 71122 Foggia, Italy

Roberto Nani, Antonio Ragnanese, Radiology and Interventional Radiology Unit, Azienda Ospedaliera Giovanni Paolo XXIII, 24128 Bergamo, Italy

Marco A Bongini, Vincenzo Mazzaferro, Hepato-biliary Surgery and Liver Transplantation Unit, National Cancer Institute, 20133 Milan, Italy

Author contributions: Greco G collected data, performed the research, wrote the manuscript and made the revision; Greco G, Cascella T, Lanocita R, Morosi C, Marchianò AV, Spreafico C and Nani R performed TACEs and designed the study; Ragnanese A, Calareso G, Vaiani M and Greco FG collected data; Facciorusso A performed statistical analysis; Bongini MA and Mazzaferro V selected the patients, performed clinical support and follow-up, performed liver transplantation; Greco G and Spreafico C evaluated imaging follow-up; Spreafico C supervised the report.

Institutional review board statement: The study was reviewed and approved by the Ethics Committee of the National Cancer Institute of Milan.

Informed consent statement: Patients were not required to give informed consent to the study because the analysis used anonymous clinical data that were obtained after each patient agreed to treatment by written consent.

Conflict-of-interest statement: We have no financial relationships to disclose.

Data sharing statement: No additional data are available.

Open-Access: This article is an open-access article which was

selected by an in-house editor and fully peer-reviewed by external reviewers. It is distributed in accordance with the Creative Commons Attribution Non Commercial (CC BY-NC 4.0) license, which permits others to distribute, remix, adapt, build upon this work non-commercially, and license their derivative works on different terms, provided the original work is properly cited and the use is non-commercial. See: <http://creativecommons.org/licenses/by-nc/4.0/>

Manuscript source: Unsolicited manuscript

Correspondence to: Giorgio Greco, MD, Department of Radiology, Interventional Radiology, Nuclear Medicine and Radiotherapy, National Cancer Institute, Via Giacomo Venezian 1, 20133 Milan, Italy. giorgio.greco@istitutotumori.mi.it
Telephone: +39-02-23903384
Fax: +39-02-23902060

Received: December 10, 2016

Peer-review started: December 13, 2016

First decision: January 16, 2017

Revised: February 23, 2017

Accepted: March 12, 2017

Article in press: March 13, 2017

Published online: May 28, 2017

Abstract**AIM**

To assess the safety and efficacy of transarterial chemoembolization (TACE) of hepatocellular carcinoma (HCC) using a new generation of 40 μ m drug eluting beads in patients not eligible for curative treatment.

METHODS

Drug eluting bead TACE (DEB-TACE) using a new generation of microspheres (embosphere tandem, 40 μ m) preloaded with 100 mg of doxorubicin was performed on 48 early or intermediate HCC patients with compensated

cirrhosis. Response to therapy was assessed with Response Evaluation Criteria in Solid Tumors (RECIST) and modified RECIST (mRECIST) guidelines applied to computed tomography or magnetic resonance imaging. Eleven out of the 48 treated patients treated progressed on to receive liver orthotopic transplantation (OLT). This allowed for histological analysis on the treated explanted nodules.

RESULTS

DEB-TACE with 40 μ m showed a good safety profile without major complications or 30-d mortality. The objective response rate of treated tumors was 72.6% and 26.7% according to mRECIST and RECIST respectively. Histological examination in 11 patients assigned to OLT showed a necrosis degree > 90% in 78.6% of cases. The overall time to progression was 13 mo (11-21).

CONCLUSION

DEB-TACE with 40 μ m particles is an effective treatment for the treatment of HCC in early-intermediate patients (Barcelona Clinic Liver Cancer stage A/B) with a good safety profile and good results in term of objective response rate and necrosis.

Key words: Embozene tandem; Drug eluting beads; Drug eluting bead transarterial chemoembolization; Transarterial chemoembolization; Hepatocellular carcinoma

© The Author(s) 2017. Published by Baishideng Publishing Group Inc. All rights reserved.

Core tip: This is the first study exploring the safety and efficacy of 40 μ m drug eluting bead transarterial chemoembolization for the treatment of hepatocellular carcinoma (HCC) in a series of 48 patients not suitable for ablation or surgical therapies. The use of microspheres smaller than 100 μ m is not common practice in the western countries due to skepticism and fear of non-target embolization. Our aim is to present our initial experiences when treating with smaller microspheres so we all can test the potential advantages inherent to them and evaluate the effectiveness in the treatment of HCC nodules.

Greco G, Cascella T, Facciorusso A, Nani R, Lanocita R, Morosi C, Vaiani M, Calareso G, Greco FG, Ragnanese A, Bongini MA, Marchianò AV, Mazzaferro V, Spreafico C. Transarterial chemoembolization using 40 μ m drug eluting beads for hepatocellular carcinoma. *World J Radiol* 2017; 9(5): 245-252 Available from: URL: <http://www.wjgnet.com/1949-8470/full/v9/i5/245.htm> DOI: <http://dx.doi.org/10.4329/wjr.v9.i5.245>

INTRODUCTION

Transarterial chemoembolization (TACE) is the current standard of care for hepatocellular carcinoma (HCC)

in patients with multinodular disease, classified as intermediate stage (stage B) of the Barcelona Clinic Liver Cancer (BCLC) staging system^[1]. Furthermore, in clinical practice, a number of patients with early stage (stage A) disease, not eligible for curative treatment (surgery, transplantation or ablation) are commonly treated with TACE^[2,3].

Conventional TACE (c-TACE) has shown superiority over basic supportive care in unresectable HCC in two randomised studies published in the early 2000s^[4,5] and in a meta-analysis published in 2003^[6].

Recently developed drug eluting beads (DEB) have the ability to bind and carry up to double the doxorubicin dose^[7,8] thus overcoming the common drawbacks of c-TACE such as the release of the chemotherapeutic agent into the systemic circulation.

DEB-TACE superiority over c-TACE or TACE superiority over transarterial embolization has not been proven in recent studies^[9,10] both in terms of survival and as objective response to treatment. These new microspheres have ensured a reduction in the systemic concentration of the loaded chemotherapeutic agent, with a lower rate of post-procedural toxicity compared to c-TACE^[11-13]. The first available microspheres had a diameter ranging between 500 and 900 μ m that has gradually reduced over the years to let DEB penetrate deeper into tumor circulation arterioles. This theory is supported by recently published controlled studies on smaller microspheres that show encouraging preliminary data on the radiological response in terms of extensive intratumoral necrosis^[14,15].

Embozene tandem 40 μ m (Boston Scientific, Minneapolis, MA, United States) are a new size of tightly calibrated spherical drug-eluting beads able to load up 100 mg of doxorubicin in a 2 mL syringe, or 150 mg in a 3 mL syringe. These biocompatible, non-resorbable, hydrogel microspheres are coated with an inorganic perfluorinated polymer (Polyzene®-F). They show a small increase in size (< 5% of the original diameter) during drug loading and storage if compared with similar DEB on the market. Dc-Beads M1 (initial diameter 70-150 μ m) show a dehydration and loss in size after loading drug; Hepashere (initial diameter 30-60 μ m), instead, show an increase in size up to 4 times of the initial diameter, resulting in a final diameter between 120-240 μ m after loading drug. Smaller microspheres theoretically allow for more distal vascular penetration and more homogeneous intratumoral drug distribution, with no meaningful evidence of better results in terms of objective response if compared to 100-300 μ m particles^[16].

The aim of this study was to assess the efficacy and safety of 40 μ m DEB-TACE in a series of 48 early-intermediate HCC patients complying with eligibility criteria. Primary endpoint was the evaluation of adverse events and complications related to TACE as well as the tumor response rate, considered as best achieved response. Secondary outcomes were the time to progressions (TTP) and time to response (TTR).

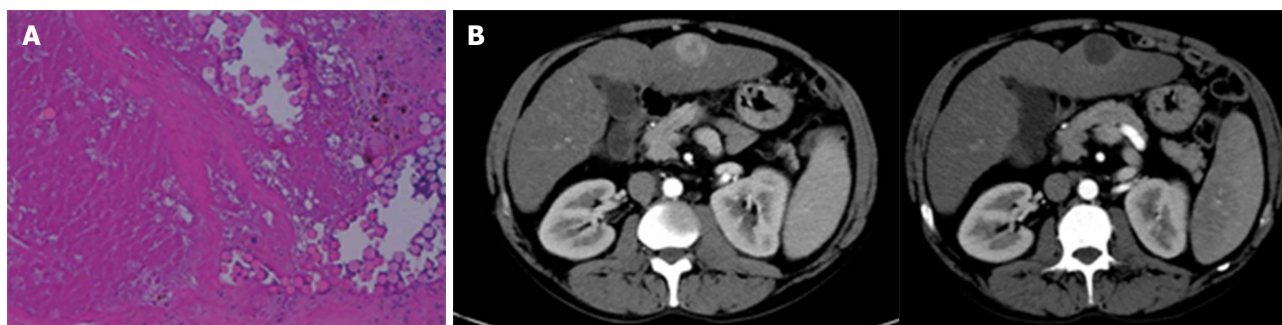


Figure 1 Patient with evidence of a ca. 32 mm tumor with arterial blood flow typical of hepatocellular carcinoma (wash-in phase at the centre of the image) in segment 3 treated with a single cycle of transarterial chemoembolization. A: The follow-up CT scan after TACE observed complete response according to mRECIST (on the right); B: Corresponding histological image of the tumor after transplantation: Particles can be seen inside the afferent arterioles of the tumor, documenting 100% necrosis. TACE: Transarterial chemoembolization; mRECIST: Modified Response Evaluation Criteria in Solid Tumors; CT: Computed tomography.

MATERIALS AND METHODS

Study population

Data from 48 early-intermediate HCC patients (BCLC stage A/B) referred to our two tertiary centers between May 2013 and May 2015 and treated with DEB-TACE using 40 μ m microspheres were retrospectively analysed (Table 1). All patients signed a dedicated informed consent form. A multidisciplinary team made up of interventional radiologists, oncologists, hepatologists, pathologists and hepatic surgeons selected candidates for the treatment.

All patients were asymptomatic at enrolment (performance status 0) with cirrhotic disease related to hepatitis C in 56.2% of cases (27/48). Fifty-six point two percent of patients were in BCLC B stage, while 43.8% were in early stage A. All patients presented with a preserved liver function (93.4% Child-Pugh A and 6.6% Child-Pugh B7). Other comorbidities were reported in approximately half of the study population (notably Diabetes, Arterial Hypertension and Chronic Obstructive Pulmonary Disease). No tumors receiving DEB-TACE had been previously treated. The mean number of tumors was 2 (range 1-4) with 30 mm (range 10-96) maximum mean diameter, and the mean sum of all maximum diameters came up to 44 mm (range 13-130).

Patient eligibility was established with the following inclusion criteria: Age > 18 years; HCC diagnosis according to the current guidelines^[1-3]; Early/intermediate patients not eligible for percutaneous or surgical ablative therapies; well compensated cirrhosis with Child-Pugh Score up to B7; performance status 0 according to the Eastern Cooperative Oncology Group.

Exclusion criteria included bilirubin > 2 mg/dL; principal (main trunk) or segmental portal thrombosis; previous treatments on target tumors (ablation, TACE, Sorafenib); intolerance to doxorubicin (leukocyte count < 3000/mm³; cardiac ejection fraction < 50%); aspartate amino transferase and alanine amino transferase levels > 270 IU/mL, and patients receiving angiogenesis agents or affected by uncorrectable coagulation disorders.

Imaging study protocols

To assess the disease extent in the liver, its vascular

pattern and possible intrahepatic vascular invasions, all patients received pre-treatment abdominal imaging with computed tomography (CT) 128 slices (Somatom Definition Flash, Siemens Healthcare, Erlangen, Germany) or with magnetic resonance imaging (MRI) 1.5 T (Achieva, Philips Healthcare, Best, the Netherlands). In addition to that, they received a CT scan of the chest for a complete staging of the extrahepatic disease.

CT image acquisition technique, before and after treatment, required both a baseline abdominal scan and the arterial, portal and late venous phase study after intravenous administration of a 120-140 mL bolus of iodinated contrast medium (Iopamiro 370 mg/dL, Bracco, Milan, Italy) at an injection flow of 4 mL/s with the Bolus Tracking technique.

The protocol for abdominal MRI required the acquisition of in-phase and out-of-phase T1 weighted sequences, T2 weighted Half-Fourier acquisition Single-shot Turbo-spin Echo (HASTE) and Fat-Saturated (FAT-SAT) sequences, diffusion study and Tissue High Resolution Isotropic Voxel Excitation sequences [T1 weighted FAT-SAT and 3D GRE (3D GradientEcho)] both before and after infusion of Gadolinium-EthOxyBenzyl-Diethylene Triamine Pentaacetic Acid (Gd-EOB-DTPA) 0.025 mmol/mL (Primovist, Bayer, Leverkusen, Germany) with acquisitions up to 20 min during the hepatospecific phase.

DEB-TACE

TACE was performed using transfemoral arterial access route with a micro-puncture system by placing a 5F vascular introducer (Boston Scientific, Natick, MA, United States). The angiographic study of the superior mesenteric artery and the celiac trunk for the characterisation of hepatic vascular anatomy was performed using an angiography unit (Axiom Angiographic Unit, Siemens Healthcare, Erlangen, Germany), and a 5F catheter (Cobra or Simmons, Boston Scientific, Natick, MA, United States). The angiographic study of extrahepatic pathological branches in some HCC tumors (usually peripheral tumors) was based on a careful study of pre-TACE imaging or on missing parts of the pathological tumor vascularization at the selective angiographic study.

Selective studies of segmental and pathological feeding vessels were also performed using a coaxial

micro catheter (Progreat 2.7F, Terumo, Tokyo, Japan), with a highly selective administration of the treatment.

In cases presenting multifocal disease, the treatment never targeted more than three hepatic segments per session. DEB-TACE was performed using a 2 mL/100 mg of doxorubicin (Adriplastina, Pfizer, New York, NY, United States) loaded dose on embosphere tandem 40 μ m microspheres.

In all performed DEB-TACE treatments embosphere tandem 40 μ m microspheres were diluted in 20-30 mL of iodinated contrast medium (Iopamiro 370 mg/dL), slowly injected manually with a 3 mL syringe, applying gentle pressure, until blood flow stasis was induced^[17].

Vasodilator drugs *via* transcatheter intra-arterial were not administered before starting chemoembolization with a view to expand to the maximum the neoplastic vascular network and theoretically increase the penetration of the particles and, accordingly, the potential effectiveness of the treatment as reported by some authors^[18]. Permanent or temporary embolizing materials were not used to complete DEB-TACE in some tumors of greater dimensions where vascular stasis with only 40 μ m drug eluting beads was not achieved. In such cases, a second treatment session has been scheduled after performing a CT/MRI investigation to assess that some conditions leading to the impossibility of repeating the treatment, such as the onset of ascites or portal vein thrombosis, had not occurred.

Access haemostasis was achieved by a mechanical system, as Exoseal (Cordis, Miami Lakes, FL, United States), and a subsequent manual compression for about 3-5 min until haemostasis was achieved.

Premedication included 100 mg of paracetamol (Paracetamol 10 mg/mL S.A.L.F., Bergamo, Italy), 8 mg of ondansetron (Ondansetron 8 mg/4 mL Hikma, Fervença, Portugal) and 50 mg of ranitidine (Ranitidina 50 mg/5 mL, S.A.L.F., Bergamo, Italy). Intravenous antibiotic prophylaxis was administered with 2 g of cefazolin (Cefamizin, Pfizer, New York, NY, United States) consistent with the hospital internal guidelines.

Hospitalization, adverse events and toxicity

Patients were discharged after a brief observation period (48-72 h). Clinical evaluation and assessment of treatment-related toxicity were performed on an outpatient basis with physician's visits and laboratory tests 12, 24 and 48 h after TACE, 4 wk later and every 3 mo thereafter. AE were defined as treatment related if occurred during hospital stay or within 30 d from treatment. Safety parameters were classified according to the Common Terminology Criteria for Adverse Events 4.0^[19] at each follow-up visit.

Imaging evaluation and follow-up

Two radiologists (Dr. Carlo Spreafico and Dr. Giorgio Greco) both experienced in interventional radiology and interventional hepatic imaging performed all radiological assessments independently.

Tumoral response to treatment was assessed according

to RECIST and mRECIST with a CT scan or MRI investigation performed 4 wk after DEB-TACE and, then, every 3 mo during the follow-up period^[20].

A second treatment session, according to the "on demand" policy, was scheduled in case of partial response (PR) or stable disease (SD) after performing blood chemistry tests documenting good preserved hepatic function and continuity in the eligibility criteria for treatment.

In case of repeated DEB-TACE sessions, only the best response was considered for analytical purposes since this has been recently proved a better predictor of survival than the initial response^[21]. In patients submitted to OLT, the treated tumors were histologically analysed during the months after treatment with targeted definition of necrosis induced by TACE.

Statistical analysis

The descriptive statistical analysis was expressed as median and range in the case of continuous variables and absolute numbers and percentage in the case of categorical ones. Time to best response and TTP were calculated with the Kaplan-Meier method, computed from the time of the first treatment and censored to the day of transplantation in transplant patients. All calculations were obtained with the SPSS software (IBM, Armonk, NY, United States). The statistical review of the study was performed by a biomedical statistician.

RESULTS

DEB-TACE and radiological tumor response

All procedures were performed without technical impediments that would prevent treatment of the target tumor. The two study sites performed an overall number of 73 TACE (47 segmental, 22 bisegmental and 4 trisegmental) on a total number of 128 tumors. 31 patients (64.7%) underwent one treatment cycle, 10 patients (20.8%) to 2 treatment cycles, 6 patients (12.5%) to 3 treatment cycles, and 1 patient to 4 treatment cycles (2%), with a mean number of treatments per patient of 1.45.

Response to treatment was assessed by classifying the tumors into three classes according to dimensional criteria, as specified in Table 2 (according to mRECIST) and Table 3 (according to RECIST). The objective response rate (CR + PR) was 26.8% and 69% for tumors smaller than 3 cm, 32.1% and 85.7% for tumors with diameters between 3 and 5 cm, 10% and 70% for tumors with diameter over 5 cm according to RECIST and mRECIST, respectively.

Considering all the treated tumors, the overall objective response rate (CR + PR) was 26.7% according to RECIST and 72.6% according to mRECIST. These data include all the 48 patients of our series. These results were calculated with RECIST and mRECIST criteria, based on the last available CT scan/MRI, with an overall mean follow-up period of 357 d (range 30-810).

Hystological tumor response in transplanted patients

Eleven patients qualified for OLT after 15 overall cycles of DEB-TACE, with a mean number of treatments per

Table 1 Demographic characteristics and tumoral parameters of the study population, *n* (%)

Age (yr)	67 (49-95)
Sex	
Male	42 (87.5)
Female	6 (13.5)
Aetiology	
HCV	27 (56.2)
HBV	9 (18.75)
Alcohol	6 (12.5)
Cryptogenetic	3 (6.25)
NASH	3 (6.25)
Child-Pugh	
A	45 (93.4)
B	3 (6.6)
MELD	8 (6-14)
BCLC	
A	21 (43.8)
B	27 (56.2)
ECOG 0	48 (100)
Portal hypertension	
Yes	22 (45.9)
No	26 (54.1)
Tumour extension	
Unilobar	29 (60.4)
Bilobar	19 (39.6)
No. of tumors (target)	
Total	128
Median	2 (1-4)
Max. diameter (mm)	30 (10-96)
Sum of diameters (mm)	44 (13-130)
TACE	
Total cycles	73
Segmental	47 (64.4)
Bisegmental	22 (30.1)
Trisegmental	4 (5.5)

TACE: Transarterial chemoembolization; HBV; Hepatitis B virus; HCV: Hepatitis C virus; NASH: Nonalcoholic steatohepatitis; MELD: Model for end-stage liver disease; BCLC: Barcelona Clinic Liver Cancer; ECOG: Eastern Cooperative Oncology Group.

patient of 1.36. Seven out of 11 patients received 1 treatment, with remaining 4 receiving 2 treatments. Median time elapsed between TACE and OLT was 4.8 mo (95%CI: 2.3-6.5). The histological examination (Table 4) performed on 11 explanted livers reported a total number of 14 tumors of HCC, 10 of which were ≤ 3 cm and 4 were between 3 and 5 cm.

Among the tumors smaller than 3 cm, 7 presented 100% necrosis and 3 presented a necrosis rate below 50%. Two out of 4 tumors > 3 cm presented a 100% necrosis rate (Figure 1), while the other 2 were above 90%.

DEB-TACE: Adverse events and toxicity

Toxicity data are reported in Table 5. All the observed AE were mild and transient, with no grade 3/4 toxicity reported. There were no cases of post procedure mortality within 30 d.

No major AE were recorded, neither systemically (pulmonary embolism, splenic infarction, gastrointestinal mucosal tumors, acute pancreatitis or cholecystitis,

Table 2 Target lesions: Modified Response Evaluation Criteria in Solid Tumors response rate

\varnothing nodules	No. of nodules	CR	PR	SD	PD
$\varnothing < 3$ cm	77	47.4%	21.6%	27.8%	3.2%
$3 \leq \varnothing \leq 5$ cm	22	42.8%	42.8%	10.8%	3.6%
$\varnothing > 5$ cm	3	40%	30%	30%	0%
Overall response	102	46%	26.6%	24.4%	3%

CR: Complete response; PR: Partial response; SD: Stable disease; PD: Progressive disease.

Table 3 Target lesions: Response Evaluation Criteria in Solid Tumors response rate

\varnothing nodules	No. of nodules	CR	PR	SD	PD
$\varnothing < 3$ cm	77	6.2%	20.6%	66%	7.2%
$3 \leq \varnothing \leq 5$ cm	22	3.5%	28.6%	64.4%	3.5%
$\varnothing > 5$ cm	3	0%	10%	90%	0%
Overall response	102	5.2%	21.5%	67.4%	5.9%

CR: Complete response; PR: Partial response; SD: Stable disease; PD: Progressive disease.

Table 4 Histological response rate of treated nodules in patients submitted to orthotopic transplantation

\varnothing nodules	Degree of necrosis		
	100%	$> 90\%$	$< 50\%$
$\varnothing < 3$ cm	7	-	3
$3 \leq \varnothing \leq 5$ cm	2	2	-
Overall necrosis	9 (64.3%)	2 (14.3%)	3 (21.4%)

spinal cord injury) related to non-target embolization nor locally (hepatic infection or abscesses, ischemic hepatitis and bile duct injuries) due to local toxicity or ischemia^[22]. Median hospital stay was 2 d (range 2-4). Post-embolization syndrome (PES) occurred in 15% of treatments (11/73). Other common AE were abdominal pain (24.6%) and nausea/vomiting (12.3%), which were treated with analgesic drugs and anti-emetics, and mild ascites (4.1%). Transient post procedure increase in transaminase levels occurred in 13.7% of cases (10/73). Other 1/2 grade laboratory tests alterations included a transient increase in bilirubin levels (6.8%).

TTR, TTP and progression free survival

The TTR for all patients was of 4 mo (95%CI: Range 1-4). Overall 24 patients (50%) experienced tumor progression through the study period. One-year progression free survival (PFS) was 64.5% whereas 2-year PFS was 52%. Median TTP was 13 mo (95%CI: Range: 11-21), calculated on mRECIST, as described in Figure 2.

DISCUSSION

DEB-TACE is the standard of care for HCC intermediate stage patients and a valuable therapeutic option in

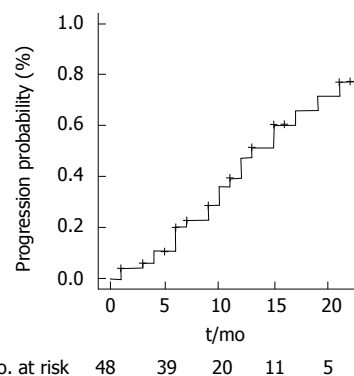
Table 5 Adverse events

Toxicity	Grade 1/2	Grade 3/4
Clinical findings		
Post embolization syndrome	11/73 (15%)	-
Ascites	3/73 (4.1%)	-
Abdominal pain	18/73 (24.6%)	-
Nausea/vomiting	9/73 (12.3%)	-
Laboratory tests		
Bilirubin	5/73 (6.8%)	-
Transaminase	10/73 (13.7%)	-

BCLC A stage when curative approach is unfeasible^[1,23]. Several consecutive sessions are usually needed for DEB-TACE to be effective, *i.e.*, the complete tumor response, so that the optimal treatment should lead to higher tumor necrosis rate with the lowest incidence of adverse event. DEB-TACE showed a low incidence of PES^[13] and systemic toxicity than in previous reports^[8], but its superiority over c-TACE is still a matter of debate^[10,24-26].

Since the diameter of chemo loaded microspheres seems to be related to their therapeutic action^[17,18], studies on pharmacological kinetics have focused on producing smaller particles that could penetrate deeper into the tumor's vascular network. The most distal penetration of these microspheres reduces the phenomenon of hypoxic-ischaemic neoangiogenesis^[27,28]. However, for embolization not associated with any drug (bland embolization), the use of particles with a diameter < 100 μ m presented a concerning rate of complications, especially in the treatment of large tumors^[29,30]. Some complications in this type of procedures are related to the "non-target embolization" that is, the unwanted escape of microspheres outside the optimal area for treatment, which can affect other organs or unwanted areas of the same organ. Acute pancreatitis (0.88%-15.2%), acute cholecystitis (0.2%-5.4%), pulmonary embolism (0.17%-2.7%), splenic infarction (0.08%-1.4%), gastro-intestinal mucosal tumors (0.22%-0.7%), spinal cord injury (0.3%-1.2%) are among the possible extrahepatic complications^[31]. Unwanted hepatic complications such as ischemic hepatitis (0.26%-15.4%), liver infarction or abscess (0.5%-2.7%) or bile duct injuries^[31] are connected to local ischemic damages. Some recent studies have proven a very high degree of safety in the use of loadable particles with diameters below 100 μ m, with good preliminary efficacy results in terms of radiological and histological response to treatment^[14,15,18].

A new generation of microspheres (embozene tandem 40 μ m) has been recently marketed for selective intra-arterial treatment even though data on the efficacy and safety profile of the product is yet to be published. To our knowledge, this is the first report on the safety and efficacy of 40 μ m particles preloaded with doxorubicin in the treatment of HCC with DEB-TACE. The overall objective response rate (CR + PR) obtained has been of 26.7% to RECIST and 72.6% to mRECIST. This is comparable to the rates according to mRECIST of two recent series carried out with 70-150 μ m^[14,15] and 30-60

**Figure 2** Time to progression.

μ m^[18] (initial diameters) particles loaded with doxorubicin by Spreafico *et al.*^[14] and Malagari *et al.*^[18] respectively.

Cases of failed response to locoregional therapy, defined as progressive disease, were around 5.9% and 3% with RECIST and mRECIST, respectively. Median TTP was 13 mo (11-21), an interesting and slightly better result if compared with previous published trials using other microspheres. Moreover, it is to be considered that we did not restrict progression analysis only to local progression of target tumors, but also distant intrahepatic progressions and/or metastases occurrence were investigated.

In 11 patients out of the recruited 48, DEB-TACE was used as bridging therapy for OLT with a complete pathological response (meant as a 100% necrosis in the histological evaluation) in 64.3% cases (9/14 tumors). Tumors smaller than 3 cm shown a better response in term of histological necrosis (70% complete necrosis), compared to those larger than 3 cm (50% complete necrosis). These histological results are consistent with those reported elsewhere^[32,33].

The best radiological response was obtained with a single cycle in 60% of patients, with two cycles in 30% of cases and with three cycles in 10% of patients, with a TTR of about 4 mo (95%CI: Range: 4-6). The effectiveness of HCC treatment using TACE on demand has been proved in our series in the event of detection of SD or PR during the follow-up by CT or MRI, in line with data in the literature. The very low toxicity rates observed in our series are probably a consequence of the high selectivity of the procedure ensured by the use of smaller particles.

The procedures were generally well tolerated. Recorded toxicity levels were lower than recent studies using larger diameter microspheres and consistent with two other studies concerning microspheres with a pre-loading diameter between 70-150 μ m^[14,15] and 30-60 μ m^[18].

The incidence of PES was to be lower than the percentages published in other series^[11,12,14,18] with particles having similar or larger dimensions, most likely due to the selectivity of the procedure and possible sparing of a larger area of peritumoral hepatic parenchyma.

To our knowledge this is the first series regarding the use of 40 μ m DEB in HCC treatment. This is interesting

for world community and especially for western countries where there is skepticism about using particles smaller than 100 μ m for DEB-TACE due to the non-target embolization danger. Our preliminary experience shows that 40 μ m DEB-TACE is a highly effective and safe technique for HCC non suitable to ablation or surgery therapies with a low rate of PES and no major complications, either local or systemic. The results are complete for all the 48 patients and for 11 of them a histologically proven response to DEB-TACE on surgical specimen is available. Objective local response reached 72.6% and 26.7% according to mRECIST and RECIST without damage to adjacent healthy liver as evidenced by imaging, histology and liver biochemistry. The study has some limitations such as the retrospective nature, the single series and the small sample of patients. Further studies with a longer follow-up period and a bigger sample should be planned to confirm our results.

The results of this retrospective study indicate that DEB-TACE with 40 μ m particles is an effective and safe treatment for early-intermediate HCC patients not eligible for curative treatment with good results in term of objective response rate and necrosis.

COMMENTS

Background

Transarterial chemoembolization (TACE) is the current standard of care for hepatocellular carcinoma (HCC) in patients with multinodular disease, classified as intermediate stage (stage B) to Barcelona Clinic Liver Cancer (BCLC) Staging System or in patients in early stage (stage A) not eligible for curative treatment (surgery, liver transplantation or percutaneous ablative treatments). Conventional TACE (c-TACE) has shown superiority over basic supportive care in unresectable HCC in literature since the early 2000s. Actually there is no evidence of superiority of drug eluting bead TACE (DEB-TACE) on c-TACE or transarterial embolization in literature. In the last fifteen years many particles with diameters gradually smaller have been developed for DEB-TACE. These new 40 μ m diameter drug eluting beads theoretically penetrate deeper into tumor circulation arterioles reducing the phenomenon of hypoxic-ischaemic neoangiogenesis due to transarterial embolization. There is no evidence in literature of DEB-TACE superiority over c-TACE in terms of efficacy. The only demonstrated advantage is the reduced rate of post embolic syndrome.

Research frontiers

The authors' report on 40 μ m DEB-TACE for HCC is the first experience in literature. The weakness points are the small sample of patients and the retrospective design of the study but it can represent an interesting report for scientific community as first evaluation of safety and efficacy of this new generation of microparticles. Further studies with a larger number of patients will be needed to confirm data and confirm or deny the theoretical benefits of this new generation of micro-particles in the treatment of HCC.

Innovations and breakthroughs

The study confirms a degree of objective response to treatment, defined as complete or partial response according to Response Evaluation Criteria in Solid Tumors (RECIST) and modified RECIST applied to computed tomography and magnetic resonance imaging, consistent with that of previous studies in the literature with a slightly higher caliber particles (40-60 and 70-150 μ m). The data is comforting when you consider the lack of intra or extrahepatic complications due to the phenomenon of non-target embolization, cause for concern in Western countries where the DEBTACE is widespread with larger gauge particles.

Applications

This study suggests that 40 μ m DEBTACE is safe and effective in early-

intermediate HCC patients with compensated cirrhosis.

Terminology

DEB-TACE: Drug eluting bead TACE; Nontarget embolization: Unwanted escape of particles outside the territory seat of treatment.

Peer-review

This paper presented about the efficacy of TACE using drug eluting beads for HCC patients. This topic could be interesting for readers.

REFERENCES

- 1 EASL-EORTC clinical practice guidelines: management of hepatocellular carcinoma. *J Hepatol* 2012; **56**: 908-943 [PMID: 22424438 DOI: 10.1016/j.jhep.2011.12.001]
- 2 Llovet JM, Bruix J. Systematic review of randomized trials for unresectable hepatocellular carcinoma: Chemoembolization improves survival. *Hepatology* 2003; **37**: 429-442 [PMID: 12540794 DOI: 10.1053/jhep.2003.50047]
- 3 Bruix J, Sherman M. Management of hepatocellular carcinoma: an update. *Hepatology* 2011; **53**: 1020-1022 [PMID: 21374666 DOI: 10.1002/hep.24199]
- 4 Llovet JM, Real MI, Montaña X, Planas R, Coll S, Aponte J, Ayuso C, Sala M, Muchart J, Solà R, Rodés J, Bruix J. Arterial embolisation or chemoembolisation versus symptomatic treatment in patients with unresectable hepatocellular carcinoma: a randomised controlled trial. *Lancet* 2002; **359**: 1734-1739 [PMID: 12049862 DOI: 10.1016/S0140-6736(02)08649-X]
- 5 Lo CM, Ngan H, Tso WK, Liu CL, Lam CM, Poon RT, Fan ST, Wong J. Randomized controlled trial of transarterial lipiodol chemoembolization for unresectable hepatocellular carcinoma. *Hepatology* 2002; **35**: 1164-1171 [PMID: 11981766 DOI: 10.1053/jhep.2002.33156]
- 6 Llovet JM, Burroughs A, Bruix J. Hepatocellular carcinoma. *Lancet* 2003; **362**: 1907-1917 [PMID: 14667750 DOI: 10.1016/S0140-6736(03)14964-1]
- 7 Poon RT, Tso WK, Pang RW, Ng KK, Woo R, Tai KS, Fan ST. A phase I/II trial of chemoembolization for hepatocellular carcinoma using a novel intra-arterial drug-eluting bead. *Clin Gastroenterol Hepatol* 2007; **5**: 1100-1108 [PMID: 17627902 DOI: 10.1016/j.cgh.2207.04.021]
- 8 Varela M, Real MI, Burrell M, Forner A, Sala M, Brunet M, Ayuso C, Castells L, Montaña X, Llovet JM, Bruix J. Chemoembolization of hepatocellular carcinoma with drug eluting beads: efficacy and doxorubicin pharmacokinetics. *J Hepatol* 2007; **46**: 474-481 [PMID: 17239480 DOI: 10.1016/j.jhep.2006.10.020]
- 9 Brown KT, Do RK, Gonen M, Covey AM, Getrajdman GI, Sofocleous CT, Jarnagin WR, D'Angelica MI, Allen PJ, Erinjeri JP, Brody LA, O'Neill GP, Johnson KN, Garcia AR, Beattie C, Zhao B, Solomon SB, Schwartz LH, DeMatteo R, Abou-Alfa GK. Randomized Trial of Hepatic Artery Embolization for Hepatocellular Carcinoma Using Doxorubicin-Eluting Microspheres Compared With Embolization With Microspheres Alone. *J Clin Oncol* 2016; **34**: 2046-2053 [PMID: 26834067 DOI: 10.1200/JCO.2015.64.0821]
- 10 Sacco R, Bargellini I, Bertini M, Bozzi E, Romano A, Petrucci P, Tumino E, Ginanni B, Federici G, Cioni R, Metrangola S, Bertoni M, Bresci G, Parisi G, Altomare E, Capria A, Bartolozzi C. Conventional versus doxorubicin-eluting bead transarterial chemoembolization for hepatocellular carcinoma. *J Vasc Interv Radiol* 2011; **22**: 1545-1552 [PMID: 21849247 DOI: 10.1016/j.jvir.2011.07.00217]
- 11 Lammer J, Malagari K, Vogl T, Pilleul F, Denys A, Watkinson A, Pitton M, Sergeant G, Pfammatter T, Terraz S, Benhamou Y, Avajon Y, Gruenberger T, Pomoni M, Langenberger H, Schuchmann M, Dumortier J, Mueller C, Chevallier P, Lencioni R. Prospective randomized study of doxorubicin-eluting-bead embolization in the treatment of hepatocellular carcinoma: results of the PRECISION V study. *Cardiovasc Intervent Radiol* 2010; **33**: 41-52 [PMID: 20101010 DOI: 10.1007/s00261-010-0510-0]

- 19908093 DOI: 10.1007/s00270-099-9711-7]
- 12 **Song MJ**, Chun HJ, Song DS, Kim HY, Yoo SH, Park CH, Bae SH, Choi JY, Chang UI, Yang JM, Lee HG, Yoon SK. Comparative study between doxorubicin-eluting beads and conventional transarterial chemoembolization for treatment of hepatocellular carcinoma. *J Hepatol* 2012; **57**: 1244-1250 [PMID: 22824821 DOI: 10.1016/j.jhep.2012.07.017]
- 13 **Facciorusso A**, Di Maso M, Muscatiello N. Drug-eluting beads versus conventional chemoembolization for the treatment of unresectable hepatocellular carcinoma: A meta-analysis. *Dig Liver Dis* 2016; **48**: 571-577 [PMID: 26965785 DOI: 10.1016/j.dld.2016.02.005]
- 14 **Spreafico C**, Cascella T, Facciorusso A, Sposito C, Rodolfo L, Morosi C, Civelli EM, Vaiani M, Bhoori S, Pellegrinelli A, Marchianò A, Mazzaferro V. Transarterial chemoembolization for hepatocellular carcinoma with a new generation of beads: clinical-radiological outcomes and safety profile. *Cardiovasc Intervent Radiol* 2015; **38**: 129-134 [PMID: 24870698 DOI: 10.1007/s00270-014-0907-0]
- 15 **Odísio BC**, Ashton A, Yan Y, Wei W, Kaseb A, Wallace MJ, Vauthey JN, Gupta S, Tam AL. Transarterial hepatic chemoembolization with 70-150 μ m drug-eluting beads: assessment of clinical safety and liver toxicity profile. *J Vasc Interv Radiol* 2015; **26**: 965-971 [PMID: 25979305 DOI: 10.1016/j.jvir.2015.03.020]
- 16 **Blümmel J**, Reinhardt S, Schäfer M, Gilbert C, Sun L, Ren J. Drug-eluting Beads in the Treatment of Hepatocellular Carcinoma and Colorectal Cancer Metastases to the Liver. *Eur Oncol Haematol* 2012; **8**: 162-166 [DOI: 10.17925/EOH.2012.08.3.162]
- 17 **Lencioni R**, de Baere T, Burrel M, Caridi JG, Lammer J, Malagari K, Martin RC, O'Grady E, Real MI, Vogl TJ, Watkinson A, Geschwind JF. Transcatheter treatment of hepatocellular carcinoma with Doxorubicin-loaded DC Bead (DEBDOX): technical recommendations. *Cardiovasc Intervent Radiol* 2012; **35**: 980-985 [PMID: 22009576 DOI: 10.1007/s00270-011-0287-7]
- 18 **Malagari K**, Pomoni M, Moschouris H, Kelekis A, Charokopakis A, Bouma E, Spyridopoulos T, Chatziioannou A, Sotirchos V, Karampelas T, Tamvakopoulos C, Filippiadis D, Karagiannis E, Marinis A, Koskinas J, Kelekis DA. Chemoembolization of hepatocellular carcinoma with HepaSphere 30-60 μ m. Safety and efficacy study. *Cardiovasc Intervent Radiol* 2014; **37**: 165-175 [PMID: 24263774 DOI: 10.1007/s00270-013-0777-x]
- 19 **National Cancer Institute**. Common terminology criteria for adverse events v4.0. NCI, NIH, DHHS. May 29, 2009. NIH publication 09-7473. Available from: URL: <http://www.hrc.govt.nz/sites/default/files/CTCAE manual - DMCC.pdf>
- 20 **Lencioni R**, Llovet JM. Modified RECIST (mRECIST) assessment for hepatocellular carcinoma. *Semin Liver Dis* 2010; **30**: 52-60 [PMID: 20175033 DOI: 10.1055/s-0030-1247132]
- 21 **Kim BK**, Kim SU, Kim KA, Chung YE, Kim MJ, Park MS, Park JY, Kim do Y, Ahn SH, Kim MD, Park SI, Won JY, Lee DY, Han KH. Complete response at first chemoembolization is still the most robust predictor for favorable outcome in hepatocellular carcinoma. *J Hepatol* 2015; **62**: 1304-1310 [PMID: 25637785 DOI: 10.1016/j.jhep.2015.01.022]
- 22 **Xia J**, Ren Z, Ye S, Sharma D, Lin Z, Gan Y, Chen Y, Ge N, Ma Z, Wu Z, Fan J, Qin L, Zhou X, Tang Z, Yang B. Study of severe and rare complications of transarterial chemoembolization (TACE) for liver cancer. *Eur J Radiol* 2006; **59**: 407-412 [PMID: 16621394 DOI: 10.1016/j.ejrad.2006.03.002]
- 23 **Malagari K**, Alexopoulou E, Chatzimichail K, Hall B, Koskinas J, Ryan S, Gallardo E, Kelekis A, Gouliamos A, Kelekis D. Transcatheter chemoembolization in the treatment of HCC in patients not eligible for curative treatments: midterm results of doxorubicin-loaded DC bead. *Abdom Imaging* 2008; **33**: 512-519 [PMID: 17938995 DOI: 10.1007/s00261-007-9334-x]
- 24 **Golfieri R**, Giampalma E, Renzulli M, Cioni R, Bargellini I, Bartolozzi C, Breatta AD, Gandini G, Nani R, Gasparini D, Cucchetti A, Bolondi L, Trevisani F. Randomised controlled trial of doxorubicin-eluting beads vs conventional chemoembolisation for hepatocellular carcinoma. *Br J Cancer* 2014; **111**: 255-264 [PMID: 24937669 DOI: 10.1038/bjc.2014.199]
- 25 **Xie ZB**, Wang XB, Peng YC, Zhu SL, Ma L, Xiang BD, Gong WF, Chen J, You XM, Jiang JH, Li LQ, Zhong JH. Systematic review comparing the safety and efficacy of conventional and drug-eluting bead transarterial chemoembolization for inoperable hepatocellular carcinoma. *Hepatol Res* 2015; **45**: 190-200 [PMID: 25388603 DOI: 10.1111/hepr.12450]
- 26 **Facciorusso A**, Mariani L, Sposito C, Spreafico C, Bongini M, Morosi C, Cascella T, Marchianò A, Camerini T, Bhoori S, Brunero F, Barone M, Mazzaferro V. Drug-eluting beads versus conventional chemoembolization for the treatment of unresectable hepatocellular carcinoma. *J Gastroenterol Hepatol* 2016; **31**: 645-653 [PMID: 26331807 DOI: 10.1111/jgh.13147]
- 27 **Wang B**, Xu H, Gao ZQ, Ning HF, Sun YQ, Cao GW. Increased expression of vascular endothelial growth factor in hepatocellular carcinoma after transcatheter arterial chemoembolization. *Acta Radiol* 2008; **49**: 523-529 [PMID: 18568538 DOI: 10.1080/02841850801958890]
- 28 **Kobayashi N**, Ishii M, Ueno Y, Kisara N, Chida N, Iwasaki T, Toyota T. Co-expression of Bcl-2 protein and vascular endothelial growth factor in hepatocellular carcinomas treated by chemoembolization. *Liver* 1999; **19**: 25-31 [PMID: 9928762]
- 29 **Bonomo G**, Pedicini V, Monfardini L, Della Vigna P, Poretti D, Orgera G, Orsi F. Bland embolization in patients with unresectable hepatocellular carcinoma using precise, tightly size-calibrated, anti-inflammatory microparticles: first clinical experience and one-year follow-up. *Cardiovasc Intervent Radiol* 2010; **33**: 552-559 [PMID: 19957182 DOI: 10.1007/s00270-009-9752-y]
- 30 **Maluccio MA**, Covey AM, Porat LB, Schubert J, Brody LA, Sofocleous CT, Getrajdman GI, Jamagin W, Dematteo R, Blumgart LH, Fong Y, Brown KT. Transcatheter arterial embolization with only particles for the treatment of unresectable hepatocellular carcinoma. *J Vasc Interv Radiol* 2008; **19**: 862-869 [PMID: 18503900 DOI: 10.1016/j.jvir.2008.02.013]
- 31 **López-Benítez R**, Richter GM, Kauczor HU, Stampfl S, Kladeck J, Radeleff BA, Neukamm M, Hallscheidt PJ. Analysis of nontarget embolization mechanisms during embolization and chemoembolization procedures. *Cardiovasc Intervent Radiol* 2009; **32**: 615-622 [PMID: 19387732 DOI: 10.1007/s00270-009-9568-9]
- 32 **Nicolini A**, Martinetti L, Crespi S, Maggioni M, Sangiovanni A. Transarterial chemoembolization with epirubicin-eluting beads versus transarterial embolization before liver transplantation for hepatocellular carcinoma. *J Vasc Interv Radiol* 2010; **21**: 327-332 [PMID: 20097098 DOI: 10.1016/j.jvir.2009.10.038]
- 33 **Nicolini D**, Svegliati-Baroni G, Candelari R, Mincarelli C, Mandolesi A, Bearzi I, Mocchegiani F, Vecchi A, Montalti R, Benedetti A, Risaliti A, Vivarelli M. Doxorubicin-eluting bead vs conventional transcatheter arterial chemoembolization for hepatocellular carcinoma before liver transplantation. *World J Gastroenterol* 2013; **19**: 5622-5632 [PMID: 24039354 DOI: 10.3748/wjg.v19.i34.5622]

P- Reviewer: Edeline J, Jin B, Ohira M **S- Editor:** Ji FF

L- Editor: A **E- Editor:** Li D





Published by **Baishideng Publishing Group Inc**
7901 Stoneridge Drive, Suite 501, Pleasanton, CA 94588, USA
Telephone: +1-925-223-8242
Fax: +1-925-223-8243
E-mail: bpgoffice@wjgnet.com
Help Desk: <http://www.f6publishing.com/helpdesk>
<http://www.wjgnet.com>



World Journal of *Radiology*

World J Radiol 2017 June 28; 9(6): 253-294





Editorial Board

2014-2017

The *World Journal of Radiology* Editorial Board consists of 365 members, representing a team of worldwide experts in radiology. They are from 36 countries, including Afghanistan (1), Argentina (2), Australia (5), Austria (7), Belgium (2), Brazil (8), Canada (6), Chile (1), China (43), Croatia (1), Denmark (4), Egypt (6), France (5), Germany (22), Greece (10), India (12), Iran (6), Ireland (2), Israel (3), Italy (47), Japan (13), Netherlands (1), New Zealand (1), Pakistan (1), Poland (2), Portugal (1), Serbia (1), Singapore (3), Slovakia (1), South Korea (18), Spain (4), Sweden (2), Switzerland (4), Thailand (1), Turkey (26), United Kingdom (11), and United States (82).

EDITORS-IN-CHIEF

Kai U Juergens, *Bremen*
Edwin JR van Beek, *Edinburgh*
Thomas J Vogl, *Frankfurt*

GUEST EDITORIAL BOARD MEMBERS

Wing P Chan, *Taipei*
Chung-Huei Hsu, *Taipei*
Chin-Chang Huang, *Taipei*
Tsong-Long Hwang, *Taoyuan*
Jung-Lung Hsu, *Taipei*
Chia-Hung Kao, *Taichung*
Yu-Ting Kuo, *Tainan*
Hon-Man Liu, *Taipei*
Hui-Lung Liang, *Kaohsiung*
Chun Chung Lui, *Kaohsiung*
Sen-Wen Teng, *Taipei*
Yung-Liang (William) Wan, *Taoyuan*

MEMBERS OF THE EDITORIAL BOARD



Afghanistan

Takao Hiraki, *Okayama*



Argentina

Patricia Carrascosa, *Vicente Lopez*
Maria C Ziadi, *Rosario*



Australia

Lourens Bester, *Sydney*
Gemma A Figtree, *Sydney*

Stuart M Grieve, *Sydney*
Wai-Kit Lee, *Fitzroy*
Prabhakar Ramachandran, *Melbourne*



Austria

Herwig R Cerwenka, *Graz*
Gudrun M Feuchtnner, *Innsbruck*
Benjamin Henninger, *Innsbruck*
Rupert Lanzenberger, *Vienna*
Shu-Ren Li, *Vienna*
Veronika Schopf, *Vienna*
Tobias De Zordo, *Innsbruck*



Belgium

Steve Majerus, *Liege*
Kathelijne Peremans, *Merelbeke*



Brazil

Clerio F Azevedo, *Rio de Janeiro*
Patrícia P Alfredo, *São Paulo*
Eduardo FC Fleury, *São Paulo*
Edward Araujo Júnior, *São Paulo*
Wellington P Martins, *Ribeirao Preto*
Ricardo A Mesquita, *Belo Horizonte*
Vera MC Salemi, *São Paulo*
Claudia Szobot, *Porto Alegre*
Lilian YI Yamaga, *São Paulo*



Canada

Marie Arsalidou, *Toronto*
Otman A Basir, *Waterloo*

Tarik Zine Belhocine, *Toronto*
James Chow, *Toronto*
Tae K Kim, *Toronto*
Anastasia Oikonomou, *Toronto*



China

Hong-Wei Chen, *Wuxi*
Feng Chen, *Hangzhou*
Jian-Ping Chu, *Guangzhou*
Guo-Guang Fan, *Shenyang*
Bu-Lang Gao, *Shijiazhuang*
Qi-Yong Gong, *Chengdu*
Ying Han, *Beijing*
Xian-Li Lv, *Beijing*
Yi-Zhuo Li, *Guangzhou*
Xiang-Xi Meng, *Harbin*
Yun Peng, *Beijing*
Jun Shen, *Guangzhou*
Ze-Zhou Song, *Hangzhou*
Wai Kwong Tang, *Hong Kong*
Gang-Hua Tang, *Guangzhou*
Jie Tian, *Beijing*
Lu-Hua Wang, *Beijing*
Xiao-bing Wang, *Xi'an*
Yi-Gen Wu, *Nanjing*
Kai Wu, *Guangzhou*
Hui-Xiong Xu, *Shanghai*
Zuo-Zhang Yang, *Kunming*
Xiao-Dan Ye, *Shanghai*
David T Yew, *Hong Kong*
Ting-He Yu, *Chongqing*
Zheng Yuan, *Shanghai*
Min-Ming Zhang, *Hangzhou*
Yudong Zhang, *Nanjing*
Dong Zhang, *Chongqing*
Wen-Bin Zeng, *Changsha*

Yue-Qi Zhu, *Shanghai*



Croatia

Goran Kusec, *Osijek*



Denmark

Poul E Andersen, *Odense*

Lars J Petersen, *Aalborg*

Thomas Z Ramsøy, *Frederiksberg*

Morten Ziebell, *Copenhagen*



Egypt

Mohamed F Bazeed, *Mansoura*

Mohamed Abou El-Ghar, *Mansoura*

Reem HA Mohamed, *Cairo*

Mohamed R Nouh, *Alexandria*

Ahmed AKA Razek, *Mansoura*

Ashraf A Zytoon, *Shebin El-Koom*



France

Sabine F Bensamoun, *Compiègne*

Romarc Loffroy, *Dijon*

Stephanie Nougaret, *Montpellier*

Hassane Oudadesse, *Rennes*

Vincent Vinh-Hung, *Fort-de-France*



Germany

Henryk Barthel, *Leipzig*

Peter Bannas, *Hamburg*

Martin Beeres, *Frankfurt*

Ilja F Ciernik, *Dessau*

A Dimitrakopoulou-Strauss, *Heidelberg*

Peter A Fasching, *Erlangen*

Andreas G Schreyer, *Regensburg*

Philipp Heusch, *Duesseldorf*

Sonja M Kirchhoff, *Munich*

Sebastian Ley, *Munich*

Adel Maataoui, *Frankfurt am Main*

Stephan M Meckel, *Freiburg*

Hans W Muller, *Duesseldorf*

Kay Raum, *Berlin*

Dirk Rades, *Luebeck*

Marc-Ulrich Regier, *Hamburg*

Alexey Surov, *Halle*

Martin Walter, *Magdeburg*

Axel Wetter, *Essen*

Christoph Zilkens, *Düsseldorf*



Greece

Panagiotis Antoniou, *Thessaloniki*

Nikos Efthimiou, *Athens*

Dimitris Karnabatidis, *Patras*

George Latsios, *Athens*

Stylianios Megremis, *Iraklion*

Alexander D Rapidis, *Athens*

Kiki Theodorou, *Larissa*

Ioannis A Tsalafoutas, *Athens*

Evanthia E Tripoliti, *Ioannina*

Athina C Tsili, *Ioannina*



India

Ritesh Agarwal, *Chandigarh*

Chandan J Das, *New Delhi*

Prathamesh V Joshi, *Mumbai*

Naveen Kalra, *Chandigarh*

Chandrasekharan Kesavadas, *Trivandrum*

Jyoti Kumar, *New Delhi*

Atin Kumar, *New Delhi*

Kaushala P Mishra, *Allahabad*

Daya N Sharma, *New Delhi*

Binit Sureka, *New Delhi*

Sanjay Sharma, *New Delhi*

Raja R Yadav, *Allahabad*



Iran

Majid Assadi, *Bushehr*

SeyedReza Najafizadeh, *Tehran*

Mohammad Ali Oghabian, *Tehran*

Amir Reza Radmard, *Tehran*

Ramin Sadeghi, *Mashhad*

Hadi Rokni Yazdi, *Tehran*



Ireland

Tadhg Gleeson, *Wexford*

Frederik JAI Vernimmen, *Cork*



Israel

Dafna Ben Bashat, *Tel Aviv*

Amit Gefen, *Tel Aviv*

Tamar Sella, *Jerusalem*



Italy

Adriano Alippi, *Rome*

Dante Amelio, *Trento*

Michele Anzidei, *Rome*

Filippo F Angileri, *Messinas*

Stefano Arcangeli, *Rome*

Roberto Azzoni, *San Donato milanese*

Tommaso V Bartolotta, *Palermo*

Tommaso Bartalena, *Imola*

Livia Bernardin, *San Bonifacio*

Federico Boschi, *Verona*

Sergio Casciaro, *Lecce*

Emanuele Casciani, *Rome*

Musa M Can, *Napoli*

Alberto Cuocolo, *Napoli*

Michele Ferrara, *Coppito*

Mauro Feola, *Fossano*

Giampiero Francica, *Castel Volturno*

Luigi De Gennaro, *Rome*

Giulio Giovannetti, *Pisa*

Francesca Iacobellis, *Napoli*

Formato Invernizzi, *Monza Brianza*

Francesco Lassandro, *Naples*

Lorenzo Livi, *Florence*

Pier P Mainenti, *Napoli*

Laura Marzetti, *Chieti*

Giuseppe Malinverni, *Crescentino*

Enrica Milanese, *Turin*

Giovanni Morana, *Treviso*

Lorenzo Monti, *Milan*

Silvia D Morbelli, *Genoa*

Barbara Palumbo, *Perugia*

Cecilia Parazzini, *Milan*

Stefano Pergolizzi, *Messina*

Antonio Pinto, *Naples*

Camillo Porcaro, *Rome*

Carlo C Quattrocchi, *Rome*

Alberto Rebonato, *Perugia*

Giuseppe Rizzo, *Rome*

Roberto De Rosa, *Naples*

Domenico Rubello, *Rovigo*

Andrea Salvati, *Bari*

Sergio Sartori, *Ferrara*

Luca M Sconfienza, *Milano*

Giovanni Storto, *Rionero*

Nicola Sverzellati, *Parma*

Alberto S Tagliafico, *Genova*

Nicola Troisi, *Florence*



Japan

Yasuhiko Hori, *Chiba*

Hidetoshi Ikeda, *Koriyama*

Masahito Kawabori, *Sapporo*

Tamotsu Kamishima, *Sapporo*

Hiro Kiyosue, *Yufu*

Yasunori Minami, *Osaka-sayama*

Yasuhiro Morimoto, *Kitakyushu*

Satoru Murata, *Tokyo*

Shigeki Nagamachi, *Miyazaki*

Hiroshi Onishi, *Yamanashi*

Morio Sato, *Wakayama Shi*

Yoshito Tsushima, *Maebashi*

Masahiro Yanagawa, *Suita*



Netherlands

Willem Jan van Rooij, *Tilburg*



New Zealand

W Howell Round, *Hamilton*



Pakistan

Wazir Muhammad, *Abbottabad*



Poland

Maciej S Baglaj, *Wroclaw*

Piotr Czauderna, *Gdansk*



Portugal

Joao Manuel RS Tavares, *Porto*



Serbia

Olivera Ciraj-Bjelac, *Belgrade*



Singapore

Gopinathan Anil, *Singapore*

Terence KB Teo, *Singapore*

Cher Heng Tan, *Singapore*



Slovakia

Stefan Sivak, *Martin*



South Korea

Ki Seok Choo, *Busan*

Seung Hong Choi, *Seoul*

Dae-Seob Choi, *Jinju*

Hong-Seok Jang, *Seoul*

Yong Jeong, *Daejeon*

Chan Kyo Kim, *Seoul*

Se Hyung Kim, *Seoul*

Joong-Seok Kim, *Seoul*

Sang Eun Kim, *Seongnam*

Sung Joon Kwon, *Seoul*

Jeong Min Lee, *Seoul*

In Sook Lee, *Busan*

Noh Park, *Goyang*

Chang Min Park, *Seoul*

Sung Bin Park, *Seoul*

Deuk Jae Sung, *Seoul*

Choongsoo Shin, *Seoul*

Kwon-Ha Yoon, *Iksan*



Spain

Miguel A De Gregorio, *Zaragoza*

Antonio Luna, *Jaén*

Enrique Marco de Lucas, *Santander*

Fernando Ruiz Santiago, *Granada*



Sweden

Dmitry Grishenkov, *Stockholm*

Tie-Qiang Li, *Stockholm*



Switzerland

Nicolau Beckmann, *Basel*

Christian Boy, *Bern*

Giorgio Treglia, *Bellinzona*

Stephan Ulmer, *Kiel*



Thailand

Sirianong Namwongprom, *Chiang Mai*



Turkey

Kubilay Aydin, *Istanbul*

Ramazan Akdemir, *Sakarya*

Serhat Avcu, *Ankara*

Ayşe Aralasmak, *Istanbul*

Oktay Algin, *Ankara*

Nevbahar Akcar, *Meselik*

Bilal Battal, *Ankara*

Zulkif Bozgeyik, *Elazig*

Nazan Ciledag, *Aakara*

Fuldem Y Donmez, *Ankara*

Gulgun Engin, *Istanbul*

Ahmet Y Goktay, *Izmir*

Oguzhan G Gumustas, *Bursa*

Kaan Gunduz, *Ankara*

Pelin Ozcan Kara, *Mersin*

Kivanc Kamburoglu, *Ankara*

Ozgur Kilickesmez, *Istanbul*

Furuzan Numan, *Istanbul*

Cem Onal, *Adana*

Ozgur Oztekin, *Izmir*

Seda Ozbek (Boruban), *Konya*

Selda Sarikaya, *Zonguldak*

Figen Taser, *Kutahya*

Baran Tokar, *Eskisehir*

Ender Uysal, *Istanbul*

Ensar Yekeler, *Istanbul*



United Kingdom

Indran Davagnanam, *London*

M DC Valdés Hernández, *Edinburgh*

Alan Jackson, *Manchester*

Suneil Jain, *Belfast*

Long R Jiao, *London*

Miltiadis Krokidis, *Cambridge*

Pradesh Kumar, *Liverpool*

Peter D Kuzmich, *Derby*

Georgios Plataniotis, *Brighton*

Vanessa Sluming, *Liverpool*



United States

Garima Agrawal, *Saint Louis*

James R Brasic, *Baltimore*

Rajendra D Badgaiyan, *Buffalo*

Ulas Bagci, *Bethesda*

Anat Biegon, *Stony Brook*

Ramon Casanova, *Winston Salem*

Wenli Cai, *Boston*

Zheng Chang, *Durham*

Corey J Chakarun, *Long Beach*

Kai Chen, *Los Angeles*

Hyun-Soon Chong, *Chicago*

Marco Cura, *Dallas*

Ravi R Desai, *Bensalem*

Delia DeBuc, *Miami*

Carlo N De Cecco, *Charleston*

Timm-Michael L Dickfeld, *Baltimore*

Subba R Digumarthy, *Boston*

Huy M Do, *Stanford*

Todd A Faasse, *Grand Rapids*

Salomao Faintuch, *Boston*

Girish M Fatterpekar, *New York*

Dhakshinamoorthy Ganesan, *Houston*

Robert J Griffin, *Little Rock*

Andrew J Gunn, *Boston*

Sandeep S Hedgire, *Boston*

Timothy J Hoffman, *Columbia*

Mai-Lan Ho, *San Francisco*

Juebin Huang, *Jackson*

Abid Irshad, *Charleston*

Matilde Inglese, *New York*

El-Sayed H Ibrahim, *Jacksonville*

Paul R Julsrud, *Rochester*

Pamela T Johnson, *Baltimore*

Ming-Hung Kao, *Tempe*

Sunil Krishnan, *Houston*

Richard A Komoroski, *Cincinnati*

Sandi A Kwee, *Honolulu*

King Kim, *Ft. Lauderdale*

Guozheng Liu, *Worcester*

Yiyan Liu, *Newark*

Venkatesh Mani, *New York*

Lian-Sheng Ma, *Pleasanton*

Rachna Madan, *Boston*

Zeyad A Metwalli, *Houston*

Yilong Ma, *Manhasset*

Hui Mao, *Atlanta*

Feroze B Mohamed, *Philadelphia*

Gul Moonis, *Boston*

John L Noshier, *New Brunswick*

Rahmi Oklu, *Boston*

Aytekun Oto, *Chicago*

Bishnuhari Paudyal, *Philadelphia*

Rajul Pandya, *Youngstown*

Chong-Xian Pan, *Sacramento*

Jay J Pillai, *Baltimore*

Neal Prakash, *Duarte*

Reza Rahbar, *Boston*

Ali S Raja, *Boston*

Gustavo J Rodriguez, *El Paso*

David J Sahn, *Portland*

Steven Schild, *Scottsdale*

Ali R Sepahdari, *Los Angeles*

Li Shen, *Indianapolis*

JP Sheehan, *Charlottesville*

Atul B Shinagare, *Boston*

Sarabjeet Singh, *Boston*

Charles J Smith, *Columbia*

Kenji Suzuki, *Chicago*

Monvadi Srichai-Parsia, *Washington*

Sree H Tirumani, *Boston*

Hebert A Vargas, *New York*

Sachit Verma, *Philadelphia*

Yoichi Watanabe, *Minneapolis*

Li Wang, *Chapel Hill*

Carol C Wu, *Boston*

Shoujun Xu, *Houston*

Min Yao, *Cleveland*

Xiaofeng Yang, *Atlanta*

Qingbao Yu, *Albuquerque*

Aifeng Zhang, *Chicago*

Chao Zhou, *Bethlehem*

Hongming Zhuang, *Philadelphia*



REVIEW

- 253 Diffusion magnetic resonance imaging: A molecular imaging tool caught between hope, hype and the real world of "personalized oncology"
Mahajan A, Deshpande SS, Thakur MH

MINIREVIEWS

- 269 Revisions to the Tumor, Node, Metastasis staging of lung cancer (8th edition): Rationale, radiologic findings and clinical implications
Kay FU, Kandathil A, Batra K, Saboo SS, Abbara S, Rajiah P

ORIGINAL ARTICLE

Retrospective Study

- 280 Cardiac magnetic resonance in patients with acute cardiac injury and unobstructed coronary arteries
Camastra GS, Sbarbati S, Danti M, Cacciotti L, Semeraro R, Della Sala SW, Ansalone G

Observational Study

- 287 Chronic antiepileptic drug use and functional network efficiency: A functional magnetic resonance imaging study
van Veenendaal TM, IJff DM, Aldenkamp AP, Lazeron RHC, Hofman PAM, de Louw AJA, Backes WH, Jansen JFA

ABOUT COVER

Editorial Board Member of *World Journal of Radiology*, Giuseppe Malinverni, MD, Director, Radiation Oncology Department, Ospedali Riuniti Marche Nord, 13044 Crescentino, Vercelli Province, Italy

AIM AND SCOPE

World Journal of Radiology (*World J Radiol*, *WJR*, online ISSN 1949-8470, DOI: 10.4329) is a peer-reviewed open access academic journal that aims to guide clinical practice and improve diagnostic and therapeutic skills of clinicians.

WJR covers topics concerning diagnostic radiology, radiation oncology, radiologic physics, neuroradiology, nuclear radiology, pediatric radiology, vascular/interventional radiology, medical imaging achieved by various modalities and related methods analysis. The current columns of *WJR* include editorial, frontier, diagnostic advances, therapeutics advances, field of vision, mini-reviews, review, topic highlight, medical ethics, original articles, case report, clinical case conference (clinicopathological conference), and autobiography.

We encourage authors to submit their manuscripts to *WJR*. We will give priority to manuscripts that are supported by major national and international foundations and those that are of great basic and clinical significance.

INDEXING/ABSTRACTING

World Journal of Radiology is now indexed in PubMed, PubMed Central, and Emerging Sources Citation Index (Web of Science).

FLYLEAF

I-III Editorial Board

EDITORS FOR THIS ISSUE

Responsible Assistant Editor: *Xiang Li*
Responsible Electronic Editor: *Huan-Liang Wu*
Proofing Editor-in-Chief: *Lian-Sheng Ma*

Responsible Science Editor: *Fang-Fang Ji*
Proofing Editorial Office Director: *Jin-Lei Wang*

NAME OF JOURNAL
World Journal of Radiology

ISSN
ISSN 1949-8470 (online)

LAUNCH DATE
January 31, 2009

FREQUENCY
Monthly

EDITORS-IN-CHIEF
Kai U Juergens, MD, Associate Professor, MRT und PET/CT, Nuklearmedizin Bremen Mitte, ZEMODI - Zentrum für morphologische und molekulare Diagnostik, Bremen 28177, Germany

Edwin JR van Beek, MD, PhD, Professor, Clinical Research Imaging Centre and Department of Medical Radiology, University of Edinburgh, Edinburgh EH16 4TJ, United Kingdom

Thomas J Vogl, MD, Professor, Reader in Health Technology Assessment, Department of Diagnostic and Interventional Radiology, Johann Wolfgang Goethe University of Frankfurt, Frankfurt 60590,

Germany

EDITORIAL BOARD MEMBERS
All editorial board members resources online at <http://www.wjgnet.com/1949-8470/editorialboard.htm>

EDITORIAL OFFICE
Xiu-Xia Song, Director
World Journal of Radiology
Baishideng Publishing Group Inc
7901 Stoneridge Drive, Suite 501, Pleasanton, CA 94588, USA
Telephone: +1-925-2238242
Fax: +1-925-2238243
E-mail: editorialoffice@wjgnet.com
Help Desk: <http://www.f6publishing.com/helpdesk>
<http://www.wjgnet.com>

PUBLISHER
Baishideng Publishing Group Inc
7901 Stoneridge Drive, Suite 501, Pleasanton, CA 94588, USA
Telephone: +1-925-2238242
Fax: +1-925-2238243
E-mail: bpgoffice@wjgnet.com
Help Desk: <http://www.f6publishing.com/helpdesk>
<http://www.wjgnet.com>

PUBLICATION DATE
June 28, 2017

COPYRIGHT
© 2017 Baishideng Publishing Group Inc. Articles published by this Open-Access journal are distributed under the terms of the Creative Commons Attribution Non-commercial License, which permits use, distribution, and reproduction in any medium, provided the original work is properly cited, the use is non commercial and is otherwise in compliance with the license.

SPECIAL STATEMENT
All articles published in journals owned by the Baishideng Publishing Group (BPG) represent the views and opinions of their authors, and not the views, opinions or policies of the BPG, except where otherwise explicitly indicated.

INSTRUCTIONS TO AUTHORS
<http://www.wjgnet.com/bpg/gerinfo/204>

ONLINE SUBMISSION
<http://www.f6publishing.com>

Diffusion magnetic resonance imaging: A molecular imaging tool caught between hope, hype and the real world of “personalized oncology”

Abhishek Mahajan, Sneha S Deshpande, Meenakshi H Thakur

Abhishek Mahajan, Sneha S Deshpande, Department of Radiodiagnosis and Imaging, Tata Memorial Hospital, Tata Memorial Centre, Mumbai 400012, Maharashtra, India

Meenakshi H Thakur, Department of Radiodiagnosis and Imaging, Tata Memorial Centre, Mumbai 400012, India

Author contributions: Guarantors of integrity of entire study, all authors; study concepts/study design or data acquisition or data analysis/interpretation, all authors; manuscript drafting or manuscript revision for important intellectual content, all authors; manuscript final version approval, all authors; literature research, all authors; and manuscript editing, all authors; all authors take responsibility for the integrity of the data and the accuracy of the data analysis.

Conflict-of-interest statement: I confirm that this manuscript is not published anywhere else and on behalf of all authors, I state that there is no conflict of interests (including none for related to commercial, personal, political, intellectual, or religious interests).

Open-Access: This article is an open-access article which was selected by an in-house editor and fully peer-reviewed by external reviewers. It is distributed in accordance with the Creative Commons Attribution Non Commercial (CC BY-NC 4.0) license, which permits others to distribute, remix, adapt, build upon this work non-commercially, and license their derivative works on different terms, provided the original work is properly cited and the use is non-commercial. See: <http://creativecommons.org/licenses/by-nc/4.0/>

Manuscript source: Invited manuscript

Correspondence to: Dr. Abhishek Mahajan, MD, Radiodiagnosis, Fellowship Cancer Imaging, MRes, Associate Professor, Department of Radiodiagnosis and Imaging, Tata Memorial Hospital, Tata Memorial Centre, Room No. 127, Dr E Borges Road, Parel, Mumbai 400012, Maharashtra, India. drabhishek.mahajan@yahoo.in
Telephone: +91-99-20210811
Fax: +91-22-24146937

Received: January 2, 2017

Peer-review started: January 4, 2017

First decision: February 17, 2017

Revised: March 24, 2017

Accepted: April 18, 2017

Article in press: April 19, 2017

Published online: June 28, 2017

Abstract

“Personalized oncology” is a multi-disciplinary science, which requires inputs from various streams for optimal patient management. Humongous progress in the treatment modalities available and the increasing need to provide functional information in addition to the morphological data; has led to leaping progress in the field of imaging. Magnetic resonance imaging has undergone tremendous progress with various newer MR techniques providing vital functional information and is becoming the cornerstone of “radiomics/radiogenomics”. Diffusion-weighted imaging is one such technique which capitalizes on the tendency of water protons to diffuse randomly in a given system. This technique has revolutionized oncological imaging, by giving vital qualitative and quantitative information regarding tumor biology which helps in detection, characterization and post treatment surveillance of the lesions and challenging the notion that “one size fits all”. It has been applied at various sites with different clinical experience. We hereby present a brief review of this novel functional imaging tool, with its application in “personalized oncology”.

Key words: Functional magnetic resonance imaging; Molecular imaging; Diffusion-weighted imaging; Tumor biology; Biomarker; Radiomics

© **The Author(s) 2017.** Published by Baishideng Publishing Group Inc. All rights reserved.

Core tip: Diffusion-weighted imaging (DWI) not only improves the sensitivity and specificity of conventional magnetic resonance imaging but provides information in regard to the tumor microenvironment that is not available from the conventional MR sequences. DWI helps in detection, characterization and post treatment surveillance of the lesions and challenges the notion that “one size fits all”. DWI provides both quantitative and qualitative information regarding tumor biology that makes it a potential reliable radiomics biomarker for personalized oncology.

Mahajan A, Deshpande SS, Thakur MH. Diffusion magnetic resonance imaging: A molecular imaging tool caught between hope, hype and the real world of “personalized oncology”. *World J Radiol* 2017; 9(6): 253-268 Available from: URL: <http://www.wjgnet.com/1949-8470/full/v9/i6/253.htm> DOI: <http://dx.doi.org/10.4329/wjcr.v9.i6.253>

INTRODUCTION

“Oncology” is a multi-disciplinary science, which requires inputs from various streams for optimal patient management. Humongous progress in the treatment modalities available and the increasing need to provide functional information in addition to the morphological data; has led to leaping progress in the field of imaging. Magnetic resonance imaging (MRI) has undergone tremendous progress with various newer MR techniques providing vital functional information and becoming a cornerstone in “radiomics or radiogenomics”^[1-3]. Diffusion-weighted imaging (DWI) is capitalizes on tendency of water protons to diffuse randomly in a given system. This technique has revolutionized oncological imaging, by giving vital qualitative and quantitative information regarding tumor biology which helps in detection, characterization and post treatment surveillance of the lesions (Figure 1).

DWI imaging challenges the notion that “one size fits all” and is becoming an integral part of “personalized oncology”^[1,2]. DWI is one of the most recent, reliable and robust imaging biomarkers for oncological imaging^[1,4,5]. The tremendous progress in MRI like higher strength of magnets used, stronger and faster gradients, multichannel coils, echoplanar imaging, faster and improved analytical software’s, etc. has expedited advancement in the acquisition of the diffusion weighted images and hence expanded the scope of DWI, especially in oncology^[1,4,5].

BASIC PRINCIPLE

DWI is based on the principle of “Brownian motion”; which states that water protons have a tendency to diffuse randomly in space^[4,5]. The backbone of DWI is Stejskal Tanner sequence^[6], which comprises of a spin

echo sequence with diffusion gradients applied before and after 180-degree pulse. The magnitude of diffusion weighting is denoted by the “b value”, an operator selected parameter which depends on the amplitude (G), separation (Δ) and duration (δ) of the diffusion gradients. The higher the “b value”, the higher the diffusion effects, which is achieved by increasing the gradient amplitude and duration and by widening the interval between the gradient pulses. The formula for “b” value is stated as

$b = \gamma^2 G^2 \delta^2 (\Delta - \delta/3)$; (where γ is the gyromagnetic ratio)

A measure of diffusion is “apparent diffusion coefficient (ADC)”^[5,6]. The ADC values are calculated from “b value zero” and using various higher “b values” and displayed as an ADC map. ADC maps are generally correlated with the DWI images to confirm diffusion restriction and negate the “T2 shine through effect”. The DWI images can be further analyzed quantitatively by assessing the ADC values. This signifies the extent of diffusion restriction and hence, is an objective evaluation tool.

Various other analytical ways are used like the ADC histogram mapping or the ADC slope analysis which gives a qualitative as well quantitative impression of the ADC in the suspicious area and comparative assessment between normal and suspicious area respectively^[7,8]. Colored maps give a better qualitative assessment of the tumor diffusivity and helps detect subtle changes in the tumor microenvironment which might be overlooked on the grey scale ADC maps. In our experience colored ADC maps are superior to the grey scale maps; especially in sub-centimeter sized lesions, and follow-up response assessment imaging^[1]. Thus, DWI forms an integral part of present era’s oncological imaging. We hereby present the various non-neuro applications of DWI in oncological imaging with a case based approach.

APPLICATIONS OF DWI IN ONCOLOGY

Head and neck tumors

“Head and neck tumors” constitute the sixth most common cancer worldwide, overall accounting for approximately 560000 new cases worldwide annually^[9]. DWI has been evaluated and applied extensively in head and neck imaging. Many studies have advocated the use of DWI in characterization of head and neck tumors (Figure 2)^[10,11]. Srinivasan *et al*^[11] concluded that the mean ADC value of malignant tumors was significantly lower than the benign lesions ($1.071 \pm 0.293 \times 10^{-3} \text{ mm}^2/\text{s}$; 95%CI: 0.864-1.277, respectively and $1.505 \pm 0.487 \times 10^{-3} \text{ mm}^2/\text{s}$; 95%CI: 1.305-1.706), and recommended a threshold value of $1.3 \times 10^{-3} \text{ mm}^2/\text{s}$ for differentiation between benign and malignant tumors on 3 T^[11]. They also reported that lymphomas have significantly lower ADC values than carcinomas, which in turn, have significantly lower ADC values than benign solid tumors. However, studies have found some overlap in the ADC values of these lesions and hence,

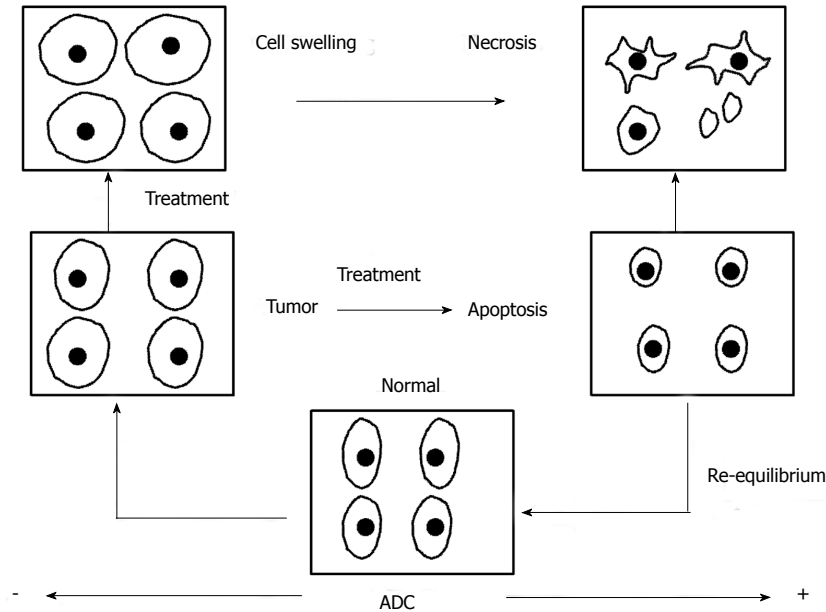


Figure 1 Diffusion imaging in oncology. The pictorial diagram depicts the diffusion changes and corresponding ADC values in correlation to the pre and post-treatment tumor microenvironment. Increased cell density in the tumor tissue leads to low ADC values as compared to the normal tissue. When subjected to antitumor therapy the cells undergo swelling in the immediate post-treatment phase which leads to further decrease in the ADC values. Once the cell death cycle sets in the cell membranes are more permeable and diffusivity increases which leads to higher ADC values. This ADC normalizes during the healing phase. ADC: Apparent diffusion coefficient.

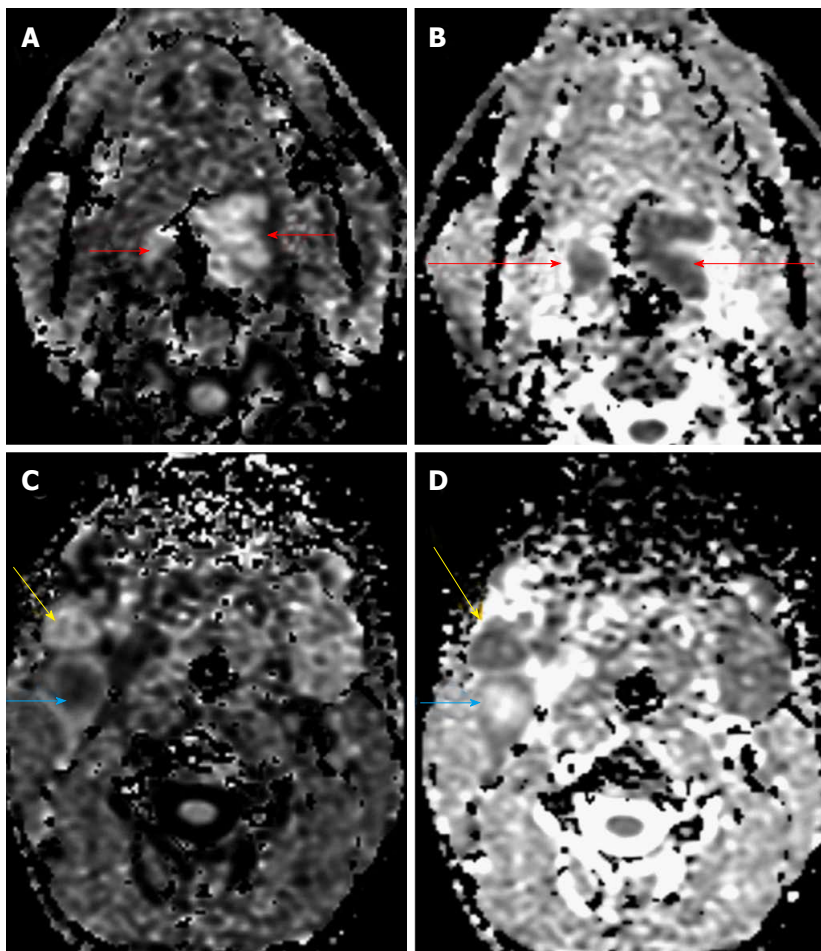


Figure 2 A 70-year-old male presented with a lesion in the base of tongue. Diffusion weighted imaging revealed restricted diffusion (A) in the primary lesion (short arrows) with reduced ADC values (B, long arrows). Restricted diffusion was also noted in the two right level II nodes with reduced ADC values (C and D) indicating nodal metastases (yellow and blue arrows). One of the nodes, showed raised central ADC values suggestive of necrosis (blue arrow). Biopsy of the primary lesion revealed squamous cell carcinoma. ADC: Apparent diffusion coefficient.

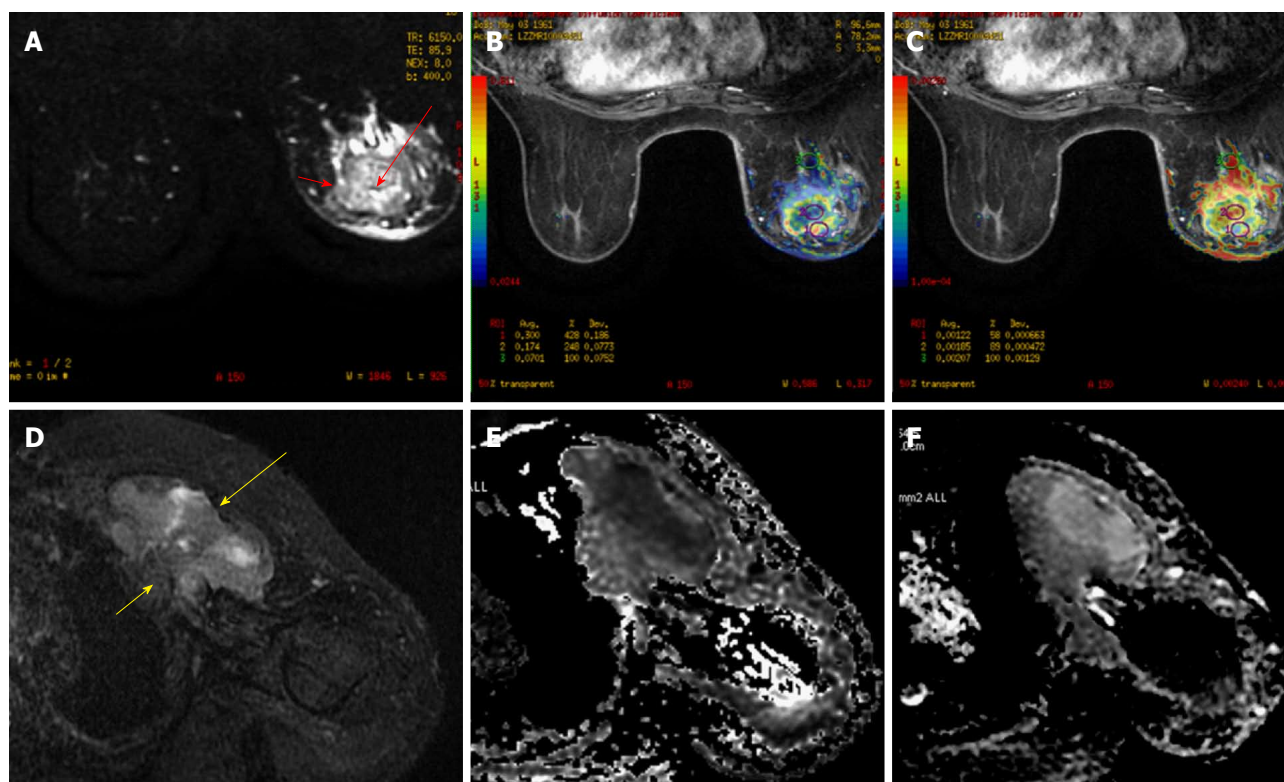


Figure 3 A 51-year-old female presented with a lump in the left breast. A: FS T2 weighted images revealed a well-defined rounded mass with smooth margins in the left breast with central hyperintensity (long red arrow) and a hypointense rim (short red arrow). Diffusion weighted imaging (B) revealed restricted diffusion in the periphery of the lesion (ROI 1) with reduced ADC values (C). The center of the lesion showed facilitated diffusion suggestive of necrotic areas (ROI 2). Biopsy revealed invasive ductal carcinoma; D: FS T2 weighted images revealed a well-defined heterogeneously hyperintense irregular mass in the left breast (long yellow arrow) with chest wall invasion (short yellow arrow). Diffusion weighted imaging (E) revealed restricted diffusion with reduced ADC values (F). Biopsy revealed invasive ductal carcinoma. ADC: Apparent diffusion coefficient.

caution needs to be executed when considering ADC values in isolation while characterizing a lesion^[12,13].

DWI contributes in predicting prognosis, since low pretreatment ADC values have been found to predict a favorable response to chemo-radiotherapy^[13,14]. DWI has also proved useful in differentiating post treatment changes from residual tumor or tumor recurrence^[15]. Tumor recurrence comprises of densely packed cells and hence reduced intercellular space. This restricts water proton motion and hence shows decreased ADC values. Post therapy changes are less cellular and with increased interstitial space; hence the higher ADC values^[16,17]. Numerous studies have shown the potential of 2-deoxy-2[F-18] fluoro-D-glucose positron emission tomography (FDG-PET) alone or hybrid PET/CT, in evaluating residual/recurrent head and neck tumors^[14,18]. However, PET results are confounded by the local inflammation post treatment, especially in early post treatment phase in nasopharyngeal cancers^[19,20]. Post treatment surveillance is routinely done by morphological imaging techniques like CT/MRI. Both of these modalities have low diagnostic sensitivity and accuracy. DWI has proved to be a useful biomarker for assessing treatment response in head and neck cancer. Pretreatment primary tumor SUV (max) and ADC values have been shown to correlate significantly and negatively with a potential to predict disease free

survival or disease events of head and neck squamous cell carcinoma^[20-23]. Role of DWI imaging has also been explored in characterizing thyroid lesions and initial results suggests that combined multimodality MRI, ultrasound and PET imaging has significant role to play in indeterminate thyroid lesions especially the Bethesda category-III^[24-26].

Breast tumors

DWI has been successfully applied to evaluate breast malignancies in both females and males (Figure 3). Sinha *et al*^[27] first concluded that the average ADC value of normal breast parenchyma ($2.37 \times 10^{-3} \text{ mm}^2/\text{s} \pm 0.27$) and benign lesions ($2.01 \times 10^{-3} \text{ mm}^2/\text{s} \pm 0.46$) is significantly higher than that of malignant breast lesions ($1.60 \times 10^{-3} \text{ mm}^2/\text{s} \pm 0.36$). In atypical lesions diffusion and multiparametric MRI has been found to increase the diagnostic accuracy for characterizing these lesions. Apart from characterizing a lesion as malignant, DWI has also shown promise in gauging the tumor grade^[28,29]. Costantini *et al*^[30] concluded that ADC values show an inverse relationship to tumor grade ($P < 0.001$), when b values of 0 and 1000 s/mm² are used. The mean ADC value of the "less aggressive" disease (Grade 1 and *in-situ* lesions) was $1.19 \times 10^{-3} \text{ mm}^2/\text{s}$, while the mean ADC value of the "more aggressive" disease group (Grade 2-Grade 3 invasive carcinomas)

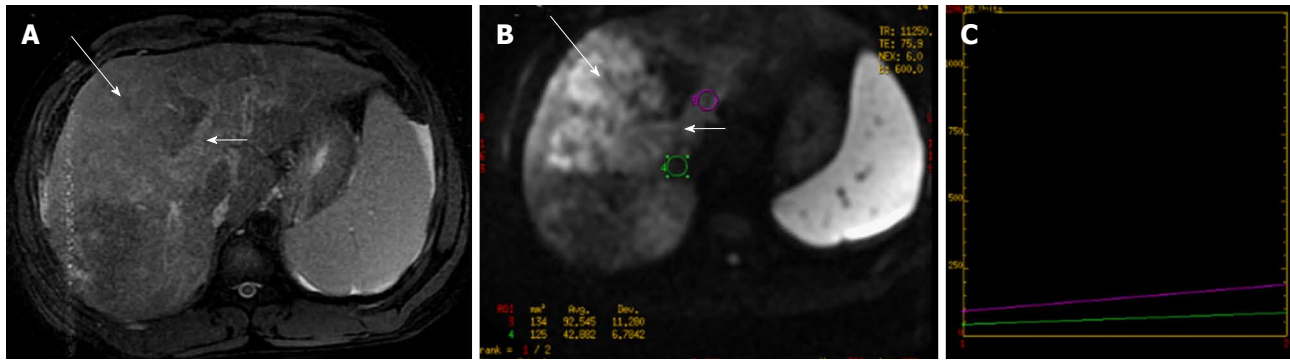


Figure 4 Pre-therapy magnetic resonance imaging in 57-year-old patient with hepatocellular carcinoma. A: DCE MR of liver showed enhancing lesion in segment V, VI, VII and VIII of the liver (long arrow-A) with enhancing portal vein thrombus (short white arrow-A). Diffusion weighted imaging revealed restricted diffusion in the hepatic lesion (long arrow-B) and the portal vein thrombus (short arrow-B) with reduced ADC values (B and C). Biopsy revealed hepatocellular carcinoma. Thus DWI helps in confirming the diagnosis of malignant portal vein thrombosis. ADC: Apparent diffusion coefficient; MR: Magnetic resonance; DWI: Diffusion-weighted imaging.

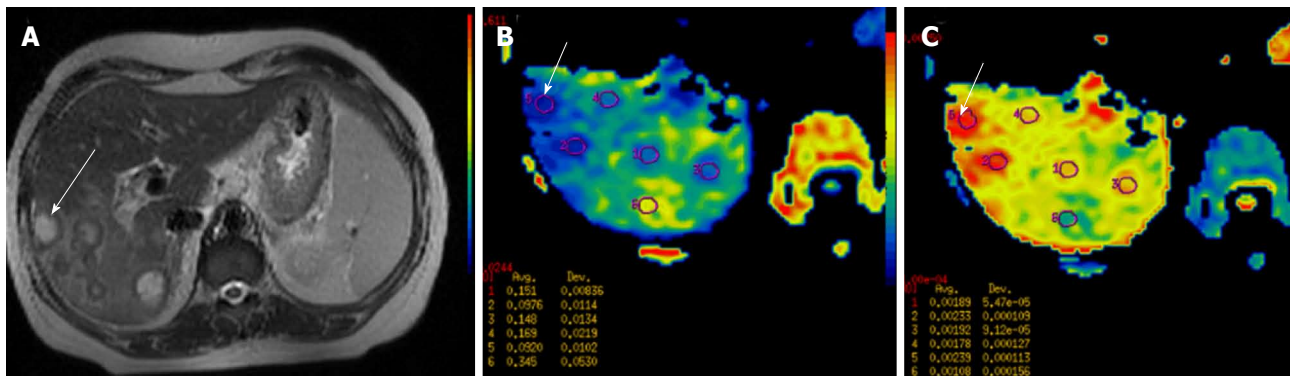


Figure 5 A 45-year-old female with ovarian malignancy, post therapy, presented with sudden onset of abdominal pain and high grade fever. A: Axial T2 W images showed well defined lesions in the right lobe of liver with central hyperintensity and hypointense rim (arrow). However, DWI showed restricted diffusion (B) in the periphery of the lesion with reduced ADC values (C) with central necrotic component which showed facilitated diffusion. The case was diagnosed as necrotic metastases. Final histopathology was hepatic metastasis. ADC: Apparent diffusion coefficient; DWI: Diffusion-weighted imaging.

was $0.96 \times 10^{-3} \text{ mm}^2/\text{s}$ ($P < 0.001$)^[30]. Ei Khouli *et al.*^[31] demonstrated a significant correlation between the expression of estrogen receptors and human epidermal growth factor receptor 2 and average ADC value of invasive ductal carcinoma of the breast. Recent studies have evaluated the utility of pre-therapy ADC values of breast cancer in the predicting tumor response to neo-adjuvant chemotherapy^[32]. Park *et al.*^[33] found that the pretherapy ADC values in responders was significantly lesser than that in non-responders and suggested a cutoff value of $1.17 \times 10^{-3} \text{ mm}^2/\text{s}$ (sensitivity of 94%, specificity of 71%). DWI with ADC quantification has been found to be more contributory in evaluating tumor response to neo-adjuvant chemotherapy than morphologic imaging parameters such as tumor volume and dynamic contrast-enhanced MRI parameters^[34,35].

Hepatic tumors

Recent advances in technology have enhanced the applications of DWI in liver imaging. Various studies have proven that images obtained using low-b-values (less than $100\text{--}150 \text{ s/mm}^2$) detect hepatic lesions better than are images obtained at a b value of 0. Parikh *et al.*^[36]

concluded that at a b value of 50 s/mm^2 , the sensitivity of DWI for detection of liver lesions was significantly higher than that of conventional T2-weighted imaging (87.7% vs 70.1% , respectively). DWI is also being evaluated as a technique, complementary to contrast imaging for lesion detection. While evaluating 50 hepatocellular carcinoma nodules, Nishie *et al.*^[37] showed that the use of superparamagnetic iron oxide-enhanced MRI combined with DWI gives a larger area under the ROC curve, than does the use of the former imaging technique alone (0.870 ± 0.04 vs 0.820 ± 0.05 , $P = 0.025$).

DWI contributes to lesion characterization when higher b values ($> 500 \text{ s/mm}^2$) and quantitative ADC assessment are used. Miller *et al.*^[38] reported that the mean ADC values for benign liver lesions was $2.5 \times 10^{-3} \text{ mm}^2/\text{s}$, whereas that of malignant lesions was $1.52 \times 10^{-3} \text{ mm}^2/\text{s}$. The ADC values however showed overlap between solid benign and malignant lesions, thus making a diagnosis based solely on DWI difficult (Figures 4 and 5). False-positive results may be obtained due to T2 shine-through effect or cellular benign lesions such as adenoma, focal nodular hyperplasia,

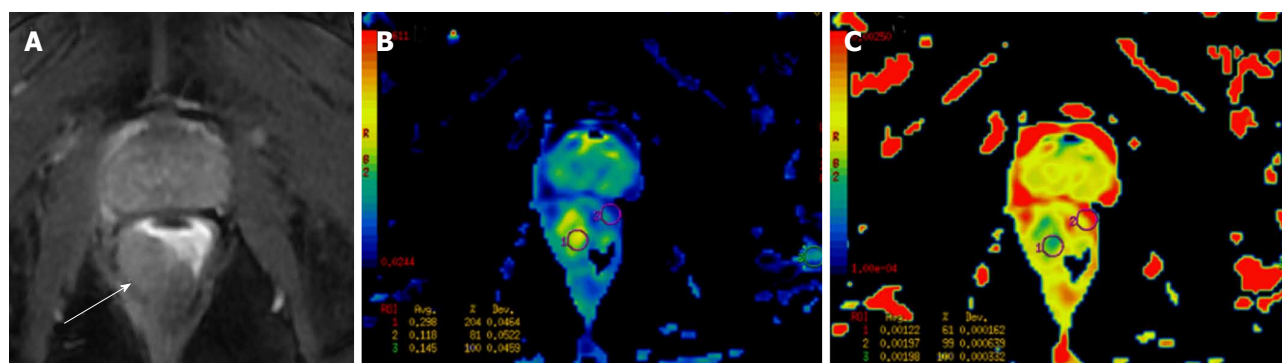


Figure 6 A 62-year-old male presented with bleeding per rectum. (A) Axial post contrast T1W fat suppressed image showed eccentric rectal wall thickening (arrow) which showed restricted diffusion (B) on diffusion weighted images (ROI 1) with reduced ADC values (C) as compared to the adjacent normal rectal wall (ROI 2). Histopathological evaluation revealed adenocarcinoma of rectum.

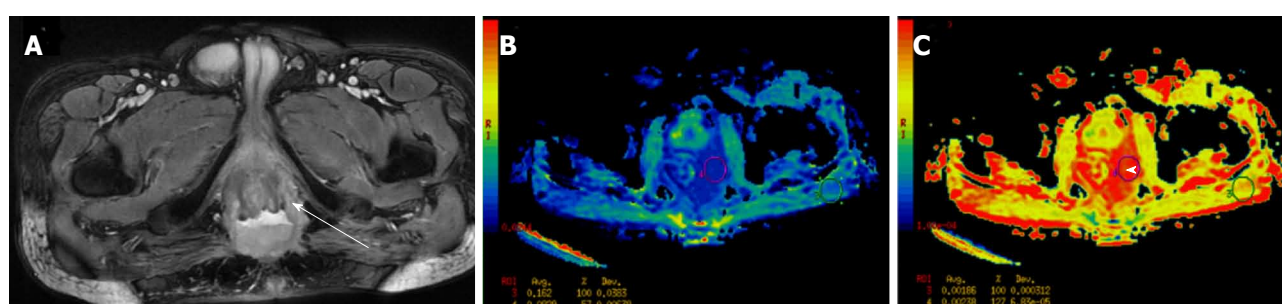


Figure 7 A 51-year-old male previously treated for rectal malignancy presented with suspected recurrence. A: Axial T2 W images showed irregular polypoidal mass lesions with necrosis within the perianal region. However, diffusion weighted images (exponential map image B and apparent diffusion map image C) showed facilitated diffusion (arrowhead, ROI 1) in both the solid polypoidal as well as the necrotic component favoring a benign etiology. A diagnosis of perianal abscess was made and patient underwent debridement which revealed ischioanal abscess.

or abscesses; whereas false-negative results may be obtained in necrotic or cystic tumors such as mucinous adenocarcinoma or well-differentiated hepatocellular adenocarcinoma^[39,40].

DWI has also proved to be useful in qualitatively and quantitatively assessing post-chemo-embolization/radio-embolization tumor response^[41,42]. Qualitative analysis is based on visually assessed changes in signal intensity in the form of increase in ADC signal in lesions that have shown response to treatment or new areas of abnormal signal intensity due to disease progression. Post-treatment DWI shows different signal intensity behaviors depending on the tissue component and the type of therapy used. After transarterial chemoembolization or radioembolization, the ADC values of a hepatocellular carcinoma may show a transient early decrease followed by increase. Transient decrease in ADC values may be due to cellular swelling, decreased extracellular space or decreased blood flow. This is followed by consistent increase, representing necrotic changes^[41,42].

Pancreatic tumors

A major diagnostic dilemma in pancreatic imaging is to differentiate mass forming pancreatitis from pancreatic tumor^[43,44]. Fattahi *et al.*^[45] evaluated application of DWI in differentiating mass forming focal pancreatitis from pancreatic tumor and found that pancreatic cancer

showed restricted diffusion with ADC values significantly lower than rest of pancreas ($1.46 \pm 0.18 \times 10^{-3} \text{ mm}^2/\text{s}$ vs $2.11 \pm 0.32 \times 10^{-3} \text{ mm}^2/\text{s}$, $P < 0.0001$). However, mass-forming FP showed no restriction of diffusion, without any significant difference between the ADC values of mass-forming focal pancreatitis and the remaining pancreas. Sandrasegaran *et al.*^[46] however found no significant difference between the signal intensity on DW images ($P = 0.82$, $P = 0.85$) or ADC values ($P = 0.51$, $P = 0.76$) between pancreatic cancer and chronic pancreatitis.

Gastrointestinal tumors

Ichikawa *et al.*^[47] concluded that DWI (at b value 1000 s/mm^2) showed 90.9% sensitivity and 100% specificity for depicting colorectal cancers. Studies have shown DWI to be useful not only in localizing, but also provide information that helps in staging and follow up after therapy of GI tumors (Figures 6 and 7). Extra-serosal spread can be seen on DWI as a hyperintense perirectal tumor extension through a thickened wall^[48,49]. Involvement of mesorectal fascia in patients with rectal cancer may also be seen as high-signal-intensity tumor extensions into the mesorectal margins. Desmoplastic changes have low signal intensity on both DWI and ADC maps. So, DWI may help distinguish between desmoplastic reaction and tumor extension^[50,51]. DWI is

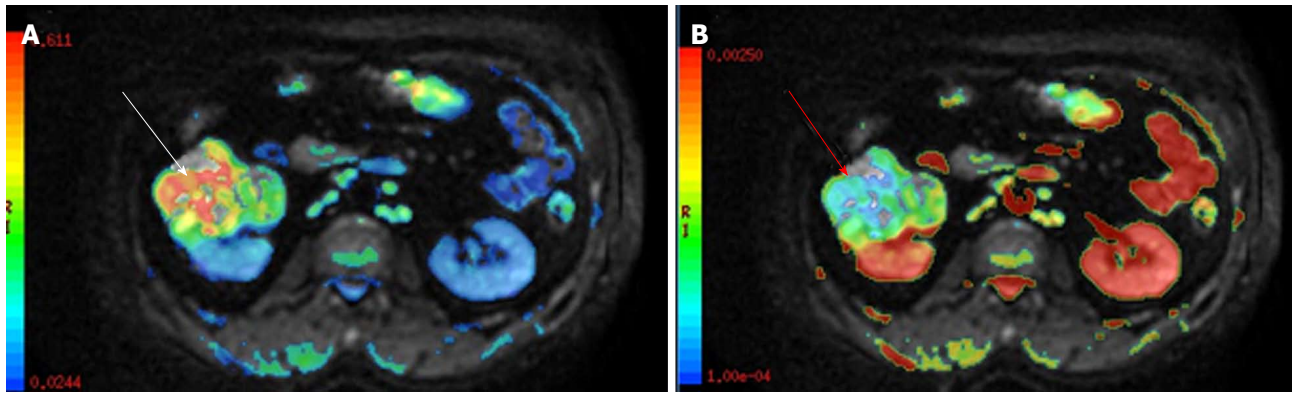


Figure 8 A 61-year-old male presented with hematuria and right sided flank pain. Superimposed DWI and T2 W images revealed a well-defined right renal mass which showed restricted diffusion (A-white arrow) with low ADC values (B-red arrow) suggestive of malignant mass. Post histopathological evaluation revealed renal cell carcinoma. ADC: Apparent diffusion coefficient; DWI: Diffusion-weighted imaging.

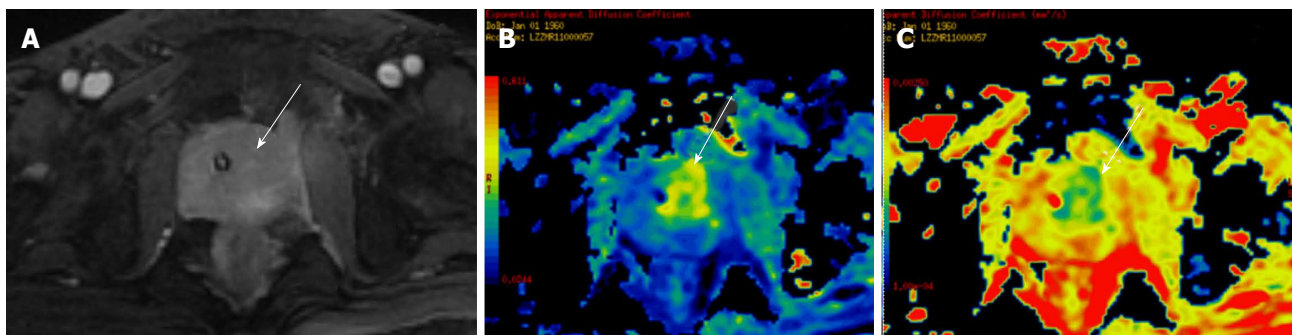


Figure 9 A 65-year-old male presented with symptoms of bladder outlet obstruction and raised serum PSA. DCE-MRI revealed a focal lesion in the central gland on the left side (white arrow in A), with restricted diffusion (white arrow in B) and low ADC values (white arrow in C) suggestive of malignancy. Biopsy revealed prostatic adenocarcinoma. ADC: Apparent diffusion coefficient; MRI: Magnetic resonance imaging.

also used in assessing patients undergoing rectal cancer treatment and to predict prognosis. DWI can also help distinguish between residual/recurrent cancer and post-RT changes, with low ADC values indicating recurrent disease while higher ADC values representing post-RT changes^[52,53]. Addition of DWI to conventional T2-weighted sequences has been found to significantly improve the diagnostic performance of MRI in the evaluation of ypCR and a high Δ ADC post-ADC pre ($> 0.3 \times 10^{-3} \text{ mm}^2/\text{s}$) is found to be predictor of ypCR (complete response)^[53].

Genito-urinary tumors

Renal tumors are commonly evaluated by morphological imaging techniques like CECT and CE-MRI. Detection of enhancing solid components in a renal lesion is highly indicative of a renal neoplasm. However, many renal neoplasms present as necrotic lesions, with few mimicking complex renal cysts. Differentiating these lesions on imaging has obvious therapeutic and prognostic implications. Solid renal tumors have lower ADCs values as compared to the necrotic or cystic tumor tissue, in which the ADCs are lower than those in benign cysts (Figure 8)^[54,55]. The recommendation is to perform DW-MRI with a maximum b value ranging from 800 to 1000 s/mm^2 at 3.0 T. Also, few studies have

reported different ADC values in tumors with differing compositions, thus possibly aiding in characterizing a renal lesion^[56]. Zhang *et al.*^[54] meta-analysis reported the differences in ADC values between benign renal lesions ($2.47 \pm 0.81 \times 10^{-3} \text{ mm}^2/\text{s}$) and malignant renal lesions ($1.81 \pm 0.41 \times 10^{-3} \text{ mm}^2/\text{s}$) with a P value < 0.001 . DWI is also studied in bladder malignancies, especially to evaluate the depth of invasion, deciding the T stage of bladder cancer which decides the management protocol^[57,58]. Management of urinary bladder cancer is primarily determined on distinguishing superficial tumors (stage T1 or lower) from invasive ones (stage T2 or higher). Takeuchi *et al.*^[58] found that the accuracy of determining the T stage diagnosis for T2-weighted images alone was 67%, for T2-weighted plus DW images was 88%, for T2-weighted plus contrast-enhanced images was 79%, and for all three image types together was 92%.

Prostate cancer

Conventional MR has been used in prostate cancer predominantly for staging (to assess Extracapsular spread and seminal vesicle involvement). However, DWI is now also used for assessing tumor location, size, and aggressiveness (Figure 9)^[59,60]. Also, the ADC values have been correlated with the Gleason's score and tumor

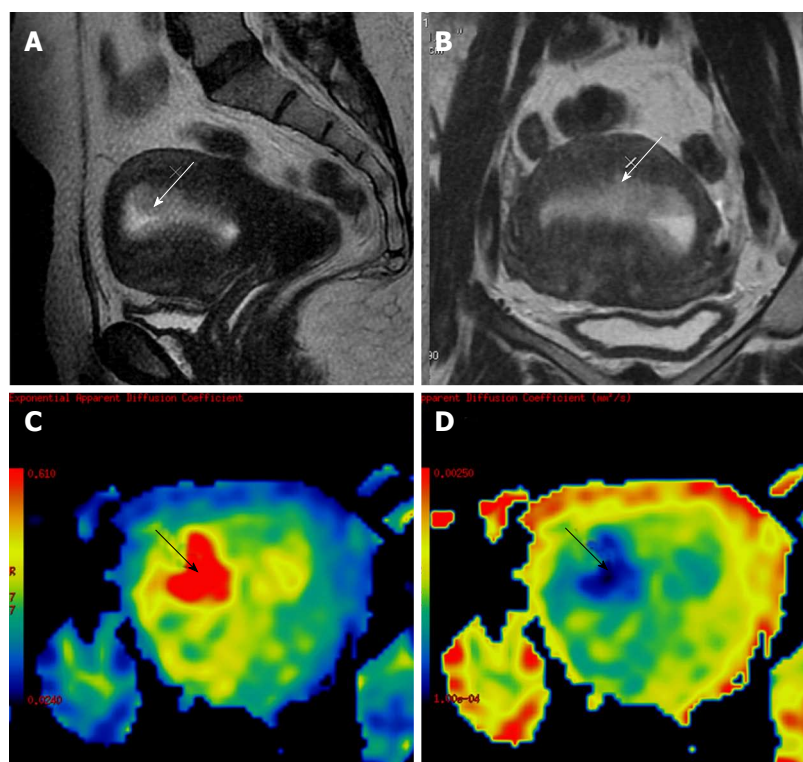


Figure 10 A 60-year-old female on tamoxifen, presented with post-menopausal bleeding. MRI revealed a heterogeneously hyperintense lesion in the endometrium (white arrow in A and B) which showed restricted diffusion (black arrow in C) with low ADC values (black arrow in D). Surgery was performed and histopathology showed tamoxifen induced hyperplasia harboring carcinoma of the endometrium. ADC: Apparent diffusion coefficient; MRI: Magnetic resonance imaging.

volume^[61]. There has been a significant overlap in the various groups due to which a consistent classification of the tumors according to the aggressiveness is not possible. Despite this, the ADC values do form a surrogate marker of the aggressiveness of the tumor and the total tumor volume^[62,63]. The lowest ADC value within tumor (ADC_{min}) is found to have an inverse correlation with the Gleason score and lower values are seen in tumors with Gleason score 3 + 4 than in the tumors with Gleason score 3 + 3 ($0.54 \pm 0.11 \times 10^{-3} \text{ mm}^2/\text{s}$ vs $0.64 \pm 0.12 \times 10^{-3} \text{ mm}^2/\text{s}$, $P < 0.05$)^[61].

Gynecological tumors

DWI has been evaluated extensively in characterization, management and follow-up female pelvic lesions. Tamai *et al.*^[64] found that uterine malignant lesions showed lower ADC values than normal myometrium or benign lesions like leiomyomas (Figure 10). Also, they demonstrated that higher grade tumors showed lower ADC values. DWI has also been fused with conventional T2 W images and used in endometrial cancers to assess the extent of myometrial invasion and thus decide stage of the lesion. Shen *et al.*^[65] found that DWI depicted multi-centricity and multi-focality in cases of uterine lesions. DWI has been applied to delineate cervical tumor especially in isointense tumors in young females, or early cervical cancer (Figure 11). A study by Naganawa *et al.*^[66] of 12 patients with cervical cancer demonstrated significantly lower mean ADC values in cervical cancer lesions ($1.09 \pm 0.20 \times 10^{-3} \text{ mm}^2/\text{s}$) than

in normal cervical tissue ($1.79 \pm 0.24 \times 10^{-3} \text{ mm}^2/\text{s}$) ($P < 0.0001$), findings that suggest the potential use of DW imaging as a tool to differentiate normal from cancerous cervical tissue. Liu *et al.*^[67] reported the ADC values of squamous carcinoma to be significantly lesser than those of adenocarcinoma ($P = 0.040$), and thus proposed the potential ability of DWI to indicate the histologic type of cervical cancer. They showed negative correlation between ADC values of cervical cancer and cellular density ($r = -0.711$, $P = 0.000$) and tumor grade ($r = -0.778$, $P = 0.000$). However, the results of studies that have used ADC values to distinguish tumor histology are mixed^[67].

Mahajan *et al.*^[68] found that in operated cervix cancer, the accuracy of diagnosing vaginal vault or local recurrent lesions was higher at combined multiparametric MRI and conventional MRI (100%) than at conventional MRI (70%) or multiparametric MRI (96.7%) alone. Restricted diffusion was seen in 23 of the 24 cases and all the benign cases showed facilitated diffusion. They found that the median ADC of recurrent carcinomas ($1.23 \pm 0.20 \times 10^{-3} \text{ mm}^2/\text{s}$) was significantly lower than benign vault tissue ($2.56 \pm 0.46 \times 10^{-3} \text{ mm}^2/\text{s}$) ($P < 0.001$)^[68]. Diffusion has also shown to aid in predicting prognosis, follow-up of these patients and detects metastatic disease with higher degree of accuracy^[69,70]. Wang *et al.*^[71] metaanalysis showed that DWI has prognostic implications and serves as a biological marker for survival in cervical cancer. Tumors with low ADC were associated with higher risks of tumor

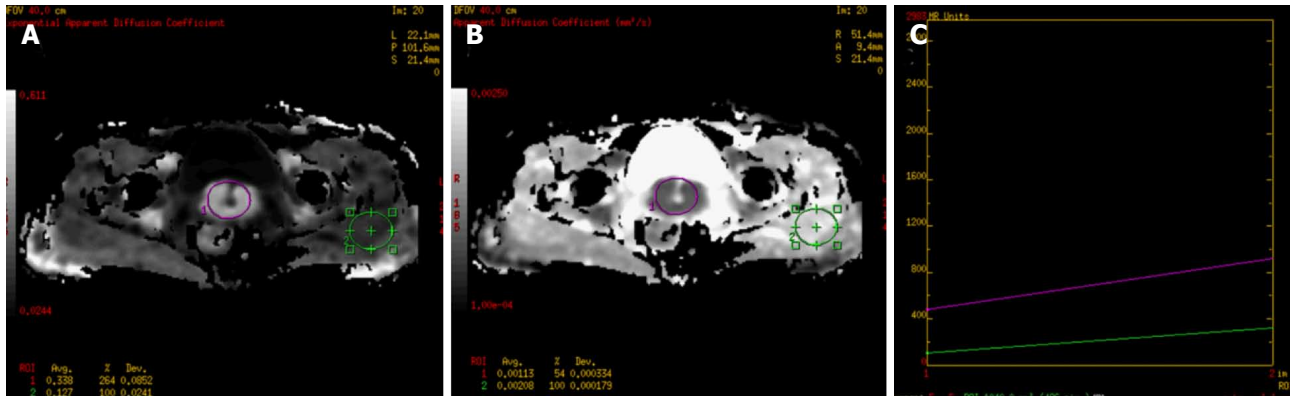


Figure 11 A 59-year-old female presented with post-menopausal bleeding. MRI revealed heterogeneously enhancing mass in the cervix which showed restricted diffusion (A-ROI 1) with low ADC (B-ROI-1) values and higher values on diffusion histogram maps (C) suggestive of malignancy. Biopsy revealed squamous cell carcinoma of the cervix. ADC: Apparent diffusion coefficient; MRI: Magnetic resonance imaging.

recurrence^[71].

DWI has been applied to evaluate ovarian lesions^[72,73]. Thomassin-Naggara *et al.*^[74] found that complex solid cystic ovarian lesions with solid components showing restricted diffusion turned out to be malignant. However, restricted diffusion is also seen in benign ovarian lesions like benign cystic teratoma, endometriomas, hemorrhagic ovarian cysts and ovarian cysts with high content of mucin^[75,76] (Figure 12). Peritoneal metastases can also be assessed with DWI, presence of which precludes surgery^[77]. The sensitivity and specificity of CT and conventional MRI decreases when a peritoneal deposit is smaller than 1 cm. DWI may depict small peritoneal deposits with high sensitivity because signal from the normal surrounding organs, ascites, and bowel is suppressed. A diffuse pattern of hyperintensity in the peritoneum may also be seen in patients with extensive peritoneal disease^[77,78]. Compared to surgical findings, DW-MRI has reported sensitivities of 71%-90% and specificities of 74%-96% for detecting peritoneal dissemination in gynecologic cancers^[77].

NODAL EVALUATION

Nodal evaluation is vital in the management of malignancies. Malignant infiltration of nodes leads to distorted nodal architecture, which may subsequently cause alterations in water diffusivity (Figure 2)^[79,80]. Thus, DWI has been largely evaluated in characterization of the nodes in oncology. Many studies have reported significant reduction in ADC values in metastatic nodes compared to benign lymph nodes^[80,81]. Vandecaveye *et al.*^[82] even found that DWI had a sensitivity of 76% and a specificity of 94% in the detection of subcentimetre sized (4-9 mm) nodes compared to the conventional MRI sequence, which had a sensitivity of 7% and a specificity of 99.5% for the same. In a study done by Sumi *et al.*^[83], however, they reported significantly higher ADC values in metastatic lymph nodes than in benign nodes, which may be due to inclusion of a large number of necrotic regions within the metastatic nodes in this study.

DWI can also contribute in evaluating enlarged

necrotic nodes; to differentiate between nodes associated with inflammation or neoplastic diseases^[84,85]. Koc *et al.*^[85] reported that abscesses and necrotic lymphadenitis appear hyperintense on DWI and exhibit lower ADC values compared to the necrotic nodal metastases that appear hypo-intense on DWI with higher ADC. A recent metaanalysis by Zhou *et al.*^[80] on role of DW-MRI in detecting nodal metastases reported a pooled sensitivity and specificity of 0.82 (95%CI: 0.76-0.87) and 0.92 (95%CI: 0.88-0.94), respectively.

Bone tumors

DWI has been applied in detection and characterization of bone and soft tissue tumors^[86,87]. Baur *et al.*^[88] first demonstrated in 1998 that DWI can help in differentiating osteoporotic and neoplastic vertebral fractures, with the neoplastic marrow showing restricted diffusion. Also, DWI has been applied to differentiate benign bone disease, bone tumors and tumor like bone lesions, for instance Ewing's sarcoma from osteomyelitis and for predicting length of tumor infiltrated marrow (Figure 13)^[89]. Moreover, measurement of ADC values can be used in the follow-up of tumors and their response to therapy^[89,90]. ADC values greater than $0.77 \times 10^{-3} \text{ mm}^2/\text{s}$ is suggestive of neoplastic marrow infiltration. This cut-off value is shown to have a sensitivity of 85% and specificity of 90% for predicting neoplastic marrow infiltration. For soft tissue tumors, a threshold ADC value of $1.34 \times 10^{-3} \text{ mm}^2/\text{s}$ is used in differentiating benign from malignant masses with an overall accuracy of 91%^[90]. DWI is also found to have a diagnostic value in evaluating patients with multiple myeloma. The reported mean ADCs for normal marrow, focal, and diffuse marrow involvement pattern is $0.360 \times 10^{-3} \text{ mm}^2/\text{s} \pm 0.110$, $1.046 \times 10^{-3} \text{ mm}^2/\text{s} \pm 0.232$, and $0.770 \times 10^{-3} \text{ mm}^2/\text{s} \pm 0.135$, respectively^[91].

RECENT ADVANCES

Whole body MR-DWI

WB-MR-DWI compliments PET imaging and has been found to contribute significantly in diagnosis, staging and

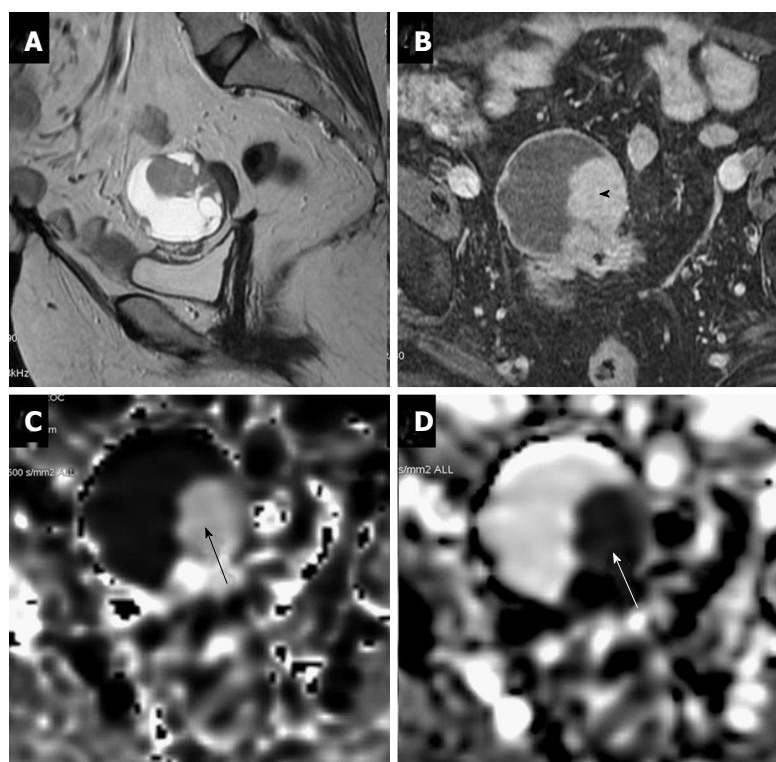


Figure 12 A 63-year-old female under evaluation for ovarian mass. (A) Sagittal T2W images showing a well-defined complex ovarian cyst showing hyperintense solid component which shows post contrast enhancement (black arrowhead-B) and restricted diffusion (black arrow-C) with low ADC values (white arrow-D). Restricted diffusion in the solid component was suggestive of this lesion to be a malignant ovarian mass. Final histopathology revealed mucinous cystadenocarcinoma..

follow-up imaging of many cancers^[92,93]. It is a fast and robust technique for tumor-detection (primary tumor, residual disease, recurrence, and metastases), tumor distribution/burden, characterization and treatment monitoring, which provides high tumor to background contrast^[94,95]. WB-DWI has been proven to be a “one stop shop” imaging tool metastatic workup both in pediatric as well as adult tumors and also in hematological malignancies such as lymphoma^[95,96]. One such technique which has been extensively developed and used in clinic is Diffusion-weighted whole-body imaging with background body signal suppression (DWIBS), which can be employed for whole body DWI in free breathing and provides high SNR. The most important clinical applications are: Relatively small primary and metastatic lesions can be accurately detected with this technique due to whole body coverage and high SNR. Other applications are similar to that of DWI like lymphoma diagnosis, staging, monitoring response to therapy and detection of tumor persistence or recurrence as opposed to post-therapeutic change^[97,98].

Intravoxel incoherent motion in diffusion-weighted MRI

When DWI is performed in well-perfused tissues at low b values (e.g., 0-100 s/mm²), both the water diffusion and microcirculation within the normal capillary network result in phase dispersion at DW-MRI and contribute to the measured signal attenuation. Le Bihan *et al.*^[99] called the behavior of protons that display signal attenuation at DW-MRI as showing

IVIM. In this IVIM model, two separate parameters have been proposed to reflect the tissue diffusivity and capillary perfusion, in the mathematical form of a bi-exponential decay function. Microcirculatory perfusion of blood within capillaries has no specific orientation and is hence termed as “pseudodiffusion”. It depends on the velocity of the flowing blood and the vascular architecture. The effect of pseudodiffusion on the signal attenuation is dependent on the b-value in each imaging voxel and the rate of signal attenuation that results from pseudodiffusion is typical for an order of magnitude greater than the tissue diffusion. This is due the larger distances of proton displacement that takes place during the application of the motion-probing gradients^[100,101]. Therefore, at higher b values in tissues that are normally perfused, pseudodiffusion contributes for a small proportion (if any) of the measured signal. At lower b values, this contribution to the DWI signal becomes more significant. The parameters derived from IVIM with biexponential analysis are: Diffusion coefficient (ADCslow), pseudo-diffusion coefficient (ADCfast) and perfusion fraction (f)^[1,102].

Stretched exponential DWI

Diffusion medium is postulated to be multi-compartmental. Bennett *et al.*^[103] introduced the stretched exponential DWI model to describe the heterogeneity of intravoxel diffusion rates and the distributed diffusion effect. Application of stretched exponential DWI model

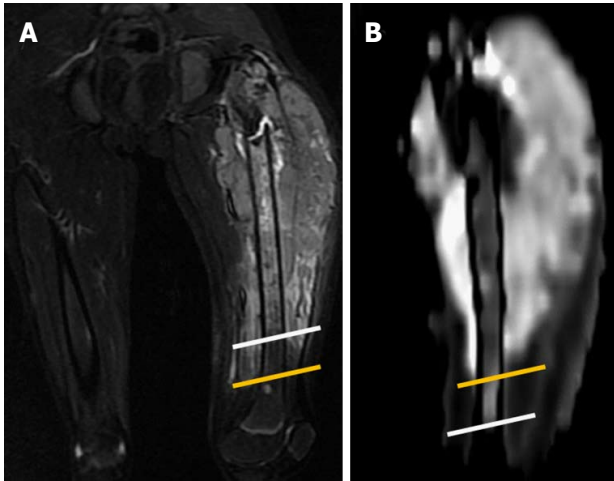


Figure 13 Case of Ewing's sarcoma in a 12-year-old boy. A: Coronal T2W-FS image showing altered marrow signal intensity in the femoral diaphysis (white line representing inferior extent) with associated soft tissue mass and surrounding edema (yellow line representing inferior extent); B: DWI shows restricted diffusion in the involved marrow which was significantly less (inferior extent represented by the white line) than that noted on the T2w Images thus differentiating the marrow edema from marrow infiltration and soft tissue edema from infiltration (yellow line representing inferior extent). The soft tissue mass shows restricted diffusion, suggestive of infiltrative tumor mass and not reactive inflammation. DWI: Diffusion-weighted imaging.

gives water molecular diffusion heterogeneity index (α) and the distributed diffusion coefficient (DDC) as follows^[103,104]: $S(b)/S(0) = \exp [-(b \cdot \text{DDC})^\alpha]$. Alpha (α) varies between 0 and 1 and is related to the intravoxel water molecular diffusion heterogeneity. A numerically high α value represents the low intravoxel diffusion heterogeneity. The DDC represents the mean intravoxel diffusion rate and represents the composite of individual ADCs, weighted by the volume fraction of water molecules in each part of the continuous distribution of ADCs. Kwee *et al.*^[105] demonstrated that the heterogeneity index of high-grade gliomas was significantly different from that of normal brain structures. Bai *et al.*^[104] demonstrated that α was significantly lower in high-grade gliomas than in low-grade gliomas, suggesting that high-grade gliomas exhibit more intravoxel diffusion heterogeneity than low-grade gliomas since they possess more histologic heterogeneity, such as heterogeneous cellularity and tortuous vascular hyperplasia. Also, Bedair *et al.*^[106] assessed early treatment response to neo-adjuvant chemotherapy in breast cancer using non-mono-exponential diffusion models. They concluded that baseline diffusion coefficients showed significant differences between complete pathological responders and non-responders, that increase in ADC and DDC at mid-treatment can discriminate responders and non-responders. And that the treatment effects can potentially be assessed by non-mono-exponential diffusion models^[106].

Diffusion kurtosis imaging

Diffusion kurtosis imaging (DKI) attempts to account for the alteration of the normative pattern of distribution

and provide more accurate model of diffusion, capturing the non-Gaussian diffusion behavior as a marker for tissue heterogeneity. Most commonly used DKI parameters are mean kurtosis (MK), the average of diffusion kurtosis along all directions; radial kurtosis (RK), the kurtosis along the radial direction of the diffusion ellipsoid and axial kurtosis (AK), the kurtosis along axial direction of diffusion ellipsoid^[107]. Studies have shown that evaluation of variant distribution pattern can provide important microstructural information about brain, especially while imaging ischemic tissue, traumatic brain injury, neoplasms, neurodegenerative and demyelinating diseases^[108-112].

To conclude, DWI is a functional imaging technique with diverse applications in "personalized oncology" and hence radiologists should now be well acquainted with the technique and various applications of DWI in Oncology. It not only improves the sensitivity and specificity of conventional MRI but provides information in regard to the tumor microenvironment that is not available from the conventional MR sequences. As a Radiomic/Radiogenomic marker it has the potential to be an imaging biomarker for "personalized oncology" and help in individualized patient management.

SUMMARY OF DIFFUSION WEIGHTED MRI IN PERSONALIZED ONCOLOGY

DWI requires no contrast and thus is useful in patients with severe renal dysfunction. DWI is an echo planar sequence, which requires less time, and hence finds its applications in diverse scan protocols. It can be acquired in the same plane as conventional MR sequences and hence provide good correlation between morphological and functional imaging.

Acquisition

The b value (s/mm^2) is an indicator of the diffusion weighting of the images. Low-b-value (e.g., $< 100\text{-}150 \text{ s/mm}^2$) provides images that are more sensitive to tissue perfusion and are recommended for IVIM imaging, whereas high b value (e.g., $> 500 \text{ s/mm}^2$) images are more specific for impaired Brownian motion that are indicative of true restricted diffusion and are recommended for DWI imaging. Typical b values used in routine oncological imaging range from 50 to 1000 s/mm^2 however from the literature review we recommend diffusion-weighted images to be obtained with b values of 0, 500 and 1000 s/mm^2 . Additional higher-b-value images (1500 s/mm^2) are suggested for MRI of the prostate and values of $700\text{-}800 \text{ s/mm}^2$ are recommended for breast and cervix imaging.

Detection of lesion

DWI offers various advantages, which justify it to be an integral part of oncological imaging; one of them being its very high sensitivity. Since, DWI reflects changes at the cellular level; it shows positive changes earlier than

the morphological imaging techniques. So, this is very sensitive technique for early lesion detection. Neoplasms are known to be more cellular than the organ of origin and hence show restricted diffusion with reduced ADC values. Not only the primary, but the nodal and distant metastases show restricted diffusion, and hence can be accurately characterized on DWI. ADC histogram mapping or the ADC slope analysis gives a qualitative as well quantitative impression of the ADC in the suspicious area and comparative assessment between normal and suspicious area respectively. Colored ADC maps are superior to the grey scale maps; especially in sub-centimeter sized lesions, and follow-up imaging.

Characterization of lesions

Differentiation of benign and malignant lesion forms the initial portal of patient management in oncology. DWI being a functional imaging modality depicts the tissue milieu at the cellular level. Malignant neoplasms are more cellular than a benign lesion, and hence show reduced ADC as compared to a benign process. The use of ADC cut off value (b value of 500 s/mm²) of 1.5×10^{-3} mm²/s and ADC cut off value (b value of 1000 s/mm²) of 1.0×10^{-3} mm²/s gives a good specificity and is recommended for differentiating malignant from benign. Also, DWI may predict the aggressiveness and grade of the tumor.

Post therapy evaluation

Oncological treatments result in tumor lysis, loss of cell membrane integrity, increased extracellular space and therefore, an increase in water diffusion. Hence, the effectiveness of the treatment can be monitored by DWI. Anti-cancer treatment like radiotherapy leads to considerable alteration in the local anatomy and hence, precludes the evaluation of the diseased area with morphological imaging. Also, it is imperative to detect residual/recurrent disease in this area, due to obvious therapeutic and prognostic implications. Morphological imaging techniques have their limitations due to altered milieu. DWI comes to the rescue in evaluation of post RT surveillance. DWI, being a functional imaging technique, detects residual/recurrent disease with high sensitivity and specificity. Also, unlike PET imaging, it is not confounded by the local inflammatory changes.

Predicting response

Research has found that tumors with low baseline pretreatment ADC values show better response to chemotherapy or radiation treatment. It is postulated that tumors with high ADC values more likely to be necrotic. Since, necrotic tumors are frequently hypoxic, acidotic, and poorly perfused, it leads to decreased sensitivity of the tumor to chemotherapy and radiation therapy.

Limitations and challenges

One of the major limitations of DWI is no standardized acquisition protocol, which precludes its successful use as a research tool. It is also very sensitive to artifacts.

The current available post-processing software tools are mostly for commercial use and do not allow complex post-processing. Lastly radiogenomics comparisons are essential in giving robust validation for its application as an imaging biomarker in personalized oncology.

REFERENCES

- 1 **Mahajan A**, Goh V, Basu S, Vaish R, Weeks AJ, Thakur MH, Cook GJ. Bench to bedside molecular functional imaging in translational cancer medicine: to image or to imagine? *Clin Radiol* 2015; **70**: 1060-1082 [PMID: 26187890 DOI: 10.1016/j.crad.2015.06.082]
- 2 **O'Connor JP**, Aboagye EO, Adams JE, Aerts HJ, Barrington SF, Beer AJ, Boellaard R, Bohndiek SE, Brady M, Brown G, Buckley DL, Chenevert TL, Clarke LP, Collette S, Cook GJ, deSouza NM, Dickson JC, Dive C, Evelhoch JL, Faivre-Finn C, Gallagher FA, Gilbert FJ, Gillies RJ, Goh V, Griffiths JR, Groves AM, Halligan S, Harris AL, Hawkes DJ, Hoekstra OS, Huang EP, Hutton BF, Jackson EF, Jayson GC, Jones A, Koh DM, Lacombe D, Lambin P, Lassau N, Leach MO, Lee TY, Leen EL, Lewis JS, Liu Y, Lythgoe MF, Manoharan P, Maxwell RJ, Miles KA, Morgan B, Morris S, Ng T, Padhani AR, Parker GJ, Partridge M, Pathak AP, Peet AC, Punwani S, Reynolds AR, Robinson SP, Shankar LK, Sharma RA, Soloviev D, Stroobants S, Sullivan DC, Taylor SA, Tofts PS, Tozer GM, van Herk M, Walker-Samuel S, Wason J, Williams KJ, Workman P, Yankeelov TE, Brindle KM, McShane LM, Jackson A, Waterton JC. Imaging biomarker roadmap for cancer studies. *Nat Rev Clin Oncol* 2017; **14**: 169-186 [PMID: 27725679 DOI: 10.1038/nrclinonc.2016.162]
- 3 **Dhingra VK**, Mahajan A, Basu S. Emerging clinical applications of PET based molecular imaging in oncology: the promising future potential for evolving personalized cancer care. *Indian J Radiol Imaging* 2015; **25**: 332-341 [PMID: 26752813 DOI: 10.4103/0971-3026.169467]
- 4 **Padhani AR**, Liu G, Koh DM, Chenevert TL, Thoeny HC, Takahara T, Dzik-Jurasz A, Ross BD, Van Cauteren M, Collins D, Hammoud DA, Rustin GJ, Taouli B, Choyke PL. Diffusion-weighted magnetic resonance imaging as a cancer biomarker: consensus and recommendations. *Neoplasia* 2009; **11**: 102-125 [PMID: 19186405]
- 5 **Galbán CJ**, Hoff BA, Chenevert TL, Ross BD. Diffusion MRI in early cancer therapeutic response assessment. *NMR Biomed* 2017; **30**: Epub 2016 Jan 15 [PMID: 26773848 DOI: 10.1002/nbm.3458]
- 6 **Stejskal EO**, Tanner JE. Spin diffusion measurements: spin-echo in the presence of a time dependent field gradient. *J ChemPhys* 1965; **42**: 288-292
- 7 **Malayeri AA**, El Khouli RH, Zaheer A, Jacobs MA, Corona-Villalobos CP, Kamel IR, Macura KJ. Principles and applications of diffusion-weighted imaging in cancer detection, staging, and treatment follow-up. *Radiographics* 2011; **31**: 1773-1791 [PMID: 21997994 DOI: 10.1148/rg.316115515]
- 8 **Hamstra DA**, Rehemtulla A, Ross BD. Diffusion magnetic resonance imaging: a biomarker for treatment response in oncology. *J Clin Oncol* 2007; **25**: 4104-4109 [PMID: 17827460]
- 9 **Ferlay J**, Soerjomataram I, Dikshit R, Eser S, Mathers C, Rebelo M, Parkin DM, Forman D, Bray F. Cancer incidence and mortality worldwide: sources, methods and major patterns in GLOBOCAN 2012. *Int J Cancer* 2015; **136**: E359-E386 [PMID: 25220842 DOI: 10.1002/ijc.29210]
- 10 **Chawla S**, Kim S, Wang S, Poptani H. Diffusion-weighted imaging in head and neck cancers. *Future Oncol* 2009; **5**: 959-975 [PMID: 19792966 DOI: 10.2217/fon.09.77]
- 11 **Srinivasan A**, Dvorak R, Perni K, Rohrer S, Mukherji SK. Differentiation of benign and malignant pathology in the head and neck using 3T apparent diffusion coefficient values: early experience. *AJNR Am J Neuroradiol* 2008; **29**: 40-44 [PMID: 17921228]
- 12 **Thoeny HC**, De Keyser F, King AD. Diffusion-weighted MR imaging in the head and neck. *Radiology* 2012; **263**: 19-32 [PMID: 22111111]

- 22438440 DOI: 10.1148/radiol.11101821]
- 13 **Hoang JK**, Choudhury KR, Chang J, Craciunescu OI, Yoo DS, Brizel DM. Diffusion-weighted imaging for head and neck squamous cell carcinoma: quantifying repeatability to understand early treatment-induced change. *AJR Am J Roentgenol* 2014; **203**: 1104-1108 [PMID: 25341151 DOI: 10.2214/AJR.14.12838]
- 14 **Varoquaux A**, Rager O, Lovblad KO, Masterson K, Dulguerov P, Ratib O, Becker CD, Becker M. Functional imaging of head and neck squamous cell carcinoma with diffusion-weighted MRI and FDG PET/CT: quantitative analysis of ADC and SUV. *Eur J Nucl Med Mol Imaging* 2013; **40**: 842-852 [PMID: 23436068 DOI: 10.1007/s00259-013-2351-9.PubMed]
- 15 **Vandecaveye V**, De Keyser F, Nuyts S, Deraedt K, Dirix P, Hamaekers P, Vander Poorten V, Delaere P, Hermans R. Detection of head and neck squamous cell carcinoma with diffusion weighted MRI after (chemo)radiotherapy: correlation between radiologic and histopathologic findings. *Int J Radiat Oncol Biol Phys* 2007; **67**: 960-971 [PMID: 17141979]
- 16 **Abdel Razek AA**, Kandeel AY, Soliman N, El-shenshawy HM, Kamel Y, Nada N, Denewar A. Role of diffusion-weighted echoplanar MR imaging in differentiation of residual or recurrent head and neck tumors and posttreatment changes. *AJNR Am J Neuroradiol* 2007; **28**: 1146-1152 [PMID: 17569975]
- 17 **Baur A**, Huber A, Arbogast S, Dürr HR, Zysk S, Wendtner C, Deimling M, Reiser M. Diffusion-weighted imaging of tumor recurrences and posttherapeutic soft-tissue changes in humans. *Eur Radiol* 2001; **11**: 828-833 [PMID: 11372617]
- 18 **Fischbein NJ**, AAssar OS, Caputo GR, Kaplan MJ, Singer MI, Price DC, Dillon WP, Hawkins RA. Clinical utility of positron emission tomography with 18F-fluorodeoxyglucose in detecting residual/recurrent squamous cell carcinoma of the head and neck. *AJNR Am J Neuroradiol* 1998; **19**: 1189-1196 [PMID: 9726451]
- 19 **Kao CH**, ChangLai SP, Chieng PU, Yen RF, Yen TC. Detection of recurrent or persistent nasopharyngeal carcinomas after radiotherapy with 18-fluoro-2-deoxyglucose positron emission tomography and comparison with computed tomography. *J Clin Oncol* 1998; **16**: 3550-3555 [PMID: 9817274]
- 20 **Law BK**, King AD, Bhatia KS, Ahuja AT, Kam MK, Ma BB, Ai QY, Mo FK, Yuan J, Yeung DK. Diffusion-Weighted Imaging of Nasopharyngeal Carcinoma: Can Pretreatment DWI Predict Local Failure Based on Long-Term Outcome? *AJNR Am J Neuroradiol* 2016; **37**: 1706-1712 [PMID: 27151750 DOI: 10.3174/ajnr.A4792]
- 21 **Zhang Y**, Liu X, Zhang Y, Li WF, Chen L, Mao YP, Shen JX, Zhang F, Peng H, Liu Q, Sun Y, Ma J. Prognostic value of the primary lesion apparent diffusion coefficient (ADC) in nasopharyngeal carcinoma: a retrospective study of 541 cases. *Sci Rep* 2015; **5**: 12242 [PMID: 26184509 DOI: 10.1038/srep12242]
- 22 **Min M**, Lee MT, Lin P, Holloway L, Wijesekera Dj, Gooneratne D, Rai R, Xuan W, Fowler A, Forstner D, Liney G. Assessment of serial multi-parametric functional MRI (diffusion-weighted imaging and R2*) with (18)F-FDG-PET in patients with head and neck cancer treated with radiation therapy. *Br J Radiol* 2016; **89**: 20150530 [PMID: 26648404 DOI: 10.1259/bjr.20150530]
- 23 **King AD**, Thoeny HC. Functional MRI for the prediction of treatment response in head and neck squamous cell carcinoma: potential and limitations. *Cancer Imaging* 2016; **16**: 23 [PMID: 27542718 DOI: 10.1186/s40644-016-0080-6]
- 24 **Chen L**, Xu J, Bao J, Huang X, Hu X, Xia Y, Wang J. Diffusion-weighted MRI in differentiating malignant from benign thyroid nodules: a meta-analysis. *BMJ Open* 2016; **6**: e008413 [PMID: 26733564 DOI: 10.1136/bmjopen-2015-008413]
- 25 **Hao Y**, Pan C, Chen W, Li T, Zhu W, Qi J. Differentiation between malignant and benign thyroid nodules and stratification of papillary thyroid cancer with aggressive histological features: Whole-lesion diffusion-weighted imaging histogram analysis. *J Magn Reson Imaging* 2016; **44**: 1546-1555 [PMID: 27093648 DOI: 10.1002/jmri.25290]
- 26 **Basu S**, Mahajan A, Arya S. Multimodality Molecular Imaging (FDG-PET/CT, US Elastography, and DWI-MRI) as Complimentary Adjunct for Enhancing Diagnostic Confidence in Reported Intermediate Risk Category Thyroid Nodules on Bethesda Thyroid Cytopathology Reporting System. *World J Nucl Med* 2016; **15**: 130-133 [PMID: 27134564 DOI: 10.4103/1450-1147.176883]
- 27 **Sinha S**, Lucas-Quesada FA, Sinha U, DeBruhl N, Bassett LW. In vivo diffusion-weighted MRI of the breast: potential for lesion characterization. *J Magn Reson Imaging* 2002; **15**: 693-704 [PMID: 12112520]
- 28 **Aribal E**, Asadov R, Ramazan A, Ugurlu MÜ, Kaya H. Multi-parametric breast MRI with 3T: Effectivity of combination of contrast enhanced MRI, DWI and 1H single voxel spectroscopy in differentiation of Breast tumors. *Eur J Radiol* 2016; **85**: 979-986 [PMID: 27130059 DOI: 10.1016/j.ejrad.2016.02.022]
- 29 **Sharma U**, Sah RG, Agarwal K, Parshad R, Seenu V, Mathur SR, Hari S, Jagannathan NR. Potential of Diffusion-Weighted Imaging in the Characterization of Malignant, Benign, and Healthy Breast Tissues and Molecular Subtypes of Breast Cancer. *Front Oncol* 2016; **6**: 126 [PMID: 27242965 DOI: 10.3389/fonc.2016.00126]
- 30 **Costantini M**, Belli P, Rinaldi P, Bufi E, Giardina G, Franceschini G, Petrone G, Bonomo L. Diffusion-weighted imaging in breast cancer: relationship between apparent diffusion coefficient and tumour aggressiveness. *Clin Radiol* 2010; **65**: 1005-1012 [PMID: 21070905 DOI: 10.1016/j.crad.2010.07.008]
- 31 **Ei Khouli RH**, Jacobs MA, Mezban SD, Huang P, Kamel IR, Macura KJ, Bluemke DA. Diffusion-weighted imaging improves the diagnostic accuracy of conventional 3.0-T breast MR imaging. *Radiology* 2010; **256**: 64-73 [PMID: 20574085 DOI: 10.1148/radiol.10091367]
- 32 **Nilsen L**, Fangberget A, Geier O, Olsen DR, Seierstad T. Diffusion-weighted magnetic resonance imaging for pretreatment prediction and monitoring of treatment response of patients with locally advanced breast cancer undergoing neoadjuvant chemotherapy. *Acta Oncol* 2010; **49**: 354-360 [PMID: 20397769 DOI: 10.3109/02841861003610184]
- 33 **Park SH**, Moon WK, Cho N, Song IC, Chang JM, Park IA, Han W, Noh DY. Diffusion-weighted MR imaging: pretreatment prediction of response to neoadjuvant chemotherapy in patients with breast cancer. *Radiology* 2010; **257**: 56-63 [PMID: 20851939 DOI: 10.1148/radiol.10092021]
- 34 **Richard R**, Thomassin I, Chapellier M, Scemama A, de Cremoux P, Varna M, Giacchetti S, Espié M, de Kerviler E, de Bazelaire C. Diffusion-weighted MRI in pretreatment prediction of response to neoadjuvant chemotherapy in patients with breast cancer. *Eur Radiol* 2013; **23**: 2420-2431 [PMID: 23652844 DOI: 10.1007/s00330-013-2850-x]
- 35 **Minarikova L**, Bogner W, Pinker K, Valković L, Zaric O, Bago-Horvath Z, Bartsch R, Helbich TH, Trattnig S, Gruber S. Investigating the prediction value of multiparametric magnetic resonance imaging at 3 T in response to neoadjuvant chemotherapy in breast cancer. *Eur Radiol* 2017; **27**: 1901-1911 [PMID: 27651141]
- 36 **Parikh T**, Drew SJ, Lee VS, Wong S, Hecht EM, Babb JS, Taouli B. Focal liver lesion detection and characterization with diffusion-weighted MR imaging: comparison with standard breath-hold T2-weighted imaging. *Radiology* 2008; **246**: 812-822 [PMID: 18223123 DOI: 10.1148/radiol.2463070432]
- 37 **Nishie A**, Tajima T, Ishigami K, Ushijima Y, Okamoto D, Hirakawa M, Nishihara Y, Taketomi A, Hatakenaka M, Irie H, Yoshimitsu K, Honda H. Detection of hepatocellular carcinoma (HCC) using super paramagnetic iron oxide (SPIO)-enhanced MRI: Added value of diffusion-weighted imaging (DWI). *J Magn Reson Imaging* 2010; **31**: 373-382 [PMID: 20099351 DOI: 10.1002/jmri.22059]
- 38 **Miller FH**, Hammond N, Siddiqi AJ, Shroff S, Khatri G, Wang Y, Merrick LB, Nikolaidis P. Utility of diffusion-weighted MRI in distinguishing benign and malignant hepatic lesions. *J Magn Reson Imaging* 2010; **32**: 138-147 [PMID: 20578020 DOI: 10.1002/jmri.22235]
- 39 **Shankar S**, Kalra N, Bhatia A, Srinivasan R, Singh P, Dhiman RK, Khandelwal N, Chawla Y. Role of Diffusion Weighted Imaging (DWI) for Hepatocellular Carcinoma (HCC) Detection and its Grading on 3T MRI: A Prospective Study. *J Clin Exp Hepatol* 2016; **6**: 303-310 [PMID: 28003720 DOI: 10.1016/j.jceh.2016.08.012]

- 40 **Yuan Z**, Zhang J, Yang H, Ye XD, Xu LC, Li WT. Diffusion-Weighted MR Imaging of Hepatocellular Carcinoma: Current Value in Clinical Evaluation of Tumor Response to Locoregional Treatment. *J Vasc Interv Radiol* 2016; **27**: 20-30; quiz 31 [PMID: 26621785 DOI: 10.1016/j.jvir.2015.10.003]
- 41 **Schelhorn J**, Best J, Reinboldt MP, Dechêne A, Gerken G, Ruhlmann M, Lauenstein TC, Antoch G, Kinner S. Does diffusion-weighted imaging improve therapy response evaluation in patients with hepatocellular carcinoma after radioembolization? comparison of MRI using Gd-EOB-DTPA with and without DWI. *J Magn Reson Imaging* 2015; **42**: 818-827 [PMID: 25515676 DOI: 10.1002/jmri.24827]
- 42 **Kokabi N**, Ludwig JM, Camacho JC, Xing M, Mittal PK, Kim HS. Baseline and Early MR Apparent Diffusion Coefficient Quantification as a Predictor of Response of Unresectable Hepatocellular Carcinoma to Doxorubicin Drug-Eluting Bead Chemoembolization. *J Vasc Interv Radiol* 2015; **26**: 1777-1786 [PMID: 26603497 DOI: 10.1016/j.jvir.2015.08.023]
- 43 **De Robertis R**, Tinazzi Martini P, Demozzi E, Dal Corso F, Bassi C, Pederzoli P, D'Onofrio M. Diffusion-weighted imaging of pancreatic cancer. *World J Radiol* 2015; **7**: 319-328 [PMID: 26516428 DOI: 10.4329/wjr.v7.i10.319]
- 44 **Negri F**, Bono NE, Barbalace S, Trunfio V, Lana S, Ganazzoli C, Marcantoni EA, Totaro M, Vallara M, Parziale R, Borgia D. Use of DWI in identification of small solid pancreatic focalities (≤ 2 cm). *Acta Biomed* 2016; **87** Suppl 3: 20-27 [PMID: 27467863]
- 45 **Fattahi R**, Balci NC, Perman WH, Hsueh EC, Alkaade S, Havlioglu N, Burton FR. Pancreatic diffusion-weighted imaging (DWI): comparison between mass-forming focal pancreatitis (FP), pancreatic cancer (PC), and normal pancreas. *J Magn Reson Imaging* 2009; **29**: 350-356 [PMID: 19161187 DOI: 10.1002/jmri.21651]
- 46 **Sandrasegaran K**, Nutakki K, Tahir B, Dhanabal A, Tann M, Cote GA. Use of diffusion-weighted MRI to differentiate chronic pancreatitis from pancreatic cancer. *AJR Am J Roentgenol* 2013; **201**: 1002-1008 [PMID: 24147470 DOI: 10.2214/AJR.12.10170]
- 47 **Ichikawa T**, Erturk SM, Motosugi U, Sou H, Iino H, Araki T, Fujii H. High-B-value diffusion-weighted MRI in colorectal cancer. *AJR Am J Roentgenol* 2006; **187**: 181-184 [PMID: 16794174]
- 48 **Nguyen TL**, Soyer P, Fornès P, Rousset P, Kianmanesh R, Hoeffel C. Diffusion-weighted MR imaging of the rectum: clinical applications. *Crit Rev Oncol Hematol* 2014; **92**: 279-295 [PMID: 25132166 DOI: 10.1016/j.critrevonc.2014.07.002.Review]
- 49 **Sinha R**, Rajiah P, Ramachandran I, Sanders S, Murphy PD. Diffusion-weighted MR imaging of the gastrointestinal tract: technique, indications, and imaging findings. *Radiographics* 2013; **33**: 655-676; discussion 676-680 [PMID: 23674768 DOI: 10.1148/r.333125042]
- 50 **Moreno CC**, Sullivan PS, Kalb BT, Tipton RG, Hanley KZ, Kitajima HD, Dixon WT, Votaw JR, Oshinski JN, Mittal PK. Magnetic resonance imaging of rectal cancer: staging and restaging evaluation. *Abdom Imaging* 2015; **40**: 2613-2629 [PMID: 25759246 DOI: 10.1007/s00261-015-0394-z]
- 51 **Moon SJ**, Cho SH, Kim GC, Kim WH, Kim HJ, Shin KM, Lee SM, Park JS, Choi GS, Kim SH. Complementary value of pre-treatment apparent diffusion coefficient in rectal cancer for predicting tumor recurrence. *Abdom Radiol (NY)* 2016; **41**: 1237-1244 [PMID: 26830420 DOI: 10.1007/s00261-016-0648-4]
- 52 **Quaia E**, Gennari AG, Ricciardi MC, Ulcigrai V, Angileri R, Cova MA. Value of percent change in tumoral volume measured at T2-weighted and diffusion-weighted MRI to identify responders after neoadjuvant chemoradiation therapy in patients with locally advanced rectal carcinoma. *J Magn Reson Imaging* 2016; **44**: 1415-1424 [PMID: 27219471 DOI: 10.1002/jmri.25310]
- 53 **Foti PV**, Privitera G, Piana S, Palmucci S, Spatola C, Bevilacqua R, Raffaele L, Salamone V, Caltabiano R, Magro G, Li Destri G, Milone P, Ettore GC. Locally advanced rectal cancer: Qualitative and quantitative evaluation of diffusion-weighted MR imaging in the response assessment after neoadjuvant chemo-radiotherapy. *Eur J Radiol Open* 2016; **3**: 145-152 [PMID: 27489868 DOI: 10.1016/j.ejro.2016.06.003]
- 54 **Zhang H**, Gan Q, Wu Y, Liu R, Liu X, Huang Z, Yuan F, Kuang M, Song B. Diagnostic performance of diffusion-weighted magnetic resonance imaging in differentiating human renal lesions (benignity or malignancy): a meta-analysis. *Abdom Radiol (NY)* 2016; **41**: 1997-2010 [PMID: 27271218 DOI: 10.1007/s00261-016-0790-z. PubMed]
- 55 **Hötter AM**, Mazaheri Y, Wibmer A, Zheng J, Moskowitz CS, Tickoo SK, Russo P, Hricak H, Akin O. Use of DWI in the Differentiation of Renal Cortical Tumors. *AJR Am J Roentgenol* 2016; **206**: 100-105 [PMID: 26700340 DOI: 10.2214/AJR.14.13923]
- 56 **Roy C**, Labani A, Alemann G, Bierry G, Lang H, Ohana M. DWI in the Etiologic Diagnosis of Excretory Upper Urinary Tract Lesions: Can It Help in Differentiating Benign From Malignant Tumors? A Retrospective Study of 98 Patients. *AJR Am J Roentgenol* 2016; **207**: 106-113 [PMID: 27064313 DOI: 10.2214/AJR.15.15652]
- 57 **Zhai N**, Wang YH, Zhu LM, Wang JH, Sun XH, Hu XB, Li X, Yu T, Wang XL, Meng N, Yan QC, Li XJ, Luo YH. Sensitivity and Specificity of Diffusion-Weighted Magnetic Resonance Imaging in Diagnosis of Bladder Cancers. *Clin Invest Med* 2015; **38**: E173-E184 [PMID: 26278427]
- 58 **Takeuchi M**, Sasaki S, Ito M, Okada S, Takahashi S, Kawai T, Suzuki K, Oshima H, Hara M, Shibamoto Y. Urinary bladder cancer: diffusion-weighted MR imaging-accuracy for diagnosing T stage and estimating histologic grade. *Radiology* 2009; **251**: 112-121 [PMID: 19332849 DOI: 10.1148/radiol.2511080873]
- 59 **Pasoglou V**, Larbi A, Collette L, Annet L, Jamar F, Machiels JP, Michoux N, Vande Berg BC, Tombal B, Lecouvet FE. One-step TNM staging of high-risk prostate cancer using magnetic resonance imaging (MRI): toward an upfront simplified "all-in-one" imaging approach? *Prostate* 2014; **74**: 469-477 [PMID: 24375774 DOI: 10.1002/pros.22764]
- 60 **Yoo S**, Kim JK, Jeong IG. Multiparametric magnetic resonance imaging for prostate cancer: A review and update for urologists. *Korean J Urol* 2015; **56**: 487-497 [PMID: 26175867 DOI: 10.4111/kju.2015.56.7.487]
- 61 **Wu X**, Reinikainen P, Vanhanen A, Kapanen M, Vierikko T, Ryymin P, Hyödynmaa S, Kellokumpu-Lehtinen PL. Correlation between apparent diffusion coefficient value on diffusion-weighted MR imaging and Gleason score in prostate cancer. *Diagn Interv Imaging* 2017; **98**: 63-71 [PMID: 27687831 DOI: 10.1016/j.diii.2016.08.009]
- 62 **Turkbey B**, Shah VP, Pang Y, Bernardo M, Xu S, Kruecker J, Locklin J, Baccala AA, Rastinehad AR, Merino MJ, Shih JH, Wood BJ, Pinto PA, Choyke PL. Is apparent diffusion coefficient associated with clinical risk scores for prostate cancers that are visible on 3-T MR images? *Radiology* 2011; **258**: 488-495 [PMID: 21177390 DOI: 10.1148/radiol.10100667]
- 63 **Faletti R**, Battisti G, Discalzi A, Grognaudi ML, Martinello S, Oderda M, Gontero P, Bergamasco L, Cassinis MC, Fonio P. Can DW-MRI, with its ADC values, be a reliable predictor of biopsy outcome in patients with suspected prostate cancer? *Abdom Radiol (NY)* 2016; **41**: 926-933 [PMID: 27193791 DOI: 10.1007/s00261-015-0574-x]
- 64 **Tamai K**, Koyama T, Saga T, Morisawa N, Fujimoto K, Mikami Y, Togashi K. The utility of diffusion-weighted MR imaging for differentiating uterine sarcomas from benign leiomyomas. *Eur Radiol* 2008; **18**: 723-730 [PMID: 17929022]
- 65 **Shen SH**, Chiou YY, Wang JH, Yen MS, Lee RC, Lai CR, Chang CY. Diffusion-weighted single-shot echo-planar imaging with parallel technique in assessment of endometrial cancer. *AJR Am J Roentgenol* 2008; **190**: 481-488 [PMID: 18212236 DOI: 10.2214/AJR.07.2155]
- 66 **Naganawa S**, Sato C, Kumada H, Ishigaki T, Miura S, Takizawa O. Apparent diffusion coefficient in cervical cancer of the uterus: comparison with the normal uterine cervix. *Eur Radiol* 2005; **15**: 71-78 [PMID: 15538578]
- 67 **Liu Y**, Bai R, Sun H, Liu H, Wang D. Diffusion-weighted magnetic resonance imaging of uterine cervical cancer. *J Comput Assist Tomogr* 2009; **33**: 858-862 [PMID: 19940650 DOI: 10.1097/RCT.0b013e31819e93af]

- 68 **Mahajan A**, Engineer R, Chopra S, Mahanshetty U, Juvekar SL, Shrivastava SK, Desekar N, Thakur MH. Role of 3T multiparametric-MRI with BOLD hypoxia imaging for diagnosis and post therapy response evaluation of postoperative recurrent cervical cancers. *Eur J Radiol Open* 2016; **3**: 22-30 [PMID: 27069975 DOI: 10.1016/j.ejro.2015.11.003]
- 69 **Zhou G**, Chen X, Tang F, Zhou J, Wang Y, Wang Z. The Value of Diffusion-Weighted Imaging in Predicting the Prognosis of Stage IB-IIA Cervical Squamous Cell Carcinoma After Radical Hysterectomy. *Int J Gynecol Cancer* 2016; **26**: 361-366 [PMID: 26807567 DOI: 10.1097/IGC.0000000000000613]
- 70 **Basu S**, Mahajan A. Psoas muscle metastasis from cervical carcinoma: Correlation and comparison of diagnostic features on FDG-PET/CT and diffusion-weighted MRI. *World J Radiol* 2014; **6**: 125-129 [PMID: 24778775 DOI: 10.4329/wjr.v6.i4.125]
- 71 **Wang YT**, Li YC, Yin LL, Pu H. Can Diffusion-weighted Magnetic Resonance Imaging Predict Survival in Patients with Cervical Cancer? A Meta-Analysis. *Eur J Radiol* 2016; **85**: 2174-2181 [PMID: 27842663 DOI: 10.1016/j.ejrad.2016.10.011]
- 72 **Gangadhar K**, Mahajan A, Sable N, Bhargava P. MR Imaging of Pelvic Masses: A Compartmental Approach. In *Seminars in Ultrasound, CT and MRI*. Available from: URL: <http://www.sem ultrasoundctmri.com/action/showFullTextImages?pii=S0887-2171%2816%2930099-3>
- 73 **Mahajan A**, Sable NP, Popat PB, Bhargava P, Gangadhar K, Thakur MH, Arya S. MR Imaging of Gynecological Malignancies: Role in Personalized Management. In *Seminars in Ultrasound, CT and MRI*. Available from: URL: [http://www.sem ultrasoundctmri.com/article/S0887-2171\(16\)30100-7/fulltext](http://www.sem ultrasoundctmri.com/article/S0887-2171(16)30100-7/fulltext)
- 74 **Thomassin-Naggara I**, Daraï E, Cuenod CA, Fournier L, Toussaint I, Marsault C, Bazot M. Contribution of diffusion-weighted MR imaging for predicting benignity of complex adnexal masses. *Eur Radiol* 2009; **19**: 1544-1552 [PMID: 19214523 DOI: 10.1007/s00330-009-1299-4]
- 75 **Basu S**, Mahajan A. Ovarian dermoid cyst serendipitously detected by pelvic radioiodine-(131)I uptake and by diffusion weighted MRI in a post-thyroidectomy case of papillary thyroid carcinoma. *Hell J Nucl Med* 2013; **16**: 62-63 [PMID: 23529395 DOI: 10.1967/s002449910073]
- 76 **Oh JW**, Rha SE, Oh SN, Park MY, Byun JY, Lee A. Diffusion-weighted MRI of epithelial ovarian cancers: correlation of apparent diffusion coefficient values with histologic grade and surgical stage. *Eur J Radiol* 2015; **84**: 590-595 [PMID: 25623826 DOI: 10.1016/j.ejrad.2015.01.005]
- 77 **Fehniger J**, Thomas S, Lengyel E, Liao C, Tenney M, Oto A, Yamada SD. A prospective study evaluating diffusion weighted magnetic resonance imaging (DW-MRI) in the detection of peritoneal carcinomatosis in suspected gynecologic malignancies. *Gynecol Oncol* 2016; **142**: 169-175 [PMID: 27103176 DOI: 10.1016/j.ygyno.2016.04.018]
- 78 **Michielsen K**, Vergote I, Op de Beeck K, Amant F, Leunen K, Moerman P, Deroose C, Souverijns G, Dymarkowski S, De Keyzer F, Vandecaveye V. Whole-body MRI with diffusion-weighted sequence for staging of patients with suspected ovarian cancer: a clinical feasibility study in comparison to CT and FDG-PET/CT. *Eur Radiol* 2014; **24**: 889-901 [PMID: 24322510 DOI: 10.1007/s00330-013-3083-8]
- 79 **Queiroz MA**, Hüllner M, Kuhn F, Huber G, Meerwein C, Kollias S, von Schulthess G, Veit-Haibach P. Use of diffusion-weighted imaging (DWI) in PET/MRI for head and neck cancer evaluation. *Eur J Nucl Med Mol Imaging* 2014; **41**: 2212-2221 [PMID: 25091219 DOI: 10.1007/s00259-014-2867-7]
- 80 **Zhou M**, Lu B, Lv G, Tang Q, Zhu J, Li J, Shi K. Differential diagnosis between metastatic and non-metastatic lymph nodes using DW-MRI: a meta-analysis of diagnostic accuracy studies. *J Cancer Res Clin Oncol* 2015; **141**: 1119-1130 [PMID: 25515409 DOI: 10.1007/s00432-014-1895-9]
- 81 **Zhong J**, Lu Z, Xu L, Dong L, Qiao H, Hua R, Gong Y, Liu Z, Hao C, Liu X, Zong C, He L, Liu J. The diagnostic value of cervical lymph node metastasis in head and neck squamous carcinoma by using diffusion-weighted magnetic resonance imaging and computed tomography perfusion. *Biomed Res Int* 2014; **2014**: 260859 [PMID: 25050333 DOI: 10.1155/2014/260859]
- 82 **Vandecaveye V**, De Keyzer F, Vander Poorten V, Dirix P, Verbeken E, Nuyts S, Hermans R. Head and neck squamous cell carcinoma: value of diffusion-weighted MR imaging for nodal staging. *Radiology* 2009; **251**: 134-146 [PMID: 19251938 DOI: 10.1148/radiol.2511080128]
- 83 **Sumi M**, Sakihama N, Sumi T, Morikawa M, Uetani M, Kabasawa H, Shigeno K, Hayashi K, Takahashi H, Nakamura T. Discrimination of metastatic cervical lymph nodes with diffusion-weighted MR imaging in patients with head and neck cancer. *AJNR Am J Neuroradiol* 2003; **24**: 1627-1634 [PMID: 13679283]
- 84 **Holzapfel K**, Duetsch S, Fauser C, Eiber M, Rummeny EJ, Gaa J. Value of diffusion-weighted MR imaging in the differentiation between benign and malignant cervical lymph nodes. *Eur J Radiol* 2009; **72**: 381-387 [PMID: 18995981 DOI: 10.1016/j.ejrad.2008.09.034]
- 85 **Koç O**, Paksoy Y, Erayman I, Kivrak AS, Arbag H. Role of diffusion weighted MR in the discrimination diagnosis of the cystic and/or necrotic head and neck lesions. *Eur J Radiol* 2007; **62**: 205-213 [PMID: 17188444]
- 86 **Mahajan A**, Azad GK, Cook GJ. PET Imaging of Skeletal Metastases and Its Role in Personalizing Further Management. *PET Clin* 2016; **11**: 305-318 [PMID: 27321034 DOI: 10.1016/j.cpet.2016.02.003]
- 87 **Subhawong TK**, Jacobs MA, Fayad LM. Insights into quantitative diffusion-weighted MRI for musculoskeletal tumor imaging. *AJR Am J Roentgenol* 2014; **203**: 560-572 [PMID: 25148158 DOI: 10.2214/AJR.13.12165]
- 88 **Baur A**, Stäbler A, Brüning R, Bartl R, Krödel A, Reiser M, Deimling M. Diffusion-weighted MR imaging of bone marrow: differentiation of benign versus pathologic compression fractures. *Radiology* 1998; **207**: 349-356 [PMID: 9577479]
- 89 43rd Congress of the International Society of Paediatric Oncology (SIOP) 2011, Auckland, New Zealand, 28th-30th October, 2011. SIOP Abstracts. *Pediatr Blood Cancer* 2011; **57**: 705-897 [PMID: 21887762 DOI: 10.1002/pbc.23299]
- 90 **Amin WM**, Kotb HT, Abdel-Kerim AA, Barakat MS, El-Malky AA, Fadel SH. Diffusion-weighted MRI and in-phase/opposed-phase sequences in the assessment of bone tumors. *J Magn Reson Imaging* 2016; **44**: 565-572 [PMID: 26934685 DOI: 10.1002/jmri.25212]
- 91 **Koutoulidis V**, Fontara S, Terpos E, Zagouri F, Matsaridis D, Christoulas D, Panourgias E, Kastritis E, Dimopoulos MA, Mouloupos LA. Quantitative Diffusion-weighted Imaging of the Bone Marrow: An Adjunct Tool for the Diagnosis of a Diffuse MR Imaging Pattern in Patients with Multiple Myeloma. *Radiology* 2017; **282**: 484-493 [PMID: 27610934 DOI: 10.1148/radiol.2016160363]
- 92 **Mahajan A**, Cook G. Physiologic and Molecular Basis of PET in Cancer Imaging. In *Basic Science of PET Imaging*. Berlin: Springer International Publishing, 2017: 399-427 [DOI: 10.1007/978-3-319-40070-9]
- 93 **Mahajan A**, Cook G. Clinical Applications of PET/CT in Oncology. In *Basic Science of PET Imaging*. Berlin: Springer International Publishing, 2017: 429-450
- 94 **Li B**, Li Q, Nie W, Liu S. Diagnostic value of whole-body diffusion-weighted magnetic resonance imaging for detection of primary and metastatic malignancies: a meta-analysis. *Eur J Radiol* 2014; **83**: 338-344 [PMID: 24355655 DOI: 10.1016/j.ejrad.2013.11.017]
- 95 **Lecouvet FE**, Michoux N, Nzeusseu Toukap A, Larbi A, Berg BV, Malghem J, Triqueneaux P, Omoumi P, Stoenoiu MS. The Increasing Spectrum of Indications of Whole-Body MRI Beyond Oncology: Imaging Answers to Clinical Needs. *Semin Musculoskelet Radiol* 2015; **19**: 348-362 [PMID: 26583363 DOI: 10.1055/s-0035-1564695]
- 96 **Balbo-Mussetto A**, Cirillo S, Bruna R, Gueli A, Saviolo C, Petracchini M, Fornari A, Lario CV, Gottardi D, De Crescenzo A, Tarella C. Whole-body MRI with diffusion-weighted imaging: a valuable alternative to contrast-enhanced CT for initial staging of aggressive lymphoma. *Clin Radiol* 2016; **71**: 271-279 [PMID: 26749081 DOI: 10.1016/j.crad.2015.11.018]
- 97 **Maggialetti N**, Ferrari C, Minoia C, Asabella AN, Ficco M, Loseto G, De Tullio G, de Fazio V, Calabrese A, Guarini A, Rubini G, Brunese

- L. Role of WB-MR/DWIBS compared to (18)F-FDG PET/CT in the therapy response assessment of lymphoma. *Radiol Med* 2016; **121**: 132-143 [PMID: 26349573 DOI: 10.1007/s11547-015-0581-6]
- 98 **Ferrari C**, Minoia C, Asabella AN, Nicoletti A, Altini C, Antonica F, Ficco M, Guarini A, Maggialletti N, Rubini G. Whole body magnetic resonance with diffusion weighted sequence with body signal suppression compared to (18)F-FDG PET/CT in newly diagnosed lymphoma. *Hell J Nucl Med* 2014; **17** Suppl 1: 40-49 [PMID: 24392468]
- 99 **Le Bihan D**, Breton E, Lallemand D, Grenier P, Cabanis E, Laval-Jeantet M. MR imaging of intravoxel incoherent motions: application to diffusion and perfusion in neurologic disorders. *Radiology* 1986; **161**: 401-407 [PMID: 3763909]
- 100 **Sakamoto J**, Imaizumi A, Sasaki Y, Kamio T, Wakoh M, Otonari-Yamamoto M, Sano T. Comparison of accuracy of intravoxel incoherent motion and apparent diffusion coefficient techniques for predicting malignancy of head and neck tumors using half-Fourier single-shot turbo spin-echo diffusion-weighted imaging. *Magn Reson Imaging* 2014; **32**: 860-866 [PMID: 24832359 DOI: 10.1016/j.mri.2014.05.002]
- 101 **Lin Y**, Li J, Zhang Z, Xu Q, Zhou Z, Zhang Z, Zhang Y, Zhang Z. Comparison of Intravoxel Incoherent Motion Diffusion-Weighted MR Imaging and Arterial Spin Labeling MR Imaging in Gliomas. *Biomed Res Int* 2015; **2015**: 234245 [PMID: 25945328 DOI: 10.1155/2015/234245]
- 102 **Liu X**, Zhou L, Peng W, Wang H, Zhang Y. Comparison of stretched-Exponential and monoexponential model diffusion-Weighted imaging in prostate cancer and normal tissues. *J Magn Reson Imaging* 2015; **42**: 1078-1085 [PMID: 25727776 DOI: 10.1002/jmri.24872]
- 103 **Bennett KM**, Schmainda KM, Bennett RT, Rowe DB, Lu H, Hyde JS. Characterization of continuously distributed cortical water diffusion rates with a stretched-exponential model. *Magn Reson Med* 2003; **50**: 727-734 [PMID: 14523958 DOI: 10.1002/mrm.10581]
- 104 **Bai Y**, Lin Y, Tian J, Shi D, Cheng J, Haacke EM, Hong X, Ma B, Zhou J, Wang M. Grading of Gliomas by Using Monoexponential, Biexponential, and Stretched Exponential Diffusion-weighted MR Imaging and Diffusion Kurtosis MR Imaging. *Radiology* 2016; **278**: 496-504 [PMID: 26230975 DOI: 10.1148/radiol.2015142173]
- 105 **Kwee TC**, Galbán CJ, Tsien C, Junck L, Sundgren PC, Ivancevic MK, Johnson TD, Meyer CR, Rehemtulla A, Ross BD, Chenevert TL. Intravoxel water diffusion heterogeneity imaging of human high-grade gliomas. *NMR Biomed* 2010; **23**: 179-187 [PMID: 19777501 DOI: 10.1002/nbm.1441]
- 106 **Bedair R**, Priest AN, Patterson AJ, McLean MA, Graves MJ, Manavaki R, Gill AB, Abeyakoon O, Griffiths JR, Gilbert FJ. Assessment of early treatment response to neoadjuvant chemotherapy in breast cancer using non-mono-exponential diffusion models: a feasibility study comparing the baseline and mid-treatment MRI examinations. *Eur Radiol* 2017; **27**: 2726-2736 [PMID: 27798751]
- 107 **Wu EX**, Cheung MM. MR diffusion kurtosis imaging for neural tissue characterization. *NMR Biomed* 2010; **23**: 836-848 [PMID: 20623793 DOI: 10.1002/nbm.1506.Review]
- 108 **Hui ES**, Fieremans E, Jensen JH, Tabesh A, Feng W, Bonilha L, Spampinato MV, Adams R, Helpert JA. Stroke assessment with diffusional kurtosis imaging. *Stroke* 2012; **43**: 2968-2973 [PMID: 22933581 DOI: 10.1161/STROKEAHA.112.657742]
- 109 **Grossman EJ**, Ge Y, Jensen JH, Babb JS, Miles L, Reaume J, Silver JM, Grossman RI, Inglesse M. Thalamus and cognitive impairment in mild traumatic brain injury: a diffusional kurtosis imaging study. *J Neurotrauma* 2012; **29**: 2318-2327 [PMID: 21639753 DOI: 10.1089/neu.2011.1763]
- 110 **Raab P**, Hattingen E, Franz K, Zanella FE, Lanfermann H. Cerebral gliomas: diffusional kurtosis imaging analysis of microstructural differences. *Radiology* 2010; **254**: 876-881 [PMID: 20089718 DOI: 10.1148/radiol.09090819]
- 111 **Falangola MF**, Jensen JH, Tabesh A, Hu C, Deardorff RL, Babb JS, Ferris S, Helpert JA. Non-Gaussian diffusion MRI assessment of brain microstructure in mild cognitive impairment and Alzheimer's disease. *Magn Reson Imaging* 2013; **31**: 840-846 [PMID: 23602730 DOI: 10.1016/j.mri.2013.02.008]
- 112 **Yoshida M**, Hori M, Yokoyama K, Fukunaga I, Suzuki M, Kamagata K, Shimoji K, Nakanishi A, Hattori N, Masutani Y, Aoki S. Diffusional kurtosis imaging of normal-appearing white matter in multiple sclerosis: preliminary clinical experience. *Jpn J Radiol* 2013; **31**: 50-55 [PMID: 23086313 DOI: 10.1007/s11604-012-0147-7]

P- Reviewer: Calvete MJF, Cerwenka HR, Chen F, Lassandro F, Plataniotis G **S- Editor:** Ji FF **L- Editor:** A **E- Editor:** Wu HL



Revisions to the Tumor, Node, Metastasis staging of lung cancer (8th edition): Rationale, radiologic findings and clinical implications

Fernando U Kay, Asha Kandathil, Kiran Batra, Sachin S Saboo, Suhny Abbara, Prabhakar Rajiah

Fernando U Kay, Asha Kandathil, Kiran Batra, Sachin S Saboo, Suhny Abbara, Prabhakar Rajiah, Department of Radiology, Cardiothoracic Imaging, UT Southwestern Medical Center, Dallas, TX 75204, United States

Author contributions: All authors equally contributed to this paper with conception and design of the study, literature review and analysis, drafting and critical revision and editing, and final approval of the final version.

Conflict-of-interest statement: All authors do not have any conflict of interest or financial disclosure relevant to this article.

Open-Access: This article is an open-access article which was selected by an in-house editor and fully peer-reviewed by external reviewers. It is distributed in accordance with the Creative Commons Attribution Non Commercial (CC BY-NC 4.0) license, which permits others to distribute, remix, adapt, build upon this work non-commercially, and license their derivative works on different terms, provided the original work is properly cited and the use is non-commercial. See: <http://creativecommons.org/licenses/by-nc/4.0/>

Manuscript source: Invited manuscript

Correspondence to: Prabhakar Rajiah, MBBS, MD, FRCR, Associate Professor, Associate Director of Cardiac CT and MRI, Department of Radiology, Cardiothoracic Imaging, UT Southwestern Medical Center, E6.120 B, Mail code 9316, 5323 Harry Hines Boulevard, Dallas, TX 75204, United States. radprabhakar@gmail.com
Telephone: +1-214-6483121

Received: January 31, 2017

Peer-review started: February 6, 2017

First decision: March 7, 2017

Revised: March 21, 2017

Accepted: April 18, 2017

Article in press: April 19, 2017

Published online: June 28, 2017

adopted by the Union for International Cancer Control (UICC) and the American Joint Committee on Cancer (AJCC), has been recently revised, with the new 8th edition of the staging manual being published in January 2017. This edition has few but important evidence-based changes to the TNM staging system used for lung cancer. Radiologists should be aware of the updated classification system to accurately provide staging information to oncologists and oncosurgeons. In this article, we discuss the rationale, illustrate the changes with relevance to Radiology, and review the clinical implications of the 8th edition of the UICC/AJCC TNM staging system with regards to lung cancer.

Key words: Lung, cancer; Tumor, Node, Metastasis; Staging; 8th edition

© **The Author(s) 2017.** Published by Baishideng Publishing Group Inc. All rights reserved.

Core tip: This article discusses the rationale, illustrates the changes with relevance to Radiology, and reviews the clinical implications of the 8th edition of the Union for International Cancer Control/American Joint Committee on Cancer Tumor, Node, Metastasis staging of lung cancer.

Kay FU, Kandathil A, Batra K, Saboo SS, Abbara S, Rajiah P. Revisions to the Tumor, Node, Metastasis staging of lung cancer (8th edition): Rationale, radiologic findings and clinical implications. *World J Radiol* 2017; 9(6): 269-279 Available from: URL: <http://www.wjgnet.com/1949-8470/full/v9/i6/269.htm> DOI: <http://dx.doi.org/10.4329/wjr.v9.i6.269>

INTRODUCTION

Lung cancer is the leading oncologic cause of mortality in both men and women in the United States. World-

Abstract

The Tumor, Node, Metastasis (TNM) staging system,

wide, Lung cancer, is the leading and the second most common cause of cancer death among men and women respectively^[1]. The American Cancer Society estimates about 224390 new cases of lung cancer in 2016, and approximately 158000 deaths^[2]. Clinical practice guidelines for lung cancer largely rely on staging models, which are used not only for predicting disease prognosis, but also to guide treatment^[3]. The Tumor, Node, Metastasis (TNM) staging system, adopted by both the Union for International Cancer Control (UICC) and the American Joint Committee on Cancer (AJCC), has been recently revised, and the new edition (8th) of the staging manual was published in January 2017^[4] (Table 1). The updated lung cancer chapter introduces few but important evidence-based changes to the prior 7th edition, derived from validation of the TNM system for staging and guiding lung cancer treatment in multidisciplinary centers.

In this article, we discuss the rationale, illustrate the changes with relevance to radiology and review the clinical implications of the 8th edition of the UICC/AJCC TNM staging system.

HISTORICAL PERSPECTIVE

Developed in France by Pierre Denoix between the years 1943 and 1952, the TNM system has been adopted by the UICC and the AJCC to help clinicians plan treatment, guide prognosis, assist in treatment evaluation, provide a common language for exchange of information, and contribute to the continuing investigation of cancer^[5]. Many iterations have led to the preceding 7th UICC/AJCC TNM edition, effective since 2009, which introduced a series of evidence-based advances in comparison with earlier versions. Radiologic reviews of the 7th TNM staging were previously published^[6]. The 7th TNM was the result of a combined effort of the International Association for the Study of Lung Cancer (IASLC), the UICC, the AJCC, and the Japanese societies against cancer^[7], and reflected the conclusions from a retrospective analysis of 81015 lung cancer patients (67725 with non-small cell lung cancer, NSCLC, and 13290 with small cell lung cancer, SCLC) treated between 1990 and 2000, from Europe (59%), North America (18%), Asia (15%), and Australia (8%). The 7th TNM edition, for the first time, encompassed small cell lung cancer (SCLC) and carcinoid tumors in the scope.

Despite these earlier efforts, some of the 7th TNM descriptors could not be validated given the lack of a tailored methodology, leading the IASLC to commission a task force responsible for gathering and analyzing a comprehensive database, composed of both retrospective and prospective cases, in an attempt to overcome prior limitations^[8]. For the first time, the database included information of 4667 patients sent *via* a specifically designed electronic data capture system, in addition to other sources (consortia, registries, or surgical series), resulting in a final cohort of 77156 lung cancer patients (70967 with NSCLC and 6189 with SCLC) from

Table 1 Lung cancer staging, Tumor, Node, Metastasis staging 8th edition

T	Primary tumor
Tx	Cannot be assessed; Tumor in sputum/bronchial washings not in imaging/bronchoscopy
To	No evidence
Tis	Carcinoma in situ
T1	≤ 3 cm surrounded by lung/visceral pleura, not involving main bronchus
T1a(mi)	Minimally invasive adenocarcinoma
T1a	≤ 1 cm
T1b	> 1 to ≤ 2 cm
T1c	> 2 to ≤ 3 cm
T2	> 3 to ≤ 5 cm or Involves main bronchus without carina involvement or Visceral pleural invasion or atelectasis/post obstructive pneumonitis extending to hilum
T2a	> 3 to ≤ 4 cm
T2b	> 4 to ≤ 5 cm
T3	> 5 to ≤ 7 cm or Separate tumor in same lobe or Direct invasion of chest wall (includes parietal pleura and superior sulcus)/parietal pericardium/phrenic nerve
T4	> 7 cm or Separate tumor in different lobe of ipsilateral lung or Invasion of heart/ great vessels/diaphragm/mediastinum/trachea/carina/esophagus/recurrent laryngeal nerve/vertebral body
N	Regional lymph node
Nx	Cannot be assessed
N0	No involvement
N1	Ipsilateral peribronchial and/or hilar nodes and intrapulmonary nodes
N2	Ipsilateral mediastinal and/or subcarinal nodes
N3	Contralateral mediastinal or hilar; ipsilateral/contralateral scalene/supraclavicular
M	Distant metastasis
M0	No distant metastasis
M1	Distant metastasis is present
M1a	Tumor (s) in contralateral lung; pleural/pericardial nodule/malignant effusion
M1b	Single extrathoracic metastasis
M1c	Multiple extrathoracic metastases, in one/more organs

35 cancer centers in 16 countries, diagnosed between 1999 and 2010 and treated with surgery or combined modalities^[9]. The resultant 8th TNM revision portrays validation of the descriptors and recommendations based on the new findings^[10].

UPDATED TUMOR DESCRIPTORS (T)

The T descriptors in the 8th TNM classification encompass size, invasion into adjacent central/mediastinal structures, and location of an additional tumor nodule in relation to the primary tumor (Table 1). The changes to the T component aim to maintain compatibility with the previous classifications, with an additional benefit of improving prognostic differentiation between the different T categories. The primary tumor is now

Table 2 Five-year survival per T stage of the 8th Tumor, Node, Metastasis staging system

	5-yr survival
T1a	92%
T1b	83%-86%
T1c	76%-81%
T2a	67%-74%
T2b	60%-65%
T3	52%-57%
T4	38%-47%

classified into 7 categories per size (*T1a*, *T1b*, *T1c*, *T2a*, *T2b*, *T3* and *T4*) as compared with the 6 categories on 7th TNM (*T1a*, *T1b*, *T2a*, *T2b*, *T3* and *T4*). The new T classification was validated on 33115 patients with NSCLC and no metastatic disease^[9,11]. Robust analysis of the survival data was performed using a log-rank statistic, which confirmed prior 7th TNM size cutoffs, and suggested further subdivision into 1-cm increments. T descriptors were analyzed using Cox regression analysis adjusted for age, sex, histologic type, and geographic region across multiple cohorts, with results showing a clear difference in 5-year survival, and hence prognosis, for each centimeter increase in tumor size between 1-5 cm (Table 2). The 5-cm cutoff remains useful to separate tumors with worse prognosis (*T3*, > 5 and ≤ 7 cm, and *T4*, > 7 cm).

The new classification subdivides *T1* lung cancers measuring ≤ 3 cm into *T1a*, *T1b*, *T1c* lesions based on specific size cutoffs (Figure 1). A superficial spreading tumor in central airways is classified as *T1a*, regardless of its location. Carcinoma *in situ* is classified as *Tis* and applies to both adenocarcinoma and squamous cell carcinoma. Minimally invasive adenocarcinomas are classified as *T1a (m)* when the invasive component is ≤ 5 mm and the noninvasive lepidic component is ≤ 3 cm (diagnoses can be only made in resected tumors).

T2 lung cancers measure > 3 and ≤ 5 cm, and are subdivided into *T2a* and *T2b* using the 4-cm cutoff (Figure 2). Additional features in the new *T2* classification include involvement of any part of the main bronchus, regardless of the distance to (but not involving) the carina. After adjusting for tumor size, partial or complete atelectasis, and pneumonitis secondary to airways invasion, these features still showed better prognosis than *T3* tumors with different descriptors. Involvement of lung hilar fat is classified as *T2* in 8th TNM, as are tumors involving the visceral pleura. However, involvement of a structure by a tumor that extends from a nodal metastasis (e.g., left recurrent laryngeal nerve involved by an aortopulmonary window node metastasis) is not regarded as T involvement^[10].

For the *T3* category, the new database analysis showed that tumors measuring > 5 and ≤ 7 cm, separate tumor nodules in the same lobe as the primary lesion, and invasion of structures such as the chest wall, phrenic nerve, and parietal pericardium had

similar 5-year survival rate. Therefore, these criteria are described in the *T3* category (Figure 3). Since the involvement of the parietal pericardium is classified as *T3*, invasion of the fat overlying the pericardium should be classified *T3* rather than *T4*.

For the *T4* descriptors, tumors measuring > 7 cm in longest diameter, and tumor nodules in the same lung but different lobes as the primary lesion are included. Invasion of the diaphragm has also been upstaged to a *T4* descriptor (previously *T3*). This is based on the 5-year survival rate, like other *T4* lesions (Figure 4). Invasion of the mediastinal fat (excluding the extrapericardial fat) is classified as *T4*, in addition to other mediastinal structures like trachea, carina, great vessels, esophagus, recurrent laryngeal nerve, and spine, since they were associated with similar 5-year survival rate and were not changed. An important change has been to eliminate the invasion of the mediastinal pleura as a descriptor in 8th TNM, given the inconsistency of this finding at both clinical and pathologic staging. However, involvement of the visceral pericardium is designated as *T4*. A superior sulcus tumor with clear involvement of the C8 or higher nerve roots or cords of the brachial plexus, subclavian vessels, and vertebral body, lamina, or spinal canal is also classified as *T4*, however a tumor is classified as *T3* if it involves only thoracic nerve roots (e.g., a tumor involving only T1 and T2 nerve roots)^[10].

When multiple T descriptors are applicable to a tumor, the highest T category should be used to determine the category. For example, a small tumor with a higher T category by invasion should be classified by the invasion, and a large tumor with a lesser degree of invasion should be categorized by the size (e.g., a 5.3-cm tumor invading the main bronchus should be classified as *T3*). Some examples on how to apply the new T descriptors are shown in Figure 5.

UPDATED NODE DESCRIPTORS (N)

In patients with NSCLC, lymph nodes measuring more than 1 cm in short axis on CT scans or MRI are abnormal. Reported sensitivity and specificity of CT scans for the detection of pathologic nodes is 51%-64% and 74%-86%, respectively^[12]. 18-FDG PET/CT has been shown to have higher accuracy than CT or MRI, with a sensitivity of 58%-94% and specificity of 76%-96% for detection of mediastinal lymph node metastasis^[13]. Contrast enhanced CT scan and 18-FDG PET/CT scans are routinely used in the clinical staging (cN) of NSCLC, whereas pathologic stage (pN) is based on histological findings.

The N staging descriptors for the 8th TNM were validated in 70336 lung cancer patients using descriptors previously used in 6th TNM and 7th TNM. No changes to the N descriptors were proposed in 8th TNM as the four N categories (N0, N1, N2, N3) based on the location of the pathologic nodes have shown to consistently predict distinct prognosis^[14] (Table 3). An illustrated scheme

T1 descriptors

Tis: Carcinoma *in situ*

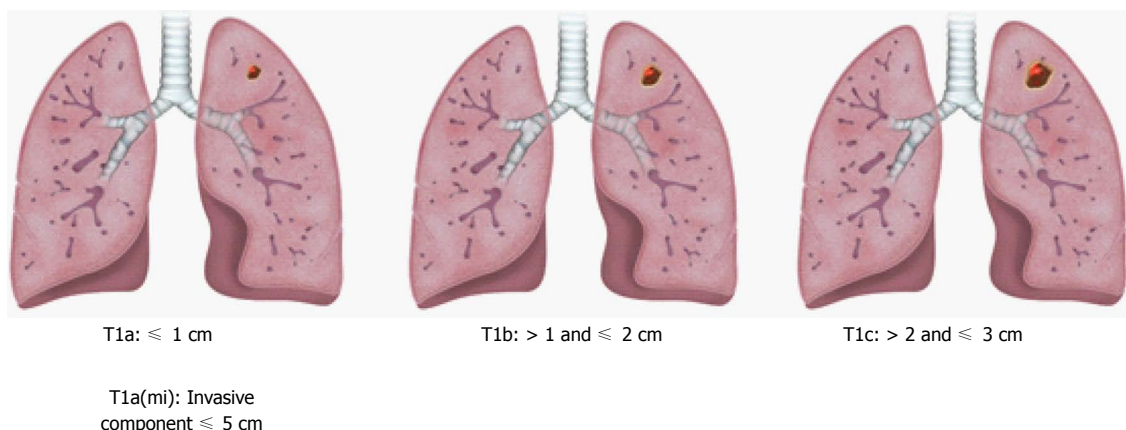


Figure 1 Illustrations demonstrating T1 descriptors.

T2 descriptors

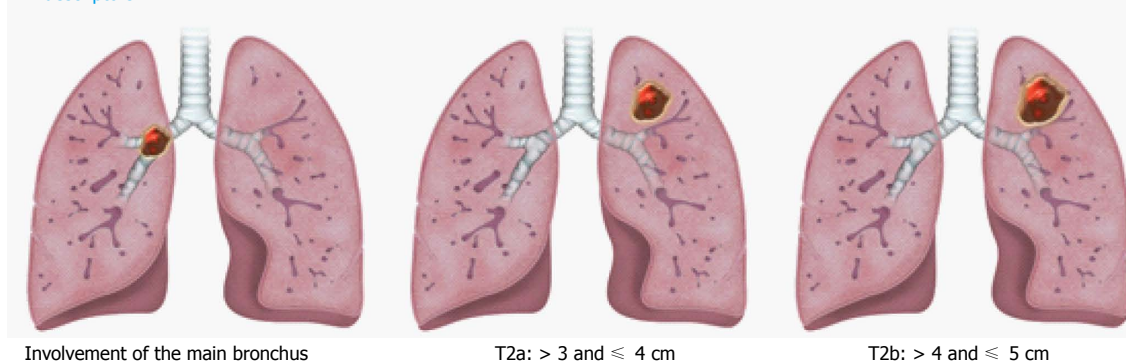


Figure 2 Illustrations demonstrating T2 descriptors.

T3 descriptors

Size: > 5 and ≤ 7 cm, or:

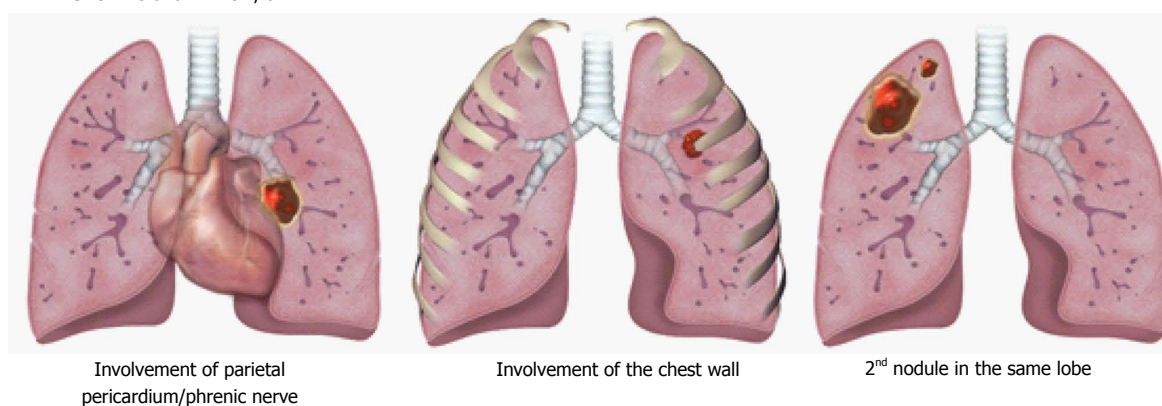


Figure 3 Illustrations demonstrating T3 descriptors.

with the current N descriptors is provided in Figure 6. Involvement of ipsilateral peribronchial and/or ipsilateral hilar nodes and intrapulmonary nodes, including direct involvement is classified as *N1*. Involvement of ipsilateral mediastinal nodes and/or subcarinal nodes is classified as *N2*. Involvement of contralateral mediastinal/hilar nodes or ipsilateral/contralateral supraclavicular/scalene

nodes is classified as *N3*. It has been suggested that addition of the number of involved nodes in *N1* and *N2* locations and presence or absence of skip metastases can improve the prognostic significance of the anatomic location of involved nodes. The international association for study of lung cancer (IASLC) recommends clinical documentation of these additional parameters in 8th TNM

T4 descriptors

Size: > 7 cm, or:

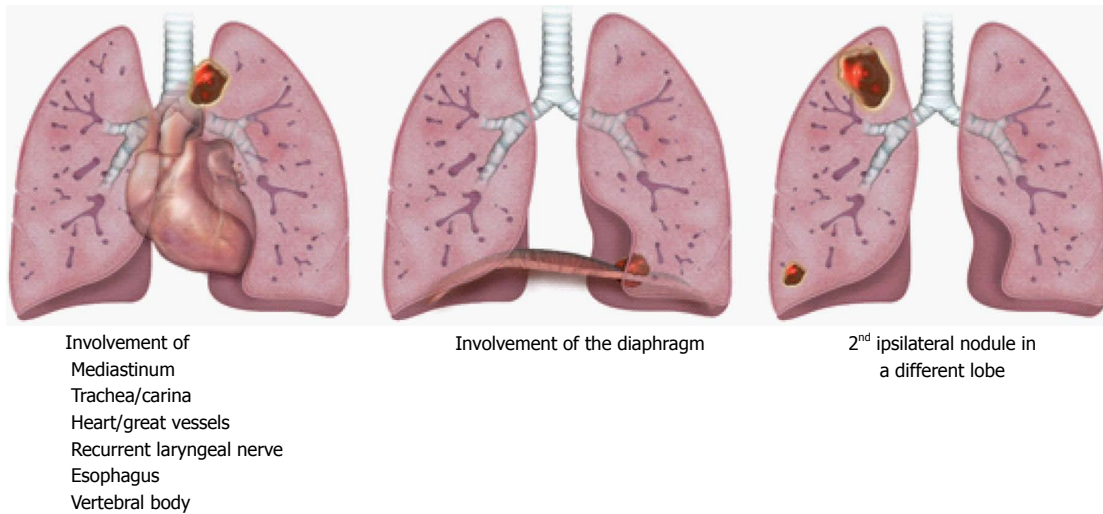


Figure 4 Illustrations demonstrating T4 descriptors.

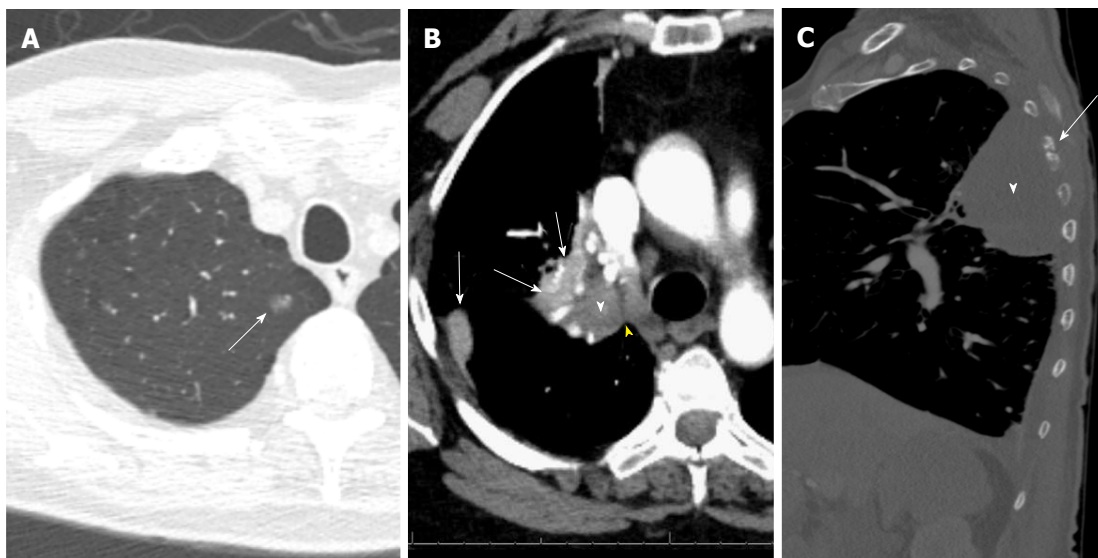


Figure 5 T descriptors. A: T1a (mi): Groundglass opacity in the apical segment of the right upper lobe (arrow) on CT lung window image; resection revealed predominantly lepidic adenocarcinoma with 3-mm invasive component and clear margins; B: T2a: 4-cm invasive squamous cell bronchogenic carcinoma of the right upper lobar bronchus (white arrowhead) with adjacent areas of atelectasis (arrows) and clear cleavage plane with the mediastinum (yellow arrowhead) on contrast-enhanced CT image; C: T4 vs T3: 8.3cm left upper lobe mass (white arrowhead), with chest wall invasion causing destruction of the adjacent left 5th rib (arrow) and small left pleural effusion. Note that the highest descriptor should be used for T staging.

for further testing.

IASLC lymph node map provides detailed anatomic and zonal definitions for all lymph node stations^[15,16]. Some examples on how to apply the new N staging descriptors are provided in Figure 7.

UPDATED METASTASIS DESCRIPTORS (M)

Metastatic disease is present in approximately 40% of patients with lung cancer at the time of initial staging with the most common sites of disease being liver, brain,

bone, adrenal gland, and contralateral lung. Lung cancer metastases can occur through different routes, including hematogenous, lymphatic, airways and through air spaces. Intrapulmonary metastasis has also been used in the context of two or more malignant pulmonary lesions and no other sites of cancer. Metastatic disease may preclude surgical resection depending on the site and number of metastases. Oligometastatic disease is defined as the limited metastatic disease that may include from 1 to 5 lesions with studies showing that patients with treated oligometastases have better clinical outcomes^[17].

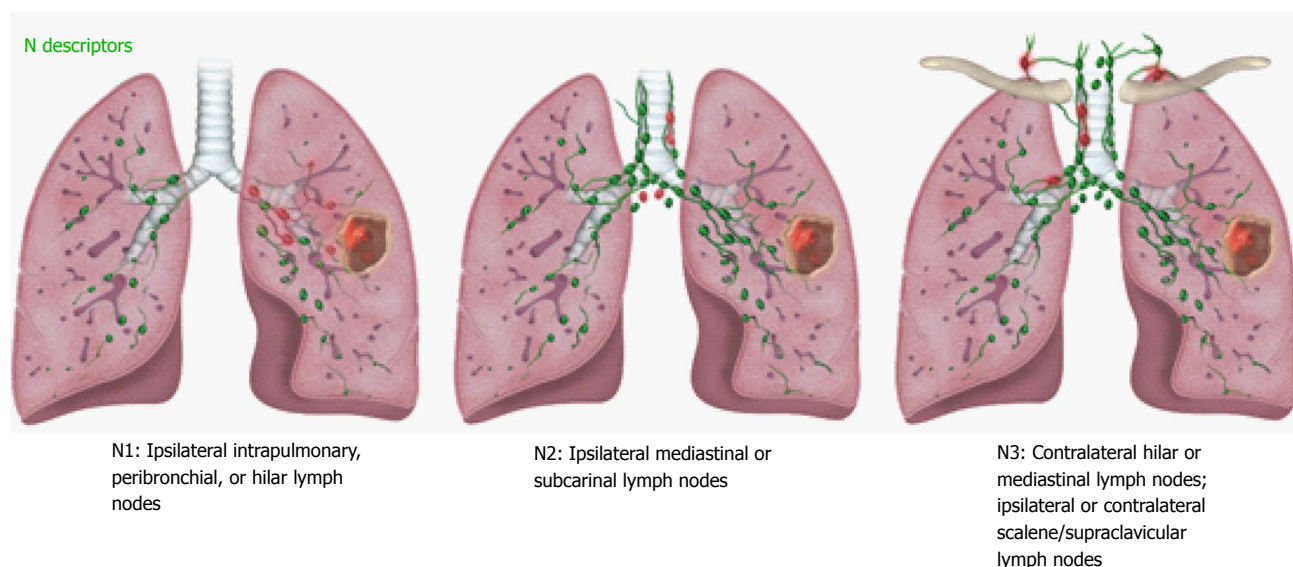


Figure 6 Illustrations demonstrating N descriptors.

Table 3 Five-year survival per N stage of the 8th Tumor, Node, Metastasis staging system

	5-yr survival
N0	60%
N1	37%
N2	23%
N3	9%

Table 4 Median survival per M stage of the 8th Tumor, Node, Metastasis Staging system

	Median survival (in months)
M1a	11.4
M1b	11.4
M1c	6.3

Proposed 8th revisions to the TNM staging system are based on significant differences in patient survival and include significant changes to the M descriptors: M0-M1 (M1 with M1a, M1b and M1c subcategories) and overall stage groupings M descriptors. An illustrated scheme of the updated M descriptors is demonstrated in Figure 8. M1a disease has not changed and comprises of intrathoracic metastases including contralateral pulmonary tumor nodules, pleural/pericardial metastatic effusion/nodules and combination of multiple of these M1a descriptors. However, extrathoracic metastatic disease has been split into M1b and M1c components based on single or multiple metastases due to significant differences in survival amongst these categories (Table 4). A single metastatic lesion involving a single distant organ is now classified as M1b category. Therefore, new M1b descriptor includes single metastatic lesion in various organs like brain, liver, bone, distant lymph node or peritoneum, skin, and adrenal. On the other hand, multiple metastases, irrespective of whether in a single distant organ or multiple distant organs, are now classified as the new M1c category. No differences in survival have been shown among different M1a descriptors or between single and multiple M1a descriptors. M1b metastatic disease is associated with survival that is similar to intrathoracic metastasis (*i.e.*, M1a disease). Averages survival rates are 11.4 mo for M1b and 6.3 mo for M1c disease^[11,17].

IASLC recommends reporting the following information during staging for metastatic disease^[17]:

- (1) identification and location of the involved site;
- (2) differentiation between intra- and extrathoracic metastasis;
- (3) number and diameter of metastatic lesions and number of involved distant organs; and
- (4) 18-FDG PET positivity (if available).

Reclassified M descriptors in the 8th revision, besides maintaining the compatibility with the M descriptors of the previous 7th edition, provide better definition of oligometastatic disease, and ability to predict prognosis, thus helping to meet the objectives of the new TNM classification^[17]. Some examples of the new M descriptors are provided in Figure 9.

UPDATED STAGE GROUPS

For the validation of the staging groups in 8th TNM, a random training set was selected from the 1999-2000 IALSC database, including 25911 and 599 cases staged M0 and M1, respectively^[18]. A tree-based model algorithm for the survival data using log-rank test statistics was used for recursive partitioning and selection of the staging groups. The 8th TNM group candidates were validated by assessing the overall survival per clinical, pathologic, and best stage. Differences in the hazard ratios between adjacent stage groups were analyzed using Cox regression analysis, adjusted for age, performance status, and cell type.

The hazard ratios between adjacent stage groups were significantly different in both 7th TNM and 8th TNM editions, albeit the latter introduces 4 additional levels of discrimination to the older system^[18]. Thus, the new

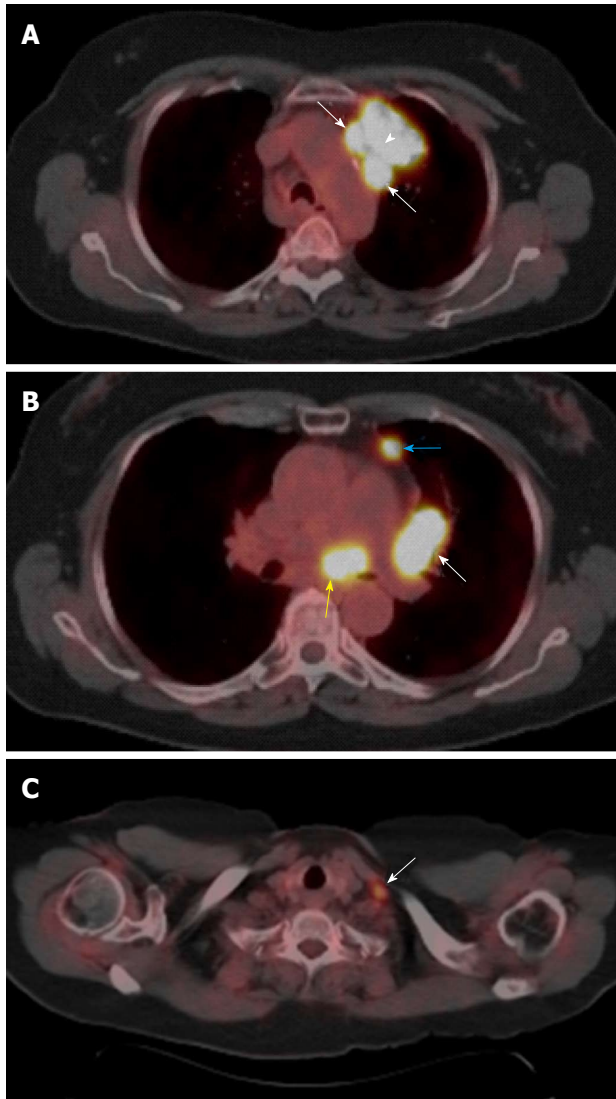


Figure 7 N descriptors. A: Primary tumor and N2: FDG-avid left upper lobe lung mass (arrowhead) invading the prevascular region of the mediastinum with adjacent FDG-avid level 6 lymph nodes suggesting nodal metastases (arrows); B: N1 and N2: Level 10L (white arrow), and 3A (blue arrow) enlarged lymph nodes with increased FDG avidity (N1 nodal metastases) and similar level 7 (yellow arrow) lymph nodes suggesting N2 nodal metastases; C: N3: FDG-avid left supraclavicular lymph node (arrow) suggesting N3 nodal metastases.

stage groups proposed by 8th TNM could determine the 5-year survival with a higher level of detail. The goodness of fit of the survival curves (R^2) were slightly better from the 7th to the 8th TNM editions for both pathologic (R^2 of 45.7 vs 46.9, respectively) and clinical stage models (R^2 of 67.5 vs 68.3, respectively). Tables 5 and 6 demonstrate the new stage groups of 8th TNM and the associated 5-year survival for clinical stages respectively.

CHALLENGES OF THE NEW STAGING SYSTEM

There are a few challenges related to the latest TNM staging system for lung cancer.

Table 5 Stage Group in the 8th Tumor, Node, Metastasis staging system (9)

		N0	N1	N2	N3
T1/M0	T1a	IA1	IIB	IIIA	IIIB
	T1b	IA2	IIB	IIIA	IIIB
	T1c	IA3	IIB	IIIA	IIIB
T2/M0	T2a	IB	IIB	IIIA	IIIB
	T2b	IIA	IIB	IIIA	IIIB
T3/M0		IIB	IIIA	IIIB	IIIC
T4/M0		IIIA	IIIA	IIIB	IIIC
TX/M1	M1a	IVA	IVA	IVA	IVA
	M1b	IVA	IVA	IVA	IVA
	M1c	IVB	IVB	IVB	IVB

Table 6 Five-year survival per stage group of the 8th Tumor, Node, Metastasis staging system (9)

	5-yr survival
IA1	92%
IA2	83%
IA3	77%
IB	68%
IIA	60%
IIB	53%
IIIA	36%
IIIB	26%
IIIC	13%
IVA	10%
IVB	0%

Small-cell lung cancer and carcinoid tumors

A single system has been proposed to stage NSCLC, small-cell lung cancer (SCLC), and bronchial carcinoids since the 7th TNM edition^[4]. The 1999-2010 IALSC database was used for validating the TNM system in 5002 cases of SCLC. Interestingly, carcinoid tumors were excluded from the analysis; therefore, validation for this histologic subtype is still lacking despite the current recommendations^[9].

Although prognostic information by T and N descriptors matched between SCLC and NSCLC, some peculiarities arose when analyzing the M descriptors. M1b patients with SCLC and single-site brain metastasis had better prognoses than those with single-site metastasis elsewhere. Likewise, the presence of pleural effusion in patients with M1b disease conferred an independent worse prognosis^[19].

Assessing multifocal pulmonary cancer

Specific guidelines have been published for addressing cases with involvement of more than one pulmonary site^[20]. IASLC recommends that patients with multiple lung lesions be assessed in a multidisciplinary tumor board. The most important question to be answered is the histology of the separate lesions. For different histologic subtypes, a second primary cancer is favored and separate T, N, and M should be provided for each tumor. If the same histologic subtype is found, a single

M descriptors

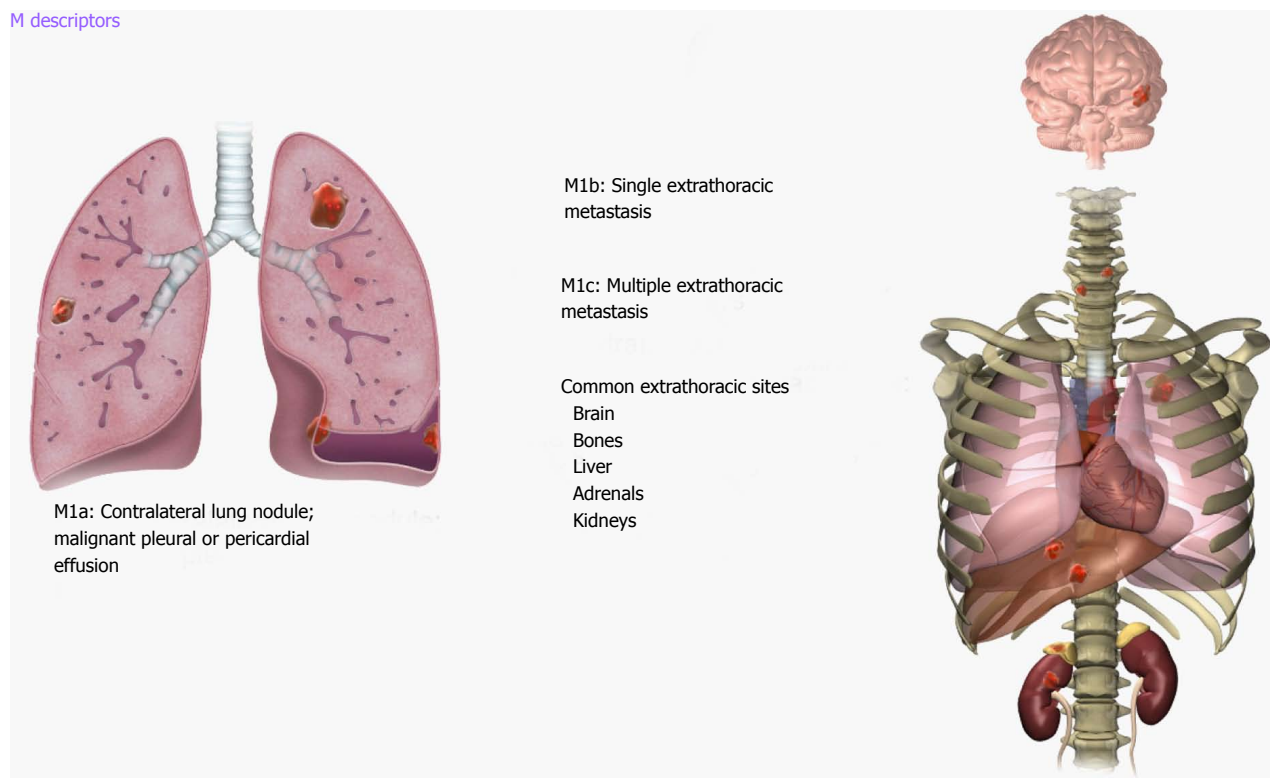


Figure 8 Illustrations demonstrating M descriptors.

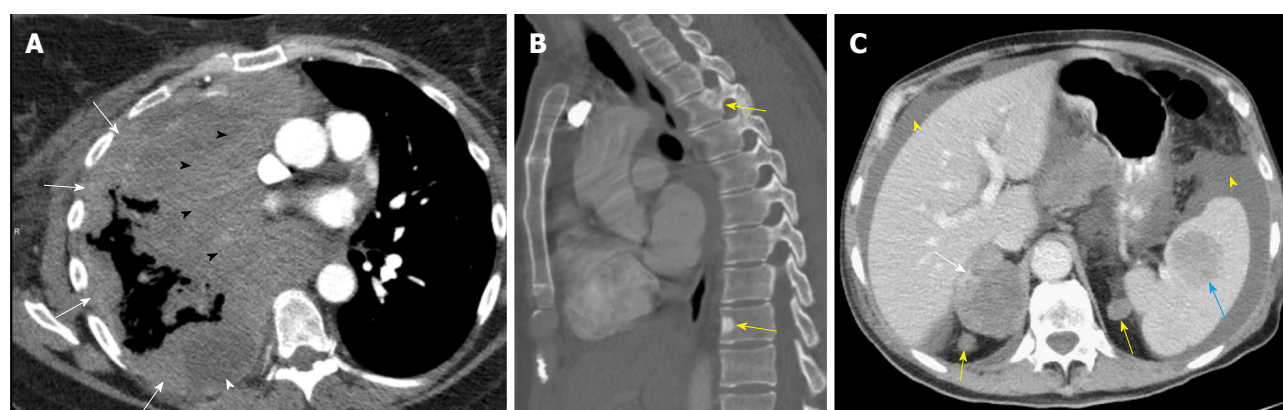


Figure 9 M descriptors. A: M1a: Nodular large heterogeneously enhancing right pleural mass like thickening (arrows) with mediastinal invasion (black arrowheads) and small right pleural effusion (white arrowhead) due to metastatic NSCLC; B: M1c: Two sclerotic metastases to thoracic spine (T3 and T9, arrows) from lung cancer; C: M1c: Multiple extrathoracic lung cancer metastases to the retroperitoneum (yellow arrows), right adrenal gland (white arrow), and spleen (blue arrow). Note the presence of malignant ascites (yellow arrowhead).

staging should be provided, with T3 descriptor used for lesions in the same lobe, T4 for ipsilateral lesions in different lobes, and M1a for contralateral lesions.

In patients with multiple groundglass lesions (lepidic tumors), the T descriptor is determined by the size and characteristics of the dominant abnormality. In this setting, the T descriptor can be listed with the total number of lesions indicated in parentheses^[20]. For example, a patient with three groundglass nodules, the largest measuring 1.4 cm, would be staged as cT1b(3), regardless of the location of the nodules (*i.e.*, same or different lobes). The *N/M* staging in this context refers to the whole set of lesions^[20].

Diffuse pneumonic-type lung cancer is categorized as T3 if in one lobe, T4 if involving multiple same-side lobes, and M1a if involving both lungs with a single *N* and *M* category for all areas of involvement.

Assessing tumor size

Specifications on how to measure the lesion size are clearly addressed in the data, although there is no clear mention about the imaging procedures that should be used to achieve this goal^[21,22]. In addition, some lesions with necrosis/cavitation, ill-defined margins, and post obstructive pneumonitis or radiation changes may create a challenge to the most experienced

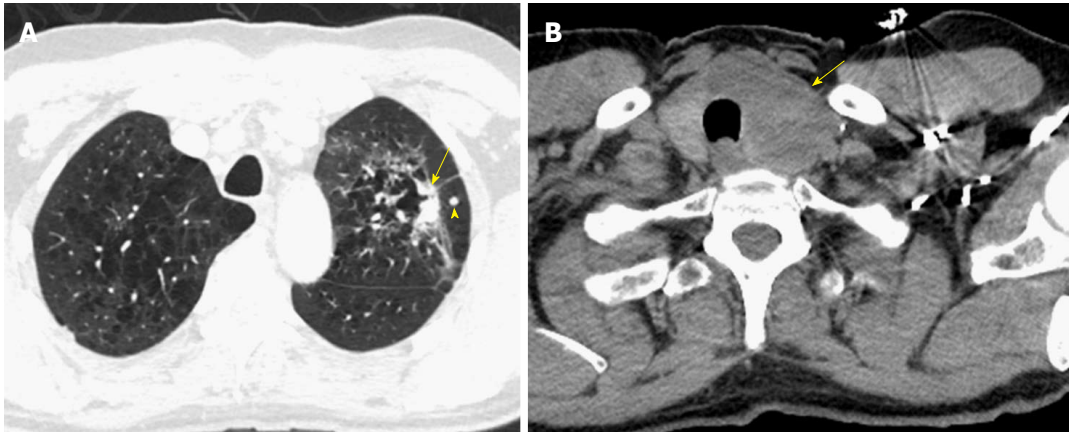


Figure 10 Challenging cases. A: A 65-year-old man with a non-calcified spiculated lesion in the left upper lobe in the region of confluent pulmonary emphysema. The lesion reveals markedly irregular shape, with the solid component measuring 2.5 cm on computed tomography (CT) (arrow), which would put the lesion in the cT1c category. A separate solid nodule in the same lobe (arrowhead) would upstage the tumor to cT3; B: CT images at the cervicothoracic junction revealed large left thyroid lobe mass (arrow). The analysis of the left lung upper lobectomy specimen revealed a 3.2 cm primary lung adenocarcinoma, with the second nodule in the thyroid representing a metastatic thyroid cancer (pT2a lung cancer).

reader^[22]. Figure 10 illustrates one challenging case for radiologists. Multiple parameters like slice-thickness, reconstruction settings, degree of inspiration, and other scanner parameters are known to affect the observed size, with significant inter and intra-observer variability for size measurements in smaller lesions^[23]. Automatic and semiautomatic 3D tools for assessing lesion size are more available, resulting in less variability^[24], and may guide future improvements in the TNM system.

For subsolid lesions, the maximum dimension of the solid component on imaging or the invasive component on microscopy is used to assign the T category^[21]. However, it is recommended that the maximum dimension of the groundglass or lepidic component be also noted.

Lymphangitis carcinomatosa

The pathologic changes seen in lymphangitis carcinomatosa are characterized by the infiltration of pulmonary lymphatics by malignant cells, usually presenting with symptoms of hypoxemia, with poor prognosis^[25]. The classic appearance on CT is thickening (smooth, irregular, or nodular) of the peribronchovascular and interlobular interstitium^[26]. Despite its potential prognostic information, lymphangitis carcinomatosa has not been added as a descriptor in neither the 7th nor the 8th TNM editions^[10,22].

Assessing number of nodes and other nodal chains

Although the N classification has not changed since the prior 7th edition, a significant limitation of the new IASLC lung cancer database must be mentioned. The anatomical location of lymph node involvement in the new database was defined by either the Naruke (for Japanese data) or Mountain-Dresler modification of the American Thoracic Society MDATS (for non-Japanese data) nodal charts, which are discrepant in the definition of subcarinal nodes. Naruke map considers subcarinal lymph nodes along the inferior border of the main stem

bronchus to be station 10 (N1), whereas MDATS map considers them station 7 (N2) nodes. Further validation of the unified nodal chart sponsored by IALSC^[15] must be pursued in the future.

In addition to the site analysis, another analysis was performed to determine the prognostic impact of adding the number of involved lymph node stations and presence of skip metastases to the present nodal categories. According to the number of involved lymph node stations (single vs multiple), *pN* categories were further subdivided: *N1* was divided into *N1*-single (*N1a*) and *N1*-multiple (*N1b*) and *N2* was divided into *N2*-single (*N2a*) and *N2*-multiple (*N2b*). *N2a* was further subdivided into single skip-metastatic *N2* node without *N1* involvement (*N2a1*) and single *N2* node with *N1* involvement (*N2a2*). Patients with *pN2* metastasis at a single lymph node station without hilar involvement (skip metastasis) had better survival than those with *pN1* metastasis at multiple stations. The number of involved nodal stations was found to have prognostic impact on pathologic staging, but was not validated in clinical staging.

There is lack of consensus in how to treat less common nodal sites of metastasis, such as internal thoracic, cardiophrenic, axillary, subpectoral, and extrathoracic chains. Some authors suggest that all chains not included in the N descriptors be considered as *M1* disease^[16,17], whereas others consider *N3* disease for specific sites (e.g., axillary chains)^[27]. Further clarification is thus necessary.

FUTURE DIRECTIONS

Metastatic disease

Although the new *M* descriptors evolved to distinguish single-site vs multiple-site metastasis, no detailed distinction is made based on the specific site or metastatic burden^[10]. However, IASLC made recommendation for recording ancillary information that may provide basis for future development, including the number of

metastatic lesions, diameter of individual metastatic lesions, and number of involved organs. Moreover, recording the histologic confirmation and/or standard uptake values from 18-FDG PET/CT of metastatic sites is also suggested for future analysis^[17].

Imaging standardization

Specific efforts to standardize imaging acquisition and interpretation protocols are necessary for improving efficacy, reproducibility, and communication of radiologic results. Pathways mapped by other radiology-led programs, such as lung cancer screening^[28], may provide future directions in lung cancer staging to be followed by radiologic societies.

CONCLUSION

The 8th edition of the TNM system for lung cancer staging consolidates and expands the base of evidence currently used for predicting prognosis and guiding patient treatment. As new stage groups are shown to demonstrate better precision for determining prognosis, it is expected that improvements in tailoring patient treatment will follow with adoption of the new staging system. It is of utmost importance that radiologists familiarize with the new system to provide accurate communication with referring physicians. Further collection of prospective data and detailed attention to unanswered questions will guide developments for future staging systems.

ACKNOWLEDGMENTS

The authors would like to acknowledge the contribution of Erin Moore, MA with illustrations for this manuscript.

REFERENCES

- 1 **Torre LA**, Siegel RL, Jemal A. Lung Cancer Statistics. *Adv Exp Med Biol* 2016; **893**: 1-19 [PMID: 26667336 DOI: 10.1007/978-3-319-24223-1_1]
- 2 **SEER NCI**. Cancer Stat Facts: Lung and Bronchus Cancer. 2016. Available from: URL: <https://seer.cancer.gov/statfacts/html/lungb.html>
- 3 **Ettinger DS**, Wood DE, Akerley W, Bazhenova LA, Borghaei H, Camidge DR, Cheney RT, Chirieac LR, D'Amico TA, Dilling TJ, Dobelbower MC, Govindan R, Hennon M, Horn L, Jahan TM, Komaki R, Lackner RP, Lanuti M, Lilenbaum R, Lin J, Loo BW, Martins R, Otterson GA, Patel JD, Pisters KM, Reckamp K, Riely GJ, Schild SE, Shapiro TA, Sharma N, Stevenson J, Swanson SJ, Tauer K, Yang SC, Gregory K, Hughes M. NCCN Guidelines Insights: Non-Small Cell Lung Cancer, Version 4.2016. *J Natl Compr Canc Netw* 2016; **14**: 255-264 [PMID: 26957612]
- 4 **Bierley JD**, Gospodarowicz MK, Wittekind C. TNM Classification of Malignant Tumours. 8th ed: Wiley, 2017
- 5 **Gospodarowicz MK**, Miller D, Groome PA, Greene FL, Logan PA, Sobin LH. The process for continuous improvement of the TNM classification. *Cancer* 2004; **100**: 1-5 [PMID: 14692017 DOI: 10.1002/cncr.11898]
- 6 **Mirsadraee S**, Oswal D, Alizadeh Y, Caulo A, van Beek E. The 7th lung cancer TNM classification and staging system: Review of the changes and implications. *World J Radiol* 2012; **4**: 128-134 [PMID: 22590666 DOI: 10.4329/wjr.v4.i4.128]
- 7 **Goldstraw P**, Crowley J, Chansky K, Giroux DJ, Groome PA, Rami-Porta R, Postmus PE, Rusch V, Sobin L. The IASLC Lung Cancer Staging Project: proposals for the revision of the TNM stage groupings in the forthcoming (seventh) edition of the TNM Classification of malignant tumours. *J Thorac Oncol* 2007; **2**: 706-714 [PMID: 17762336 DOI: 10.1097/JTO.0b013e31812f3c1a]
- 8 **Giroux DJ**, Rami-Porta R, Chansky K, Crowley JJ, Groome PA, Postmus PE, Rusch V, Sculier JP, Shepherd FA, Sobin L, Goldstraw P. The IASLC Lung Cancer Staging Project: data elements for the prospective project. *J Thorac Oncol* 2009; **4**: 679-683 [PMID: 19461401 DOI: 10.1097/JTO.0b013e3181a52370]
- 9 **Rami-Porta R**, Bolejack V, Giroux DJ, Chansky K, Crowley J, Asamura H, Goldstraw P. The IASLC lung cancer staging project: the new database to inform the eighth edition of the TNM classification of lung cancer. *J Thorac Oncol* 2014; **9**: 1618-1624 [PMID: 25436796 DOI: 10.1097/JTO.0000000000000334]
- 10 **Detterbeck FC**, Boffa DJ, Kim AW, Tanoue LT. The Eighth Edition Lung Cancer Stage Classification. *Chest* 2017; **151**: 193-203 [PMID: 27780786 DOI: 10.1016/j.chest.2016.10.010]
- 11 **Detterbeck FC**, Chansky K, Groome P, Bolejack V, Crowley J, Shemanski L, Kennedy C, Krasnik M, Peake M, Rami-Porta R. The IASLC Lung Cancer Staging Project: Methodology and Validation Used in the Development of Proposals for Revision of the Stage Classification of NSCLC in the Forthcoming (Eighth) Edition of the TNM Classification of Lung Cancer. *J Thorac Oncol* 2016; **11**: 1433-1446 [PMID: 27448762 DOI: 10.1016/j.jtho.2016.06.028]
- 12 **Walker CM**, Chung JH, Abbott GF, Little BP, El-Sherief AH, Shepard JA, Lanuti M. Mediastinal lymph node staging: from noninvasive to surgical. *AJR Am J Roentgenol* 2012; **199**: W54-W64 [PMID: 22733932 DOI: 10.2214/AJR.11.7446]
- 13 **Schimmer C**, Neukam K, Elert O. Staging of non-small cell lung cancer: clinical value of positron emission tomography and mediastinoscopy. *Interact Cardiovasc Thorac Surg* 2006; **5**: 418-423 [PMID: 17670605 DOI: 10.1510/icvts.2006.129478]
- 14 **Asamura H**, Chansky K, Crowley J, Goldstraw P, Rusch VW, Vansteenkiste JF, Watanabe H, Wu YL, Zielinski M, Ball D, Rami-Porta R. The International Association for the Study of Lung Cancer Lung Cancer Staging Project: Proposals for the Revision of the N Descriptors in the Forthcoming 8th Edition of the TNM Classification for Lung Cancer. *J Thorac Oncol* 2015; **10**: 1675-1684 [PMID: 26709477 DOI: 10.1097/JTO.0000000000000678]
- 15 **Rusch VW**, Asamura H, Watanabe H, Giroux DJ, Rami-Porta R, Goldstraw P. The IASLC lung cancer staging project: a proposal for a new international lymph node map in the forthcoming seventh edition of the TNM classification for lung cancer. *J Thorac Oncol* 2009; **4**: 568-577 [PMID: 19357537 DOI: 10.1097/JTO.0b013e3181a0d82e]
- 16 **El-Sherief AH**, Lau CT, Wu CC, Drake RL, Abbott GF, Rice TW. International association for the study of lung cancer (IASLC) lymph node map: radiologic review with CT illustration. *Radiographics* 2014; **34**: 1680-1691 [PMID: 25310423 DOI: 10.1148/rg.346130097]
- 17 **Eberhardt WE**, Mitchell A, Crowley J, Kondo H, Kim YT, Turrisi A, Goldstraw P, Rami-Porta R. The IASLC Lung Cancer Staging Project: Proposals for the Revision of the M Descriptors in the Forthcoming Eighth Edition of the TNM Classification of Lung Cancer. *J Thorac Oncol* 2015; **10**: 1515-1522 [PMID: 26536193 DOI: 10.1097/JTO.0000000000000673]
- 18 **Goldstraw P**, Chansky K, Crowley J, Rami-Porta R, Asamura H, Eberhardt WE, Nicholson AG, Groome P, Mitchell A, Bolejack V, International Association for the Study of Lung Cancer Staging and Prognostic Factors Committee, Advisory Boards, and Participating Institutions. The IASLC Lung Cancer Staging Project: Proposals for Revision of the TNM Stage Groupings in the Forthcoming (Eighth) Edition of the TNM Classification for Lung Cancer. *J Thorac Oncol* 2016; **11**: 39-51 [PMID: 26762738 DOI: 10.1016/j.jtho.2015.09.009]
- 19 **Nicholson AG**, Chansky K, Crowley J, Beyruti R, Kubota K, Turrisi A, Eberhardt WE, van Meerbeeck J, Rami-Porta R. The International Association for the Study of Lung Cancer Lung Cancer Staging Project: Proposals for the Revision of the Clinical and Pathologic Staging of Small Cell Lung Cancer in the Forthcoming Eighth Edition of the TNM Classification for Lung Cancer. *J Thorac Oncol* 2016; **11**: 300-311 [PMID: 26723244 DOI: 10.1016/j.jtho.2015.10.008]

- 20 **Detterbeck FC**, Marom EM, Arenberg DA, Franklin WA, Nicholson AG, Travis WD, Girard N, Mazzone PJ, Donington JS, Tanoue LT, Rusch VW, Asamura H, Rami-Porta R. The IASLC Lung Cancer Staging Project: Background Data and Proposals for the Application of TNM Staging Rules to Lung Cancer Presenting as Multiple Nodules with Ground Glass or Lepidic Features or a Pneumonic Type of Involvement in the Forthcoming Eighth Edition of the TNM Classification. *J Thorac Oncol* 2016; **11**: 666-680 [PMID: 26940527 DOI: 10.1016/j.jtho.2015.12.113]
- 21 **Travis WD**, Asamura H, Bankier AA, Beasley MB, Detterbeck F, Flieder DB, Goo JM, MacMahon H, Naidich D, Nicholson AG, Powell CA, Prokop M, Rami-Porta R, Rusch V, van Schil P, Yatabe Y. The IASLC Lung Cancer Staging Project: Proposals for Coding T Categories for Subsolid Nodules and Assessment of Tumor Size in Part-Solid Tumors in the Forthcoming Eighth Edition of the TNM Classification of Lung Cancer. *J Thorac Oncol* 2016; **11**: 1204-1223 [PMID: 27107787 DOI: 10.1016/j.jtho.2016.03.025]
- 22 **Carter BW**, Godoy MC, Wu CC, Erasmus JJ, Truong MT. Current Controversies in Lung Cancer Staging. *J Thorac Imaging* 2016; **31**: 201-214 [PMID: 27306388 DOI: 10.1097/RTI.0000000000000213]
- 23 **Brandman S**, Ko JP. Pulmonary nodule detection, characterization, and management with multidetector computed tomography. *J Thorac Imaging* 2011; **26**: 90-105 [PMID: 21508732 DOI: 10.1097/RTI.0b013e31821639a9]
- 24 **Petrick N**, Kim HJ, Clunie D, Borradaile K, Ford R, Zeng R, Gavrielides MA, McNitt-Gray MF, Lu ZQ, Fenimore C, Zhao B, Buckler AJ. Comparison of 1D, 2D, and 3D nodule sizing methods by radiologists for spherical and complex nodules on thoracic CT phantom images. *Acad Radiol* 2014; **21**: 30-40 [PMID: 24331262 DOI: 10.1016/j.acra.2013.09.020]
- 25 **Bruce DM**, Heys SD, Eremin O. Lymphangitis carcinomatosa: a literature review. *J R Coll Surg Edinb* 1996; **41**: 7-13 [PMID: 8930034]
- 26 **Munk PL**, Müller NL, Miller RR, Ostrow DN. Pulmonary lymphangitic carcinomatosis: CT and pathologic findings. *Radiology* 1988; **166**: 705-709 [PMID: 3340765 DOI: 10.1148/radiology.166.3.3340765]
- 27 **Nair A**, Klusmann MJ, Jogeessvaran KH, Grubnic S, Green SJ, Vlahos I. Revisions to the TNM staging of non-small cell lung cancer: rationale, clinicoradiologic implications, and persistent limitations. *Radiographics* 2011; **31**: 215-238 [PMID: 21257943 DOI: 10.1148/rg.311105039]
- 28 **McKee BJ**, Regis SM, McKee AB, Flacke S, Wald C. Performance of ACR Lung-RADS in a clinical CT lung screening program. *J Am Coll Radiol* 2015; **12**: 273-276 [PMID: 25176499 DOI: 10.1016/j.jacr.2014.08.004]

P- Reviewer: Tirumani SH, van Beek EJR **S- Editor:** Ji FF
L- Editor: A **E- Editor:** Wu HL



Retrospective Study

Cardiac magnetic resonance in patients with acute cardiac injury and unobstructed coronary arteries

Giovanni Salvatore Camastra, Stefano Sbarbati, Massimiliano Danti, Luca Cacciotti, Raffaella Semeraro, Sabino Walter Della Sala, Gerardo Ansalone

Giovanni Salvatore Camastra, Stefano Sbarbati, Massimiliano Danti, Luca Cacciotti, Raffaella Semeraro, Sabino Walter Della Sala, Gerardo Ansalone, Department of Cardiology and of Radiology M.G. Vannini Hospital, 00177 Roma, Italy

Author contributions: Camastra GS, Sbarbati S and Danti M performed the research and wrote the paper; Cacciotti L, Semeraro R, Della Sala SW and Ansalone G contributed to the analysis and supervised the report.

Institutional review board statement: This study was reviewed and approved by the Hospital review board. Ethics Committee approval is not requested for retrospective studies in our institution.

Informed consent statement: Patients were not required to give informed consent for participation in the study as the analyses used anonymous clinical data that were obtained after each patient agreed to treatment *via* written consent.

Conflict-of-interest statement: We have no financial relationship in disclosure.

Data sharing statement: No additional data are available.

Open-Access: This article is an open-access article which was selected by an in-house editor and fully peer-reviewed by external reviewers. It is distributed in accordance with the Creative Commons Attribution Non Commercial (CC BY-NC 4.0) license, which permits others to distribute, remix, adapt, build upon this work non-commercially, and license their derivative works on different terms, provided the original work is properly cited and the use is non-commercial. See: <http://creativecommons.org/licenses/by-nc/4.0/>

Manuscript source: Invited manuscript

Correspondence to: Giovanni Salvatore Camastra, MD, Department of Cardiology and of Radiology M.G. Vannini Hospital, via di acqua Bullicante 4, 00177 Roma, Italy. gcamastra@virgilio.it
Telephone: +39-062-4291386
Fax: +39-062-4291418

Received: January 4, 2017

Peer-review started: January 7, 2017

First decision: February 17, 2017

Revised: May 9, 2017

Accepted: May 18, 2017

Article in press: May 19, 2017

Published online: June 28, 2017

Abstract**AIM**

To define the role of cardiac magnetic resonance (CMR) by analyzing a particular group of patients with suspected acute coronary syndrome (ACS) and normal coronary angiogram.

METHODS

From January 2009 to December 2015, we examined 220 patients with clinical suspicion of ACS, Troponin elevation [the threshold used to define a positive Troponin T test (TnT) was 0.1 ng/mL] and no significant coronary disease at angiography (the patients were considered to have significant angiographic disease only a 50% stenosis was detected in any of their coronary arteries). The role of CMR with the late gadolinium enhancement was evaluated.

RESULTS

CMR was performed to 190 patients (86%) of this group which reveals: Myocarditis in 90 patients (47%); apical ballooning (Tako-Tsubo syndrome) in 32 patients (17%); myocardial infarction (MI) in 40 patients (21%) and no clear diagnosis identified by CMR in 28 patients (15%). A comparison with previous studies was also made. Clinical and echocardiographic follow-ups were performed at 12 ± 2 mo and no major adverse cardiac events were revealed.

CONCLUSION

There is a group of patients with clinical suspicion of ACS displaying normal coronary angiograms. CMR was demonstrated to be a valuable tool in the differential diagnosis evaluation of myocarditis, apical ballooning and MI.

Key words: Magnetic resonance; Acute coronary syndrome; Troponin; Myocarditis; Coronary angiography

© The Author(s) 2017. Published by Baishideng Publishing Group Inc. All rights reserved.

Core tip: In some patients with suspected acute coronary syndrome and elevated Troponin, the subsequent coronary angiography reveals normal coronaries. These patients represent an obscure and difficult field of diagnosis and investigation. There are several potential causes of this uncertainty, such as myocardial infarction with a recanalized coronary artery, myocarditis, different cardiomyopathies, and other rare conditions. Cardiac magnetic resonance offers a new and more appropriate method in distinguishing between different chest pain etiologies.

Camastra GS, Sbarbati S, Danti M, Cacciotti L, Semeraro R, Della Sala SW, Ansalone G. Cardiac magnetic resonance in patients with acute cardiac injury and unobstructed coronary arteries. *World J Radiol* 2017; 9(6): 280-286 Available from: URL: <http://www.wjgnet.com/1949-8470/full/v9/i6/280.htm> DOI: <http://dx.doi.org/10.4329/wjr.v9.i6.280>

INTRODUCTION

Troponin can accurately predict the presence of acute coronary syndrome (ACS) in patients with coronary artery disease (CAD) and is usually used in the risk assessment of patients presenting acute chest pain. In some patients with chest pain and an elevated Troponin, the subsequent Coronary Angiography reveals normal coronaries or some un-obstructed coronary arteries (defined as a < 50% stenosis in the main and side branch arteries). Previous reports have shown a prevalence of patients with suspected ACS and normal coronary arteries of 2.6%-12%^[1-3].

These patients represent an obscure and difficult field of diagnosis and investigation^[4,5]. There are several potential causes of this uncertainty, such as myocardial infarction (MI) with a recanalized coronary artery^[6], myocarditis, different cardiomyopathies, aortic disease, pulmonary embolism, arrhythmias, valvular heart disease, sepsis, and other rare conditions. With the aim of establishing a different cause of the Troponin elevation, cardiac magnetic resonance (CMR) offers a new and more appropriate technique thanks to its ability in identifying areas of inflammation and fibrosis with high spatial resolution. Using a combination of available

sequences, CMR was shown to have a good ability in distinguishing between different etiologies of chest pain with elevated levels of Troponin and ECG modifications in cases such as acute infarction, myocarditis and other cardiomyopathies^[7]. We hypothesized that CMR offers an incremental diagnostic value in determining the underlying etiology of patients with clinical suspicion of ACS with regards to optimizing the pharmacological dosage and to define the appropriate therapy according to specific etiological diagnosis.

MATERIALS AND METHODS

Patient population

From January 2009 to December 2015, we selected 220 patients with new-onset chest pain, elevated Troponin and normal coronary arteries. The patients presented various ECGs which included ST elevation, ST depression, negative T wave, as well as normal ECGs. We assigned these patients to CMR in order to exclude MI and to provide an alternative diagnosis which would explain the clinical presentation. All CMR scans were performed at admission, and the average interval time between clinical presentation and the administration of CMR were 4 ± 2 d (range 1-14 d). A coronary angiogram was performed on all these patients. Thirty patients were excluded, seven of whom due to severe claustrophobia and twenty-three patients due to their cardiac history in cases such as myocarditis, MI, impaired left-ventricular (LV) function, pulmonary embolism or renal failure. The final number of patients included in our study was 190. Clinical and echocardiograph follow-ups were performed on all patients within 12 ± 2 mo.

CMR

CMR was performed by breath-hold using a 1.5-T MRI system (INTERA, Philips Medical Systems, Best, the Netherlands). Both cine and contrast-enhanced short-axis MRI images were detected at every 10 mm from base to apex with slice thickness of 8 mm. In plane-resolution 1.2 mm × 1.8 mm. Cine MRI was performed using a steady-state free-precession sequence (SSFP). T2 STIR was performed with the following parameters: repetition times 2 R-R intervals, slice thickness 8 mm. T2-weighted images were considered abnormal if increased signal was observed within the myocardium. Contrast MRI images were also obtained on average 10 to 15 min after a contrast injection, using a segmented Inversion Recovery-Gradient Echo (IR-GE) technique adjusting inversion time to null normal myocardium. The contrast dose [Magnevist (gadoteridol), Shering AG] was 0.1 mmol/kg. Endocardial and epicardial borders were outlined on the short axis cine images. The extension of the late gadolinium enhancement (LGE) was measured on the short-axis contrast images detecting the increased image intensity level ≥ 2 SD above the average of normal myocardium enhancement

Table 1 Demographic characteristics of the study group

Patient: 190
Age (median \pm SD) years: 50 \pm 20
Gender
Male 92 (48%)
Female 98 (52%)
ECG at presentation
Normal in 11 patients (6%)
ST-segment elevation in 130 patients (68%)
ST-segment depression in 40 patients (21%)
Negative T-waves in 9 patients (5%)
Mean time interval from presentation to CMR 4 \pm 2 d (median \pm SD); 1-14 d (range)

CMR: Cardiac magnetic resonance.

in order to define the abnormal contrast enhancement. The location of LE was classified in accordance with the AHA segmentation. Regional parameters were assessed using a model dividing each short axis into 6 circumferential segments. The extension of contrast enhancement and the left ventricular ejection fraction, were measured using the freely available software segment on the website (<http://segment.heiberg.se>)^[8]. The CMR studies were assessed by two independent observers.

Clinical data

Clinical data including clinical history, physical examination, Troponin levels, ECG recordings, transthoracic echocardiography and coronary angiography, overall were reviewed by a single experienced observer in order to include these patients to our study. The Troponin tests were performed at Vannini Hospital using an internal laboratory with normal range values and *measurement units*. A "false positive" of rising serum Troponin level, was considered in patients with a single Troponin rise followed by a second normal value within 24 h.

Statistical analysis

Continuous data were expressed as a mean SD. Categorical variables were respectively expressed as number and percentage. The statistical review of the study was performed by a biomedical statistician

RESULTS

Baseline characteristic

The average age of patients was 50 \pm 20 years and the gender prevalence was 52% female (98 patients), 48% male (Table 1). None of the patients had a previous history of MI or myocarditis or renal failure before presenting acute chest pain. About 94% of the cohort had an abnormal ECG at presentation, and ST-segment elevation being the most common abnormality. In particular ECG was: Normal in 11 patients, ST-segment elevation in 130 patients, ST-segment depression in 40 patients, while T-waves were negative in 9 patients. There was a low prevalence of cardiac risk factors. The

Table 2 Results

Tako-tsubo: 32 patients (17%)	LGE: Absent
Myocarditis: 90 patients (47%)	LGE: Epicardial or intramycocardial
Myocardial infarction: 40 patients (21%)	LGE: Subendocardial or transmural
No clear diagnosis: 28 patients (15%)	LGE: Absent

LGE: Late gadolinium enhancement.

average interval time between the presentation of chest pain to the CMR was 4 \pm 2 d (range 1-14 d).

CMR results

The T2-STIR-weighted images were performed to detect areas of high signal intensity which are compatible with myocardial edema^[9]. On the short-axis post-contrast images, the LGE enhancement patterns were classified as subendocardial, midwall, subepicardial, and transmural or any combination of these (Table 2). Areas of edema were detected in the same segments of late enhancement in all the patients. We found intramycocardial or subepicardial LGEs suggestive of myocarditis in 90 patients (47%); absence of LGEs with apical edema suggesting apical ballooning (Tako-Tsubo syndrome) in 32 patients (17%); subendocardial LGEs indicating MI in 40 patients (21%) and an absence of LGEs and edema in 28 patients (15%) with no clear diagnosis identified in the CMR.

DISCUSSION

Diagnosis was based on assessment of LV size, regional and global wall motion, and the presence and pattern of LGE. Our aim was to assess and to compare the LGE patterns caused by MI with other myocardial diseases that are not related to ischemic disease. The evidence of edema represents an additional value of LGE imaging in identifying the underlying etiology. In MI we have the subendocardial or transmural LGE. LGE in non-ischemic cardiomyopathy generally does not correspond to any particular coronary artery distribution and is located mostly in the mid-wall to subepicardial layer. The patients who presented areas of subendocardial and transmural LGE had a diagnosis of MI (Figure 1). With regards to cardiac inflammation (Myocarditis), the regional distribution of edema usually does not reflect the coronary perfusion areas and typically appears within a sub-epicardial distribution. In our study we found areas of edema in the same segments of late enhancement in all the patients. The presence of LGE in an area that does not correspond to any particular coronary artery distribution and is located mostly in the mid-wall to subepicardial layer correlates strongly with myocarditis in the correct clinical setting. Myocarditis lesions occur predominantly in the lateral free wall and originate from the epicardial layer of the ventricular wall. The patients who presented areas of subepicardial or intramycocardial LGEs were

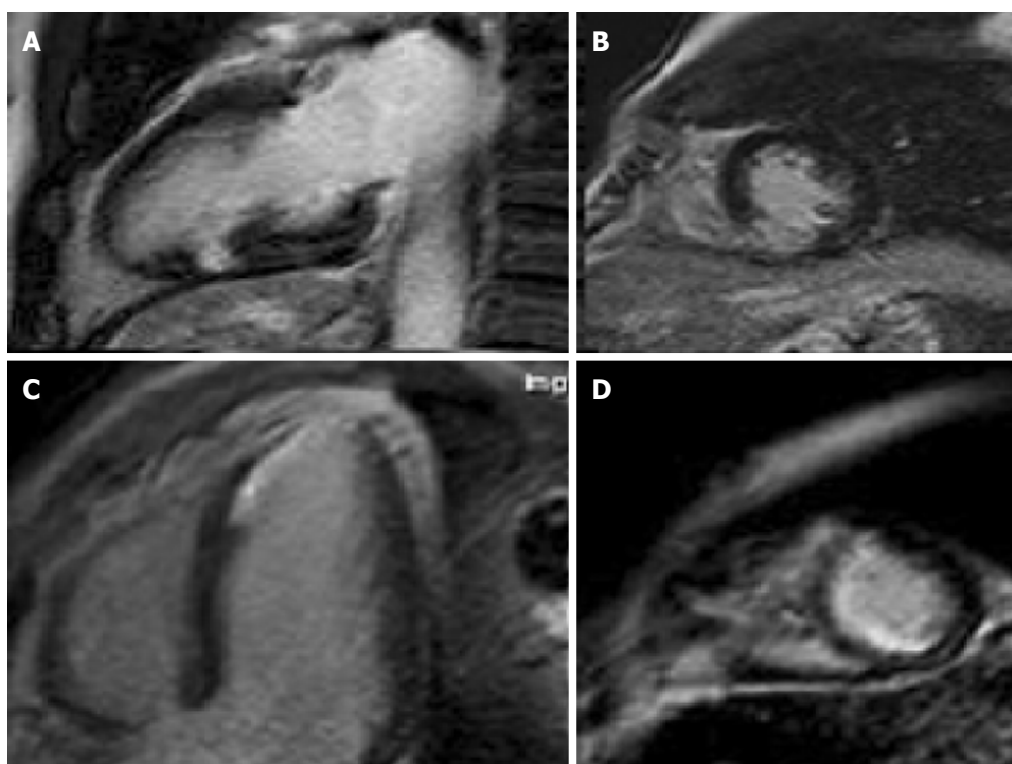


Figure 1 Cardiac magnetic resonance in myocardial infarction: Areas of subendocardial late gadolinium enhancement.

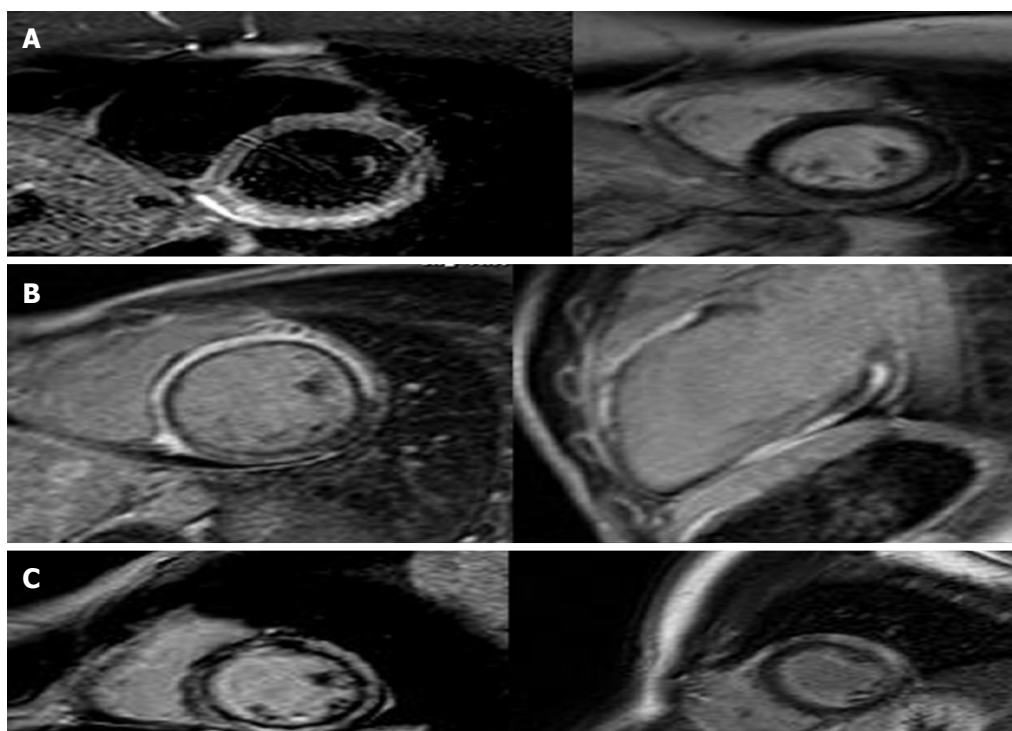


Figure 2 Cardiac magnetic resonance in myocarditis: (A) area of subepicardial edema (B-C) post contrast images show enhancement in the same area.

given a diagnosis of myocarditis (Figure 2)^[10-13]. The Tako-tsubo cardiomyopathy was characterized by a global apical and mid ventricular edema matching the distribution of LV dysfunction in the absence of LGE (Figure 3)^[14-16]. In these cases CMR provided a new

diagnosis in 85% of patients; the remaining patients had no detectable infarction or inflammation and no additional new diagnoses were made. MI was diagnosed in 21% of patients, while Myocarditis was diagnosed in 47%. We observed a peculiar distribution pattern of

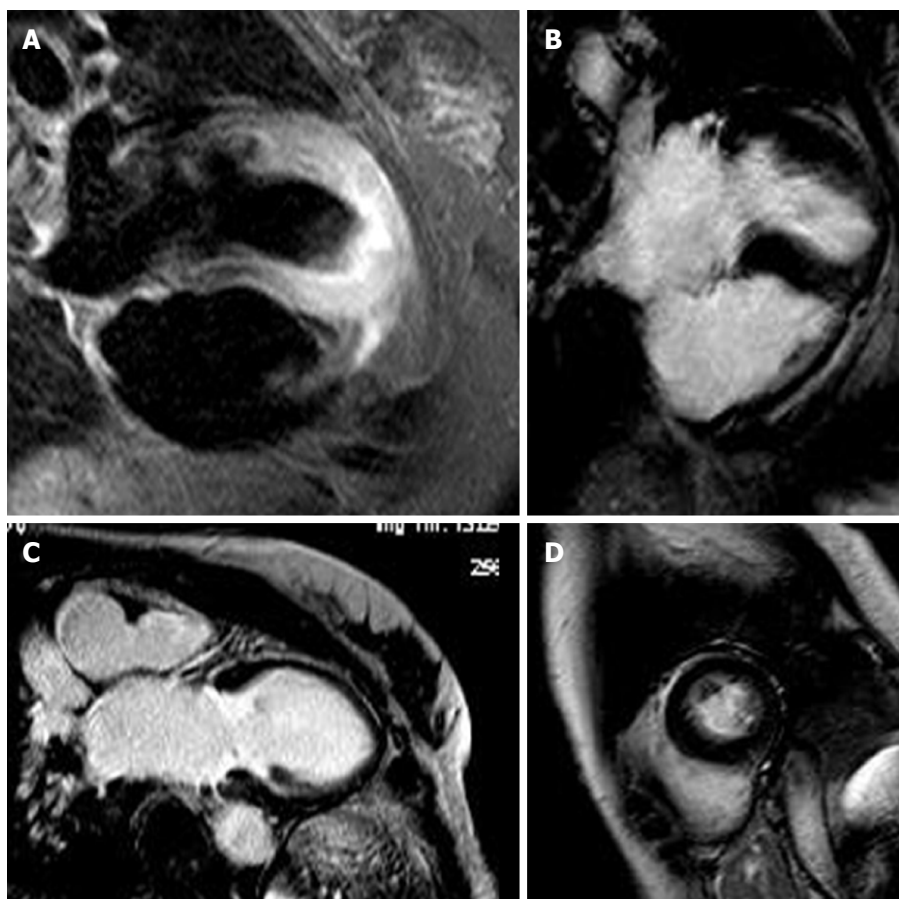


Figure 3 Cardiac magnetic resonance in apical ballooning: T2 images show edema in the apical segments (A), cine-MR shows akinesia (B: Diastole; C: Systole) in the same segments without (D) late gadolinium enhancement in the postcontrast images.

myocarditis lesions, as they always originate from the epicardial layer of the ventricular walls and moreover they are frequently located at the mid and distal portion of the lateral free wall. Patients with myocarditis are generally young men. In 32 patients with recent stress and minimal ST elevation in the anterior leads at the ECG, CMR revealed severe apical dysfunction with preserved basal LV function and no LGE, so a diagnosis of “Tako-tsubo” cardiomyopathy (apical ballooning) was made. This diagnosis was confirmed in the clinical and echocardiographic follow-ups which revealed a complete normalization of LV function. In 28 patients (15%) CMR did not reveal any structural or myocardial tissue abnormalities. In the follow-up examinations over a 1 year period adverse cardiac events were not detected. Echocardiography revealed complete recovery of contractility in patients with tako-tsubo syndrome and parameters remained unchanged in the remaining patients. We can affirm that an increase in Troponin usually reveals a myocardial necrosis. The great majority of patients presenting acute chest pain, elevated troponin levels and ECG abnormalities were correctly diagnosed and treated for ACS and therefore, coronary angiographies revealed significant coronary stenoses. On the other hand those patients with normal coronary angiography represented this study’s clinical challenge as there are a large number of other

reasons for Troponin elevation without obstructive CAD, such as Myocarditis, stress Cardiomyopathy, cardiac contusion, congestive heart failure, infarction and other non-cardiological causes. CMR has a potential role in evaluating the etiology of Troponin elevation, since it is able to provide detailed information on myocardial tissue characteristics, such that it has become the gold standard for *in vivo* detection of scarring associated with MI and other non-ischemic conditions. The high degree of CMR spatial resolution and contrast allows for the identification of very small areas of infarction. Our study demonstrates that CMR is able to identify the etiology of Troponin elevation in 85% of patients presenting ACS-like symptoms with normal coronary arteries. In this group the most common cause was Myocarditis (47%). Currently, no single clinical or imaging methods confirm a diagnosis of myocarditis with any certainty, thus requiring invasive diagnostic methods such as endomyocardial biopsy (EMB). However, EMB underestimates the true incidence of myocarditis and is not free of complications. EMB is currently indicated only in severe LV dysfunction or refractory arrhythmia and the patients in our study had no indications for EMB in accordance with therapeutic guidelines. In such patients, CMR appears to be suitable in identifying significant ongoing inflammation. We observed a peculiar distribution pattern of myocarditis lesions, with the lateral wall being

Table 3 Comparison with previous studies

Ref.	Year	No. of patients	Age of patients	Time from presentation to CMR (d)	Diagnosis				
					Infarction	Myocarditis	Tako-tsubo	Other	No diagnosis
[8]	2007	60	44 ± 17	1-90 (mean 14.5)	11.6%	50%	1.70%	1.70%	35%
[18]	2009	80	48	4	15%	63%	11%	5.50%	5.50%
[19]	2011	49	45 ± 14	1	0	29%	10%	43%	18%
[20]	2011	130	54 ± 17	6.2 ± 5.3	28.5%	26.1%	21.50%	0.80%	23.10%

CMR: Cardiac magnetic resonance.

the preferred location. The mechanism responsible for LGE has not been fully elucidated. In our series apical ballooning was detected in 17% of patients; it was diagnosed on the basis of cardiac symptoms and the presence of emotional stress. In these patients, the pattern of left ventricular dysfunction is characterized by apical and mid-ventricular contractile abnormalities, absence of LGE, minimal elevation of cardiac enzymes despite the presence of large regions of focal akinesia in the myocardium and finally the absence of coronary stenosis. Edema was present in myocardial segments with the most impaired function. MI was diagnosed in 21% of patients who presented areas of subendocardial and trans-mural LGE. The mechanism responsible for MI in these patients may be due to coronary artery spasm or coronary embolism. In a small percentage (15%) of cases with lower troponin levels it was impossible to evidence or to define a correct diagnosis. In the follow-up examination at 1 year, adverse cardiac events were not detected.

Comparison with previous studies

We reviewed the literature beginning from 2007 with the study of Assomull *et al.*^[7] regarding the role of CMR in patients with suspected ACS, raised Troponin and normal coronary arteries (Table 3). It is important to emphasize that most of these studies were single-center reports, had a small sample size and variable inclusion criteria. The CMR studies were performed at variable time points after the onset of disease and with non-uniform patient populations (age and gender). Our data are not in line with the previous study of Assomull *et al.*^[7] due to the high prevalence of Takotsubo cardiomyopathy (17% vs 1.7%) in our population, this difference is probably due to the gender differences of the two groups of patients (52% females in our group vs 28% females in Assomull's group). If we compare our results with the study of Laraudogoitia Zaldumbide *et al.*^[17] there are some similarities despite the gender differences of the two groups of patients (52% females in our group vs 19% females in Laraudogoitia's group). The Tako-tsubo cardiomyopathy predominantly affects women, while myocarditis predominantly affects men, thus explaining the variability reflected in the different studies, and the relatively lower frequency indicated in

our work. If we correlate this data by gender, the results would be more consistent. We must also consider the average age of different populations (higher in our group compared to the group of Assomull) that can explain the different prevalence of various diseases in our work because myocarditis is most common in young people and Takotsubo cardiomyopathy is more common in older women. In the study conducted by Stensaeth *et al.*^[18] MI was not detected, therefore, it is not possible to compare it with other studies. If we compare our results with the study of Gerbaud *et al.*^[19] we find a higher percentage of myocarditis (47% vs 26.1%) and a lower percentage of no diagnosis (15% vs 23.1%) in our patients. The review of literature reveals a great variability in the incidence of "no diagnosis" varying from 5.5% (Laraudogoitia) to 35% (Assomull). In our study, we found a average level of no diagnosis (15%).

Limitations

A limiting effect on our study was the small number of patients. It should be considered that CMR presents technical and procedural limitations in particular cases. In patients with irregular breathing patterns or significant arrhythmia, image quality may be reduced. The prognostic value of CMR was not analyzed. Another limitation is the lack of provocative tests for detecting coronary spasms and a lack of EMB although this is currently indicated only in severe LV dysfunction or refractory arrhythmia. None of the patients in our study had these features.

Conclusions

There are non-ischemic disorders that can present a similar clinical picture to ACS such as myocarditis or Tako-tsubo cardiomyopathy. CMR offers an incremental diagnostic value in determining the underlying etiology of patients with suspected ACS, with the aim of optimizing pharmacological therapy as well as in defining the correct therapy in accordance with a specific etiological diagnosis.

COMMENTS

Background

There are non-ischemic disorders that can present a similar clinical picture to acute coronary syndrome (ACS). In some patients with chest pain and an

elevated Troponin levels the subsequent coronary angiography reveals normal coronaries or some un-obstructed coronary arteries. These patients do not have a defined diagnosis and represent an obscure and difficult field of investigation.

Research frontiers

Cardiac magnetic resonance (CMR) with T2-STIR-weighted images can detect areas of myocardial edema and with late gadolinium enhancement (LGE) images can detect areas of myocardial necrosis related to an increase in troponin.

Innovations and breakthroughs

The patients who presented areas of subendocardial and transmural LGE were given a diagnosis of myocardial infarction while the patients who presented areas of subepicardial or intramyocardial LGE were given a diagnosis of myocarditis. In Tako-tsubo cardiomyopathy the pattern of edema was characterized by a global apical and mid ventricular edema matching the distribution of LV dysfunction in the absence of LGE.

Applications

CMR offers incremental diagnostic value in determining the underlying etiology of patients with suspected ACS.

Terminology

CMR: Cardiac magnetic resonance; LGE: Late gadolinium enhancement; ACS: Acute coronary syndrome.

Peer-review

The authors present an interesting study, investigating the differential diagnosis of patients with myocardial infarction and normal coronary arteries by CMR. The study seems to be well designed.

REFERENCES

- 1 **Kang WY**, Jeong MH, Ahn YK, Kim JH, Chae SC, Kim YJ, Hur SH, Seong IW, Hong TJ, Choi DH, Cho MC, Kim CJ, Seung KB, Chung WS, Jang YS, Rha SW, Bae JH, Cho JG, Park SJ. Are patients with angiographically near-normal coronary arteries who present as acute myocardial infarction actually safe? *Int J Cardiol* 2011; **146**: 207-212 [PMID: 19664828 DOI: 10.1016/j.ijcard.2009.07.001]
- 2 **Widimsky P**, Stellova B, Groch L, Aschermann M, Branny M, Zelizko M, Stasek J, Formanek P. Prevalence of normal coronary angiography in the acute phase of suspected ST-elevation myocardial infarction: experience from the PRAGUE studies. *Can J Cardiol* 2006; **22**: 1147-1152 [PMID: 17102833]
- 3 **Larsen AI**, Galbraith PD, Ghali WA, Norris CM, Graham MM, Knudtson ML. Characteristics and outcomes of patients with acute myocardial infarction and angiographically normal coronary arteries. *Am J Cardiol* 2005; **95**: 261-263 [PMID: 15642564 DOI: 10.1016/j.amjcard.2004.09.014]
- 4 **Kardasz I**, De Caterina R. Myocardial infarction with normal coronary arteries: a conundrum with multiple aetiologies and variable prognosis: an update. *J Intern Med* 2007; **261**: 330-348 [PMID: 17391108 DOI: 10.1111/j.1365-2796.2007.01788.x]
- 5 **Korff S**, Katus HA, Giannitsis E. Differential diagnosis of elevated troponins. *Heart* 2006; **92**: 987-993 [PMID: 16775113 DOI: 10.1136/hrt.2005.071282]
- 6 **Dokainish H**, Pillai M, Murphy SA, DiBattiste PM, Schweiger MJ, Lotfi A, Morrow DA, Cannon CP, Braunwald E, Lakkis N. Prognostic implications of elevated troponin in patients with suspected acute coronary syndrome but no critical epicardial coronary disease: a TACTICS-TIMI-18 substudy. *J Am Coll Cardiol* 2005; **45**: 19-24 [PMID: 15629367 DOI: 10.1016/j.jacc.2004.09.056]

- 7 **Assomull RG**, Lyne JC, Keenan N, Gulati A, Bunce NH, Davies SW, Pennell DJ, Prasad SK. The role of cardiovascular magnetic resonance in patients presenting with chest pain, raised troponin, and unobstructed coronary arteries. *Eur Heart J* 2007; **28**: 1242-1249 [PMID: 17478458 DOI: 10.1093/eurheartj/ehm113]
- 8 **Heiberg E**, Sjögren J, Ugander M, Carlsson M, Engblom H, Arheden H. Design and validation of Segment--freely available software for cardiovascular image analysis. *BMC Med Imaging* 2010; **10**: 1 [PMID: 20064248 DOI: 10.1186/1471-2342-10-1]
- 9 **Wince WB**, Kim RJ. Molecular imaging: T2-weighted CMR of the area at risk--a risky business? *Nat Rev Cardiol* 2010; **7**: 547-549 [PMID: 20865026 DOI: 10.1038/nrcardio.2010.124]
- 10 **Friedrich MG**, Strohm O, Schulz-Menger J, Marciniak H, Luft FC, Dietz R. Contrast media-enhanced magnetic resonance imaging visualizes myocardial changes in the course of viral myocarditis. *Circulation* 1998; **97**: 1802-1809 [PMID: 9603535 DOI: 10.1161/01.CIR.97.18.1802]
- 11 **Mahrholdt H**, Goedecke C, Wagner A, Meinhardt G, Athanasiadis A, Vogelsberg H, Fritz P, Klingel K, Kandolf R, Sechtem U. Cardiovascular magnetic resonance assessment of human myocarditis: a comparison to histology and molecular pathology. *Circulation* 2004; **109**: 1250-1258 [PMID: 14993139 DOI: 10.1161/01.CIR.000.00118493.13323.81]
- 12 **Camasta GS**, Cacciotti L, Marconi F, Sbarbati S, Pironi B, Ansalone G. Late enhancement detected by cardiac magnetic resonance imaging in acute myocarditis mimicking acute myocardial infarction: location patterns and lack of correlation with systolic function. *J Cardiovasc Med (Hagerstown)* 2007; **8**: 1029-1033 [PMID: 18163015 DOI: 10.2459/JCM.0b013e3281053a83]
- 13 **Danti M**, Sbarbati S, Alsadi N, Di Filippo A, Gangitano G, Giglio L, Salvini V, Amoroso M, Camasta GS, Ansalone G, Della Sala S. Cardiac magnetic resonance imaging: diagnostic value and utility in the follow-up of patients with acute myocarditis mimicking myocardial infarction. *Radiol Med* 2009; **114**: 229-238 [PMID: 19082782 DOI: 10.1007/s11547-008-0353-7]
- 14 **Mitchell JH**, Hadden TB, Wilson JM, Achari A, Muthupillai R, Flamm SD. Clinical features and usefulness of cardiac magnetic resonance imaging in assessing myocardial viability and prognosis in Takotsubo cardiomyopathy (transient left ventricular apical ballooning syndrome). *Am J Cardiol* 2007; **100**: 296-301 [PMID: 17631086 DOI: 10.1016/j.amjcard.2007.02.091]
- 15 **Camasta GS**, Cacciotti L, Kol A, Ansalone G. Stress cardiomyopathy with apical thrombosis promptly diagnosed with cardiovascular MRI. *Cardiology* 2006; **105**: 108-109 [PMID: 16352872 DOI: 10.1159/000090143]
- 16 **Cacciotti L**, Camasta GS, Beni S, Giannantonio P, Musarò S, Proietti I, De Angelis L, Semeraro R, Ansalone G. A new variant of Tako-tsubo cardiomyopathy: transient mid-ventricular ballooning. *J Cardiovasc Med (Hagerstown)* 2007; **8**: 1052-1054 [PMID: 18163020 DOI: 10.2459/JCM.0b013e32803cab4a]
- 17 **Laraudogoitia Zaldumbide E**, Pérez-David E, Larena JA, Velasco del Castillo S, Rumoroso Cuevas JR, Onaindia JJ, Lekuona Goya I, García-Fernández MA. The value of cardiac magnetic resonance in patients with acute coronary syndrome and normal coronary arteries. *Rev Esp Cardiol* 2009; **62**: 976-983 [PMID: 19712618]
- 18 **Stensaeth KH**, Fossum E, Hoffmann P, Mangschau A, Klow NE. Clinical characteristics and role of early cardiac magnetic resonance imaging in patients with suspected ST-elevation myocardial infarction and normal coronary arteries. *Int J Cardiovasc Imaging* 2011; **27**: 355-365 [PMID: 20652637 DOI: 10.1007/s10554-010-9671-7]
- 19 **Gerbaud E**, Harcaut E, Coste P, Erickson M, Lederlin M, Labèque JN, Perron JM, Cochet H, Dos Santos P, Durrieu-Jaïs C, Laurent F, Montaudon M. Cardiac magnetic resonance imaging for the diagnosis of patients presenting with chest pain, raised troponin, and unobstructed coronary arteries. *Int J Cardiovasc Imaging* 2012; **28**: 783-794 [PMID: 21538065 DOI: 10.1007/s10554-011-9879-1]

P- Reviewer: Korosoglou G, Lin GM **S- Editor:** Ji FF **L- Editor:** A
E- Editor: Wu HL



Observational Study

Chronic antiepileptic drug use and functional network efficiency: A functional magnetic resonance imaging study

Tamar M van Veenendaal, Dominique M IJff, Albert P Aldenkamp, Richard H C Lazeron, Paul A M Hofman, Anton J A de Louw, Walter H Backes, Jacobus F A Jansen

Tamar M van Veenendaal, Dominique M IJff, Albert P Aldenkamp, Paul A M Hofman, Walter H Backes, Jacobus F A Jansen, School for Mental Health and Neuroscience, Maastricht University, 6200 MD, Maastricht, The Netherlands

Tamar M van Veenendaal, Paul A M Hofman, Walter H Backes, Jacobus F A Jansen, Departments of Radiology and Nuclear Medicine, Maastricht University Medical Center, 6202 AZ, Maastricht, The Netherlands

Dominique M IJff, Albert P Aldenkamp, Richard H C Lazeron, Paul A M Hofman, Anton J A de Louw, Departments of Neurology and Neuropsychology, Epilepsy Center Kempenhaeghe, 5590 AB, Heeze, The Netherlands

Albert P Aldenkamp, Department of Neurology, Gent University Hospital, 9000 Gent, Belgium

Albert P Aldenkamp, Anton J A de Louw, Department of Neurology, Maastricht University Medical Center, 6202 AZ, Maastricht, The Netherlands

Albert P Aldenkamp, Anton J A de Louw, Faculty of Electrical Engineering, University of Technology Eindhoven, 5600 MB, Eindhoven, The Netherlands

Author contributions: Aldenkamp AP, Lazeron RHC, Backes WH and Jansen JFA designed to research; IJff DM and Lazeron RHC included patients; van Veenendaal TM and IJff DM performed the research; van Veenendaal TM, IJff DM, Hofman PAM, de Louw AJA, Backes WH and Jansen JFA analyzed the data; van Veenendaal TM, Backes WH and Jansen JFA wrote the paper.

Institutional review board statement: This observational study was reviewed and approved by the Medical Ethical Committee of Maastricht University Medical Center.

Informed consent statement: All study participants provided written informed consent prior to study enrollment.

Conflict-of-interest statement: There are no conflicts of interest to disclose for this study.

Data sharing statement: No additional data are available.

Open-Access: This article is an open-access article which was selected by an in-house editor and fully peer-reviewed by external reviewers. It is distributed in accordance with the Creative Commons Attribution Non Commercial (CC BY-NC 4.0) license, which permits others to distribute, remix, adapt, build upon this work non-commercially, and license their derivative works on different terms, provided the original work is properly cited and the use is non-commercial. See: <http://creativecommons.org/licenses/by-nc/4.0/>

Manuscript source: Invited manuscript

Correspondence to: Jacobus F A Jansen, PhD, Departments of Radiology and Nuclear Medicine, Maastricht University Medical Center, PO Box 5800, 6202 AZ, Maastricht, The Netherlands. jacobus.jansen@mumc.nl
Telephone: +31-043-3874908
Fax: +31-043-3876909

Received: October 15, 2016

Peer-review started: October 19, 2016

First decision: January 16, 2017

Revised: February 24, 2017

Accepted: March 23, 2017

Article in press: March 24, 2017

Published online: June 28, 2017

Abstract

AIM

To increase our insight in the neuronal mechanisms underlying cognitive side-effects of antiepileptic drug (AED) treatment.

METHODS

The relation between functional magnetic resonance-acquired brain network measures, AED use, and cognitive function was investigated. Three groups of

patients with epilepsy with a different risk profile for developing cognitive side effects were included: A "low risk" category (lamotrigine or levetiracetam, $n = 16$), an "intermediate risk" category (carbamazepine, oxcarbazepine, phenytoin, or valproate, $n = 34$) and a "high risk" category (topiramate, $n = 5$). Brain connectivity was assessed using resting state functional magnetic resonance imaging and graph theoretical network analysis. The Computerized Visual Searching Task was used to measure central information processing speed, a common cognitive side effect of AED treatment.

RESULTS

Central information processing speed was lower in patients taking AEDs from the intermediate and high risk categories, compared with patients from the low risk category. The effect of risk category on global efficiency was significant ($P < 0.05$, ANCOVA), with a significantly higher global efficiency for patient from the low category compared with the high risk category ($P < 0.05$, *post-hoc* test). Risk category had no significant effect on the clustering coefficient (ANCOVA, $P > 0.2$). Also no significant associations between information processing speed and global efficiency or the clustering coefficient (linear regression analysis, $P > 0.15$) were observed.

CONCLUSION

Only the four patients taking topiramate show aberrant network measures, suggesting that alterations in functional brain network organization may be only subtle and measureable in patients with more severe cognitive side effects.

Key words: Antiepileptic drugs; Cognitive side effects; Brain networks; Resting state; Functional magnetic resonance imaging; Graph analysis

© **The Author(s) 2017.** Published by Baishideng Publishing Group Inc. All rights reserved.

Core tip: Slowed information processing is a commonly observed cognitive side-effect of antiepileptic drug (AED) treatment. We aimed to increase our insight in the neuronal mechanisms underlying this side-effect. Therefore, the relation between functional MR-acquired brain network measures, AED use, and cognitive function was investigated. No associations were found between information processing speed and graph measures, and only the four patients taking topiramate (with a high risk on cognitive side effects) showed aberrant network measures. The results suggest that alterations in functional brain network organization may be only subtle and measureable in patients with more severe cognitive side effects.

van Veenendaal TM, IJff DM, Aldenkamp AP, Lazeron RHC, Hofman PAM, de Louw AJA, Backes WH, Jansen JFA. Chronic antiepileptic drug use and functional network efficiency: A functional magnetic resonance imaging study. *World J Radiol* 2017; 9(6): 287-294 Available from: URL: <http://www.wjgnet.com>

com/1949-8470/full/v9/i6/287.htm DOI: <http://dx.doi.org/10.4329/wjcr.v9.i6.287>

INTRODUCTION

Epilepsy is generally treated with antiepileptic drugs (AEDs). A persistent problem in AED treatment is the occurrence of adverse events among which cognitive side effects are commonly seen^[1,2]. The cognitive side effects account for a high percentage of the disease burden^[3] and lead to early drug discontinuation^[4]. The prevalence and severity of the cognitive side effects varies among different AEDs. Several AEDs, such as topiramate, are associated with cognitive problems such as language deficit (anomia), while other AEDs such as lamotrigine seem to induce less cognitive side effects or even have activating effects^[5]. Despite specific differences, a decreased central information processing speed is commonly observed among the different AEDs to some extent^[2].

AEDs control epileptic seizures *via* several distinct mechanisms, such as enhancement of GABAergic inhibition, reduction of glutamatergic neurotransmission, or modulation of the voltage-gated ion channels^[6]. Changes in brain metabolic processes also affect healthy brain activity, and are likely to be responsible for cognitive side effects^[1]. Functional magnetic resonance imaging (fMRI) enables assessment of this brain activity, and can be employed to measure combined effects of different mechanism of action of AEDs^[7]. Several fMRI studies have shown altered brain activity patterns in healthy participants^[8] or patients with epilepsy^[9,10] treated with AEDs. For instance, altered brain activity patterns appeared to be associated with language impairments when taking topiramate^[11-13].

Cognitive functions are mediated by the concerted action of multiple and distributed brain regions. These brain regions show correlations of their fMRI time signals, which is commonly interpreted as functional connectivity. Collectively, these functional connections form a brain network, which can be analyzed and characterized using graph theoretical analysis. Brain networks appear to be efficient networks, characterized by a high functional segregation and integration, *i.e.*, different brain regions form densely interconnected groups, enabling specialized information processing, and also rapid communication between distributed brain regions. Several graph measures are available to quantify these characteristics^[14].

Cognitive performance has been associated with the efficiency of functional brain networks^[15,16], while impaired functional brain networks have been associated with cognitive decline in epilepsy^[17,18]. Furthermore, associations between drug load, cognition and graph measures were shown in one of these studies, although this was not the main focus of the current study^[17]. Another study associated the use of carbamazepine with altered graph measures when compared with

other AEDs, but did not investigate the relation with cognitive effects^[19]. In the current study, we aim to test whether chronic use of AEDs, associated with a high risk for cognitive side-effects, affects functional resting-state network measures differently than long-term use of AEDs associated with milder cognitive side-effects. Furthermore, we will test whether functional resting-state network measures are associated with impaired cognitive functioning.

MATERIALS AND METHODS

Patients

Three groups of patients with epilepsy were compared in this observational, cross-sectional study^[20]. These groups were subdivided based on the AEDs that were being used, in accordance with Samarasekera *et al.*^[21]. The first group, the low risk category, consisted of patients using lamotrigine or levetiracetam. Patients taking carbamazepine, oxcarbazepine, phenytoin, or valproate were included in the intermediate risk category, while the high risk category comprised patients taking topiramate. Patients on polytherapy took at most two different AEDs and were categorized according to their AED associated with the greatest cognitive risk. By including patients with AEDs from the three risk groups, a range in slowing of information processing speed is realized.

All patients were clinically diagnosed with localization-related epilepsy and aged between 18 and 70 years. The patients were recruited from our tertiary epilepsy referral center. Participants not eligible for MRI, because of metal implants, claustrophobia, or pregnancy, were excluded from this study. Furthermore, patients did not experience seizures at least 12 h prior to MRI. This study was approved by the local Medical Ethical Committee and all participants provided written informed consent.

Neuropsychological investigation

Cognitive functioning was assessed by two neuropsychological tasks. The Computerized Visual Searching Task (CVST) was used to measure visual (complex) information processing speed^[22]. Slowing of this central information processing speed is a common side effect of AEDs^[2], and therefore the CVST is considered to be sensitive for treatment effects^[23]. With the CVST, a centered grid is shown surrounded by 24 other grid patterns. Participants have to find the (only) grid identical to the centered one as fast as possible.

The Raven Standard Progressive Matrices was administered to assess global cognitive performance. This is a non-verbal reasoning test which gives an indication of fluid intelligence^[24]. Previous studies suggested that intelligence stays relatively unaffected by AEDs^[23].

Epilepsy severity

As several epilepsy related characteristics might affect functional brain networks^[25], a score was composed to account for these effects. This epilepsy severity score

was assessed in all patients and compared between the different risk categories. Epilepsy severity was characterized using a summarized score between zero and seven, composed by the sum of subscores for seizure type (tonic-clonic: 1, other: 0), previous occurrence of status epilepticus (yes: 1, no: 0), seizure-related injury (yes: 1, no: 0) and seizure frequency (seizure free: 0, yearly: 1, monthly: 2, weekly: 3, daily: 4).

MRI data acquisition

MRI data were acquired on a 3.0T MRI scanner equipped with an 8-channel head coil (Philips Achieva, Philips Medical Systems, Best, The Netherlands). The scanning protocol included resting-state functional MRI and a T1-weighted scan. Functional MRI data were acquired using whole-brain single-shot multi-slice echo planar imaging sequence sensitive to the blood-oxygen-level-dependent (BOLD) effect (195 volumes, 32 slices, in-plane resolution 2 mm × 2 mm, 4 mm thick slices, repetition time 2000 ms, echo time 35 ms, flip angle: 90°, acquisition time: 7 min). A 3D T1-weighted scan was acquired for anatomic reference (voxel size 1 mm × 1 mm × 1 mm, repetition time 8.3 ms, echo time 4.8 ms, inversion time 1022 ms, 180 slices, flip angle 8°, acquisition time 6 min).

Data preprocessing

Preprocessing of the functional images was performed using SPM8 (Wellcome Department of Cognitive Neurology, London, United Kingdom). The functional images were corrected for differences in slice timing and head movement, coregistered to the T1 image and spatially (FWHM 6 mm) and temporally filtered (band pass 0.01-0.1 Hz). The BOLD signal originating from the white matter and ventricles, which is assumed to reflect physiological noise^[26], and the six translation and rotation parameters obtained from the motion correction were deregressed from the BOLD signal.

The T1-weighted scan was parcellated into 82 cortical and subcortical brain regions using FreeSurfer v5.1.0 (The General Hospital Corporation, Boston MA, United States). Subsequently, a connectivity matrix was created by calculating the Pearson's correlation coefficient between the average (deregressed) BOLD time signal of each combination of two regions. Negative correlations were set to zero. The correlation values were thresholded, based on the average connectivity matrix, to obtain connectivity matrices with only the strongest connections. The number of included connections was varied, with sparsity levels ranging from 0 to 0.9 (0 is fully connected, whereas 1 indicates no connections).

Data analysis

The Brain Connectivity Toolbox^[14] was employed to compute graph measures for each individual connectivity matrix. The clustering coefficient and the characteristic path length are commonly used to characterize the functional segregation and integration, respectively. The

Table 1 Patient characteristics for the three risk categories¹

	Low risk (<i>n</i> = 16)	Intermediate risk (<i>n</i> = 34)	High risk (<i>n</i> = 5)
General			
Male/female	5/11 (31%/69%)	16/18 (47%/53%)	0/5 (0%/100%)
Age (yr) ²	39.5 ± 13.4	50.7 ± 12.5 ^a	42.4 ± 15.8
Educational level ³	5 (range 2-6)	5 (range 2-7)	5 (range 4-6)
Epilepsy-related			
Symptomatic/non-symptomatic epilepsy	2/14 (13/88%)	15/19 (44/56%)	0/5
Seizure frequency			
Weekly	0	1 (3%)	0
Monthly	4 (25%)	3 (9%)	0
Yearly	2 (13%)	6 (18%)	2 (40%)
Seizure free	10 (63%)	24 (71%)	3 (60%)
Years since epilepsy onset ²	22.7 ± 11.7	30.4 ± 13.4	26.8 ± 23.3
Epilepsy severity score ²	1.4 ± 0.8	1.2 ± 1.0	1.0 ± 0.7
AED-related			
Mono-/polytherapy	16/0	8/26 (24/77%) ^a	3/2 (60/40%) ^b
Medication type			
CBZ	0	17 (50%)	1 (20%)
LEV	7 (44%)	6 (18%)	0
LTG	9 (56%)	10 (29%)	1 (20%)
OXC	0	4 (12%)	0
PHT	0	16 (47%)	0
TPM	0	0	5 (100%)
VPA	0	7 (21%)	1 (20%)
Drug load ^{2,4}	1.3 ± 0.6	1.8 ± 0.7 ^a	1.2 ± 1.0

Differences between the risk groups were tested using a Fisher's exact test (gender, symptomatic epilepsy, number of different AEDs), a Mann-Whitney test (educational level, seizure frequency, epilepsy severity score), or a student's *t* test (all remaining variables). ^aIndicates significant differences between the low and intermediate risk category (*P* < 0.05); ^bIndicates differences between the low and high risk category (*P* < 0.05). ¹Low risk: Lamotrigine (LTG), levetiracetam (LEV); Intermediate risk: Valproate (VPA), carbamazepine (CBZ), oxcarbazepine (OXC) and phenytoin (PHT); High risk: Topiramate (TPM); ²Mean ± SD; ³Median (range). Scores are according to Verhage^[30], range 1 (did not finish primary school) to 7 (Master's degree); ⁴The drug load is defined as the ratio of the prescribed daily dose to the defined daily dose^[29]. AED: Antiepileptic drug.

clustering coefficient quantifies the fraction of a node's neighbor that is also connected to each other. The characteristic path length is defined as the average shortest distance (the inverse correlation coefficient) between all pairs of nodes. As, in sparse networks, a single weak connection can result in a large, or even infinite average path lengths, global efficiency was computed instead of characteristic path length, which avoids this effect by using inverse path lengths^[27]. One hundred null models of the connectivity matrices were computed by randomizing the connections of the original matrices, while preserving the degree and weight distribution^[28]. The graph measures were divided by the mean global efficiency and clustering coefficient of these null models, providing a normalized global efficiency (*E_g*) and clustering coefficient (*γ*).

Statistical analysis

To test whether the clustering coefficient and global efficiency differed between the risk categories, an analysis of covariance (ANCOVA) was applied with the graph measures as outcome, cognitive risk category as fixed factor and age as covariate. Associations with cognition were assessed with linear regression analysis, with CVST time as outcome, and *E_g* or *γ*, age, and the percentage correct answers in the Raven test as independent variables. To assess whether these results were affected by confounders, these analyses were

repeated with gender, epilepsy severity score, or drug load (ratio of prescribed daily dose to defined daily dose^[29]) added to the regression analyses as additional covariates. All statistical analyses were performed in MATLAB (version R2012b). *P* values lower than 0.05 were considered significant.

RESULTS

Patient characteristics

In total, 58 patients were included in this study. Three of these patients did not finish the procedures due to claustrophobia, resulting in 16 patients taking AEDs from the low risk category, 34 taking AEDs from the intermediate risk category, and 5 taking high risk AEDs. The age and drug load were significantly higher in the intermediate risk category than in the low risk category (Table 1). Also the number of patients on polytherapy was significantly higher in the intermediate risk category compared with the low risk category, while the high and low risk categories significantly differed in number of patients on polytherapy. The risk categories did not differ in gender distribution, educational level, or epilepsy severity.

Neuropsychological assessment

The results of the CVST and the Raven task are summarized in Table 2. The CVST reaction time was slower

Table 2 Results of the neuropsychological investigation, represented as mean \pm SD for each risk category

Risk category	Cognitive test results	
	CVST (s) ¹	Raven ²
Low risk	11.5 \pm 2.9	71.7% \pm 10.3%
Intermediate risk	15.7 \pm 6.4	73.2% \pm 10.1%
High risk	20.2 \pm 6.7	71.7% \pm 3.1%
P value ³	0.008	0.85

¹Mean reaction time on the Computerized Visual Searching Task (CVST)^[22].²Percentage correct answers on the Raven Standard Progressive Matrices^[24].³Tested with ANOVA.

than the normal range (range: 7.3 to 30.8 s, while the mean \pm SD was 10.3 \pm 4.1 s in normal population^[31]). A significant effect of risk category on CVST reaction time was observed, which remained significant when controlling for age, gender, and global cognitive level ($P = 0.009$, ANCOVA). Post-hoc tests showed significant differences in CVST between the low and intermediate risk category ($P = 0.035$, estimated adjusted mean difference 3.5 s), and between the low and high risk category ($P = 0.004$, adjusted mean difference 7.8 s). No significant differences were found between the percentage correct answers Raven scores of the different risk categories.

Network topology

Of the 55 included patients, seven were excluded from further analysis: One patient was excluded because of excessive head motion (maximum head movement of 8.0 mm, while the maximum head movement was below 1.5 mm in all other patients), one because of a deeper large lesion mass, and five patients were excluded because of a failure to automatically parcellate the cortex, due to cortical abnormalities. The analysis was therefore performed on 48 patients: 15 patients taking AEDs from the low-risk category, 29 patients taking AEDs from the intermediate risk category and 4 patients taking the high risk medication. The maximum head displacement did not differ between the three risk categories.

The functional networks were fully connected and showed small-world characteristics within the sparsity range 0.32-0.66 (which was defined as γ/λ significantly larger than one, with γ the normalized clustering coefficient, and λ the normalized characteristic path length). Only the sparsity levels within this range were considered for further analyses. The ANCOVA test revealed significant effects of risk category on Eg at most sparsities within this sparsity range (Figure 1). Post-hoc tests showed a significantly higher Eg for patients from the low category ($n = 14$) compared with the high risk category ($n = 4$), and for patients from the intermediate category ($n = 29$) compared with the high risk category ($n = 4$). Eg or γ did not differ significantly between patients from the low and intermediate risk categories ($P > 0.2$ at all sparsity levels), and no

significant associations were observed between γ or Eg and CVST time ($P > 0.15$ at all sparsity levels). Gender, epilepsy severity score, or drug load were not significantly associated with the γ , Eg , or CVST reaction time, and the results of these adjusted analyses were consistent with the results of the analyses without these additional covariates ($< 10\%$ change in effect size of the variable of interest).

DISCUSSION

The current study investigated whether patients taking AEDs with a different risk for cognitive side-effects have different functional brain topologies. To this end, we included epilepsy patients with chronic AED treatment with different risk profiles, *i.e.*, a low risk category, intermediate-risk, and high risk category. Furthermore, we assessed whether cognitive problems, in terms of a decreased central information processing speed, could be associated with the functional brain organization.

A higher global efficiency was shown in patients taking TPM ($n = 4$, the high risk category), compared with patients taking the low ($n = 14$) and intermediate risk AEDs ($n = 29$). The directionality of this difference is strikingly, as this result seems to contradict the cognitive side effects of TPM. The global efficiency is suggested to be particularly important for more complex cognitive tasks, for which different brain areas are involved^[32]. The "better" global efficiency in TPM users might however be interpreted as a compensatory mechanism, or could be explained by a "survivor effect". As patients with side effects are more likely to switch to other AEDs, it is likely that these patients are less vulnerable for cognitive problems. The higher global efficiency in the high-risk group might therefore reflect a lower susceptibility for cognitive side effects of these patients^[33,34]. However, these patients did have a lower processing speed compared with the other patients, which argues against this explanation and in favor of a compensatory mechanism.

No differences in graph measures were observed between the patients groups taking AEDs from the low and from the intermediate risk category. It is possible that the effects of TPM on brain organization are more pronounced compared with effects of other AEDs, but TPM can also have distinctive effects on brain organization. TPM is suggested to have a unique cognitive profile, with specific effects on verbal fluency. Moreover, it has multiple mechanisms of action, and both these mechanisms and its chemical structure differ from other AEDs^[35].

Furthermore, no associations were found between processing speed and graph measures, in contrast to a previous study that showed not only associations between intellectual decline and a lowered clustering coefficient in patients with epilepsy, but also with increasing drug load^[17]. The latter suggests that the intellectual decline (which was based on intelligence tests) was a side effect of the AED treatment, but

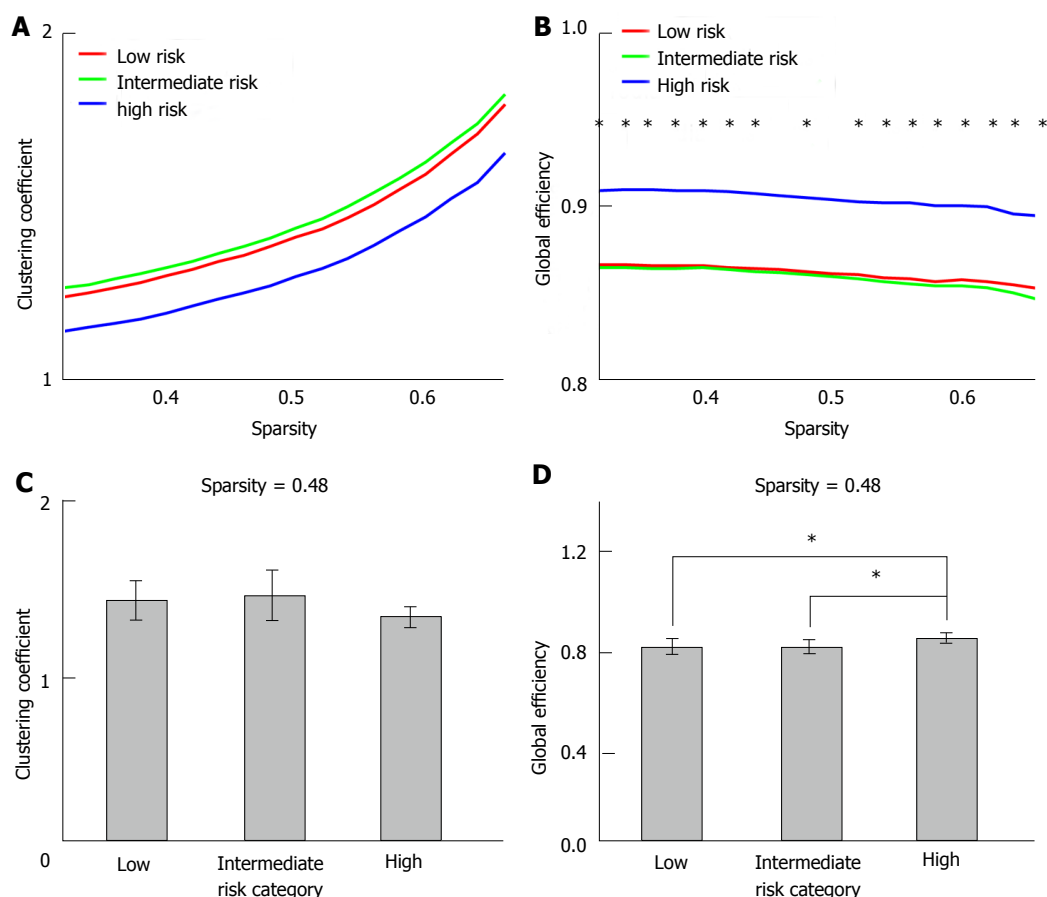


Figure 1 Mean clustering coefficient (A and C) and global efficiency (B and D) for each risk category. Both clustering coefficient and global efficiency are normalized, *i.e.*, the measures are divided by the clustering coefficient and global efficiency of random networks. A and B show the graph measures as a function of sparsity, while C and D show the results at a single sparsity level. Error bars show standard deviations, while the “*” indicate significant differences between the risk categories ($P < 0.05$, with age included as covariate).

this could also result from differences in epilepsy characteristics. That study included more patients with a high drug load (15% of the patients had a drug load higher than 3) than the current study (no drug loads higher than 3 in the included patients), thus it is possible that the effects on graph measures are only measureable in patients with higher drug loads or AEDs with high risks on cognitive complaints.

The measured information processing speed covered the whole range from normal to a clearly affected processing speed, and patients taking AEDs known to induce cognitive side effects, showed lower processing speeds than patients with lower risk AEDs. These results could therefore not explain the lack of associations between graph measures and information processing speed, or the lack of differences in graph measures between the low and intermediate risk category. Also no trends were shown, while the total number of participants (48), and the number of patients in the low (16) and intermediate risk categories (34) were relatively large, making it unlikely that this lack of findings were due to limited power.

All included patients in the current study were diagnosed with localization-related epilepsy. Epilepsy is associated with a decreased global efficiency and

increased clustering coefficient, although some studies showed a decreased clustering coefficient in patients with epilepsy^[36]. It is therefore plausible that the functional brain networks of all three groups of patients in this study were already altered compared with healthy participants, irrespective of AED treatment.

This study has several limitations. Although we tried to include comparable patient groups, the risk categories differed in age and drug load, suggesting that our study population is biased. Therefore, the analyses were corrected for these characteristics by including age and drug load as covariates. Besides these characteristics, also other factors could have confounded our results, such as the location of the epileptic focus or effects of AEDs on the neurovascular coupling, which should be assessed in separate studies^[37]. Finally, no information is available about changes over time and causality due to the cross-sectional design.

No differences in functional network graph measures could be detected between patients with epilepsy after chronic use of AEDs with a different risks on cognitive side effects. Only the four patients taking TPM, which has a high risk for developing cognitive side effects, showed a more efficient brain network topology, which might be a compensatory mechanism. Also no associations

were found between the graph measures and the measured cognitive impairments, specifically slowing of central information processing. Alterations in functional brain network organization may be only subtle and measureable in patients with more severe cognitive side-effects.

ACKNOWLEDGMENTS

The authors thank Berting R for his assistance with the image acquisition and Geerlings M and Slenter J for continuous hardware and software support.

COMMENTS

Background

A persistent problem in antiepileptic drug (AED) treatment is the occurrence of adverse events among which cognitive side effects are commonly seen. The prevalence and severity of the cognitive side effects varies among different AEDs, but a decreased central information processing speed is commonly observed among the different AEDs to some extent.

Research frontiers

Functional brain network analysis is being applied to study cognitive processes and cognitive problems.

Innovations and breakthroughs

This is the first study that specifically assessed the relation between functional brain network measures and cognitive problems in patients taking different types of AEDs.

Applications

To summarize the practical applications of your research findings, so that readers may understand the perspectives by which this study will affect the field and future research.

Terminology

AED: Antiepileptic drug; Clustering coefficient: Network measure; indication of segregation of a network; Global efficiency: Network measure; indication of integration of a network; CVST: Computerized Visual Searching Task; measures visual (complex) information processing speed.

Peer-review

The manuscript is well written.

REFERENCES

- 1 **Perucca P**, Gilliam FG. Adverse effects of antiepileptic drugs. *Lancet Neurol* 2012; **11**: 792-802 [PMID: 22832500 DOI: 10.1016/S1474-4422(12)70153-9]
- 2 **Ijff DM**, Aldenkamp AP. Cognitive side-effects of antiepileptic drugs in children. *Handb Clin Neurol* 2013; **111**: 707-718 [PMID: 23622218 DOI: 10.1016/B978-0-444-52891-9.00073-7]
- 3 **Helmstaedter C**, Aldenkamp AP, Baker GA, Mazarati A, Ryvlin P, Sankar R. Disentangling the relationship between epilepsy and its behavioral comorbidities - the need for prospective studies in new-onset epilepsies. *Epilepsy Behav* 2014; **31**: 43-47 [PMID: 24333577 DOI: 10.1016/j.yebeh.2013.11.010]
- 4 **Bootsma HP**, Ricker L, Hekster YA, Hulsman J, Lambrechts D, Majoie M, Schellekens A, de Krom M, Aldenkamp AP. The impact of side effects on long-term retention in three new antiepileptic drugs. *Seizure* 2009; **18**: 327-331 [PMID: 19110447 DOI: 10.1016/j.seizure.2008.11.006]
- 5 **Kwan P**, Brodie MJ. Neuropsychological effects of epilepsy and antiepileptic drugs. *Lancet* 2001; **357**: 216-222 [PMID: 11213111 DOI: 10.1016/S0140-6736(00)03600-x]
- 6 **Rogawski MA**, Löscher W. The neurobiology of antiepileptic drugs. *Nat Rev Neurosci* 2004; **5**: 553-564 [PMID: 15208697 DOI: 10.1038/nrn1430]
- 7 **van Veenendaal TM**, Ijff DM, Aldenkamp AP, Hofman PA, Vlooswijk MC, Rouhl RP, de Louw AJ, Backes WH, Jansen JF. Metabolic and functional MR biomarkers of antiepileptic drug effectiveness: A review. *Neurosci Biobehav Rev* 2015; **59**: 92-99 [PMID: 26475992 DOI: 10.1016/j.neubiorev.2015.10.004]
- 8 **Li X**, Ricci R, Large CH, Anderson B, Nahas Z, Bohning DE, George MS. Interleaved transcranial magnetic stimulation and fMRI suggests that lamotrigine and valproic acid have different effects on corticolumbic activity. *Psychopharmacology (Berl)* 2010; **209**: 233-244 [PMID: 20195575 DOI: 10.1007/s00213-010-1786-y]
- 9 **Jokeit H**, Okujava M, Woermann FG. Carbamazepine reduces memory induced activation of mesial temporal lobe structures: a pharmacological fMRI-study. *BMC Neurol* 2001; **1**: 6 [PMID: 11710962 DOI: 10.1186/1471-2377-1-6]
- 10 **Wandschneider B**, Stretton J, Sidhu M, Centeno M, Kozák LR, Symms M, Thompson PJ, Duncan JS, Koepp MJ. Levetiracetam reduces abnormal network activations in temporal lobe epilepsy. *Neurology* 2014; **83**: 1508-1512 [PMID: 25253743 DOI: 10.1212/WNL.0000000000000910]
- 11 **Jansen JF**, Aldenkamp AP, Marian Majoie HJ, Reijs RP, de Krom MC, Hofman PA, Eline Kooi M, Nicolay K, Backes WH. Functional MRI reveals declined prefrontal cortex activation in patients with epilepsy on topiramate therapy. *Epilepsy Behav* 2006; **9**: 181-185 [PMID: 16793345 DOI: 10.1016/j.yebeh.2006.05.004]
- 12 **De Ciantis A**, Muti M, Piccolini C, Principi M, Di Renzo A, De Ciantis R, Frondizi D, Iannone G, Ottaviano P, Piccirilli M. A functional MRI study of language disturbances in subjects with migraine headache during treatment with topiramate. *Neurol Sci* 2008; **29** Suppl 1: S141-S143 [PMID: 18545916 DOI: 10.1007/s10072-008-0906-5]
- 13 **Yasuda CL**, Centeno M, Vollmar C, Stretton J, Symms M, Cendes F, Mehta MA, Thompson P, Duncan JS, Koepp MJ. The effect of topiramate on cognitive fMRI. *Epilepsy Res* 2013; **105**: 250-255 [PMID: 23333471 DOI: 10.1016/j.eplepsyres.2012.12.007]
- 14 **Rubinov M**, Sporns O. Complex network measures of brain connectivity: uses and interpretations. *Neuroimage* 2010; **52**: 1059-1069 [PMID: 19819337 DOI: 10.1016/j.neuroimage.2009.10.003]
- 15 **van den Heuvel MP**, Stam CJ, Kahn RS, Hulshoff Pol HE. Efficiency of functional brain networks and intellectual performance. *J Neurosci* 2009; **29**: 7619-7624 [PMID: 19515930 DOI: 10.1523/JNEUROSCI.1443-09.2009]
- 16 **Giessing C**, Thiel CM, Alexander-Bloch AF, Patel AX, Bullmore ET. Human brain functional network changes associated with enhanced and impaired attentional task performance. *J Neurosci* 2013; **33**: 5903-5914 [PMID: 23554472 DOI: 10.1523/JNEUROSCI.4854-12.2013]
- 17 **Vlooswijk MC**, Vaessen MJ, Jansen JF, de Krom MC, Majoie HJ, Hofman PA, Aldenkamp AP, Backes WH. Loss of network efficiency associated with cognitive decline in chronic epilepsy. *Neurology* 2011; **77**: 938-944 [PMID: 21832213 DOI: 10.1212/WNL.0b013e31822cfc2f]
- 18 **Bonilha L**, Tabesh A, Dabbs K, Hsu DA, Stafstrom CE, Hermann BP, Lin JJ. Neurodevelopmental alterations of large-scale structural networks in children with new-onset epilepsy. *Hum Brain Mapp* 2014; **35**: 3661-3672 [PMID: 24453089 DOI: 10.1002/hbm.22428]
- 19 **Haneef Z**, Levin HS, Chiang S. Brain Graph Topology Changes Associated with Anti-Epileptic Drug Use. *Brain Connect* 2015; **5**: 284-291 [PMID: 25492633 DOI: 10.1089/brain.2014.0304]
- 20 **van Veenendaal TM**, Ijff DM, Aldenkamp AP, Lazeron RH, Puts NA, Edden RA, Hofman PA, de Louw AJ, Backes WH, Jansen JF. Glutamate concentrations vary with antiepileptic drug use and mental slowing. *Epilepsy Behav* 2016; **64**: 200-205 [PMID: 27744245 DOI: 10.1016/j.yebeh.2016.08.027]
- 21 **Samarasekera SR**, Helmstaedter C, Reuber M. Cognitive impairment in adults with epilepsy: The relationship between subjective and

- objective assessments of cognition. *Epilepsy Behav* 2015; **52**: 9-13 [PMID: 26398591 DOI: 10.1016/j.yebeh.2015.08.013]
- 22 **Aldenkamp AP**, Arends J, de la Parra NM, Migchelbrink EJ. The cognitive impact of epileptiform EEG discharges and short epileptic seizures: relationship to characteristics of the cognitive tasks. *Epilepsy Behav* 2010; **17**: 205-209 [PMID: 20056494 DOI: 10.1016/j.yebeh.2009.11.024]
- 23 **Grevers E**, Breuer LE, IJff DM, Aldenkamp AP. Mental slowing in relation to epilepsy and antiepileptic medication. *Acta Neurol Scand* 2016; **134**: 116-122 [PMID: 26918421 DOI: 10.1111/ane.12517]
- 24 **Raven J**, Raven JC, Court JH. Manual for Raven's Progressive Matrices and Vocabulary Scales. Section 3: The Standard Progressive Matrices. San Antonio, TX: Harcourt Assessment, 2000
- 25 **van Diessen E**, Diederens SJ, Braun KP, Jansen FE, Stam CJ. Functional and structural brain networks in epilepsy: what have we learned? *Epilepsia* 2013; **54**: 1855-1865 [PMID: 24032627 DOI: 10.1111/epi.12350]
- 26 **Murphy K**, Birn RM, Bandettini PA. Resting-state fMRI confounds and cleanup. *Neuroimage* 2013; **80**: 349-359 [PMID: 23571418 DOI: 10.1016/j.neuroimage.2013.04.001]
- 27 **Bullmore ET**, Bassett DS. Brain graphs: graphical models of the human brain connectome. *Annu Rev Clin Psychol* 2011; **7**: 113-140 [PMID: 21128784 DOI: 10.1146/annurev-clinpsy-040510-143934]
- 28 **Rubinov M**, Sporns O. Weight-conserving characterization of complex functional brain networks. *Neuroimage* 2011; **56**: 2068-2079 [PMID: 21459148 DOI: 10.1016/j.neuroimage.2011.03.069]
- 29 **Lammers MW**, Hekster YA, Keyser A, Meinardi H, Renier WO, van Lier H. Monotherapy or polytherapy for epilepsy revisited: a quantitative assessment. *Epilepsia* 1995; **36**: 440-446 [PMID: 7614920 DOI: 10.1111/j.1528-1157.1995.tb00484.x]
- 30 **Verhage F**. Intelligentie en leeftijd: Onderzoek bij Nederlanders van twaalf tot zevenenzeventig jaar. Assen: Van Gorcum, 1964
- 31 **Alpherts W**, Aldenkamp A. FePsy: the iron psyche. Heemstede: Instituut voor Epilepsiebestrijding, 1994
- 32 **Giessing C**, Thiel CM. Pro-cognitive drug effects modulate functional brain network organization. *Front Behav Neurosci* 2012; **6**: 53 [PMID: 22973209 DOI: 10.3389/fnbeh.2012.00053]
- 33 **Hahn A**, Kranz GS, Sladky R, Ganger S, Windischberger C, Kasper S, Lanzenberger R. Individual diversity of functional brain network economy. *Brain Connect* 2015; **5**: 156-165 [PMID: 25411715 DOI: 10.1089/brain.2014.0306]
- 34 **Santarnecchi E**, Rossi S, Rossi A. The smarter, the stronger: intelligence level correlates with brain resilience to systematic insults. *Cortex* 2015; **64**: 293-309 [PMID: 25569764 DOI: 10.1016/j.cortex.2014.11.005]
- 35 **Mula M**. Topiramate and cognitive impairment: evidence and clinical implications. *Ther Adv Drug Saf* 2012; **3**: 279-289 [PMID: 25083242 DOI: 10.1177/2042098612455357]
- 36 **van Diessen E**, Zweiphenning WJ, Jansen FE, Stam CJ, Braun KP, Otte WM. Brain Network Organization in Focal Epilepsy: A Systematic Review and Meta-Analysis. *PLoS One* 2014; **9**: e114606 [PMID: 25493432 DOI: 10.1371/journal.pone.0114606]
- 37 **Kida I**, Smith AJ, Blumenfeld H, Behar KL, Hyder F. Lamotrigine suppresses neurophysiological responses to somatosensory stimulation in the rodent. *Neuroimage* 2006; **29**: 216-224 [PMID: 16112588 DOI: 10.1016/j.neuroimage.2005.07.015]

P- Reviewer: Altamura C, Kilickesmez O, Razek AAKA

S- Editor: Ji FF **L- Editor:** A **E- Editor:** Wu HL





Published by **Baishideng Publishing Group Inc**
7901 Stoneridge Drive, Suite 501, Pleasanton, CA 94588, USA
Telephone: +1-925-223-8242
Fax: +1-925-223-8243
E-mail: bpgoffice@wjgnet.com
Help Desk: <http://www.f6publishing.com/helpdesk>
<http://www.wjgnet.com>



World Journal of *Radiology*

World J Radiol 2017 July 28; 9(7): 295-320





Editorial Board

2014-2017

The *World Journal of Radiology* Editorial Board consists of 365 members, representing a team of worldwide experts in radiology. They are from 36 countries, including Afghanistan (1), Argentina (2), Australia (5), Austria (7), Belgium (2), Brazil (8), Canada (6), Chile (1), China (43), Croatia (1), Denmark (4), Egypt (6), France (5), Germany (22), Greece (10), India (12), Iran (6), Ireland (2), Israel (3), Italy (47), Japan (13), Netherlands (1), New Zealand (1), Pakistan (1), Poland (2), Portugal (1), Serbia (1), Singapore (3), Slovakia (1), South Korea (18), Spain (4), Sweden (2), Switzerland (4), Thailand (1), Turkey (26), United Kingdom (11), and United States (82).

EDITORS-IN-CHIEF

Kai U Juergens, *Bremen*
Edwin JR van Beek, *Edinburgh*
Thomas J Vogl, *Frankfurt*

GUEST EDITORIAL BOARD MEMBERS

Wing P Chan, *Taipei*
Chung-Huei Hsu, *Taipei*
Chin-Chang Huang, *Taipei*
Tsong-Long Hwang, *Taoyuan*
Jung-Lung Hsu, *Taipei*
Chia-Hung Kao, *Taichung*
Yu-Ting Kuo, *Tainan*
Hon-Man Liu, *Taipei*
Hui-Lung Liang, *Kaohsiung*
Chun Chung Lui, *Kaohsiung*
Sen-Wen Teng, *Taipei*
Yung-Liang (William) Wan, *Taoyuan*

MEMBERS OF THE EDITORIAL BOARD



Afghanistan

Takao Hiraki, *Okayama*



Argentina

Patricia Carrascosa, *Vicente Lopez*
Maria C Ziadi, *Rosario*



Australia

Lourens Bester, *Sydney*
Gemma A Figtree, *Sydney*



Austria

Herwig R Cerwenka, *Graz*
Gudrun M Feuchtnner, *Innsbruck*
Benjamin Henninger, *Innsbruck*
Rupert Lanzenberger, *Vienna*
Shu-Ren Li, *Vienna*
Veronika Schopf, *Vienna*
Tobias De Zordo, *Innsbruck*



Belgium

Steve Majerus, *Liege*
Kathelijne Peremans, *Merelbeke*



Brazil

Clerio F Azevedo, *Rio de Janeiro*
Patrícia P Alfredo, *São Paulo*
Eduardo FC Fleury, *São Paulo*
Edward Araujo Júnior, *São Paulo*
Wellington P Martins, *Ribeirao Preto*
Ricardo A Mesquita, *Belo Horizonte*
Vera MC Salemi, *São Paulo*
Claudia Szobot, *Porto Alegre*
Lilian YI Yamaga, *São Paulo*



Canada

Marie Arsalidou, *Toronto*
Otman A Basir, *Waterloo*

Tarik Zine Belhocine, *Toronto*
James Chow, *Toronto*
Tae K Kim, *Toronto*
Anastasia Oikonomou, *Toronto*



China

Hong-Wei Chen, *Wuxi*
Feng Chen, *Hangzhou*
Jian-Ping Chu, *Guangzhou*
Guo-Guang Fan, *Shenyang*
Bu-Lang Gao, *Shijiazhuang*
Qi-Yong Gong, *Chengdu*
Ying Han, *Beijing*
Xian-Li Lv, *Beijing*
Yi-Zhuo Li, *Guangzhou*
Xiang-Xi Meng, *Harbin*
Yun Peng, *Beijing*
Jun Shen, *Guangzhou*
Ze-Zhou Song, *Hangzhou*
Wai Kwong Tang, *Hong Kong*
Gang-Hua Tang, *Guangzhou*
Jie Tian, *Beijing*
Lu-Hua Wang, *Beijing*
Xiao-bing Wang, *Xi'an*
Yi-Gen Wu, *Nanjing*
Kai Wu, *Guangzhou*
Hui-Xiong Xu, *Shanghai*
Zuo-Zhang Yang, *Kunming*
Xiao-Dan Ye, *Shanghai*
David T Yew, *Hong Kong*
Ting-He Yu, *Chongqing*
Zheng Yuan, *Shanghai*
Min-Ming Zhang, *Hangzhou*
Yudong Zhang, *Nanjing*
Dong Zhang, *Chongqing*
Wen-Bin Zeng, *Changsha*

Yue-Qi Zhu, *Shanghai*



Croatia

Goran Kusec, *Osijek*



Denmark

Poul E Andersen, *Odense*

Lars J Petersen, *Aalborg*

Thomas Z Ramsøy, *Frederiksberg*

Morten Ziebell, *Copenhagen*



Egypt

Mohamed F Bazeed, *Mansoura*

Mohamed Abou El-Ghar, *Mansoura*

Reem HA Mohamed, *Cairo*

Mohamed R Nouh, *Alexandria*

Ahmed AKA Razek, *Mansoura*

Ashraf A Zytoon, *Shebin El-Koom*



France

Sabine F Bensamoun, *Compiègne*

Romarc Loffroy, *Dijon*

Stephanie Nougaret, *Montpellier*

Hassane Oudadesse, *Rennes*

Vincent Vinh-Hung, *Fort-de-France*



Germany

Henryk Barthel, *Leipzig*

Peter Bannas, *Hamburg*

Martin Beeres, *Frankfurt*

Ilja F Ciernik, *Dessau*

A Dimitrakopoulou-Strauss, *Heidelberg*

Peter A Fasching, *Erlangen*

Andreas G Schreyer, *Regensburg*

Philipp Heusch, *Duesseldorf*

Sonja M Kirchhoff, *Munich*

Sebastian Ley, *Munich*

Adel Maataoui, *Frankfurt am Main*

Stephan M Meckel, *Freiburg*

Hans W Muller, *Duesseldorf*

Kay Raum, *Berlin*

Dirk Rades, *Luebeck*

Marc-Ulrich Regier, *Hamburg*

Alexey Surov, *Halle*

Martin Walter, *Magdeburg*

Axel Wetter, *Essen*

Christoph Zilkens, *Düsseldorf*



Greece

Panagiotis Antoniou, *Thessaloniki*

Nikos Efthimiou, *Athens*

Dimitris Karnabatidis, *Patras*

George Latsios, *Athens*

Stylianios Megremis, *Iraklion*

Alexander D Rapidis, *Athens*

Kiki Theodorou, *Larissa*

Ioannis A Tsalafoutas, *Athens*

Evanthia E Tripoliti, *Ioannina*

Athina C Tsili, *Ioannina*



India

Ritesh Agarwal, *Chandigarh*

Chandan J Das, *New Delhi*

Prathamesh V Joshi, *Mumbai*

Naveen Kalra, *Chandigarh*

Chandrasekharan Kesavadas, *Trivandrum*

Jyoti Kumar, *New Delhi*

Atin Kumar, *New Delhi*

Kaushala P Mishra, *Allahabad*

Daya N Sharma, *New Delhi*

Binit Sureka, *New Delhi*

Sanjay Sharma, *New Delhi*

Raja R Yadav, *Allahabad*



Iran

Majid Assadi, *Bushehr*

SeyedReza Najafizadeh, *Tehran*

Mohammad Ali Oghabian, *Tehran*

Amir Reza Radmard, *Tehran*

Ramin Sadeghi, *Mashhad*

Hadi Rokni Yazdi, *Tehran*



Ireland

Tadhg Gleeson, *Wexford*

Frederik JAI Vernimmen, *Cork*



Israel

Dafna Ben Bashat, *Tel Aviv*

Amit Gefen, *Tel Aviv*

Tamar Sella, *Jerusalem*



Italy

Adriano Alippi, *Rome*

Dante Amelio, *Trento*

Michele Anzidei, *Rome*

Filippo F Angileri, *Messinas*

Stefano Arcangeli, *Rome*

Roberto Azzoni, *San Donato milanese*

Tommaso V Bartolotta, *Palermo*

Tommaso Bartalena, *Imola*

Livia Bernardin, *San Bonifacio*

Federico Boschi, *Verona*

Sergio Casciaro, *Lecce*

Emanuele Casciani, *Rome*

Musa M Can, *Napoli*

Alberto Cuocolo, *Napoli*

Michele Ferrara, *Coppito*

Mauro Feola, *Fossano*

Giampiero Francica, *Castel Volturno*

Luigi De Gennaro, *Rome*

Giulio Giovannetti, *Pisa*

Francesca Iacobellis, *Napoli*

Formato Invernizzi, *Monza Brianza*

Francesco Lassandro, *Naples*

Lorenzo Livi, *Florence*

Pier P Mainenti, *Napoli*

Laura Marzetti, *Chieti*

Giuseppe Malinverni, *Crescentino*

Enrica Milanese, *Turin*

Giovanni Morana, *Treviso*

Lorenzo Monti, *Milan*

Silvia D Morbelli, *Genoa*

Barbara Palumbo, *Perugia*

Cecilia Parazzini, *Milan*

Stefano Pergolizzi, *Messina*

Antonio Pinto, *Naples*

Camillo Porcaro, *Rome*

Carlo C Quattrocchi, *Rome*

Alberto Rebonato, *Perugia*

Giuseppe Rizzo, *Rome*

Roberto De Rosa, *Naples*

Domenico Rubello, *Rovigo*

Andrea Salvati, *Bari*

Sergio Sartori, *Ferrara*

Luca M Sconfienza, *Milano*

Giovanni Storto, *Rionero*

Nicola Sverzellati, *Parma*

Alberto S Tagliafico, *Genova*

Nicola Troisi, *Florence*



Japan

Yasuhiko Hori, *Chiba*

Hidetoshi Ikeda, *Koriyama*

Masahito Kawabori, *Sapporo*

Tamotsu Kamishima, *Sapporo*

Hiro Kiyosue, *Yufu*

Yasunori Minami, *Osaka-sayama*

Yasuhiro Morimoto, *Kitakyushu*

Satoru Murata, *Tokyo*

Shigeki Nagamachi, *Miyazaki*

Hiroshi Onishi, *Yamanashi*

Morio Sato, *Wakayama Shi*

Yoshito Tsushima, *Maebashi*

Masahiro Yanagawa, *Suita*



Netherlands

Willem Jan van Rooij, *Tilburg*



New Zealand

W Howell Round, *Hamilton*



Pakistan

Wazir Muhammad, *Abbottabad*



Poland

Maciej S Baglaj, *Wroclaw*

Piotr Czauderna, *Gdansk*



Portugal

Joao Manuel RS Tavares, *Porto*



Serbia

Olivera Ciraj-Bjelac, *Belgrade*



Singapore

Gopinathan Anil, *Singapore*

Terence KB Teo, *Singapore*

Cher Heng Tan, *Singapore*



Slovakia

Stefan Sivak, *Martin*



South Korea

Ki Seok Choo, *Busan*

Seung Hong Choi, *Seoul*

Dae-Seob Choi, *Jinju*

Hong-Seok Jang, *Seoul*

Yong Jeong, *Daejeon*

Chan Kyo Kim, *Seoul*

Se Hyung Kim, *Seoul*

Joong-Seok Kim, *Seoul*

Sang Eun Kim, *Seongnam*

Sung Joon Kwon, *Seoul*

Jeong Min Lee, *Seoul*

In Sook Lee, *Busan*

Noh Park, *Goyang*

Chang Min Park, *Seoul*

Sung Bin Park, *Seoul*

Deuk Jae Sung, *Seoul*

Choongsoo Shin, *Seoul*

Kwon-Ha Yoon, *Iksan*



Spain

Miguel A De Gregorio, *Zaragoza*

Antonio Luna, *Jaén*

Enrique Marco de Lucas, *Santander*

Fernando Ruiz Santiago, *Granada*



Sweden

Dmitry Grishenkov, *Stockholm*

Tie-Qiang Li, *Stockholm*



Switzerland

Nicolau Beckmann, *Basel*

Christian Boy, *Bern*

Giorgio Treglia, *Bellinzona*

Stephan Ulmer, *Kiel*



Thailand

Sirianong Namwongprom, *Chiang Mai*



Turkey

Kubilay Aydin, *Istanbul*

Ramazan Akdemir, *Sakarya*

Serhat Avcu, *Ankara*

Ayşe Aralasmak, *Istanbul*

Oktay Algin, *Ankara*

Nevbahar Akcar, *Meselik*

Bilal Battal, *Ankara*

Zulkif Bozgeyik, *Elazig*

Nazan Ciledag, *Aakara*

Fuldem Y Donmez, *Ankara*

Gulgun Engin, *Istanbul*

Ahmet Y Goktay, *Izmir*

Oguzhan G Gumustas, *Bursa*

Kaan Gunduz, *Ankara*

Pelin Ozcan Kara, *Mersin*

Kivanc Kamburoglu, *Ankara*

Ozgur Kilickesmez, *Istanbul*

Furuzan Numan, *Istanbul*

Cem Onal, *Adana*

Ozgur Oztekin, *Izmir*

Seda Ozbek (Boruban), *Konya*

Selda Sarikaya, *Zonguldak*

Figen Taser, *Kutahya*

Baran Tokar, *Eskisehir*

Ender Uysal, *Istanbul*

Ensar Yekeler, *Istanbul*



United Kingdom

Indran Davagnanam, *London*

M DC Valdés Hernández, *Edinburgh*

Alan Jackson, *Manchester*

Suneil Jain, *Belfast*

Long R Jiao, *London*

Miltiadis Krokidis, *Cambridge*

Pradesh Kumar, *Liverpool*

Peter D Kuzmich, *Derby*

Georgios Plataniotis, *Brighton*

Vanessa Sluming, *Liverpool*



United States

Garima Agrawal, *Saint Louis*

James R Brasic, *Baltimore*

Rajendra D Badgaiyan, *Buffalo*

Ulas Bagci, *Bethesda*

Anat Biegon, *Stony Brook*

Ramon Casanova, *Winston Salem*

Wenli Cai, *Boston*

Zheng Chang, *Durham*

Corey J Chakarun, *Long Beach*

Kai Chen, *Los Angeles*

Hyun-Soon Chong, *Chicago*

Marco Cura, *Dallas*

Ravi R Desai, *Bensalem*

Delia DeBuc, *Miami*

Carlo N De Cecco, *Charleston*

Timm-Michael L Dickfeld, *Baltimore*

Subba R Digumarthy, *Boston*

Huy M Do, *Stanford*

Todd A Faasse, *Grand Rapids*

Salomao Faintuch, *Boston*

Girish M Fatterpekar, *New York*

Dhakshinamoorthy Ganesan, *Houston*

Robert J Griffin, *Little Rock*

Andrew J Gunn, *Boston*

Sandeep S Hedgire, *Boston*

Timothy J Hoffman, *Columbia*

Mai-Lan Ho, *San Francisco*

Juebin Huang, *Jackson*

Abid Irshad, *Charleston*

Matilde Inglese, *New York*

El-Sayed H Ibrahim, *Jacksonville*

Paul R Julsrud, *Rochester*

Pamela T Johnson, *Baltimore*

Ming-Hung Kao, *Tempe*

Sunil Krishnan, *Houston*

Richard A Komoroski, *Cincinnati*

Sandi A Kwee, *Honolulu*

King Kim, *Ft. Lauderdale*

Guozheng Liu, *Worcester*

Yiyan Liu, *Newark*

Venkatesh Mani, *New York*

Lian-Sheng Ma, *Pleasanton*

Rachna Madan, *Boston*

Zeyad A Metwalli, *Houston*

Yilong Ma, *Manhasset*

Hui Mao, *Atlanta*

Feroze B Mohamed, *Philadelphia*

Gul Moonis, *Boston*

John L Noshier, *New Brunswick*

Rahmi Oklu, *Boston*

Aytekun Oto, *Chicago*

Bishnuhari Paudyal, *Philadelphia*

Rajul Pandya, *Youngstown*

Chong-Xian Pan, *Sacramento*

Jay J Pillai, *Baltimore*

Neal Prakash, *Duarte*

Reza Rahbar, *Boston*

Ali S Raja, *Boston*

Gustavo J Rodriguez, *El Paso*

David J Sahn, *Portland*

Steven Schild, *Scottsdale*

Ali R Sepahdari, *Los Angeles*

Li Shen, *Indianapolis*

JP Sheehan, *Charlottesville*

Atul B Shinagare, *Boston*

Sarabjeet Singh, *Boston*

Charles J Smith, *Columbia*

Kenji Suzuki, *Chicago*

Monvadi Srichai-Parsia, *Washington*

Sree H Tirumani, *Boston*

Hebert A Vargas, *New York*

Sachit Verma, *Philadelphia*

Yoichi Watanabe, *Minneapolis*

Li Wang, *Chapel Hill*

Carol C Wu, *Boston*

Shoujun Xu, *Houston*

Min Yao, *Cleveland*

Xiaofeng Yang, *Atlanta*

Qingbao Yu, *Albuquerque*

Aifeng Zhang, *Chicago*

Chao Zhou, *Bethlehem*

Hongming Zhuang, *Philadelphia*

**MINIREVIEWS**

- 295 Interventional radiology treatment for pulmonary embolism
De Gregorio MA, Guirola JA, Lahuerta C, Serrano C, Figueredo AL, Kuo WT

ORIGINAL ARTICLE**Retrospective Study**

- 304 Incidental extravascular findings in computed tomographic angiography for planning or monitoring endovascular aortic aneurysm repair: Smoker patients, increased lung cancer prevalence?
Mazzei MA, Guerrini S, Gentili F, Galzerano G, Setacci F, Benevento D, Mazzei FG, Volterrani L, Setacci C

SYSTEMATIC REVIEWS

- 312 Preoperative [18]fluorodeoxyglucose-positron emission tomography/computed tomography in early stage breast cancer: Rates of distant metastases
Vinh-Hung V, Everaert H, Farid K, Djassemi N, Baudin-Veronique J, Bougas S, Michailovich Y, Joachim-Contaret C, Cécilia-Joseph E, Verschraegen C, Nguyen NP

ABOUT COVER

Editorial Board Member of *World Journal of Radiology*, Ozgur Oztekin, MD, Associate Professor, Radiology Department, Tepecik Research and Education Hospital, 35540 Izmir, Turkey

AIM AND SCOPE

World Journal of Radiology (*World J Radiol*, *WJR*, online ISSN 1949-8470, DOI: 10.4329) is a peer-reviewed open access academic journal that aims to guide clinical practice and improve diagnostic and therapeutic skills of clinicians.

WJR covers topics concerning diagnostic radiology, radiation oncology, radiologic physics, neuroradiology, nuclear radiology, pediatric radiology, vascular/interventional radiology, medical imaging achieved by various modalities and related methods analysis. The current columns of *WJR* include editorial, frontier, diagnostic advances, therapeutics advances, field of vision, mini-reviews, review, topic highlight, medical ethics, original articles, case report, clinical case conference (clinicopathological conference), and autobiography.

We encourage authors to submit their manuscripts to *WJR*. We will give priority to manuscripts that are supported by major national and international foundations and those that are of great basic and clinical significance.

INDEXING/ABSTRACTING

World Journal of Radiology is now indexed in PubMed, PubMed Central, and Emerging Sources Citation Index (Web of Science).

FLYLEAF

I-III Editorial Board

EDITORS FOR THIS ISSUE

Responsible Assistant Editor: *Xiang Li*
Responsible Electronic Editor: *Ya-Jing Lu*
Proofing Editor-in-Chief: *Lian-Sheng Ma*

Responsible Science Editor: *Fang-Fang Ji*
Proofing Editorial Office Director: *Jin-Lei Wang*

NAME OF JOURNAL
World Journal of Radiology

ISSN
ISSN 1949-8470 (online)

LAUNCH DATE
January 31, 2009

FREQUENCY
Monthly

EDITORS-IN-CHIEF
Kai U Juergens, MD, Associate Professor, MRT und PET/CT, Nuklearmedizin Bremen Mitte, ZEMODI - Zentrum für morphologische und molekulare Diagnostik, Bremen 28177, Germany

Edwin JR van Beek, MD, PhD, Professor, Clinical Research Imaging Centre and Department of Medical Radiology, University of Edinburgh, Edinburgh EH16 4TJ, United Kingdom

Thomas J Vogl, MD, Professor, Reader in Health Technology Assessment, Department of Diagnostic and Interventional Radiology, Johann Wolfgang Goethe University of Frankfurt, Frankfurt 60590,

Germany

EDITORIAL BOARD MEMBERS
All editorial board members resources online at <http://www.wjnet.com/1949-8470/editorialboard.htm>

EDITORIAL OFFICE
Xiu-Xia Song, Director
World Journal of Radiology
Baishideng Publishing Group Inc
7901 Stoneridge Drive, Suite 501, Pleasanton, CA 94588, USA
Telephone: +1-925-2238242
Fax: +1-925-2238243
E-mail: editorialoffice@wjnet.com
Help Desk: <http://www.f6publishing.com/helpdesk>
<http://www.wjnet.com>

PUBLISHER
Baishideng Publishing Group Inc
7901 Stoneridge Drive, Suite 501, Pleasanton, CA 94588, USA
Telephone: +1-925-2238242
Fax: +1-925-2238243
E-mail: bpgoffice@wjnet.com
Help Desk: <http://www.f6publishing.com/helpdesk>
<http://www.wjnet.com>

PUBLICATION DATE
July 28, 2017

COPYRIGHT
© 2017 Baishideng Publishing Group Inc. Articles published by this Open-Access journal are distributed under the terms of the Creative Commons Attribution Non-commercial License, which permits use, distribution, and reproduction in any medium, provided the original work is properly cited, the use is non commercial and is otherwise in compliance with the license.

SPECIAL STATEMENT
All articles published in journals owned by the Baishideng Publishing Group (BPG) represent the views and opinions of their authors, and not the views, opinions or policies of the BPG, except where otherwise explicitly indicated.

INSTRUCTIONS TO AUTHORS
<http://www.wjnet.com/bpg/gerinfo/204>

ONLINE SUBMISSION
<http://www.f6publishing.com>

Interventional radiology treatment for pulmonary embolism

Miguel A De Gregorio, Jose A Guirola, Celia Lahuerta, Carolina Serrano, Ana L Figueredo, William T Kuo

Miguel A De Gregorio, CIBER BBN - Bioengineering, Biomaterials and Nanomedicine [CIBER de Bioingeniería, Biomateriales y Nanomedicina (CIBER-BBN), Centro de Investigación Biomédica en Red] C/Monforte de Lemos 3-5, 28029 Madrid, Spain

Miguel A De Gregorio, Jose A Guirola, Celia Lahuerta, Carolina Serrano, Minimally Invasive Techniques Research Group (GITMI), Facultad de Medicina, 50009 Zaragoza, Spain

Ana L Figueredo, Department of Respiratory, Hospital Miguel Servet, 50009 Zaragoza, Spain

William T Kuo, Division of Vascular and Interventional Radiology, Department of Radiology, Stanford University Medical Center, Stanford, CA 94305, United States

Author contributions: All authors were involved in the planning the design and conduct of the review paper; each equally revises the manuscript and approve the final version; De Gregorio MA and Kuo WT conducted the initial research.

Conflict-of-interest statement: Miguel A De Gregorio, Jose A Guirola, Celia Lahuerta, Carolina Serrano, Ana L Figueredo and William T Kuo have no conflicts of interest or financial to disclose related to this review.

Open-Access: This article is an open-access article which was selected by an in-house editor and fully peer-reviewed by external reviewers. It is distributed in accordance with the Creative Commons Attribution Non Commercial (CC BY-NC 4.0) license, which permits others to distribute, remix, adapt, build upon this work non-commercially, and license their derivative works on different terms, provided the original work is properly cited and the use is non-commercial. See: <http://creativecommons.org/licenses/by-nc/4.0/>

Manuscript source: Invited manuscript

Correspondence to: Miguel A De Gregorio, MD, PhD, EBIR, FCIRSE, FSIR, Full Professor and Chairman of Interventional Radiology, Minimally Invasive Techniques Research Group (GITMI), Facultad de Medicina, Calle Domingo Miral s/n, 50009 Zaragoza, Spain. mgregori@unizar.es
Telephone: +34-976-765768
Fax: +34-976-765768

Received: January 19, 2017

Peer-review started: January 19, 2017

First decision: March 27, 2017

Revised: April 29, 2017

Accepted: May 18, 2017

Article in press: May 18, 2017

Published online: July 28, 2017

Abstract

Venous thromboembolism (VTE) is an illness that has a potentially life-threatening condition that affects a large percentage of the global population. VTE with pulmonary embolism (PE) is the third leading cause of death after myocardial infarction and stroke. In the first three months after an acute PE, there is an estimated 15% mortality among submassive PE, and 68% mortality in massive PE. Current guidelines suggest fibrinolytic therapy regarding the clinical severity, however some studies suggest a more aggressive treatment approach. This review will summarize the available endovascular treatments and the different techniques with its indications and outcomes.

Key words: Pulmonary embolism; Massive pulmonary embolism; Venous thromboembolism; Pulmonary embolism treatment; Submassive pulmonary embolism; Catheter directed therapy; Interventional radiology

© The Author(s) 2017. Published by Baishideng Publishing Group Inc. All rights reserved.

Core tip: Venous thromboembolism (VTE) is an illness that is potentially life-threatening condition that affects a large percentage of the global population. VTE is the third leading cause of death related with cardiovascular pathology after myocardial infarction and stroke. This article summarizes the clinical management and emphasizes which interventional treatments that exist and the most effective ones to treat massive and submassive pulmonary embolism.

De Gregorio MA, Guirola JA, Lahuerta C, Serrano C, Figueredo

AL, Kuo WT. Interventional radiology treatment for pulmonary embolism. *World J Radiol* 2017; 9(7): 295-303 Available from: URL: <http://www.wjgnet.com/1949-8470/full/v9/i7/295.htm> DOI: <http://dx.doi.org/10.4329/wjrr.v9.i7.295>

INTRODUCTION

Venous thromboembolism (VTE) is a life-threatening condition that affects a large percentage of the global population; VTE includes the deep vein thrombosis (DVT) and pulmonary embolism (PE). The incidence rate of VTE is 100 cases per 100000 inhabitants in Europe^[1] and 160 per 100000 inhabitants in the United States^[2]. VTE is the third leading cause of death after myocardial infarction and stroke. In the first three months after an acute PE, there is an estimated of 15% mortality among submassive PE, and 68% mortality in massive PE^[3]. Acute PE is also the leading cause of pulmonary hypertension and right ventricular failure^[4].

From the clinical point of view, two different situations need to be considered, prognosis and therapeutic management. For a massive PE there are three different treatments options: (1) systemic thrombolysis; (2) Surgical pulmonary embolectomy; and (3) Endovascular techniques^[5]. Other authors also advocate to implant an inferior vena cava filter (IVCF) in massive PE to prevent further thrombus migration and avoid higher thrombotic load or avoid anticoagulation therapy. According to the clinical guidelines of the American College of Chest Physicians (ACCP) an interventional approach, in an acute massive PE, currently is only considered the treatment of choice when a systemic thrombolysis therapy fails or is contraindicated^[6]; however other authors advocate the use of the following procedures: Catheter directed therapy (CDT), mechanical fragmentation, thrombectomy procedures as a more aggressive therapeutic management that can provide excellent results in a massive PE^[7-10]. Since there are a variety of CDT and thrombectomy methods, more prospective studies are still needed to refine the interventional approach protocol and determine the safest techniques in larger cohorts. This review will outline the different clinical presentation of PE, and will summarize the available endovascular treatments and the different techniques with its indications and outcomes.

TYPES AND DEFINITIONS OF PE

The two main subtypes of PE that are necessary to address are the submassive (intermediate risk) and massive PE (high risk). The most frequent clinical symptoms are dyspnea (82%) and chest pain (49%), but it can also present: Cough (20%), syncope(14%) and Hemoptysis (7%)^[3].

Massive PE is defined as an hemodynamically unstable condition which has clinical presentation with

low blood pressure (systolic pressure < 90 mmHg or a decrease of more than 40 mmHg in baseline systolic pressure) and may develop a cardiac arrest. Other clinical manifestations related to hypotension may be present, such as tissue hypoperfusion and hypoxemia^[11].

Submassive PE (intermediate risk) is defined as a hemodynamically stable condition (normal blood pressure) with a right ventricular dysfunction or elevated cardiac biomarkers which can develop a reduced workload and an increased strain on the heart^[5].

It should not be confused with the radiological definitions of "massive" PE in which the criteria are related to the quantity of thrombus within the pulmonary trunk or the arterial pulmonary branches instead of the clinical presentation of the PE. A "massive" PE, from the radiological point of view, is described as a reduction of lung perfusion in one lung (> 90%) or total occlusion of a main pulmonary artery diagnosed with a pulmonary CT angiography^[12].

Mortality in massive PE patients with hemodynamic shock can reach a 68% in the first hours after diagnosis^[13]. However In submassive PE the mortality is lower compared to a massive PE.

The American College of Chest Physicians in their guidelines differentiates the considered treatment for both situations^[6]. While in the massive PE, thrombolysis (Class II a, Level of Evidence B) is recommended as the first option, in a submassive PE the thrombolysis is controversial. Thrombolysis may be indicated in submassive PE with a poor prognosis (RV dysfunction, severe respiratory failure, myocardial necrosis) and low risk of bleeding (Class II b level of evidence C). In the rest, thrombolysis is not recommended (Class III, level of evidence B).

PATHOPHYSIOLOGY OF MASSIVE PE

The severity of a massive PE is directly related to the amount of thrombus occluding the pulmonary arteries and the underlying cardiopulmonary status of the patient, which causes hemodynamic instability^[14]. A significant obstruction of the pulmonary vascular bed produces hypoxemia and results in the release of potent vasoconstricting substances that further aggravate the systemic hypoxia, with an increase in pulmonary arterial resistance that can cause an elevated right ventricular afterload^[15]. Right ventricular overload produces hypokinesia and ventricular dilatation with tricuspid regurgitation; in which can eventually lead to right ventricular failure. Increased pressure in the right ventricle (RV) may cause alteration in the cardiac wall with ischemia or myocardial infarction due to an increase in the demand for oxygen and a decrease in the supply. In addition, stress on the myocardial wall along with systemic arterial hypotension decreases the perfusion to the coronary arteries, which can also lead to RV ischemia with or without infarction^[16]. All of

Table 1 Predictive factors of severity and 30-d mortality

Predictors of 30-d mortality
Cardiac failure
COPD
Systolic pressure < 100 mmHg
Age over 70 yr
Heart rate > 100 bpm
ECG signs of RV dysfunction
Elevated cardiac biomarkers (Troponins, BNP, H-FABP)
CT findings: RV enlargement
Echocardiography findings:
RV hypokinesis and dilatation
Deviation of the interventricular septum
Tricuspid regurgitation > 2.6 m/s
Loss of inspiratory collapse of the inferior vena cava
Patent foramen ovale

Modified from Pizza *et al*^[16]. COPD: Chronic obstructive pulmonary disease; bpm: Beat per minute; ECG: Electrocardiogram; BNP: Brain-type natriuretic peptide; H-FABP: Heart-type fatty acid-binding protein; RV: Right ventricle; CT: Computed tomography.

these changes may lead to RV failure, diminished left ventricular output and life-threatening hemodynamic shock^[13].

MASSIVE PE DIAGNOSIS

Clinical manifestations play an important role in the differential diagnosis between massive PE and non-massive PE. Hemodynamic instability with suspected PE (blood pressure < 90 mmHg) establishes the diagnosis of massive PE, while to diagnose a submassive PE it is essential to rule out right ventricular dysfunction by echocardiography and/or elevated cardiac biomarkers. Computed tomography pulmonary angiography (CTPA) should report the size of the thrombus and percentage of occlusion of the pulmonary arteries. The amount and size of the thrombus should not be used to differentiate between clinical massive and submassive PE. If the patient has a good pulmonary reserve, a massive embolism (high thrombotic load) does not always have an hemodynamic repercussion. CTPA also provides information on pulmonary vascular perfusion as well as other chest findings such as pleural effusion, pneumonic foci, neoplasia, *etc.* Finally CTPA can also describe RV failure by comparison of the diameter of the RV with the left ventricle (LV) and determine RV dilatation (RV/LV ratio > 1)^[17]. The main echocardiographic signs of submassive PE are RV dilation and septum deviation to the LV^[16,18]. Clinical history and physical examination are the key to establish the prognostic signs of severity. The International Cooperative Pulmonary Embolism Registry (ICOPER) identifies many clinical factors that can predict an increased mortality at 30 d (Table 1)^[3]. Ventilation/perfusion (V/Q) scanning is reserve as a diagnostic tool only in patients in whom CTPA is contraindicated or inconclusive and V/Q scanning should only be performed in patients with normal chest radiograph^[19].

Other supportive diagnostic tools include elevated

d-dimer, cardiac biomarkers, DVT diagnosed with lower limb duplex, and RV dysfunction and elevated pulmonary pressure with echocardiography^[20].

MEDICAL TREATMENT AND SUPPORT IN MASSIVE AND SUBMASSIVE PE

It is important from the outset to establish if the PE has hemodynamic stability, and to choose the appropriate therapeutic guideline. The ACCP^[6] in its guidelines for the treatment and management of pulmonary PE recommends systemic fibrinolytic agent for massive PE with hemodynamic instability and low bleeding risk (Grade 1B). While a patient with a low risk PE it is only recommended anticoagulation therapy. However, the treatment of submassive PE is controversial. For submassive PE, the ACCP currently recommends, in selected patients with acute PE who deteriorate after starting anticoagulant therapy but have yet not develop a hypotension and who have a low bleeding risk, they suggest systemically administered fibrinolytic therapy. In patients who have a higher risk of bleeding with systemic fibrinolytic therapy, the physicians with access to CDT are likely to choose this treatment over systemic fibrinolytic therapy^[6].

Massive and submassive PE has an important mortality in the first few hours, therefore urgent diagnosis and therapeutic approach is required^[13]. It has been established that more than 25% of patients diagnosed with massive PE with hemodynamic instability die within the first two weeks^[3,7]. The first therapeutic measures with fluid therapy and vasoactive drugs (dopamine, noradrenaline, *etc.*) should be directed to correct the hypotension and the RV failure. It is important to maintain patent airway with good oxygen supply, if necessary with tracheal intubation and mechanical ventilation, to improve oxygenation and prevent respiratory failure.

Anticoagulation treatment, if there is no contraindication, should be administered immediately. Low-molecular-weight heparin (LMWH) or unfractionated heparin can be used in therapeutic range. ACCP recommends systemic thrombolysis in the case of massive PE with haemodynamic instability, and low bleeding risk. Urokinase (UK) and recombinant tissue plasminogen activator (r-TPA) are used as fibrinolytic substances. For massive PE, standard doses are: UK 4400 IU/kg per hour in 12-24 h, streptokinase 250000 IU bolus and then 100000 U/h for 12-24 h, or 1500000 U over 2 h, and 100 mg r-TPA over 2 h. The UKEP study did not demonstrate significant differences between 12 and 24-h therapeutic regimens in terms of safety and efficacy^[21]. Other studies have used higher doses of UK (3 million IU) and streptokinase (1.5 million IU) in two hours with similar efficacy and safety results (Table 2)^[22,23].

Currently the ACCP guidelines^[6] recommend short treatments of 2 h of fibrinolytic agents for massive PE

Table 2 Fibrinolytic treatments used in massive pulmonary embolism

Fibrinolytic agent	Infusion treatment 12-24 h	Short infusion treatment
Urokinase	4400 IU/kg (bolus/30 min) +	3 million IU/2 h
Streptokinase	4400 IU/kg per hour 12-24 h 250000 IU (bolus/15 min) +	1.5 million IU/2 h
r-tPA	100000 IU/h 12-24 h N/A	100 mg/2 h

N/A: Not applicable.

(Recommendation Grade 2C). In submassive PE, the ACCP^[6] recommends the use of fibrinolytics only in cases of clinical deterioration despite anticoagulation. In this case the doses to be used will be the same as for the massive PE, however some advocate for half-dose of r-TPA to decrease the bleeding risk.

Regarding the route of administration, the systemic effect is recommended in severe PE. However, when the patient has a high risk of bleeding or the systemic therapy hasn't been effective, a lower-dose fibrinolytic therapy can be administered *via* catheter placed within the pulmonary artery or directly in the thrombus; this procedure may be performed with or without thrombectomy and/or clot fragmentation. Regarding massive PE, Kuo *et al.*^[9] in their recent multicenter study, showed that a catheter-directed therapy (CDT) improves pulmonary hypertension and RV function effectively without more complications.

When pharmacological treatment (anticoagulant or thrombolysis) fails or is contraindicated, an IVCf can be implanted to prevent the migration of thrombi to the lung from a previous DVT (Recommendation Grade 1B). There are many types of filters on the market with similar efficacy and safety, although there are few comparative studies^[7]. The development of the retrievable filters has expanded its use since it is possible to recover the IVCf once as filtration is no longer necessary or the risk of embolism has been resolved^[24,25]. In the long term, The IVCf may become a thrombogenic device as and therefore may require long-term anticoagulant treatment to mitigate the risk of filter-related thrombosis^[26]. The FDA in 2010 issued a recommendation advising the recovery of every IVCf as soon as possible, once they had fulfilled their clinical mission^[27]. Only temporary IVCf should be implanted based on the available evidence and routinely removed within 25-54 d according to the guidelines of the USFDA^[28].

ENDOVASCULAR TECHNIQUES FOR THE TREATMENT OF MASSIVE PE

The first objective in a massive PE is to remove the artery obstruction in order to reduce pulmonary hy-

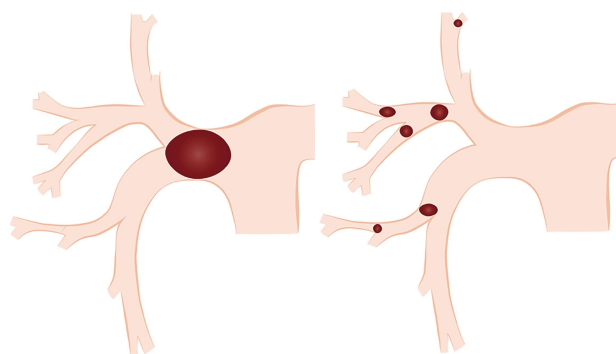


Figure 1 Schematic representation of thrombus fragmentation by a mechanical thrombolysis resulting a distal embolization of smaller thrombi, creating a larger surface area of the clot improving the efficacy of the thrombolytic agent therapy.

pertension and RV failure. Endovascular treatment by different devices of fragmentation or thrombectomy can help reduce the thrombotic load and improve the reperfusion of the vascular system. At the same time, thrombus fragmentation exposes a larger surface area of clot, producing a superior efficacy of the fibrinolytic therapy (Figure 1)^[29].

Systemic fibrinolytic therapy has demonstrated to flow in other continuous patent vessels without acting directly into the clogged vessel. Some studies have shown a more precise action of these drugs when it was administered directly within the thrombus with excellent results^[30]. Several devices have been used to perform a CDT with different levels of efficacy^[12,29,31-41].

The simplest and most widespread technique is the use of pigtail catheters to fragment the thrombus by continuous rotation of the catheter^[42]. The proximal fragmentation of the thrombus leads to distal embolization of smaller thrombi (Figure 1), however some authors have reported pulmonary hypertension with the use of this technique^[43]; other authors or many years had shown the contrary^[8,34,44,45]. Other devices like balloon catheters of different sizes are inflated and deflated successively for the fragmentation of the thrombi. The aspiration of thrombi located in the pulmonary arteries can also be attempted with aspiration of large caliber catheters (8 French or more)^[14]. All of them are used in combination with locally administered fibrinolytic agents through an intra-thrombus catheter. The great advantage of these devices although of dubious effectiveness, is that they are simple to use and available at a low price (Figure 2).

The mechanical devices of thrombectomy or endovascular aspiration can be classified by their mechanism of action in: Rheolytic, rotational, aspiration and fragmentation (Table 3)^[39].

The AngioJet (Boston Scientific Voisins-le-Bretonneux, France) rheolytic system is a thrombectomy designed to aspirate the thrombus using the Venturi-Bernoulli effect. With high-pressure jets and velocity in the distal holes of the system, it creates a zone of low pressure and a suction effect. The system

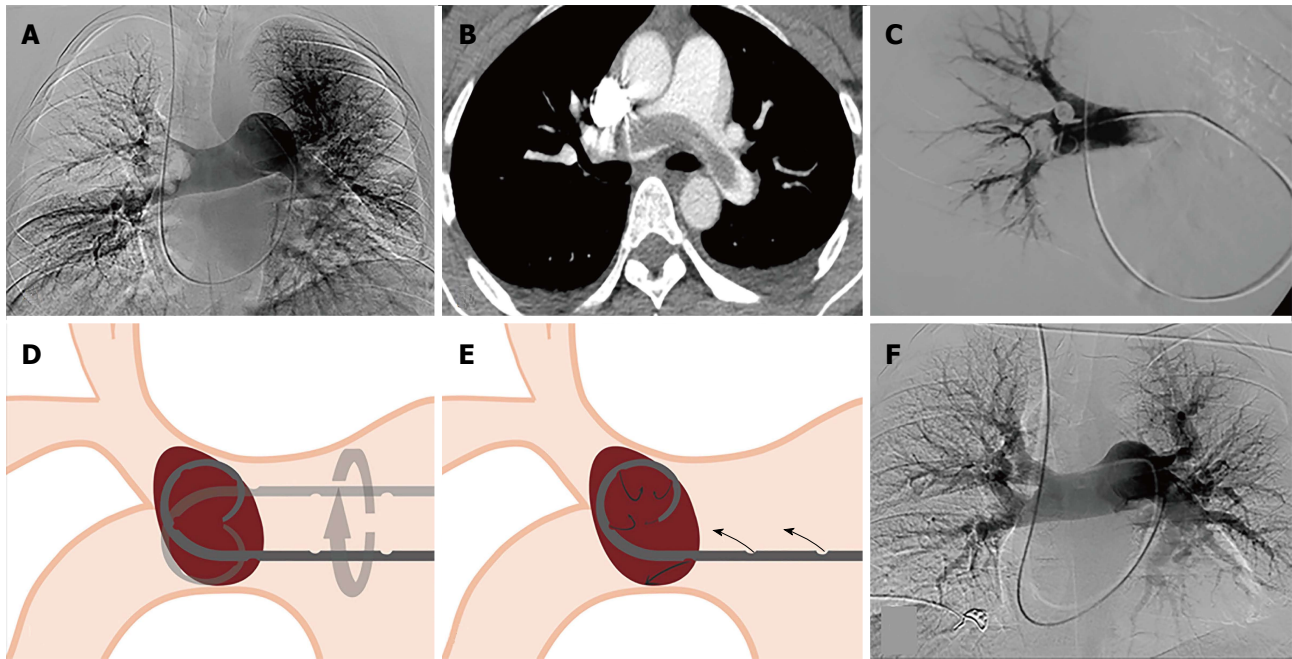


Figure 2 The great advantage of these devices although of dubious effectiveness, is that they are simple to use and available at a low price. A, B: Pulmonary angiography and CT angiography, of a 37-year-old male patient diagnosed with a massive pulmonary embolism; C: Catheter drug therapy, and mechanical thrombolysis; D, E: Schematic representation of mechanical thrombolysis and the infusion of fibrinolytic agents through the pigtail catheter; F: Pulmonary angiography after 24 h of perfusion with 100000.00 UI/h of urokinase, showing no residual occlusion.

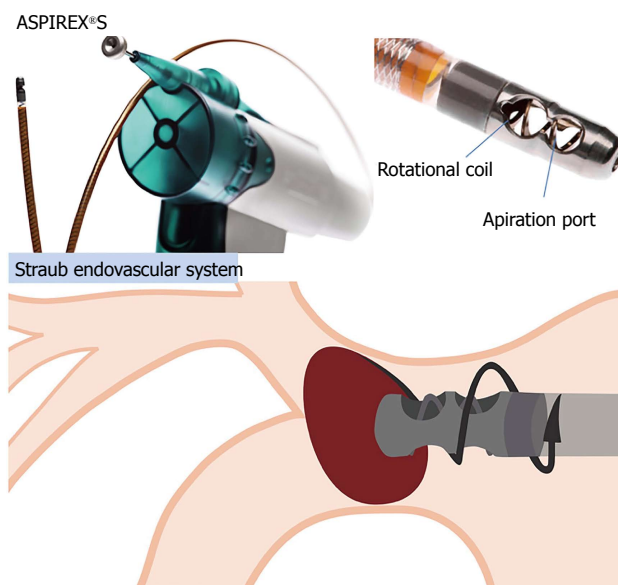


Figure 3 Aspirex®S by Straub Endovascular System. Mechanism of thrombectomy in which has a screw that rotates inside the catheter lumen, and this spiral movement is generated by an active motor that produces a thrombus aspiration.

has been associated with multiple complications including bradycardia, blockage, hemoglobinuria, renal insufficiency, severe hemoptysis, even procedural death^[29], which the FDA advises against its use as the first therapeutic option in PE^[32,46].

The Helix Clot Buster (Medtronic Minneapolis, United States), formerly known as the Amplatz thrombectomy

device, is an FDA-approved device for the endovascular treatment to treat dialysis grafts and AV fistulas, but hasn't been used for thrombectomy in PE. It is a reinforced polyurethane catheter of 7 Fr with lengths from 75 to 120 cm. At its distal end it has a metal impeller that is connected to a motor that rotates more than 140000 rpm, which generates a pressure of 30-35 psi that allows the suction of the thrombus^[33].

Two relatively new devices are Aspirex and Rotarex (Straub, Wangs, Switzerland). The Aspirex catheter acts as the archimedean screw, that rotates inside the catheter lumen; this spiral mechanism is connected to an active motor producing a thrombus aspiration. A catheter system transports the aspirated material to a manifold. Its clinical results are promising but there are no controlled studies that can support it (Figure 3)^[18].

The Indigo mechanical aspiration system (Penumbra Alameda, United States) is an aspiration thrombectomy catheter system. A large caliber (8 Fr) catheter with dirigible and soft tip, allows easy aspiration of the thrombi housed in the pulmonary arteries due to the great suction power of the suction pump. Several studies are being performed to evaluate safety and efficacy of this device (Figure 4).

The EKOSonic system (Ekosonic endovascular System BTG Riverside Way, Watchmoor Park, United Kingdom) is the only device approved by the FDA to treat PE. This system generates an acoustic pulse fibrinolytic agent, which have shown satisfactory results to treat massive and submassive PE. The catheter lodges in its interior a sophisticated catheter with an

Table 3 Fragmentation and aspiration devices used in the endovascular treatment of pulmonary embolism

Endovascular mechanisms of thrombectomy and thrombolysis	Rheolytic	Rotational	Aspiration	Fragmentation	Ultrasound
Devices	Angio Jet Boston Scientific Hydrolyzer Cordis	Rotarex Aspirex Straub Medical	Indigo Penumbra	Fogarty arterial balloon embolectomy catheter Edwards Pig-tail Catheter Cook Medical	Ekos Sonic BTG
Mechanism	Pressurized saline or fibrinolytic agent injection through the catheter in the distal tip, and the remaining fragmented thrombus is aspirated	High-speed rotation coil within the catheter, creating a negative pressure and aspiration of the thrombus	Aspiration pump that provides a high negative pressure of suction with a guide-wire (separator) to create fragmentation of the thrombus	Performing balloon sweeps or manually rotation of the standard Pig-tail to fragment the thrombus	Ultrasound emitting catheter localized within the thrombus to generate an acoustic field creating a more lytic dispersion of the drug infused

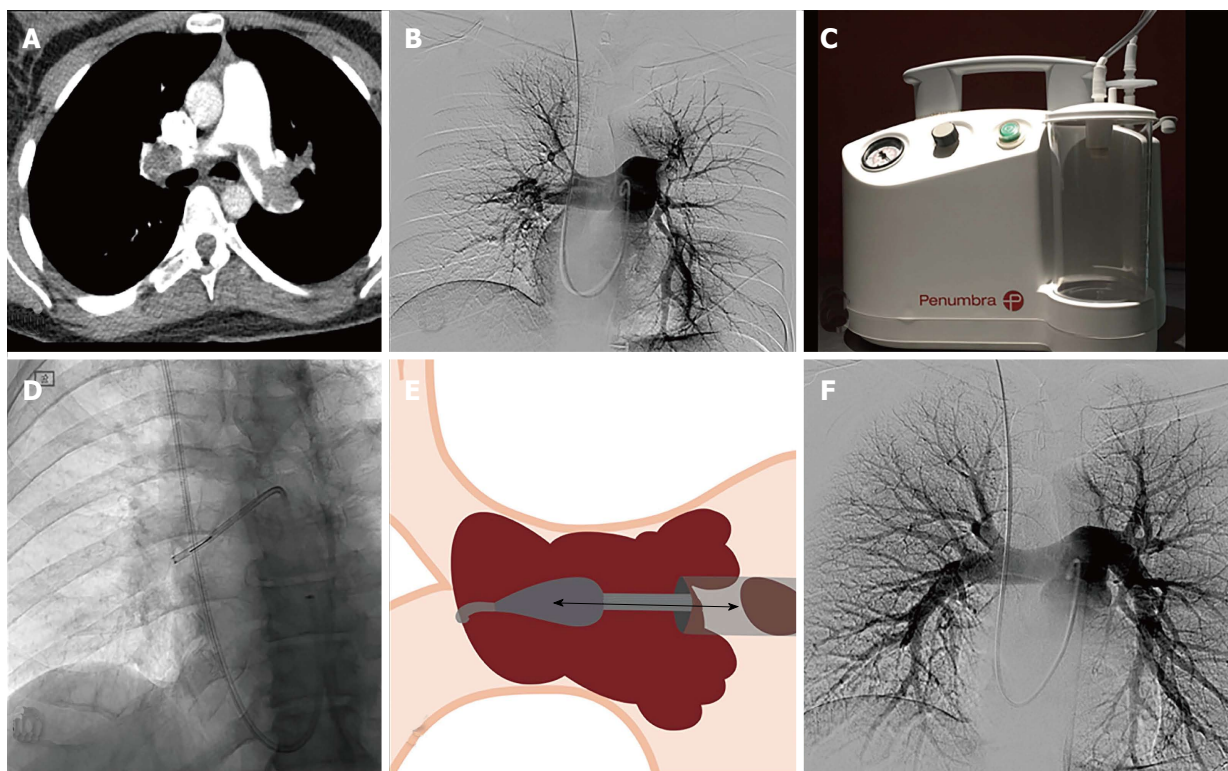
Modified from Barjaktarevic *et al*^[39].

Figure 4 The Indigo mechanical aspiration system (Penumbra Alameda, United States) is an aspiration thrombectomy catheter system. A, B: Pulmonary angiography and CT angiography, of a 37-year-old male patient diagnosed with a massive pulmonary embolism, 24-year-old female patient diagnosed with massive pulmonary embolism; C-F: Treated with CAT8 and SEP8 Indigo System® by PENUMBRA and catheter directed therapy with Pig-tail catheter with an infusion of 1200000.00 UI urokinase administered in 12 h. CT: Computed tomography.

ultrasonic core to effectively target an entire clot. This catheter uses two systems, the ultrasound and the infusion of the fibrinolytic agent. It consists of a 5.4 Fr catheter and has a functional distal tip ranging from 6 to 50 cm in length^[41]. However, acoustic field catheters may accelerate dispersion, clinical advantage vs standard infusion catheters is unclear and unproven (Figure 5).

RESULTS OF ENDOVASCULAR TECHNIQUES FOR THE TREATMENT OF PE

There are few randomized studies comparing both types of fibrinolytic administration (systemic vs CDT)^[47]. The first study on which the ACCP recommendations

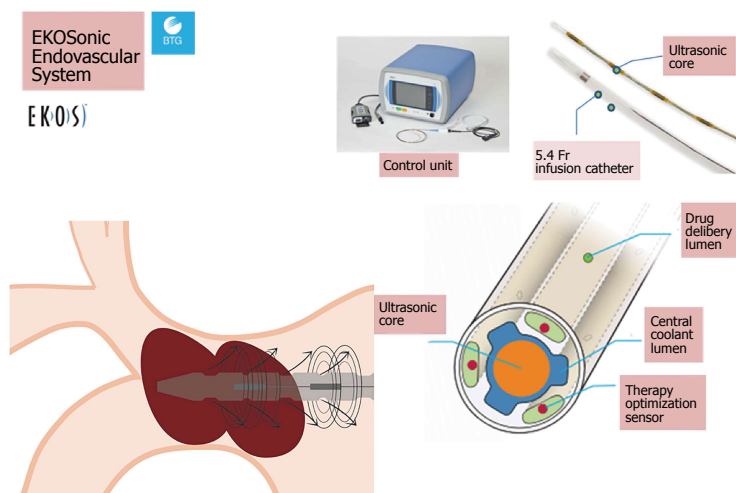


Figure 5 EKOSonic Endovascular System by BTG. Specialized catheter that lodges in its interior a sophisticated mechanism that has an ultrasonic core to effectively target an entire clot producing thrombolysis effect, and also helps the infusion of the fibrinolytic agent work faster and more efficient.

are based, was published by Verstraete *et al.*^[48]. In this study, 34 patients were treated with local or systemic thrombolysis and did not observe significant differences between the two groups in terms of efficacy and complications. It should be noted that in the CDT group, the fibrinolytic agent was administered from the catheter located in a non intra-thrombus approach within the pulmonary artery. The meta-analysis published in 2008 about 35 studies, indicates that 594 patients with PE were treated with CDT and of them 67% received intra-thrombotic thrombolysis during CDT^[31]. Treatment with CDT with or without thrombolysis produced a clinical success of 86.5% (356/535). Similar results have now been obtained by combining local fibrinolytic agent with thrombus fragmentation or aspiration^[8,49]. PERFECT, a multicenter trial with a total of 101 patients were treated with CDT and achieved a clinical success of 85.7% of the patients diagnosed with massive PE and 97.3% in submassive PE^[9]. The use of new devices for fragmentation and/or aspiration of the thrombi can improve these results. The use of ultrasound through a 5.4 Fr catheter with infusion of fibrinolytic leads to rapid lysis of the thrombi located in the pulmonary artery^[40,50,51]. Seattle II, a prospective study of 150 patients diagnosed with massive or submassive PE using EKO-sonic and a low dose of r-TPA through CDT, reduced the RV/LV ratio measured with CT by 25% in 48 h, showed a 30% improvement of the systolic pressure and another 30% in the pulmonary artery obstruction^[41]. These results, however, according to several authors, do not represent significant differences with those obtained by the standard CDT^[49,52].

COMPLICATION

In a randomized study of 1006 patients with submassive PE the risk of intracranial hemorrhage also with systemic thrombolysis is 3%-5% in the various studies^[3,53]. Other complications have been described such as: Bradyarrhythmia, cardiac tamponade, rupture or dissection of the pulmonary arteries, severe

hemoptysis, renal failure and hemoglobinuria. Major complications (major bleeding and death) ranged from 0%-3%^[9,45,49]. A meta-analysis of PE treated with CDT had a 2.4% of major complications and 7.9% of minor complications^[29].

CONCLUSION

CDT is an accepted therapeutic technique for the treatment of acute massive PE and cases of submassive PE with RV dysfunction or failure. However it requires a well-trained medical and interventional team to achieve best results. Further clinical studies are needed to analyze the CDT protocol for massive and submassive PE, define which submassive PE patients should be treated with early CDT, and determine if early CDT treatment can decrease the long-term risk of developing chronic thromboembolic pulmonary hypertension.

REFERENCES

- 1 Cushman M, Tsai AW, White RH, Heckbert SR, Rosamond WD, Enright P, Folsom AR. Deep vein thrombosis and pulmonary embolism in two cohorts: the longitudinal investigation of thromboembolism etiology. *Am J Med* 2004; **117**: 19-25 [PMID: 15210384]
- 2 Cohen AT, Agnelli G, Anderson FA, Arcelus JJ, Bergqvist D, Brecht JG, Greer IA, Heit JA, Hutchinson JL, Kakkar AK, Mottier D, Oger E, Samama MM, Spannagl M; VTE Impact Assessment Group in Europe (VITAE). Venous thromboembolism (VTE) in Europe. The number of VTE events and associated morbidity and mortality. *Thromb Haemost* 2007; **98**: 756-764 [PMID: 17938798]
- 3 Goldhaber SZ, Visani L, De Rosa M. Acute pulmonary embolism: clinical outcomes in the International Cooperative Pulmonary Embolism Registry (ICOPER) *Lancet* 1999; **353**: 1386-1389 [PMID: 10227218]
- 4 Piazza G, Goldhaber SZ. The acutely decompensated right ventricle: pathways for diagnosis and management. *Chest* 2005; **128**: 1836-1852 [PMID: 16162794]
- 5 Dudzinski DM, Giri J, Rosenfield K. Interventional Treatment of Pulmonary Embolism. *Circ Cardiovasc Interv* 2017; **10**: e004345 [PMID: 28213377 DOI: 10.1161/CIRCINTERVENTIONS.116.004345]
- 6 Kearon C, Akl EA, Ornelas J, Blaivas A, Jimenez D, Bounameaux H, Huisman M, King CS, Morris TA, Sood N, Stevens SM, Vintch JR, Wells P, Woller SC, Moores L. Antithrombotic Therapy for VTE Disease: CHEST Guideline and Expert Panel Report. *Chest* 2016; **149**: 315-352 [PMID: 26867832 DOI: 10.1016/j.chest.2015.11.026]

- 7 **Emmerich J**, Meyer G, Decousus H, Agnelli G. Role of fibrinolysis and interventional therapy for acute venous thromboembolism. *Thromb Haemost* 2006; **96**: 251-257 [PMID: 16953264]
- 8 **de Gregorio MA**, Laborda A, de Blas I, Medrano J, Mainar A, Oribe M. Endovascular treatment of a haemodynamically unstable massive pulmonary embolism using fibrinolysis and fragmentation. Experience with 111 patients in a single centre. Why don't we follow ACCP recommendations? *Arch Bronconeumol* 2011; **47**: 17-24 [PMID: 21208705 DOI: 10.1016/j.arbres.2010.08.004]
- 9 **Kuo WT**, Banerjee A, Kim PS, DeMarco FJ, Levy JR, Facchini FR, Unver K, Bertini MJ, Sista AK, Hall MJ, Rosenberg JK, De Gregorio MA. Pulmonary Embolism Response to Fragmentation, Embolectomy, and Catheter Thrombolysis (PERFECT): Initial Results From a Prospective Multicenter Registry. *Chest* 2015; **148**: 667-673 [PMID: 25856269 DOI: 10.1378/chest.15-0119]
- 10 **Zuin M**, Kuo WT, Rigatelli G, Daggubati R, Vassiliev D, Roncon L. Catheter-directed therapy as a first-line treatment strategy in hemodynamically unstable patients with acute pulmonary embolism: Yes or no? *Int J Cardiol* 2016; **225**: 14-15 [PMID: 27694031 DOI: 10.1016/j.ijcard.2016.09.104]
- 11 **Pelliccia F**, Schiariti M, Terzano C, Keyhani AM, D'Agostino DC, Speziale G, Greco C, Gaudio C. Treatment of acute pulmonary embolism: update on newer pharmacologic and interventional strategies. *Biomed Res Int* 2014; **2014**: 410341 [PMID: 25025049 DOI: 10.1155/2014/410341]
- 12 **Reekers JA**, Baarslag HJ, Koolen MG, Van Delden O, van Beek EJ. Mechanical thrombectomy for early treatment of massive pulmonary embolism. *Cardiovasc Intervent Radiol* 2003; **26**: 246-250 [PMID: 14562972]
- 13 **Wood KE**. Major pulmonary embolism: review of a pathophysiologic approach to the golden hour of hemodynamically significant pulmonary embolism. *Chest* 2002; **121**: 877-905 [PMID: 11888976]
- 14 **Kuo WT**. Endovascular therapy for acute pulmonary embolism. *J Vasc Interv Radiol* 2012; **23**: 167-179.e4; quiz 179 [PMID: 22192633 DOI: 10.1016/j.jvir.2011.10.012]
- 15 **ten Wolde M**, Söhne M, Quak E, Mac Gillavry MR, Büller HR. Prognostic value of echocardiographically assessed right ventricular dysfunction in patients with pulmonary embolism. *Arch Intern Med* 2004; **164**: 1685-1689 [PMID: 15302640]
- 16 **Piazza G**, Goldhaber SZ. Fibrinolysis for acute pulmonary embolism. *Vasc Med* 2010; **15**: 419-428 [PMID: 20926501 DOI: 10.1177/1358863X10380304]
- 17 **Furlan A**, Aghayev A, Chang CC, Patil A, Jeon KN, Park B, Fetzer DT, Saul M, Roberts MS, Bae KT. Short-term mortality in acute pulmonary embolism: clot burden and signs of right heart dysfunction at CT pulmonary angiography. *Radiology* 2012; **265**: 283-293 [PMID: 22993221]
- 18 **Kucher N**, Rossi E, De Rosa M, Goldhaber SZ. Prognostic role of echocardiography among patients with acute pulmonary embolism and a systolic arterial pressure of 90 mm Hg or higher. *Arch Intern Med* 2005; **165**: 1777-1781 [PMID: 16087827]
- 19 **PIOPED Investigators**. Value of the ventilation/perfusion scan in acute pulmonary embolism. Results of the prospective investigation of pulmonary embolism diagnosis (PIOPED). *JAMA* 1990; **263**: 2753-2759 [PMID: 2332918]
- 20 **Jarrett H**, Bashir R. Interventional Management of Venous Thromboembolism: State of the Art. *AJR Am J Roentgenol* 2017; **208**: 891-906 [PMID: 28225642 DOI: 10.2214/AJR.16.17064]
- 21 The UKEP study: multicentre clinical trial on two local regimens of urokinase in massive pulmonary embolism. The UKEP Study Research Group. *Eur Heart J* 1987; **8**: 2-10 [PMID: 3545842]
- 22 **Meneveau N**, Schiele F, Metz D, Valette B, Attali P, Vuilleminot A, Grollier G, Elaerts J, Mossard JM, Viel JF, Bassand JP. Comparative efficacy of a two-hour regimen of streptokinase versus alteplase in acute massive pulmonary embolism: immediate clinical and hemodynamic outcome and one-year follow-up. *J Am Coll Cardiol* 1998; **31**: 1057-1063 [PMID: 9562007]
- 23 **Meneveau N**, Schiele F, Vuilleminot A, Valette B, Grollier G, Bernard Y, Bassand JP. Streptokinase vs alteplase in massive pulmonary embolism. A randomized trial assessing right heart haemodynamics and pulmonary vascular obstruction. *Eur Heart J* 1997; **18**: 1141-1148 [PMID: 9243149]
- 24 **De Gregorio MA**, Gamboa P, Bonilla DL, Sanchez M, Higuera MT, Medrano J, Mainar A, Lostalé F, Laborda A. Retrieval of Gunther Tulip optional vena cava filters 30 days after implantation: a prospective clinical study. *J Vasc Interv Radiol* 2006; **17**: 1781-1789 [PMID: 17142708]
- 25 **Lee MJ**, Valenti D, de Gregorio MA, Minocha J, Rimón U, Pellerin O. The CIRSE Retrievable IVC Filter Registry: Retrieval Success Rates in Practice. *Cardiovasc Intervent Radiol* 2015; **38**: 1502-1507 [PMID: 25933644 DOI: 10.1007/s00270-015-1112-5]
- 26 **PREPIC Study Group**. Eight-year follow-up of patients with permanent vena cava filters in the prevention of pulmonary embolism: the PREPIC (Prevention du Risque d'Embolie Pulmonaire par Interruption Cave) randomized study. *Circulation* 2005; **112**: 416-422 [PMID: 16009794]
- 27 Inferior Vena Cava (IVC) Filters: Initial Communication: Risk of Adverse Events with Long Term Use [Internet]. [accessed 2017 May 27]. Available from: URL: <https://wayback.archive-it.org/7993/20161023081037/http://www.fda.gov/Safety/MedWatch/SafetyInformation/SafetyAlertsforHumanMedicalProducts/ucm221707.htm>
- 28 **Arous EJ**, Messina LM. Temporary Inferior Vena Cava Filters: How Do We Move Forward? *Chest* 2016; **149**: 1143-1145 [PMID: 27012891 DOI: 10.1016/j.chest.2016.03.015]
- 29 **Kuo WT**, Gould MK, Louie JD, Rosenberg JK, Sze DY, Hofmann LV. Catheter-directed therapy for the treatment of massive pulmonary embolism: systematic review and meta-analysis of modern techniques. *J Vasc Interv Radiol* 2009; **20**: 1431-1440 [PMID: 19875060 DOI: 10.1016/j.jvir.2009.08.002]
- 30 **Schmitz-Rode T**, Kilbinger M, Günther RW. Simulated flow pattern in massive pulmonary embolism: significance for selective intrapulmonary thrombolysis. *Cardiovasc Intervent Radiol* 2008; **21**: 199-204 [PMID: 9626434]
- 31 **Kuo WT**, van den Bosch MA, Hofmann LV, Louie JD, Kothary N, Sze DY. Catheter-directed embolectomy, fragmentation, and thrombolysis for the treatment of massive pulmonary embolism after failure of systemic thrombolysis. *Chest* 2008; **134**: 250-254 [PMID: 18682455 DOI: 10.1378/chest.07-2846]
- 32 **Kuo WT**, Sze DY, Hofmann LV. Catheter-directed intervention for acute pulmonary embolism: a shining saber. *Chest* 2008; **133**: 317-318; author reply 318 [PMID: 18187767 DOI: 10.1378/chest.07-2278]
- 33 **Uflacker R**, Strange C, Vujic I. Massive pulmonary embolism: preliminary results of treatment with the Amplatz thrombectomy device. *J Vasc Interv Radiol* 1996; **7**: 519-528 [PMID: 8855528]
- 34 **Fava M**, Loyola S, Huete I. Massive pulmonary embolism: treatment with the hydrolyser thrombectomy catheter. *J Vasc Interv Radiol* 2000; **11**: 1159-1164 [PMID: 11041472]
- 35 **Siablis D**, Karnabatidis D, Katsanos K, Kagadis GC, Zabakis P, Hahalis G. AngioJet rheolytic thrombectomy versus local intrapulmonary thrombolysis in massive pulmonary embolism: a retrospective data analysis. *J Endovasc Ther* 2005; **12**: 206-214 [PMID: 15823068 DOI: 10.1583/04-1378.1]
- 36 **Yoshida M**, Inoue I, Kawagoe T, Ishihara M, Shimatani Y, Kurisu S, Kusano KF, Ohe T. Novel percutaneous catheter thrombectomy in acute massive pulmonary embolism: rotational bidirectional thrombectomy (ROBOT). *Catheter Cardiovasc Interv* 2006; **68**: 112-117 [PMID: 16755594 DOI: 10.1002/ccd.20747]
- 37 **Chamsuddin A**, Nazzal L, Kang B, Best I, Peters G, Panah S, Martin L, Lewis C, Zeinati C, Ho JW, Venbrux AC. Catheter-directed thrombolysis with the Endowave system in the treatment of acute massive pulmonary embolism: a retrospective multicenter case series. *J Vasc Interv Radiol* 2008; **19**: 372-376 [PMID: 18295696 DOI: 10.1016/j.jvir.2007.10.019]
- 38 **Liu S**, Shi HB, Gu JP, Yang ZQ, Chen L, Lou WS, He X, Zhou WZ, Zhou CG, Zhao LB, Xia JG, Li LS. Massive pulmonary embolism: treatment with the rotarex thrombectomy system. *Cardiovasc Intervent Radiol* 2011; **34**: 106-113 [PMID: 20454793 DOI: 10.1007/s00270-010-9878-y]
- 39 **Barjaktarevic I**, Friedman O, Ishak C, Sista AK. Catheter-directed clot fragmentation using the Cleaner™ device in a patient presenting

- with massive pulmonary embolism. *J Radiol Case Rep* 2014; **8**: 30-36 [PMID: 24967017 DOI: 10.3941/jrcr.v8i2.1455]
- 40 **Garcia MJ.** Endovascular Management of Acute Pulmonary Embolism Using the Ultrasound-Enhanced EkoSonic System. *Semin Intervent Radiol* 2015; **32**: 384-387 [PMID: 26622102 DOI: 10.1055/s-0035-1564707]
 - 41 **Piazza G,** Hohlfelder B, Jaff MR, Ouriel K, Engelhardt TC, Sterling KM, Jones NJ, Gurley JC, Bhatheja R, Kennedy RJ, Goswami N, Natarajan K, Rundback J, Sadiq IR, Liu SK, Bhalla N, Raja ML, Weinstock BS, Cynamon J, Elmasri FF, Garcia MJ, Kumar M, Ayerdi J, Soukas P, Kuo W, Liu PY, Goldhaber SZ; SEATTLE II Investigators. A Prospective, Single-Arm, Multicenter Trial of Ultrasound-Facilitated, Catheter-Directed, Low-Dose Fibrinolysis for Acute Massive and Submassive Pulmonary Embolism: The SEATTLE II Study. *JACC Cardiovasc Interv* 2015; **8**: 1382-1392 [PMID: 26315743 DOI: 10.1016/j.jcin.2015.04.020]
 - 42 **Schmitz-Rode T,** Janssens U, Duda SH, Erley CM, Günther RW. Massive pulmonary embolism: percutaneous emergency treatment by pigtail rotation catheter. *J Am Coll Cardiol* 2000; **36**: 375-380 [PMID: 10933345]
 - 43 **Nakazawa K,** Tajima H, Murata S, Kumita SI, Yamamoto T, Tanaka K. Catheter fragmentation of acute massive pulmonary thromboembolism: distal embolisation and pulmonary arterial pressure elevation. *Br J Radiol* 2008; **81**: 848-854 [PMID: 18941044 DOI: 10.1259/bjr/93840362]
 - 44 **de Gregorio MA,** Fava M. [Fragmentation and fibrinolysis in pulmonary thromboembolism]. *Arch Bronconeumol* 2001; **37**: 513 [PMID: 11734143]
 - 45 **De Gregorio MA,** Gimeno MJ, Mainar A, Herrera M, Tobio R, Alfonso R, Medrano J, Fava M. Mechanical and enzymatic thrombolysis for massive pulmonary embolism. *J Vasc Interv Radiol* 2002; **13**: 163-169 [PMID: 11830622]
 - 46 **Kuo WT,** Hofmann LV. Drs. Kuo and Hofmann respond. *J Vasc Interv Radiol* 2010; **21**: 1776-1777 [DOI: 10.1016/j.jvir.2010.08.001]
 - 47 **Macovei L,** Presura RM, Arsenescu Georgescu C. Systemic or local thrombolysis in high-risk pulmonary embolism. *Cardiol J* 2015; **22**: 467-474 [PMID: 25563712 DOI: 10.5603/CJ.a2014.0103]
 - 48 **Verstraete M,** Miller GA, Bounameaux H, Charbonnier B, Colle JP, Lecorff G, Marbet GA, Mombaerts P, Olsson CG. Intravenous and intrapulmonary recombinant tissue-type plasminogen activator in the treatment of acute massive pulmonary embolism. *Circulation* 1988; **77**: 353-360 [PMID: 3123091]
 - 49 **Liang NL,** Chaer RA, Marone LK, Singh MJ, Makaroun MS, Avgerinos ED. Midterm outcomes of catheter-directed interventions for the treatment of acute pulmonary embolism. *Vascular* 2017; **25**: 130-136 [PMID: 27271537 DOI: 10.1177/1708538116654638]
 - 50 **Ozmen C,** Deniz A, Akilli RE, Deveci OS, Cagliyan CE, Aktas H, Celik AI, Akpınar AA, Disel NR, Balli HT, Hanta İ, Demir M, Usal A, Kanadasi M. Ultrasound Accelerated Thrombolysis May Be an Effective and Safe Treatment Modality for Intermediate Risk/ Submassive Pulmonary Embolism. *Int Heart J* 2016; **57**: 91-95 [PMID: 26673444 DOI: 10.1536/ihj.15-271]
 - 51 **Teleb M,** Porres-Aguilar M, Rivera-Lebron B, Ngamdu KS, Botrus G, Anaya-Ayala JE, Mukherjee D. Ultrasound-Assisted Catheter-Directed Thrombolysis: A Novel and Promising Endovascular Therapeutic Modality for Intermediate-Risk Pulmonary Embolism. *Angiology* 2016; **68**: 494-501 [PMID: 27609936]
 - 52 **Tafur AJ,** Shamoun FE, Patel SI, Tafur D, Donna F, Murad MH. Catheter-Directed Treatment of Pulmonary Embolism. *Clin Appl Thromb Hemost* 2016; Epub ahead of print [PMID: 27481877 DOI: 10.1177/1076029616661414]
 - 53 **Fiumara K,** Kucher N, Fanikos J, Goldhaber SZ. Predictors of major hemorrhage following fibrinolysis for acute pulmonary embolism. *Am J Cardiol* 2006; **97**: 127-129 [PMID: 16377297]

P- Reviewer: Gao BL, Pereira-Vega A, Schoenhagen P, Tawfik MM

S- Editor: Song XX **L- Editor:** A **E- Editor:** Lu YJ



Retrospective Study

Incidental extravascular findings in computed tomographic angiography for planning or monitoring endovascular aortic aneurysm repair: Smoker patients, increased lung cancer prevalence?

Maria Antonietta Mazzei, Susanna Guerrini, Francesco Gentili, Giuseppe Galzerano, Francesco Setacci, Domenico Benevento, Francesco Giuseppe Mazzei, Luca Volterrani, Carlo Setacci

Maria Antonietta Mazzei, Susanna Guerrini, Francesco Gentili, Luca Volterrani, Department of Medical, Surgical and Neuro Sciences, Diagnostic Imaging, University of Siena, Azienda Ospedaliera Universitaria Senese, 53100 Siena, Italy

Giuseppe Galzerano, Francesco Setacci, Carlo Setacci, Department of Medical, Surgical and Neuro Sciences, Vascular and Endovascular Unit, University of Siena, Azienda Ospedaliera Universitaria Senese, 53100 Siena, Italy

Domenico Benevento, Vascular and Endovascular Unit, Azienda Ospedaliera Universitaria Senese, 53100 Siena, Italy

Francesco Giuseppe Mazzei, Diagnostic Imaging, Azienda Ospedaliera Universitaria Senese, 53100 Siena, Italy

Author contributions: All authors contributed equally to this work; Mazzei MA, Guerrini S, Gentili F, Galzerano G and Mazzei FG performed the research and wrote the manuscript; Mazzei MA, Guerrini S, Gentili F, Galzerano G, Setacci F, Benevento D and Mazzei FG contributed to the conception and design of the study and to the acquisition and interpretation of the data; Mazzei MA, Guerrini S, Gentili F and Mazzei FG contributed to the acquisition of the data; Mazzei MA revised the article critically for important intellectual content; Mazzei MA, Volterrani L and Setacci C designed the research and approved the final version for publication; all authors have read and approved the final version to be published.

Institutional review board statement: The study was reviewed and approved by the University of Siena Institutional Review Board.

Informed consent statement: All study participants, or their legal guardian, provided informed written consent prior to study enrollment.

Conflict-of-interest statement: None.

Data sharing statement: No additional data are available.

Open-Access: This article is an open-access article which was selected by an in-house editor and fully peer-reviewed by external reviewers. It is distributed in accordance with the Creative Commons Attribution Non Commercial (CC BY-NC 4.0) license, which permits others to distribute, remix, adapt, build upon this work non-commercially, and license their derivative works on different terms, provided the original work is properly cited and the use is non-commercial. See: <http://creativecommons.org/licenses/by-nc/4.0/>

Manuscript source: Invited manuscript

Correspondence to: Maria Antonietta Mazzei, MD, Associate Professor of Radiology, Department of Medical, Surgical and Neuro Sciences, Diagnostic Imaging, University of Siena, Azienda Ospedaliera Universitaria Senese, Viale Bracci 10, 53100 Siena, Italy. mariaantonietta.mazzei@unisi.it
Telephone: +39-05-77585700
Fax: +39-05-7744496

Received: December 27, 2016

Peer-review started: December 31, 2016

First decision: March 28, 2017

Revised: April 16, 2017

Accepted: May 30, 2017

Article in press: June 1, 2017

Published online: July 28, 2017

Abstract**AIM**

To validate the feasibility of high resolution computed tomography (HRCT) of the lung prior to computed tomography angiography (CTA) in assessing incidental thoracic findings during endovascular aortic aneurysm repair (EVAR) planning or follow-up.

METHODS

We conducted a retrospective study among 181 patients (143 men, mean age 71 years, range 50-94) referred to our centre for CTA EVAR planning or follow-up. HRCT and CTA were performed before or after 1 or 12 mo respectively to EVAR in all patients. All HRCT examinations were reviewed by two radiologists with 15 and 8 years experience in thoracic imaging. The results were compared with histology, bronchoscopy or follow-up HRCT in 12, 8 and 82 nodules respectively.

RESULTS

There were a total of 102 suspected nodules in 92 HRCT examinations, with a mean of 1.79 nodules per patient and an average diameter of 9.2 mm (range 4-56 mm). Eighty-nine out of 181 HRCTs resulted negative for the presence of suspected nodules with a mean smoking history of 10 pack-years (p-y, range 5-18 p-y). Eighty-two out of 102 (76.4%) of the nodules met criteria for computed tomography follow-up, to exclude the malignant evolution. Of the remaining 20 nodules, 10 out of 20 (50%) nodules, suspected for malignancy, underwent biopsy and then surgical intervention that confirmed the neoplastic nature: 4 (20%) adenocarcinomas, 4 (20%) squamous cell carcinomas, 1 (5%) small cell lung cancer and 1 (5%) breast cancer metastasis; 8 out of 20 (40%) underwent bronchoscopy (8 pneumonia) and 2 out of 20 (10%) underwent biopsy with the diagnosis of sarcoidosis.

CONCLUSION

HRCT in EVAR planning and follow-up allows to correctly identify patients requiring additional treatments, especially in case of lung cancer.

Key words: Computed tomography angiography; Aorta; Endovascular aortic aneurysm repair; Cigarette smoking; Lung cancer

© The Author(s) 2017. Published by Baishideng Publishing Group Inc. All rights reserved.

Core tip: Nowadays the use of high resolution computed tomography in endovascular aortic aneurysm repair (EVAR) patients planning and follow up is not yet recommended. Our study demonstrates the possibility to early diagnose lung cancer during EVAR follow-up or planning in smoker patients, overcoming the concept of dose radiation induced neoplasms, especially in over 65 years old patients.

Mazzei MA, Guerrini S, Gentili F, Galzerano G, Setacci F, Benevento D, Mazzei FG, Volterrani L, Setacci C. Incidental extravascular findings in computed tomographic angiography for planning or monitoring endovascular aortic aneurysm repair: Smoker patients, increased lung cancer prevalence? *World J Radiol* 2017; 9(7): 304-311 Available from: URL: <http://www.wjgnet.com/1949-8470/full/v9/i7/304.htm> DOI: <http://dx.doi.org/10.4329/wjr.v9.i7.304>

INTRODUCTION

Vascular diseases cover an extended selection of pathologies comprising cardiovascular, thoracoabdominal, peripheral vascular and cerebrovascular disease^[1]. Smoking is considered one of the main risk factors for the development of atherosclerosis and, in particular, oxidative stress and inflammation that constitute the physiological connection between smoking and vascular diseases. Polycyclic aromatic hydrocarbons (PAH) represent the main carcinogenic compound found in cigarettes, produced during the incomplete combustion of organic matter. Many articles demonstrate the double activity of PAH, both carcinogenic (lung and other tissues) and inflammatory, provoking endothelial dysfunction and several studies demonstrate that oxidants directly impair endothelial function, increasing nitric oxide scavenging by oxygen free radicals^[2-6]. In the literature it is well known that cardiovascular diseases are often diagnosed on the basis of imaging findings, such as suspected atherosclerotic plaques of the chest in computed tomography (CT), also incidentally^[7-9]. A similar approach should be used to identify extravascular findings, when the CT examination is required to explore vascular diseases. In particular, since cigarette smoking is the main risk factor for both vascular and neoplastic lung diseases, radiologists should examine the chest in evaluation of vascular patients with many risk factors suggesting possible synchronous pathologies. It has been reported that CTs requested for the exclusion of pulmonary embolism give a high yield of chest abnormalities, such as mediastinal adenopathy, paratracheal adenopathy, atelectasis, emphysema and pulmonary nodules or masses^[10,11]. Although not the target of the investigation, lung abnormalities, especially lung cancer, could become the main finding with prognostic relevance in terms of life-long survivor risk in vascular patients. Furthermore, even if many articles over the last decade have reported the problem of unsuspected thoracic findings in CTs, performed for suspected pulmonary embolism or thoracic aortic pathology, the possibility of finding chest pathology, and in particular lung cancer, in smoker patients suffering from vascular disease has been underestimated^[12,13]. Moreover, several articles have reported a high cumulative radiation dose in patients treated with endovascular aneurysm repair (EVAR), both during the interventional procedure and CT follow-up, suggesting a possible role of radiation exposure in developing cancer in these patients^[14-16]. On the contrary, there have been no articles to date about the discovery of lung cancer during EVAR planning or surveillance in smokers suggesting that smoking rather than the exposure of patients to radiation is the main risk factor for lung cancer. Considering the previous statements, the purpose of this study is to assess the prevalence of lung cancer in patients with a smoking

attitude, who underwent computed tomography angiography (CTA) for planning or monitoring EVAR in our department.

MATERIALS AND METHODS

Patient characteristics

Institutional review board approval was obtained for this retrospective study, as well as informed consent from all subjects. We reviewed the report results of 250 CTs of patients referred to our department for EVAR planning or follow-up between June 2014 and May 2016, searching for lung abnormalities in the patients who underwent high resolution computed tomography (HRCT) of the lung before contrast agent administration. Patients were identified throughout a digital radiological database (Picture Archive and Communication System, PACS) which registers all radiological studies performed by the Department of Radiology. The mean age of patients at the time of CT was 71 years, in a range from 50 to 94, and 38 (21%) were female. Sixty-nine (26.6%) patients were excluded for the following reasons: 30 (43.5%) because of the absence of synchronous chest HRCT, 21 (30.4%) because of lack of proven histological findings of lung cancer or HRCT follow-up examinations, and 18 (26.1%) because of non-smoking attitude. The CTA and HRCT were performed simultaneously in all selected cases to avoid interpretation bias. Seventy-four (40.8%) CTs were performed for EVAR planning and 107 for EVAR surveillance (67 at 1 mo and 40 at 12 mo after EVAR). All the selected patients had a documented history of smoking [number of pack-years (p-y)]^[17-19].

Imaging technique

All the CTs were performed with a 64-detector row CT scanner (Discovery HD 750, General Electric Healthcare, and Milwaukee, United States). HRCTs were acquired at end of inspiration using volumetric technique in the caudocranial direction from the basis to the apex of the lung; patients were in supine position. The following technical parameters were used: Effective slice thickness 3.75 mm, collimation 40 mm, beam pitch 0.969, reconstruction interval 1 mm, tube voltage 140 kVp and reference mAs 250/400. Automatic tube current modulation was used to minimise radiation exposure. Chest CTs were acquired using a standard algorithm, then data were reconstructed by using a high spatial-frequency algorithm (bone plus), with 1.25 mm slice thickness. Abdominal CT angiography (CTA) was performed with a spiral technique in the caudocranial direction (from the pelvic brim to the lung bases) with the patients supine. Patients were instructed to hold their breath during helical imaging to avoid motion artefacts. After a scout-view scan, intravenous injection of 1.5 mL/kg non-ionic contrast material (Iomeprol 400 mg iodine/mL; Iomeron 400, Bracco Diagnostics, Milan, Italy) followed by 40 mL saline solution was administered with an 18-gauge needle in the antecubital

vein, using a dual-barrel injector (4 mL/s flow rate, CT Motion, Ulrich Medical, Ulm, Germany). Arterial phase images were obtained 4 seconds after bolus detection in the suprarenal aorta. The following technical parameters were used: Effective slice thickness 1.25 mm, collimation 40 mm, beam pitch 0.969, reconstruction interval 0.8 mm, tube voltage 140 kVp and reference mAs 250/700. A standard reconstruction algorithm was used. In 24 out of 181 patients (13.2%), the contrast CT was extended to the thorax using the same technical parameters. Automatic tube current modulation was also used to minimise radiation exposure in the post-contrast examination^[16].

Image analysis

All images were analysed independently and blindly by two readers with 15 and 8 years' experience in chest-imaging respectively. HRCT scans were analysed on a reconstruction and image interpretation console (Advantage Workstation 4.4, GE Healthcare, Milwaukee, Wis, United States), adjusting the image level, window and enlargement values each time, and routinely using a 2D multiplanar reconstruction technique (coronal, sagittal and oblique planes). Pulmonary HRCT findings included: Pleural effusion, atelectasis/pneumonia, pericardial effusion, cardiomegaly, coronary artery calcifications, bone findings, hiatal hernia, emphysema, mediastinal or hilar adenopathy, pulmonary micronodule (< 4 mm), pulmonary nodule (> 4 mm and < 30 mm) and pulmonary mass (> 30 mm). The readers recorded any incidental finding, with particular attention to pulmonary nodules or masses and differences were resolved by consensus. All nodules were characterised by number, size (measured in their greatest diameter) and CT characteristic appearance (solid, ground-glass or partially solid, edge characteristics, speculated or smooth, presence or absence of pleural-tag, bronchus sign, calcifications, intralesional fat or intralesional air) and reviewed with the smoking history of the patient. According to Fleischner Society guidelines, all suspected nodules were addressed to CT biopsy or surgical intervention, whereas nodules with a CT low risk appearance for lung cancer were addressed to CT follow-up^[20] (Table 1). All previous medical reports, clinical notes, discharges summaries and medical histories of patients were examined to potentially define every mass or nodule as a new incidental finding.

Statistical analysis

The lung findings detected by the readers were collected, and the results expressed as mean \pm SD. A descriptive statistical analysis was performed; the quantitative variables were expressed as means and range whereas the qualitative values as percentages. The statistical review of the study was performed by a biomedical statistician. The analysis was performed using Stata version 8.0 (Stata Corp, College Station, Texas).

Table 1 Recommendations for follow-up and management of nodules and micronodules^[20]

Nodule size (mm)	Low risk patient ¹	High risk patient ²
≤ 4	No FU needed	Follow-up CT at 12 mo; if unchanged, no further follow-up
> 4-6	FU CT at 12 mo; if unchanged, no further FU	Initial follow-up CT at 6-12 mo then at 18-24 mo if no change
> 6-8	Initial FU CT at 6-12 mo then at 18-24 mo if no change	Initial follow-up CT at 3-6 mo then at 9-12 and 24 mo if no change
> 8	FU CT at around 3, 9, and 24 mo, dynamic contrast-enhanced CT, PET, and or biopsy	Same as for low-risk patient

¹Minimal or absent history of smoking and of other known risk factors; ²History of smoking or of other known risk factors. CT: Computed tomography; FU: Follow-up; PET: Positron emission tomography.

Table 2 Incidental findings

Patients (n)	Findings
31	Pleural effusion
5	Atelectasis
8	Pneumonia
16	Pericardial effusion
48	Cardiomegaly
57	Coronary artery calcifications
0	Bone findings
23	Hiatal hernia
94	Emphysema
39	Mediastinal or hilar adenopathy

Table 3 Computed tomography nodules characteristics

Nodules size	n (tot 102)
Pulmonary micronodule (< 4 mm)	43
Pulmonary nodule (> 4 mm and < 30 mm)	51
Pulmonary mass (> 30 mm)	8
Nodules characteristics	n
Solid	73
Ground-glass	21
Partially solid	8
Spiculated	9
Smooth	4
Pleural tag	3
Bronchus sign	6
Calcifications	7
Intralesion fat	4
Intralesional air	2

RESULTS

A total of 181 HRCTs were reviewed. The incidental lung findings reported on chest CT are shown in Table 2. There were a total of 102 (56%) nodules in 92 out of 181 (50.8%) HRCTs, with a mean of 1.79 nodules per patient and an average diameter of 9.2 mm, ranging from 4 to 56 mm. All the CT nodules characteristics are reported in Table 3. After radiologists' review, 82 (76.4%) of the nodules met criteria for CT follow-up and were submitted to a second HRCT examination (performed between 6-12 mo), to exclude the possibility of malignant evolution. Of the remaining 20 nodules, 10 out of the 20 (50%) suspected for malignancy underwent biopsy and then surgical intervention which confirmed the following neoplastic nature: 4 (20%) adenocarcinomas (Figure 1), 4 (20%) squamous cell carcinomas, 1 (5%) small cell lung cancer and 1 (5%) breast cancer metastasis (Figure 2); 8 out of 20 (40%) underwent bronchoscopy (8 pneumonia) and 2 out of 20 (10%) underwent biopsy with the diagnosis of sarcoidosis. All the patients diagnosed with lung cancer (1 female and 8 males) had a smoking history with a mean quantity of 60 p-y (range 45-83 p-y). The remaining patients with non-neoplastic nodules had a smoking history with a mean quantity of 35 p-y (range 20-46 p-y) per patient. Eighty-nine out of 181 HRCTs resulted negative for the presence of suspected nodules with a mean smoking history of 10 p-y (range 5-18 p-y).

DISCUSSION

EVAR currently represents a safe and effective treat-

ment for abdominal aortic aneurysms exclusion with an increase in the choice of this treatment over traditional open repair, especially in elderly patients^[21,22]. In particular, EVAR is also becoming the method of choice for aneurysmal sac exclusion in vascular patients with difficult vascular anatomies due to its favourable outcomes, customised approach and easy technical execution^[23-25]. Despite these advantages some articles debate the risk of long-term lifelong EVAR CT follow-up, with a remarkable amount of radiation exposure carrying the risk of developing cancers; moreover they report the need of dose optimisations using new targeted CT protocols, considering that the absorbed dose by the patient differs on the basis different scanners, patient body size and age^[26-28]. However to our knowledge there are no articles discussing the prevalence of lung cancer, prior to EVAR treatment, in patients with a smoking attitude. Furthermore, lung cancer represents the most important cause of death in the world, and the majority of patients suffering from lung cancer present mild or no symptoms, with nodular lesions being the most common presentation of peripheral lung adenocarcinoma^[12]. Moreover, a large number of patients with vascular disease have a smoking history and, in particular, smoking is one of the major risk factors for developing vascular diseases. At the same time, smoking also represents the main risk factor for lung cancer due to the activation of the same inflammatory pathway with continuous endothelial damage. In our study we assess the prevalence of

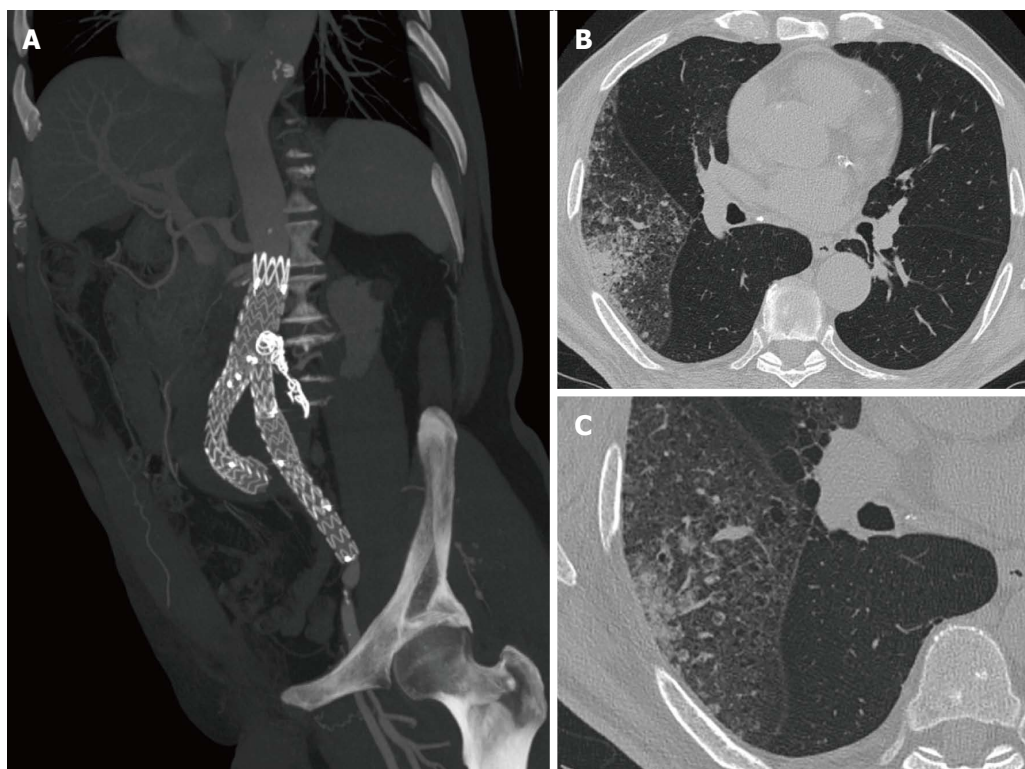


Figure 1 Lepidic predominant adenocarcinoma diagnosed during endovascular aortic aneurysm repair follow-up. A-C: A 80-year-old male with a LPA of the right upper lobe diagnosed during endovascular aortic aneurysm repair follow-up for a type II endoleak treated with glue and coils (A). HRCT images (B and C) demonstrate the lepidic growth of the tumor and aerogenous metastases in the same lobe. LPA: Lepidic predominant adenocarcinoma; HRCT: High resolution computed tomography.

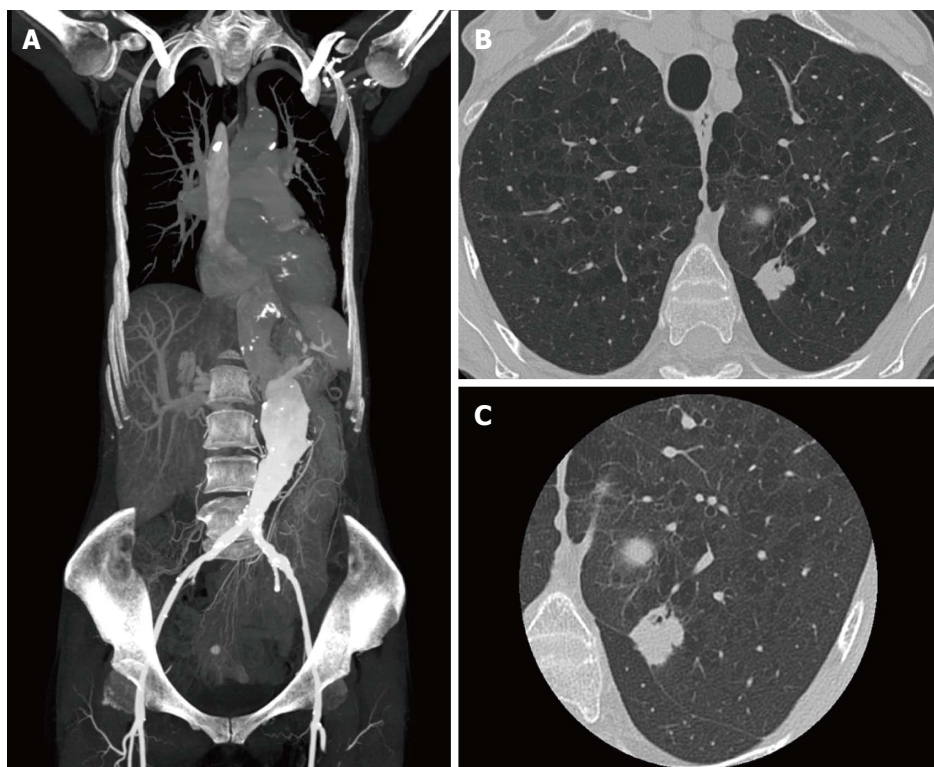


Figure 2 Breast cancer lung metastasis diagnosed during endovascular aortic aneurysm repair planning. A-C: A-63-year-old woman, with a history of breast cancer (10 year before, pT1c, N0, M), addressed to our institution for vascular planning due to an abdominal aortic aneurysm (A). HRCT image (B) performed before the contrast media administration showed diffuse emphysema in upper lobes and the presence in the left upper lobe of a solid nodule (18 mm) with spiculated margins and bronchus sign, confirmed at small FOV reconstruction (C). Histological evaluation, after surgical intervention, demonstrated a breast cancer lung metastasis. HRCT: High resolution computed tomography.

lung nodules through HRCT in a cohort of smoker patients who underwent abdominal CTA for planning or follow-up EVAR; considering the mean advanced age of patients (71 years), stochastic radiation damage deriving from the extra dose of HRCT (respectively mean CTDI 12.6 mGy (range 9.4-15.2) for HRCT vs 22.3 mGy (19.8-24.3) for abdominal CTA) can be considered negligible, comparing to the benefit of early tumor detection; in fact 9 out of 102 nodules (8.8%) in 9 out of 181 (4.9%) patients were finally diagnosed as lung cancer with consequent surgery (6 patients), chemotherapeutic treatment (1 patient) or both (2 patients), with a free survivor rate of 100% at one years. All the other patients were correctly addressed to the appropriate treatment or follow-up. In this context, performing HRCT of the lung to optimise morphological evaluation of lung nodules and/or adding advanced imaging procedure such as CT perfusion or CT volumetric assessment of lung nodules during CTA for the evaluation of vascular aneurysm, offers radiologists the possibility of performing a differential diagnosis between benign or malignant nodules, choosing the correct management for each patient^[29-33]. Moreover, CTA can be performed in the emergency setting to exclude or confirm the presence of aneurysmal sac or EVAR complications or to investigate an abdominal pain after a doubtful ultrasound examination; incidental findings can also occur in that setting^[34-37].

In fact several articles in the literature have reported the possibility of discovering coexistent neoplasms such as gastrointestinal and gall bladder cancers during CT examination of vascular patients^[38-40].

Our study had some limitations. First of all, it is a retrospective study with some possible bias in patient selection, although the database used to find the patients was complete in medical records. Secondly, not all the patients underwent a prior chest radiography that could exclude patients with negative reports from the study. Additionally, a prospective study is mandatory to test the real impact of incidental findings in smoker patients who underwent EVAR planning or follow-up, in order to support the introduction of HRCT of the lung in the CT protocol for smoker patients.

In conclusion, this study actually demonstrates the possibility of early diagnosis of lung cancers during CTA EVAR planning or follow-up, overcoming the concept of dose radiation induced neoplasms, especially in patients over the age of 65.

COMMENTS

Background

Vascular diseases include an extended selection of pathologies (cardiovascular disease, thoraco-abdominal, peripheral vascular disease and brain vascular disease) and smoking is considered one of the main risk factor for the development of atherosclerosis and in particular oxidative stress and inflammation that provide the physiological connection between smoking and vascular diseases. Even if many articles reported the problem of unsuspected thoracic findings at computed tomographies, performed for suspected pulmonary

embolism or thoracic aortic pathology, the possibility to find chest pathology, and in particular lung cancer, in smoker patients suffering from vascular disease is underestimated.

Research frontiers

Nowadays the use of high resolution computed tomography (HRCT) in endovascular aortic aneurysm repair (EVAR) patients planning and follow up is not yet recommended but this study demonstrates the possibility to early diagnose lung cancers during EVAR planning or follow-up, overcoming the concept of dose radiation induced neoplasms, especially in over 65 years old patients.

Innovations and breakthroughs

To be known, this is the first study using HRCT for the evaluation of vascular patients during EVAR planning or follow-up.

Applications

HRCT could play a key role in the diagnosis of incidental lung findings during the evaluation of vascular patients (EVAR planning or follow-up) and surely in the management. In particular HRCT can discriminate patients with urgent lung surgical evaluation for the presence of malignancy, from patients in which a follow-up can be proposed, increasing lifelong patients expectancy.

Terminology

HRCT (high resolution computed tomography of the lung) before contrast agent administration, can lead a better evaluation of lung abnormalities enhancing nodule morphology and shape; CTA (computed tomography angiography) allow a better evaluation of vascular lumen during surgical planning and a correct assessment in cases of EVAR follow-up complications.

Peer-review

The manuscript is well written.

REFERENCES

- 1 Pini A, Bocalini G, Baccari MC, Becatti M, Garella R, Fiorillo C, Calosi L, Bani D, Nistri S. Protection from cigarette smoke-induced vascular injury by recombinant human relaxin-2 (serelaxin). *J Cell Mol Med* 2016; **20**: 891-902 [PMID: 26915460 DOI: 10.1111/jcmm.12802]
- 2 Michael Pittilo R. Cigarette smoking, endothelial injury and cardiovascular disease. *Int J Exp Pathol* 2000; **81**: 219-230 [PMID: 10971743 DOI: 10.1046/j.1365-2613.2000.00162.x]
- 3 Burke A, Fitzgerald GA. Oxidative stress and smoking-induced vascular injury. *Prog Cardiovasc Dis* 2003; **46**: 79-90 [PMID: 12920701 DOI: 10.1016/S0033-0620(03)00076-8]
- 4 Paraskevas KI, Mikhailidis DP, Veith FJ. Patients with peripheral arterial disease, abdominal aortic aneurysms and carotid artery stenosis are at increased risk for developing lung and other cancers. *Int Angiol* 2012; **31**: 404-405 [PMID: 22801408]
- 5 Ambrose JA, Barua RS. The pathophysiology of cigarette smoking and cardiovascular disease: an update. *J Am Coll Cardiol* 2004; **43**: 1731-1737 [PMID: 15145091 DOI: 10.1016/j.jacc.2003.12.047]
- 6 Messner B, Bernhard D. Smoking and cardiovascular disease: mechanisms of endothelial dysfunction and early atherogenesis. *Arterioscler Thromb Vasc Biol* 2014; **34**: 509-515 [PMID: 24554606 DOI: 10.1161/ATVBAHA.113.300156]
- 7 Bruzzi JF, Rémy-Jardin M, Delhay D, Teisseire A, Khalil C, Rémy J. When, why, and how to examine the heart during thoracic CT: Part 1, basic principles. *AJR Am J Roentgenol* 2006; **186**: 324-332 [PMID: 16423934 DOI: 10.2214/AJR.05.0717]
- 8 Sverzellati N, Arcadi T, Salvolini L, Dore R, Zompatori M, Mereu M, Battista G, Martella I, Toni F, Cardinale L, Maffei E, Maggi F, Cademartiri F, Pirroni T. Under-reporting of cardiovascular findings on chest CT. *Radiol Med* 2016; **121**: 190-199 [PMID: 26519045 DOI: 10.1007/s11547-015-0595-0]

- 9 **Lee SH**, Seo JB, Kang JW, Chae EJ, Park SH, Lim TH. Incidental cardiac and pericardial abnormalities on chest CT. *J Thorac Imaging* 2008; **23**: 216-226 [PMID: 18728554 DOI: 10.1097/RTI.0b013e318166a485]
- 10 **Hall WB**, Truitt SG, Scheunemann LP, Shah SA, Rivera MP, Parker LA, Carson SS. The prevalence of clinically relevant incidental findings on chest computed tomographic angiograms ordered to diagnose pulmonary embolism. *Arch Intern Med* 2009; **169**: 1961-1965 [PMID: 19933956 DOI: 10.1001/archinternmed.2009.360]
- 11 **Richman PB**, Courtney DM, Friese J, Matthews J, Field A, Petri R, Kline JA. Prevalence and significance of nonthromboembolic findings on chest computed tomography angiography performed to rule out pulmonary embolism: a multicenter study of 1,025 emergency department patients. *Acad Emerg Med* 2004; **11**: 642-647 [PMID: 15175202 DOI: 10.1111/j.1553-2712.2004.tb00717.x]
- 12 **Kino A**, Boisselle PM, Raptopoulos V, Hatabu H. Lung cancer detected in patients presenting to the Emergency Department studies for suspected pulmonary embolism on computed tomography pulmonary angiography. *Eur J Radiol* 2006; **58**: 119-123 [PMID: 16377113 DOI: 10.1016/j.ejrad.2005.11.008]
- 13 **Kasirajan K**, Dayama A. Incidental findings in patients evaluated for thoracic aortic pathology using computed tomography angiography. *Ann Vasc Surg* 2012; **26**: 306-311 [PMID: 22321476 DOI: 10.1016/j.avsg.2011.08.017]
- 14 **Nyheim T**, Staxrud LE, Jørgensen JJ, Jensen K, Olerud HM, Sandbæk G. Radiation exposure in patients treated with endovascular aneurysm repair: what is the risk of cancer, and can we justify treating younger patients? *Acta Radiol* 2017; **58**: 323-330 [PMID: 27279268 DOI: 10.1177/0284185116651002]
- 15 **Dindyal S**, Rahman S, Kyriakides C. Review of the Use of Ionizing Radiation in Endovascular Aneurysm Repair. *Angiology* 2015; **66**: 607-612 [PMID: 25225195 DOI: 10.1177/0003319714548564]
- 16 **Mazzei MA**, Guerrini S, Mazzei FG, Cioffi Squitieri N, Notaro D, de Donato G, Galzerano G, Sacco P, Setacci F, Volterrani L, Setacci C. Follow-up of endovascular aortic aneurysm repair: Preliminary validation of digital tomosynthesis and contrast enhanced ultrasound in detection of medium- to long-term complications. *World J Radiol* 2016; **8**: 530-536 [PMID: 27247719 DOI: 10.4329/wjr.v8.i5.530]
- 17 **National Cancer Institute**. NCI Dictionary of Cancer Terms. Available from: URL: <http://www.cancer.gov/dictionary?Cdrid=306510>
- 18 **De Silva L**, Ginter T, Forbush T. Extraction and quantification of pack-years and classification of smoker information in semi-structured Medical Records. Bellevue WA - USA: Proceedings of the 28th International Conference on Machine Learning, 2011
- 19 **NCCN**. National Comprehensive Cancer Network (NCCN): guidelines for patients/lung cancer screening. USA: National Comprehensive Cancer Network, 2014
- 20 **MacMahon H**, Naidich DP, Goo JM, Lee KS, Leung AN, Mayo JR, Mehta AC, Ohno Y, Powell CA, Prokop M, Rubin GD, Schaefer-Prokop CM, Travis WD, Van Schil PE, Bankier AA. Guidelines for Management of Incidental Pulmonary Nodules Detected on CT Images: From the Fleischner Society 2017. *Radiology* 2017; **23**: 161659 [PMID: 28240562 DOI: 10.1148/radiol.2017161659]
- 21 **Setacci F**, Sirignano P, de Donato G, Chisci E, Galzerano G, Cappelli A, Palasciano G, Setacci C. Endovascular approach for ruptured abdominal aortic aneurysms. *J Cardiovasc Surg (Torino)* 2010; **51**: 313-317 [PMID: 20523280]
- 22 **de Donato G**, Setacci C, Chisci E, Setacci F, Giubolini M, Sirignano P, Galzerano G, Cappelli A, Pieraccini M, Palasciano G. Abdominal aortic aneurysm repair in octogenarians: myth or reality? *J Cardiovasc Surg (Torino)* 2007; **48**: 697-703 [PMID: 17947926]
- 23 **Setacci F**, Sirignano P, de Donato G, Chisci E, Iacoponi F, Galzerano G, Palasciano G, Cappelli A, Setacci C. AAA with a challenging neck: early outcomes using the Endurant stent-graft system. *Eur J Vasc Endovasc Surg* 2012; **44**: 274-279 [PMID: 22705160 DOI: 10.1016/j.ejvs.2012.04.031]
- 24 **Setacci F**, Sirignano P, de Donato G, Galzerano G, Messina G, Guerrini S, Mazzei MA, Setacci C. Two-year-results of Endurant stent-graft in challenging aortic neck morphologies versus standard anatomies. *J Cardiovasc Surg (Torino)* 2014; **55**: 85-92 [PMID: 24356050]
- 25 **Speziale F**, Sirignano P, Setacci F, Menna D, Capoccia L, Mansour W, Galzerano G, Setacci C. Immediate and two-year outcomes after EVAR in "on-label" and "off-label" neck anatomies using different commercially available devices: analysis of the experience of two Italian vascular centers. *Ann Vasc Surg* 2014; **28**: 1892-1900 [PMID: 25011083 DOI: 10.1016/j.avsg.2014.06.057]
- 26 **Motaganahalli R**, Martin A, Feliciano B, Murphy MP, Slaven J, Dalsing MC. Estimating the risk of solid organ malignancy in patients undergoing routine computed tomography scans after endovascular aneurysm repair. *J Vasc Surg* 2012; **56**: 929-937 [PMID: 22784414 DOI: 10.1016/j.jvs.2012.02.061]
- 27 **Walsh C**, O'Callaghan A, Moore D, O'Neill S, Madhavan P, Colgan MP, Haider SN, O'Reilly A, O'Reilly G. Measurement and optimization of patient radiation doses in endovascular aneurysm repair. *Eur J Vasc Endovasc Surg* 2012; **43**: 534-539 [PMID: 22342015 DOI: 10.1016/j.ejvs.2012.01.028]
- 28 **Li X**, Samei E, Segars WP, Sturgeon GM, Colsher JG, Toncheva G, Yoshizumi TT, Frush DP. Patient-specific radiation dose and cancer risk estimation in CT: part II. Application to patients. *Med Phys* 2011; **38**: 408-419 [PMID: 21361209 DOI: 10.1118/1.3515864]
- 29 **Mazzei MA**, Scialpi M, Mazzei FG, Giacobone G, Volterrani L. Three-dimensional volumetric assessment with thoracic CT: a reliable approach for noncalcified lung nodules? *Radiology* 2010; **254**: 634; author reply 635 [PMID: 20093537 DOI: 10.1148/radiol.091655]
- 30 **Volterrani L**, Mazzei MA, Fedi M, Scialpi M. Computed tomography perfusion using first pass methods for lung nodule characterization: limits and implications in radiologic practice. *Invest Radiol* 2009; **44**: 124; author reply 124 [PMID: 19238004 DOI: 10.1097/01.rli.0000344907.14010.c4]
- 31 **Mazzei MA**, Cioffi Squitieri N, Guerrini S, Di Crescenzo V, Rossi M, Fonio P, Mazzei FG, Volterrani L. [Quantitative CT perfusion measurements in characterization of solitary pulmonary nodules: new insights and limitations]. *Recenti Prog Med* 2013; **104**: 430-437 [PMID: 24042423 DOI: 10.1701/1315.14591]
- 32 **Mazzei MA**, Squitieri NC, Sani E, Guerrini S, Imbriaco G, Di Lucia D, Guasti A, Mazzei FG, Volterrani L. Differences in perfusion CT parameter values with commercial software upgrades: a preliminary report about algorithm consistency and stability. *Acta Radiol* 2013; **54**: 805-811 [PMID: 23612426 DOI: 10.1177/0284185113484643]
- 33 **Eguchi T**, Fukui D, Takasuna K, Wada Y, Amano J, Yoshida K. Successful lung lobectomy for a lung cancer following thoracic endovascular aortic repair for a thoracic aortic aneurysm: report of a case. *Surg Today* 2014; **44**: 940-943 [PMID: 23266753 DOI: 10.1007/s00595-012-0470-8]
- 34 **Mazzei MA**, Guerrini S, Cioffi Squitieri N, Cagini L, Macarini L, Coppolino F, Giganti M, Volterrani L. The role of US examination in the management of acute abdomen. *Crit Ultrasound J* 2013; **5** Suppl 1: S6 [PMID: 23902801 DOI: 10.1186/2036-7902-5-S1-S6]
- 35 **Scaglione M**, Salvolini L, Casciani E, Giovagnoni A, Mazzei MA, Volterrani L. The many faces of aortic dissections: Beware of unusual presentations. *Eur J Radiol* 2008; **65**: 359-364 [PMID: 17950552 DOI: 10.1016/j.ejrad.2007.09.021]
- 36 **Mazzei MA**, Guerrini S, Cioffi Squitieri N, Imbriaco G, Mazzei FG, Volterrani L. Non-obstructive mesenteric ischemia after cardiovascular surgery: not so uncommon. *Ann Thorac Cardiovasc Surg* 2014; **20**: 253-255 [PMID: 23445796 DOI: 10.5761/atcs.le.12.02154]
- 37 **Setacci C**, De Donato G, Setacci F, Chisci E, Perulli A, Galzerano G, Sirignano P. Management of abdominal endograft infection. *J Cardiovasc Surg (Torino)* 2010; **51**: 33-41 [PMID: 20081760]
- 38 **Jung HJ**, Lee SS. Hybrid Treatment of Coexisting Renal Artery Aneurysm and Abdominal Aortic Aneurysm in a Gallbladder Cancer Patient. *Vasc Specialist Int* 2014; **30**: 68-71 [PMID: 26217619 DOI: 10.5758/vsi.2014.30.2.68]
- 39 **Kouvelos GN**, Patelis N, Antoniou GA, Lazaris A, Bali C, Matsagkas M. Management of concomitant abdominal aortic aneurysm and

colorectal cancer. *J Vasc Surg* 2016; **63**: 1384-1393 [PMID: 27005754
DOI: 10.1016/j.jvs.2016.01.026]

40 **Mohandas S**, Malik HT, Syed I. Concomitant abdominal aortic

aneurysm and gastrointestinal malignancy: evolution of treatment
paradigm in the endovascular era - review article. *Int J Surg* 2013; **11**:
112-115 [PMID: 23266417 DOI: 10.1016/j.ijvs.2012.11.022]

P- Reviewer: Gao BL, Razek AAKA, Tarazov PG **S- Editor:** Ji FF
L- Editor: A **E- Editor:** Lu YJ



Preoperative [18]fluorodeoxyglucose-positron emission tomography/computed tomography in early stage breast cancer: Rates of distant metastases

Vincent Vinh-Hung, Hendrik Everaert, Karim Farid, Navid Djassemi, Jacqueline Baudin-Veronique, Stefanos Bougas, Yuriy Michailovich, Clarisse Joachim-Contaret, Elsa Cécilia-Joseph, Claire Verschraegen, Nam P Nguyen

Vincent Vinh-Hung, Stefanos Bougas, Department of Radiation Oncology, University Hospital of Martinique, Fort-de-France 97200, Martinique

Hendrik Everaert, Department of Nuclear Medicine, Universitair Ziekenhuis Brussel, Brussels 1090, Belgium

Karim Farid, Department of Nuclear Medicine, University Hospital of Martinique, Fort-de-France 97200, Martinique

Navid Djassemi, Ross University School of Medicine, Miramar, FL 33027, United States

Jacqueline Baudin-Veronique, Cancer Research Department, University Hospital of Martinique, Fort-de-France 97200, Martinique

Yuriy Michailovich, Cancer Control Department, National Cancer Institute, Kyiv 03022, Ukraine

Clarisse Joachim-Contaret, Cancer Registry of the Martinique, Fort-de-France 97200, Martinique

Elsa Cécilia-Joseph, Biostatistics, Sciences Department, Schoelcher Campus of the University of the French West Indies, 97233 Schoelcher, Martinique

Claire Verschraegen, Department of Medical Oncology, Ohio State University Comprehensive Cancer Center, Columbus, OH 43210, United States

Nam P Nguyen, Department of Radiation Oncology, Howard University, Washington, DC 20060, United States

Author contributions: Vinh-Hung V and Nguyen NP conceptualized and designed the review; Nguyen NP carried out the analysis and drafted the initial manuscript; Cécilia-Joseph E reviewed the statistics; Vinh-Hung V, Everaert H, Farid K, Djassemi N, Baudin-Veronique J, Bougas S, Michailovich Y, Joachim-Contaret C, Cécilia-Joseph E and Verschraegen C contributed to the literature search, interpretation of the data, and critical revisions; all

authors reviewed and approved the final manuscript as submitted.

Conflict-of-interest statement: The authors declare no conflicts of interests for this article.

Data sharing statement: No additional data are available.

Open-Access: This article is an open-access article which was selected by an in-house editor and fully peer-reviewed by external reviewers. It is distributed in accordance with the Creative Commons Attribution Non Commercial (CC BY-NC 4.0) license, which permits others to distribute, remix, adapt, build upon this work non-commercially, and license their derivative works on different terms, provided the original work is properly cited and the use is non-commercial. See: <http://creativecommons.org/licenses/by-nc/4.0/>

Manuscript source: Invited manuscript

Correspondence to: Vincent Vinh-Hung, MD, PhD, Chair, Department of Radiation Oncology, University Hospital of Martinique, Bld Pasteur, Fort-de-France 97200, Martinique. vincent.vinh-hung@chu-martinique.fr
Telephone: +596-696-542019

Received: March 28, 2017

Peer-review started: March 29, 2017

First decision: April 18, 2017

Revised: May 20, 2017

Accepted: June 19, 2017

Article in press: June 20, 2017

Published online: July 28, 2017

Abstract

AIM

To investigate rates of distant metastases (DM) detected with [18]fluorodeoxyglucose-positron emission

tomography/computed tomography (¹⁸FDG-PET/CT) in early stage invasive breast cancer.

METHODS

We searched the English language literature databases of PubMed, EMBASE, ISI Web of Knowledge, Web of Science and Google Scholar, for publications on DM detected in patients who had ¹⁸FDG-PET/CT scans as part of the staging for early stages of breast cancer (stage I and II), prior to or immediately following surgery. Reports published between 2011 and 2017 were considered. The systematic review was conducted according to the PRISMA guidelines.

RESULTS

Among the 18 total studies included in the analysis, the risk of DM ranged from 0% to 8.3% and 0% to 12.9% for stage I and II invasive breast cancer, respectively. Among the patients with clinical stage II, the rate of occult metastases diagnosed by ¹⁸FDG-PET/CT was 7.2% (range, 0%-19.6%) for stage II A and 15.8% (range, 0%-40.8%) for stage II B. In young patients (< 40-year-old), ¹⁸FDG-PET/CT demonstrated a higher prevalence of DM at the time of diagnosis for those with aggressive histology (*i.e.*, triple-negative receptors and poorly differentiated grade).

CONCLUSION

Young patients with poorly differentiated tumors and stage II B triple-negative breast cancer may benefit from ¹⁸FDG-PET/CT at initial staging to detect occult DM prior to surgery.

Key words: Breast cancer; Early stage; Staging workup; Distant metastases; [18]fluorodeoxyglucose-positron emission tomography/computed tomography scan

© **The Author(s) 2017.** Published by Baishideng Publishing Group Inc. All rights reserved.

Core tip: This systematic review identifies groups of patients with early stage breast cancer who might benefit most from [18]fluorodeoxyglucose-positron emission tomography/computed tomography (commonly known as ¹⁸FDG-PET/CT) scan at initial staging, prior to surgery.

Vinh-Hung V, Everaert H, Farid K, Djassemi N, Baudin-Veronique J, Bougas S, Michailovich Y, Joachim-Contaret C, Cécilia-Joseph E, Verschraegen C, Nguyen NP. Preoperative [18]fluorodeoxyglucose-positron emission tomography/computed tomography in early stage breast cancer: Rates of distant metastases. *World J Radiol* 2017; 9(7): 312-320 Available from: URL: <http://www.wjgnet.com/1949-8470/full/v9/i7/312.htm> DOI: <http://dx.doi.org/10.4329/wjr.v9.i7.312>

INTRODUCTION

Breast cancer is the most common cancer in women

worldwide^[1]. Mortality of breast cancer has declined notably in the United States, with death rates in 2012 decreasing 36% from peak rates as a result of improvements in early detection and treatment^[2]. Yet, there remains considerable heterogeneity in the outcomes of early stage breast cancer^[3]. The rate of death at 7 year due to stage I breast cancer was 2.1% in women aged 40 years or younger (as compared to 1.6% in women aged over 50) and was 3.8% in women with negative estrogen receptor status (as compared to 1.1% in those with positive estrogen receptor status)^[3].

There is a large consensus that imaging should be limited to patients with apparent advanced disease or clinical suspicion of metastases^[4-7]. Accordingly, staging scans are seldom performed^[6,8]. The question arises, then, as to whether the excess mortality observed in "early stage" patients^[3] is due to unfavorable biological factors or instead to the initial misclassification as "early stage". We hypothesize that some clinically early stage breast cancer patients could benefit from a formal staging workup.

[18]fluorodeoxyglucose-positron emission tomography (¹⁸FDG-PET) scan is a valuable, well established tool for diagnostic staging in numerous cancer sites^[9-12], as well as for locally advanced breast cancer to detect distant metastases (DM)^[13-15]. Even though PET imaging is more sensitive for detection of loco-regional spread and metastatic disease in breast cancer compared to computed tomography (CT) scan alone, its high cost precludes the routine use of PET scan in clinical practice. Thus, a review of the literature is necessary for future guidelines about the benefit of PET scan in early stage breast cancer.

Standard-of-care for early stage breast cancer is surgery, either alone or followed by adjuvant radiotherapy and/or systemic therapy, depending on the pathologic stage and the type of surgery to be performed. The presence or absence of axillary lymph node metastases in patients with clinically non-palpable lymph nodes is routinely assessed through sentinel lymph node sampling or axillary lymph node dissection. Alternatively, PET scan could be most helpful in assessing the presence of DM in early stage breast cancer, which would preclude first-line surgery^[16]. The prevalence of occult DM diagnosed by PET scan in patients with early stage breast cancer has not been analyzed and was the topic of this literature review. In particular, we sought to identify subsets of early stage breast cancer patients who might benefit most from PET scan, prior to surgery.

MATERIALS AND METHODS

Literature search strategy

Electronic searches were performed in the following databases: PubMed, EMBASE, ISI Web of Knowledge (Web of Science), and Google Scholar. The following terms were explored and used in each database search: "Breast cancer", "surgery", "PET scan", "distant

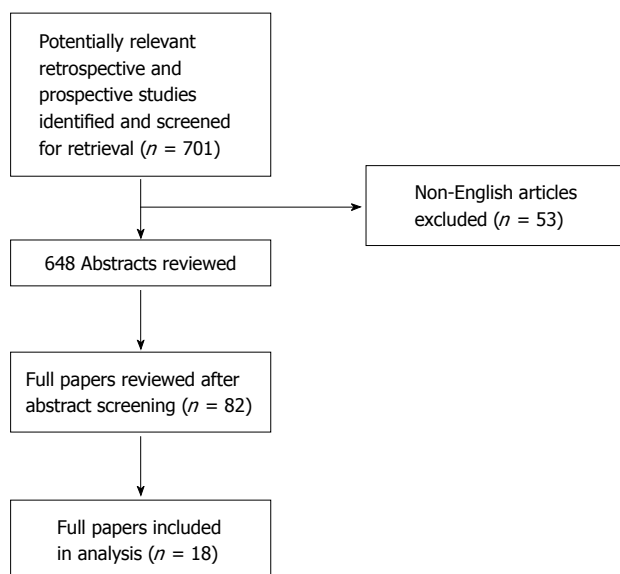


Figure 1 PRISMA flow diagram of the included studies.

metastases", and "stage I (T1N0M0) and II (T0-2N1M0, T3N0M0)". All relevant articles were accessed in full-text. The reference lists of relevant papers were then searched for additional publications.

Selection criteria

Eligible studies over the past 6 year (2011-2017) in the present review included those in which patients had ¹⁸FDG-PET/CT scan as part of their workup prior to or immediately after surgery for histologically-proven breast cancer, regardless of age or sex, and in which the rates of DM were reported by ¹⁸FDG-PET/CT scan. All patients had clinical stage I or stage II breast cancer. Only studies reported in English were considered. Duplicated studies were excluded.

Data extraction and critical appraisal

Prevalence of DM was extracted from each study and correlated to the disease stage. The influence of age, histology (e.g., lobular vs ductal), tumor grade (e.g., well differentiated vs poorly differentiated), and receptor status on the rate of DM (if reported) was also analyzed using descriptive summaries.

RESULTS

Number of reports analyzed

Figure 1 summarizes the search strategy. A total of 701 reports published between 2011 and 2017 were considered. Out of the 82 full papers that were assessed according to their potential for consisting of information relevant to the review, 18 were found to match the selection criteria and were selected for study inclusion. ¹⁸FDG-PET/CT scanning had been performed in addition to the clinical staging with or without conventional imaging in those 18 studies, either through a retrospective review or within a prospective protocol.

As none of the studies was randomized, bias could not be excluded. Publications reviewing patients with early stage invasive breast cancer were included.

Prevalence of DM diagnosed by ¹⁸FDG-PET/CT scan according to patient characteristics

Clinical stage: The rates of DM ranged from 0% to 30%^[17-34] for the entire group of reported patients. However, only 9 of the studies correlated DM rates detected by ¹⁸FDG-PET/CT with the clinical stage^[17,22-24,27,29,31,32,34]. The rate of DM was lowest among studies of patients with invasive lobular cancer compared to studies that had included a mixture of other histologies, such as invasive ductal carcinoma^[18] (Tables 1 and 2).

Overall, the rate of DM for presumed stage I was low for all cancer types but non-negligible, ranging from 0% to 8.3%^[22,27,29,31,32,34]. Among the 9 studies that reported the rate of DM in patients with stage II breast cancer separately, the prevalence ranged from 0% to 12.4%^[17,22,24,27,29,31,32,34]. Patients with large tumors and/or axillary lymph node metastases appeared to be at increased risk of DM; specifically, the rate of DM was 7.2% (range, 0%-19.6%) and 15.8% (range, 0%-40.8%) for stage II A and stage II B, respectively^[17,22,24,27,31,32,34].

Tumor size: Among studies that included a significant proportion of patients with large tumors (T2 and/or T3), the DM rate was higher and ranged from 8% to 8.4%^[18,19], as compared to the range of 1.5% to 4.8% in studies including patients with smaller tumors^[21,23,28]. However, since those latter studies also included a small proportion of patients with stage III disease and did not analyze the metastatic rate in relation to the clinical stage, the correlation between tumor size and DM rate remains unclear.

Nodal status: Patients who presented with N1 disease also presented with a higher risk of having DM. The rate of DM was 6% and 20% for N0 and N1 disease, respectively^[31].

Receptor status: Among the 232 patients with triple-negative breast cancer, the DM rate was 0% and 10.9% for clinical stage I and stage II diseases, respectively, but there was no comparison performed with receptor-positive cases^[32]. Other studies did not report the rates of DM according to receptor status.

Age: Two studies reported the influence of age on DM rate^[27,33]. In the first study, among 134 young patients (< 40-year-old), the DM rate was 5% and 10.9% for clinical stage I and stage II, respectively^[27]. In the second study, among 214 stage I-III patients, the DM rates did not differ significantly between the age groups of < 40-year-old and ≥ 40-year-old^[33]. However, the DM rates in the younger age group were 8% in stage I, 9% in stage II A and 17% in stage II B, equating to 2x's

Table 1 Prevalence of distant metastases in patients with invasive breast cancer who had [¹⁸F]fluorodeoxyglucose-positron emission tomography scan as part of the workup before or immediately after surgery

Ref.	Subjects, <i>n</i>	Stage	Age, median	Histology	Tumor grade	Tumor receptors	Distant metastases	2 nd primaries
Groheux <i>et al</i> ^[17]	131	II: 84 III: 47 T1: 2 T2: 71 T3: 58 N0: 50 N1: 59 N2: 18	NS	IDC: 114 ILC: 8 Other: 9	1: 9 2: 5 3: 53 NS: 4	ER+: 82 HER2+: 30	5.90% (II)	1% (II)
Bernsdorf <i>et al</i> ^[18]	103	T2 or higher	55 (24-81)	IDC: 83 ILC: 14 Other: 6	1: 11 2: 54 3: 37 NS: 1	ER+: 74 HER2+: 22 TN: 13	8%	1.90%
Choi <i>et al</i> ^[19]	154	I: 69 II: 51 III: 21 IV: 13 T1: 89 T2: 51 T3: 14	52 (30-81)	IDC: 141 ILC: 4 Other: 9	NS: 154	NS	8.40%	NS
Garami <i>et al</i> ^[20]	115	T1: 56 T2: 48 NS: 11 N0: 57 N+: 46 NS: 12	55.7	IDC: 92 ILC: 11 Other: 12	1: 16 2: 50 3: 48 NS: 1	ER+: 89 ER-: 26	6.90%	2.60%
Groves <i>et al</i> ^[21]	70	T1: 34 T2: 30 N1: 24	61	IDC: 45 ILC: 10 Other: 5	1: 02 2: 33 3: 25	ER+: 64 HER+: 15	2.80%	NS
Gunalp <i>et al</i> ^[22]	141	I: 19 II: 100 III: 14	47 (28-78)	NS	2 + 3: 141	NS	5% (I) 30% (II)	NS
Pritchard <i>et al</i> ^[23]	325	T1: 207 T2: 110 T3: 8 N0: 325	56 (28-83)	IDC: 290 ILC: 35	1: 68 2: 158 3: 92	NS	1.50%	NS
Cochet <i>et al</i> ^[24]	142	II: 79 III: 46 IV: 17 T2 or Higher	51 (25-85)	IDC: 128 ILC: 11 Other: 3	1+2: 81 3: 56 NS: 3	ER+/HER2-: 63 HER2+: 33 TN: 31	7.5% (II)	NS
Jeong <i>et al</i> ^[25]	178	N0: 178 T1: 108 T2: 64 T3: 6	54.9 (33-82)	IDC: 145 ILC: 11 DCIS: 12 Other: 10	NS	NS	0%	2.80%
Koolen <i>et al</i> ^[26]	62	I: 35 II: 25 III: 2 T1: 62	59.8 (26-75)	IDC: 58 ILC: 1 Other: 3	1: 21 2: 29 3: 09 NS: 3	ER+/HER2-: 48 TN: 7 HER2+: 7	16%	3%
Riedl <i>et al</i> ^[27]	134	I: 20 II: 91 III: 19	36.2 (22-39)	IDC: 124 ILC: 1 Other: 9	1: 01 2: 23 3: 110	ER+/HER2-: 75 HER2+: 26	5% (I) 10.9% (II)	4%
Zhang <i>et al</i> ^[28]	164	T1: 127 T2: 35 T3: 2 N0: 123 N1: 29 N2: 9 N3: 3	45 (21-70)	IDL: 150 ILC: 14	1: 23 2-3: 141	ER+: 140 HER2+: 18	4.80%	NS
Hogan <i>et al</i> ^[29]	146	I: 8 II: 50 III: 88	57 (34-92)	ILC: 146	NS	ER+/HER2-: 132 HER2+: 8 TN: 5	0% (I) 4% (II)	NS
Krammer <i>et al</i> ^[30]	101	II: 75 III: 15 IV: 11 T1: 7	54	IDC: 80 ILC: 15 Other: 9	1: 05 2: 48 3: 45 NS: 6	ER+: 67 HER2+: 56	15.80%	NS

Nursal <i>et al</i> ^[31]	419	T2: 69 T3: 4 T4: 5	51.5	IDC: 305 ILC: 29 Other: 85	NS	NS	2.9% (I) 12.4% (II)	NS
		I : 104						
		II : 315						
		T1: 127 T2: 270 T3: 20						
Ulaner <i>et al</i> ^[32]	232	I : 23	51 (25-93)	IDC: 217 ILC: 2	2: 8 3: 217 NS: 7	TN: 232	0% (I) 10% (II)	NS
		II : 169						
		III: 40						
Lebon <i>et al</i> ^[33]	214	I : 24	45.2	IDC: 181 ILC: 10 Other: 23	1: 13 2: 68 3: 133	HR+/HER2-: 89 HER2+: 61 TN: 63 NS: 1	8.3% (I) 12.9% (II)	NS
		II : 124						
		III: 66						
Ulaner <i>et al</i> ^[34]	483	I : 36	52.7 (23.6-89.5)	IDC: 414 ILC: 41 Other: 28	1: 5 2: 55 3: 400 NS: 23	ER+: 402 HER2+: 245 TN: 0	2.8% (I) 9.7% (II) 24.1% (III)	1.40%
		II : 331						
		III: 116						

DCIS: Ductal carcinoma *in situ*; ER: Estrogen receptor; ¹⁸FDG-PET: [18]fluorodeoxyglucose-positron emission tomography; HER2: Human epidermal growth factor receptor 2; IDC: Invasive ductal carcinoma; ILC: Invasive lobular carcinoma; NS: Not specified; PR: Progesterone receptor; TN: Triple-negative.

Table 2 Prevalence of occult distant metastases in clinical stage II patients who had [18]fluorodeoxyglucose-positron emission tomography scan as part of a staging workup before or immediately after surgery

Ref.	Subjects, <i>n</i>	Age, median	Distant metastases rate		
			II A	II B	All
Grobeux <i>et al</i> ^[17]	84	NS	2.80% (1/36)	8.30% (4/48)	5.95%
Gunalp <i>et al</i> ^[22]	100	51	19.60% (10/51)	40.80% (20/49)	30%
Cochet <i>et al</i> ^[24]	142	51	9.10% (2/22)	7.00% (4/57)	7.60%
Jeong <i>et al</i> ^[25]	70	54.9	0% (0/64)	0% (0/6)	0%
Riedl <i>et al</i> ^[27]	91	36.2	5% (2/44)	17% (8/47)	10.90%
Nursal <i>et al</i> ^[31]	315	51.5	9.50% (19/199)	17.20% (20/116)	12.40%
Ulaner <i>et al</i> ^[32]	169	51	5% (4/82)	15% (13/87)	9.50%
Lebon <i>et al</i> ^[33]	124	45.2	11% (7/64)	15% (9/60)	12.90%
Ulaner <i>et al</i> ^[34]	483	52.7	4.20% (6/143)	13.80% (26/188)	9.70%
All	1578	47.8	7.20% (0%-19.6%)	15.80% (0%-40.8%)	11.40% (0%-12.9%)

¹⁸FDG-PET: [18]fluorodeoxyglucose-positron emission tomography; NS: Not specified.

higher than those found in the first study.

Histologic grade: Histologic grade of the tumor may also be associated with increased risk of developing DM. Among 141 patients with moderate to poorly differentiated invasive breast cancers, the rate of DM was 30% for stage II patients^[22]. However, correlation between tumor histologic grade and DM risk was not investigated in other studies^[17-21,23,24,26-33].

DISCUSSION

This article reviews the role of ¹⁸FDG-PET/CT scan in the detection of DM in patients with early stages (*i.e.*, I and II) of invasive breast cancer. The findings might represent important information applicable to discussions with patients about the utility of the scan. In contrast to stage III breast cancer, the role of ¹⁸FDG-PET/CT scan in identifying patients with clinical stages I and II who are at high risk of DM is

controversial. Even though ¹⁸FDG-PET/CT scan may also be capable of identifying a second primary cancer, its main role in patients with breast cancer is the detection of DM, which could preclude upfront surgery^[16]. Furthermore, the detection of DM could be of critical importance for the correct classification of patients and in the evaluation of treatment outcomes.

As the risk of DM is low in "early stage" asymptomatic breast cancer patients, an expensive imaging study, such as with the ¹⁸FDG-PET/CT scan, is not justified for the staging workup of all patients^[6,35]. However, breast cancer is a heterogeneous disease, with some subgroups of patients at risk of developing DM even at the early stage. Subgroups of breast cancer patients with worse outcome include younger patients^[36] and patients that have tumors with a more aggressive biological profile^[37]. Rare histologic subtypes, such as metaplastic carcinoma of breast and invasive micropapillary carcinoma, are also more frequently associated with poor prognosis because of the high

rate of axillary lymph node involvement and DM^[38,39]. Genomic classification of risk, such as the oncotype DX and Perou's studies, also identified the risk of distant recurrence^[40-42]. Thus, those patients at high risk of systemic spread may benefit from early diagnosis of DM, for which chemotherapy may be initiated in a timely manner and unnecessary surgery may be avoided. The benefit of ¹⁸FDG-PET scan may outweigh its cost in those circumstances.

In patients with clinical stage I breast cancer, regardless of age, tumor grade or aggressive histology, the risk of DM as diagnosed by ¹⁸FDG-PET scan ranged from 0% to 8.3%^[22,27,29,31-34]. This low, though not negligible, metastatic rate has been corroborated in studies with a high proportion of patients with T1 and N0 disease^[21,23]. Even though the number of patients with stage I disease in those studies was small, preliminary evidence suggested that ¹⁸FDG-PET scan may not be cost effective for clinical stage I patients.

In patients with clinical stage II breast cancer, the prevalence of occult DM detected through ¹⁸FDG-PET scan ranged from 0% to 12.4%^[17,22,24,27,29,31,32,34]. As stage II breast cancer patients also comprise a heterogeneous group, the risk of DM is higher for patients with stage II B disease (T3N0M0, T2N1M0) than for those with stage II A (T1N1M0, T2N0M0) disease. Discounting the one study that included only 6 patients with stage II B disease^[25], the risk of unsuspected DM diagnosed by ¹⁸FDG-PET scan ranged from 2.8% to 19.6% for stage II A and 9.1% to 40% for stage II B, respectively^[17,22,27,31,32,34] (Table 2).

Patients with stage II B have larger tumors than those with stage II A. As tumor size has been reported to be correlated with an increased risk of DM, this may be one of the reasons underlying the higher rate of DM at diagnosis^[43]. Other studies have corroborated the increased prevalence of DM diagnosed with ¹⁸FDG-PET scan for patients with large tumors compared to those with smaller tumors^[18-21,23,28]. It is likely that other factors, like axillary lymph node metastases and tumor biology, may also lead to a high rate of DM at diagnosis^[22,24,27,29,31].

Patients with triple-negative breast cancer frequently have a worse prognosis than their counterparts who harbor other subtypes because of the high rate of DM^[44]. A 10% rate of unsuspected DM was seen on ¹⁸FDG-PET scan compared to conventional imaging for patients with clinical stage II breast cancer^[32]. However, even among those triple-negative breast cancer patients, the rate of DM remained low for stage II A disease. Specifically, the DM rate was 5% and 15% for stage II A and II B triple-negative breast cancers, respectively.

Another prognostic factor that has been reported in the literature is the patient age at diagnosis. Young patients (< 40-year-old) may have a more aggressive tumor biology that translates to a lower survival rate compared to older patients^[36]. Among young patients with breast cancer, those with stage II B disease had

a 17% rate of DM compared to 5% for stage II A. The incidence of DM in patients with clinical stage II A with moderate to poorly differentiated grade carcinoma climbs to 19.6% after ¹⁸FDG-PET scanning^[22]. Tumor biology needs to be taken into account beyond the conventional TNM staging. In patients with invasive micropapillary carcinoma, for example, a high rate of DM detected by ¹⁸FDG-PET scan before surgery has been reported. Among 16 patients with invasive micropapillary carcinoma who underwent ¹⁸FDG-PET scan when the tumor was diagnosed, axillary lymph node metastases and DM were observed in 12 (75% of cases)^[45].

To date, this is the first study looking at the impact of ¹⁸FDG-PET on the management of invasive micropapillary carcinoma, a rare tumor with a high rate of axillary lymph node invasion and DM, even in the case of a relatively small tumor. Moreover, no study has been performed yet to investigate the role of ¹⁸FDG-PET scan for the diagnosis of occult DM in patients who had surgery for metaplastic carcinoma of the breast, another rare tumor with a poor survival rate associated with a high propensity to metastasize to distant sites.

Our study was restricted by the limited availability of the data correlating clinical stages and biology with the risk of DM diagnosed with ¹⁸FDG-PET/CT scan in patients with early stage breast cancer. Ki-67 is a known prognostic marker^[46] but was not reported in any of the recent and largest studies^[31-34]. Most studies were retrospective. The classification of patients into stages was usually done after the ¹⁸FDG-PET/CT image acquisition, which might have affected the selection of patients. Some studies included the more advanced stages, stage III and IV, and a few studies included post-operative patients. Many issues of importance are relevant for breast cancer, notably the emerging role of PET/MRI and its comparison with PET/CT^[47], the use of PET in the monitoring of neoadjuvant therapy^[48], the use for staging and restaging^[49], the standardized uptake values (commonly known as SUVs) and how they relate to lymph node status^[50], the prognostic role of FDG-PET^[51] and the suitability for treatment planning^[52]; all these represent immensely exciting domains of breast cancer research, but would have confused the scope of the present study, namely the rates of DM.

In summary, the current review suggests a need for future prospective studies looking at subgroups of patients who would most likely benefit from PET scan before surgery-stage II B, poorly differentiated tumors, rare tumors with aggressive biology, such as invasive micropapillary carcinoma, and young age. These patients would most likely receive systemic therapy. Detection of DM could help in selecting the optimal sequence of therapies and the monitoring thereof. Incorporating biomarkers such as c-erbB2 and genetic arrays in those studies may further help the clinician to define the risk of DM at diagnosis for patients with early stage breast cancer.

Conclusion

In patients with clinical stage I breast cancer, the systematic use of ¹⁸FDG-PET/CT scan for staging is not cost effective because the yield of ¹⁸FDG-PET/CT-detected DM in clinical stage I is low. In young patients with stage II B triple-negative and/or poorly differentiated breast cancer, ¹⁸FDG-PET/CT scan identifies a substantial rate of DM and should therefore be considered for these patients. Finally, the role of ¹⁸FDG-PET for stage II breast cancer and for rare tumors with aggressive biology needs to be defined in future prospective studies.

ACKNOWLEDGMENTS

The authors would like to express their heartfelt gratitude to Carl Leak, for revising the language of this manuscript, to Jessica Malki, Olga Morgan, Brentwood Oftedal, Yeoshina Pillay and Andrew Westfall of the RUSM Oncology Society, Ross University School of Medicine, Dominica, West Indies for their enthusiastic interest and partaking in the discussion and the writing.

COMMENTS

Background

Staging of cancer is the process of identifying and classifying the extent of the disease. Staging is important to aid the clinician in planning treatment, to inform the patient on prognosis, to evaluate the results of treatment, and to facilitate the exchange of information between treatment centers. Initial staging is based on all evidence acquired before treatment. The evidence arises from physical examination, imaging, pathology, and/or endoscopic or surgical exploration.

Research frontiers

In early breast cancer (small tumor and no symptom), previous diagnostic studies rarely detected metastases. The contentious issue is that the earlier studies were based on the use of conventional imaging with poor detection performance. Metastatic disease might have been missed.

Innovations and breakthroughs

[¹⁸F]fluorodeoxyglucose-positron emission tomography/computed tomography (¹⁸FDG-PET/CT) combines metabolic and anatomic imaging. It requires a dual competence in radiology and in nuclear medicine. Negative reviews of its role in breast cancer confounded it with ¹⁸FDG-PET alone, did not have the joint nuclear-radiologist's expertise to analyze the images, or focused only on the detection of regional lymph node involvement. There has been no pooled evaluation of the rates of distant metastases detected with ¹⁸FDG-PET/CT. This study fills the gap.

Applications

The present review identifies groups of patients with early breast cancer, who are at high risk for distant metastases, notably those with stage II B or aggressive histologies, in whom it might be prudent to reconsider the role of ¹⁸FDG-PET/CT.

Terminology

¹⁸FDG is a radioactively labeled glucose analog. It allows the detection of tissues that have a high glucose uptake, such as tumors with a high metabolic activity. Imaging with ¹⁸FDG, the ¹⁸FDG-PET, shows areas of high activity. The ¹⁸FDG-PET imaging combined with CT imaging shows where the areas of high activity are distributed in the body; N1 disease: Cancer that has spread to regional lymph nodes; Distant metastases: Cancer that has spread beyond the breast and regional lymph nodes to distant organs or distant lymph nodes;

Triple-negative breast cancer: Breast tumor that tested negative for the estrogen receptor, the progesterone receptor, and the human epidermal growth receptor HER2. Triple negative tumors might respond to chemotherapy but will not to receptor targeted treatments.

Peer-review

A well-written review article, summarising important information to the field.

REFERENCES

- 1 **Schnitt SJ**, Lakhani SR. Breast Cancer in: World Cancer Report 2014. Lyon, France: International Agency for Research on Cancer, 2014: 362-373
- 2 **Siegel RL**, Miller KD, Jemal A. Cancer statistics, 2016. *CA Cancer J Clin* 2016; **66**: 7-30 [PMID: 26742998 DOI: 10.3322/caac.21332]
- 3 **Iqbal J**, Ginsburg O, Rochon PA, Sun P, Narod SA. Differences in breast cancer stage at diagnosis and cancer-specific survival by race and ethnicity in the United States. *JAMA* 2015; **313**: 165-173 [PMID: 25585328 DOI: 10.1001/jama.2014.17322]
- 4 **Barrett T**, Bowden DJ, Greenberg DC, Brown CH, Wishart GC, Britton PD. Radiological staging in breast cancer: which asymptomatic patients to image and how. *Br J Cancer* 2009; **101**: 1522-1528 [PMID: 19861999 DOI: 10.1038/sj.bjc.6605323]
- 5 **Senkus E**, Kyriakides S, Ohno S, Penault-Llorca F, Poortmans P, Rutgers E, Zackrisson S, Cardoso F. Primary breast cancer: ESMO Clinical Practice Guidelines for diagnosis, treatment and follow-up. *Ann Oncol* 2015; **26** Suppl 5: v8-30 [PMID: 26314782 DOI: 10.1093/annonc/mdv298]
- 6 **Merrill SA**, Stevens P, Verschraegen C, Wood ME. Utility and Costs of Routine Staging Scans in Early-Stage Breast Cancer. *Am J Hematol Oncol* 2016; **12**: 4
- 7 **Schnipper LE**, Smith TJ, Raghavan D, Blayney DW, Ganz PA, Mulvey TM, Wollins DS. American Society of Clinical Oncology identifies five key opportunities to improve care and reduce costs: the top five list for oncology. *J Clin Oncol* 2012; **30**: 1715-1724 [PMID: 22493340 DOI: 10.1200/JCO.2012.42.8375]
- 8 **Chand N**, Cutress RI, Oeppen RS, Agrawal A. Staging Investigations in Breast Cancer: Collective Opinion of UK Breast Surgeons. *Int J Breast Cancer* 2013; **2013**: 506172 [PMID: 24349790 DOI: 10.1155/2013/506172]
- 9 **Zhang Y**, Feng B, Zhang GL, Hu M, Fu Z, Zhao F, Zhang XL, Kong L, Yu JM. Value of 18F-FDG PET-CT in surveillance of postoperative colorectal cancer patients with various carcinoembryonic antigen concentrations. *World J Gastroenterol* 2014; **20**: 6608-6614 [PMID: 24914384 DOI: 10.3748/wjg.v20.i21.6608]
- 10 **Tantiwongkosi B**, Yu F, Kanard A, Miller FR. Role of (18)F-FDG PET/CT in pre and post treatment evaluation in head and neck carcinoma. *World J Radiol* 2014; **6**: 177-191 [PMID: 24876922 DOI: 10.4329/wjrv.v6.i5.177]
- 11 **Sun L**, Wan Y, Lin Q, Sun YH, Zhao L, Luo ZM, Wu H. Multiple primary malignant tumors of upper gastrointestinal tract: a novel role of 18F-FDG PET/CT. *World J Gastroenterol* 2010; **16**: 3964-3969 [PMID: 20712059 DOI: 10.3748/wjg.v16.i31.3964]
- 12 **Abuodeh Y**, Naghavi AO, Ahmed KA, Venkat PS, Kim Y, Kis B, Choi J, Biebel B, Sweeney J, Anaya DA, Kim R, Malafa M, Frakes JM, Hoffe SE, El-Haddad G. Prognostic value of pre-treatment F-18-FDG PET-CT in patients with hepatocellular carcinoma undergoing radioembolization. *World J Gastroenterol* 2016; **22**: 10406-10414 [PMID: 28058021 DOI: 10.3748/wjg.v22.i47.10406]
- 13 **Groheux D**, Giacchetti S, Delord M, Hindié E, Vercellino L, Cuvier C, Toubert ME, Merlet P, Hennequin C, Espié M. 18F-FDG PET/CT in staging patients with locally advanced or inflammatory breast cancer: comparison to conventional staging. *J Nucl Med* 2013; **54**: 5-11 [PMID: 23213197 DOI: 10.2967/jnumed.112.106864]
- 14 **Champion L**, Lerebours F, Cherel P, Edeline V, Giraudet AL, Wartski M, Bellet D, Alberini JL. 18F-FDG PET/CT imaging versus dynamic contrast-enhanced CT for staging and prognosis of inflammatory breast cancer. *Eur J Nucl Med Mol Imaging* 2013; **40**: 1206-1213 [PMID: 23640467 DOI: 10.1007/s00259-013-2405-z]
- 15 **Liu Y**. Role of FDG PET-CT in evaluation of locoregional nodal

- disease for initial staging of breast cancer. *World J Clin Oncol* 2014; **5**: 982-989 [PMID: 25493234 DOI: 10.5306/wjco.v5.i5.982]
- 16 **Badwe R**, Hawaldar R, Nair N, Kaushik R, Parmar V, Siddique S, Budrukkar A, Mittra I, Gupta S. Locoregional treatment versus no treatment of the primary tumour in metastatic breast cancer: an open-label randomised controlled trial. *Lancet Oncol* 2015; **16**: 1380-1388 [PMID: 26363985 DOI: 10.1016/S1470-2045(15)00135-7]
 - 17 **Groheux D**, Giacchetti S, Espié M, Vercellino L, Hamy AS, Delord M, Berenger N, Toubert ME, Misset JL, Hindié E. The yield of 18F-FDG PET/CT in patients with clinical stage IIA, IIB, or IIIA breast cancer: a prospective study. *J Nucl Med* 2011; **52**: 1526-1534 [PMID: 21880576 DOI: 10.2967/jnumed.111.093864]
 - 18 **Bernsdorf M**, Berthelsen AK, Wielenga VT, Kroman N, Teilum D, Binderup T, Tange UB, Andersson M, Kjær A, Loft A, Graff J. Preoperative PET/CT in early-stage breast cancer. *Ann Oncol* 2012; **23**: 2277-2282 [PMID: 22357250 DOI: 10.1093/annonc/mds002]
 - 19 **Choi YJ**, Shin YD, Kang YH, Lee MS, Lee MK, Cho BS, Kang YJ, Park JS. The Effects of Preoperative (18)F-FDG PET/CT in Breast Cancer Patients in Comparison to the Conventional Imaging Study. *J Breast Cancer* 2012; **15**: 441-448 [PMID: 23346174 DOI: 10.4048/jbc.2012.15.4.441]
 - 20 **Garami Z**, Hascsi Z, Varga J, Dinya T, Tanyi M, Garai I, Damjanovich L, Galuska L. The value of 18-FDG PET/CT in early-stage breast cancer compared to traditional diagnostic modalities with an emphasis on changes in disease stage designation and treatment plan. *Eur J Surg Oncol* 2012; **38**: 31-37 [PMID: 21937190 DOI: 10.1016/j.ejso.2011.09.002]
 - 21 **Groves AM**, Shastry M, Ben-Haim S, Kayani I, Malhotra A, Davidson T, Kelleher T, Whittaker D, Meagher M, Holloway B, Warren RM, Ell PJ, Keshtgar MR. Defining the role of PET-CT in staging early breast cancer. *Oncologist* 2012; **17**: 613-619 [PMID: 22539550 DOI: 10.1634/theoncologist.2011-0270]
 - 22 **Gunalp B**, Ince S, Karacalioglu AO, Ayan A, Emer O, Alagoz E. Clinical impact of (18)F-FDG PET/CT on initial staging and therapy planning for breast cancer. *Exp Ther Med* 2012; **4**: 693-698 [PMID: 23170128 DOI: 10.3892/etm.2012.659]
 - 23 **Pritchard KI**, Julian JA, Holloway CM, McCready D, Gulenchyn KY, George R, Hodgson N, Lovrics P, Perera F, Elavathil L, O'Malley FP, Down N, Bodurtha A, Shelley W, Levine MN. Prospective study of 2-[18F]fluorodeoxyglucose positron emission tomography in the assessment of regional nodal spread of disease in patients with breast cancer: an Ontario clinical oncology group study. *J Clin Oncol* 2012; **30**: 1274-1279 [PMID: 22393089 DOI: 10.1200/JCO.2011.38.1103]
 - 24 **Cochet A**, Dygai-Cochet I, Riedinger JM, Humbert O, Berriolo-Riedinger A, Toubreau M, Guiu S, Coutant C, Coudert B, Fumoleau P, Brunotte F. 18F-FDG PET/CT provides powerful prognostic stratification in the primary staging of large breast cancer when compared with conventional explorations. *Eur J Nucl Med Mol Imaging* 2014; **41**: 428-437 [PMID: 24196916 DOI: 10.1007/s00259-013-2595-4]
 - 25 **Jeong YJ**, Kang DY, Yoon HJ, Son HJ. Additional value of F-18 FDG PET/CT for initial staging in breast cancer with clinically negative axillary nodes. *Breast Cancer Res Treat* 2014; **145**: 137-142 [PMID: 24682676 DOI: 10.1007/s10549-014-2924-8]
 - 26 **Koolen BB**, van der Leij F, Vogel WV, Rutgers EJ, Vrancken Peeters MJ, Elkhuizen PH, Valdés Olmos RA. Accuracy of 18F-FDG PET/CT for primary tumor visualization and staging in T1 breast cancer. *Acta Oncol* 2014; **53**: 50-57 [PMID: 23672678 DOI: 10.3109/0284186X.2013.783714]
 - 27 **Riedl CC**, Slobod E, Jochelson M, Morrow M, Goldman DA, Gonen M, Weber WA, Ulaner GA. Retrospective analysis of 18F-FDG PET/CT for staging asymptomatic breast cancer patients younger than 40 years. *J Nucl Med* 2014; **55**: 1578-1583 [PMID: 25214641 DOI: 10.2967/jnumed.114.143297]
 - 28 **Zhang X**, Wu F, Han P. The role of (18)F-FDG PET/CT in the diagnosis of breast cancer and lymph nodes metastases and micrometastases may be limited. *Hell J Nucl Med* 2014; **17**: 177-183 [PMID: 25526754]
 - 29 **Hogan MP**, Goldman DA, Dashevsky B, Riedl CC, Gonen M, Osborne JR, Jochelson M, Hudis C, Morrow M, Ulaner GA. Comparison of 18F-FDG PET/CT for Systemic Staging of Newly Diagnosed Invasive Lobular Carcinoma Versus Invasive Ductal Carcinoma. *J Nucl Med* 2015; **56**: 1674-1680 [PMID: 26294295 DOI: 10.2967/jnumed.115.161455]
 - 30 **Krammer J**, Schnitzer A, Kaiser CG, Buesing KA, Sperk E, Brade J, Wasgindt S, Suetterlin M, Schoenberg SO, Sutton EJ, Wasser K. (18)F-FDG PET/CT for initial staging in breast cancer patients - Is there a relevant impact on treatment planning compared to conventional staging modalities? *Eur Radiol* 2015; **25**: 2460-2469 [PMID: 25680729 DOI: 10.1007/s00330-015-3630-6]
 - 31 **Nursal GN**, Nursal TZ, Aytac HO, Hasbay B, Torun N, Reyhan M, Yapar AF. Is PET/CT Necessary in the Management of Early Breast Cancer? *Clin Nucl Med* 2016; **41**: 362-365 [PMID: 26914560 DOI: 10.1097/RLU.0000000000001165]
 - 32 **Ulaner GA**, Castillo R, Goldman DA, Wills J, Riedl CC, Pinker-Domenig K, Jochelson MS, Gonen M. (18)F-FDG-PET/CT for systemic staging of newly diagnosed triple-negative breast cancer. *Eur J Nucl Med Mol Imaging* 2016; **43**: 1937-1944 [PMID: 27129866 DOI: 10.1007/s00259-016-3402-9]
 - 33 **Lebon V**, Alberini JL, Pierga JY, Diéras V, Jehanno N, Wartski M. Rate of Distant Metastases on 18F-FDG PET/CT at Initial Staging of Breast Cancer: Comparison of Women Younger and Older Than 40 Years. *J Nucl Med* 2017; **58**: 252-257 [PMID: 27587709 DOI: 10.2967/jnumed.116.178749]
 - 34 **Ulaner GA**, Castillo R, Wills J, Gonen M, Goldman DA. (18)F-FDG-PET/CT for systemic staging of patients with newly diagnosed ER-positive and HER2-positive breast cancer. *Eur J Nucl Med Mol Imaging* 2017; Epub ahead of print [PMID: 28456837 DOI: 10.1007/s00259-017-3709-1]
 - 35 **Debald M**, Wolfgarten M, Kreklau P, Abramian A, Kaiser C, Höller T, Leutner C, Keyver-Paik MD, Braun M, Kuhn W. Staging of primary breast cancer is not indicated in asymptomatic patients with early tumor stages. *Oncol Res Treat* 2014; **37**: 400-405 [PMID: 25138300 DOI: 10.1159/000363528]
 - 36 **Ribnikar D**, Ribeiro JM, Pinto D, Sousa B, Pinto AC, Gomes E, Moser EC, Cardoso MJ, Cardoso F. Breast cancer under age 40: a different approach. *Curr Treat Options Oncol* 2015; **16**: 16 [PMID: 25796377 DOI: 10.1007/s11864-015-0334-8]
 - 37 **Braunstein LZ**, Niemierko A, Shenouda MN, Truong L, Sadek BT, Abi Raad R, Wong JS, Punglia RS, Taghian AG, Bellon JR. Outcome following local-regional recurrence in women with early-stage breast cancer: impact of biologic subtype. *Breast J* 2015; **21**: 161-167 [PMID: 25559656 DOI: 10.1111/tbj.12371]
 - 38 **Chen HL**, Ding A. Comparison of invasive micropapillary and triple negative invasive ductal carcinoma of the breast. *Breast* 2015; **24**: 723-731 [PMID: 26392199 DOI: 10.1016/j.breast.2015.09.001]
 - 39 **Lai HW**, Tseng LM, Chang TW, Kuo YL, Hsieh CM, Chen ST, Kuo SJ, Su CC, Chen DR. The prognostic significance of metaplastic carcinoma of the breast (MCB)--a case controlled comparison study with infiltrating ductal carcinoma. *Breast* 2013; **22**: 968-973 [PMID: 23787124 DOI: 10.1016/j.breast.2013.05.010]
 - 40 **Sorlie T**, Perou CM, Tibshirani R, Aas T, Geisler S, Johnsen H, Hastie T, Eisen MB, van de Rijn M, Jeffrey SS, Thorsen T, Quist H, Matese JC, Brown PO, Botstein D, Lønning PE, Børresen-Dale AL. Gene expression patterns of breast carcinomas distinguish tumor subclasses with clinical implications. *Proc Natl Acad Sci USA* 2001; **98**: 10869-10874 [PMID: 11553815 DOI: 10.1073/pnas.191367098]
 - 41 **Reis-Filho JS**, Pusztai L. Gene expression profiling in breast cancer: classification, prognostication, and prediction. *Lancet* 2011; **378**: 1812-1823 [PMID: 22098854 DOI: 10.1016/S0140-6736(11)61539-0]
 - 42 **Cardoso F**, van't Veer LJ, Bogaerts J, Slaets L, Viale G, Delaloge S, Pierga JY, Brain E, Causeret S, DeLorenzi M, Glas AM, Goulioti V, Goulioti T, Knox S, Matos E, Meulemans B, Neijenhuis PA, Nitz U, Passalacqua R, Ravdin P, Rubio IT, Saghatian M, Smilde TJ, Sotiriou C, Stork L, Strahle C, Thomas G, Thompson AM, van der Hoeven JM, Vuylsteke P, Bernards R, Tryfonidis K, Rutgers E, Piccart M. 70-Genome Signature as an Aid to Treatment Decisions in Early-Stage Breast Cancer. *N Engl J Med* 2016; **375**: 717-729 [PMID: 27557300 DOI: 10.1056/NEJMoa1602253]
 - 43 **Fei F**, Messina C, Slaets L, Chakiba C, Cameron D, Bogaerts J, Bonnefoi

- H. Tumour size is the only predictive factor of distant recurrence after pathological complete response to neoadjuvant chemotherapy in patients with large operable or locally advanced breast cancers: a sub-study of EORTC 10994/BIG 1-00 phase III trial. *Eur J Cancer* 2015; **51**: 301-309 [PMID: 25578377 DOI: 10.1016/j.ejca.2014.11.023]
- 44 **Kast K**, Link T, Friedrich K, Petzold A, Niedostatek A, Schoffer O, Werner C, Klug SJ, Werner A, Gatzweiler A, Richter B, Baretton G, Wimberger P. Impact of breast cancer subtypes and patterns of metastasis on outcome. *Breast Cancer Res Treat* 2015; **150**: 621-629 [PMID: 25783184 DOI: 10.1007/s10549-015-3341-3]
 - 45 **Yun SU**, Choi BB, Shu KS, Kim SM, Seo YD, Lee JS, Chang ES. Imaging findings of invasive micropapillary carcinoma of the breast. *J Breast Cancer* 2012; **15**: 57-64 [PMID: 22493629 DOI: 10.4048/jbc.2012.15.1.57]
 - 46 **de Azambuja E**, Cardoso F, de Castro G, Colozza M, Mano MS, Durbecq V, Sotiriou C, Larsimont D, Piccart-Gebhart MJ, Paesmans M. Ki-67 as prognostic marker in early breast cancer: a meta-analysis of published studies involving 12,155 patients. *Br J Cancer* 2007; **96**: 1504-1513 [PMID: 17453008 DOI: 10.1038/sj.bjc.6603756]
 - 47 **Tabouret-Viaud C**, Botsikas D, Delattre BM, Mainta I, Amzalag G, Rager O, Vinh-Hung V, Miralbell R, Ratib O. PET/MR in Breast Cancer. *Semin Nucl Med* 2015; **45**: 304-321 [PMID: 26050658 DOI: 10.1053/j.semnuclmed.2015.03.003]
 - 48 **Rousseau C**, Devillers A, Sagan C, Ferrer L, Bridji B, Champion L, Ricaud M, Bourbouloux E, Doutriaux I, Clouet M, Berton-Rigaud D, Bouriel C, Delecroix V, Garin E, Rouquette S, Resche I, Kerbrat P, Chatal JF, Campone M. Monitoring of early response to neoadjuvant chemotherapy in stage II and III breast cancer by [¹⁸F]fluorodeoxyglucose positron emission tomography. *J Clin Oncol* 2006; **24**: 5366-5372 [PMID: 17088570 DOI: 10.1200/JCO.2006.05.7406]
 - 49 **Groheux D**, Cochet A, Humbert O, Alberini JL, Hindié E, Mankoff D. ¹⁸F-FDG PET/CT for Staging and Restaging of Breast Cancer. *J Nucl Med* 2016; **57** Suppl 1: 17S-26S [PMID: 26834096 DOI: 10.2967/jnumed.115.157859]
 - 50 **Futamura M**, Asano T, Kobayashi K, Morimitsu K, Nawa M, Kanematsu M, Morikawa A, Mori R, Yoshida K. Prediction of macrometastasis in axillary lymph nodes of patients with invasive breast cancer and the utility of the SUV lymph node/tumor ratio using FDG-PET/CT. *World J Surg Oncol* 2015; **13**: 49 [PMID: 25885028 DOI: 10.1186/s12957-014-0424-2]
 - 51 **Vinh-Hung V**, Everaert H, Lamote J, Voordeckers M, van Parijs H, Vanhoeij M, Verfaillie G, Fontaine C, Veas H, Ratib O, Vlastos G, De Ridder M. Diagnostic and prognostic correlates of preoperative FDG PET for breast cancer. *Eur J Nucl Med Mol Imaging* 2012; **39**: 1618-1627 [PMID: 22777335 DOI: 10.1007/s00259-012-2181-1]
 - 52 **Bral S**, Vinh-Hung V, Everaert H, De Coninck P, Storme G. The use of molecular imaging to evaluate radiation fields in the adjuvant setting of breast cancer: a feasibility study. *Strahlenther Onkol* 2008; **184**: 100-104 [PMID: 18259702 DOI: 10.1007/s00066-008-1769-7]

P- Reviewer: Bilir C, Wang L, Wang SK **S- Editor:** Ji FF

L- Editor: A **E- Editor:** Lu YJ





Published by **Baishideng Publishing Group Inc**
7901 Stoneridge Drive, Suite 501, Pleasanton, CA 94588, USA
Telephone: +1-925-223-8242
Fax: +1-925-223-8243
E-mail: bpgoffice@wjgnet.com
Help Desk: <http://www.f6publishing.com/helpdesk>
<http://www.wjgnet.com>



World Journal of *Radiology*

World J Radiol 2017 August 28; 9(8): 321-338





Editorial Board

2014-2017

The *World Journal of Radiology* Editorial Board consists of 365 members, representing a team of worldwide experts in radiology. They are from 36 countries, including Afghanistan (1), Argentina (2), Australia (5), Austria (7), Belgium (2), Brazil (8), Canada (6), Chile (1), China (43), Croatia (1), Denmark (4), Egypt (6), France (5), Germany (22), Greece (10), India (12), Iran (6), Ireland (2), Israel (3), Italy (47), Japan (13), Netherlands (1), New Zealand (1), Pakistan (1), Poland (2), Portugal (1), Serbia (1), Singapore (3), Slovakia (1), South Korea (18), Spain (4), Sweden (2), Switzerland (4), Thailand (1), Turkey (26), United Kingdom (11), and United States (82).

EDITORS-IN-CHIEF

Kai U Juergens, *Bremen*
Edwin JR van Beek, *Edinburgh*
Thomas J Vogl, *Frankfurt*

GUEST EDITORIAL BOARD MEMBERS

Wing P Chan, *Taipei*
Chung-Huei Hsu, *Taipei*
Chin-Chang Huang, *Taipei*
Tsong-Long Hwang, *Taoyuan*
Jung-Lung Hsu, *Taipei*
Chia-Hung Kao, *Taichung*
Yu-Ting Kuo, *Tainan*
Hon-Man Liu, *Taipei*
Hui-Lung Liang, *Kaohsiung*
Chun Chung Lui, *Kaohsiung*
Sen-Wen Teng, *Taipei*
Yung-Liang (William) Wan, *Taoyuan*

MEMBERS OF THE EDITORIAL BOARD



Afghanistan

Takao Hiraki, *Okayama*



Argentina

Patricia Carrascosa, *Vicente Lopez*
Maria C Ziadi, *Rosario*



Australia

Lourens Bester, *Sydney*
Gemma A Figtree, *Sydney*



Austria

Herwig R Cerwenka, *Graz*
Gudrun M Feuchtnner, *Innsbruck*
Benjamin Henninger, *Innsbruck*
Rupert Lanzenberger, *Vienna*
Shu-Ren Li, *Vienna*
Veronika Schopf, *Vienna*
Tobias De Zordo, *Innsbruck*



Belgium

Steve Majerus, *Liege*
Kathelijne Peremans, *Merelbeke*



Brazil

Clerio F Azevedo, *Rio de Janeiro*
Patrícia P Alfredo, *São Paulo*
Eduardo FC Fleury, *São Paulo*
Edward Araujo Júnior, *São Paulo*
Wellington P Martins, *Ribeirao Preto*
Ricardo A Mesquita, *Belo Horizonte*
Vera MC Salemi, *São Paulo*
Claudia Szobot, *Porto Alegre*
Lilian YI Yamaga, *São Paulo*



Canada

Marie Arsalidou, *Toronto*
Otman A Basir, *Waterloo*

Tarik Zine Belhocine, *Toronto*
James Chow, *Toronto*
Tae K Kim, *Toronto*
Anastasia Oikonomou, *Toronto*



China

Hong-Wei Chen, *Wuxi*
Feng Chen, *Hangzhou*
Jian-Ping Chu, *Guangzhou*
Guo-Guang Fan, *Shenyang*
Bu-Lang Gao, *Shijiazhuang*
Qi-Yong Gong, *Chengdu*
Ying Han, *Beijing*
Xian-Li Lv, *Beijing*
Yi-Zhuo Li, *Guangzhou*
Xiang-Xi Meng, *Harbin*
Yun Peng, *Beijing*
Jun Shen, *Guangzhou*
Ze-Zhou Song, *Hangzhou*
Wai Kwong Tang, *Hong Kong*
Gang-Hua Tang, *Guangzhou*
Jie Tian, *Beijing*
Lu-Hua Wang, *Beijing*
Xiao-bing Wang, *Xi'an*
Yi-Gen Wu, *Nanjing*
Kai Wu, *Guangzhou*
Hui-Xiong Xu, *Shanghai*
Zuo-Zhang Yang, *Kunming*
Xiao-Dan Ye, *Shanghai*
David T Yew, *Hong Kong*
Ting-He Yu, *Chongqing*
Zheng Yuan, *Shanghai*
Min-Ming Zhang, *Hangzhou*
Yudong Zhang, *Nanjing*
Dong Zhang, *Chongqing*
Wen-Bin Zeng, *Changsha*

Yue-Qi Zhu, *Shanghai*



Croatia

Goran Kusec, *Osijek*



Denmark

Poul E Andersen, *Odense*

Lars J Petersen, *Aalborg*

Thomas Z Ramsøy, *Frederiksberg*

Morten Ziebell, *Copenhagen*



Egypt

Mohamed F Bazeed, *Mansoura*

Mohamed Abou El-Ghar, *Mansoura*

Reem HA Mohamed, *Cairo*

Mohamed R Nouh, *Alexandria*

Ahmed AKA Razek, *Mansoura*

Ashraf A Zytoon, *Shebin El-Koom*



France

Sabine F Bensamoun, *Compiègne*

Romarc Loffroy, *Dijon*

Stephanie Nougaret, *Montpellier*

Hassane Oudadesse, *Rennes*

Vincent Vinh-Hung, *Fort-de-France*



Germany

Henryk Barthel, *Leipzig*

Peter Bannas, *Hamburg*

Martin Beeres, *Frankfurt*

Ilja F Ciernik, *Dessau*

A Dimitrakopoulou-Strauss, *Heidelberg*

Peter A Fasching, *Erlangen*

Andreas G Schreyer, *Regensburg*

Philipp Heusch, *Duesseldorf*

Sonja M Kirchhoff, *Munich*

Sebastian Ley, *Munich*

Adel Maataoui, *Frankfurt am Main*

Stephan M Meckel, *Freiburg*

Hans W Muller, *Duesseldorf*

Kay Raum, *Berlin*

Dirk Rades, *Luebeck*

Marc-Ulrich Regier, *Hamburg*

Alexey Surov, *Halle*

Martin Walter, *Magdeburg*

Axel Wetter, *Essen*

Christoph Zilkens, *Düsseldorf*



Greece

Panagiotis Antoniou, *Thessaloniki*

Nikos Efthimiou, *Athens*

Dimitris Karnabatidis, *Patras*

George Latsios, *Athens*

Stylianios Megremis, *Iraklion*

Alexander D Rapidis, *Athens*

Kiki Theodorou, *Larissa*

Ioannis A Tsalafoutas, *Athens*

Evanthia E Tripoliti, *Ioannina*

Athina C Tsili, *Ioannina*



India

Ritesh Agarwal, *Chandigarh*

Chandan J Das, *New Delhi*

Prathamesh V Joshi, *Mumbai*

Naveen Kalra, *Chandigarh*

Chandrasekharan Kesavadas, *Trivandrum*

Jyoti Kumar, *New Delhi*

Atin Kumar, *New Delhi*

Kaushala P Mishra, *Allahabad*

Daya N Sharma, *New Delhi*

Binit Sureka, *New Delhi*

Sanjay Sharma, *New Delhi*

Raja R Yadav, *Allahabad*



Iran

Majid Assadi, *Bushehr*

SeyedReza Najafizadeh, *Tehran*

Mohammad Ali Oghabian, *Tehran*

Amir Reza Radmard, *Tehran*

Ramin Sadeghi, *Mashhad*

Hadi Rokni Yazdi, *Tehran*



Ireland

Tadhg Gleeson, *Wexford*

Frederik JAI Vernimmen, *Cork*



Israel

Dafna Ben Bashat, *Tel Aviv*

Amit Gefen, *Tel Aviv*

Tamar Sella, *Jerusalem*



Italy

Adriano Alippi, *Rome*

Dante Amelio, *Trento*

Michele Anzidei, *Rome*

Filippo F Angileri, *Messinas*

Stefano Arcangeli, *Rome*

Roberto Azzoni, *San Donato milanese*

Tommaso V Bartolotta, *Palermo*

Tommaso Bartalena, *Imola*

Livia Bernardin, *San Bonifacio*

Federico Boschi, *Verona*

Sergio Casciaro, *Lecce*

Emanuele Casciani, *Rome*

Musa M Can, *Napoli*

Alberto Cuocolo, *Napoli*

Michele Ferrara, *Coppito*

Mauro Feola, *Fossano*

Giampiero Francica, *Castel Volturno*

Luigi De Gennaro, *Rome*

Giulio Giovannetti, *Pisa*

Francesca Iacobellis, *Napoli*

Formato Invernizzi, *Monza Brianza*

Francesco Lassandro, *Naples*

Lorenzo Livi, *Florence*

Pier P Mainenti, *Napoli*

Laura Marzetti, *Chieti*

Giuseppe Malinverni, *Crescentino*

Enrica Milanese, *Turin*

Giovanni Morana, *Treviso*

Lorenzo Monti, *Milan*

Silvia D Morbelli, *Genoa*

Barbara Palumbo, *Perugia*

Cecilia Parazzini, *Milan*

Stefano Pergolizzi, *Messina*

Antonio Pinto, *Naples*

Camillo Porcaro, *Rome*

Carlo C Quattrocchi, *Rome*

Alberto Rebonato, *Perugia*

Giuseppe Rizzo, *Rome*

Roberto De Rosa, *Naples*

Domenico Rubello, *Rovigo*

Andrea Salvati, *Bari*

Sergio Sartori, *Ferrara*

Luca M Sconfienza, *Milano*

Giovanni Storto, *Rionero*

Nicola Sverzellati, *Parma*

Alberto S Tagliafico, *Genova*

Nicola Troisi, *Florence*



Japan

Yasuhiko Hori, *Chiba*

Hidetoshi Ikeda, *Koriyama*

Masahito Kawabori, *Sapporo*

Tamotsu Kamishima, *Sapporo*

Hiro Kiyosue, *Yufu*

Yasunori Minami, *Osaka-sayama*

Yasuhiro Morimoto, *Kitakyushu*

Satoru Murata, *Tokyo*

Shigeki Nagamachi, *Miyazaki*

Hiroshi Onishi, *Yamanashi*

Morio Sato, *Wakayama Shi*

Yoshito Tsushima, *Maebashi*

Masahiro Yanagawa, *Suita*



Netherlands

Willem Jan van Rooij, *Tilburg*



New Zealand

W Howell Round, *Hamilton*



Pakistan

Wazir Muhammad, *Abbottabad*



Poland

Maciej S Baglaj, *Wroclaw*

Piotr Czauderna, *Gdansk*



Portugal

Joao Manuel RS Tavares, *Porto*



Serbia

Olivera Ciraj-Bjelac, *Belgrade*



Singapore

Gopinathan Anil, *Singapore*

Terence KB Teo, *Singapore*

Cher Heng Tan, *Singapore*



Slovakia

Stefan Sivak, *Martin*



South Korea

Ki Seok Choo, *Busan*

Seung Hong Choi, *Seoul*

Dae-Seob Choi, *Jinju*

Hong-Seok Jang, *Seoul*

Yong Jeong, *Daejeon*

Chan Kyo Kim, *Seoul*

Se Hyung Kim, *Seoul*

Joong-Seok Kim, *Seoul*

Sang Eun Kim, *Seongnam*

Sung Joon Kwon, *Seoul*

Jeong Min Lee, *Seoul*

In Sook Lee, *Busan*

Noh Park, *Goyang*

Chang Min Park, *Seoul*

Sung Bin Park, *Seoul*

Deuk Jae Sung, *Seoul*

Choongsoo Shin, *Seoul*

Kwon-Ha Yoon, *Iksan*



Spain

Miguel A De Gregorio, *Zaragoza*

Antonio Luna, *Jaén*

Enrique Marco de Lucas, *Santander*

Fernando Ruiz Santiago, *Granada*



Sweden

Dmitry Grishenkov, *Stockholm*

Tie-Qiang Li, *Stockholm*



Switzerland

Nicolau Beckmann, *Basel*

Christian Boy, *Bern*

Giorgio Treglia, *Bellinzona*

Stephan Ulmer, *Kiel*



Thailand

Sirianong Namwongprom, *Chiang Mai*



Turkey

Kubilay Aydin, *Istanbul*

Ramazan Akdemir, *Sakarya*

Serhat Avcu, *Ankara*

Ayşe Aralasmak, *Istanbul*

Oktay Algin, *Ankara*

Nevbahar Akcar, *Meselik*

Bilal Battal, *Ankara*

Zulkif Bozgeyik, *Elazig*

Nazan Ciledag, *Aakara*

Fuldem Y Donmez, *Ankara*

Gulgun Engin, *Istanbul*

Ahmet Y Goktay, *Izmir*

Oguzhan G Gumustas, *Bursa*

Kaan Gunduz, *Ankara*

Pelin Ozcan Kara, *Mersin*

Kivanc Kamburoglu, *Ankara*

Ozgur Kilickesmez, *Istanbul*

Furuzan Numan, *Istanbul*

Cem Onal, *Adana*

Ozgur Oztekin, *Izmir*

Seda Ozbek (Boruban), *Konya*

Selda Sarikaya, *Zonguldak*

Figen Taser, *Kutahya*

Baran Tokar, *Eskisehir*

Ender Uysal, *Istanbul*

Ensar Yekeler, *Istanbul*



United Kingdom

Indran Davagnanam, *London*

M DC Valdés Hernández, *Edinburgh*

Alan Jackson, *Manchester*

Suneil Jain, *Belfast*

Long R Jiao, *London*

Miltiadis Krokidis, *Cambridge*

Pradesh Kumar, *Liverpool*

Peter D Kuzmich, *Derby*

Georgios Plataniotis, *Brighton*

Vanessa Sluming, *Liverpool*



United States

Garima Agrawal, *Saint Louis*

James R Brasic, *Baltimore*

Rajendra D Badgaiyan, *Buffalo*

Ulas Bagci, *Bethesda*

Anat Biegon, *Stony Brook*

Ramon Casanova, *Winston Salem*

Wenli Cai, *Boston*

Zheng Chang, *Durham*

Corey J Chakarun, *Long Beach*

Kai Chen, *Los Angeles*

Hyun-Soon Chong, *Chicago*

Marco Cura, *Dallas*

Ravi R Desai, *Bensalem*

Delia DeBuc, *Miami*

Carlo N De Cecco, *Charleston*

Timm-Michael L Dickfeld, *Baltimore*

Subba R Digumarthy, *Boston*

Huy M Do, *Stanford*

Todd A Faasse, *Grand Rapids*

Salomao Faintuch, *Boston*

Girish M Fatterpekar, *New York*

Dhakshinamoorthy Ganesan, *Houston*

Robert J Griffin, *Little Rock*

Andrew J Gunn, *Boston*

Sandeep S Hedgire, *Boston*

Timothy J Hoffman, *Columbia*

Mai-Lan Ho, *San Francisco*

Juebin Huang, *Jackson*

Abid Irshad, *Charleston*

Matilde Inglese, *New York*

El-Sayed H Ibrahim, *Jacksonville*

Paul R Julsrud, *Rochester*

Pamela T Johnson, *Baltimore*

Ming-Hung Kao, *Tempe*

Sunil Krishnan, *Houston*

Richard A Komoroski, *Cincinnati*

Sandi A Kwee, *Honolulu*

King Kim, *Ft. Lauderdale*

Guozheng Liu, *Worcester*

Yiyan Liu, *Newark*

Venkatesh Mani, *New York*

Lian-Sheng Ma, *Pleasanton*

Rachna Madan, *Boston*

Zeyad A Metwalli, *Houston*

Yilong Ma, *Manhasset*

Hui Mao, *Atlanta*

Feroze B Mohamed, *Philadelphia*

Gul Moonis, *Boston*

John L Noshier, *New Brunswick*

Rahmi Oklu, *Boston*

Aytekun Oto, *Chicago*

Bishnuhari Paudyal, *Philadelphia*

Rajul Pandya, *Youngstown*

Chong-Xian Pan, *Sacramento*

Jay J Pillai, *Baltimore*

Neal Prakash, *Duarte*

Reza Rahbar, *Boston*

Ali S Raja, *Boston*

Gustavo J Rodriguez, *El Paso*

David J Sahn, *Portland*

Steven Schild, *Scottsdale*

Ali R Sepahdari, *Los Angeles*

Li Shen, *Indianapolis*

JP Sheehan, *Charlottesville*

Atul B Shinagare, *Boston*

Sarabjeet Singh, *Boston*

Charles J Smith, *Columbia*

Kenji Suzuki, *Chicago*

Monvadi Srichai-Parsia, *Washington*

Sree H Tirumani, *Boston*

Hebert A Vargas, *New York*

Sachit Verma, *Philadelphia*

Yoichi Watanabe, *Minneapolis*

Li Wang, *Chapel Hill*

Carol C Wu, *Boston*

Shoujun Xu, *Houston*

Min Yao, *Cleveland*

Xiaofeng Yang, *Atlanta*

Qingbao Yu, *Albuquerque*

Aifeng Zhang, *Chicago*

Chao Zhou, *Bethlehem*

Hongming Zhuang, *Philadelphia*

**MINIREVIEWS**

- 321** Imaging of the treated breast post breast conservation surgery/oncoplasty: Pictorial review

Ramani SK, Rastogi A, Mahajan A, Nair N, Shet T, Thakur MH

ORIGINAL ARTICLE**Observational Study**

- 330** Clinical-radiological-pathological correlation of cavernous sinus hemangioma: Incremental value of diffusion-weighted imaging

Mahajan A, Rao VRK, Anantaram G, Polnaya AM, Desai S, Desai P, Vadapalli R, Panigrahi M

Contents

World Journal of Radiology
Volume 9 Number 8 August 28, 2017

ABOUT COVER

Editorial Board Member of *World Journal of Radiology*, XW Cui, PhD, Professor, Department of Medical Ultrasound, Tongji Hospital of Tongji Medical College, Huazhong University of Science and Technology, Wuhan 430030, Hubei Province, China

AIM AND SCOPE

World Journal of Radiology (*World J Radiol*, *WJR*, online ISSN 1949-8470, DOI: 10.4329) is a peer-reviewed open access academic journal that aims to guide clinical practice and improve diagnostic and therapeutic skills of clinicians.

WJR covers topics concerning diagnostic radiology, radiation oncology, radiologic physics, neuroradiology, nuclear radiology, pediatric radiology, vascular/interventional radiology, medical imaging achieved by various modalities and related methods analysis. The current columns of *WJR* include editorial, frontier, diagnostic advances, therapeutics advances, field of vision, mini-reviews, review, topic highlight, medical ethics, original articles, case report, clinical case conference (clinicopathological conference), and autobiography.

We encourage authors to submit their manuscripts to *WJR*. We will give priority to manuscripts that are supported by major national and international foundations and those that are of great basic and clinical significance.

INDEXING/ABSTRACTING

World Journal of Radiology is now indexed in PubMed, PubMed Central, and Emerging Sources Citation Index (Web of Science).

FLYLEAF

I-III Editorial Board

EDITORS FOR THIS ISSUE

Responsible Assistant Editor: *Xiang Li*
Responsible Electronic Editor: *Ya-Jing Lu*
Proofing Editor-in-Chief: *Lian-Sheng Ma*

Responsible Science Editor: *Jin-Xin Kong*
Proofing Editorial Office Director: *Jin-Lei Wang*

NAME OF JOURNAL
World Journal of Radiology

ISSN
ISSN 1949-8470 (online)

LAUNCH DATE
January 31, 2009

FREQUENCY
Monthly

EDITORS-IN-CHIEF
Kai U Juergens, MD, Associate Professor, MRT und PET/CT, Nuklearmedizin Bremen Mitte, ZEMODI - Zentrum für morphologische und molekulare Diagnostik, Bremen 28177, Germany

Edwin JR van Beek, MD, PhD, Professor, Clinical Research Imaging Centre and Department of Medical Radiology, University of Edinburgh, Edinburgh EH16 4TJ, United Kingdom

Thomas J Vogl, MD, Professor, Reader in Health Technology Assessment, Department of Diagnostic and Interventional Radiology, Johann Wolfgang Goethe University of Frankfurt, Frankfurt 60590,

Germany

EDITORIAL BOARD MEMBERS
All editorial board members resources online at <http://www.wjgnet.com/1949-8470/editorialboard.htm>

EDITORIAL OFFICE
Xiu-Xia Song, Director
World Journal of Radiology
Baishideng Publishing Group Inc
7901 Stoneridge Drive, Suite 501, Pleasanton, CA 94588, USA
Telephone: +1-925-2238242
Fax: +1-925-2238243
E-mail: editorialoffice@wjgnet.com
Help Desk: <http://www.f6publishing.com/helpdesk>
<http://www.wjgnet.com>

PUBLISHER
Baishideng Publishing Group Inc
7901 Stoneridge Drive, Suite 501, Pleasanton, CA 94588, USA
Telephone: +1-925-2238242
Fax: +1-925-2238243
E-mail: bpgoffice@wjgnet.com
Help Desk: <http://www.f6publishing.com/helpdesk>
<http://www.wjgnet.com>

PUBLICATION DATE
August 28, 2017

COPYRIGHT
© 2017 Baishideng Publishing Group Inc. Articles published by this Open-Access journal are distributed under the terms of the Creative Commons Attribution Non-commercial License, which permits use, distribution, and reproduction in any medium, provided the original work is properly cited, the use is non commercial and is otherwise in compliance with the license.

SPECIAL STATEMENT
All articles published in journals owned by the Baishideng Publishing Group (BPG) represent the views and opinions of their authors, and not the views, opinions or policies of the BPG, except where otherwise explicitly indicated.

INSTRUCTIONS TO AUTHORS
<http://www.wjgnet.com/bpg/gerinfo/204>

ONLINE SUBMISSION
<http://www.f6publishing.com>

Imaging of the treated breast post breast conservation surgery/oncoplasty: Pictorial review

Subhash K Ramani, Ashita Rastogi, Abhishek Mahajan, Nita Nair, Tanuja Shet, Meenakshi H Thakur

Subhash K Ramani, Department of Radiodiagnosis, JJ Hospital, Mumbai 400008, India

Telephone: +91-99-69492798
Fax: +91-22-24146937

Subhash K Ramani, Ashita Rastogi, Abhishek Mahajan, Meenakshi H Thakur, Department of Radiodiagnosis and Imaging, Tata Memorial Centre, Mumbai 400012, India

Received: January 20, 2017
Peer-review started: January 20, 2017
First decision: March 27, 2017
Revised: May 1, 2017
Accepted: May 12, 2017
Article in press: May 15, 2017
Published online: August 28, 2017

Nita Nair, Department of Surgical Oncology, Tata Memorial Centre, Mumbai 400012, India

Tanuja Shet, Department of Pathology, Tata Memorial Centre, Mumbai 400012, India

Author contributions: All authors are the guarantors of integrity of entire study; Ramani SK designed the study; Ramani SK, Rastogi A, Mahajan A and Thakur MH performed data analysis/interpretation; Ramani SK and Rastogi A performed the literature research; all authors contributed to manuscript drafting or manuscript revision for important intellectual content; all authors gave manuscript final version approval and manuscript editing; all authors take responsibility for the integrity of the data and the accuracy of the data analysis.

Conflict-of-interest statement: This manuscript is not published anywhere else; all authors conform that there is no conflict of interests (including none for related to commercial, personal, political, intellectual, or religious interests).

Open-Access: This article is an open-access article which was selected by an in-house editor and fully peer-reviewed by external reviewers. It is distributed in accordance with the Creative Commons Attribution Non Commercial (CC BY-NC 4.0) license, which permits others to distribute, remix, adapt, build upon this work non-commercially, and license their derivative works on different terms, provided the original work is properly cited and the use is non-commercial. See: <http://creativecommons.org/licenses/by-nc/4.0/>

Manuscript source: Invited manuscript

Correspondence to: Dr. Ashita Rastogi, DNB, Radiodiagnosis, Fellowship Cancer Imaging, Assistant Professor, Department of Radiodiagnosis and Imaging, Tata Memorial Centre, Room No. 117, Dr E Borges Road, Parel, Mumbai 400012, India. rastogia@tmc.gov.in

Abstract

Mammographic appearance of the normal breast is altered in the post-operative setting. It is essential to be aware of the normal findings as well as to identify features of recurrent disease with particular emphasis on radiological-pathological concordance. Digital breast tomosynthesis and volumetric breast density add incremental value in this clinical setting. We present a pictorial review of various cases to illustrate normal post-operative findings as well as mammographic features suspicious for recurrent disease.

Key words: Mammography; Digital breast tomosynthesis; Breast conservation surgery; Post breast-conserving therapy imaging; Breast cancer

© **The Author(s) 2017.** Published by Baishideng Publishing Group Inc. All rights reserved.

Core tip: Mammographic imaging in patients after breast conservation surgery is challenging because surgery alters the normal breast architecture. The distinction of normal post-operative changes from true findings of recurrence becomes demanding even for a breast imager making it essential to update our knowledge in the subject. In the recent times digital breast tomosynthesis and volumetric breast density are adding an incremental value in this clinical setting.

Ramani SK, Rastogi A, Mahajan A, Nair N, Shet T, Thakur MH. Imaging of the treated breast post breast conservation surgery/oncoplasty: Pictorial review. *World J Radiol* 2017; 9(8): 321-329 Available from: URL: <http://www.wjgnet.com/1949-8470/full/v9/i8/321.htm> DOI: <http://dx.doi.org/10.4329/wjr.v9.i8.321>

INTRODUCTION

Breast conservation surgery (BCS) is the most commonly employed management of breast cancer in current practice and aims at surgical excision of the tumor while conserving the patient's breast appearance and form. Breast radiologists need to update their knowledge of typical and atypical appearances of the treated breast in order to detect abnormalities signifying recurrence as well as to not raise unnecessary concern over benign course of post-operative change.

The expected changes on mammography after breast conservative surgery include skin thickening or edema, parenchymal edema, post-operative fluid collection, scar, fat necrosis and dystrophic calcifications which are more marked up to six months after therapy. Recurrence on mammographic imaging may be observed as a mass or microcalcifications, increase in skin thickening, increase in breast density, scar enlargement, axillary nodal recurrence or Paget's disease. We present various mammography images to illustrate findings which may be left alone and those which require further intervention.

LEAVE-ME-ALONE FEATURES

Skin thickening and parenchymal edema

Normal skin thickness of the breast as seen on mammogram is 2 mm^[1,2]. Skin thickening (more than 2 mm) is the most common finding after breast-conserving therapy (BCT), reported in up to 90% of patients^[3]. On imaging it manifests as skin and trabecular thickening or overall increased breast density due to parenchymal edema which decrease on follow up studies and return to normal by 2 to 3 years (Figure 1)^[2]. Post radiation edema occurs more commonly after external beam radiotherapy (EBRT) than intraoperative radiotherapy^[4,5]. Less commonly the skin thickening and parenchymal edema may be a consequence of lymphedema (secondary to axillary node dissection) or mastitis^[3].

Post-operative collection

Fluid with or without blood which collects in the post-operative cavity appears as an oval or round circumscribed mass on mammography. When viewed on ultrasound, a mixed echogenic collection with variable fluid (anechoic) and haemorrhagic (echogenic) contents is observed. Post-operative fluid collections are seen in about half the patients at 1 mo after surgery and may remain in up to a fourth of cases till 6 mo^[2] though in a few patients these may persist for years^[6]. On sequential

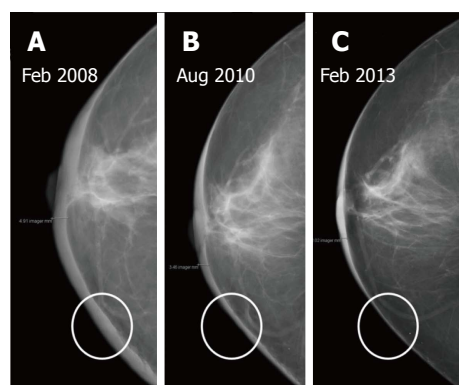


Figure 1 Patient underwent lumpectomy followed by radiation therapy. A-C: (A) Diffuse increase in skin thickness is seen in first post therapy mammogram which decreased on subsequent mammograms at two (B) and five (C) years respectively.

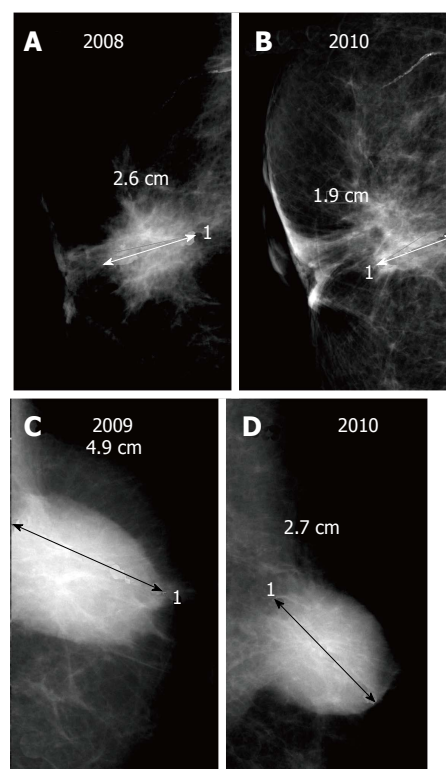


Figure 2 Two different patients post breast conservation. A and B demonstrate retraction of scar in right breast on follow up while C and D reveal serial decrease in size of a post-operative collection (seroma) in left breast.

mammograms, the lesion becomes smaller, irregular and denser as the seroma retracts and is replaced by fibrous tissue (Figure 2). However an increase in size on follow-up merits further evaluation to exclude a recurrent mass.

Post-surgical scar

A post-surgical scar appears as an area of architectural distortion contiguous with contour deformity of surgery. In comparison to a true recurrence which appears same on all mammographic views and has a dense centre; on different projections a scar has varied appearances (appearing less distorted on one) and demonstrates

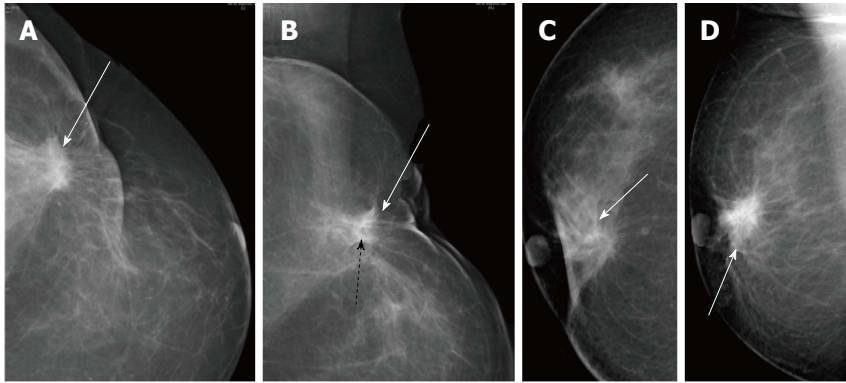


Figure 3 The scar usually decreases in density and/or size on serial imaging. A and B demonstrate a post-surgical scar in left breast which is contiguous with the skin contour deformity. Fat lucency (black dashed arrow) within the scar is seen on the MLO view in (B); C and D show the post-surgery scar (white arrow) on CC and MLO views having different morphology respectively; it opens up on CC view (C).

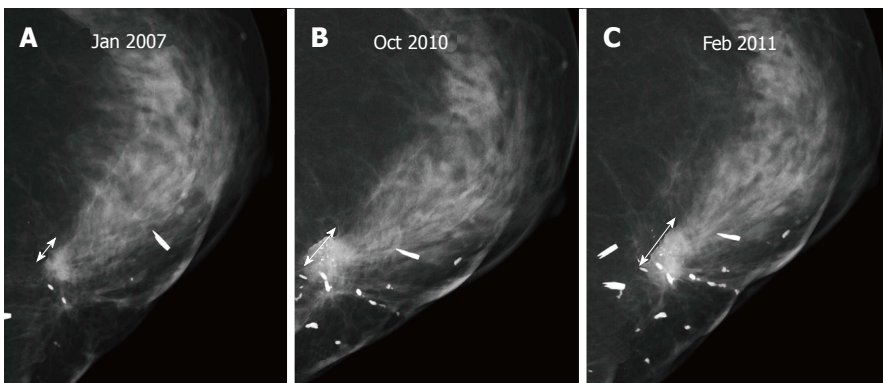


Figure 4 In a patient post breast-conserving therapy, scar (double headed arrow) is seen to increase in size at three (B) and four (C) years as compared to the initial mammogram shown in (A) which suggests recurrence.

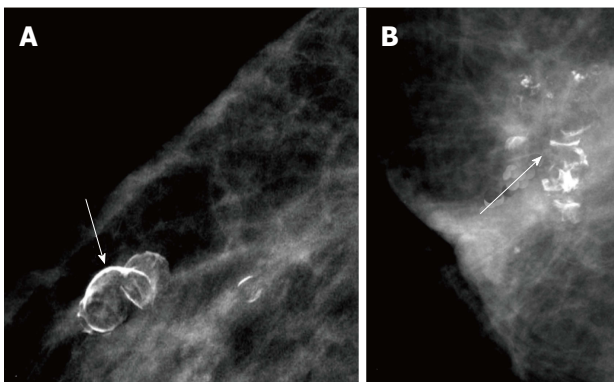


Figure 5 Calcifications associated with fat necrosis demonstrate a typical curvilinear or arc-like (arrows) morphology (A and B).

fat lucencies within^[3]. These features may be better imaged on spot compression or magnification views. As with a seroma, the scar usually decreases in density and/or size on serial imaging (Figure 3) or remains stable while an increase in size or density is suspicious for recurrence (Figure 4).

Dystrophic calcifications and fat necrosis

Benign calcifications are seen on mammography in about a third of treated breasts beginning 2 to 3 years after completion of therapy due to a combination of surgical trauma and radiation. Morphologically these calcifications are large (> 5 mm) and irregular in outline with central lucencies, with no associated mass/density

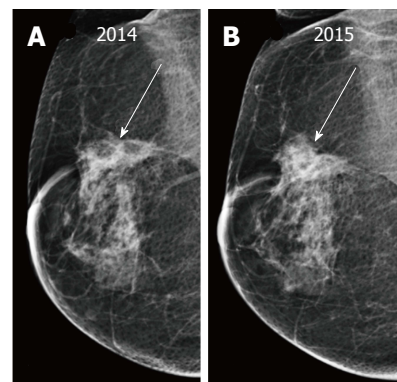


Figure 6 (A) Post breast-conserving therapy scar is seen in the right breast which appears to have increased in size on follow up mammogram after one year seen in (B). However fat lucencies are still seen within the lesion (which was better appreciated on tomography images). Patient underwent biopsy because of clinical suspicion of recurrence.

and always occur at the site of surgery^[7].

Fat necrosis is tissue necrosis resulting from damage to the intima of arteries from surgery and radiation. It more commonly manifests as an oval or round lucency with curvilinear or arc-like peripheral calcifications which are characteristic for the same (Figure 5). It is a common complication of myocutaneous flaps usually seen after 6-12 mo of treatment^[3] and may clinically present as a palpable mass that is firm or hard^[8]. When it presents as a palpable lesion with atypical appearance on mammography, sonography followed by biopsy may become requisite to confirm the diagnosis (Figure 6)^[9].

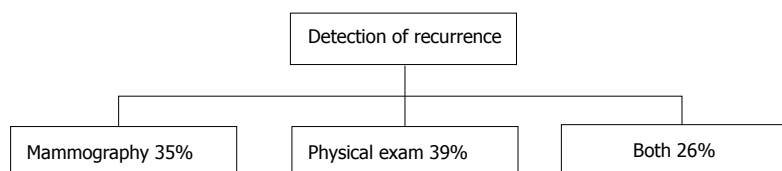


Figure 7 How are recurrences detected on follow up.

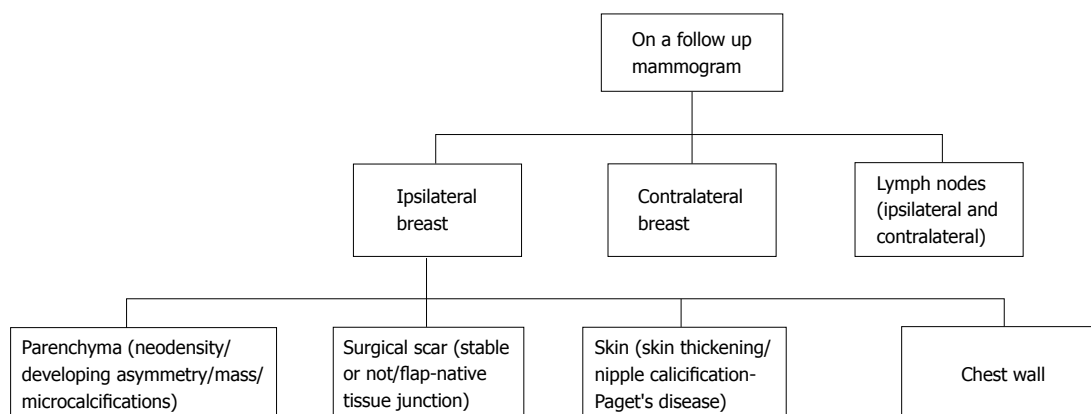


Figure 8 Sites for recurrent lesions.

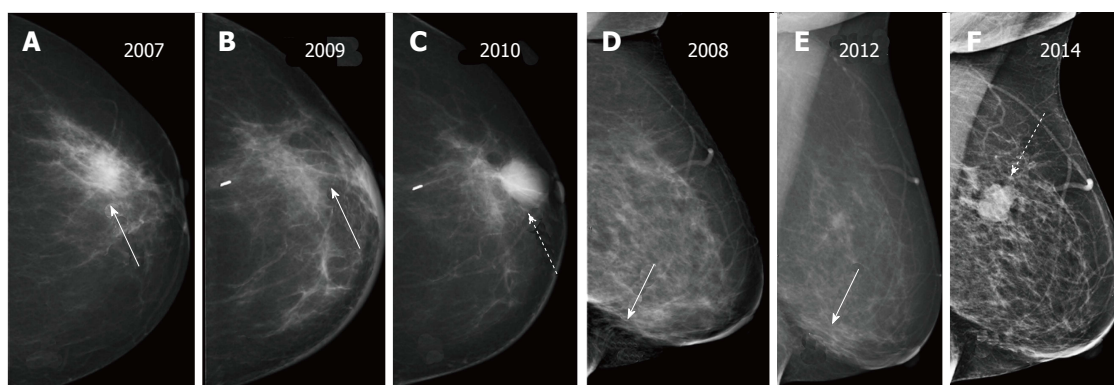


Figure 9 Two patients post breast-conserving therapy with recurrent masses. A-C show a recurrent mass (dashed arrow in C) appearing at the scar site (solid arrow in A and B) two years after surgery; D-F demonstrate a post-surgical scar in the lower aspect (arrow in D and E) and a recurrent mass (dashed arrow in F) in upper aspect - different quadrant than the primary.

WORRISOME MAMMOGRAPHY FINDINGS, I.E., "RED FLAGS"

Recurrences may present at clinical examination or, may be detected only on mammography (Figure 7) as suspicious microcalcifications or masses. The rate of local recurrence after breast cancer surgery is 1%-2% per year^[10]. Stability is defined as no interval change on two successive mammographic studies^[7] and is generally observed at around 2-3 years after the completion of radiation therapy. Any retrograde change in imaging findings such as a new mass, microcalcifications, architectural distortion or an area of increased density at the scar site post stability should raise suspicion for tumor recurrence. Figure 8 lists the sites of recurrences to be looked for in conservatively

treated breast on follow up.

Masses

Palpable recurrences usually manifest as masses and even when seen as microcalcifications on a mammogram, they have associated densities. The temporal changes from prior mammogram determine the approach to patients^[11]. Recurrences may be perceived as an increasing asymmetry or an enlarging mass within the operative bed or a new mass (neodensity) away from operative site^[10] (Figure 9). Any neodensity at mammography should be evaluated on ultrasound to determine whether it is solid or cystic (Figure 10), and solid lesions should be biopsied (Figure 11).

Up to 65% of early recurrences occur at or within a few centimetres of the site of original tumor, usually

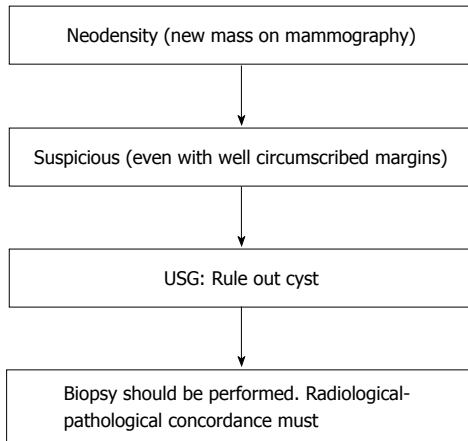


Figure 10 Approach to a neodensity.

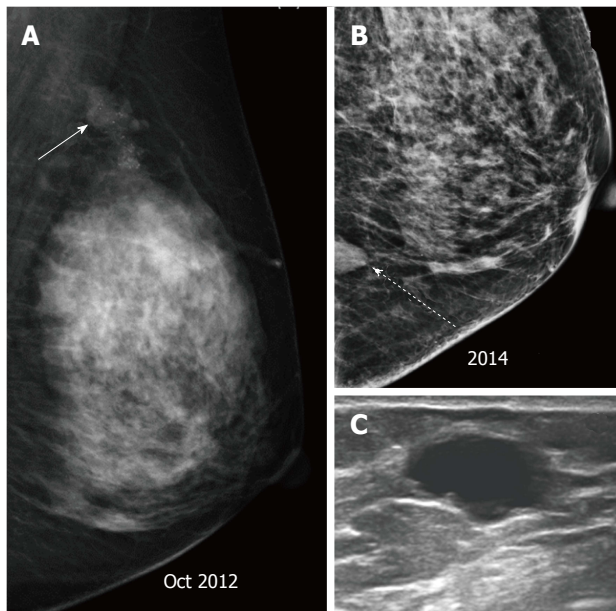


Figure 11 Patient with a left breast mass (arrow), who underwent breast-conserving therapy (A), (B) follow up mammogram at 2 years revealed a neodensity (dashed arrow) which on ultrasound (C) was found to be a cyst.

within 6-7 years of treatment^[1]. At follow up imaging, it is essential to ensure that scar site is visible in two views (CC and MLO or additional views), at least in the first decade after surgery^[6]. A new lesion or a neodensity which is suspicious may remain stable due to ongoing hormonal treatment, and stability does not indicate benign finding. Morphology is the most important criteria, and it is necessary to achieve a radiological-pathological concordance (Figure 12). Recurrence in the form of a developing asymmetry (Figure 13) has a 27% likelihood of cancer post BCT^[12]. Post-oncoplastic or breast reconstruction, locoregional tumor recurrence is seen in 2.3%. The most common site of tumor recurrence is the contact line, at the junction of the flap with the native tissue^[13] (Figure 14).

Microcalcifications

Microcalcifications that are casting, fine linear or

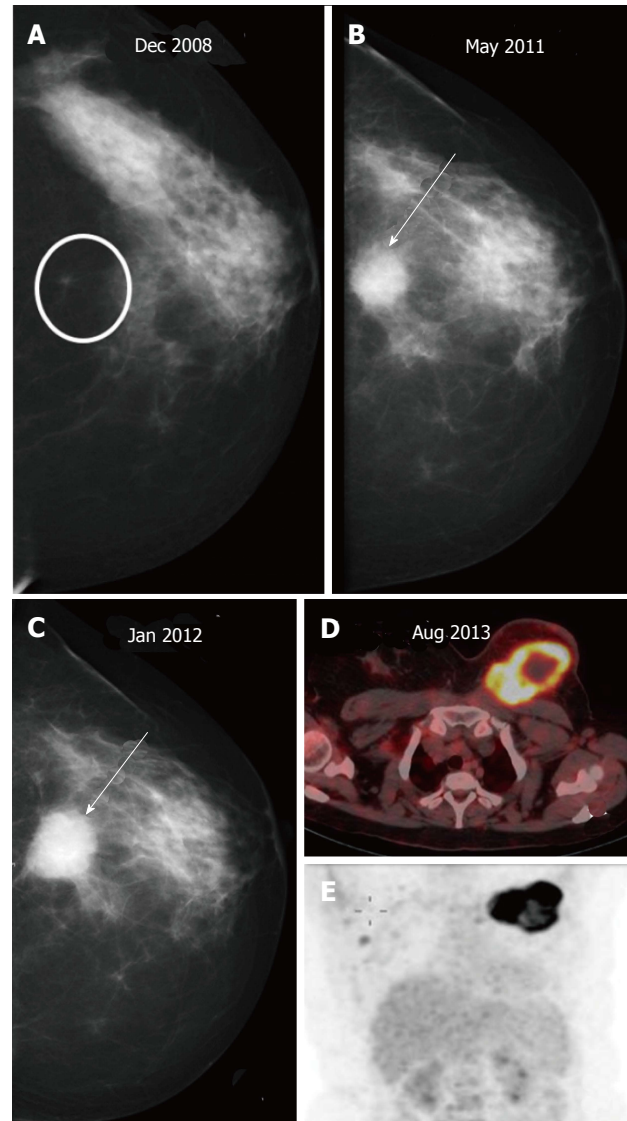


Figure 12 Morphology is the most important criteria, and it is necessary to achieve a radiological-pathological concordance. A-C: Patient underwent breast-conserving therapy for left breast carcinoma and on follow up imaging was found to have a developing asymmetry (circle in A) progressing to a mass (arrows in B and C). Biopsy and histopathology showed no evidence of malignancy however there was radiological and pathological discordance; D and E: Patient presented a year later with a large necrotic FDG-avid mass in the left breast. FDG: Fluoro-2-deoxyglucose.

linear branching and not typical of fat necrosis are suspicious. They are frequently similar in morphology to the primary cancer^[7] (Figure 15). In an area of fat necrosis, fat like lucency is noted around or within the calcific densities, while in calcifications associated with recurrence, an associated mass density is seen in the region (Figure 16).

Skin thickening

Progression of breast edema or skin thickening after the first post-surgical, post radiation therapy mammogram is abnormal and should be investigated^[14]. Increasing skin thickening is better appreciated on digital mammography as compared to screen film mammography.

Radiation induced sarcoma is a rare complication

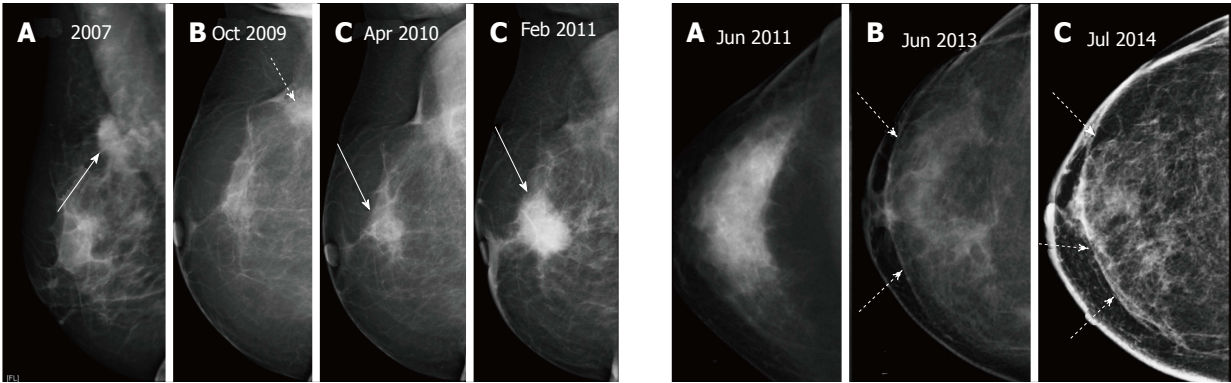


Figure 13 Patient with a right breast mass (arrow in A) who underwent breast-conserving therapy shows a normal post therapy mammogram at two years (B) with a post-surgical scar (dashed arrow), follow up imaging demonstrates a developing asymmetry in the retro-areolar region at three (C) years post therapy which subsequently developed into a frank mass (D).

which manifests as thickening of the skin or prominent trabecular pattern^[15]. Angiosarcoma presents as a painless mass that may be associated with overlying blue or purplish discoloration of the skin (Figure 17).

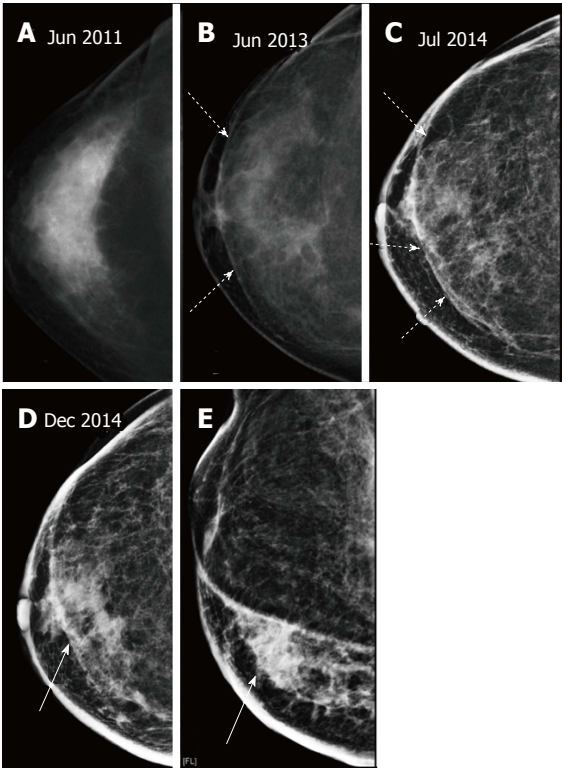
Paget's disease: Incidence of Paget's disease in ipsilateral breast tumor recurrences ranges from 3.1% to 10.6%. Paget's disease following BCT or subcutaneous mastectomy and reconstruction in patients presenting with nipple changes is not uncommon and should prompt early biopsy of what could be considered post-RT nipple changes^[16]. Microcalcifications in the nipple-areola region may be seen on the mammogram (Figure 18).

Axillary recurrence

Axillary nodal recurrence is relatively rare after adequate nodal dissection (of level I and II) has been done, occurring in 1%-3% of women^[17]. Patients who present with axillary recurrence have metastatic disease at other sites in about fifty percent. On mammogram enlarged nodes may be seen (Figure 19).

ROLE OF DIGITAL BREAST TOMOSYNTHESIS AND VOLUMETRIC BREAST DENSITY

Digital breast tomosynthesis (DBT) as a technique entails imaging of the breast tissue in multiple sections (at varied angles) instead of a two-dimensional image as with conventional mammography. The overlap of parenchymal tissues is resolved thus reducing the false positives as well as adequately identifying true lesions thus increasing the sensitivity of a mammogram. DBT not only helps in triangulation of a lesion but also reduces the requirement for additional views and lowers the patient call-back rate. Studies related to digital breast tomosynthesis to date have primarily focussed on screening with fewer reports on its utility in diagnostic mammography. Most studies have concluded a definite advantage of DBT in dense breasts (*i.e.*,



Per subject	Per breast		Per image	
F	29-12-2014		02-07-2014	
	R	L	R	L
Quantra				
Vfg (cm ³)	143	125	111	108
Vb (cm ³)	734	580	768	529
Vbd (%)	19	14	20	

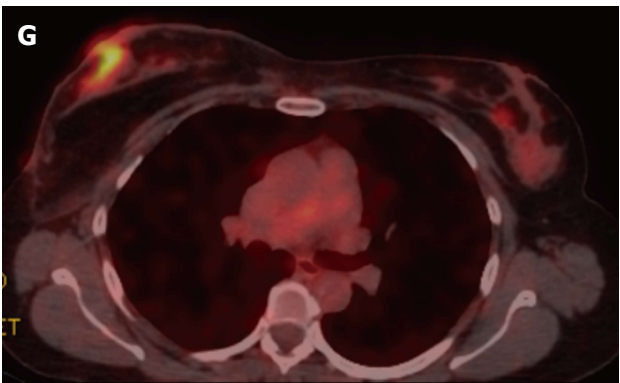


Figure 14 The most common site of tumor recurrence is the contact line, at the junction of the flap with the native tissue. A-C: Patient post right lumpectomy (A) underwent subcutaneous mastectomy with LD flap (dashed arrows in B and C); D-F: At three year follow up patient presented with a skin nodule which was seen as an asymmetric density at the junction of flap with native breast tissue (arrows in D and E) and an increase in volumetric density of right breast (F); FDG-PET study (G) showed that the nodule was FDG avid. Histology - IDC grade 3. FDG-PET: Fluoro-2-deoxyglucose-positron emission tomography.

patients who have types 3 and 4 breast parenchymal

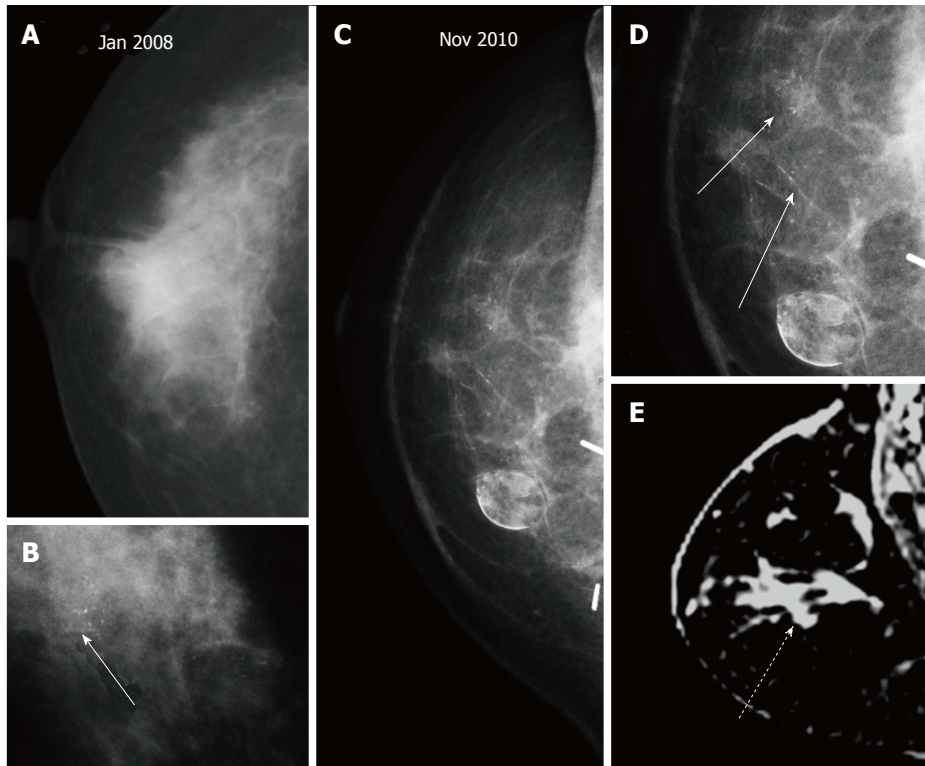


Figure 15 Microcalcifications. A, B: Patient presented with a right breast mass with microcalcifications (arrow in B) and underwent right breast-conserving therapy with latissimus dorsi flap; C, D: At two years post treatment casting microcalcifications developed similar to the index lesion, better appreciated on magnified view (arrows in D) are seen around the scar site; E: Breast MRI revealed non-mass enhancement (dashed arrow) in the right breast. Histopathology of the recurrence showed DCIS. MRI: Magnetic resonance imaging.

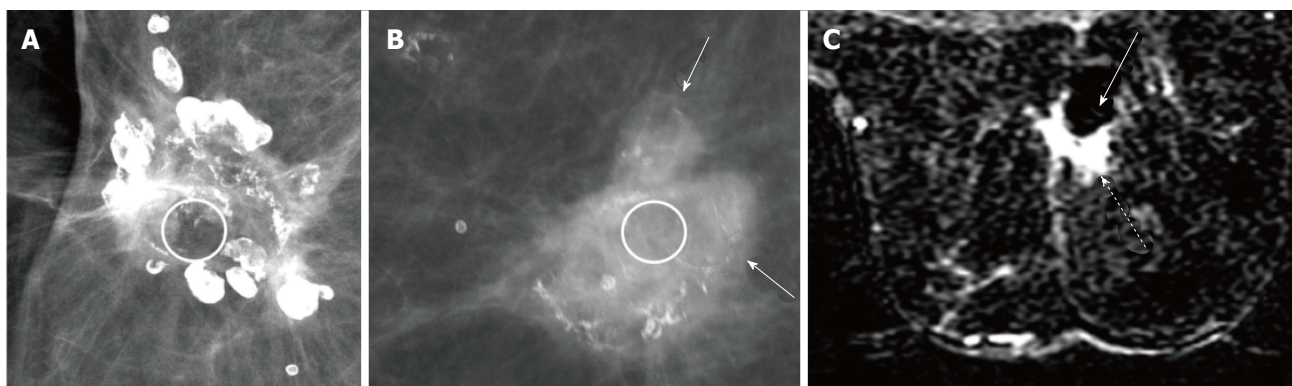


Figure 16 In dystrophic or benign calcifications, fat lucency (circle) is present within as seen in (A) while in calcifications associated with recurrence (arrows), the centre appears dense (circle) as shown in (B), (C) subtracted post contrast MRI image of the patient in (B) shows a seroma cavity (solid arrow) with an enhancing solid component (dashed arrow) in the periphery anteriorly.

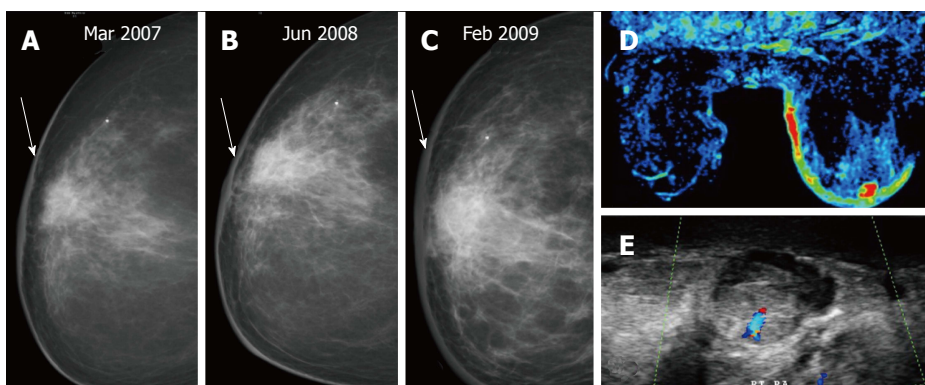


Figure 17 (A) In a post breast-conserving therapy patient, the skin thickness increases at one-year (B) and two-year (C) follow up mammograms; (D) dynamic MR perfusion reveals increased perfusion along the skin of the right breast and an enhancing focus, on ultrasound (E) an oval hypoechoic mass with increased vascularity is seen in the retroareolar region corresponding to the enhancing focus on breast MRI. Histopathology: Angiosarcoma. MRI: Magnetic resonance imaging.

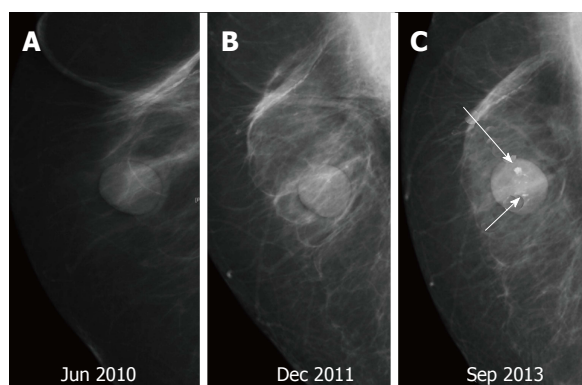


Figure 18 Microcalcifications in the nipple-areola region may be seen on the mammogram. A: Three year post breast-conserving therapy mammogram - normal. Patient presented with unilateral yellowish nipple discharge and no clinically palpable abnormality at five year follow up. MMG revealed microcalcification (arrows in C) in the nipple-areola region. Histopathology: Paget's disease of nipple; B: On retrospective evaluation, a tiny speck of calcification is seen in the nipple-areola region.

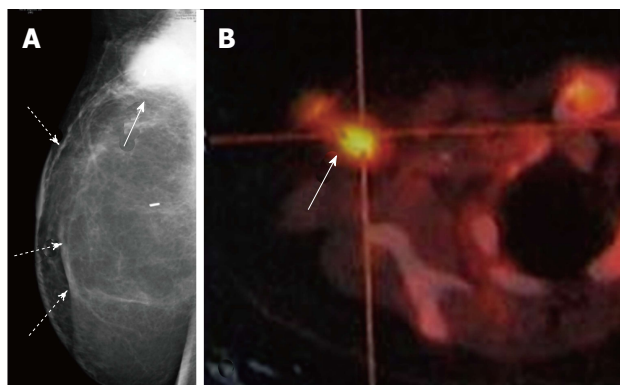


Figure 19 Patient underwent right skin sparing mastectomy with Deep Inferior Epigastric Perforator Flap (dashed arrows in A) and axillary and apical clearance, one year later she presented with right axillary nodes (arrow) on mammogram (A) which were FDG-avid on PET (B).

density) in terms of lesion characterisation^[18].

Similar to screening mammography, DBT also helps resolve post conservation changes such as a scar or other asymmetric densities due to parenchymal edema from a true recurrence^[19]. A recent study by Sia *et al.*^[20] also reported that DBT decreases the rate of indeterminate findings in surveillance imaging of conservatively treated breasts. The fat density within the scar and that associated with benign calcification is better appreciated on DBT (Figure 20) whereas a true recurrence would demonstrate a mass. Increase in the volumetric breast density (Vbd) allows for a quantitative assessment for recurrences particularly where the presentation is without a definite mass (Figure 21).

CONCLUSION

To conclude, mammographic appearance of the breast is altered in the post-operative setting and breast radiologists should be cognisant of features suggestive

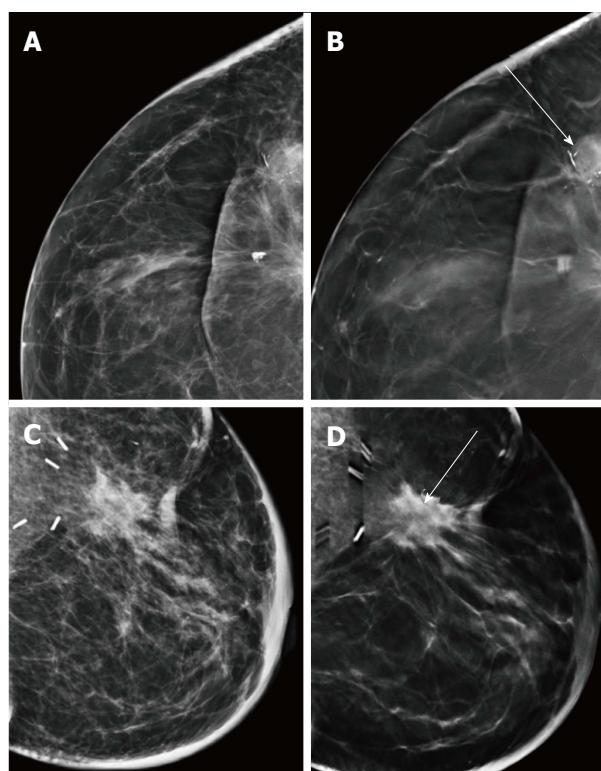


Figure 20 (A) and (B) represent conventional or 2D mammographic (A) and digital breast tomosynthesis (B) views of the scar site recurrence wherein mass density within the lesion is better appreciated on digital breast tomosynthesis (arrow); (C) and (D) show appearance of a scar on conventional or 2D mammogram (C) and digital breast tomosynthesis (D) where the fat lucency at the scar site is confirmed (arrow) on digital breast tomosynthesis.

of recurrent disease to identify it early. It is just as essential to be aware of the normal evolution of post therapy changes to avoid unnecessary further workup and stress to the patient. DBT and Vbd add incremental value in characterising normal and abnormal findings in this clinical setting. Not many studies have assessed the value of DBT over digital mammography with scope for research in this area in future.

REFERENCES

- 1 Mendelson EB. Evaluation of the postoperative breast. *Radiol Clin North Am* 1992; **30**: 107-138 [PMID: 1732922]
- 2 Krishnamurthy R, Whitman GJ, Stelling CB, Kushwaha AC. Mammographic findings after breast conservation therapy. *Radiographics* 1999; **19** Spec No: S53-S62; quiz S262-S263 [PMID: 10517443 DOI: 10.1148/radiographics.19.suppl_1.g99oc16s53]
- 3 Chansakul T, Lai KC, Slanetz PJ. The postconservation breast: part 1, Expected imaging findings. *AJR Am J Roentgenol* 2012; **198**: 321-330 [PMID: 22268174 DOI: 10.2214/AJR.10.7298]
- 4 Rivera R, Smith-Bronstein V, Villegas-Mendez S, Rayhanabad J, Sheth P, Rashtian A, Holmes DR. Mammographic findings after intraoperative radiotherapy of the breast. *Radiol Res Pract* 2012; **2012**: 758371 [PMID: 22550585 DOI: 10.1155/2012/758371]
- 5 Elsberger B, Romsauerova A, Vinnicombe S, Whelehan P, Brown DC, Dewar JA, Thompson AM, Evans A. Comparison of mammographic findings after intraoperative radiotherapy or external beam whole breast radiotherapy. *Eur J Surg Oncol* 2014; **40**: 163-167 [PMID: 24332581 DOI: 10.1016/j.ejso.2013.11.011]
- 6 Dershaw DD. Breast imaging and the conservative treatment of breast

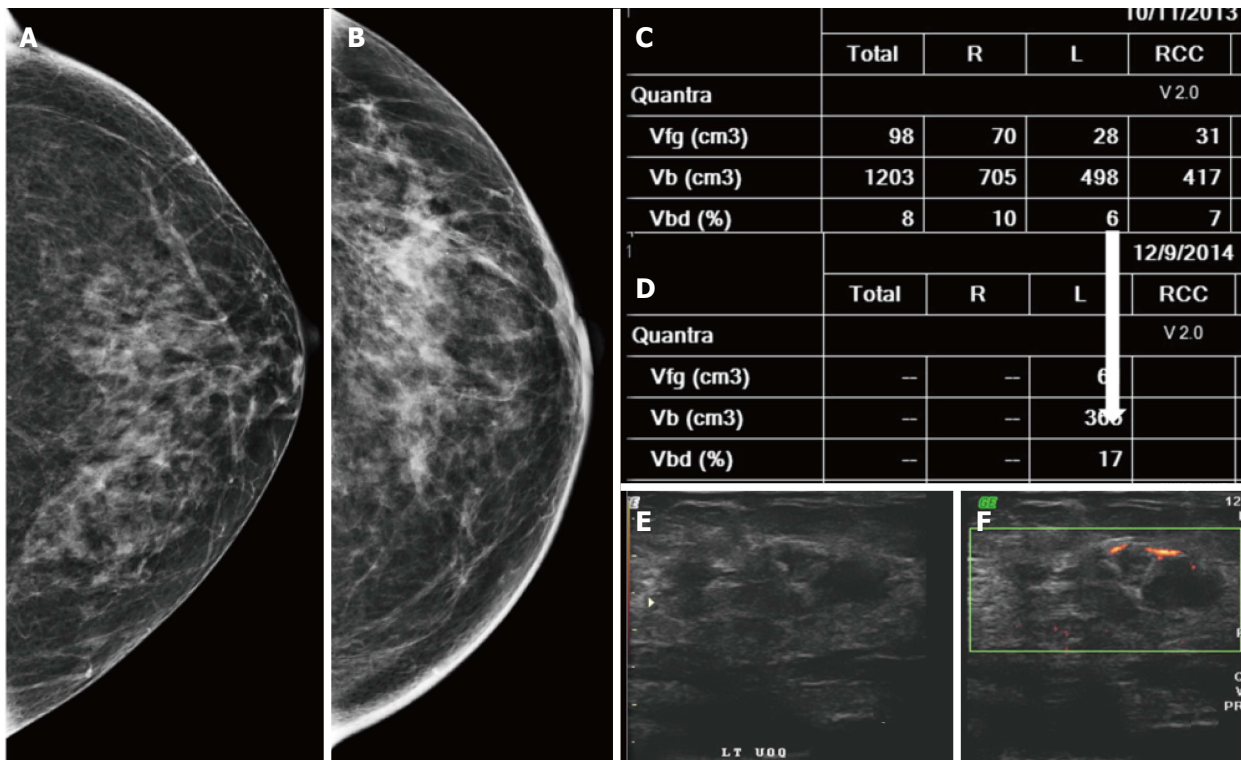


Figure 21 Patient underwent left breast-conserving therapy. On follow-up mammograms at five (A) and six (B) years a subtle increase in density is noted. On volumetric assessment (C and D), the left breast density increased from 6 to 17; E and F: Ultrasound and color Doppler revealed a heterogeneously hypoechoic mass in left upper outer quadrant with peripheral vascularity. Histology: IDC.

- cancer. *Radiol Clin North Am* 2002; **40**: 501-516 [PMID: 12117189]
- 7 **Gutierrez R**, Horst KC, Dirbas FM, Ikeda DM. Breast imaging following breast conservation therapy. In: Dirbas FM and Scott-Conner CEH. Breast surgical techniques and interdisciplinary management. New York: Springer Science Business Media, 2011: 975-995
- 8 **Hogge JP**, Zuurbier RA, de Paredes ES. Mammography of autologous myocutaneous flaps. *Radiographics* 1999; **19** Spec No: S63-S72 [PMID: 10517444 DOI: 10.1148/radiographics.19.suppl_1.g99oc12s63]
- 9 **Hedegard W**, Niell B, Specht M, Winograd J, Rafferty E. Breast reconstruction with a deep inferior epigastric perforator flap: imaging appearances of the normal flap and common complications. *AJR Am J Roentgenol* 2013; **200**: W75-W84 [PMID: 23255774 DOI: 10.2214/AJR.12.9270]
- 10 **Chansakul T**, Lai KC, Slanetz PJ. The postconservation breast: part 2, Imaging findings of tumor recurrence and other long-term sequelae. *AJR Am J Roentgenol* 2012; **198**: 331-343 [PMID: 22268175 DOI: 10.2214/AJR.11.6881]
- 11 **Hadjiiski L**, Sahiner B, Chan HP, Petrick N, Helvie MA, Gurcan M. Analysis of temporal changes of mammographic features: computer-aided classification of malignant and benign breast masses. *Med Phys* 2001; **28**: 2309-2317 [PMID: 11764038 DOI: 10.1118/1.1412242]
- 12 **Leung JW**, Sickles EA. Developing asymmetry identified on mammography: correlation with imaging outcome and pathologic findings. *AJR Am J Roentgenol* 2007; **188**: 667-675 [PMID: 17312052 DOI: 10.2214/AJR.06.0413]
- 13 **Farras Roca JA**, Dao TH, Lantieri L, Lepage C, Bosc R, Meyblum E, Pigneur F, Beaussart P, Assaf E, Totobenazara JL, Calitchi E, Belkacemi Y, Rahmouni A, Luciani A. Ipsilateral breast cancer recurrence after Deep Inferior Epigastric Perforator (DIEP) flap reconstruction: Incidence and radiological presentation. *Diagn Interv Imaging* 2016; **97**: 203-209 [PMID: 26282051 DOI: 10.1016/j.diii.2015.06.021]
- 14 **Gage I**, Schnitt SJ, Recht A, Abner A, Come S, Shulman LN, Monson JM, Silver B, Harris JR, Connolly JL. Skin recurrences after breast-conserving therapy for early-stage breast cancer. *J Clin Oncol* 1998; **16**: 480-486 [PMID: 9469331 DOI: 10.1200/jco.1998.16.2.480]
- 15 **Yi A**, Kim HH, Shin HJ, Huh MO, Ahn SD, Seo BK. Radiation-induced complications after breast cancer radiation therapy: a pictorial review of multimodality imaging findings. *Korean J Radiol* 2009; **10**: 496-507 [PMID: 19721835 DOI: 10.3348/kjr.2009.10.5.496]
- 16 **Plastaras JP**, Harris EE, Solin LJ. Paget's disease of the nipple as local recurrence after breast-conservation treatment for early-stage breast cancer. *Clin Breast Cancer* 2005; **6**: 349-353 [PMID: 16277886 DOI: 10.3816/CBC.2005.n.039]
- 17 **Clemons M**, Danson S, Hamilton T, Goss P. Locoregionally recurrent breast cancer: incidence, risk factors and survival. *Cancer Treat Rev* 2001; **27**: 67-82 [PMID: 11319846 DOI: 10.1053/ctrv.2000.0204]
- 18 **Margolis L**, Cohen A, Sonnenblick E, Mandeli J, Schmidt PH, Szabo J, Patel N, Hermann G, Weltz C, Port E. Digital breast tomosynthesis changes management in patients seen at a tertiary care breast center. *ISRN Radiol* 2014; **2014**: 658929 [PMID: 24967297 DOI: 10.1155/2014/658929]
- 19 **Curran J**. How effective is mammography in detecting breast cancer recurrence in women after Breast Conservation Therapy (BCT) - A systematic literature review. *Radiography* 2016; **22**: 252-256 [DOI: 10.1016/j.radi.2016.02.001]
- 20 **Sia J**, Moodie K, Bressel M, Lau E, Gyorki D, Skandarajah A, Chua B. A prospective study comparing digital breast tomosynthesis with digital mammography in surveillance after breast cancer treatment. *Eur J Cancer* 2016; **61**: 122-127 [PMID: 27163158 DOI: 10.1016/j.ejca.2016.04.007]

P- Reviewer: Langdon S, Medina-Franco H, Olsha O
S- Editor: Song XX **L- Editor:** A **E- Editor:** Lu YJ



Observational Study

Clinical-radiological-pathological correlation of cavernous sinus hemangioma: Incremental value of diffusion-weighted imaging

Abhishek Mahajan, Vedula Rajni Kanth Rao, Gudipati Anantaram, Ashwin M Polnaya, Sandeep Desai, Paresh Desai, Rammohan Vadapalli, Manas Panigrahi

Abhishek Mahajan, Ashwin M Polnaya, Department of Radiodiagnosis, Tata Memorial Centre, Mumbai 400012, India

Vedula Rajni Kanth Rao, Gudipati Anantaram, Department of Radiology, Krishna Institute of Medical Sciences, Secunderabad 500003, India

Sandeep Desai, Department of Radiodiagnosis Clumax Imaging, Bangalore 560011, India

Paresh Desai, Department of Radiology, Apollo Victor Hospital, Goa 403601, India

Rammohan Vadapalli, Department of Radiology, Vijaya Diagnostics, Hyderabad, Secunderabad 500003, India

Manas Panigrahi, Department of Neurosurgery, Krishna Institute of Medical Sciences, Secunderabad 500003, India

Author contributions: Guarantors of integrity of entire study by all authors; study concepts/study design or data acquisition or data analysis/interpretation by all authors; manuscript drafting or manuscript revision for important intellectual content by all authors; manuscript final version approval by all authors; literature research by all authors; manuscript editing by all authors; all authors take responsibility for the integrity of the data and the accuracy of the data analysis.

Institutional review board statement: The study was reviewed and approved by the Institutional review board.

Informed consent statement: Participants gave informed consent for data sharing.

Conflict-of-interest statement: I confirm that this manuscript is not published anywhere else and on behalf of all authors, I state that there is no conflict of interests (including none for related to commercial, personal, political, intellectual, or religious interests).

Data sharing statement: All the cases presented in this article belong to the authors and have not been copied or borrowed from any published material. Technical appendix, statistics, and dataset available from the corresponding author Dr V R K Rao (vedula@gmail.com). The authors whose names are listed above certify that they have no affiliations with or involvement in any organization or entity with any financial interest or non-financial interest in the subject matter or materials discussed in this manuscript. The authors certify that a manuscript on the same or similar material has not already been published or has not been or will not be submitted to another journal or by colleagues at their institution before their work appears in your journal.

Open-Access: This article is an open-access article which was selected by an in-house editor and fully peer-reviewed by external reviewers. It is distributed in accordance with the Creative Commons Attribution Non Commercial (CC BY-NC 4.0) license, which permits others to distribute, remix, adapt, build upon this work non-commercially, and license their derivative works on different terms, provided the original work is properly cited and the use is non-commercial. See: <http://creativecommons.org/licenses/by-nc/4.0/>

Manuscript source: Invited manuscript

Correspondence to: Vedula Rajni Kanth Rao, MD, DMRD, Department of Radiology, Krishna Institute of Medical Sciences, Minister Road, Secunderabad 500003, India. drvedula@kimshospitals.co.in
Telephone: +91-99-89773473
Fax: +91-40-27840980

Received: February 21, 2017
Peer-review started: February 26, 2017
First decision: March 27, 2017
Revised: May 8, 2017
Accepted: May 22, 2017
Article in press: May 24, 2017
Published online: August 28, 2017

Abstract

AIM

To elucidate the clinical, magnetic resonance imaging (MRI), pathological features of these lesions and assess the incremental value of diffusion-weighted imaging (DWI) in diagnosing them.

METHODS

Fifteen consecutive patients (11 females and 4 males; mean age 40.93 years; age range 13-63 years) with cavernous sinus hemangiomas (CSH) who underwent examination between November 2008 and May 2016 were included for the analysis. MRI, clinical and surgical findings of each patient was retrospectively reviewed. DWI were also analysed and mean-apparent diffusion coefficient (ADC) value was calculated. Eleven patients underwent surgical removal of the lesion and 2 patients had biopsy only. Diagnosis of CSH was confirmed histologically in 13 patients.

RESULTS

Eleven patients (73%) presented with headaches and 10 (66%) had cranial nerve involvement. Extra cavernous sinus extension was noted in 14 (94%). Surgery was performed in 13 (87%) and post-operative radiation was given to 4 (28%) patients. Thirteen patients remained asymptomatic on follow up. Three conspicuous imaging features were highly suggestive of the diagnosis: Lack of diffusion restriction (100%), homogeneous hyperintensity on T2 weighted image sequences (93.3%) and intense post-contrast enhancement (100%). The mean ADC was $1.82 \times 10^{-3} \pm 0.2186 \text{ cm}^2/\text{s}$.

CONCLUSION

T1-weighted hypointensity with homogeneous hyperintensity on T2-weighted sequences, intense enhancement and absence of hemosiderin within the lesion on GRE sequence favour the diagnosis. Facilitated diffusion on DWI differentiates CSH from other solid cavernous sinus lesions and significantly improves the diagnostic accuracy, a critical factor for planning surgery.

Key words: Cavernous sinus hemangioma; Cavernous sinus; Magnetic resonance imaging; Diffusion weighted imaging

© **The Author(s) 2017.** Published by Baishideng Publishing Group Inc. All rights reserved.

Core tip: Cavernous hemangioma in the cavernous sinus are rare lesions with significant female preponderance. This article highlights the diagnostic magnetic resonance imaging features of cavernous sinus hemangiomas (CSH). T1-weighted hypointensity with homogeneous hyperintensity on T2-weighted sequence, absence of hemosiderin within the lesion on GRE sequence and intense post contrast enhancement favour the diagnosis. On diffusion-weighted imaging CSH shows facilitated diffusion and is nearly 100% specific for CSH. Markedly hypointense hemangioma on T1 weighted images

suggests schirrous nature of the lesion and is amenable to complete surgical excision.

Mahajan A, Rao VRK, Anantaram G, Polnaya AM, Desai S, Desai P, Vadapalli R, Panigrahi M. Clinical-radiological-pathological correlation of cavernous sinus hemangioma: Incremental value of diffusion-weighted imaging. *World J Radiol* 2017; 9(8): 330-338 Available from: URL: <http://www.wjgnet.com/1949-8470/full/v9/i8/330.htm> DOI: <http://dx.doi.org/10.4329/wjr.v9.i8.330>

INTRODUCTION

Cavernous hemangioma in the cavernous sinus has an estimated prevalence of 1% incidence with significant female preponderance, considered to be due to hormonal influence^[1,2]. The lesion is rare in occurrence closely mimicking commonly encountered cavernous sinus lesions such as schwannoma, meningioma, chordoma, granuloma, carotid aneurysm and lymphoproliferative conditions^[3,4]. Microscopically cavernous sinus hemangioma (CSH) consists of multiple vascular channels lined by a single layer of endothelium without muscular layer and any intervening neural tissue^[2]. Magnetic resonance imaging (MRI) is the imaging modality of choice for evaluating cavernous sinus lesions. On MR imaging, CSH shows hypointense signal on T1 weighted images (T1-W) and hyperintense signal on T2 weighted images (T2-W) that is indistinguishable from the other lesions which have high cellular matrix and/or necrotic components^[3,4]. T2 prolongation resulting in extremely high signal intensity has been considered a definite sign of a cavernous hemangioma^[4,5]. Hence, even at MRI, the diagnosis of a cavernous hemangioma can still be in doubt, with the main differential diagnosis being a schwannoma of the V nerve or meningioma^[3,6]. The study aimed to elucidate the clinical, MRI, pathological features of these lesions and assess the incremental value of diffusion-weighted imaging (DWI) in diagnosing them.

MATERIALS AND METHODS

This retrospective interpretation of data was approved by the hospital internal review board and informed consent was waived. A total of 15 consecutive patients with CSH who underwent MRI examination between December 2008 and May 2016 were included for the analysis. MRI, clinical, and surgical findings of each patient were retrospectively reviewed. Imaging was performed on both 1.5-T and 3-T systems (HDxt GE, Siemens Medical, Philips Ingenia) using 8 channel high resolution dedicated brain coil. The imaging protocol included spin-echo T1-W, fast spin-echo T2-W, fluid-attenuated inversion recovery imaging (FLAIR) and contrast-enhanced spin-echo T1-W was performed following gadolinium injection. Fast Imaging Employing

Table 1 Signal intensities and other features on conventional and special magnetic resonance imaging sequences

Case No.	T1W	T2W	T2 FLAIR	Post-contrast	Flow voids	Extension beyond cavernous sinus	Vessel encasement	DWI	Blooming on GRE
1	Hypo	Hyper	Hyper	Intense enhancement	Yes	Moderate	Yes	Hypointense	No
2	Hypo	Hyper	Hyper	Intense enhancement	No	Moderate	Yes	Hypointense	No
3	Hypo	Hyper	Hyper	Intense enhancement	No	Moderate	Yes	Hypointense	No
4	Hypo	Hyper	Hyper	Intense enhancement	No	Extensive	Yes	Not done	No
5	Hypo	Hyper	Hyper	Intense enhancement	No	Extensive	Displaced only	Hypointense	Not done
6	Hypo	Hyper	Hyper	Intense enhancement	No	Nil	Displaced only	Not done	Not done
7	Hypo	Hyper	Hyper	Intense enhancement	Yes	Mild	Yes	Hypointense	No
8	Hypo	Hyper	Hyper	Intense enhancement	Centripetal filling	Moderate	Yes	Hypointense	-
9	Iso intense	Mildly hyper	Not done	Intense enhancement	No	Moderate	Yes	Hypointense	Not done
10	Hypo	Hyper	Not done	Intense enhancement	No	Mild	Yes	Not done	Not done
11	Hypo	Hyper	Hyper	Not available	No	Moderate	No	Not done	Not done
12	Hypo	Hyper	Hyper	Intense enhancement	Vascular supply from left ICA	Extensive	Yes	Hypointense	No
13	Hypo	Hyper	Hyper	Intense enhancement	No	Mild	Yes	Hypointense	No
14	Hypo	Hyper	Hyper	Intense enhancement	No	Extensive	Yes	Hypointense	Not done
15	Hypo	Hyper	Hyper	Intense enhancement	Yes	Extensive	Yes	Not done	Not done

T1-W: T1 weighted image; T2-W: T2 weighted image; FLAIR: Fluid attenuated inversion recovery; DWI: Diffusion-weighted imaging; GRE: Gradient recalled echo.

Steady-state Acquisition (FIESTA) and susceptibility weighted imaging (SWI) were added to the routine sequences in two patients. Diffusion weighted imaging was performed in ten patients and GRE imaging in seven. MR angiography and digital subtraction angiography (DSA) were performed in four and two patients respectively.

Imaging parameters used for various sequences were as follows: (1) repetition time (TR) ms/echo time (TE) msec, 375/11; flip angle, 90°; and matrix, 296 × 205 for spin-echo T1-W; (w) 3000/90; flip angle, 90°; and matrix, 492 × 479 for fast spin echo T2-W; and (3) 10000/125; 90°; and matrix, 300 × 205 for fluid-attenuated inversion recovery imaging. The other parameters were as follows: 5-mm section thickness with a 1.5-2.2 mm intersection gap and 230 mm × 250 mm field of view. Echo-planar DW MR imaging [2921/82.4 ($b = 0$ and 1000 s/mm²); 24 sections; bandwidth, 2501 Hz per voxel; section thickness, 4 mm; intersection gap, 1.5-2.5 mm; field of view, 230 mm × 230 mm; matrix, 120 × 90; three signals acquired; voxel resolution, 2.05 mm × 2.53 mm × 4 mm) was performed in the axial plane before contrast material injection.

Diffusion weighted imaging was performed in 10 patients [apparent diffusion coefficient (ADC) values

of 5 cases were listed in Table 1]. DW images were acquired at b value = 1000 mm²/s in three orthogonal directions and combined into a trace image. DW images were visually inspected and classified as hyperintense, isointense and hypointense as compared with normal white matter. The mean ADC values (10⁻³ cm²/s) were calculated on a voxel-by-voxel basis with the software incorporated into the MR imaging unit. Manual ROIs were placed using T2 weighted and contrast enhanced images as the guide.

A fat-suppression pulse was added to the axial T1-weighted sequences following contrast enhancement. The intravenous manual bolus dose of gadolinium based contrast medium given at 0.2 mL/kg (0.1 mmol/kg) body weight. T1-weighted 3D spin-echo sequences without fat suppression were performed with identical imaging parameters after contrast agent administration. Post contrast Spoiled Gradient Echo (SPGR) sequences were obtained using repetition time /echo time 5/10 ms; flip angle, 80; matrix, 492 × 479; slice thickness, 1 mm; slice interval, 0 and FOV, 240 × 240.

MRI images were reviewed by three neuroradiologists (R.K., R.M., AM.) by consensus agreements. Signal intensities in T1-W, T2-FSE and FLAIR were tabulated as hyper, hypo, isointensities. GRE and DWI sequences were assessed for blooming and restriction of dif-

Table 2 Mean apparent diffusion coefficient values in 5 patients

Case number	mean ADC ($10^{-3} \text{ cm}^2/\text{s}$)
Case 1	1.98 ± 0.227
Case 2	1.67 ± 0.19
Case 3	1.184 ± 0.127
Case 7	2.774 ± 0.299
Case 9	1.54 ± 0.287
Mean	1.8296 ± 0.2038

ADC: Apparent diffusion coefficient.

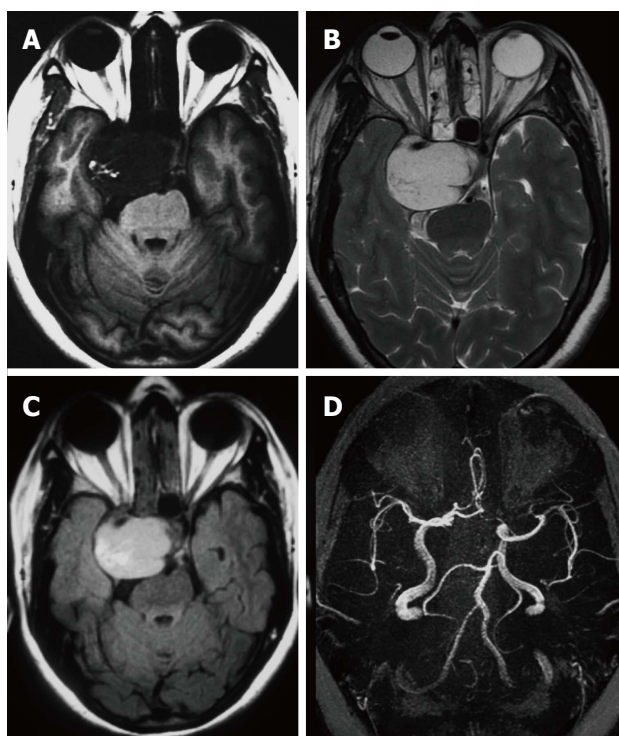


Figure 1 T1 weighted image, T2 weighted image and fluid-attenuated inversion recovery imaging images. A: Axial MRI image shows well defined lobulated hypointense mass on T1-W sequence image in the right cavernous sinus; B: Homogeneous hyperintensity of the mass is noted in the T2-W axial image; C: T2-W FLAIR axial image demonstrates marked hyperintense signal of the lesion; D: MRA reveals laterally stretched and displaced cavernous carotid segment. T1-W: T1 weighted image; T2-W: T2 weighted image; FLAIR: Fluid attenuated inversion recovery; MRI: Magnetic resonance imaging; MRA: Magnetic resonance angiography.

fusion. Degree of enhancement was noted from the contrast enhanced T1-Fat Suppressed sequences. The medical case files were reviewed retrospectively. The demography is detailed in Table 2. The age at presentation ranged from 13 to 63 years with a mean of 40.93 ± 13.82 years. There were 11 female and 4 male patients with a female preponderance. The mean age of female cohort was 42.27 ± 11.064 years. Diagnosis of cavernous hemangioma in the cavernous sinus was verified from the surgical and pathology notes. Eleven patients underwent surgical removal of the lesion and 2 patients had biopsy only. Diagnosis of CSH was confirmed histologically in 13 patients.

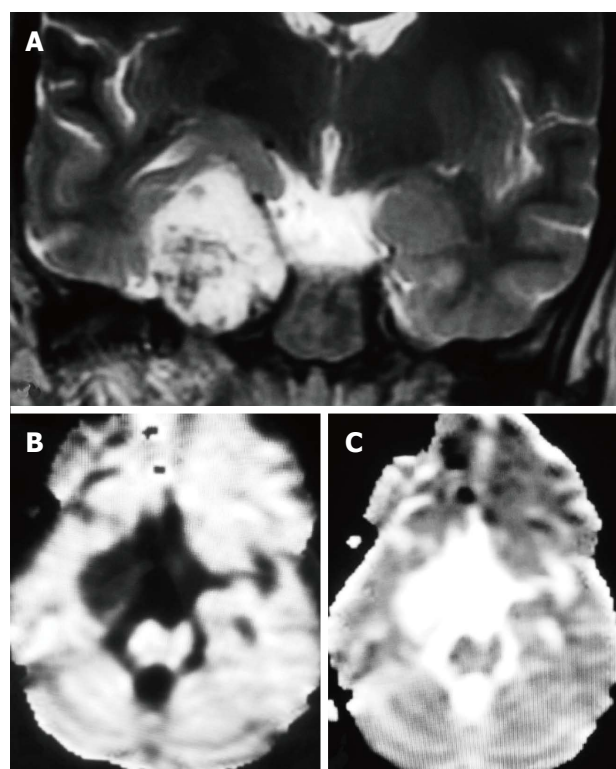


Figure 2 T2 weighted image coronal, diffusion-weighted imaging and apparent diffusion coefficient map images. A: T2-W coronal image demonstrates multiple flow voids within the CSH in the right cavernous sinus; B: DWI image shows hypointense signal on diffusion-weighted map (B) and corresponding hyperintensity on ADC maps (C) suggestive of facilitated diffusion. T2-W: T2 weighted image; CSH: Cavernous sinus hemangioma; DWI: Diffusion-weighted imaging; ADC: Apparent diffusion coefficient.

RESULTS

Headache was the constant feature and 7 patients had no visual symptoms despite large size of the lesion (Table 2). Papilledema was observed in one patient only. One patient had painful ophthalmoplegia in spite of a small sub-centimeter lesion occupying the small posterior segment of the cavernous sinus. Pre-operative MR imaging features are summarised in Table 3. Fourteen of the 15 patients showed well defined hypointense lesions occupying the cavernous sinus on T1-W imaging and all of these lesions showed homogeneous hyperintensity in T2-W and FLAIR imaging sequences (Figure 1). Significant extension beyond cavernous sinus into the Meckel's cave, prepontine cistern and impression onto the peduncle was seen in 14 of 15 patients and correlated with the presenting complaints.

In the ten patients who had DW imaging, hypointense signal on DWI images was a consistent finding suggestive of facilitated diffusion (Table 3, Figure 2). The ADC maps in these lesions were hyperintense in comparison with contralateral brain parenchyma and the mean ADC value (5 patients) was $1.82 \times 10^{-3} \pm 0.2186 \text{ cm}^2/\text{s}$. GRE images in seven patients did not show any blooming (Figure 3). Intense enhancement of the lesion was noted in all patients (14 of 14). Centripetal

Table 3 Demography, clinical features, treatment and follow up

Case number	1 ^a	2 ^a	3 ^a	4 ^a	5	6	7	8	9	10	11	12	13	14	15
Age	51	26	38	47	52	63	26	33	59	51	50	34	38	33	13
Sex	F	M	F	F	F	F	F	F	M	M	F	F	F	F	M
Location	Right	Right	Left	Right	Left	Left	Right	Left	Right	Left	Right	Left	Left	Left	Left
Headache	1 yr	2 yr	Yes	4 yr	Yes	No	Yes	3 mo	Yes	Yes	Not available	No	No	6 mo	4 mo
Visual symptoms	Yes	12 mo	Blurring	6 mo	Nil	Nil	Blurring	Nil	6 mo	Nil	Not available	Nil	2 mo	6 mo	Nil
Cranial nerve involvement ^b	3 rd , 4 th , 6 th	6 th	No	3 rd	No	3 rd , 4 th , 6 th	No	No	No	6 th	Not available	Numbness face	No	No	3 rd , 6 th
Operative details	Sub total	Sub total	Biopsy	Sub total	No surgery	Sub total	Biopsy	Sub total	No surgery	Complete excision	Sub total	Sub total	Sub total	Sub total	Complete excision
Follow up	No symptoms	No symptoms	No symptoms	No symptoms	No symptoms	Not available	No symptoms	No symptoms	Not available	No symptoms	Not available	No symptoms	No symptoms	No symptoms	No symptoms

^aReceived radiotherapy: Case no 1: 45 Gy in 25 fractions; case no 2: 25 Gy in 5 fractions; case 3: Stereotactic radiosurgery - 13 Gy in single fraction; case 4: Received adjuvant radiotherapy; ^bCranial nerves 3 (oculomotor), 4 (trochlear), and 6 (abducens). F: Female; M: Male.

enhancement was observed progressively increasing in intensity in a young female patient. DSA examination demonstrated stretching and irregular narrowing of the internal carotid artery. Multiple venous channels were seen persisting in the venous phase (Figure 4). Contrast enhanced MRI performed after two years demonstrated significant shrinkage with thrombosis of the center of the lesion in one patient and total regression in another (Figure 5). Complete resection of CSH was possible in two patients (Figure 6). One patient had a sub-centimeter lesion in the left cavernous sinus presenting with painful ophthalmoplegia (Figure 7).

Three conspicuous imaging features were considered highly suggestive of the diagnosis: Homogeneous hyperintensity on T2-W sequences (14/15, 93.3%) facilitated diffusion (10/10, 100%) and intense contrast enhancement (14/14, 100%). Of the 13 patients who received surgery, subtotal excision or biopsy in 11 and complete excision in 2 patients were performed. Four patients received radiation therapy (Table 2). Eleven patients had serial follow-up ranging from 10 mo to 90 mo (mean 2.5 years) and all were asymptomatic on the serial follow-up.

DISCUSSION

Extracerebral CSH are rare in occurrence with a definite female preponderance. They are usually attached to the outer wall of cavernous sinus or located in the Meckel's cave or cerebellopontine angle^[1,2]. Eleven of fifteen patients in our study were females and their preponderance is considered to be due to influence of estrogen. Symptoms are slow and insidious presenting with headaches, ophthalmoplegia, proptosis, cranial nerve palsy and endocrine disturbances^[7,8]. In our series headache was the most common presenting complaint followed by vision abnormality and cranial nerve palsy. Imaging findings of meningiomas and schwannomas in this location overlap significantly. Typically, the lesion is not demonstrable on angiography in spite of the adjacent tortuous and serpentine arterial feeders and venous drainage. Degeneration into thrombosis, calcification, hyaline changes and hemorrhage are revealed by MR imaging^[7-9].

Extension beyond cavernous sinus is noted in large lesions which may be seen also in meningioma, epidermoid, neurogenic tumors and granulomatous masses^[3,7]. Extension beyond cavernous sinus was seen in all sizable lesions in our series and five lesions showed extensive para-cavernous extension. It was interesting to note, one of our CSH extended into the superior orbital fissure anteriorly, superiority into the suprasellar region, greater wing of sphenoid bone and pterygoid fossa inferolaterally

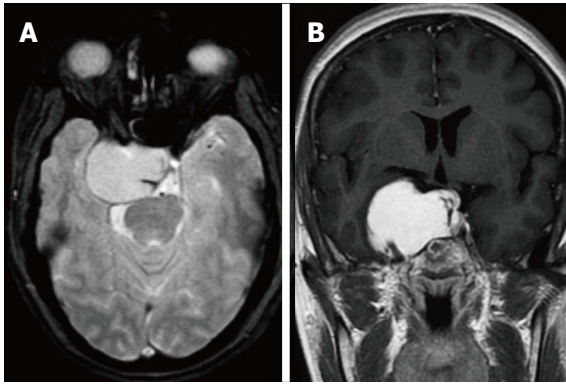


Figure 3 Axial gradient recalled echo and contrast enhanced T1 weighted image axial magnetic resonance images. A: Axial gradient recalled echo sequence does not show any blooming; B: Contrast enhanced coronal T1 weighted image shows intensely enhancing lesion encasing the internal carotid artery.

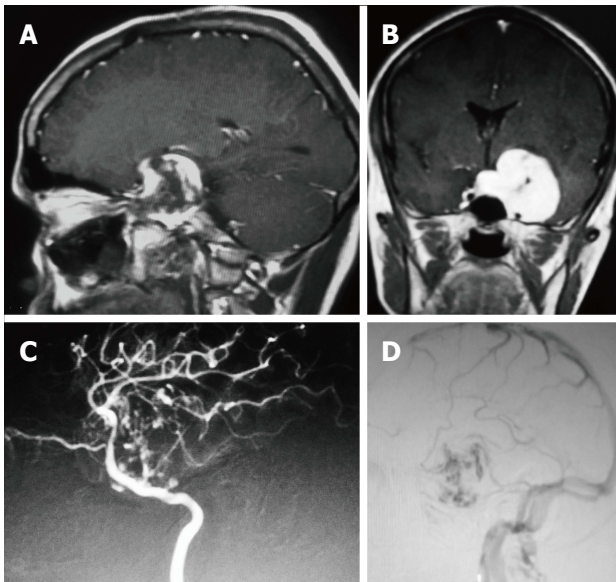


Figure 4 Contrast enhanced sagittal and coronal T1 weighted images and lateral views of digital subtraction angiography arterial and venous phases of left internal carotid angiogram. A, B: Centripetal filling of the CSH in the left cavernous sinus is demonstrated; C: Arterial phase of DSA shows diffuse irregularity and stretching of C3 to C5 segments; D: Venous phase shows stasis in the venous channels within the CSH. CSH: Cavernous sinus hemangioma; DSA: Digital subtraction angiography.

and into retroclival region posteriorly indistinguishable from a granulomatous or a neurogenic lesion^[3,8]. Multiple cranial nerves and both internal carotid arteries traversing the cavernous sinus preclude complete surgical resection in addition to the risk of profuse bleeding. Tiny branches from the cavernous segment of the internal carotid artery may be revealed on digital subtraction angiography which are otherwise not appreciable on routine anatomical imaging^[7,8]. Hypertrophied pial arteries, tumor stain and large draining veins were described in the intra-axial cavernous hemangioma closely resembling a highly vascular neoplasm^[10,11].

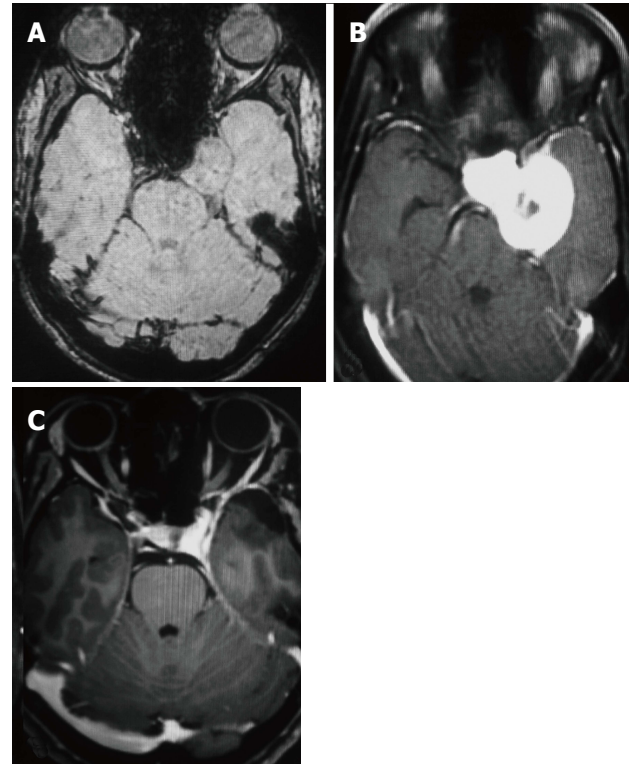


Figure 5 Contrast enhanced axial, susceptibility weighted imaging and 2 years follow up axial CE images. A: SWI axial image shows isointense signal of the CSH; B: Contrast enhanced axial T1-W image demonstrates the postero-inferior extension of the CSH; C: Two years post-operative surveillance axial contrast enhanced T1-W image shows complete resolution of the lesion. T1-W: T1 weighted image; SWI: Susceptibility weighted image; CSH: Cavernous sinus hemangioma.

On MR imaging, the lesions are seen as well-defined hypointense mass on T1-W and markedly hyperintense mass on T2-W sequence. In our series 14 of 15 patients (93%) showed these findings^[3,4]. Schwannomas exhibit high signal intensity on T2-W and display heterogeneous enhancement following the expected course of the nerves from which they arise. Meningiomas show similar signal intensity to gray matter on T2-W unlike the CSH^[3,12]. Delayed T1-W Gd-DTPA imaging confirms the temporal course of enhancement of the lesion. Uniformly intense and homogeneous contrast enhancement of all our CSH distinctly differ from the intra axial cavernous hemangiomas which mostly do not show enhancement^[9,12,13]. Hypointense hemosiderin rim is not a common feature which is otherwise seen in intra-axial cavernous hemangioma. Bowing and displacement of the lateral wall of the cavernous sinus is clearly depicted on MR imaging indicating the extradural extension^[5,12] and extensive extradural extension was seen in 5 patients in our series.

Lack of restriction to diffusion may be explained due to slow flow within the lesion which allows free diffusion of water molecules. There are no intervening neural/cellular elements outside the vascular channels which can prevent free movement of the protons and cause restriction of diffusion in the extravascular spaces

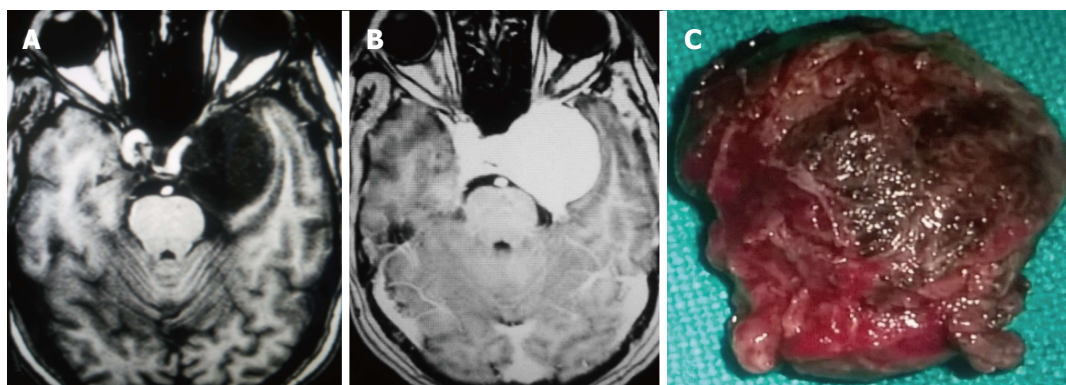


Figure 6 T1 weighted image plain, contrast enhanced axial magnetic resonance images and specimen photograph. A: Axial plain T1-W image shows large hypointense lesion in the left cavernous sinus; B: Contrast enhancement is intense in the axial T1-W image; C: The surgical specimen shows a well lobulated reddish mass resected entirely. T1-W: T1 weighted image.

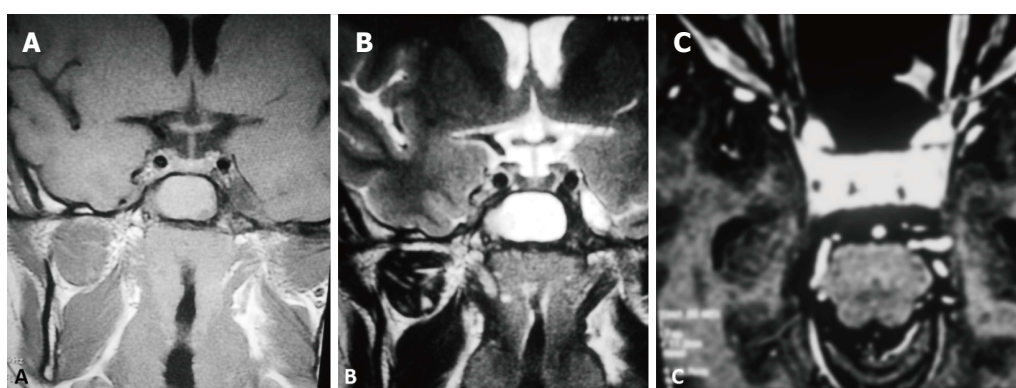


Figure 7 T2 weighted image coronal plain and contrast enhanced T1 weighted images. A: T1-W coronal unenhanced image shows an isointense to hypointense signal in the left cavernous sinus without affecting the internal carotid artery; B: Coronal T2-W shows small heterogeneous signal intensity in the left cavernous sinus; C: T1-W contrast enhancement shows homogeneous enhancement of the small lesion causing painful ophthalmoplegia. T1-W: T1 weighted image; T2-W: T2 weighted image.

as well. Hence these lesions are iso or hypointense to brain parenchyma on DWI images^[4,14,15]. One hundred percent patients in our series showed hypointense signal on DW imaging suggesting facilitated diffusion (mean $ADC = 1.8296 \pm 0.2038 \times 10^{-3} \text{ cm}^2/\text{s}$). Our series is the largest series which has looked into the incremental value of DW imaging in diagnosing CSH and results of our series suggest that facilitated diffusion is a consistent finding in CSH. However, at the b value = $1000 \text{ mm}^2/\text{s}$ used in our series, effect of intravoxel incoherent motion is less though it cannot be eliminated completely which might have contributed to low signal on DWI and high ADC values^[14,15]. False negative results may be seen in CSH with hemorrhage within and may cause a diagnostic dilemma, which was not seen in our series. CSH should be entertained in the differential diagnosis of a homogeneously enhancing cavernous sinus lesion that does not show evidence of hemorrhage and shows facilitated diffusion^[15-17].

Blood flowing in the CSH is not exactly venous blood as it has not passed through a tissue and hence there is no oxygen extraction. Since the blood within the CSH behaves as oxygenated blood there is no susceptibility induced signal loss on SWI imaging,

as noted in our series. Similar signal intensities are observed in the cavernous hemangioma elsewhere in the body, unless there are phleboliths or thrombosed areas^[9,13,14]. Hemorrhage has been reported in CSH^[18]. Concentric layers of hemosiderin are the hallmark of intra-axial lesions due to recurrent hemorrhages into the wall of the lesion causing slow growth. None of the cases in our series showed this finding. At least two thirds of cavernous hemangiomas exhibit some degree of vascular blush unlike the parenchymal cavernous angiomas which are occult to catheter angiography^[8,10,12]. Microscopically CSH consists of multiple vascular channels lined by a single layer of endothelium without muscular layer. In our series, vascular blush was noted from distal branches of middle meningeal artery and meningeal branches of internal carotid artery in 3 patients while one lesion was avascular on DSA as reported by Krief *et al*^[19]. Delayed SPECT imaging of the red blood pool scintigrams demonstrate increased activity persistently in contrast to the photopenic areas in meningioma, chordoma and chondrosarcoma^[18,19].

Sclerosing CSH is a less aggressive solid/semisolid entity in the spectrum of lesions of the cavernous sinus.

Aversa do Souto *et al*^[20] and Shi *et al*^[21] successfully operated a less aggressive CSH in the cavernous sinus by internal decompression without any life-threatening intraoperative bleeding similar to the case 10 in this series. Connective tissue proliferation between the vascular spaces evolves into a more densely packed solid or semisolid sclerosing Type-B CSH over a period of time. On imaging the subtype B of CSH is hyperintense on T2W and shows heterogeneous contrast enhancement while subtype-A is soft and pulsatile having thin walled blood spaces with a propensity to bleed profusely during surgery. Due to the abundant vascularization of these lesions, surgery is extremely complex and is associated with high morbidity such as cranial neuropathies^[20,22]. CSH respond to radiation unlike the extraaxial cavernous angiomas. Gamma Knife surgery is a safe and effective primary as well as adjuvant treatment modality for CSH^[23,24]. In one series the reported post-therapy shrinkage of CSH using gamaknife surgery was reported to be 84.6% at 12 mo follow-up^[25]. Two-year follow-up of four patients in this series after stereotactic radiotherapy were asymptomatic. The mean follow-up in our series was 2.5 years and all patients had no symptoms over the serial follow-up. However, there are limitations of this study, as this was a retrospective study of a relatively small sample size we could not estimate the inter observer variability.

MR imaging findings reported in this study are characteristic and diagnostic of CSH. T1-W hypointensity, homogeneous hyperintensity on T2-W sequences, intense enhancement following gadolinium injection and facilitated diffusion on DW imaging establish the diagnosis prior to surgery. Absence of hemosiderin within the lesion on GRE with facilitated diffusion significantly increases the diagnostic accuracy. With the characteristic and favourable MR imaging evidence followed by an open biopsy, attempt for radical excision is unwarranted since CSH responds well to stereotactic radiation.

COMMENTS

Background

Even though magnetic resonance imaging (MRI) is the modality of choice for characterising lesions at the cavernous sinus, the diagnosis of a cavernous hemangioma can still be in doubt, with the main differential diagnosis being a schwannoma of the V nerve or meningioma.

Research frontiers

The study aimed to elucidate the clinical, MRI, pathological features of these lesions and assess the incremental value of diffusion-weighted imaging (DWI) in diagnosing them.

Innovations and breakthroughs

This is one of the largest series of cavernous sinus hemangiomas that have clinical-radiological and pathological correlation as well as follow-up details. The study also highlights the incremental value of DWI imaging and the apparent diffusion coefficient value in these lesions which has not elucidated in the existing literature.

Applications

T1-weighted hypointensity with homogeneous hyperintensity on T2-weighted sequence, absence of hemosiderin within the lesion on GRE sequence and intense post contrast enhancement favour the diagnosis of cavernous sinus hemangioma (CSH). On DW imaging CSH shows facilitated diffusion and is nearly 100% specific for CSH. Markedly hypointense hemangioma on T1W images suggests schirrous nature of the lesion and are amenable to complete surgical excision.

Terminology

Cavernous hemangioma in the cavernous sinus has an estimated prevalence of 1% incidence. The lesion is rare in occurrence closely mimicking commonly encountered cavernous sinus lesions such as schwannoma, meningioma, chordoma, granuloma, carotid aneurysm and lympho-proliferative conditions. Microscopically cavernous sinus hemangioma (CSH) consist of multiple vascular channels lined by a single layer of endothelium without muscular layer without any intervening neural tissue. Diffusion weighted MR imaging measures the diffusivity of the water molecules in the tissue. Hindrance of water molecule movement gives a hyperintense signal on diffusion imaging interpreted as restricted diffusion and indicates high cellularity of the tissue. CSH shows facilitated diffusion on DWI.

Peer-review

Cavernous sinus hemangiomas (CSHs) is a benign vascular malformation which belong to Intracranial-extraaxial cavernous hemangiomas. Radiosurgery can effectively control the growth of smaller CSHs. Diagnosing CSH preoperatively is very important, but its radiological differential diagnosis is difficult. In this paper, the MRI sequence is abundant. Especially the number of DWI cases has a large proportion, which can provide valuable information for the diagnosis of CSH.

REFERENCES

- 1 Simard JM, Garcia-Bengochea F, Ballinger WE, Mickle JP, Quisling RG. Cavernous angioma: a review of 126 collected and 12 new clinical cases. *Neurosurgery* 1986; **18**: 162-172 [PMID: 3960293 DOI: 10.1227/00006123-198602000-00008]
- 2 Del Curling O, Kelly DL, Elster AD, Craven TE. An analysis of the natural history of cavernous angiomas. *J Neurosurg* 1991; **75**: 702-708 [PMID: 1919691 DOI: 10.3171/jns.1991.75.5.0702]
- 3 Razek AA, Castillo M. Imaging lesions of the cavernous sinus. *AJNR Am J Neuroradiol* 2009; **30**: 444-452 [PMID: 19095789 DOI: 10.3174/ajnr.A1398]
- 4 Yadav RR, Boruah DK, Yadav G, Pandey R, Phadke RV. Imaging characteristics of cavernous sinus cavernous hemangiomas. *Neuroradiol J* 2012; **25**: 515-524 [PMID: 24029085 DOI: 10.1177/197140091202500503]
- 5 Sohn CH, Kim SP, Kim IM, Lee JH, Lee HK. Characteristic MR imaging findings of cavernous hemangiomas in the cavernous sinus. *AJNR Am J Neuroradiol* 2003; **24**: 1148-1151 [PMID: 12812943]
- 6 Yao Z, Feng X, Chen X, Zee C. Magnetic resonance imaging characteristics with pathological correlation of cavernous malformation in cavernous sinus. *J Comput Assist Tomogr* 2006; **30**: 975-979 [PMID: 17082705 DOI: 10.1097/01.rct.0000221953.06135.3e]
- 7 Zhou LF, Mao Y, Chen L. Diagnosis and surgical treatment of cavernous sinus hemangiomas: an experience of 20 cases. *Surg Neurol* 2003; **60**: 31-36; discussion 36-37 [PMID: 12865008 DOI: 10.1016/S0090-3019(03)00190-3]
- 8 Linskey ME, Sekhar LN. Cavernous sinus hemangiomas: a series, a review, and an hypothesis. *Neurosurgery* 1992; **30**: 101-108 [PMID: 1738435 DOI: 10.1227/00006123-199201000-00018]
- 9 Gonzalez LF, Lekovic GP, Eschbacher J, Coons S, Porter RW, Spetzler RF. Are cavernous sinus hemangiomas and cavernous malformations different entities? *Neurosurg Focus* 2006; **21**: e6 [PMID: 16859259 DOI: 10.3171/foc.2006.21.1.7]
- 10 Rao VR, Pillai SM, Shenoy KT, Radhakrishnan VV, Mathews G. Hypervascular cavernous angioma at angiography. *Neuroradiology* 1979; **18**: 211-214 [PMID: 530433 DOI: 10.1007/BF00345728]
- 11 Numaguchi Y, Kishikawa T, Fukui M, Sawada K, Kitamura K,

- Matsuura K, Russell WJ. Prolonged injection angiography for diagnosing intracranial cavernous hemangiomas. *Radiology* 1979; **131**: 137-138 [PMID: 424574 DOI: 10.1148/131.1.137]
- 12 **McEvoy SH**, Farrell M, Brett F, Looby S. Haemangioma, an uncommon cause of an extradural or intradural extramedullary mass: case series with radiological pathological correlation. *Insights Imaging* 2016; **7**: 87-98 [PMID: 26385689 DOI: 10.1007/s13244-015-0432-y]
- 13 **Jinhu Y**, Jianping D, Xin L, Yuanli Z. Dynamic enhancement features of cavernous sinus cavernous hemangiomas on conventional contrast-enhanced MR imaging. *AJNR Am J Neuroradiol* 2008; **29**: 577-581 [PMID: 18065511 DOI: 10.3174/ajnr.A0845]
- 14 **Korchi AM**, Cuvinciuc V, Caetano J, Becker M, Lovblad KO, Vargas MI. Imaging of the cavernous sinus lesions. *Diagn Interv Imaging* 2014; **95**: 849-859 [PMID: 23763988 DOI: 10.1016/j.diii.2013.04.013]
- 15 **Ginat DT**, Mangla R, Yeane G, Ekholm S. Diffusion-weighted imaging of skull lesions. *J Neurol Surg B Skull Base* 2014; **75**: 204-213 [PMID: 25072014 DOI: 10.1055/s-0034-1371362]
- 16 **Bansal S**, Suri A, Singh M, Kale SS, Agarwal D, Sharma MS, Mahapatra AK, Sharma BS. Cavernous sinus hemangioma: a fourteen year single institution experience. *J Clin Neurosci* 2014; **21**: 968-974 [PMID: 24524951 DOI: 10.1016/j.jocn.2013.09.008]
- 17 **Mathur A**, Jain N, Kesavadas C, Thomas B, Kapilamoorthy TR. Imaging of skull base pathologies: Role of advanced magnetic resonance imaging techniques. *Neuroradiol J* 2015; **28**: 426-437 [PMID: 26427895 DOI: 10.1177/1971400915609341]
- 18 **Salanitri GC**, Stuckey SL, Murphy M. Extracerebral cavernous hemangioma of the cavernous sinus: diagnosis with MR imaging and labeled red cell blood pool scintigraphy. *AJNR Am J Neuroradiol* 2004; **25**: 280-284 [PMID: 14970031]
- 19 **Krief O**, Sichez JP, Chedid G, Bencherif B, Zouaoui A, Le Bras F, Marsault C. Extraaxial cavernous hemangioma with hemorrhage. *AJNR Am J Neuroradiol* 1991; **12**: 988-990 [PMID: 1950936]
- 20 **Aversa do Souto A**, Marcondes J, Reis da Silva M, Chimelli L. Sclerosing Cavernous Hemangioma in the Cavernous Sinus: Case Report. *Skull Base* 2003; **13**: 93-99 [PMID: 15912165 DOI: 10.1055/s-2003-820564]
- 21 **Shi J**, Hang C, Pan Y, Liu C, Zhang Z. Cavernous hemangiomas in the cavernous sinus. *Neurosurgery* 1999; **45**: 1308-1313; discussion 1308-1313 [PMID: 10598697 DOI: 10.1097/00006123-199912000-00006]
- 22 **Anqi X**, Zhang S, Jiahe X, Chao Y. Cavernous sinus cavernous hemangioma: imaging features and therapeutic effect of Gamma Knife radiosurgery. *Clin Neurol Neurosurg* 2014; **127**: 59-64 [PMID: 25459244 DOI: 10.1016/j.clineuro.2014.09.025]
- 23 **Tang X**, Wu H, Wang B, Zhang N, Dong Y, Ding J, Dai J, Yu T, Pan L. A new classification and clinical results of Gamma Knife radiosurgery for cavernous sinus hemangiomas: a report of 53 cases. *Acta Neurochir (Wien)* 2015; **157**: 961-969; discussion 969 [PMID: 25862173 DOI: 10.1007/s00701-015-2417-5]
- 24 **Wang Y**, Li P, Zhang XJ, Xu YY, Wang W. Gamma Knife Surgery for Cavernous Sinus Hemangioma: A Report of 32 Cases. *World Neurosurg* 2016; **94**: 18-25 [PMID: 27373416 DOI: 10.1016/j.wneu.2016.06.094]
- 25 **Park CK**, Choi SK, Kang IH, Choi MK, Park BJ, Lim YJ. Radiosurgical considerations for cavernous sinus hemangioma: long-term clinical outcomes. *Acta Neurochir (Wien)* 2016; **158**: 313-318 [PMID: 26658989 DOI: 10.1007/s00701-015-2657-4]

P- Reviewer: Chowdhury FH, Xie Q **S- Editor:** Song XX
L- Editor: A **E- Editor:** Lu YJ



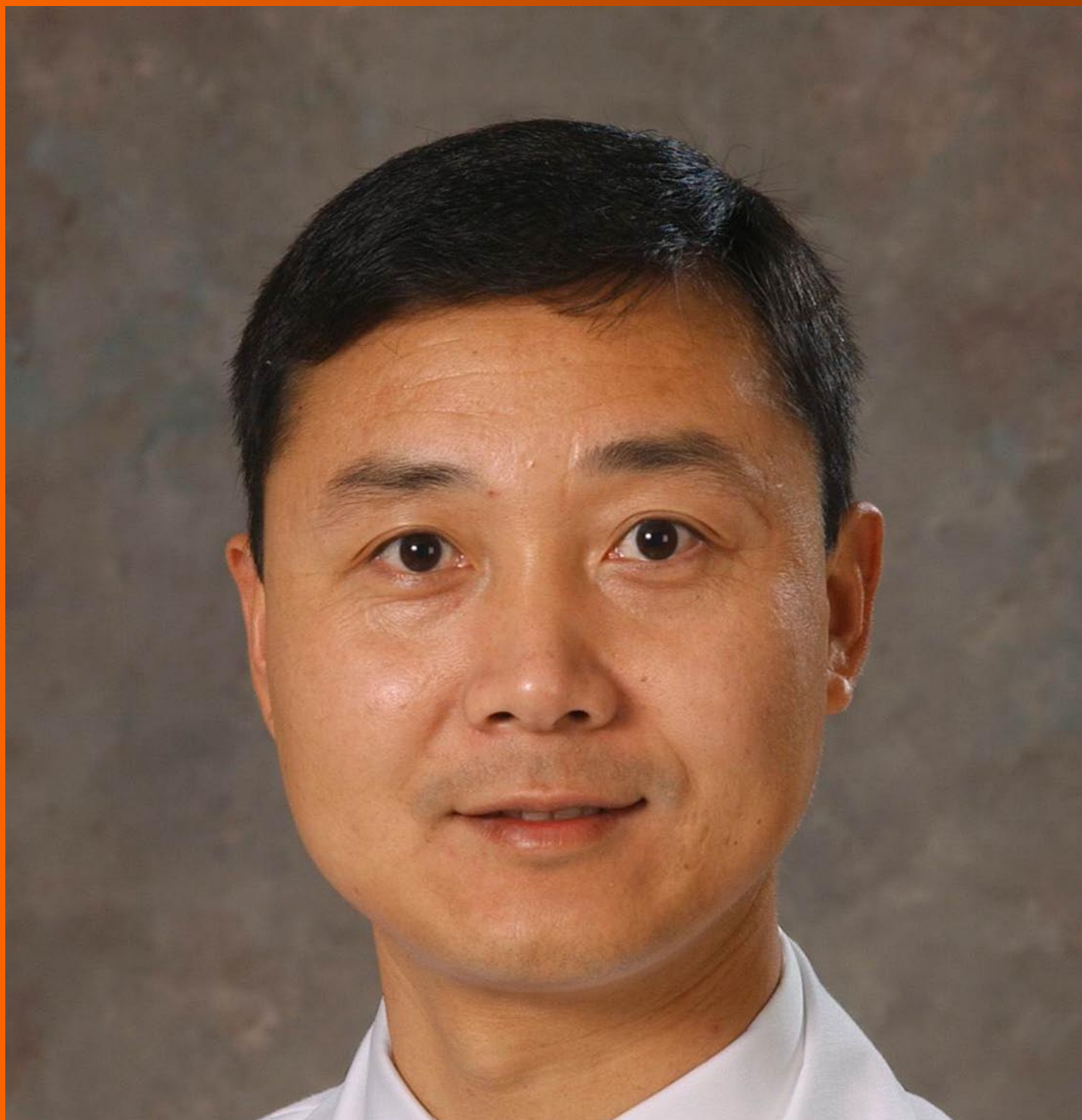


Published by **Baishideng Publishing Group Inc**
7901 Stoneridge Drive, Suite 501, Pleasanton, CA 94588, USA
Telephone: +1-925-223-8242
Fax: +1-925-223-8243
E-mail: bpgoffice@wjgnet.com
Help Desk: <http://www.f6publishing.com/helpdesk>
<http://www.wjgnet.com>



World Journal of *Radiology*

World J Radiol 2017 September 28; 9(9): 339-370





Editorial Board

2014-2017

The *World Journal of Radiology* Editorial Board consists of 365 members, representing a team of worldwide experts in radiology. They are from 36 countries, including Afghanistan (1), Argentina (2), Australia (5), Austria (7), Belgium (2), Brazil (8), Canada (6), Chile (1), China (43), Croatia (1), Denmark (4), Egypt (6), France (5), Germany (22), Greece (10), India (12), Iran (6), Ireland (2), Israel (3), Italy (47), Japan (13), Netherlands (1), New Zealand (1), Pakistan (1), Poland (2), Portugal (1), Serbia (1), Singapore (3), Slovakia (1), South Korea (18), Spain (4), Sweden (2), Switzerland (4), Thailand (1), Turkey (26), United Kingdom (11), and United States (82).

EDITORS-IN-CHIEF

Kai U Juergens, *Bremen*
Edwin JR van Beek, *Edinburgh*
Thomas J Vogl, *Frankfurt*

GUEST EDITORIAL BOARD MEMBERS

Wing P Chan, *Taipei*
Chung-Huei Hsu, *Taipei*
Chin-Chang Huang, *Taipei*
Tsong-Long Hwang, *Taoyuan*
Jung-Lung Hsu, *Taipei*
Chia-Hung Kao, *Taichung*
Yu-Ting Kuo, *Tainan*
Hon-Man Liu, *Taipei*
Hui-Lung Liang, *Kaohsiung*
Chun Chung Lui, *Kaohsiung*
Sen-Wen Teng, *Taipei*
Yung-Liang (William) Wan, *Taoyuan*

MEMBERS OF THE EDITORIAL BOARD



Afghanistan

Takao Hiraki, *Okayama*



Argentina

Patricia Carrascosa, *Vicente Lopez*
Maria C Ziadi, *Rosario*



Australia

Lourens Bester, *Sydney*
Gemma A Figtree, *Sydney*



Austria

Herwig R Cerwenka, *Graz*
Gudrun M Feuchtnner, *Innsbruck*
Benjamin Henninger, *Innsbruck*
Rupert Lanzenberger, *Vienna*
Shu-Ren Li, *Vienna*
Veronika Schopf, *Vienna*
Tobias De Zordo, *Innsbruck*



Belgium

Steve Majerus, *Liege*
Kathelijne Peremans, *Merelbeke*



Brazil

Clerio F Azevedo, *Rio de Janeiro*
Patrícia P Alfredo, *São Paulo*
Eduardo FC Fleury, *São Paulo*
Edward Araujo Júnior, *São Paulo*
Wellington P Martins, *Ribeirao Preto*
Ricardo A Mesquita, *Belo Horizonte*
Vera MC Salemi, *São Paulo*
Claudia Szobot, *Porto Alegre*
Lilian YI Yamaga, *São Paulo*



Canada

Marie Arsalidou, *Toronto*
Otman A Basir, *Waterloo*

Tarik Zine Belhocine, *Toronto*
James Chow, *Toronto*
Tae K Kim, *Toronto*
Anastasia Oikonomou, *Toronto*



China

Hong-Wei Chen, *Wuxi*
Feng Chen, *Hangzhou*
Jian-Ping Chu, *Guangzhou*
Guo-Guang Fan, *Shenyang*
Bu-Lang Gao, *Shijiazhuang*
Qi-Yong Gong, *Chengdu*
Ying Han, *Beijing*
Xian-Li Lv, *Beijing*
Yi-Zhuo Li, *Guangzhou*
Xiang-Xi Meng, *Harbin*
Yun Peng, *Beijing*
Jun Shen, *Guangzhou*
Ze-Zhou Song, *Hangzhou*
Wai Kwong Tang, *Hong Kong*
Gang-Hua Tang, *Guangzhou*
Jie Tian, *Beijing*
Lu-Hua Wang, *Beijing*
Xiao-bing Wang, *Xi'an*
Yi-Gen Wu, *Nanjing*
Kai Wu, *Guangzhou*
Hui-Xiong Xu, *Shanghai*
Zuo-Zhang Yang, *Kunming*
Xiao-Dan Ye, *Shanghai*
David T Yew, *Hong Kong*
Ting-He Yu, *Chongqing*
Zheng Yuan, *Shanghai*
Min-Ming Zhang, *Hangzhou*
Yudong Zhang, *Nanjing*
Dong Zhang, *Chongqing*
Wen-Bin Zeng, *Changsha*

Yue-Qi Zhu, *Shanghai*



Croatia

Goran Kusec, *Osijek*



Denmark

Poul E Andersen, *Odense*

Lars J Petersen, *Aalborg*

Thomas Z Ramsøy, *Frederiksberg*

Morten Ziebell, *Copenhagen*



Egypt

Mohamed F Bazeed, *Mansoura*

Mohamed Abou El-Ghar, *Mansoura*

Reem HA Mohamed, *Cairo*

Mohamed R Nouh, *Alexandria*

Ahmed AKA Razek, *Mansoura*

Ashraf A Zytoon, *Shebin El-Koom*



France

Sabine F Bensamoun, *Compiègne*

Romarc Loffroy, *Dijon*

Stephanie Nougaret, *Montpellier*

Hassane Oudadesse, *Rennes*

Vincent Vinh-Hung, *Fort-de-France*



Germany

Henryk Barthel, *Leipzig*

Peter Bannas, *Hamburg*

Martin Beeres, *Frankfurt*

Ilja F Ciernik, *Dessau*

A Dimitrakopoulou-Strauss, *Heidelberg*

Peter A Fasching, *Erlangen*

Andreas G Schreyer, *Regensburg*

Philipp Heusch, *Duesseldorf*

Sonja M Kirchhoff, *Munich*

Sebastian Ley, *Munich*

Adel Maataoui, *Frankfurt am Main*

Stephan M Meckel, *Freiburg*

Hans W Muller, *Duesseldorf*

Kay Raum, *Berlin*

Dirk Rades, *Luebeck*

Marc-Ulrich Regier, *Hamburg*

Alexey Surov, *Halle*

Martin Walter, *Magdeburg*

Axel Wetter, *Essen*

Christoph Zilkens, *Düsseldorf*



Greece

Panagiotis Antoniou, *Thessaloniki*

Nikos Efthimiou, *Athens*

Dimitris Karnabatidis, *Patras*

George Latsios, *Athens*

Stylianios Megremis, *Iraklion*

Alexander D Rapidis, *Athens*

Kiki Theodorou, *Larissa*

Ioannis A Tsalafoutas, *Athens*

Evanthia E Tripoliti, *Ioannina*

Athina C Tsili, *Ioannina*



India

Ritesh Agarwal, *Chandigarh*

Chandan J Das, *New Delhi*

Prathamesh V Joshi, *Mumbai*

Naveen Kalra, *Chandigarh*

Chandrasekharan Kesavadas, *Trivandrum*

Jyoti Kumar, *New Delhi*

Atin Kumar, *New Delhi*

Kaushala P Mishra, *Allahabad*

Daya N Sharma, *New Delhi*

Binit Sureka, *New Delhi*

Sanjay Sharma, *New Delhi*

Raja R Yadav, *Allahabad*



Iran

Majid Assadi, *Bushehr*

SeyedReza Najafizadeh, *Tehran*

Mohammad Ali Oghabian, *Tehran*

Amir Reza Radmard, *Tehran*

Ramin Sadeghi, *Mashhad*

Hadi Rokni Yazdi, *Tehran*



Ireland

Tadhg Gleeson, *Wexford*

Frederik JAI Vernimmen, *Cork*



Israel

Dafna Ben Bashat, *Tel Aviv*

Amit Gefen, *Tel Aviv*

Tamar Sella, *Jerusalem*



Italy

Adriano Alippi, *Rome*

Dante Amelio, *Trento*

Michele Anzidei, *Rome*

Filippo F Angileri, *Messinas*

Stefano Arcangeli, *Rome*

Roberto Azzoni, *San Donato milanese*

Tommaso V Bartolotta, *Palermo*

Tommaso Bartalena, *Imola*

Livia Bernardin, *San Bonifacio*

Federico Boschi, *Verona*

Sergio Casciaro, *Lecce*

Emanuele Casciani, *Rome*

Musa M Can, *Napoli*

Alberto Cuocolo, *Napoli*

Michele Ferrara, *Coppito*

Mauro Feola, *Fossano*

Giampiero Francica, *Castel Volturno*

Luigi De Gennaro, *Rome*

Giulio Giovannetti, *Pisa*

Francesca Iacobellis, *Napoli*

Formato Invernizzi, *Monza Brianza*

Francesco Lassandro, *Naples*

Lorenzo Livi, *Florence*

Pier P Mainenti, *Napoli*

Laura Marzetti, *Chieti*

Giuseppe Malinverni, *Crescentino*

Enrica Milanese, *Turin*

Giovanni Morana, *Treviso*

Lorenzo Monti, *Milan*

Silvia D Morbelli, *Genoa*

Barbara Palumbo, *Perugia*

Cecilia Parazzini, *Milan*

Stefano Pergolizzi, *Messina*

Antonio Pinto, *Naples*

Camillo Porcaro, *Rome*

Carlo C Quattrocchi, *Rome*

Alberto Rebonato, *Perugia*

Giuseppe Rizzo, *Rome*

Roberto De Rosa, *Naples*

Domenico Rubello, *Rovigo*

Andrea Salvati, *Bari*

Sergio Sartori, *Ferrara*

Luca M Sconfienza, *Milano*

Giovanni Storto, *Rionero*

Nicola Sverzellati, *Parma*

Alberto S Tagliafico, *Genova*

Nicola Troisi, *Florence*



Japan

Yasuhiko Hori, *Chiba*

Hidetoshi Ikeda, *Koriyama*

Masahito Kawabori, *Sapporo*

Tamotsu Kamishima, *Sapporo*

Hiro Kiyosue, *Yufu*

Yasunori Minami, *Osaka-sayama*

Yasuhiro Morimoto, *Kitakyushu*

Satoru Murata, *Tokyo*

Shigeki Nagamachi, *Miyazaki*

Hiroshi Onishi, *Yamanashi*

Morio Sato, *Wakayama Shi*

Yoshito Tsushima, *Maebashi*

Masahiro Yanagawa, *Suita*



Netherlands

Willem Jan van Rooij, *Tilburg*



New Zealand

W Howell Round, *Hamilton*



Pakistan

Wazir Muhammad, *Abbottabad*



Poland

Maciej S Baglaj, *Wroclaw*

Piotr Czauderna, *Gdansk*



Portugal

Joao Manuel RS Tavares, *Porto*



Serbia

Olivera Ciraj-Bjelac, *Belgrade*



Singapore

Gopinathan Anil, *Singapore*

Terence KB Teo, *Singapore*

Cher Heng Tan, *Singapore*



Slovakia

Stefan Sivak, *Martin*



South Korea

Ki Seok Choo, *Busan*

Seung Hong Choi, *Seoul*

Dae-Seob Choi, *Jinju*

Hong-Seok Jang, *Seoul*

Yong Jeong, *Daejeon*

Chan Kyo Kim, *Seoul*

Se Hyung Kim, *Seoul*

Joong-Seok Kim, *Seoul*

Sang Eun Kim, *Seongnam*

Sung Joon Kwon, *Seoul*

Jeong Min Lee, *Seoul*

In Sook Lee, *Busan*

Noh Park, *Goyang*

Chang Min Park, *Seoul*

Sung Bin Park, *Seoul*

Deuk Jae Sung, *Seoul*

Choongsoo Shin, *Seoul*

Kwon-Ha Yoon, *Iksan*



Spain

Miguel A De Gregorio, *Zaragoza*

Antonio Luna, *Jaén*

Enrique Marco de Lucas, *Santander*

Fernando Ruiz Santiago, *Granada*



Sweden

Dmitry Grishenkov, *Stockholm*

Tie-Qiang Li, *Stockholm*



Switzerland

Nicolau Beckmann, *Basel*

Christian Boy, *Bern*

Giorgio Treglia, *Bellinzona*

Stephan Ulmer, *Kiel*



Thailand

Sirianong Namwongprom, *Chiang Mai*



Turkey

Kubilay Aydin, *Istanbul*

Ramazan Akdemir, *Sakarya*

Serhat Avcu, *Ankara*

Ayşe Aralasmak, *Istanbul*

Oktay Algin, *Ankara*

Nevbahar Akcar, *Meselik*

Bilal Battal, *Ankara*

Zulkif Bozgeyik, *Elazig*

Nazan Ciledag, *Aakara*

Fuldem Y Donmez, *Ankara*

Gulgun Engin, *Istanbul*

Ahmet Y Goktay, *Izmir*

Oguzhan G Gumustas, *Bursa*

Kaan Gunduz, *Ankara*

Pelin Ozcan Kara, *Mersin*

Kivanc Kamburoglu, *Ankara*

Ozgur Kilickesmez, *Istanbul*

Furuzan Numan, *Istanbul*

Cem Onal, *Adana*

Ozgur Oztekin, *Izmir*

Seda Ozbek (Boruban), *Konya*

Selda Sarikaya, *Zonguldak*

Figen Taser, *Kutahya*

Baran Tokar, *Eskisehir*

Ender Uysal, *Istanbul*

Ensar Yekeler, *Istanbul*



United Kingdom

Indran Davagnanam, *London*

M DC Valdés Hernández, *Edinburgh*

Alan Jackson, *Manchester*

Suneil Jain, *Belfast*

Long R Jiao, *London*

Miltiadis Krokidis, *Cambridge*

Pradesh Kumar, *Liverpool*

Peter D Kuzmich, *Derby*

Georgios Plataniotis, *Brighton*

Vanessa Sluming, *Liverpool*



United States

Garima Agrawal, *Saint Louis*

James R Brasic, *Baltimore*

Rajendra D Badgaiyan, *Buffalo*

Ulas Bagci, *Bethesda*

Anat Biegon, *Stony Brook*

Ramon Casanova, *Winston Salem*

Wenli Cai, *Boston*

Zheng Chang, *Durham*

Corey J Chakarun, *Long Beach*

Kai Chen, *Los Angeles*

Hyun-Soon Chong, *Chicago*

Marco Cura, *Dallas*

Ravi R Desai, *Bensalem*

Delia DeBuc, *Miami*

Carlo N De Cecco, *Charleston*

Timm-Michael L Dickfeld, *Baltimore*

Subba R Digumarthy, *Boston*

Huy M Do, *Stanford*

Todd A Faasse, *Grand Rapids*

Salomao Faintuch, *Boston*

Girish M Fatterpekar, *New York*

Dhakshinamoorthy Ganesan, *Houston*

Robert J Griffin, *Little Rock*

Andrew J Gunn, *Boston*

Sandeep S Hedgire, *Boston*

Timothy J Hoffman, *Columbia*

Mai-Lan Ho, *San Francisco*

Juebin Huang, *Jackson*

Abid Irshad, *Charleston*

Matilde Inglese, *New York*

El-Sayed H Ibrahim, *Jacksonville*

Paul R Julsrud, *Rochester*

Pamela T Johnson, *Baltimore*

Ming-Hung Kao, *Tempe*

Sunil Krishnan, *Houston*

Richard A Komoroski, *Cincinnati*

Sandi A Kwee, *Honolulu*

King Kim, *Ft. Lauderdale*

Guozheng Liu, *Worcester*

Yiyan Liu, *Newark*

Venkatesh Mani, *New York*

Lian-Sheng Ma, *Pleasanton*

Rachna Madan, *Boston*

Zeyad A Metwalli, *Houston*

Yilong Ma, *Manhasset*

Hui Mao, *Atlanta*

Feroze B Mohamed, *Philadelphia*

Gul Moonis, *Boston*

John L Noshier, *New Brunswick*

Rahmi Oklu, *Boston*

Aytekun Oto, *Chicago*

Bishnuhari Paudyal, *Philadelphia*

Rajul Pandya, *Youngstown*

Chong-Xian Pan, *Sacramento*

Jay J Pillai, *Baltimore*

Neal Prakash, *Duarte*

Reza Rahbar, *Boston*

Ali S Raja, *Boston*

Gustavo J Rodriguez, *El Paso*

David J Sahn, *Portland*

Steven Schild, *Scottsdale*

Ali R Sepahdari, *Los Angeles*

Li Shen, *Indianapolis*

JP Sheehan, *Charlottesville*

Atul B Shinagare, *Boston*

Sarabjeet Singh, *Boston*

Charles J Smith, *Columbia*

Kenji Suzuki, *Chicago*

Monvadi Srichai-Parsia, *Washington*

Sree H Tirumani, *Boston*

Hebert A Vargas, *New York*

Sachit Verma, *Philadelphia*

Yoichi Watanabe, *Minneapolis*

Li Wang, *Chapel Hill*

Carol C Wu, *Boston*

Shoujun Xu, *Houston*

Min Yao, *Cleveland*

Xiaofeng Yang, *Atlanta*

Qingbao Yu, *Albuquerque*

Aifeng Zhang, *Chicago*

Chao Zhou, *Bethlehem*

Hongming Zhuang, *Philadelphia*

**MINIREVIEWS**

- 339 Radiographic and magnetic resonances contrast agents: Essentials and tips for safe practices

Nouh MR, El-Shazly MA

ORIGINAL ARTICLE**Retrospective Cohort Study**

- 350 Clinical significance of prostate ¹⁸F-labelled fluorodeoxyglucose uptake on positron emission tomography/computed tomography: A five-year review

Chetan MR, Barrett T, Gallagher FA

Retrospective Study

- 359 Reliability of the pronator quadratus fat pad sign to predict the severity of distal radius fractures

Loesaus J, Wobbe I, Stahlberg E, Barkhausen J, Goltz JP

CASE REPORT

- 365 Imatinib response of gastrointestinal stromal tumor patients with germline mutation on *KIT* exon 13: A family report

Engin G, Eraslan S, Kayserili H, Kapran Y, Akman H, Akyuz A, Aykan NF

ABOUT COVER

Editorial Board Member of *World Journal of Radiology*, XW Cui, PhD, Professor, Department of Medical Ultrasound, Tongji Hospital of Tongji Medical College, Huazhong University of Science and Technology, Wuhan 430030, Hubei Province, China

AIM AND SCOPE

World Journal of Radiology (*World J Radiol*, *WJR*, online ISSN 1949-8470, DOI: 10.4329) is a peer-reviewed open access academic journal that aims to guide clinical practice and improve diagnostic and therapeutic skills of clinicians.

WJR covers topics concerning diagnostic radiology, radiation oncology, radiologic physics, neuroradiology, nuclear radiology, pediatric radiology, vascular/interventional radiology, medical imaging achieved by various modalities and related methods analysis. The current columns of *WJR* include editorial, frontier, diagnostic advances, therapeutics advances, field of vision, mini-reviews, review, topic highlight, medical ethics, original articles, case report, clinical case conference (clinicopathological conference), and autobiography.

We encourage authors to submit their manuscripts to *WJR*. We will give priority to manuscripts that are supported by major national and international foundations and those that are of great basic and clinical significance.

INDEXING/ABSTRACTING

World Journal of Radiology is now indexed in PubMed, PubMed Central, and Emerging Sources Citation Index (Web of Science).

FLYLEAF

I-III Editorial Board

EDITORS FOR THIS ISSUE

Responsible Assistant Editor: Xiang Li
Responsible Electronic Editor: Li-Min Zhao
Proofing Editor-in-Chief: Lian-Sheng Ma

Responsible Science Editor: Jin-Xin Kong
Proofing Editorial Office Director: Jin-Lei Wang

NAME OF JOURNAL
World Journal of Radiology

ISSN
ISSN 1949-8470 (online)

LAUNCH DATE
January 31, 2009

FREQUENCY
Monthly

EDITORS-IN-CHIEF
Kai U Juergens, MD, Associate Professor, MRT und PET/CT, Nuklearmedizin Bremen Mitte, ZEMODI - Zentrum für morphologische und molekulare Diagnostik, Bremen 28177, Germany

Edwin JR van Beek, MD, PhD, Professor, Clinical Research Imaging Centre and Department of Medical Radiology, University of Edinburgh, Edinburgh EH16 4TJ, United Kingdom

Thomas J Vogl, MD, Professor, Reader in Health Technology Assessment, Department of Diagnostic and Interventional Radiology, Johann Wolfgang Goethe University of Frankfurt, Frankfurt 60590,

Germany

EDITORIAL BOARD MEMBERS
All editorial board members resources online at <http://www.wjgnet.com/1949-8470/editorialboard.htm>

EDITORIAL OFFICE
Xiu-Xia Song, Director
World Journal of Radiology
Baishideng Publishing Group Inc
7901 Stoneridge Drive, Suite 501, Pleasanton, CA 94588, USA
Telephone: +1-925-2238242
Fax: +1-925-2238243
E-mail: editorialoffice@wjgnet.com
Help Desk: <http://www.f6publishing.com/helpdesk>
<http://www.wjgnet.com>

PUBLISHER
Baishideng Publishing Group Inc
7901 Stoneridge Drive, Suite 501, Pleasanton, CA 94588, USA
Telephone: +1-925-2238242
Fax: +1-925-2238243
E-mail: bpgoffice@wjgnet.com
Help Desk: <http://www.f6publishing.com/helpdesk>
<http://www.wjgnet.com>

PUBLICATION DATE
September 28, 2017

COPYRIGHT
© 2017 Baishideng Publishing Group Inc. Articles published by this Open-Access journal are distributed under the terms of the Creative Commons Attribution Non-commercial License, which permits use, distribution, and reproduction in any medium, provided the original work is properly cited, the use is non commercial and is otherwise in compliance with the license.

SPECIAL STATEMENT
All articles published in journals owned by the Baishideng Publishing Group (BPG) represent the views and opinions of their authors, and not the views, opinions or policies of the BPG, except where otherwise explicitly indicated.

INSTRUCTIONS TO AUTHORS
<http://www.wjgnet.com/bpg/gerinfo/204>

ONLINE SUBMISSION
<http://www.f6publishing.com>

Radiographic and magnetic resonances contrast agents: Essentials and tips for safe practices

Mohamed R Nouh, Mohamed A El-Shazly

Mohamed R Nouh, Mohamed A El-Shazly, Department of Radiology and Clinical Imaging, Faculty of Medicine, Alexandria University, Alexandria 21563, Egypt

Author contributions: Nouh MR and El-Shazly MA had been having the idea of the manuscript; both authors had been equally reviewed the literature, drafted the manuscript and critically revised it; both authors approved the manuscript in its current final form.

Conflict-of-interest statement: The authors declare no conflict of interest.

Open-Access: This article is an open-access article which was selected by an in-house editor and fully peer-reviewed by external reviewers. It is distributed in accordance with the Creative Commons Attribution Non Commercial (CC BY-NC 4.0) license, which permits others to distribute, remix, adapt, build upon this work non-commercially, and license their derivative works on different terms, provided the original work is properly cited and the use is non-commercial. See: <http://creativecommons.org/licenses/by-nc/4.0/>

Manuscript source: Invited manuscript

Correspondence to: Mohamed R Nouh, MD, Assistant Professor, Department of Radiology and Clinical Imaging, Faculty of Medicine, Alexandria University, 1 Kolyat El-Teb Street, Mahata El-Ramel, Alexandria 21563, Egypt. mohamed.nouh@alexmed.edu.eg
Telephone: +20-11-16590365
Fax: +20-3-4869754

Received: January 24, 2017
Peer-review started: February 2, 2017
First decision: May 11, 2017
Revised: June 14, 2017
Accepted: June 19, 2017
Article in press: June 20, 2017
Published online: September 28, 2017

Abstract

With extended and continued expansion of medical

imaging utilization in modern medical practice over last decade, radiologists as well as other faculty staff dealing with radiographic and magnetic resonances contrast media (CM) have to be well oriented with their potential hypersensitivity reactions and recognize high-risk groups liable to develop it so as to enable early recognition. Radiologists and other medical staff involved in administration and dealing with CM have to be ready to implement prompt, practical and effective management plan to deal with these scenarios should they emerge. Strategies to prevent potential contrast-induced acute and delayed renal injuries have to be routinely exercised. Paying attention to the pregnant and nursing women, pediatrics, diabetics, as well as other fragile populations is of utmost importance for patient safety during contrast administrations. Radiologists should play a pivotal role in orienting patients about necessity to use CM for their imaging studies, in case it is needed, and assure them about its safety. Moreover, they have to be oriented with the medico-legal issues related to use of CM. These will pay as improved patient safety as well as safe daily working environment at different levels of radiology practices.

Key words: Radiographic; Magnetic resonances; Contrast; Safe practice; Medico-legal

© **The Author(s) 2017.** Published by Baishideng Publishing Group Inc. All rights reserved.

Core tip: Radiologists have to be oriented with the potential hypersensitivity reactions of radiographic and magnetic resonances contrast media (CM) and able to recognize high-risk groups liable to develop such reactions. Effective management plans have to be ready to implement should these scenarios emerge. Strategies to prevent potential contrast-induced acute and delayed renal injuries have to be exercised. Caring for special considerations as well as other fragile populations is of utmost importance for patients' safety. Moreover, radiologists should be oriented with

the medico-legal issues related to use of CM. These will be conveyed as improved patients' safety and safe radiology practices.

Nouh MR, El-Shazly MA. Radiographic and magnetic resonances contrast agents: Essentials and tips for safe practices. *World J Radiol* 2017; 9(9): 339-349 Available from: URL: <http://www.wjgnet.com/1949-8470/full/v9/i9/339.htm> DOI: <http://dx.doi.org/10.4329/wjcr.v9.i9.339>

INTRODUCTION

Advances in the field of medical imaging over last decade, notably for multi-detector computed tomography (MDCT) and magnetic resonances imaging (MRI) have been associated with increased use of contrast media (CM). Likewise, the extended spectrum of therapeutic/interventional procedures in different body organs, using imaging guidance tools, has expanded the use of CM.

Although CM are generally safe, their allergy-like reactions may be mild needing just observation and patient reassurance or may rarely result in potential life threatening conditions. These situations impose a day to day challenge for radiologists and allied medical staff at different levels of radiology practices. Hence, radiologists and medical personnel involved in CM administration have to be oriented to the justifications for their use and stratification of risk factors that increase the likelihood of patients to develop adverse reactions to CM. Moreover, they have to be able to recognize these adverse reactions once they show up and promptly as well as effectively deal with it for patient safety. Besides, radiology practice personnel have to familiarize themselves to the medico-legal caveats associated with their practices. They should develop their own protocols for safe practice should CM administration be required. This review aims to highlight an updated discussion about these aforementioned hot issues related to use of CM in our daily work.

CM: ESSENTIAL KNOWLEDGE

CM are pharmaceutical formulas that have been used to supplement the capabilities of various medical imaging modalities. They can be administered *via* different routes; the most widely used, and subject of the current review, is the intravenous access.

Describing the different types, classifications, uses and route of administrations is beyond the scope of this review. However, a summary of the essential knowledge, for every radiologist, about current available CM will be underscored briefly in the next paragraphs.

Based on the differential attenuation of iodine by ionizing radiation, iodine-based contrast agents are

used for contrast-enhanced radiographic and MDCT procedures^[1]. Physico-chemically; iodine-based contrast agents may be grouped according to their: (1) ionicity (to ionic or nonionic CM); (2) osmolality into high osmolar CM (HOCM), low-osmolar (LOCM), or iso-osmolar (IOCM); and (3) the number of benzene rings (either monomeric or dimeric CM)^[2]. Owing to the contemporary implementation of non-ionic IOCM and LOCM in clinical imaging practices worldwide with withdrawal of HOCM, our discussion on iodinated CM will focus onto the non-ionic (iso- and low-osmolar) CM.

On the other hand, gadolinium-based contrast agents (GBCAs) are used to enhance MR examinations, thanks to their ability to alter the relaxivity of infused tissues; largely^[3]. However, they can provide physiologic data derived from proton density and flow within the induced field depending of the weighting of the image^[4].

Likewise, GBCAs are commonly grouped according to their: (1) pharmacokinetics (either extracellular or organ specific and the extracellular GBCAs may be further sub-classified into blood-pool agents and; interstitial extra-cellular agents); (2) the chelating ligand molecular design (either; macrocyclic or linear); and (3) their ionicity (ionic or nonionic)^[2].

EPIDEMIOLOGY OF CM REACTIONS

In general, CM (both iodinated and gadolinium based) are safe drugs with very low incidence of adverse reactions^[5]. Hypersensitivity reactions to CM are generally sporadic and unpredictable^[2,5-7]. The incidences of mild to moderate CM reactions are commoner for iodinated CM than gadolinium-based chelates^[2,6,7]. Moreover, the hypersensitivity to non-ionic iodinated CM is far rare compared to their ionic correspondents^[2,5,6] (Table 1). highlights the salient predisposing risk factors and populations at risk for development of acute adverse reaction to CM. Age extremes populations are at high risk for developing mild to moderate hypersensitivity reactions to CM^[8,9]. The incidence of severe sensitivity reaction doesn't differ between different CM agents including the gadolinium chelates^[10,11].

An overall major determinant of patient's intolerance to CM administration is a history of a previous severe reaction to a contrast agent^[8,9]. This increases the likelihood of the patient to develop a life-threatening hypersensitivity reaction by 3-6 fold^[2]. Other major determinants are active generalized allergic tendencies (*e.g.*, asthma, hay fever, *etc.*) and compromised renal functions^[5,10,12]. However, controlled atopies; including asthma don't preclude patients to have intravenous CM when necessary^[12].

Recognizing these factors could be achieved *via* scrutinizing patient's history cautiously. Thomsen^[2] proposed a simplified questionnaire to simply identify high-risk patients liable to suffer CM-induced renal complications by asking the patient seven critical

Table 1 Risk factors that predispose patients to contrast medium reactions

Patients with a prior history of allergy to CM (3-6 folds)
Patients with a prior history of allergic reactions to drugs and foods
Patients with generalized atopic tendencies (<i>e.g.</i> , asthma and hay fever)
Dehydration states
Age extremes (less than 5 yr and older than 60 yr)
Serious illness and chronic debilitating conditions, <i>e.g.</i> , CVS diseases and renal failure
Anemia
Certain co-medications, <i>e.g.</i> , β -blockers and metformin
Malignancies
Patient's anxiety due to public concerns about CM-induced reaction

CM: Contrast media; CVS: Cardiovascular.

Table 2 Co-morbidities indicating renal profile checkup prior to contrast agent administration

Age extremes	Older than 60 yr and less than 5 yr
History of relevant renal disorders	Anatomic variations: Solitary kidney and horse-shoe kidney Renal surgeries Renal endangering medications, <i>e.g.</i> , NSAIDs and chemotherapy Renal-induced nephropathy (prior) History of prior renal dialysis Renal malignancies
Nephropathy-associated chronic diseases	<i>E.g.</i> , uncontrolled DM, hypertension and hyperuricemia
Drugs interfering with renal excretions	Metformin

NSAIDs: Nonsteroidal antiinflammatory drugs; DM: Diabetes mellitus.

questions: Whether the patient had or has: (1) renal disease; (2) previous renal surgery; (3) proteinuria; (4) diabetes mellitus; (5) hypertension; (6) gout; and (7) recent administration of nephrotoxic drugs]. The authors thought that adding two more critical questions, which are (1) whether the patient had undergone a contrast-enhanced imaging study or not? and (2) if any, what was his/her experience with it? May expand the benefit of this questionnaire to be more global for identification of most high-risk patients are prone to develop CM induced hypersensitivity.

PATHOGENESIS OF CM HYPERSENSITIVITY

In spite of different postulations, the exact nature of CM hypersensitivity reactions is not clearly understood yet. The osmolality and chemotoxicity of a contrast agent are thought to be major determinants of its adverse reaction liability^[13,14].

For immediate hypersensitivity reactions, both the Ig-G mediated mechanisms (allergy-like) and the unpredictable non-allergic (idiosyncratic) mechanisms,

thought to depend on the chemotoxic effects and physico-chemical properties of the agent, are plausible. For either pathway, cell-membrane injury of basophils and mast cell with subsequent release of histamine; bradykinins; and other inflammatory mediators is the main event^[14,15]. Also, activation of the clotting factor XII with subsequent activation of kinin system as well as cyclo-oxygenase and lipoxygenase inflammatory pathways and production of bradykinin, prostaglandins and leukotrienes is thought to mediate the CM induced respiratory and cardiovascular manifestations presented in moderate and severe hypersensitivity reactions^[13,16].

Recent research revealed that iodine is the initiating factor in immediate and delayed sensitivity reactions to iodinated CM^[17]. Consequently, hyper-osmolar contrast agent use has been largely replaced in clinical imaging practices, over last two decades, with worldwide shift towards their non-ionic counterparts (whether; iso- or low-osmolar CM) thanks to improved safety profiles of these agents^[18].

Similarly, recent researches emphasized that immediate and moderate hypersensitivity reactions to GBCA may occur with high incidence in females, patients with history of allergies and previous reactions to CM^[6]. Notably, severe hypersensitivity reactions to GBCA were higher for abdominal examinations rather than brain and spines^[6]. Although an Ig-E mediated mechanism was suggested, the exact mechanism hasn't been elucidated. Interestingly, these hypersensitivity reactions seem to vary between various GBCA in different studies with no solid evidence whether it depends on the specific characteristics of gadolinium-based structure or not, at least for the GBCA immediate reactions^[7,19,20]. On the contrary, delayed CM hypersensitivity reactions are thought to be T-cell mediated^[10,14].

SERUM CREATININE SCREENING BEFORE CM EXAMINATIONS

Based on the safety profile of CM in clinical use nowadays, adequate screening questions as mentioned earlier, mitigates the need to have recent serum creatinine level done in normal average adults in most radiology practices^[2,5,10,21]. However, having a laboratory renal profile for fragile patients due to senility and/or chronic debilitating disorders is highly advisable, especially in elective examination. Many patient co-morbidities require intentional lookup of the patient's renal profile (Table 2).

Renal creatinine is the widely acceptable indicator for renal function. The agreed upon simple general practices are to administer CM in patients with creatinine ≤ 1.5 mg/dL, be cautious in patients with creatinine in the range of 1.6-2.0 mg/dL, and to avoid contrast in patients with creatinine > 2.0 mg/dL^[8,9].

Other groups suggested relying on estimated glomerular filtration rate (eGFR) as reliable indicators

Table 3 Common elective premedication protocols for high-risk patients to develop iodinated contrast medium hypersensitivity reactions

Lasser protocol	Elective Greenberger protocol ¹	Emergency IV protocols (in descending order of desirability)
Oral prednisone 50 mg at 13/7 and 1 h before contrast medium injection	Oral methylprednisolone 32 mg at 12 and 2 h before contrast medium injection +/-	Methylprednisolone sodium succinate 40 mg
		OR
		hydrocortisone sodium succinate 200 mg every 4 h till examination
		+ diphenhydramine 50 mg IV - 1 h
+ (oral/IM or IV) diphenhydramine 50 mg just 1 h before examination	+/- (oral/IM or IV) diphenhydramine 50 mg just 1 h before examination	No corticosteroids at all (not preferable)
		Only diphenhydramine 50 mg IV

¹IV hydrocortisone 200 mg may be a substitute for oral prednisone, if the patient cannot tolerate oral medication.

of renal function in adults, as it consider age, gender and ethnic variations^[22,23]. eGFRs between 30 and 60 mL/min per 1.73 m² requires precautions to be practiced to avoid contrast induced renal injuries and needs close post-procedural monitoring of renal functions^[8,9,22,23].

In emergency examinations requiring CM administration, reliance on urine dipstick check for creatinine done in the emergency room was suggested as a predict for serum creatinine along with adequate history taking^[24,25]. Although no consensus exists regarding serum creatinine and CM administration time window, a renal profile done within last 30 d is an acceptable recent documentation in general^[9,26]. The authors recommend shorter time-intervals for high-risk groups, however.

Concerns about volume of used iodinated CM and the usage of absolute rather than the absolute and relative creatinine levels are on the rise, more recently, to avoid systematic inaccuracies in assessment of renal function and avoid contrast-induced nephropathy^[27,28].

PRE-MEDICATIONS FOR PATIENTS AT RISK

Premedication before IV contrast administration is a well-known and widely practiced protocol that aims to reduce the incidence of mild to moderate adverse reactions to iodinated CM, primarily^[29,30]. However, the possibility of severe reactions occurrence albeit rare is unaffected by premedication regimens^[16].

Corticosteroids are the critical component of any premedication regime. The use of antihistamine alone or as a supplement to corticosteroids is a customary practice^[8,9]. The mechanism of action of both drug groups is still controversial yet they are thought to interfere with the mechanisms of antigen-antibody response and actions of the released mediators^[31]. However, the sole use of antihistamines did not

prove to be working alone in prevention of contrast-induced hypersensitivity reactions^[32]. Two common elective premedication protocols, the Lasser^[33] and the Greenberger^[34] (Table 3), are widely implemented and supported by recognized bodies^[8,9].

HYDRATION (EXTRACELLULAR VOLUME EXPANSION)

The osmolality of iodinated CM was postulated to cause extracellular fluid shifts, leading to cell dehydration and increased intracellular fluid viscosity, which precipitates cellular dysfunction^[35].

Volume expansion appears to be an amenable effective strategy to obviate contrast induced nephropathy (CIN). A practical hydration regime has to be initiated before and be continued for several hours after CM administration^[36]. Various hydrations regimens either *via* oral and/or IV administration of crystalline solutions are available including normal and half-strength saline's, sodium bicarbonates infusion, N-acetylcysteine and statins^[37]. Yet the privileges of one over another have not been effectively established; thanks to limited studies done in patients receiving IV CM for diagnostic purposes^[36,37].

ADVERSE REACTIONS TO CM

CM adverse reactions are usually grouped according to their emergence and necessity for intervention into: (1) acute; happening during or within the 1st hour following injection; (2) late, presenting up to 1 week thereafter; and (3) very late group that surfaces weeks to months following contrast administration. However; for easy academic deliberation, we will consider it under two main categories, the (1) immediate (acute) adverse reactions; occurring up to one hour from injection; and the (2) non-immediate (delayed) reactions; occurring later on. Furthermore, for the increased awareness

Table 4 Severity scale, signs, symptoms and management options of adverse reactions to contrast media

Category of reaction	Symptoms	Treatment
Mild (self-limited without evidence of progression)	Hives, rashes and sweats Nasal symptoms Nausea, vomiting Pallor Cough Flushing Warmth Chills Headache and/or Dizziness Self limited anxiety	Patient reassurance usually suffices in some cases Close observation till resolution of symptoms May require symptomatic treatment in some cases
Moderate (signs and symptoms are more pronounced)	Generalized or diffuse erythema Tachycardia/bradycardia Bronchospasm, wheezing and/or dyspnea Hypo- or hyper-tension Voice hoarseness	Requires prompt treatment Requires close, careful observation for possible progression to a life-threatening event
Severe (sign and symptoms are often life-threatening)	Laryngeal edema (severe or rapidly progressing) Convulsions Profound hypotension Unresponsiveness Clinically manifest arrhythmias Cardiopulmonary arrest	Requires hospitalization and aggressive treatment by emergency teams

by renal side effects of different CM these will be sub-classified into renal and non-renal reactions.

IMMEDIATE NON-RENAL ADVERSE REACTIONS TO CM

From practical point of view we will describe it as mild, moderate and severe reactions. Table 4 shows the immediate non-renal adverse reactions and their common manifestations as well as the general guidelines that every radiologist and/or medical staff dealing with CM reactions have to be oriented with.

In general, the majority of reactions to CM are of the mild form in form of hives and nausea^[5-7] and occurs within the first minutes following CM administration while severe and potentially life-threatening reactions to intravascular CM occur within 20 min after contrast administration^[5,6,11,19]. It is recommended to keep patients under observation for 20-30 min in the radiology department after contrast medium injection^[8,9]. This is of special consideration for the pediatric population who can't verbally communicate. Mild reactions may require no more than observation, patient reassurance and/or a dose of an antihistaminic. In moderate to severe adverse reactions more therapeutic interventions will be implemented.

Every radiology practice has to be equipped with a general emergency cart loaded with up to date medications and instrumentations used in dealing with CM-induced reactions^[8-10]. A cooperative plan with concerned emergency teams should be put into effect

in hospitals to deal with severe reactions to CM.

BREAKTHROUGH REACTION

A breakthrough reaction refers to a reaction that occurs after iodinated CM injection in patients who have already been intentionally pre-medicated to prevent CM sensitivity reaction^[31]. So, they are patients who are principally labeled as being at high risk for a reaction. Severity of reaction is more or less similar to those of the initial reaction and needs likewise treatment. Practically, these patients should be advised that they are likely to be at increased risk for more severe reactions if iodinated contrast material is administered in the future. Furthermore, radiologists have to recommend other alternative safe imaging modalities to help with their diagnoses.

IMMEDIATE RENAL ADVERSE REACTIONS TO CM

Iodinated CM may cause disturbed renal functions known as contrast induced-acute kidney injury (CI-AKI), that is commonly defined as "abrupt deterioration in kidney function, manifested by an increase in serum creatinine level with or without reduced urine output"^[38]. There are more specific diagnostic criteria for diagnosing (CI-AKI) delineated by the consensus of concerned major concerned bodies (Table 5)^[39]. Dehydrated, debilitated and high-risk chronic illness fragile patients, especially the diabetics, are more prone to develop CI-AKI^[22,40-42]. CI-AKI is likely to

Table 5 The criteria for diagnosing contrast induced-acute kidney injury

Absolute serum creatinine increase of greater than or equal to 0.3 mg/dL (> 26.4 μmol/L)
An increase in the percentage of serum creatinine of greater than or equal to 50%
Urine output reduced to less than or equal to 0.5 mL/kg per hour for at least 6 h

Table 6 European medicines agency nephrogenic systemic fibrosis-risk stratification categorization of gadolinium-based contrast agent

GBCA NSF-risk class	Scientific (generic) name
Highest risk of NSF	Gadodiamide (Omniscan®) Gadopentetate dimeglumine (Magnevist®) Gadoversetamide (Optimark®)
Intermediate risk of NSF	Gadobenate dimeglumine (Multihance®) Gadofosveset trisodium (Vasovist®, Ablavar®) Gadoxetate disodium (Primovist®, Eovist®)
Lowest risk of NSF	Gadobutrol (Gadovist®) Gadoterate meglumine (Dotarem®) Gadoteridol (Prohance®)

NSF: Nephrogenic systemic fibrosis; GBCA: Gadolinium-based contrast agent.

be the result of burden of coexistent morbidity rather than the CM itself. Moreover, this depends on the base line renal profile^[22,42,43]. Moreover, it was noticed that CI-AKI is more likely to develop in patients undergoing intra-arterial use of contrast above the level of renal arteries more than in patients undergoing IV administration of the CM^[41].

EXTRAVASATION

Extravasation refers to the escape of contrast material from the vascular lumen with infiltration of the interstitial tissue around injection site during injection. It is reported to be less than 1% and is not directly correlated with injection^[44]. The physician has to promptly recognize and evaluate it to reduce the chance and severity of injury. The staff in charge of CM injections should: (1) check the adequacy of vascular access; (2) adjust injection rate; (3) counsel the patient to report any unpleasant sensations at the injection site; and (4) monitor the injection site during and/or following the procedure.

If extravasation commences the injection should be withheld, assessment is done. Small and limited extravasations are self limited and just need monitoring, reassurance, hot and cold foment. Large injurious extravasations may require surgical intervention^[45].

DELAYED NON-RENAL ADVERSE REACTIONS TO CM

Delayed contrast hypersensitivity is defined as a reaction that occurs 1 h to 1 wk following iodinated contrast administration. They are usually limited to skin

rashes and occasionally mild and self limited. Originally, these reactions were reported to be associated with the non-ionic iso-osmolar iodinated CM^[8,9]. However, recent reports addressed its occurrence following GBCA^[11,19].

Iodine-provoked thyroid dysfunction

Iodinated CM have a free iodine content that is greatly higher than average daily human needs^[46]. In general, it is contraindicated to administer iodine based CM intra-vascularly to patients at risk of thyrotoxicosis^[2,9].

Iodine-provoked thyroid dysfunction is a self-limited, relatively rare entity of transient altered thyroid hormones in the blood in response to high load of free iodine following intravenous administration of iodinated CM (disrupted auto-regulation)^[46,47]. Subjects with normal thyroid function are not at risk^[47,48]. The problem is for patients with hyperthyroid states, *e.g.*, thyroid autonomy and graves' disease who become deprived of thyroid hormones and need treatment adjustments. Theoretically speaking; long term suppression may end with hypothyroidism^[46].

Another caveat is patients planned for radio-active iodine scanning. In this population, the use of iodinated contrast agents has to be postponed after planned radioactive iodine imaging or therapy. Excess free iodine following IV administration of iodinated CM will saturate its receptors and result in sub-optimal or non-diagnostic studies and/or management of their disease^[2]. A noteworthy point to mention here, is that iodinated CM used during ¹⁸FDG-PET/CT do not have a dumping effect on the clinical assessment of these studies^[49,50].

Reports about iodine-provoked thyroid dysfunction following non-vascular uses have emerged recently and the issue has to be monitored by radiologists^[51-53].

DELAYED RENAL ADVERSE REACTIONS TO CM (NEPHROGENIC SYSTEMIC FIBROSIS)

Actually, all iodinated CM have a nephrotoxic potential yet variable potentialities exist for GBCA^[10,11,19]. Table 6 shows the popular classification of commercially available GBCA by European Medicines Agency EMA^[54].

Nephrogenic systemic fibrosis (NSF) is a serious progressive clinico-pathologic entity that may progress to be fatal. It has no associated imaging findings. NSF came into attention more than a decade earlier and has been described to develop in patients with compromised renal functions^[55-57]. Clinically, it is a diagnosis of exclusion that can be suspected in patients showing variable skin rashes up to subcutaneous scleroderma-like plaques as well as variable systemic manifestations who received a GBCA^[57,58]. However, these should be coupled with histological findings^[58]. Although its pathogenesis has not been agreed upon, postulations assumed that weak stability of gadolinium chelates leads to its free dissociation in tissues and incite a fibrotic response in different body tissue. Association with linear; more than the macro-

Table 7 Strategies for safe clinical practice of contrast media to reduce risk for renal complications in patients with renal problems

Patients with SCr ≥ 2 g/dL and/or eGFR ≤ 60 mL/min per 1.73 m^2	Withhold contrast whenever possible and use alternative imaging modalities if feasible Adequate hydration
Patients with end-stage renal disease who still produce urine	Consider alternative diagnostic study if feasible Avoid use of CM whenever possible Use lowest possible dose of contrast Use intermediate to low osmolar and/or low risk GBCA followed by prompt dialysis if the patient is already undergoing dialysis
Patients with end-stage renal disease who are anuric	Can receive routine volumes of intravenous contrast material without risk for further renal damage or the need for urgent dialysis

GBCA: Gadolinium-based contrast agent; CM: Contrast media; eGFR: Estimated glomerular filtration rate.

Table 8 Practical guidelines for safe contrast media-metformin interaction

Renal function (eGFR-indexed)	Action
Patients with normal renal function (eGFR ≥ 60 mL/min per 1.73 m^2)	No need to withhold metformin
Patients with compromised renal function (eGFR ≥ 30 but ≤ 60 mL/min per 1.73 m^2)	Withhold metformin for 48 h Re-institution after renal function monitoring
Patients with compromised renal function (eGFR < 30 mL/min per 1.73 m^2)	Have not to be on metformin Consult nephrologist

eGFR: Estimated glomerular filtration rate.

cyclic; formulas of GBCA is supportive for these assumptions^[59,60].

POPULATIONS WITH SPECIAL CONSIDERATIONS

Patients liable to and/or actually have renal compromise

It is of utmost importance for radiologists to identify patients with renal compromise in advance using same screening tips for identifying high risk groups, discussed in earlier section (Table 1). So radiologists can adhere to some precious strategies for safe clinical practice of CM to reduce risk for NSF (Table 7).

The use of renal protective agents such as N-acetylcysteine, sodium bicarbonate, diuretics, and theophylline is debatable and has not proven great benefits^[36]. The previous recommendations of hemodialysis in patients at high risk for CM-associated complications are no longer sound and consulting a nephrologist is a wisdom practice^[61].

METFORMIN

Metformin is an oral anti-hyperglycemic agent, commonly, used to treat patients with non-insulin-dependent diabetes mellitus. Metformin is excreted unchanged in the urine. However, in the presence of renal failure, either pre-existing or induced by iodinated contrast medium, metformin may potentially accumulate in sufficient amounts to cause lactic acidosis. Hence, radiologists have to cautiously approach those patients for safe practices considering the potentiality for contrast-induced renal injury with subsequent metformin use co-morbidity (Table 8)^[2,8,9]. For GBCA, there is no necessity to discontinue metformin before examinations, however^[9].

PREGNANT AND NURSING WOMEN

Although iodinated contrast agents and gadolinium cross the placenta in little traces reaching the fetus, no definite gene mutation or teratogenic effects have been reported in human^[62,63]. The large scientific bodies in radiology^[8,9] recommend that, no contrast should be administered to the pregnant mother unless there is prudent need to intervene to save both mother and baby, based on these contrast-enhanced studies. Furthermore, post-natal assessment of neonatal thyroid function has to be carried if the administered CM was iodine-based^[53,64] while this is not of clinical utility for the GBCA^[8,9,63].

Small traces of iodinated contrast material or GBCA are excreted in breast milk and absorbed by the infant with no reports of fetal reactions to the best of author's knowledge. So, breast feeding abstinence following contrast studies of nursing women is not recommended^[8,9,26].

PEDIATRICS

Due to limited number of studies, estimating the incidence of reactions to CM in children is difficult. Special considerations have to be weighted when dealing with infants and young children. These include: Fluid shifts in neonates, low weights, immaturity of their renal function, lower (eGFR), fragile vascular access and lack of communicability. Most CM reactions in children are mild and in the form of skin and respiratory reactions. Warming of iodinated CM before administration to children is recommended to increase their viscosity and diminish rates of contrast reaction^[65,66]. Other recommendations may include, use of low-osmolality contrast agents, diminishing the volume of contrast given, avoid nephrotoxic drugs and adequate hydration of the patient^[67].

GBCA reactions are rare in children and exclusively presented in children with pre-existing renal problems^[68]. However, GBCAs use should be limited in children and only used when necessary^[9]. Recent

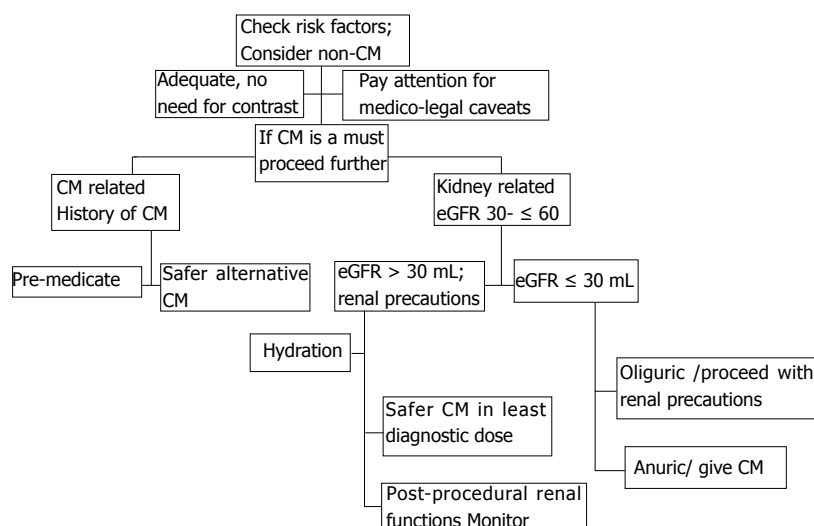


Figure 1 Procedural infographic display for safe clinical practice use of iodinated and gadolinium-based contrast agent for IV use in clinical imaging. CM: Contrast media; eGFR: Estimated glomerular filtration rate.

reports recommended the use of gadobenate dimeglumine (Multihance) in pediatrics of different ages^[69].

CM: MEDICO-LEGAL CAVEATS

Informed consent is defined as "a process of a patient-physician communication that results in the patient's authorization or agreement to undergo a specific medical intervention"^[70]. The aim of informed consent is to gather relevant information that makes the procedure both safe and comfortable as possible^[26].

With increased daily implementation of different clinical imaging modalities worldwide, obtaining an informed consent remains a practical caveat as it is not possible to achieve its requirements for every running contrast-enhanced imaging procedures^[71]. Practically, this is compromised by patient's unfamiliarity with the invisible nature of radiation, its measurements and the probability of its stochastic effects compared to orientation with incisions and intubations for example^[72]. Moreover, informed consent timing, work list scheduling and radiologists' discomfort, about discussing CM complications with their patients are added limitations for the classic informed consent process^[73]. After all, the patient-radiologist relationship which is brief and episodic, especially for the outpatients basis^[72,73].

Based on the aforementioned highlights and the documented evidences that CM are largely safe drugs, a ready to sign informed consent form, by the patient or his/her guardian, is a customary practice worldwide in most radiology practices^[26,73]. Previous reports emphasized that adoption of adequate interactive verbal communication, along with providing multimedia approaches, *e.g.*, on-site videos, leaflets, educational seminars, *etc.*, explaining the benefits of CM use, the rarity of their hypersensitivity reactions,

the propensity of these reactions to be mild and transient, the populations at risk for developing it, can effectively relieve the patient's apprehensions and confusions for elective diagnostic imaging as well as interventional procedures requiring the administration of CM^[74-76].

The authors thought that conducting those steps along with providing an easy to tick, short targeted questionnaire fulfills the aim of informed consent, by identifying high-risk populations to develop CM reactions, and make the process of gaining it a time-effective and easy routine. Undoubtedly, these routine practices relieve the patient's anxiety and mitigate an important provoking element thought to be involved in developing reactions to CM^[77].

Justification for the use of CM based on clinical concerns is the sole responsibility of the radiologist in charge based on regional laws, institutional and departmental policies^[8,9].

Another medico-legal caveat is the off-label contrast media (OLCM) which are defined as CM that are used in otherwise originally tested, indicated and licensed purposes, *e.g.*, CT and/or MR angiographic, cardiac and arthrographic procedures^[73,78]. Although, these applications are proved by recognized scientific bodies^[8,9] as well as scientifically-based well conducted large population and multicenter studies^[7]; to be clinically beneficial and are widely used since decades, the use of CM for these examinations remains outside legal boundaries^[78,79]. This imparts medico-legal responsibility to the radiologist in charge to divulge exhaustive information to patients and get a documented informed consent from patients before proceeding into such procedures. Shortly, most scientific societies and regulatory bureaus ascertain that radiologists using CM for an off-label indication should judge his/her use based on sound scientific medical evidences and should maintain a record of the

products used and their effects^[80].

Lastly, a simple applicable working safety practice hierarchical info-graph for administrating radiographic and MR CM is suggested by the authors (Figure 1).

CONCLUSION

In conclusion, radiologists as well as faculty staffs dealing with radiographic and MR CM have to be well oriented with the potential CM hypersensitivity reactions, high-risk groups liable to develop it and their early recognition. They have to be ready to implement prompt and effective management plan to deal with these reactions should they emerge. Faculty staff dealing with radiographic and MR contrast administrations have to exercise strategies to prevent potential contrast-induced acute and delayed renal injuries and pay attention to the pregnant and nursing women, pediatrics, diabetics, as well as other fragile populations for optimized patient safety. Moreover, radiologists should be oriented with the medico-legal issues related to use of CM and play pivotal role in patient learning and assurance about CM safety. These will pay dividends as improved patient safety as well as safe radiology practices and working environment.

ACKNOWLEDGMENTS

The authors would thank to Dr. Tariq Saeed, FRCS, Neurosurgery Consultant, Armed force Hospital, King Abdulaziz Airbase, Dhahran, Saudi Arabia, for his critical linguistic revision of the final manuscript.

REFERENCES

- 1 **Lusic H**, Grinstaff MW. X-ray-computed tomography contrast agents. *Chem Rev* 2013; **113**: 1641-1666 [PMID: 23210836 DOI: 10.1021/cr200358s]
- 2 **Thomsen HS**. Contrast media safety-an update. *Eur J Radiol* 2011; **80**: 77-82 [PMID: 21856102 DOI: 10.1016/j.ejrad.2010.12.104]
- 3 **Kirsch JE**. Basic principles of magnetic resonance contrast agents. *Top Magn Reson Imaging* 1991; **3**: 1-18 [PMID: 2025431]
- 4 **Lee DH**. Mechanisms of contrast enhancement in magnetic resonance imaging. *Can Assoc Radiol J* 1991; **42**: 6-12 [PMID: 2001531]
- 5 **Hunt CH**, Hartman RP, Hesley GK. Frequency and severity of adverse effects of iodinated and gadolinium contrast materials: retrospective review of 456,930 doses. *AJR Am J Roentgenol* 2009; **193**: 1124-1127 [PMID: 19770337 DOI: 10.2214/AJR.09.2520]
- 6 **Prince MR**, Zhang H, Zou Z, Staron RB, Brill PW. Incidence of immediate gadolinium contrast media reactions. *AJR Am J Roentgenol* 2011; **196**: W138-W143 [PMID: 21257854 DOI: 10.2214/AJR.10.4885]
- 7 **Bruder O**, Schneider S, Pilz G, van Rossum AC, Schwitter J, Nothnagel D, Lombardi M, Buss S, Wagner A, Petersen S, Greulich S, Jensen C, Nagel E, Sechtem U, Mahrholdt H. 2015 Update on Acute Adverse Reactions to Gadolinium based Contrast Agents in Cardiovascular MR. Large Multi-National and Multi-Ethnic Population Experience With 37788 Patients From the EuroCMR Registry. *J Cardiovasc Magn Reson* 2015; **17**: 58 [PMID: 26170152 DOI: 10.1186/s12968-015-0168-3]
- 8 **European Society of Urogenital Radiology**. [accessed 2017 Jan 3]. Available from: URL: <http://www.esur.org/guidelines/>
- 9 **Manual on Contrast Media v10.2** - American College of Radiology. [accessed 2016 Aug 12]. Available from: URL: <http://www.acr.org/quality-safety/resources/contrast-manual>
- 10 **Namasivayam S**, Kalra MK, Torres WE, Small WC. Adverse reactions to intravenous iodinated contrast media: a primer for radiologists. *Emerg Radiol* 2006; **12**: 210-215 [PMID: 16688432 DOI: 10.1007/s10140-006-0488-6]
- 11 **Jung JW**, Kang HR, Kim MH, Lee W, Min KU, Han MH, Cho SH. Immediate hypersensitivity reaction to gadolinium-based MR contrast media. *Radiology* 2012; **264**: 414-422 [PMID: 22550309 DOI: 10.1148/radiol.12112025]
- 12 **Bettmann MA**, Heeren T, Greenfield A, Goudey C. Adverse events with radiographic contrast agents: results of the SCVIR Contrast Agent Registry. *Radiology* 1997; **203**: 611-620 [PMID: 9169677 DOI: 10.1148/radiology.203.3.9169677]
- 13 **Cochran ST**, Bomyea K, Sayre JW. Trends in adverse events after IV administration of contrast media. *AJR Am J Roentgenol* 2001; **176**: 1385-1388 [PMID: 11373197 DOI: 10.2214/ajr.176.6.1761385]
- 14 **Brockow K**, Sánchez-Borges M. Hypersensitivity to contrast media and dyes. *Immunol Allergy Clin North Am* 2014; **34**: 547-564, viii [PMID: 25017677 DOI: 10.1016/j.jiac.2014.04.002]
- 15 **Brockow K**, Ring J. Classification and pathophysiology of radiocontrast media hypersensitivity. *Chem Immunol Allergy* 2010; **95**: 157-169 [PMID: 20519888 DOI: 10.1159/000315949]
- 16 **Morcos SK**. Review article: Acute serious and fatal reactions to contrast media: our current understanding. *Br J Radiol* 2005; **78**: 686-693 [PMID: 16046418 DOI: 10.1259/bjr/26301414]
- 17 **Scherer K**, Harr T, Bach S, Bircher AJ. The role of iodine in hypersensitivity reactions to radio contrast media. *Clin Exp Allergy* 2010; **40**: 468-475 [PMID: 20210815 DOI: 10.1111/j.1365-2222.2009.03361.x]
- 18 **Wilmot A**, Mehta N, Jha S. The adoption of low-osmolar contrast agents in the United States: historical analysis of health policy and clinical practice. *AJR Am J Roentgenol* 2012; **199**: 1049-1053 [PMID: 23096178 DOI: 10.2214/AJR.11.8426]
- 19 **Aran S**, Shaqdan KW, Abujudeh HH. Adverse allergic reactions to linear ionic gadolinium-based contrast agents: experience with 194, 400 injections. *Clin Radiol* 2015; **70**: 466-475 [PMID: 25626627 DOI: 10.1016/j.crad.2014.12.011]
- 20 **Bruder O**, Schneider S, Nothnagel D, Pilz G, Lombardi M, Sinha A, Wagner A, Dill T, Frank H, van Rossum A, Schwitter J, Nagel E, Senges J, Sabin G, Sechtem U, Mahrholdt H. Acute adverse reactions to gadolinium-based contrast agents in CMR: multicenter experience with 17,767 patients from the EuroCMR Registry. *JACC Cardiovasc Imaging* 2011; **4**: 1171-1176 [PMID: 22093267 DOI: 10.1016/j.jcmg.2011.06.019]
- 21 **Tippins RB**, Torres WE, Baumgartner BR, Baumgarten DA. Are screening serum creatinine levels necessary prior to outpatient CT examinations? *Radiology* 2000; **216**: 481-484 [PMID: 10924574 DOI: 10.1148/radiology.216.2.r00au23481]
- 22 **Davenport MS**, Khalatbari S, Cohan RH, Ellis JH. Contrast medium-induced nephrotoxicity risk assessment in adult inpatients: a comparison of serum creatinine level- and estimated glomerular filtration rate-based screening methods. *Radiology* 2013; **269**: 92-100 [PMID: 23579047 DOI: 10.1148/radiol.13122462]
- 23 **McDonald JS**, McDonald RJ, Carter RE, Katzberg RW, Kallmes DF, Williamson EE. Risk of intravenous contrast material-mediated acute kidney injury: a propensity score-matched study stratified by baseline-estimated glomerular filtration rate. *Radiology* 2014; **271**: 65-73 [PMID: 24475854 DOI: 10.1148/radiol.13130775]
- 24 **Firestone D**, Vos A, Killeen JP, Chan TC, Guluma K, Davis DP, Vilke GM. Can urine dipstick be used as a surrogate for serum creatinine in emergency department patients who undergo contrast studies? *J Emerg Med* 2007; **33**: 119-122 [PMID: 17692759 DOI: 10.1016/j.jemermed.2007.02.021]
- 25 **Firestone DN**, Band RA, Hollander JE, Castillo E, Vilke GM. Use of a urine dipstick and brief clinical questionnaire to predict an abnormal serum creatinine in the emergency department. *Acad Emerg Med* 2009; **16**: 699-703 [PMID: 19500077 DOI: 10.1111/j.1553-2712.2009.00421.x]
- 26 **Bettmann MA**. Frequently asked questions: iodinated contrast

- agents. *Radiographics* 2004; **24** Suppl 1: S3-10 [PMID: 15486247 DOI: 10.1148/rg.24si045519]
- 27 **Barbieri L**, Verdoia M, Marino P, Suryapranata H, De Luca G. Contrast volume to creatinine clearance ratio for the prediction of contrast-induced nephropathy in patients undergoing coronary angiography or percutaneous intervention. *Eur J Prev Cardiol* 2016; **23**: 931-937 [PMID: 26525064 DOI: 10.1177/2047487315614493]
- 28 **Liu Y**, Liu YH, Chen JY, Tan N, Zhou YL, Duan CY, Yu DQ, Xie NJ, Li HL, Chen PY. Safe contrast volumes for preventing contrast-induced nephropathy in elderly patients with relatively normal renal function during percutaneous coronary intervention. *Medicine* (Baltimore) 2015; **94**: e615 [PMID: 25816028 DOI: 10.1097/MD.0000000000000615]
- 29 **Lasser EC**, Berry CC, Mishkin MM, Williamson B, Zheutlin N, Silverman JM. Pretreatment with corticosteroids to prevent adverse reactions to nonionic contrast media. *AJR Am J Roentgenol* 1994; **162**: 523-526 [PMID: 8109489 DOI: 10.2214/ajr.162.3.8109489]
- 30 **Kim SH**, Lee SH, Lee SM, Kang HR, Park HW, Kim SS, Cho SH, Min KU, Kim YY, Chang YS. Outcomes of premedication for non-ionic radio-contrast media hypersensitivity reactions in Korea. *Eur J Radiol* 2011; **80**: 363-367 [PMID: 20619990 DOI: 10.1016/j.ejrad.2010.06.014]
- 31 **Schopp JG**, Iyer RS, Wang CL, Petscavage JM, Paladin AM, Bush WH, Dighe MK. Allergic reactions to iodinated contrast media: premedication considerations for patients at risk. *Emerg Radiol* 2013; **20**: 299-306 [PMID: 23430296 DOI: 10.1007/s10140-012-1081-9]
- 32 **Davies P**, Roberts MB, Roylance J. Acute reactions to urographic contrast media. *Br Med J* 1975; **2**: 434-437 [PMID: 236064]
- 33 **Lasser EC**, Berry CC, Talner LB, Santini LC, Lang EK, Gerber FH, Stolberg HO. Pretreatment with corticosteroids to alleviate reactions to intravenous contrast material. *N Engl J Med* 1987; **317**: 845-849 [PMID: 3627208 DOI: 10.1056/NEJM198710013171401]
- 34 **Greenberger PA**, Patterson R. The prevention of immediate generalized reactions to radiocontrast media in high-risk patients. *J Allergy Clin Immunol* 1991; **87**: 867-872 [PMID: 2013681]
- 35 **Almén T**. The etiology of contrast medium reactions. *Invest Radiol* 1994; **29** Suppl 1: S37-S45 [PMID: 8071042]
- 36 **Thomsen HS**, Morcos SK, Barrett BJ. Contrast-induced nephropathy: the wheel has turned 360 degrees. *Acta Radiol* 2008; **49**: 646-657 [PMID: 18568557 DOI: 10.1080/02841850801995413]
- 37 **Subramaniam RM**, Suarez-Cuervo C, Wilson RF, Turban S, Zhang A, Sherrod C, Aboagye J, Eng J, Choi MJ, Hutfless S, Bass EB. Effectiveness of Prevention Strategies for Contrast-Induced Nephropathy: A Systematic Review and Meta-analysis. *Ann Intern Med* 2016; **164**: 406-416 [PMID: 26830221 DOI: 10.7326/M15-1456]
- 38 **Rahman M**, Shad F, Smith MC. Acute kidney injury: a guide to diagnosis and management. *Am Fam Physician* 2012; **86**: 631-639 [PMID: 23062091]
- 39 **Lewington A**, MacTier R, Sutton A, Smith D, Downes M. Prevention of Contrast Induced Acute Kidney Injury (CI-AKI) In Adult Patients on behalf of The Renal Association, British Cardiovascular Intervention Society and Royal College of Radiologists. 2013. [accessed 2017 Jan 9]. Available from: URL: <http://www.renal.org/docs/default-source/guidelines-resources/joint-guidelines/Prevention of Contrast Induced Acute Kidney Injury CI-AKI In Adult Patients.pdf>
- 40 **Huang MK**, Hsu TF, Chiu YH, Chiang SC, Kao WF, Yen DH, Huang MS. Risk factors for acute kidney injury in the elderly undergoing contrast-enhanced computed tomography in the emergency department. *J Chin Med Assoc* 2013; **76**: 271-276 [PMID: 23683260 DOI: 10.1016/j.jcma.2013.01.007]
- 41 **Katzberg RW**, Newhouse JH. Intravenous contrast medium-induced nephrotoxicity: is the medical risk really as great as we have come to believe? *Radiology* 2010; **256**: 21-28 [PMID: 20574082 DOI: 10.1148/radiol.10092000]
- 42 **Moos SI**, van Vemde DN, Stoker J, Bipat S. Contrast induced nephropathy in patients undergoing intravenous (IV) contrast enhanced computed tomography (CECT) and the relationship with risk factors: a meta-analysis. *Eur J Radiol* 2013; **82**: e387-e399 [PMID: 23711425 DOI: 10.1016/j.ejrad.2013.04.029]
- 43 **McDonald RJ**, McDonald JS, Bida JP, Carter RE, Fleming CJ, Misra S, Williamson EE, Kallmes DF. Intravenous contrast material-induced nephropathy: causal or coincident phenomenon? *Radiology* 2013; **267**: 106-118 [PMID: 23360742 DOI: 10.1148/radiol.12121823]
- 44 **Wang CL**, Cohan RH, Ellis JH, Adusumilli S, Dunnick NR. Frequency, management, and outcome of extravasation of nonionic iodinated contrast medium in 69,657 intravenous injections. *Radiology* 2007; **243**: 80-87 [PMID: 17392249 DOI: 10.1148/radiol.2431060554]
- 45 **Tonolini M**, Campari A, Bianco R. Extravasation of radiographic contrast media: prevention, diagnosis, and treatment. *Curr Probl Diagn Radiol* 2012; **41**: 52-55 [PMID: 22285002 DOI: 10.1067/j.cpradiol.2011.07.004]
- 46 **Rhee CM**, Bhan I, Alexander EK, Brunelli SM. Association between iodinated contrast media exposure and incident hyperthyroidism and hypothyroidism. *Arch Intern Med* 2012; **172**: 153-159 [PMID: 22271121 DOI: 10.1001/archinternmed.2011.677]
- 47 **Leger AF**, Massin JP, Laurent MF, Vincens M, Auriol M, Helal OB, Chomette G, Savoie JC. Iodine-induced thyrotoxicosis: analysis of eighty-five consecutive cases. *Eur J Clin Invest* 1984; **14**: 449-455 [PMID: 6441722]
- 48 **Savoie JC**, Massin JP, Thomopoulos P, Leger F. Iodine-induced thyrotoxicosis in apparently normal thyroid glands. *J Clin Endocrinol Metab* 1975; **41**: 685-691 [PMID: 1176580 DOI: 10.1210/jcem-41-4-685]
- 49 **Abdul Razak HR**, Nordin AJ, Ackerly T, Van Every B, Martin R, Geso M. Quantifying the effects of iodine contrast media on standardised uptake values of FDG PET/CT images: an anthropomorphic phantom study. *Australas Phys Eng Sci Med* 2011; **34**: 367-374 [PMID: 21786083 DOI: 10.1007/s13246-011-0088-y]
- 50 **Prechtel HW**, Verburg FA, Palmowski M, Krohn T, Pietsch H, Kuhl CK, Mottaghy FM, Behrendt FF. Different intravenous contrast media concentrations do not affect clinical assessment of 18F-fluorodeoxyglucose positron emission tomography/computed tomography scans in an intraindividual comparison. *Invest Radiol* 2012; **47**: 497-502 [PMID: 22820678 DOI: 10.1097/RLI.0b013e31825d676e]
- 51 **Mekaru K**, Kamiyama S, Masamoto H, Sakumoto K, Aoki Y. Thyroid function after hysterosalpingography using an oil-soluble iodinated contrast medium. *Gynecol Endocrinol* 2008; **24**: 498-501 [PMID: 18958768 DOI: 10.1080/09513590802246364]
- 52 **Kaneshige T**, Arata N, Harada S, Ohashi T, Sato S, Umehara N, Saito T, Saito H, Murashima A, Sago H. Changes in serum iodine concentration, urinary iodine excretion and thyroid function after hysterosalpingography using an oil-soluble iodinated contrast medium (lipiodol). *J Clin Endocrinol Metab* 2015; **100**: E469-E472 [PMID: 25546154 DOI: 10.1210/jc.2014-2731]
- 53 **Lombard F**, Dalla-Vale F, Veyrac C, Plan O, Cambonie G, Picaud JC. Severe hypothyroidism after contrast enema in premature infants. *Eur J Pediatr* 2009; **168**: 499-500 [PMID: 18618140 DOI: 10.1007/s00431-008-0782-2]
- 54 **European Medicines Agency**. Human medicines - Gadolinium-containing contrast agents [Internet]. Gadolinium-Containing Contrast Agents, 2010. [accessed 2017 Jan 10]. Available from: URL: http://www.ema.europa.eu/ema/index.jsp?curl=pages/medicines/human/referrals/Gadolinium-containing_contrast_agents/human_referral_000182.jsp&mid=WC0b01ac05805c516f
- 55 **Cowper SE**, Robin HS, Steinberg SM, Su LD, Gupta S, LeBoit PE. Scleromyxoedema-like cutaneous diseases in renal-dialysis patients. *Lancet* 2000; **356**: 1000-1001 [PMID: 11041404 DOI: 10.1016/S0140-6736(00)02694-5]
- 56 **Daram SR**, Cortese CM, Bastani B. Nephrogenic fibrosing dermopathy/nephrogenic systemic fibrosis: report of a new case with literature review. *Am J Kidney Dis* 2005; **46**: 754-759 [PMID: 16183432 DOI: 10.1053/j.ajkd.2005.06.024]
- 57 **Introcaso CE**, Hivnor C, Cowper S, Werth VP. Nephrogenic fibrosing dermopathy/nephrogenic systemic fibrosis: a case series of nine patients and review of the literature. *Int J Dermatol* 2007; **46**: 447-452 [PMID: 17472669 DOI: 10.1111/j.1365-4632.2007.03301.x]

- 58 **Khawaja AZ**, Cassidy DB, Al Shakarchi J, McGrogan DG, Inston NG, Jones RG. Revisiting the risks of MRI with Gadolinium based contrast agents-review of literature and guidelines. *Insights Imaging* 2015; **6**: 553-558 [PMID: 26253982 DOI: 10.1007/s13244-015-0420-2]
- 59 **Frenzel T**, Lengsfeld P, Schirmer H, Hütter J, Weinmann HJ. Stability of gadolinium-based magnetic resonance imaging contrast agents in human serum at 37 degrees C. *Invest Radiol* 2008; **43**: 817-828 [PMID: 19002053 DOI: 10.1097/RLI.0b013e3181852171]
- 60 **Thomsen HS**, Marckmann P. Extracellular Gd-CA: differences in prevalence of NSF. *Eur J Radiol* 2008; **66**: 180-183 [PMID: 18342468 DOI: 10.1016/j.ejrad.2008.01.024]
- 61 **Rodby RA**. Preventing complications of radiographic contrast media: is there a role for dialysis? *Semin Dial* 2007; **20**: 19-23 [PMID: 17244114 DOI: 10.1111/j.1525-139X.2007.00233.x]
- 62 **Vanhaesebrouck P**, Verstraete AG, De Praeter C, Smets K, Zecic A, Craen M. Transplacental passage of a nonionic contrast agent. *Eur J Pediatr* 2005; **164**: 408-410 [PMID: 15798909 DOI: 10.1007/s00431-005-1659-2]
- 63 **De Santis M**, Straface G, Cavaliere AF, Carducci B, Caruso A. Gadolinium periconceptional exposure: pregnancy and neonatal outcome. *Acta Obstet Gynecol Scand* 2007; **86**: 99-101 [PMID: 17230297 DOI: 10.1080/00016340600804639]
- 64 **Satoh M**, Aso K, Katagiri Y. Thyroid Dysfunction in Neonates Born to Mothers Who Have Undergone Hysterosalpingography Involving an Oil-Soluble Iodinated Contrast Medium. *Horm Res Paediatr* 2015; **84**: 370-375 [PMID: 26402613 DOI: 10.1159/000439381]
- 65 **Vergara M**, Seguel S. Adverse reactions to contrast media in CT: effects of temperature and ionic property. *Radiology* 1996; **199**: 363-366 [PMID: 8668779 DOI: 10.1148/radiology.199.2.8668779]
- 66 **Davenport MS**, Wang CL, Bashir MR, Neville AM, Paulson EK. Rate of contrast material extravasations and allergic-like reactions: effect of extrinsic warming of low-osmolality iodinated CT contrast material to 37 degrees C. *Radiology* 2012; **262**: 475-484 [PMID: 22106356 DOI: 10.1148/radiol.11111282]
- 67 **Cohen MD**. Safe use of imaging contrast agents in children. *J Am Coll Radiol* 2009; **6**: 576-581 [PMID: 19643386 DOI: 10.1016/j.jacr.2009.04.003]
- 68 **Nardone B**, Saddleton E, Laumann AE, Edwards BJ, Raisch DW, McKoy JM, Belknap SM, Bull C, Haryani A, Cowper SE, Abu-Alfa AK, Miller FH, Godinez-Puig V, Dharnidharka VR, West DP. Pediatric nephrogenic systemic fibrosis is rarely reported: a RADAR report. *Pediatr Radiol* 2014; **44**: 173-180 [PMID: 24057195 DOI: 10.1007/s00247-013-2795-x]
- 69 **Schneider G**, Schürholz H, Kirchin MA, Bückner A, Fries P. Safety and adverse effects during 24 hours after contrast-enhanced MRI with gadobenate dimeglumine (MultiHance) in children. *Pediatr Radiol* 2013; **43**: 202-211 [PMID: 23179483 DOI: 10.1007/s00247-012-2498-8]
- 70 **American Medical Association**. Code of Medical Ethics/Opinions on patient-Physician Relationships [Internet]. Httpswwwama-assnorgabout-uscode-Med-Ethics. [accessed 2017 Jan 6]. Available from: URL: https://www.ama-assn.org/about-us/code-medical-ethics
- 71 **Berlin L**. Informed consent for contrast media and gadolinium injections. *AJR Am J Roentgenol* 2011; **197**: W359 [PMID: 21785067 DOI: 10.2214/AJR.10.5551]
- 72 **Cardinal JS**, Gunderman RB, Tarver RD. Informing patients about risks and benefits of radiology examinations: a review article. *J Am Coll Radiol* 2011; **8**: 402-408 [PMID: 21636054 DOI: 10.1016/j.jacr.2010.09.007]
- 73 **Pomara C**, Pascale N, Maglietta F, Neri M, Riezzi I, Turillazzi E. Use of contrast media in diagnostic imaging: medico-legal considerations. *Radiol Med* 2015; **120**: 802-809 [PMID: 26082145 DOI: 10.1007/s11547-015-0549-6]
- 74 **Hopper KD**, Zajdel M, Hulse SF, Yoanidis NR, TenHave TR, Labuski MR, Houts PS, Brensinger CM, Hartman DS. Interactive method of informing patients of the risks of intravenous contrast media. *Radiology* 1994; **192**: 67-71 [PMID: 8208968 DOI: 10.1148/radiology.192.1.8208968]
- 75 **Winterton RI**, Alaani A, Loke D, Bem C. Role of information leaflets in improving the practice of informed consent for patients undergoing septoplasty. *J Laryngol Otol* 2007; **121**: 134-137 [PMID: 17040592 DOI: 10.1017/S002221510600257X]
- 76 **Cowan EA**, Calderon Y, Gennis P, Macklin R, Ortiz C, Wall SP. Spanish and English video-assisted informed consent for intravenous contrast administration in the emergency department: a randomized controlled trial. *Ann Emerg Med* 2007; **49**: 221-230, 230.e1-230.e3 [PMID: 17011074 DOI: 10.1016/j.annemergmed.2006.07.934]
- 77 **Yucel A**, Gecici O, Emul M, Oyar O, Gulsoy UK, Dayanir YO, Acar M, Degirmenci B, Haktanir A. Effect of informed consent for intravascular contrast material on the level of anxiety: how much information should be given? *Acta Radiol* 2005; **46**: 701-707 [PMID: 16372689]
- 78 **Reimer P**, Vosschenrich R. Off-label use of contrast agents. *Eur Radiol* 2008; **18**: 1096-1101 [PMID: 18274752 DOI: 10.1007/s00330-008-0886-0]
- 79 **Thomsen HS**. For whom? *Acta Radiol* 2013; **54**: 473-475 [PMID: 24879877 DOI: 10.1177/0284185113479331]
- 80 **Walton SM**, Schumock GT, Alexander GC, Meltzer D, Stafford RS. Importance of distinguishing supported and unsupported off-label drug use. *Arch Intern Med* 2010; **170**: 657-658; author reply 658 [PMID: 20386014 DOI: 10.1001/archinternmed.2010.69]

P- Reviewer: Chen F, Li YZ, Sureka B **S- Editor:** Ji FF
L- Editor: A **E- Editor:** Zhao LM



Retrospective Cohort Study

Clinical significance of prostate ¹⁸F-labelled fluorodeoxyglucose uptake on positron emission tomography/computed tomography: A five-year review

Madhurima R Chetan, Tristan Barrett, Ferdia A Gallagher

Madhurima R Chetan, School of Clinical Medicine, University of Cambridge, Cambridge CB2 0SP, United Kingdom

Tristan Barrett, Ferdia A Gallagher, Department of Radiology, Addenbrooke's Hospital and University of Cambridge, Cambridge CB2 0QQ, United Kingdom

Author contributions: Chetan MR, Barrett T and Gallagher FA designed the research; Chetan MR performed the research; Chetan MR, Barrett T and Gallagher FA analysed the data; Chetan MR wrote the paper; Barrett T and Gallagher FA critically revised the manuscript for important intellectual content.

Institutional review board statement: The study was reviewed and approved by Addenbrooke's Hospital, Cambridge.

Informed consent statement: The requirement for informed consent for data analysis was waived.

Conflict-of-interest statement: The authors have no competing interests.

Data sharing statement: No additional data available.

Open-Access: This article is an open-access article which was selected by an in-house editor and fully peer-reviewed by external reviewers. It is distributed in accordance with the Creative Commons Attribution Non Commercial (CC BY-NC 4.0) license, which permits others to distribute, remix, adapt, build upon this work non-commercially, and license their derivative works on different terms, provided the original work is properly cited and the use is non-commercial. See: <http://creativecommons.org/licenses/by-nc/4.0/>

Manuscript source: Unsolicited manuscript

Correspondence to: Tristan Barrett, MB BS, BSc, MRCP, FRCR, Department of Radiology, Addenbrooke's Hospital and University of Cambridge, Box 218, Cambridge CB2 0QQ, United Kingdom. tb507@medschl.cam.ac.uk
Telephone: +44-1223-336890

Fax: +44-1223-330915

Received: September 20, 2016

Peer-review started: September 23, 2016

First decision: November 21, 2016

Revised: February 20, 2017

Accepted: March 21, 2017

Article in press: March 22, 2017

Published online: September 28, 2017

Abstract

AIM

To determine the significance and need for investigation of incidental prostatic uptake in men undergoing ¹⁸F-labelled fluorodeoxyglucose (¹⁸F-FDG) positron emission tomography/computed tomography (PET/CT) for other indications.

METHODS

Hospital databases were searched over a 5-year period for patients undergoing both PET/CT and prostate magnetic resonance imaging (MRI). For the initial analysis, the prostate was divided into six sectors and suspicious or malignant sectors were identified using MRI and histopathology reports respectively. Maximum and mean ¹⁸F-FDG standardised uptake values were measured in each sector by an investigator blinded to the MRI and histopathology findings. Two age-matched controls were selected per case. Results were analysed using a paired t-test and one-way ANOVA. For the second analysis, PET/CT reports were searched for prostatic uptake reported incidentally and these patients were followed up.

RESULTS

Over a 5-year period, 15 patients underwent both PET/

CT and MRI and had biopsy-proven prostate cancer. Malignant prostatic sectors had a trend to higher ^{18}F -FDG uptake than benign sectors, however this was neither clinically nor statistically significant (3.13 ± 0.58 vs 2.86 ± 0.68 , $P > 0.05$). ^{18}F -FDG uptake showed no correlation with the presence or histopathological grade of tumour. ^{18}F -FDG uptake in cases with prostate cancer was comparable to that from age-matched controls. Forty-six (1.6%) of 2846 PET/CTs over a 5-year period reported incidental prostatic uptake. Of these, 18 (0.6%) were investigated by PSA, 9 (0.3%) were referred to urology, with 3 (0.1%) undergoing MRI and/or biopsy. No cases of prostate cancer were diagnosed in patients with incidental ^{18}F -FDG uptake in our institute over a 5-year period.

CONCLUSION

^{18}F -FDG uptake overlaps significantly between malignant and benign prostatic conditions. Subsequent patient management was not affected by the reporting of incidental focal prostatic uptake in this cohort.

Key words: ^{18}F -labelled fluorodeoxyglucose; Positron emission tomography reporting; Positron emission tomography/computed tomography; Prostate cancer; Magnetic resonance imaging

© The Author(s) 2017. Published by Baishideng Publishing Group Inc. All rights reserved.

Core tip: ^{18}F -labelled fluorodeoxyglucose (^{18}F -FDG) uptake overlaps significantly between malignant and benign prostatic conditions. In a cohort of nearly 3000 patients over a 5-year period, the reporting of incidental elevated prostatic ^{18}F -FDG uptake did not affect subsequent clinical management or patient outcomes.

Chetan MR, Barrett T, Gallagher FA. Clinical significance of prostate ^{18}F -labelled fluorodeoxyglucose uptake on positron emission tomography/computed tomography: A five-year review. *World J Radiol* 2017; 9(9): 350-358 Available from: URL: <http://www.wjgnet.com/1949-8470/full/v9/i9/350.htm> DOI: <http://dx.doi.org/10.4329/wjcr.v9.i9.350>

INTRODUCTION

Positron emission tomography of ^{18}F -labelled fluorodeoxyglucose uptake combined with computed tomography (^{18}F -FDG PET/CT) is a mainstay of oncologic imaging. PET/CT imaging is well-tolerated and therefore has become a powerful tool for the diagnosis, staging and monitoring of many metabolically-active cancers. However, ^{18}F -FDG PET/CT imaging is not routinely used for detecting prostate cancer for both biological and technical reasons. Firstly, glucose uptake in well-differentiated prostatic adenocarcinoma is less avid than in many other

cancers due to low glycolytic activity^[1]. Secondly, urinary excretion of ^{18}F -FDG in the bladder and urethra can mask pathological uptake in the adjacent prostate. Thirdly, there is a large overlap in ^{18}F -FDG uptake between malignant disease, benign hyperplasia and inflammation of the prostate^[1].

In men undergoing ^{18}F -FDG PET/CT for unrelated reasons, incidental prostatic uptake is found in 0.6%-2.8% of studies^[1-5]. Although this is a small percentage of cases, it affects a large number of men given the growing number of PET/CT studies performed per year: 50000 annually in the UK and 2 million annually in the United States^[6,7]. The significance of such incidental uptake, together with the need for further investigation, is both uncertain and controversial.

A previous meta-analysis of prostatic uptake on ^{18}F -FDG PET/CT imaging showed that PET/CT cannot reliably differentiate benign from malignant disease, although only a small percentage of these patients underwent a definitive biopsy^[8]. The published positive predictive value of ^{18}F -FDG uptake for detecting prostate cancer ranges between 30% (in a low-risk population of men with bladder cancer undergoing radical prostatectomy) to 65% [in a high-risk population of men undergoing prostate magnetic resonance imaging (MRI)]^[9,10]. Some studies argue that the positive predictive value is increased if ^{18}F -FDG uptake shows a high SUV_{max} , the lesion is in a peripheral location and the CT demonstrates a lack of calcification^[11-13]. However, these features all show considerable overlap between malignant and benign disease.

Serum prostate-specific antigen (PSA), multiparametric prostate magnetic resonance imaging (mpMRI) and prostate biopsy can be used to investigate incidental prostatic ^{18}F -FDG uptake to determine if the patient has significant prostate cancer^[5,9]. However, there is no consensus on the management of patients with incidental prostatic ^{18}F -FDG uptake^[9].

In order to better understand the significance of incidental prostatic ^{18}F -FDG uptake, we investigated both the correlation of prostatic ^{18}F -FDG uptake with findings from MRI and histopathology, and the impact on patient management of reporting increased ^{18}F -FDG uptake in the prostate.

MATERIALS AND METHODS

Study design and patient population

This single-institution retrospective study was approved locally, with the need for informed consent for data analysis waived. The hospital radiology database was searched to identify a total of 2846 ^{18}F -FDG PET/CT studies performed on male patients in the period January 2010 to September 2015. For the first part of the study, 23 eligible men were identified who had both a prostate MRI and an ^{18}F -FDG PET/CT study. 15 of these men had prostate adenocarcinoma on

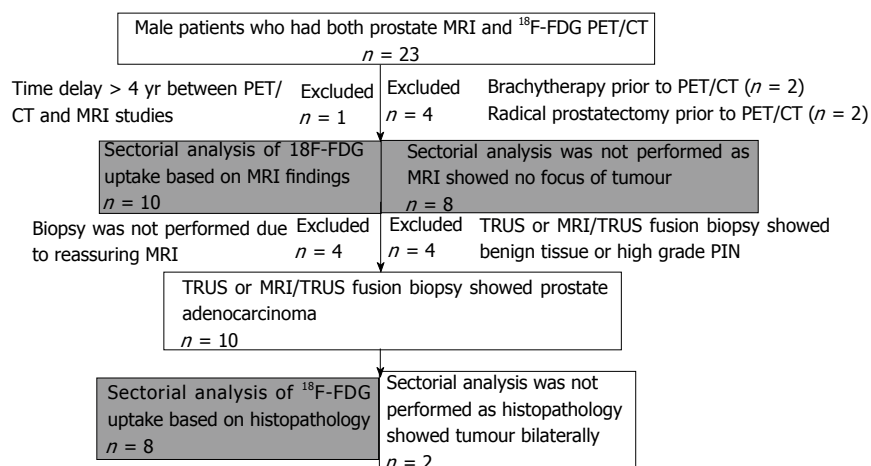


Figure 1 Flowchart showing inclusion and exclusion criteria for selection of cases for sector-based analysis.

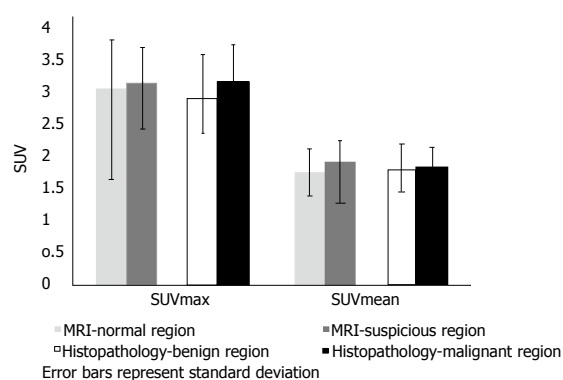


Figure 2 Sectorial analysis comparing ¹⁸F-labelled fluorodeoxyglucose uptake in sectors found to be suspicious on magnetic resonance imaging or malignant on histopathology with ¹⁸F-labelled fluorodeoxyglucose uptake in the remaining sectors. Mean values and standard deviations have been shown.

ultrasound-guided biopsy or MRI/ultrasound fusion biopsy. Five men were excluded (the prostate cancer was treated prior to undergoing PET/CT in 4 patients, and one patient had > 4 years between MRI and PET/CT). For the second part of the study, the ¹⁸F-FDG PET/CT reports were searched to identify patients with incidentally reported focal prostatic ¹⁸F-FDG uptake. Patient records were examined for details of follow-up investigations and management. Two cases were included in both the first and second parts of the study.

MRI and ¹⁸F-FDG PET/CT analysis

A proprietary workstation and software (Volume Viewer, Advantage Workstation, GE Healthcare, Milwaukee, WI, United States) were used to review the ¹⁸F-FDG PET/CT images. The prostate was divided into six sectors: Left and right sides at the apex, mid-zone and base of the gland. Standardised uptake values (SUV) in each sector were measured by an investigator who was blinded to the MRI and histopathological findings. A threshold of 75% of the SUV_{max} was used to

calculate the SUV_{mean}^[14].

MRI reports were used to identify the prostatic sectors that were suspicious for tumour. Histopathology reports were used to identify the prostatic lobe(s) in which cancer had been detected. Sectorial analysis could not be performed for patients with no tumour focus on MRI, or bilateral tumour on histopathology (Figure 1).

Age-matched controls undergoing ¹⁸F-FDG PET/CT but without prostate cancer were randomly selected for each case from PET/CT studies recently undertaken in the department; two controls for each case were acquired. Age matching within 18 mo was used as the criterion, and patients with a known tumour close to the prostate were excluded.

Statistical analysis

A paired two-tailed student's *t*-test was used to compare the ¹⁸F-FDG uptake within suspicious or malignant sectors, with that in the remaining prostate for each individual patient. A paired two-tailed student's *t*-test was also used to compare prostatic ¹⁸F-FDG uptake in patients with that from the controls. A one-way ANOVA was used to compare prostatic ¹⁸F-FDG uptake between histopathological subgroups. Statistical analyses were performed using GraphPad Prism version 6.00 (GraphPad Software, La Jolla, CA, United States).

RESULTS

Eighteen patients who had both ¹⁸F-FDG PET/CT and prostate MRI studies were included in the first part of the study. The median age was 72 years, median PSA was 7.30 ng/mL and median time difference between the ¹⁸F-FDG PET/CT and the prostate MRI was 11.5 mo. See Table 1 for patient characteristics.

There was a trend for a higher ¹⁸F-FDG uptake in prostatic sectors shown to be suspicious on MRI or

Table 1 Characteristics of patients who had both ¹⁸F-labelled fluorodeoxyglucose positron emission tomography/computed tomography and prostate magnetic resonance imaging studies

Age (yr)	MRI before or after PET/CT?	¹⁸ F-FDG PET/CT indication	Prostate SUV _{max}	Prostate MRI indication	MRI result	PSA (ng/mL)	Biopsy result
73	2 mo before	Bone metastases (prostate primary)	3.4	Negative TRUS biopsy	T2aNxMx	20.8	Gleason 4 + 5 = 9
72	11 mo after	Non-Hodgkin lymphoma	2.7	Elevated PSA, negative TRUS biopsy	T2aNxMx	8.8	Gleason 5 + 3 = 8
62	3 mo after	Cancer of unknown primary	3.9	Prostate cancer staging	T3bNxMx	37	Gleason 4 + 3 = 7
75	46 mo after	Head and neck cancer	3.4	Active surveillance	T1NxMx	2.28	Gleason 4 + 3 = 7
76	6 mo before	Gastrointestinal stromal tumour	3	Elevated PSA, negative TRUS biopsy	T2bNxMx	150	Gleason 3 + 4 = 7
79	22 mo after	Non-Hodgkin lymphoma	2.9	Elevated PSA	T2aNxMx	5.4	Gleason 3 + 4 = 7
66	30 mo after	Non-Hodgkin lymphoma	3.1	Active surveillance	T2cNxMx	4.8	Gleason 3 + 4 = 7
73	26 mo after	Oesophageal cancer	2.4	Active surveillance	T2cNxMx	7.8	Gleason 3 + 3 = 6
68	18 mo after	Cancer of unknown primary	3.9	Elevated PSA	T2aNxMx	6.1	Gleason 3 + 3 = 6
74	5 mo before	Oesophageal cancer	3.9	Elevated PSA	T1NxMx	7.3	Gleason 3 + 3 = 6
68	5 mo before	Hodgkin lymphoma	9.9	Elevated PSA, negative biopsy	No focus of tumour	4.7	High-grade PIN
65	39 mo before	Colorectal cancer	5.2	Elevated PSA, negative TRUS biopsy	No focus of tumour	8.6	High-grade PIN
76	34 mo before	Non-Hodgkin lymphoma	4.2	Elevated PSA	Suspicious foci bilaterally	15	Benign
67	4 mo before	Non-Hodgkin lymphoma	4.1	Incidental prostatic ¹⁸ F-FDG uptake	Suspicious foci bilaterally	5.5	Benign
72	16 mo after	Pyrexia of unknown origin	2.7	Chronic urinary infection	Likely prostatitis	Not done	Biopsy not performed
78	1 mo after	Non-Hodgkin lymphoma	3.1	Elevated PSA	No focus of tumour	11.4	Biopsy not performed
61	12 mo after	Lung nodule	5.2	Elevated PSA, positive family history	No focus of tumour	4.5	Biopsy not performed
68	7 mo after	Colorectal cancer	8.8	Incidental prostatic ¹⁸ F-FDG uptake	No focus of tumour	3	Biopsy not performed

SUV: Standardised uptake value, PSA: Prostate specific antigen, TRUS: Transrectal ultrasound.

Table 2 Sectorial analysis, case-control analysis and subgroup analysis showed no significant difference in ¹⁸F-labelled fluorodeoxyglucose uptake

	Mean SUV _{max}	Mean SUV _{mean}
Sectorial analysis		
MRI - normal prostatic sectors	3.02	1.74
MRI - suspicious prostatic sectors	3.1	1.89
Histopathology - benign prostatic lobe	2.86	1.79
Histopathology - malignant prostatic lobe	3.13	1.82
Case-control analysis		
Age-matched controls	3.09	1.83
Cases with prostate cancer	3.26	1.81
Subgroup analysis		
Biopsy not performed	4.95	1.91
Benign disease and high-grade PIN	5.85	2.86
Low-grade prostate cancer (Gleason ≤ 3 + 4)	3.2	1.83
High-grade prostate cancer (Gleason score ≥ 4 + 3)	3.35	1.78

SUV: Standardised uptake value, PIN: Prostatic intraepithelial neoplasia.

malignant on histopathology, compared to those in the

remainder of the prostate, but this was not statistically significant (Figure 2). There was no significant difference in ¹⁸F-FDG uptake between cases with prostate cancer and age-matched controls undergoing PET/CT who did not have prostate cancer. Patients were classified into the following subgroups according to histopathology findings: biopsy not performed ($n = 4$), benign biopsy or high-grade prostatic intraepithelial neoplasia (PIN) ($n = 4$), low-grade prostate cancer with Gleason score $\leq 3 + 4$ ($n = 6$), and high-grade prostate cancer with Gleason score $\geq 4 + 3$ ($n = 4$). ¹⁸F-FDG uptake was not significantly different between subgroups; we therefore found no correlation between prostatic ¹⁸F-FDG uptake and the presence or grade of tumour confirmed on histopathology. Figure 3 illustrates a representative case of a 70-year-old man with high-grade prostate cancer that showed no uptake on PET/CT. See Table 2 for mean values of SUV_{max} and SUV_{mean} derived from sectorial, case-control and subgroup analysis.

For the second part of the study, 2846 male patients undergoing ¹⁸F-FDG PET/CT over a 5-year period were followed-up. 46 men (1.6%) had an

Table 3 Characteristics of patients in whom elevated prostatic ^{18}F -labelled fluorodeoxyglucose uptake was investigated

Age (yr)	^{18}F -FDG PET/CT indication	Prostate SUVmax	PSA (ng/mL)	Urology referral made	Urology outcome
68	Adrenal nodule	10.4	3	Yes	MRI - no suspicious foci
77	Lung nodule	4.5	2.78	Yes	Biopsy - high-grade PIN
67	Non-Hodgkin lymphoma	4.5	5.5	Yes	MRI - suspicious foci Biopsy - benign
68	Colorectal cancer	5.9	3.04	Yes	PSA monitoring
58	Colorectal cancer	7.6	1.38	Yes	PSA monitoring
64	Non-Hodgkin lymphoma	5.4	1.84	Yes	PSA monitoring
58	Non-Hodgkin lymphoma	19.9	7.44	Yes	PSA monitoring
81	Cholangiocarcinoma	10.3	18	Yes	Lost to follow up
75	Hepatic metastases (colorectal primary)	8	-	Yes	Lost to follow up
61	Colorectal cancer	14	1.47	No - PSA normal	
55	Paraneoplastic syndrome	4.8	0.62	No - PSA normal	
61	Non-Hodgkin lymphoma	5.8	2.85	No - PSA normal	
68	Gastrointestinal stromal tumour	13.2	1.48	No - PSA normal	
71	Hepatic metastases (colorectal primary)	9.2	4.9	No - palliative care	
87	Oesophageal cancer	5.3	11.86	No - palliative care	
82	Colorectal cancer	15.4	3.85	No - palliative care	
35	Hodgkin lymphoma	11.8	3.04	No - suspected prostatitis	
71	Oesophageal cancer	7.3	4.58	No - likely urethral uptake	

SUV: Standardised uptake value; PSA: Prostate specific antigen; PIN: Prostatic intraepithelial neoplasia.

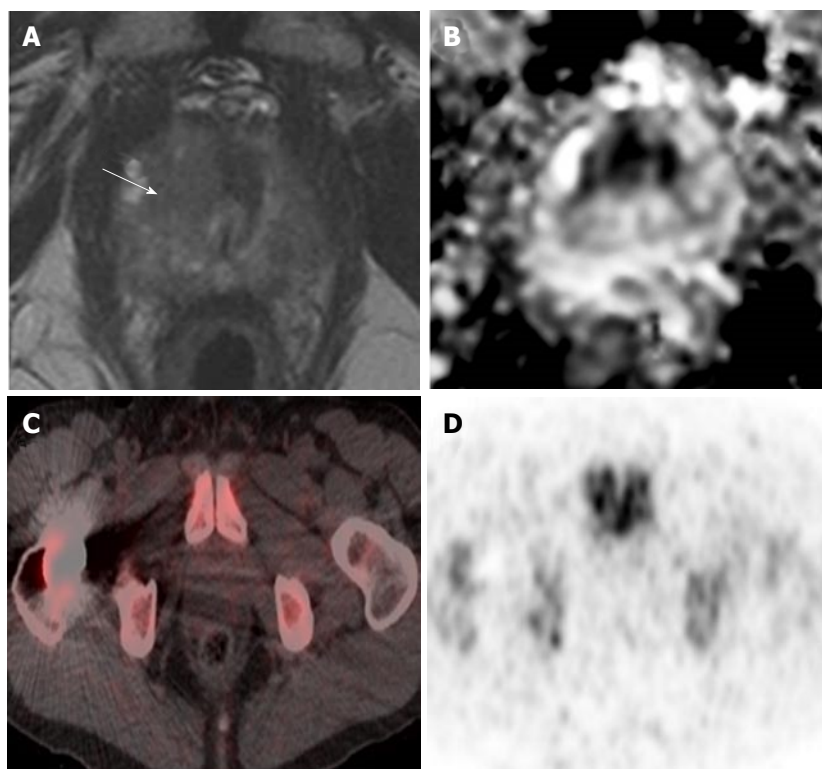


Figure 3 High-grade prostate cancer showing no increased uptake on positron emission tomography/computed tomography in a 73-year-old man. A, B: Prostate MRI performed for raised PSA (19 ng/mL) showed a high probability lesion in the right apex transition zone (arrow in A) with matching restricted diffusion on the ADC map (B). Subsequent targeted transperineal biopsy confirmed Gleason 4 + 5 disease in 40% of cores; C, D: PET/CT performed after a two-month interval and no intervening treatment showed no focal uptake in this region shown as both fused PET/CT imaging (C) and PET alone (D). PET/CT: Positron emission tomography/computed tomography; MRI: Magnetic resonance imaging; ADC: Apparent diffusion co-efficient; PSA: Prostate specific antigen.

incidental and unexplained finding of elevated prostatic ^{18}F -FDG uptake. 18 (0.6%) of these patients underwent further investigation. They had a median age of 68 years, median prostatic SUV_{max} of 7.80 and median PSA of 3.04 ng/mL. See Table 3 for patient characteristics.

Of these 18 men, 9 (0.3%) were referred to urology. Two men had a prostate biopsy, which showed benign disease and high-grade PIN respectively (Figure 4). No cases of prostate cancer were diagnosed in the 5-year period. See Figure 5 for more detailed clinical outcomes.

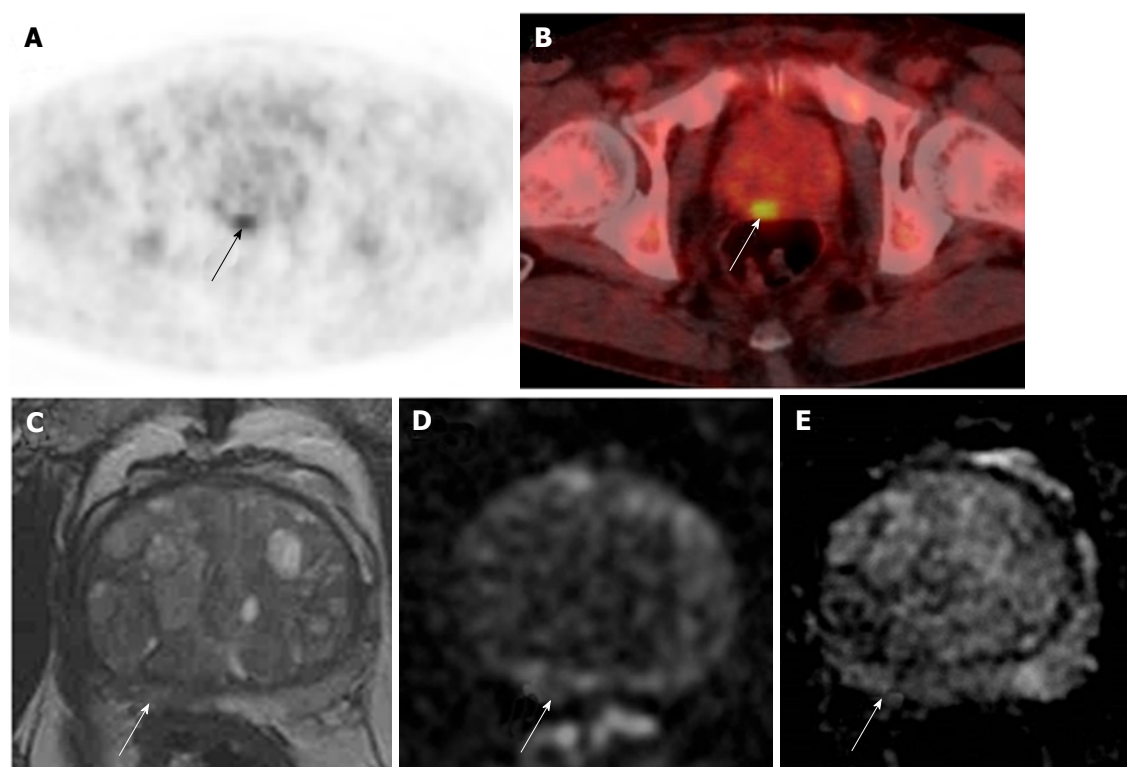


Figure 4 Incidental prostatic ^{18}F -labelled fluorodeoxyglucose uptake in a 67-year-old patient with Stage IV diffuse large B-cell lymphoma. A, B: Focal uptake in the posterior right peripheral zone of the prostate at the level of the mid-gland as demonstrated on PET (A) and fused PET/CT (B); SUV_{max} = 4.5; C-E: Prostate MRI shows non-specific geographical intermediate signal on T2-weighted imaging (C), but with no matching restricted diffusion on b-1400 diffusion-weighted images (D) or ADC maps (E). The MRI findings are low probability for tumour. Subsequent transrectal ultrasound-guided biopsy showed no cancer. PET/CT: Positron emission tomography/computed tomography; MRI: Magnetic resonance imaging; ADC: Apparent diffusion co-efficient.

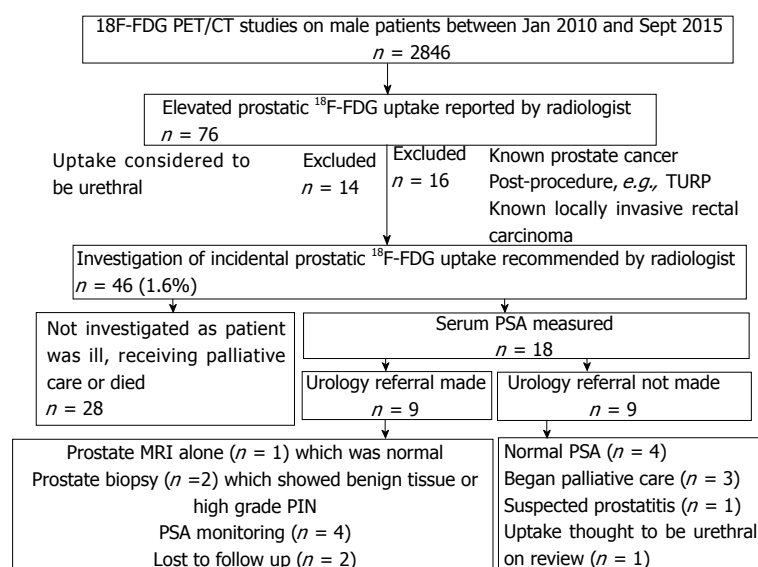


Figure 5 Flowchart showing clinical outcomes in patients with elevated prostatic ^{18}F -labelled fluorodeoxyglucose uptake.

DISCUSSION

Prostate cancer is the commonest male cancer^[15]. There is therefore a potentially high incidence of synchronous prostatic tumour in patients undergoing ^{18}F -FDG PET/CT for other indications. However, PET/CT lacks specificity and sensitivity for primary detection

of prostate cancer; consequently it is unclear how patients with incidental tracer uptake in the prostate should be managed. Our study has shown that focal ^{18}F -FDG uptake is not indicative of prostate cancer in this cohort, with SUV_{mean} and SUV_{max} values significantly overlapping between malignant and benign conditions, and that the reporting of incidental prostatic uptake

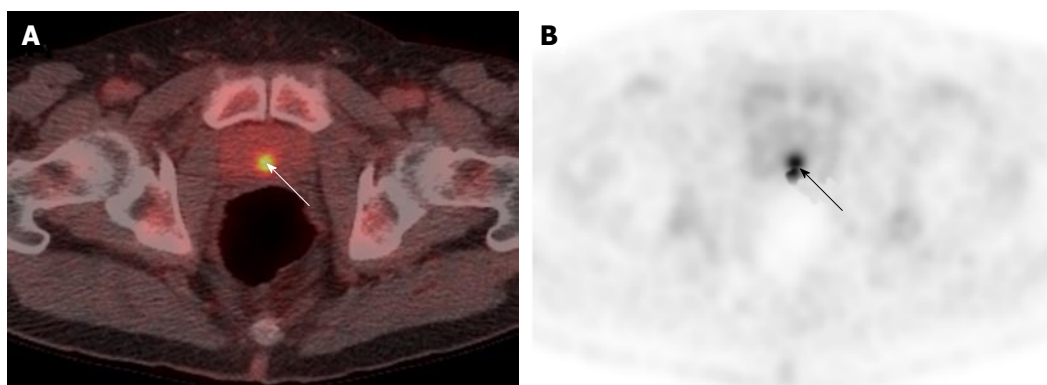


Figure 6 Midline uptake on ^{18}F -labelled fluorodeoxyglucose positron emission tomography/computed tomography in a 71-year-old man with oesophageal carcinoma and serum prostate specific antigen of 4.58 ng/mL. A, B: Fused PET/CT and PET-only imaging shows focal uptake in the midline of the prostate (arrowed). The uptake was considered to be tracer in the urethra given its anatomical location. PET/CT: Positron emission tomography/computed tomography.

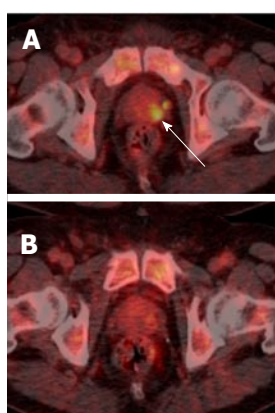


Figure 7 Resolving focal prostatic uptake in a 61-year-old man with Stage IV high-grade non-Hodgkin's lymphoma and serum prostate-specific antigen of 2.85 ng/mL. A: Fused PET/CT imaging performed after 2 cycles of chemotherapy shows focal uptake (arrowed) in the left side of the prostate at the level of the midgland on fused PET/CT; B: Repeat PET/CT performed 4 mo later following completing of 6 cycles of chemotherapy demonstrates resolution of this focal uptake. PET/CT: Positron emission tomography/computed tomography.

did not affect subsequent clinical management of any patient in our institute over a 5-year period.

Sector-based analysis showed that, in individual patients, malignant prostatic sectors had a trend to higher ^{18}F -FDG uptake than benign sectors. However, this difference was not statistically significant and total prostate ^{18}F -FDG uptake in men with prostate cancer was comparable to that from age-matched controls. Comparison of ^{18}F -FDG uptake across patient subgroups showed no correlation between ^{18}F -FDG uptake and histopathological findings. Although some authors have suggested that ^{18}F -FDG uptake weakly correlates with Gleason score, the small numbers in our study did not demonstrate this finding^[9,16]. In fact, we observed a higher SUV_{max} and SUV_{mean} in patients with no biopsy, benign biopsy or high grade PIN than in patients with prostate cancer. This may be partially explained by increased ^{18}F -FDG uptake in prostatitis, where there is also increased glucose uptake within the inflammatory tissue^[17].

Incidental and unexplained prostate uptake was found in 1.6% of all ^{18}F -FDG PET/CT studies in male patients, which is comparable to the rate reported previously^[3-5]. These patients had a median SUV_{max} of 7.8, which is suspicious for tumour; other authors have suggested an SUV_{max} greater than 6.0 should be considered as a cut-off value for high-grade prostate cancer^[9]. Only 40% of patients with incidental and unexplained prostatic uptake were investigated with a serum PSA. Twenty percent of patients were referred to a urologist, and only one-third of these patients underwent further investigation with either biopsy or MRI. This may reflect the fact that the existing cancer diagnosis is the primary factor in determining clinical prognosis, and that the subsequent detection of prostate cancer would not significantly affect patient management due to unsuitability for radical therapy. Another possibility is a reluctance to perform a transrectal prostate biopsy in patients undergoing chemotherapy due to the risk of sepsis. In some patients, incidental prostatic uptake was not investigated for different reasons, *e.g.*, uptake was thought to represent tracer in the urethra upon review (Figure 6), or uptake resolved on repeat PET/CT (Figure 7). Ultimately over a 5-year period in our centre, involving nearly three thousand ^{18}F -FDG PET/CT studies, no change in patient management occurred as a result of an incidental finding of elevated prostatic ^{18}F -FDG uptake. Therefore, our retrospective study questions the need to investigate incidental prostatic uptake of ^{18}F -FDG in men undergoing PET/CT.

Our study has some limitations. Firstly, as a retrospective study our population consisted of patients who underwent ^{18}F -FDG PET/CT primarily for other malignancies, and therefore the time difference between PET/CT and MRI was long in some cases (up to 46 mo). This timescale is similar to previously reported retrospective studies and given that the natural history of prostate cancer is one of a slow-growing tumour, most prostate cancers will be present for years before clinical presentation^[10,18]. Secondly,

the number of eligible patients in our study was small. Thirdly, patients in our study had ultrasound-guided biopsy or MRI/ultrasound fusion biopsy, which are less sensitive in detecting prostate cancer than whole-mount histology derived from prostatectomy samples.

In conclusion, ¹⁸F-FDG uptake has low clinical utility in distinguishing benign and malignant prostatic disease. Reporting incidental prostatic uptake did not affect subsequent patient management or clinical outcomes in this cohort of patients. This study suggests there may be little benefit in investigating incidental elevated prostatic ¹⁸F-FDG uptake on PET/CT which should be addressed with future large prospective studies.

COMMENTS

Background

¹⁸F-labelled fluorodeoxyglucose (¹⁸F-FDG) uptake on positron emission tomography/computed tomography (PET/CT) is used extensively in the diagnosis, staging and monitoring of many cancers. Incidental elevated prostatic ¹⁸F-FDG uptake is found in a significant proportion of men undergoing PET/CT for unrelated reasons. ¹⁸F-FDG PET/CT is not routinely used in prostate cancer because of the relatively low metabolic activity of prostate cancer, the proximity to tracer in the urethra and the presence of significant ¹⁸F-FDG uptake in benign and inflammatory prostatic disease.

Research frontiers

The significance of incidental prostatic uptake, together with the need for further investigation, is unclear.

Innovations and breakthroughs

The results suggest that incidental prostatic uptake has no significant correlation with prostate magnetic resonance imaging or biopsy findings. In a cohort of nearly 3000 men over 5 years, reporting incidental prostatic ¹⁸F-FDG uptake did not alter patient management or clinical outcomes.

Applications

The results suggest there is little benefit in investigating incidental elevated prostatic ¹⁸F-FDG uptake.

Peer-review

This is an interesting study which investigates the clinical significance of incidental FDG uptake. Although the number of eligible patients was small, this is an well written retrospective study.

REFERENCE

- 1 Takahashi N, Inoue T, Lee J, Yamaguchi T, Shizukuishi K. The roles of PET and PET/CT in the diagnosis and management of prostate cancer. *Oncology* 2007; **72**: 226-233 [PMID: 18176088 DOI: 10.1159/000112946]
- 2 Picchio M, Mapelli P, Panebianco V, Castellucci P, Incerti E, Briganti A, Gandaglia G, Kirienko M, Barchetti F, Nanni C, Montorsi F, Gianolli L, Fanti S. Imaging biomarkers in prostate cancer: role of PET/CT and MRI. *Eur J Nucl Med Mol Imaging* 2015; **42**: 644-655 [PMID: 25595344 DOI: 10.1007/s00259-014-2982-5]
- 3 Kang PM, Seo WI, Lee SS, Bae SK, Kwak HS, Min K, Kim W, Kang DI. Incidental abnormal FDG uptake in the prostate on 18-fluoro-2-deoxyglucose positron emission tomography-computed tomography scans. *Asian Pac J Cancer Prev* 2014; **15**: 8699-8703 [PMID: 25374193 DOI: 10.7314/APJCP.2014.15.20.8699]
- 4 Seino H, Ono S, Miura H, Morohashi S, Wu Y, Tsushima F, Takai Y, Kijima H. Incidental prostate ¹⁸F-FDG uptake without calcification indicates the possibility of prostate cancer. *Oncol Rep* 2014; **31**: 1517-1522 [PMID: 24503866 DOI: 10.3892/or.2014.3011]
- 5 Kwon T, Jeong IG, You D, Hong JH, Ahn H, Kim CS. Prevalence and clinical significance of incidental (18F)-fluoro-2-deoxyglucose uptake in prostate. *Korean J Urol* 2015; **56**: 288-294 [PMID: 25874042]
- 6 NHS England. NHS Commissioning B02. PET-CT. [accessed 2016 Jan 22]. Available from: URL: <https://www.england.nhs.uk/commissioning/spec-services/npc-crg/group-b/b02/>
- 7 Czernin J, Allen-Auerbach M, Nathanson D, Herrmann K. PET/CT in Oncology: Current Status and Perspectives. *Curr Radiol Rep* 2013; **1**: 177-190 [PMID: 24883234 DOI: 10.1007/s40134-013-0016-x]
- 8 Bertagna F, Sadeghi R, Giovannella L, Treglia G. Incidental uptake of 18F-fluorodeoxyglucose in the prostate gland. Systematic review and meta-analysis on prevalence and risk of malignancy. *Nuklearmedizin* 2014; **53**: 249-258 [PMID: 25170975 DOI: 10.3413/Nukmed-0668-14-05]
- 9 Reesink DJ, Fransen van de Putte EE, Vegt E, De Jong J, van Werkhoven E, Mertens LS, Bex A, van der Poel HG, van Rhijn BW, Horenblas S, Meijer RP. Clinical Relevance of Incidental Prostatic Lesions on FDG-Positron Emission Tomography/Computerized Tomography-Should Patients Receive Further Evaluation? *J Urol* 2016; **195**: 907-912 [PMID: 26598424 DOI: 10.1016/j.juro.2015.11.025]
- 10 Brown AM, Lindenberg ML, Sankineni S, Shih JH, Johnson LM, Pruthy S, Kurdziel KA, Merino MJ, Wood BJ, Pinto PA, Choyke PL, Turkbey B. Does focal incidental 18F-FDG PET/CT uptake in the prostate have significance? *Abdom Imaging* 2015; **40**: 3222-3229 [PMID: 26239399 DOI: 10.1007/s00261-015-0520-y]
- 11 Hwang I, Chong A, Jung SI, Hwang EC, Kim SO, Kang TW, Kwon DD, Park K, Ryu SB. Is further evaluation needed for incidental focal uptake in the prostate in 18-fluoro-2-deoxyglucose positron emission tomography-computed tomography images? *Ann Nucl Med* 2013; **27**: 140-145 [PMID: 23076866 DOI: 10.1007/s12149-012-0663-7]
- 12 Yang Z, Hu S, Cheng J, Xu J, Shi W, Zhu B, Zhang Y, Yao Z, Pan H, Zhang Y. Prevalence and risk of cancer of incidental uptake in prostate identified by fluorine-18 fluorodeoxyglucose positron emission tomography/computed tomography. *Clin Imaging* 2014; **38**: 470-474 [PMID: 24629790 DOI: 10.1016/j.clinimag.2014.01.019]
- 13 Han EJ, H O J, Choi WH, Yoo IR, Chung SK. Significance of incidental focal uptake in prostate on 18-fluoro-2-deoxyglucose positron emission tomography CT images. *Br J Radiol* 2010; **83**: 915-920 [PMID: 20965901 DOI: 10.1259/bjr/19887771]
- 14 Gerety EL, Lawrence EM, Wason J, Yan H, Hilborne S, Buscombe J, Cheow HK, Shaw AS, Bird N, Fife K, Heard S, Lomas DJ, Matakidou A, Soloviev D, Eisen T, Gallagher FA. Prospective study evaluating the relative sensitivity of 18F-NaF PET/CT for detecting skeletal metastases from renal cell carcinoma in comparison to multidetector CT and 99mTc-MDP bone scintigraphy, using an adaptive trial design. *Ann Oncol* 2015; **26**: 2113-2118 [PMID: 26202597 DOI: 10.1093/annonc/mdv289]
- 15 Siegel R, Ma J, Zou Z, Jemal A. Cancer statistics, 2014. *CA Cancer J Clin* 2014; **64**: 9-29 [PMID: 24399786 DOI: 10.3322/caac.21208]
- 16 Chang JH, Lim Joon D, Lee ST, Hiew CY, Esler S, Gong SJ, Wada M, Clouston D, O'Sullivan R, Goh YP, Tochon-Danguy H, Chan JG, Bolton D, Scott AM, Khoo V, Davis ID. Diffusion-weighted MRI, 11C-choline PET and 18F-fluorodeoxyglucose PET for predicting the Gleason score in prostate carcinoma. *Eur Radiol* 2014; **24**: 715-722 [PMID: 24192979 DOI: 10.1007/s00330-013-3045-1]
- 17 Lin KH, Chen YS, Hu G, Tsay DG, Peng NJ. Chronic bacterial prostatitis detected by FDG PET/CT in a patient presented with fever of unknown origin. *Clin Nucl Med* 2010; **35**: 894-895 [PMID: 20940554 DOI: 10.1097/RLU.0b013e3181f49e57]
- 18 Draisma G, Etzioni R, Tsodikov A, Mariotto A, Wever E, Gulati

R, Feuer E, de Koning H. Lead time and overdiagnosis in prostate-specific antigen screening: importance of methods and context.

J Natl Cancer Inst 2009; **101**: 374-383 [PMID: 19276453 DOI: 10.1093/jnci/djp001]

P- Reviewer: Kucherlapati MH, Lim SM **S- Editor:** Kong JX
L- Editor: A **E- Editor:** Zhao LM



Retrospective Study

Reliability of the pronator quadratus fat pad sign to predict the severity of distal radius fractures

Julia Loesaus, Isabel Wobbe, Erik Stahlberg, Joerg Barkhausen, Jan Peter Goltz

Julia Loesaus, Isabel Wobbe, Erik Stahlberg, Joerg Barkhausen, Jan Peter Goltz, Department for Radiology, Neuroradiology and Nuclear Medicine, University Hospital of Schleswig-Holstein, 23538 Lübeck, Germany

Author contributions: Loesaus J and Goltz JP contributed to study conception and design; Loesaus J and Goltz JP contributed to acquisition of data; Loesaus J and Stahlberg E contributed to analysis and interpretation of data; Loesaus J and Goltz JP contributed to drafting of manuscript; Wobbe I and Barkhausen J contributed to critical revision.

Institutional review board statement: This study was reviewed and approved by the University Hospital of Schleswig-Holstein.

Informed consent statement: All study participants, or their legal guardian, provided informed written consent prior to study enrollment.

Conflict-of-interest statement: The authors certify that they have no affiliations with or involvement in any organization or entity with any financial interest, or any non-financial interest in the subject matter or materials discussed in this manuscript.

Data sharing statement: Technical appendix, statistical code, and dataset available from the corresponding author at j.loesaus@gmail.com. Participants gave informed consent for data sharing.

Open-Access: This article is an open-access article which was selected by an in-house editor and fully peer-reviewed by external reviewers. It is distributed in accordance with the Creative Commons Attribution Non Commercial (CC BY-NC 4.0) license, which permits others to distribute, remix, adapt, build upon this work non-commercially, and license their derivative works on different terms, provided the original work is properly cited and the use is non-commercial. See: <http://creativecommons.org/licenses/by-nc/4.0/>

Manuscript source: Unsolicited manuscript

Correspondence to: Julia Loesaus, MD, Department for Radiology, Neuroradiology and Nuclear Medicine, University Hospital of Schleswig-Holstein, Campus Lübeck, Ratzeburger

Allee 160, 23538 Lübeck, Germany. loesausj@klifue.de
Telephone: +49-451-50017001
Fax: +49-451-50017004

Received: January 19, 2017

Peer-review started: January 20, 2017

First decision: May 22, 2017

Revised: June 26, 2017

Accepted: July 14, 2017

Article in press: July 17, 2017

Published online: September 28, 2017

Abstract

AIM

To evaluate the reliability of pronator quadratus fat pad sign to detect distal radius fracture and to predict its severity.

METHODS

Retrospectively we identified 89 consecutive patients (41 female, mean age 49 ± 18 years) who had X-ray (CR) and computed tomography (CT) within 24 h following distal forearm trauma. Thickness of pronator quadratus fat pad complex (PQC) was measured using lateral views (CR) and sagittal reconstructions (CT). Pearson's test was used to determine the correlation of the PQC thickness in CR and CT. A positive pronator quadratus sign (PQS) was defined as a PQC > 8.0 mm (female) or > 9.0 mm (male). Frykman classification was utilized to assess the severity of fractures.

RESULTS

Forty-four/89 patients (49%) had a distal radius fracture (Frykman I $n = 3$, II $n = 0$, III $n = 10$, IV $n = 5$, V $n = 2$, VI $n = 2$, VII $n = 9$, VIII $n = 13$). Mean thickness of the PQC thickness can reliably be measured on X-ray views and was 7.5 ± 2.8 mm in lateral views (CR), respectively 9.4 ± 3.0 mm in sagittal reconstructions (CT), resulting in a significant correlation coefficient

of 0.795. A positive PQS at CR was present in 21/44 patients (48%) with distal radius fracture and in 2/45 patients (4%) without distal radius fracture, resulting in a specificity of 96% and a sensitivity of 48% for the detection of distal radius fractures. There was no correlation between thickness of the PQC and severity of distal radius fractures.

CONCLUSION

A positive PQS shows high specificity but low sensitivity for detection of distal radius fractures. The PQC thickness cannot predict the severity of distal radius fractures.

Key words: Pronator quadratus fat pad sign; Pronator quadratus complex; Distal radius fracture; Frykman classification; Conventional radiograph; Computed tomography

© The Author(s) 2017. Published by Baishideng Publishing Group Inc. All rights reserved.

Core tip: This study evaluated reliability of pronator quadratus fat pad sign (PQS) to detect distal radius fracture and to predict its severity. Therefore correlation of measurements of pronator quadratus complex (PQC) on conventional lateral radiographs (CR) and sagittal reconstructions of computed tomographies (CT), also regarding the severity of fractures were analyzed. In conclusion PQC thickness can reliably be measured on lateral CR and correlates with CT. Sensitivity of PQS for detecting fractures is low, but specificity is high. Therefore a positive PQS in putative negative radiograph should trigger further investigations, *e.g.*, CT scan. PQC thickness cannot predict severity of wrist fractures.

Loesaus J, Wobbe I, Stahlberg E, Barkhausen J, Goltz JP. Reliability of the pronator quadratus fat pad sign to predict the severity of distal radius fractures. *World J Radiol* 2017; 9(9): 359-364 Available from: URL: <http://www.wjgnet.com/1949-8470/full/v9/i9/359.htm> DOI: <http://dx.doi.org/10.4329/wjcr.v9.i9.359>

INTRODUCTION

Soft tissue alterations or signs may be helpful when radiographs are assessed for fractures and have been used to detect occult bone injuries^[1]. Regarding the wrist the "navicular fat stripe" and the "pronator quadratus sign" (PQS) have been described. Mac Ewan was first to characterize the pronator quadratus fat pad sign consisting of a radiolucent (fat containing) stripe which runs parallel to the pronator quadratus muscle covering the distal radius and ulnar (Figure 1)^[1,2]. Studies on healthy subjects have shown that thickness of the pronator quadratus complex (PQC) is significantly greater in men (values up to 9 mm) than

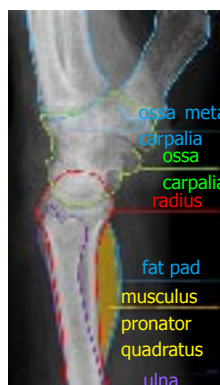


Figure 1 Anatomical sketch of conventional radiograph on lateral view of wrist.

in women (values up to 8 mm) and increases with age^[3,4].

In the case of a trauma to the distal radius or ulna this radiolucent stripe may be deformed or displaced, probably related to edema or hematoma within the pronator quadratus muscle^[5,6]. In the majority of lateral conventional radiographs this fat pad can be identified. In the past several studies have analyzed the usefulness of the PQS to detect subtle fractures or inflammation of adjacent e in their detecting^[7]. Sensitivity of the PQS measured on lateral X-rays to detect occult fractures^[3,4,5,7]. While earlier studies described the PQS as a useful adjunctive to detect subtle fractures^[1], more recent studies, which used MRI as a reference, have found this sign to be unreliable. Distal forearm fractures has been reported to range between 26% and 65%. Specificity however has been found to be 69%-70%^[4,8], indicating that absence of the PQS does not necessarily exclude an (occult) fracture, while its presence should trigger further investigations to rule out an underlying pathology. More recent data suggest that a certain muscle-to-bone ratio (maximum pronator quadratus thickness and distal radial thickness at same levels) might be a useful index for the diagnosis of non-displaced and occult distal forearm fracture^[9]. Besides detection of a distal radius fracture, classification and evaluation of the injury extent play a role during work-up of extremity trauma cases. So far conventional X-ray underestimates the severity of distal radius fracture when compared to computed tomography or the intraoperative situs^[10,11]. In this context the PQS has not been evaluated for predicting the severity of an underlying fracture to the distal radius up to today.

Therefore the presented study analyzes: (1) the correlation of measurements of the pronator quadratus complex on conventional lateral radiographs and sagittal reconstructions of computed tomographies; (2) the sensitivity and specificity of the PQS on conventional lateral radiographs with computed tomography as the reference; and (3) the reliability of the PQS to predict the severity of an underlying fracture.

Table 1 Distribution ($n = 44$) of distal radius fractures according to the Frykman classification

Frykman-classification	
I	3
II	0
III	10
IV	5
V	2
VI	2
VII	9
VIII	13

Table 2 Thickness of the pronator quadratus complex measured on lateral conventional radiographs and sagittal reconstructions of a computed tomography

	Total ($n = 89$)	With fracture ($n = 44$)	Without fracture ($n = 45$)
CR (mm)	7.5 ± 2.8	8.8 ± 2.9	6.2 ± 1.8
CT (mm)	9.4 ± 3.0	10.9 ± 3.1	7.8 ± 2.0
Correlation coefficient	0.795	0.74	0.695

CR: Conventional radiographs; CT: Computed tomography.

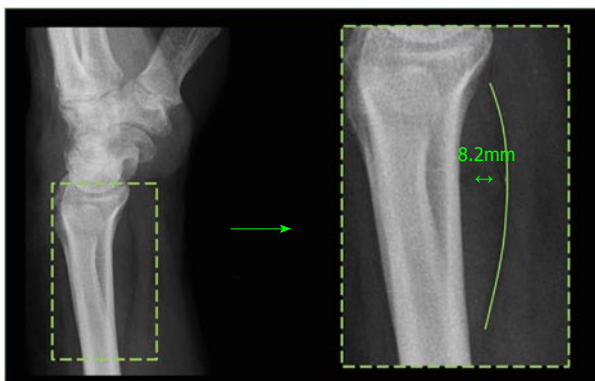


Figure 2 Measurement of the pronator quadratus complex on a lateral conventional radiograph.

MATERIALS AND METHODS

Institutional Review Board approval (Ethic votum No. 15-097A) was granted. Between 01/2010 and 08/2013 we retrospectively identified 89 patients (41 women, 48 men, mean age 49 ± 18 years) with conventional radiographs of the wrist, who had undergone an additional computed tomography within 24 h after suffering a forearm trauma. Inclusion criteria for this study were a distal forearm trauma in patients older than 18 years who had both a conventional X-ray as well as a CT scan of the wrist within 24 h of the time of trauma. Exclusion criteria included age below 18 years, diabetic patients, patients under treatment with corticosteroid, patients with previous forearm fractures as well as musculo-skeletal (muscular dystrophy osteoporosis) and neurological disorders (polyneuropathy, multiple sclerosis).

Thickness of the pronator quadratus complex was measured by two radiologists (three and eight years of experience with musculoskeletal imaging) on lateral radiographs (Figure 2) and on sagittal reconstructions of CTs (Figure 3). The thickest part of the pronator quadratus complex was identified, and the musculus pronator quadratus as well as the adjacent layer of fat were measured together. Inter-observer variability between the two readers was analyzed using Cohen's kappa.

Correlation of measurements of the pronator quadratus complex on conventional lateral radiographs and sagittal reconstructions of computed tomographies was evaluated using the Pearson product-moment correlation coefficient. The Pearson product-moment correlation coefficient is a dimensionless parameter of the strength of the linear relationship between two variables. It can take values between -1 and +1, where +1 (or -1) is a completely positive (or negative) linear relationship between the observed values. Values at 0 indicate no linear correlation.

A (positive) pronator quadratus sign was defined if the pronator quadratus complex measured more than 8 mm in women or 9 mm in men^[4]. Severity of distal radius fractures was classified using the Frykman classification^[12].

For statistical analysis SPSS (Statistics 21, SPSS Inc, IBM Company) was used. Significance level was set at 0.05. Sensitivity, specificity, positive and negative predictive values for a positive fat pad sign were calculated.

RESULTS

Of 89 patients 44 (49%) had a distal radius fracture. Of these, 24 (55%) patients had a Colles-fracture and ten (23%) patients had a Smith-fracture. Furthermore there were four (9%) patients with dorsal Barton fracture and one (2%) patient with reversed Barton fracture. Two (5%) patients had a Chauffeur fracture and two (5%) had a compressed plurifragmentary fracture. Figures 4 and 5 highlight case examples from the analyzed patient cohort. Table 1 highlights the distribution of fractures according to the Frykman classification.

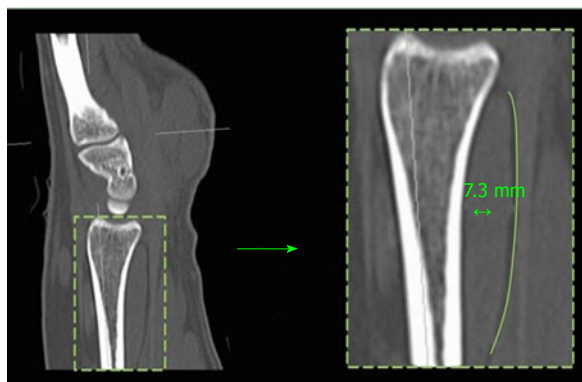
The group without fractures included 45 patients (21 female, 24 male) and served as control group. Mean age was 47.0 ± 17.5 years. One patient had an underlying malignant disease. The group with a fracture consisted of 44 patients (20 female, 24 male) with a mean age of 51.8 ± 18.2 years.

Mean thickness of the pronator quadratus complex on lateral radiographs was 7.5 ± 2.8 mm and 9.4 ± 3.0 mm on sagittally reconstructed CT respectively. Table 2 depicts measurements in patients with and without an accompanying fracture. Cohen's kappa was used and showed an almost perfect agreement between the measurement of the two radiographs (0.887, $P < 0.01$).

Regarding thickness measurements we found a

Table 3 Frequency of a positive and negative fat pad sign depending on the absence or presence of a fracture

CR pronator quadratus fat pad sign				
Radius fracture		Positive	Negative	Total
Yes		21	23	44
No		2	43	45
Total		23	66	89

**Figure 3** Measurement of the pronator quadratus complex on a sagittal reconstructed computed tomography.

significant correlation ($P < 0.01$) with a Pearson product-moment correlation coefficient of 0.795 between lateral radiographs and sagittal reconstructions of the CT scans.

Table 3 depicts the distribution of a normal or increased thickness (positive fat pad sign) of the pronator quadratus complex depending on the presence of a fracture (as confirmed or excluded by CT). On lateral radiographs 21/44 patients (47.7%) with a fracture had a positive fat pad sign. On the other hand we found 2/45 patients (4.4%) with a positive fat pad sign in the group without a fracture. Sensitivity and specificity were 48% and 96%, respectively. Positive and negative predictive values for detection of fracture using the fat pad sign was 91% and 65%, respectively (Tables 3 and 4). No significant correlation was found if the thickness of the pronator quadratus complex was used to determine the severity of a fracture, neither on lateral radiographs (Pearson product-moment correlation coefficient 0.038) nor on sagittal reconstructions of CT (0.006) scans.

DISCUSSION

Based on the results of our study we consider two messages to be of importance: A positive fat pad sign has a high specificity but low sensitivity for detection of a wrist fracture. We found no significant correlation between the thickness of the PQC and the severity of a fracture.

Early reports have suggested that a positive PQS should arouse suspicion of an occult fracture^[7]. However more recent studies have reported sensitivity

**Figure 4** No fracture on lateral radiographs (A), but positive fat pad sign and confirmed fracture on computed tomography study (B). A 48-year-old lady, who had a distal forearm trauma. On lateral radiographs no fracture can be detected, but detailed analysis of the CR shows a thickened pronator quadratus complex measuring 8.5 mm (positive fat pad sign without verification of a wrist fracture on CR) (A). Computed tomography however reveals a fissural epiphyseal fracture (B).

for the positive fat pad sign to detect an occult fracture as low as 26%-65%^[4,8], judging it unreliable. One reason may be that in those studies MRI was used as reference - a method which is very sensitive for depicting bone injuries. Moreover, false negative results may be attributed to a dorsal location of the fracture which would not displace the pronator quadratus muscle, or to a poor image quality of the radiographs which do not allow evaluation of the fat pad sign and, last but not least, to a short interval between the injury and the generation of the radiographs so that the soft tissue is not swollen to such a degree that it may be detectable^[1]. A recent study has suggested utilization of a muscle-to-bone ratio (maximum pronator muscle thickness divided by the maximum bone thickness of the distal radius at corresponding levels): With a ratio above 0.4 an occult distal forearm trauma seems likely and should be further evaluated^[9].

For the first time, but in a setting similar to the above-mentioned studies, the presented evaluation used computed tomography scans as reference standard. CT is also known to be sensitive in detecting fractures and we too found a poor sensitivity of 46% for a positive PQS in predicting a distal radius fracture. Specificity of a positive PQS however has been calculated around 70%^[4,8] and thus found to

Table 4 Sensitivity and specificity of the positive fat pad sign for detection of a fracture

	Sensitivity	Specificity	Positive predictive value	Negative predictive value
Positive fat pad sign for detection of a fracture	48.00%	96.00%	91.00%	65.00%

**Figure 5 Non-thickened pronator quadratus complex (7 mm) in spite of an obvious fracture in a 27-year-old patient following distal forearm trauma.**

range higher than sensitivity. In our study specificity was 96%, indicating that absence of the PQS does not necessarily exclude an (occult) fracture, while presence of it should trigger further investigations to rule out an underlying pathology, as proposed by others^[13].

So far correlation of the PQS on conventional X-rays and CT or MRI has not been evaluated: In this context the presented study found a significant correlation of the thickness of the pronator quadratus complex on lateral radiographs and sagittal reconstruction of CT scans of the wrist. From this one may conclude that measurements on lateral radiographs are reproducible and may therefore be used for further studies.

Radiographs in a.p. and lateral views have been used as standard and been judged to be sufficient for evaluation of wrist fractures^[10]. Several classifications have been used to group wrist fractures, with AO and Frykman classification as the most common. However both classifications are unreliable regarding reproducibility^[14]. Moreover it has been reported that these systems, when compared to CT or intraoperative evaluation, underestimate the severity of wrist fractures, *e.g.*, involvement of bearing areas, which again may be associated with worse outcome for involved patients^[10,11]. In this context the present study aimed at evaluation of PQS as an aid to the assessment of lateral radiographs by predicting the severity of an underlying wrist fracture. As no correlation could be found between the thickness of the PQC and the severity of the underlying fracture as assessed by Frykman classification, there seems to be no relevant role for the evaluating of the PQS in predicting the grade or severity of a wrist fracture.

There are main limitations to this study. First, the sample size is small, which prevents us from

generalizing on the basis of the results of our series. Second, this study is retrospective and lacks randomization. Therefore a patient selection bias may have played a role. Third, true lateral radiographs of the distal radius might be hard to achieve constantly throughout a study collective and this circumstance might therefore be a slight source of error.

In conclusion, there is a strong correlation of measurements of the pronator quadratus complex on lateral radiographs and sagittal reconstructions from computed tomography scans. Sensitivity of the PQS for detecting wrist fractures is low, but specificity is high. Therefore a positive PQS in a putative negative radiograph should trigger further investigations, *e.g.*, a CT scan. The thickness of the PQC does not correlate with the severity of wrist fractures.

COMMENTS

Background

Conventional radiography is a fast, easy and feasible diagnostic tool to detect fractures. Indirect fracture signs which can be detected on conventional X-ray studies play their role in the detection of occult bone injuries, and might trigger further investigations as, *e.g.*, a computed tomography (CT) scan. The present study evaluates the reliability of such an indirect sign, namely the pronator quadratus fat pad sign, for the detection of distal radius fractures and prediction of its severity.

Research frontiers

The main conclusion of the present study is that a positive pronator quadratus sign (PQS) shows high specificity but low sensitivity for detection of distal radius fractures and that the Pronator quadratus complex (PQC) thickness cannot predict the severity of distal radius fractures. However, there are main limitations to this study. First, the sample size is small, which prevents us from generalizing on the basis of the results of our series. Second, this study is retrospective and lacks randomization. Therefore a patient selection bias may have played a role.

Innovations and breakthroughs

For the first time, but in a setting similar to other studies, the presented evaluation used computed tomography scans as reference standard. When compared to other studies we too found a poor sensitivity of 46% for a positive PQS in predicting a distal radius fracture. In this study specificity was 96%, indicating that absence of the PQS does not necessarily exclude an (occult) fracture, while presence of it should trigger further investigations to rule out an underlying pathology, as proposed by other articles. However configuration of the PQS does not give any information on the severity of an underlying fracture.

Applications

There is a strong correlation of measurements of the pronator quadratus complex on lateral radiographs and sagittal reconstructions from computed tomography scans. It can therefore be reliably used for further research purposes regarding this topic. Sensitivity of the PQS for detecting wrist fractures is low, but specificity is high. Therefore a positive PQS in a putative negative radiograph should trigger further investigations, *e.g.*, a CT scan. A certain thickness of the PQS cannot help to adjudicate the severity of the underlying fracture.

Terminology

There are two terms which are important for a clear understanding of this article. First, this study pays attention to the PQC, which consists of the pronator quadratus muscle covering the distal radius and ulnar and can be identified on the lateral view of the wrist and a radiolucent (fat containing) stripe, which runs parallel to the pronator quadratus muscle. Second, the authors analyzed a positive (and negative) PQS. A positive pronator quadratus sign is defined as thickness of the pronator quadratus complex above 9 mm in men and below 8

mm in women.

Peer-review

It is very interesting study which investigated the relationship between pronator quadratus fat pad sign and distal radius fractures.

REFERENCES

- 1 **Zimmers TE**. Fat plane radiological signs in wrist and elbow trauma. *Am J Emerg Med* 1984; **2**: 526-532 [PMID: 6529466 DOI: 10.1016/0735-6757(84)90079-2]
- 2 **Macewan DW**. Changes due to trauma in the fat plane overlying the pronator quadratus muscle: a radiologic sign. *Radiology* 1964; **82**: 879-886 [PMID: 14153680 DOI: 10.1148/82.5.879]
- 3 **Zammit-Maempel I**, Bisset RA, Morris J, Forbes WS. The value of soft tissue signs in wrist trauma. *Clin Radiol* 1988; **39**: 664-668 [PMID: 3243059 DOI: 10.1016/S0009-9260(88)80089-8]
- 4 **Fallahi F**, Jafari H, Jefferson G, Jennings P, Read R. Explorative study of the sensitivity and specificity of the pronator quadratus fat pad sign as a predictor of subtle wrist fractures. *Skeletal Radiol* 2013; **42**: 249-253 [PMID: 22684408 DOI: 10.1007/s00256-012-1451-0]
- 5 **Sasaki Y**, Sugioka Y. The pronator quadratus sign: its classification and diagnostic usefulness for injury and inflammation of the wrist. *J Hand Surg Br* 1989; **14**: 80-83 [PMID: 2926229 DOI: 10.1016/0266-7681(89)90021-1]
- 6 **Sato J**, Ishii Y, Noguchi H, Takeda M, Toyabe S. Sonographic appearance of the pronator quadratus muscle in healthy volunteers. *J Ultrasound Med* 2014; **33**: 111-117 [PMID: 24371105 DOI: 10.7863/ultra.33.1.111]
- 7 **Curtis DJ**, Downey EF Jr, Brower AC, Cruess DF, Herrington WT, Ghaed N. Importance of soft-tissue evaluation in hand and wrist trauma: statistical evaluation. *AJR Am J Roentgenol* 1984; **142**: 781-788 [PMID: 6608240 DOI: 10.2214/ajr.142.4.781]
- 8 **Annamalai G**, Raby N. Scaphoid and pronator fat stripes are unreliable soft tissue signs in the detection of radiographically occult fractures. *Clin Radiol* 2003; **58**: 798-800 [PMID: 14521890 DOI: 10.1016/S0009-9260(03)00230-7]
- 9 **Sun B**, Zhang D, Gong W, Huang S, Luan Q, Yang J, Wang D, Tian J. Diagnostic value of the radiographic muscle-to-bone thickness ratio between the pronator quadratus and the distal radius at the same level in undisplaced distal forearm fracture. *Eur J Radiol* 2016; **85**: 452-458 [PMID: 26781151 DOI: 10.1016/j.ejrad.2015.12.002]
- 10 **Metz VM**, Gilula LA. Imaging techniques for distal radius fractures and related injuries. *Orthop Clin North Am* 1993; **24**: 217-228 [PMID: 8479720]
- 11 **Dahlen HC**, Franck WM, Sabauri G, Amlang M, Zwipp H. [Incorrect classification of extra-articular distal radius fractures by conventional X-rays. Comparison between biplanar radiologic diagnostics and CT assessment of fracture morphology]. *Unfallchirurg* 2004; **107**: 491-498 [PMID: 15060773 DOI: 10.1007/s00113-004-0747-5]
- 12 **Frykman G**. Fracture of the distal radius including sequelae--shoulder-hand-finger syndrome, disturbance in the distal radio-ulnar joint and impairment of nerve function. A clinical and experimental study. *Acta Orthop Scand* 1967; **Suppl 108**: 1-153 [PMID: 4175195]
- 13 **Moosikasuwan JB**. The pronator quadratus sign. *Radiology* 2007; **244**: 927-928 [PMID: 17709842 DOI: 10.1148/radiol.2443042063]
- 14 **Illarramendi A**, González Della Valle A, Segal E, De Carli P, Maignon G, Gallucci G. Evaluation of simplified Frykman and AO classifications of fractures of the distal radius. Assessment of interobserver and intraobserver agreement. *Int Orthop* 1998; **22**: 111-115 [PMID: 9651777]

P- Reviewer: Liu JY, Zhang L S- Editor: Ji FF L- Editor: A
E- Editor: Zhao LM



Imatinib response of gastrointestinal stromal tumor patients with germline mutation on *KIT* exon 13: A family report

Gulgun Engin, Serpil Eraslan, Hülya Kayserili, Yersu Kapran, Haluk Akman, Ali Akyuz, Nuri Faruk Aykan

Gulgun Engin, Oncology Institute, Istanbul University, 34390 Capa, Istanbul, Turkey

Serpil Eraslan, Hülya Kayserili, Medical Genetics Department, Koç University, School of Medicine (KUSoM), 34010 Topkapı, Istanbul, Turkey

Yersu Kapran, Pathology Department, Koç University, School of Medicine (KUSoM), 34010 Topkapı, Istanbul, Turkey

Haluk Akman, International Hospital, Yesilkoy, 34662 Bakirkoy, Istanbul, Turkey

Ali Akyuz, Acıbadem University, Acıbadem International Hospital, 34149 Bakirkoy, Istanbul, Turkey

Nuri Faruk Aykan, Istinye University, Liv Hospital, 34510 Esenyurt, Istanbul, Turkey

Author contributions: Engin G analysed data, designed and wrote the paper; Eraslan S performed molecular analysis and made the last revision of the report; Kayserili H performed genetic work-up and made the last revision of the report; Kapran Y performed the pathologic analyses; Akman H performed the computed tomography; Akyuz A performed surgical operations and Aykan NF collected the clinical data of patients, performed medical treatments and made the last revision of the report.

Institutional review board statement: This case report was approved by the Institutional Review Board of Istanbul University Oncology Institute in Istanbul.

Informed consent statement: The patients involved in this study gave their written informed consent authorizing use and disclosure of them protected health information.

Conflict-of-interest statement: All the authors have no conflicts of interests to declare.

Open-Access: This article is an open-access article which was selected by an in-house editor and fully peer-reviewed by external reviewers. It is distributed in accordance with the Creative Commons Attribution Non Commercial (CC BY-NC 4.0) license,

which permits others to distribute, remix, adapt, build upon this work non-commercially, and license their derivative works on different terms, provided the original work is properly cited and the use is non-commercial. See: <http://creativecommons.org/licenses/by-nc/4.0/>

Manuscript source: Invited manuscript

Correspondence to: Gulgun Engin, MD, Oncology Institute, Istanbul University, Millet Street, 34390 Capa, Istanbul, Turkey. gengin@istanbul.edu.tr
Telephone: +90-212-4142000
Fax: +90-212-5348078

Received: January 27, 2017

Peer-review started: February 9, 2017

First decision: June 12, 2017

Revised: July 24, 2017

Accepted: August 2, 2017

Article in press: August 2, 2017

Published online: September 28, 2017

Abstract

Familial gastrointestinal stromal tumor (GIST) is a rare autosomal dominant disorder associated with mutations in the *KIT* gene in the majority of cases. Although, exon 11 appears to be the hot spot region for approximately 95% of germline mutations, pathogenic variations have also been identified in exon 8, 13 and 17. Exon 13 germline mutations are extremely rare amongst familial GISTs and seven families with a germline mutation have been reported to date. Moreover, the role of imatinib mesylate in this rare familiar settings is not completely known so far. We describe here clinical, imaging, pathological and genetic findings of a family with four affected members; grandmother, his son and two grand-sons having a germline gain-of-function mutation of *KIT* in exon 13 and discuss the imatinib mesylate treatment surveillance outcomes towards

disease management.

Key words: Gastrointestinal stromal tumor; Familial; Germline mutation; Imatinib; Response

© **The Author(s) 2017.** Published by Baishideng Publishing Group Inc. All rights reserved.

Core tip: Familial gastrointestinal stromal tumor (GIST) with exon 13 germline mutations are extremely rare. Moreover, there are only a few reports describing the response to imatinib in familial GISTs. The data on the role of imatinib in familial GISTs is still limited. Understanding the role of imatinib is important for the appropriate management of mutation positive familial GISTs. It is also crucial to be able to determine the role of specific germline *KIT* mutations in. We hereby report our findings in consideration of up-to-date information.

Engin G, Eraslan S, Kayserili H, Kapran Y, Akman H, Akyuz A, Aykan NF. Imatinib response of gastrointestinal stromal tumor patients with germline mutation on *KIT* exon 13: A family report. *World J Radiol* 2017; 9(9): 365-370 Available from: URL: <http://www.wjgnet.com/1949-8470/full/v9/i9/365.htm> DOI: <http://dx.doi.org/10.4329/wjcr.v9.i9.365>

INTRODUCTION

Gastrointestinal stromal tumors (GISTs) are the most common mesenchymal tumors originating in the gastrointestinal tract. GISTs constitute 1%-3% of all malignant gastrointestinal tumors and the majority of cases are sporadic^[1]. Familial GIST is an extremely rare autosomal dominant condition which is predominantly due to germline gain-of-function mutations of *KIT* and to a lesser extent of *PDGFRA*^[2]. Diffuse proliferation of interstitial cells of Cajal (ICCs) in the myenteric plexus layer of the intestine has been described in patients with familial GISTs^[3].

Familial GISTs, associated with germline gain-of-function mutations of *KIT* have been described in 35 families^[2,4,5]. Somatic *KIT* mutations are reported in approximately 60% of all sporadic GISTs, and almost 95% of all mutations are located in exon 11^[6]. In patients with familial GISTs, most germline mutations are also located in exon 11^[4]. Familial GISTs with exon 13 mutations are extremely rare, the range of frequency of exon 13 mutations is between 0.8% to 4.1%. Seven families with a germline gain-of-function mutation of *KIT* in exon 13 have been reported to date^[7-12].

Surgery is the primary treatment for localized GISTs. Imatinib mesylate, which is a tyrosine kinase inhibitor, is administered as adjuvant therapy for high-risk groups after the operation or as neoadjuvant therapy for the management of advanced GISTs which are not candidates for surgery at initial diagnosis^[13,14]. There are only a few reports describing the response to

imatinib in familial GISTs confirming it as a promising therapeutic option^[4,5,10].

We here describe clinical, imaging, pathological and genetic findings of a family with four affected members, grandmother, his son and two grandsons having a germline gain-of-function mutation of *KIT* in exon 13 and discuss the imatinib treatment surveillance outcomes towards disease management.

CASE REPORT

We describe a family, father and two sons, with multiple GISTs. Grandmother was reported as being operated at the age of 62 and staged as advanced GIST. Genetic analysis was carried out on DNA obtained from peripheral blood samples from three affected individuals, and there was no DNA available from the grandmother (Figure 1). Sequence analysis of *KIT* gene (RefSeq ID: NM_000222.2; NP_000213.1) revealed a heterozygous exon 13 c.1924A>G (p.Lys642Glu; p.K642E) gain-of-function mutation in all three cases (Figure 2). This result was in concordance with the familial GIST diagnosis.

All three had been operated and found to have low risk, grade 1 multiple GISTs (T2N0M0). Immunohistochemical studies of the tumors showed strong positivity for CD117 (c-kit) (Figure 3). The father and older sibling were treated with imatinib for rest tumors after resection and showed a partial response to treatment.

Patient 1 (III-1; 36 years)

The patient has been hospitalized due to massive GIS bleeding at the age of 20 and was operated at the age of 27 after an intensive rectal bleeding. Mesenteric angiography showed bleeding from proximal jejunal branches and tumoral staining. The bleeding branches embolized. Abdominal computed tomography (CT) revealed proximal jejunal wall thickening and nodular solid lesions with 2.5 cm in diameter. Laparoscopic jejunal resection was made and histopathological examination showed low risk grade 1 GIST with strong positivity for CD117(c-kit) (pT2N0M0). Postoperative follow-up PET-CT demonstrated normal findings. He was, thereafter, treated with imatinib (400 mg/d) for five years due to residual multiple, milimetric GISTs and annual follow-up PET-CT showed no recurrence during that period. Imatinib treatment was terminated upon patient's request, end of five years treatment, in 2012. A recent follow-up PET-CT scan identified two nodular lesions in jejunum, 2 cm (SUVmax: 4.69) and 1.5 cm (SUVmax: 1.68) in diameters, which were consistent with GIST recurrence (Figure 4). Abdominal CT revealed multiple duodenal, jejunal and ileal contrast enhanced solid, nodular lesions with maximum 3 cm in diameter. The patient rejected the operation and preferred the re-treatment of imatinib (400 mg/d). A partial response was obtained again in the following 3 mo (Figure 5). The proband had multiple nevi on palms and soles which showed

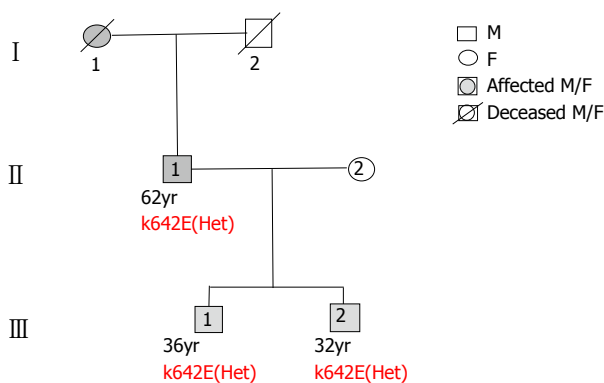


Figure 1 Pedigree of the family shows vertical transmission of *KIT* exon 13 c.1924A>G (p.Lys642Glu; p.K642E) mutation. Het: Heterozygous.

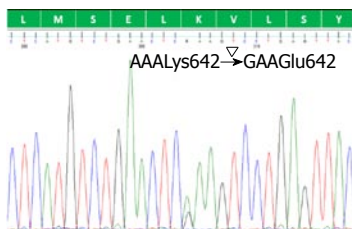


Figure 2 Electropherogram shows exon 13 c.1924A>G missense mutation leading to a change of lysine at position 642 to glutamine (p.Lys642Glu; p.K642E) (dbSNP: 121913512) of *KIT* gene at heterozygote state in three affected family members.

regression after the initiation of the treatment and had hypopigmentation of skin in general.

Patient 2 (III-2; 32 years)

He was referred due to abdominal distension and dysphagia at the age of 32. Gastroduodenal endoscopic examination and endoscopic ultrasonography (EUS) showed a gastric submucosal 1.4 cm tumor in diameter on the small curvature of prepyloric antrum. Colonoscopy showed normal findings. ¹⁸F-FDG PET-CT revealed two lesions, one at the prepyloric antrum 1.5 cm in diameter with a SUVmax: 5.0 and another at jejunum 2.2 cm in diameter with a SUVmax: 5.39. Abdominal CT showed multiple solid, contrast enhanced mass lesions maximum 3.5 cm in diameter located at the jejunum in addition to the prepyloric antral mass. Partial jejunal resection, multiple wedge resection of stomach and jejunum was performed. Histopathological examination showed low risk grade 1, multifocal masses, two, in stomach at 2.5 cm in diameter and multiple in jejunum, more than 20 with a maximum diameter of 4 cm). Tumors showed strong positivity for CD117 (c-kit) (pT2N0M0). The patient opted for no adjuvant therapy and decided to be followed up by routine annual PET-CT.

Patient 3 (III-3; 62 years)

The father had been treated for gastrointestinal bleeding at the age of 18 and preoperatively diagnosed

as GIST at the age of 25. He had Billroth operation at the age of 28 and had bleeding episodes thereafter and is on imatinib for the past eight years. At the age of 53, abdominal CT revealed multiple solid lesions with heterogenous contrast enhancement at the distal duodenum, max 5.2 cm in diameter, proximal and middle jejunum, max 5.0 cm in diameter. Three similar solid lesions were further identified at the esophageal wall of the esophago-gastric junction level (2.0 cm in diameter), at the colonic wall of the splenic flexura level (1.2 cm in diameter) and of the rectosigmoid junction level (1.0 cm in diameter), respectively. There was no additional pathologic finding in the liver, peritoneal or retroperitoneal areas. Partial jejunal resection and multiple wedge resections from the esophagus, colon and rectum were performed. Histopathological examination showed low risk grade 1 multifocal GIST with strong positive CD117 (c-kit) (pT2N0M0). After the operation, the patient has been treated with imatinib (400 mg/d) for 8 years due to residual multiple, milimetric GISTs without recurrence on annual follow-up PET-CT.

DISCUSSION

We present an extremely rare condition of autosomal dominant familial GIST with heterozygous c.1924A>G (p.Lys642Glu; p.K642E) germline *KIT* mutation in exon 13 (K642E). All three patients had been operated and two of them were treated with imatinib due to residual multiple, milimetric GISTs to which they all showed partial response.

Surgery is the initial treatment for primary and localized GISTs, targeting complete resection with macroscopic and microscopic negative margins and functional preservation by wedge resection, whenever applicable. The management of a positive microscopic margin after macroscopic complete resection is not well defined, and options may include re-excision, watchful waiting, and adjuvant imatinib therapy. Imatinib mesylate is a first-line standard therapy for inoperable, metastatic, or recurrent GISTs. It is also indicated as adjuvant treatment for intermediate or high risk group of GISTs^[14].

Only about half of the patients with sporadic GIST respond to imatinib treatment; 12%-14% show primary resistance to imatinib, and 40%-50% experience secondary resistance and disease progression within 2-3 years from the beginning of therapy^[5]. With regard to familial GISTs, there are only 12 reports on the use of imatinib in 24 patients with *KIT* germline mutations^[8,10,15-24].

The effect of imatinib on the inhibition of *KIT* activation is dependent on the site of the mutation within the *KIT* gene^[5,25]. Previous studies described that the best responses were obtained in GISTs with exon 11 mutations with a daily dose of 400 mg while a daily double dose of 800 mg is required in cases with exon 9 mutation^[5,26,27]. Clinical data on the effect of imatinib against sporadic GISTs with exon 13

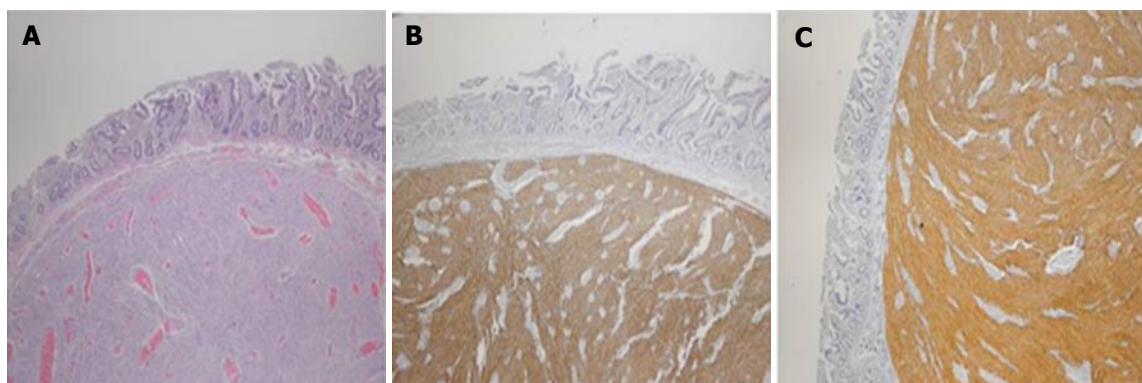


Figure 3 Microscopic findings of gastrointestinal stromal tumor located in the proximal jejunum. Hematoxylin and Eosin staining revealed spindle cells in small bowel submucosa and wall (A). Immunohistochemistry for DOG1 (B) and c-KIT (C) showed immun activity in the tumor cell (original magnification: A, B and C, 40 ×).

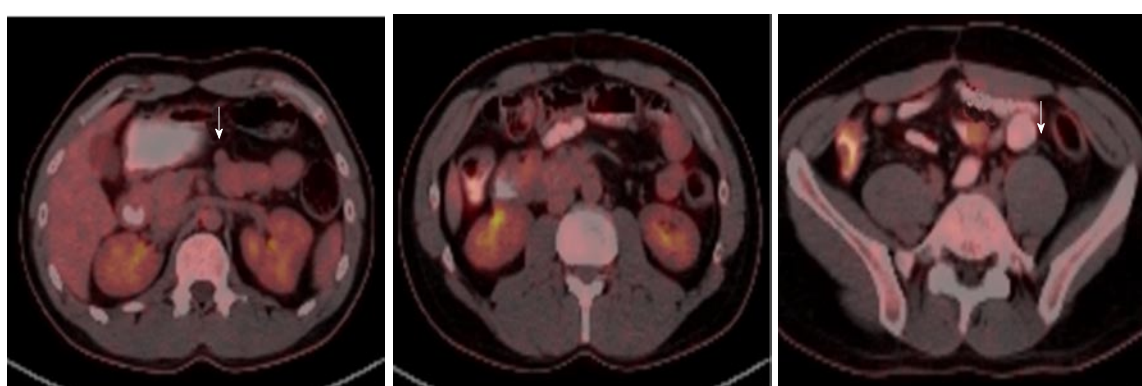


Figure 4 ^{18}F -fluorodeoxyglucose positron emission tomography-computerized tomography scans of the gastrointestinal stromal tumors recurrence. Serial ^{18}F -FDG PET-CT scans showed submucosal, solid lesions in jejunum (SUVmax: 1.68-1.50) (A, B) and ileum (SUVmax: 4.69) (C) with maximum 2 cm in diameter, consisted with GIST recurrence on the follow-up (arrows). ^{18}F -FDG: ^{18}F -fluorodeoxyglucose; PET-CT: Positron emission tomography-computerized tomography; GIST: Gastrointestinal stromal tumors.

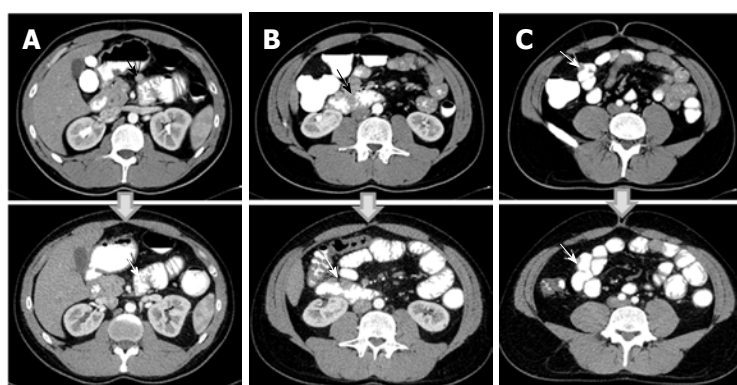


Figure 5 Imatinib response evaluation of the gastrointestinal stromal tumors using contrast-enhanced abdominal computerized tomography. Pre- and post-treatment CT images are shown on upper and lower series respectively. A partial response is seen in jejunal (A, B) and ileal (C) GISTs in the following 3 mo after imatinib therapy (arrows). CT: Computerized tomography; GIST: Gastrointestinal stromal tumors.

mutations are limited. However, it has been proven that imatinib is effective in controlling the progression of sporadic GISTs in patients with K642E mutation. *In vitro* assays also showed that activation of K642E is inhibited by imatinib^[26,27].

Several research and follow-up studies has shown that twelve exon 11 positive patients on 400 mg/d

imatinib had stable outcome, lasting from 12 to 58 mo^[10,19-21,23]. Three out of four exon 17 mutated patients^[22,24], two out of three exon 13 mutated patients^[8,10] and one exon 8 mutated patient^[15] also reported to be stable after imatinib treatment initiation.

In our family, the father and the older son were treated with imatinib (400 mg/d) without recurrence.

There were no signs of recurrence in the father. However, the older son showed recurrence four years after the cessation of imatinib treatment upon patient's request. Imatinib was re-administered with a daily dose of 400 mg and CT scan showed a significant decrease in the tumor size, after three months of the treatment.

We conclude that, *KIT* mutation analysis is advisable prior to initiation of imatinib treatment, as it can help predicting the tumor response. However, data on the role of imatinib in familial GISTs is still limited. We believe that case studies will contribute to our understanding the significance of mutation analysis in regard to the drug dosage, duration of treatment, drug response and follow-up studies of imatinib therapy in familial GISTs. The prognostic comparison of the outcome of imatinib treatment in sporadic GISTs and familial GISTs may play a role in defining the underlying mechanisms and pathways.

COMMENTS

Case characteristics

A family, a father (62-year-old) and two sons (32 and 36 years old) having multiple gastrointestinal stromal tumor (GIST) are described.

Clinical diagnosis

Massive GIS hemorrhage in the father and his older son, abdominal distension and dysphagia in the younger son.

Differential diagnosis

Gastric varices, Mallory-Weiss tear, neoplasm and hemorrhagic gastritis in upper GIS; bleeding, diverticulosis, angiodysplasia, colitis (infectious or ischemic), inflammatory bowel disease, colon cancer in lower GIS bleeding. Dysphagia can be seen in mechanical obstruction or neuromuscular motility disorders.

Laboratory diagnosis

All labs were within normal limits.

Imaging diagnosis

Imaging computed tomography showed multiple, submucosal, solid masses in 2-5 cm sizes in the upper and lower gastrointestinal tract. ¹⁸F-FDG PET-CT revealed high FDG activity (SUVmax 5.0-5.4) in the solid lesions.

Pathological diagnosis

Immunohistochemistry for DOG1 and c-kit showed immun activity in the tumor cell. Sequence analysis of *KIT* gene revealed a heterozygous exon 13 c.1924A>G gain-of-function mutation in all three cases in concordance with the familial GIST diagnosis.

Related reports

Exon 13 germline mutations are extremely rare amongst familial GISTs and seven families with a germline mutation have been reported to date. Moreover, there are only a few reports describing the response to imatinib in familial GISTs confirming it as a promising therapeutic option.

Term explanation

Familial gastrointestinal stromal tumor (GIST) is a rare autosomal dominant disorder associated with mutations in the *KIT* gene in the majority of cases presents multiple GIST. Although surgery is the primary treatment for localized GISTs, imatinib mesylate is used as adjuvant or neoadjuvant therapy in high risk or advanced GIST groups.

Experiences and lessons

We conclude that *KIT* mutation analysis is advisable prior to initiation of imatinib

treatment in familial GIST, as it can help predicting the tumor response. We believe that case studies will contribute to our understanding the significance of mutation analysis in regard to the drug dosage, duration of treatment, drug response and follow-up studies of imatinib therapy in familial GISTs.

Peer-review

The authors describe three members of a family treated with surgery and imatinib due to a familiar GIST with a rare mutation. The role of imatinib in this rare familiar settings is not completely known so far. The paper is interesting, addresses a novel topic and adds further knowledge to literature.

REFERENCES

- 1 **Cassier PA**, Ducimetière F, Lurkin A, Ranchère-Vince D, Scoazec JY, Bringuier PP, Decouvelaere AV, Méus P, Cellier D, Blay JY, Ray-Coquard I. A prospective epidemiological study of new incident GISTs during two consecutive years in Rhône Alpes region: incidence and molecular distribution of GIST in a European region. *Br J Cancer* 2010; **103**: 165-170 [PMID: 20588273 DOI: 10.1038/sj.bjc.6605743]
- 2 **Hirota S**, Nishida T, Isozaki K, Taniguchi M, Nishikawa K, Ohashi A, Takabayashi A, Obayashi T, Okuno T, Kinoshita K, Chen H, Shinomura Y, Kitamura Y. Familial gastrointestinal stromal tumors associated with dysphagia and novel type germline mutation of *KIT* gene. *Gastroenterology* 2002; **122**: 1493-1499 [PMID: 11984533]
- 3 **Hirota S**, Isozaki K, Moriyama Y, Hashimoto K, Nishida T, Ishiguro S, Kawano K, Hanada M, Kurata A, Takeda M, Muhammad Tunio G, Matsuzawa Y, Kanakura Y, Shinomura Y, Kitamura Y. Gain-of-function mutations of c-kit in human gastrointestinal stromal tumors. *Science* 1998; **279**: 577-580 [PMID: 9438854]
- 4 **Bamba S**, Hirota S, Inatomi O, Ban H, Nishimura T, Shioya M, Imaeda H, Nishida A, Sasaki M, Murata S, Andoh A. Familial and multiple gastrointestinal stromal tumors with fair response to a half-dose of imatinib. *Intern Med* 2015; **54**: 759-764 [PMID: 25832938 DOI: 10.2169/internalmedicine.54.3585]
- 5 **Gupta D**, Chandrashekar L, Larizza L, Colombo EA, Fontana L, Gervasini C, Thappa DM, Rajappa M, Rajendiran KS, Sreenath GS, Kate V. Familial gastrointestinal stromal tumors, lentigines, and café-au-lait macules associated with germline c-kit mutation treated with imatinib. *Int J Dermatol* 2017; **56**: 195-201 [PMID: 28074523 DOI: 10.1111/ijd.13516]
- 6 **Hirota S**, Ohashi A, Nishida T, Isozaki K, Kinoshita K, Shinomura Y, Kitamura Y. Gain-of-function mutations of platelet-derived growth factor receptor alpha gene in gastrointestinal stromal tumors. *Gastroenterology* 2003; **125**: 660-667 [PMID: 12949711]
- 7 **Yamanoi K**, Higuchi K, Kishimoto H, Nishida Y, Nakamura M, Sudoh M, Hirota S. Multiple gastrointestinal stromal tumors with novel germline c-kit gene mutation, K642T, at exon 13. *Hum Pathol* 2014; **45**: 884-888 [PMID: 24565205 DOI: 10.1016/j.humpath.2013.11.009]
- 8 **Bachet JB**, Landi B, Laurent-Puig P, Italiano A, Le Cesne A, Lévy P, Safar V, Duffaud F, Blay JY, Emile JF. Diagnosis, prognosis and treatment of patients with gastrointestinal stromal tumour (GIST) and germline mutation of *KIT* exon 13. *Eur J Cancer* 2013; **49**: 2531-2541 [PMID: 23648119 DOI: 10.1016/j.ejca.2013.04.005]
- 9 **Isozaki K**, Terris B, Belghiti J, Schifmann S, Hirota S, Vanderwinden JM. Germline-activating mutation in the kinase domain of *KIT* gene in familial gastrointestinal stromal tumors. *Am J Pathol* 2000; **157**: 1581-1585 [PMID: 11073817 DOI: 10.1016/S0002-9440(10)64795-5]
- 10 **Graham J**, Debiec-Rychter M, Corless CL, Reid R, Davidson R, White JD. Imatinib in the management of multiple gastrointestinal stromal tumors associated with a germline *KIT* K642E mutation. *Arch Pathol Lab Med* 2007; **131**: 1393-1396 [PMID: 17824795 DOI: 10.1043/1543-2165(2007)131[1393:ITMOM]2.0.CO;2]
- 11 **Vilain RE**, Dudding T, Braye SG, Groombridge C, Meldrum C, Spigelman AD, Ackland S, Ashman L, Scott RJ. Can a familial gastrointestinal tumour syndrome be allelic with Waardenburg syndrome? *Clin Genet* 2011; **79**: 554-560 [PMID: 20636395 DOI: 10.1111/j.1399-0004.2010.01489.x]
- 12 **Peña-Irún A**, Villa-Puente M, García-Espinosa R, Cavadas-López A. [Familial gastrointestinal stroma tumor due to mutation in exon 13 (K642E) of the *KIT* gene]. *Med Clin (Barc)* 2012; **139**: 512-513

- [PMID: 22626674 DOI: 10.1016/j.medcli.2012.03.018]
- 13 **Wadt K**, Andersen MK, Hansen TV, Gerdes AM. [A new genetic diagnosis of familial gastrointestinal stromal tumour]. *Ugeskr Laeger* 2012; **174**: 1462-1464 [PMID: 22640790]
 - 14 **Nishida T**, Blay JY, Hirota S, Kitagawa Y, Kang YK. The standard diagnosis, treatment, and follow-up of gastrointestinal stromal tumors based on guidelines. *Gastric Cancer* 2016; **19**: 3-14 [PMID: 26276366 DOI: 10.1007/s10120-015-0526-8]
 - 15 **Speight RA**, Nicolle A, Needham SJ, Verrill MW, Bryon J, Panter S. Rare, germline mutation of KIT with imatinib-resistant multiple GI stromal tumors and mastocytosis. *J Clin Oncol* 2013; **31**: e245-e247 [PMID: 23610110 DOI: 10.1200/JCO.2012.42.0133]
 - 16 **Adela Avila S**, Peñaloza J, González F, Abdo I, Rainville I, Root E, Carrero Valenzuela RD, Garber J. Dysphagia, melanosis, gastrointestinal stromal tumors and a germinal mutation of the KIT gene in an Argentine family. *Acta Gastroenterol Latinoam* 2014; **44**: 9-15 [PMID: 24847623]
 - 17 **Jones DH**, Caracciolo JT, Hodul PJ, Strosberg JR, Coppola D, Bui MM. Familial gastrointestinal stromal tumor syndrome: report of 2 cases with KIT exon 11 mutation. *Cancer Control* 2015; **22**: 102-108 [PMID: 25504284]
 - 18 **Wozniak A**, Floris G, Debiec-Rychter M, Sciort R, Schöffski P. Implications of mutational analysis for the management of patients with gastrointestinal stromal tumors and the application of targeted therapies. *Cancer Invest* 2010; **28**: 839-848 [PMID: 20690803 DOI: 10.3109/07357907.2010.494322]
 - 19 **Lasota J**, Miettinen M. A new familial GIST identified. *Am J Surg Pathol* 2006; **30**: 1342 [PMID: 17001171 DOI: 10.1097/01.pas.0000213364.56498.3b]
 - 20 **Kleinbaum EP**, Lazar AJ, Tamborini E, Mcauliffe JC, Sylvestre PB, Sonnenberg TD, Strong L, Chen LL, Choi H, Benjamin RS, Zhang W, Trent JC. Clinical, histopathologic, molecular and therapeutic findings in a large kindred with gastrointestinal stromal tumor. *Int J Cancer* 2008; **122**: 711-718 [PMID: 17943734 DOI: 10.1002/ijc.23137]
 - 21 **Woźniak A**, Rutkowski P, Sciort R, Ruka W, Michej W, Debiec-Rychter M. Rectal gastrointestinal stromal tumors associated with a novel germline KIT mutation. *Int J Cancer* 2008; **122**: 2160-2164 [PMID: 18183595 DOI: 10.1002/ijc.23338]
 - 22 **Thalheimer A**, Schlemmer M, Bueter M, Merkelbach-Bruse S, Schildhaus HU, Buettner R, Hartung E, Thiede A, Meyer D, Fein M, Maroske J, Wardelmann E. Familial gastrointestinal stromal tumors caused by the novel KIT exon 17 germline mutation N822Y. *Am J Surg Pathol* 2008; **32**: 1560-1565 [PMID: 18724244 DOI: 10.1097/PAS.0b013e318172ce6f]
 - 23 **Campbell T**, Felsten L, Moore J. Disappearance of lentiginos in a patient receiving imatinib treatment for familial gastrointestinal stromal tumor syndrome. *Arch Dermatol* 2009; **145**: 1313-1316 [PMID: 19917964 DOI: 10.1001/archdermatol.2009.263]
 - 24 **Veiga I**, Silva M, Vieira J, Pinto C, Pinheiro M, Torres L, Soares M, Santos L, Duarte H, Bastos AL, Coutinho C, Dinis J, Lopes C, Teixeira MR. Hereditary gastrointestinal stromal tumors sharing the KIT Exon 17 germline mutation p.Asp820Tyr develop through different cytogenetic progression pathways. *Genes Chromosomes Cancer* 2010; **49**: 91-98 [PMID: 19847891 DOI: 10.1002/gcc.20720]
 - 25 **Ashman LK**, Griffith R. Therapeutic targeting of c-KIT in cancer. *Expert Opin Investig Drugs* 2013; **22**: 103-115 [PMID: 23127174 DOI: 10.1517/13543784.2013.740010]
 - 26 **Heinrich MC**, Corless CL, Demetri GD, Blanke CD, von Mehren M, Joensuu H, McGreevey LS, Chen CJ, Van den Abbeele AD, Druker BJ, Kiese B, Eisenberg B, Roberts PJ, Singer S, Fletcher CD, Silberman S, Dimitrijevic S, Fletcher JA. Kinase mutations and imatinib response in patients with metastatic gastrointestinal stromal tumor. *J Clin Oncol* 2003; **21**: 4342-4349 [PMID: 14645423 DOI: 10.1200/JCO.2003.04.190]
 - 27 **Debiec-Rychter M**, Sciort R, Le Cesne A, Schlemmer M, Hohenberger P, van Oosterom AT, Blay JY, Leyvraz S, Stul M, Casali PG, Zalcberg J, Verweij J, Van Glabbeke M, Hagemijer A, Judson I; EORTC Soft Tissue and Bone Sarcoma Group; Italian Sarcoma Group; Australasian GastroIntestinal Trials Group. KIT mutations and dose selection for imatinib in patients with advanced gastrointestinal stromal tumours. *Eur J Cancer* 2006; **42**: 1093-1103 [PMID: 16624552 DOI: 10.1016/j.ejca.2006.01.030]

P- Reviewer: Vallicelli C S- Editor: Kong JX L- Editor: A
E- Editor: Zhao LM





Published by **Baishideng Publishing Group Inc**
7901 Stoneridge Drive, Suite 501, Pleasanton, CA 94588, USA
Telephone: +1-925-223-8242
Fax: +1-925-223-8243
E-mail: bpgoffice@wjgnet.com
Help Desk: <http://www.f6publishing.com/helpdesk>
<http://www.wjgnet.com>



World Journal of *Radiology*

World J Radiol 2017 October 28; 9(10): 371-404





Editorial Board

2014-2017

The *World Journal of Radiology* Editorial Board consists of 365 members, representing a team of worldwide experts in radiology. They are from 36 countries, including Afghanistan (1), Argentina (2), Australia (5), Austria (7), Belgium (2), Brazil (8), Canada (6), Chile (1), China (43), Croatia (1), Denmark (4), Egypt (6), France (5), Germany (22), Greece (10), India (12), Iran (6), Ireland (2), Israel (3), Italy (47), Japan (13), Netherlands (1), New Zealand (1), Pakistan (1), Poland (2), Portugal (1), Serbia (1), Singapore (3), Slovakia (1), South Korea (18), Spain (4), Sweden (2), Switzerland (4), Thailand (1), Turkey (26), United Kingdom (11), and United States (82).

EDITORS-IN-CHIEF

Kai U Juergens, *Bremen*
Edwin JR van Beek, *Edinburgh*
Thomas J Vogl, *Frankfurt*

GUEST EDITORIAL BOARD MEMBERS

Wing P Chan, *Taipei*
Chung-Huei Hsu, *Taipei*
Chin-Chang Huang, *Taipei*
Tsong-Long Hwang, *Taoyuan*
Jung-Lung Hsu, *Taipei*
Chia-Hung Kao, *Taichung*
Yu-Ting Kuo, *Tainan*
Hon-Man Liu, *Taipei*
Hui-Lung Liang, *Kaohsiung*
Chun Chung Lui, *Kaohsiung*
Sen-Wen Teng, *Taipei*
Yung-Liang (William) Wan, *Taoyuan*

MEMBERS OF THE EDITORIAL BOARD



Afghanistan

Takao Hiraki, *Okayama*



Argentina

Patricia Carrascosa, *Vicente Lopez*
Maria C Ziadi, *Rosario*



Australia

Lourens Bester, *Sydney*
Gemma A Figtree, *Sydney*

Stuart M Grieve, *Sydney*
Wai-Kit Lee, *Fitzroy*
Prabhakar Ramachandran, *Melbourne*



Austria

Herwig R Cerwenka, *Graz*
Gudrun M Feuchtnner, *Innsbruck*
Benjamin Henninger, *Innsbruck*
Rupert Lanzenberger, *Vienna*
Shu-Ren Li, *Vienna*
Veronika Schopf, *Vienna*
Tobias De Zordo, *Innsbruck*



Belgium

Steve Majerus, *Liege*
Kathelijne Peremans, *Merelbeke*



Brazil

Clerio F Azevedo, *Rio de Janeiro*
Patrícia P Alfredo, *São Paulo*
Eduardo FC Fleury, *São Paulo*
Edward Araujo Júnior, *São Paulo*
Wellington P Martins, *Ribeirão Preto*
Ricardo A Mesquita, *Belo Horizonte*
Vera MC Salemi, *São Paulo*
Claudia Szobot, *Porto Alegre*
Lilian YI Yamaga, *São Paulo*



Canada

Marie Arsalidou, *Toronto*
Otman A Basir, *Waterloo*

Tarik Zine Belhocine, *Toronto*
James Chow, *Toronto*
Tae K Kim, *Toronto*
Anastasia Oikonomou, *Toronto*



China

Hong-Wei Chen, *Wuxi*
Feng Chen, *Hangzhou*
Jian-Ping Chu, *Guangzhou*
Guo-Guang Fan, *Shenyang*
Bu-Lang Gao, *Shijiazhuang*
Qi-Yong Gong, *Chengdu*
Ying Han, *Beijing*
Xian-Li Lv, *Beijing*
Yi-Zhuo Li, *Guangzhou*
Xiang-Xi Meng, *Harbin*
Yun Peng, *Beijing*
Jun Shen, *Guangzhou*
Ze-Zhou Song, *Hangzhou*
Wai Kwong Tang, *Hong Kong*
Gang-Hua Tang, *Guangzhou*
Jie Tian, *Beijing*
Lu-Hua Wang, *Beijing*
Xiao-bing Wang, *Xi'an*
Yi-Gen Wu, *Nanjing*
Kai Wu, *Guangzhou*
Hui-Xiong Xu, *Shanghai*
Zuo-Zhang Yang, *Kunming*
Xiao-Dan Ye, *Shanghai*
David T Yew, *Hong Kong*
Ting-He Yu, *Chongqing*
Zheng Yuan, *Shanghai*
Min-Ming Zhang, *Hangzhou*
Yudong Zhang, *Nanjing*
Dong Zhang, *Chongqing*
Wen-Bin Zeng, *Changsha*

Yue-Qi Zhu, *Shanghai*



Croatia

Goran Kusec, *Osijek*



Denmark

Poul E Andersen, *Odense*

Lars J Petersen, *Aalborg*

Thomas Z Ramsøy, *Frederiksberg*

Morten Ziebell, *Copenhagen*



Egypt

Mohamed F Bazeed, *Mansoura*

Mohamed Abou El-Ghar, *Mansoura*

Reem HA Mohamed, *Cairo*

Mohamed R Nouh, *Alexandria*

Ahmed AKA Razek, *Mansoura*

Ashraf A Zytoon, *Shebin El-Koom*



France

Sabine F Bensamoun, *Compiègne*

Romarc Loffroy, *Dijon*

Stephanie Nougaret, *Montpellier*

Hassane Oudadesse, *Rennes*

Vincent Vinh-Hung, *Fort-de-France*



Germany

Henryk Barthel, *Leipzig*

Peter Bannas, *Hamburg*

Martin Beeres, *Frankfurt*

Ilja F Ciernik, *Dessau*

A Dimitrakopoulou-Strauss, *Heidelberg*

Peter A Fasching, *Erlangen*

Andreas G Schreyer, *Regensburg*

Philipp Heusch, *Duesseldorf*

Sonja M Kirchhoff, *Munich*

Sebastian Ley, *Munich*

Adel Maataoui, *Frankfurt am Main*

Stephan M Meckel, *Freiburg*

Hans W Muller, *Duesseldorf*

Kay Raum, *Berlin*

Dirk Rades, *Luebeck*

Marc-Ulrich Regier, *Hamburg*

Alexey Surov, *Halle*

Martin Walter, *Magdeburg*

Axel Wetter, *Essen*

Christoph Zilkens, *Düsseldorf*



Greece

Panagiotis Antoniou, *Thessaloniki*

Nikos Efthimiou, *Athens*

Dimitris Karnabatidis, *Patras*

George Latsios, *Athens*

Stylianios Megremis, *Iraklion*

Alexander D Rapidis, *Athens*

Kiki Theodorou, *Larissa*

Ioannis A Tsalafoutas, *Athens*

Evanthia E Tripoliti, *Ioannina*

Athina C Tsili, *Ioannina*



India

Ritesh Agarwal, *Chandigarh*

Chandan J Das, *New Delhi*

Prathamesh V Joshi, *Mumbai*

Naveen Kalra, *Chandigarh*

Chandrasekharan Kesavadas, *Trivandrum*

Jyoti Kumar, *New Delhi*

Atin Kumar, *New Delhi*

Kaushala P Mishra, *Allahabad*

Daya N Sharma, *New Delhi*

Binit Sureka, *New Delhi*

Sanjay Sharma, *New Delhi*

Raja R Yadav, *Allahabad*



Iran

Majid Assadi, *Bushehr*

SeyedReza Najafizadeh, *Tehran*

Mohammad Ali Oghabian, *Tehran*

Amir Reza Radmard, *Tehran*

Ramin Sadeghi, *Mashhad*

Hadi Rokni Yazdi, *Tehran*



Ireland

Tadhg Gleeson, *Wexford*

Frederik JAI Vernimmen, *Cork*



Israel

Dafna Ben Bashat, *Tel Aviv*

Amit Gefen, *Tel Aviv*

Tamar Sella, *Jerusalem*



Italy

Adriano Alippi, *Rome*

Dante Amelio, *Trento*

Michele Anzidei, *Rome*

Filippo F Angileri, *Messinas*

Stefano Arcangeli, *Rome*

Roberto Azzoni, *San Donato milanese*

Tommaso V Bartolotta, *Palermo*

Tommaso Bartalena, *Imola*

Livia Bernardin, *San Bonifacio*

Federico Boschi, *Verona*

Sergio Casciaro, *Lecce*

Emanuele Casciani, *Rome*

Musa M Can, *Napoli*

Alberto Cuocolo, *Napoli*

Michele Ferrara, *Coppito*

Mauro Feola, *Fossano*

Giampiero Francica, *Castel Volturno*

Luigi De Gennaro, *Rome*

Giulio Giovannetti, *Pisa*

Francesca Iacobellis, *Napoli*

Formato Invernizzi, *Monza Brianza*

Francesco Lassandro, *Naples*

Lorenzo Livi, *Florence*

Pier P Mainenti, *Napoli*

Laura Marzetti, *Chieti*

Giuseppe Malinverni, *Crescentino*

Enrica Milanese, *Turin*

Giovanni Morana, *Treviso*

Lorenzo Monti, *Milan*

Silvia D Morbelli, *Genoa*

Barbara Palumbo, *Perugia*

Cecilia Parazzini, *Milan*

Stefano Pergolizzi, *Messina*

Antonio Pinto, *Naples*

Camillo Porcaro, *Rome*

Carlo C Quattrocchi, *Rome*

Alberto Rebonato, *Perugia*

Giuseppe Rizzo, *Rome*

Roberto De Rosa, *Naples*

Domenico Rubello, *Rovigo*

Andrea Salvati, *Bari*

Sergio Sartori, *Ferrara*

Luca M Sconfienza, *Milano*

Giovanni Storto, *Rionero*

Nicola Sverzellati, *Parma*

Alberto S Tagliafico, *Genova*

Nicola Troisi, *Florence*



Japan

Yasuhiko Hori, *Chiba*

Hidetoshi Ikeda, *Koriyama*

Masahito Kawabori, *Sapporo*

Tamotsu Kamishima, *Sapporo*

Hiro Kiyosue, *Yufu*

Yasunori Minami, *Osaka-sayama*

Yasuhiro Morimoto, *Kitakyushu*

Satoru Murata, *Tokyo*

Shigeki Nagamachi, *Miyazaki*

Hiroshi Onishi, *Yamanashi*

Morio Sato, *Wakayama Shi*

Yoshito Tsushima, *Maebashi*

Masahiro Yanagawa, *Suita*



Netherlands

Willem Jan van Rooij, *Tilburg*



New Zealand

W Howell Round, *Hamilton*



Pakistan

Wazir Muhammad, *Abbottabad*



Poland

Maciej S Baglaj, *Wroclaw*

Piotr Czauderna, *Gdansk*



Portugal

Joao Manuel RS Tavares, *Porto*



Serbia

Olivera Ciraj-Bjelac, *Belgrade*



Singapore

Gopinathan Anil, *Singapore*

Terence KB Teo, *Singapore*

Cher Heng Tan, *Singapore*



Slovakia

Stefan Sivak, *Martin*



South Korea

Ki Seok Choo, *Busan*

Seung Hong Choi, *Seoul*

Dae-Seob Choi, *Jinju*

Hong-Seok Jang, *Seoul*

Yong Jeong, *Daejeon*

Chan Kyo Kim, *Seoul*

Se Hyung Kim, *Seoul*

Joong-Seok Kim, *Seoul*

Sang Eun Kim, *Seongnam*

Sung Joon Kwon, *Seoul*

Jeong Min Lee, *Seoul*

In Sook Lee, *Busan*

Noh Park, *Goyang*

Chang Min Park, *Seoul*

Sung Bin Park, *Seoul*

Deuk Jae Sung, *Seoul*

Choongsoo Shin, *Seoul*

Kwon-Ha Yoon, *Iksan*



Spain

Miguel A De Gregorio, *Zaragoza*

Antonio Luna, *Jaén*

Enrique Marco de Lucas, *Santander*

Fernando Ruiz Santiago, *Granada*



Sweden

Dmitry Grishenkov, *Stockholm*

Tie-Qiang Li, *Stockholm*



Switzerland

Nicolau Beckmann, *Basel*

Christian Boy, *Bern*

Giorgio Treglia, *Bellinzona*

Stephan Ulmer, *Kiel*



Thailand

Sirianong Namwongprom, *Chiang Mai*



Turkey

Kubilay Aydin, *Istanbul*

Ramazan Akdemir, *Sakarya*

Serhat Avcu, *Ankara*

Ayşe Aralasmak, *Istanbul*

Oktay Algin, *Ankara*

Nevbahar Akcar, *Meselik*

Bilal Battal, *Ankara*

Zulkif Bozgeyik, *Elazig*

Nazan Ciledag, *Aakara*

Fuldem Y Donmez, *Ankara*

Gulgun Engin, *Istanbul*

Ahmet Y Goktay, *Izmir*

Oguzhan G Gumustas, *Bursa*

Kaan Gunduz, *Ankara*

Pelin Ozcan Kara, *Mersin*

Kivanc Kamburoglu, *Ankara*

Ozgur Kilickesmez, *Istanbul*

Furuzan Numan, *Istanbul*

Cem Onal, *Adana*

Ozgur Oztekin, *Izmir*

Seda Ozbek (Boruban), *Konya*

Selda Sarikaya, *Zonguldak*

Figen Taser, *Kutahya*

Baran Tokar, *Eskisehir*

Ender Uysal, *Istanbul*

Ensar Yekeler, *Istanbul*



United Kingdom

Indran Davagnanam, *London*

M DC Valdés Hernández, *Edinburgh*

Alan Jackson, *Manchester*

Suneil Jain, *Belfast*

Long R Jiao, *London*

Miltiadis Krokidis, *Cambridge*

Pradesh Kumar, *Liverpool*

Peter D Kuzmich, *Derby*

Georgios Plataniotis, *Brighton*

Vanessa Sluming, *Liverpool*



United States

Garima Agrawal, *Saint Louis*

James R Brasic, *Baltimore*

Rajendra D Badgaiyan, *Buffalo*

Ulas Bagci, *Bethesda*

Anat Biegon, *Stony Brook*

Ramon Casanova, *Winston Salem*

Wenli Cai, *Boston*

Zheng Chang, *Durham*

Corey J Chakarun, *Long Beach*

Kai Chen, *Los Angeles*

Hyun-Soon Chong, *Chicago*

Marco Cura, *Dallas*

Ravi R Desai, *Bensalem*

Delia DeBuc, *Miami*

Carlo N De Cecco, *Charleston*

Timm-Michael L Dickfeld, *Baltimore*

Subba R Digumarthy, *Boston*

Huy M Do, *Stanford*

Todd A Faasse, *Grand Rapids*

Salomao Faintuch, *Boston*

Girish M Fatterpekar, *New York*

Dhakshinamoorthy Ganesan, *Houston*

Robert J Griffin, *Little Rock*

Andrew J Gunn, *Boston*

Sandeep S Hedgire, *Boston*

Timothy J Hoffman, *Columbia*

Mai-Lan Ho, *San Francisco*

Juebin Huang, *Jackson*

Abid Irshad, *Charleston*

Matilde Inglese, *New York*

El-Sayed H Ibrahim, *Jacksonville*

Paul R Julsrud, *Rochester*

Pamela T Johnson, *Baltimore*

Ming-Hung Kao, *Tempe*

Sunil Krishnan, *Houston*

Richard A Komoroski, *Cincinnati*

Sandi A Kwee, *Honolulu*

King Kim, *Ft. Lauderdale*

Guozheng Liu, *Worcester*

Yiyan Liu, *Newark*

Venkatesh Mani, *New York*

Lian-Sheng Ma, *Pleasanton*

Rachna Madan, *Boston*

Zeyad A Metwalli, *Houston*

Yilong Ma, *Manhasset*

Hui Mao, *Atlanta*

Feroze B Mohamed, *Philadelphia*

Gul Moonis, *Boston*

John L Noshier, *New Brunswick*

Rahmi Oklu, *Boston*

Aytekun Oto, *Chicago*

Bishnuhari Paudyal, *Philadelphia*

Rajul Pandya, *Youngstown*

Chong-Xian Pan, *Sacramento*

Jay J Pillai, *Baltimore*

Neal Prakash, *Duarte*

Reza Rahbar, *Boston*

Ali S Raja, *Boston*

Gustavo J Rodriguez, *El Paso*

David J Sahn, *Portland*

Steven Schild, *Scottsdale*

Ali R Sepahdari, *Los Angeles*

Li Shen, *Indianapolis*

JP Sheehan, *Charlottesville*

Atul B Shinagare, *Boston*

Sarabjeet Singh, *Boston*

Charles J Smith, *Columbia*

Kenji Suzuki, *Chicago*

Monvadi Srichai-Parsia, *Washington*

Sree H Tirumani, *Boston*

Hebert A Vargas, *New York*

Sachit Verma, *Philadelphia*

Yoichi Watanabe, *Minneapolis*

Li Wang, *Chapel Hill*

Carol C Wu, *Boston*

Shoujun Xu, *Houston*

Min Yao, *Cleveland*

Xiaofeng Yang, *Atlanta*

Qingbao Yu, *Albuquerque*

Aifeng Zhang, *Chicago*

Chao Zhou, *Bethlehem*

Hongming Zhuang, *Philadelphia*

**REVIEW**

- 371 Cerebellum and neurodegenerative diseases: Beyond conventional magnetic resonance imaging

Mormina E, Petracca M, Bommarito G, Piaggio N, Cocozza S, Inglese M

- 389 Lymph node imaging in initial staging of prostate cancer: An overview and update

Zarzour JG, Galgano S, McConathy J, Thomas JV, Rais-Bahrami S

CASE REPORT

- 400 MR neurography in intraosseous median nerve entrapment

Aggarwal A, Jana M, Kumar V, Srivastava DN, Garg K

ABOUT COVER

Editorial Board Member of *World Journal of Radiology*, Stefano Arcangeli, MD, Assistant Professor, Department of Radiotherapy, Azienda Ospedaliera S. Camillo-Forlanini, Rome 00152, Italy

AIM AND SCOPE

World Journal of Radiology (*World J Radiol*, *WJR*, online ISSN 1949-8470, DOI: 10.4329) is a peer-reviewed open access academic journal that aims to guide clinical practice and improve diagnostic and therapeutic skills of clinicians.

WJR covers topics concerning diagnostic radiology, radiation oncology, radiologic physics, neuroradiology, nuclear radiology, pediatric radiology, vascular/interventional radiology, medical imaging achieved by various modalities and related methods analysis. The current columns of *WJR* include editorial, frontier, diagnostic advances, therapeutics advances, field of vision, mini-reviews, review, topic highlight, medical ethics, original articles, case report, clinical case conference (clinicopathological conference), and autobiography.

We encourage authors to submit their manuscripts to *WJR*. We will give priority to manuscripts that are supported by major national and international foundations and those that are of great basic and clinical significance.

INDEXING/ABSTRACTING

World Journal of Radiology is now indexed in PubMed, PubMed Central, and Emerging Sources Citation Index (Web of Science).

FLYLEAF

I-III Editorial Board

EDITORS FOR THIS ISSUE

Responsible Assistant Editor: *Xiang Li*
Responsible Electronic Editor: *Ya-Jing Lu*
Proofing Editor-in-Chief: *Lian-Sheng Ma*

Responsible Science Editor: *Li-Jun Cui*
Proofing Editorial Office Director: *Xiu-Xia Song*

NAME OF JOURNAL
World Journal of Radiology

ISSN
ISSN 1949-8470 (online)

LAUNCH DATE
January 31, 2009

FREQUENCY
Monthly

EDITORS-IN-CHIEF
Kai U Juergens, MD, Associate Professor, MRT und PET/CT, Nuklearmedizin Bremen Mitte, ZEMODI - Zentrum für morphologische und molekulare Diagnostik, Bremen 28177, Germany

Edwin JR van Beek, MD, PhD, Professor, Clinical Research Imaging Centre and Department of Medical Radiology, University of Edinburgh, Edinburgh EH16 4TJ, United Kingdom

Thomas J Vogl, MD, Professor, Reader in Health Technology Assessment, Department of Diagnostic and Interventional Radiology, Johann Wolfgang Goethe University of Frankfurt, Frankfurt 60590,

Germany

EDITORIAL BOARD MEMBERS
All editorial board members resources online at <http://www.wjnet.com/1949-8470/editorialboard.htm>

EDITORIAL OFFICE
Xiu-Xia Song, Director
World Journal of Radiology
Baishideng Publishing Group Inc
7901 Stoneridge Drive, Suite 501, Pleasanton, CA 94588, USA
Telephone: +1-925-2238242
Fax: +1-925-2238243
E-mail: editorialoffice@wjnet.com
Help Desk: <http://www.f6publishing.com/helpdesk>
<http://www.wjnet.com>

PUBLISHER
Baishideng Publishing Group Inc
7901 Stoneridge Drive, Suite 501, Pleasanton, CA 94588, USA
Telephone: +1-925-2238242
Fax: +1-925-2238243
E-mail: bpgoffice@wjnet.com
Help Desk: <http://www.f6publishing.com/helpdesk>
<http://www.wjnet.com>

PUBLICATION DATE
October 28, 2017

COPYRIGHT
© 2017 Baishideng Publishing Group Inc. Articles published by this Open-Access journal are distributed under the terms of the Creative Commons Attribution Non-commercial License, which permits use, distribution, and reproduction in any medium, provided the original work is properly cited, the use is non commercial and is otherwise in compliance with the license.

SPECIAL STATEMENT
All articles published in journals owned by the Baishideng Publishing Group (BPG) represent the views and opinions of their authors, and not the views, opinions or policies of the BPG, except where otherwise explicitly indicated.

INSTRUCTIONS TO AUTHORS
<http://www.wjnet.com/bpg/gerinfo/204>

ONLINE SUBMISSION
<http://www.f6publishing.com>

Cerebellum and neurodegenerative diseases: Beyond conventional magnetic resonance imaging

Enricomaria Mormina, Maria Petracca, Giulia Bommarito, Niccolò Piaggio, Sirio Coccozza, Matilde Inglese

Enricomaria Mormina, Maria Petracca, Giulia Bommarito, Sirio Coccozza, Matilde Inglese, Department of Neurology, Icahn School of Medicine at Mount Sinai, New York, NY 10029, United States

Enricomaria Mormina, Neuroradiology Unit, Department of Biomedical Sciences and Morphological and Functional Images, University of Messina, 98100 Messina, Italy

Maria Petracca, Department of Neuroscience, Reproductive Sciences and Odontostomatology, University of Naples Federico II, 80138 Naples, Italy

Giulia Bommarito, Niccolò Piaggio, Matilde Inglese, Department of Neuroscience, Rehabilitation, Ophthalmology, Genetics and Maternal and Child Health (DINOEMI), University of Genoa, 16132 Genoa, Italy

Niccolò Piaggio, Department of Neuroradiology, San Martino Hospital, 16132 Genoa, Italy

Sirio Coccozza, Department of Advanced Biomedical Sciences, University of Naples Federico II, 80138 Naples, Italy

Author contributions: Inglese M takes responsibility for the integrity and accuracy of the review; Study concept and design: Mormina E, Petracca M and Inglese M; Literature review: All authors; Drafting and critical revision of the manuscript for important intellectual content: All authors; Study supervision: Inglese M.

Conflict-of-interest statement: No potential conflicts of interest. No financial support.

Open-Access: This article is an open-access article which was selected by an in-house editor and fully peer-reviewed by external reviewers. It is distributed in accordance with the Creative Commons Attribution Non Commercial (CC BY-NC 4.0) license, which permits others to distribute, remix, adapt, build upon this work non-commercially, and license their derivative works on different terms, provided the original work is properly cited and the use is non-commercial. See: <http://creativecommons.org/licenses/by-nc/4.0/>

Manuscript source: Invited manuscript

Correspondence to: Matilde Inglese, MD, PhD, Associate Professor, Director of Neurology Imaging Laboratory, Department of Neurology, Icahn School of Medicine at Mount Sinai, Annenberg 14, Box 1137, One Gustave L. Levy Place, New York, NY 10029, United States. matilde.inglese@mssm.edu
Telephone: +1-212-8249310
Fax: +1-212-3481310

Received: January 27, 2017

Peer-review started: February 12, 2017

First decision: April 17, 2017

Revised: July 18, 2017

Accepted: August 2, 2017

Article in press: August 2, 2017

Published online: October 28, 2017

Abstract

The cerebellum plays a key role in movement control and in cognition and cerebellar involvement is described in several neurodegenerative diseases. While conventional magnetic resonance imaging (MRI) is widely used for brain and cerebellar morphologic evaluation, advanced MRI techniques allow the investigation of cerebellar microstructural and functional characteristics. Volumetry, voxel-based morphometry, diffusion MRI based fiber tractography, resting state and task related functional MRI, perfusion, and proton MR spectroscopy are among the most common techniques applied to the study of cerebellum. In the present review, after providing a brief description of each technique's advantages and limitations, we focus on their application to the study of cerebellar injury in major neurodegenerative diseases, such as multiple sclerosis, Parkinson's and Alzheimer's disease and hereditary ataxia. A brief introduction to the pathological substrate of cerebellar involvement is provided for each disease, followed by the review of MRI studies exploring structural and functional cerebellar abnormalities and by a discussion of the clinical relevance of MRI measures of cerebellar damage in terms of both clinical status and cognitive performance.

Key words: Cerebellum; Neurodegenerative disease; Ataxia; Multiple sclerosis; Parkinson's disease; Diffusion magnetic resonance imaging; Tractography; Volumetry; Functional magnetic resonance imaging; Alzheimer's disease

© **The Author(s) 2017.** Published by Baishideng Publishing Group Inc. All rights reserved.

Core tip: The cerebellum is involved in movement control and cognition. Conventional and advanced magnetic resonance imaging (MRI) techniques are widely used for the morphologic evaluation and the microstructural and functional investigation of the cerebellum. In this review we show the state of the art of advanced MRI techniques in the investigation of cerebellum alterations, especially in patients affected by neurodegenerative diseases. In particular, we evaluated advantages, limitations and future perspective of these techniques in multiple sclerosis, Parkinson's disease and Parkinsonisms, Alzheimer's disease and hereditary ataxia, highlighting how the investigation of cerebellum may play a key role in the assessment of motor performance and clinical status of these diseases.

Mormina E, Petracca M, Bommarito G, Piaggio N, Cocozza S, Inglese M. Cerebellum and neurodegenerative diseases: Beyond conventional magnetic resonance imaging. *World J Radiol* 2017; 9(10): 371-388 Available from: URL: <http://www.wjgnet.com/1949-8470/full/v9/i10/371.htm> DOI: <http://dx.doi.org/10.4329/wjor.v9.i10.371>

INTRODUCTION

The cerebellum plays a key role in normal brain function and its structural and functional involvement in several neurological diseases is associated with the impairment of both motor and non-motor functions such as cognition, mood and behavior. Imaging studies have been challenged in the past by the complex cerebellar anatomical structure and by its location in the posterior fossa. The advent of high-field magnets and the development of new algorithms for image acquisition and analysis have, at least in part, improved the study of cerebellar structure and functions. This review provides a brief description of cerebellar macro- and microscopic anatomy and functions and focuses on the imaging methods and segmentation tools for the analysis of the cerebellum with emphasis on each method's advantages and limitations. Further, the clinical implications of the cerebellar involvement in neurological diseases such as multiple sclerosis, hereditary ataxias, Parkinson's and Alzheimer's disease are discussed.

Anatomy and function

The cerebellum is a large folded structure consisting of two cerebellar hemispheres, united by a central part known as vermis located in the posterior cranial fossa, lying dorsal to the brainstem and inferior occipital lobes.

It is separated from the cerebrum by a dura mater layer known as tentorium cerebelli and it is surrounded postero-laterally and infero-medially by venous structures, respectively transverse and sigmoid sinuses. The cerebellar cortex is tightly folded and composed by three layers: Molecular layer, Purkinje cell layer and granular layer. Each ridge or gyrus of gray matter is called folium. Underneath these layer of gray matter there is a central mass of white matter, also called corpus midollare or arbor vitae (tree of life), in which are embedded the three deep gray matter cerebellar nuclei: Fastigial nucleus, interposed nucleus (composed by the emboliform and globose nuclei) and dentate nucleus. Three white matter peduncles (superior, middle and inferior) connect the cerebellum to the brainstem, respectively to the midbrain, pons and medulla oblongata. In addition to the above reported macro- and microscopic description, cerebellar structure can be further characterized from a morphologic, phylogenetic and functional perspective. The morphologic classification describes, without any functional basis, a division into three lobes: Anterior, posterior and flocculonodular lobe, while the phylogenetic classification divides the cerebellum into archicerebellum (the most ancient portion), paleocerebellum (developed after archicerebellum) and neocerebellum (the newest portion). The functional classification divides the cerebellum in three regions: Vestibulocerebellum, spinocerebellum and cerebrocerebellum based on the location of the afferent and efferent neurons^[1,2]. The vestibulocerebellum corresponds to the flocculonodular lobe, with afferents neurons arising from vestibular nuclei (and some portion of visual cortex) and efferents neurons going to vestibular nuclei. It modulates gait balance and eye movements. The spinocerebellum is formed by the superior and inferior portion of the vermis (with the exception of the nodule) and by a bilateral paravermian portion, located on both sides of the vermis. The vermian part of the spinocerebellum has its afferent neurons arising from the spinal cord, vestibular, visual and acoustic nuclei and has its efferents neurons going through the fastigial nucleus. It modulates head and neck muscle movement as well as trunk and limb proximal portions. The paravermian part of the spinocerebellum has its afferents neurons arising from the spinal cord and trigeminal sensory nuclei, and its efferents neurons going through the interposed nucleus. It completes movement modulation performed by the vermian part, acting on limb distal portions. The cerebrocerebellum is composed by the two cerebellar hemispheres and receives afferent neurons from most of the neocortex (frontal, parietal, temporal, and occipital lobes) through the pons nuclei, sending its efferent neurons to thalamus and cerebral cortex through the dentate nucleus. Functional specificity is granted by the presence of multiple close-loop circuits between cerebral and cerebellar cortex, in which the same brain area that is the major target of output from the cerebro-cerebellar circuit it is also its major source of input^[3,4]. In each loop, a specific cortical area projects through the pontine nuclei to a distinct region

of the cerebellar cortex. A specific portion of the dentate nucleus projects then to a specific cortical area through a distinct thalamic region, thus closing the cerebro-cerebellar loop^[5,6]. According to studies conducted on primates, the dentate nucleus is topographically organized in a ventral portion, projecting to the prefrontal and posterior parietal cortex, and a dorsal portion, projecting to the motor cortex^[7]. Both motor and non-motor domains of the dentate also project to the striatum (input stage of basal ganglia processing), raising the hypothesis that cerebellum could also modulate basal ganglia facilitation of voluntary movements^[8]. The cerebrocerebellum is the largest part of the cerebellum and accounts for motor planning and motor learning. It is responsible for the transition from controlled to automatic movement: Once motor memories storage has been achieved in the cerebellar cortex, the execution of movements can be triggered by sparse high-level command from cerebral cortex^[9]. The ability of the cerebellum to adjust performance according to context, automatically integrating interoception with perception and internal models, does not apply only to movements controls but also to cognitive function, as proved by the occurrence of the cerebellar cognitive-affective syndrome following acute cerebellar lesions of the posterior lobe^[10]. In particular, lesions of the posterolateral hemispheres cause cognitive disturbances, while vermis lesions induce behavioral and affective alterations. Cerebrocerebellum is considered an essential modulator of cognitive abilities, such as language processing and visuospatial perception (respectively lateralized in the right and left cerebellar hemisphere), as well as high order functions as emotions, behaviors and personality. For example, thanks to its connection to the prefrontal cortex, the cerebellum is involved in the execution of abstract rules that govern response selection, regardless of whether they specifically relate to the selection of actions^[11,12].

MRI of the posterior cranial fossa

The posterior cranial fossa (PCF) is located between the tentorium cerebelli and foramen magnum and houses the cerebellum and the brainstem. For its peculiar conformation, small dimensions and contained structures, an accurate study by means of computed tomography (CT) and MRI had always represented a great challenge^[13-15]. However, several progresses have been made in this field to avoid the artifacts related to the X-ray beam hardening and the partial volume effects (which is non-linear) caused by the thickness and the irregularity of the skull-base bones. Specifically, the introduction of thin-section spiral multidetector CT, which allows the acquisition of isotropic voxel scans and the use of MRI scanners which allow the acquisition of multiplanar and multiparametric images have contributed to minimize PCF artifacts^[16-23]. Most of PCF artifacts are related to blood flow pulsation, inflow/outflow of cerebro-spinal fluid (CSF) and to the brain-bone-air interfaces^[24-30].

Artifacts related to vessels blood pulsation generate a signal that is displaced from its correct anatomical

position causing a wrong/inappropriate image, also called "ghost" artifacts^[31]. Transverse sinuses blood-flow related artifact, which often generate a false image projecting onto cerebellar parenchyma, may lead to an inaccurate or inappropriate interpretation of MR images. Artifacts related to the inflow and outflow of CSF inside PCF from the superior or inferior regions can be minimized by the use of fluid attenuated inversion recovery (FLAIR) images where the CSF signal is nulled out by setting a proper inversion pulse. Unfortunately, these artifacts can still be present if the inversion pulse is spatially selective, allowing a partial suppression^[30,32]. As shown by Baksi *et al.*^[30] and Lavdas *et al.*^[33] this type of artifact may mimic or hide a brain parenchymal lesion due to the presence, along with the phase encoding direction, of a redundant CSF signal.

The brain-bone-air interfaces artifact represents one of the magnetic susceptibility artifacts that are often present on gradient-echo sequences^[28], especially in regions like the skull base, petrous temporal bone, paranasal sinuses and orbits^[34,35].

It should be noted that some MRI sequences are more prone to specific artifacts than others: *i.e.*, gradient-echo for susceptibility artifacts (since this sequence does not use a refocusing 180° pulse and signal dephases fast due to field inhomogeneity), inversion recovery (*e.g.*, short tau inversion recovery and FLAIR) for pulsatile artifacts, or 2D time-of-flight for slow-flow artefactual gaps in non-dominant transverse sinus^[13,30,33,36]. Nonetheless, some of these artifacts are routinely exploited for diagnostic purposes: Susceptibility weighted images (and in general T2*w gradient-echo images) thanks to its capability of being susceptible to paramagnetic molecules, is able to recognize small amounts of blood degradation products better than other sequences and to distinguish between parenchymal calcifications and blood products^[37].

Although the combined use of MRI and CT is recommended for the diagnosis of PCF pathologies, MR is preferred to CT in order to evaluate soft tissue structures and to determinate their spatial relationship. While MRI provides higher accuracy in detecting bone marrow changes, brain parenchyma, meningeal infiltration, perineural and perivascular spread caused by tumors^[14,38,39], CT is more sensitive for the evaluation of bone structures, PFC tumoral and non-tumoral conditions^[14,40].

High and ultra-high field MRI

The possibility to study the brain at high and ultra-high field strength has become quite common after the United States FDA approval of MR magnets up to 4 Tesla (T) for clinical use. Currently, the term ultra-high field is used for MR scanners with a magnetic field strength higher than 3T. The application of high and ultra-high static magnetic field strength can improve the visualization of brain anatomy and the study of changes in brain structure and function in several neuropsychiatric diseases. For example, the higher signal-to-noise ratio (SNR) of 3T scanners allows not only to perform faster imaging compared to 1.5T scanners (doubling the strength of the

magnetic field would theoretically lead to a reduction of acquisition time of a factor of four), but also to acquire images at higher spatial resolution, that turns be very useful in the evaluation of small structures such as the cerebellum and the brainstem. It has been shown that higher spatial resolution is helpful in studying the cerebellar cortex, whose thickness is lower than cerebral thickness (< 0.5 mm vs the 3-4 mm, respectively)^[41,42].

In the research field, 7T MR scanners have proven to be of great use for the identification and the study of each cerebellar folia (which are approximatively 260)^[43] and for the study of cerebellar cortical layers. Specifically, the granular and molecular cerebellar layers, whose thickness is approximatively 240 μ m, are well recognized and morphologically studied at 7T which has the unique advantage to allow an in-plane voxel size of 120 μ m not possible at low-field MR scanners^[44]. It is important to bear in mind that higher magnetic fields bring the inherit heavy burden of several artifacts and limitations. For instance chemical shift imaging and susceptibility artifacts, are only some of the artifacts that will increase with high magnetic field. These phenomena, which may cause images misinterpretation, can also be exploited, leading for example to a better separation of metabolites in spectroscopy, a better performance in perfusion weighted imaging, or a better blood products detection. Further, when using high and ultra-high magnetic fields in humans, the specific absorption rate (SAR) should also be carefully evaluated, since it will be quadruplicate with the doubling of the field strength, limiting the use of some sequences and making some parameter modulation necessary in order not to exceed the SAR threshold limit given by International Electrotechnical Commission^[45].

MRI techniques available for the study of cerebellum **Conventional morphologic techniques**

The remarkable wide range of MR sequences available for the study of the PCF and the cerebellum comes with the difficulty of making the optimal selection based on the clinical or research question. In a standard clinical study the MRI protocol should include a turbo spin-echo (TSE) T1weighted (T1w) sequence to assess shape and dimension of the cerebellum and of the PCF, TSE-T2w and FLAIR-T2w sequences to detect potential white matter (WM) lesions. The choice of an isotropic voxel (≤ 1 mm) should always be preferred when available or when a high-resolution multiplanar evaluation is needed. For example, it has been showed that, in comparison to TSE-T2/proton density sequences, isotropic 3D-FLAIR is more accurate in detecting not only white matter lesions but also cortical and infratentorial lesions in patients with multiple sclerosis (MS)^[46]. 3D FLAIR has advantages even when acquired at ultra-high magnetic field, such as in the study of Kilsdonk *et al*^[47] in which cortical gray matter (GM) lesions were better detected at 7T with 3D FLAIR than with GM-Specific 3D double inversion recovery (DIR) or with 2D-T2w and 3D-T1w. Finally, quantitative T1 and proton density (ρ) magnetic resonance imaging at 3T

provide a good visualization of deep cerebellar nuclei, like dentate nuclei at 1.5T^[48]. Similarly, susceptibility weighted imaging (SWI) allows a better detection of the dentate nuclei at 1.5T while higher magnetic field allows visualization of the dentate wall corrugation, which is the iron-poorer dorsal portion of it^[49].

Volumetric techniques

There is an ever-increasing interest in the evaluation of cerebellar volume as a potential correlate of motor and cognitive performance and as a biomarker of progression and/or treatment outcome in neurodegenerative disorders^[50].

Several computerized methods with specific advantages and limitations are available to perform cerebellar segmentation, lobule parcellation and thus to assess global cerebellar volume, regional or lobular volumes and GM and WM volume. Although manual volume segmentation is considered the "gold standard", this option is extremely time-consuming and its reliability may vary with the experience of the raters^[51]. Several semi-automatic computerized methods have been developed and validated in order to minimize operator-dependent limitation. We will focus on the methods that have been more extensively applied in clinical studies and will describe each method's advantages and limitations.

SUIT (spatially unbiased atlas template of the cerebellum and brainstem) is a Statistical Parametric mapping software (SPM) toolbox for MATLAB, based on a nonlinear coregistration of MRI images to a high-resolution cerebellum template obtained from images of healthy controls^[52]. This method allows the parcellation of the cerebellum in at least 28 lobules, thus measuring GM volume for each lobule and the global GM volume as the sum of all lobule volumes (Figure 1). SUIT has been applied to the study of several diseases such as multiple sclerosis (MS), autism spectrum disorder, attention deficit hyperactivity disorder, developmental dyslexia and primary craniocervical dystonia, and it has been shown that it has higher sensibility to volume changes than conventional whole-brain voxel-based morphometry (VBM) methods^[50,53,54]. The main advantage of SUIT is that it provides an optimal overlap of the cerebellar lobules, preserving anatomical details, and thanks to its cropping step avoids results bias from supratentorial structures^[50,53,54]. However, Bogovic *et al*^[51] reported that SUIT accuracy may decrease in patients with severe cerebellar atrophy especially with regard to lobule specific segmentation.

Cerebellar analysis toolkit (CATK) is based on a Bayesian framework of FMRIB's Integrated Registration and Segmentation Tool^[55]. Using hand-delineated examples, active appearance models are created in order to perform cerebellar labeling and segmentation. CATK has shown a high reliability (Intraclass Correlation Coefficients, ICCs, of 0.96 for test-retest) a good manual segmentation agreement (ICC 0.87) and a better performance than other softwares, such as SUIT (v 2.7) and Freesurfer when compared to manual segmentation



Figure 1 SUIE atlas (top) and template (bottom) showing the central cerebellar slice in the sagittal, coronal and axial planes. The atlas does not explicitly identify white matter apart from the dentate nuclei (from Ref. [55]).

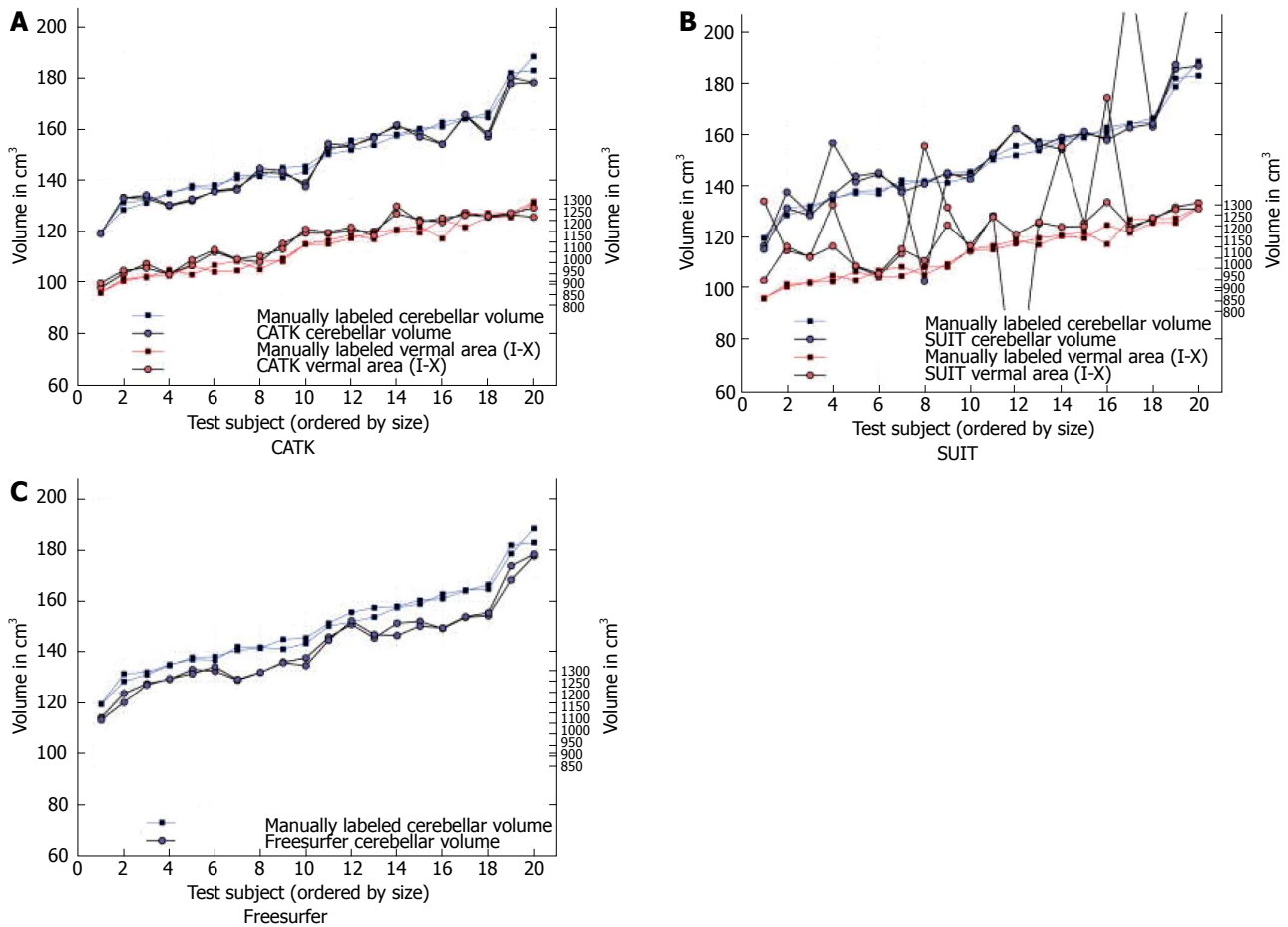


Figure 2 Comparative plots of total cerebellar volumes and combined vermal areas are shown against manually labeled examples, in 20 subjects with (A) CATK, (B) SUIE and (C) Freesurfer. Both test and retest are plotted, illustrating the repeatability of each method (from Ref. [55]).

(gold standard). However, the main limitation when compared to other softwares, is that CATK does not allow cerebellar hemisphere parcellation, although Price *et al.*^[55] in their paper stated a pending further improvement which would solve this issue and which would give higher image delineation (Figure 2).

ECCET is a semiautomatic toolkit based on a manually drawn region of interest ROI software. It is able to perform a fast semiautomatic segmentation after a manual outline drawing of few brainstem slices. It allows, when needed, manual editing in a 3D volume rendering mode (https://www.eccet.de/projects/neuro_en.html). This method has shown a good interobserver (ICC =

0.98, 95%CI = 0.74-0.99) and test-retest reliability (ICC = 0.99, 95%CI = 0.98-0.99) and the capability of avoiding some segmentation errors such as the inclusion of venous sinuses without the need of manual editing^[56].

Unfortunately, to date, all the above-mentioned softwares provide pipelines for one time point evaluation (cross-sectional), but not for longitudinal analysis along time. This gap has been fulfilled by Freesurfer, which is a software that allows a reliable automatic whole brain segmentation, with up to 40 subcortical structures, labelling each voxel in a normalized space of the brain volume^[57]. In addition to the cross-sectional analysis, Freesurfer comprises a longitudinal stream where each

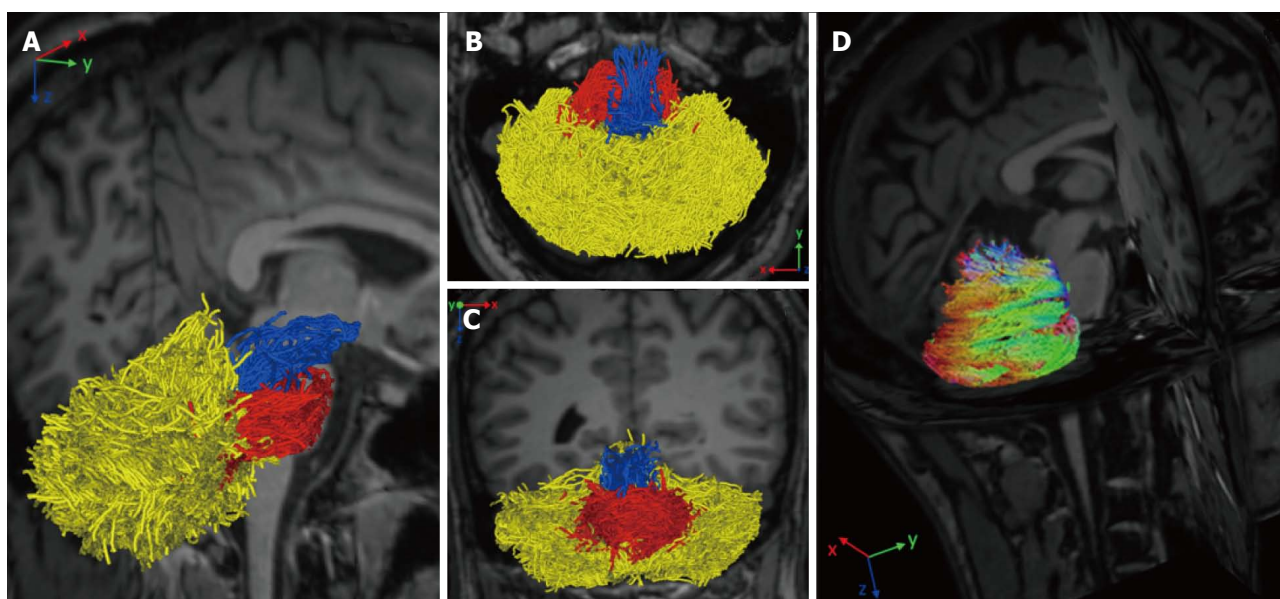


Figure 3 Reconstruction of cerebellar white matter tracts using constrained spherical deconvolution. Sagittal rotated view (A), superior axial view (B), and coronal view (C) show each fiber bundle manually colored: Superior cerebellar peduncle (blue), middle cerebellar peduncle (red), and hemispheric cerebellar tracts (yellow). The tridimensional sagittal rotated view shows color-coded cerebellar hemispheric streamlines according to the principal eigenvector's direction (with permission of Springer, from Ref. [63]).

time-point is co-registered to a subject-specific template by creating an average segmentation along time points, resulting in volume and GM thickness estimation^[57]. Although Freesurfer presents this important advantage, it does not allow sub-regional segmentation in cerebellar lobules^[55]. Moreover, manual editing of segmentation outputs is needed in order to improve volume evaluation reliability^[58]. Although the editing can be performed manually, resulting in a very time-consuming (up to 4h) and operator-dependent approach, Wang *et al.*^[58], in a recent paper, proposed an accurate and efficient new machine-learning based method in order to overcome this issue.

Diffusion weighted imaging and fiber tractography

Diffusion magnetic resonance imaging (dMRI) is a MRI technique able to detect water molecules diffusion inside brain tissue. While diffusion of water molecules in GM is isotropic, diffusion in WM is anisotropic, *i.e.*, it occurs in one main direction due to the presence of myelin barriers^[59]. The evaluation of diffusion in a three dimensional space and along at least 6 directions, allows the creation of a diffusion tensor matrix, which provides the bases of tractographic reconstruction of brain neural circuitry^[60]. Diffusion tensor imaging (DTI) and more advanced approaches (such as diffusion spectrum imaging or constrained spherical deconvolution) have been applied to determine cerebellar pathways and their connection with other supratentorial areas^[61-63] (Figure 3). Although conventional DTI techniques are the most used technique to reconstruct cerebellar pathways by means of tractography, they are also well known for their limitations in the study of connectivity. DTI, indeed, is limited by the inability to discriminate different fiber

populations with complex configurations at a voxel level (kissing fibers, bridging fibers, merging fibers, crossing fibers), thus leading to artefacts in fiber reconstructions and connectivity evaluations. Methods such as diffusion spectrum imaging and Q-ball imaging have been developed over the last few years to overcome these limitations; however, the more complex hardware set up and the longer acquisition times have limited so far their application in the clinical setting^[64]. Other promising techniques, such as diffusion kurtosis imaging (DKI), neurite orientation dispersion and density imaging (NODDI) and constrained spherical deconvolution can be performed within clinically feasible acquisition times^[65] (Figure 3). Moreover, all these techniques can be analyzed with both deterministic and probabilistic fiber reconstruction models. While deterministic models reconstruct streamlines (virtual fiber tracts) taking into account the principle eigenvector of fractional anisotropy (FA) in each voxel, probabilistic models generate a connectivity map from a larger numbers of possible pathways, obtaining the probability of each voxel to be connected to another^[66]. Regardless of the used approach, tractographic output can be used not only to reconstruct the spatial configuration of fiber tracts but also to measure diffusion parameters (*i.e.*, FA or mean diffusivity) at voxel level. However, it has been proved that, not only parameters' quantification but also the accuracy of tractographic results may be affected by the poor quality of the acquired data that can lead to the detection of false connections or to miss detection of a real connections between structures^[59]. Therefore, a better data quality, optimized in terms of SNR, spatial resolution, number of diffusion directions, and number and values of *b* values, with the choice of a proper tractography method, may improve the method performance avoiding

inaccuracy in structural connectivity analysis^[67]. Since cerebellar pathways tracking is particularly difficult due to the presence of sharp turning angles along their crossing, the assessment of cerebro-cerebellar and intra-cerebellar connectivity could especially benefit from data quality improvement^[61,63].

Resting state and task related fMRI

Functional MRI (fMRI) is based on the detection of the blood oxygen level-dependent (BOLD) changes that take place as a consequence of neuronal activity. An increase in neural activity leads to an increase in the arterial blood flow, in order to increase the activity itself. To this increase in the amount of oxygenated blood does not correspond a similar increase in oxygen extraction at the level of capillary bed, leading to a relative decrease of deoxyhemoglobin levels, that directly affects the MR signal.

fMRI experiments can be divided in task and rest-related. The first measure brain activity during a task performance, the second evaluate the interaction between different brain regions without the execution of any specific task, in a rest condition (resting-state fMRI - RS-fMRI).

With regard to task-based fMRI studies, two main experimental paradigms are commonly used^[68]. The first one is the so-called block design experiment, in which stimuli are presented to the subject in blocks of variable length alternated to blocks of rest, in which the stimulus is removed. MRI signals are then compared between the two conditions, in order to extrapolate the areas that show more activation during the execution of the task. The second is the event-related experimental design, in which the stimuli and the resting blocks are not alternated in a set sequence, but the administration, as well as the duration of the stimulus, are randomized.

RS-fMRI experiments can be analyzed using two major approaches. The first one is the seed-based approach, in which a region of interest is selected and the corresponding time-activity curve is extracted. Then, voxels with similar activation are searched whole brain, and are assumed to be functionally correlated to the chosen seed^[69]. The second method is the independent component analysis (ICA), a mathematical algorithm that allows to subdivide a multivariate and noisy signal in its subcomponents^[70]. In this approach, no a priori seeds are chosen, but the operator is asked to identify the component of interest, and discard those obtained from noise or physiological signals. ICA analysis has allowed the identification of preferential connections between specific cerebral structures, that take the name of resting state networks^[71]. Cerebellar lobules are not only hubs of several of these resting state networks (*i.e.*, lobule IX in the default mode network, crus I and II in the executive control network or lobule VI in the salience network)^[72], but also an entire and separate cerebellar network is recognized among the major resting state networks^[71].

With this knowledge, it is easy to understand how future improvement is warranted to increase the of

functional changes with respect of the cerebellar lobular anatomy. In particular, the possibility of increasing spatial resolution in fMRI experiments is a future challenge for investigating cerebellar functional connectivity due to the characteristic lobular anatomy. The increase in spatial resolution could further help in elucidating the exact functional lobular topography of the cerebellum, with regards to specific motor and cognitive functions^[73].

Proton magnetic resonance spectroscopy

Proton magnetic resonance spectroscopy (¹H-MRS) is an analytical method that allows the investigation of brain metabolites. Every metabolite at sufficient concentration level generates a specific peak in function of its resonance frequency^[74]. Since metabolic abnormalities occur earlier than structural MRI alterations, ¹H-MRS can provide a valid tool for early diagnosis and for monitoring of neurological diseases^[75].

The most commonly studied brain metabolites are the N-acetylaspartate, a marker of neuroaxonal integrity, choline containing compounds, a marker of membrane turnovers, creatine/phosphocreatine, a marker of energy metabolism, and myo-inositol, a marker of astroglial activation. From a quantification point of view, metabolites' levels are expressed as absolute quantifications or as ratios where the denominator is the creatine level which is assumed to be stable in normal as well as in many pathologic states^[76].

Although the infratentorial structures are often involved in neurodegenerative processes, strong B0 inhomogeneities due to nearby skull bone, scalp lipids and tissue/air interfaces constitute a technical challenge for the ¹H-MRS acquisition. In addition, the small size of cerebellum increases the risk of partial volume effects^[77], which can be accounted for by combining spectroscopic data with structural MRI segmentation^[78]. Nevertheless, ¹H-MRS of the infratentorial fossa is feasible^[79] and could provide an early biomarker of neuronal damage in cerebellar diseases, with even increased specificity when used in combination with other techniques^[80].

Perfusion MRI

Perfusion weighted imaging (PWI) allows the measurement of blood perfusion in brain tissue and it is categorized as: "minimally invasive" if requiring gadolinium injection (*i.e.*, dynamic susceptibility contrast MRI or DSC-MRI and dynamic contrast enhanced MRI or DCE-MRI) or "non-invasive" if no contrast agent is needed (*i.e.*, arterial spin labelling or ASL-MRI)^[81]. Data from either technique above is subsequently processed and normalized to estimate the well-known perfusion values: cerebral blood flow (CBF), cerebral blood volume (CBV), mean transit time (MTT), Ktrans and *etc.*, which are all representable on parametric color maps.

Cerebellar tissue is subject to a great blood supply, and measurement of local variations of blood request/availability is clinically relevant in the assessment of neurodegenerative diseases. Specifically, cerebral blood flow (CBF) alterations (*i.e.*, general or local CBF

reduction) appear to precede structural abnormalities (for example: atrophy). Moreover, the cerebellum has been used as a reference region for intensity normalization of “relative” Cerebral Blood Volume (rCBV), based on the assumption that its CBV is not affected in neurocognitive disorders^[82]. Although hard to eradicate, this assumption is nowadays obsolete, as alternative reference regions have recently been proposed and validated^[83].

With respect to the study of the cerebellum and the PCF, DSC-MRI provides higher spatial resolution, high sensitivity in transit time and whole-brain coverage in shorter scan times, and it is preferred in all situations where a fast assessment is required. DCE-MRI has the advantage of reducing artifacts especially for the measurement of CBV and Ktrans. ASL-MRI is often preferred in the study of neurodegenerative diseases for its complete lack of invasiveness, vessel selective capability^[84] and the best accuracy in absolute tissue perfusion quantification^[81]. Particular care in placing the “labeling plane” is essential to avoid artifacts in the lower cerebellar sections^[85]. Another limit of ASL-MRI is WM assessment, which is particularly challenging due to the low blood transit and the consequent low SNR^[86].

Unfortunately, despite the theoretical indications of each method, in the routine clinical settings, is the availability and practicality of the techniques that forces the choice, rather than its potential performance. This could explain the more frequent use of DSC and DCE imaging, faster, easy to perform and widely installed on most clinical scanners, compared to the use of ASL.

MRI AND CLINICAL APPLICATIONS ON NEURODEGENERATIVE DISEASES

Multiple sclerosis

Multiple Sclerosis (MS) is an inflammatory/demyelinating disease of the central nervous system (CNS) characterized by heterogeneous symptoms and signs that can present a relapsing remitting (RR) or a progressive course. In 1877 Jean Martin Charcot first described the disease as a triad of symptoms consisting of nystagmus, dysarthria and ataxia^[87], thus underlining the dominant role of cerebellar deficits. Not only is the cerebellum frequently involved by the disease pathological processes but the presence of MRI visible infratentorial lesions provides high specificity to the diagnostic criteria for MS^[88]. Indeed, 31% of patients with a clinically isolated syndrome (CIS) present with at least one infratentorial lesion and about 20.5% with a cerebellar lesion. The detection of a cerebellar lesion at onset is associated with an increased risk of conversion to MS^[89]. In patients with a clinically defined MS, cerebellar lesions have been described in up to 49% of cases and patients with a progressive form have an increased number of PCF lesions when compared to patients with a RR type^[90]. Disease pathology involves not only the cerebellar WM but also the GM; in fact, cortical cerebellar lesions are

observed in patients with MS, even at the early stages of the disease, and correlate with the cerebellar functional score of the expanded disability status scale (EDSS)^[91]. Longitudinal studies have shown cerebellar GM volume loss and an increased number of cortical lesions in both CIS, RR and progressive patients^[92,93].

Volumetry changes

Along with cerebral atrophy, also cerebellar volume loss occurs in patients with MS, at all the disease stages. Edwards and coworkers found reduced global cerebellar volumes in patients with a secondary progressive (SP) form when compared to RR patients, and in both groups when compared to healthy controls^[94]. However, in a more recent study, when compared to healthy controls only MS patients with a SP form, but not RR or patients with benign MS, showed lower cerebellar volumes^[50]. When cerebellar WM and GM are considered separately, study results are discordant. Ramasamy *et al.*^[95] found a reduced cerebellar WM but not GM volume in CIS and MS patients when compared to healthy controls. However, Anderson and coworkers detected a reduced cerebellar GM volume in RR and SP MS patients versus controls and only a trend of significance, when comparing WM volumes, between SP MS and controls^[96]. In the latter study, cerebellar GM and WM volumes were related with performance at the nine-hole peg test, highlighting the clinical relevance of measures of cerebellar volumes. A greater loss of GM in patients with a progressive course and its correlation with measures of clinical outcome are findings mirroring the process at the whole brain level.

Structural connectivity changes

DTI has been widely used for the study of cerebellar WM, in particular to evaluate the damage of the cerebellar peduncles and its clinical impact. Anderson *et al.*^[97] found reduced FA and increased radial diffusivity values in the middle cerebellar peduncle in patients with primary progressive (PP) MS; DTI metrics correlated with clinical impairment both of the upper and lower limbs. A study on a cohort of patients at different stages of the disease revealed greater mean, axial and radial diffusivity and reduced FA in MS patients, when compared to healthy controls, at the level of the middle and superior cerebellar peduncles; moreover, when compared to cerebellar peduncles T2 lesion load or atrophy, diffusivity measures better distinguished between patients with a worse EDSS score^[98]. Disability in RR patients also correlated with the FA values of the cerebellar normal appearing WM^[99].

Functional MR changes

MS is characterized by a reorganization of the functional connectivity. Functional MR studies with motor tasks revealed an increased activation in several cortical areas within the sensorimotor network, including the cerebellum, in patients when compared to healthy controls^[100,101] (Figure 4). The altered functional cerebellar connectivity could represent a compensatory mechanism to WM

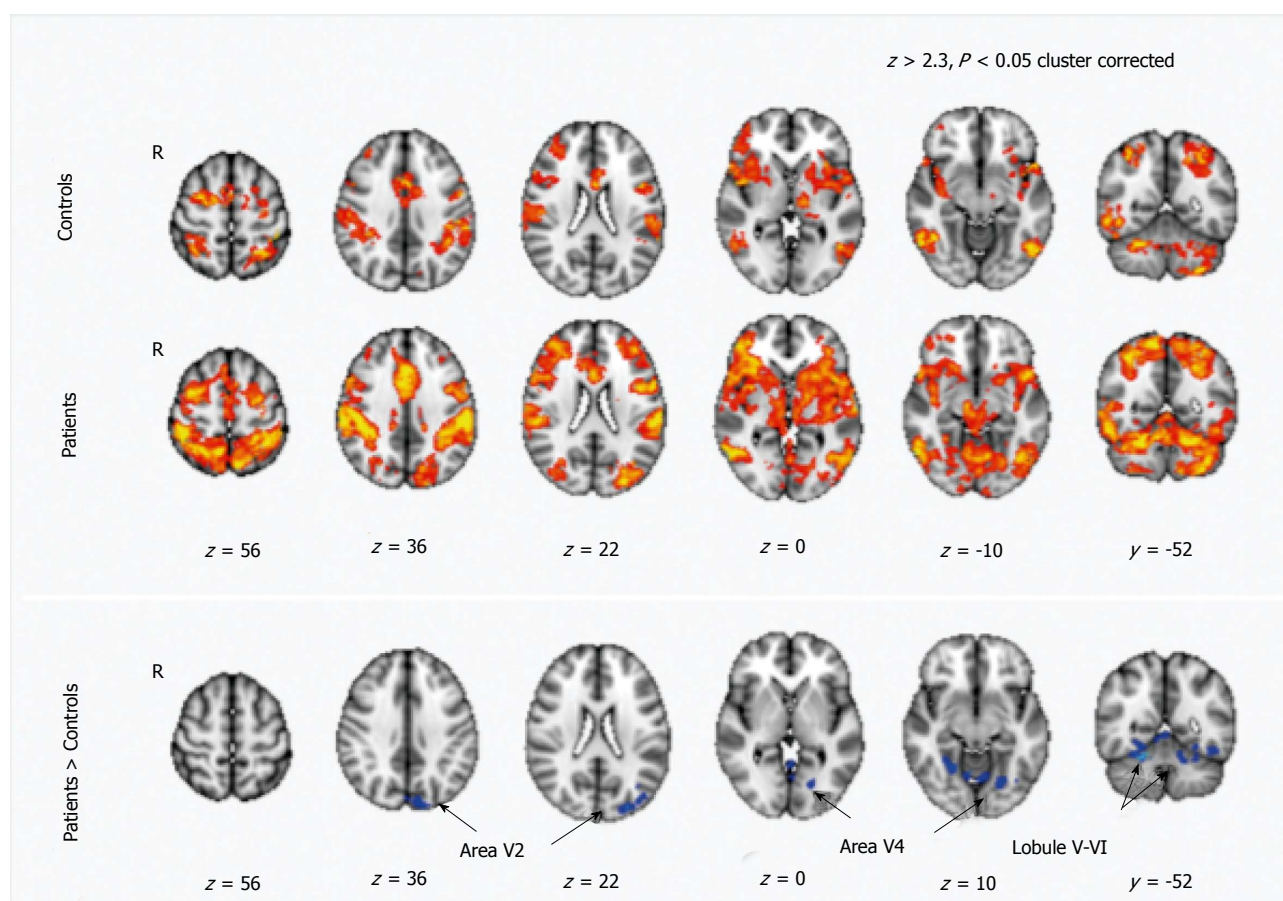


Figure 4 Motor training-dependent functional magnetic resonance imaging signal changes in healthy volunteers and in MS patients. Maps of training-related functional magnetic resonance imaging signal changes are reported in healthy volunteers (indicated as controls) and in patients ($Z > 2.3$, $P < 0.05$, cluster corrected). Comparison between patients and controls show a higher signal reduction in the patients in regions corresponding to the secondary visual areas (V2 and V4) and in the cerebellum (lobule V-VI) (from Ref. [100]). V5: Visual cortex; R5: Right hemisphere; fMRI: Functional magnetic resonance imaging.

damage; accordingly, in RR MS patients a damage in the dentatorubrothalamic tract, assessed by means of DTI, was related to an increased functional connectivity between right sensorimotor cortex and cerebellum^[101]. The cerebellum activation is also increased in patients with greater perceived fatigue where fatigue is conceived as a correlate of an increased resource demand for motor activities^[102].

Cerebellum and cognitive impairment

Besides the classical motor clinical features associated with cerebellar dysfunction, lately more attention has been focused on the role of cerebellum in cognitive impairment. MS patients with cerebellar signs perform worse at the symbol digit modalities test (SDMT) and the paced auditory serial addition test (PASAT); moreover, the PASAT execution is predicted by cerebellar lesion volume^[103]. In particular the posterior cerebellum has been implicated in cognitive processing; in MS patients, a reduced posterior volume predicted a worse cognitive performance^[50]. Information processing speed impairment has been associated with GM atrophy of the posterior lobules, especially at the level of the vermis VI^[104]. As with

motor tasks, a functional reorganization could also occur in response to the impairment of cognitive processes. Recently, a greater functional connectivity of the dentate nucleus with frontal and parietal cortical areas was detected in MS patients versus controls^[105,106] and the increased connectivity was related to a better cognitive performance. Moreover, an increased connectivity between anterior cingulate cortex and cerebellum was also associated with a better performance at PASAT in CIS, RR and SP patients versus controls and authors suggested an adaptive mechanism^[107].

Dentate nuclei hyperintensity

The hyperintense signal on T1-weighted images at the level of dentate nucleus has been detected in almost 50% of patients with a secondary progressive phase of the disease, in contrast to what found in the RR or PP form^[108]. Although this change in signal could be related to the reduction in the number and axosomatic synapses in the dentate nucleus as documented by pathological studies^[109], an association between the nuclei hyperintensity in T1-weighted images and Gadolinium retention has recently received greater attention^[110].

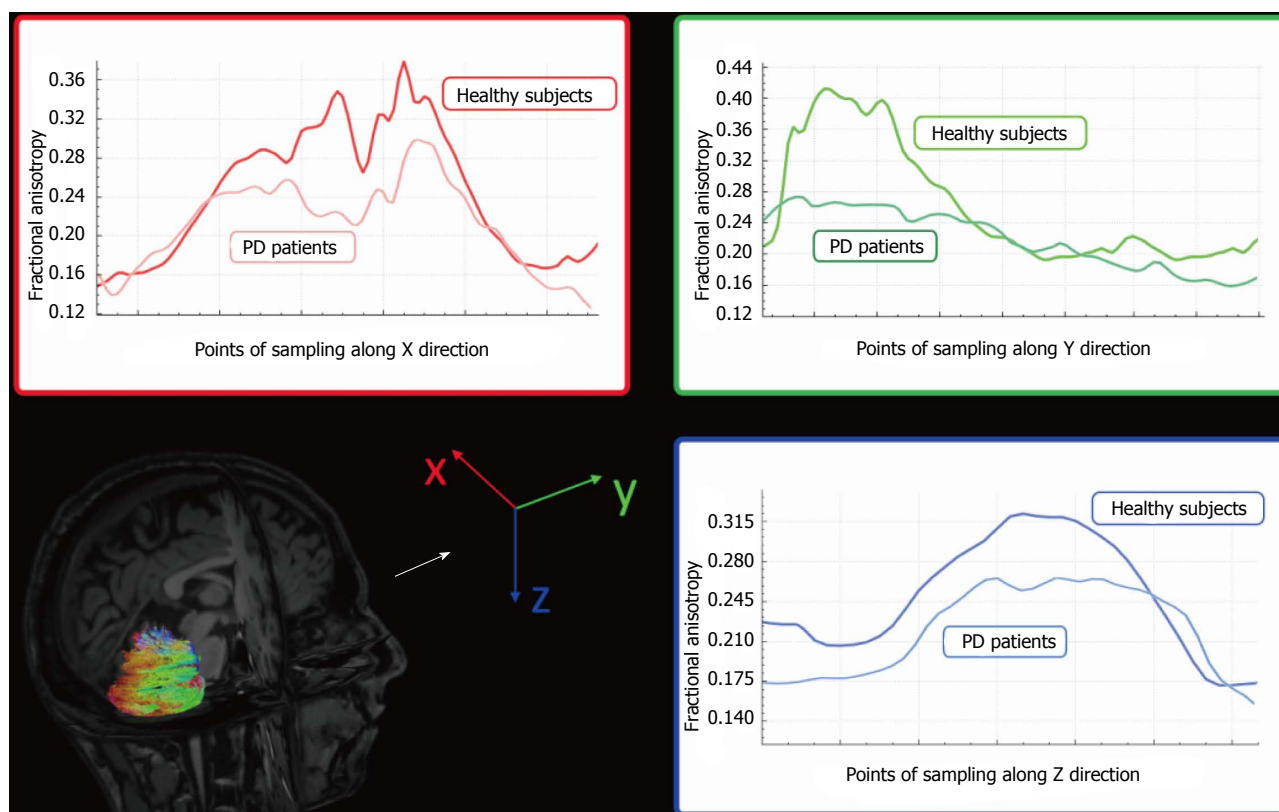


Figure 5 Graphic representations of Fractional Anisotropy mean decrement along X (red), Y (green), and Z (blue) direction samplings of Parkinson's disease patients compared to healthy subjects. Colors follow principal eigenvector's directions (with permission of Springer, from Ref. [63]). PD: Parkinson's disease.

PARKINSON'S DISEASE AND OTHER MOVEMENT DISORDERS

Parkinson's disease

Parkinson's disease (PD) is a neurodegenerative disorder pathologically characterized by the loss of dopaminergic neurons of the pars compacta of the substantia nigra; clinical features include motor, in particular rest tremor, bradykinesia and rigidity, and non-motor symptoms. The role of cerebellum in the physiopathology of this frequent neurodegenerative disorder has received increasing interest. Studies on monkeys discovered direct anatomical connections between cerebellum and basal ganglia, in particular with the subthalamic nuclei and the striatum^[8,111]. Such findings have been confirmed with a DTI study in humans^[112]. Interestingly, patients receiving deep brain stimulation had a clinical benefit when the electrode was positioned nearby one of these basal ganglia-cerebellum connections, in particular the dentato-thalamic tract.

Volumetry changes

Cerebellar atrophy has been documented in patients with PD. MRI morphometric studies have shown cerebellar volume loss at the level of the left cerebellum when compared to controls^[113], and at the level of the right quadrangular lobe and declive in patients with tremor compared to those without, thus suggesting a possible role of cerebellum in the genesis of rest tremor^[114]. A more

recent study confirmed cerebellar GM atrophy, which correlated with a reduced connectivity between cerebellum and sensorimotor, dorsal attention and default networks and an increased connectivity with the frontoparietal network^[115]. Altogether these results confirm the role of cerebellum in the physiopathology of motor symptoms in PD. Atrophy occurs since cerebellum is involved in the neurodegenerative pathological process of the disease, with the accumulation of α -synuclein and neuronal loss.

Structural connectivity changes

DTI studies have detected decreased FA in the cerebellar hemispheres of patients with PD when compared to healthy controls (Figure 5)^[63,116]. Although no differences in DTI parameters in superior and middle cerebellar peduncles have been detected between patients with PD and healthy subjects^[63], DTI metrics of the superior cerebellar peduncles could be helpful in differentiating PD and other parkinsonism, such as progressive supranuclear palsy (PSP)^[117].

Functional MR changes

Cerebellar hyperactivation has been showed and confirmed in several studies on patients with PD, both with akinesia-rigidity subtype and with tremor subtype. Whether the contribution of cerebellum is mostly an adaptive mechanism or a primary pathologic change of the disease is still a matter of debate. In a resting-state fMRI study, Wu *et al.*^[118] observed an increased activation

in the cerebellum in PD patients versus healthy controls; moreover, the altered pattern of activation was normalized after levodopa administration. A substitutive hyperactivity of the cerebello-thalamo-cortical circuit has been proposed as a mechanism to compensate the hypoactivation of the striato-thalamo-cortical circuit in hypokinetic patients; however, for PD tremor subtype, a dysfunction in the cerebello-thalamo-cortical circuit has been advanced as a physiopathologic mechanism for rest tremor^[118,119].

Multiple systemic atrophy

Multiple systemic atrophy (MSA) is a movement disorder, with a poor prognosis, which has two clinical phenotypes: one with a prominent akinetic-rigid parkinsonism (parkinsonian variant, MSA-P) and the other with a progressive ataxia (cerebellar variant, MSA-C). It has been suggested that imaging of cerebellum could be useful in the differential diagnosis of MSA. Atrophy of the middle cerebellar peduncles is frequent in patients with MSA and reduced volume of basal ganglia, middle and inferior cerebellar peduncles and pons have been found in the parkinsonian subtype of MSA, when compared with controls and PD patients^[120]. Moreover, both MSA-P and MSA-C patients were found to have higher MD values in cerebellar hemispheres when compared to PD and PSP patients^[121]. Brainstem and middle cerebellar peduncles atrophy have also been found to be very specific for the cerebellar subtype of MSA when compared to idiopathic late-onset cerebellar ataxia^[122].

Dystonia

Dystonia is a disorder characterized by sustained and abnormal spontaneous muscle contractions. It can be classified according to the etiology (inherited or acquired) or the topographic distribution. Cerebellar dysfunction has been implicated in the physiopathology of dystonia. Morphological cerebellar abnormalities have been reported in 14% of patients with cervical or segmental dystonia^[123]. Focal cerebellar lesions have been associated with dystonia and cerebellar atrophy has been described in patients with writer's cramp^[124]. Besides morphological studies, several functional studies have shown an increased activation in cerebellum in patients with writer's cramp^[125] and in patients with blepharospasm^[126].

Hereditary ataxias

Ataxias are an heterogeneous group of conditions characterized by slowly progressive incoordination of gait, often associated with a reduction of coordination of hands, speech, and oculomotor signs^[127]. Ataxias can be subdivided, basing on the etiology behind the development of the condition, in three major groups: acquired ataxias, nonhereditary degenerative ataxias and hereditary ataxias (HA), which can be further divided in dominant and recessive^[127]. Spinocerebellar ataxia type 3 (SCA3) is the most frequent type of dominant ataxia, followed by SCA2 and SCA6, while Friedreich Ataxia (FRDA) and ataxia-telangiectasia (AT) are respectively the first and the second most

common type of recessive ataxias, with FRDA that is, independently from the inheritance, the most frequent ataxia in terms of incidence^[128].

Volumetry changes

Atrophy of the cerebellar cortex is not a distinguish feature of all the HA. Different patterns of atrophy can be identified, depending on the degree of cerebellar atrophy and the involvement of midbrain structures. In particular, SCA3 and SCA2 are characterized by the presence of cortical, cerebellar and pons atrophy^[129]. On the other hand, SCA6 shows a pattern of pure cortical cerebellar atrophy, with a relative sparing of midbrain structures^[130]. With regard to recessive ataxias, FRDA is characterized by a prominent spinal cord atrophy^[131] compared to cerebellar cortical structures^[132], with atrophy that, when significant, affects mainly the lateral cerebellar hemispheres^[133]. Finally, AT is characterized by superior cerebellar hemispheres atrophy, in particular of the vermis, which appears hypoplastic in its inferior portion^[134-137].

Structural connectivity changes

Unlike volumetric measures, almost all the major HA show similar microstructural changes affecting infratentorial WM tracts. Indeed, SCA3 patients showed a significant FA reduction in different cerebellar areas, including both anterior and posterior cerebellar lobes, nodule, culmen, dentate, fastigial, lingual, and all three cerebellar peduncles, as well as in pons and midbrain^[138]. These abnormalities were correlated with clinical variables, such as scale for the assessment and rating of ataxia (SARA) scores or disease duration^[138,139]. In SCA2, significant microstructural changes were present in cerebellar WM, brainstem and cerebellar peduncle^[140,141], with changes in the mode of anisotropy that were lower in SCA2 patients compared to healthy controls in a longitudinal evaluation^[141]. Unlike in SCA3, no correlation with clinical variables emerged for these infratentorial clusters of microstructural changes in SCA2. In FRDA, microstructural changes were found to affect predominantly cerebellar peduncles^[142-145], as well as cerebellar hemispheres and vermis^[144] and to be associated with clinical disability^[142-144]. Finally, in AT patients a reduction of mean diffusivity was reported within cerebellar peduncle regions^[146] (Figure 6).

Functional MR changes

Similar to structural connectivity, functional connectivity changes are present in almost all HA. However, these modifications are not limited to a somehow expected reduction of FC in HA patients compared to healthy controls, but also increase in FC are reported in some HA, probably due to compensatory phenomena, reflecting the known heterogeneity of this group of conditions. Indeed, a significant increase of activation of the ventral part of the dentate nuclei, but not of the cerebellar cortex, was found during an hand-movement task fMRI experiment in SCA3 patients compared to healthy controls, suggesting a

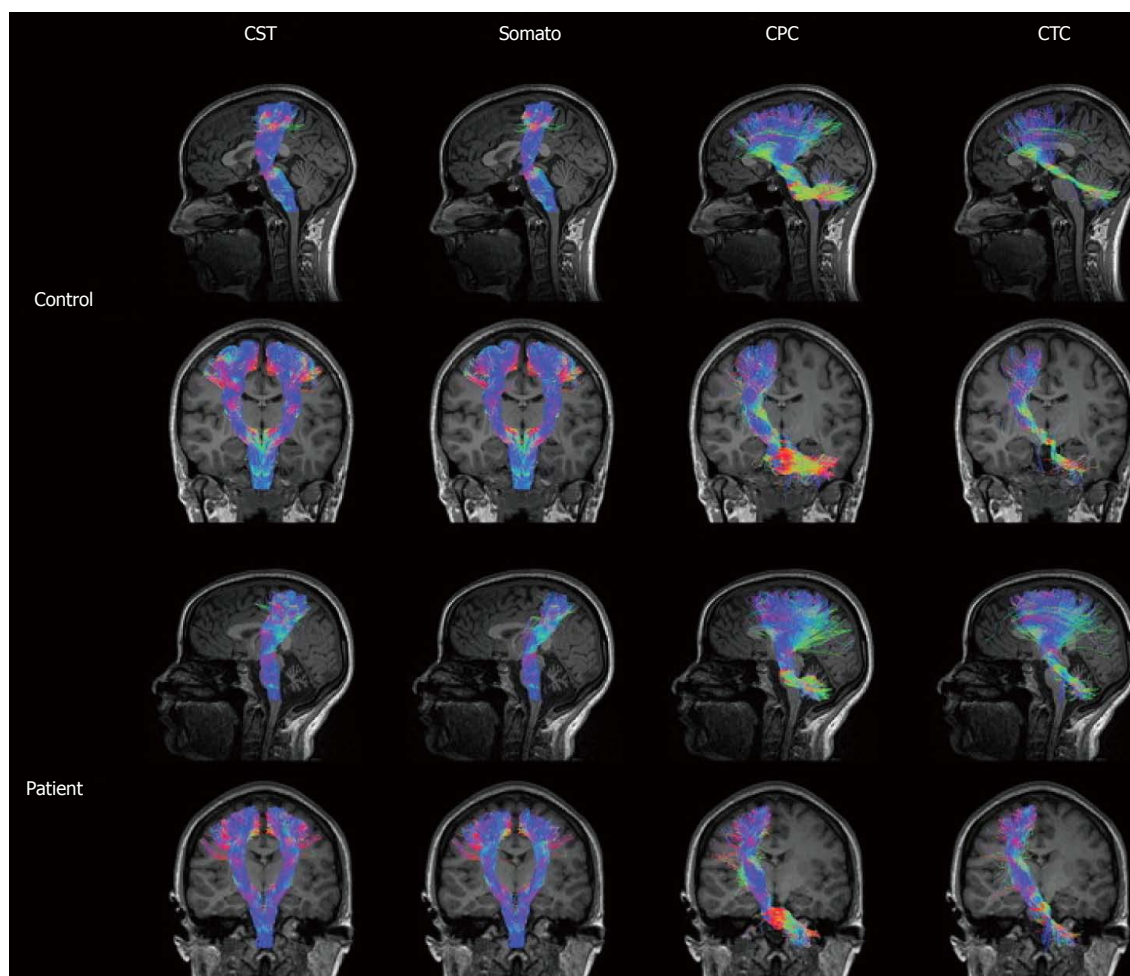


Figure 6 Somatosensory motor tracts in a representative control and ataxia telangiectasia (A-T) subject (age 23). Control tracts are displayed in the first and second rows comprising the left sagittal (first row) tracts, left and right coronal (second row) corticospinal (CST) and somatosensory tracts, and left coronal (second row) cortico-ponto-cerebellar (CPC) and cerebellar-thalamo-cortical (CTC) tracts. Patient tracts are displayed in the third and fourth rows comprising the left sagittal (third row) tracts, left and right coronal (fourth row) CST and somatosensory tracts, and left coronal (fourth row) CPC and CTC tracts. Tract colors are based on the direction of water diffusion (Blue: Ascending–descending diffusion; Red: Left–right diffusion; Green: Anterior–posterior diffusion). Compared to motor pathways in age matched controls, A-T CST and somatosensory pathways display a morphological thinning of tracts at the level of the thalamus in the coronal view. In addition, A-T CPC and CTC pathways display morphological thinning of tracts in the cerebellum at the position of the medial cerebellar peduncles (from Ref. [147]).

compensatory phenomenon of the *cerebrocerebellum* to a prominent damage of the *spinocerebellum*^[147]. Moreover, a recent fMRI study, involving a bilateral audiopaced thumb movements paradigm, showed a diminished movement synchronization in SCA3 patients^[148] that would suggest the presence of functional reorganization of the motor network and a potential role of fMRI as a tool to monitor the disease^[148]. In SCA2, a seed-based fMRI analysis showed a decreased putaminal connection with the pons, together with a decreased connectivity between the rostral sensorimotor area and both cerebellum and pons^[149]. Furthermore, a decrease of the functional connectivity of the cerebellar components of the default mode, executive and right fronto-parietal networks was described in SCA2, unrelated to the cortical gray matter volume loss^[150], with some authors that showed a significant correlation between both motor and neuropsychological scores and the abnormal cerebellar functional connectivity strength^[151]. In SCA6 patients, a significantly higher activation at the level of the lobules V and VI, as well as in the dentate

nuclei, was detected compared to controls when performing a hand-movement task fMRI experiment^[147]. Likewise, in FRDA patients the same motor task showed a higher activation mainly prominent at the level of lobules V and VI and dentate nuclei, compared to healthy control^[147]. Furthermore, a working memory task fMRI experiment showed that FRDA patients had a decrease functional connectivity between cerebellum and prefrontal areas, with a correlation between disease severity and cerebellar dysfunction^[152].

Alzheimer's disease

Alzheimer's disease (AD) is the most common cause of dementia and it is preceded by a predementia phase, called mild cognitive impairment (MCI), characterized by a deficit in one or more cognitive domains. The role of cerebellum involvement in AD is controversial. While a volumetric MRI study in patients with AD, MCI and healthy controls found a volume loss at the level of the posterior cerebellar lobes in AD patients compared to healthy

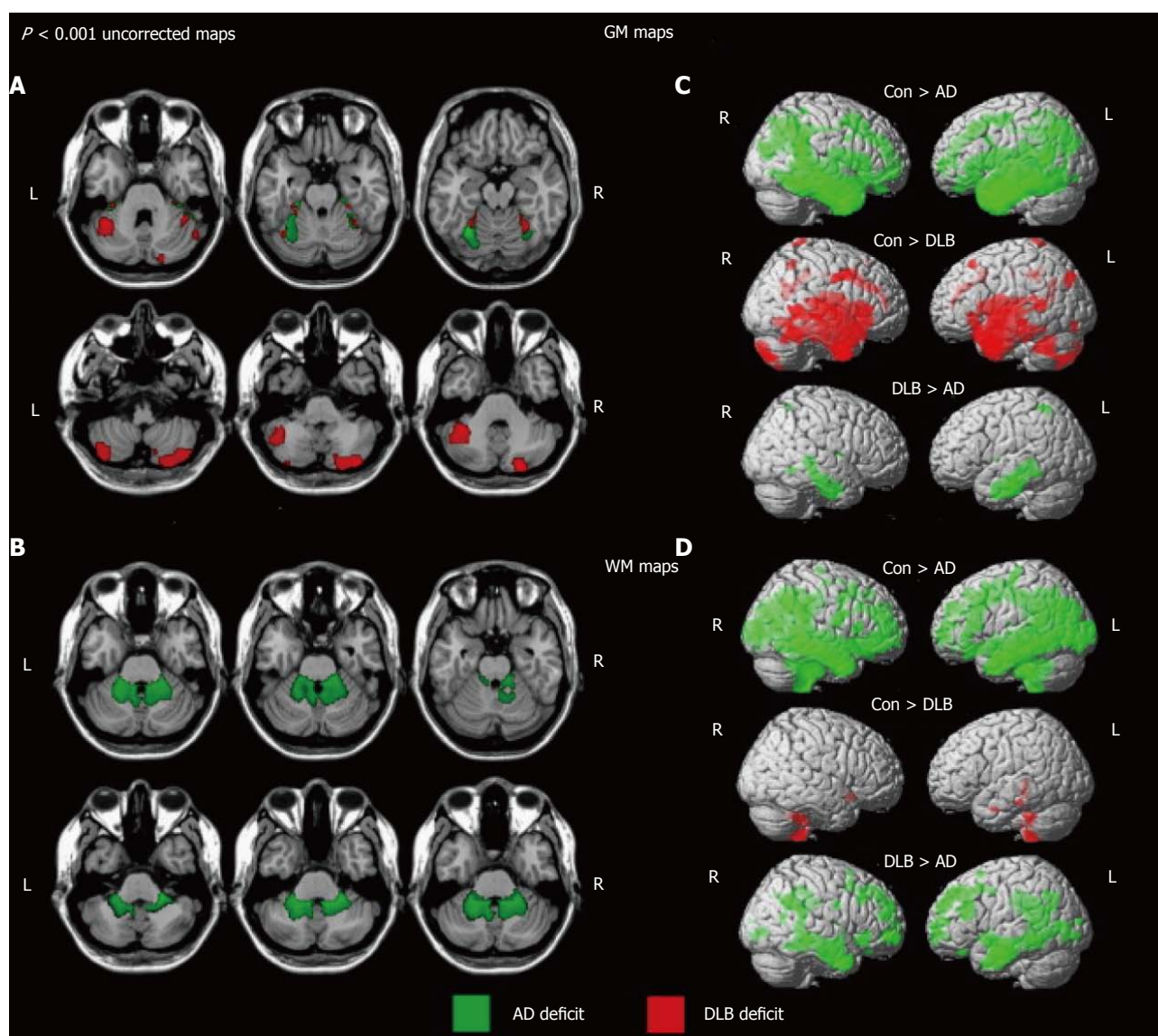


Figure 7 Significant cerebellar GM and WM loss in Alzheimer's disease. A: Significant cerebellar GM loss in Alzheimer's disease (green) and dementia with Lewy bodies (red) relative to healthy older subjects; B: Significant cerebellar WM loss in AD relative to healthy older subjects; C and D: Whole brain maps depicting significant regions of GM (C) and WM (D) loss between groups. Results superimposed on a MRI T1 brain template image (L = left, R = right). AD: Alzheimer's disease; DLB: Dementia with Lewy bodies (from Ref. [154]). GM: Gray matter; WM: White matter.

controls, no significant differences were showed between patients with MCI and healthy controls^[153]. Another study detected a regional GM atrophy in cerebellar lobule VI in patients with AD^[154] (Figure 7). These findings were not confirmed^[155] in a more recent study, suggesting that the decrease of cerebellar volume could be influenced by the patients' age. This is supported by the findings of cerebellar atrophy in patients with a late-onset, but not early-onset AD^[156] and by the presence of cerebellar atrophy in cognitively preserved old subjects^[157].

CONCLUSION

The cerebellum plays a key role in the control of motor and cognitive functions due to the multiple connections to the forebrain, the thalamus, and the spinal cord. However, the cerebellar complex anatomical structure and its

location in the posterior fossa represent a challenge for *in vivo* structural and cerebellar neuroimaging. The recent advancement in MRI hardware and software and the development of more accurate and robust algorithms for image analysis have improved the structural and functional assessment of the cerebellum. This is of paramount importance due to the frequent and early involvement of the cerebellum in several neurodegenerative diseases. Therefore, MRI measures of cerebellar structure and function could serve as early and sensitive marker of disease progression and help monitor response to current or experimental treatments.

REFERENCES

- 1 Nieuwenhuys R, Voogd J, Huijzen Cv. The human central nervous system. 4th ed. New York: Springer, 2008: 807-840 [DOI: 10.1007/97

- 8-3-540-34686-9]
- 2 **Barahona ML MJ**, Querol Pascual R, Alvarez-Linera Prado J, Gañan Presmanes Y, Fernández Gil MÁ. Structural and Functional anatomy of cerebellum. More than a motor conception. Poster No: C-0497 Congress: ECR 2011 Type: Educational Exhibit 2011 [DOI: 10.1594/ecr2011/C-0497]
- 3 **Glickstein M**, May JG 3rd, Mercier BE. Corticopontine projection in the macaque: the distribution of labelled cortical cells after large injections of horseradish peroxidase in the pontine nuclei. *J Comp Neurol* 1985; **235**: 343-359 [PMID: 3998215 DOI: 10.1002/cne.902350306]
- 4 **Schmahmann JD**. From movement to thought: anatomic substrates of the cerebellar contribution to cognitive processing. *Hum Brain Mapp* 1996; **4**: 174-198 [PMID: 20408197 DOI: 10.1002/(SICI)1097-0193(1996)4:3<174::AID-HBM3>3.0.CO;2-0]
- 5 **Strick PL**, Dum RP, Fiez JA. Cerebellum and nonmotor function. *Annu Rev Neurosci* 2009; **32**: 413-434 [PMID: 19555291 DOI: 10.1146/annurev.neuro.31.060407.125606]
- 6 **Milardi D**, Arrigo A, Anastasi G, Cacciola A, Marino S, Mormina E, Calamuneri A, Bruschetta D, Cutroneo G, Trimarchi F, Quartarone A. Extensive Direct Subcortical Cerebellum-Basal Ganglia Connections in Human Brain as Revealed by Constrained Spherical Deconvolution Tractography. *Front Neuroanat* 2016; **10**: 29 [PMID: 27047348 DOI: 10.3389/fnana.2016.00029]
- 7 **Dum RP**, Strick PL. An unfolded map of the cerebellar dentate nucleus and its projections to the cerebral cortex. *J Neurophysiol* 2003; **89**: 634-639 [PMID: 12522208 DOI: 10.1152/jn.00626.2002]
- 8 **Hoshi E**, Tremblay L, Féger J, Carras PL, Strick PL. The cerebellum communicates with the basal ganglia. *Nat Neurosci* 2005; **8**: 1491-1493 [PMID: 16205719 DOI: 10.1038/nn1544]
- 9 **Marr D**. A theory of cerebellar cortex. *J Physiol* 1969; **202**: 437-470 [PMID: 5784296 DOI: 10.1113/jphysiol.1969.sp008820]
- 10 **Schmahmann JD**, Sherman JC. The cerebellar cognitive affective syndrome. *Brain* 1998; **121** (Pt 4): 561-579 [PMID: 9577385 DOI: 10.1093/brain/121.4.561]
- 11 **Balsters JH**, Ramnani N. Symbolic representations of action in the human cerebellum. *Neuroimage* 2008; **43**: 388-398 [PMID: 18692577 DOI: 10.1016/j.neuroimage.2008.07.010]
- 12 **Balsters JH**, Ramnani N. Cerebellar plasticity and the automation of first-order rules. *J Neurosci* 2011; **31**: 2305-2312 [PMID: 21307266 DOI: 10.1523/JNEUROSCI.4358-10.2011]
- 13 **Raut AA**, Naphade PS, Chawla A. Imaging of skull base: Pictorial essay. *Indian J Radiol Imaging* 2012; **22**: 305-316 [PMID: 23833423 DOI: 10.4103/0971-3026.111485]
- 14 **Borges A**. Imaging of the central skull base. *Neuroimaging Clin N Am* 2009; **19**: 669-696 [PMID: 19959012 DOI: 10.1016/j.nic.2009.11.001]
- 15 **Laine FJ**, Nadel L, Braun IF. CT and MR imaging of the central skull base. Part 2. Pathologic spectrum. *Radiographics* 1990; **10**: 797-821 [PMID: 2217972 DOI: 10.1148/radiographics.10.5.2217972]
- 16 **Ertl-Wagner B**, Eftimov L, Blume J, Bruening R, Becker C, Cormack J, Brueckmann H, Reiser M. Cranial CT with 64-, 16-, 4- and single-slice CT systems-comparison of image quality and posterior fossa artifacts in routine brain imaging with standard protocols. *Eur Radiol* 2008; **18**: 1720-1726 [PMID: 18389247 DOI: 10.1007/s00330-008-0937-6]
- 17 **Jones TR**, Kaplan RT, Lane B, Atlas SW, Rubin GD. Single- versus multi-detector row CT of the brain: quality assessment. *Radiology* 2001; **219**: 750-755 [PMID: 11376264 DOI: 10.1148/radiology.219.3.r01jn47750]
- 18 **Kamalian S**, Atkinson WL, Florin LA, Pomerantz SR, Lev MH, Romero JM. Emergency department CT screening of patients with nontraumatic neurological symptoms referred to the posterior fossa: comparison of thin versus thick slice images. *Emerg Radiol* 2014; **21**: 251-256 [PMID: 24469596 DOI: 10.1007/s10140-014-1194-4]
- 19 **Rozeik C**, Kotterer O, Preiss J, Schütz M, Dingler W, Deininger HK. Cranial CT artifacts and gantry angulation. *J Comput Assist Tomogr* 1991; **15**: 381-386 [PMID: 2026796 DOI: 10.1097/00004728-199105000-00007]
- 20 **Levy JM**, Hupke R. Composite addition technique: a new method in CT scanning of the posterior fossa. *AJNR Am J Neuroradiol* 1991; **12**: 686-688 [PMID: 1882744]
- 21 **Moström U**, Ytterbergh C. Artifacts in computed tomography of the posterior fossa: a comparative phantom study. *J Comput Assist Tomogr* 1986; **10**: 560-566 [PMID: 3734195 DOI: 10.1097/00004728-198607000-00002]
- 22 **Glover GH**, Pelc NJ. Nonlinear partial volume artifacts in x-ray computed tomography. *Med Phys* 1980; **7**: 238-248 [PMID: 7393149 DOI: 10.1118/1.594678]
- 23 **Joseph PM**, Spital RD. A method for correcting bone induced artifacts in computed tomography scanners. *J Comput Assist Tomogr* 1978; **2**: 100-108 [PMID: 670461 DOI: 10.1097/00004728-197801000-00017]
- 24 **Morelli JN**, Runge VM, Ai F, Attenberger U, Vu L, Schmeets SH, Nitz WR, Kirsch JE. An image-based approach to understanding the physics of MR artifacts. *Radiographics* 2011; **31**: 849-866 [PMID: 21571661 DOI: 10.1148/rg.313105115]
- 25 **Hwang DY**, Silva GS, Furie KL, Greer DM. Comparative sensitivity of computed tomography vs. magnetic resonance imaging for detecting acute posterior fossa infarct. *J Emerg Med* 2012; **42**: 559-565 [PMID: 22305149 DOI: 10.1016/j.jemermed.2011.05.101]
- 26 **Young IR**, Bydder GM, Hall AS, Steiner RE, Worthington BS, Hawkes RC, Holland GN, Moore WS. The role of NMR imaging in the diagnosis and management of acoustic neuroma. *AJNR Am J Neuroradiol* 1983; **4**: 223-224 [PMID: 6410706 DOI: 10.1097/00004728-198302000-00049]
- 27 **Wilms G**, Decrop E, Plets C, Demaerel P, Marchal G, Van Hecke P, Baert AL. Magnetic resonance imaging in acoustic neurinoma. Comparison with CT. *J Belge Radiol* 1989; **72**: 151-158 [PMID: 2793814]
- 28 **Wenz F**, Hess T, Knopp MV, Weisser G, Blüml S, Schad LR, Hawighorst H, van Kaick G. 3D MPRAGE evaluation of lesions in the posterior cranial fossa. *Magn Reson Imaging* 1994; **12**: 553-558 [PMID: 8057759 DOI: 10.1016/0730-725X(94)92449-X]
- 29 **Kallmes DF**, Hui FK, Mugler JP 3rd. Suppression of cerebrospinal fluid and blood flow artifacts in FLAIR MR imaging with a single-slab three-dimensional pulse sequence: initial experience. *Radiology* 2001; **221**: 251-255 [PMID: 11568348 DOI: 10.1148/radiol.2211001712]
- 30 **Bakshi R**, Caruthers SD, Janardhan V, Wasay M. Intraventricular CSF pulsation artifact on fast fluid-attenuated inversion-recovery MR images: analysis of 100 consecutive normal studies. *AJNR Am J Neuroradiol* 2000; **21**: 503-508 [PMID: 10730642]
- 31 **Winkelmann R**, Börmert P, Dössel O. Ghost artifact removal using a parallel imaging approach. *Magn Reson Med* 2005; **54**: 1002-1009 [PMID: 16155885 DOI: 10.1002/mrm.20640]
- 32 **Rydborg JN**, Hammond CA, Grimm RC, Erickson BJ, Jack CR Jr, Huston J 3rd, Riederer SJ. Initial clinical experience in MR imaging of the brain with a fast fluid-attenuated inversion-recovery pulse sequence. *Radiology* 1994; **193**: 173-180 [PMID: 8090888 DOI: 10.1148/radiology.193.1.8090888]
- 33 **Lavdas E**, Tsougos I, Kogia S, Gratsias G, Svolos P, Roka V, Fezoulidis IV, Kapsalaki E. T2 FLAIR artifacts at 3-T brain magnetic resonance imaging. *Clin Imaging* 2014; **38**: 85-90 [PMID: 24359643 DOI: 10.1016/j.clinimag.2013.10.004]
- 34 **Schaefer PW**, Grant PE, Gonzalez RG. Diffusion-weighted MR imaging of the brain. *Radiology* 2000; **217**: 331-345 [PMID: 11058626 DOI: 10.1148/radiology.217.2.r00nv24331]
- 35 **Holodny AI**, Ollenschläger M. Diffusion imaging in brain tumors. *Neuroimaging Clin N Am* 2002; **12**: 107-124, x [PMID: 11998248 DOI: 10.1016/S1052-5149(03)00072-8]
- 36 **Ayanzen RH**, Bird CR, Keller PJ, McCully FJ, Theobald MR, Heiserman JE. Cerebral MR venography: normal anatomy and potential diagnostic pitfalls. *AJNR Am J Neuroradiol* 2000; **21**: 74-78 [PMID: 10669228]
- 37 **Wu Z**, Mittal S, Kish K, Yu Y, Hu J, Haacke EM. Identification of calcification with MRI using susceptibility-weighted imaging: a case study. *J Magn Reson Imaging* 2009; **29**: 177-182 [PMID: 19097156 DOI: 10.1002/jmri.21617]
- 38 **Lesser FD**, Derbyshire SG, Lewis-Jones H. Can computed tomography and magnetic resonance imaging differentiate between malignant pathology and osteomyelitis in the central skull base? *J Laryngol Otol* 2015; **129**: 852-859 [PMID: 26314320 DOI: 10.1017/

- S0022215115001991]
- 39 **Fischbein NJ**, Kaplan MJ. Magnetic resonance imaging of the central skull base. *Top Magn Reson Imaging* 1999; **10**: 325-346 [PMID: 10643825 DOI: 10.1097/00002142-199910000-00005]
 - 40 **Curtin HD**, Chavali R. Imaging of the skull base. *Radiol Clin North Am* 1998; **36**: 801-817, v-vi [PMID: 9747190 DOI: 10.1016/S0033-8389(05)70065-8]
 - 41 **Marques JP**, Gruetter R, van der Zwaag W. In vivo structural imaging of the cerebellum, the contribution of ultra-high fields. *Cerebellum* 2012; **11**: 384-391 [PMID: 20596807 DOI: 10.1007/s12311-010-0189-2]
 - 42 **Hawkes R**, Blyth S, Chockkan V, Tano D, Ji Z, Mascher C. Structural and molecular compartmentation in the cerebellum. *Can J Neurol Sci* 1993; **20** Suppl 3: S29-S35 [PMID: 8334590]
 - 43 **Manto M**. The cerebellum, cerebellar disorders, and cerebellar research—two centuries of discoveries. *Cerebellum* 2008; **7**: 505-516 [PMID: 18855093 DOI: 10.1007/s12311-008-0063-7]
 - 44 **Marques JP**, van der Zwaag W, Granziera C, Krueger G, Gruetter R. Cerebellar cortical layers: in vivo visualization with structural high-field-strength MR imaging. *Radiology* 2010; **254**: 942-948 [PMID: 20177104 DOI: 10.1148/radiol.09091136]
 - 45 **Tanenbaum LN**. Clinical 3T MR imaging: mastering the challenges. *Magn Reson Imaging Clin N Am* 2006; **14**: 1-15 [PMID: 16530631 DOI: 10.1016/j.mric.2005.12.004]
 - 46 **Gramsch C**, Nensa F, Kastrup O, Maderwald S, Deuschl C, Ringelstein A, Schelhorn J, Forsting M, Schlamann M. Diagnostic value of 3D fluid attenuated inversion recovery sequence in multiple sclerosis. *Acta Radiol* 2015; **56**: 622-627 [PMID: 24867222 DOI: 10.1177/0284185114534413]
 - 47 **Kilsdonk ID**, de Graaf WL, Soriano AL, Zwanenburg JJ, Visser F, Kuijter JP, Geurts JJ, Pouwels PJ, Polman CH, Castelijns JA, Luijten PR, Barkhof F, Wattjes MP. Multicontrast MR imaging at 7T in multiple sclerosis: highest lesion detection in cortical gray matter with 3D-FLAIR. *AJNR Am J Neuroradiol* 2013; **34**: 791-796 [PMID: 23042930 DOI: 10.3174/ajnr.A3289]
 - 48 **Deoni SC**, Catani M. Visualization of the deep cerebellar nuclei using quantitative T1 and rho magnetic resonance imaging at 3 Tesla. *Neuroimage* 2007; **37**: 1260-1266 [PMID: 17702607 DOI: 10.1016/j.neuroimage.2007.06.036]
 - 49 **Maderwald S**, Thürling M, Küper M, Theysohn N, Müller O, Beck A, Aurich V, Ladd ME, Timmann D. Direct visualization of cerebellar nuclei in patients with focal cerebellar lesions and its application for lesion-symptom mapping. *Neuroimage* 2012; **63**: 1421-1431 [PMID: 22892334 DOI: 10.1016/j.neuroimage.2012.07.063]
 - 50 **D'Ambrosio A**, Pagani E, Riccitelli GC, Colombo B, Rodegher M, Falini A, Comi G, Filippi M, Rocca MA. Cerebellar contribution to motor and cognitive performance in multiple sclerosis: An MRI sub-regional volumetric analysis. *Mult Scler* 2017; **23**: 1194-1203 [PMID: 27760859 DOI: 10.1177/1352458516674567]
 - 51 **Bogovic JA**, Jedynak B, Rigg R, Du A, Landman BA, Prince JL, Ying SH. Approaching expert results using a hierarchical cerebellum parcellation protocol for multiple inexperienced human raters. *Neuroimage* 2013; **64**: 616-629 [PMID: 22975160 DOI: 10.1016/j.neuroimage.2012.08.075]
 - 52 **Diedrichsen J**. A spatially unbiased atlas template of the human cerebellum. *Neuroimage* 2006; **33**: 127-138 [PMID: 16904911 DOI: 10.1016/j.neuroimage.2006.05.056]
 - 53 **Stoodley CJ**. Distinct regions of the cerebellum show gray matter decreases in autism, ADHD, and developmental dyslexia. *Front Syst Neurosci* 2014; **8**: 92 [PMID: 24904314 DOI: 10.3389/fnsys.2014.00092]
 - 54 **Piccinin CC**, Santos MC, Piovesana LG, Campos LS, Guimarães RP, Campos BM, Torres FR, França MC, Amato-Filho AC, Lopes-Cendes I, Cendes F, D'Abreu A. Infratentorial gray matter atrophy and excess in primary craniocervical dystonia. *Parkinsonism Relat Disord* 2014; **20**: 198-203 [PMID: 24262871 DOI: 10.1016/j.parkreldis.2013.10.026]
 - 55 **Price M**, Cardenas VA, Fein G. Automated MRI cerebellar size measurements using active appearance modeling. *Neuroimage* 2014; **103**: 511-521 [PMID: 25192657 DOI: 10.1016/j.neuroimage.2014.08.047]
 - 56 **Weier K**, Beck A, Magon S, Amann M, Naegelin Y, Penner IK, Thürling M, Aurich V, Derfuss T, Radue EW, Stippich C, Kappos L, Timmann D, Sprenger T. Evaluation of a new approach for semi-automatic segmentation of the cerebellum in patients with multiple sclerosis. *J Neurol* 2012; **259**: 2673-2680 [PMID: 22711160 DOI: 10.1007/s00415-012-6569-4]
 - 57 **Reuter M**, Schmansky NJ, Rosas HD, Fischl B. Within-subject template estimation for unbiased longitudinal image analysis. *Neuroimage* 2012; **61**: 1402-1418 [PMID: 22430496 DOI: 10.1016/j.neuroimage.2012.02.084]
 - 58 **Wang JY**, Ngo MM, Hessel D, Hagerman RJ, Rivera SM. Robust Machine Learning-Based Correction on Automatic Segmentation of the Cerebellum and Brainstem. *PLoS One* 2016; **11**: e0156123 [PMID: 27213683 DOI: 10.1371/journal.pone.0156123]
 - 59 **Knösche TR**, Anwender A, Liptrot M, Dyrby TB. Validation of tractography: Comparison with manganese tracing. *Hum Brain Mapp* 2015; **36**: 4116-4134 [PMID: 26178765 DOI: 10.1002/hbm.22902]
 - 60 **Le Bihan D**. Diffusion MRI: what water tells us about the brain. *EMBO Mol Med* 2014; **6**: 569-573 [PMID: 24705876 DOI: 10.1002/emmm.201404055]
 - 61 **Keser Z**, Hasan KM, Mwangi BI, Kamali A, Ucisik-Keser FE, Riascos RF, Yozbatiran N, Francisco GE, Narayana PA. Diffusion tensor imaging of the human cerebellar pathways and their interplay with cerebral macrostructure. *Front Neuroanat* 2015; **9**: 41 [PMID: 25904851 DOI: 10.3389/fnana.2015.00041]
 - 62 **Mormina E**, Briguglio M, Morabito R, Arrigo A, Marino S, Di Rosa G, Micalizzi A, Valente EM, Salpietro V, Vinci SL, Longo M, Granata F. A rare case of cerebellar agenesis: a probabilistic Constrained Spherical Deconvolution tractographic study. *Brain Imaging Behav* 2016; **10**: 158-167 [PMID: 25832852 DOI: 10.1007/s11682-015-9377-5]
 - 63 **Mormina E**, Arrigo A, Calamuneri A, Granata F, Quartarone A, Ghilardi MF, Inglese M, Di Rocco A, Milardi D, Anastasi GP, Gaeta M. Diffusion tensor imaging parameters' changes of cerebellar hemispheres in Parkinson's disease. *Neuroradiology* 2015; **57**: 327-334 [PMID: 25479963 DOI: 10.1007/s00234-014-1473-5]
 - 64 **Mormina E**, Longo M, Arrigo A, Alafaci C, Tomasello F, Calamuneri A, Marino S, Gaeta M, Vinci SL, Granata F. MRI Tractography of Corticospinal Tract and Arcuate Fasciculus in High-Grade Gliomas Performed by Constrained Spherical Deconvolution: Qualitative and Quantitative Analysis. *AJNR Am J Neuroradiol* 2015; **36**: 1853-1858 [PMID: 26113071 DOI: 10.3174/ajnr.A4368]
 - 65 **Neto Henriques R**, Correia MM, Nunes RG, Ferreira HA. Exploring the 3D geometry of the diffusion kurtosis tensor—impact on the development of robust tractography procedures and novel biomarkers. *Neuroimage* 2015; **111**: 85-99 [PMID: 25676915 DOI: 10.1016/j.neuroimage.2015.02.004]
 - 66 **Jenabi M**, Peck KK, Young RJ, Brennan N, Holodny AI. Identification of the Corticobulbar Tracts of the Tongue and Face Using Deterministic and Probabilistic DTI Fiber Tracking in Patients with Brain Tumor. *AJNR Am J Neuroradiol* 2015; **36**: 2036-2041 [PMID: 26251424 DOI: 10.3174/ajnr.A4430]
 - 67 **Behrens TE**, Berg HJ, Jbabdi S, Rushworth MF, Woolrich MW. Probabilistic diffusion tractography with multiple fibre orientations: What can we gain? *Neuroimage* 2007; **34**: 144-155 [PMID: 17070705 DOI: 10.1016/j.neuroimage.2006.09.018]
 - 68 **Gore JC**. Principles and practice of functional MRI of the human brain. *J Clin Invest* 2003; **112**: 4-9 [PMID: 12840051 DOI: 10.1172/JCI19010]
 - 69 **Biswal B**, Yetkin FZ, Haughton VM, Hyde JS. Functional connectivity in the motor cortex of resting human brain using echo-planar MRI. *Magn Reson Med* 1995; **34**: 537-541 [PMID: 8524021 DOI: 10.1002/mrm.1910340409]
 - 70 **Damoiseaux JS**, Rombouts SA, Barkhof F, Scheltens P, Stam CJ, Smith SM, Beckmann CF. Consistent resting-state networks across healthy subjects. *Proc Natl Acad Sci USA* 2006; **103**: 13848-13853 [PMID: 16945915 DOI: 10.1073/pnas.0601417103]
 - 71 **Smith SM**, Fox PT, Miller KL, Glahn DC, Fox PM, Mackay CE, Filippini N, Watkins KE, Toro R, Laird AR, Beckmann CF. Correspondence of the brain's functional architecture during activation

- and rest. *Proc Natl Acad Sci USA* 2009; **106**: 13040-13045 [PMID: 19620724 DOI: 10.1073/pnas.0905267106]
- 72 **Habas C**, Kamdar N, Nguyen D, Prater K, Beckmann CF, Menon V, Greicius MD. Distinct cerebellar contributions to intrinsic connectivity networks. *J Neurosci* 2009; **29**: 8586-8594 [PMID: 19571149 DOI: 10.1523/JNEUROSCI.1868-09.2009]
 - 73 **Yacoub E**, Shmuel A, Pfeuffer J, Van De Moortele PF, Adriany G, Andersen P, Vaughan JT, Merkle H, Ugurbil K, Hu X. Imaging brain function in humans at 7 Tesla. *Magn Reson Med* 2001; **45**: 588-594 [PMID: 11283986 DOI: 10.1002/mrm.1080]
 - 74 **Jansen JF**, Backes WH, Nicolay K, Kooi ME. 1H MR spectroscopy of the brain: absolute quantification of metabolites. *Radiology* 2006; **240**: 318-332 [PMID: 16864664 DOI: 10.1148/radiol.2402050314]
 - 75 **Oz G**, Alger JR, Barker PB, Bartha R, Bizzi A, Boesch C, Bolan PJ, Brindle KM, Cudalbu C, Dinçer A, Dydak U, Emir UE, Frahm J, González RG, Gruber S, Gruetter R, Gupta RK, Heerschap A, Henning A, Hetherington HP, Howe FA, Hüppi PS, Hurd RE, Kantarci K, Klomp DW, Kreis R, Kruiskamp MJ, Leach MO, Lin AP, Luijten PR, Marjańska M, Maudsley AA, Meyerhoff DJ, Mountford CE, Nelson SJ, Pamir MN, Pan JW, Peet AC, Poptani H, Posse S, Pouwels PJ, Ratai EM, Ross BD, Scheenen TW, Schuster C, Smith IC, Soher BJ, Tkáč I, Vigneron DB, Kauppinen RA; MRS Consensus Group. Clinical proton MR spectroscopy in central nervous system disorders. *Radiology* 2014; **270**: 658-679 [PMID: 24568703 DOI: 10.1148/radiol.13130531]
 - 76 **Li BS**, Wang H, Gonen O. Metabolite ratios to assumed stable creatine level may confound the quantification of proton brain MR spectroscopy. *Magn Reson Imaging* 2003; **21**: 923-928 [PMID: 14599543 DOI: 10.1016/S0730-725X(03)00181-4]
 - 77 **Mascalchi M**, Brugnoli R, Guerrini L, Belli G, Nistri M, Politi LS, Gavazzi C, Lolli F, Argenti G, Villari N. Single-voxel long TE 1H-MR spectroscopy of the normal brainstem and cerebellum. *J Magn Reson Imaging* 2002; **16**: 532-537 [PMID: 12412029 DOI: 10.1002/jmri.10189]
 - 78 **Weber-Fahr W**, Ende G, Braus DF, Bachert P, Soher BJ, Henn FA, Büchel C. A fully automated method for tissue segmentation and CSF-correction of proton MRSI metabolites corroborates abnormal hippocampal NAA in schizophrenia. *Neuroimage* 2002; **16**: 49-60 [PMID: 11969317 DOI: 10.1006/nimg.2002.1057]
 - 79 **Currie S**, Hadjivassiliou M, Wilkinson ID, Griffiths PD, Hoggard N. Magnetic resonance spectroscopy of the normal cerebellum: what degree of variability can be expected? *Cerebellum* 2013; **12**: 205-211 [PMID: 22987337 DOI: 10.1007/s12311-012-0415-1]
 - 80 **Sajja BR**, Wolinsky JS, Narayana PA. Proton magnetic resonance spectroscopy in multiple sclerosis. *Neuroimaging Clin N Am* 2009; **19**: 45-58 [PMID: 19064199 DOI: 10.1016/j.nic.2008.08.002]
 - 81 **Jahng GH**, Li KL, Ostergaard L, Calamante F. Perfusion magnetic resonance imaging: a comprehensive update on principles and techniques. *Korean J Radiol* 2014; **15**: 554-577 [PMID: 25246817 DOI: 10.3348/kjr.2014.15.5.554]
 - 82 **Talbot PR**, Lloyd JJ, Snowden JS, Neary D, Testa HJ. Choice of reference region in the quantification of single-photon emission tomography in primary degenerative dementia. *Eur J Nucl Med* 1994; **21**: 503-508 [PMID: 8082664 DOI: 10.1007/BF00173036]
 - 83 **Lacalle-Aurioles M**, Alemán-Gómez Y, Guzmán-De-Villoria JA, Cruz-Orduña I, Olazarán J, Mateos-Pérez JM, Martino ME, Desco M. Is the cerebellum the optimal reference region for intensity normalization of perfusion MR studies in early Alzheimer's disease? *PLoS One* 2013; **8**: e81548 [PMID: 24386081 DOI: 10.1371/journal.pone.0081548]
 - 84 **Hartkamp NS**, Petersen ET, De Vis JB, Bokkers RP, Hendrikse J. Mapping of cerebral perfusion territories using territorial arterial spin labeling: techniques and clinical application. *NMR Biomed* 2013; **26**: 901-912 [PMID: 22807022 DOI: 10.1002/nbm.2836]
 - 85 **Grade M**, Hernandez Tamames JA, Pizzini FB, Achten E, Golay X, Smits M. A neuroradiologist's guide to arterial spin labeling MRI in clinical practice. *Neuroradiology* 2015; **57**: 1181-1202 [PMID: 26351201 DOI: 10.1007/s00234-015-1571-z]
 - 86 **van Gelderen P**, de Zwart JA, Duyn JH. Pitfalls of MRI measurement of white matter perfusion based on arterial spin labeling. *Magn Reson Med* 2008; **59**: 788-795 [PMID: 18383289 DOI: 10.1002/mrm.21515]
 - 87 **Compston A**, Lassmann H, McDonald I. Chapter 1 - The story of multiple sclerosis. In: McAlpine's Multiple Sclerosis (Fourth Edition). Edinburgh: Churchill Livingstone, 2006: 3-68 [DOI: 10.1016/B978-0-443-07271-0.50003-3]
 - 88 **Tintore M**, Otero-Romero S, Río J, Arrambide G, Pujal B, Tur C, Galán I, Comabella M, Nos C, Arévalo MJ, Vidal-Jordana A, Castelló J, Rodríguez-Acevedo B, Midaglia L, Mitjana R, Auger C, Sastre-Garriga J, Rovira À, Montalban X. Contribution of the symptomatic lesion in establishing MS diagnosis and prognosis. *Neurology* 2016; **87**: 1368-1374 [PMID: 27566747 DOI: 10.1212/WNL.0000000000003144]
 - 89 **Fazekas F**, Offenbacher H, Fuchs S, Schmidt R, Niederkorn K, Horner S, Lechner H. Criteria for an increased specificity of MRI interpretation in elderly subjects with suspected multiple sclerosis. *Neurology* 1988; **38**: 1822-1825 [PMID: 3057397]
 - 90 **Ormerod IE**, Miller DH, McDonald WI, du Boulay EP, Rudge P, Kendall BE, Moseley IF, Johnson G, Tofts PS, Halliday AM. The role of NMR imaging in the assessment of multiple sclerosis and isolated neurological lesions. A quantitative study. *Brain* 1987; **110** (Pt 6): 1579-1616 [PMID: 3427402]
 - 91 **Favaretto A**, Lazzarotto A, Poggiali D, Rolma G, Causin F, Rinaldi F, Perini P, Gallo P. MRI-detectable cortical lesions in the cerebellum and their clinical relevance in multiple sclerosis. *Mult Scler* 2016; **22**: 494-501 [PMID: 26163070 DOI: 10.1177/1352458515594043]
 - 92 **Calabrese M**, Reynolds R, Magliozzi R, Castellaro M, Morra A, Scalfari A, Farina G, Romualdi C, Gajofatto A, Pitteri M, Benedetti MD, Monaco S. Regional Distribution and Evolution of Gray Matter Damage in Different Populations of Multiple Sclerosis Patients. *PLoS One* 2015; **10**: e0135428 [PMID: 26267665 DOI: 10.1371/journal.pone.0135428]
 - 93 **Bendfeldt K**, Kuster P, Traud S, Egger H, Winkhofer S, Mueller-Lenke N, Naegelin Y, Gass A, Kappos L, Matthews PM, Nichols TE, Radue EW, Borgwardt SJ. Association of regional gray matter volume loss and progression of white matter lesions in multiple sclerosis - A longitudinal voxel-based morphometry study. *Neuroimage* 2009; **45**: 60-67 [PMID: 19013533 DOI: 10.1016/j.neuroimage.2008.10.006]
 - 94 **Edwards SG**, Gong QY, Liu C, Zvartau ME, Jaspan T, Roberts N, Blumhardt LD. Infratentorial atrophy on magnetic resonance imaging and disability in multiple sclerosis. *Brain* 1999; **122** (Pt 2): 291-301 [PMID: 10071057]
 - 95 **Ramasamy DP**, Benedict RH, Cox JL, Fritz D, Abdelrahman N, Hussein S, Minagar A, Dwyer MG, Zivadinov R. Extent of cerebellum, subcortical and cortical atrophy in patients with MS: a case-control study. *J Neurol Sci* 2009; **282**: 47-54 [PMID: 19201003 DOI: 10.1016/j.jns.2008.12.034]
 - 96 **Anderson VM**, Fisniku LK, Altmann DR, Thompson AJ, Miller DH. MRI measures show significant cerebellar gray matter volume loss in multiple sclerosis and are associated with cerebellar dysfunction. *Mult Scler* 2009; **15**: 811-817 [PMID: 19465449 DOI: 10.1177/1352458508101934]
 - 97 **Anderson VM**, Wheeler-Kingshott CA, Abdel-Aziz K, Miller DH, Toosy A, Thompson AJ, Ciccarelli O. A comprehensive assessment of cerebellar damage in multiple sclerosis using diffusion tractography and volumetric analysis. *Mult Scler* 2011; **17**: 1079-1087 [PMID: 21511688 DOI: 10.1177/1352458511403528]
 - 98 **Preziosa P**, Rocca MA, Mesaros S, Pagani E, Drulovic J, Stosic-Opincal T, Dackovic J, Copetti M, Caputo D, Filippi M. Relationship between damage to the cerebellar peduncles and clinical disability in multiple sclerosis. *Radiology* 2014; **271**: 822-830 [PMID: 24555637 DOI: 10.1148/radiol.13132142]
 - 99 **Deppe M**, Tabelow K, Krämer J, Tenberge JG, Schiffer P, Bittner S, Schwindt W, Zipp F, Wiendl H, Meuth SG. Evidence for early, non-lesional cerebellar damage in patients with multiple sclerosis: DTI measures correlate with disability, atrophy, and disease duration. *Mult Scler* 2016; **22**: 73-84 [PMID: 25921041 DOI: 10.1177/1352458515579439]
 - 100 **Tomassini V**, d'Ambrosio A, Petsas N, Wise RG, Sbardella E, Allen M, Tona F, Fanelli F, Foster C, Cami M, Gallo A, Pantano P, Pozzilli C. The effect of inflammation and its reduction on brain plasticity

- in multiple sclerosis: MRI evidence. *Hum Brain Mapp* 2016; **37**: 2431-2445 [PMID: 26991559 DOI: 10.1002/hbm.23184]
- 101 **Rocca MA**, Pagani E, Absinta M, Valsasina P, Falini A, Scotti G, Comi G, Filippi M. Altered functional and structural connectivities in patients with MS: a 3-T study. *Neurology* 2007; **69**: 2136-2145 [PMID: 18056577 DOI: 10.1212/01.wnl.0000295504.92020.ca]
 - 102 **Pardini M**, Bonzano L, Roccatagliata L, Mancardi GL, Bove M. The fatigue-motor performance paradox in multiple sclerosis. *Sci Rep* 2013; **3**: 2001 [PMID: 23774178 DOI: 10.1038/srep02001]
 - 103 **Weier K**, Penner IK, Magon S, Amann M, Naegelin Y, Andelova M, Derfuss T, Stippich C, Radue EW, Kappos L, Sprenger T. Cerebellar abnormalities contribute to disability including cognitive impairment in multiple sclerosis. *PLoS One* 2014; **9**: e86916 [PMID: 24466290 DOI: 10.1371/journal.pone.0086916]
 - 104 **Damasceno A**, Damasceno BP, Cendes F. The clinical impact of cerebellar grey matter pathology in multiple sclerosis. *PLoS One* 2014; **9**: e96193 [PMID: 24789257 DOI: 10.1371/journal.pone.0096193]
 - 105 **Yeoman LJ**, Howarth L, Britten A, Cotterill A, Adam EJ. Gantry angulation in brain CT: dosage implications, effect on posterior fossa artifacts, and current international practice. *Radiology* 1992; **184**: 113-116 [PMID: 1609066 DOI: 10.1148/radiology.184.1.1609066]
 - 106 **Sbardella E**, Upadhyay N, Tona F, Prosperini L, De Giglio L, Petsas N, Pozzilli C, Pantano P. Dentate nucleus connectivity in adult patients with multiple sclerosis: functional changes at rest and correlation with clinical features. *Mult Scler* 2017; **23**: 546-555 [PMID: 27411700 DOI: 10.1177/1352458516657438]
 - 107 **Loitfelder M**, Filippi M, Rocca M, Valsasina P, Ropele S, Jehna M, Fuchs S, Schmidt R, Neuper C, Fazekas F, Enzinger C. Abnormalities of resting state functional connectivity are related to sustained attention deficits in MS. *PLoS One* 2012; **7**: e42862 [PMID: 22912754 DOI: 10.1371/journal.pone.0042862]
 - 108 **Roccatagliata L**, Vuolo L, Bonzano L, Pichiecchio A, Mancardi GL. Multiple sclerosis: hyperintense dentate nucleus on unenhanced T1-weighted MR images is associated with the secondary progressive subtype. *Radiology* 2009; **251**: 503-510 [PMID: 19401576 DOI: 10.1148/radiol.2511081269]
 - 109 **Albert M**, Barrantes-Freer A, Lohrberg M, Antel JP, Prineas JW, Palkovits M, Wolff JR, Brück W, Stadelmann C. Synaptic pathology in the cerebellar dentate nucleus in chronic multiple sclerosis. *Brain Pathol* 2016; Epub ahead of print [PMID: 27706868 DOI: 10.1111/bpa.12450]
 - 110 **Tedeschi E**, Palma G, Canna A, Cocozza S, Russo C, Borrelli P, Lanzillo R, Angelini V, Postiglione E, Morra VB, Salvatore M, Brunetti A, Quarantelli M. In vivo dentate nucleus MRI relaxometry correlates with previous administration of Gadolinium-based contrast agents. *Eur Radiol* 2016; **26**: 4577-4584 [PMID: 26905870 DOI: 10.1007/s00330-016-4245-2]
 - 111 **Bostan AC**, Dum RP, Strick PL. The basal ganglia communicate with the cerebellum. *Proc Natl Acad Sci USA* 2010; **107**: 8452-8456 [PMID: 20404184 DOI: 10.1073/pnas.1000496107]
 - 112 **Sweet JA**, Walter BL, Gunalan K, Chaturvedi A, McIntyre CC, Miller JP. Fiber tractography of the axonal pathways linking the basal ganglia and cerebellum in Parkinson disease: implications for targeting in deep brain stimulation. *J Neurosurg* 2014; **120**: 988-996 [PMID: 24484226 DOI: 10.3171/2013.12.JNS131537]
 - 113 **Borghammer P**, Østergaard K, Cumming P, Gjedde A, Rodell A, Hall N, Chakravarty MM. A deformation-based morphometry study of patients with early-stage Parkinson's disease. *Eur J Neurol* 2010; **17**: 314-320 [PMID: 19912319 DOI: 10.1111/j.1468-1331.2009.02807.x]
 - 114 **Benninger DH**, Thees S, Kollias SS, Bassetti CL, Waldvogel D. Morphological differences in Parkinson's disease with and without rest tremor. *J Neurol* 2009; **256**: 256-263 [PMID: 19219572 DOI: 10.1007/s00415-009-0092-2]
 - 115 **O'Callaghan C**, Hornberger M, Balsters JH, Halliday GM, Lewis SJ, Shine JM. Cerebellar atrophy in Parkinson's disease and its implication for network connectivity. *Brain* 2016; **139**: 845-855 [PMID: 26794597 DOI: 10.1093/brain/awv399]
 - 116 **Zhang K**, Yu C, Zhang Y, Wu X, Zhu C, Chan P, Li K. Voxel-based analysis of diffusion tensor indices in the brain in patients with Parkinson's disease. *Eur J Radiol* 2011; **77**: 269-273 [PMID: 19692193 DOI: 10.1016/j.ejrad.2009.07.032]
 - 117 **Nicoletti G**, Caligiuri ME, Cherubini A, Morelli M, Novellino F, Arabia G, Salsone M, Quattrone A. A Fully Automated, Atlas-Based Approach for Superior Cerebellar Peduncle Evaluation in Progressive Supranuclear Palsy Phenotypes. *AJNR Am J Neuroradiol* 2017; **38**: 523-530 [PMID: 28034996 DOI: 10.3174/ajnr.A5048]
 - 118 **Wu T**, Long X, Zang Y, Wang L, Hallett M, Li K, Chan P. Regional homogeneity changes in patients with Parkinson's disease. *Hum Brain Mapp* 2009; **30**: 1502-1510 [PMID: 18649351 DOI: 10.1002/hbm.20622]
 - 119 **Dirkx MF**, den Ouden H, Aarts E, Timmer M, Bloem BR, Toni I, Helmich RC. The Cerebral Network of Parkinson's Tremor: An Effective Connectivity fMRI Study. *J Neurosci* 2016; **36**: 5362-5372 [PMID: 27170132 DOI: 10.1523/JNEUROSCI.3634-15.2016]
 - 120 **Planetta PJ**, Kurani AS, Shukla P, Prodoehl J, Corcos DM, Comella CL, McFarland NR, Okun MS, Vaillancourt DE. Distinct functional and macrostructural brain changes in Parkinson's disease and multiple system atrophy. *Hum Brain Mapp* 2015; **36**: 1165-1179 [PMID: 25413603 DOI: 10.1002/hbm.22694]
 - 121 **Nicoletti G**, Rizzo G, Barbagallo G, Tonon C, Condino F, Manners D, Messina D, Testa C, Arabia G, Gambardella A, Lodi R, Quattrone A. Diffusivity of cerebellar hemispheres enables discrimination of cerebellar or parkinsonian multiple system atrophy from progressive supranuclear palsy-Richardson syndrome and Parkinson disease. *Radiology* 2013; **267**: 843-850 [PMID: 23329659 DOI: 10.1148/radiol.12120364]
 - 122 **Lin DJ**, Hermann KL, Schmahmann JD. The Diagnosis and Natural History of Multiple System Atrophy, Cerebellar Type. *Cerebellum* 2016; **15**: 663-679 [PMID: 26467153 DOI: 10.1007/s12311-015-0728-y]
 - 123 **Batla A**, Sánchez MC, Erro R, Ganos C, Stamelou M, Balint B, Brugger F, Antelmi E, Bhatia KP. The role of cerebellum in patients with late onset cervical/segmental dystonia?--evidence from the clinic. *Parkinsonism Relat Disord* 2015; **21**: 1317-1322 [PMID: 26385708 DOI: 10.1016/j.parkreldis.2015.09.013]
 - 124 **Delmaire C**, Vidailhet M, Elbaz A, Bourdain F, Bleton JP, Sangla S, Meunier S, Terrier A, LeHérisy S. Structural abnormalities in the cerebellum and sensorimotor circuit in writer's cramp. *Neurology* 2007; **69**: 376-380 [PMID: 17646630 DOI: 10.1212/01.wnl.0000266591.49624.1a]
 - 125 **Preibisch C**, Berg D, Hofmann E, Solymosi L, Naumann M. Cerebral activation patterns in patients with writer's cramp: a functional magnetic resonance imaging study. *J Neurol* 2001; **248**: 10-17 [PMID: 11266013]
 - 126 **Baker RS**, Andersen AH, Morecraft RJ, Smith CD. A functional magnetic resonance imaging study in patients with benign essential blepharospasm. *J Neuroophthalmol* 2003; **23**: 11-15 [PMID: 12616082]
 - 127 **Klockgether T**. Update on degenerative ataxias. *Curr Opin Neurol* 2011; **24**: 339-345 [PMID: 21734495 DOI: 10.1097/WCO.0b013e32834875ba]
 - 128 **Ruano L**, Melo C, Silva MC, Coutinho P. The global epidemiology of hereditary ataxia and spastic paraplegia: a systematic review of prevalence studies. *Neuroepidemiology* 2014; **42**: 174-183 [PMID: 24603320 DOI: 10.1159/000358801]
 - 129 **Bürk K**, Abele M, Fetter M, Dichgans J, Skalej M, Laccone F, Didierjean O, Brice A, Klockgether T. Autosomal dominant cerebellar ataxia type I clinical features and MRI in families with SCA1, SCA2 and SCA3. *Brain* 1996; **119** (Pt 5): 1497-1505 [PMID: 8931575 DOI: 10.1093/brain/119.5.1497]
 - 130 **Schulz JB**, Borkert J, Wolf S, Schmitz-Hübsch T, Rakowicz M, Mariotti C, Schöls L, Timmann D, van de Warrenburg B, Dürr A, Pandolfo M, Kang JS, Mandly AG, Nägele T, Grisoli M, Boguslawska R, Bauer P, Klockgether T, Hauser TK. Visualization, quantification and correlation of brain atrophy with clinical symptoms in spinocerebellar ataxia types 1, 3 and 6. *Neuroimage* 2010; **49**: 158-168 [PMID: 19631275 DOI: 10.1016/j.neuroimage.2009.07.027]
 - 131 **Klockgether T**, Petersen D, Grodd W, Dichgans J. Early onset cerebellar ataxia with retained tendon reflexes. Clinical, electrophysiological and MRI observations in comparison with Friedreich's ataxia. *Brain* 1991;

- 114 (Pt 4): 1559-1573 [PMID: 1884166 DOI: 10.1093/brain/114.4.1559]
- 132 **Mascalchi M.** The cerebellum looks normal in Friedreich ataxia. *AJNR Am J Neuroradiol* 2013; **34**: E22 [PMID: 23328073 DOI: 10.3174/ajnr.A3480]
- 133 **Selvadurai LP**, Harding IH, Corben LA, Stagnitti MR, Storey E, Egan GF, Delatycki MB, Georgiou-Karistianis N. Cerebral and cerebellar grey matter atrophy in Friedreich ataxia: the IMAGE-FRDA study. *J Neurol* 2016; **263**: 2215-2223 [PMID: 27522354 DOI: 10.1007/s00415-016-8252-7]
- 134 **Al-Maawali A**, Blaser S, Yoon G. Diagnostic approach to childhood-onset cerebellar atrophy: a 10-year retrospective study of 300 patients. *J Child Neurol* 2012; **27**: 1121-1132 [PMID: 22764178 DOI: 10.1177/0883073812448680]
- 135 **Lin DD**, Barker PB, Lederman HM, Crawford TO. Cerebral abnormalities in adults with ataxia-telangiectasia. *AJNR Am J Neuroradiol* 2014; **35**: 119-123 [PMID: 23886747 DOI: 10.3174/ajnr.A3646]
- 136 **Sardanelli F**, Parodi RC, Ottonello C, Renzetti P, Saitta S, Lignana E, Mancardi GL. Cranial MRI in ataxia-telangiectasia. *Neuroradiology* 1995; **37**: 77-82 [PMID: 7708196 DOI: 10.1007/BF00588526]
- 137 **Tavani F**, Zimmerman RA, Berry GT, Sullivan K, Gatti R, Bingham P. Ataxia-telangiectasia: the pattern of cerebellar atrophy on MRI. *Neuroradiology* 2003; **45**: 315-319 [PMID: 12740724 DOI: 10.1007/s00234-003-0945-9]
- 138 **Guimarães RP**, D'Abreu A, Yasuda CL, França MC Jr, Silva BH, Cappabianco FA, Bergo FP, Lopes-Cendes IT, Cendes F. A multimodal evaluation of microstructural white matter damage in spinocerebellar ataxia type 3. *Mov Disord* 2013; **28**: 1125-1132 [PMID: 23553599 DOI: 10.1002/mds.25451]
- 139 **Kang JS**, Klein JC, Baudrexel S, Deichmann R, Nolte D, Hilker R. White matter damage is related to ataxia severity in SCA3. *J Neurol* 2014; **261**: 291-299 [PMID: 24272589 DOI: 10.1007/s00415-013-7186-6]
- 140 **Hernandez-Castillo CR**, Vaca-Palomares I, Galvez V, Campos-Romo A, Diaz R, Fernandez-Ruiz J. Cognitive Deficits Correlate with White Matter Deterioration in Spinocerebellar Ataxia Type 2. *J Int Neuropsychol Soc* 2016; **22**: 486-491 [PMID: 26888086 DOI: 10.1017/S1355617716000084]
- 141 **Mascalchi M**, Toschi N, Giannelli M, Ginestroni A, Della Nave R, Nicolai E, Bianchi A, Tessa C, Salvatore E, Aiello M, Soricelli A, Diciotti S. Progression of microstructural damage in spinocerebellar ataxia type 2: a longitudinal DTI study. *AJNR Am J Neuroradiol* 2015; **36**: 1096-1101 [PMID: 25882284 DOI: 10.3174/ajnr.A4343]
- 142 **Clemm von Hohenberg C**, Schocke MF, Wigand MC, Nachbauer W, Guttman CR, Kubicki M, Shenton ME, Boesch S, Egger K. Radial diffusivity in the cerebellar peduncles correlates with clinical severity in Friedreich ataxia. *Neurol Sci* 2013; **34**: 1459-1462 [PMID: 23640016 DOI: 10.1007/s10072-013-1402-0]
- 143 **Della Nave R**, Ginestroni A, Tessa C, Salvatore E, Bartolomei I, Salvi F, Dotti MT, De Michele G, Piacentini S, Mascalchi M. Brain white matter tracts degeneration in Friedreich ataxia. An in vivo MRI study using tract-based spatial statistics and voxel-based morphometry. *Neuroimage* 2008; **40**: 19-25 [PMID: 18226551 DOI: 10.1016/j.neuroimage.2007.11.050]
- 144 **Rizzo G**, Tonon C, Valentino ML, Manners D, Fortuna F, Gellera C, Pini A, Ghezzi A, Baruzzi A, Testa C, Malucelli E, Barbiroli B, Carelli V, Lodi R. Brain diffusion-weighted imaging in Friedreich's ataxia. *Mov Disord* 2011; **26**: 705-712 [PMID: 21370259 DOI: 10.1002/mds.23518]
- 145 **Vieira Karuta SC**, Raskin S, de Carvalho Neto A, Gasparetto EL, Doring T, Teive HA. Diffusion tensor imaging and tract-based spatial statistics analysis in Friedreich's ataxia patients. *Parkinsonism Relat Disord* 2015; **21**: 504-508 [PMID: 25801908 DOI: 10.1016/j.parkreldis.2015.02.021]
- 146 **Sahama I**, Sinclair K, Fiori S, Doecke J, Pannek K, Reid L, Lavin M, Rose S. Motor pathway degeneration in young ataxia telangiectasia patients: A diffusion tractography study. *Neuroimage Clin* 2015; **9**: 206-215 [PMID: 26413479 DOI: 10.1016/j.nicl.2015.08.007]
- 147 **Stefanescu MR**, Dohnalek M, Maderwald S, Thürling M, Minnerop M, Beck A, Schlamann M, Diedrichsen J, Ladd ME, Timmann D. Structural and functional MRI abnormalities of cerebellar cortex and nuclei in SCA3, SCA6 and Friedreich's ataxia. *Brain* 2015; **138**: 1182-1197 [PMID: 25818870 DOI: 10.1093/brain/awv064]
- 148 **Duarte JV**, Faustino R, Lobo M, Cunha G, Nunes C, Ferreira C, Januário C, Castelo-Branco M. Parametric fMRI of paced motor responses uncovers novel whole-brain imaging biomarkers in spinocerebellar ataxia type 3. *Hum Brain Mapp* 2016; **37**: 3656-3668 [PMID: 27273236 DOI: 10.1002/hbm.23266]
- 149 **Wu T**, Wang C, Wang J, Hallett M, Zang Y, Chan P. Preclinical and clinical neural network changes in SCA2 parkinsonism. *Parkinsonism Relat Disord* 2013; **19**: 158-164 [PMID: 23000299 DOI: 10.1016/j.parkreldis.2012.08.011]
- 150 **Cocozza S**, Saccà F, Cervo A, Marsili A, Russo CV, Giorgio SM, De Michele G, Filla A, Brunetti A, Quarantelli M. Modifications of resting state networks in spinocerebellar ataxia type 2. *Mov Disord* 2015; **30**: 1382-1390 [PMID: 26094751 DOI: 10.1002/mds.26284]
- 151 **Hernandez-Castillo CR**, Galvez V, Mercadillo RE, Díaz R, Yescas P, Martinez L, Ochoa A, Velazquez-Perez L, Fernandez-Ruiz J. Functional connectivity changes related to cognitive and motor performance in spinocerebellar ataxia type 2. *Mov Disord* 2015; **30**: 1391-1399 [PMID: 26256273 DOI: 10.1002/mds.26320]
- 152 **Harding IH**, Corben LA, Storey E, Egan GF, Stagnitti MR, Poudel GR, Delatycki MB, Georgiou-Karistianis N. Fronto-cerebellar dysfunction and dysconnectivity underlying cognition in friedreich ataxia: The IMAGE-FRDA study. *Hum Brain Mapp* 2016; **37**: 338-350 [PMID: 26502936 DOI: 10.1002/hbm.23034]
- 153 **Thomann PA**, Schäfer C, Seidl U, Santos VD, Essig M, Schröder J. The cerebellum in mild cognitive impairment and Alzheimer's disease - a structural MRI study. *J Psychiatr Res* 2008; **42**: 1198-1202 [PMID: 18215400 DOI: 10.1016/j.jpsychires.2007.12.002]
- 154 **Colloby SJ**, O'Brien JT, Taylor JP. Patterns of cerebellar volume loss in dementia with Lewy bodies and Alzheimer's disease: A VBM-DARTEL study. *Psychiatry Res* 2014; **223**: 187-191 [PMID: 25037902 DOI: 10.1016/j.psychres.2014.06.006]
- 155 **Łojkowska W**, Witkowski G, Bednarska-Makaruk M, Wehr H, Sienkiewicz-Jarosz H, Graban A, Bochyńska A, Wiśniewska A, Gugała M, Sławińska K, Sawicka B, Poniatowska R, Ryglewicz D. Correlations between cerebellar and brain volumes, cognitive impairments, ApoE levels, and APOE genotypes in patients with AD and MCI. *Curr Alzheimer Res* 2013; **10**: 964-972 [PMID: 24117117 DOI: 10.2174/15672050113106660161]
- 156 **Möller C**, Vrenken H, Jiskoot L, Versteeg A, Barkhof F, Scheltens P, van der Flier WM. Different patterns of gray matter atrophy in early- and late-onset Alzheimer's disease. *Neurobiol Aging* 2013; **34**: 2014-2022 [PMID: 23561509 DOI: 10.1016/j.neurobiolaging.2013.02.013]
- 157 **Raji CA**, Lopez OL, Kuller LH, Carmichael OT, Becker JT. Age, Alzheimer disease, and brain structure. *Neurology* 2009; **73**: 1899-1905 [PMID: 19846828 DOI: 10.1212/WNL.0b013e3181c3f293]

P- Reviewer: Quattrocchi CC S- Editor: Kong JX L- Editor: A
E- Editor: Lu YJ



Lymph node imaging in initial staging of prostate cancer: An overview and update

Jessica G Zarzour, Sam Galgano, Jonathan McConathy, John V Thomas, Soroush Rais-Bahrami

Jessica G Zarzour, Sam Galgano, Jonathan McConathy, John V Thomas, Soroush Rais-Bahrami, Department of Radiology, University of Alabama at Birmingham, Birmingham, AL 35249, United States

Soroush Rais-Bahrami, Department of Urology, University of Alabama at Birmingham, Birmingham, AL 35249, United States

Author contributions: Zarzour JG was responsible for the conception and design of the article, drafting and revision of the article, gives approval for the final version of the article, and serves as the corresponding author; Galgano S, McConathy J and Thomas JV contributed to the design of the project, participated in drafting and revising, and gives approval for the final version of the manuscript; and Rais-Bahrami S served as the supervision author, contributed to the design of the article, participated in drafting and revisions, and gives approval for the final version of the article.

Supported by Eli Lilly/Avid; AbbVie, consulting for GE Healthcare, Siemens Healthcare and Blue Earth Diagnostics.

Conflict-of-interest statement: The authors have no conflicts of interests to declare.

Open-Access: This article is an open-access article which was selected by an in-house editor and fully peer-reviewed by external reviewers. It is distributed in accordance with the Creative Commons Attribution Non Commercial (CC BY-NC 4.0) license, which permits others to distribute, remix, adapt, build upon this work non-commercially, and license their derivative works on different terms, provided the original work is properly cited and the use is non-commercial. See: <http://creativecommons.org/licenses/by-nc/4.0/>

Manuscript source: Invited manuscript

Correspondence to: Jessica G Zarzour, MD, Department of Radiology, University of Alabama at Birmingham, JTN 357, 619 19th Street South, Birmingham, AL 35294, United States. jgzarzour@uabmc.edu
Telephone: +1-205-9343166
Fax: +1-205-9753540

Received: February 10, 2017

Peer-review started: February 15, 2017

First decision: May 7, 2017

Revised: May 26, 2017

Accepted: July 14, 2017

Article in press: July 17, 2017

Published online: October 28, 2017

Abstract

Accurate nodal staging at the time of diagnosis of prostate cancer is crucial in determining a treatment plan for the patient. Pelvic lymph node dissection is the most reliable method, but is less than perfect and has increased morbidity. Cross sectional imaging with computed tomography (CT) and magnetic resonance imaging (MRI) are non-invasive tools that rely on morphologic characteristics such as shape and size of the lymph nodes. However, lymph nodes harboring metastatic disease may be normal sized and non-metastatic lymph nodes may be enlarged due to reactive hyperplasia. The optimal strategy for preoperative staging remains a topic of ongoing research. Advanced imaging techniques to assess lymph nodes in the setting of prostate cancer utilizing novel MRI contrast agents as well as positron emission tomography (PET) tracers have been developed and continue to be studied. Magnetic resonance lymphography utilizing ultra-small super paramagnetic iron oxide has shown promising results in detection of metastatic lymph nodes. Combining MRL with diffusion-weighted imaging may also improve accuracy. Considerable efforts are being made to develop effective PET radiotracers that are performed using hybrid-imaging systems that combine PET with CT or MRI. PET tracers that will be reviewed in this article include [¹⁸F]fluoro-D-glucose, sodium [¹⁸F]fluoride, [¹⁸F]choline, [¹¹C]choline, prostate specific membrane antigen binding ligands, [¹¹C]acetate, [¹⁸F]fluciclovine, gastrin releasing peptide receptor ligands, and androgen binding receptors. This article will review these advanced imaging modalities and ability to detect prostate cancer metastasis to lymph nodes. While more research is

needed, these novel techniques to image lymph nodes in the setting of prostate cancer show a promising future in improving initial lymph node staging.

Key words: Prostate cancer; Staging; Magnetic resonance imaging; Ultra-small super paramagnetic iron oxide; Molecular imaging; Positron emission tomography; Lymph nodes

© **The Author(s) 2017.** Published by Baishideng Publishing Group Inc. All rights reserved.

Core tip: Accurate nodal staging at time of prostate cancer diagnosis is crucial in determining a treatment plan for the patient. This review article highlights the newest imaging techniques that have been and are being developed for imaging of lymph nodes in the initial staging of prostate cancer. Magnetic resonance lymphography utilizing ultra-small super paramagnetic iron oxide has shown to detect metastatic disease in normal sized lymph nodes. Considerable efforts are being made in molecular imaging to develop effective positron emission tomography radiotracers that may be combined with computed tomography or magnetic resonance to detect prostate metastasis as well as potential therapeutic applications.

Zarzour JG, Galgano S, McConathy J, Thomas JV, Rais-Bahrami S. Lymph node imaging in initial staging of prostate cancer: An overview and update. *World J Radiol* 2017; 9(10): 389-399 Available from: URL: <http://www.wjgnet.com/1949-8470/full/v9/i10/389.htm> DOI: <http://dx.doi.org/10.4329/wjr.v9.i10.389>

INTRODUCTION

Prostate cancer is the most common cancer in American men and is associated with a significant likelihood of cure when patients have organ-confined disease through the use of local definitive therapy such as radical prostatectomy or radiation therapy^[1]. However, once prostate cancer spreads beyond the gland to the lymphatic tissues, the opportunity for cure with a local therapy is lost in most cases and significantly diminished in others^[1]. Due to the adverse prognostic implications associated with lymph node metastasis, detection of clinically occult lymph node metastasis is of extreme importance^[2]. Risk assessment tools are used to predict patients who are at risk for higher pathologic stage and use inputs such as PSA, biopsy Gleason sum, percent positive biopsies, and magnetic resonance imaging (MRI) findings^[3-5]. The prostate health index (PHI) test utilizes three forms of PSA (total PSA, free PSA and p2PSA) and the 4K panel (total PSA, free PSA, single chain intact PSA, and human kallikrein 2) have been shown to more accurately predict higher-grade prostate cancer^[6,7]. Patients who are deemed low risk, defined as a predicted < 5% (or in some more conservative guidelines ≤ 2%) for lymph node metastasis usually undergo definitive treatment with curative intent without

any further radiological imaging or lymph node dissection^[1]. Patients determined to be at higher risk for systemic disease need to undergo nodal staging. The most reliable method is pelvic lymph node dissection; however, this is invasive and may be associated with increased morbidity and risk of complications^[1]. Furthermore, pelvic lymph node dissection is less than perfect as several studies have reported positive lymph nodes outside the routine dissection template^[8-11]. Even extended pelvic lymph node dissections have been shown to miss up to 13% of metastatic lymph nodes^[12].

Cross sectional imaging is a non-invasive tool utilized for nodal staging and largely relies on morphologic characteristics such as size and shape. A meta-analysis found a pooled sensitivity of 42% and specificity of 82% for computed tomography (CT) imaging and similar 39% sensitivity and 82% specificity for MR imaging for detection of metastatic lymph nodes^[1]. Utilizing CT and MRI, determination of metastatic lymph nodes is determined largely by size. A threshold of 1.0 cm in short axis of oval nodes and 0.8 cm for round nodes are generally used as indicators of likely metastatic disease^[13]. However, more than half of lymph nodes involved with metastatic prostate cancer may be less than 1 cm^[14]. Moreover, non-metastatic nodes may be enlarged due to reactive hyperplasia. Given the lack of sensitivity of both CT and MRI based on size criteria alone, new techniques of MR lymphography (MRL) have been developed as well as molecular imaging techniques. Herein, we will discuss these modalities for improved prostate cancer lymph node staging.

LYMPH NODE IMAGING WITH MRI

MRL

High resolution MRI utilizing ultra-small super paramagnetic iron oxide (USPIO) has been utilized to improve sensitivity for detection of metastatic lymph nodes^[15,16]. Lymphotropic superparamagnetic nanoparticles are avidly taken up by lymph nodes where they are internalized by macrophages^[17]. Malignant nodes have a relatively paucity of macrophages compared to benign lymph nodes. The intracellular iron-containing particles cause benign lymph nodes to lose signal (appear dark) on T2* images (Figure 1) while lymph nodes affected by metastatic disease do not take up the USPIO as effectively due to the decreased macrophages and hence appear bright^[18]. This evaluation of macrophage function does not rely on nodal size to detect metastasis^[19]. Moreover, it does not depend on the functional activity of cancer in the lymph nodes as it labels normal macrophages in the lymph nodes^[20]. Given the high spatial resolution of MRI, more lymph nodes at smaller sizes can be detected and accurately characterized as benign or malignant with macrophage replacement by metastatic cancer cells^[20].

USPIO particles have been used extensively as a lymphotropic contrast agent for detection of metastatic prostate cancer in numerous clinical trials^[16,21-26]. In an initial study that utilized USPIO (ferumoxtran-10), nodes

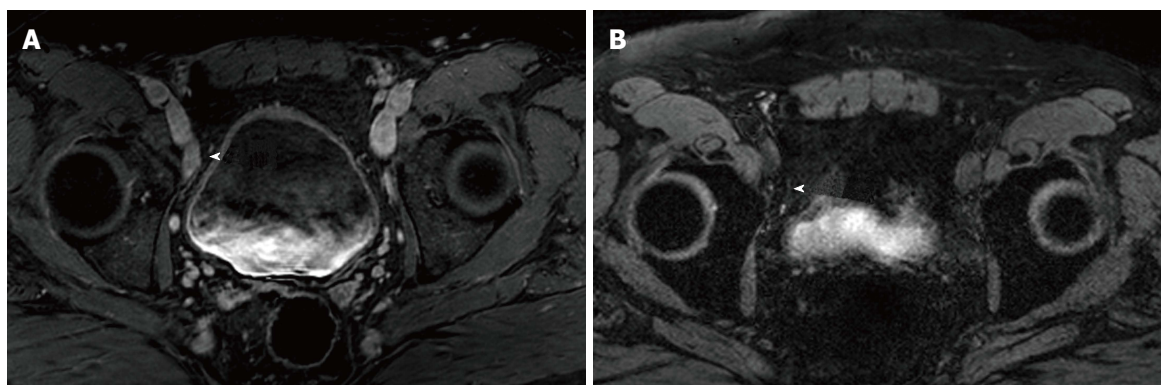


Figure 1 Selected images from a ferumoxytol enhanced magnetic resonance imaging in a 59-year-old man who underwent transrectal ultrasonography prostate biopsy for elevated PSA (10.8 ng/mL) which showed Gleason 3 + 4 disease of 4 cores. A: Initial prostate multiparametric T1 weighted post gadolinium magnetic resonance imaging (MRI) showed a 1.8 cm × 0.9 cm right external iliac chain lymph node that was suspicious based on size criteria (arrowhead); B: 24 h post injection of ferumoxytol (7.5 Fe/kg dose), T2* weighted MRI showed decreased signal intensity within the node (arrowhead), consistent with uptake of ferumoxytol. This was considered a benign lymph node based on these results. The patient underwent computed tomography guided biopsy for confirmation and the node was negative for malignancy.

were considered malignant when one of the following three criteria are present: (1) A decrease in signal intensity of less than 30 percent on T2-weighted fast spin-echo or gradient-echo sequences after the administration of USPIO; (2) a heterogeneous signal (giving the entire node a mottled appearance), discrete focal defects (isolated islands of high signal intensity), or both on gradient echo imaging; and (3) nodes with a central area of hyperintensity (excluding a fatty hilum) but a peripheral decrease in signal intensity^[15]. This initial study utilizing ferumoxtran-10 demonstrated a sensitivity for detection of malignant lymph nodes with short axis diameter of 5-10 mm was increased with use of USPIO compared to MRI alone (96.4% vs 28.5%, respectively)^[15]. Other studies have confirmed the ability of MR ferumoxtran-10-enhanced lymphography to detect metastatic disease in non-pathologically enlarged lymph nodes (< 7 mm) with high sensitivity and specificity^[20,23,24,27-30].

Meijer *et al.*^[31] showed a better prognosis in a subset of patients with MRL positive lymph nodes that were < 8 mm and better outcomes in patients in whom all MRL positive lymph nodes were resected. This highlights a window of opportunity for cure in these patients as those with MRL-detected positive nodes that were entirely removed had a five-year distant metastatic disease free survival of 80% compared to 35% in the patients who did not have all MRL-detected positive nodes removed^[31].

Additionally, the potential for MRL to detect metastatic lymph nodes outside of the routine dissection margin has potential for great clinical value including surgical and radiation therapy planning. In series of 269 men with moderate to high risk for nodal metastasis, 41% were found to have lymph node metastasis outside of the routine dissection area that were identified with MR ferumoxtran-10-enhanced lymphography^[24]. MRL has been utilized to guide radiation therapy as another study showed that 53% of prostate cancer patients had

MRL positive lymph nodes outside of the target volume for pelvic radiation^[32]. Salvage radiation therapy is associated with some toxicity^[33], and improved selection of patients and detection of nodal targets can decrease morbidity and improve cure rates^[25]. However, despite these promising results, ferumoxtran-10 failed to achieve Food and Drug Administration (FDA) approval and production was halted^[34].

Ferumoxytol is a newly released USPIO agent that has been more recently utilized in detection of malignant lymph nodes^[35]. Ferumoxytol is a compound closely related to ferumoxtran-10 that is FDA approved as iron replacement therapy in patients with chronic kidney failure with the recommended clinical dose of 1020 mg (two doses of 510 mg administered intravenously 3-8 d apart)^[35,36]. In phase I and II clinical trials, ferumoxytol was associated with low adverse event rate which the most common events including nausea, dizziness, and diarrhea^[37], although more serious reactions such as hypotension and anaphylaxis have been reported^[38,39]. This has led to the FDA releasing a safety communication recommending modifications to give ferumoxytol as a dilute infusion^[40].

Due to its large size, ferumoxytol remains in a relatively steady concentration within the intravascular space for several hours (circulating half-life is 14-15 h) and then is gradually cleared by macrophages from the blood pool over several days^[41]. Following macrophage breakdown, the iron oxide particles are taken up by the reticuloendothelial system^[41]. In a recent phase I dose escalation trial, it was shown that the signal intensity of normal lymph nodes drop in a dose dependent manner with the optimal dose determined to be 7.5 mg Fe/kg^[35]. A pilot study quantitatively compared the ability of ferumoxytol and ferumoxtran-10 to suppress signal intensity in normal lymph nodes (in patients with high risk prostate cancer) and showed that signal suppression was weaker for ferumoxytol MRL than for ferumoxtran-10 MRL^[42]. This study was limited in that

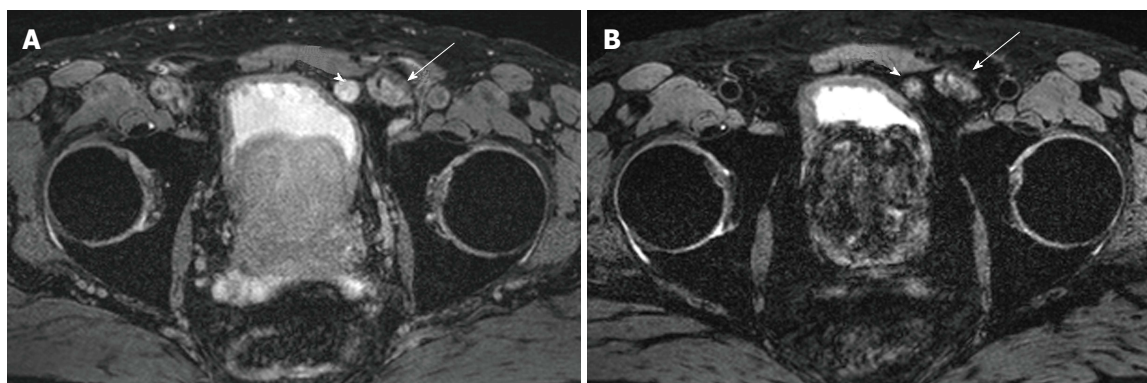


Figure 2 Selected images from a ferumoxytol enhanced magnetic resonance imaging in a 65 years old man status post magnetic resonance imaging/ultrasound fusion guided prostate biopsy revealing 3 + 3 prostate cancer and PSA 16.6 ng/mL. A: Baseline T2* weighted magnetic resonance imaging (MRI) showed a rounded lymph node anterior to the bladder (arrowhead) that measured 1.5 cm and was hyperintense. Lobular mass like lesion (arrow) lateral to the suspicious lymph node corresponds to hernia mesh; B: 24 h post injection of ferumoxytol (7.5 Fe/kg dose) enhanced MRI shows persistent heterogeneous hyperintensity within the node (arrowhead). The lack of ferumoxytol uptake within the node was suspicious for malignant involvement. Pathology revealed castleman's disease (false positive). Arrow again indicates hernia mesh.

only 4 patients received ferumoxytol and the dose was 6.0 mg Fe/kg, but further research is needed to validate the accuracy of ferumoxytol MRL^[42]. Ferumoxytol MRL has also been preliminarily evaluated in non-human primates for use as an intraprostatic injection to directly map lymph nodes draining the prostate gland, with a potential of guiding lymphatic drainage patterns for specific gland segments^[43].

MRL may have false positive results in the setting of reactive nodal hyperplasia or granulomatous diseases in which there are decreased number of macrophages in otherwise benign lymph nodes that may lead to mischaracterization of lymph nodes as malignant suspicion on imaging^[44] (Figure 2).

Diffusion-weighted imaging

In diffusion-weighted imaging (DWI), the Brownian motion of water molecules within a voxel of tissue is imaged and can be quantitatively expressed using the apparent diffusion coefficient (ADC) value. DWI can be performed quickly without the need of a contrast medium. Malignant tissue tends to have increased cellularity with enlarged nuclei and an abundance of macromolecular proteins, resulting in restricted diffusion^[45]. Typical malignant lesions appear hyperintense on images acquired at high b-values (800-1000 s/mm²) and hypointense on the corresponding ADC maps.

Malignant lymph nodes have been shown to have a lower ADC value when compared to benign lymph nodes^[46,47], but show less promising results in normal sized lymph nodes with a wide range of ADC values^[45,48]. In a study of 29 patients with prostate cancer and a total of 118 lymph nodes evaluated by DWI-MRI, a cut off value of 1.3×10^{-3} mm²/s yielded a sensitivity of 86% and specificity of 85%^[46]. ADC values can be elevated in necrotic nodes due to the free diffusion of water, which can lead to misclassification^[49]. While some authors have reporting the combination of nodal size and the relative ADC value nodes is more useful in

detecting pelvic lymph node metastasis^[50], others have found less promising results^[45]. Nevertheless, there can be an overlap of ADC values in benign and malignant lymph nodes^[51].

In a more recent prospective study utilizing a 3T MRI system and a non-quantitative approach to evaluation DWI and ADC maps, revealed 94% specificity and 41% sensitivity for anatomical region based analysis (mean positive lymph node size was 1.2 cm)^[52]. In a prospective evaluation of detection of normal sized metastatic lymph nodes in initial staging of prostate and bladder carcinoma, there was increased detection utilizing DWI when compared to conventional cross-section imaging techniques with detection of metastasis in 64%-79% of patients^[51]. Evaluating additional morphologic features at MR imaging such as round shape, irregular border, low T2 signal may improve specificity than relying only on diffusion weighted imaging^[51]. Further advances in DWI-MRI technique will require standardization of the technique, image acquisition and sequence parameters of different scanner platforms^[53].

Combining DWI-MRI with other techniques such as USPIO or choline show perhaps the most promising results^[30,54]. In a study evaluating 2,993 normal sized lymph nodes in patients with prostate or bladder cancer, combining DWI-MRI with USPIO improved sensitivity and specificity (65%-75% and 93%-96%; compared to 55%-65% and 71%-91%, respectively) and decreased imaging interpretation time compared to USPIO alone^[30].

PET TRACERS FOR INITIAL NODAL STAGING OF PROSTATE CANCER

PET

Considerable efforts are currently being made to develop effective radiotracers to image prostate cancer in both the setting of primary staging as well as biochemical recurrence. Although not the focus of this paper, there is substantial evidence supporting the use of PET tracers for

Table 1 Selected positron emission tomography tracers used for prostate cancer imaging

PET tracers	Mechanism of action
[¹⁸ F]FDG	Glucose metabolism
Sodium [¹⁸ F]fluoride	Chemisorption to bone matrix
[¹⁸ F]choline, [¹¹ C]choline	Cell membrane metabolism
[¹⁸ F]DCFBC, [⁶⁸ Ga]HBED-CC	PSMA binding
[¹¹ C]acetate	Fatty acid metabolism
[¹⁸ F]fluciclovine	Amino acid transport
[⁶⁸ Ga]DOTA-bombesin	GRPR receptor binding
[¹⁸ F]FDHT	Androgen receptor binding

PET: Positron emission tomography; [¹⁸F]FDG: (¹⁸F)fluoro-D-glucose; [¹⁸F]DCFBC: (¹⁸F)fluorobenzyl-L-cysteine; GRPR: Gastrin-releasing peptide receptor.

biochemical recurrence, and two PET tracers [(¹¹C)choline and (¹⁸F)fluciclovine] have been approved by the FDA for the detection and staging of biochemical recurrence. However, there has been less investigation regarding the use of PET in the initial nodal staging of prostate cancer. A wide range of PET tracers have been developed and investigated for prostate cancer imaging, and this section summarizes PET tracers that have demonstrated utility for detecting lymph node metastases from prostate cancer. These tracers and their key properties are summarized in Table 1.

Positron emission tomography (PET) is currently performed using hybrid imaging systems that combine PET with CT or MRI for attenuation correction and anatomic localization of the PET findings. In PET imaging, a positron emitting radiotracer is administered to the patient, which then emits 511 keV gamma rays through annihilation of the positron with an electron in the tissue which can be localized through coincidence detection^[55]. Compared to conventional planar scintigraphy and single photon computed tomography (SPECT), PET provides higher spatial and temporal resolution. One of the limitations of PET is resolution, with decreased sensitivity of the detection and characterization of PET tracer uptake in lesions less than 8 mm. However, the use of hybrid imaging PET/CT or PET/MRI allows the combination of anatomical imaging from the CT or MRI with molecular information from PET.

PET tracers for prostate cancer imaging have been labeled with several different radionuclides that vary in terms of their physical half-life ($t_{1/2}$) and their chemistries. PET radionuclides include are carbon-11 ($t_{1/2}$ = 20 min), fluorine-18 ($t_{1/2}$ = 110 min), and gallium-68 ($t_{1/2}$ = 68 min). Carbon-11 and fluorine-18 are produced using cyclotrons while gallium-68 is produced using a generator system. Fluorine-18 is widely available, and its long half-life facilitates production of large batches of PET tracers and distribution to sites that do not have onsite production capabilities.

The most commonly used radiotracer for clinical oncologic imaging is 2-deoxy-2-(¹⁸F)fluoro-D-glucose (FDG), but this tracer is of limited utility for the initial staging of prostate cancer due to the low metabolic activity in the early phase of the disease which results

in poor sensitivity^[56]. Another disadvantage of FDG is urinary excretion, potentially decreasing sensitivity for pelvic lymph nodes^[57]. For the evaluation of bony metastases, sodium(¹⁸F) fluoride (NaF) has been used for skeletal scintigraphy which takes advantage of higher spatial resolution when compared with conventional planar (^{99m}Tc)methyldiphosphinate (MDP). Several studies have demonstrated that cross-sectional skeletal scintigraphy with fluoride-PET/CT or MDP-SPECT/CT have superior sensitivity and specificity for detection of osseous metastases when compared to conventional planar bone scans (96% and 98%, respectively)^[58]. The uptake of (¹⁸F)fluoride is based on bone turnover with increased binding to newly deposited mineralize bone matrix that occurs in bone metastases, particularly osteoblastic metastases. While (¹⁸F)fluoride-PET/CT may be useful in preoperative skeletal staging in prostate cancer, this tracer is not useful for the detection of lymph node metastases.

Choline is a naturally-occurring small molecule that is incorporated into tumor cells after phosphorylation by choline kinase, which is up regulated in prostate cancer^[59]. (¹¹C)choline uptake in metastatic lymph nodes occurs in the presence of viable malignant tissue, and (¹¹C)choline has been approved by the FDA for use in the detection and localization of suspected biochemically recurrent prostate cancer. This PET tracer has been used for prostate cancer with a pooled sensitivity of 49.2% and specificity of 95% for detection lymph node metastasis^[60]. Results are better for larger nodes, but sensitivity is limited in lymph nodes smaller than 7 mm^[20]. Several studies combining (¹¹C)choline PET/CT and diffusion weighted MRI showed that sensitivity remained too low to be clinically useful for initial staging^[54,61].

Fluorinated analogues of choline have been developed to take advantage of the longer half-life of fluorine-18 [e.g., (¹⁸F)fluorocholine and 2-(¹⁸F)fluoroethyl choline]. However, these fluorinated choline analogues have similar limited capability in detecting lymph node metastasis (sensitivity 40% and specificity 96%)^[62,63]. Combining ¹⁸F-choline PET and MRI may help improve the results of choline PET imaging, but further research is needed^[64,65]. The value of choline for the detection of recurrent prostate cancer in patients with low PSA levels (< 2.5 ng/mL) is limited^[66,67]. Additionally, ¹⁸F-labeled analogues of choline are eliminated *via* the kidney and urinary tract activity, which is undesirable for pelvic imaging.

Acetate is a naturally occurring metabolic substrate that can enter the fatty acid metabolic pathway which is overexpressed in prostate cancer cells^[68]. Most research has been done with (¹¹C)acetate and has shown sensitivity of 68% and specificity of 78% in one study of intermediate and high risk prostate cancer^[69], but has the disadvantage of requiring an on onsite cyclotron to due to the short half-life of 20 min.

Prostate specific membrane antigen (PSMA) is a protein expressed by the prostate and overexpressed in prostate cancer^[70]. The initial molecular imaging

agent targeting PSMA that gained widespread use was (^{111}In)indium capromab pendetide, a radiolabeled monoclonal antibody that targets the intracellular portion of PSMA and is imaged utilizing SPECT/CT. While initial results showed improvement over conventional techniques, there was limited sensitivity and specificity^[71,72]. However with the additional of MRI, sensitivity and specificity were increased^[73]. The main disadvantage of (^{111}In)indium capromab pendetide is that it targets an intracellular protein making imaging only a possibility upon apoptosis or necrosis and not in viable tissue^[55,70,74]. Additionally, the slow kinetics of (^{111}In)indium capromab pendetide requires imaging 5–7 d after injection. More recently, a great deal of research has been focused on small molecule ligands that bind to the extracellular portion of PSMA^[75,76].

Novel small molecule imaging PSMA ligands have been developed such as *N*-{*N*-[(*S*)-1,3-dicarboxypropyl] carbamoyl}-4-(^{18}F)fluorobenzyl-L-cysteine [(^{18}F)DCFBC], which binds irreversibly to the extracellular component of PSMA and has been shown to improve detection of metastatic prostate cancer^[77,78]. The most commonly used PSMA ligand in Europe is ^{68}Ga -N,N'-bis [2-hydroxy-5-(carboxyethyl)benzyl] ethylenediamine-N,N'-diacetic acid (HBED-CC) (Figure 3). In a study utilizing ^{68}Ga -labeled PSMA ligand (HBED-CC), there was improved accuracy of lymph node staging over conventional imaging with 65.9% sensitivity and 98.9% specificity^[79]. A retrospective study examining ^{68}Ga -PSMA PET/CT in initial staging of patients with high risk of lymph node metastasis found 33.3% sensitivity and 100% specificity (mean size of true positive nodes was 13.6 cm and of false positive node was 4.3 mm)^[80].

Amino acid radiotracers can accumulate in prostate cancer cells through the upregulation of transmembrane amino acid transport in prostate cancer^[81]. The most work with a synthetic amino acid PET radiotracer for prostate cancer has been with (^{18}F)fluciclovine for detection of recurrent disease, and this PET tracer was approved by the FDA for use in biochemically recurrent prostate cancer in 2016 (Figure 4). Preliminary studies have reported results for initial staging^[81,82]. In a multicenter phase IIb clinical trial for staging of initial prostate cancer, diagnostic accuracy of (^{18}F)fluciclovine PET/CT was compared to conventional imaging with CT and bone scan^[83]. Overall accuracies were similar (85.5% for (^{18}F)fluciclovine PET/CT and 87.3% for conventional imaging); however, (^{18}F)fluciclovine PET/CT was positive in 5–9 mm nodes and skeletal lesions that were not detected by conventional imaging.

An additional molecular target that is currently under investigation is the gastrin-releasing peptide receptor (GRPR) which is overexpressed in prostate but has lower levels in benign prostate tissue including benign prostatic hyperplasia^[84]. Initial studies demonstrate GRPR overexpression in 63%–100% of primary prostate carcinomas and 50%–85% of nodal and osseous metastases^[85]. A number of peptide based ligands for GRPR have been developed including the 14 amino acid peptide bombesin, as well as analogues of the 27-amino

acid gastrin releasing peptide (GRP)^[86]. A single human trial utilizing a ^{68}Ga -labeled GRPR antagonist for pre-operative staging has been completed^[87]. This trial enrolled 11 patients with primary prostate carcinoma and three patients with evidence of biochemical recurrence, demonstrating a sensitivity of 88% and specificity of 81% for detection of the primary lesion (within a sextant level) and found evidence of biochemical recurrence in lymph nodes and the prostate bed in two out of three patients^[88].

Androgen sensitivity and receptor expression remain a mainstay in the diagnosis and treatment of prostate carcinoma. Importantly, androgen receptor expression plays a role in both initial treatment strategies and in the setting for treatment for biochemical recurrence/metastatic disease. Preliminary human imaging studies have been performed using the androgen receptor ligand 16β -(^{18}F)fluoro-5 α -dihydrotestosterone (FDHT). The initial human study compared FDHT and FDG, which demonstrated FDHT uptake in 46/59 lesions in seven patients with progressive metastatic prostate cancer (compared to FDG uptake in 57/59)^[89]. The role, if any, of (^{18}F)FDHT in the pre-operative evaluation of prostate cancer is not yet defined.

An interesting future in targeted molecular imaging of metastatic prostate carcinoma is the use of PSMA and bombesin agents for targeted therapy with alpha-emitters or beta-emitters (including ^{90}Y and ^{177}Lu). These agents are currently being utilized in clinical trials for patients with biochemical recurrence, but are not currently approved for use in the United States^[90,91]. These compounds may play a future role in adjuvant therapy post prostatectomy as the previously described molecular targeted PET agents become established for initial staging.

An exciting development that may increase the impact of molecular imaging for prostate carcinoma is the recent FDA approval of hybrid PET/MRI scanners. These scanners can acquire PET and MRI data simultaneously and combine targeted molecular imaging with PET with the soft tissue contrast and anatomic detail provided by pelvic MRI. The MRI component of PET/MRI can significantly increase detection of lesions compared to the non-contrast CT typically performed with conventional PET/CT. Evaluation of the prostate bed can also be significantly improved utilizing PET/MRI vs PET/CT. Given the established role of MRI for prostate cancer staging and lesion detection, PET/MRI may become the preferred platform for prostate cancer imaging in certain clinical scenarios. However, more data are needed to define the role of PET/MRI in the initial staging of prostate cancer.

CONCLUSION

Conventional imaging (CT and MRI) cannot depict small metastases in normal sized and normal appearing lymph nodes. The optimal strategy for the preoperative staging of prostate cancer remains a topic of ongoing

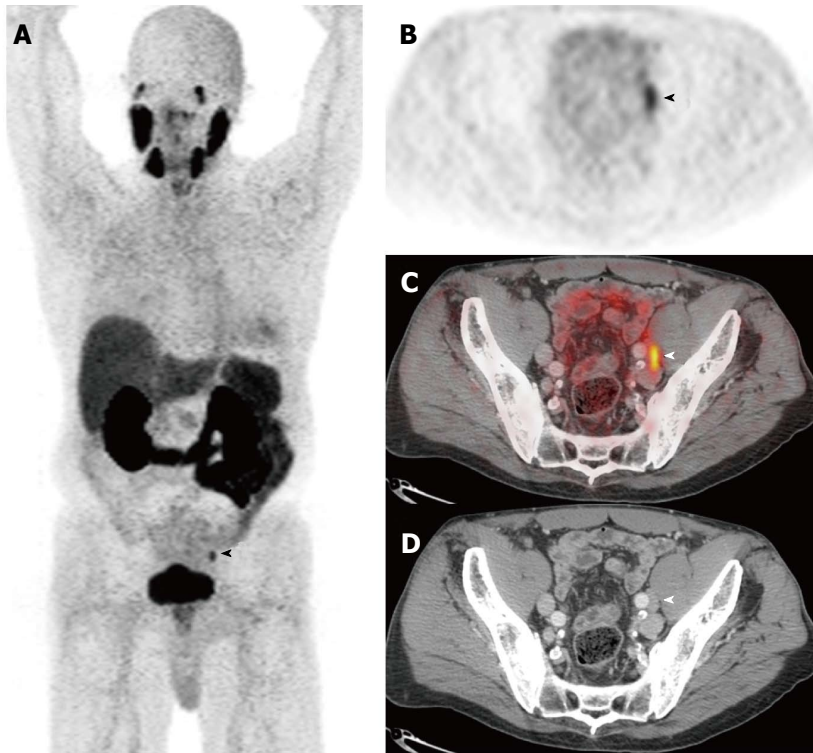


Figure 3 Prostate specific membrane antigen. Selected images from a [^{68}Ga]PSMA-11-PET/CT study performed prior to therapy in a man with biopsy-proven Gleason 9 prostate adenocarcinoma, a serum PSA of 11.6 ng/mL, and a clinical tumor stage of cT2b. The anterior maximum intensity projection (MIP) image (A) and the axial PET (B), fusion (C), and CT (D) images through the pelvis demonstrate focal activity in a left external iliac lymph node. This appearance is highly suspicious for a lymph node metastasis. Images courtesy of Tom Hope, MD, University of California San Francisco, Department of Radiology. PSMA: Prostate specific membrane antigen; PET/CT: Positron emission tomography/computed tomography.

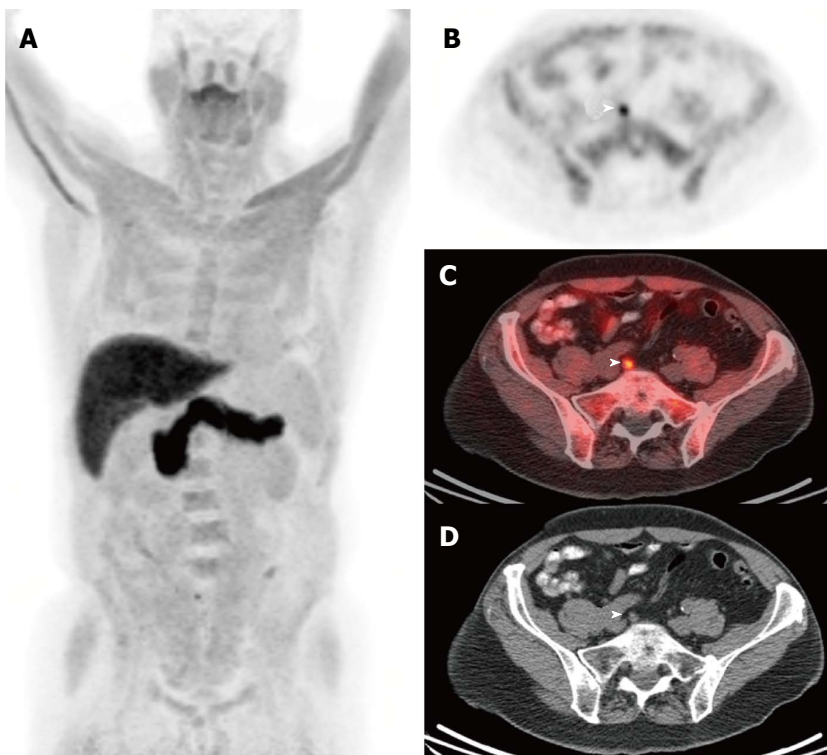


Figure 4 Fluciclovine. Selected images from a (^{18}F)fluciclovine-positron emission tomography/computed tomography study performed in a man who underwent prostatectomy for Gleason 8 prostate adenocarcinoma 11 years ago. He developed biochemical recurrence with a serum PSA of 0.8 ng/mL and a PSA doubling time of 14 mo at the time of the (^{18}F)fluciclovine-PET/CT study. The anterior maximum intensity projection (MIP) image (A) and the axial PET (B), fusion (C), and CT (D) images near the level of the pelvic inlet demonstrate focal activity in a subcentimeter right common iliac lymph node. This appearance is highly suspicious for a lymph node metastasis. Images courtesy of Ephraim Parent MD, PhD, and David Schuster, MD, Emory University, Department of Radiology. PET/CT: Positron emission tomography/computed tomography.

research. Advanced imaging techniques to assess lymph nodes in the setting of prostate cancer utilizing novel MRI contrast agents as well as PET tracers have been developed and continue to be studied. MRL utilizing USPIO has shown high sensitivity and specificity in detection of normal sized lymph nodes containing metastatic disease and thus a positive finding may alter the treatment course for the patient. Ongoing research is occurring in molecular imaging and continues to show a promising future for detection of prostate metastasis as well as potential therapeutic applications.

REFERENCES

- Hövels AM, Heesakkers RA, Adang EM, Jager GJ, Strum S, Hoogeveen YL, Severens JL, Barentsz JO. The diagnostic accuracy of CT and MRI in the staging of pelvic lymph nodes in patients with prostate cancer: a meta-analysis. *Clin Radiol* 2008; **63**: 387-395 [PMID: 18325358 DOI: 10.1016/j.crad.2007.05.022]
- Kothari PS, Scardino PT, Ohori M, Kattan MW, Wheeler TM. Incidence, location, and significance of periprostatic and periseminal vesicle lymph nodes in prostate cancer. *Am J Surg Pathol* 2001; **25**: 1429-1432 [PMID: 11684961]
- Makarov DV, Trock BJ, Humphreys EB, Mangold LA, Walsh PC, Epstein JI, Partin AW. Updated nomogram to predict pathologic stage of prostate cancer given prostate-specific antigen level, clinical stage, and biopsy Gleason score (Partin tables) based on cases from 2000 to 2005. *Urology* 2007; **69**: 1095-1101 [PMID: 17572194 DOI: 10.1016/j.urol.2007.03.042]
- D'Amico AV, Whittington R, Malkowicz SB, Schultz D, Schnall M, Tomaszewski JE, Wein A. Combined modality staging of prostate carcinoma and its utility in predicting pathologic stage and postoperative prostate specific antigen failure. *Urology* 1997; **49**: 23-30 [PMID: 9123732]
- D'Amico AV. Combined-modality staging for localized adenocarcinoma of the prostate. *Oncology* (Williston Park) 2001; **15**: 1049-1059; discussion 1060-106, 1064-1065, 1069-1070, 1073-1075 [PMID: 11548976]
- Loeb S, Catalona WJ. The Prostate Health Index: a new test for the detection of prostate cancer. *Ther Adv Urol* 2014; **6**: 74-77 [PMID: 24688603 DOI: 10.1177/1756287213513488]
- McDonald ML, Parsons JK. 4-Kallikrein Test and Kallikrein Markers in Prostate Cancer Screening. *Urol Clin North Am* 2016; **43**: 39-46 [PMID: 26614027 DOI: 10.1016/j.ucl.2015.08.004]
- Allaf ME, Palapattu GS, Trock BJ, Carter HB, Walsh PC. Anatomical extent of lymph node dissection: impact on men with clinically localized prostate cancer. *J Urol* 2004; **172**: 1840-1844 [PMID: 15540734]
- Burkhard FC, Studer UE. The role of lymphadenectomy in prostate cancer. *Urol Oncol* 2004; **22**: 198-202; discussion 202-204 [PMID: 15271316 DOI: 10.1016/j.urolonc.2004.04.032]
- McDowell GC 2nd, Johnson JW, Tenney DM, Johnson DE. Pelvic lymphadenectomy for staging clinically localized prostate cancer. Indications, complications, and results in 217 cases. *Urology* 1990; **35**: 476-482 [PMID: 2353374]
- Schuessler WW, Pharand D, Vancaillie TG. Laparoscopic standard pelvic node dissection for carcinoma of the prostate: is it accurate? *J Urol* 1993; **150**: 898-901 [PMID: 8345606]
- Joniau S, Van den Bergh L, Lerut E, Deroose CM, Haustermans K, Oyen R, Budiharto T, Ameye F, Bogaerts K, Van Poppel H. Mapping of pelvic lymph node metastases in prostate cancer. *Eur Urol* 2013; **63**: 450-458 [PMID: 22795517 DOI: 10.1016/j.eururo.2012.06.057]
- Jager GJ, Barentsz JO, Oosterhof GO, Witjes JA, Ruijs SJ. Pelvic adenopathy in prostatic and urinary bladder carcinoma: MR imaging with a three-dimensional T1-weighted magnetization-prepared-rapid gradient-echo sequence. *AJR Am J Roentgenol* 1996; **167**: 1503-1507 [PMID: 8956585 DOI: 10.2214/ajr.167.6.8956585]
- Davis GL. Sensitivity of frozen section examination of pelvic lymph nodes for metastatic prostate carcinoma. *Cancer* 1995; **76**: 661-668 [PMID: 8625162]
- Harisinghani MG, Barentsz J, Hahn PF, Deserno WM, Tabatabaei S, van de Kaa CH, de la Rosette J, Weissleder R. Noninvasive detection of clinically occult lymph-node metastases in prostate cancer. *N Engl J Med* 2003; **348**: 2491-2499 [PMID: 12815134 DOI: 10.1056/NEJMoa022749]
- Bellin MF, Roy C, Kinkel K, Thoumas D, Zaim S, Vanel D, Tuchmann C, Richard F, Jacqmin D, Delcourt A, Challier E, Lebre T, Cluzel P. Lymph node metastases: safety and effectiveness of MR imaging with ultrasmall superparamagnetic iron oxide particles--initial clinical experience. *Radiology* 1998; **207**: 799-808 [PMID: 9609907 DOI: 10.1148/radiology.207.3.9609907]
- Weissleder R, Elizondo G, Wittenberg J, Lee AS, Josephson L, Brady TJ. Ultrasmall superparamagnetic iron oxide: an intravenous contrast agent for assessing lymph nodes with MR imaging. *Radiology* 1990; **175**: 494-498 [PMID: 2326475 DOI: 10.1148/radiology.175.2.2326475]
- Wunderbaldinger P, Josephson L, Bremer C, Moore A, Weissleder R. Detection of lymph node metastases by contrast-enhanced MRI in an experimental model. *Magn Reson Med* 2002; **47**: 292-297 [PMID: 11810672]
- Hricak H, Choyke PL, Eberhardt SC, Leibel SA, Scardino PT. Imaging prostate cancer: a multidisciplinary perspective. *Radiology* 2007; **243**: 28-53 [PMID: 17392247 DOI: 10.1148/radiol.2431030580]
- Fortuin AS, Deserno WM, Meijer HJ, Jager GJ, Takahashi S, Debats OA, Reske SN, Schick C, Krause BJ, van Oort I, Witjes AJ, Hoogeveen YL, van Lin EN, Barentsz JO. Value of PET/CT and MR lymphography in treatment of prostate cancer patients with lymph node metastases. *Int J Radiat Oncol Biol Phys* 2012; **84**: 712-718 [PMID: 22417806 DOI: 10.1016/j.ijrobp.2011.12.093]
- Harisinghani MG, Saini S, Slater GJ, Schnall MD, Rifkin MD. MR imaging of pelvic lymph nodes in primary pelvic carcinoma with ultrasmall superparamagnetic iron oxide (Combixen): preliminary observations. *J Magn Reson Imaging* 1997; **7**: 161-163 [PMID: 9039609]
- Harisinghani MG, Saksena MA, Hahn PF, King B, Kim J, Torabi MT, Weissleder R. Ferumoxtran-10-enhanced MR lymphangiography: does contrast-enhanced imaging alone suffice for accurate lymph node characterization? *AJR Am J Roentgenol* 2006; **186**: 144-148 [PMID: 16357394 DOI: 10.2214/AJR.04.1287]
- Heesakkers RA, Hövels AM, Jager GJ, van den Bosch HC, Witjes JA, Raat HP, Severens JL, Adang EM, van der Kaa CH, Fütterer JJ, Barentsz J. MRI with a lymph-node-specific contrast agent as an alternative to CT scan and lymph-node dissection in patients with prostate cancer: a prospective multicohort study. *Lancet Oncol* 2008; **9**: 850-856 [PMID: 18708295 DOI: 10.1016/S1470-2045[08]70203-1]
- Heesakkers RA, Jager GJ, Hövels AM, de Hoop B, van den Bosch HC, Raat F, Witjes JA, Mulders PF, van der Kaa CH, Barentsz JO. Prostate cancer: detection of lymph node metastases outside the routine surgical area with ferumoxtran-10-enhanced MR imaging. *Radiology* 2009; **251**: 408-414 [PMID: 19401573 DOI: 10.1148/radiol.2512071018]
- Ross RW, Zietman AL, Xie W, Coen JJ, Dahl DM, Shipley WU, Kaufman DS, Islam T, Guimaraes AR, Weissleder R, Harisinghani M. Lymphotropic nanoparticle-enhanced magnetic resonance imaging (LNMRI) identifies occult lymph node metastases in prostate cancer patients prior to salvage radiation therapy. *Clin Imaging* 2009; **33**: 301-305 [PMID: 19559353 DOI: 10.1016/j.clinimag.2009.01.013]
- Froehlich JM, Triantafyllou M, Fleischmann A, Vermathen P, Thalmann GN, Thoeny HC. Does quantification of USPIO uptake-related signal loss allow differentiation of benign and malignant normal-sized pelvic lymph nodes? *Contrast Media Mol Imaging* 2012; **7**: 346-355 [PMID: 22539405 DOI: 10.1002/cmmi.503]
- Thoeny HC, Triantafyllou M, Birkhaeuser FD, Froehlich JM, Tshering DW, Binser T, Fleischmann A, Vermathen P, Studer UE. Combined ultrasmall superparamagnetic particles of iron oxide-enhanced and diffusion-weighted magnetic resonance imaging reliably detect pelvic lymph node metastases in normal-sized nodes of bladder

- and prostate cancer patients. *Eur Urol* 2009; **55**: 761-769 [PMID: 19144456 DOI: 10.1016/j.eururo.2008.12.034]
- 28 **Triantafyllou M**, Studer UE, Birkhäuser FD, Fleischmann A, Bains LJ, Petralia G, Christe A, Froehlich JM, Thoeny HC. Ultrasmall superparamagnetic particles of iron oxide allow for the detection of metastases in normal sized pelvic lymph nodes of patients with bladder and/or prostate cancer. *Eur J Cancer* 2013; **49**: 616-624 [PMID: 23084842 DOI: 10.1016/j.ejca.2012.09.034]
 - 29 **Heesakkers RA**, Fütterer JJ, Hövels AM, van den Bosch HC, Scheenen TW, Hoogeveen YL, Barentsz JO. Prostate cancer evaluated with ferumoxtran-10-enhanced T2*-weighted MR Imaging at 1.5 and 3.0 T: early experience. *Radiology* 2006; **239**: 481-487 [PMID: 16641354 DOI: 10.1148/radiol.2392050411]
 - 30 **Birkhäuser FD**, Studer UE, Froehlich JM, Triantafyllou M, Bains LJ, Petralia G, Vermathen P, Fleischmann A, Thoeny HC. Combined ultrasmall superparamagnetic particles of iron oxide-enhanced and diffusion-weighted magnetic resonance imaging facilitates detection of metastases in normal-sized pelvic lymph nodes of patients with bladder and prostate cancer. *Eur Urol* 2013; **64**: 953-960 [PMID: 23916692 DOI: 10.1016/j.eururo.2013.07.032]
 - 31 **Meijer HJ**, Debats OA, van Lin EN, Witjes JA, Kaanders JH, Barentsz JO. A retrospective analysis of the prognosis of prostate cancer patients with lymph node involvement on MR lymphography: who might be cured. *Radiat Oncol* 2013; **8**: 190 [PMID: 23898991 DOI: 10.1186/1748-717X-8-190]
 - 32 **Meijer HJ**, Debats OA, Kunze-Busch M, van Kollenburg P, Leer JW, Witjes JA, Kaanders JH, Barentsz JO, van Lin EN. Magnetic resonance lymphography-guided selective high-dose lymph node irradiation in prostate cancer. *Int J Radiat Oncol Biol Phys* 2012; **82**: 175-183 [PMID: 21075555 DOI: 10.1016/j.ijrobp.2010.09.023]
 - 33 **Pisansky TM**, Kozelsky TF, Myers RP, Hillman DW, Blute ML, Buskirk SJ, Cheville JC, Ferrigni RG, Schild SE. Radiotherapy for isolated serum prostate specific antigen elevation after prostatectomy for prostate cancer. *J Urol* 2000; **163**: 845-850 [PMID: 10687990]
 - 34 **George AK**, Turkbey B, Valayil SG, Muthigi A, Mertan F, Kongnyuy M, Pinto PA. A urologist's perspective on prostate cancer imaging: past, present, and future. *Abdom Radiol (NY)* 2016; **41**: 805-816 [PMID: 27138438 DOI: 10.1007/s00261-016-0751-6]
 - 35 **Turkbey B**, Agarwal HK, Shih J, Bernardo M, McKinney YL, Daar D, Griffiths GL, Sankineni S, Johnson L, Grant KB, Weaver J, Rais-Bahrami S, Harisinghani M, Jacobs P, Dahut W, Merino MJ, Pinto PA, Choyke PL. A Phase I Dosing Study of Ferumoxetyl for MR Lymphography at 3 T in Patients With Prostate Cancer. *AJR Am J Roentgenol* 2015; **205**: 64-69 [PMID: 26102381 DOI: 10.2214/AJR.14.13009]
 - 36 **Vasanawala SS**, Nguyen KL, Hope MD, Bridges MD, Hope TA, Reeder SB, Bashir MR. Safety and technique of ferumoxetyl administration for MRI. *Magn Reson Med* 2016; **75**: 2107-2111 [PMID: 26890830 DOI: 10.1002/mrm.26151]
 - 37 **Pai AB**, Garba AO. Ferumoxetyl: a silver lining in the treatment of anemia of chronic kidney disease or another dark cloud? *J Blood Med* 2012; **3**: 77-85 [PMID: 22973119 DOI: 10.2147/JBM.S29204]
 - 38 **Bailie GR**. Comparison of rates of reported adverse events associated with i.v. iron products in the United States. *Am J Health Syst Pharm* 2012; **69**: 310-320 [PMID: 22302256 DOI: 10.2146/ajhp.110262]
 - 39 **Santosh S**, Podaralla P, Miller B. Anaphylaxis with elevated serum tryptase after administration of intravenous ferumoxetyl. *NDT Plus* 2010; **3**: 341-342 [PMID: 25949425 DOI: 10.1093/ndtplus/sfq084]
 - 40 FDA Drug Safety Communication: FDA strengthens warnings and changes prescribing instructions to decrease the risk of serious allergic reactions with anemia drug Feraheme. 2015, accessed December 5 2016. Available from: URL: <https://www.fda.gov/Drugs/DrugSafety/ucm440138.htm>
 - 41 **Bashir MR**, Bhatti L, Marin D, Nelson RC. Emerging applications for ferumoxetyl as a contrast agent in MRI. *J Magn Reson Imaging* 2015; **41**: 884-898 [PMID: 24974785 DOI: 10.1002/jmri.124691]
 - 42 **Debats OA**, Fortuin AS, Meijer HJ, Hambroek T, Litjens GJ, Barentsz JO, Huisman HJ. Intrnodal signal suppression in pelvic MR lymphography of prostate cancer patients: a quantitative comparison of ferumoxtran-10 and ferumoxetyl. *PeerJ* 2016; **4**: e2471 [PMID: 27781154 DOI: 10.7717/peerj.2471]
 - 43 **Sankineni S**, Smedley J, Bernardo M, Brown AM, Johnson L, Muller B, Griffiths GL, Kobayashi H, Rais-Bahrami S, Pinto PA, Wood BJ, Keele B, Choyke PL, Turkbey B. Ferumoxetyl as an intraprostatic MR contrast agent for lymph node mapping of the prostate: a feasibility study in non-human primates. *Acta Radiol* 2016; **57**: 1396-1401 [PMID: 26013022 DOI: 10.1177/0284185115586023]
 - 44 **Saokar A**, Braschi M, Harisinghani M. Lymphotropic nanoparticle enhanced MR imaging (LNMRI) for lymph node imaging. *Abdom Imaging* 2006; **31**: 660-667 [PMID: 16680506 DOI: 10.1007/s00261-006-9006-2]
 - 45 **Roy C**, Bierry G, Matau A, Bazille G, Pasquali R. Value of diffusion-weighted imaging to detect small malignant pelvic lymph nodes at 3 T. *Eur Radiol* 2010; **20**: 1803-1811 [PMID: 20182732 DOI: 10.1007/s00330-010-1736-4]
 - 46 **Eiber M**, Beer AJ, Holzapfel K, Tauber R, Ganter C, Weirich G, Krause BJ, Rummeny EJ, Gaa J. Preliminary results for characterization of pelvic lymph nodes in patients with prostate cancer by diffusion-weighted MR-imaging. *Invest Radiol* 2010; **45**: 15-23 [PMID: 19996762 DOI: 10.1097/RLI.0b013e3181bbdc2f]
 - 47 **Akduman EI**, Momtahan AJ, Balci NC, Mahajann N, Havlioglu N, Wolverson MK. Comparison between malignant and benign abdominal lymph nodes on diffusion-weighted imaging. *Acad Radiol* 2008; **15**: 641-646 [PMID: 18423322 DOI: 10.1016/j.acra.2007.12.023]
 - 48 **Budiharto T**, Joniau S, Lerut E, Van den Bergh L, Mottaghy F, Deroose CM, Oyen R, Ameye F, Bogaerts K, Haustermans K, Van Poppel H. Prospective evaluation of 11C-choline positron emission tomography/computed tomography and diffusion-weighted magnetic resonance imaging for the nodal staging of prostate cancer with a high risk of lymph node metastases. *Eur Urol* 2011; **60**: 125-130 [PMID: 21292388 DOI: 10.1016/j.eururo.2011.01.015]
 - 49 **Sumi M**, Van Cauteren M, Nakamura T. MR microimaging of benign and malignant nodes in the neck. *AJR Am J Roentgenol* 2006; **186**: 749-757 [PMID: 16498102 DOI: 10.2214/AJR.04.1832]
 - 50 **Choi EK**, Kim JK, Choi HJ, Park SH, Park BW, Kim N, Kim JS, Im KC, Cho G, Cho KS. Node-by-node correlation between MR and PET/CT in patients with uterine cervical cancer: diffusion-weighted imaging vs size-based criteria on T2WI. *Eur Radiol* 2009; **19**: 2024-2032 [PMID: 19277675 DOI: 10.1007/s00330-009-1350-5]
 - 51 **Thoeny HC**, Froehlich JM, Triantafyllou M, Huesler J, Bains LJ, Vermathen P, Fleischmann A, Studer UE. Metastases in normal-sized pelvic lymph nodes: detection with diffusion-weighted MR imaging. *Radiology* 2014; **273**: 125-135 [PMID: 24893049 DOI: 10.1148/radiol.14132921]
 - 52 **von Below C**, Daouacher G, Wassberg C, Grzegorek R, Gestblom C, Sörensen J, Ahlström H, Waldén M. Validation of 3 T MRI including diffusion-weighted imaging for nodal staging of newly diagnosed intermediate- and high-risk prostate cancer. *Clin Radiol* 2016; **71**: 328-334 [PMID: 26774372 DOI: 10.1016/j.crad.2015.12.001]
 - 53 **Giannarini G**, Petralia G, Thoeny HC. Potential and limitations of diffusion-weighted magnetic resonance imaging in kidney, prostate, and bladder cancer including pelvic lymph node staging: a critical analysis of the literature. *Eur Urol* 2012; **61**: 326-340 [PMID: 22000497 DOI: 10.1016/j.eururo.2011.09.019]
 - 54 **Heck MM**, Souvatzoglou M, Retz M, Nawroth R, Kübler H, Maurer T, Thalgott M, Gramer BM, Weirich G, Rondak IC, Rummeny EJ, Schwaiger M, Gschwend JE, Krause B, Eiber M. Prospective comparison of computed tomography, diffusion-weighted magnetic resonance imaging and [11C]choline positron emission tomography/computed tomography for preoperative lymph node staging in prostate cancer patients. *Eur J Nucl Med Mol Imaging* 2014; **41**: 694-701 [PMID: 24297503 DOI: 10.1007/s00259-013-2634-1]
 - 55 **Fortuin A**, Rooij Md, Zamecnik P, Haberkorn U, Barentsz J. Molecular and functional imaging for detection of lymph node metastases in prostate cancer. *Int J Mol Sci* 2013; **14**: 13842-13875 [PMID: 23823804 DOI: 10.3390/ijms140713842]
 - 56 **Ghanem N**, Uhl M, Brink I, Schäfer O, Kelly T, Moser E, Langer M. Diagnostic value of MRI in comparison to scintigraphy, PET, MS-CT and PET/CT for the detection of metastases of bone. *Eur J Radiol*

- 2005; **55**: 41-55 [PMID: 15950100 DOI: 10.1016/j.ejrad.2005.01.016]
- 57 **Shreve PD**, Grossman HB, Gross MD, Wahl RL. Metastatic prostate cancer: initial findings of PET with 2-deoxy-2-[F-18]fluoro-D-glucose. *Radiology* 1996; **199**: 751-756 [PMID: 8638000 DOI: 10.1148/radiology.199.3.8638000]
 - 58 **Tateishi U**, Morita S, Taguri M, Shizukuishi K, Minamimoto R, Kawaguchi M, Murano T, Terauchi T, Inoue T, Kim EE. A meta-analysis of (18)F-Fluoride positron emission tomography for assessment of metastatic bone tumor. *Ann Nucl Med* 2010; **24**: 523-531 [PMID: 20559896 DOI: 10.1007/s12149-010-0393-7]
 - 59 **Ackerstaff E**, Glunde K, Bhujwalla ZM. Choline phospholipid metabolism: a target in cancer cells? *J Cell Biochem* 2003; **90**: 525-533 [PMID: 14523987 DOI: 10.1002/jcb.10659]
 - 60 **Evangelista L**, Guttilla A, Zattoni F, Muzzio PC, Zattoni F. Utility of choline positron emission tomography/computed tomography for lymph node involvement identification in intermediate- to high-risk prostate cancer: a systematic literature review and meta-analysis. *Eur Urol* 2013; **63**: 1040-1048 [PMID: 23036576 DOI: 10.1016/j.eururo.2012.09.039]
 - 61 **Van den Bergh L**, Lerut E, Haustermans K, Deroose CM, Oyen R, Isebaert S, Budiharto T, Ameye F, Mottaghy FM, Bogaerts K, Van Poppel H, Joniau S. Final analysis of a prospective trial on functional imaging for nodal staging in patients with prostate cancer at high risk for lymph node involvement. *Urol Oncol* 2015; **33**: 109.e23-109.e31 [PMID: 25655681 DOI: 10.1016/j.urolonc.2014.11.008]
 - 62 **Tilki D**, Reich O, Graser A, Hacker M, Silchinger J, Becker AJ, Khoder W, Bartenstein P, Stief CG, Loidl W, Seitz M. 18F-Fluoroethylcholine PET/CT identifies lymph node metastasis in patients with prostate-specific antigen failure after radical prostatectomy but underestimates its extent. *Eur Urol* 2013; **63**: 792-796 [PMID: 22902037 DOI: 10.1016/j.eururo.2012.08.003]
 - 63 **Vali R**, Loidl W, Pirich C, Langesteger W, Beheshti M. Imaging of prostate cancer with PET/CT using (18)F-Fluorocholine. *Am J Nucl Med Mol Imaging* 2015; **5**: 96-108 [PMID: 25973332]
 - 64 **Wetter A**, Lipponer C, Nensa F, Beiderwellen K, Olbricht T, Rübhen H, Bockisch A, Schlosser T, Heusner TA, Lauenstein TC. Simultaneous 18F choline positron emission tomography/magnetic resonance imaging of the prostate: initial results. *Invest Radiol* 2013; **48**: 256-262 [PMID: 23462678 DOI: 10.1097/RLI.0b013e318282c654]
 - 65 **Pinaquy JB**, De Clermont-Galleran H, Pasticier G, Rigou G, Alberti N, Hindie E, Mokrane Y, Fernandez P. Comparative effectiveness of [(18)F]-fluorocholine PET-CT and pelvic MRI with diffusion-weighted imaging for staging in patients with high-risk prostate cancer. *Prostate* 2015; **75**: 323-331 [PMID: 25393215 DOI: 10.1002/pros.22921]
 - 66 **Rinnab L**, Simon J, Hautmann RE, Cronauer MV, Hohl K, Buck AK, Reske SN, Mottaghy FM. [(11)C]choline PET/CT in prostate cancer patients with biochemical recurrence after radical prostatectomy. *World J Urol* 2009; **27**: 619-625 [PMID: 19234708 DOI: 10.1007/s00345-009-0371-7]
 - 67 **Giovacchini G**, Picchio M, Coradeschi E, Bettinardi V, Gianolli L, Scattoni V, Cozzarini C, Di Muzio N, Rigatti P, Fazio F, Messa C. Predictive factors of [(11)C]choline PET/CT in patients with biochemical failure after radical prostatectomy. *Eur J Nucl Med Mol Imaging* 2010; **37**: 301-309 [PMID: 19756592 DOI: 10.1007/s00259-009-1253-3]
 - 68 **Våvere AL**, Kridel SJ, Wheeler FB, Lewis JS. 1-11C-acetate as a PET radiopharmaceutical for imaging fatty acid synthase expression in prostate cancer. *J Nucl Med* 2008; **49**: 327-334 [PMID: 18199615 DOI: 10.2967/jnumed.107.046672]
 - 69 **Haseebuddin M**, Dehdashti F, Siegel BA, Liu J, Roth EB, Nepple KG, Siegel CL, Fischer KC, Kibel AS, Andriole GL, Miller TR. 11C-acetate PET/CT before radical prostatectomy: nodal staging and treatment failure prediction. *J Nucl Med* 2013; **54**: 699-706 [PMID: 23471311 DOI: 10.2967/jnumed.112.111153]
 - 70 **Ghosh A**, Heston WD. Tumor target prostate specific membrane antigen (PSMA) and its regulation in prostate cancer. *J Cell Biochem* 2004; **91**: 528-539 [PMID: 14755683 DOI: 10.1002/jcb.10661]
 - 71 **Rosenthal SA**, Haseman MK, Polascik TJ. Utility of capromab pendetide (ProstaScint) imaging in the management of prostate cancer. *Tech Urol* 2001; **7**: 27-37 [PMID: 11272670]
 - 72 **Ponsky LE**, Cherullo EE, Starkey R, Nelson D, Neumann D, Zippe CD. Evaluation of preoperative ProstaScint scans in the prediction of nodal disease. *Prostate Cancer Prostatic Dis* 2002; **5**: 132-135 [PMID: 12497003 DOI: 10.1038/sj.pcan.4500570]
 - 73 **Hardie AD**, Rieter WJ, Bradshaw ML, Gordon LL, Young MA, Keane TE. Improved performance of SPECT-CT In-111 capromab pendetide by correlation with diffusion-weighted magnetic resonance imaging for identifying metastatic pelvic lymphadenopathy in prostate cancer. *World J Urol* 2013; **31**: 1327-1332 [PMID: 23595605 DOI: 10.1007/s00345-013-1079-2]
 - 74 **Troyer JK**, Beckett ML, Wright GL Jr. Location of prostate-specific membrane antigen in the LNCaP prostate carcinoma cell line. *Prostate* 1997; **30**: 232-242 [PMID: 9111600]
 - 75 **Osborne JR**, Akhtar NH, Vallabhajosula S, Anand A, Deh K, Tagawa ST. Prostate-specific membrane antigen-based imaging. *Urol Oncol* 2013; **31**: 144-154 [PMID: 22658884 DOI: 10.1016/j.urolonc.2012.04.016]
 - 76 **Rowe SP**, Gorin MA, Allaf ME, Pienta KJ, Tran PT, Pomper MG, Ross AE, Cho SY. PET imaging of prostate-specific membrane antigen in prostate cancer: current state of the art and future challenges. *Prostate Cancer Prostatic Dis* 2016; **19**: 223-230 [PMID: 27136743 DOI: 10.1038/pcan.2016.13]
 - 77 **Rowe SP**, Macura KJ, Ciarallo A, Mena E, Blackford A, Nadal R, Antonarakis ES, Eisenberger MA, Carducci MA, Ross AE, Kantoff PW, Holt DP, Dannals RF, Mease RC, Pomper MG, Cho SY. Comparison of Prostate-Specific Membrane Antigen-Based 18F-DCFC PET/CT to Conventional Imaging Modalities for Detection of Hormone-Naïve and Castration-Resistant Metastatic Prostate Cancer. *J Nucl Med* 2016; **57**: 46-53 [PMID: 26493203 DOI: 10.2967/jnumed.115.163782]
 - 78 **Eder M**, Eisenhut M, Babich J, Haberkorn U. PSMA as a target for radiolabelled small molecules. *Eur J Nucl Med Mol Imaging* 2013; **40**: 819-823 [PMID: 23463331 DOI: 10.1007/s00259-013-2374-2]
 - 79 **Maurer T**, Gschwend JE, Rauscher I, Souvatzoglou M, Haller B, Weirich G, Wester HJ, Heck M, Kübler H, Beer AJ, Schwaiger M, Eiber M. Diagnostic Efficacy of (68)Gallium-PSMA Positron Emission Tomography Compared to Conventional Imaging for Lymph Node Staging of 130 Consecutive Patients with Intermediate to High Risk Prostate Cancer. *J Urol* 2016; **195**: 1436-1443 [PMID: 26682756 DOI: 10.1016/j.juro.2015.12.025]
 - 80 **Budäus L**, Leyh-Bannurah SR, Salomon G, Michl U, Heinzer H, Huland H, Graefen M, Steuber T, Rosenbaum C. Initial Experience of (68)Ga-PSMA PET/CT Imaging in High-risk Prostate Cancer Patients Prior to Radical Prostatectomy. *Eur Urol* 2016; **69**: 393-396 [PMID: 26116958 DOI: 10.1016/j.eururo.2015.06.010]
 - 81 **Schuster DM**, Nanni C, Fanti S. Evaluation of Prostate Cancer with Radiolabeled Amino Acid Analogs. *J Nucl Med* 2016; **57**: 61S-66S [PMID: 27694174 DOI: 10.2967/jnumed.115.170209]
 - 82 **Odevole OA**, Tade FI, Nieh PT, Savir-Baruch B, Jani AB, Master VA, Rossi PJ, Halkar RK, Osunkoya AO, Akin-Akintayo O, Zhang C, Chen Z, Goodman MM, Schuster DM. Recurrent prostate cancer detection with anti-3-[(18)F]FACBC PET/CT: comparison with CT. *Eur J Nucl Med Mol Imaging* 2016; **43**: 1773-1783 [PMID: 27091135 DOI: 10.1007/s00259-016-3383-8]
 - 83 **Suzuki H**, Inoue Y, Fujimoto H, Yonese J, Tanabe K, Fukasawa S, Inoue T, Saito S, Ueno M, Otaka A. Diagnostic performance and safety of NMK36 (trans-1-amino-3-[18F] fluorocyclobutanecarboxylic acid)-PET/CT in primary prostate cancer: multicenter Phase IIb clinical trial. *Jpn J Clin Oncol* 2017; **47**: 283 [PMID: 27920097 DOI: 10.1093/jco/hyw177]
 - 84 **Wibmer AG**, Burger IA, Sala E, Hricak H, Weber WA, Vargas HA. Molecular Imaging of Prostate Cancer. *Radiographics* 2016; **36**: 142-159 [PMID: 26587888 DOI: 10.1148/rg.2016150059]
 - 85 **Mansi R**, Fleischmann A, Mäcke HR, Reubi JC. Targeting GRPR in urological cancers--from basic research to clinical application. *Nat Rev Urol* 2013; **10**: 235-244 [PMID: 23507930 DOI: 10.1038/nrurol.2013.42]
 - 86 **Dijkgraaf I**, Franssen GM, McBride WJ, D'Souza CA, Laverman P, Smith CJ, Goldenberg DM, Oyen WJ, Boerman OC. PET of tumors expressing gastrin-releasing peptide receptor with an 18F-labeled bombesin analog. *J Nucl Med* 2012; **53**: 947-952 [PMID: 22570329]

DOI: 10.2967/jnumed.111.100891]

- 87 **Zhang H**, Abiraj K, Thorek DL, Waser B, Smith-Jones PM, Honer M, Reubi JC, Maecke HR. Evolution of bombesin conjugates for targeted PET imaging of tumors. *PLoS One* 2012; **7**: e44046 [PMID: 23024746 DOI: 10.1371/journal.pone.0044046]
- 88 **Kähkönen E**, Jambor I, Kemppainen J, Lehtiö K, Grönroos TJ, Kuisma A, Luoto P, Sipilä HJ, Tolvanen T, Alanen K, Silén J, Kallajoki M, Roivainen A, Schäfer N, Schibli R, Dragic M, Johayem A, Valencia R, Borkowski S, Minn H. In vivo imaging of prostate cancer using [68Ga]-labeled bombesin analog BAY86-7548. *Clin Cancer Res* 2013; **19**: 5434-5443 [PMID: 23935037 DOI: 10.1158/1078-0432.CCR-12-3490]
- 89 **Larson SM**, Morris M, Gunther I, Beattie B, Humm JL, Akhurst TA, Finn RD, Erdi Y, Pentlow K, Dyke J, Squire O, Bornmann W, McCarthy T, Welch M, Scher H. Tumor localization of 16beta-18F-fluoro-5alpha-dihydrotestosterone vs 18F-FDG in patients with progressive, metastatic prostate cancer. *J Nucl Med* 2004; **45**: 366-373 [PMID: 15001675]
- 90 **Rahbar K**, Ahmadzadehfard H, Kratochwil C, Haberkorn U, Schäfers M, Essler M, Baum RP, Kulkarni HR, Schmidt M, Drzezga A, Bartenstein P, Pfestroff A, Luster M, Lützen U, Marx M, Prasad V, Brenner W, Heinzel A, Mottaghy FM, Ruf J, Meyer PT, Heuschkel M, Eveslage M, Bögemann M, Fendler WP, Krause BJ. German Multicenter Study Investigating 177Lu-PSMA-617 Radioligand Therapy in Advanced Prostate Cancer Patients. *J Nucl Med* 2017; **58**: 85-90 [PMID: 27765862 DOI: 10.2967/jnumed.116.183194]
- 91 **Chatalic KL**, Konijnenberg M, Nonnekens J, de Blois E, Hoebe S, de Ridder C, Brunel L, Fehrentz JA, Martinez J, van Gent DC, Nock BA, Maina T, van Weerden WM, de Jong M. In Vivo Stabilization of a Gastrin-Releasing Peptide Receptor Antagonist Enhances PET Imaging and Radionuclide Therapy of Prostate Cancer in Preclinical Studies. *Theranostics* 2016; **6**: 104-117 [PMID: 26722377 DOI: 10.7150/thno.13580]

P- Reviewer: Arcangeli S, Huang SP S- Editor: Kong JX

L- Editor: A E- Editor: Lu YJ



MR neurography in intraosseous median nerve entrapment

Ankita Aggarwal, Manisha Jana, Vijay Kumar, Deep Narayan Srivastava, Kanwaljeet Garg

Ankita Aggarwal, Manisha Jana, Deep Narayan Srivastava,
Department of Radiodiagnosis, All India Institute of Medical
Sciences, New Delhi 110029, India

Vijay Kumar, Department of Orthopedics, All India Institute of
Medical Sciences, New Delhi 110029, India

Kanwaljeet Garg, Department of Neurosurgery, All India Institute
of Medical Sciences, New Delhi 110029, India

Author contributions: Aggarwal A and Srivastava DN designed
the research; Aggarwal A, Jana M and Srivastava DN performed
the research; Kumar V and Srivastava DN provided administrative
support; Aggarwal A and Garg K prepared the manuscript.

Institutional review board statement: Ethics clearance for this
study was taken from the Ethics Committee of All India Institute
of Medical Sciences, New Delhi, India.

Informed consent statement: All study participants, or their
legal guardian, provided informed written consent prior to study
enrollment.

Conflict-of-interest statement: The authors do not have any
conflict of interest.

Open-Access: This article is an open-access article which was
selected by an in-house editor and fully peer-reviewed by external
reviewers. It is distributed in accordance with the Creative
Commons Attribution Non Commercial (CC BY-NC 4.0) license,
which permits others to distribute, remix, adapt, build upon this
work non-commercially, and license their derivative works on
different terms, provided the original work is properly cited and
the use is non-commercial. See: [http://creativecommons.org/
licenses/by-nc/4.0/](http://creativecommons.org/licenses/by-nc/4.0/)

Manuscript source: Unsolicited manuscript

Correspondence to: Deep Narayan Srivastava, Professor,
Department of Radiodiagnosis, All India Institute of Medical
Sciences, Room No 69, Ground Floor, Near South Extension, New
Delhi 110029, India. drdeepsrivastava@rediffmail.com
Telephone: +91-98-99245764

Received: February 13, 2017

Peer-review started: February 14, 2017

First decision: April 19, 2017

Revised: June 24, 2017

Accepted: July 7, 2017

Article in press: July 10, 2017

Published online: October 28, 2017

Abstract

Intraosseous entrapment of the median nerve is an uncommon complication of elbow dislocation and fractures. The condition is seen to occur in adolescent age group with a remote history of trauma. We report two rare cases of type 2 intraosseous median nerve entrapment. Though the diagnosis of median neuropathy is made with clinical tests and neurophysiological studies, however exact site of entrapment and presurgical mapping of nerve is done accurately with MR neurography. Imaging thus plays a pivotal role in management of this condition.

Key words: Intraosseous; MR neurography; Median nerve

© **The Author(s) 2017.** Published by Baishideng Publishing Group Inc. All rights reserved.

Core tip: Intraosseous entrapment of median nerve at the level of elbow joint is rare but serious complication of closed reduction of posterior elbow dislocation. We report two cases of type 2 intraosseous median nerve entrapment (wherein the median nerve gets entrapped in fractured medial epicondyle) and discuss the role of MR neurography. MR delineates the posterior course of median nerve with altered signal intensity, thickening and loss of fascicular pattern. In addition, secondary denervation changes in muscles supplied by median nerve is indirect evidence of nerve pathology. Management of such cases would differ depending on the time of diagnosis.

Aggarwal A, Jana M, Kumar V, Srivastava DN, Garg K. MR neurography in intraosseous median nerve entrapment. *World J Radiol* 2017; 9(10): 400-404 Available from: URL: <http://www.wjgnet.com/1949-8470/full/v9/i10/400.htm> DOI: <http://dx.doi.org/10.4329/wjr.v9.i10.400>

INTRODUCTION

Intraosseous entrapment of the median nerve at the level of elbow joint is a rare but serious complication of closed reduction of posterior elbow dislocation^[1]. The diagnosis often gets delayed due to subtle symptoms which leads to grave damage to nerve. Imaging plays a major role preoperatively determining the site of entrapment. We report two cases of type 2 intraosseous median nerve entrapment and discuss their MR neurography findings.

CASE REPORT

Case 1

An 18-year-old male suffered fracture of medial epicondyle of left humerus along with elbow dislocation after he fell from rooftop about two years back. He was managed with closed reduction of elbow, followed by cast immobilization and physiotherapy. After removal of cast, he progressively started having symptoms of median neuropathy in the form of numbness and paresthesia along the median nerve distribution in forearm and hand with inability to form a fist and weak hand movements (Figure 1A). Gradually there was thinning of the forearm muscles. On clinical examination, there was atrophy of forearm muscles (of the anterior compartment) and of thenar muscles (Figure 1B). He had weakness of small hand muscles as well in the median nerve distribution. Clinical impression was median nerve palsy. Ulnar and radial nerve function was normal on clinical examination. Nerve conduction studies revealed median nerve neuropathy at the level of elbow.

High resolution USG was done, which revealed grossly thickened and hypoechoic median nerve in the region of distal arm with an abrupt cut off at the level of elbow (Figure 1C). The nerve fibers were seen coursing posteriorly and distal median nerve could not be traced. Limited MR neurography of the elbow was done for further confirmation of diagnosis. It revealed the median nerve to be swollen and having abnormal signal intensity (hyperintense on T2) in the distal arm (Figures 1D and 2). It was seen to have an altered course as the median nerve was seen to course posteriorly through the fractured medial epicondyle and subsequently was entrapped between the olecranon of ulna and olecranon fossa of humerus. Thereafter, the nerve was not visualized for some distance after which it reappeared with decreased calibre in its normal course in forearm with normal signal intensity. The muscles of the anterior compartment, supplied by median nerve, showed hyperintense signal on T1w and T2w sequence suggesting chronic denervation with fatty infiltration. These features were suggestive of type 2 median nerve entrapment.

Case 2

A 20-year-old patient suffered supracondylar fracture

of humerus 1 year back. The patient was managed conservatively by immobilization. Patient noticed weakness of hand grip and hand movements and decreased sensations of lateral half of forearm and lateral half of hand after immobilization was removed.

On examination, there was atrophy of anterior compartment muscles of right forearm and thenar eminence of hand. There was weakness of lateral half of hand fingers. All tests for median nerve were also positive in this case. NCV confirmed median neuropathy with likely site to be at elbow.

MR neurography revealed markedly thickened median nerve and was T2 hyperintense in the region of arm proximal to fracture site and traversed through the fractured fragment of humerus and coursed posteriorly (Figure 3). The nerve was entrapped between the olecranon and olecranon fossa and was seen coursing anteriorly back to its normal course with normal intensity and mildly decreased thickness. There was secondary atrophy of flexor digitorum profundus (lateral belly), flexor digitorum superficialis, flexor pollicis longus, pronator teres and of thenar muscles with fatty change s/o chronic insult.

DISCUSSION

Intraosseous median nerve entrapment is relatively rare complication of elbow dislocation and fractures of lower end humeral, frequency of which varies from 1%-12.5%^[2]. It was first described by Gurdjian and Smathers^[3] in 1945. The condition is seen to occur in a relative younger age group (adolescents) with a slight male predominance^[4].

Four types of intraosseous median nerve entrapment are described^[5]. The first three types have been described by Hallet while type IV was described by al-Danielsson *et al*^[6], Hallett *et al*^[7], Steiger *et al*^[8], Ozkoç *et al*^[9], Noonan *et al*^[10]. In type 1 intraosseous median nerve entrapment, the medial collateral ligament is torn and the median nerve slips posteriorly adhering to the posterior surface of humerus and gets entrapped between trochlea and olecranon process. In type 2, median nerve is entrapped in the fractured medial epicondyle. Type 3 is when nerve gets entrapped between the distal end of humerus and ulna in the ulno-humeral joint without any fracture. Type 4 is combination of type 1 and 2^[11]. Both our cases were of type 2 variety; the median nerve was entrapped in the fractured medial epicondyle. Both the patients were young adolescent males having a remote history of trauma and were managed non-operatively.

Intraosseous entrapment of the median nerve should be suspected when there is failure of concentric reduction, presence of joint widening post reduction or the clinical symptoms persist or if there occurs cortical depression with surrounding sclerotic changes in the distal metaphysis of humerus (Matter sign)^[1,12,13].

Imaging played a pivotal role in preoperative diagnosis of this condition. Altered signal intensity and thickening of the median nerve with loss of fascicular

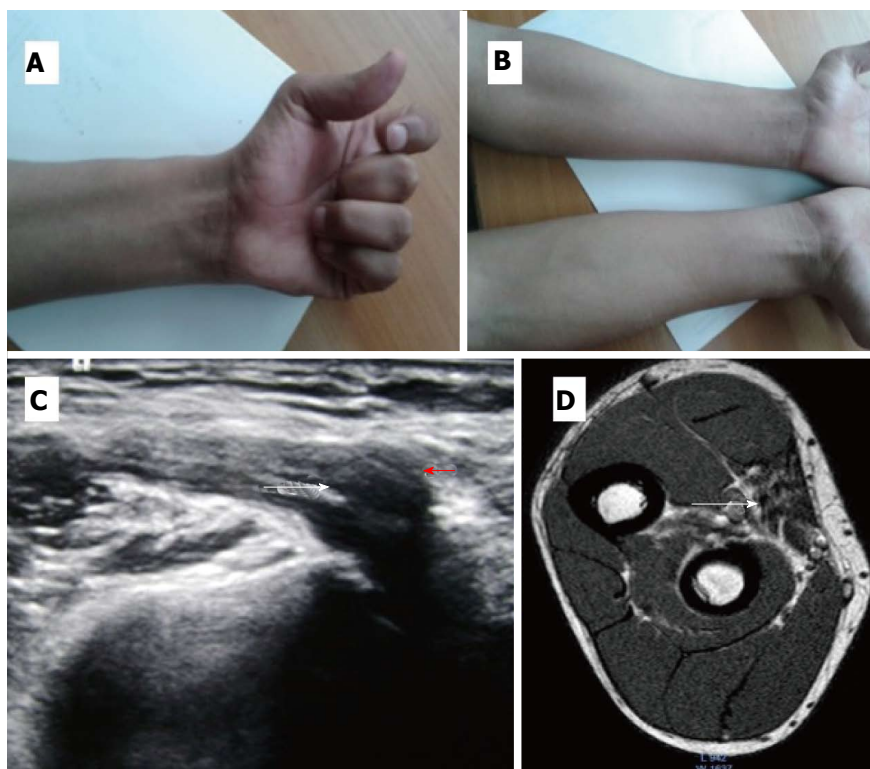


Figure 1 Images of first patient with intraosseous median nerve entrapment. A: Clinical Photograph showing inability to close fist completely with partial flexion of the index finger; B: Atrophy of anterior compartment muscles of left forearm; C: Sonogram shows thickened and hypoechoic median nerve (arrow), coursing posteriorly through the fractured bone; D: SE T1 W MR axial image shows atrophy of anterior compartment muscles of forearm with fatty infiltration s/o chronic denervation changes (arrow).

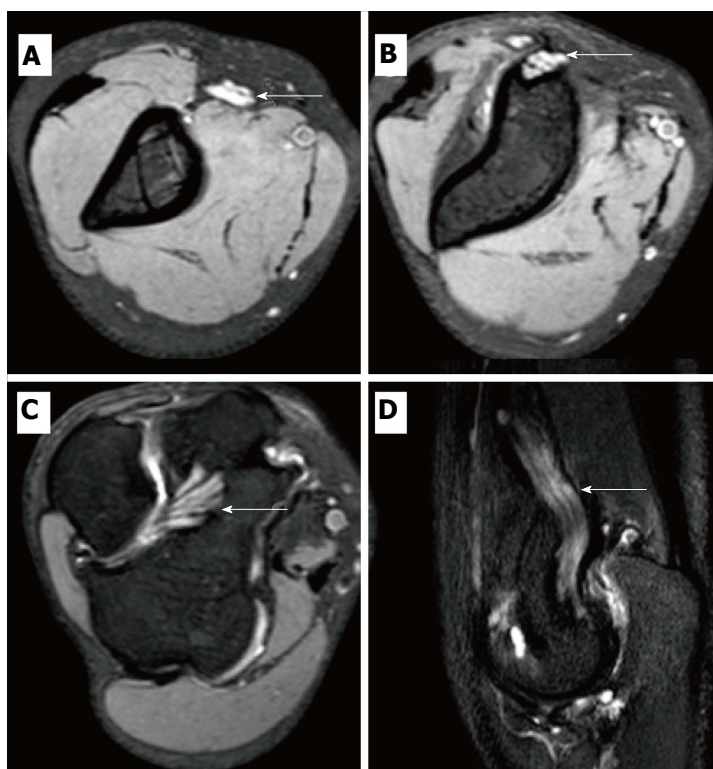


Figure 2 Images of second patient with intraosseous median nerve entrapment. A-C: 3D GRE T2W images showing markedly thickened and hyperintense entrapped median nerve (arrow), coursing posteriorly through the fractured medial epicondyle; D: STIR Coronal image showing markedly thickened and hyperintense median nerve (arrow).



Figure 3 Images of third patient with intraosseous median nerve entrapment. A-D: SE T2W FS axial MR image shows markedly thickened and hyperintense nerve coursing through the fractured medial epicondyle; E: STIR coronal MR image shows entrapped median nerve coursing posteriorly; F: DWIBS coronal reformat highlights the abnormal median nerve.

pattern pointed towards the abnormality of the nerve. MRI clearly delineated the posterior course of the median nerve. In addition, secondary denervation changes in muscles supplied by median nerve were also seen.

Management of such cases would differ depending on the time of diagnosis. Usually the symptoms of median nerve entrapment are mild hence detection of this neuropathy is delayed. If detected early, relocation of the nerve from posterior to anterior compartment is done. If detected later then excision of the diseased segment with either nerve repair (end to end) or nerve grafting is done (with sural nerve graft). Early diagnosis and treatment ensures better prognosis. Both the cases we encountered were of chronic insult due to delayed diagnosis. The first case was lost to follow up and the second underwent nerve grafting.

MR neurography plays a vital role in the diagnosis of intraosseous entrapment of median nerve following medial epicondyle fracture by clearly demonstrating its altered course in the posterior compartment leading to its entrapment. In addition, presurgical mapping of the nerve can be accurately done with MRI and it also helps in deciding the correct management of the patient.

COMMENTS

Case characteristics

Numbness and paresthesia along the median nerve distribution in forearm and hand with inability to form a fist, and weak hand movements with gradual thinning of the forearm muscles.

Clinical diagnosis

Weakness and atrophy of muscles of median nerve distribution.

Differential diagnosis

Traumatic/entrapment/infectious/inflammatory neuropathy.

Laboratory diagnosis

Nerve conduction study will reveal reduced velocity across the median nerve.

Imaging diagnosis

MR delineates the posterior course of median nerve with altered signal intensity, thickening and loss of fascicular pattern.

Pathological diagnosis

Neuropathy at the fracture level.

Treatment

If detected early, relocation of the nerve from posterior to anterior compartment is done and if detected later then excision of the diseased segment with either nerve repair (end to end) or nerve grafting is done (with sural nerve graft).

Related reports

Four types of intraosseous median nerve entrapment are described. Intraosseous entrapment of the median nerve should be suspected when there is failure of concentric reduction, presence of joint widening post reduction or the clinical symptoms persist or if there occurs cortical depression with surrounding sclerotic changes in the distal metaphysis of humerus (matev sign). MRI clearly delineated the posterior course of the median nerve. In addition, secondary denervation changes in muscles supplied by median nerve were also seen.

Term explanation

Intraosseous entrapment of the median nerve is a rare complication of closed reduction of posterior elbow dislocation.

Experiences and lessons

MR neurography plays a vital role in the diagnosis of intraosseous entrapment of median nerve following medial epicondyle fracture by clearly demonstrating its altered course in the posterior compartment leading to its entrapment.

Peer-review

The case studies are described clearly and it is easy for the reader to follow.

REFERENCES

- 1 Gurdjian ES, Smathers HM. Peripheral nerve injury in fractures

- and dislocations of long bones. *J Neurosurg* 1945; **2**: 202-219 [DOI: 10.3171/jns.1945.2.3.0202]
- 2 **Landin LA**, Danielsson LG. Elbow fractures in children. An epidemiological analysis of 589 cases. *Acta Orthop Scand* 1986; **57**: 309-312 [PMID: 3788491 DOI: 10.3109/17453678608994398]
- 3 **Fourrier P**, Levai JP, Collin JP. [Median nerve entrapment in elbow dislocation]. *Rev Chir Orthop Reparatrice Appar Mot* 1977; **63**: 13-16 [PMID: 141697]
- 4 **al-Qattan MM**, Zuker RM, Weinberg MJ. Type 4 median nerve entrapment after elbow dislocation. *J Hand Surg Br* 1994; **19**: 613-615 [PMID: 7822921 DOI: 10.1016/0266-7681(94)90127-9]
- 5 **Ayala H**, De Pablos J, Gonzalez J, Martinez A. Entrapment of the median nerve after posterior dislocation of the elbow. *Microsurgery* 1983; **4**: 215-220 [DOI: 10.1002/micr.1920040403]
- 6 **Danielsson LG**. Median nerve entrapment in elbow dislocation. A case report. *Acta Orthop Scand* 1986; **57**: 450-452 [PMID: 3811894 DOI: 10.3109/17453678609014770]
- 7 **Hallett J**. Entrapment of the median nerve after dislocation of the elbow. A case report. *J Bone Joint Surg Br* 1981; **63-B**: 408-412 [PMID: 7263756]
- 8 **Steiger RN**, Larrick RB, Meyer TL. Median-nerve entrapment following elbow dislocation in children. A report of two cases. *J Bone Joint Surg Am* 1969; **51**: 381-385 [PMID: 5767328 DOI: 10.2106/0004623-196951020-00017]
- 9 **Ozkoç G**, Akpınar S, Hersekli MA, Ozalay M, Uysal M, Tandoğan NR. Type 4 median nerve entrapment in a child after elbow dislocation. *Arch Orthop Trauma Surg* 2003; **123**: 555-557 [PMID: 12920535 DOI: 10.1007/s00402-003-0565-1]
- 10 **Noonan KJ**, Blair WF. Chronic median-nerve entrapment after posterior fracture-dislocation of the elbow. A case report. *J Bone Joint Surg Am* 1995; **77**: 1572-1575 [PMID: 7593068 DOI: 10.2106/00004623-199510000-00014]
- 11 **Webb S**, Lourie J. Median nerve entrapment in an unreduced fracture-dislocation of the elbow: case report. *P N G Med J* 1986; **29**: 185-187 [PMID: 3465102]
- 12 **Matev I**. A radiological sign of entrapment of the median nerve in the elbow joint after posterior dislocation. A report of two cases. *J Bone Joint Surg Br* 1976; **58**: 353-355 [PMID: 956256]
- 13 **Simon D**, Masquijo JJ, Duncan MJ, Kontio K. Intra-articular median nerve incarceration after spontaneous reduction of a pediatric elbow dislocation: case report and review of the literature. *J Pediatr Orthop* 2010; **30**: 125-129 [PMID: 20179558 DOI: 10.1097/BPO.0b013e3181cf3bfd]

P- Reviewer: Demonacos C **S- Editor:** Ji FF **L- Editor:** A
E- Editor: Lu YJ





Published by **Baishideng Publishing Group Inc**
7901 Stoneridge Drive, Suite 501, Pleasanton, CA 94588, USA
Telephone: +1-925-223-8242
Fax: +1-925-223-8243
E-mail: bpgoffice@wjgnet.com
Help Desk: <http://www.f6publishing.com/helpdesk>
<http://www.wjgnet.com>



World Journal of *Radiology*

World J Radiol 2017 November 28; 9(11): 405-415





Editorial Board

2014-2017

The *World Journal of Radiology* Editorial Board consists of 365 members, representing a team of worldwide experts in radiology. They are from 36 countries, including Afghanistan (1), Argentina (2), Australia (5), Austria (7), Belgium (2), Brazil (8), Canada (6), Chile (1), China (43), Croatia (1), Denmark (4), Egypt (6), France (5), Germany (22), Greece (10), India (12), Iran (6), Ireland (2), Israel (3), Italy (47), Japan (13), Netherlands (1), New Zealand (1), Pakistan (1), Poland (2), Portugal (1), Serbia (1), Singapore (3), Slovakia (1), South Korea (18), Spain (4), Sweden (2), Switzerland (4), Thailand (1), Turkey (26), United Kingdom (11), and United States (82).

EDITORS-IN-CHIEF

Kai U Juergens, *Bremen*
Edwin JR van Beek, *Edinburgh*
Thomas J Vogl, *Frankfurt*

GUEST EDITORIAL BOARD MEMBERS

Wing P Chan, *Taipei*
Chung-Huei Hsu, *Taipei*
Chin-Chang Huang, *Taipei*
Tsong-Long Hwang, *Taoyuan*
Jung-Lung Hsu, *Taipei*
Chia-Hung Kao, *Taichung*
Yu-Ting Kuo, *Tainan*
Hon-Man Liu, *Taipei*
Hui-Lung Liang, *Kaohsiung*
Chun Chung Lui, *Kaohsiung*
Sen-Wen Teng, *Taipei*
Yung-Liang (William) Wan, *Taoyuan*

MEMBERS OF THE EDITORIAL BOARD



Afghanistan

Takao Hiraki, *Okayama*



Argentina

Patricia Carrascosa, *Vicente Lopez*
Maria C Ziadi, *Rosario*



Australia

Lourens Bester, *Sydney*
Gemma A Figtree, *Sydney*



Austria

Herwig R Cerwenka, *Graz*
Gudrun M Feuchtnner, *Innsbruck*
Benjamin Henninger, *Innsbruck*
Rupert Lanzenberger, *Vienna*
Shu-Ren Li, *Vienna*
Veronika Schopf, *Vienna*
Tobias De Zordo, *Innsbruck*



Belgium

Steve Majerus, *Liege*
Kathelijne Peremans, *Merelbeke*



Brazil

Clerio F Azevedo, *Rio de Janeiro*
Patrícia P Alfredo, *São Paulo*
Eduardo FC Fleury, *São Paulo*
Edward Araujo Júnior, *São Paulo*
Wellington P Martins, *Ribeirao Preto*
Ricardo A Mesquita, *Belo Horizonte*
Vera MC Salemi, *São Paulo*
Claudia Szobot, *Porto Alegre*
Lilian YI Yamaga, *São Paulo*



Canada

Marie Arsalidou, *Toronto*
Otman A Basir, *Waterloo*

Tarik Zine Belhocine, *Toronto*
James Chow, *Toronto*
Tae K Kim, *Toronto*
Anastasia Oikonomou, *Toronto*



China

Hong-Wei Chen, *Wuxi*
Feng Chen, *Hangzhou*
Jian-Ping Chu, *Guangzhou*
Guo-Guang Fan, *Shenyang*
Bu-Lang Gao, *Shijiazhuang*
Qi-Yong Gong, *Chengdu*
Ying Han, *Beijing*
Xian-Li Lv, *Beijing*
Yi-Zhuo Li, *Guangzhou*
Xiang-Xi Meng, *Harbin*
Yun Peng, *Beijing*
Jun Shen, *Guangzhou*
Ze-Zhou Song, *Hangzhou*
Wai Kwong Tang, *Hong Kong*
Gang-Hua Tang, *Guangzhou*
Jie Tian, *Beijing*
Lu-Hua Wang, *Beijing*
Xiao-bing Wang, *Xi'an*
Yi-Gen Wu, *Nanjing*
Kai Wu, *Guangzhou*
Hui-Xiong Xu, *Shanghai*
Zuo-Zhang Yang, *Kunming*
Xiao-Dan Ye, *Shanghai*
David T Yew, *Hong Kong*
Ting-He Yu, *Chongqing*
Zheng Yuan, *Shanghai*
Min-Ming Zhang, *Hangzhou*
Yudong Zhang, *Nanjing*
Dong Zhang, *Chongqing*
Wen-Bin Zeng, *Changsha*

Yue-Qi Zhu, *Shanghai*



Croatia

Goran Kusec, *Osijek*



Denmark

Poul E Andersen, *Odense*

Lars J Petersen, *Aalborg*

Thomas Z Ramsøy, *Frederiksberg*

Morten Ziebell, *Copenhagen*



Egypt

Mohamed F Bazeed, *Mansoura*

Mohamed Abou El-Ghar, *Mansoura*

Reem HA Mohamed, *Cairo*

Mohamed R Nouh, *Alexandria*

Ahmed AKA Razek, *Mansoura*

Ashraf A Zytoon, *Shebin El-Koom*



France

Sabine F Bensamoun, *Compiègne*

Romarc Loffroy, *Dijon*

Stephanie Nougaret, *Montpellier*

Hassane Oudadesse, *Rennes*

Vincent Vinh-Hung, *Fort-de-France*



Germany

Henryk Barthel, *Leipzig*

Peter Bannas, *Hamburg*

Martin Beeres, *Frankfurt*

Ilja F Ciernik, *Dessau*

A Dimitrakopoulou-Strauss, *Heidelberg*

Peter A Fasching, *Erlangen*

Andreas G Schreyer, *Regensburg*

Philipp Heusch, *Duesseldorf*

Sonja M Kirchhoff, *Munich*

Sebastian Ley, *Munich*

Adel Maataoui, *Frankfurt am Main*

Stephan M Meckel, *Freiburg*

Hans W Muller, *Duesseldorf*

Kay Raum, *Berlin*

Dirk Rades, *Luebeck*

Marc-Ulrich Regier, *Hamburg*

Alexey Surov, *Halle*

Martin Walter, *Magdeburg*

Axel Wetter, *Essen*

Christoph Zilkens, *Düsseldorf*



Greece

Panagiotis Antoniou, *Thessaloniki*

Nikos Efthimiou, *Athens*

Dimitris Karnabatidis, *Patras*

George Latsios, *Athens*

Stylianios Megremis, *Iraklion*

Alexander D Rapidis, *Athens*

Kiki Theodorou, *Larissa*

Ioannis A Tsalafoutas, *Athens*

Evanthia E Tripoliti, *Ioannina*

Athina C Tsili, *Ioannina*



India

Ritesh Agarwal, *Chandigarh*

Chandan J Das, *New Delhi*

Prathamesh V Joshi, *Mumbai*

Naveen Kalra, *Chandigarh*

Chandrasekharan Kesavadas, *Trivandrum*

Jyoti Kumar, *New Delhi*

Atin Kumar, *New Delhi*

Kaushala P Mishra, *Allahabad*

Daya N Sharma, *New Delhi*

Binit Sureka, *New Delhi*

Sanjay Sharma, *New Delhi*

Raja R Yadav, *Allahabad*



Iran

Majid Assadi, *Bushehr*

SeyedReza Najafizadeh, *Tehran*

Mohammad Ali Oghabian, *Tehran*

Amir Reza Radmard, *Tehran*

Ramin Sadeghi, *Mashhad*

Hadi Rokni Yazdi, *Tehran*



Ireland

Tadhg Gleeson, *Wexford*

Frederik JAI Vernimmen, *Cork*



Israel

Dafna Ben Bashat, *Tel Aviv*

Amit Gefen, *Tel Aviv*

Tamar Sella, *Jerusalem*



Italy

Adriano Alippi, *Rome*

Dante Amelio, *Trento*

Michele Anzidei, *Rome*

Filippo F Angileri, *Messinas*

Stefano Arcangeli, *Rome*

Roberto Azzoni, *San Donato milanese*

Tommaso V Bartolotta, *Palermo*

Tommaso Bartalena, *Imola*

Livia Bernardin, *San Bonifacio*

Federico Boschi, *Verona*

Sergio Casciaro, *Lecce*

Emanuele Casciani, *Rome*

Musa M Can, *Napoli*

Alberto Cuocolo, *Napoli*

Michele Ferrara, *Coppito*

Mauro Feola, *Fossano*

Giampiero Francica, *Castel Volturno*

Luigi De Gennaro, *Rome*

Giulio Giovannetti, *Pisa*

Francesca Iacobellis, *Napoli*

Formato Invernizzi, *Monza Brianza*

Francesco Lassandro, *Naples*

Lorenzo Livi, *Florence*

Pier P Mainenti, *Napoli*

Laura Marzetti, *Chieti*

Giuseppe Malinverni, *Crescentino*

Enrica Milanese, *Turin*

Giovanni Morana, *Treviso*

Lorenzo Monti, *Milan*

Silvia D Morbelli, *Genoa*

Barbara Palumbo, *Perugia*

Cecilia Parazzini, *Milan*

Stefano Pergolizzi, *Messina*

Antonio Pinto, *Naples*

Camillo Porcaro, *Rome*

Carlo C Quattrocchi, *Rome*

Alberto Rebonato, *Perugia*

Giuseppe Rizzo, *Rome*

Roberto De Rosa, *Naples*

Domenico Rubello, *Rovigo*

Andrea Salvati, *Bari*

Sergio Sartori, *Ferrara*

Luca M Sconfienza, *Milano*

Giovanni Storto, *Rionero*

Nicola Sverzellati, *Parma*

Alberto S Tagliafico, *Genova*

Nicola Troisi, *Florence*



Japan

Yasuhiko Hori, *Chiba*

Hidetoshi Ikeda, *Koriyama*

Masahito Kawabori, *Sapporo*

Tamotsu Kamishima, *Sapporo*

Hiro Kiyosue, *Yufu*

Yasunori Minami, *Osaka-sayama*

Yasuhiro Morimoto, *Kitakyushu*

Satoru Murata, *Tokyo*

Shigeki Nagamachi, *Miyazaki*

Hiroshi Onishi, *Yamanashi*

Morio Sato, *Wakayama Shi*

Yoshito Tsushima, *Maebashi*

Masahiro Yanagawa, *Suita*



Netherlands

Willem Jan van Rooij, *Tilburg*



New Zealand

W Howell Round, *Hamilton*



Pakistan

Wazir Muhammad, *Abbottabad*



Poland

Maciej S Baglaj, *Wroclaw*

Piotr Czauderna, *Gdansk*



Portugal

Joao Manuel RS Tavares, *Porto*



Serbia

Olivera Ciraj-Bjelac, *Belgrade*



Singapore

Gopinathan Anil, *Singapore*

Terence KB Teo, *Singapore*

Cher Heng Tan, *Singapore*



Slovakia

Stefan Sivak, *Martin*



South Korea

Ki Seok Choo, *Busan*

Seung Hong Choi, *Seoul*

Dae-Seob Choi, *Jinju*

Hong-Seok Jang, *Seoul*

Yong Jeong, *Daejeon*

Chan Kyo Kim, *Seoul*

Se Hyung Kim, *Seoul*

Joong-Seok Kim, *Seoul*

Sang Eun Kim, *Seongnam*

Sung Joon Kwon, *Seoul*

Jeong Min Lee, *Seoul*

In Sook Lee, *Busan*

Noh Park, *Goyang*

Chang Min Park, *Seoul*

Sung Bin Park, *Seoul*

Deuk Jae Sung, *Seoul*

Choongsoo Shin, *Seoul*

Kwon-Ha Yoon, *Iksan*



Spain

Miguel A De Gregorio, *Zaragoza*

Antonio Luna, *Jaén*

Enrique Marco de Lucas, *Santander*

Fernando Ruiz Santiago, *Granada*



Sweden

Dmitry Grishenkov, *Stockholm*

Tie-Qiang Li, *Stockholm*



Switzerland

Nicolau Beckmann, *Basel*

Christian Boy, *Bern*

Giorgio Treglia, *Bellinzona*

Stephan Ulmer, *Kiel*



Thailand

Sirianong Namwongprom, *Chiang Mai*



Turkey

Kubilay Aydin, *Istanbul*

Ramazan Akdemir, *Sakarya*

Serhat Avcu, *Ankara*

Ayşe Aralasmak, *Istanbul*

Oktay Algin, *Ankara*

Nevbahar Akcar, *Meselik*

Bilal Battal, *Ankara*

Zulkif Bozgeyik, *Elazig*

Nazan Ciledag, *Aakara*

Fuldem Y Donmez, *Ankara*

Gulgun Engin, *Istanbul*

Ahmet Y Goktay, *Izmir*

Oguzhan G Gumustas, *Bursa*

Kaan Gunduz, *Ankara*

Pelin Ozcan Kara, *Mersin*

Kivanc Kamburoglu, *Ankara*

Ozgur Kilickesmez, *Istanbul*

Furuzan Numan, *Istanbul*

Cem Onal, *Adana*

Ozgur Oztekin, *Izmir*

Seda Ozbek (Boruban), *Konya*

Selda Sarikaya, *Zonguldak*

Figen Taser, *Kutahya*

Baran Tokar, *Eskisehir*

Ender Uysal, *Istanbul*

Ensar Yekeler, *Istanbul*



United Kingdom

Indran Davagnanam, *London*

M DC Valdés Hernández, *Edinburgh*

Alan Jackson, *Manchester*

Suneil Jain, *Belfast*

Long R Jiao, *London*

Miltiadis Krokidis, *Cambridge*

Pradesh Kumar, *Liverpool*

Peter D Kuzmich, *Derby*

Georgios Plataniotis, *Brighton*

Vanessa Sluming, *Liverpool*



United States

Garima Agrawal, *Saint Louis*

James R Brasic, *Baltimore*

Rajendra D Badgaiyan, *Buffalo*

Ulas Bagci, *Bethesda*

Anat Biegon, *Stony Brook*

Ramon Casanova, *Winston Salem*

Wenli Cai, *Boston*

Zheng Chang, *Durham*

Corey J Chakarun, *Long Beach*

Kai Chen, *Los Angeles*

Hyun-Soon Chong, *Chicago*

Marco Cura, *Dallas*

Ravi R Desai, *Bensalem*

Delia DeBuc, *Miami*

Carlo N De Cecco, *Charleston*

Timm-Michael L Dickfeld, *Baltimore*

Subba R Digumarthy, *Boston*

Huy M Do, *Stanford*

Todd A Faasse, *Grand Rapids*

Salomao Faintuch, *Boston*

Girish M Fatterpekar, *New York*

Dhakshinamoorthy Ganesan, *Houston*

Robert J Griffin, *Little Rock*

Andrew J Gunn, *Boston*

Sandeep S Hedgire, *Boston*

Timothy J Hoffman, *Columbia*

Mai-Lan Ho, *San Francisco*

Juebin Huang, *Jackson*

Abid Irshad, *Charleston*

Matilde Inglese, *New York*

El-Sayed H Ibrahim, *Jacksonville*

Paul R Julsrud, *Rochester*

Pamela T Johnson, *Baltimore*

Ming-Hung Kao, *Tempe*

Sunil Krishnan, *Houston*

Richard A Komoroski, *Cincinnati*

Sandi A Kwee, *Honolulu*

King Kim, *Ft. Lauderdale*

Guozheng Liu, *Worcester*

Yiyan Liu, *Newark*

Venkatesh Mani, *New York*

Lian-Sheng Ma, *Pleasanton*

Rachna Madan, *Boston*

Zeyad A Metwalli, *Houston*

Yilong Ma, *Manhasset*

Hui Mao, *Atlanta*

Feroze B Mohamed, *Philadelphia*

Gul Moonis, *Boston*

John L Noshier, *New Brunswick*

Rahmi Oklu, *Boston*

Aytekun Oto, *Chicago*

Bishnuhari Paudyal, *Philadelphia*

Rajul Pandya, *Youngstown*

Chong-Xian Pan, *Sacramento*

Jay J Pillai, *Baltimore*

Neal Prakash, *Duarte*

Reza Rahbar, *Boston*

Ali S Raja, *Boston*

Gustavo J Rodriguez, *El Paso*

David J Sahn, *Portland*

Steven Schild, *Scottsdale*

Ali R Sepahdari, *Los Angeles*

Li Shen, *Indianapolis*

JP Sheehan, *Charlottesville*

Atul B Shinagare, *Boston*

Sarabjeet Singh, *Boston*

Charles J Smith, *Columbia*

Kenji Suzuki, *Chicago*

Monvadi Srichai-Parsia, *Washington*

Sree H Tirumani, *Boston*

Hebert A Vargas, *New York*

Sachit Verma, *Philadelphia*

Yoichi Watanabe, *Minneapolis*

Li Wang, *Chapel Hill*

Carol C Wu, *Boston*

Shoujun Xu, *Houston*

Min Yao, *Cleveland*

Xiaofeng Yang, *Atlanta*

Qingbao Yu, *Albuquerque*

Aifeng Zhang, *Chicago*

Chao Zhou, *Bethlehem*

Hongming Zhuang, *Philadelphia*

**ORIGINAL ARTICLE****Retrospective Study**

- 405 Comparison of seldinger and trocar techniques in the percutaneous treatment of hydatid cysts
Turan HG, Özdemir M, Acu R, Küçükay F, Özdemir FAE, Hekimoğlu B, Yıldırım UM

LETTERS TO THE EDITOR

- 413 Naso-jejunal tube insertion - interface between radiology and endoscopy
Riddel N, Thoufeeq MH

ABOUT COVER

Editorial Board Member of *World Journal of Radiology*, Nicola Sverzellati, MD, Academic Research, Department of Surgical Sciences, Section of Radiology, University of Parma, Parma 43121, Italy

AIM AND SCOPE

World Journal of Radiology (*World J Radiol*, *WJR*, online ISSN 1949-8470, DOI: 10.4329) is a peer-reviewed open access academic journal that aims to guide clinical practice and improve diagnostic and therapeutic skills of clinicians.

WJR covers topics concerning diagnostic radiology, radiation oncology, radiologic physics, neuroradiology, nuclear radiology, pediatric radiology, vascular/interventional radiology, medical imaging achieved by various modalities and related methods analysis. The current columns of *WJR* include editorial, frontier, diagnostic advances, therapeutics advances, field of vision, mini-reviews, review, topic highlight, medical ethics, original articles, case report, clinical case conference (clinicopathological conference), and autobiography.

We encourage authors to submit their manuscripts to *WJR*. We will give priority to manuscripts that are supported by major national and international foundations and those that are of great basic and clinical significance.

INDEXING/ABSTRACTING

World Journal of Radiology is now indexed in Emerging Sources Citation Index (Web of Science), and PubMed, PubMed Central.

FLYLEAF

I-III Editorial Board

EDITORS FOR THIS ISSUE

Responsible Assistant Editor: *Xiang Li*
Responsible Electronic Editor: *Li-Min Zhao*
Proofing Editor-in-Chief: *Lian-Sheng Ma*

Responsible Science Editor: *Li-Jun Cai*
Proofing Editorial Office Director: *Xiu-Xia Song*

NAME OF JOURNAL
World Journal of Radiology

ISSN
ISSN 1949-8470 (online)

LAUNCH DATE
January 31, 2009

FREQUENCY
Monthly

EDITORS-IN-CHIEF
Kai U Juergens, MD, Associate Professor, MRT und PET/CT, Nuklearmedizin Bremen Mitte, ZEMODI - Zentrum für morphologische und molekulare Diagnostik, Bremen 28177, Germany

Edwin JR van Beek, MD, PhD, Professor, Clinical Research Imaging Centre and Department of Medical Radiology, University of Edinburgh, Edinburgh EH16 4TJ, United Kingdom

Thomas J Vogl, MD, Professor, Reader in Health Technology Assessment, Department of Diagnostic and Interventional Radiology, Johann Wolfgang Goethe University of Frankfurt, Frankfurt 60590,

Germany

EDITORIAL BOARD MEMBERS
All editorial board members resources online at <http://www.wjnet.com/1949-8470/editorialboard.htm>

EDITORIAL OFFICE
Xiu-Xia Song, Director
World Journal of Radiology
Baishideng Publishing Group Inc
7901 Stoneridge Drive, Suite 501, Pleasanton, CA 94588, USA
Telephone: +1-925-2238242
Fax: +1-925-2238243
E-mail: editorialoffice@wjnet.com
Help Desk: <http://www.f6publishing.com/helpdesk>
<http://www.wjnet.com>

PUBLISHER
Baishideng Publishing Group Inc
7901 Stoneridge Drive, Suite 501, Pleasanton, CA 94588, USA
Telephone: +1-925-2238242
Fax: +1-925-2238243
E-mail: bpgoffice@wjnet.com
Help Desk: <http://www.f6publishing.com/helpdesk>
<http://www.wjnet.com>

PUBLICATION DATE
November 28, 2017

COPYRIGHT
© 2017 Baishideng Publishing Group Inc. Articles published by this Open-Access journal are distributed under the terms of the Creative Commons Attribution Non-commercial License, which permits use, distribution, and reproduction in any medium, provided the original work is properly cited, the use is non commercial and is otherwise in compliance with the license.

SPECIAL STATEMENT
All articles published in journals owned by the Baishideng Publishing Group (BPG) represent the views and opinions of their authors, and not the views, opinions or policies of the BPG, except where otherwise explicitly indicated.

INSTRUCTIONS TO AUTHORS
<http://www.wjnet.com/bpg/gerinfo/204>

ONLINE SUBMISSION
<http://www.f6publishing.com>

Retrospective Study

Comparison of seldinger and trocar techniques in the percutaneous treatment of hydatid cysts

Hilal Gülsüm Turan, Mustafa Özdemir, Ruşen Acı, Fahrettin Küçükay, Fatma Ayça Edis Özdemir, Baki Hekimoğlu, Utku Mahir Yıldırım

Hilal Gülsüm Turan, Department of Radiology, Çekirge State Hospital, Bursa 16090, Turkey

Mustafa Özdemir, Fatma Ayça Edis Özdemir, Department of Interventional Radiology, Türkiye Yüksek İhtisas Hospital, Ankara 06230, Turkey

Ruşen Acı, Department of Radiology, Batman Bölge Hospital, Batman 72070, Turkey

Fahrettin Küçükay, Department of Interventional Radiology, Eskişehir Osman Gazi University, Eskişehir 26030, Turkey

Baki Hekimoğlu, Department of Interventional Radiology, Dışkapı Education And Research Hospital, Ankara 06110, Turkey

Utku Mahir Yıldırım, Department of Interventional Radiology, İzmir University Hospital, Ankara 35575, Turkey

Author contributions: Turan HG and Özdemir M designed the study, wrote this paper; Acı R contributed to the analysis and supervised the report; Küçükay F revised the paper; Özdemir FAE contributed to the analysis and supervised the report; Hekimoğlu B and Yıldırım UM designed the study.

Institutional review board statement: This retrospective study was reviewed and approved by the Dışkapı Education and Research Hospital institutional review board.

Informed consent statement: Written informed consent was obtained for each procedure from all patients.

Conflict-of-interest statement: All authors have no conflict-of-interest related to this study.

Data sharing statement: Participants gave informed consent for data sharing, and no additional data are available.

Open-Access: This article is an open-access article which was selected by an in-house editor and fully peer-reviewed by external reviewers. It is distributed in accordance with the Creative

Commons Attribution Non Commercial (CC BY-NC 4.0) license, which permits others to distribute, remix, adapt, build upon this work non-commercially, and license their derivative works on different terms, provided the original work is properly cited and the use is non-commercial. See: <http://creativecommons.org/licenses/by-nc/4.0/>

Manuscript source: Unsolicited manuscript

Correspondence to: Hilal Gülsüm Turan, MD, Department of Radiology, Çekirge State Hospital, Mutluevler Street, Doburca Avenue, Osmangazi, Bursa 16090, Turkey. h.turanozsoy@saglik.gov.tr
Telephone: +90-224-2948100
Fax: +90-224-2610888

Received: January 4, 2017

Peer-review started: January 7, 2017

First decision: February 17, 2017

Revised: May 25, 2017

Accepted: June 12, 2017

Article in press: June 13, 2017

Published online: November 28, 2017

Abstract

AIM

To comparatively evaluate Seldinger and Trocar techniques in the percutaneous treatment of hydatid disease.

METHODS

Trocar and Seldinger techniques were used for 49 and 56 cysts, respectively, among 106 hydatid cysts in 88 patients. The number of males and females were 22 and 66, respectively with a mean age of 44.9 years (range, 15-87). Follow-up studies included cyst diameter, cyst contents, and morphological changes in

the cyst wall, local recurrence, and secondary invasion, using ultrasound, computerized tomography and chest X-rays.

RESULTS

The positive criteria of healing were a decrease in cyst diameter, progressive solidification of the cyst contents, and disappearance of the cyst. Local recurrence was defined as an increase in the cyst diameter and contents, and appearance of daughter cysts in the primary cavity, while secondary dissemination was defined as the appearance of new cysts outside the treated cyst. Mean duration of follow-up was 19.23 mo (range, 18-26 mo). Follow-up results demonstrated that no significant differences were present between the Trocar and Seldinger techniques in the percentage of decrease in the cyst volume, rate of early complications, local recurrence and secondary dissemination ($P = 0.384, 0.069, 0.215$ and 0.533 , respectively).

CONCLUSION

There are no differences between the Seldinger and Trocar techniques that gain entry to the cyst cavity in terms of the efficacy of the treatment and the rates of early and late complications.

Key words: Percutaneous treatment; Trocar technique; Liver; Cyst hydatid; Seldinger technique

© **The Author(s)** 2017. Published by Baishideng Publishing Group Inc. All rights reserved.

Core tip: Although various methods have been developed as interventional procedures, there is no knowledge in the literature on which technique should be used when entering the cyst hydatid cavity. In this study, no differences have been found between the Seldinger and Trocar techniques that gain entry to the cyst hydatid cavity in terms of the efficacy of the treatment and the rates of early and late complications. Although trocar technique is a practical method that is easier and more economical to apply compared with the drainage procedure conducted using Seldinger technique, it should not be considered in post-surgical and elderly patients.

Turan HG, Özdemir M, Acu R, Küçükay F, Özdemir FAE, Hekimoğlu B, Yıldırım UM. Comparison of seldinger and trocar techniques in the percutaneous treatment of hydatid cysts. *World J Radiol* 2017; 9(11): 405-412 Available from: URL: <http://www.wjgnet.com/1949-8470/full/v9/i11/405.htm> DOI: <http://dx.doi.org/10.4329/wjr.v9.i11.405>

INTRODUCTION

Although surgery is a long-standing conventional treatment for the hydatid cysts, non-surgical alternative options have been used instead due to its remarkable

rate of complications and the risk of recurrence^[1,2]. Drugs containing benzimidazole constitute an alternative treatment, but the success rate is low and are not curative when used alone^[3,4]. Endoscopic treatment is limited to hydatid cysts with biliary tract invasion^[5].

Development in interventional radiology and the successful application of percutaneous methods for other intra-abdominal lesions resulted in the percutaneous approach being used for the treatment of cystic echinococcosis, and studies over the past 30 years have proved that these lesions could be successfully treated using the percutaneous approach^[6-18].

Although various methods have been developed as interventional procedures, there is no knowledge in the literature on which technique should be used when entering the cyst cavity. The aim of this study is to compare two different techniques for percutaneous entry and to evaluate their efficacy.

MATERIALS AND METHODS

Eighty-eight patients with hydatid cysts treated between January 2009 and February 2012, were retrospectively evaluated. One hundred and six hydatid cysts in these patients were treated using the percutaneous approach. The patients were followed up until February 2013. The mean duration of follow-up was 19.23 mo (range, 18-26). The number of males and females were 22 and 66, respectively, with a mean age of 44.9 years (range, 15-87). Hydatid cysts were classified according to the criteria of Gharbi *et al*^[19]. Type 1 and type 2 cysts were included in the study, while type 3 cysts were included only in cases where daughter cysts constituted a small part of the cyst. Type 4 and 5 cysts were excluded from the study. Also, three cysts that were initially diagnosed as hydatid cyst but were later detected to be non-parasitic cysts, were excluded from the study. Among these cysts, 99 had the appearance of type 1 cyst, four were type 2, and three were type 3 cysts. And 104 and two cases were located in the liver and the peritoneal cavity next to the liver, respectively. The volume of the cysts varied between 22.5 and 6840 mL (mean volume, 504.4 mL).

Percutaneous drainage technique

Oral albendazole at a dose of 10 mg/kg per day was administered to the patients for a week prior to the procedure in order to prevent secondary dissemination. Albendazole treatment was continued for prophylaxis for two further weeks following the procedure^[9,20]. Catheter placement was performed using two different techniques: the Seldinger technique and the Trocar technique. An 18-22 G (gauge) Chiba needle, 6-10 F percutaneous drainage catheter or 5.7-8 F trocar tip (one-step) drainage catheter was used. The Seldinger

technique was used in 56 cysts (53%) and the Trocar technique was used in 50 cysts (47%).

Seldinger technique

This is a two-step procedure. Standard wires and guide wires were used for drainage. The cyst was approached primarily through an intervention needle. Subsequently, a guide wire was sent through this needle and the needle was withdrawn. Thus, the guide wire could be located in the area of intervention. With dilators of various diameters sent through this guide wire, a hole was created that would permit the passage of the catheter through both the skin and the region of drainage. Finally, the drainage catheter was placed into the target area over the same guide wire, and the guide wire was withdrawn.

Trocar technique

This is a single step procedure and a standard trocar tip drainage catheter is composed of a sheath needle and a catheter coaxial system. A catheter and a straightening cannula of the same size were placed in the catheter and a needle 2-3 mm longer than the catheter was placed one in the other. Through this system, a direct puncture was made and it was forwarded to the field of drainage. Subsequently, the cannula and needle was withdrawn with the catheter remaining inside.

Following the first puncture, the cyst fluid was sent for cytological examination. Mobile scolexes in the cyst, seen under direct microscopy, were accepted as evidence of viability. Cysts without presence of evidence of viability, such as that of laminar membrane fragments and scolex hooks in cytological examination and separation of the endocyst in radiological evaluation, were excluded from the study. We applied Puncture Aspiration Injection Reaspiration (PAIR) in cysts with a diameter of less than 6 cm and catheterization method in larger cysts^[21-31]. Sixty-two cysts (58%) in 88 patients were treated using the PAIR technique, while the catheterization technique was used in the remaining 44 (42%) cysts^[22].

Follow-up studies included the cyst diameter and morphological changes in the cyst wall, local recurrence and secondary dissemination. Follow-up with US was performed at the 1, 3, 6, 12, 18 and 24 mo after the procedure. Annual whole abdominal CT and chest X-ray examinations were also performed. Positive criteria of healing were accepted to be a decrease in cyst diameter, progressive solidification of the cyst contents and disappearance of the cyst. Local recurrence was defined as increased cyst diameter and contents, and the appearance of daughter cysts in the primary cavity, while secondary dissemination was defined as the appearance of new cysts outside the treated cyst.

Statistical analysis

SPSS 14.0 statistics software package program (SPSS

Inc, Chicago, IL, United States) was used for statistical analysis. The analysis of difference in volume between Trocar and Seldinger methods was performed using Mann-Whitney U test. Differences between the two techniques in terms of the rates of complication, local recurrence and secondary dissemination were analyzed using the χ^2 test. $P < 0.05$ was accepted as statistically significant.

RESULTS

Separation of the endocyst from the pericyst was observed in 104 out of 106 cysts following injection of the sclerosing agent. The cyst was drained without observation of membrane separation in one case, due to severe abdominal pain subsequent to hypertonic saline injection. In another patient, the procedure was terminated due to the development of anaphylaxis before the cyst contents could be aspirated, following catheter insertion.

Daughter cysts were ruptured following hypertonic saline injection in two type 3 cysts including daughter cysts among the three type 3 cysts in the total series and they were ruptured with the manipulation of the catheter/guide wire in one of the type 3 cysts. Cytological examination confirmed the diagnosis of hydatid cyst in 106 cysts, while viability was detected in 98 cysts.

The Trocar technique was used in 50 cysts (47%) for entry to the cavity, while the Seldinger technique was used in 56 cysts (53%). Sclerotherapy was used in 98 cysts. Sclerotherapy was not performed in eight cysts, although they were catheterized due to contraindications of biliary fistula ($n = 4$), intra-abdominal extravasation ($n = 2$), anaphylaxis ($n = 1$), and absence of cellular elements in histopathological examination ($n = 1$). Mean duration of catheterization in 62 patients was 2.43 (range, 1- 45) d.

The mean duration of the follow-up of the 106 hydatid cysts in 88 patients was 19.23 mo (range, 18-26). Floating membranes were observed in the cyst fluid during the follow-up US examinations 12 mo after the percutaneous treatment, while none of the cysts had a pure anechoic image, which included dense internal echoes. At 12-14 mo follow-up, the cavity was seen to have collapsed, the cyst wall had thickened, and the cyst fluid was indiscernible. Finally, at the previous cyst, solid pseudotumors developed in many cases, which was seen to be iso- or hyperechoic with the liver parenchyma (Figure 1). No statistically significant difference was found in the cyst volume ($P = 0.384$) between the Trocar and Seldinger techniques (Table 1).

Thirteen early complications developed in a total of 12 patients. The early complications were anaphylaxis in one patient, biliary fistula in four, minor reaction in one (chills and tachycardia), abdominal pain in three, fever without signs of infection, entry site infection in

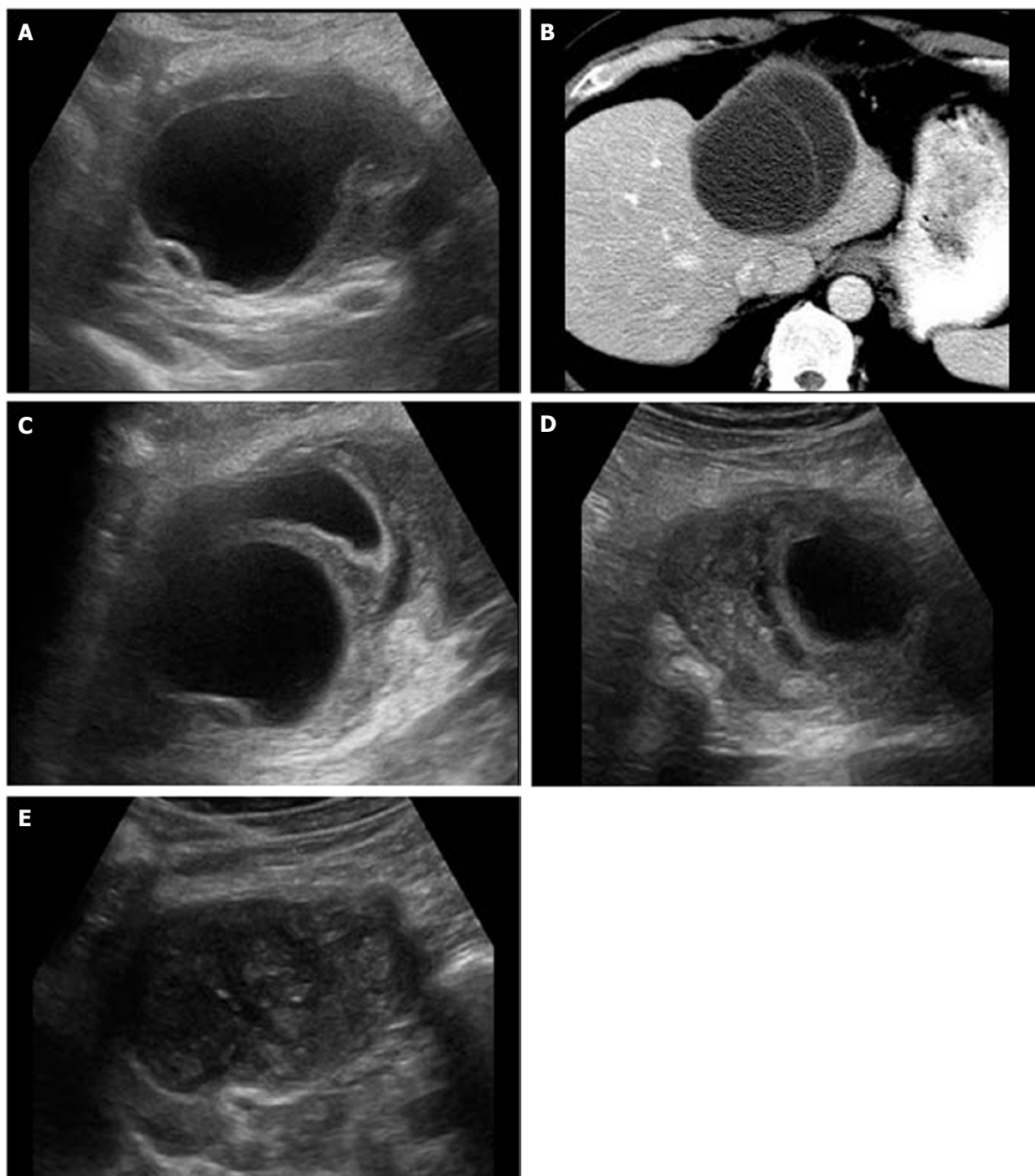


Figure 1 Type 1 hydatid cyst follow-up examinations conducted one to 1-18 mo after the procedure. A: US image prior to the procedure; B: CT image prior to the procedure; C: US image 6 mo after the procedure, wall thickness and irregularity of the cyst is seemed to be increased; D: US image 12 mo after the procedure, cyst dimension and tension is seemed to be markedly decreased and the contents can could be seen to have solidified; E: US image 18 mo after percutaneous drainage. Cyst can could be seen to have completely collapsed and solidified in the image and a pseudotumor image is formed. US: Ultrasound; CT: Computerized tomography.

one patient, infection in the cyst cavity (abscess) in one patient, in whom a biliary fistula also developed, and intra-abdominal extravasation in one patient. Late complications developed in three patients that were secondary dissemination in one and local recurrence in two patients.

During entry to the cavity with the Seldinger technique, following catheter placement and before

aspiration of the cyst contents, anaphylaxis developed in a 17-year-old male patient with a type 1 cyst. The patient's vital signs returned to normal following immediate treatment. With the Seldinger technique, the catheter was placed in all cysts in which biliary fistula had developed. These cysts were big cysts with a mean diameter of 8 cm (range, 5-11.5 cm). Due to severe abdominal pain, the procedure was terminated

Table 1 Statistical evaluation comparison of the changes in cyst volume between trocar and seldinger techniques (Mann-Whitney *U* test)

Method	<i>n</i>	Mean rank	Lower and upper- median	Mann-Whitney <i>U</i>	<i>P</i> value	Difference
Trocar	50	50.23	-165.00 and 97.00 61	1236.5	0.384	None
Seldinger	56	55.42	-29.00 and 100.00 70.5			

Table 2 Association of the techniques used and rate of complications (χ^2 analysis)

		Trocar	Seldinger	Total	χ^2	<i>P</i> value
Development of complications	Yes, <i>n</i>	3	10	13	3317	0.069
	(%)	6.1	17.9	12.4		
	No, <i>n</i>	47	46	93		
	(%)	93.9	82.1	87.6		
Total	<i>n</i>	50	56	106		
	(%)	100	100			

Table 3 Association of the techniques used and rate of local recurrence (χ^2 analysis)

		Trocar	Seldinger	Total	χ^2	<i>P</i> value
Local recurrence, present, <i>n</i>					2330	0.215
	(%)	2	0	2		
Local recurrence, none, <i>n</i>		4	0	1.9		
	(%)	48	56	104		
Total, <i>n</i>		96	100	98.1		
	(%)	50	56	106		
		100	100	100		

in two patients treated with the Seldinger technique and in one patient treated with the Trocar technique. Fever, chills and tachycardia developed in one patient with the Seldinger technique; however these signs resolved spontaneously without any medical treatment. Entry site infection was seen in a patient using the Seldinger technique, and the patient was treated with antibiotics. Cystography revealed leakage into the peritoneal cavity in two cysts subcapsularly located at the dome of the right lobe of the liver in a patient using the Seldinger technique. This patient was treated with albendazole for three months and no peritoneal cysts were detected during the 24-mo follow-up period.

Local recurrence developed in two patients using the Seldinger technique, including the presence of multiple daughter cysts and increased dimensions in a cyst cavity that had collapsed and solidified. These two patients underwent surgical treatment. Two new lesions (secondary dissemination and recurrence) were found at the 12 mo follow-up visit in a patient using Seldinger technique. These lesions were also treated by percutaneous methods.

Complication rates, local recurrence and secondary dissemination were statistically similar between the

patients using the Seldinger and Trocar techniques (Tables 2-4).

DISCUSSION

Hydatid cyst disease should be treated, due to the risks of severe infection, invasion to the biliary system and peritoneum and dissemination into other organs. Although surgery is the gold standard treatment, various types of percutaneous treatment provide alternatives for the elimination of the parasite and preventing the disease from reoccurring^[23-25,32]. In different series, the success rate of percutaneous procedures has been reported to be 95%-100%^[6-19,23,26].

The two step Seldinger technique or single step Trocar technique may be used for entry to the cyst cavity. The disadvantages in using the hydrophilic coated drainage catheters placed percutaneously with a guide wire, as required by the Seldinger technique, are the necessity for two individuals to perform the procedure and the relatively high cost of the technique. Trocar type catheters can be placed by a single individual and are more cost effective. However, secondary to aging, the pleura and peritoneum lose their elasticity after surgery, making the insertion of

Table 4 Association of the techniques used and rate of secondary dissemination (χ^2 analysis)

	Trocar	Seldinger	Total	χ^2	P value
Secondary dissemination, present, <i>n</i>	0	1	1	0.883	0.533
(%)	0	1.8	1		
Secondary dissemination, none, <i>n</i>	50	55	105		
(%)	100	98.2	99		
Total, <i>n</i>	50	56	106		
(%)	100	100	100		

trocar type catheters difficult in such cases. There is no publication in the literature reporting whether a difference exists between the two techniques used for the entry to the cyst cavity in terms of the efficacy of treatment and the development of complications^[15,31,32]. In the present study, Seldinger and Trocar techniques were used in 56 (53%) and 50 (47%) cysts, respectively, and the differences between the two techniques in terms of the efficacy of treatment and complications, if any, were evaluated.

A significant decrease was found in the cyst volume during the follow-up period. Furthermore, no statistically significant difference was found in the volume changes between the two techniques ($P = 0.384$).

The most frequently seen early complication of percutaneous treatment is fever without signs of infection and minor hypersensitivity reactions probably due to signs that develop secondary to the antigenic stimulus of the parasite, and are treated successfully with symptomatic treatment, as was the case in the present study and in other series previously reported in the literature^[3,8,22]. Fistula may develop between the cavity and the biliary system, due to the percutaneous procedure or prolonged drainage. Some of the fistulae may close spontaneously, while some necessitate an endoscopic approach in the treatment^[8,23,28]. In the present study, biliary fistula developed in four patients, all of whom had undergone percutaneous drainage with the Seldinger technique. In large patient series in the literature, the rate of development of anaphylaxis has been reported to be approximately 1%-2% with both percutaneous and surgical techniques^[27-29]. When we looked into the cases reported in the literature, spontaneous rupture does not always result in anaphylaxis^[30]. In the present study, an anaphylactic reaction developed in one patient during the PAIR procedure following catheter placement with Seldinger technique, however the medical treatment was successful. No statistically significant differences between the two techniques used for the entry to the cyst were found in terms of the rates of development of early complications, such as anaphylaxis, biliary fistula, minor reactions, abdominal pain, entry site infection, infection in the cyst cavity and intraabdominal

extravasation ($P = 0.069$).

Rates of local recurrence and secondary dissemination were reported to be 0%-4% in the literature^[3,6,22]. In the present study, local recurrence and secondary dissemination occurred in two patients and one patient, respectively. No statistically significant association was found in the rates of local recurrence and secondary dissemination between the two techniques ($P = 0.215$, $P = 0.533$).

In conclusion, no differences were found between the Seldinger and Trocar techniques that might be used in the entry to cyst cavity, in terms of the efficacy of the treatment and the rates of early and late complications. Although percutaneous cyst drainage, conducted with a trocar type catheter, is a practical method that is easier and more economical to apply compared with the drainage procedure conducted using a Seldinger needle, guide wire and a catheter, it should be considered in post-surgical and elderly patients that the trocar type catheter placement might be more difficult to apply, due to decreased elasticity of the pleura and peritoneum in such cases.

COMMENTS

Background

Although various methods have been developed as interventional procedures, there is no knowledge in the literature on which technique should be used when entering the liver cyst hydatid cavity. Two step Seldinger technique or single step Trocar technique may be used for entry to the cavity. The objective of this study was to compare two different techniques of percutaneous entry and to evaluate their efficacy.

Research frontiers

The weakness points are the small sample of patients and the retrospective design of the study but it can represent an interesting report for literature as first evaluation comparing two different techniques of percutaneous entry. Further studies with a larger number of patients will be needed to confirm the data.

Innovations and breakthroughs

No differences were found between the seldinger and Trocar techniques that might be used in the entry to cyst cavity, in terms of the efficacy of the treatment and the rates of early and late complications. Although percutaneous cyst drainage, conducted with a trocar type catheter, is a practical method that is easier and more economical to apply compared with the drainage procedure conducted using a Seldinger needle, guide wire and a catheter, it should be considered in post-surgical and elderly patients that the trocar type catheter

placement might be more difficult to apply, due to decreased elasticity of the pleura and peritoneum, in such cases.

Applications

Seldinger technique is a two-step procedure, and standard wires and guide wires were used for drainage. Trocar technique is a single step procedure, and a standard trocar tip drainage catheter is composed of a sheath needle and a catheter coaxial system.

Terminology

PAIR technique: The Puncture Aspiration Injection Reaspiration technique is performed using either ultrasound or CT guidance, involves aspiration of the cyst contents via a special cannula, followed by injection of a scolical agent and then reaspiration of the cystic contents. US: Ultrasound; CT: Computerized tomography.

Peer-review

This study compared two percutaneous techniques on treatment of hydatid cysts.

REFERENCES

- 1 **Rozanes I**, Güven K, Acunaş B, Emre A. Cystic echinococcal liver disease: new insights into an old disease and an algorithm for therapy planning. *Cardiovasc Intervent Radiol* 2007; **30**: 1112-1116 [PMID: 17533534 DOI: 10.1007/s00270-007-9081-y]
- 2 **Giorgio A**, Tarantino L, Francica G, Mariniello N, Aloisio T, Soscia E, Pierri G. Unilocular hydatid liver cysts: treatment with US-guided, double percutaneous aspiration and alcohol injection. *Radiology* 1992; **184**: 705-710 [PMID: 1509053 DOI: 10.1148/radiology.184.3.1509053]
- 3 **Khuroo MS**, Dar MY, Yattoo GN, Zargar SA, Javaid G, Khan BA, Boda MI. Percutaneous drainage versus albendazole therapy in hepatic hydatidosis: a prospective, randomized study. *Gastroenterology* 1993; **104**: 1452-1459 [PMID: 8482455 DOI: 10.1016/0016-5085(93)90355-G]
- 4 **Akkiz H**, Akinoglu A, Colakoglu S, Demiryurek H, Yagmur O. Endoscopic management of biliary hydatid disease. *Can J Surg* 1996; **39**: 287-292 [PMID: 8697318]
- 5 **Al Karawi MA**, Mohamed AR, Yasawy I, Haleem A. Non-surgical endoscopic trans-papillary treatment of ruptured echinococcus liver cyst obstructing the biliary tree. *Endoscopy* 1987; **19**: 81-83 [PMID: 3569154 DOI: 10.1055/s-2007-1013021]
- 6 **Akhan O**, Ozmen MN, Dinçer A, Sayek I, Göçmen A. Liver hydatid disease: long-term results of percutaneous treatment. *Radiology* 1996; **198**: 259-264 [PMID: 8539390 DOI: 10.1148/radiology.198.1.8539390]
- 7 **Men S**, Hekimoğlu B, Yücesoy C, Arda IS, Baran I. Percutaneous treatment of hepatic hydatid cysts: an alternative to surgery. *AJR Am J Roentgenol* 1999; **172**: 83-89 [PMID: 9888745 DOI: 10.2214/ajr.172.1.9888745]
- 8 **Khuroo MS**, Zargar SA, Mahajan R. Echinococcus granulosus cysts in the liver: management with percutaneous drainage. *Radiology* 1991; **180**: 141-145 [PMID: 2052682 DOI: 10.1148/radiology.180.1.2052682]
- 9 **Nasseri-Moghaddam S**, Abrishami A. Percutaneous needle aspiration, injection, and reaspiration with or without benzimidazole coverage for uncomplicated hepatic hydatid cysts. *The Cochrane Library* 2009; **1**: 1-20
- 10 **Kabaalioglu A**, Ceken K, Alimoglu E, Apaydin A. Percutaneous imaging-guided treatment of hydatid liver cysts: do long-term results make it a first choice? *Eur J Radiol* 2006; **59**: 65-73 [PMID: 16513311 DOI: 10.1016/j.ejrad.2006.01.014]
- 11 **Sayek I**, Tirnaksiz MB, Dogan R. Cystic hydatid disease: current trends in diagnosis and management. *Surg Today* 2004; **34**: 987-996 [PMID: 15580379 DOI: 10.1007/s00595-004-2830-5]
- 12 **Bosanac ZB**, Lisanin L. Percutaneous drainage of hydatid cyst in the liver as a primary treatment: review of 52 consecutive cases with long-term follow-up. *Clin Radiol* 2000; **55**: 839-848 [PMID: 11069739 DOI: 10.1053/crad.2000.0543]
- 13 **Duță C**, Păscuț M, Bordoș D. Percutaneous treatment of the liver hydatid cysts under sonographic guidance. *Chirurgia (Bucur)* 2002; **97**: 173-177 [PMID: 12731228]
- 14 **Peláez V**, Kugler C, Correa D, Del Carpio M, Guangirolí M, Molina J, Marcos B, Lopez E. PAIR as percutaneous treatment of hydatid liver cysts. *Acta Trop* 2000; **75**: 197-202 [PMID: 10708659 DOI: 10.1016/S0001-706X(00)00058-9]
- 15 **WHO Informal Working Group on Echinococcosis**. Guidelines for treatment of cystic and alveolar echinococcosis in humans. WHO Informal Working Group on Echinococcosis. *Bull World Health Organ* 1996; **74**: 231-242 [PMID: 8789923]
- 16 **Khuroo MS**. Hydatid disease: current status and recent advances. *Ann Saudi Med* 2002; **22**: 56-64 [PMID: 17259768 DOI: 10.5144/0256-4947.2002.56]
- 17 **Eckert J**, Gemmel MA, Meslin F-X, Pawlowski ZS (Eds). WHO/OIE Manual on Echinococcosis in Humans and Animals: a Public Health Problem of Global Concern. Geneva, Paris, 2001
- 18 **Larrieu E**, Del Carpio M, Salvitti JC, Mercapide C, Sustersic J, Panomarenko H, Costa M, Bigatti R, Labanchi J, Herrero E, Cantoni G, Perez A, Odriozola M. Ultrasonographic diagnosis and medical treatment of human cystic echinococcosis in asymptomatic school age carriers: 5 years of follow-up. *Acta Trop* 2004; **91**: 5-13 [PMID: 15158684 DOI: 10.1016/j.actatropica.2004.02.006]
- 19 **Gharbi HA**, Hassine W, Brauner MW, Dupuch K. Ultrasound examination of the hydatid liver. *Radiology* 1981; **139**: 459-463 [PMID: 7220891 DOI: 10.1148/radiology.139.2.7220891]
- 20 **El-On J**. Benzimidazole treatment of cystic echinococcosis. *Acta Trop* 2003; **85**: 243-252 [PMID: 12606103 DOI: 10.1016/S0001-706X(02)00217-6]
- 21 **Ben Amor N**, Gargouri M, Gharbi HA, Golvan YJ, Ayachi K, Kchouk H. [Trial therapy of inoperable abdominal hydatid cysts by puncture]. *Ann Parasitol Hum Comp* 1986; **61**: 689-692 [PMID: 3566087]
- 22 **Akhan O**, Dincer A, Gököz A, Sayek I, Havlioglu S, Abbasoglu O, Eryilmaz M, Besim A, Baris I. Percutaneous treatment of abdominal hydatid cysts with hypertonic saline and alcohol. An experimental study in sheep. *Invest Radiol* 1993; **28**: 121-127 [PMID: 8444568 DOI: 10.1097/00004424-199302000-00008]
- 23 **Smego RA**, Sebanego P. Treatment options for hepatic cystic echinococcosis. *Int J Infect Dis* 2005; **9**: 69-76 [PMID: 15708321 DOI: 10.1016/j.ijid.2004.08.001]
- 24 **Chautems R**, Buhler L, Gold B, Chilcott M, Morel P, Mentha G. Long term results after complete or incomplete surgical resection of liver hydatid disease. *Swiss Med Wkly* 2003; **133**: 258-262 [PMID: 12833196]
- 25 **Gupta N**, Javed A, Puri S, Jain S, Singh S, Agarwal AK. Hepatic hydatid: PAIR, drain or resect? *J Gastrointest Surg* 2011; **15**: 1829-1836 [PMID: 21826545 DOI: 10.1007/s11605-011-1649-9]
- 26 **Odev K**, Paksoy Y, Arslan A, Aygün E, Sahin M, Karaköse S, Baykan M, Arikoglu H, Aksoy F. Sonographically guided percutaneous treatment of hepatic hydatid cysts: long-term results. *J Clin Ultrasound* 2000; **28**: 469-478 [PMID: 11056024 DOI: 10.1002/1097-0096(200011/12)28:9<469::AID-JCU4>3.3.CO;2-6]
- 27 **Ormeçi N**, Soykan I, Bektas A, Sanoğlu M, Palabiyikoğlu M, Hadi Yasa M, Dökmeci A, Uzunalimoğlu O. A new percutaneous approach for the treatment of hydatid cysts of the liver. *Am J Gastroenterol* 2001; **96**: 2225-2230 [PMID: 11467657 DOI: 10.1111/j.1572-0241.2001.03886.x]
- 28 **Etlik O**, Arslan H, Bay A, Sakarya ME, Harman M, Temizoz O, Kayan M, Bakan V, Unal O. Abdominal hydatid disease: long-term results of percutaneous treatment. *Acta Radiol* 2004; **45**: 383-389 [PMID: 15323389 DOI: 10.1080/02841850410005651]
- 29 **Hofstetter C**, Segovia E, Vara-Thorbeck R. Treatment of uncomplicated hydatid cyst of the liver by closed marsupialization and fibrin glue obliteration. *World J Surg* 2004; **28**: 173-178 [PMID: 15323389 DOI: 10.1080/02841850410005651]

- 14708059 DOI: 10.1007/s00268-003-6932-9]
- 30 **Saenz de San Pedro B**, Cazaña JL, Cobo J, Serrano CL, Quiralte J, Contreras J, Martinez F. Anaphylactic shock by rupture of hydatid hepatic cyst. Follow-up by specific IgE serum antibodies. *Allergy* 1992; **47**: 568-570 [PMID: 1485662 DOI: 10.1111/j.1398-9995.1992.tb00683.x]
- 31 **WHO**. PAIR: Puncture, Aspiration, Injection, ReAspiration. An option for the treatment of Cystic Echinococcosis. Available from: URL: <http://wholibdoc.who.int/hq/2001>
- 32 **Gomez I Gavara C**, López-Andújar R, Belda Ibáñez T, Ramia Ángel JM, Moya Herraiz Á, Orbis Castellanos F, Pareja Ibars E, San Juan Rodríguez F. Review of the treatment of liver hydatid cysts. *World J Gastroenterol* 2015; **21**: 124-131 [PMID: 25574085 DOI: 10.3748/wjg.v21.i1.124]

P- Reviewer: Liu F **S- Editor:** Ji FF **L- Editor:** A
E- Editor: Zhao LM



Naso-jejunal tube insertion - interface between radiology and endoscopy

Naomi Riddel, Mo Hameed Thoufeeq

Naomi Riddel, Peterborough Hospitals NHS Trust, Peterborough PE3 9GZ, United Kingdom

Mo Hameed Thoufeeq, Department of Endoscopy, Sheffield Teaching Hospitals, Sheffield S5 7AU, United Kingdom

Author contributions: Riddel N and Thoufeeq MH were involved in writing the letter.

Conflict-of-interest statement: None.

Open-Access: This article is an open-access article which was selected by an in-house editor and fully peer-reviewed by external reviewers. It is distributed in accordance with the Creative Commons Attribution Non Commercial (CC BY-NC 4.0) license, which permits others to distribute, remix, adapt, build upon this work non-commercially, and license their derivative works on different terms, provided the original work is properly cited and the use is non-commercial. See: <http://creativecommons.org/licenses/by-nc/4.0/>

Manuscript source: Unsolicited manuscript

Correspondence to: Dr. Mo Hameed Thoufeeq, Consultant Gastroenterologist, Department of Endoscopy, Sheffield Teaching Hospitals, Huntsman Building, Herries Road, Sheffield S5 7AU, United Kingdom. mo.thoufeeq@sth.nhs.uk
Telephone: +44-11-43052586

Received: June 6, 2017

Peer-review started: June 12, 2017

First decision: July 11, 2017

Revised: July 17, 2017

Accepted: August 2, 2017

Article in press: August 2, 2017

Published online: November 28, 2017

Abstract

A survey was performed to identify the practice associated with endoscopic placement of naso-jejunal (NJ) tubes. We had a total of 236 responses, of which 228 responded to the frequency of requesting X-ray

after placing NJ tubes. The responses suggested that there was a strong variation in the practice. The practice was independent on clinicians' area of interest, hospital setting or experience in endoscopy. Currently there are no accepted guidelines on this. Hence, we advise hospitals to have robust local guidelines until there is internationally agreed consensus.

Key words: Decision making; X-rays; Naso-jejunal tube; Nutrition; Documentation

© **The Author(s) 2017.** Published by Baishideng Publishing Group Inc. All rights reserved.

Core tip: Endoscopy and interventional radiology complement each other given the advances in both fields. Enteral feeding has been found to be useful in patients with poor oral intake. This may be achieved by placing jejunal tubes either endoscopically or by radiological guidance without the need for surgery. In order to ascertain if clinicians recommend radiological confirmation after placing jejunal tube endoscopically, we did a survey. We had 236 responses; wherein we found that there was strong variation in the practice. Clinical area of interest, years of experience in endoscopy and type of clinical setting made no significant change to the practice.

Riddel N, Thoufeeq MH. Naso-jejunal tube insertion - interface between radiology and endoscopy. *World J Radiol* 2017; 9(11): 413-415 Available from: URL: <http://www.wjgnet.com/1949-8470/full/v9/i11/413.htm> DOI: <http://dx.doi.org/10.4329/wjr.v9.i11.413>

To the Editor

We read Ray *et al* article Complementary roles of interventional radiology and therapeutic endoscopy

Table 1 Results of the survey

	I always ask for X-ray confirmation	I sometimes ask for X-ray confirmation	I ask for X-ray confirmation on the rare occasion	I never ask for X-ray confirmation	Analysis (χ^2 test)
All responders to the frequency of Requesting X-rays ($n = 228$)	26.80%	22.80%	21.00%	29.40%	
> 10 yr endoscopy experience ($n = 152$)	29.60%	25.70%	19.70%	25.00%	$P = 0.13$
6-10 yr Endoscopy experience ($n = 46$)	26.10%	19.50%	17.40%	37.00%	
3-5 yr endoscopy experience ($n = 19$)	15.80%	5.30%	26.30%	52.60%	
0-2 yr endoscopy experience ($n = 8$)	12.50%	25.00%	50.00%	12.50%	
Gastroenterologist with interest in a Speciality other than nutrition ($n = 100$)	28.00%	20.00%	20.00%	32.00%	$P = 0.23$
Gastroenterologist with nutrition Interest ($n = 81$)	27.20%	29.60%	21.00%	22.20%	
Gastroenterology trainee ($n = 28$)	14.30%	17.90%	21.40%	46.40%	$P = 0.06$
Practicing at general hospitals ($n = 140$)	28.10%	27.30%	17.30%	27.30%	
Practicing at academic hospitals ($n = 82$)	22.00%	15.90%	28.00%	34.10%	

in gastroenterology with interest. Besides what's been highlighted in the article, nasojunal tube (NJ) placement also has complementary roles of radiology and endoscopy. Enteral feeding has been known to be associated with excellent outcomes particularly in patients with poor oral intake^[1].

We did a survey to identify the practice associated with endoscopic placement (EP) of NJ tube. A survey prepared using survey monkey® was sent as an email to endoscopy members of BAPEN (British association of parenteral and enteral nutrition) and members of BSG (British society of gastroenterology). Email to BSG members were sent directly whilst the email to BAPEN members were sent through the assistance of BAPEN office.

Respondents were asked to provide information about their current practice. We had a total of 236 responses, of which 228 responded to the frequency of requesting X-ray after placing NJ tubes. BAPEN directly sent the invitation themselves, hence we are unable to comment on how many clinicians were invited to participate. We found that there was a variation in practice of requesting X-ray after placing NJ tubes. There was no statistical significance noted with regards to the practice of recommending X-ray confirmation based on the clinicians' experience in endoscopy, clinicians' area of expertise or places of work, *i.e.*, an academic unit or a general hospital. The practice was no different if the clinician had a special interest in nutrition.

Results are enclosed in the following Table 1. NJ tubes have been placed endoscopically since 1984^[2]. They can be safely placed without any significant complications^[3]. Our study shows that there is a variation in the practice associated with the practice of X-ray confirmation following EP of NJ tube.

The protagonists of the practice suggest that it

will be useful for documentation purposes and to detect inadvertent slippage of the tube into the airway following placement. Adverse events secondary to medical care seriously affect mortality and morbidity^[4]. However, as it is placed under direct view there are other endoscopists who suggest that it is unnecessary and it exposes patients to unnecessary radiation and delays decision to start feeding if X-ray confirmation is made mandatory prior to use. There is also an argument of increasing the workload of the already over-stretched radiology department. Studies which looked at EP NJ tubes placement where radiological confirmation was done have showed near perfect concordance between re-endoscopy and X-ray^[5]. These suggest that radiological confirmation may not be necessary.

There are different endoscopic techniques by which NJ tubes are placed. In the over-the-guidewire method, a guidewire is passed through the biopsy channel with the endoscope into the small bowel. Following this, the scope is removed, with the guidewire left in place and oronasal transfer of the wire is performed. The feeding tube is advanced over the wire into the jejunum^[6].

In the "through-the-scope" method (Figure 1), the feeding tube is passed through the working (biopsy) channel of the endoscope into the jejunum^[7]. Following this, the endoscope is withdrawn, but the tube is left in place. The procedure is completed after an oral to nasal tube transfer is performed.

A pragmatic approach might be to mainly request X-ray confirmation if the procedure had been difficult particularly if the procedure had taken longer time than usual or if there's narrowing of gastro-intestinal lumen.

It will be useful to have society guidelines pertaining to need for X-ray confirmation following EP of NJ tubes in order avoid variation in the practice.

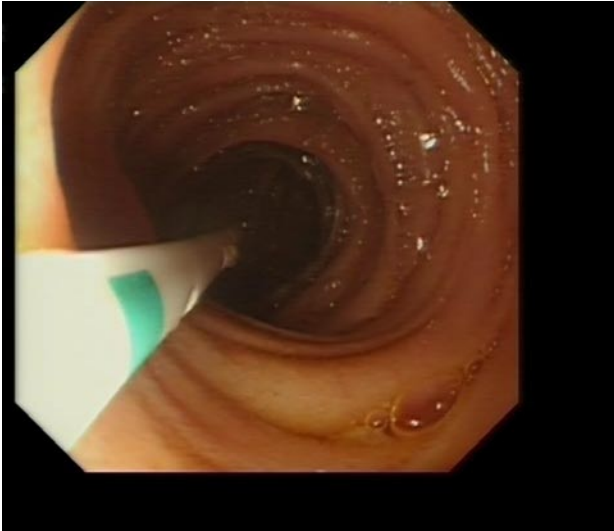


Figure 1 Endoscopic image showing a jejunal tube.

Until then we advise clinicians to follow local guidelines and to use a multi-disciplinary approach in decision making.

REFERENCES

- 1 **Pearce CB**, Duncan HD. Enteral feeding. Nasogastric, nasojejunal, percutaneous endoscopic gastrostomy, or jejunostomy: its indications and limitations. *Postgrad Med J* 2002; **78**: 198-204 [PMID: 11930022 DOI: 10.1136/pmj.78.918.198]
- 2 **Mann NS**, Nair PK, Mann SK, Lehman BH, Harder GL, Knox AL, Howland CC, Reddy AB. Nasoenteral feeding tube insertion via fiberoptic endoscope for enteral hyperalimentation. *J Am Coll Nutr* 1984; **3**: 333-339 [PMID: 6438209 DOI: 10.1080/07315724.1984.10720057]
- 3 **Byrne KR**, Fang JC. Endoscopic placement of enteral feeding catheters. *Curr Opin Gastroenterol* 2006; **22**: 546-550 [PMID: 16891888 DOI: 10.1097/01.mog.0000239871.12081.7f]
- 4 **Jha AK**, Larizgoitia I, Audera-Lopez C, Prasopa-Plaizier N, Waters H, Bates DW. The global burden of unsafe medical care: analytic modelling of observational studies. *BMJ Qual Saf* 2013; **22**: 809-815 [PMID: 24048616 DOI: 10.1136/bmjqs-2012-001748]
- 5 **O'Keefe SJ**, Foody W, Gill S. Transnasal endoscopic placement of feeding tubes in the intensive care unit. *JPEN J Parenter Enteral Nutr* 2003; **27**: 349-354 [PMID: 129771735 DOI: 10.1177/0148607103027005349]
- 6 **Rafferty GP**, Tham TC. Endoscopic placement of enteral feeding tubes. *World J Gastrointest Endosc* 2010; **2**: 155-164 [PMID: 21160743 DOI: 10.4253/wjge.v2.i5.155]
- 7 **DiSario JA**. Endoscopic approaches to enteral nutritional support. *Best Pract Res Clin Gastroenterol* 2006; **20**: 605-630 [PMID: 16782532 DOI: 10.1015/J.BPG.2006.02.002]

P- Reviewer: Gao BL, Li YZ, Schoenhagen P **S- Editor:** Ji FF
L- Editor: A **E- Editor:** Zhao LM





Published by **Baishideng Publishing Group Inc**
7901 Stoneridge Drive, Suite 501, Pleasanton, CA 94588, USA
Telephone: +1-925-223-8242
Fax: +1-925-223-8243
E-mail: bpgoffice@wjgnet.com
Help Desk: <http://www.f6publishing.com/helpdesk>
<http://www.wjgnet.com>



World Journal of *Radiology*

World J Radiol 2017 December 28; 9(12): 416-458





Editorial Board

2014-2017

The *World Journal of Radiology* Editorial Board consists of 365 members, representing a team of worldwide experts in radiology. They are from 36 countries, including Afghanistan (1), Argentina (2), Australia (5), Austria (7), Belgium (2), Brazil (8), Canada (6), Chile (1), China (43), Croatia (1), Denmark (4), Egypt (6), France (5), Germany (22), Greece (10), India (12), Iran (6), Ireland (2), Israel (3), Italy (47), Japan (13), Netherlands (1), New Zealand (1), Pakistan (1), Poland (2), Portugal (1), Serbia (1), Singapore (3), Slovakia (1), South Korea (18), Spain (4), Sweden (2), Switzerland (4), Thailand (1), Turkey (26), United Kingdom (11), and United States (82).

EDITORS-IN-CHIEF

Kai U Juergens, *Bremen*
Edwin JR van Beek, *Edinburgh*
Thomas J Vogl, *Frankfurt*

GUEST EDITORIAL BOARD MEMBERS

Wing P Chan, *Taipei*
Chung-Huei Hsu, *Taipei*
Chin-Chang Huang, *Taipei*
Tsong-Long Hwang, *Taoyuan*
Jung-Lung Hsu, *Taipei*
Chia-Hung Kao, *Taichung*
Yu-Ting Kuo, *Tainan*
Hon-Man Liu, *Taipei*
Hui-Lung Liang, *Kaohsiung*
Chun Chung Lui, *Kaohsiung*
Sen-Wen Teng, *Taipei*
Yung-Liang (William) Wan, *Taoyuan*

MEMBERS OF THE EDITORIAL BOARD



Afghanistan

Takao Hiraki, *Okayama*



Argentina

Patricia Carrascosa, *Vicente Lopez*
Maria C Ziadi, *Rosario*



Australia

Lourens Bester, *Sydney*
Gemma A Figtree, *Sydney*

Stuart M Grieve, *Sydney*
Wai-Kit Lee, *Fitzroy*
Prabhakar Ramachandran, *Melbourne*



Austria

Herwig R Cerwenka, *Graz*
Gudrun M Feuchtnner, *Innsbruck*
Benjamin Henninger, *Innsbruck*
Rupert Lanzenberger, *Vienna*
Shu-Ren Li, *Vienna*
Veronika Schopf, *Vienna*
Tobias De Zordo, *Innsbruck*



Belgium

Steve Majerus, *Liege*
Kathelijne Peremans, *Merelbeke*



Brazil

Clerio F Azevedo, *Rio de Janeiro*
Patrícia P Alfredo, *São Paulo*
Eduardo FC Fleury, *São Paulo*
Edward Araujo Júnior, *São Paulo*
Wellington P Martins, *Ribeirao Preto*
Ricardo A Mesquita, *Belo Horizonte*
Vera MC Salemi, *São Paulo*
Claudia Szobot, *Porto Alegre*
Lilian YI Yamaga, *São Paulo*



Canada

Marie Arsalidou, *Toronto*
Otman A Basir, *Waterloo*

Tarik Zine Belhocine, *Toronto*
James Chow, *Toronto*
Tae K Kim, *Toronto*
Anastasia Oikonomou, *Toronto*



China

Hong-Wei Chen, *Wuxi*
Feng Chen, *Hangzhou*
Jian-Ping Chu, *Guangzhou*
Guo-Guang Fan, *Shenyang*
Bu-Lang Gao, *Shijiazhuang*
Qi-Yong Gong, *Chengdu*
Ying Han, *Beijing*
Xian-Li Lv, *Beijing*
Yi-Zhuo Li, *Guangzhou*
Xiang-Xi Meng, *Harbin*
Yun Peng, *Beijing*
Jun Shen, *Guangzhou*
Ze-Zhou Song, *Hangzhou*
Wai Kwong Tang, *Hong Kong*
Gang-Hua Tang, *Guangzhou*
Jie Tian, *Beijing*
Lu-Hua Wang, *Beijing*
Xiao-bing Wang, *Xi'an*
Yi-Gen Wu, *Nanjing*
Kai Wu, *Guangzhou*
Hui-Xiong Xu, *Shanghai*
Zuo-Zhang Yang, *Kunming*
Xiao-Dan Ye, *Shanghai*
David T Yew, *Hong Kong*
Ting-He Yu, *Chongqing*
Zheng Yuan, *Shanghai*
Min-Ming Zhang, *Hangzhou*
Yudong Zhang, *Nanjing*
Dong Zhang, *Chongqing*
Wen-Bin Zeng, *Changsha*

Yue-Qi Zhu, *Shanghai*



Croatia

Goran Kusec, *Osijek*



Denmark

Poul E Andersen, *Odense*

Lars J Petersen, *Aalborg*

Thomas Z Ramsøy, *Frederiksberg*

Morten Ziebell, *Copenhagen*



Egypt

Mohamed F Bazeed, *Mansoura*

Mohamed Abou El-Ghar, *Mansoura*

Reem HA Mohamed, *Cairo*

Mohamed R Nouh, *Alexandria*

Ahmed AKA Razek, *Mansoura*

Ashraf A Zytoon, *Shebin El-Koom*



France

Sabine F Bensamoun, *Compiègne*

Romarc Loffroy, *Dijon*

Stephanie Nougaret, *Montpellier*

Hassane Oudadesse, *Rennes*

Vincent Vinh-Hung, *Fort-de-France*



Germany

Henryk Barthel, *Leipzig*

Peter Bannas, *Hamburg*

Martin Beeres, *Frankfurt*

Ilja F Ciernik, *Dessau*

A Dimitrakopoulou-Strauss, *Heidelberg*

Peter A Fasching, *Erlangen*

Andreas G Schreyer, *Regensburg*

Philipp Heusch, *Duesseldorf*

Sonja M Kirchhoff, *Munich*

Sebastian Ley, *Munich*

Adel Maataoui, *Frankfurt am Main*

Stephan M Meckel, *Freiburg*

Hans W Muller, *Duesseldorf*

Kay Raum, *Berlin*

Dirk Rades, *Luebeck*

Marc-Ulrich Regier, *Hamburg*

Alexey Surov, *Halle*

Martin Walter, *Magdeburg*

Axel Wetter, *Essen*

Christoph Zilkens, *Düsseldorf*



Greece

Panagiotis Antoniou, *Thessaloniki*

Nikos Efthimiou, *Athens*

Dimitris Karnabatidis, *Patras*

George Latsios, *Athens*

Stylianios Megremis, *Iraklion*

Alexander D Rapidis, *Athens*

Kiki Theodorou, *Larissa*

Ioannis A Tsalafoutas, *Athens*

Evanthia E Tripoliti, *Ioannina*

Athina C Tsili, *Ioannina*



India

Ritesh Agarwal, *Chandigarh*

Chandan J Das, *New Delhi*

Prathamesh V Joshi, *Mumbai*

Naveen Kalra, *Chandigarh*

Chandrasekharan Kesavadas, *Trivandrum*

Jyoti Kumar, *New Delhi*

Atin Kumar, *New Delhi*

Kaushala P Mishra, *Allahabad*

Daya N Sharma, *New Delhi*

Binit Sureka, *New Delhi*

Sanjay Sharma, *New Delhi*

Raja R Yadav, *Allahabad*



Iran

Majid Assadi, *Bushehr*

SeyedReza Najafizadeh, *Tehran*

Mohammad Ali Oghabian, *Tehran*

Amir Reza Radmard, *Tehran*

Ramin Sadeghi, *Mashhad*

Hadi Rokni Yazdi, *Tehran*



Ireland

Tadhg Gleeson, *Wexford*

Frederik JAI Vernimmen, *Cork*



Israel

Dafna Ben Bashat, *Tel Aviv*

Amit Gefen, *Tel Aviv*

Tamar Sella, *Jerusalem*



Italy

Adriano Alippi, *Rome*

Dante Amelio, *Trento*

Michele Anzidei, *Rome*

Filippo F Angileri, *Messinas*

Stefano Arcangeli, *Rome*

Roberto Azzoni, *San Donato milanese*

Tommaso V Bartolotta, *Palermo*

Tommaso Bartalena, *Imola*

Livia Bernardin, *San Bonifacio*

Federico Boschi, *Verona*

Sergio Casciaro, *Lecce*

Emanuele Casciani, *Rome*

Musa M Can, *Napoli*

Alberto Cuocolo, *Napoli*

Michele Ferrara, *Coppito*

Mauro Feola, *Fossano*

Giampiero Francica, *Castel Volturno*

Luigi De Gennaro, *Rome*

Giulio Giovannetti, *Pisa*

Francesca Iacobellis, *Napoli*

Formato Invernizzi, *Monza Brianza*

Francesco Lassandro, *Naples*

Lorenzo Livi, *Florence*

Pier P Mainenti, *Napoli*

Laura Marzetti, *Chieti*

Giuseppe Malinverni, *Crescentino*

Enrica Milanese, *Turin*

Giovanni Morana, *Treviso*

Lorenzo Monti, *Milan*

Silvia D Morbelli, *Genoa*

Barbara Palumbo, *Perugia*

Cecilia Parazzini, *Milan*

Stefano Pergolizzi, *Messina*

Antonio Pinto, *Naples*

Camillo Porcaro, *Rome*

Carlo C Quattrocchi, *Rome*

Alberto Rebonato, *Perugia*

Giuseppe Rizzo, *Rome*

Roberto De Rosa, *Naples*

Domenico Rubello, *Rovigo*

Andrea Salvati, *Bari*

Sergio Sartori, *Ferrara*

Luca M Sconfienza, *Milano*

Giovanni Storto, *Rionero*

Nicola Sverzellati, *Parma*

Alberto S Tagliafico, *Genova*

Nicola Troisi, *Florence*



Japan

Yasuhiko Hori, *Chiba*

Hidetoshi Ikeda, *Koriyama*

Masahito Kawabori, *Sapporo*

Tamotsu Kamishima, *Sapporo*

Hiro Kiyosue, *Yufu*

Yasunori Minami, *Osaka-sayama*

Yasuhiro Morimoto, *Kitakyushu*

Satoru Murata, *Tokyo*

Shigeki Nagamachi, *Miyazaki*

Hiroshi Onishi, *Yamanashi*

Morio Sato, *Wakayama Shi*

Yoshito Tsushima, *Maebashi*

Masahiro Yanagawa, *Suita*



Netherlands

Willem Jan van Rooij, *Tilburg*



New Zealand

W Howell Round, *Hamilton*



Pakistan

Wazir Muhammad, *Abbottabad*



Poland

Maciej S Baglaj, *Wroclaw*

Piotr Czauderna, *Gdansk*



Portugal

Joao Manuel RS Tavares, *Porto*



Serbia

Olivera Ciraj-Bjelac, *Belgrade*



Singapore

Gopinathan Anil, *Singapore*

Terence KB Teo, *Singapore*

Cher Heng Tan, *Singapore*



Slovakia

Stefan Sivak, *Martin*



South Korea

Ki Seok Choo, *Busan*

Seung Hong Choi, *Seoul*

Dae-Seob Choi, *Jinju*

Hong-Seok Jang, *Seoul*

Yong Jeong, *Daejeon*

Chan Kyo Kim, *Seoul*

Se Hyung Kim, *Seoul*

Joong-Seok Kim, *Seoul*

Sang Eun Kim, *Seongnam*

Sung Joon Kwon, *Seoul*

Jeong Min Lee, *Seoul*

In Sook Lee, *Busan*

Noh Park, *Goyang*

Chang Min Park, *Seoul*

Sung Bin Park, *Seoul*

Deuk Jae Sung, *Seoul*

Choongsoo Shin, *Seoul*

Kwon-Ha Yoon, *Iksan*



Spain

Miguel A De Gregorio, *Zaragoza*

Antonio Luna, *Jaén*

Enrique Marco de Lucas, *Santander*

Fernando Ruiz Santiago, *Granada*



Sweden

Dmitry Grishenkov, *Stockholm*

Tie-Qiang Li, *Stockholm*



Switzerland

Nicolau Beckmann, *Basel*

Christian Boy, *Bern*

Giorgio Treglia, *Bellinzona*

Stephan Ulmer, *Kiel*



Thailand

Sirianong Namwongprom, *Chiang Mai*



Turkey

Kubilay Aydin, *Istanbul*

Ramazan Akdemir, *Sakarya*

Serhat Avcu, *Ankara*

Ayşe Aralasmak, *Istanbul*

Oktay Algin, *Ankara*

Nevbahar Akcar, *Meselik*

Bilal Battal, *Ankara*

Zulkif Bozgeyik, *Elazig*

Nazan Ciledag, *Aakara*

Fuldem Y Donmez, *Ankara*

Gulgun Engin, *Istanbul*

Ahmet Y Goktay, *Izmir*

Oguzhan G Gumustas, *Bursa*

Kaan Gunduz, *Ankara*

Pelin Ozcan Kara, *Mersin*

Kivanc Kamburoglu, *Ankara*

Ozgur Kilickesmez, *Istanbul*

Furuzan Numan, *Istanbul*

Cem Onal, *Adana*

Ozgur Oztekin, *Izmir*

Seda Ozbek (Boruban), *Konya*

Selda Sarikaya, *Zonguldak*

Figen Taser, *Kutahya*

Baran Tokar, *Eskisehir*

Ender Uysal, *Istanbul*

Ensar Yekeler, *Istanbul*



United Kingdom

Indran Davagnanam, *London*

M DC Valdés Hernández, *Edinburgh*

Alan Jackson, *Manchester*

Suneil Jain, *Belfast*

Long R Jiao, *London*

Miltiadis Krokidis, *Cambridge*

Pradesh Kumar, *Liverpool*

Peter D Kuzmich, *Derby*

Georgios Plataniotis, *Brighton*

Vanessa Sluming, *Liverpool*



United States

Garima Agrawal, *Saint Louis*

James R Brasic, *Baltimore*

Rajendra D Badgaiyan, *Buffalo*

Ulas Bagci, *Bethesda*

Anat Biegon, *Stony Brook*

Ramon Casanova, *Winston Salem*

Wenli Cai, *Boston*

Zheng Chang, *Durham*

Corey J Chakarun, *Long Beach*

Kai Chen, *Los Angeles*

Hyun-Soon Chong, *Chicago*

Marco Cura, *Dallas*

Ravi R Desai, *Bensalem*

Delia DeBuc, *Miami*

Carlo N De Cecco, *Charleston*

Timm-Michael L Dickfeld, *Baltimore*

Subba R Digumarthy, *Boston*

Huy M Do, *Stanford*

Todd A Faasse, *Grand Rapids*

Salomao Faintuch, *Boston*

Girish M Fatterpekar, *New York*

Dhakshinamoorthy Ganesan, *Houston*

Robert J Griffin, *Little Rock*

Andrew J Gunn, *Boston*

Sandeep S Hedgire, *Boston*

Timothy J Hoffman, *Columbia*

Mai-Lan Ho, *San Francisco*

Juebin Huang, *Jackson*

Abid Irshad, *Charleston*

Matilde Inglese, *New York*

El-Sayed H Ibrahim, *Jacksonville*

Paul R Julsrud, *Rochester*

Pamela T Johnson, *Baltimore*

Ming-Hung Kao, *Tempe*

Sunil Krishnan, *Houston*

Richard A Komoroski, *Cincinnati*

Sandi A Kwee, *Honolulu*

King Kim, *Ft. Lauderdale*

Guozheng Liu, *Worcester*

Yiyan Liu, *Newark*

Venkatesh Mani, *New York*

Lian-Sheng Ma, *Pleasanton*

Rachna Madan, *Boston*

Zeyad A Metwalli, *Houston*

Yilong Ma, *Manhasset*

Hui Mao, *Atlanta*

Feroze B Mohamed, *Philadelphia*

Gul Moonis, *Boston*

John L Noshier, *New Brunswick*

Rahmi Oklu, *Boston*

Aytekun Oto, *Chicago*

Bishnuhari Paudyal, *Philadelphia*

Rajul Pandya, *Youngstown*

Chong-Xian Pan, *Sacramento*

Jay J Pillai, *Baltimore*

Neal Prakash, *Duarte*

Reza Rahbar, *Boston*

Ali S Raja, *Boston*

Gustavo J Rodriguez, *El Paso*

David J Sahn, *Portland*

Steven Schild, *Scottsdale*

Ali R Sepahdari, *Los Angeles*

Li Shen, *Indianapolis*

JP Sheehan, *Charlottesville*

Atul B Shinagare, *Boston*

Sarabjeet Singh, *Boston*

Charles J Smith, *Columbia*

Kenji Suzuki, *Chicago*

Monvadi Srichai-Parsia, *Washington*

Sree H Tirumani, *Boston*

Hebert A Vargas, *New York*

Sachit Verma, *Philadelphia*

Yoichi Watanabe, *Minneapolis*

Li Wang, *Chapel Hill*

Carol C Wu, *Boston*

Shoujun Xu, *Houston*

Min Yao, *Cleveland*

Xiaofeng Yang, *Atlanta*

Qingbao Yu, *Albuquerque*

Aifeng Zhang, *Chicago*

Chao Zhou, *Bethlehem*

Hongming Zhuang, *Philadelphia*

**REVIEW**

- 416 Dynamic contrast-enhanced magnetic resonance imaging of prostate cancer: A review of current methods and applications

Mazaheri Y, Akin O, Hricak H

- 426 Endovascular treatment of pulmonary embolism: Selective review of available techniques

Nosher JL, Patel A, Jagpal S, Gribbin C, Gendel V

MINIREVIEWS

- 438 Imaging features of intrathoracic complications of lung transplantation: What the radiologists need to know

Chia E, Babawale SN

CASE REPORT

- 448 Aggressive blood pressure treatment of hypertensive intracerebral hemorrhage may lead to global cerebral hypoperfusion: Case report and imaging perspective

Gavito-Higuera J, Khatri R, Qureshi IA, Maud A, Rodriguez GJ

- 454 Case of victims of modern imaging technology: Increased information noise concealing the diagnosis

Mahajan A, Santhoshkumar GV, Kawthalkar AS, Vaish R, Sable N, Arya S, Desai S

ABOUT COVER

Editorial Board Member of *World Journal of Radiology*, Guo-Guang Fan, MD, PhD, Professor, Department of Radiology, First hospital of China Medical University, Shenyang 110001, Liaoning Province, China

AIM AND SCOPE

World Journal of Radiology (*World J Radiol*, *WJR*, online ISSN 1949-8470, DOI: 10.4329) is a peer-reviewed open access academic journal that aims to guide clinical practice and improve diagnostic and therapeutic skills of clinicians.

WJR covers topics concerning diagnostic radiology, radiation oncology, radiologic physics, neuroradiology, nuclear radiology, pediatric radiology, vascular/interventional radiology, medical imaging achieved by various modalities and related methods analysis. The current columns of *WJR* include editorial, frontier, diagnostic advances, therapeutics advances, field of vision, mini-reviews, review, topic highlight, medical ethics, original articles, case report, clinical case conference (clinicopathological conference), and autobiography.

We encourage authors to submit their manuscripts to *WJR*. We will give priority to manuscripts that are supported by major national and international foundations and those that are of great basic and clinical significance.

INDEXING/ABSTRACTING

World Journal of Radiology is now indexed in PubMed, PubMed Central, and Emerging Sources Citation Index (Web of Science).

FLYLEAF

I-III Editorial Board

EDITORS FOR THIS ISSUE

Responsible Assistant Editor: *Xiang Li*
Responsible Electronic Editor: *Ya-Jing Lu*
Proofing Editor-in-Chief: *Lian-Sheng Ma*

Responsible Science Editor: *Li-Jun Cui*
Proofing Editorial Office Director: *Xiu-Xia Song*

NAME OF JOURNAL
World Journal of Radiology

ISSN
ISSN 1949-8470 (online)

LAUNCH DATE
January 31, 2009

FREQUENCY
Monthly

EDITORS-IN-CHIEF
Kai U Juergens, MD, Associate Professor, MRT und PET/CT, Nuklearmedizin Bremen Mitte, ZEMODI - Zentrum für morphologische und molekulare Diagnostik, Bremen 28177, Germany

Edwin JR van Beek, MD, PhD, Professor, Clinical Research Imaging Centre and Department of Medical Radiology, University of Edinburgh, Edinburgh EH16 4TJ, United Kingdom

Thomas J Vogl, MD, Professor, Reader in Health Technology Assessment, Department of Diagnostic and Interventional Radiology, Johann Wolfgang Goethe University of Frankfurt, Frankfurt 60590,

Germany

EDITORIAL BOARD MEMBERS
All editorial board members resources online at <http://www.wjgnet.com/1949-8470/editorialboard.htm>

EDITORIAL OFFICE
Xiu-Xia Song, Director
World Journal of Radiology
Baishideng Publishing Group Inc
7901 Stoneridge Drive, Suite 501, Pleasanton, CA 94588, USA
Telephone: +1-925-2238242
Fax: +1-925-2238243
E-mail: editorialoffice@wjgnet.com
Help Desk: <http://www.f6publishing.com/helpdesk>
<http://www.wjgnet.com>

PUBLISHER
Baishideng Publishing Group Inc
7901 Stoneridge Drive, Suite 501, Pleasanton, CA 94588, USA
Telephone: +1-925-2238242
Fax: +1-925-2238243
E-mail: bpgoffice@wjgnet.com
Help Desk: <http://www.f6publishing.com/helpdesk>
<http://www.wjgnet.com>

PUBLICATION DATE
December 28, 2017

COPYRIGHT
© 2017 Baishideng Publishing Group Inc. Articles published by this Open-Access journal are distributed under the terms of the Creative Commons Attribution Non-commercial License, which permits use, distribution, and reproduction in any medium, provided the original work is properly cited, the use is non commercial and is otherwise in compliance with the license.

SPECIAL STATEMENT
All articles published in journals owned by the Baishideng Publishing Group (BPG) represent the views and opinions of their authors, and not the views, opinions or policies of the BPG, except where otherwise explicitly indicated.

INSTRUCTIONS TO AUTHORS
<http://www.wjgnet.com/bpg/gerinfo/204>

ONLINE SUBMISSION
<http://www.f6publishing.com>

Dynamic contrast-enhanced magnetic resonance imaging of prostate cancer: A review of current methods and applications

Yousef Mazaheri, Oguz Akin, Hedvig Hricak

Yousef Mazaheri, Department of Medical Physics and Radiology, Memorial Sloan Kettering Cancer Center, New York, NY 10065, United States

Oguz Akin, Hedvig Hricak, Department of Radiology, Memorial Sloan Kettering Cancer Center, New York, NY 10065, United States

ORCID number: Yousef Mazaheri (0000-0002-8493-1608); Oguz Akin (0000-0002-2041-6199); Hedvig Hricak (0000-0003-2240-9694).

Author contributions: All authors are the guarantors of integrity of entire study; Mazaheri Y designed the study; Mazaheri Y and Akin O performed data analysis/interpretation; Mazaheri Y and Akin O performed the literature research; all authors contributed to manuscript drafting or manuscript revision for important intellectual content; all authors gave manuscript final version approval and manuscript editing; all authors take responsibility for the integrity of the data and the accuracy of the data analysis.

Conflict-of-interest statement: This manuscript is not published anywhere else; all authors conform that there is no conflict of interests (including none for related to commercial, personal, political, intellectual, or religious interests).

Open-Access: This article is an open-access article which was selected by an in-house editor and fully peer-reviewed by external reviewers. It is distributed in accordance with the Creative Commons Attribution Non Commercial (CC BY-NC 4.0) license, which permits others to distribute, remix, adapt, build upon this work non-commercially, and license their derivative works on different terms, provided the original work is properly cited and the use is non-commercial. See: <http://creativecommons.org/licenses/by-nc/4.0/>

Manuscript source: Unsolicited manuscript

Correspondence to: Yousef Mazaheri, PhD, Department of Medical Physics and Radiology, Memorial Sloan Kettering Cancer Center, 1275 York Avenue, New York, NY 10065, United States. mazahery@mskcc.org
Telephone: +1-646-8884520
Fax: +1-646-8885139

Received: May 17, 2017

Peer-review started: May 19, 2017

First decision: July 3, 2017

Revised: August 3, 2017

Accepted: October 17, 2017

Article in press: October 17, 2017

Published online: December 28, 2017

Abstract

In many areas of oncology, dynamic contrast-enhanced magnetic resonance imaging (DCE-MRI) has proven to be a clinically useful, non-invasive functional imaging technique to quantify tumor vasculature and tumor perfusion characteristics. Tumor angiogenesis is an essential process for tumor growth, proliferation, and metastasis. Malignant lesions demonstrate rapid extravasation of contrast from the intravascular space to the capillary bed due to leaky capillaries associated with tumor neovascularity. DCE-MRI has the potential to provide information regarding blood flow, areas of hypoperfusion, and variations in endothelial permeability and microvessel density to aid treatment selection, enable frequent monitoring during treatment and assess response to targeted therapy following treatment. This review will discuss the current status of DCE-MRI in cancer imaging, with a focus on its use in imaging prostate malignancies as well as weaknesses that limit its widespread clinical use. The latest techniques for quantification of DCE-MRI parameters will be reviewed and compared.

Key words: Prostate cancer; Prostate magnetic resonance imaging; Tumor angiogenesis; Dynamic contrast-enhanced magnetic resonance imaging; K_{ep} = rate constant between extracellular extravascular space and plasma space; K^{trans} = volume transfer constant

© The Author(s) 2017. Published by Baishideng Publishing Group Inc. All rights reserved.

Core tip: Dynamic contrast-enhanced magnetic resonance imaging (DCE-MRI) of prostate cancer can characterize tissue vascularity with important clinical application including aid in the detection, localization and staging, assessment of tumor aggressiveness, and assessment of treatment response. The current lack of standardized acquisition and analysis methods should be addressed to encourage more wide spread use of DCE-MRI in prostate cancer imaging.

Mazaheri Y, Akin O, Hricak H. Dynamic contrast-enhanced magnetic resonance imaging of prostate cancer: A review of current methods and applications. *World J Radiol* 2017; 9(12): 416-425 Available from: URL: <http://www.wjgnet.com/1949-8470/full/v9/i12/416.htm> DOI: <http://dx.doi.org/10.4329/wjr.v9.i12.416>

INTRODUCTION

This review describes dynamic contrast-enhanced magnetic resonance imaging (DCE-MRI) techniques for aiding prostate cancer management. First, we review methodologies for the acquisition and analysis of DCE-MRI data, including a commonly used model for the quantification of DCE-MRI data sets. Second, we discuss several current and potential future clinical applications of DCE-MRI and pharmacokinetic parametric maps in prostate cancer imaging. These include: (1) Primary tumor detection, localization, and staging; (2) risk assessment; (3) treatment planning; (4) treatment response assessment; and (5) detection of residual or locally recurrent cancer after treatment. Finally, we present an overview of the challenges of DCE-MRI in the management of prostate cancer and future directions.

BASIC CONCEPTS

To characterize tumor vasculature, a number of paramagnetic agents have been approved for routine clinical use. The most commonly-used contrast agents are gadolinium (Gd) chelates of low molecular weight. The mechanism of most T₁ methods involves characterization of the influxes and out-fluxes of the contrast agent and of the extracellular extravascular volume fraction within the tumor vasculature. In conventional contrast-enhanced imaging, data are acquired before contrast administration and again one or two times after contrast administration. An intravenous line may be set up during or prior to the exam to allow the injection of gadolinium contrast [gadolinium-diethylenetriamine pentaacetic acid (Gd-DTPA)] during a magnetic resonance (MR) acquisition. For some patients, Gd-DTPA may be injected into the arm by a nurse, just as is done for many routine clinical MRI exams. Gd-DTPA is administered into the right antecubital vein.

DCE-MRI is the acquisition of sequential images during the passage of a contrast agent within a tissue

of interest. DCE-MRI data are acquired rapidly during imaging following IV injection of the contrast agent and allow modeling of the passage of the contrast agent. Numerous pharmacokinetic models have been proposed for quantitative analysis of the observed signal intensity changes following contrast agent administration and for estimating pharmacokinetic parameters^[1,2]. For a comprehensive review of DCE-MRI tracer kinetic models see^[3] as well as a recent article by Sourbron and Buckley^[4].

IMAGING STRATEGIES: RAPID DYNAMIC CONTRAST-ENHANCED IMAGING

In “dynamic” contrast-enhanced MR imaging, 3D T₁-weighted fast spoiled gradient-echo MRI sequences are obtained every 5-10 s before, during, and several minutes after administration of contrast in a sequential or “dynamic” fashion for a period of up to 10 min. Acquisition times of greater than 15 s are generally not used due to difficulty detecting early enhancement and capillary transit time of < 5 s. Contrast agents create shorter relaxation times, resulting in a brightening of T₁ signal on images. Contrast signal depends on both extravasation of contrast as well as velocity of blood flow to the target area^[5,6]. There is no consensus on the best method for acquiring DCE-MRI data.

QUANTIFICATION OF DCE-MRI DATA

The assessment of signal enhancement after contrast injection can be performed through a semi-quantitative analysis of signal intensity changes over time. In this approach parameters, including curve shape, maximum signal intensity, wash-in (or upslope) and washout rates, as well as the initial area under the signal intensity curve or contrast medium concentration (IAUGC) curve, are estimated. Alternatively, it is possible to use a quantitative approach, which is based on pharmacokinetic modeling of the contrast agent. Numerous pharmacokinetic models have been proposed for quantitative analysis of signal intensity changes and for estimating pharmacokinetic parameters^[1,2].

Semi-quantitative/model-free method

Data modeling impacts the accuracy of parameters derived from DCE-MR images, which depends on both temporal sampling and signal intensity from the injected contrast agent. As an alternative to data modeling, data can be compared in a semi-quantitative method by using pixel-by-pixel analysis^[4,6]. From the corresponding signal intensity-time curves, enhancement kinetic parameters, semi-quantitative parameters are estimated. The typical parameters estimated for the semi-quantitative or non-model-based analysis include peak enhancement (PE), time-to-peak (TTP), wash-in, washout, and IAUGC. PE refers to the maximum signal intensity value between contrast arrivals, normalized by subtraction of the baseline

signal intensity. The quantity TTP is the corresponding time when the peak-enhancement is observed. The enhancement-slope and washout-slope allow for the quantitative evaluation of the wash-in and wash-out of the contrast agent and refer to the steepness of the curve during wash-in and wash-out (until the end of the acquisition), respectively. Semi-quantitative parameters are readily calculated with post-processing software available from the manufacturer of the MR unit and do not require measurement of arterial input function or tissue T_1 relaxation. One notable disadvantage of semi-quantitative parameters is that they are estimated directly from the signal intensity measurements (or concentration if in addition T_1 maps are generated) without a physiological or empirical model. Another disadvantage is that these parameters are dependent on experimental factors such as hardware, sequence parameters, and contrast dose, which limit their comparability across different sites or different acquisitions under different experimental conditions.

The semi-quantitative analyses provide parameters of area under the curve, time to peak, maximum enhancement, and slope of regions of interest. Advantages of these analytical parameters are their ease of acquisition, good visual image quality, and the fact that they do not require additional information such as tissue T_1 or measurement of the arterial input function. However, variability in dosing, bolus time, sequence parameters, tissue characteristics or other factors could affect reproducibility, presenting problems when utilizing these descriptive parameters. Models have been utilized to quantify and standardize parameters of contrast agents.

Quantitative analysis of DCE-MRI

A number of methods have been presented in the literature for the acquisition and analysis of DCE-MRI data sets. In this section we will review the basic principles of DCE-MRI analysis and introduce a few widely used analysis methods.

Relationship between MR signal and contrast agent concentration

In contrast-enhanced MRI, the relationship between signal and contrast agent concentration is not linear. To estimate contrast agent concentration, required for quantification of DCE-MRI parameters, the relationship between T_1 , signal intensity, and contrast agent concentration is applied. The signal intensity for a spoiled gradient echo in steady-state is given by: $S(\alpha) = M_0 [(1-E_1) \sin(\alpha)]/[1-E_1 \cos(\alpha)] \times e^{(-TE/T_2^*)}$ [1].

Where $E_1 = e^{-(TE/T_1)}$, α is the flip angle, M_0 is the proton density, TR is the repetition time, TE is the echo time, and T_2^* is the effective transversal relaxation time. The change in relaxation rate per unit of contrast agent concentration is given by^[7], assuming that the tracer concentration is to be linearly proportional to the change in the relaxation rate under the assumption of a fast exchange limit: $C(t) = (1/R_1) \{[1/T_1(t)] - [1/T_1(0)]\}$ [2].

Where $T_1(t)$ and $T_1(t)$ are the relaxation times with contrast agent at time t , and pre-enhancement, R_1 is the relaxivity in $(\text{mM}\cdot\text{s})^{-1}$ taken to equal 4.5 mmol/s at 1.5-Tesla field strength, and $C(t)$ is the concentration of the contrast agent.

Tofts model

Following the convention proposed by Tofts *et al.*^[8], a simple one-compartmental model of the tumor is used to predict the flow of the contrast agent into the EES as a function of time (Figure 1): $[dC_t(t)]/dt = K^{\text{trans}} \times \{C_p(t) - [C_t(t)/v_e]\}$ [8].

Where $C_p(t)$ is the tracer concentration in blood plasma $C_p = C_b/(1-\text{Hct})$, and the hematocrit (Hct) in tumors is typically assumed to equal 0.25^[9]. K^{trans} (min) is the volume transfer constant between the blood plasma and the EES; K_{ep} (min) is the rate constant between the EES and the blood plasma and is given by: $K_{ep} = (K^{\text{trans}}/v_e)$ where v_e is the fractional volume of the EES. Intuitively, K^{trans} describes the diffusive transport of the contrast agent across the capillary endothelium. The solution to Eq.^[8], with the assumption that the contribution to the concentration of the contrast agent due to plasma is negligible, is given by the following (referred to as the original Tofts model): $C_p(t) = K^{\text{trans}} \int_0^t C_p(u) \times \exp\{-[K^{\text{trans}}(t-u)]/v_e\} du$ [9].

Extended Tofts model (ETM)

In the case of tumors, the above-mentioned assumption is not valid, and thus the two-compartment extension of the Tofts model is required, where the tissue concentration is the sum of the contribution due to the plasma volume, v_p , as well as the fractional volume of the EES, v_e : $C_t(t) = v_p C_p(t) + v_e C_e(t)$ [10].

The extended Tofts model corresponds to two compartments with the assumption that the concentration of the contrast agent is derived from the EES and plasma, given by: $C_t(t) = K^{\text{trans}} \int_0^t C_p(u) \times \exp\{-[K^{\text{trans}}(t-u)]/v_e\} du + v_p C_p(t)$ [11].

Additional considerations in quantitative DCE-MRI

A number of factors need to be taken into account in the estimation of parameters from DCE-MRI.

Choice of arterial input function

Measurement of the patient-specific arterial input function (AIF) or plasma concentration requires localization of a large vessel that delivers blood to the organ of interest. Alternatively a bi-exponential AIF, $C_p(t)$, can be generated assuming a bi-exponent model given by^[10] (Figure 2): $C_p(t) = D [a_1 \exp(-m_1 t) + a_2 \exp(-m_2 t)]$ [10].

Where D is the dose of the contrast agent (mmol/kg of body weight). This is referred to as a model-based AIF. The first term in this expression corresponds to the equilibration of contrast agent between blood and extracellular space (fast), while the second term

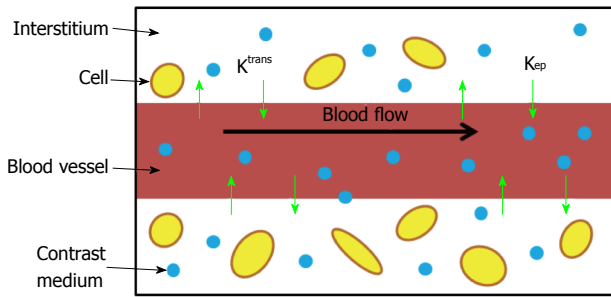


Figure 1 Schematic diagram of the Tofts kinetic model with the commonly used estimated parameters K^{trans} and k_{ep} .

corresponds to the removal of contrast agent from the plasma by the kidneys (slow). Substituting Eq.^[10] into Eq.^[8] and solving for $C_t(t)$ in the tumor tissue we obtain: $C_p(t) = D \times K^{trans} \sum_{i=1}^2 \{ [a_1 \exp(-\lambda_1 t) + a_2 \exp(-\lambda_2 t)] / K_{ep} - m_i \}$ [11].

An alternative to calculating the bi-exponential AIF is to derive the AIF in a select population and extend it to future studies. This is referred to as a population average AIF. One study compared prostate DCE-MRI parameters obtained at 3 Tesla before biopsy using three AIF estimates: Patient-specific or individual AIF, population average AIF, and model-based AIF^[11]. The study found patient-specific and population average AIFs had the highest sensitivity in predicting the biopsy results in prostate cancer, while the model-based bi-exponential AIF had the highest specificity. The areas under the ROC curves were not significantly different between any of the AIFs. In another study^[12], investigators compared the effects of using population based AIF or semi-automated or fully automated image-based patient-specific AIF to calculate DCE-MRI parameters in the prostate; they found that K^{trans} estimates were more sensitive to the choice between population vs patient-specific AIF as compared to k_{ep} .

T₁ mapping

An estimate of the voxel contrast concentration in DCE-MRI requires T_1 estimation in order to convert signal intensity to T_1 values. T_1 relaxation times can be estimated from T_1 maps acquired prior to the injection of contrast. Typically, before contrast agent administration, a series of spoiled gradient echo volumes at different flip angles are acquired^[13]. The steady-state signal is given by Eq.[1], which can be rearranged to yield: $S(\alpha)/\sin(\alpha) = E_1 [S(\alpha)/\tan(\alpha)] + M_0 \times (1-E_1) \times e^{(-TE/T^*2)}$ [12].

With a series of acquisitions at different flip angles, a linear fit of $S(\alpha)/\sin(\alpha)$ vs $S(\alpha)/\tan(\alpha)$ will allow estimation of T_1 from a linear fit $T_1 = -TR/\ln(m)$, where m is the slope between measurement points. At least two flip angles are required to estimate T_1 maps.

DCE-MRI of prostate

Studies on the use of dynamic or conventional contrast-enhanced MRI for prostate cancer have focused on localization and staging, assessment of prostate cancer

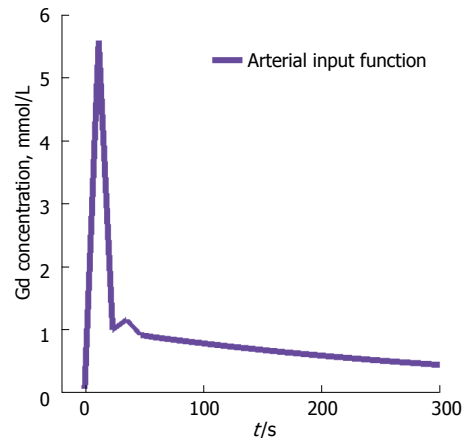


Figure 2 Model-based arterial input function. Shown is the model-based arterial input function, based on the Parker function.

aggressiveness, and assessment of treatment response (Figure 3). These studies suggest the many ways that contrast-enhanced MRI could be used to augment the value of a prostate MRI exam.

Localization and staging

Numerous studies have investigated the accuracy of DCE-MRI in localization and staging of prostate cancer using DCE-MRI (Figures 4 and 5). In a study performed at 1.5 Tesla, the accuracy of DCE-MRI in tumor localization was found to be significantly higher than that of T2-weighted imaging (as well as significantly higher than that of quantitative spectroscopic imaging)^[14]. The same group reported that accuracy in prostate cancer localization (again at 1.5 Tesla) was significantly higher with DCE-MRI and 3D MRSI than with T2-weighted imaging^[14,15]. Using a 3.0-Tesla system, Kim *et al.*^[16] found that detection of prostate cancer in the peripheral zone was better with DCE-MRI than with T2-weighted imaging. Sensitivity, specificity, and accuracy were 55%, 88% and 70%, respectively, with T2-weighted MRI as compared to 73%, 77%, and 75%, respectively, with dynamic contrast-enhanced imaging. In another study phased-array coils were used for signal homogeneity to image patients on a 1.5 T system before biopsy; based on early and intense enhancement areas on T1-weighted DCE images, sensitivity, specificity, and positive and negative predictive values were 90%, 88%, 77% and 95%, respectively for the detection of foci greater than 0.5 cc vs 77%, 91%, 86% and 85% for the detection of foci greater than 0.2 cc^[17]. Ocak *et al.*^[18] found the forward volume transfer constant (K^{trans}), the reverse reflux rate constant between extracellular space and plasma (k_{ep}), and the area under the gadolinium curve (AUGC) to be significantly higher in cancer than in the normal PZ. Engelbrecht *et al.*^[19] identified relative peak enhancement in the PZ and washout rate in the central gland as DCE-MRI parameters useful for prostate cancer detection and localization, but they did not find strong correlations between dynamic parameters in prostate

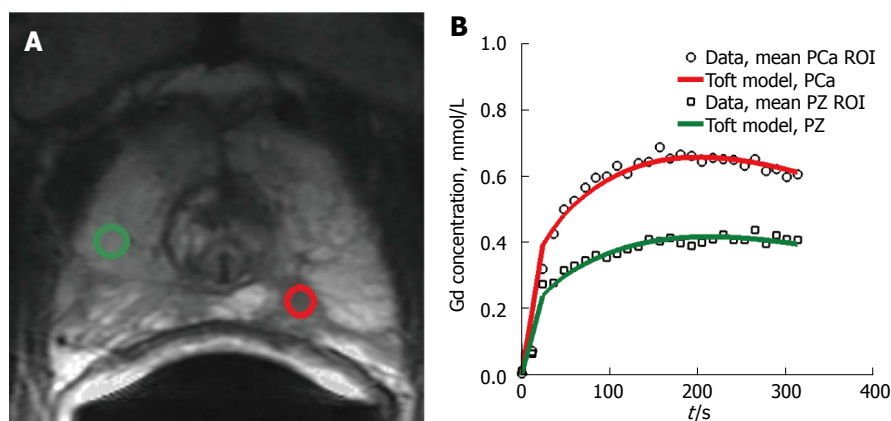


Figure 3 Example of enhancement kinetics pattern from two regions-of-interest. A: Transverse T2-weighted image. The green regions-of-interest (ROIs) corresponds to a benign PZ region. The red ROI corresponds to region with prostate cancer; B: Contrast curves of the two ROIs shown in A. The curves are characteristic of the types of time-intensity curves obtained with dynamic contrast-enhanced MRI. The green ROI shows moderately slow and slight enhancement wash-in pattern. This is characteristic for many benign, enhancing tissues, such as normal prostate tissue. The red ROI shows a rapid rise in signal intensity with subsequent wash-out as is typical in tumors.

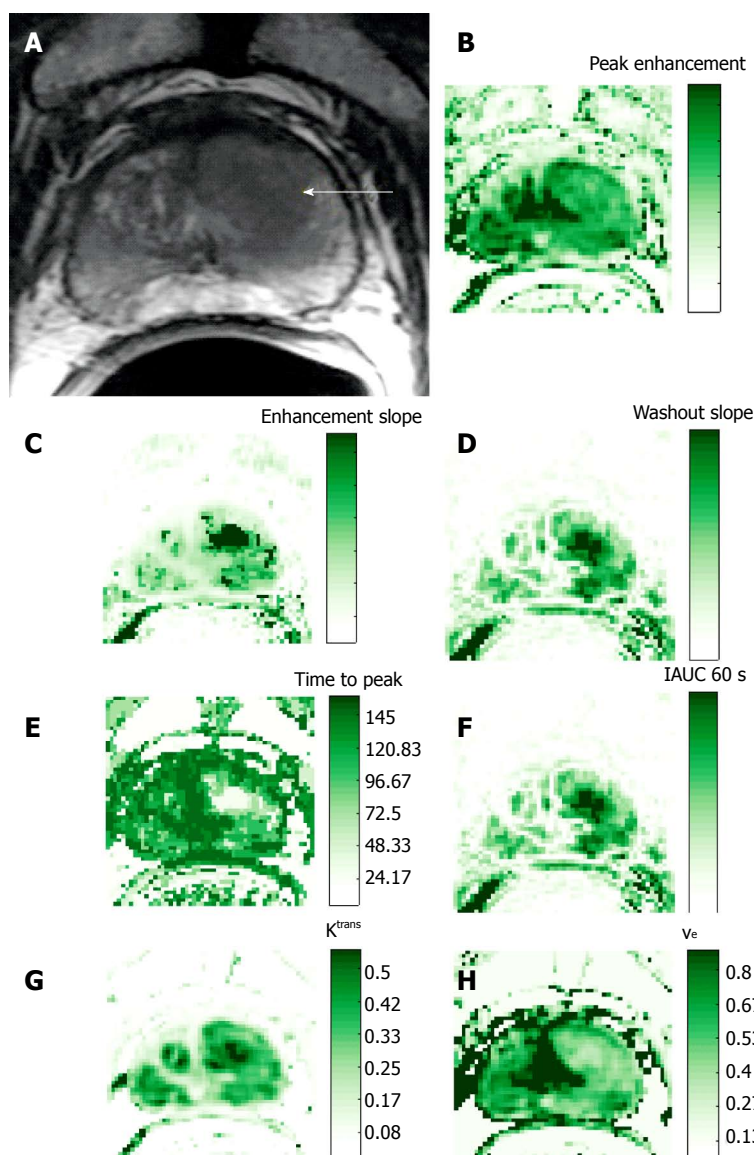


Figure 4 Representative 3T data in 63-year-old patient with prostate cancer (presurgical prostate-specific antigen level, 3.4 ng/mL). A: Transverse T2-weighted image. Pharmacokinetic parameter maps based on the semi-quantitative method and the Toft's kinetic model. Parametric maps for the semi-quantitative parameters, including; B: Peak-enhancement; C: Enhancement slope; D: Wash-out slope; E: Time-to-peak; and F: Intensity curve or contrast medium concentration at 60 s. Using the Toft's kinetic model, the pharmacokinetic parameter maps for G K^{trans} and H V_e are shown.

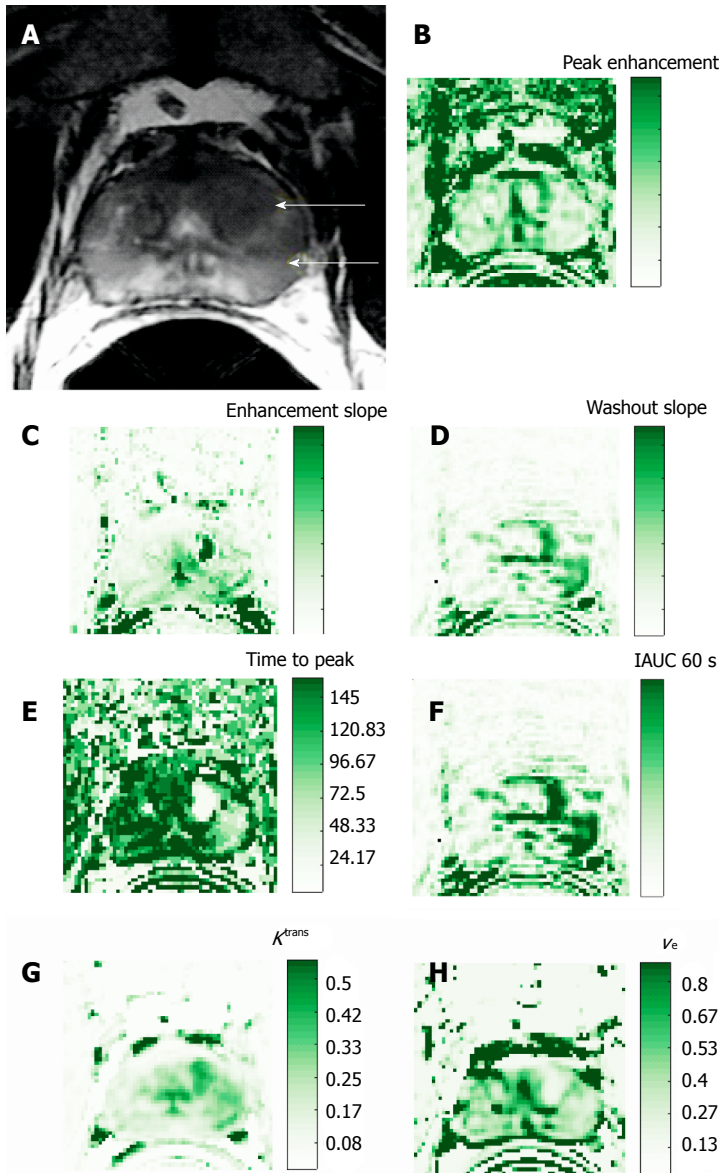


Figure 5 Representative 3T data in a 54-year-old prostate cancer patient [presurgical prostate-specific antigen level, 4.7 ng/mL; biopsy Gleason score, 7 (3 + 4)]. Pharmacokinetic parameter maps based on the semi-quantitative method and the Toft's kinetic model. Parametric maps for the semi-quantitative parameters, including B: Peak-enhancement; C: Enhancement slope; D: Wash-out slope; E: Time-to-peak; and F: Intensity curve or contrast medium concentration at 60 s. Using the Toft's kinetic model, the pharmacokinetic parameter maps for G K^{trans} and H v_e are shown.

cancer regions and tumor stage, Gleason score, patient age, tumor volume, or prostate-specific antigen. Alonzi *et al.*^[20] provided a table summarizing the early literature on prostate tumor localization.

With regard to staging of prostate cancer with DCE-MRI, one study compared the performance of an experienced reader to that of a less experienced reader^[21]. The investigators found that for the experienced reader, the sensitivity, specificity, and accuracy of staging with dynamic contrast-enhanced MR imaging were 69%, 97%, and 87%, respectively, and were not significantly different from the corresponding values obtained with T2-weighted imaging alone. However, for the less experienced reader, the use of DCE-MRI parametric maps resulted in a significant improvement in the area under the receiver operating characteristic curve as compared to T2-weighted imaging alone. Bloch *et al.*^[22] presented findings from

1.5-Tesla high-spatial-resolution T2-weighted imaging and DCE-MR imaging in 32 patients. When the T2-weighted imaging and DCE-MR imaging data sets were combined, the mean sensitivity, specificity, *P* value, and negative predictive values for the assessment of extracapsular extension (ECE) were 86%, 95%, 90%, and 93%, respectively; the determination of ECE was significantly better when the data sets were combined than when T2-weighted imaging was used alone.

ROLE OF DCE-MRI IN THE PI-RADS (PROSTATE IMAGING REPORTING AND DATA SYSTEM) CLASSIFICATION

The European Society of Urogenital Radiology (ESUR) has provided a set of guidelines for MR imaging of the

prostate^[23]. These guidelines provide recommendations for minimum standards of MR protocols as well outlining a structured reporting scheme, referred to as PI-RADS which are based on the BI-RADS classification for breast imaging. The reporting provides scores ranging from 1 to 5. The PI-RADS classification of DCE-MRI uses the time-resolved signal intensity curve to provide a qualitative analysis of the shape of the signal intensity curve. A score of 1 is assigned when the signal intensity curve increases gradually (Type I curve). Score of 2 is assigned when there is progressive signal intensity stabilization followed by a slight and late decrease in signal intensity (Type II curve). Score of 3 is assigned if the signal intensity curve demonstrates rapid washout after reaching peak enhancement (Type III curve). Focal lesions which enhance according to Type II or III curves are assigned an additional point. Asymmetric lesions or unusually located lesions which enhance according to Type II or III curves receive an additional point^[24].

Assessment of prostate cancer aggressiveness

The Gleason score, determined by histopathology, characterizes prostate cancer aggressiveness based on the microscopic appearance of the cancer tissue^[25]. Together with other parameters, the Gleason score is used for prostate cancer staging, assessment of the patient's prognosis and treatment selection. Most commonly, the Gleason score is determined by biopsy, which is performed when an elevated serum prostate-specific antigen (PSA) level and/or an abnormal digital rectal examination (DRE) suggest that the patient may have prostate cancer. The biopsy Gleason score and the amount of cancer in each biopsy core are both important predictors of prostate cancer aggressiveness and rate of progression^[26,27]. However, biopsy underestimates the Gleason score relative to the prostatectomy Gleason score in as many as 50% of cases^[28]. Moreover, sextant biopsy samples mostly the posterior peripheral zone of the prostate, thereby potentially missing tumors in anterior portions of the gland.

A review of prior studies to identify associations between MRI perfusion parameters and Gleason score suggests no such associations have been consistently found^[29-33]. An earlier study by Padhani *et al.*^[29] found only a weak correlation between MRI tumor stage and tumor vascular permeability. However, no correlation was observed between enhancement patterns (*i.e.*, both quantitative and semi-quantitative parameters) and Gleason score or PSA levels. Another study used an enhanced inversion-prepared dual-contrast gradient-echo sequence at 1.5 Tesla to perform DCE-MRI combined with dynamic susceptibility contrast (DSC) MR imaging, which allows simultaneous calculation of the parameters blood volume, blood flow, and interstitial volume. Subsequently, the parameters were correlated with histologic mean vessel density (MVD), mean vessel area (MVA), and mean interstitial area (MIA), and it was found that the measured quantities of blood volume and interstitial volume did not reliably correlate with

the histologic parameters^[30]. Chen *et al.*^[31] performed both semi-quantitative and quantitative analysis of DCE-MRI and correlated the parameters with Gleason score; they found that only the washout gradient correlated significantly with Gleason score. Another study using quantitative analysis of DCE-MRI was also unable to identify any significant correlations with Gleason score or vascular endothelial growth factor (VEGF) expression, although k_{ep} was found to correlate moderately with microvessel density^[32]. Recently, a study at 3 Tesla found that both semi-quantitative and quantitative parameters (mean and 75th percentile values of wash-in, mean wash-out, and 75th percentile of K^{trans}), differed significantly between low-grade (Gleason grades 2 and 3 present) and high-grade prostate cancer (primary Gleason grade of 4 and/or any 5 component) in the peripheral zone^[33]. Two factors which were identified as being important in acquisition of data for optimal modeling were: (1) the use of high temporal resolution imaging (temporal resolution = 3 s), which allowed the investigators to more accurately probe the early phase of enhancement; and (2) the use of patient-specific AIF rather than population-based AIF.

ASSESSMENT OF TREATMENT RESPONSE

Androgen deprivation therapy

VEGF also called vascular permeability factor, is a stimulus of tumor neo-angiogenesis^[34]. It has been shown that androgens induce the stimulation of vascular endothelial growth factor production in human prostate cancer^[35]. A study of 56 patients measured the effects of androgen deprivation therapy (ADT) on prostatic morphology and vascular permeability^[36] and found a significant reduction in tumor permeability surface area product in the peripheral zone, central gland and tumor, as well as changes in washout patterns^[36]. The authors also reported significant reductions in K^{trans} in the peripheral zone and central gland as well as a weak correlation between tumor K^{trans} and tumor volume change.

Another study examined the effect of ADT on prostate tumor blood flow by comparing quantitative parametric maps of the prostate for blood flow, blood volume, and blood oxygenation [intrinsic relaxivity (R_2^*)], measured using a DSC-MRI acquisition and analysis, and K^{trans} and v_e , measured using a DCE-MRI acquisition and analysis; values acquired before ADT was administered were compared to those acquired after 1 mo and 3 mo of therapy^[37]. The study found significant decreases in tumor blood volume and flow in the first month after treatment, and significant increases in R_2^* of the prostate tumor by three months; the study also found significant reductions in tumor K^{trans} from baseline at both 1 and 3 mo. Another study looking at monitoring response with both DCE and DWI found that DCE-MRI parameters (K^{trans} , v_e , v_p , IAUGC-90) measured in tumor after 3 mo of therapy were significantly reduced as compared to those

measured before treatment, whereas normal-appearing peripheral zone tissue showed no significant change^[38].

External-beam radiation therapy

When local recurrence is suspected after radiation treatment, MRI may be used to identify a target for biopsy and estimate the location and extent of the tumor. In an early study by Rouvière *et al.*^[39] assessing the value of DCE-MRI in patients with suspected recurrent prostate cancer after external beam radiotherapy (EBRT), readers interpreted contrast-enhanced images during the early phases, when prostatic tissue showed some degree of enhancement (the images were referred to as arterial phase images). They found that as compared to T2-weighted imaging, contrast-enhanced MRI localized recurrent cancer after EBRT more accurately and with less inter-observer variability. A later study found that in the localization of recurrent prostate cancer by sextant in patients with suspected relapse after EBRT, the sensitivity, positive predictive value and negative predictive value of DCE-MRI were significantly higher than those of T2-weighted imaging^[40]. Although the investigators found that DCE-MRI had excellent sensitivity, negative predictive value (both of 100%), and good accuracy (82%) for the detection of prostate cancer recurrence after EBRT, the positive predictive value was not very high (46%), even though it was higher than that of T2-weighted imaging. Multi-parametric approaches have also been investigated^[41,42]. One recent study found multi-parametric methods to be superior to T2-weighted imaging in the detection of recurrent prostate cancer after image-guided radiation therapy; however, there was no additional benefit when DCE-MRI was added to combined T2-weighted imaging and diffusion-weighted MRI (DW-MRI)^[42].

High-dose-rate brachytherapy

A recent article retrospectively evaluated the ability of multiphase (specifically, 5-phase) dynamic contrast-enhanced MRI obtained every 30 s (as well as DW-MRI) to detect local recurrence after high-dose-rate brachytherapy^[43]. Whereas the sensitivity, specificity, and accuracy of T2-weighted imaging were 27%, 99%, and 87%, respectively, those of DCE-MRI were 50%, 98%, and 90%, respectively. The authors found that a multi-parametric approach combining T2-weighted MRI, DW-MRI and DCE-MRI achieved the highest sensitivity (77%) with a slight reduction in specificity (92%) as compared to DW-MRI.

High-intensity focused ultrasound

For the treatment of patients with localized prostate cancer, a nonsurgical, noninvasive treatment referred to as transrectal high-intensity focused ultrasound (HIFU) can be considered^[44,45]. DCE-MRI (combined with T2-weighted imaging) can have a role in detecting local cancer recurrences after HIFU. It can assist in distinguishing residual or recurrent cancers within 2-5 d after HIFU treatment^[46] which are typically hypervascular from post-HIFU fibrosis which are often homogeneous and

hypovascular^[47] and can guide post-HIFU biopsy towards areas of recurrent cancer. One study found that although Gadolinium-enhanced MRI can accurately determine the extend of tissue damage following HIFU, it cannot predict histological results^[46].

Surgery

A study by Casciani *et al.*^[48] to determine the ability of endorectal MRI (T1- and T2-weighted imaging) combined with DCE-MRI to detect local recurrence after radical prostatectomy found that all recurrences showed signal enhancement after gadolinium administration. In most cases of recurrence (22/24), tumors display rapid and early signal enhancement. The study found a significant improvement in the detection of recurrence with combined MRI and DCE-MRI as compared to MRI alone. Similarly, Sciarra *et al.*^[49] found that the use of DCE-MRI alone or in combination with spectroscopic imaging was accurate for identifying local prostate cancer recurrence in patients with biochemical progression after radical prostatectomy.

CHALLENGES AND FUTURE DIRECTIONS

Limitations in DCE-MRI specific to prostate cancer include motion artifact, specifically from rectal and colonic peristalsis. Further, hyperintense findings on MRI may correlate not only with abnormal tumor tissue but any changes in vascularity including BPH nodules, post-biopsy changes, and prostatitis. At present, an additional limitation of DCE-MRI of the prostate, which also applies to the imaging of all other organ systems, is the lack of standardization of sequences and analysis parameters^[5]. With the availability of a wide range of imaging sequences on most MR units, a defining objective of many studies today is to identify the role of DCE-MRI as part of a multi-parametric examination^[50].

CONCLUSION

We have reviewed DCE-MRI acquisition and data analysis methods for the detection and monitoring of cancer in the prostate. Potential clinical applications of DCE-MRI for prostate cancer include detection, localization and staging, assessment of tumor aggressiveness, and assessment of treatment response. Limitations include lack of standardized acquisition and analysis methods which can results in variability in the results. We expect that with the standardization of these methods will encourage more wide spread use of DCE-MRI in prostate cancer imaging.

REFERENCES

1. **Padhani AR**, Husband JE. Dynamic contrast-enhanced MRI studies in oncology with an emphasis on quantification, validation and human studies. *Clin Radiol* 2001; **56**: 607-620 [PMID: 11467863 DOI: 10.1053/crad.2001.0762]
2. **Knopp MV**, Giesel FL, Marcos H, von Tengg-Koblighk H, Choyke P. Dynamic contrast-enhanced magnetic resonance imaging in oncology.

- Top Magn Reson Imaging* 2001; **12**: 301-308 [PMID: 11687716]
- 3 **Tofts PS**, Brix G, Buckley DL, Evelhoch JL, Henderson E, Knopp MV, Larsson HB, Lee TY, Mayr NA, Parker GJ, Port RE, Taylor J, Weisskoff RM. Estimating kinetic parameters from dynamic contrast-enhanced T(1)-weighted MRI of a diffusable tracer: standardized quantities and symbols. *J Magn Reson Imaging* 1999; **10**: 223-232 [PMID: 10508281]
- 4 **Sourbron SP**, Buckley DL. Classic models for dynamic contrast-enhanced MRI. *NMR Biomed* 2013; **26**: 1004-1027 [PMID: 23674304 DOI: 10.1002/nbm.2940]
- 5 **Verma S**, Turkbey B, Muradyan N, Rajesh A, Cornud F, Haider MA, Choyke PL, Harisinghani M. Overview of dynamic contrast-enhanced MRI in prostate cancer diagnosis and management. *AJR Am J Roentgenol* 2012; **198**: 1277-1288 [PMID: 22623539 DOI: 10.2214/AJR.12.8510]
- 6 **Ferl GZ**, Port RE. Quantification of antiangiogenic and antivascular drug activity by kinetic analysis of DCE-MRI data. *Clin Pharmacol Ther* 2012; **92**: 118-124 [PMID: 22588603 DOI: 10.1038/clpt.2012.63]
- 7 **Donahue KM**, Burstein D, Manning WJ, Gray ML. Studies of Gd-DTPA relaxivity and proton exchange rates in tissue. *Magn Reson Med* 1994; **32**: 66-76 [PMID: 8084239]
- 8 **Tofts PS**. Modeling tracer kinetics in dynamic Gd-DTPA MR imaging. *J Magn Reson Imaging* 1997; **7**: 91-101 [PMID: 9039598]
- 9 **Brix G**, Bahner ML, Hoffmann U, Horvath A, Schreiber W. Regional blood flow, capillary permeability, and compartmental volumes: measurement with dynamic CT--initial experience. *Radiology* 1999; **210**: 269-276 [PMID: 9885619 DOI: 10.1148/radiology.210.1.r99ja46269]
- 10 **Weinmann HJ**, Laniado M, Mützel W. Pharmacokinetics of GdDTPA/dimeglumine after intravenous injection into healthy volunteers. *Physiol Chem Phys Med NMR* 1984; **16**: 167-172 [PMID: 6505043]
- 11 **Meng R**, Chang SD, Jones EC, Goldenberg SL, Kozlowski P. Comparison between population average and experimentally measured arterial input function in predicting biopsy results in prostate cancer. *Acad Radiol* 2010; **17**: 520-525 [PMID: 20074982 DOI: 10.1016/j.acra.2009.11.006]
- 12 **Fedorov A**, Fluckiger J, Ayers GD, Li X, Gupta SN, Tempny C, Mulkern R, Yankeelov TE, Fennessy FM. A comparison of two methods for estimating DCE-MRI parameters via individual and cohort based AIFs in prostate cancer: a step towards practical implementation. *Magn Reson Imaging* 2014; **32**: 321-329 [PMID: 24560287 DOI: 10.1016/j.mri.2014.01.004]
- 13 **Fennessy FM**, Fedorov A, Gupta SN, Schmidt EJ, Tempny CM, Mulkern RV. Practical considerations in T1 mapping of prostate for dynamic contrast enhancement pharmacokinetic analyses. *Magn Reson Imaging* 2012; **30**: 1224-1233 [PMID: 22898681 DOI: 10.1016/j.mri.2012.06.011]
- 14 **Fütterer JJ**, Heijmink SW, Scheenen TW, Veltman J, Huisman HJ, Vos P, Hulsbergen-Van de Kaa CA, Witjes JA, Krabbe PF, Heerschap A, Barentsz JO. Prostate cancer localization with dynamic contrast-enhanced MR imaging and proton MR spectroscopic imaging. *Radiology* 2006; **241**: 449-458 [PMID: 16966484 DOI: 10.1148/radiol.2412051866]
- 15 **Fütterer JJ**, Heijmink SW, Scheenen TW, Jager GJ, Hulsbergen-Van de Kaa CA, Witjes JA, Barentsz JO. Prostate cancer: local staging at 3-T endorectal MR imaging--early experience. *Radiology* 2006; **238**: 184-191 [PMID: 16304091 DOI: 10.1148/radiol.2381041832]
- 16 **Kim CK**, Park BK, Kim B. Localization of prostate cancer using 3T MRI: comparison of T2-weighted and dynamic contrast-enhanced imaging. *J Comput Assist Tomogr* 2006; **30**: 7-11 [PMID: 16365565]
- 17 **Villers A**, Puech P, Mouton D, Leroy X, Ballereau C, Lemaitre L. Dynamic contrast enhanced, pelvic phased array magnetic resonance imaging of localized prostate cancer for predicting tumor volume: correlation with radical prostatectomy findings. *J Urol* 2006; **176**: 2432-2437 [PMID: 17085122 DOI: 10.1016/j.juro.2006.08.007]
- 18 **Ocak I**, Bernardo M, Metzger G, Barrett T, Pinto P, Albert PS, Choyke PL. Dynamic contrast-enhanced MRI of prostate cancer at 3 T: a study of pharmacokinetic parameters. *AJR Am J Roentgenol* 2007; **189**: 849 [PMID: 17885055 DOI: 10.2214/AJR.06.1329]
- 19 **Engelbrecht MR**, Huisman HJ, Laheij RJ, Jager GJ, van Leenders GJ, Hulsbergen-Van De Kaa CA, de la Rosette JJ, Blickman JG, Barentsz JO. Discrimination of prostate cancer from normal peripheral zone and central gland tissue by using dynamic contrast-enhanced MR imaging. *Radiology* 2003; **229**: 248-254 [PMID: 12944607 DOI: 10.1148/radiol.2291020200]
- 20 **Alonzi R**, Padhani AR, Allen C. Dynamic contrast enhanced MRI in prostate cancer. *Eur J Radiol* 2007; **63**: 335-350 [PMID: 17689907 DOI: 10.1016/j.ejrad.2007.06.028]
- 21 **Fütterer JJ**, Engelbrecht MR, Huisman HJ, Jager GJ, Hulsbergen-van De Kaa CA, Witjes JA, Barentsz JO. Staging prostate cancer with dynamic contrast-enhanced endorectal MR imaging prior to radical prostatectomy: experienced versus less experienced readers. *Radiology* 2005; **237**: 541-549 [PMID: 16244263 DOI: 10.1148/radiol.2372041724]
- 22 **Bloch BN**, Furman-Haran E, Helbich TH, Lenkinski RE, Degani H, Kratzik C, Susani M, Haitel A, Jaromi S, Ngo L, Rofsky NM. Prostate cancer: accurate determination of extracapsular extension with high-spatial-resolution dynamic contrast-enhanced and T2-weighted MR imaging--initial results. *Radiology* 2007; **245**: 176-185 [PMID: 17717328 DOI: 10.1148/radiol.2451061502]
- 23 **Barentsz JO**, Richenberg J, Clements R, Choyke P, Verma S, Villeirs G, Rouviere O, Logager V, Fütterer JJ; European Society of Urogenital Radiology. ESUR prostate MR guidelines 2012. *Eur Radiol* 2012; **22**: 746-757 [PMID: 22322308 DOI: 10.1007/s00330-011-2377-y]
- 24 **Röthke M**, Blondin D, Schlemmer HP, Franiel T. [PI-RADS classification: structured reporting for MRI of the prostate]. *Rofo* 2013; **185**: 253-261 [PMID: 23404430]
- 25 **Gleason DF**, Mellinger GT. Prediction of prognosis for prostatic adenocarcinoma by combined histological grading and clinical staging. *J Urol* 1974; **111**: 58-64 [PMID: 4813554]
- 26 **Epstein JI**, Allsbrook WC Jr, Amin MB, Egevad LL. Update on the Gleason grading system for prostate cancer: results of an international consensus conference of urologic pathologists. *Adv Anat Pathol* 2006; **13**: 57-59 [PMID: 16462155 DOI: 10.1097/01.pap.0000202017.78917.18]
- 27 **Epstein JI**. What's new in prostate cancer disease assessment in 2006? *Curr Opin Urol* 2006; **16**: 146-151 [PMID: 16679850 DOI: 10.1097/01.mou.0000193389.31727.9b]
- 28 **Bak JB**, Landas SK, Haas GP. Characterization of prostate cancer missed by sextant biopsy. *Clin Prostate Cancer* 2003; **2**: 115-118 [PMID: 15040873]
- 29 **Padhani AR**, Gapinski CJ, Macvicar DA, Parker GJ, Suckling J, Revell PB, Leach MO, Dearnaley DP, Husband JE. Dynamic contrast enhanced MRI of prostate cancer: correlation with morphology and tumour stage, histological grade and PSA. *Clin Radiol* 2000; **55**: 99-109 [PMID: 10657154 DOI: 10.1053/crad.1999.0327]
- 30 **Franiel T**, Lüdemann L, Rudolph B, Rehbein H, Stephan C, Taupitz M, Beyersdorff D. Prostate MR imaging: tissue characterization with pharmacokinetic volume and blood flow parameters and correlation with histologic parameters. *Radiology* 2009; **252**: 101-108 [PMID: 19561252 DOI: 10.1148/radiol.2521081400]
- 31 **Chen M**, Dang HD, Wang JY, Zhou C, Li SY, Wang WC, Zhao WF, Yang ZH, Zhong CY, Li GZ. Prostate cancer detection: comparison of T2-weighted imaging, diffusion-weighted imaging, proton magnetic resonance spectroscopic imaging, and the three techniques combined. *Acta Radiol* 2008; **49**: 602-610 [PMID: 18568549 DOI: 10.1080/02841850802004983]
- 32 **Oto A**, Kayhan A, Jiang Y, Tretiakova M, Yang C, Antic T, Dahi F, Shalhav AL, Karczmars G, Stadler WM. Prostate cancer: differentiation of central gland cancer from benign prostatic hyperplasia by using diffusion-weighted and dynamic contrast-enhanced MR imaging. *Radiology* 2010; **257**: 715-723 [PMID: 20843992 DOI: 10.1148/radiol.10100021]
- 33 **Vos EK**, Litjens GJ, Kobus T, Hambroek T, Hulsbergen-van de Kaa CA, Barentsz JO, Huisman HJ, Scheenen TW. Assessment of prostate cancer aggressiveness using dynamic contrast-enhanced magnetic resonance imaging at 3 T. *Eur Urol* 2013; **64**: 448-455 [PMID: 23751135 DOI: 10.1016/j.eururo.2013.05.045]

- 34 **Dvorak HF**, Brown LF, Detmar M, Dvorak AM. Vascular permeability factor/vascular endothelial growth factor, microvascular hyperpermeability, and angiogenesis. *Am J Pathol* 1995; **146**: 1029-1039 [PMID: 7538264]
- 35 **Hägström S**, Lissbrant IF, Bergh A, Damber JE. Testosterone induces vascular endothelial growth factor synthesis in the ventral prostate in castrated rats. *J Urol* 1999; **161**: 1620-1625 [PMID: 10210429]
- 36 **Padhani AR**, MacVicar AD, Gapinski CJ, Deamaley DP, Parker GJ, Suckling J, Leach MO, Husband JE. Effects of androgen deprivation on prostatic morphology and vascular permeability evaluated with mr imaging. *Radiology* 2001; **218**: 365-374 [PMID: 11161148 DOI: 10.1148/radiology.218.2.r01ja04365]
- 37 **Alonzi R**, Padhani AR, Taylor NJ, Collins DJ, D'Arcy JA, Stirling JJ, Saunders MI, Hoskin PJ. Antivascular effects of neoadjuvant androgen deprivation for prostate cancer: an in vivo human study using susceptibility and relaxivity dynamic MRI. *Int J Radiat Oncol Biol Phys* 2011; **80**: 721-727 [PMID: 20630668 DOI: 10.1016/j.ijrobp.2010.02.060]
- 38 **Barrett T**, Gill AB, Kataoka MY, Priest AN, Joubert I, McLean MA, Graves MJ, Stearn S, Lomas DJ, Griffiths JR, Neal D, Gnanapragasam VJ, Sala E. DCE and DW MRI in monitoring response to androgen deprivation therapy in patients with prostate cancer: a feasibility study. *Magn Reson Med* 2012; **67**: 778-785 [PMID: 22135228]
- 39 **Rouvière O**, Valette O, Grivolat S, Colin-Pangaud C, Bouvier R, Chapelon JY, Gelet A, Lyonnet D. Recurrent prostate cancer after external beam radiotherapy: value of contrast-enhanced dynamic MRI in localizing intraprostatic tumor--correlation with biopsy findings. *Urology* 2004; **63**: 922-927 [PMID: 15134982 DOI: 10.1016/j.urol.2003.12.017]
- 40 **Haider MA**, Chung P, Sweet J, Toi A, Jhaveri K, Ménard C, Warde P, Trachtenberg J, Lockwood G, Milosevic M. Dynamic contrast-enhanced magnetic resonance imaging for localization of recurrent prostate cancer after external beam radiotherapy. *Int J Radiat Oncol Biol Phys* 2008; **70**: 425-430 [PMID: 17881141 DOI: 10.1016/j.ijrobp.2007.06.029]
- 41 **Akin O**, Gultekin DH, Vargas HA, Zheng J, Moskowitz C, Pei X, Sperling D, Schwartz LH, Hricak H, Zelefsky MJ. Incremental value of diffusion weighted and dynamic contrast enhanced MRI in the detection of locally recurrent prostate cancer after radiation treatment: preliminary results. *Eur Radiol* 2011; **21**: 1970-1978 [PMID: 21533634]
- 42 **Donati OF**, Jung SI, Vargas HA, Gultekin DH, Zheng J, Moskowitz CS, Hricak H, Zelefsky MJ, Akin O. Multiparametric prostate MR imaging with T2-weighted, diffusion-weighted, and dynamic contrast-enhanced sequences: are all pulse sequences necessary to detect locally recurrent prostate cancer after radiation therapy? *Radiology* 2013; **268**: 440-450 [PMID: 23481164 DOI: 10.1148/radiol.13122149]
- 43 **Tamada T**, Sone T, Higashi H, Jo Y, Yamamoto A, Kanki A, Ito K. Prostate cancer detection in patients with total serum prostate-specific antigen levels of 4-10 ng/mL: diagnostic efficacy of diffusion-weighted imaging, dynamic contrast-enhanced MRI, and T2-weighted imaging. *AJR Am J Roentgenol* 2011; **197**: 664-670 [PMID: 21862809 DOI: 10.2214/AJR.10.5923]
- 44 **Uchida T**, Ohkusa H, Yamashita H, Shoji S, Nagata Y, Hyodo T, Satoh T. Five years experience of transrectal high-intensity focused ultrasound using the Sonablate device in the treatment of localized prostate cancer. *Int J Urol* 2006; **13**: 228-233 [PMID: 16643614]
- 45 **Poissonnier L**, Chapelon JY, Rouvière O, Curiel L, Bouvier R, Martin X, Dubernard JM, Gelet A. Control of prostate cancer by transrectal HIFU in 227 patients. *Eur Urol* 2007; **51**: 381-387 [PMID: 16857310 DOI: 10.1016/j.eururo.2006.04.012]
- 46 **Rouvière O**, Lyonnet D, Raudrant A, Colin-Pangaud C, Chapelon JY, Bouvier R, Dubernard JM, Gelet A. MRI appearance of prostate following transrectal HIFU ablation of localized cancer. *Eur Urol* 2001; **40**: 265-274 [PMID: 11684842]
- 47 **Rouvière O**, Girouin N, Glas L, Ben Cheikh A, Gelet A, Mège-Lechevallier F, Rabilloud M, Chapelon JY, Lyonnet D. Prostate cancer transrectal HIFU ablation: detection of local recurrences using T2-weighted and dynamic contrast-enhanced MRI. *Eur Radiol* 2010; **20**: 48-55 [PMID: 19690866 DOI: 10.1007/s00330-009-1520-5]
- 48 **Casciani E**, Poletini E, Carminini E, Floriani I, Masselli G, Bertini L, Gualdi GF. Endorectal and dynamic contrast-enhanced MRI for detection of local recurrence after radical prostatectomy. *AJR Am J Roentgenol* 2008; **190**: 1187-1192 [PMID: 18430830 DOI: 10.2214/AJR.07.3032]
- 49 **Sciarra A**, Panebianco V, Salciccia S, Osimani M, Lisi D, Ciccariello M, Passariello R, Di Silverio F, Gentile V. Role of dynamic contrast-enhanced magnetic resonance (MR) imaging and proton MR spectroscopic imaging in the detection of local recurrence after radical prostatectomy for prostate cancer. *Eur Urol* 2008; **54**: 589-600 [PMID: 18226441 DOI: 10.1016/j.eururo.2007.12.034]
- 50 **Puech P**, Sufana-Iancu A, Renard B, Lemaitre L. Prostate MRI: can we do without DCE sequences in 2013? *Diagn Interv Imaging* 2013; **94**: 1299-1311 [PMID: 24211261 DOI: 10.1016/j.diii.2013.09.010]

P- Reviewer: Arcangeli S, Shoji S **S- Editor:** Cui LJ **L- Editor:** A
E- Editor: Lu YJ



Endovascular treatment of pulmonary embolism: Selective review of available techniques

John L Noshier, Arjun Patel, Sugeet Jagpal, Christopher Gribbin, Vyacheslav Gendel

John L Noshier, Arjun Patel, Christopher Gribbin, Vyacheslav Gendel, Division of Interventional Radiology, Department of Radiology, Rutgers Robert Wood Johnson Medical School, New Brunswick, NJ 08901, United States

Sugeet Jagpal, Division of Pulmonary and Critical Care Medicine, Department of Medicine, Rutgers Robert Wood Johnson Medical School, New Brunswick, NJ 08901, United States

ORCID number: John L Noshier (0000-0002-9358-5057); Arjun Patel (0000-0003-1088-6880); Sugeet Jagpal (0000-0002-8076-7652); Christopher Gribbin (0000-0002-6952-7252); Vyacheslav Gendel (0000-0002-8765-4626).

Author contributions: All authors equally contributed to this paper with conception and design of the study, literature review and analysis, drafting, critical revision and editing, and final approval of the final version.

Conflict-of-interest statement: No potential conflicts of interest. No financial support.

Open-Access: This article is an open-access article which was selected by an in-house editor and fully peer-reviewed by external reviewers. It is distributed in accordance with the Creative Commons Attribution Non Commercial (CC BY-NC 4.0) license, which permits others to distribute, remix, adapt, build upon this work non-commercially, and license their derivative works on different terms, provided the original work is properly cited and the use is non-commercial. See: <http://creativecommons.org/licenses/by-nc/4.0/>

Manuscript source: Unsolicited manuscript

Correspondence to: John L Noshier, MD, Division of Interventional Radiology, Department of Radiology, Rutgers Robert Wood Johnson Medical School, 1 Robert Wood Johnson Place, MEB404, New Brunswick, NJ 08901, United States. noshier@rwjms.rutgers.edu
Telephone: +1-732-2357721

Received: July 18, 2017

Peer-review started: July 20, 2017

First decision: August 4, 2017

Revised: August 11, 2017

Accepted: September 3, 2017

Article in press: September 3, 2017

Published online: December 28, 2017

Abstract

Acute pulmonary embolism (PE) is the third most common cause of death in hospitalized patients. The development of sophisticated diagnostic and therapeutic modalities for PE, including endovascular therapy, affords a certain level of complexity to the treatment of patients with this important clinical entity. Furthermore, the lack of level I evidence for the safety and effectiveness of catheter directed therapy brings controversy to a promising treatment approach. In this review paper, we discuss the pathophysiology and clinical presentation of PE, review the medical and surgical treatment of the condition, and describe in detail the tools that are available for the endovascular therapy of PE, including mechanical thrombectomy, suction thrombectomy, and fibrinolytic therapy. We also review the literature available to date on these methods, and describe the function of the Pulmonary Embolism Response Team.

Key words: Pulmonary embolism; Thrombolysis; Endovascular; Interventional radiology; Thrombectomy; Fibrinolysis

© The Author(s) 2017. Published by Baishideng Publishing Group Inc. All rights reserved.

Core tip: Endovascular treatment of pulmonary embolism (PE) represents several methods of minimally invasive therapy of this important clinical entity, including mechanical thrombectomy, suction thrombectomy, and fibrinolytic therapy. With this paper, we hope to provide a detailed review of these methods, which is critical to understanding the tools that are available to the clinician for the treatment of PE.

Noshier JL, Patel A, Jagpal S, Gribbin C, Gendel V. Endovascular

treatment of pulmonary embolism: Selective review of available techniques. *World J Radiol* 2017; 9(12): 426-437 Available from: URL: <http://www.wjgnet.com/1949-8470/full/v9/i12/426.htm> DOI: <http://dx.doi.org/10.4329/wjr.v9.i12.426>

INTRODUCTION

Acute pulmonary embolism (PE) is the third most common cause of death in hospitalized patients^[1]. The development of sophisticated diagnostic and therapeutic modalities for PE, including medical and surgical treatment as well as newly developed endovascular therapy, affords a certain level of complexity to the treatment of patients with this important clinical entity.

Pathophysiology

PE, by definition, involves emboli to the pulmonary arterial circulation, which can induce acute pulmonary arterial hypertension, right heart strain, and in some patients, right ventricular infarction^[2]. Angiographic studies have demonstrated that pulmonary artery pressures increase when the embolic load occludes more than 30%-50% of the cross sectional area of the pulmonary arterial bed^[3]. Clot burden alone does not determine the degree of pulmonary hypertension. The disruption of the alveolar capillary membrane by thrombus results in disruption of the diffusion of oxygen, with subsequent decreased oxygen binding to hemoglobin. Both hypoxia and the release of vasoconstrictors precipitate vasoconstriction of the pulmonary circulation, which contributes to the acute development of pulmonary hypertension^[4]. This pulmonary hypertension leads to right ventricular dilatation and subsequent right ventricular failure. Underlying cardiopulmonary disease influences the ability of the right heart to adapt to increased pulmonary artery pressure.

Clinical presentation

The majority of pulmonary emboli are clinically silent. This is due to the dual blood supply of the lung through the bronchial and pulmonary arteries, as well as the fact that most emboli to the lung are small and resolve before the manifestation of any physical signs and symptoms. The clinical presentation of PE depends upon its severity, which tends to vary widely. Patients with PE can range from being completely asymptomatic to presenting with cardiovascular collapse^[5]. According to the Prospective Investigation of Pulmonary Embolism Diagnosis II (PIOPED II) study, the most commonly occurring complaints in patients with PE were sudden onset dyspnea, pleuritic chest pain, cough, orthopnea, calf/thigh pain with associated swelling, erythema, edema, tenderness and palpable cords, wheezing, and hemoptysis^[6]. On physical exam, the most common presenting signs were tachypnea and tachycardia. Less commonly seen, but still significant, were rales, decreased breath sounds, an accentuated pulmonic component of the second heart sound, jugular venous

distension, and fever. Patients with massive PE may present with acute right ventricular failure leading to increased jugular venous pressure, a right-sided third heart sound, parasternal lift, cyanosis, hypotension, and shock^[7,8].

Cardiovascular collapse is the product of a large sized or saddle embolus, and therefore an uncommon presenting sign, given that most pulmonary emboli are small. It should still be noted, however, that in patients with comorbid severe pulmonary hypertension who suffer a small PE, entry into shock is still a strong possibility^[7,8]. Syncope is a less common but clinically significant initial presenting sign of PE that occurs in approximately 10% of patients^[9]. As PE causes a ventilation/perfusion (V/Q) mismatch, patients present with hypoxemia that results in hyperventilation, and ultimately hypocapnia, which leads to respiratory alkalosis. These findings, along with a widened alveolar-arterial oxygen gradient, are the most common findings on arterial blood gas analysis. Electrocardiographic abnormalities include nonspecific ST segment or T wave changes^[10]. On chest radiography, parenchymal abnormality may be found^[10]; however, cardiomegaly is the most common radiographic abnormality associated with acute PE^[11]. Myocardial stretching, a marker of increased pulmonary pressures can be detected in the serum *via* elevated troponin and pro-BNP levels and are markers for increased risk of right heart failure and potentially right ventricular infarct^[12].

Of the 80% of patients with PE who are normotensive, it is estimated that 27%-55% have echocardiographic evidence of RV dysfunction^[13,14]. Normotensive patients with RV dysfunction have an increased risk of death from PE and recurrent PE^[14]. The impact of RV dysfunction on mortality has been demonstrated in two multi-center registries. In the International Cooperative Pulmonary Embolism registry of 2454 patients with PE in the normotensive group with RV hypokinesis, the all-cause mortality was doubled at 3 mo^[15]. In the Management Strategy and Prognosis of Pulmonary Embolism Registry, normotensive patients with RV dysfunction had an in-hospital mortality of 7.1% and a rate of recurrent PE of 14%^[16].

The current mainstays in the imaging diagnosis of PE are computed tomographic pulmonary angiography (CTPA) and echocardiography, which aid in determining the significance of PE on right ventricular function. Historically, the diagnosis was often made by ventilation/perfusion nuclear medicine scans, which is still employed for patients who cannot receive iodinated contrast material. Catheter based pulmonary angiography, the "gold standard" for the diagnosis of PE, has been supplanted by CTPA and is now performed almost exclusively only prior to a catheter based intervention. Depending on the institution, patients with suspected PE who present in shock or are severely ill may be first evaluated with echocardiography in the emergency room. Evidence of right ventricular dysfunction, such as paradoxical septal bowing or an elevated right ventricle to left ventricle ratio (RV/LV) may then be triaged rapidly

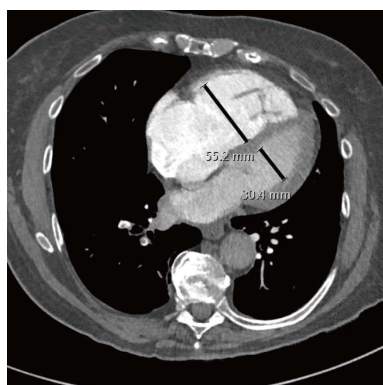


Figure 1 Right/left ventricular ratio greater than 0.9, measured in the basal portion of the ventricles at the level of the atrioventricular valve.

for CTPA or, if the diagnosis is sufficiently strong clinically and the patient is unstable, straight for angiography and intervention. In these patients, echocardiography may also disclose the presence of free floating clot in the right heart which, if available, may indicate surgical or large bore catheter intervention. More commonly, patients who are more stable will first be evaluated with CTPA. This, along with troponin and pro-BNP assays, permits assignment of patients to massive, submassive or low risk categories of PE. In addition to demonstrating the extent and distribution of PE, the CTPA can provide a sufficient indication of RV dysfunction, in the absence of echocardiography. Signs of RV dysfunction on CTPA include an elevated RV/LV ratio (generally shown to be > 0.9), septal bowing and reflux of contrast into the hepatic veins (Figure 1).

MEDICAL TREATMENT

The American Heart Association (AHA) divides PE into three categories: Massive PE, submassive PE, and low risk PE^[12]. Massive PE is defined as acute PE with sustained hypotension (systolic BP < 90 mmHg for at least 15 min or requiring inotropic support), pulselessness, or persistent profound bradycardia (heart rate < 40 beats per minute with signs or symptoms of shock). Submassive PE presents with signs of right ventricular dysfunction including right ventricular dilatation on chest CTA (Figure 1), echocardiographic signs of right ventricular (RV) dysfunction, and/or serum markers consistent with myocardial stretching such as troponin and pro-BNP. Low risk PE shows no signs of RV dysfunction or biomarker evidence of strain^[12]. Current treatment recommendations are for full anticoagulation for all three categories of PE, with thrombolysis for massive PE and to be considered in submassive PE^[12]. Class III, Level B evidence recommends against fibrinolysis for low risk PE^[12]. Catheter embolectomy and fragmentation or surgical embolectomy are alternatives for patients with massive PE with a contraindication for fibrinolysis^[12]. In general, mechanical embolectomy should be reserved for main and lobar pulmonary arterial branches^[12].

Organization of pulmonary emboli begins with adherence of clot to the vessel wall and the formation of a thin lining of endothelial cells over its surface, followed by ingrowth of cells from the intima media and capillary buds into the thrombus^[17]. Serial imaging has demonstrated that reduction in amount of thrombus is 10% after 24 h, 40% after 7 d, and 50% after 2 to 4 wk^[18]. Complete resolution is likely achieved in 70%-85% of patients at 6 to 12 mo after initial PE diagnosis^[19]. The resolution of thrombi appears to plateau after 3 mo of adequate treatment, and only small amounts of improvement are seen after that time^[20]. This forms the basis of recommendations for anticoagulation for 6 mo.

Unresolved thrombi can result in persistent perfusion defects and subsequently lead to chronic thromboembolic pulmonary hypertension (CTEPH). CTEPH following 3 mo of effective anticoagulation is defined by: (1) invasively measured mean pulmonary artery pressure > 25 mmHg with a pulmonary capillary wedge pressure < 15 mmHg; and (2) at least one segmental perfusion defect^[21]. Patients with PE can have residual symptoms of reduced functional status, persistent thrombi, limitations of cardiopulmonary function, and CTEPH. The incidence of CTEPH is low, seen in 3.1% of patients at 1 year and in 3.8% of patients at 2 years in a cohort of 223 patients with confirmed PE, as reported by Pengo *et al.*^[22]. Although patients with CTEPH are a very small component of the total PE population, they unfortunately have the most functional impairment, and pulmonary endarterectomy and PAH Group 1 therapies are often discussed in this population^[12].

SURGICAL TREATMENT

Several surgical treatment options are available for the management of PE. Historically, surgical pulmonary embolectomy has been indicated in patients who are hemodynamically unstable secondary to acute massive PE. Candidates for surgical embolectomy have failed or are not candidates for thrombolytic therapy. Surgical pulmonary embolectomy is also recommended for patients with persistent hemodynamic instability, or in patients with RV dysfunction that persists despite the use of fibrinolytic therapy^[23]. There are reports in which surgical embolectomy is shown to be superior in the long term compared to thrombolysis in hemodynamically comparable patients. In a 2006 study by Meneveau *et al.*^[24], 488 patients with PE underwent thrombolysis, 40 of whom did not respond to the therapy. Of these 40 patients failing thrombolytic therapy, 14 patients were treated by rescue surgical embolectomy, and 26 were treated by repeat thrombolysis. Ultimately, rescue surgical embolectomy led to a better in-hospital course when compared with repeat thrombolysis in patients with massive PE who did not respond to thrombolysis^[24]. In experienced centers, surgical embolectomy is considered to be a safe procedure with low mortality, providing improved postoperative right ventricular function and

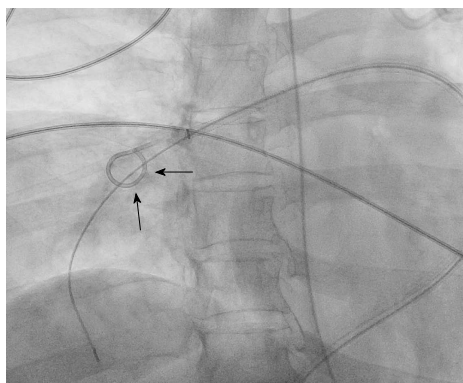


Figure 2 A pigtail catheter in the right pulmonary artery is rotated to fragment and then disperse clot into the larger volume peripheral circulation.

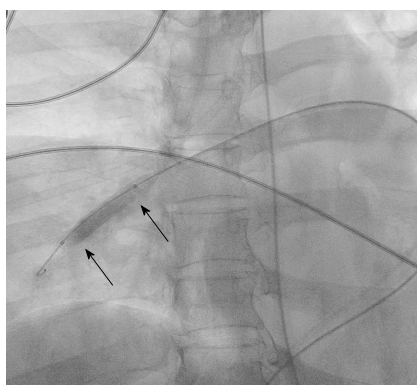


Figure 3 An angioplasty balloon catheter in the right pulmonary artery being used to fragment and disperse clot into the larger volume peripheral circulation.

pulmonary pressure as well as improved long-term outcome^[25]. In a study of 37 consecutive cases, Edelman *et al*^[25] demonstrated that elimination of a large portion of the clot burden could be life-saving. They concluded that pulmonary embolectomy should be considered as an initial treatment strategy in patients with massive or submassive pulmonary embolus with a large burden of proximal clot^[25].

CATHETER DIRECTED THERAPY

Catheter directed therapy of PE includes mechanical thrombectomy/fragmentation, mechanical thrombectomy plus thrombolytic therapy, and catheter delivered thrombolytic therapy. The goal of catheter directed therapy is to decrease afterload on the right ventricle while reducing clot burden and long-term sequelae of CTEPH. Displacement of centrally occlusive thrombus to a more peripheral distribution in pulmonary arterial branches may decrease afterload in the right ventricle but may not address clot burden. We will not attempt to discuss all devices but limit discussion to the devices most reported for use in the pulmonary arteries. Given the large number of existing devices, it is clear that an ideal device is not currently available.

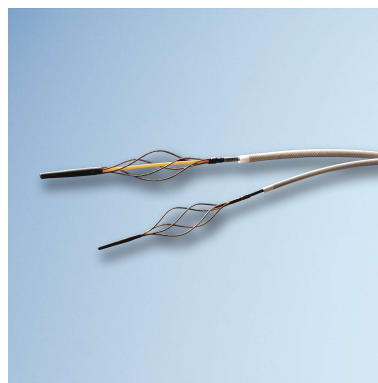


Figure 4 Trerotola thrombolytic device (Permission to use image granted by Teleflex Inc., Wayne, PA, United States).

Mechanical thrombectomy

Purely mechanical approaches to central pulmonary emboli include clot fragmentation, fragmentation with aspiration, and rheolytic thrombectomy^[26,27]. Clot fragmentation has been achieved with procedures as simple as rotation of a pigtail catheter within the thrombus either manually or with mechanical assistance (Figure 2). Angioplasty balloons inflated within clot provide an alternative approach to fragmentation (Figure 3). Other mechanical devices such as the Trerotola Mechanical Thrombectomy Device (Teleflex Inc., Wayne, PA, United States) designed for use in thrombosed dialysis grafts have been used in the pulmonary arteries with mixed results (Figure 4).

There are several rheolytic thrombectomy devices, which have been used off label in the pulmonary arteries. The Amplatzer thrombectomy device (Microvena, White Bear Lake, MN) is a 6-French catheter that incorporates a high-pressure air-driven high-speed impeller, creating a vacuum vortex-pulling clot into the distal tip of the catheter, fragmenting the thrombus, then expelling particles, most of which measure 50 μm or less^[26,27].

The Angiojet catheter (Boston Scientific, Marlborough, MA, United States) is one of the most frequently used devices, which provides both clot fragmentation and aspiration of clot fragments. Saline jets directed into the clot at the distal end of the catheter result in clot fragmentation. These jets may also be used to distribute thrombolytic agents into the clot in the "power pulse mode". At the same time, aspiration of clot fragments is achieved at catheter sideports from high velocity saline looping back into a second lumen creating a Venturi effect (Figure 5). These procedures displace obstructive emboli from a central location into the larger volume peripheral pulmonary arterial vasculature, resulting in reduction of pulmonary artery pressure and afterload on the right heart^[28]. Frequently, mechanical approaches are combined with infusion systems delivering low dose thrombolytics into residual thrombus.

Suction thrombectomy

Suction thrombectomy was one of the earliest ap-

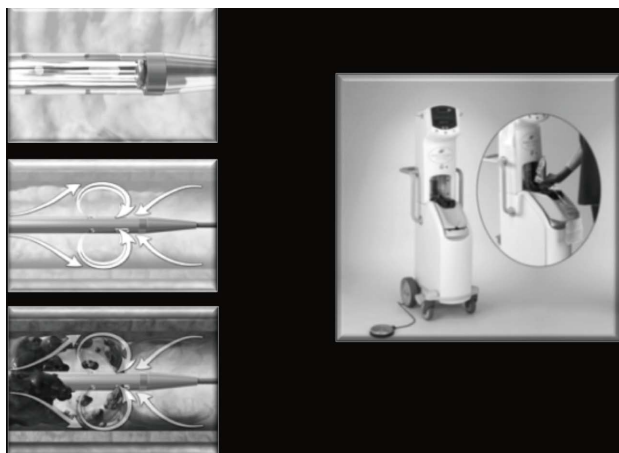


Figure 5 Angiojet rheolytic thrombectomy device (Boston Scientific, Marlborough, MA, United States). Distal Saline jets fragment clots and high velocity saline loops into a second lumen, aspirating fragments of clot into the sideports through the Venturi effect (Image provided courtesy of Boston Scientific. ©2017 Boston Scientific Corporation or its affiliates. All rights reserved).

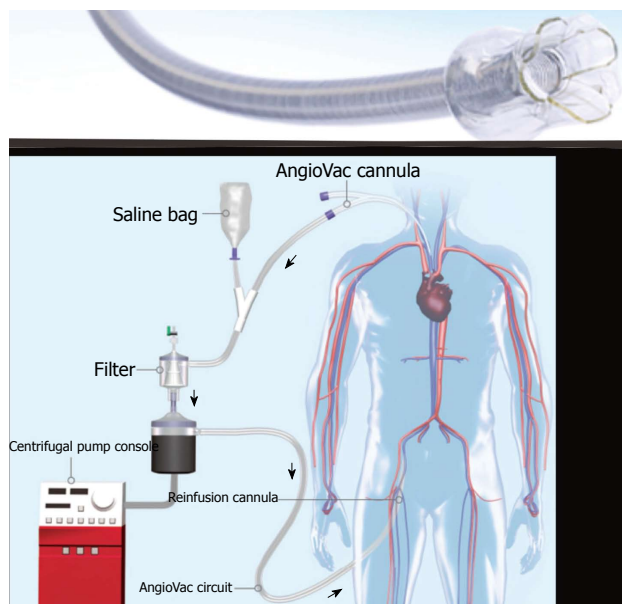


Figure 6 Angiovac catheter (Angiodynamics, Inc., Latham, NY, United States) and reperfusion circuit, in which aspirated clot is filtered from aspirated blood, which is subsequently returned to the patient (permission to use image granted by Angiodynamics, Inc.).

proaches to transcatheter treatment of pulmonary emboli, introduced by Greenfield, using a 12-French catheter with a cup on its distal end. Suction was applied to the catheter hub with a large volume syringe. A portion of thrombus was engaged in the cup and removed along with trailing adherent thrombus through a large diameter vascular sheath in either the femoral or jugular veins.

More recent approaches involve aspiration of thrombus into the lumen of an aspiration catheter of varying diameters with discharge into an aspiration container. The Angiovac system (Angiodynamics Inc., Latham, NY) consists of a 22-French coil reinforced cannula with

a balloon actuated expandable funnel-shaped distal tip. The catheter is part of a veno-venous recirculation system with aspirated thrombus and blood separated and returned to the patient through a large central venous return cannula (Figure 6). The system requires a perfusionist to be present during the procedure and the added time required to assemble this team.

An alternative large lumen suction device is the FlowTrieve system (Inari Medical, Irvine, CA, United States), in which a large bore (20-French) sheath is introduced for placement of suction catheter, which is connected to a retraction aspirator, providing a vacuum for clot aspiration. Blood admixed with clot does not have a means to return to the circulation (Figure 7). The advantage of the large bore catheters is the ability to remove large volumes of thrombus rapidly; however, their size and rigidity makes access to pulmonary artery branches more difficult. In addition, stiffness increases the possibility of injury to the heart or to the pulmonary artery.

The Penumbra system (Penumbra Inc., Alameda, CA, United States) is a suction aspiration system first used in the endovascular treatment of stroke. The Penumbra INDIGO CAT 8 system is a flexible 8-French aspiration catheter, which is connected to a continuous suction vacuum system. A wire separator in the catheter lumen facilitates clot retrieval (Figure 8). As with the FlowTrieve device, the Penumbra lacks a means to return blood to the patient and can lead to significant blood loss if not embedded in clot. None of the suction systems is FDA approved in the United States for the treatment of PE, and their use is considered "off label". The FlowTrieve system has received approval from the FDA for the FLARE IDE clinical trial for patients with submassive pulmonary emboli and is currently recruiting.

Fibrinolytic therapy

Fibrinolysis is most effective when the agent is delivered directly into the thrombus. There are several catheter systems available for delivery of fibrinolytic agents directly into the thrombus. The Unifuse infusion system (Angiodynamics, Latham, NY, United States) consists of a multi-hole catheter with an end hole and side holes distributed in variable lengths along the distal catheter. Their distribution is defined by radiopaque markers. The catheter is introduced over a standard guidewire. Following desired placement in the clot, an occluding ball guide wire is introduced to obstruct the end hole, thereby forcing the infusate out the side holes. This catheter can be used to simply infuse or pulse spray fibrinolytics by forcible injection at the catheter hub (Figure 9).

Ultrasound assisted infusion of thrombolytics through the Ekos system (Ekos Corp., Bothel, WA, United States) utilizes an ultrasonic core to generate an acoustic field dispersing the fibrinolytic agent into the clot. In addition, this acoustic field is felt to disaggregate thrombus with separation of fibrin crosslinks, accelerating clot lysis. The system consists of a 5.4-French infusion catheter with markers delineating the active area, an ultrasound core

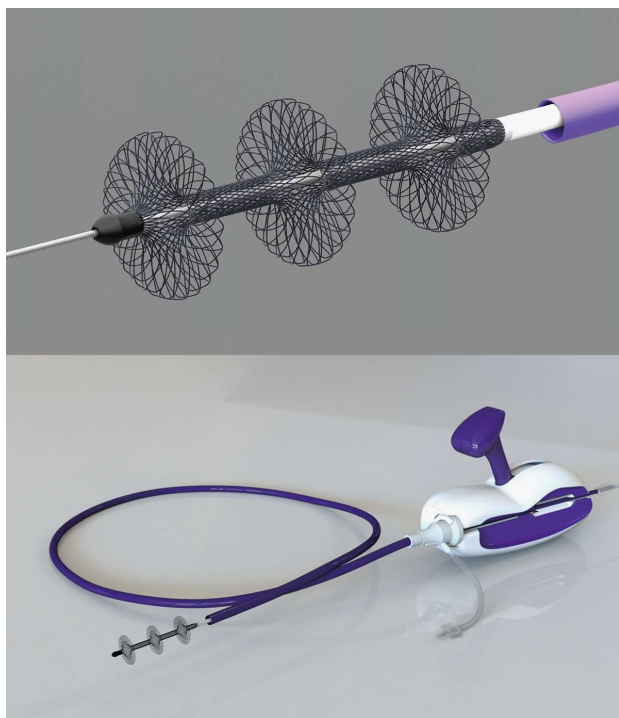


Figure 7 Flowtriever device (Inari Medical, Irvine, CA, United States) with three braided nitinol disks to engage clot and pull it into the aspiration guide catheter for evacuation by the retraction aspirator (Permission to use image granted by Inari Medical).

transducer, and a control unit. The catheter has both a drug delivery lumen and a central coolant channel (Figure 10).

REVIEW OF RESULTS

In spite of greater than 30 years of experience with catheter directed therapy for acute PE, controversy still exists as to its precise role. This is primarily related to the lack of level I evidence of its safety and effectiveness. Most evidence is based on small non-controlled cohort studies with non-consecutive recruitment and varying criteria for success (Table 1).

Any review of results of studies dealing with PE treatment should begin with a brief explanation of the Miller score, which is one of several scoring systems that attempt to objectively quantify the magnitude of PE (Figure 11). Described in 1975^[29] and based on pulmonary arteriography it is the sum of obstruction and perfusion scores. The obstruction index divides the lung into nine segments on the right and seven on the left. Thrombus in any segment is given a score of 1. Thrombus proximal to segmental branches is given a score of the number of branches peripheral to the thrombus (*i.e.*, right lower lobe pulmonary artery = 4, saddle embolus = 16). The perfusion index divides each lung into upper, middle and lower zones scored as no perfusion (3), severely reduced perfusion (2), mildly reduced perfusion (1), and normal perfusion (0). Therefore the worst Miller index combining obstruction

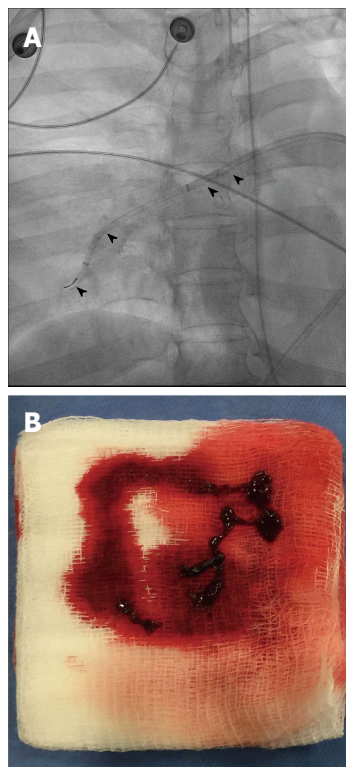


Figure 8 Penumbra device. A: Penumbra Indigo CAT-8 (Penumbra, Inc., Alameda, CA, United States) in the right pulmonary artery. The guiding catheter (arrowheads) is in the right main pulmonary artery and the aspiration catheter (arrows) is in the right lower lobe pulmonary artery. The separator wire used to promote aspiration is exiting the aspiration catheter; B: Small volume clot aspirated with the Penumbra Indigo CAT-8 system.

and perfusion is 34.

Suction thrombectomy

The earliest reports were those describing suction embolectomy with the Greenfield suction embolectomy catheter. Greenfield reported 46 patients treated with the 12-French suction catheter^[30]. Of these patients, 33 had sustained massive pulmonary emboli, 4 submassive, and 9 chronic. Mean pulmonary arterial pressure was reduced from 32 to 24 mmHg in 31 patients, in whom it was measured with clinical success in 36/46 patients. After the adoption of prophylactic inferior vena cava (IVC) filters following the procedure, the 30 d survival increased from 50% in the first 10 patients to 70% in the subsequent 36 patients. Because of the size and difficulty of placement of the Greenfield suction embolectomy catheter, the device fell out of favor.

Currently, two large bore aspiration catheters are available. The Angiovac system, approved for use in treating thrombi in the venous system, is being used off-label in the pulmonary arteries. There have been case reports and small series reporting the use of this device with mixed results^[31]. A retrospective review of five consecutive patients in whom the Angiovac was used included four patients with massive PE and one with submassive PE^[32]. Technical success, defined as

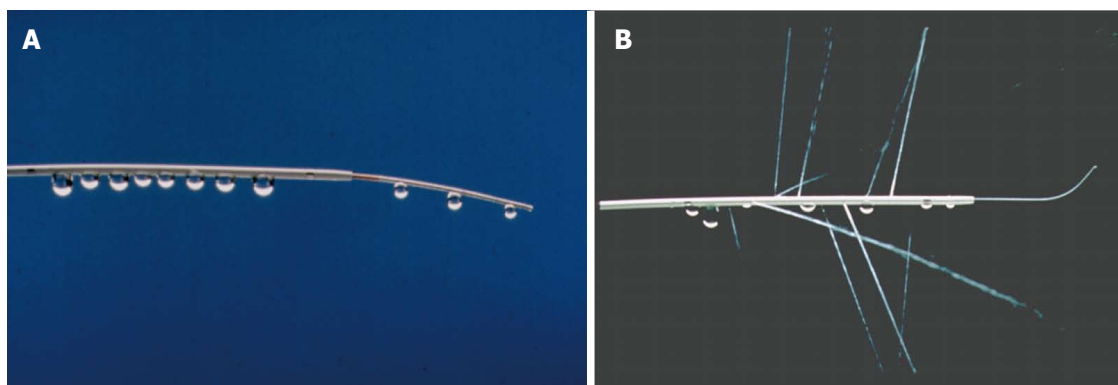


Figure 9 Multiholed infusion catheter. A: A multiholed infusion catheter with sideholes dispersing infusate within clot and infusion wire further distributing the infusate while also occluding the endhole of the infusion catheter, forcing flow out of the sideholes of the catheter (Permission to use image granted by Angiodynamics, Inc.); B: A multiholed infusion catheter with sideholes dispersing infusate within clot and infusion wire further distributing the infusate while also occluding the endhole of the infusion catheter, forcing flow out of the sideholes of the catheter (Permission to use image granted by Angiodynamics, Inc.).

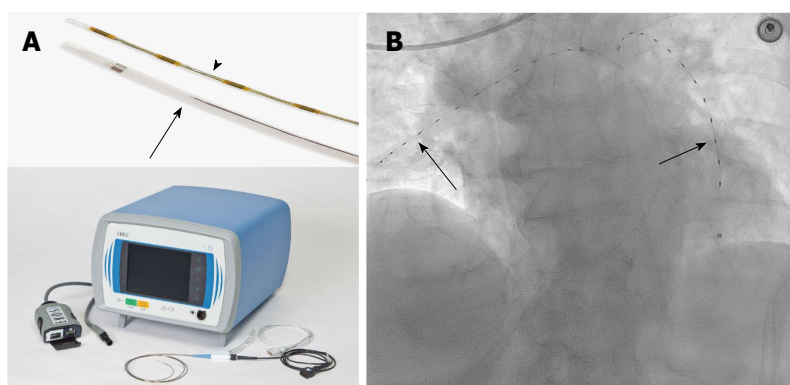


Figure 10 Ekos system. A: Ekos system with multiholed infusion catheter (arrow), ultrasonic core transducer (arrowhead) and control unit (Permission to use image granted by Ekos Corp., Bothell, WA, United States); B: Ekos catheters (arrows) with ultrasonic core transducers in place in the right and left pulmonary arteries.

successful removal of some thrombus combined with reduction of the Miller score by greater than or equal to 5 was achieved in two of the four patients with massive PE. Four patients died at a mean of 7.3 d, all having presented with massive PE. One death was related to catheter perforation of the right ventricular free wall. In another small series of three patients in whom thrombectomy of the pulmonary arteries was attempted, the procedure was unsuccessful in two of the three patients. Lack of success was attributed to size, stiffness and lack of maneuverability of the device.

There is even less information on the use of the FlowTriever device in the pulmonary arteries. A single case of success in a saddle embolus in the pulmonary artery was recently reported^[33]. It is uncertain if similar problems with stiffness and lack of maneuverability are encountered with this device. The FlowTriever FLARE trial will help clarify these issues in a larger cohort of patients. Unfortunately this trial excludes patients with massive PE - a group of patients in whom suction embolectomy is most appropriate.

The Penumbra device is another suction device currently available in an 8-French system, providing the flexibility for placement in segmental branches of the pulmonary artery. However, luminal diameter limits the

volume of clot aspirated. There is no evidence available at the current time to support its use.

Mechanical thrombectomy

The Amplatz thrombectomy device has been used in the pulmonary arteries and reported about in small series. A report by Muller-Hulsbeck included 9 patients, out of which, 5 were treated with additional tPA^[34]. Miller index was reduced from 18 to 11. Of interest, the mean pulmonary arterial pressure was reduced from 57 to 55 mmHg after mechanical thrombectomy. The addition of fibrinolytic therapy achieved further reduction of mean pulmonary arterial pressure to 39 mmHg, raising question of the value of the mechanical component of the procedure.

The Angiojet device is the most studied rheolytic thrombectomy device. A study by Nassiri *et al.*^[35] reviewed experience with 15 consecutive patients, one with massive and 14 with submassive pulmonary emboli. Adjunctive tPA was administered in 10 patients. Completion angiography was used to assess success. Significant clot resolution (> 75%) was observed in 9 patients, moderate (50%-75%) in 5 patients, and minimal (< 50%) in 1 patient. All patients receiving adjunctive tPA had significant or moderate clot resolution.

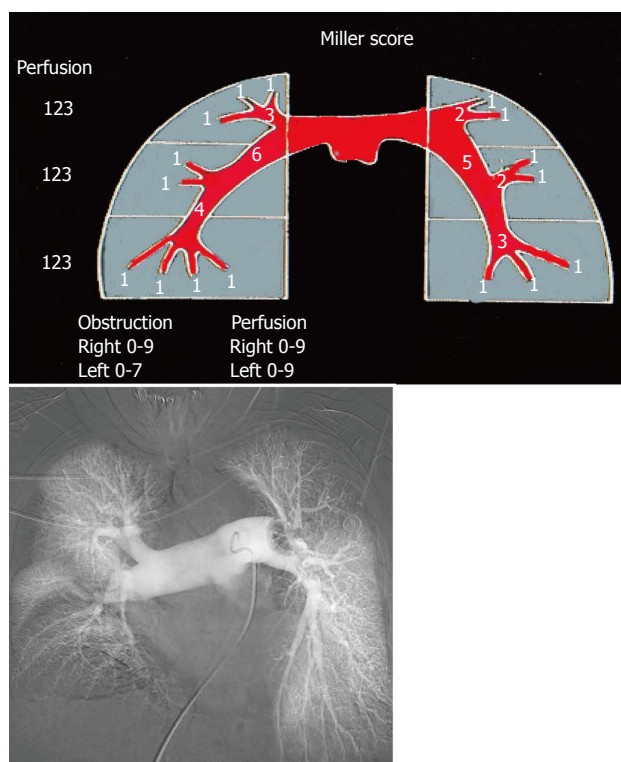


Figure 11 Miller Score. Pulmonary arteriogram demonstrating left main pulmonary artery embolus (obstruction score 7) and severely reduced perfusion of the upper and middle zones of the left lung (perfusion index 2 + 2). There is occlusion of the left lower lobe pulmonary and middle lobe pulmonary artery (obstructive score 4 + 2) with perfusion severely reduced in the lower lobe and mildly reduced in the middle lobe (perfusion index 2 + 1). This patient's combined Miller score is therefore 20.

There were no in-hospital deaths or recurrent pulmonary emboli. Two patients had post procedural renal failure and there was one case of cardiopulmonary arrest.

Chechi retrospectively reviewed 51 patients presenting with massive (in 22 patients) or submassive (in 29 patients) pulmonary emboli^[36]. Technical success determined by angiography was achieved in 92% of cases, with mean reduction of the Miller index by 51%. Adjunctive fibrinolytic therapy was performed in 21% of patients. The in-hospital mortality was 42% in patients presenting with shock, 12% in patients with hypotension, and 3.4% in patients with submassive pulmonary emboli. Renal failure was reported in 24% of patients, while bradycardia requiring transvenous pacing was reported in 8%.

Systemic complications of renal insufficiency, bradycardia, and asystole are frequently reported with the Angiojet device. Both complications stem from red blood cell destruction leading to the release of adenosine, causing bradycardia and asystole. Some operators limit activation of the device to five-second intervals, separating the intervals to limit the amount of adenosine in the circulation. Renal insufficiency is felt to result from hemoglobinuria and resultant acute tubular necrosis. Aggressive hydration and administration of bicarbonate to raise urine pH to above 6.5 may diminish the tubular toxicity of hemoglobin^[37].

Fibrinolytic therapy

Patients with massive PE who have failed systemic thrombolysis, have absolute contraindications to thrombolysis, or cannot await the two hour time interval for administration of systemic thrombolytics are clearly candidates for either catheter directed therapy or surgical thrombo-embolectomy. Unfortunately few centers are equipped for urgent surgical thrombo-embolectomy and few will achieve the survival outcomes of centers with expertise in pulmonary thrombo-embolectomy.

A meta-analysis of catheter directed treatment of PE by Tafur^[38] included 24 studies, enrolling 700 patients, of whom 653 received endovascular treatment. Pooled data estimated risk of death in non-ultrasound assisted thrombolysis (USAT) studies at 9% and 4% in the USAT group. In studies using risk stratification, the Miller index decreased from 19.4 to 9.9 following intervention. In studies including pulmonary artery pressures, mean pressures were reduced from 57 to 36 mmHg. The main safety outcome of major bleeding was 4% in the USAT studies and 10% in the non-USAT group.

A review of data of a nationwide inpatient sample of 72230 patients with PE who were considered unstable reported a case fatality rate of 47% in patients not receiving thrombolytic therapy and 15% in patients receiving thrombolytics. However 70% of these patients were denied thrombolytics for various reasons^[39]. Given this data randomization of patients with massive PE and contraindications to systemic thrombolysis to catheter directed intervention vs no therapy raises both ethical concerns and recruitment challenges and is unlikely to occur.

Catheter directed therapy in massive PE

There is evidence supporting the use of catheter directed therapy in patients with massive PE. A meta-analysis of catheter directed therapy in 2009^[40] identified a subset 594 patients from 35 uncontrolled studies treated for massive PE defined by hypotension. Clinical success was determined by stabilization of hemodynamics, resolution of hypoxia, and survival. Ninety six percent of patients did not receive thrombolytics before catheter directed therapy. Thirty three percent of patients received mechanical thrombectomy alone, while 60%-67% received both mechanical thrombectomy and pharmacologic thrombolysis. Mechanical technique most often used was pigtail catheter fragmentation in 69% of patients; used alone in 53%. Clinical success was achieved in 86.5% of patients. Clinical success was higher in studies in which patients received catheter directed thrombolytic therapy compared to those in which thrombolytic was less frequently given. The pooled risk of minor complications was 7.9% and major complication 2.4%. Of interest, five procedural related deaths were all associated with use of the Angiojet device.

Given the fatality rate that approaches 50%, as reported for untreated patients with massive PE, and subset analysis of catheter directed therapy in patients with massive PE reporting mortality rates as low as

Table 1 Comparison of pulmonary embolism treatment devices based on currently available evidence

Treatment method	Type of device	No. of patients	Outcomes
Suction thrombectomy	Greenfield suction embolectomy catheter	$n = 46^{[32]}$	Mean PAP reduction from 32 to 24 mmHg in 31 patients
		33 with massive PE	
		4 with submassive PE	
	Angiovac	9 with chronic PE	Technical success in 2 of the 4 patients with massive PE
		$n = 5^{[34]}$	
		4 with massive PE	
Mechanical thrombectomy	Flowtriever	1 with submassive PE	Procedure successful
		$n = 1^{[35]}$	
		FLARE trial - ongoing	
	Penumbra Amplatz thrombectomy device	None	None
		$n = 9^{[36]}$	
		(5 were treated with tPA)	
Catheter directed fibrinolysis	Angiojet	$n = 15^{[37]}$	9 patients - significant clot resolution 5 patients - moderate clot resolution 1 patient - minimal clot resolution
		10 were treated with tPA	
	Angiojet	$n = 51^{[38]}$	92% technical success Mean reduction of Miller index by 51%
		22 patients - massive PE 29 patients - submassive PE	
Catheter directed fibrinolysis	USAT	$n = 59^{[47]}$ (ULTIMA trial)	Greater mean decrease of RV/LV ratio in the UFH + USAT group <i>vs</i> UFH alone (0.30 <i>vs</i> 0.03)
		29 patients - UFH alone 30 patients - unfractionated heparin + USAT	

PE: Pulmonary embolism; USAT: Ultrasound-assisted thrombolysis; PAP: Pulmonary arterial pressure; RV/LV: Right ventricle to left ventricle ratio; UFH: Unfractionated heparin.

15%, this therapy appears to be appropriate. Since many if not most of these patients had received both mechanical as well as pharmaco-mechanical treatment, it is therefore difficult to predict the effectiveness of mechanical thrombo-dispersion-thrombectomy alone. Certainly the next generation of thrombectomy devices will facilitate access to the main pulmonary arteries and segmental branches, improving the efficacy of mechanical thrombectomy. Currently, there is no data supporting the addition of catheter directed therapy to systemic therapy for patients who have responded to systemic therapy in spite of its ability to further decrease clot burden and the sequelae of CTEPH.

Catheter directed therapy in submassive PE

For patients with submassive PE, there is controversy as to the role of both systemic or catheter directed therapy. A meta-analysis of randomized controlled trials comparing systemic thrombolytic therapy with heparin alone in patients with PE showed a benefit only in patients with massive PE^[41]. In contrast, the MAPPET-3 trial^[42] randomized 256 patients with sub-massive PE into heparin plus tPA (118 patients) *vs* heparin plus placebo (138 patients). The primary endpoint of in hospital mortality or clinical deterioration requiring an escalation of treatment was significantly higher in the heparin plus placebo group primarily due to the need for treatment escalation (26% *vs* 10%). Mortality in both groups was low: 3.4% in the heparin plus tPA group and 2.2% in the heparin plus placebo group. No fatal or intracranial hemorrhage was observed.

The PEITHO trial^[43] randomized 1006 patients with submassive PE to systemic tenecteplase (30-50 mg) as a single bolus or placebo with both groups receiving intravenous heparin. The primary endpoints were death, hemodynamic decompensation, confirmed recurrent PE within 7 d, death within 30 d, and major adverse events within 30 d. Death or hemodynamic decompensation occurred in 2.6% of patients in the tenecteplase group and in 5.6% in the placebo group ($P = 0.02$). Extracranial bleeding occurred in 6.3% of the tenecteplase group and in 1.2% of the placebo group ($P \leq 0.001$). Stroke occurred in 2.4% of the tenecteplase group and in 0.2% of the placebo group. At 30 d, the mortality was 2.4% and 3.2% in the tenecteplase and placebo groups, respectively. Thrombolytic therapy decreased the need for escalation of care with no difference in mortality but at the expense of increased bleeding complications including hemorrhagic stroke.

The MOPETT trial^[44] randomized 121 patients with moderate PE to receive a "safe dose" of systemic thrombolytic (50 mg tPA) in 61 patients or anticoagulation alone in 60 patients. The primary end point was pulmonary hypertension and composite endpoints of pulmonary hypertension and recurrent PE at 28 mo. Secondary endpoints included total mortality, duration of hospital stay, and bleeding during hospitalization. Pulmonary hypertension and the composite endpoint of pulmonary hypertension and recurrent PE occurred in 16% of the thrombolytic group and in 57% of the control group ($P \leq 0.001$). Death and recurrent PE occurred in 1.6% and 10% of the tPA and control groups respectively.

There was no major bleeding in either group. When death or recurrent PE were assessed independently there was no difference between the groups. There have been numerous papers published on the delivery of fibrinolytic agents through infusion catheters placed directly into pulmonary artery thrombus. The most compelling evidence for the effectiveness of catheter directed treatment of PE comes from the ULTIMA trial^[45]. In this prospective randomized trial, USAT was compared to heparin alone in patients with submassive PE. A dose of 10-20 mg recombinant tissue plasminogen activator (rtPA) was infused over 15 h (approximately 0.75 to 1.5 mg/h) in the USAT group. RV/LV ratio showed a mean decrease at 24 h of 0.30 vs 0.03 in the heparin alone group ($P < 0.001$). At 90 d, there was one death from pancreatic cancer in the heparin group. There was no major bleeding and 4 episodes of minor bleeding: 3 in the USAT group, 1 in the heparin alone group ($P = 0.61$). Criticism of this trial includes failure to randomize patients with perhaps the greatest need for catheter directed therapy, the elderly and those with cancer; a low recruitment rate; and failure to follow patients to 6 mo when the heparin alone group may have additionally benefited from physiologic thrombolysis.

There is conflicting evidence as to whether ultrasound assisted delivery of fibrinolytic agents is more effective than infusion alone. In the PREFECT registry^[46], 101 consecutive patients were enrolled at 7 sites. Twenty-eight patients had massive PE (28%) and 73 had submassive PE (73%). Patients with massive PE were treated with mechanical thrombectomy or pharmaco-mechanical thrombectomy with clinical success in 24/28 patients and 14% mortality. Clinical success in the submassive group was 97% with 3% mortality. While the device choices for mechanical thrombectomy are not mentioned in the study, the Angiojet device was not used because of reported complications. In a subgroup analysis, comparing USAT with CDT there was no difference in post treatment pulmonary artery pressures, average pressure change, thrombolytic dose, raising the question of the added expense of USAT.

Looking at the evidence of systemic and catheter directed therapy in patients with submassive PE, it appears that patients receiving lytic therapy have a decreased need for escalation of care compared to those with heparin administration alone, a more rapid resolution of afterload on the right heart, but no significant survival advantage. However, there may be greater improvement in pulmonary artery pressures in the long term. The advantages of catheter directed therapies over systemic administration are thrombolytic delivery directly into the clot and the requirement of a lower dose of thrombolytics, which may decrease hemorrhagic complications. In light of the effectiveness of thrombolytics alone, one questions the need for mechanical thrombectomy in submassive PE, unless there is a contraindication to thrombolysis.

Pulmonary embolism response teams

As treatment options for patients with PE have evolved,

the concept of bringing together experts from different disciplines in an urgent manner to create the best treatment plan for patients presenting with PE has led to the creation of Pulmonary Embolism Response Teams (PERT)^[47]. Similar multidisciplinary collaborations have been employed to facilitate patients presenting with stroke (the "Stroke Team")^[48] or cardiac events (the "Heart Team").

The manner in which clinicians are summoned to make decisions about treatment varies considerably from institution to institution. It may involve alerting the members of the team through a beeper system that a patient has presented, or it may involve protocols which dictate how triage should be accomplished, with the necessary members alerted as needed^[49]. Members involved typically include pulmonary/critical care, cardiology, vascular/cardiothoracic surgery and interventional radiology or cardiology. Additional members who may be involved include anesthesiologists, perfusionists, diagnostic radiologists, and pharmacists. Activation may involve several or all of the members converging at the patient's bedside. In some instances, this may be done *via* videoconference with subsequent in-person activation of the physicians relevant to the particular patient's situation^[50].

An important function of the PERT process is data collection and the refinement of treatment protocols. By examining outcomes and correlating them with initial data collected, such as high and low heart rates, blood pressure, oxygen saturation, number of segments with thrombus, RV/LV ratio, *etc.*, triage of patients to different treatment arms may be optimized. Ideally, patients may subsequently be seen in follow up in a dedicated PERT clinic. Long term follow up can then be introduced to the PERT database. Centers with PERT programs have the opportunity to share data with each other allowing for more rapid determination of critical treatment parameters. Collaboration regarding data sharing is evolving through multicenter affiliations such as the PERT Consortium^[51].

In addition to streamlined treatment, another function of the PERT process is data collection, which will lead to the refinement of treatment protocols. Members of the national PERT Consortium will have the opportunity to share data advancing the understanding of PE and its treatment. The success of a PERT program requires extensive education of referring physicians, house staff, nursing staff, ED and ICU staff, pharmacy, and the community.

CONCLUSION

Currently, the precise role of catheter directed therapy in the treatment of both massive and submassive PE remains to be established through well-designed prospective controlled trials. For patients with massive PE in whom there is an absolute contraindication for systemic thrombolysis, a failure of systemic thrombolysis or no time for the 2 h of administration of systemic

thrombolytic agents, mechanical thrombectomy provides the primary alternative to surgical thrombectomy. With respect to submassive PE, catheter directed therapy decreases the need for treatment escalation, decreases the time for clinical improvement, but does not increase overall survival. An overall reduction in clot burden may decrease the incidence of CETPH and improve quality of life.

REFERENCES

- 1 Pulido T**, Aranda A, Zevallos MA, Bautista E, Martínez-Guerra ML, Santos LE, Sandoval J. Pulmonary embolism as a cause of death in patients with heart disease: an autopsy study. *Chest* 2006; **129**: 1282-1287 [PMID: 16685020 DOI: 10.1378/chest.129.5.1282]
- 2 McIntyre KM**, Sasahara AA. The hemodynamic response to pulmonary embolism in patients without prior cardiopulmonary disease. *Am J Cardiol* 1971; **28**: 288-294 [PMID: 5155756 DOI: 10.1016/0002-9149(71)90116-0]
- 3 McIntyre KM**, Sasahara AA. Determinants of right ventricular function and hemodynamics after pulmonary embolism. *Chest* 1974; **65**: 534-543 [PMID: 4826027 DOI: 10.1378/chest.65.5.534]
- 4 Stratmann G**, Gregory GA. Neurogenic and humoral vasoconstriction in acute pulmonary thromboembolism. *Anesth Analg* 2003; **97**: 341-354 [PMID: 12873915 DOI: 10.1213/01.ANE.0000068983.18131.F0]
- 5 Corrigan D**, Prucnal C, Kabrhel C. Pulmonary embolism: the diagnosis, risk-stratification, treatment and disposition of emergency department patients. *Clin Exp Emerg Med* 2016; **3**: 117-125 [PMID: 27752629 DOI: 10.15441/ceem.16.146]
- 6 Stein PD**, Beemath A, Matta F, Weg JG, Yusen RD, Hales CA, Hull RD, Leeper KV Jr, Sostman HD, Tapson VF, Buckley JD, Gottschalk A, Goodman LR, Wakefield TW, Woodard PK. Clinical characteristics of patients with acute pulmonary embolism: data from PIONEER II. *Am J Med* 2007; **120**: 871-879 [PMID: 17904458 DOI: 10.1016/j.amjmed.2007.03.024]
- 7 Guidelines on diagnosis and management of acute pulmonary embolism.** Task Force on Pulmonary Embolism, European Society of Cardiology. *Eur Heart J* 2000; **21**: 1301-1336 [PMID: 10952823 DOI: 10.1053/euhj.2000.2250]
- 8 Kucher N**, Goldhaber SZ. Management of massive pulmonary embolism. *Circulation* 2005; **112**: e28-e32 [PMID: 16009801 DOI: 10.1161/CIRCULATIONAHA.105.55.551374]
- 9 Castelli R**, Tarsia P, Tantarini C, Pantaleo G, Guariglia A, Porro F. Syncope in patients with pulmonary embolism: comparison between patients with syncope as the presenting symptom of pulmonary embolism and patients with pulmonary embolism without syncope. *Vasc Med* 2003; **8**: 257-261 [PMID: 15125486 DOI: 10.1191/1358863.x03vm510oa]
- 10 Stein PD**, Terrin ML, Hales CA, Palevsky HI, Saltzman HA, Thompson BT, Weg JG. Clinical, laboratory, roentgenographic, and electrocardiographic findings in patients with acute pulmonary embolism and no pre-existing cardiac or pulmonary disease. *Chest* 1991; **100**: 598-603 [PMID: 1909617 DOI: 10.1378/chest.100.3.604]
- 11 Elliott CG**, Goldhaber SZ, Visani L, DeRosa M. Chest radiographs in acute pulmonary embolism. Results from the International Cooperative Pulmonary Embolism Registry. *Chest* 2000; **118**: 33-38 [PMID: 10893356 DOI: 10.1378/chest.118.1.33]
- 12 Jaff MR**, McMurtry MS, Archer SL, Cushman M, Goldenberg N, Goldhaber SZ, Jenkins JS, Kline JA, Michaels AD, Thistlethwaite P, Vedantham S, White RJ, Zierler BK; American Heart Association Council on Cardiopulmonary, Critical Care, Perioperative and Resuscitation; American Heart Association Council on Peripheral Vascular Disease; American Heart Association Council on Arteriosclerosis, Thrombosis and Vascular Biology. Management of massive and submassive pulmonary embolism, iliofemoral deep vein thrombosis, and chronic thromboembolic pulmonary hypertension: a scientific statement from the American Heart Association. *Circulation* 2011; **123**: 1788-1830 [PMID: 21422387 DOI: 10.1161/CIR.0b013e318214914f]
- 13 Grifoni S**, Olivetto I, Cecchini P, Pieralli F, Camaiti A, Santoro G, Conti A, Agnelli G, Berni G. Short-term clinical outcome of patients with acute pulmonary embolism, normal blood pressure, and echocardiographic right ventricular dysfunction. *Circulation* 2000; **101**: 2817-2822 [PMID: 10859287 DOI: 10.1161/01.CIR.101.24.2817]
- 14 Kreit JW**. The impact of right ventricular dysfunction on the prognosis and therapy of normotensive patients with pulmonary embolism. *Chest* 2004; **125**: 1539-1545 [PMID: 15078772 DOI: 10.1378/chest.125.4.1539]
- 15 Goldhaber SZ**, Visani L, De Rosa M. Acute pulmonary embolism: clinical outcomes in the International Cooperative Pulmonary Embolism Registry (ICOPER). *Lancet* 1999; **353**: 1386-1389 [PMID: 10227218 DOI: 10.1016/S0140-6736(98)07534-5]
- 16 Kasper W**, Konstantinides S, Geibel A, Olschewski M, Heinrich F, Grosser KD, Rauber K, Iversen S, Redeker M, Kienast J. Management strategies and determinants of outcome in acute major pulmonary embolism: results of a multicenter registry. *J Am Coll Cardiol* 1997; **30**: 1165-1171 [PMID: 9350909 DOI: 10.1016/S0735-1097(97)00319-7]
- 17 Wagenvoort CA**. Pathology of pulmonary thromboembolism. *Chest* 1995; **107**: 10S-17S [PMID: 7813322 DOI: 10.1378/chest.107.1_Sup.p10S]
- 18 Dong BR**, Hao Q, Yue J, Wu T, Liu GJ. Thrombolytic therapy for pulmonary embolism. *Cochrane Database Syst Rev* 2009; **8**: CD004437 [PMID: 19588357 DOI: 10.1002/14651858.CD004437.pub3]
- 19 Alonso-Martínez JL**, Annicchero-Sánchez FJ, Urbietta-Echezarreta MA, García-Sanchotena JL, Herrero HG. Residual pulmonary thromboemboli after acute pulmonary embolism. *Eur J Intern Med* 2012; **23**: 379-383 [PMID: 22560390 DOI: 10.1016/j.ejim.2011.08.018]
- 20 Stein PD**, Yaekoub AY, Matta F, Janjua M, Patel RM, Goodman LR, Gross ML, Denier JE. Resolution of pulmonary embolism on CT pulmonary angiography. *AJR Am J Roentgenol* 2010; **194**: 1263-1268 [PMID: 20410413 DOI: 10.2214/AJR.09.3410]
- 21 Lang IM**, Pesavento R, Bonderman D, Yuan JX. Risk factors and basic mechanisms of chronic thromboembolic pulmonary hypertension: a current understanding. *Eur Respir J* 2013; **41**: 462-468 [PMID: 22700839 DOI: 10.1183/09031936.00049312]
- 22 Pengo V**, Lensing AW, Prins MH, Marchiori A, Davidson BL, Tiozzo F, Albanese P, Biasiolo A, Pegoraro C, Iliceto S, Prandoni P; Thromboembolic Pulmonary Hypertension Study Group. Incidence of chronic thromboembolic pulmonary hypertension after pulmonary embolism. *N Engl J Med* 2004; **350**: 2257-2264 [PMID: 15163775 DOI: 10.1056/NEJMoa032274]
- 23 Moorjani N**, Price S. Massive pulmonary embolism. *Cardiol Clin* 2013; **31**: 503-518, vii [PMID: 24188217 DOI: 10.1016/j.ccl.2013.07.005]
- 24 Meneveau N**, Séronde MF, Blonde MC, Legallier P, Didier-Petit K, Briand F, Caulfield F, Schiele F, Bernard Y, Bassand JP. Management of unsuccessful thrombolysis in acute massive pulmonary embolism. *Chest* 2006; **129**: 1043-1050 [PMID: 16608956 DOI: 10.1378/chest.129.4.1043]
- 25 Edelman JJ**, Okiwelu N, Anvardeen K, Joshi P, Murphy B, Sanders LH, Newman MA, Passage J. Surgical Pulmonary Embolectomy: Experience in a Series of 37 Consecutive Cases. *Heart Lung Circ* 2016; **25**: 1240-1244 [PMID: 27423976 DOI: 10.1016/j.hlc.2016.03.010]
- 26 Sharafuddin MJ**, Hicks ME. Current status of percutaneous mechanical thrombectomy. Part I. General principles. *J Vasc Interv Radiol* 1997; **8**: 911-921 [PMID: 9399459 DOI: 10.1016/S1051-0443(97)70687-0]
- 27 Sharafuddin MJ**, Hicks ME. Current status of percutaneous mechanical thrombectomy. Part II. Devices and mechanisms of action. *J Vasc Interv Radiol* 1998; **9**: 15-31 [PMID: 9468392 DOI: 10.1016/S1051-0443(98)70477-4]
- 28 Dawson CA**, Rickaby DA, Linehan JH, Bronikowski TA. Distributions of vascular volume and compliance in the lung. *J Appl Physiol* (1985) 1988; **64**: 266-273 [PMID: 3356646]

- 29 **Tibbitt DA**, Fletcher EW, Thomas L, Sutton GC, Miller GA. Evaluation of a method for quantifying the angiographic severity of major pulmonary embolism. *Am J Roentgenol Radium Ther Nucl Med* 1975; **125**: 895-899 [PMID: 1211520 DOI: 10.2214/ajr.125.4.895]
- 30 **Greenfield LJ**, Proctor MC, Williams DM, Wakefield TW. Long-term experience with transvenous catheter pulmonary embolectomy. *J Vasc Surg* 1993; **18**: 450-457; discussion 457-458 [PMID: 8377239 DOI: 10.1067/mva.1993.48033]
- 31 **Donaldson CW**, Baker JN, Narayan RL, Provias TS, Rassi AN, Giri JS, Sakhuja R, Weinberg I, Jaff MR, Rosenfield K. Thrombectomy using suction filtration and veno-venous bypass: single center experience with a novel device. *Catheter Cardiovasc Interv* 2015; **86**: E81-E87 [PMID: 24975395 DOI: 10.1002/ccd.25583]
- 32 **Al-Hakim R**, Park J, Bansal A, Genshaft S, Moriarty JM. Early Experience with AngioVac Aspiration in the Pulmonary Arteries. *J Vasc Interv Radiol* 2016; **27**: 730-734 [PMID: 27106647 DOI: 10.1016/j.jvir.2016.01.012]
- 33 **Weinberg AS**, Dohad S, Ramzy D, Madyoon H, Tapson VF. Clot Extraction With the FlowTriever Device in Acute Massive Pulmonary Embolism. *J Intensive Care Med* 2016; **3**: 676-679 [PMID: 27601482 DOI: 10.1177/0885066616666031]
- 34 **Müller-Hülsbeck S**, Brossmann J, Jahnke T, Grimm J, Reuter M, Bewig B, Heller M. Mechanical thrombectomy of major and massive pulmonary embolism with use of the Amplatz thrombectomy device. *Invest Radiol* 2001; **36**: 317-322 [PMID: 11410751 DOI: 10.1097/0004424-200106000-00003]
- 35 **Nassiri N**, Jain A, McPhee D, Mina B, Rosen RJ, Giangola G, Carroccio A, Green RM. Massive and submassive pulmonary embolism: experience with an algorithm for catheter-directed mechanical thrombectomy. *Ann Vasc Surg* 2012; **26**: 18-24 [PMID: 21885244 DOI: 10.1016/j.avsg.2011.05.026]
- 36 **Chechi T**, Vecchio S, Spaziani G, Giuliani G, Giannotti F, Arcangeli C, Rubboli A, Margheri M. Rheolytic thrombectomy in patients with massive and submassive acute pulmonary embolism. *Catheter Cardiovasc Interv* 2009; **73**: 506-513 [PMID: 19235240 DOI: 10.1002/ccd.21858]
- 37 **Dukkipati R**, Yang EH, Adler S, Vintch J. Acute kidney injury caused by intravascular hemolysis after mechanical thrombectomy. *Nat Clin Pract Nephrol* 2009; **5**: 112-116 [PMID: 19092794 DOI: 10.1038/ncpneph1019]
- 38 **Tafur AJ**, Shamoun FE, Patel SI, Tafur D, Donna F, Murad MH. Catheter-Directed Treatment of Pulmonary Embolism. *Clin Appl Thromb Hemost* 2016; **1**: 1076029616661414 [PMID: 27481877 DOI: 10.1177/1076029616661414]
- 39 **Stein PD**, Matta F. Thrombolytic therapy in unstable patients with acute pulmonary embolism: saves lives but underused. *Am J Med* 2012; **125**: 465-470 [PMID: 22325236 DOI: 10.1016/j.amjmed.2011.10.015]
- 40 **Kuo WT**, Gould MK, Louie JD, Rosenberg JK, Sze DY, Hofmann LV. Catheter-directed therapy for the treatment of massive pulmonary embolism: systematic review and meta-analysis of modern techniques. *J Vasc Interv Radiol* 2009; **20**: 1431-1440 [PMID: 19875060 DOI: 10.1016/j.jvir.2009.08.002]
- 41 **Wan S**, Quinlan DJ, Agnelli G, Eikelboom JW. Thrombolysis compared with heparin for the initial treatment of pulmonary embolism: a meta-analysis of the randomized controlled trials. *Circulation* 2004; **110**: 744-749 [PMID: 15262836 DOI: 10.1161/01.CIR.0000137826.09715.9C]
- 42 **Konstantinides S**, Geibel A, Heusel G, Heinrich F, Kasper W; Management Strategies and Prognosis of Pulmonary Embolism-3 Trial Investigators. Heparin plus alteplase compared with heparin alone in patients with submassive pulmonary embolism. *N Engl J Med* 2002; **347**: 1143-1150 [PMID: 12374874 DOI: 10.1056/NEJMoa021274]
- 43 **Meyer G**, Vicaut E, Danays T, Agnelli G, Becattini C, Beyer-Westendorf J, Bluhmki E, Bouvaist H, Brenner B, Couturaud F, Dellas C, Empen K, Franca A, Galliè N, Geibel A, Goldhaber SZ, Jimenez D, Kozak M, Kupatt C, Kucher N, Lang IM, Lankeit M, Meneveau N, Pacouret G, Palazzini M, Petris A, Pruszczyk P, Rugolotto M, Salvi A, Schellong S, Sebbane M, Sobkowicz B, Stefanovic BS, Thiele H, Torbicki A, Verschuren F, Konstantinides SV; PEITHO Investigators. Fibrinolysis for patients with intermediate-risk pulmonary embolism. *N Engl J Med* 2014; **370**: 1402-1411 [PMID: 24716681 DOI: 10.1056/NEJMoa1302097]
- 44 **Sharifi M**, Bay C, Skrocki L, Rahimi F, Mehdipour M; "MOPETT" Investigators. Moderate pulmonary embolism treated with thrombolysis (from the "MOPETT" Trial). *Am J Cardiol* 2013; **111**: 273-277 [PMID: 23102885 DOI: 10.1016/j.amjcard.2012.09.027]
- 45 **Kucher N**, Boekstegers P, Müller OJ, Kupatt C, Beyer-Westendorf J, Heitzer T, Tebbe U, Horstkotte J, Müller R, Blessing E, Greif M, Lange P, Hoffmann RT, Werth S, Barmeyer A, Härtel D, Grünwald H, Empen K, Baumgartner I. Randomized, controlled trial of ultrasound-assisted catheter-directed thrombolysis for acute intermediate-risk pulmonary embolism. *Circulation* 2014; **129**: 479-486 [PMID: 24226805 DOI: 10.1161/CIRCULATIONAHA.113.005544]
- 46 **Kuo WT**, Banerjee A, Kim PS, DeMarco FJ Jr, Levy JR, Facchini FR, Unver K, Bertini MJ, Sista AK, Hall MJ, Rosenberg JK, De Gregorio MA. Pulmonary Embolism Response to Fragmentation, Embolectomy, and Catheter Thrombolysis (PERFECT): Initial Results From a Prospective Multicenter Registry. *Chest* 2015; **148**: 667-673 [PMID: 25856269 DOI: 10.1378/chest.15-0119]
- 47 **Dudzinski DM**, Piazza G. Multidisciplinary Pulmonary Embolism Response Teams. *Circulation* 2016; **133**: 98-103 [PMID: 26719388 DOI: 10.1161/CIRCULATIONAHA.115.015086]
- 48 **Jauch EC**, Saver JL, Adams HP Jr, Bruno A, Connors JJ, Demaerschalk BM, Khatri P, McMullan PW Jr, Qureshi AI, Rosenfield K, Scott PA, Summers DR, Wang DZ, Wintermark M, Yonas H; American Heart Association Stroke Council; Council on Cardiovascular Nursing; Council on Peripheral Vascular Disease; Council on Clinical Cardiology. Guidelines for the early management of patients with acute ischemic stroke: a guideline for healthcare professionals from the American Heart Association/American Stroke Association. *Stroke* 2013; **44**: 870-947 [PMID: 23370205 DOI: 10.1161/STR.0b013e318284056a]
- 49 **Provias T**, Dudzinski DM, Jaff MR, Rosenfield K, Channick R, Baker J, Weinberg I, Donaldson C, Narayan R, Rassi AN, Kabrhel C. The Massachusetts General Hospital Pulmonary Embolism Response Team (MGH PERT): creation of a multidisciplinary program to improve care of patients with massive and submassive pulmonary embolism. *Hosp Pract* (1995) 2014; **42**: 31-37 [PMID: 24566594 DOI: 10.3810/hp.2014.02.1089]
- 50 **Kabrhel C**, Jaff MR, Channick RN, Baker JN, Rosenfield K. A multidisciplinary pulmonary embolism response team. *Chest* 2013; **144**: 1738-1739 [PMID: 24189880 DOI: 10.1378/chest.13-1562]
- 51 **PERT**. The National Consortium of Pulmonary Embolism Response Teams: Developing effective solutions to a devastating illness. Available from: URL: <http://pertconsortium.org>

P- Reviewer: Gao BL, Gumustas OG, Shen J, van Beek EJR, Yazdi HR

S- Editor: Ji FF **L- Editor:** A **E- Editor:** Lu YJ



Imaging features of intrathoracic complications of lung transplantation: What the radiologists need to know

Elisa Chia, Simeon Niyi Babawale

Elisa Chia, Simeon Niyi Babawale, Department of Radiology, Royal Perth Hospital, Wellington Street Campus, Perth, WA 6001, Australia

ORCID number: Elisa Chia (0000-0003-1110-6524); Simeon Niyi Babawale (0000-0002-3482-3158).

Author contributions: Chia E collated imaging used in the manuscript after obtaining consent from the patients and contributed to the drafting and editing of the manuscript; Babawale SN contributed to the writing of the manuscript, manuscript editing and review of the imaging.

Conflict-of-interest statement: No conflicts of interest were noted in the making of this manuscript. There is no financial support or relationships associated with the authors of this work that may pose a conflict of interest.

Open-Access: This article is an open-access article which was selected by an in-house editor and fully peer-reviewed by external reviewers. It is distributed in accordance with the Creative Commons Attribution Non Commercial (CC BY-NC 4.0) license, which permits others to distribute, remix, adapt, build upon this work non-commercially, and license their derivative works on different terms, provided the original work is properly cited and the use is non-commercial. See: <http://creativecommons.org/licenses/by-nc/4.0/>

Manuscript source: Unsolicited manuscript

Correspondence to: Elisa Chia, MBBS, Department of Radiology, Royal Perth Hospital, Wellington Street Campus, GPO Box X2213, Perth, WA 6001, Australia. elisa.chia@health.wa.gov.au
Telephone: +61-08-92242244
Fax: +61-08-92242912

Received: July 2, 2017

Peer-review started: July 3, 2017

First decision: August 7, 2017

Revised: October 20, 2017

Accepted: November 8, 2017

Article in press: November 8, 2017

Published online: December 28, 2017

Abstract

Lung transplantation has been a method for treating end stage lung disease for decades. Despite improvements in the preoperative assessment of recipients and donors as well as improved surgical techniques, lung transplant recipients are still at a high risk of developing post-operative complications which tend to impact negatively the patients' outcome if not recognised early. The recognised complications post lung transplantation can be broadly categorised into acute and chronic complications. Recognising the radiological features of these complications has a significant positive impact on patients' survival post transplantation. This manuscript provides a comprehensive review of the radiological features of post lung transplantations complications over a time continuum.

Key words: Lung transplantation; Post-surgical features of lung transplantation; Complication of lung transplantation; Imaging features; Early and late complications

© The Author(s) 2017. Published by Baishideng Publishing Group Inc. All rights reserved.

Core tip: Lung transplantation is a common method of treating end stage lung disease. However, despite advances in surgical techniques, complications are still common and can occur years after lung transplantation. Radiological imaging plays an essential role in characterising many post-transplantation complications. It is crucial for radiologists to identify early signs of common complications on imaging to ensure that appropriate treatments are instituted early.

Chia E, Babawale SN. Imaging features of intrathoracic complications of lung transplantation: What the radiologists need to know. *World J Radiol* 2017; 9(12): 438-447 Available from: URL: <http://www.wjgnet.com/1949-8470/full/v9/i12/438.htm> DOI: <http://dx.doi.org/10.4329/wjr.v9.i12.438>

INTRODUCTION

Lung transplantation is an accepted treatment modality for end stage lung disease with over 3614 transplantations performed worldwide between July 2013 and June 2014^[1]. In Australia alone, over 163 of lung transplantations were performed in 2014^[2]. During the early 1960s when human lung transplantation was explored, multiple attempts at the procedure often failed rapidly due to rejection and issues with bronchial and vessel anastomoses. However, over years, this measure of treatment has achieved remarkable outcomes.

Given the inherent risks associated with lung transplantation, patients are carefully selected for their suitability for treatment. Improved outcomes have been associated with advancing surgical techniques, appropriate patient selection, cautious harvesting and preservation of organs, and improved immunosuppressive therapy^[3]. Despite the pre-transplant strict selection criteria, complications are still frequent.

Postoperative complications can be categorised broadly into: Early complications; including but not limited to reperfusion oedema and acute rejection; and late complications including infections, anastomotic complications and chronic graft rejection. Understanding the timeline of post-operative complications is a key to making accurate diagnosis for early intervention.

EARLY COMPLICATIONS

Early complications of lung transplantation generally occur within few weeks post-operatively. These account for the significant proportion of mortality in patients who undergo lung transplantation.

Donor lung and recipient thorax mismatch

Donor lung and recipient thoracic cage mismatch is a potential underlying cause of some of the early complications of lung transplantation. Therefore, meticulous attention to details in selecting appropriate donor lung is a crucial initial step in obviating the likelihood of complications relating to donor-recipient mismatch. These complications include pleural effusion and pneumothorax, which have been shown to develop especially if the donor lung is too small for the recipient thorax. These complications may, in certain cases require interventions such as thoracentesis and antibiotic therapy. This contributes to a prolonged hospitalisation and increased overall cost of lung transplantation.

However, deliberately mismatching the donor lung and the recipient's thorax may have some potential benefits. Moderately oversized donor lung has been shown to reduce the risk of early primary graft dysfunction^[4]. However, in cases where the donor lung is too large in size, atelectasis and impaired ventilation may

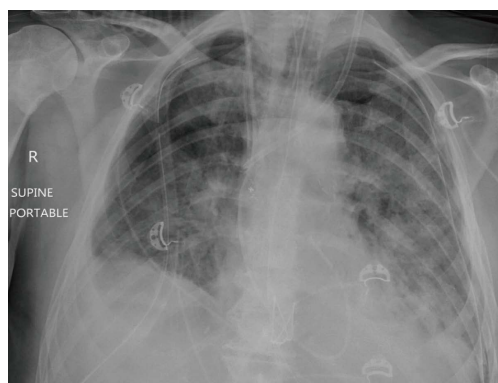


Figure 1 Chest X-ray of a 64-year-old male 3 d post transplantation showing reperfusion oedema. Bilateral airspace opacity predominantly in the mid to lower zones with associated bilateral pleural effusions.

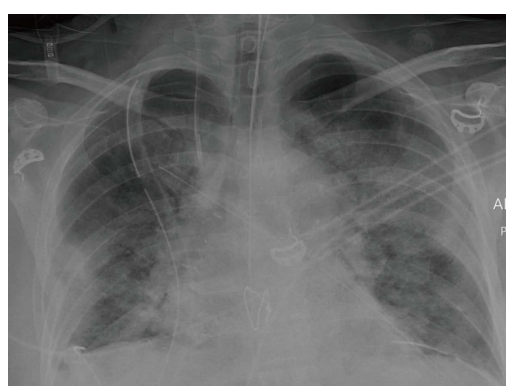


Figure 2 Chest X-ray 3 d post transplantation shows reperfusion oedema. Bilateral airspace opacity in the mid to lower zones and sub-pleural consolidation in the lower zone of the right lower lobe.

ensue^[4].

Ischaemia-reperfusion injury

Ischaemic-reperfusion injury, also known as primary graft dysfunction is a frequent complication following lung transplantation. It is one of the leading causes of early post-transplant morbidity and mortality. It is a severe acute lung injury syndrome that develops within the first 48-72 h post lung transplantation^[5].

Reperfusion oedema has variable imaging features. On chest X-ray, it may present with hazy peri-hilar airspace opacity in milder cases, and dense peri-hilar consolidations with air bronchograms in more severe cases^[6] (Figures 1 and 2).

High resolution computerised tomography (HRCT) will demonstrate the above features in greater details, even though these are not specific only to pulmonary oedema. Perihilar ground-glass opacities, peribronchovascular thickening and reticulations with predilection for the middle and lower lobes are elegantly demonstrable on HRCT^[7,8].

Acute rejection

Acute cellular rejection occurs generally within the first

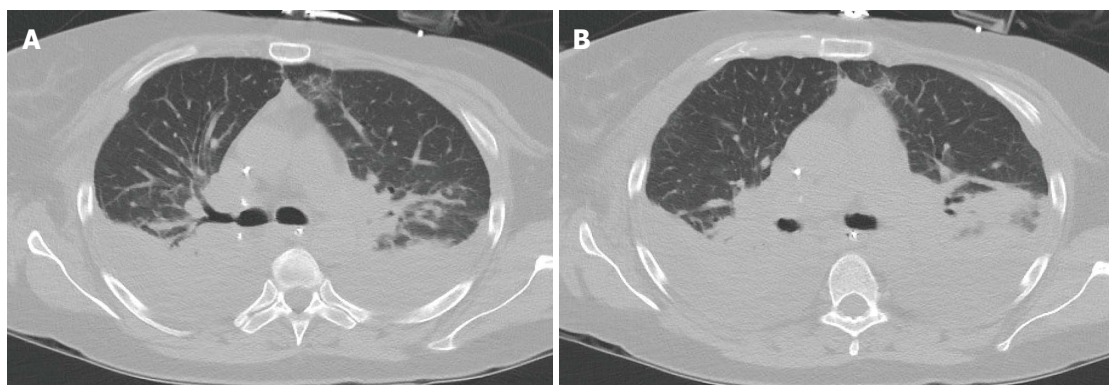


Figure 3 Computerised tomography images of the chest 4 wk post-transplantation showing acute rejection. Bilateral basal predominant consolidation, diffuse ground glass opacity and atelectasis with large bilateral pleural effusions. A: Axial slice of CT chest image showing bilateral basal consolidations; B: Axial slice of CT chest image illustrating extensive bilateral pleural effusions with pulmonary atelectasis. CT: Computerised tomography.



Figure 4 Acute rejection in a 50-year-old female 3 wk post-transplantation. CT scan of the chest shows bilateral diffuse ground glass opacity, linear atelectases, bilateral pleural effusion and bilateral peribronchial thickening. A: Coronal slice of CT chest image showing bilateral ground glass opacities and linear atelectasis; B: Axial slice of CT chest image highlighting bilateral pleural effusions; C: Axial slice of CT chest image highlighting peribronchial thickening. CT: Computerised tomography.



Figure 5 Chest X-ray shows increased lucency of the costophrenic angles on both sides (deep sulcus sign) in keeping with bilateral supine pneumothoraces.

2 wk post-lung transplantation. This complication is a potential cause of significant morbidity. Acute cellular rejection is a cell-mediated immune response to human leukocyte antigen (HLA) complex expressed in the donor lung. This immune response leads to perivascular lymphocytic infiltrate^[9-11].

Imaging findings in the mild acute rejection may be very subtle and, hence, trans-bronchial lung biopsy is the gold standard for diagnosis in this setting. Normal

findings on chest X-rays, therefore, does not exclude the diagnosis of acute rejection, especially in the mild form^[10]. Radiological findings, demonstrable on HRCT, include lower lobe predominant peri-hilar ground glass opacities, peri-bronchial cuffing, interlobular septal thickening, and new or increasing pleural effusions^[9,11] (Figures 3 and 4). Notably, the absence of ground glass opacities in HRCT within the first few weeks post lung transplantation virtually excludes the diagnosis of severe acute rejection^[7].

Pleural complications

The spectrums of acute pleural complications include minor air leaks, haemothorax, pneumothorax, chylothorax and pleural effusions. Air leaks may occur transiently following lung transplantation or persist for quite a while. Pleural leaks (Figure 5) are considered transient if spontaneous resolution occurs within 7 d post-transplantation. Air leaks that are unresolved after 7 d post-transplantation are dubbed persistent and may signify more serious complications such as significant bronchial dehiscence or airway ischaemia. This may eventually lead to pneumomediastinum, persistent pneumothorax or subcutaneous emphysema^[9].

Pleural effusion may persist for few months. At 3 mo, approximately 59% of patients may have some pleural

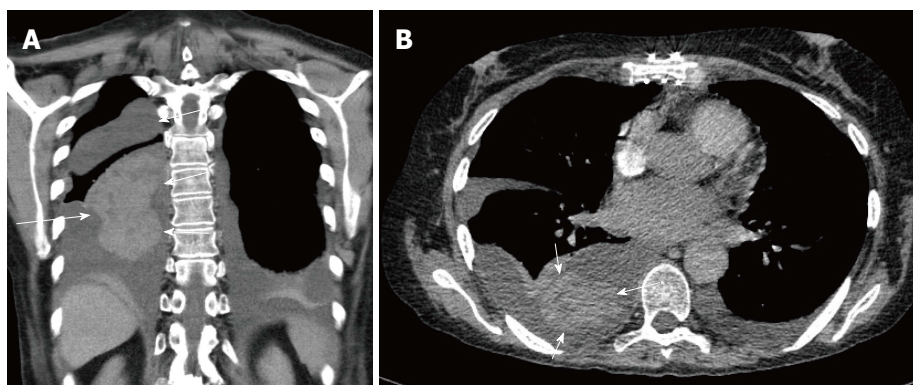


Figure 6 Computerised tomography scan of the chest in a 63-year-old female performed 16 d post bilateral lung transplant showing a coronal slice and an axial slice of a left pleural effusion and right haemothorax with clotted blood component (arrow). A: Coronal slice; B: Axial slice.

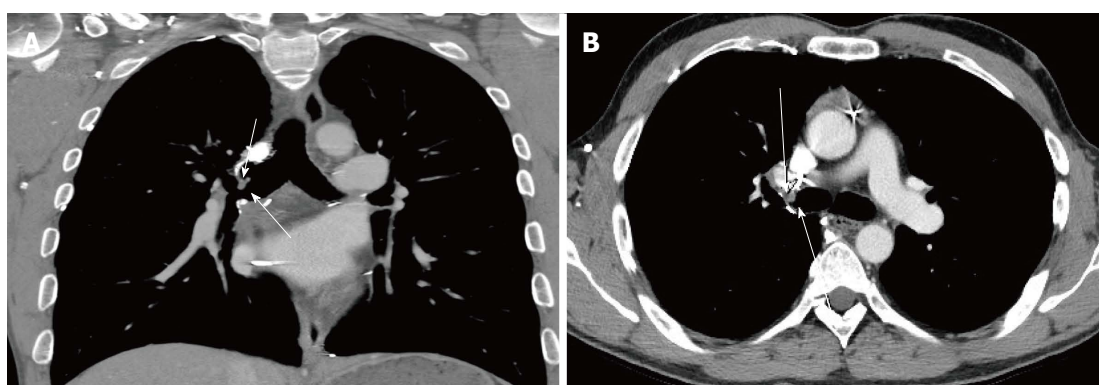


Figure 7 Computerised tomography scan images of a 37-year-old man performed 18 mo post-transplantation showing a coronal slice and an axial slice of a stenosis of the right main stem bronchus (arrow). A: Coronal slice; B: Axial slice.

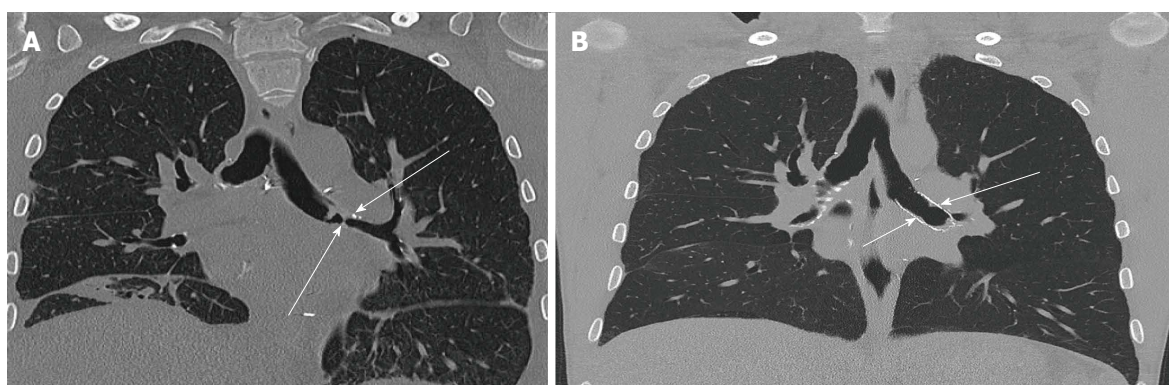


Figure 8 Computerised tomography scan of the chest showing a left main stem bronchial stenosis (arrow) in a 36-year-old male 2 mo post lung transplantation. A: Coronal slice of CT chest image before insertion of bronchial stent; B: Coronal slice of CT chest image after insertion of bronchial stent. CT: Computerised tomography.

effusions detectable on imaging study, especially on computerised tomography (CT) scan. However, majority of pleural effusion resolve completely by 12 mo (8%)^[12]. Pleural thickening and calcification may manifest as a long-term complication. Figure 6 illustrates some of the more common pleural complications.

Bronchial anastomotic complications

Bronchial dehiscence, bronchial stenosis, bronchomalacia and bronchopleural fistulas are some of the airway

anastomotic complications that can occur. The most frequent of these complications is bronchial stenosis. There are two patterns of bronchial stenosis: Surgical site anastomotic stenosis and segmental non-anastomotic bronchial stenosis.

Bronchial stenosis is easily demonstrable in chest X-ray. Bronchial stenosis may be severe enough to cause the atelectasis of the affected lobe^[13]. As demonstrated in Figures 7 and 8, helical CT with multiplanar reconstruction will demonstrate this and

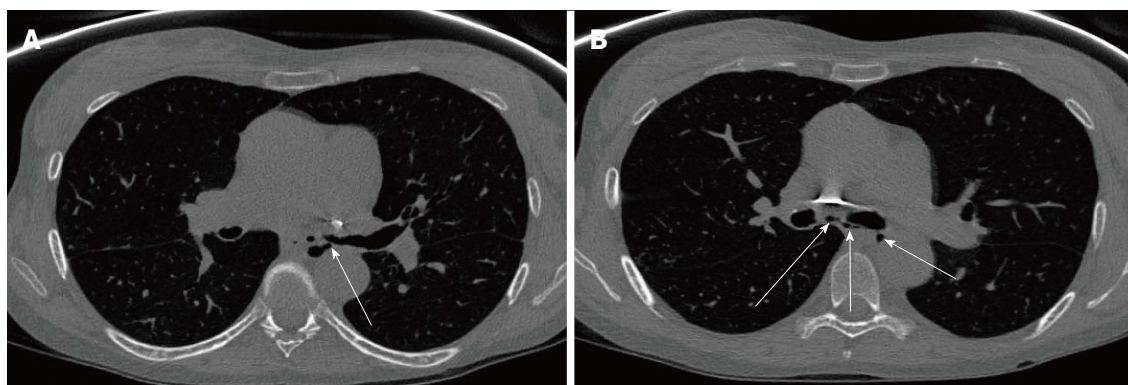


Figure 9 Computerised tomography scan of the chest in a 51-year-old female performed nearly 3 years post bilateral lung transplantation shows left main bronchial dehiscence resulting in gas locules tracking from the left main stem bronchus to the mediastinum causing pneumomediastinum. A: Axial slice of CT chest image showing gas leaks (arrow) from the left main stem bronchus; B: Axial slice of CT chest image showing multiple gas locules (arrow) causing pneumomediastinum. CT: Computerised tomography.

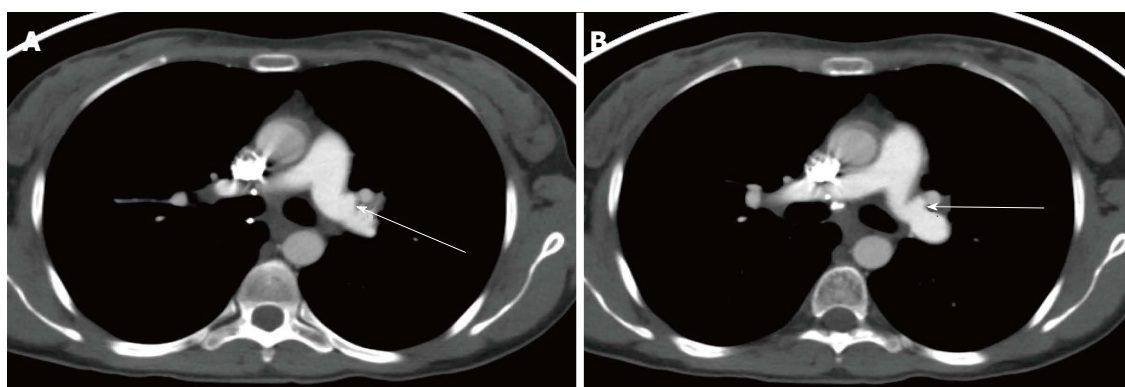


Figure 10 Computerised tomography scan of the chest in a 31-year-old female 3 mo post bilateral lung transplantation showing peri-anastomotic left pulmonary artery saccular aneurysm. A: Axial slice of CT chest image showing a left pulmonary artery saccular aneurysm (arrow); B: Axial slice of CT chest image showing a left pulmonary artery saccular aneurysm (arrow). CT: Computerised tomography.

other associated features more elegantly and is said to have an accuracy of 94% for detecting bronchial stenosis^[13].

Bronchial dehiscence results from ongoing mucosal necrosis of the donor bronchus secondary to disruption of the bronchial circulation^[7]. Chest radiography is unreliable for the diagnosis of bronchial dehiscence due to the presence of peri-bronchial air that may obscure the major airways.

CT scan is more sensitive and readily able to identify the features of bronchial dehiscence including bronchial wall defects, fixed or dynamic bronchial narrowing, and peribronchial air around the anastomosis^[13] (Figure 9).

Bronchopleural fistula manifests as progressive increase in the intrapleural air, new or progressing hydro-pneumothorax and changes in the already present air-fluid levels. In severe cases, tension pneumothorax may occur with imaging demonstrating contralateral mediastinal shift, flattening of the ipsilateral diaphragm, ipsilateral widening of intercostal spaces and atelectasis of the contralateral lung.

Vascular anastomotic complications

Complications involving the vasculature anastomotic sites post lung transplantation are much less frequent

compared to airway anastomotic complications. Vascular complications include pulmonary artery stenosis, kinking of the pulmonary artery and pulmonary vein thrombosis. Peri-anastomotic pulmonary artery aneurysm is an unusual complication (Figure 10).

Pulmonary artery stenosis can occur early or late after lung transplantation and is generally a result of incongruent lengths of the donor and recipient segments, technical narrowing or twisting of the anastomosis^[14].

CT angiogram is the acceptable imaging modality for investigating these complications. Narrowing or occlusion of the affected artery is readily demonstrable with CT angiogram. Diminished opacification of the corresponding pulmonary segment may indicate atelectasis or evolving pulmonary infarction^[15].

Infections

Pulmonary infection after lung transplantation remains an important complication that is associated with high rates of morbidity and mortality. The incidence of infection is far more frequent in the lung transplant recipients than any other organ transplant recipients^[9]. This is due to the higher level of immunosuppression and loss of local pulmonary host defences characterised by the reduction in lymphatic drainage, and reduced mucociliary

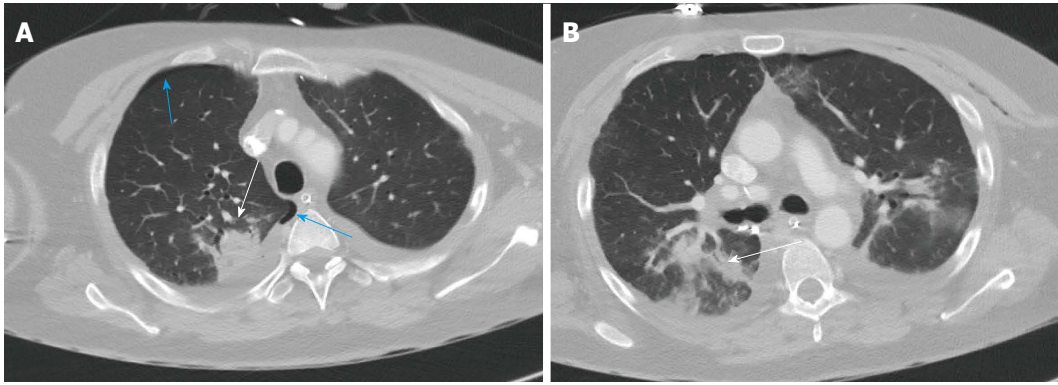


Figure 11 Computerised tomography scan of the chest 2 wk post-transplantation shows consolidation in the right upper lobe posteriorly with air bronchogram in keeping with pneumonia. Associated right sided pneumothorax. A: Axial slice of CT chest showing right upper lobe consolidation (white arrow), and right sided pneumothorax (blue arrows); B: Axial slice showing consolidation on the right upper lobe with air bronchogram (arrow). CT: Computerised tomography.



Figure 12 Chest computerised tomography scan of a 57-year-old male performed 2 years post-transplantation shows pseudomonas lung infection. Geographic area of ground glass opacity with associated diffuse centrilobular ground glass opacities and bronchiolar thickening mainly in the basal segment of the left upper lobe. A: Axial slice of CT chest image showing ground glass opacity (arrow); B: Axial slice of CT chest image highlighting diffuse centrilobular ground glass opacities on the left; C: Axial slice of CT chest image showing bronchiolar wall thickening in the left upper lobe (arrow). CT: Computerised tomography.

clearance.

Bacterial pneumonia accounts for approximately 36% of pneumonias^[16] occurring post lung transplantation. *Staphylococcus aureus*, *pseudomonas aeruginosa* and *Enterobacteriaceae* are the most common bacterial culprits.

Radiographic manifestation of bacterial pneumonia (Figures 11 and 12) may be nonspecific with the occurrence of patchy or confluent consolidation, ground-glass opacity, septal thickening and pleural effusions^[16]. These features and the presence of tree-in-bud opacity on chest radiograph, in conjunction with the appropriate clinical picture, makes the radiographic diagnosis of pneumonia fairly obvious. Pleural effusion is nonspecific. It may be indicative of haemorrhage, rejection or empyema^[17].

LATE COMPLICATIONS

Late complications post lung transplantation can occur anytime from months to years. It is vitally important to have a high index of suspicion in recognising the signs of late complications as these largely contribute to the patients' morbidity and mortality.

Chronic rejection

Chronic allograft rejection is one of the causes attributed

to the increased rate of mortality and morbidity post lung transplantation, whether single lung transplantation or bilateral. Chronic allograft rejection is described clinically as bronchiolitis obliterans syndrome. Cryptogenic organising pneumonia may also be seen. Patho-physiologically, chronic rejection is typified by inflammatory and fibrotic processes. Eosinophilic hyaline fibrosis of the small airways leads to progressive concentric bronchiolar luminal narrowing and eventually bronchiolar occlusion^[7].

Plain radiograph is of limited diagnostic value in chronic graft rejection. Non-specific features in plain radiograph that can suggest chronic rejection include pulmonary hyperinflation, decreased vascular markings, regional volume loss, subsegmental atelectasis, linear opacities and bronchiectasis^[7].

Chest CT is the imaging of choice for demonstrating the features of small airway and interstitial lung parenchymal changes that occur in chronic graft rejection (Figure 13). Some of these features, which are readily demonstrable on chest CT, include bronchial wall thickening, interlobular septal thickening, reticulo-nodular opacity, ground-glass opacity with mosaic attenuation, air trapping and peripherally predominant bronchiectasis^[7,9,18].

Atypical infections

Iatrogenic immunosuppression post lung transplantation

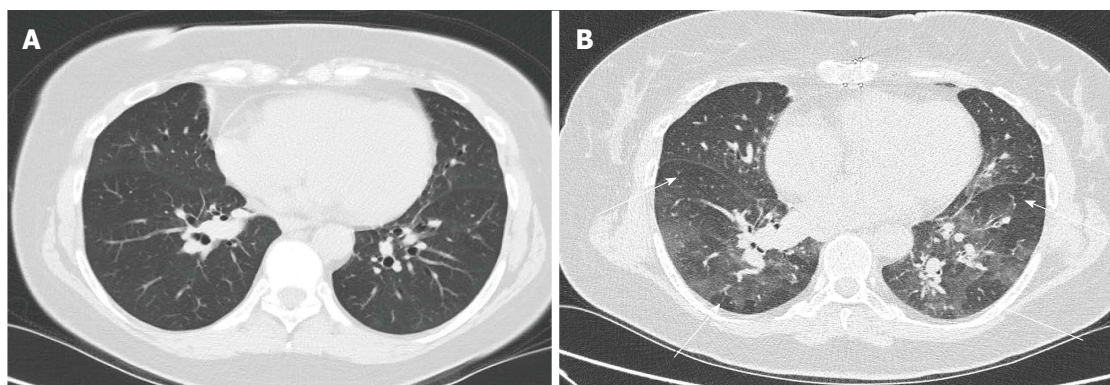


Figure 13 Bronchiolitis/small airway disease. CT scan of the chest performed 8 years post-transplantation shows patchy multifocal air trapping with bronchiolar thickening. A: Axial slice of CT chest image showing bronchiolar thickening; B: Axial slice of CT chest image showing multifocal areas of patchy air trapping. CT: Computerised tomography.



Figure 14 Chest computerised tomography scan of a 30-year-old male performed 2 mo after lung transplantation shows fungal infection. Two partly solid nodules in the right lung (one in the basal segment of the right upper lobe and the other in the right lower lobe. A: Axial slice of CT chest image showing right lower lobe nodule (arrow); B: Coronal slice of CT chest image showing 2 nodules on the lower segment of the right upper lobe (blue arrow) and right lower lobe (white arrow); C: Axial slice of CT chest image showing partially solid nodule (arrow). CT: Computerised tomography.

is an important predisposing factor for infection with atypical organisms such as viruses, fungi and mycobacterium.

Viruses, particularly cytomegalovirus (CMV), are largely opportunistic infections and are a risk factor for the development of transplant rejection. Lung transplant recipients are particularly susceptible to CMV infection and the rate of infection in these patients can be as high as 50%^[7]. Other viral culprits include parainfluenza virus, respiratory syncytia virus and adenovirus.

Features of viral chest infections are nonspecific. It is usually patchy with no particular lobar predilection. Nodular opacities, patchy consolidation, diffuse ground-glass opacity and bronchiolar thickening can be seen in viral chest infections. Adenoviral pneumonia imaging findings typically are more extensive compared to those caused by other viral infections^[19].

Fungal infection post lung transplantation is less frequent than bacterial and viral infections, however they are associated with high mortality rates. *Aspergillus* and *Candida* species are the most common causes of fungal infections in lung transplant recipients (Figure 14). Colonisation of the airways by aspergillus species is a common occurrence in lung transplant recipients, particularly those with underlying cystic fibrosis. Colonisation with these organisms increase the risk of

developing invasive aspergillosis which could be fatal and may result in as high as 55% mortality in lung transplant recipients if not aggressively treated^[20].

Fungal chest infections have various chest CT features including consolidation, lung nodules and cavitating nodules or masses. Ground glass opacity surrounding a lung nodule or mass (Figures 15 and 16) dubbed as a halo sign is highly suggestive, although not specific, of fungal infection in appropriate clinical settings^[7].

Rate of tuberculosis infections usually vary by geographic location. However, tuberculosis infection has been shown to be significantly higher in transplant recipients compared to the general population irrespective of geographic location^[21]. It presents commonly as a reactivation of the latent infection in the transplant recipients, but can also be acquired from unrecognised infected donor lung. Pulmonary tuberculosis is commonly seen radiologically as focal infiltrates or in a miliary pattern^[22].

Thromboembolism

Thromboembolism (including pulmonary embolism and deep vein thrombosis) is a common complication that tends to occur within few months post-transplantation. It is important to recognise this since up to 27% of lung transplant recipients are prone to this complication^[23]. This

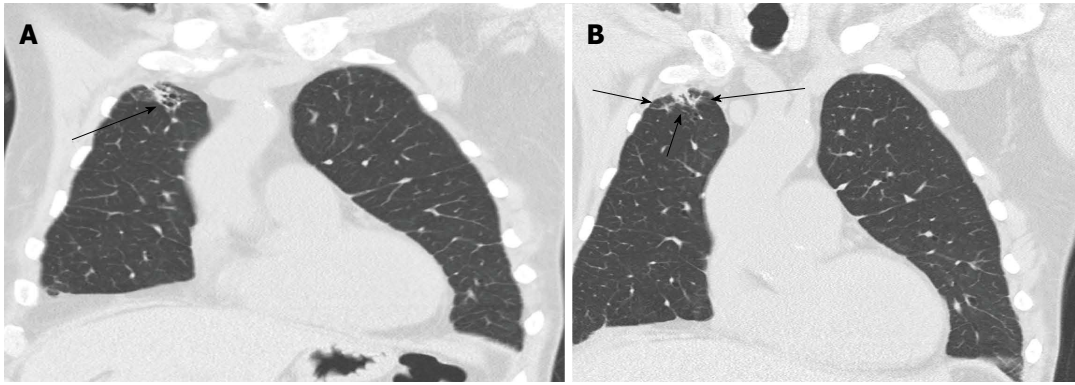


Figure 15 Broncho-alveolar lavage proven aspergillosis. CT scan of the chest shows right lung apex sub-pleural nodule with surrounding ground glass opacity and focal bronchiectasis. A: Coronal slice of CT chest showing right apical sub-pleural nodule (arrow); B: Coronal slice of CT chest showing surrounding ground glass opacity and focal bronchiectasis (arrow) around a sub-pleural nodule. CT: Computerised tomography.

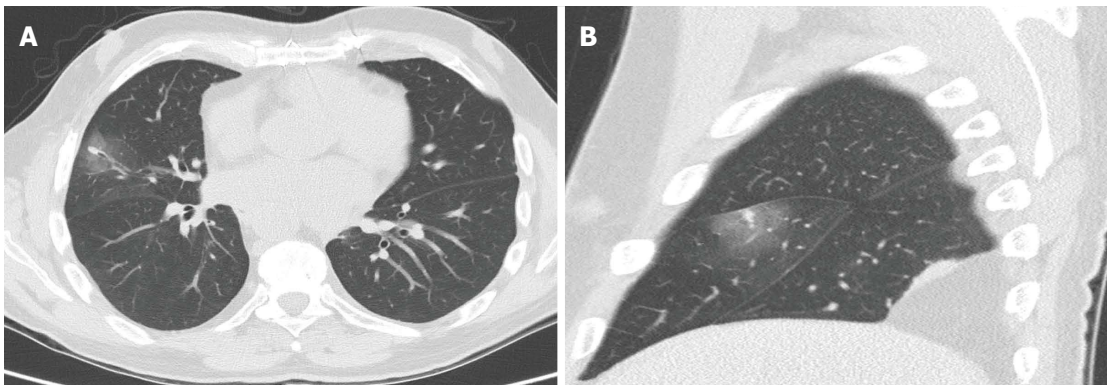


Figure 16 Computerised tomography scan of the chest performed 1 year post bilateral lung transplant shows pulmonary aspergillosis. An axial slice (A) and sagittal slice (B) showing a middle lobe small solid nodule with relatively large peripheral halo of ground glass opacity known as a "halo sign" (arrow). Bronchoscopy confirmed aspergillosis. A: Axial slice; B: Sagittal slice.

has been suggested to be due to the hypercoagulable state caused by the inflammatory response to the donor organ^[11]. Potential thrombogenic surfaces, such as the pulmonary artery anastomotic site and central lines, also act as sources of venous thromboembolisms^[23].

Lung transplant recipients are more susceptible to thromboembolic induced pulmonary infarcts due to a deficient dual blood supply (bronchial and pulmonary arterial supply) in the early post-operative period. Clues suggesting pulmonary thromboembolism on chest radiography include segmental oligemia, pleural effusion, dilated central pulmonary arteries and cardiomegaly^[7]. Wedge shaped sub-pleural opacity representing lung infarct is readily demonstrable on chest radiograph.

CT pulmonary angiogram is the gold standard for diagnosing pulmonary embolism. Filling defects with segmental partial or total occlusion in the central or segmental branches of the pulmonary arteries are the most reliable direct signs of thromboembolism^[7,10]. Indirect features include consolidation in specific vascular territories, mosaic perfusion, atelectasis and pleural effusions^[7,10]. Ventilation perfusion scans is a viable alternative in patients who have contraindications to CT pulmonary angiogram.

Transplant related lymphoproliferative disorder

A diverse number of lymphoproliferative diseases may develop post lung transplantation. These are collectively termed post-transplantation lymphoproliferative disorders (PTLD) and occur in approximately 5% of lung transplant recipients^[24]. Patho-physiologically, transplant recipients are predisposed to Epstein-Barr virus (EBV) which induces B-cell proliferative responses leading to PTLD, usually within a year after transplantation.

CT features of PTLD are variable, and may be seen as a single or multiple pulmonary nodules or masses with or without mediastinal, hilar and extra-thoracic adenopathy^[25].

Primary lung carcinoma

Primary lung carcinomas occurring in the lung allograft are rare^[26]. This is attributable in part to the comprehensive screening process prior to transplantation aiming at excluding donors with underlying parenchymal lung disease and those with significant smoking history. The risk of developing primary pulmonary carcinoma in transplant recipients is therefore the same as the general population.

Nevertheless, in cases where primary lung allograft

carcinomas arise, tumours tend to be more aggressive^[26]. This is likely due to immunosuppression, and can be challenging radiologically to distinguish from an infectious process.

Recurrence of primary disease

Despite lung transplantation being the only available therapy for end-stage lung disease, a number of diseases have been reported to recur in the lung allograft. Sarcoidosis has been demonstrated to have a high recurrence rate^[27]. Lymphangioleiomyomatosis and diffuse panbronchiolitis and pulmonary alveolar proteinosis have also been reported to recur post lung transplantation. Radiological findings of these diseases, however, have slight morphological differences at recurrence compared with pre-transplantation^[27].

CONCLUSION

Lung transplantation is essentially the only viable option for treating end stage lung disease. Despite this advanced procedure, it poses a diverse list of complications that are associated with morbidity and mortality for transplant recipients. Although radiological manifestations of post-lung transplant complications may be non-specific, understanding the main features of post-transplant complications over a time continuum is the key to improving patients' survival. By recognising these radiological features, early treatment can be instituted.

REFERENCES

- 1 **International Society for Heart and Lung Transplantation.** The registry of the international society for heart and lung transplantation: Thirty-second annual report. Available from: URL: <https://www.ishlt.org/downloadables/slides/2015/introduction.pptx>
- 2 **ANZOD Committee.** ANZOD Registry Annual Report 2015. Australia and New Zealand Organ Donation Registry. Available from: URL: http://www.anzdata.org.au/anzod/ANZODReport/2015/2015ANZOD_annrpt.pdf
- 3 **O'Donovan PB.** Imaging of complications of lung transplantation. *Radiographics* 1993; **13**: 787-796 [PMID: 8356268 DOI: 10.1148/radiographics.13.4.8356268]
- 4 **Eberlein M, Permutt S, Chahla MF, Bolukbas S, Nathan SD, Shlobin OA, Shelhamer JH, Reed RM, Pearse DB, Orens JB, Brower RG.** Lung size mismatch in bilateral lung transplantation is associated with allograft function and bronchiolitis obliterans syndrome. *Chest* 2012; **141**: 451-460 [PMID: 21799025 DOI: 10.1378/chest.11-0767]
- 5 **Kundu S, Herman SJ, Winton TL.** Reperfusion edema after lung transplantation: radiographic manifestations. *Radiology* 1998; **206**: 75-80 [PMID: 9423654 DOI: 10.1148/radiology.206.1.9423654]
- 6 **Herman SJ, Rappaport DC, Weisbrod GL, Olscamp GC, Patterson GA, Cooper JD.** Single-lung transplantation: imaging features. *Radiology* 1989; **170**: 89-93 [PMID: 2642351 DOI: 10.1148/radiology.170.1.2642351]
- 7 **Krishnam MS, Suh RD, Tomasian A, Goldin JG, Lai C, Brown K, Batra P, Aberle DR.** Postoperative complications of lung transplantation: radiologic findings along a time continuum. *Radiographics* 2007; **27**: 957-974 [PMID: 17620461 DOI: 10.1148/rg.274065141]
- 8 **Belmaati EO, Steffensen I, Jensen C, Kofoed KF, Mortensen J, Nielsen MB, Iversen M.** Radiological patterns of primary graft dysfunction after lung transplantation evaluated by 64-multi-slice computed tomography: a descriptive study. *Interact Cardiovasc Thorac Surg* 2012; **14**: 785-791 [PMID: 22378316 DOI: 10.1093/icvts/ivs065]
- 9 **Diez Martinez P, Pakkal M, Prenovault J, Chevrier MC, Chalaoui J, Gorgos A, Ferraro P, Poirier C, Chartrand-Lefebvre C.** Postoperative imaging after lung transplantation. *Clin Imaging* 2013; **37**: 617-623 [PMID: 23557663 DOI: 10.1016/j.clinimag.2013.02.008]
- 10 **Hochhegger B, Irion KL, Marchiori E, Bello R, Moreira J, Camargo JJ.** Computed tomography findings of postoperative complications in lung transplantation. *J Bras Pneumol* 2009; **35**: 266-274 [PMID: 19390726 DOI: 10.1590/S1806-37132009000300012]
- 11 **Ahmad S, Shlobin OA, Nathan SD.** Pulmonary complications of lung transplantation. *Chest* 2011; **139**: 402-411 [PMID: 21285054 DOI: 10.1378/chest.10-1048]
- 12 **Ferrer J, Roldan J, Roman A, Bravo C, Monforte V, Pallisa E, Gic I, Sole J, Morell F.** Acute and chronic pleural complications in lung transplantation. *J Heart Lung Transplant* 2003; **22**: 1217-1225 [PMID: 14585383 DOI: 10.1016/S1053-2498(02)01230-5]
- 13 **Santacruz JF, Mehta AC.** Airway complications and management after lung transplantation: ischemia, dehiscence, and stenosis. *Proc Am Thorac Soc* 2009; **6**: 79-93 [PMID: 19131533 DOI: 10.1513/pats.200808-094GO]
- 14 **Anaya-Ayala JE, Loebe M, Davies MG.** Endovascular management of early lung transplant-related anastomotic pulmonary artery stenosis. *J Vasc Interv Radiol* 2015; **26**: 878-882 [PMID: 25851200 DOI: 10.1016/j.jvir.2015.02.017]
- 15 **Madan R, Chansakul T, Goldberg HJ.** Imaging in lung transplants: Checklist for the radiologist. *Indian J Radiol Imaging* 2014; **24**: 318-326 [PMID: 25489125 DOI: 10.4103/0971-3026.143894]
- 16 **Collins J, Müller NL, Kazerooni EA, Paciocco G.** CT findings of pneumonia after lung transplantation. *AJR Am J Roentgenol* 2000; **175**: 811-818 [PMID: 10954472 DOI: 10.2214/ajr.175.3.1750811]
- 17 **Judson MA, Handy JR, Sahn SA.** Pleural effusions following lung transplantation. Time course, characteristics, and clinical implications. *Chest* 1996; **109**: 1190-1194 [PMID: 8625665 DOI: 10.1378/chest.109.5.1190]
- 18 **Bankier AA, Van Muylem A, Scillia P, De Maertelaer V, Estenne M, Gevenois PA.** Air trapping in heart-lung transplant recipients: variability of anatomic distribution and extent at sequential expiratory thin-section CT. *Radiology* 2003; **229**: 737-742 [PMID: 14657310 DOI: 10.1148/radiol.2293020827]
- 19 **Matar LD, McAdams HP, Palmer SM, Howell DN, Henshaw NG, Davis RD, Tapson VF.** Respiratory viral infections in lung transplant recipients: radiologic findings with clinical correlation. *Radiology* 1999; **213**: 735-742 [PMID: 10580947 DOI: 10.1148/radiology.213.3.r99dc25735]
- 20 **Singh N, Husain S.** Aspergillus infections after lung transplantation: clinical differences in type of transplant and implications for management. *J Heart Lung Transplant* 2003; **22**: 258-266 [PMID: 12633692 DOI: 10.1016/S1053-2498(02)00477-1]
- 21 **Morales P, Briones A, Torres JJ, Solé A, Pérez D, Pastor A.** Pulmonary tuberculosis in lung and heart-lung transplantation: fifteen years of experience in a single center in Spain. *Transplant Proc* 2005; **37**: 4050-4055 [PMID: 16386624 DOI: 10.1016/j.transproceed.2005.09.144]
- 22 **Singh N, Paterson DL.** Mycobacterium tuberculosis infection in solid-organ transplant recipients: impact and implications for management. *Clin Infect Dis* 1998; **27**: 1266-1277 [PMID: 9827281 DOI: 10.1086/514993]
- 23 **Krivokuca I, van de Graaf EA, van Kessel DA, van den Bosch JM, Grutters JC, Kwakkel-van Erp JM.** Pulmonary embolism and pulmonary infarction after lung transplantation. *Clin Appl Thromb Hemost* 2011; **17**: 421-424 [PMID: 20547546 DOI: 10.1177/1076029610371474]
- 24 **Kremer BE, Reshef R, Misleh JG, Christie JD, Ahya VN, Blumenthal NP, Kotloff RM, Hadjiliadis D, Stadtmayer EA, Schuster SJ, Tsai DE.** Post-transplant lymphoproliferative disorder after lung transplantation: a review of 35 cases. *J Heart Lung Transplant* 2012; **31**: 296-304 [PMID: 22112992 DOI: 10.1016/j.healun.2011.10.013]
- 25 **Rappaport DC, Chamberlain DW, Shepherd FA, Hutcheon MA.** Lymphoproliferative disorders after lung transplantation: imaging

- features. *Radiology* 1998; **206**: 519-524 [PMID: 9457207 DOI: 10.1148/radiology.206.2.9457207]
- 26 **Grewal AS**, Padera RF, Boukedes S, Divo M, Rosas IO, Camp PC, Fuhlbrigge A, Goldberg H, El-Chemaly S. Prevalence and outcome of lung cancer in lung transplant recipients. *Respir Med* 2015; **109**: 427-433 [PMID: 25616348 DOI: 10.1016/j.rmed.2014.12.013]
- 27 **Collins J**, Hartman MJ, Warner TF, Müller NL, Kazerooni EA, McAdams HP, Slone RM, Parker LA. Frequency and CT findings of recurrent disease after lung transplantation. *Radiology* 2001; **219**: 503-509 [PMID: 11323479 DOI: 10.1148/radiology.219.2.r01ma12503]

P- Reviewer: Cerwenka H, Li YZ **S- Editor:** Ji FF **L- Editor:** A
E- Editor: Lu YJ



Aggressive blood pressure treatment of hypertensive intracerebral hemorrhage may lead to global cerebral hypoperfusion: Case report and imaging perspective

Jose Gavito-Higuera, Rakesh Khatri, Ihtesham A Qureshi, Alberto Maud, Gustavo J Rodriguez

Jose Gavito-Higuera, Rakesh Khatri, Ihtesham A Qureshi, Alberto Maud, Gustavo J Rodriguez, Department of Neurology, Paul L. Foster School of Medicine, Texas Tech University of Health Sciences Center, El Paso, TX 79905, United States

Author contributions: All authors contributed equally.

Informed consent statement: Informed consent was obtained from the family of the patient for the purpose of publication.

Conflict-of-interest statement: None.

Open-Access: This article is an open-access article which was selected by an in-house editor and fully peer-reviewed by external reviewers. It is distributed in accordance with the Creative Commons Attribution Non Commercial (CC BY-NC 4.0) license, which permits others to distribute, remix, adapt, build upon this work non-commercially, and license their derivative works on different terms, provided the original work is properly cited and the use is non-commercial. See: <http://creativecommons.org/licenses/by-nc/4.0/>

Manuscript source: Invited manuscript

Correspondence to: Rakesh Khatri, MD, Assistant Professor, Department of Neurology, Paul L. Foster School of Medicine, Texas Tech University of Health Sciences Center, 5001 El Paso Drive, El Paso, TX 79905, United States. rakesh.khatri@ttuhsc.edu
Telephone: +1-915-2155900
Fax: +1-915-5456705

Received: February 8, 2017

Peer-review started: February 12, 2017

First decision: May 17, 2017

Revised: August 22, 2017

Accepted: November 29, 2017

Article in press: November 29, 2017

Published online: December 28, 2017

Abstract

Hypoperfusion injury related to blood pressure decrease in

acute hypertensive intracerebral hemorrhage continues to be a controversial topic. Aggressive treatment is provided with the intent to stop the ongoing bleeding. However, there may be additional factors, including autoregulation and increased intracranial pressure, that may limit this approach. We present here a case of acute hypertensive intracerebral hemorrhage, in which aggressive blood pressure management to levels within the normal range led to global cerebral ischemia within multiple border zones. Global cerebral ischemia may be of concern in the management of hypertensive hemorrhage in the presence of premonitory poorly controlled blood pressure and increased intracranial pressure.

Key words: Intracranial hemorrhage; Neurocritical care; Stroke management; Perihematoma ischemia

© **The Author(s) 2017.** Published by Baishideng Publishing Group Inc. All rights reserved.

Core tip: The current case report highlights the risk of aggressive management of acute hypertension in the setting of intracerebral hemorrhage causing global cerebral hypoperfusion, despite maintenance of cerebral perfusion pressure above the lower threshold of autoregulation. The authors suggest the use of accurate method to measure cerebral oxygenation, such as brain-tissue oxygen monitoring, which could help individualize aggressive blood pressure control in patients with acute hypertensive intracerebral hemorrhage.

Gavito-Higuera J, Khatri R, Qureshi IA, Maud A, Rodriguez GJ. Aggressive blood pressure treatment of hypertensive intracerebral hemorrhage may lead to global cerebral hypoperfusion: Case report and imaging perspective. *World J Radiol* 2017; 9(12): 448-453 Available from: URL: <http://www.wjgnet.com/1949-8470/full/v9/i12/448.htm> DOI: <http://dx.doi.org/10.4329/wjr.v9.i12.448>

INTRODUCTION

Up to one-third of spontaneous intracerebral hemorrhages (ICHs) expand, typically, within the first 6 h after the ictus. This expansion contributes to clinical deterioration and worse outcome^[1-3]. Persistent high blood pressure may promote recurrent early bleeding^[4-6]. Despite several reports that supported aggressive blood pressure control, reducing the risk of bleeding and improving the outcome, recent randomized larger trials have failed to prove it^[7-9]. The safety of this approach has been questioned, mainly based on the concern that the perihematoma region may already be ischemic, due to local tissue pressure and have impaired autoregulation. But it may also be because autoregulation may be globally impaired after the ictus, or autoregulation may be retained but shifted substantially toward higher perfusion pressures. Based on these concerns, aggressive blood pressure reduction might lead to local or global ischemia.

There is evidence suggesting that autoregulation is retained locally in the perihematoma region. Blood flow decreases in areas adjacent to the hematoma; although, there is an accompanying decrease in metabolism without evidence of ischemia^[10]. Cerebral autoregulation has been shown to be preserved in small- and medium-sized hematomas; however, it is variably shifted to higher levels in patients with chronic hypertension^[11,12]. Determining whether blood pressure management prevents hematoma growth after ICH and how blood pressure reduction can be safely performed are key research priorities^[13].

We present herein a case of spontaneous ICH, for which aggressive treatment of hypertension did not lead to infarction around the hematoma but globally in multiple border zone areas.

CASE REPORT

A 52-year-old black woman suddenly developed slurred speech and mild right hemiparesis. Medical history included poorly controlled chronic hypertension, and no known history of atrial fibrillation. In the emergency department, the initial blood pressure reading was 264/218 mmHg. The patient had right hemiparesis and dysarthria, and it was also noted that she was confused. After an episode of emesis she became lethargic, requiring emergent endotracheal intubation. A computerized tomography (CT) scan of the head showed a left thalamic hemorrhage (volume 36 mL, $A \times B \times C/2$) with intraventricular extension and developing hydrocephalus. Treatment to control blood pressure included intravenous labetalol boluses and nitroprusside infusion. External ventricular drainage was placed to manage hydrocephalus, and intracranial pressure and cerebral perfusion pressure were then monitored (Figure 1).

The patient underwent CT angiography of the head on arrival, which revealed no vessel occlusion. In addition, further work-up including continuous

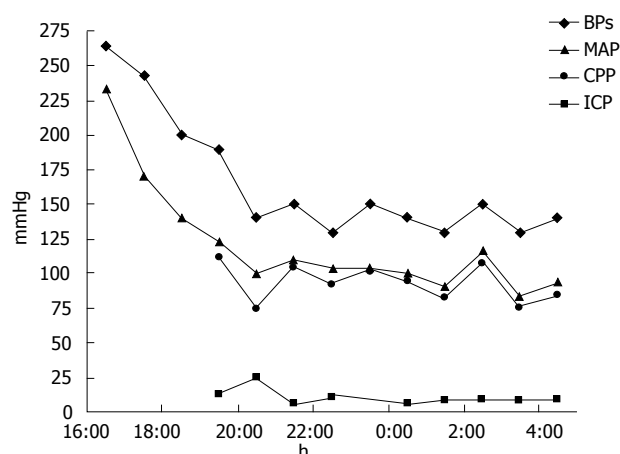


Figure 1 Diagram showing the evolution of systolic blood pressure, mean arterial blood pressure, cerebral perfusion pressure and intracranial pressure within the first 12 h. BP: Blood pressure; MAP: Mean arterial blood pressure; CPP: Cerebral perfusion pressure; ICP: Intracranial pressure.

cardiac monitoring in telemetry unit in the intensive care unit (ICU) for several days, electrocardiogram and echocardiogram did not reveal any cardioembolic etiology, except for left ventricular hypertrophy. For the following days, the patient remained comatose, although examination was limited due to sedation. A follow-up CT of the head at 96 h post-admission showed a cerebellar hypodensity. Magnetic resonance imaging (MRI) of the brain showed areas of restricted diffusion consistent with acute ischemia in multiple internal border zone areas of bilateral cerebral and cerebellar hemispheres (Figure 2). No significant stenosis was found in the magnetic angiography of the neck or brain. Cerebral perfusion pressure was above 70 mmHg, except for two measurements (68 mmHg on day 2 and 62 mmHg on day 4). On day 2, intraventricular thrombolytics were administered and the ventriculostomy was clamped. On day 4, blood pressure was 110/55 (the lowest recorded) and the nitroprusside drip was reduced with rapid improvement. The patient survived, but was aphasic and right hemiparetic at the time of discharge to a nursing home.

DISCUSSION

Two features in this case are to be discussed. First, global cerebral ischemia after aggressive blood pressure reduction seemed more a concern than the presence of ischemia around the hematoma; and, second, global ischemia developed despite maintenance of cerebral perfusion pressure above the lower threshold of autoregulation in normals.

The fact that the region around the hematoma was spared, with a mean arterial pressure reduction of about 50%, goes along with recent work by Powers *et al.*^[12] and Zazulia *et al.*^[14]. Although ischemia around the hematoma was initially thought to be present and to contribute to secondary brain injury based on experimental animal models^[15-17], nowadays it is

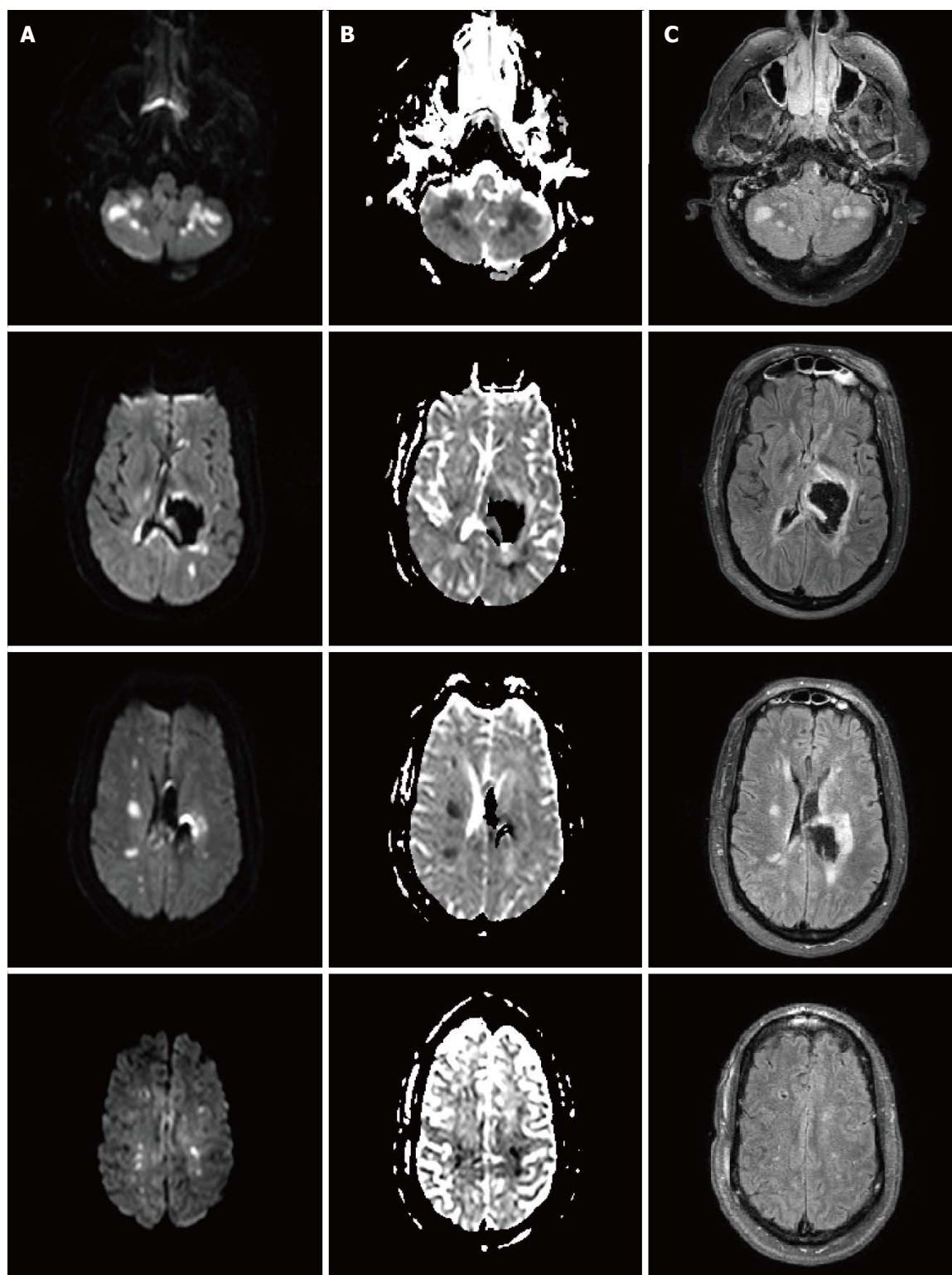


Figure 2 Brain magnetic resonance imaging with diffusion weighted imaging (A), apparent diffusion coefficient (B) and FLAIR sequences (C) showing multiple areas of infarction in the internal border zone areas of bilateral cerebral and cerebellar hemispheres. There is no evidence of perihematoma infarction. MRI: Magnetic resonance imaging.

more controversial and it is becoming more evident about its absence, based on human studies. Using MRI, no markers of ischemia were associated with the perihematoma region in acute ICH^[18,19]. Positron emission tomography (PET) studies also reported

perihematoma cerebral blood flow reductions, without evidence of ischemia^[20]. Reduced perihematoma cerebral blood flow was associated with a decreased metabolic rate of oxygen and oxygen extraction fraction, suggesting that flow changes represent hypoactive

rather than ischemic tissue^[14].

On the basis of evidence derived from laboratory and clinical studies, three phases have been identified^[10]. The hibernation phase, an acute period of concomitant hypoperfusion and hypometabolism, predominantly involves the perihematoma region and occurs during the first 2 d. The reperfusion phase is observed between days 2 and 14, with a heterogeneous pattern of cerebral blood flow, consisting of areas of relatively normal flow, persistent hypoperfusion and hyperperfusion. And, the normalization phase is observed thereafter, with normal cerebral blood flow reestablished in all viable regions. In this case, hypometabolism in the area around the hematoma might have prevented the tissue from infarction.

The reduction of about 50% in the mean arterial pressure may seem unsafe; although, once the intracranial pressure was monitored, the cerebral perfusion pressure (CPP) could be calculated, and in fact it was kept above the lower range for normals. Nevertheless, strong evidence-based guidelines for the management of blood pressure in patients with spontaneous ICH with systolic blood pressure more than 220 mm Hg are not clearly established. The writing group of the stroke council for the American Heart Association encourages in their guidelines, aggressive treatment of high blood pressure to prevent ongoing bleeding with the caveat that aggressive treatment may decrease cerebral perfusion and worsen brain damage, especially^[21-23]. Based on these two rationales, the recommendation is for patients presenting with a systolic blood pressure between 150 and 220 mmHg, acute lowering of systolic blood pressure to 140 mmHg is safe (Class I ; Level of Evidence A); however, if the systolic blood pressure at presentation is above 220 mmHg, the recommendation of aggressive reduction is less clear (Class II b; Level of Evidence C). Intracranial pressure monitoring is also considered in patients with significant intraventricular hemorrhage or hydrocephalus, with a reasonable goal CPP between 50-70 mmHg (Class II b; Level of Evidence C).

Cerebral autoregulation maintains cerebral blood flow by modifying the cerebrovascular resistance when cerebral perfusion pressure fluctuates, keeping cerebral blood flow constant in normal subjects at a CPP between 50-70 mmHg^[24]. In chronic hypertension, cerebral autoregulation is shifted to higher levels and the degree correlates with the severity of hypertension. Thickening in the vascular wall increases the resistance, providing tissue protection if CPP is high; however, the ability to dilate when CPP lowers is lessened^[25,26]. While perfusion pressure is calculable at bedside, quantitative tissue flow cannot be measured without employing a method such PET or a more invasive one using brain-tissue oxygen monitors^[27]. Recently, it has been shown in traumatic brain injury that up to one-third of patients may demonstrate low brain tissue oxygen despite adequate CPP^[28,29].

The patient presented herein developed multiple

cerebral border zone infarcts after aggressive but carefully monitored treatment of blood pressure with labetalol and nitroprusside. Several modern imaging studies suggest that an internal watershed infarction is primarily caused by hypoperfusion as seen in our patient; this should not be confused with cortical watershed infarct, which is primarily caused by microembolism^[30-33].

We hypothesize that the lower limit of autoregulation was shifted to higher levels secondary to chronic untreated hypertension. What is an adequate cerebral perfusion pressure in a normal subject was not so in her case, resulting in insufficient cerebral blood flow and ischemia. Alternatively, decreased cerebral perfusion pressure could have occurred during treatment of hypertension prior to intracranial pressure monitoring (Figure 2).

In conclusion, aggressive management of acute hypertension in ICH is controversial. Global but not perihematoma hypoperfusion may be of more concern in this approach, since cerebral autoregulation in chronic hypertensive patients is variably shifted to higher levels. An accurate method to measure cerebral oxygenation, such as brain-tissue oxygen monitoring, could help individualize aggressive blood pressure control in patients with acute hypertensive ICH.

ARTICLE HIGHLIGHTS

Case characteristics

This case illustrates diffuse border zone infarcts caused by rapid and dramatic reduction in blood pressure in a patient presenting with intracerebral hemorrhage and chronic uncontrolled hypertension.

Clinical diagnosis

Stroke, sudden onset of slurred speech, right-sided hemiparesis, dysarthria, lethargy, blood pressure of 264/218.

Differential diagnosis

Ischemic stroke, hemorrhagic stroke, transient ischemic attack, hypoglycemia, Todd's paralysis, intracerebral aneurysm rupture.

Laboratory diagnosis

No laboratory test was diagnostic; the patient, however, presented with very elevated blood pressure levels, and normal blood sugar levels.

Imaging diagnosis

Non-contrast computed tomography (CT) scan of the head showed left thalamic hemorrhage with intraventricular extension and developing hydrocephalus. Follow-up non-contrast CT scan of the head at 96 h showed a cerebellar hypodensity. Electrocardiogram revealed normal sinus rhythm. Echocardiogram did not reveal any cardioembolic etiology, except for left ventricular hypertrophy. Magnetic resonance imaging of the brain showed areas of restricted diffusion consistent with acute ischemia in multiple internal border zone areas of bilateral cerebral and cerebellar hemispheres; the location in the border zone areas makes embolic etiology of the ischemia unlikely. Magnetic resonance angiography of the brain and neck revealed no significant stenosis that could have contributed to the cerebral ischemia.

Treatment

Blood pressure control with intravenous labetalol boluses and nitroprusside infusion. For the management of hydrocephalus and monitoring of intracranial and cerebral perfusion pressures, external ventricular drain was placed.

Intraventricular thrombolytics were given to prevent clot formation in the ventricles and facilitate the cerebrospinal fluid drainage.

Related reports

There are several randomized controlled trials that have focused on blood pressure control in the setting of intracerebral hemorrhage; however, strong evidence-based guidelines for the management of blood pressure in patients with spontaneous intracerebral hemorrhage and systolic blood pressure more than 220 mmHg are not clearly established.

Term explanation

Hematoma expansion: An increase in size of the initial intracerebral hemorrhage that occurs in up to one-third of the patients, usually within the first 24 h. **Borderline or watershed infarctions:** Those that occur in areas shared by two vascular territories; those areas are more susceptible to perfusion reduction as it happens with blood pressure reduction and/or shifted cerebral autoregulation. **Cerebral autoregulation:** A physiological mechanism that maintains cerebral blood flow at different blood pressure levels. In patients with chronic hypertension, the curve shifts to the right ("right shifted"); autoregulation is used for higher blood pressure levels, and it is more protective to elevated blood pressure but fails to react in case of lower blood pressure levels.

Experiences and lessons

Caution should be advised when blood pressure reduction is considered in patients with intracerebral hemorrhage, especially if arriving with very elevated blood pressure and known to have untreated chronic hypertension. In addition, the presence of concomitant increased intracranial pressure due to the mass effect and/or hydrocephalus after intraventricular extension increases the intracranial pressure and thus decreases the cerebral perfusion pressure. Cerebral autoregulation shifts to the right in patients with chronic untreated hypertension and a reduction in blood pressure may not be tolerated leading to ischemia; therefore, such intervention in certain cases may be unsafe, as described in the article.

REFERENCES

- 1 **Brott T**, Broderick J, Kothari R, Barsan W, Tomsick T, Sauerbeck L, Spilker J, Duldner J, Khoury J. Early hemorrhage growth in patients with intracerebral hemorrhage. *Stroke* 1997; **28**: 1-5 [PMID: 8996478 DOI: 10.1161/01.STR.28.1.1]
- 2 **Kazui S**, Naritomi H, Yamamoto H, Sawada T, Yamaguchi T. Enlargement of spontaneous intracerebral hemorrhage. Incidence and time course. *Stroke* 1996; **27**: 1783-1787 [PMID: 8841330 DOI: 10.1161/01.STR.27.10.1783]
- 3 **Broderick JP**, Brott TG, Tomsick T, Barsan W, Spilker J. Ultra-early evaluation of intracerebral hemorrhage. *J Neurosurg* 1990; **72**: 195-199 [PMID: 2295917 DOI: 10.3171/jns.1990.72.2.0195]
- 4 **Kazui S**, Minematsu K, Yamamoto H, Sawada T, Yamaguchi T. Predisposing factors to enlargement of spontaneous intracerebral hematoma. *Stroke* 1997; **28**: 2370-2375 [PMID: 9412616 DOI: 10.1161/01.STR.28.12.2370]
- 5 **Becker KJ**, Baxter AB, Bybee HM, Tirschwell DL, Abouelsaad T, Cohen WA. Extravasation of radiographic contrast is an independent predictor of death in primary intracerebral hemorrhage. *Stroke* 1999; **30**: 2025-2032 [PMID: 10512902 DOI: 10.1161/01.STR.30.10.2025]
- 6 **Ohwaki K**, Yano E, Nagashima H, Hirata M, Nakagomi T, Tamura A. Blood pressure management in acute intracerebral hemorrhage: relationship between elevated blood pressure and hematoma enlargement. *Stroke* 2004; **35**: 1364-1367 [PMID: 15118169 DOI: 10.1161/01.STR.0000128795.38283.4b]
- 7 **Anderson CS**, Heeley E, Huang Y, Wang J, Stapf C, Delcourt C, Lindley R, Robinson T, Lavados P, Neal B, Hata J, Arima H, Parsons M, Li Y, Wang J, Heritier S, Li Q, Woodward M, Simes RJ, Davis SM, Chalmers J; INTERACT2 Investigators. Rapid blood-pressure lowering in patients with acute intracerebral hemorrhage. *N Engl J Med* 2013; **368**: 2355-2365 [PMID: 23713578 DOI: 10.1056/NEJMoa1214609]
- 8 **Qureshi AI**. Antihypertensive Treatment of Acute Cerebral Hemorrhage (ATACH): rationale and design. *Neurocrit Care* 2007; **6**: 56-66 [PMID: 17356194 DOI: 10.1385/NCC.6:1:56]
- 9 **Qureshi AI**, Palesch YY, Barsan WG, Hanley DF, Hsu CY, Martin RL, Moy CS, Silbergleit R, Steiner T, Suarez JJ, Toyoda K, Wang Y, Yamamoto H, Yoon BW; ATACH-2 Trial Investigators and the Neurological Emergency Treatment Trials Network. Intensive Blood-Pressure Lowering in Patients with Acute Cerebral Hemorrhage. *N Engl J Med* 2016; **375**: 1033-1043 [PMID: 27276234 DOI: 10.1056/NEJMoa1603460]
- 10 **Qureshi AI**, Hanel RA, Kirmani JF, Yahia AM, Hopkins LN. Cerebral blood flow changes associated with intracerebral hemorrhage. *Neurosurg Clin N Am* 2002; **13**: 355-370 [PMID: 12486925 DOI: 10.1016/S1042-3680(02)00012-8]
- 11 **Strandgaard S**. Autoregulation of cerebral blood flow in hypertensive patients. The modifying influence of prolonged antihypertensive treatment on the tolerance to acute, drug-induced hypotension. *Circulation* 1976; **53**: 720-727 [PMID: 815061 DOI: 10.1161/01.CIR.53.4.720]
- 12 **Powers WJ**, Zazulia AR, Videen TO, Adams RE, Yundt KD, Aiyagari V, Grubb RL Jr, Diringner MN. Autoregulation of cerebral blood flow surrounding acute (6 to 22 hours) intracerebral hemorrhage. *Neurology* 2001; **57**: 18-24 [PMID: 11445622 DOI: 10.1212/WNL.57.1.18]
- 13 **NINDS ICH Workshop Participants**. Priorities for clinical research in intracerebral hemorrhage: report from a National Institute of Neurological Disorders and Stroke workshop. *Stroke* 2005; **36**: e23-e41 [PMID: 15692109 DOI: 10.1161/01.STR.0000155685.77775.4c]
- 14 **Zazulia AR**, Diringner MN, Videen TO, Adams RE, Yundt K, Aiyagari V, Grubb RL Jr, Powers WJ. Hypoperfusion without ischemia surrounding acute intracerebral hemorrhage. *J Cereb Blood Flow Metab* 2001; **21**: 804-810 [PMID: 11435792 DOI: 10.1097/00004647-200107000-00005]
- 15 **Kobari M**, Gotoh F, Tomita M, Tanahashi N, Shinohara T, Terayama Y, Mihara B. Bilateral hemispheric reduction of cerebral blood volume and blood flow immediately after experimental cerebral hemorrhage in cats. *Stroke* 1988; **19**: 991-996 [PMID: 3400110 DOI: 10.1161/01.STR.19.8.991]
- 16 **Bullock R**, Brock-Utne J, van Dellen J, Blake G. Intracerebral hemorrhage in a primate model: effect on regional cerebral blood flow. *Surg Neurol* 1988; **29**: 101-107 [PMID: 3336844 DOI: 10.1016/0090-3019(88)90065-1]
- 17 **Nehls DG**, Mendelow AD, Graham DI, Sinar EJ, Teasdale GM. Experimental intracerebral hemorrhage: progression of hemodynamic changes after production of a spontaneous mass lesion. *Neurosurgery* 1988; **23**: 439-444 [PMID: 3200374]
- 18 **Butcher KS**, Baird T, MacGregor L, Desmond P, Tress B, Davis S. Perihematomal edema in primary intracerebral hemorrhage is plasma derived. *Stroke* 2004; **35**: 1879-1885 [PMID: 15178826 DOI: 10.1161/01.STR.0000131807.54742.1a]
- 19 **Schellinger PD**, Fiebach JB, Hoffmann K, Becker K, Orakcioglu B, Kollmar R, Jüttler E, Schramm P, Schwab S, Sartor K, Hacke W. Stroke MRI in intracerebral hemorrhage: is there a perihemorrhagic penumbra? *Stroke* 2003; **34**: 1674-1679 [PMID: 12805502 DOI: 10.1161/01.STR.0000076010.10696.55]
- 20 **Hirano T**, Read SJ, Abbott DF, Sachinidis JJ, Tochon-Danguy HJ, Egan GF, Bladin CF, Scott AM, McKay WJ, Donnan GA. No evidence of hypoxic tissue on 18F-fluoromisonidazole PET after intracerebral hemorrhage. *Neurology* 1999; **53**: 2179-2182 [PMID: 10599802 DOI: 10.1212/WNL.53.9.2179]
- 21 **Hemphill JC 3rd**, Greenberg SM, Anderson CS, Becker K, Bendok BR, Cushman M, Fung GL, Goldstein JN, Macdonald RL, Mitchell PH, Scott PA, Selim MH, Woo D; American Heart Association Stroke Council; Council on Cardiovascular and Stroke Nursing; Council on Clinical Cardiology. Guidelines for the Management of Spontaneous Intracerebral Hemorrhage: A Guideline for Healthcare Professionals From the American Heart Association/American Stroke Association. *Stroke* 2015; **46**: 2032-2060 [PMID: 26022637 DOI: 10.1161/STR.0000000000000069]
- 22 **D'Amore C**, Paciaroni M. Border-zone and watershed infarctions. *Front Neurol Neurosci* 2012; **30**: 181-184 [PMID: 22377891 DOI: 10.1159/000333638]

- 23 **Gerraty RP**, Gilford EJ, Gates PC. Watershed cerebral infarction associated with perioperative hypotension. *Clin Exp Neurol* 1993; **30**: 82-89 [PMID: 7712632]
- 24 **Aaslid R**, Lindegaard KF, Sorteberg W, Nornes H. Cerebral autoregulation dynamics in humans. *Stroke* 1989; **20**: 45-52 [PMID: 2492126 DOI: 10.1161/01.STR.20.1.45]
- 25 **Baumbach GL**, Heistad DD. Cerebral circulation in chronic arterial hypertension. *Hypertension* 1988; **12**: 89-95 [PMID: 3044994 DOI: 10.1161/01.HYP.12.2.89]
- 26 **Agnoli A**, Fieschi C, Bozzao L, Battistini N, Prencipe M. Autoregulation of cerebral blood flow. Studies during drug-induced hypertension in normal subjects and in patients with cerebral vascular diseases. *Circulation* 1968; **38**: 800-812 [PMID: 5677964 DOI: 10.1161/01.CIR.38.4.800]
- 27 **Powers WJ**, Zazulia AR. The use of positron emission tomography in cerebrovascular disease. *Neuroimaging Clin N Am* 2003; **13**: 741-758 [PMID: 15024958]
- 28 **Stiefel MF**, Udoetuk JD, Spiotta AM, Gracias VH, Goldberg A, Maloney-Wilensky E, Bloom S, Le Roux PD. Conventional neurocritical care and cerebral oxygenation after traumatic brain injury. *J Neurosurg* 2006; **105**: 568-575 [PMID: 17044560 DOI: 10.3171/jns.2006.105.4.568]
- 29 **Stocchetti N**, Chieregato A, De Marchi M, Croci M, Benti R, Grimoldi N. High cerebral perfusion pressure improves low values of local brain tissue O₂ tension (PtiO₂) in focal lesions. *Acta Neurochir Suppl* 1998; **71**: 162-165 [PMID: 9779173 DOI: 10.1007/978-3-7091-6475-4_47]
- 30 **Zheng M**, Sun A, Sun Q, Zhang H, Fan D. Clinical and Imaging Analysis of a Cerebellar Watershed Infarction. *Chinese Medicine* 2015; **6**: 54-60 [DOI: 10.4236/cm.2015.61006]
- 31 **Moriwaki H**, Matsumoto M, Hashikawa K, Oku N, Ishida M, Seike Y, Watanabe Y, Hougaku H, Handa N, Nishimura T. Hemodynamic aspect of cerebral watershed infarction: assessment of perfusion reserve using iodine-123-iodoamphetamine SPECT. *J Nucl Med* 1997; **38**: 1556-1562 [PMID: 9379192]
- 32 **Lee PH**, Bang OY, Oh SH, Joo IS, Huh K. Subcortical white matter infarcts: comparison of superficial perforating artery and internal border-zone infarcts using diffusion-weighted magnetic resonance imaging. *Stroke* 2003; **34**: 2630-2635 [PMID: 14563962 DOI: 10.1161/01.STR.0000097609.66185.05]
- 33 **Gould B**, McCourt R, Gioia LC, Kate M, Hill MD, Asdaghi N, Dowlathshahi D, Jeerakathil T, Coutts SB, Demchuk AM, Emery D, Shuaib A, Butcher K; ICH ADAPT Investigators. Acute blood pressure reduction in patients with intracerebral hemorrhage does not result in borderzone region hypoperfusion. *Stroke* 2014; **45**: 2894-2899 [PMID: 25147326 DOI: 10.1161/STROKEAHA.114.005614]

P- Reviewer: Kim MS, Llompert-Pou JA, Shen J, Zavras N
S- Editor: Kong JX **L- Editor:** Filipodia **E- Editor:** Lu YJ



Case of victims of modern imaging technology: Increased information noise concealing the diagnosis

Abhishek Mahajan, G V Santhoshkumar, Ameya Shirish Kawthalkar, Richa Vaish, Nilesh Sable, Supreeta Arya, Subhash Desai

Abhishek Mahajan, G V Santhoshkumar, Ameya Shirish Kawthalkar, Richa Vaish, Nilesh Sable, Supreeta Arya, Subhash Desai, Department of Radiodiagnosis and Imaging, Tata Memorial Hospital, Mumbai 400012, India

ORCID number: Abhishek Mahajan (0000-0001-6606-6537); G V Santhoshkumar (0000-0001-5426-5651); Ameya Shirish Kawthalkar (0000-0002-3248-325X); Richa Vaish (0000-0002-3384-9380); Nilesh Sable (0000-0002-3384-9380); Supreeta Arya (0000-0002-0483-9095); Subhash Desai (0000-0003-2525-0690).

Author contributions: All authors contributed to study concepts/ study design, data acquisition or data analysis/interpretation, manuscript drafting or manuscript revision for important intellectual content, manuscript final version approval, literature research, manuscript editing and integrity of the data/ the accuracy of the data analysis.

Informed consent statement: Participant gave informed consent for data sharing.

Conflict-of-interest statement: I confirm that this manuscript is not published anywhere else and on behalf of all authors, I state that there is no conflict of interests (including none for related to commercial, personal, political, intellectual, or religious interests).

Open-Access: This article is an open-access article which was selected by an in-house editor and fully peer-reviewed by external reviewers. It is distributed in accordance with the Creative Commons Attribution Non Commercial (CC BY-NC 4.0) license, which permits others to distribute, remix, adapt, build upon this work non-commercially, and license their derivative works on different terms, provided the original work is properly cited and the use is non-commercial. See: <http://creativecommons.org/licenses/by-nc/4.0/>

Manuscript source: Unsolicited manuscript

Correspondence to: Abhishek Mahajan, MRes, MD, Radiodiagnosis, Fellowship in Cancer Imaging, Associate professor, Department of Radiodiagnosis and Imaging, Tata Memorial Hospital, Room No. 127, Dr E Borges Road, Parel, Mumbai

400012, India. mahajana@tmc.gov.in
Telephone: +91-99-20210811

Received: September 13, 2017

Peer-review started: September 19, 2017

First decision: October 23, 2017

Revised: November 9, 2017

Accepted: November 27, 2017

Article in press: November 27, 2017

Published online: December 28, 2017

Abstract

We present a case of tubercular arthritis who underwent numerous unnecessary investigations what is known as "victims of modern imaging technology" or VOMIT. Today there is an exponential rise in the volume of the medical imaging, part of which is contributed by unnecessary and unjustified indications. We discuss about the untoward effects of the uninhibited and careless use of modern imaging modalities and possible ways to avoid. Skeletal manifestation of the tuberculosis is still common in the endemic countries like India. Although the final diagnosis of the skeletal tuberculosis like tubercular arthritis is made by bacteriological and histological studies, few demographic, clinical and radiological features might help making early diagnosis.

Key words: Radiology; Modern imaging; Patient care; Healthcare costs; Tubercular arthritis; Diagnostic imaging overuse

© **The Author(s) 2017.** Published by Baishideng Publishing Group Inc. All rights reserved.

Core tip: The primary objective is to highlight the possible consequences of the irrational use of imaging investigations. In this case report, we want to explain about an anxious patient undergoing some myriad

investigations for an uncommon presentation of common presentations. It is important to optimally use available resources with improved communication with referring physicians and increasing the awareness regarding the utility and indications for various imaging.

Mahajan A, Santhoshkumar GV, Kawthalkar AS, Vaish R, Sable N, Arya S, Desai S. Case of victims of modern imaging technology: Increased information noise concealing the diagnosis. *World J Radiol* 2017; 9(12): 454-458 Available from: URL: <http://www.wjgnet.com/1949-8470/full/v9/i12/454.htm> DOI: <http://dx.doi.org/10.4329/wjr.v9.i12.454>

INTRODUCTION

With modern medical imaging boom and exponential rise of its volume as well as with increasing accuracy from these imaging, it is small wonder that the examples of victims of modern imaging technology or VOMIT are on the rise^[1,2]. While radiology and imaging are influencing patient management and treatment decisions like never before, unscrupulous and careless use of newer imaging techniques is detrimental to the patient's as well as hospital's resources and, contributes significantly to patient's anxiety if a grave diagnosis is mistakenly made.

Skeletal tuberculosis is uncommon in third world countries with Appendicular joint affection being uncommon than spinal tuberculosis^[3]. The few cases of distal small joint affectations are all prior to 1980^[4]. Two cases of tubercular arthritis mimicking neoplasm have been reported^[5]. However, there is no case reported of carcinomatous arthropathy of the first metacarpophalangeal joint^[6]. As an example of VOMIT in the modern era, we wish to highlight a rare case of tubercular arthritis of the first metacarpophalangeal joint masquerading as skeletal metastasis, which demonstrates the ill-effects of unwarranted excessive medical imaging.

CASE REPORT

A 40-year-old male presented with pain and swelling of the left thumb in the past 1 mo along with vague bone and joint pains and associated swelling in the neck. Clinical evaluation for the midline neck swelling revealed an indeterminate heteroechoic 15 mm thyroid lesion on sonography (Figure 1). His routine blood investigations and serum biochemistry were normal. The radiograph of his left thumb revealed destruction of the left first metacarpophalangeal joint. A Tc-99m pertechnetate thyroid scan showed focal low-grade uptake in the thyroid in the same location. Assuming this thyroid lesion as a primary carcinoma and the thumb lesion as metastatic, the patient was advised a fluoride-18 bone scan for the multiple vague bone and joint pains that showed a focus of intense tracer uptake at the left first

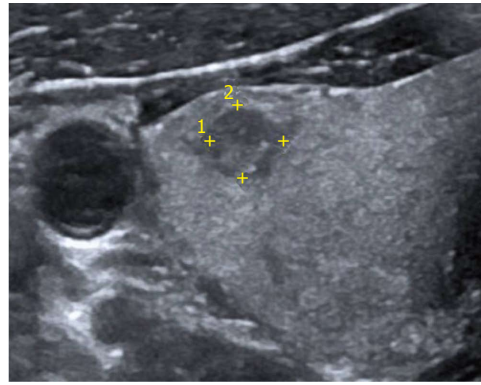


Figure 1 High resolution ultrasonography of the neck reveals a well-defined heteroechoic lesion in the right lobe of thyroid gland which appeared indeterminate on imaging (TIRADS 4B).

metacarpophalangeal joint accompanied by varying degrees of uptake at multiple sites in the appendicular and axial skeleton. The patient was thus referred to our tertiary cancer institute for further management.

Our Head and Neck Surgical Oncology OPD advised sonography-guided thyroid FNAC that was reported as benign colloid goiter (Bethesda category II). The CT-guided biopsy of hand lesion (Figure 2) reported necrotic tissue with calcification and reparative changes, along with few lymphoid cells and, suggested evaluation for any parathyroid pathology. On sonography, the parathyroids were normal and he had normal levels of rheumatoid factor, serum uric acid, and parathormone levels. ESR was marginally elevated (42 mm/h).

An FDG positron emission tomography- computed tomography (PET-CT) was performed to confirm/rule out malignancy, which revealed a lytic destructive lesion of the first metacarpophalangeal joint with a soft tissue component, having a maximum standardized uptake value (SUV) of 17.2. No uptake was noted elsewhere in the appendicular or axial skeleton. The lung images showed diffuse ground glass opacities with multiple subcentimeter sized soft tissue density nodules, fibrotic changes and calcified granulomas in both the lungs (Figure 3). Considering the patient's demographic and clinical background these were most likely suggestive of active pulmonary tuberculosis.

MR of the affected hand suggested by our orthopedic surgeons revealed altered marrow signal intensity involving the left first MCP joint with associated articular cortical destruction, synovitis, active enhancing pannus formation and rim-enhancing soft tissue component (abscesses) (Figure 4). A review of the previous radiograph showed joint destruction and peri-articular osteopenia (Figure 5). Malignancy being ruled out, the differentials narrowed down to an infective or traumatic arthropathy. Correlating the radiographic, PET-CT and MR findings, a provisional diagnosis of tubercular arthritis secondary to active pulmonary tuberculosis was made.

A pathology review of the CT guided biopsy sample was asked with real time polymerase chain reaction

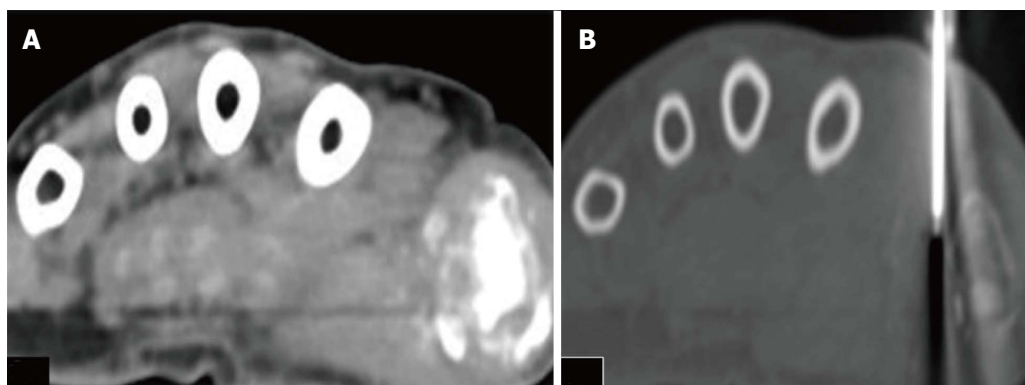


Figure 2 Axial computed tomography of the hand. The patient is positioned in prone position. A: Axial CT scan image in soft tissue window; B: Axial CT scan image in bone window is showing Trucut biopsy needle taking tissue sample from the soft tissue component surrounding the area of lytic destructive lesion at the first metacarpo-phalangeal joint. CT: Computed tomography.

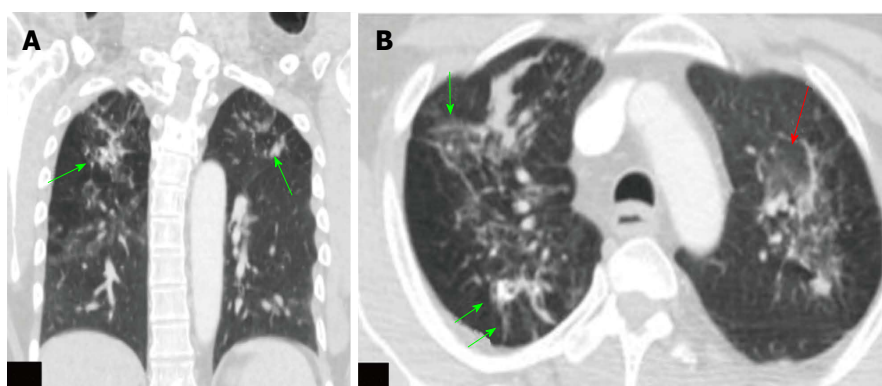


Figure 3 Computed tomography thorax images of the positron emission tomography-computed tomography scan. A: Coronal CT scan image of the thorax in lung window; B: Axial CT scan image of the thorax in lung window at upper thorax. These images show ground glass opacities (red arrow) with multiple soft tissue density nodules (green arrow), fibrotic changes and calcified granulomas in both the lungs. Features are suggestive of active tuberculosis. CT: Computed tomography.

(RT-PCR). This test revealed evidence of mycobacterium tuberculosis within the biopsy sample, thus establishing the diagnosis of tubercular arthritis of the left first metacarpophalangeal joint.

At the end of all these diagnostic investigations which included radiological, biochemical and histological tests, patient spent a significant amount of money and time. He also paid for travel expenses and registration and consultation charges in various hospitals. Added to this he must have underwent mental turmoil of anxiety and frustration. Not only these were costing him, there was waste of resources and time of hospitals/country which might have been used for patient in need.

DISCUSSION

It's been a while that the concept of VOMIT was put forth to prevent patients from needless diagnostic costs and mental anguish after being put through a battery of expensive and misdirected imaging tests^[1,2]. Still cases such as these are routinely found in clinical practice; the primary reason is our inability to discern pertinent data from the flood of information provided by myriad new imaging studies.

In this century and in endemic countries like India, primary bone tuberculosis is not as common; spine and large joint afflictions are seen, but those of small joints are infrequent^[3,4]. The mean age of presentation is 20 to 40 years and presenting with pain and swelling of affected joint; mostly metacarpal of the little finger^[7]. Radiologically, the key to diagnosis is the Phemister's triad that includes juxta-articular osteopenia, subarticular erosions and joint space narrowing, with or without soft tissue component^[2]. Key magnetic resonance imaging (MRI) features include synovitis, joint effusion, subarticular erosions, active and chronic pannus, abscesses, hypointense synovium and bone chips^[8].

The final diagnosis of tuberculous arthritis is based on bacteriology and histological studies. The differential diagnosis of tuberculous arthritis includes gout, sarcoidosis, osteomyelitis and tumors^[9]. Inflammatory and infective lesions may show high grade FDG uptake, and every lesion which demonstrates high SUV should not be labeled as a malignancy^[10]. Metastatic arthropathy is a rare occurrence with only a handful of cases reported in the literature^[5,6]. For joint disease in patients with a known primary, other etiologies should always be considered first in the differential diagnosis.

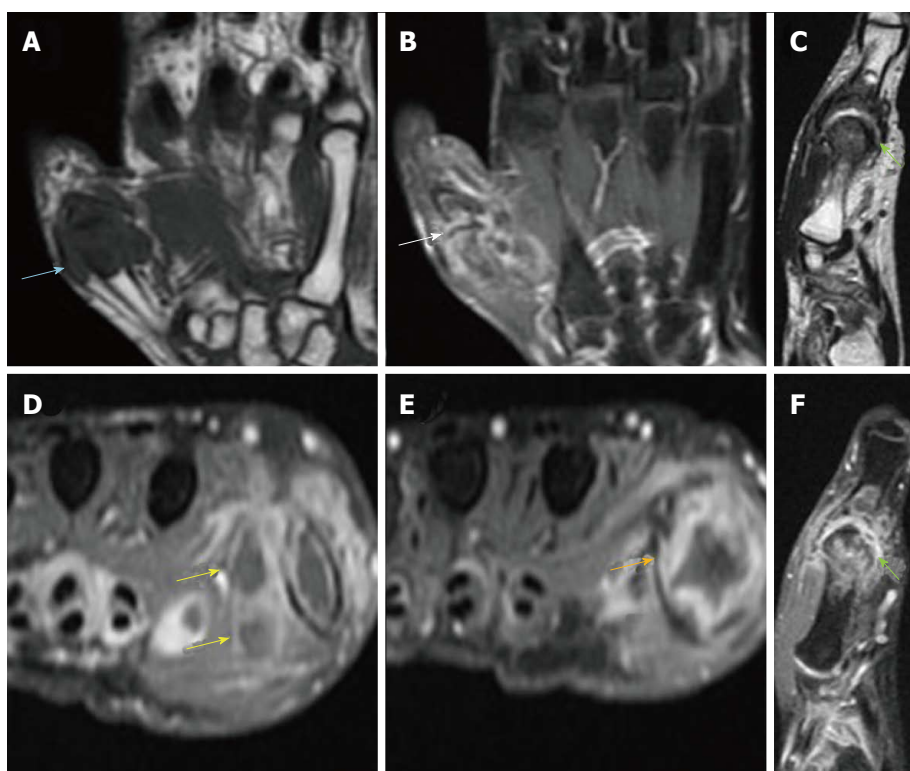


Figure 4 Plain and contrast enhanced magnetic resonance imaging images of proximal hand. A: Coronal T1W. Hypointense soft-tissue is noted surrounding the first MCP joint with hypointense marrow changes; B: Coronal STIR. Irregular hyperintensities are seen surrounding the first MCP joint along with hyperintensity within the peri-articular bone marrow; C: Sagittal T2W. Mild joint effusion is seen with hypertrophied T2 hypointense synovium and pannus formation; D-F: Axial and sagittal post-contrast Fat Sat T1W. Arrows indicate peripherally enhancing abscesses adjacent to the first MCP joint. Also noted in the vicinity is enhancing proliferative pannus. MCP: Metacarpophalangeal.



Figure 5 Radiograph of left thumb shows destruction of left first metacarpophalangeal joint with juxta-articular osteopenia and foci of calcification. In view of this appearance gout was also considered in the differential. However in view of normal serum uric acid levels, infective arthropathy was the most likely diagnosis.

To conclude, radiologists should improve communication with referring physicians and increase their awareness regarding the utility and indications for various imaging tests^[11]. Radiologists should also themselves act as true imaging gatekeepers, preventing unnecessary overuse of imaging and striving to overcome commoditization of imaging modalities^[12].

While making of provisional diagnosis, a radiologist should think of common disease over uncommon dis-

eases. With high prevalence of common disease, a radiologist making a diagnosis of common disease, statistically will be correct in most of the cases. But it should be kept in mind that not to miss a grave or medico legally important condition even it might be uncommon.

It is always worth to follow protocol in certain conditions, which are made for standardization, streamlining the workflow, increase the accuracy as well better communication among clinicians and radiologist. A good example for a well-accepted protocol is Breast Imaging Reporting and Data System (BIRADS). At times a radiologist giving a BIRADS category of 3, he might be more than 98% accurate in diagnosis (BIRADS category 3 translates to “probably benign”. The likelihood of malignancy is 0%-2%). To address this small portion of likelihood of malignancy, it is advised to have a short interval follow up, rather than further investigations to confirm the benignity.

A referring clinician needs to know what imaging study is suitable to ascertain a particular condition. An open and free discussion with the radiologist regarding patient disease condition, availability of imaging resources, benefits and limitation of diagnostic modality should be encouraged.

There is a need for setting objective benchmarks for missed diagnoses in the field of radiology. There must be greater knowledge sharing, targeted instruction and team-working among various clinical fields.

ARTICLE HIGHLIGHTS

Case characteristics

A case of tubercular arthritis who underwent a number of investigations in suspicion of malignancy, each one adding to the confusion rather than helping in arriving diagnosis.

Clinical diagnosis

Infective arthritis of hand.

Differential diagnosis

Rheumatoid arthritis; Septic arthritis; Primary or secondary malignancy.

Laboratory diagnosis

Demonstration of Mycobacterium tuberculosis on culture of bone tissue/positive Ziehl-Neelsen staining/rapid PCR DNA detection.

Imaging diagnosis

Radiography: Juxta-articular osteopenia, subarticular erosions and joint space narrowing, with or without soft tissue component. MRI: Synovitis, joint effusion, subarticular erosions, active and chronic pannus, abscesses, hypo-intense synovium and bone chips.

Pathological diagnosis

Features favoring tubercular infection as granulomas with caseous necrosis in synovial tissue and bone.

Treatment

Skeletal tuberculosis including arthritis are treated with 9-12 mo of anti-tubercular drug regimen.

Related reports

Several cases of tubercular involvement of small joints of hand are reported in literature. In most of the cases, septic and rheumatoid arthritis were considered as differential diagnosis. Two cases of tubercular arthritis mimicking neoplasm have been reported.

Term explanation

VOMIT: Victims of modern imaging technology; Phemister's triad: Juxta-articular osteopenia, subarticular erosions and joint space narrowing.

Experiences and lessons

Following standardized guidelines reduces the errors in diagnostic and

treatment workflow. While making of provisional diagnosis, a radiologist should think of common disease over uncommon diseases. A free and open discussion among clinicians, radiologists and pathologists should be encouraged.

REFERENCES

- 1 **Hayward R.** VOMIT (victims of modern imaging technology)-an acronym for our times. *BMJ* 2003; **326**: 1273 [DOI: 10.1136/bmj.326.7401.1273]
- 2 **Shaikh U, Lewis-Jones H.** Commercial CT scans: VOMIT victim of medical investigative technology. *BMJ* 2008; **336**: 8 [PMID: 18174573 DOI: 10.1136/bmj.39435.572731.3A]
- 3 **Harisinghani MG, McCloud TC, Shepard JA, Ko JP, Shroff MM, Mueller PR.** Tuberculosis from head to toe. *Radiographics* 2000; **20**: 449-470; quiz 528-529, 532 [PMID: 10715343 DOI: 10.1148/radiographics.20.2.g00mc12449]
- 4 **Martini M.** Tuberculosis of the Upper-Limb Joints. Tuberculosis of the Bones and Joints. Switzerland: Springer, 1988: 80-110 [DOI: 10.1007/978-3-642-61358-6_10]
- 5 **Fukasawa H, Suzuki H, Kato A, Yamamoto T, Fujigaki Y, Yonemura K, Hishida A.** Tuberculous arthritis mimicking neoplasm in a hemodialysis patient. *Am J Med Sci* 2001; **322**: 373-375 [PMID: 11780697 DOI: 10.1097/00000441-200112000-00012]
- 6 **Gutiérrez-Polo RA, López-Medina S, Cabrera-Pozuelo E, González-Vela C, Gutiérrez-Polo MD, Peña-Sagredo JL, Martínez-Taboada VM.** Metastatic arthropathy report of two cases and review of the literature. *J Clin Rheumatol* 1997; **3**: 162-167 [PMID: 19078177 DOI: 10.1097/00124743-199706000-00011]
- 7 **Kotwal PP, Khan SA.** Tuberculosis of the hand: clinical presentation and functional outcome in 32 patients. *J Bone Joint Surg Br* 2009; **91**: 1054-1057 [PMID: 19651833 DOI: 10.1302/0301-620X.91B8.22074]
- 8 **Sawani V, Chandra T, Mishra RN, Aggarwal A, Jain UK, Gujral RB.** MRI features of tuberculosis of peripheral joints. *Clin Radiol* 2003; **58**: 755-762 [PMID: 14521883 DOI: 10.1016/S0009-9260(03)00271-X]
- 9 **Hassan FO.** Tuberculous dactylitis pseudotumor of an adult thumb: a case report. *Strategies Trauma Limb Reconstr* 2010; **5**: 53-56 [PMID: 20360878 DOI: 10.1007/s11751-010-0080-1]
- 10 **Kobayashi K, Bhargava P, Raja S, Nasser F, Al-Balas HA, Smith DD, George SP, Vij MS.** Image-guided biopsy: what the interventional radiologist needs to know about PET/CT. *Radiographics* 2012; **32**: 1483-1501 [PMID: 22977031 DOI: 10.1148/rg.325115159]
- 11 **FitzGerald R.** Radiological error: analysis, standard setting, targeted instruction and teamworking. *Eur Radiol* 2005; **15**: 1760-1767 [PMID: 15726377 DOI: 10.1007/s00330-005-2662-8]
- 12 **Jain SN.** Are radiologists true medical imaging gatekeepers? *Indian J Radiol Imaging* 2014; **24**: 315-316 [PMID: 25489123 DOI: 10.4103/0971-3026.143892]

P- Reviewer: Arcangeli S, Chow J, Gao BL **S- Editor:** Ji FF

L- Editor: A **E- Editor:** Lu YJ





Published by **Baishideng Publishing Group Inc**
7901 Stoneridge Drive, Suite 501, Pleasanton, CA 94588, USA
Telephone: +1-925-223-8242
Fax: +1-925-223-8243
E-mail: bpgoffice@wjgnet.com
Help Desk: <http://www.f6publishing.com/helpdesk>
<http://www.wjgnet.com>

